FINAL SAFETY ANALYSIS REPORT

for the

HOLTEC INTERNATIONAL

STORAGE, TRANSPORT,

AND REPOSITORY CASK SYSTEM

(HI-STAR 100 CASK SYSTEM)

DOCKET 72-1008

LIST OF EFFECTIVE PAGES FOR HI-STAR 100 FSAR REVISION 3

Page(s)	Revision
i through xxvii	3

LIST OF EFFECTIVE PAGES FOR HI-STAR 100 FSAR REVISION 3

Page(s)	Revision
1.0-1 through 1.0-25	3
1.1-1	0
Fig. 1.1.1 and 1.1.2	0
1.2-1 through 1.2-21	2
Fig. 1.2.1 and 1.2.2	0
Fig. 1.2.3	0 (deleted)
Fig. 1.2.4	1
Fig. 1.2.5 through 1.2.9	0
Fig. 1.2.10	1 (deleted)
Fig. 1.2.11a through 11c	0
Fig. 1.2.12a through 12c	0
1.3-1	0
1.4-1 and 1.4-2	0
Fig. 1.4.1	0
1.5-1	2
Drawings	See Section 1.5
1.6-1	0
1.7-1	0
1.A-1 through 1.A-7	2
Fig. 1.A.1 through 1.A.5	0
1.B-1 through 1.B-4	0
1.C-1 through 1.C-8	0

LIST OF EFFECTIVE PAGES FOR HI-STAR 100 FSAR REVISION 3

Page(s)	Revision
2.0-1 through 2.0-20	3
2.1-1 through 2.1-25	2
Fig. 2.1.1	1
Fig. 2.1.2 and 2.1.2A	0
Fig. 2.1.3 through 2.1.6	0
Fig. 2.1.7	0 (deleted)
Fig. 2.1.8	0
2.2-1 through 2.2-40	2
2.3-1 through 2.3-7	1
2.4-1 through 2.4-3	1
2.5-1	0
2.6-1 and 2.6-2	0

LIST OF EFFECTIVE PAGES FOR HI-STAR 100 FSAR REVISION 3

Page(s)	Revision
3.0-1 through 3.0-10	1
3.1-1 through 3.1-38	2
Fig. 3.1.1 through 3.1.3	0
3.2-1 through 3.2-5	2
Fig. 3.2.1	0
3.3-1 through 3.3-8	2
3.4-1 through 3.4-88	3
Fig. 3.4.1 through 3.4.3	0
Fig. 3.4.4	0 (deleted)
Fig. 3.4.5 and 3.4.6	0
Fig. 3.4.7	0 (deleted)
Fig. 3.4.8 and 3.4.9	0
Fig. 3.4.10	0 (deleted)
Fig. 3.4.11 through 3.4.28	0
Fig. 3.4.29 and 3.4.30	0 (deleted)
Fig. 3.4.31 through 3.4.34	0
Fig. 3.4.35	0 (deleted)
Fig. 3.4.36 through 3.4.45	0
Fig. 3.4.46	1
3.5-1	0
3.6-1 through 3.6-9	1
3.7-1 through 3.7-8	2
3.8-1 and 3.8-2	0
3.A-1 through 3.A-18	2
Fig. 3.A.1 and 3.A.11	0
Fig. 3.A.12 and 3.A.13	0 (deleted)
Fig. 3.A.14 through 3.A.19	0
3.B-1 through 3.B-8	1
3.C-1 through 3.C-8	0
Fig. 3.C.1 through 3.C.3	0
3.D-1 through 3.D-10	0
Fig. 3.D.1 and 3.D.2	0
3.E-1 through 3.E-11	1
Fig. 3.E.1 and 3.E.2	0
3.F-1 through 3.F-23	1
3.G-1 through 3.G-15	0
Fig. 3.G.1 through 3.G.6	0
3.H-1 through 3.H-35	1
3.I-1 through 3.I-7	0
Fig. 3.I.1	0
3.J-1 through 3.J-24	1
3.K-1 through 3.K-10	0
3.L-1 through 3.L-3	0
Fig. 3.L.1 and 3.L.2	0
3.M-1 through 3.M-17	3
Fig. 3.M.1 and 3.M.2	0
Appendix 3.N	1 (deleted)
Appendix 3.O	1 (deleted)
Appendix 3.P	0 (deleted)
Appendix 3.Q	0 (deleted)
Appendix 3.R	1 (deleted)

Appendix 3.S	1 (deleted)
Appendix 3.T	1 (deleted)
3.U-1 through 3.U-16	0
Fig. 3.U.1	0
Appendix 3.V	0 (deleted)
3.W-1 through 3.W-16	0
Fig. 3.W.1	0
3.X-1 through 3.X-9	0
Fig. 3.X.1 and 3.X.6	0
3.Y-1 through 3.Y-8	0
Fig. 3.Y.1 through 3.Y.3	0
Fig. 3.Y.4a through 3.Y.4e	0
3.Z-1 through 3.Z-7	1
Fig. 3.Z.1 and 3.Z.2	0
Appendix 3.AA	1 (deleted)
Appendix 3.AB	1 (deleted)
Appendix 3.AC	1 (deleted)
3.AD-1 through 3.AD-9	0
Fig. 3.AD.1	0
3.AE-1 through 3.AE-12	2
3.AF-1 through 3.AF-13	2
3.AG-1 through 3.AG-6	1
3.AH-1 through 3.AH-6	1
3.AI-1 through 3.AI-11	0

LIST OF EFFECTIVE PAGES FOR HI-STAR 100 FSAR REVISION 3

Page(s)	Revision
4.0-1 and 4.0-2	0
4.1-1 through 4.1-3	1
4.2-1 through 4.2-10	1
4.3-1 through 4.3-16	1
4.4-1 through 4.4-58	1
Fig. 4.4.1 through 4.4.3	0
Fig. 4.4.4	1
Fig. 4.4.5 through 4.4.9	0
Fig. 4.4.10	0 (deleted)
Fig. 4.4.11	1
Fig. 4.4.12 through 4.4.15	0
Fig. 4.4.16	0 (deleted)
Fig. 4.4.17 through 4.4.19	0
Fig. 4.4.20	0 (deleted)
Fig. 4.4.21 and 4.4.22	0
Fig. 4.4.23	0 (deleted)
Fig. 4.4.24 and 4.4.25	0
4.5-1 and 4.5-2	0
4.6-1 and 4.6-2	0

LIST OF EFFECTIVE PAGES FOR HI-STAR 100 FSAR REVISION 3

Page(s)	Revision
5.0-1 through 5.0-3	0
5.1-1 through 5.1-15	1
Fig. 5.1.1 and 5.1.2	0
5.2-1 through 5.2-44	1
5.3-1 through 5.3-10	1
Fig. 5.3.1	0 (deleted)
Fig. 5.3.2 and 5.3.3	0
Fig. 5.3.4	0 (deleted)
Fig. 5.3.5 and 5.3.9	0
Fig. 5.3.10 and 5.3.11	1
5.4-1 through 5.4-28	1
Fig. 5.4.1	0
5.5-1	0
5.6-1 and 5.6-2	0
5.A-1 through 5.A-3	0
5.B-1 through 5.B-6	0
5.C-1 through 5.C-35	0

LIST OF EFFECTIVE PAGES FOR HI-STAR 100 FSAR REVISION 3

Page(s)	Revision
6.1-1 through 6.1-10	1
6.2-1 through 6.2-55	1
6.3-1 through 6.3-11	1
Fig. 6.3.1	1
Fig. 6.3.2	0 (deleted)
Fig. 6.3.3	0
Fig. 6.3.4	1
Fig. 6.3.5	0 (deleted)
Fig. 6.3.6 and 6.3.7	0
6.4-1 through 6.4-13	1
Fig. 6.4.1	0 (deleted)
Fig. 6.4.2 through 6.4.10	0
6.5-1	0
6.6-1	0
6.7-1 and 6.7-2	1
6.A-1 through 6.A-20	2
Fig. 6.A.1 through 6.A.5	0
Fig. 6.A.6	2
6.B-1 and 6.B-2	0
6.C-1 through 6.C-8	1
6.D-1 through 6.D-46	1

LIST OF EFFECTIVE PAGES FOR HI-STAR 100 FSAR REVISION 3

Page(s)	Revision
7.0-1	0
7.1-1 through 7.1-8	2
Fig. 7.1.1 through 7.1.2	0
Fig 7.1.3	2 (deleted)
7.2-1 through 7.2-7	1
7.3-1 through 7.3-16	1
7.4-1 and 7.4-2	0
7.5-1 and 7.5-2	0
7.A-1 through 7.A-46	0

LIST OF EFFECTIVE PAGES FOR HI-STAR 100 FSAR REVISION 3

Page(s)	Revision
8.0-1 through 8.0-6	2
8.1-1 through 8.1-35	3
Fig. 8.1.1	0
Fig. 8.1.2a through 8.1.2c	0
Fig. 8.1.3 through 8.1.11	0
Fig. 8.1.12	1
Fig. 8.1.13 through 8.1.16	0
Fig. 8.1.17 and 8.1.18	1
Fig. 8.1.19	0
Fig. 8.1.20	0 (deleted)
Fig. 8.1.21	1
Fig. 8.1.22	0
Fig. 8.1.23	1
Fig. 8.1.24 through 8.1.31	0
8.2-1	0
8.3-1 through 8.3-8	2
Fig. 8.3.1	0
Fig. 8.3.2a through 8.3.2c	0
Fig. 8.3.3 and 8.3.4	0
Fig. 8.3.5	1
8.4-1	0
8.5-1	0
8.6-1	2

LIST OF EFFECTIVE PAGES FOR HI-STAR 100 FSAR REVISION 3

Page(s)	Revision
9.1-1 through 9.1-28	3
Fig. 9.1.1	0 (deleted)
Fig. 9.1.2 through 9.1.4	0
9.2-1 through 9.2-3	0
9.3-1	0
9.4-1 and 9.4-2	0

LIST OF EFFECTIVE PAGES FOR HI-STAR 100 FSAR REVISION 3

Page(s)	Revision
10.1-1 through 10.1-7	2
Fig. 10.1.1	0
Fig. 10.1.2	1
Fig. 10.1.3 through 10.1.6	0
10.2-1	0
10.3-1 through 10.3-8	1
10.4-1 through 10.4-3	0
10.5-1	0
10.6-1	0

LIST OF EFFECTIVE PAGES FOR HI-STAR 100 FSAR REVISION 3

Page(s)	Revision
11.1-1 through 11.1-10	0
11.2-1 through 11.2-38	1
Fig. 11.2.1 through 11.2.4	0
11.3-1	0
11.4-1	0

LIST OF EFFECTIVE PAGES FOR HI-STAR 100 FSAR REVISION 3

Page(s)	Revision
12.1-1 through 12.1-3	0
12.2-1 through 12.2-4	0
12.3-1	0
12.4-1	0
12.5-1	0
Appendix 12.A (37 Pages)	0
Appendix 12.B (95 Pages)	0

LIST OF EFFECTIVE PAGES FOR HI-STAR 100 FSAR REVISION 3

Page(s)	Revision
13.0-1	3
13.1-1 and 13.1.2	1(deleted)
13.2-1	0(deleted)
13.3-1 through 13.3-15	1(deleted)
13.4-1	1(deleted)
13.5-1 and 13.5.2	0(deleted)
13.6-1	3

TABLE OF CONTENTS

TABLE OF CONTENTS

TABLE OF CONTENTS

TABLE OF CONTENTS

TABLE OF CONTENTS

TABLE OF CONTENTS

TABLE OF CONTENTS

TABLE OF CONTENTS

TABLE OF CONTENTS

TABLE OF CONTENTS

TABLE OF CONTENTS

TABLE OF CONTENTS

TABLE OF CONTENTS

LIST OF FIGURES

LIST OF FIGURES (continued)

LIST OF FIGURES (continued)

LIST OF FIGURES (continued)

LIST OF FIGURES (continued)

LIST OF FIGURES (continued)

LIST OF FIGURES (continued)

LIST OF FIGURES (continued)

LIST OF FIGURES (continued)

LIST OF FIGURES (continued)

LIST OF FIGURES (continued)

LIST OF FIGURES (continued)

LIST OF FIGURES (continued)

CHAPTER 1: GENERAL DESCRIPTION

1.0 GENERAL INFORMATION

This Final Safety Analysis Report (FSAR) for Holtec International's HI-STAR 100 System is a compilation of information and analyses to support a United States Nuclear Regulatory Commission (NRC) licensing review as a spent nuclear fuel dry storage cask under the requirements specified in 10CFR72 [1.0.1]. This FSAR describes the basis for NRC approval and issuance of a Certificate of Compliance (C of C) for storage under provisions of 10CFR72, Subpart L for the HI-STAR 100 to safely store spent nuclear fuel (SNF) at an Independent Spent Fuel Storage Installation (ISFSI) facility. This report has been prepared in the format and content suggested in NRC Regulatory Guide 3.61 [1.0.2] and NUREG-1536 Standard Review Plan for Dry Cask Storage Systems [1.0.3] to facilitate the NRC review process.

The purpose of this chapter is to provide a general description of the design features and storage capabilities of the HI-STAR 100 System, drawings of the structures, systems, and components important to safety, and the qualifications of the certificate holder. This report is also suitable for incorporation into a site-specific Safety Analysis Report which may be submitted by an applicant for a site-specific 10 CFR 72 license to store SNF at an ISFSI or a facility similar in objective and scope. Table 1.0.1 contains a listing of the terminology and notation used in this FSAR.

To aid NRC review, additional tables and references have been added to facilitate the location of information requested by NUREG-1536. Table 1.0.2 provides a matrix of the topics in NUREG-1536 and Regulatory Guide 3.61, the corresponding 10CFR72 requirements, and a reference to the applicable FSAR section that addresses each topic.

The HI-STAR 100 FSAR is in full compliance with the intent of all regulatory requirements listed in Section III of each chapter of NUREG-1536. However, an exhaustive review of the provisions in NUREG-1536, particularly Section IV (Acceptance Criteria) and Section V (Review Procedures) has identified certain deviations from verbatim compliance with all requirements. A list of all such items, along with a discussion of their intent and Holtec International's approach for compliance with the underlying intent is presented in Table 1.0.3 herein. Table 1.0.3 also contains the justification for the alternative method for compliance adopted in this FSAR. The justification may be in the form of a supporting analysis, established industry practice, or other NRC guidance documents. Each chapter in this FSAR provides a clear statement with respect to the extent of compliance to the NUREG-1536 provisions.

Chapter 1 is in full compliance with NUREG-1536; no exceptions are taken.

The generic design basis and the corresponding safety analysis of the HI-STAR 100 System contained in this FSAR are intended to bound the SNF characteristics, design, conditions, and interfaces that exist in the vast majority of domestic power reactor sites and potential away-from-reactor storage sites in the contiguous United States. This FSAR also provides the basis for component fabrication and acceptance, and the requirements for safe operation and maintenance of the components, consistent with the design basis and safety analysis documented herein. In accordance with 10CFR72, Subpart K, site-specific implementation of the generically certified HI-

STAR 100 System requires that the licensee perform a site-specific evaluation, as defined in 10CFR72.212. The HI-STAR 100 System FSAR identifies a limited number of conditions that are necessarily site-specific and are to be addressed in the licensee's 10CFR72.212 evaluation. These include:

- Siting of the ISFSI and design of the storage pad and security system. Site-specific demonstration of compliance with regulatory dose limits. Implementation of a site-specific ALARA program.

- An evaluation of site-specific hazards and design conditions that may exist at the ISFSI site or the transfer route between the plant's cask receiving bay and the ISFSI. These include, but are not limited to, explosion and fire hazards, flooding conditions, land slides, and lightning protection.

- Determination that the physical and nucleonic characteristics and the condition of the SNF assemblies to be dry stored meet the fuel acceptance requirements of the Certificate of Compliance.

- An evaluation of interface and design conditions that exist within the plant's fuel building in which canister fuel loading, canister closure, and cask handling operations are to be conducted in accordance with the applicable 10CFR50 requirements and technical specifications for the plant.

- Detailed site-specific operating, maintenance, and inspection procedures prepared in accordance with the generic procedures and requirements provided in Chapters 8 and 9, and the technical specifications provided in the Certificate of Compliance.

- Performance of pre-operational testing.

- Implementation of a safeguards and accountability program in accordance with 10CFR73. Preparation of a physical security plan in accordance with 10CFR73.55.

- Review of the reactor emergency plan, quality assurance (QA) program, training program, and radiation protection program.

The generic safety analyses contained in the HI-STAR 100 FSAR may be used as input and for guidance by the licensee in performing a 10CFR72.212 evaluation.

Within this report, all figures, tables and references cited are identified by the double decimal system m.n.i, where m is the chapter number, n is the section number, and i is the sequential number. Thus, for example, Figure 1.2.3 is the third figure in Section 1.2 of Chapter 1.

Revision 0 of this FSAR, issued in March 2001, included information supporting changes to CoC 72-1008 made in Amendment 1 (effective December 26, 2000), as well as information from the original version of the CoC that did not change as a result of that amendment. This is because the

safety analysis report updating requirements of 10 CFR 72.248 did not become effective until after the original version of CoC 72-1008 became effective in October 1999. Therefore, a Final Safety Analysis Report (FSAR) was never issued to replaced Revision 10 of the HI-STAR 100 Topical Safety Analysis Report (TSAR).

1.0.1 Engineering Change Orders

The changes authorized by the following Holtec Engineering Change Orders (ECOs) are reflected in Revision 3 of this FSAR:

General FSAR Changes: ECOs 5014- 112, 116, 126, 134, 142.

Table 1.0.1

TERMINOLOGY AND NOTATION

ALARA is an acronym for As Low As Reasonably Achievable.

Boral is a generic term to denote an aluminum-boron carbide cermet manufactured in accordance with U.S. Patent No. 4027377. The individual material supplier may use another trade name to refer to the same product.

Boral^{TM} means Boral manufactured by AAR Advanced Structures.

BWR is an acronym for boiling water reactor.

C.G. is an acronym for center of gravity.

Confinement Boundary means the outline formed by the sealed, cylindrical enclosure of the multi-purpose canister (MPC) shell welded to a solid baseplate, a lid welded around the top circumference of the shell wall, the port cover plates welded to the lid, and the closure ring welded to the lid and MPC shell.

Confinement System means the HI-STAR 100 multi-purpose canister (MPC) which encloses and confines the spent nuclear fuel during storage.

Controlled Area means that area immediately surrounding an ISFSI for which the owner/user exercises authority over its use and within which operations are performed.

DBE means Design Basis Earthquake.

DCSS is an acronym for Dry Cask Storage System.

Damaged Fuel Assembly is defined as a fuel assembly with known or suspected cladding defects, as determined by a review of records, greater than pinhole leaks or hairline cracks, missing fuel rods that are not replaced with dummy fuel rods, or those that cannot be handled by normal means. Fuel assemblies that cannot be handled by normal means due to fuel cladding damage are considered fuel debris.

Damaged Fuel Container means a specially designed enclosure for damaged fuel or fuel debris which permits gaseous and liquid media to escape while minimizing dispersal of gross particulates. DFCs authorized for use in the HI-STAR 100 System are the Holtec design or the Transnuclear Dresden Unit 1 design.

Enclosure Vessel means the pressure vessel defined by the cylindrical shell, baseplate, port cover plates, lid, and closure ring which provides confinement for the helium gas contained within the MPC. The Enclosure Vessel (EV) and the fuel basket together constitute the multi-purpose canister.

Fuel Basket means a honeycomb structural weldment with square openings that can accept a fuel assembly of the type for which it is designed.

Fuel Debris is defined as ruptured fuel rods, severed fuel rods, loose fuel pellets, or fuel assemblies with known or suspected defects which cannot be handled by normal means due to fuel cladding damage.

FSAR is an acronym for Final Safety Analysis Report (10CFR72).

Helium Retention Boundary means the enclosure formed by the overpack inner shell welded to a bottom plate and top main flange plus the bolted closure plate and port plugs with metallic seals. The helium retention boundary is an additional independent confinement boundary, however, no credit is taken for this additional barrier. The helium retention boundary maintains an inert helium atmosphere around the MPC.

HI-STAR 100 MPC means the sealed spent nuclear fuel container which consists of a honeycombed fuel basket contained in a cylindrical canister shell which is welded to a baseplate, lid with welded port cover plates, and closure ring. MPC is an acronym for multi-purpose canister. There are different MPCs with different fuel basket geometries for storing PWR or BWR fuel, but all MPCs have identical exterior dimensions. The MPC is the confinement boundary for storage conditions.

HI-STAR 100 overpack or overpack means the cask that receives and contains the sealed multi-purpose canisters containing spent nuclear fuel. It provides the retention boundary for the helium atmosphere, gamma and neutron shielding, and a set each of lifting and pocket trunnions. It is not defined as the confinement boundary for the radioactive material during storage.

HI-STAR 100 System consists of the HI-STAR 100 MPC sealed within the HI-STAR 100 overpack.

Holtite^{TM} is the trade name for all present and future neutron shielding materials formulated under Holtec International's R&D program dedicated to developing shielding materials for application in dry storage and transport systems. The Holtite development program is an ongoing experimentation effort to identify neutron shielding materials with enhanced shielding and temperature tolerance characteristics. Holtite-A^{TM} is the first, and only shielding material qualified under the Holtec R&D program. As such, the terms Holtite and Holtite-A may be used inter changeably throughout this FSAR.

Holtite-A^{TM} is a trademarked Holtec International neutron shield material.

Important to Safety (ITS) means a function or condition required to store spent nuclear fuel safely; to prevent damage to spent nuclear fuel during handling and storage, and to provide reasonable assurance that spent nuclear fuel can be received, handled, packaged, stored, and retrieved without undue risk to the health and safety of the public.

Independent Spent Fuel Storage Installation (ISFSI) means a facility designed, constructed, and licensed for the interim storage of spent nuclear fuel and other radioactive materials associated with spent fuel storage in accordance with 10CFR72.

Intact Fuel Assembly is defined as a fuel assembly without known or suspected cladding defects greater than pinhole leaks and hairline cracks, and which can be handled by normal means. Partial fuel assemblies, that is fuel assemblies from which fuel rods are missing, shall not be classified as intact fuel assemblies unless dummy fuel rods used to displace an amount of water greater than or equal to that displaced by the original fuel rod(s).

Maximum Reactivity means the highest possible k-effective including bias, uncertainties, and calculational statistics evaluated for the worst-case combination of fuel basket manufacturing tolerances.

MGDS is an acronym for Mined Geological Depository System.

Multi-Purpose Canister (MPC) means the sealed canister which consists of a honeycombed fuel basket for spent nuclear fuel storage, contained in a cylindrical canister shell which is welded to a baseplate, lid with welded port cover plates, and closure ring. There are different MPCs with different fuel basket geometries for storing PWR or BWR fuel, but all MPCs have identical exterior dimensions. The MPC is the confinement boundary for storage conditions. MPC is an acronym for multi-purpose canister. The MPCs used as part of the HI-STORM 100 System (Docket No. 72-1014) are identical to the HI-STAR 100 MPCs evaluated in the HI-STAR 100 storage (Docket No. 72-1008) and transport (Docket No. 71-9261) applications.

MPC Fuel Basket means the honeycombed composite cell structure utilized to maintain subcriticality of the spent nuclear fuel. The number and size of the storage cells depends on the type of spent nuclear fuel to be stored. Each MPC fuel basket has sheathing welded to the storage cell walls for retaining the Boral neutron absorber. Boral is a commercially-available thermal neutron poison material composed of boron carbide and aluminum.

Neutron Shielding means Holtite or Holtite-A, a material used in the HI-STAR overpack to thermalize and capture neutrons emanating from the radioactive spent nuclear fuel.

PWR is an acronym for pressurized water reactor.

Reactivity is used synonymously with effective multiplication factor or k-effective.

SAR is an acronym for Safety Analysis Report (10CFR71).

Single Failure Proof means that the handling system is designed so that a single failure will not result in the loss of the capability of the system to safely retain the load.

SNF is an acronym for spent nuclear fuel.

Table 1.0.1 (continued)

TERMINOLOGY AND NOTATION

SSC is an acronym for Structures, Systems and Components.

STP is Standard Temperature (298°K) and Pressure (1 atm) conditions.

ZPA is an acronym for zero period acceleration.

Table 1.0.2

HI-STAR 100 SYSTEM FSAR REGULATORY COMPLIANCE
CROSS-REFERENCE MATRIX

Regulatory Guide 3.61 Section and Content	Associated NUREG-1536 Review Criteria	Applicable 10CFR72 or 10CFR20 Requirement	HI-STAR FSAR
1. General Description			
1.1 Introduction	1.III.1 General Description & Operational Features	10CFR72.24(b)	1.1
1.2 General Description	1.III.1 General Description & Operational Features	10CFR72.24(b)	1.2
1.2.1 Cask Characteristics	1.III.1 General Description & Operational Features	10CFR72.24(b)	1.2.1
1.2.2 Operational Features	1.III.1 General Description & Operational Features	10CFR72.24(b)	1.2.2
1.2.3 Cask Contents	1.III.3 DCSS Contents	10CFR72.2(a)(1) 10CFR72.236(a)	1.2.3
1.3 Identification of Agents & Contractors	1.III.4 Qualification of the Applicant	10CFR72.24(j) 10CFR72.28(a)	1.3
1.4 Generic Cask Arrays	1.III.1 General Description & Operational Features	10CFR72.24(c)(3)	1.4
1.5 Supplemental Data	1.III.2 Drawings	10CFR72.24(c)(3)	1.5
NA	1.III.6 Consideration of Transport Requirements	10CFR72.230(b) 10CFR72.236(m)	1.1
NA	1.III.5 Quality Assurance	10CFR72.24(n)	1.3
2. Principal Design Criteria			
2.1 Spent Fuel To Be Stored	2.III.2.a Spent Fuel Specifications	10CFR72.2(a)(1) 10CFR72.236(a)	2.1
2.2 Design Criteria for Environmental Conditions and Natural Phenomena	2.III.2.b External Conditions, 2.III.3.b Structural, 2.III.3.c Thermal	0CFR71.122(b)	2.2
		10CFR72.122(c)	2.2.3.3, 2.2.3.10
		10CFR72.122(b)(1)	2.2
		10CFR72.122(b)(2)	2.2.3.11
		10CFR72.122(h)(1)	2.0
2.2.1 Tornado and Wind Loading	2.III.2.b External Conditions	10CFR72.122(b)	2.2.3.5

Table 1.0.2 (continued)

HI-STAR 100 SYSTEM FSAR REGULATORY COMPLIANCE CROSS-REFERENCE MATRIX

Regulatory Guide 3.61 Section and Content	Associated NUREG-1536 Review Criteria	Applicable 10CFR72 or 10CFR20 Requirement	HI-STAR FSAR
2.2.2 Water Level (Flood)	2.III.2.b External Conditions 2.III.3.b Structural	10CFR72.122(b)(2)	2.2.3.6
2.2.3 Seismic	2.III.3.b Structural	10CFR72.102(f) 10CFR72.122(b)(2)	2.2.3.7
2.2.4 Snow and Ice	2.III.2.b External Conditions 2.III.3.b Structural	10CFR72.122(b)	2.2.1.6
2.2.5 Combined Load	2.III.3.b Structural	10CFR72.24(d) 10CFR72.122(b)(2)(ii)	2.2.7
NA	2.III.1 Structures, Systems, and Components Important to Safety	10CFR72.122(a) 10CFR72.24(c)(3)	2.2.4
NA	2.III.2 Design Criteria for Safety Protection Systems	10CFR72.236(g) 10CFR72.24(c)(1) 10CFR72.24(c)(2) 10CFR72.24(c)(4) 10CFR72.120(a) 10CFR72.236(b)	2.0, 2.2
NA	2.III.3.c Thermal	10CFR72.128(a)(4)	2.3.2.2, 4.0
NA	2.III.3.f Operating Procedures	10CFR72.24(f) 10CFR72.128(a)(5)	10.0, 8.0
		10CFR72.236(h)	8.0
		10CFR72.24 (l)(2)	1.2.1, 1.2.2
		10CFR72.236(l)	2.3.2.1
		10CFR72.24(e) 10CFR72.104(b)	10.0, 8.0
	2.III.3.g Acceptance Tests & Maintenance	10CFR72.122 (l) 10CFR72.236 (g) 10CFR72.122 (f) 10CFR72.128 (a)(1)	9.0
2.3 Safety Protection Systems	--	--	2.3
2.3.1 General	--	--	2.3
2.3.2 Protection by Multiple Confinement Barriers and Systems	2.III.3.b Structural	10CFR72.236(1)	2.3.2.1
	2.III.3.c Thermal	10CFR72.236(f)	2.3.2.2
	2.III.3.d Shielding/ Confinement/ Radiation Protection	10CFR72.126(a) 10CFR72.128(a)(2)	2.3.5.2
		10CFR72.128(a)(3)	2.3.2.1
		10CFR72.236(d)	2.3.2.1, 2.3.5.2

Table 1.0.2 (continued)

HI-STAR 100 SYSTEM FSAR REGULATORY COMPLIANCE CROSS-REFERENCE MATRIX

Regulatory Guide 3.61 Section and Content	Associated NUREG-1536 Review Criteria	Applicable 10CFR72 or 10CFR20 Requirement	HI-STAR FSAR
		10CFR72.236(e)	2.3.2.1
2.3.3 Protection by Equipment & Instrument Selection	2.III.3.d Shielding/ Confinement/ Radiation Protection	10CFR72.122(h)(4) 10CFR72.122(i) 10CFR72.128(a)(1)	2.3.5
2.3.4 Nuclear Criticality Safety	2.III.3.e Criticality	10CFR72.124(a) 10CFR72.236(c) 10CFR72.124(b)	2.3.4, 6.0
2.3.5 Radiological Protection	2.III.3.d Shielding/ Confinement/ Radiation Protection	10CFR72.24(d) 10CFR72.104(a) 10CFR72.236(d)	10.4.1
		10CFR72.24(d) 10CFR72.106(b) 10CFR72.236(d)	10.4.2
		10CFR72.24(m)	2.3.2.1
2.3.6 Fire and Explosion Protection	2.III.3.b Structural	10CFR72.122(c)	2.3.6, 2.2.3.10
2.4 Decommissioning Considerations	2.III.3.h Decommissioning	10CFR72.24(f) 10CFR72.130 10CFR72.236 (h)	2.4
	14.III.1 Design	10CFR72.130	2.4
	14.III.2 Cask Decontamination	10CFR72.236(i)	2.4
	14.III.3 Financial Assurance & Record Keeping	10CFR72.30	(1)
	14.III.4 License Termination	10CFR72.54	(1)
3. Structural Evaluation			
3.1 Structural Design	3.III.1 SSC Important to Safety	10CFR72.24(c)(3) 10CFR72.24(c)(4)	3.1
	3.III.6 Concrete Structures	10CFR72.182 (b) 10CFR72.182 (c)	3.1
3.2 Weights and Centers of Gravity	3.V.1.b.2 Structural Design Features	--	3.2
3.3 Mechanical Properties of Materials	3.V.1.c Structural Materials	10CFR72.24(c)(3)	3.3
	3.V.2.c Structural Materials		
NA	3.III.2 Radiation Shielding, Confinement, and Subcriticality	10CFR72.24(d) 10CFR72.124(a) 10CFR72.236(c) 10CFR72.236(d) 10CFR72.236(l)	3.4.4.3 3.4.7.3 3.4.10

Table 1.0.2 (continued)

HI-STAR 100 SYSTEM FSAR REGULATORY COMPLIANCE CROSS-REFERENCE MATRIX

Regulatory Guide 3.61 Section and Content	Associated NUREG-1536 Review Criteria	Applicable 10CFR72 or 10CFR20 Requirement	HI-STAR FSAR
NA	3.III.3 Ready Retrieval	10CFR72.122(f) 10CFR72.122(h) 10CFR72.122(l)	3.4.4.3
NA	3.III.4 Design-Basis Earthquake	10CFR72.24(c) 10CFR72.236(g)	3.4.7
NA	3.III.5 20 Year Minimum Design Length	10CFR72.24(c) 10CFR72.182(b) 10CFR72.182(c)	3.4.11 3.4.12
3.4 General Standards for Casks	--	--	3.4
3.4.1 Chemical and Galvanic Reactions	3.V.1.b.2 Structural Design Features	--	3.4.1
3.4.2 Positive Closure	--	--	3.4.2
3.4.3 Lifting Devices	3.V.1.ii(4)(a) Trunnions	--	3.4.3, Appendices 3.E, 3AC, 3.D
3.4.4 Heat	3.V.1.d Structural Analysis	10CFR72.24(d) 10CFR72.122(b) 10CFR72.236(g)	3.4.4, Appendices 3.U, 3.W, 3.AD
3.4.5 Cold	3.V.1.d Structural Analysis	10CFR72.24(d) 10CFR72.102(f) 10CFR72.122(b) 10CFR72.122(c) 10CFR72.236(g)	3.4.5
3.5 Fuel Rods	--	10CFR72.122(h)(1)	3.5
4. Thermal Evaluation			
4.1 Discussion	4.III Regulatory Requirements	10CFR72.24(c)(3) 10CFR72.128(a)(4) 10CFR72.236(f)	4.1, 4.5
		10CFR72.236(h)	
4.2 Summary of Thermal Properties of Materials	4.V.4.b Material Properties	--	4.2
4.3 Specifications for Components	4.IV Acceptance Criteria	10CFR72.122(h)(1)	4.3
4.4 Thermal Evaluation for Normal Conditions of Storage	4.IV Acceptance Criteria	10CFR72.24(d) 10CFR72.236(g)	4.4
NA	4.IV Acceptance Criteria	10CFR72.24(d) 10CFR72.122(c)	11.1, 11.2

Table 1.0.2 (continued)

HI-STAR 100 SYSTEM FSAR REGULATORY COMPLIANCE CROSS-REFERENCE MATRIX

Regulatory Guide 3.61 Section and Content	Associated NUREG-1536 Review Criteria	Applicable 10CFR72 or 10CFR20 Requirement	HI-STAR FSAR
4.5 Supplemental Data	4.V.6 Supplemental Info.	--	--
5. Shielding Evaluation			
5.1 Discussion and Results	--	10CFR72.104(a) 10CFR72.106(b)	5.1
5.2 Source Specification	5.V.2 Radiation Source Definition	--	5.2
5.2.1 Gamma Source	5.V.2.a Gamma Source	--	5.2.1, 5.2.3
5.2.2 Neutron Source	5.V.2.b Neutron Source	--	5.2.2, 5.2.3
5.3 Model Specification	5.V.3 Shielding Model Specification	--	5.3
5.3.1 Description of the Radial and Axial Shielding Configuration	5.V.3.a Configuration of the Shielding and Source	10CFR72.24(c)(3)	5.3.1
5.3.2 Shield Regional Densities	5.V.3.b Material Properties	10CFR72.24(c)(3)	5.3.2
5.4 Shielding Evaluation	5.V.4 Shielding Analysis	10CFR72.24(d) 10CFR72.104(a) 10CFR72.106(b) 10CFR72.128(a)(2) 10CFR72.236(d)	5.4
5.5 Supplemental Data	5.V.5 Supplemental Info.	--	Appendices 5.A, 5.B, and 5.C
6. Criticality Evaluation			
6.1 Discussion and Results	--	--	6.1
6.2 Spent Fuel Loading	6.V.2 Fuel Specification	--	6.1, 6.2
6.3 Model Specifications	6.V.3 Model Specification	--	6.3
6.3.1 Description of Calculational Model	6.V.3.a Configuration	10CFR72.124(b) 10CFR72.24(c)(3)	6.3.1
6.3.2 Cask Regional Densities	6.V.3.b Material Properties	10CFR72.24(c)(3) 10CFR72.124(b) 10CFR72.236(g)	6.3.2
6.4 Criticality Calculations	6.V.4 Criticality Analysis	10CFR72.124	6.4
6.4.1 Calculational or Experimental Method	6.V.4.a Computer Programs and 6.V.4.b Multiplication Factor	10CFR72.124	6.4.1
6.4.2 Fuel Loading or Other	6.V.3.a Configuration	--	6.4.2

Table 1.0.2 (continued)

HI-STAR 100 SYSTEM FSAR REGULATORY COMPLIANCE CROSS-REFERENCE MATRIX

Regulatory Guide 3.61 Section and Content		Associated NUREG-1536 Review Criteria		Applicable 10CFR72 or 10CFR20 Requirement	HI-STAR FSAR
	Contents Loading Optimization				
6.4.3	Criticality Results	6.IV	Acceptance Criteria	10CFR72.24(d) 10CFR72.124 10CFR72.236(c)	6.1, 6.2, 6.3.1, 6.3.2
6.5	Critical Benchmark Experiments	6.V.4.c	Benchmark Comparisons	--	6.5, Appendix 6.A, 6.4.3
6.6	Supplemental Data	6.V.5	Supplemental Info.		Appendices 6.B, 6.C, and 6.D
7. Confinement					
7.1	Confinement Boundary	7.III.1	Description of Structures, Systems, and Components Important to Safety	10CFR72.24(c)(3) 10CFR72.24(l)	7.0, 7.1
7.1.1	Confinement Vessel	7.III.2	Protection of Spent Fuel Cladding	10CFR72.122(h)(l)	7.1, 7.1.1, 7.2.2
7.1.2	Confinement Penetrations	--		--	7.1.2
7.1.3	Seals and Welds	--		--	7.1.3
7.1.4	Closure	7.III.3	Redundant Sealing	10CFR72.236(e)	7.1.1, 7.1.4
7.2	Requirements for Normal Conditions of Storage	7.III.7	Evaluation of Confinement System	10CFR72.24(d) 10CFR72.236(l)	7.2
7.2.1	Release of Radioactive Material	7.III.6	Release of Nuclides to the Environment	10CFR72.24(l)(1)	7.2.1
		7.III.4	Monitoring of Confinement System	10CFR72.122(h)(4) 10CFR72.128(a)(l)	7.1.4
		7.III.5	Instrumentation	10CFR72.24(l) 10CFR72.122(i)	7.1.4
		7.III.8	Annual Dose	10CFR72.104(a)	7.3.5
7.2.2	Pressurization of Confinement Vessel	--		--	7.2.2
7.3	Confinement Requirements for Hypothetical Accident Conditions	7.III.7	Evaluation of Confinement System	10CFR72.24(d) 10CFR72.122(b) 10CFR72.236(l)	7.3
7.3.1	Fission Gas Products	--		--	7.3.1
7.3.2	Release of Contents	--		--	7.3.3
NA		--		10CFR72.106(b)	7.3

Table 1.0.2 (continued)

HI-STAR 100 SYSTEM FSAR REGULATORY COMPLIANCE CROSS-REFERENCE MATRIX

Regulatory Guide 3.61 Section and Content		Associated NUREG-1536 Review Criteria		Applicable 10CFR72 or 10CFR20 Requirement	HI-STAR FSAR
7.4	Supplemental Data	7.V	Supplemental Info.	--	--
8. Operating Procedures					
8.1	Procedures for Loading the Cask	8.III.1	Develop Operating Procedures	10CFR72.40(a)(5)	8.1 to 8.5
		8.III.2	Operational Restrictions for ALARA	10CFR72.24(e) 10CFR72.104(b)	8.1.5
		8.III.3	Radioactive Effluent Control	10CFR72.24(l)(2)	8.1.5, 8.5.2
		8.III.4	Written Procedures	10CFR72.212(b)(9)	8.0
		8.III.5	Establish Written Procedures and Tests	10CFR72.234(f)	8.0
		8.III.6	Wet or Dry Loading and Unloading Compatibility	10CFR72.236(h)	8.0
		8.III.7	Cask Design to Facilitate Decon	10CFR72.236(i)	8.1, 8.3
8.2	Procedures for Unloading the Cask	8.III.1	Develop Operating Procedures	10CFR72.40(a)(5)	8.3
		8.III.2	Operational Restrictions for ALARA	10CFR72.24(e) 10CFR72.104(b)	--
		8.III.3	Radioactive Effluent Control	10CFR72.24(l)(2)	8.3.3
		8.III.4	Written Procedures	10CFR72.212(b)(9)	8.0
		8.III.5	Establish Written Procedures and Tests	10CFR72.234(f)	8.0
		8.III.6	Wet or Dry Loading and Unloading Compatibility	10CFR72.236(h)	8.0
		8.III.8	Ready Retrieval	10CFR72.122(l)	8.3
8.3	Preparation of the Cask	--		--	8.3.2
8.4	Supplemental Data	--		--	Tables 8.1.1 to 8.1.10
	NA	8.III.9	Design To Minimize Radwaste	10CFR72.24(f) 10CFR72.128(a)(5)	8.1, 8.3
		8.III.10	SSCs Permit Inspection, Maintenance, and Testing	10CFR72.122(f)	Table 8.1.6

Table 1.0.2 (continued)

HI-STAR 100 SYSTEM FSAR REGULATORY COMPLIANCE CROSS-REFERENCE MATRIX

Regulatory Guide 3.61 Section and Content	Associated NUREG-1536 Review Criteria	Applicable 10CFR72 or 10CFR20 Requirement	HI-STAR FSAR
9. Acceptance Criteria and Maintenance Program			
9.1 Acceptance Criteria	9.III.1.a Preoperational Testing & Initial Operations	10CFR72.24(p)	8.1, 9.1
	9.III.1.c SSCs Tested and Maintained to Appropriate Quality Standards	10CFR72.24(c) 10CFR72.122(a)	9.1
	9.III.1.d Test Program	10CFR72.162	9.1
	9.III.1.e Appropriate Tests	10CFR72.236(l)	9.1
	9.III.1.f Inspection for Cracks, Pinholes, Voids and Defects	10CFR72.236(j)	9.1
	9.III.1.g Provisions that Permit Commission Tests	10CFR72.232(b)	9.1[(2)]
9.2 Maintenance Program	9.III.1.b Maintenance	10CFR72.236(g)	9.2
	9.III.1.c SSCs Tested and Maintained to Appropriate Quality Standards	10CFR72.122(f) 10CFR72.128(a)(l)	9.2
	9.III.1.h Records of Maintenance	10CFR72.212(b)(8)	9.2
NA	9.III.2 Resolution of Issues Concerning Adequacy of Reliability	10CFR72.24(i)	[(3)]
	9.III.1.d Submit Pre-Op Test Results to NRC	10CFR72.82(e)	[(4)]
	9.III.1.i Casks Conspicuously and Durably Marked	10CFR72.236(k)	9.1.7, 9.1.1.(12)
	9.III.3 Cask Identification		
10. Radiation Protection			
10.1 Ensuring that Occupational Exposures Are As Low As Reasonably Achievable (ALARA)	10.III.4 ALARA	10CFR20.1101 10CFR72.24(e) 10CCR72.104(b) 10CFR72.126(a)	10.1
10.2 Radiation Protection Design Features	10.V.1.b Design Features	10CFR72.126(a)(6)	10.2
10.3 Estimated Onsite Collective Dose Assessment	10.III.2 Occupational Exposures	10CFR20.1201 10CFR20.1207 10CFR20.1208 10CFR20.1301	10.3

Table 1.0.2 (continued)

HI-STAR 100 SYSTEM FSAR REGULATORY COMPLIANCE
CROSS-REFERENCE MATRIX

Regulatory Guide 3.61 Section and Content	Associated NUREG-1536 Review Criteria	Applicable 10CFR72 or 10CFR20 Requirement	HI-STAR FSAR
NA	10.III.3 Public Exposure	10CFR72.104 10CFR72.106	
	10.III.1 Effluents and Direct Radiation	10CFR72.104	10.4
11. Accident Analyses			
11.1 Off-Normal Operations	11.III.2 Meet Dose Limits for Anticipated Events	10CFR72.24(d) 10CFR72.104(a) 10CFR72.236(d)	11.1
	11.III.4 Maintain Subcritical Condition	10CFR72.124(a) 10CFR72.236(c)	11.1
	11.III.7 Instrumentation and Control for Off-Normal Condition	10CFR72.122(i)	11.1
11.2 Accidents	11.III.1 SSCs Important to Safety Designed for Accidents	10CFR72.24(d)(2) 10CFR72.122(b)(2) 10CFR72.122(b)(3) 10CFR72.122(d) 10CFR72.122(g)	11.2
	11.III.5 Maintain Confinement for Accident	10CFR72.236(l)	11.2
	11.III.4 Maintain Subcritical Condition	10CFR72.124(a) 10CFR72.236(c)	11.2, 6.0
	11.III.3 Meet Dose Limits for Accidents	10CFR72.24(d)(2) 10CFR72.24(m) 10CFR72.106(b)	11.2, 5.1.2, 7.3
	11.III.6 Retrieval	10CFR72.122(l)	8.3
	11.III.7 Instrumentation and Control for Accident Conditions	10CFR72.122(i)	(5)
NA	11.III.8 Confinement Monitoring	10CFR72.122(h)(4)	7.1.4
12. Operating Controls and Limits			
12.1 Proposed Operating Controls and Limits	--	10CFR72.44(c)	12.0
	12.III.1.e Administrative Controls	10CFR72.44(c)(5)	12.0
12.2 Development of Operating Controls and Limits	12.III.1 General Requirement for Technical Specifications	10CFR72.24(g) 10CFR72.26 10CFR72.44(c) 10CFR72 Subpart F 10CFR72 Subpart F	12.0
12.2.1 Functional and	12.III.1.a Functional/	10CFR72.44(c)(l)	Appendix

Table 1.0.2 (continued)

HI-STAR 100 SYSTEM FSAR REGULATORY COMPLIANCE
CROSS-REFERENCE MATRIX

Regulatory Guide 3.61 Section and Content	Associated NUREG-1536 Review Criteria	Applicable 10CFR72 or 10CFR20 Requirement	HI-STAR FSAR
Operating Limits, Monitoring Instruments, and Limiting Control Settings	Operating Units, Monitoring Instruments and Limiting Controls		12.A
12.2.2 Limiting Conditions for Operation	12.III.1.b Limiting Controls	10CFR72.44(c)(2)	Appendix 12.A
	12.III.2.a Type of Spent Fuel	10CFR72.236(a)	Appendix 12.A
	12.III.2.b Enrichment		
	12.III.2.c Burnup		
	12.III.2.d Minimum Acceptable Cooling Time		
	12.III.2.f Maximum Spent Fuel Loading Limit		
	12.III.2.g Weights and Dimensions		
	12.III.2.h Condition of Spent Fuel		
	12.III.2.e Maximum Heat Dissipation	10CFR72.236(a)	Appendix 12.A
	12.III.2.i Inerting Atmosphere Requirements	10CFR72.236(a)	Appendix 12.A
12.2.3 Surveillance Specifications	12.III.1.c Surveillance Requirements	10CFR72.44(c)(3)	Chapter 12
12.2.4 Design Features	12.III.1.d Design Features	10CFR72.44(c)(4)	Chapter 12
12.2.5 Suggested Format for Operating Controls and Limits	--	--	Appendix 12.A
NA	12.III.2 SCC Design Bases and Criteria	10CFR72.236(b)	2.0
NA	12.III.2 Criticality Control	10CFR72.236(c)	2.3.4, 6.0
NA	12.III.2 Shielding and Confinement	10CFR20 10CFR72.236(d)	2.3.5, 7.0, 5.0, 10.0
NA	12.III.2 Redundant Sealing	10CFR72.236(e)	7.1, 2.3.2
NA	12.III.2 Passive Heat Removal	10CFR72.236(f)	2.3.2.2, 4.0

Table 1.0.2 (continued)

HI-STAR 100 SYSTEM FSAR REGULATORY COMPLIANCE
CROSS-REFERENCE MATRIX

Regulatory Guide 3.61 Section and Content	Associated NUREG-1536 Review Criteria	Applicable 10CFR72 or 10CFR20 Requirement	HI-STAR FSAR
NA	12.III.2 20 Year Storage and Maintenance	10CFR72.236(g)	1.2.1.5, 9.0, 3.4.10, 3.4.11
NA	12.III.2 Decontamination	10CFR72.236(i)	8.0, 10.1
NA	12.III.2 Wet or Dry Loading	10CFR72.236(h)	8.0
NA	12.III.2 Confinement Effectiveness	10CFR72.236(j)	9.0
NA	12.III.2 Evaluation for Confinement	10CFR72.236(l)	7.1, 7.2, 9.0
13. Quality Assurance			
13.1 Quality Assurance	13.III Regulatory Requirements	10CFR72.24 (m)	13.0
	13.IV Acceptance Criteria	10CFR72, Subpart G	

Table 1.0.2 (continued)

HI-STAR 100 SYSTEM FSAR REGULATORY COMPLIANCE
CROSS-REFERENCE MATRIX

Notes:

(1) The stated requirement is the responsibility of the licensee (i.e., utility) as part of the ISFSI pad and is therefore not addressed in this application.

(2) It is assumed that approval of the FSAR by the NRC is the basis for the Commission's acceptance of the tests defined in Chapter 9.

(3) Not applicable to HI-STAR 100 System. The functional adequacy of all-important to safety components is demonstrated by analyses.

(4) The stated requirement is the responsibility of licensee (i.e., utility) as part of the ISFSI and is therefore not addressed in this application.

(5) The stated requirement is not applicable to the HI-STAR 100 System. No monitoring is required for accident conditions.

"--" There is no corresponding NUREG-1536 criteria, no applicable 10CFR72 or 10CFR20 regulatory requirement, or the item is not addressed in the FSAR.

"NA" There is no Regulatory Guide 3.61 section that corresponds to the NUREG-1536, 10CFR72, or 10CFR20 requirement being addressed.

Table 1.0.3

HI-STAR 100 SYSTEM FSAR CLARIFICATIONS AND EXCEPTIONS TO NUREG –1536

NUREG-1536 Requirement	Alternate Method to Meet NUREG-1536 Intent	Justification
2.V.2.(b)(1) "The NRC accepts as the maximum and minimum "normal" temperatures the highest and lowest ambient temperatures recorded in each year, averaged over the years of record."	Exception: Section 2.2.1.4 for environmental temperatures utilizes an upper bounding value of 80°F on the annual average ambient temperatures for the United States.	The 80°F temperature set forth in Table 2.2.2 is greater than the annual average ambient temperature at any location in the continental United States. Inasmuch as the primary effect of the environmental temperature is on the computed fuel cladding temperature to establish long-term fuel cladding integrity, the annual average ambient temperature for each ISFSI site should be below 80°F. The large thermal inertia of the HI-STAR 100 System ensures that the daily fluctuations in temperatures do not affect the temperatures of the system. Additionally, the 80°F ambient temperature is combined with insolation in accordance with 10CFR71.71 averaged over 24 hours.
2.V.2.(b)(3)(f) "10CFR Part 72 identifies several other natural phenomena events (including seiche, tsunami, and hurricane) that should be addressed for spent fuel storage."	Clarification: A site-specific safety analysis of the effects of seiche, tsunami, and hurricane on the HI-STAR 100 System must be performed prior to use if these events are applicable to the site.	In accordance with NUREG-1536, 2.V.(b)(3)(f), if seiche, tsunami, and hurricane are not addressed in the SAR and they prove to be applicable to the site, a safety analysis is required prior to approval for use of the DCSS under either a site specific, or general license.
3.V.(d), page 3-11, "Drops with the axis generally vertical should be analyzed for both the conditions of a flush impact and an initial impact at a corner of the cask..."	Clarification: As stated in NUREG-1536, 3.V.(d), page 3-11, "Generally, applicants establish the design basis in terms of the maximum height to which the cask is lifted outside the spent fuel building, or the maximum deceleration that the cask could experience in a drop." The maximum deceleration for a corner drop is specified as 60g's for the HI-STAR overpack. No carry height limit is specified for the corner drop.	In Chapter 3, the MPC is evaluated under a 60g radial and axial loading while in the HI-STAR overpack and is shown to meet ASME Code allowable stress limits. Therefore, the HI-STAR 100 System is qualified for a 60g loading as a result of a corner drop. Depending on the type of rigging used, the administrative vertical carry height limit, and the stiffness of the impacted surface, site-specific analyses are required to demonstrate that the deceleration limit of 60g's is not exceeded.

Table 1.0.3 (continued)

HI-STAR 100 SYSTEM FSAR CLARIFICATIONS AND EXCEPTIONS TO NUREG –1536

NUREG-1536 Requirement	Alternate Method to Meet NUREG-1536 Intent	Justification
4.IV.5, Page 4-2 "for each fuel type proposed for storage, the DCSS should ensure a very low probability (e.g., 0.5 percent per fuel rod) of cladding breach during long-term storage." 4.IV.1, Page 4-3, Para. 1 "the staff should verify that cladding temperatures for each fuel type proposed for storage will be below the expected damage thresholds for normal conditions of storage." 4.IV.1, Page 4-3, Para. 2 "fuel cladding limits for each fuel type should be defined in the SAR with thermal restrictions in the DCSS technical specifications." 4.V.1, Page 4-3, Para. 4 "the applicant should verify that these cladding temperature limits are appropriate for all fuel types proposed for storage, and that the fuel cladding temperatures will remain below the limit for facility operations (e.g., fuel transfer) and the worst-case credible accident."	Clarification: As described in Section 4.3, all fuel array types authorized for storage have been evaluated for the peak fuel cladding temperature.	As described in Section 4.3, all fuel array types authorized for storage have been evaluated for the peak fuel cladding temperature. All major variations in fuel parameters are considered in the determination of the peak fuel cladding temperatures. Minor variations in fuel parameters within an array type are bounded by the conservative determination of the allowable peak fuel cladding temperature.

Table 1.0.3 (continued)

HI-STAR 100 SYSTEM FSAR CLARIFICATIONS AND EXCEPTIONS TO NUREG –1536

NUREG-1536 Requirement	Alternate Method to Meet NUREG-1536 Intent	Justification
4.V.4.a, Page 4-6, Para. 3 "applicants seeking NRC approval of specific internal convection models should propose, in the SAR, a comprehensive test program to demonstrate the adequacy of the cask design and validation of the convection models."	Exception: The natural convection model described in Subsection 4.4.1.1.5 is based on classical correlations for natural convection in differentially heated cavities which have been validated by many experimental studies. Therefore, no additional test program is proposed.	Many experimental studies of this mechanism have been performed by others and reported in open literature sources. As discussed in Subsection 4.4.1.1.5, natural convection has been limited to the relatively large MPC basket to shell peripheral gap. Subsection 4.4.1.1.5 provides sufficient references to experiments which document the validity of the classical correlation used in the analysis.
4.V.4.a, Page 4-6, Para. 6 "the basket wall temperature of the hottest assembly can then be used to determine the peak rod temperature of the hottest assembly using the Wooten-Epstein correlation."	Clarification: As discussed in Subsection 4.4.2, conservative maximum fuel temperatures are obtained directly from the cask thermal analysis. The peak fuel cladding temperatures are then used to determine the corresponding peak basket wall temperatures using a finite-element based update of Wooten-Epstein (described in Subsection 4.4.1.1.2)	The finite-element based thermal conductivity is greater than a Wooten-Epstein based value. This larger thermal conductivity minimizes the fuel-to-basket temperature difference. Since the basket temperature is less than the fuel temperature, minimizing the temperature difference conservatively maximizes the basket wall temperature.
4.V.4.b, Page 4-7, Para. 2 "if the thermal model is axisymmetric or three-dimensional, the longitudinal thermal conductivity should generally be limited to the conductivity of the cladding (weighted fractional area) within the fuel assembly."	Clarification: As described in Subsection 4.4.1.1.4, the axial thermal conductivity of the fuel basket is set equal to the cross-sectional thermal conductivity.	Due to the large number of gaps in the cross-sectional heat transfer paths, use of the fuel basket cross-sectional thermal conductivity for the axial thermal conductivity severely underpredicts the axial thermal conductivity of the fuel basket region. This imposed axial thermal conductivity restriction is even more limiting than that imposed by this requirement of NUREG-1536.
4.V.4.b, Page 4-7, Para. 2 "high burnup effects should also be considered in determining the fuel region effective thermal conductivity."	Exception: All calculations of fuel assembly effective thermal conductivities, described in Subsection 4.4.1.1.2, use nominal fuel design dimensions, neglecting wall thinning associated with high burnup.	Within Subsection 4.4.1.1.2, the calculated effective thermal conductivities based on nominal design fuel dimensions are compared with available literature values and are demonstrated to be conservative by a substantial margin.

Table 1.0.3 (continued)

HI-STAR 100 SYSTEM FSAR CLARIFICATIONS AND EXCEPTIONS TO NUREG –1536

NUREG-1536 Requirement	Alternate Method to Meet NUREG-1536 Intent	Justification
4.V.4.c, Page 4-7, Para. 5 "a heat balance on the surface of the cask should be given and the results presented."	Clarification: No additional heat balance is performed or provided.	The FLUENT computational fluid dynamics program used to perform evaluations of the HI-STAR 100 System, which uses a discretized numerical solution algorithm, enforces an energy balance on all discretized volumes throughout the computational domain. This solution method, therefore, ensures a heat balance at the surface of the cask.
4.V.5.a, Page 4-8, Para. 2 "the SAR should include input and output file listings for the thermal evaluations."	Exception: No input or output file listings are provided in Chapter 4.	A complete set of computer program input and output files would be in excess of three hundred pages. All computer files are considered proprietary because they provide details of the design and analysis methods. In order to eliminate proprietary information in the FSAR, computer files are provided in the proprietary calculation packages.
4.V.5.c, Page 4-10, Para. 3 "free volume calculations should account for thermal expansion of the cask internal components and the fuel when subjected to accident temperatures.	Exception: All free volume calculations use nominal confinement boundary dimensions, but the volume occupied by the MPC internals (i.e., fuel assemblies, fuel basket, etc.) are calculated using maximum weights and minimum densities.	Calculating the volume occupied by the MPC internals (i.e., fuel assemblies, fuel basket, etc.) using maximum weights and minimum densities conservatively overpredicts the volume occupied by the internal components and correspondingly underpredicts the remaining free volume.

Table 1.0.3 (continued)

HI-STAR 100 SYSTEM FSAR CLARIFICATIONS AND EXCEPTIONS TO NUREG –1536

NUREG-1536 Requirement	Alternate Method to Meet NUREG-1536 Intent	Justification
7.V.4.c "Because the leak is assumed to be instantaneous, the plume meandering factor of Regulatory Guide 1.145 is not typically applied." and "Note that for an instantaneous release (and instantaneous exposure), the time that an individual remains at the controlled area boundary is not a factor in the dose calculation."	Exception: As described in Section 7.3, in lieu of an instantaneous release, the assumed leakage rate is set equal to the MPC leakage rate acceptance criteria ($5x10^{-6}$ cm^3/s) plus the sensitivity ($2.5x10^{-6}$ cm^3/s), which yields an assumed leakage rate of $7.5x10^{-6}$ cm^3/s. Because the release is assumed to be a leakage rate, the individual is assumed to be at the controlled area boundary for 720 hours. Additionally, the atmospheric dispersion factors of Regulatory Guide 1.145 are applied.	The MPC uses redundant closures to assure that there is no release of radioactive materials under all credible conditions. Analyses presented in Chapters 3 and 11 demonstrate that the confinement boundary does not degrade under all normal, off-normal, and accident conditions. Multiple inspection methods are used to verify the integrity of the confinement boundary (e.g., helium leakage, hydrostatic, and volumetric (or multi-layer liquid penetrant) weld inspection). The HI-STAR overpack provides an additional barrier to the release of radionuclides. The NRC letter to Holtec International dated 9/15/97, Subject: Supplemental Request for Additional Information - HI-STAR 100 Dual Purpose Cask System (TAC No. L22019), RAI 7.3 states "use the verified confinement boundary leakage rate in lieu of the assumption that the confinement boundary fails."
9.V.1.a, Page 9-4, Para. 4 "Acceptance criteria should be defined in accordance with NB/NC-5330, "Ultrasonic Acceptance Standards"."	Clarification: Section 9.1.1.1 and the Design Drawings specify that the ASME Code, Section III, Subsection NB, Article NB-5332 will be used for the acceptance criteria for the volumetric examination of the MPC lid-to-shell weld.	In accordance with the first line on page 9-4, the NRC endorses the use of "...appropriate acceptance criteria as defined by either the ASME code, or an alternative approach..." The ASME Code, Section III, Subsection NB, Paragraph NB-5332 is appropriate acceptance criteria for pre-service examination.

Table 1.0.3 (continued)

HI-STAR 100 SYSTEM FSAR CLARIFICATIONS AND EXCEPTIONS TO NUREG –1536

NUREG-1536 Requirement	Alternate Method to Meet NUREG-1536 Intent	Justification
9.V.1.d, Para. 1 "Tests of the effectiveness of both the gamma and neutron shielding may be required if, for example, the cask contains a poured lead shield or a special neutron absorbing material."	Exception: Subsection 9.1.5 describes the control of special processes, such as shield material installation and post-loading shield effectiveness testing, to be performed in lieu of scanning or probing with neutron sources.	The dimensional compliance of all neutron shielding cavities is verified by inspection to Design Drawing requirements prior to shield installation. The neutron shield is installed in accordance with written, approved, and qualified special process procedures. The composition of the neutron shielding material is confirmed by inspection and tests prior to first use. Following the first loading of each HI-STAR overpack, a shield effectiveness test is performed in accordance with written approved procedures, as specified in the Technical Specifications.
13.III, " the application must include, at a minimum, a description that satisfies the requirements of 10 CFR Part 72, Subpart G, 'Quality Assurance'..."	Exception: Section 13.0 incorporates the NRC-approved Holtec International Quality Assurance Program Manual by reference rather than describing the Holtec QA program in detail.	The NRC has approved the Holtec Quality Assurance Program Manual under 10 CFR 71 (NRC QA Program Approval for Radioactive Material Packages No. 0784, Rev. 3). Pursuant to 10 CFR 72.140(d), Holtec will apply this QA program to all important-to-safety dry storage cask activities. Incorporating the Holtec QA Program Manual by reference eliminates duplicate documentation.

1.1 INTRODUCTION

HI-STAR 100 (acronym for Holtec International Storage, Transport and Repository) is a spent nuclear fuel (SNF) packaging designed to be in general compliance with the U.S. Department of Energy's (DOE) design procurement specifications for multi-purpose canisters and large transportation casks [1.1.1], [1.1.2]. The annex "100" is a model number designation which denotes a system weighing in the range of 100 tons. The HI-STAR 100 System consists of a sealed metallic canister, herein abbreviated as the "MPC", contained within an overpack. Figure 1.1.1 depicts the HI-STAR 100.

The HI-STAR 100 System is designed to accommodate a wide variety of spent fuel assemblies in a single overpack by utilizing different MPCs. The external dimensions of all MPCs are identical to allow the use of a single overpack design. Each of the MPCs has different internals (baskets) to accommodate distinct fuel characteristics. Each MPC is identified by the maximum quantity of fuel assemblies it is capable of receiving. The MPC-24 can contain a maximum of 24 PWR assemblies and the MPC-68 can contain a maximum of 68 BWR assemblies. Figure 1.1.2 depicts the HI-STAR 100 with two of its major constituents, the MPC and the overpack, in a cutaway view.

The HI-STAR 100 is designed for both storage and transport. The HI-STAR 100 System's multi-purpose design reduces SNF handling operations and thereby enhances radiological protection. Once the SNF is loaded and the MPC and cask are sealed, the HI-STAR 100 System can be positioned on-site for temporary or long-term storage or transported directly off-site. The HI-STAR 100 System's ability to both store and transport SNF eliminates repackaging.

The HI-STAR 100 System is a completely passive stand-alone storage system which provides SNF confinement, radiation shielding, structural integrity, criticality control, and heat removal independent of any other facility, structures or components. This Final Safety Analysis Report (FSAR) provides bounding values for design criteria to facilitate NRC review and evaluation for both General License use under 10CFR72, Subpart K, and as reference for a site-specific storage facility application.

This FSAR demonstrates the inherent safety of one loaded overpack as well as interactions among an array of overpacks at an ISFSI. The HI-STAR 100 System can be used alone or as part of a multi-unit array at an ISFSI. The site for the ISFSI can be located either at a reactor or away from a reactor.

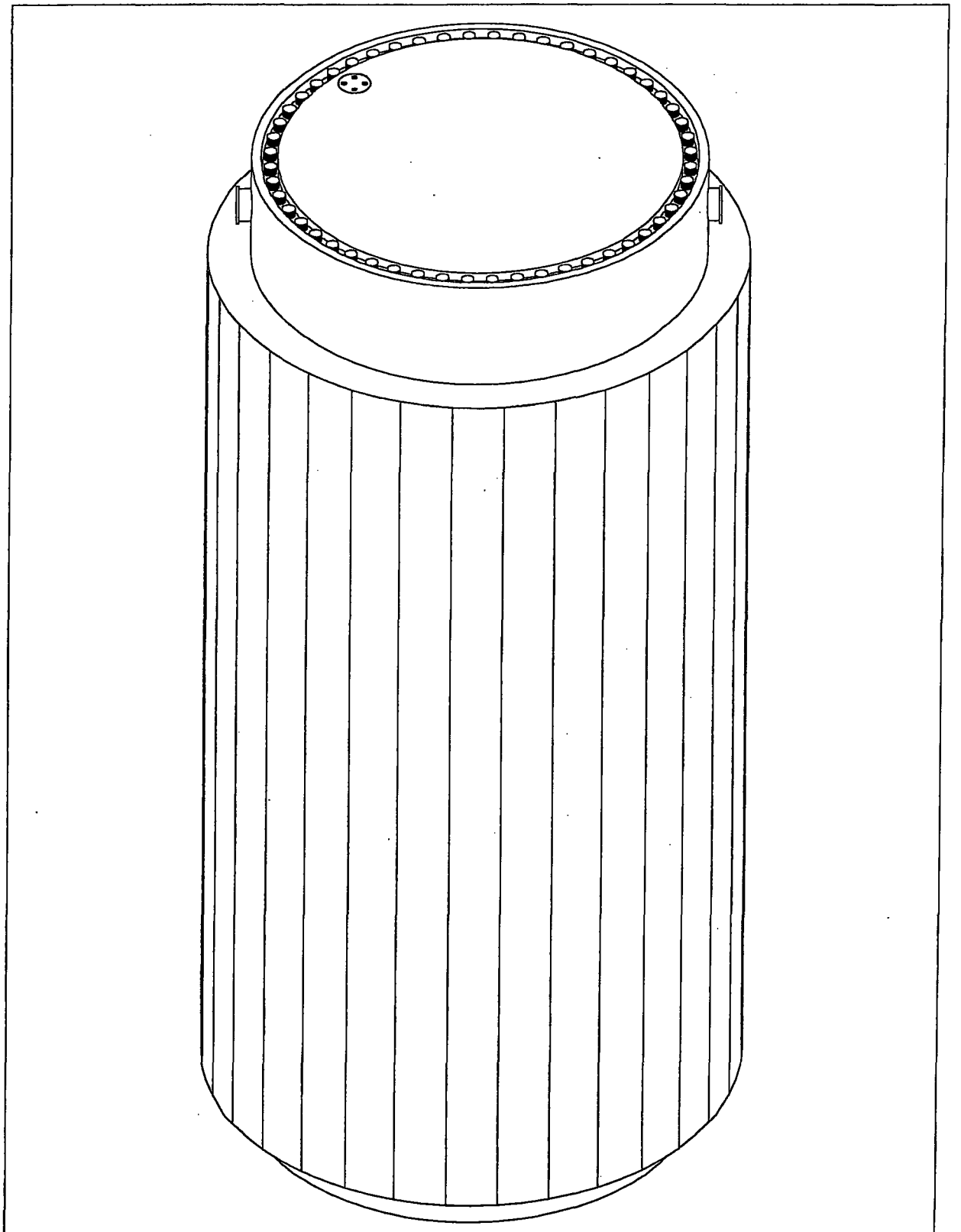

FIGURE 1.1.1; PICTORIAL VIEW OF HI-STAR 100

REPORT HI-2012610 REVISION 0

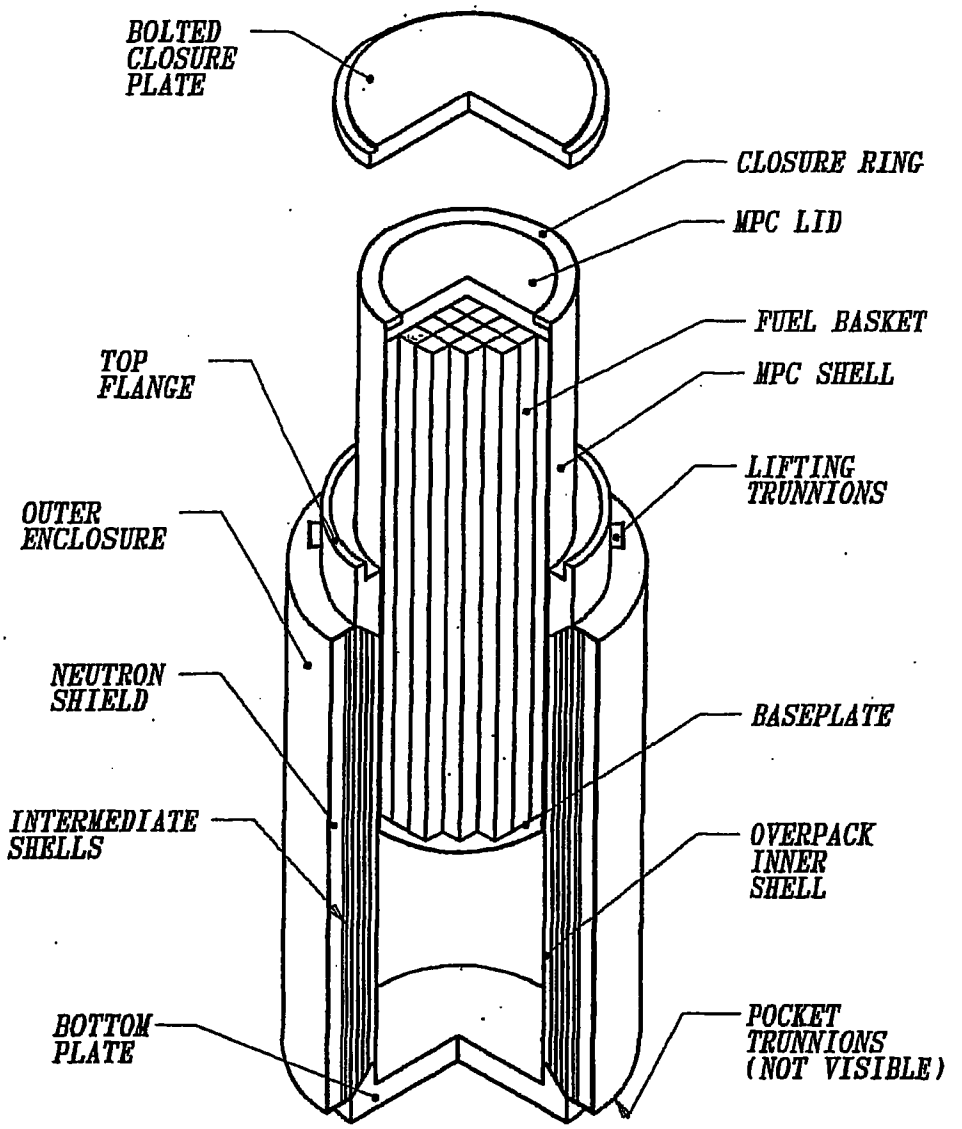

Figure 1.1.2; HI-STAR 100 OVERPACK WITH MPC PARTIALLY INSERTED

REPORT HI-2012610 REVISION 0

1.2 GENERAL DESCRIPTION AND OPERATING FEATURES OF HI-STAR 100

1.2.1 System Characteristics

The complete HI-STAR 100 System for storage of spent nuclear fuel is comprised of two discrete components:

- the multi-purpose canister (MPC), and
- the storage/transport overpack

Necessary auxiliaries required to deploy the HI-STAR 100 System for storage are:

- lifting and handling systems
- welding equipment
- vacuum drying system and helium backfill system with leak detector
- a heavy haul transfer device (to move the cask from the fuel building to the cask pad)

The HI-STAR 100 System consists of interchangeable MPCs which constitute the confinement boundary for BWR or PWR spent nuclear fuel, and an overpack which provides the helium retention boundary. Tables 1.2.1 and 1.2.2 contain the key parameters for the HI-STAR 100 MPCs. Figure 1.2.1 provides a cross sectional elevation view of the HI-STAR 100 System in storage.

All MPCs have identical exterior dimensions which render them interchangeable. The outer diameter of the MPC is nominally 68-3/8 inches and the length is approximately 190-1/2 inches. Due to the differing storage contents of each of the MPCs, the maximum loaded weight differs between each MPC. However, the maximum weight of a loaded MPC is approximately 44-1/2 tons.

A single overpack design is provided which is capable of storing each type of MPC. The inner diameter of the overpack is approximately 68-3/4 inches and the height of the cavity is nominally 191-1/8 inches. The overpack inner cavity is sized to accommodate the MPCs. The outer diameter of the overpack is approximately 96 inches and the height is approximately 203-1/8 inches. The weight of the overpack without an MPC is approximately 77 tons.

Before proceeding to present detailed physical data on the HI-STAR 100 System, it is contextual to summarize the design attributes which set it apart from the prior generation of casks. There are several features in the HI-STAR 100 System design which increase its effectiveness with respect to the safe storage and transport of spent nuclear fuel (SNF). Some of the principal features of the HI-STAR 100 System which enhance its effectiveness as an SNF storage device and a safe SNF confinement structure are:

- the honeycomb design of the MPC fuel basket
- the effective distribution of neutron and gamma shielding materials within the system
- the high heat expulsion capability
- the structural robustness of the multi-shell overpack construction

The honeycomb design of the MPC fuel baskets renders the basket into a multi-flange plate weldment where all structural elements (box walls) are arrayed in two orthogonal sets of plates. Consequently, the walls of the cells are either completely co-planar (no offset) or orthogonal with each other. There is complete edge-to-edge continuity between the contiguous cells.

Among the many benefits of the honeycomb construction is the uniform distribution of the metal mass of the basket over the body of the basket (in contrast to the "box and spacer disk" construction where the support plates are localized mass points). Physical reasoning suggests that a uniformly distributed mass provides a more effective shielding barrier than can be obtained from a nonuniform (box and spacer disk) basket. In other words, the honeycomb basket is a more effective radiation attenuation device.

The complete cell-to-cell connectivity inherent in the honeycomb basket structure provides an uninterrupted heat transmission path, making the HI-STAR 100 MPC an effective heat rejection device.

Finally, the multilayer shell construction in the overpack provides a natural barrier against crack propagation in the radial direction through the overpack structure. If, during a mechanical accident (drop) event, a crack was initiated in one layer, the crack could not propagate to the adjacent layer. Additionally, it is less likely that a crack would initiate as the thinner layers are more ductile than a thicker plate.

A description of each of the HI-STAR components is provided in the following subsections, along with information with respect to its fabrication and safety features. This discussion is supplemented with the full set of drawings in Section 1.5.

1.2.1.1 Multi-Purpose Canisters

The HI-STAR 100 MPCs are welded cylindrical structures with flat ends as shown in cross sectional views of Figures 1.2.2 and 1.2.4. Each MPC is an assembly consisting of a honeycombed fuel basket, a baseplate, canister shell, a lid, and a closure ring, as depicted in the MPC cross section elevation view, Figure 1.2.5. The outer diameter and cylindrical height of each MPC is fixed. However, the number of spent nuclear fuel storage locations in each of the MPCs depends on the fuel assembly characteristics. Drawings of the MPCs are provided in Section 1.5.

The MPC provides the confinement boundary for the stored fuel. Figure 1.2.6 provides an elevation view of the MPC confinement boundary. The confinement boundary is a seal-welded enclosure constructed entirely of stainless steel.

The construction features of the PWR MPC-24 and the BWR MPC-68 are similar. However, the PWR MPC-24 canister in Figure 1.2.4, which is designed for highly enriched PWR fuel without credit for soluble boron, differs in construction from the MPC-68 in one important aspect: The fuel storage cells are physically separated from one another by a "flux trap" between each storage cell for criticality control. All MPC baskets are formed from an array of plates welded to each other, such

that a honeycomb structure is created which resembles a multiflanged, closed-section beam in its

structural characteristics.

The MPC fuel basket is positioned and supported within the MPC shell by a basket support structure welded to the inside of the MPC shell. Between the periphery of the basket, the MPC shell, and the basket supports, heat conduction elements are installed. These heat conduction elements are fabricated from thin aluminum alloy 1100 in shapes and a design which allow a snug fit in the confined spaces and ease of installation. The heat conduction elements are installed along the full length of the MPC basket, except at the drain pipe location, to create a nonstructural thermal connection which facilitates heat transfer from the basket to shell. In their operating condition, the heat conduction elements will conform to and contact the MPC shell and basket walls.

Lifting lugs attached to the inside surface of the MPC canister shell serve to permit lifting and placement of the empty MPC into the overpack. The lifting lugs also serve to axially locate the lid prior to welding. These internal lifting lugs are not used to handle a loaded MPC. Since the MPC lid is installed prior to any handling of the loaded MPC, there is no access to the lifting lugs once the MPC is loaded.

The top end of the HI-STAR 100 MPC incorporates a redundant closure system. Figure 1.2.6 provides a sketch of the MPC closure details. The MPC lid is a circular plate (fabricated from one piece, or two pieces - split top and bottom) edge-welded to the MPC outer shell. If the two-piece lid design is employed, only the top piece is analyzed as part of the enclosure vessel pressure boundary. The bottom piece acts as a radiation shield and is attached to the top piece with a non-structural, non-pressure retaining weld. This lid is equipped with vent and drain ports which are utilized to remove moisture and air from the MPC, and backfill the MPC with a specified pressure of inert gas (helium). The vent and drain ports are covered and welded before the closure ring is installed. The closure ring is a circular ring edge-welded to the MPC shell and lid. The MPC lid provides sufficient rigidity to allow the entire MPC loaded with SNF to be lifted by threaded holes in the MPC lid.

For fuel assemblies that are shorter than the design basis length, upper and lower fuel spacers (as appropriate) maintain the axial position of the fuel assembly within the MPC basket. The upper fuel spacers are threaded into the underside of the MPC lid as shown in Figure 1.2.5. The lower fuel spacers are placed in the bottom of each fuel basket cell. The upper and lower fuel spacers are designed to withstand normal, off-normal, and accident conditions of storage. An axial clearance of approximately 2 to 2-1/2 inches is provided to account for the irradiation and thermal growth of the fuel assemblies. The suggested values for the upper and lower fuel spacer lengths are listed in Tables 2.1.9 and 2.1.10 for each fuel assembly type.

The MPC is constructed entirely from stainless steel alloy materials (except for the neutron absorber and aluminum heat conduction elements). No carbon steel parts are permitted in the MPC. Concerns regarding interaction of coated carbon steel materials and various MPC operating environments [1.2.1] are not applicable to the MPC. All structural components in a MPC shall be made of Alloy X, a designation which warrants further explanation.

Alloy X is a material which is expected to be acceptable as a Mined Geological Depository System (MGDS) waste package and which meets the thermophysical properties set forth in this document.

At this time, there is considerable uncertainty with respect to the material of construction for an MPC which would be acceptable as a waste package for the MGDS. Candidate materials being considered for acceptability by the DOE include:

- Type 316
- Type 316LN
- Type 304
- Type 304LN

The DOE material selection process is primarily driven by corrosion resistance in the potential environment of the MGDS. As the decision regarding a suitable material to meet disposal requirements is not imminent, the MPC design allows the use of any one of the four Alloy X materials.

For the MPC design and analysis, Alloy X (as defined in this FSAR) may be one of the following materials. Any steel part in an MPC may be fabricated from any of the acceptable Alloy X materials listed below, except that the steel pieces comprising the MPC shell (i.e., the 1/2" thick cylinder) must be fabricated from the same Alloy X stainless steel type. .

- Type 316
- Type 316LN
- Type 304
- Type 304LN

The Alloy X approach is accomplished by qualifying the MPC for all mechanical, structural, neutronic, radiological, and thermal conditions using material thermophysical properties which are the least favorable for the entire group for the analysis in question. For example, when calculating the rate of heat rejection to the outside environment, the value of thermal conductivity used is the lowest for the candidate material group. Similarly, the stress analysis calculations use the lowest value of the ASME Code allowable stress intensity for the entire group. Stated differently, we have defined a material, which is referred to as Alloy X, whose thermophysical properties, from the MPC design perspective, are the least favorable of the candidate materials.

The evaluation of the Alloy X constituents to determine the least favorable properties is provided in Appendix 1.A.

The Alloy X approach is conservative because no matter which material is ultimately utilized in the MPC construction, the Alloy X approach guarantees that the performance of the MPC will exceed the analytical predictions contained in this document.

1.2.1.2 HI-STAR 100 Overpack

The HI-STAR 100 overpack is a heavy-walled steel cylindrical vessel. Figure 1.2.7 provides a cross sectional elevation view of the HI-STAR 100 overpack. The overpack helium retention boundary is formed by an inner shell welded at the bottom to a cylindrical forging and, at the top, to a heavy main flange with bolted closure plate. Two concentric grooves are machined into the closure plate for the metallic seals. The closure plate is recessed into the top flange and the bolted joint is configured to provide maximum protection to the closure bolts and seals in the event of a drop accident. The closure plate has a vent port which is sealed by a threaded port plug with a seal. The bottom plate has a drain port which is sealed by a threaded port plug with a seal. The inner surfaces of the HI-STAR overpack form an internal cylindrical cavity for housing the MPC.

As shown in Figure 1.2.8, the outer surface of the overpack inner shell is buttressed with intermediate shells of gamma shielding which are installed in a manner to ensure a permanent state of contact between adjacent layers. Besides serving as an effective gamma shield, these layers provide additional strength to the overpack to resist potential punctures or penetrations from external missiles. Radial channels are vertically welded to the outside surface of the outermost intermediate shell at equal intervals around the circumference. These radial channels act as fins for improved heat conduction to the overpack outer enclosure shell surface and as cavities for retaining and protecting the neutron shielding. The enclosure shell is formed by welding enclosure shell panels between each of the channels to form additional cavities. Neutron shielding material is placed into each of the radial cavity segments formed by the radial channels, the outermost intermediate shell, and the enclosure shell panels. The exterior flats of the radial channels and the enclosure shell panels form the overpack outer enclosure shell. Atop the outer enclosure shell, rupture disks are positioned in a recessed area. The rupture disks relieve internal pressure which may develop as a result of the fire accident and subsequent off-gassing of the neutron shield material. Within each radial channel, a layer of silicone sponge is positioned to act as a thermal expansion foam to compress as the neutron shield expands. Appendix 1.C provides material information on the thermal expansion foam. Figure 1.2.9 contains a mid-plane cross section of the overpack depicting the inner shell, intermediate shells, radial channels, outer enclosure shell, and neutron shield.

The exposed steel surfaces of the overpack are coated with paint to prevent corrosion. The paint is specified on the design drawings and the material data on the paint is provided in Appendix 1.C. The inner cavity of the overpack is coated with a paint appropriate to its higher temperatures and the exterior of the overpack is coated with a paint appropriate for fuel pool operations and environmental exposure.

Lifting trunnions are attached to the overpack top flange forging for lifting and for rotating the cask body between vertical and horizontal positions. The lifting trunnions are located 180° apart in the sides of the top flange. Pocket trunnions are welded to the lower side of the overpack to provide a pivoting axis for rotation. The pocket trunnions are located slightly off-center to ensure the proper rotation direction of the overpack. As shown in Figure 1.2.7, the lifting trunnions do not protrude beyond the cylindrical envelope of the overpack enclosure shell. This feature reduces the potential for a direct impact on a trunnion in the event of an overpack side impact.

1.2.1.3 Shielding

The HI-STAR 100 System is provided with sufficient shielding to ensure that the external radiation requirements in 10CFR72.126, 10CFR72.104, and 10CFR72.106 are met. This shielding is an important factor in minimizing personnel doses from gamma and neutron sources in the spent nuclear fuel for ALARA considerations during loading, handling, and storage operations.

The initial attenuation of gamma and neutron radiation emitted by the radioactive spent fuel is provided by the fuel basket structure built from inter-welded intersecting plates and Boral neutron poison panels attached to the fuel storage cell walls. The MPC canister shell, baseplate, and lid provide additional thicknesses of steel to further reduce gamma radiation and, to a smaller extent, neutron radiation at the outer MPC surfaces.

The primary HI-STAR 100 shielding is located in the overpack and consists of neutron shielding and additional layers of steel for gamma shielding. Neutron shielding is provided around the outer circumferential surface of the overpack. Gamma shielding is provided by the overpack inner, intermediate, and enclosure shells with additional axial shielding provided by the bottom plate and the closure plate.

1.2.1.3.1 Boral Neutron Absorber

Boral is a thermal neutron poison material composed of boron carbide and aluminum (aluminum powder and plate). Boron carbide is a compound having a high boron content in a physically stable and chemically inert form. The boron carbide contained in Boral is a fine granulated powder that conforms to ASTM C-750-80 nuclear grade Type III. The Boral cladding is made of alloy aluminum, a lightweight metal with high tensile strength which is protected from corrosion by a highly resistant oxide film. The two materials, boron carbide and aluminum, are chemically compatible and ideally suited for long-term use in the radiation, thermal, and chemical environment of a nuclear reactor, spent fuel pool, or dry cask.

The documented historical applications of Boral, in environments comparable to those in spent fuel pools and fuel storage casks, dates to the early 1950s (the U.S. Atomic Energy Commission's AE-6 Water-Boiler Reactor [1.2.2]). Technical data on the material was first printed in 1949, when the report "Boral: A New Thermal Neutron Shield" was published [1.2.3]. In 1956, the first edition of the Reactor Shielding Design Manual [1.2.4] contains a section on Boral and its properties.

In the research and test reactors built during the 1950s and 1960s, Boral was frequently the material of choice for control blades, thermal-column shutters, and other items requiring very good thermal-neutron absorption properties. It is in these reactors that Boral has seen its longest service in environments comparable to today's applications.

Boral found other uses in the 1960s, one of which was a neutron poison material in baskets used in the shipment of irradiated, enriched fuel rods from Canada's Chalk River laboratories to Savannah River. Use of Boral in shipping containers continues, with Boral serving as the poison in current British Nuclear Fuels Limited casks and the Storable Transport Cask by Nuclear Assurance Corporation [1.2.5].

Boral has been licensed by the USNRC for use in numerous BWR and PWR spent fuel storage racks and has been extensively used in international nuclear installations.

Boral has been exclusively used in fuel storage applications in recent years. Its use in spent fuel pools as a neutron absorbing material can be attributed to its proven performance and several unique characteristics, such as:

- Boron carbide, in the form of fine particles, is homogeneously dispersed throughout the central layer of the Boral panels.
- The neutron absorbing central layer of Boral is clad with permanently bonded surfaces of aluminum.
- The content and placement of boron carbide provides a very high removal cross section for thermal neutrons.
- The boron carbide and aluminum materials in Boral do not degrade as a result of long-term exposure to radiation.
- Boral is stable, strong, durable, and corrosion resistant.

Boral absorbs thermal neutrons without physical change or degradation of any sort from the anticipated exposure to gamma radiation and heat. The material does not suffer loss of neutron attenuation capability when exposed to high levels of radiation dose.

Holtec International's QA Program ensures that Boral is manufactured under the control and surveillance of a Quality Assurance/Quality Control Program that conforms to the requirements of 10CFR72, Subpart G. Holtec International has procured over 200,000 panels of Boral from AAR Advanced Structures in over 20 projects. Boral has always been purchased with a minimum ^{10}B loading requirement. Coupons extracted from production runs were tested using the wet chemistry procedure. The actual ^{10}B loading, out of thousands of coupons tested, has never been found to fall below the design specification. The size of this coupon data base is sufficient to provide confidence that all future procurements will continue to yield Boral in full compliance with the stipulated minimum loading. Furthermore, the surveillance, coupon testing, and material tracking processes which have so effectively controlled the quality of Boral are expected to continue to yield Boral of similar quality in the future. Nevertheless, to add another layer of insurance, only 75% ^{10}B credit of the fixed neutron absorber is assumed in the criticality analysis consistent with Chapter 6.0, IV, 4.c of NUREG-1536, Standard Review Plan for Dry Cask Storage Systems.

Operating experience in nuclear plants with fuel loading of Boral equipped MPCs as well as laboratory test data indicate that the aluminium used in the manufacture of the Boral may react with water, resulting in the generation of hydrogen. The numerous variables (i.e., aluminium particle size, pool temperature, pool chemistry, etc.) that influence the extent of the hydrogen produced make it impossible to predict the amount of hydrogen that may be generated during MPC loading or unloading at a particular plant. Therefore, due to the variability in hydrogen generation from the

Boral-water reaction, the operating procedures in Chapter 8 require monitoring for combustible gases and either exhausting or purging the space beneath the MPC lid during loading and unloading operations when an ignition event could occur (i.e., when the space beneath the MPC lid is open to the welding or cutting operation).

1.2.1.3.2 Holtite™ Neutron Shielding

The specification of the overpack neutron shield material is predicated on functional performance criteria. These criteria are:

- Attenuation of neutron radiation and associated neutron capture to appropriate levels;
- Durability of the shielding material under normal conditions, in terms of thermal, chemical, mechanical, and radiation environments;
- Stability of the homogeneous nature of the shielding material matrix;
- Stability of the shielding material in mechanical or thermal accident conditions to the desired performance levels; and
- Predictability of the manufacturing process under adequate procedural control to yield an in-place neutron shield of desired function and uniformity.

Other aspects of a shielding material, such as ease of handling and prior nuclear industry use, are also considered, within the limitations of the main criteria. Final specification of a shield material is a result of optimizing the material properties with respect to the main criteria, along with the design of the shield system, to achieve the desired shielding results.

Holtite-A is the only approved neutron shield material which fulfills the aforementioned criteria. Holtite-A is a poured-in-place solid borated synthetic neutron-absorbing polymer. Holtite-A is specified with a nominal B_4C loading of 1 weight percent for the HI-STAR 100 System. Appendix 1.B provides the Holtite-A material properties germane to its function as a neutron shield. Holtec has performed confirmatory qualification tests on Holtite-A under the company's QA program.

In the following, a brief summary of the performance characteristics and properties of Holtite-A is provided.

Density

The specific gravity of Holtite-A is 1.68 g/cm^3 as specified in Appendix 1.B. To conservatively bound any potential weight loss at the design temperature and any inability to reach the theoretical density, the density is reduced by 4% to 1.61 g/cm^3. The density used for the shielding analysis is conservatively assumed to be 1.61 g/cm^3 to underestimate the shielding capabilities of the neutron shield.

Hydrogen

The weight concentration of hydrogen is 6.0%. However, all shielding analyses conservatively assume 5.9% hydrogen by weight in the calculations.

Boron Carbide

Boron carbide dispersed within Holtite-A in finely dispersed powder form is present in 1% weight concentration. Holtite-A may be specified with a B_4C content of up to 6.5 weight percent. For the HI-STAR 100 System, Holtite-A is specified with a nominal B_4C weight percent of 1%.

Design Temperature

The design temperature of Holtite-A is set at 300°F. The maximum spatial temperature of Holtite-A under all normal operating conditions must be demonstrated to be below this design temperature.

Thermal Conductivity

It is evident from Figure 1.2.9 that Holtite-A is directly in the path of heat transmission from the inside of the overpack to its outside surface. For conservatism, however, the design basis thermal conductivity of Holtite-A under heat rejection conditions is set equal to zero. The reverse condition occurs under a postulated fire event when the thermal conductivity of Holtite-A aids in the influx of heat to the stored fuel in the fuel basket. The thermal conductivity of Holtite-A is conservatively set at 1 Btu/hr-ft-°F for all fire event evaluations.

The Holtite-A neutron shielding material is stable below the design temperature for long-term use and provides excellent shielding properties for neutrons.

1.2.1.3.3 Gamma Shielding Material

For gamma shielding, HI-STAR 100 utilizes carbon steel in plate stock form. Instead of utilizing a thick forging, the gamma shield design in the HI-STAR 100 overpack borrows from the concept of layered vessels from the field of ultra-high pressure vessel technology. The shielding is made from successive layers of plate stock. The fabrication of the shell begins by rolling the inner shell plate and making the longitudinal weld seam. Each layer of the intermediate shells are constructed from two halves. The two halves of the shell shall be precision sheared, bevelled, and rolled to the required radii. The two halves of the second layer are wrapped around the first shell. Each shell half is positioned in its location and while applying pressure using a specially engineered fixture, the halves are tack welded. The bevelled edges to be joined will be positioned to make contact or have a slight root gap. The second layer is made by joining the two halves using two longitudinal welds. Successive layers are assembled in a like manner. Thus, the welding of every successive shell provides a certain inter-layer contact (Figure 1.2.8). The longitudinal and circumferential welds of the intermediate shells are offset from the previous layer, as shown on the drawings in Section 1.5. A thick structural component radiation barrier is thus constructed with four key features, namely:

- The number of layers can be increased as necessary to realize the required design objectives.

- The layered construction is ideal to stop propagation of flaws.
- The thinner plate stock is much more ductile than heavy forgings.
- Post-weld heat treatment is not required by the ASME Code, simplifying fabrication.

1.2.1.4 Lifting Devices

The HI-STAR 100 overpack is equipped with two lifting trunnions located in the top flange. The trunnions are manufactured from a high strength alloy and are installed in tapped openings. The lifting trunnions are designed in accordance with NUREG-0612 and ANSI N14.6. The trunnions are secured in position by a locking pad shaped to make conformal contact with the curved overpack. Once the locking pad is bolted in position, the locking pad inner diameter is sized to restrain the trunnion from backing out.

The lifting, upending, and downending of the HI-STAR 100 System requires the use of external handling devices. A lift yoke is utilized when the cask is to be lifted or set in a vertical orientation. Rotation cradles provide rotation trunnions which interface with pocket trunnions to provide a pivot axis. The lift yoke is connected to the lifting trunnions and the crane hook is used for upending or downending the HI-STAR 100 System by rotating on the rear pocket trunnions.

The top of the MPC lid is equipped with four threaded holes that allow lifting of the loaded MPC. These holes allow the loaded MPC to be raised/lowered from the HI-STAR overpack. MPC handling operations are performed using a HI-TRAC transfer cask of the HI-STORM 100 System (Docket No. 72-1014). The HI-TRAC transfer cask allows the sealed MPC loaded with spent fuel to be transferred from the HI-STORM Overpack (storage-only) to the HI-STAR Overpack, or vice versa. The threaded holes in the MPC lid are designed in accordance with NUREG-0612 and ANSI N14.6.

1.2.1.5 Design Life

The design life of the HI-STAR 100 System is 40 years. This is accomplished by using materials of construction with a long proven history in the nuclear industry and specifying materials known to withstand their operating environments with little to no degradation. A maintenance program, as specified in Chapter 9, is also implemented to ensure the HI-STAR 100 System will exceed its design life of 40 years. The design considerations that assure the HI-STAR 100 System performs as designed throughout the service life include the following:

HI-STAR Overpack

- Exposure to Environmental Effects
- Material Degradation
- Maintenance and Inspection Provisions

MPC

- Corrosion
- Structural Fatigue Effects
- Maintenance of Helium Atmosphere
- Allowable Fuel Cladding Temperatures
- Neutron Absorber Boron Depletion

The adequacy of the HI-STAR 100 System for its design life is discussed in Sections 3.4.10 and 3.4.11.

1.2.2 Operational Characteristics

1.2.2.1 Design Features

The HI-STAR 100 System is engineered to store different types of MPCs for varying PWR and BWR fuel characteristics.

The HI-STAR 100 System can safely store spent nuclear fuel with minimum cooling times. The maximum thermal decay heat load and SNF enrichments for each of the MPCs are identified in Chapter 2. The decay heat emitted by the spent nuclear fuel is dissipated in an entirely passive mode without any mechanical or forced cooling.

Both the free volume of the HI-STAR 100 MPCs and the annulus between the external surface of the MPC and the inside surface of the overpack are inerted with 99.995% pure helium gas during the spent nuclear fuel loading operations. Table 1.2.2 specifies the helium pressure to be placed in the MPC internal cavity.

The primary heat transfer mechanisms are metal conduction and surface radiation for the HI-STAR 100 System. The MPC internal helium atmosphere, in addition to providing a noncorrosive dry atmosphere for the fuel cladding, provides for heat transfer through helium conduction. The most adverse temperature profiles and thermal gradients for the HI-STAR 100 System with each of the MPCs are discussed in detail in Chapter 4.

The criticality control features of the HI-STAR 100 are designed to maintain the neutron multiplication factor k-effective (including uncertainties and calculational bias) at less than 0.95 under all normal, off-normal, and accident conditions of storage as analyzed in Chapter 6.

1.2.2.2 Sequence of Operations

Table 1.2.6 provides the basic sequence of operations necessary to defuel a spent fuel pool using the HI-STAR 100 System. The detailed sequence of steps for storage-related loading and handling operations is provided in Chapter 8 and is supported by the drawings in Section 1.5. A summary of general actions needed for the loading and unloading operations is provided below. Figures 1.2.11 and 1.2.12 provide a pictorial view of the loading and unloading operations, respectively.

Loading Operations

At the start of loading operations, the overpack is configured with the closure plate removed. The lift yoke is used to position the overpack in the designated preparation area or setdown area for overpack inspection and MPC insertion. The annulus is filled with plant demineralized water and an inflatable annulus seal is installed. The inflatable seal prevents contact between spent fuel pool water and the MPC shell reducing the possibility of contaminating the outer surfaces of the MPC. The MPC is then filled with spent fuel pool water or plant demineralized water. The overpack and MPC are lowered into the spent fuel pool for fuel loading using the lift yoke. Pre-selected assemblies are loaded into the MPC and a visual verification of the assembly identification is performed.

While still underwater, a thick shielding lid (the MPC lid) is installed. The lift yoke is remotely engaged to the overpack lifting trunnions and is used to lift the overpack close to the spent fuel pool surface. As an ALARA measure, dose rates are measured on the top of the overpack and MPC prior to removal from the pool to check for activated debris on the top surface. The MPC lift bolts (securing the MPC lid to the lift yoke) are removed. As the overpack is removed from the spent fuel pool, the lift yoke and overpack are sprayed with demineralized water to help remove contamination.

The overpack is removed from the pool and placed in the designated preparation area. The top surfaces of the MPC lid and the top flange of the overpack are decontaminated. The inflatable annulus seal is removed, and an annulus shield is installed. The annulus shield provides additional personnel shielding at the top of the annulus and also prevents small items from being dropped into the annulus. Dose rates are measured to ensure that the dose rates are within expected values. The Automated Welding System baseplate shield is installed to reduce dose rates around the top of the cask. The MPC water level is lowered slightly and the MPC lid is seal-welded using the Automated Welding System (AWS). Liquid penetrant examinations are performed on the root and final passes.

A volumetric (or multi-layer liquid penetrant) examination is also performed on the MPC lid-to-shell weld. The water level is raised to the top of the MPC and the weld is hydrostatically tested. Then a small volume of the water is displaced with helium gas. The helium gas is used for leakage testing. A helium leakage rate test is performed on the MPC lid confinement weld (lid-to-shell) to verify weld integrity and to ensure that required leakage rates are within acceptance criteria. The MPC water is displaced from the MPC by blowing pressurized helium or nitrogen gas into the vent port of the MPC, thus displacing the water through the drain line.

The Vacuum Drying System (VDS) is connected to the MPC and is used to remove all residual water from the MPC in a stepped evacuation process. The stepped evacuation process is used to preclude the formation of ice in the MPC and VDS lines. The internal pressure is reduced and held

for a duration to ensure that all liquid water has evaporated.

Following this dryness test, the VDS is disconnected, the Helium Backfill System (HBS) is attached, and the MPC is backfilled with a predetermined amount of helium gas. The helium backfill ensures adequate heat transfer during storage, provides an inert atmosphere for long-term fuel integrity, and provides the means of future leakage rate testing of the MPC confinement boundary welds. Cover plates are installed and seal-welded over the MPC vent and drain ports with liquid penetrant examinations performed on the root and final passes. The cover plates are helium leakage tested to confirm that they meet the established leakage rate criteria.

The MPC closure ring is then placed on the MPC, aligned, tacked in place, and seal welded, providing redundant closure of the MPC confinement cavity closure welds. Tack welds are visually examined, and the root and final welds are inspected using the liquid penetrant examination technique to ensure weld integrity. The annulus shield is removed and the remaining water in the annulus is drained. The AWS Baseplate shield is removed. The MPC lid and accessible areas of the top of the MPC shell are smeared for removable contamination and overpack dose rates are measured. The overpack closure plate is installed and the bolts are torqued. The overpack annulus is dried using the VDS, and backfilled with helium gas for heat transfer and seal testing. Concentric metallic seals in the overpack closure plate prevent the leakage of the helium gas from the annulus and provide an additional confinement boundary to the release of radioactive materials. The seals on the overpack vent and drain port plugs are leak tested along with the overpack closure plate inner seal. Cover plates with metallic seals are installed over the overpack vent and drain ports to provide redundant closure of the overpack penetrations. A port plug with a metallic seal is installed in the overpack closure plate test port to provide fully redundant closure of all potential leakage paths in the overpack penetrations.

The overpack is secured to the transporter and moved to the ISFSI pad. The overpack may be moved using a number of methods as long as the handling height limitations listed in the Technical Specifications are not exceeded.

The HI-STAR 100 System can also be remotely loaded at a specially-designed dry loading facility (i.e., hot cell) with appropriate modifications to the loading procedures.

Unloading Operations

The HI-STAR 100 System unloading procedures describe the general actions necessary to prepare the MPC for unloading, cool the stored fuel assemblies in the MPC, flood the MPC cavity, remove the lid welds, unload the spent fuel assemblies, and recover the overpack and empty MPC. Special precautions are outlined to ensure personnel safety during the unloading operations, and to prevent the risk of MPC overpressurization and thermal shock to the stored spent fuel assemblies.

The overpack and MPC are returned to the designated preparation area from the ISFSI. At the site's discretion, a gas sample is drawn from the annulus and analyzed. The gas sample provides an indication of MPC confinement performance. The annulus is depressurized, the overpack closure plate is removed, and the annulus is filled with plant demineralized water. The annulus and overpack top surface are protected from debris that will be produced by removing the MPC lid.

The MPC closure ring and vent and drain port cover plates are core drilled. Local ventilation is established round the MPC ports. The RVOAs are attached to the vent and drain ports. The RVOAs allow access to the inner cavity of the MPC, while providing a hermetic seal. The MPC is cooled using a closed loop heat exchanger to reduce the MPC internal temperature to allow water flooding. Following fuel cooldown, the MPC is flooded with water. The MPC lid-to-shell weld is removed. Then all weld removal equipment is removed with the MPC lid left in place.

The inflatable annulus seal is installed and pressurized. The MPC lid is rigged to the lift yoke and the lift yoke is engaged to overpack lifting trunnions. The overpack is placed in the spent fuel pool and the MPC lid is removed. All fuel assemblies are returned to the spent fuel storage racks and the MPC fuel cells are vacuumed to remove any assembly debris. The overpack and MPC are returned to the designated preparation area where the MPC water is pumped back into the spent fuel pool. The annulus water is drained and the MPC and overpack are decontaminated in preparation for re-utilization.

The HI-STAR 100 System can also be remotely unloaded at a specially designed dry unloading facility (i.e., hot cell) with appropriate modifications to the unloading procedures.

1.2.2.3 Identification of Subjects for Safety and Reliability Analysis

1.2.2.3.1 Criticality Prevention

Criticality is controlled by geometry and neutron absorption materials in the fuel basket. The MPC-24 and MPC-68 do not rely on soluble boron credit or the assurance that water cannot enter the MPC to meet the stipulated criticality limits.

The MPC-68 basket is equipped with Boral with a minimum ^{10}B areal density of 0.0372 g/cm^2. The MPC-24 basket is equipped with Boral with a minimum ^{10}B areal density of 0.0267 g/cm^2. Due to the lower reactivity of the fuel to be stored in the MPC-68F as specified by the Technical Specifications, the MPC-68F is equipped with Boral with a minimum ^{10}B areal density of 0.01 g/cm^2.

1.2.2.3.2 Chemical Safety

There are no chemical safety hazards associated with operations of the HI-STAR 100 dry storage system. A detailed evaluation is provided in Section 3.4.

1.2.2.3.3 Operation Shutdown Modes

The HI-STAR 100 System is totally passive and consequently, operation shutdown modes are unnecessary. Guidance is provided in Chapter 8, which outlines the HI-STAR 100 unloading procedures, and Chapter 11, which outlines the corrective course of action in the wake of all postulated accidents.

1.2.2.3.4 Instrumentation

As stated earlier, the HI-STAR 100 confinement boundary is the MPC, which is seal welded, volumetrically (or multi-layer liquid penetrant) examined, hydrostatically tested, and leak tested. Including the overpack, there are three completely independent barriers to the release of radioactivity to the outside environment. These barriers, proven through decades of use in numerous industries, are arrayed in a sequential manner, making the escape of radioactivity to the outside environment unlikely. The HI-STAR 100 is a completely passive system with appropriate margins of safety; therefore, it is not necessary to deploy any instrumentation to monitor the cask in the storage mode, and none is provided.

1.2.2.3.5 Maintenance Technique

Because of their passive nature, the HI-STAR 100 Systems require minimal maintenance over their lifetime. Chapter 9 describes the acceptance criteria and maintenance program set forth for the HI-STAR 100 System.

1.2.3 Cask Contents

The HI-STAR 100 System is designed to house different types of MPCs. The MPCs are designed to store both BWR and PWR spent nuclear fuel assemblies. Tables 1.2.1 and 1.2.2 provide key design parameters for the MPCs. A description of acceptable fuel assemblies for storage in the MPCs is provided in Chapter 2.

Fuel assemblies classified as damaged fuel or fuel debris (assembly array/class 6x6A, 6x6B, 6x6C, 7x7A, and 8x8A as specified in Table 1.2.11) have been evaluated. Damaged fuel assemblies and fuel debris shall be placed in damaged fuel containers (see Figure 2.1.1) for storage in the MPC to facilitate handling and contain loose components. Damaged fuel assemblies in damaged fuel containers may be stored in the standard MPC-68. The MPC-68 design to store fuel debris is identical to the MPC-68 design to store intact or damaged fuel. The sole additional restriction imposed on an MPC-68 to load damaged fuel containers with fuel assemblies classified as fuel debris is a stricter leakage rate criteria prior to shipment. Therefore, an MPC-68 which is to store damaged fuel containers with fuel assemblies classified as fuel debris must be designated during fabrication to ensure the proper leakage rate criteria is applied. To distinguish an MPC-68, which is fabricated to store damaged fuel containers with fuel assemblies classified as fuel debris, the MPC shall be designated as an "MPC-68F".

Up to 4 damaged fuel containers containing specified fuel debris may be stored within an MPC-68F.

Table 1.2.1

KEY SYSTEM DATA FOR HI-STAR 100

ITEM	QUANTITY	NOTES
Types of MPCs included in this revision of the submittal	2	1 for PWR 1 for BWR
MPC storage capacity:	MPC-24	Up to 24 intact zircaloy or stainless steel clad PWR fuel assemblies
	MPC-68	Up to 68 intact zircaloy or intact stainless steel clad BWR fuel assemblies or damaged zircaloy clad fuel assemblies in damaged fuel containers in the MPC-68 or Up to 4 damaged fuel containers with zircaloy clad BWR fuel debris and the complement intact or damaged zircaloy clad BWR fuel assemblies within an MPC-68F.

Table 1.2.2

KEY PARAMETERS FOR HI-STAR 100 MULTI-PURPOSE CANISTERS

	PWR	BWR
Pre-disposal service life (years)	40	40
Design temperature, max./min. (°F)	725 °F /-40°C	725 °F /-40 °C
Design internal pressure (psig) Normal conditions Off-normal conditions Accident Conditions	 100 100 125	 100 100 125
Total heat load, max. (kW)	19.0 (MPC-24)	18.5 (MPC-68)
Maximum permissible peak fuel cladding temperature: Normal (°F) Short Term & Accident (°F)	 See Table 2.2.3 1058	 See Table 2.2.3 1058
MPC internal environment Helium fill (psig)	 $\leq$ 22.2	 $\leq$ 28.5
MPC external environment/overpack internal pressure Helium fill initial pressure (psig, at STP)	 10	 10
Maximum permissible reactivity including all uncertainties and biases	<0.95	<0.95
Boral ^{10}B Areal Density (g/cm^2)	0.0267 (MPC-24)	0.0372 (MPC-68) 0.01 (MPC-68F)
End closure(s)	Welded	Welded
Fuel handling	Opening compatible with standard grapples	Opening compatible with standard grapples
Heat dissipation	Passive	Passive

Table 1.2.3

INTENTIONALLY DELETED

Table 1.2.4

INTENTIONALLY DELETED

Table 1.2.5

INTENTIONALLY DELETED

Table 1.2.6

HI-STAR 100 OPERATIONS DESCRIPTION

Site-specific handling and operations procedures will be prepared, reviewed, and approved by each owner/user.	
1	Overpack and MPC lowered into the fuel pool without closure plate and MPC lid
2	Fuel assemblies transferred into the MPC fuel basket
3	MPC lid lowered onto the MPC
4	Overpack/MPC assembly moved to the decon pit and MPC lid welded in place, volumetrically (or multi-layer liquid penetrant) examined, hydrostatically tested, and leak tested
5	MPC dewatered, vacuum dried, backfilled with helium and the vent/drain port cover plates and closure ring welded
6	Overpack drained and external surfaces decontaminated
7	Overpack seals and closure plate installed and bolts torqued
8	Overpack cavity dried, backfilled with helium, and helium leak tested
9	HI-STAR 100 loaded onto transporter and moved to the ISFSI pad for on-site storage
10	HI-STAR 100 emplaced onto the ISFSI pad at its designated location

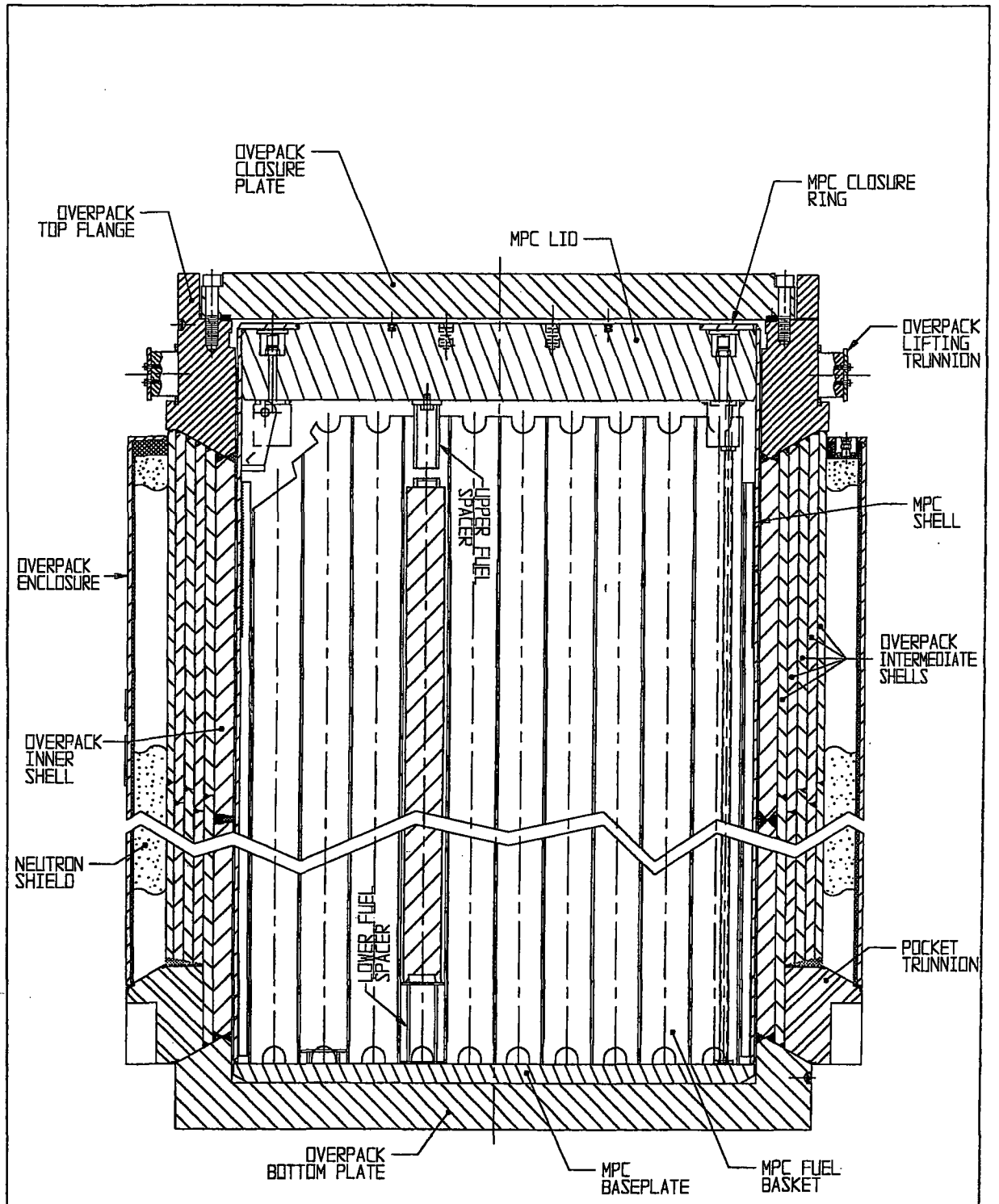

FIGURE 1.2.1; CROSS SECTION ELEVATION VIEW OF HI-STAR 100 SYSTEM

REPORT HI-2012610 | REVISION 0

F:\PROJECTS\GENERIC\HI2012610\CH. 1

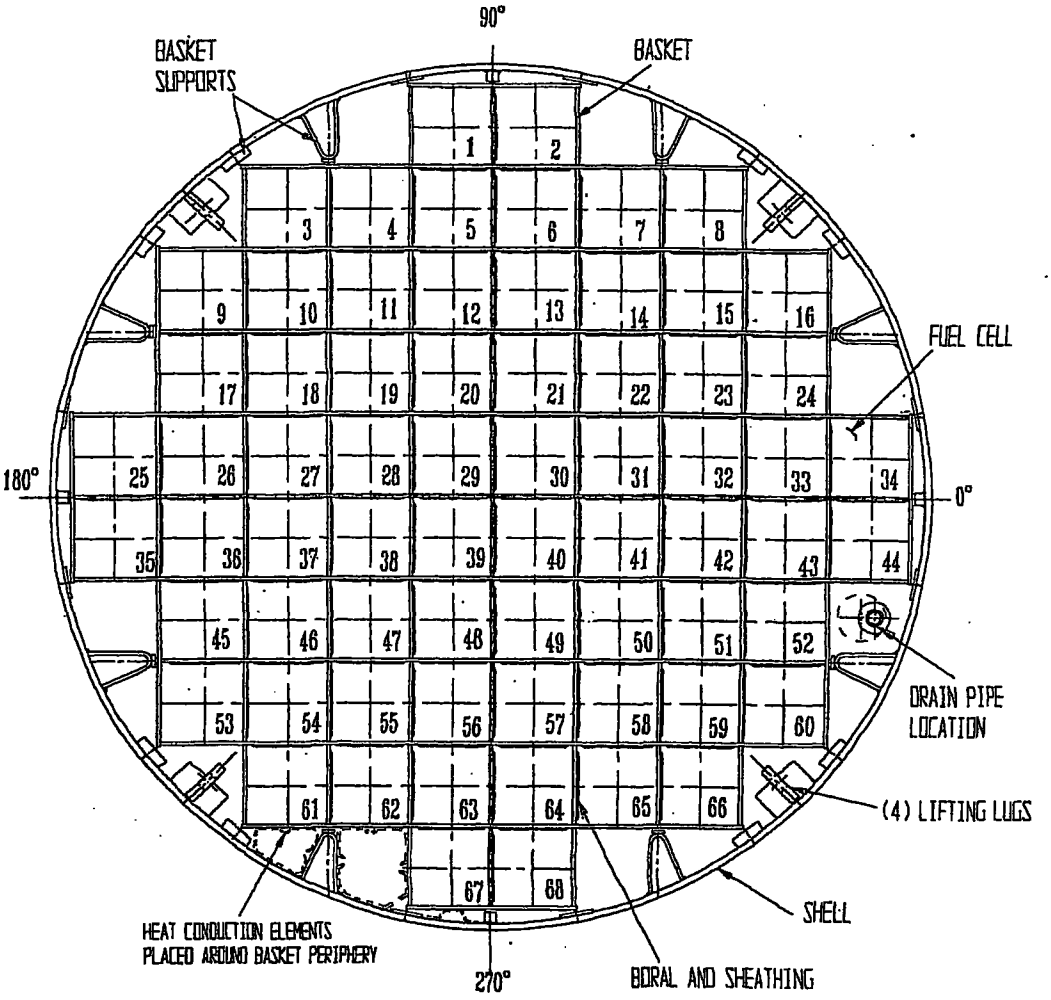

FIGURE 1.2.2; MPC-68 CROSS SECTION VIEW

REPORT HI-2012610 | REVISION 0

F:\PROJECTS\GENERIC\HI2012610\CH. 1

DELETED

FIGURE 1.2.3; MPC-32 CROSS SECTION

REPORT HI-2012610 REV. 0

\PROJECTS\GENERIC\HI2012610NCH.1\1_2_3

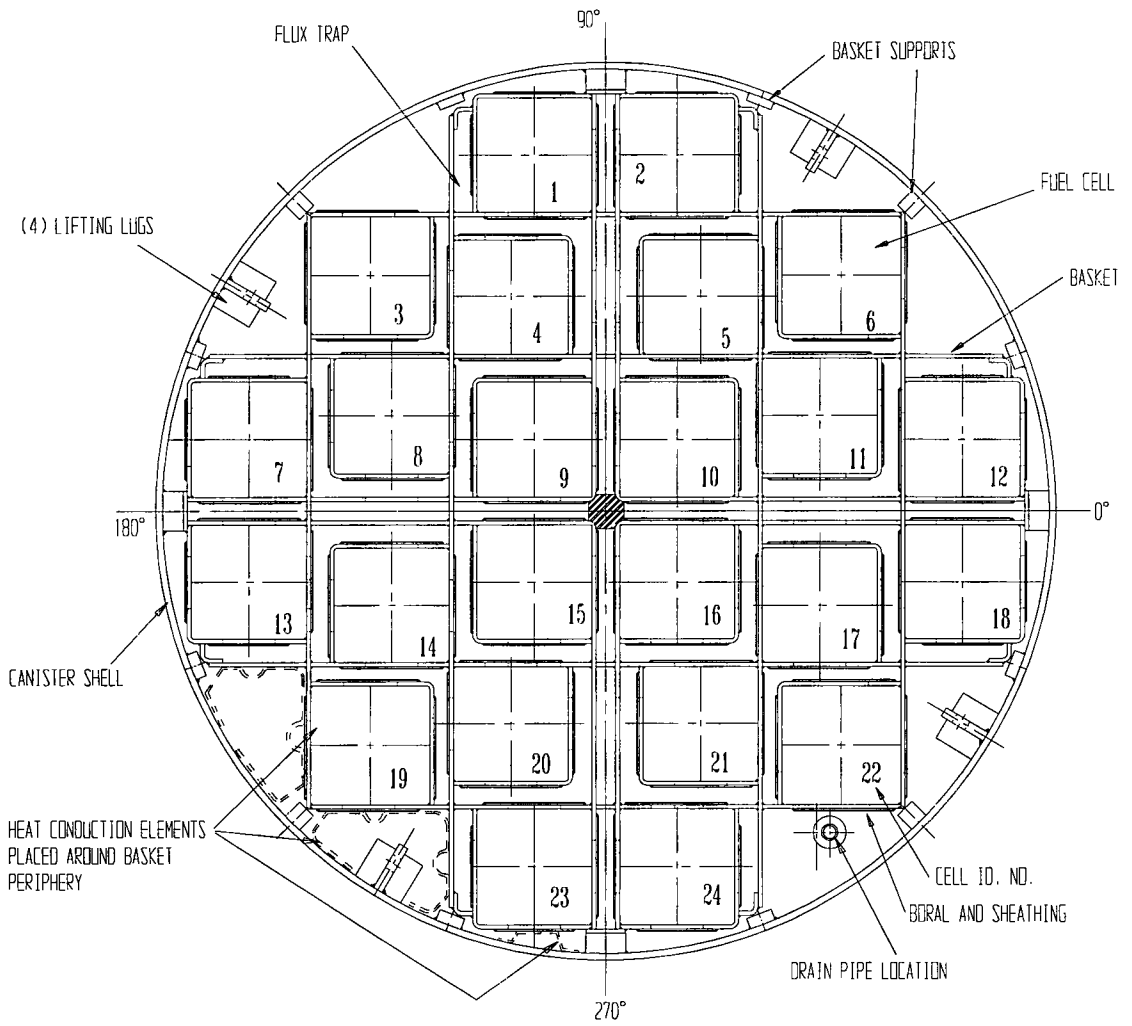

FIGURE 1.2.4; MPC-24 CROSS SECTION VIEW

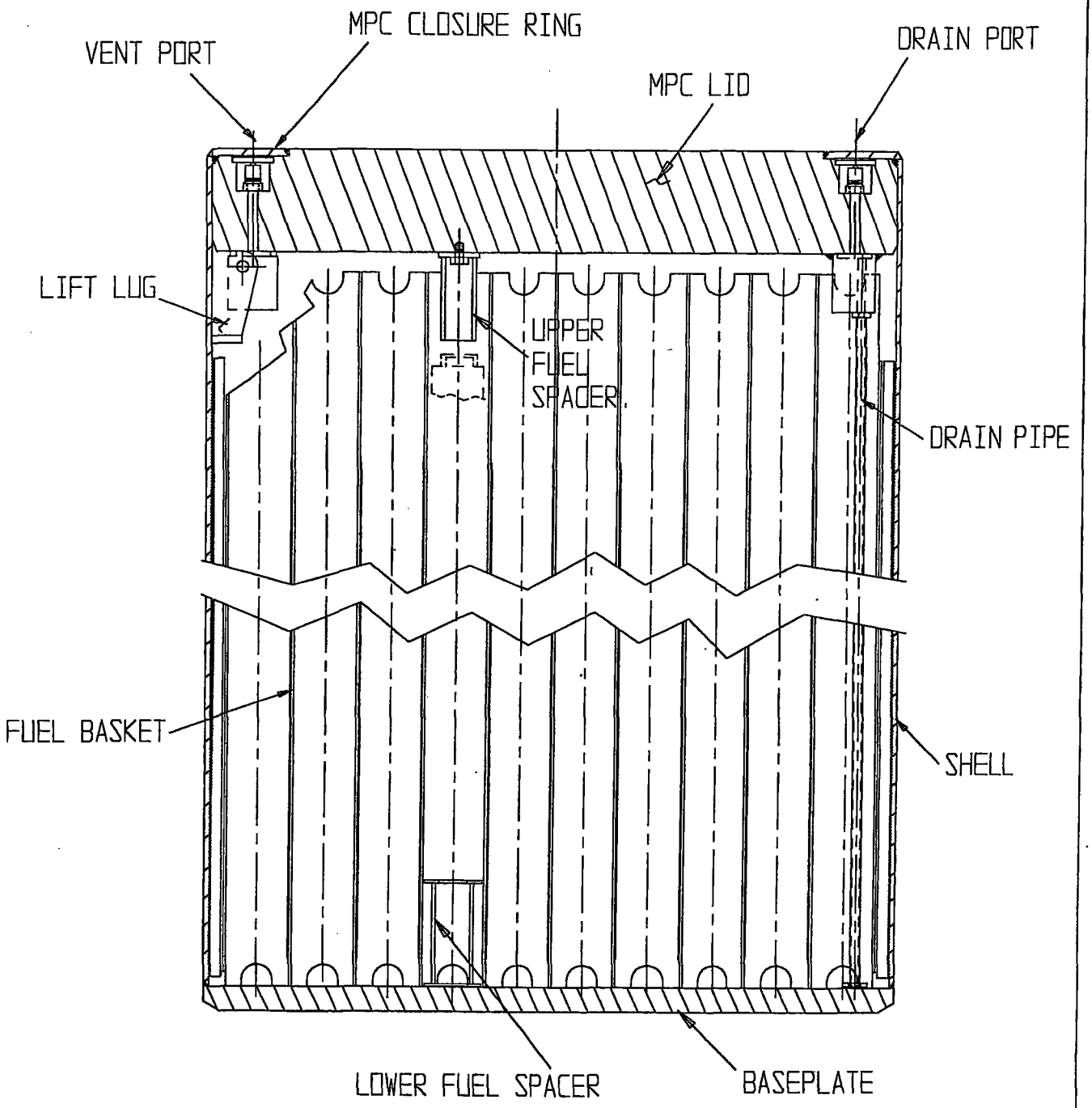

FIGURE 1.2.5; CROSS SECTION ELEVATION VIEW OF MPC

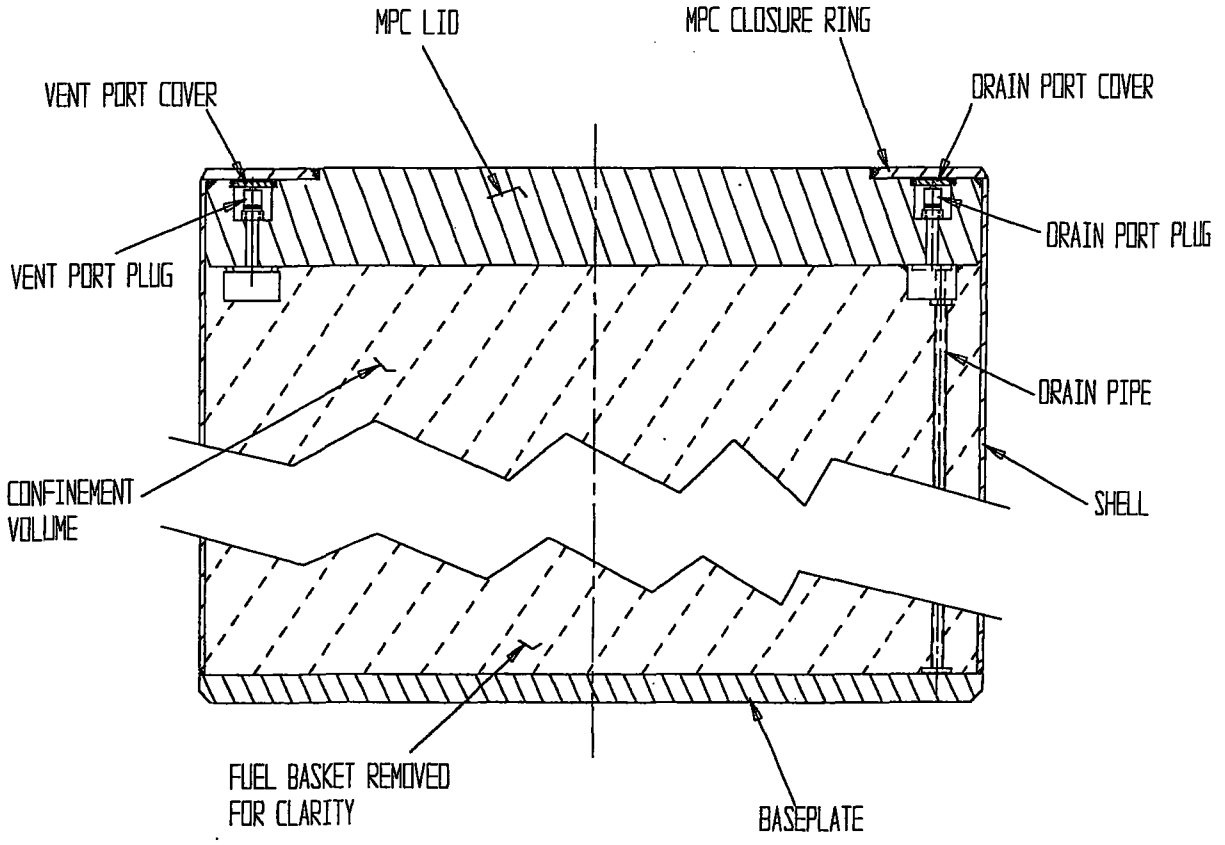

FIGURE 1.2.6; MPC CONFINEMENT BOUNDARY

REPORT HI-2012610 REV. 0

\PROJECTS\GENERIC\HI2012610\CH. 1\1 2 6

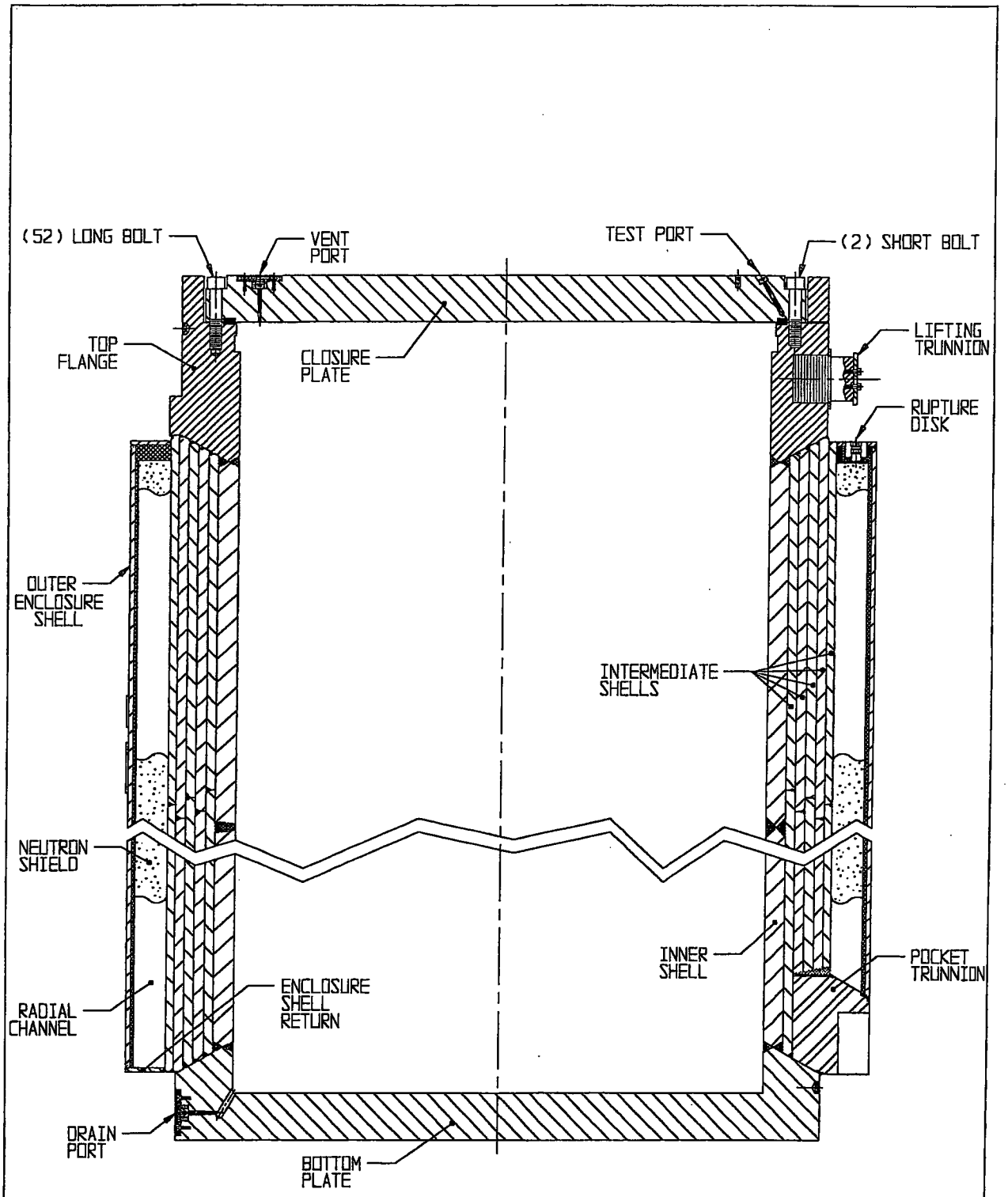

FIGURE 1.2.7; CROSS SECTION ELEVATION VIEW OF OVERPACK

REPORT HI-2012610 REV. 0

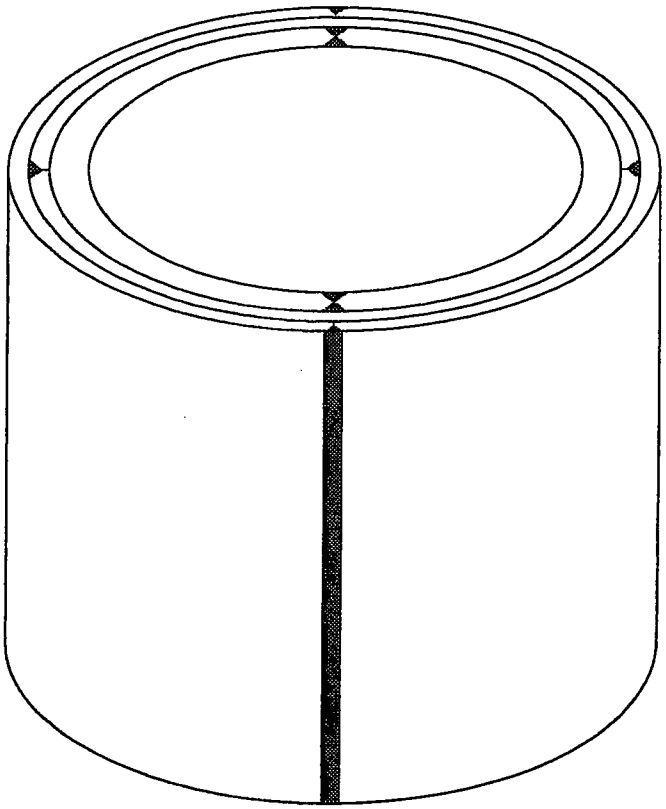

ISOMETRIC VIEW OF CENTRAL REGION OF THE OVERPACK

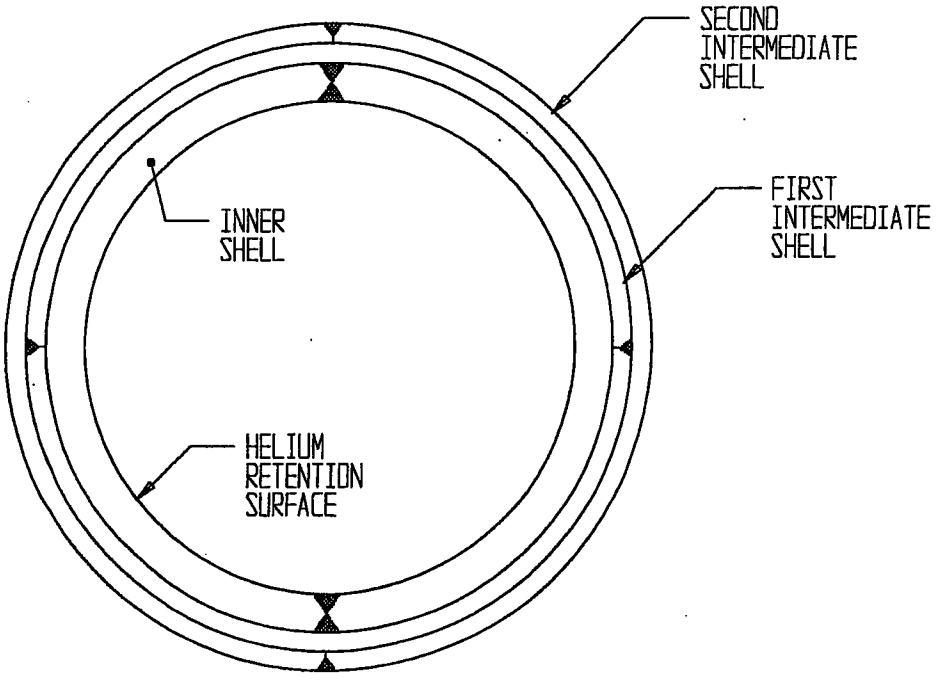

CROSS SECTION AT MID-HEIGHT

FIGURE 1.2.8; HI-STAR 100 OVERPACK SHELL LAYERING

REPORT HI-2012610 REVISION 0

\PROJECTS\GENERIC\HI2012610\CH. 1\ 1_2_8

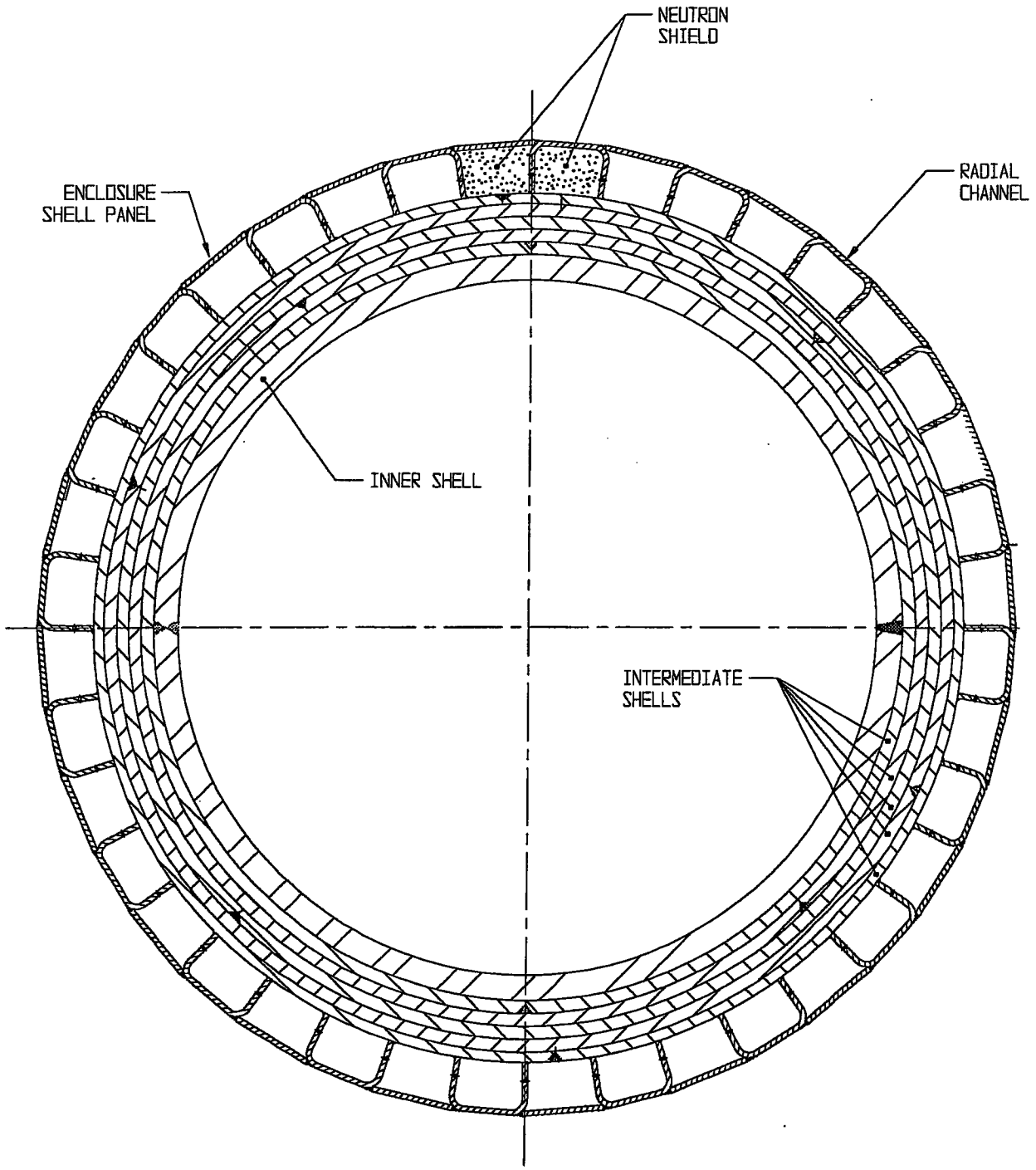

FIGURE 1.2.9; OVERPACK MID-PLANE CROSS SECTION

FIGURE 1.2.10

INTENTIONALLY DELETED

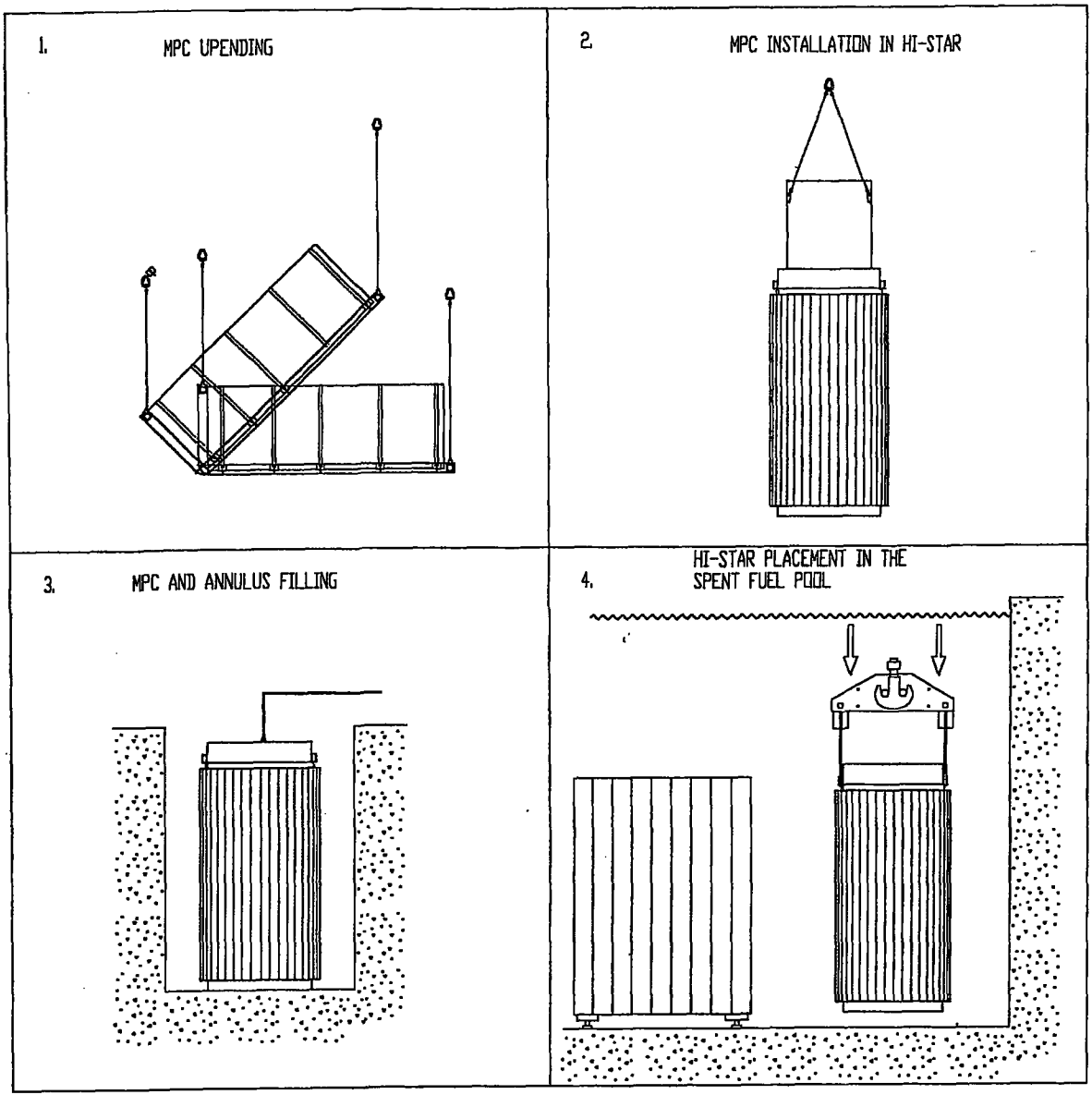

Figure 1.2.11a; Major HI-STAR 100 Loading Operations (Sheet 1 of 3)

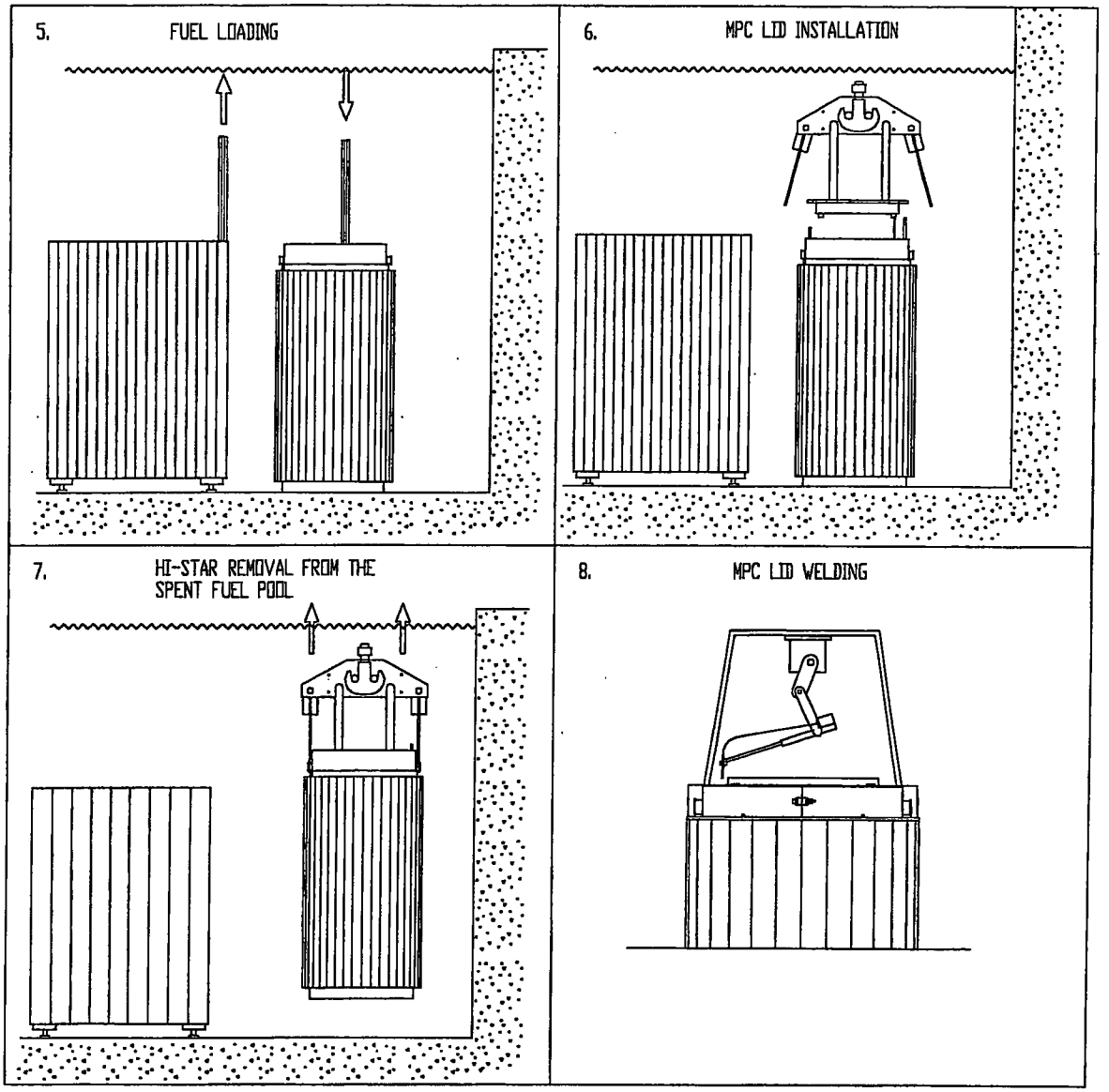

Figure 1.2.11b; Major HI-STAR 100 Loading Operations (Sheet 2 of 3)

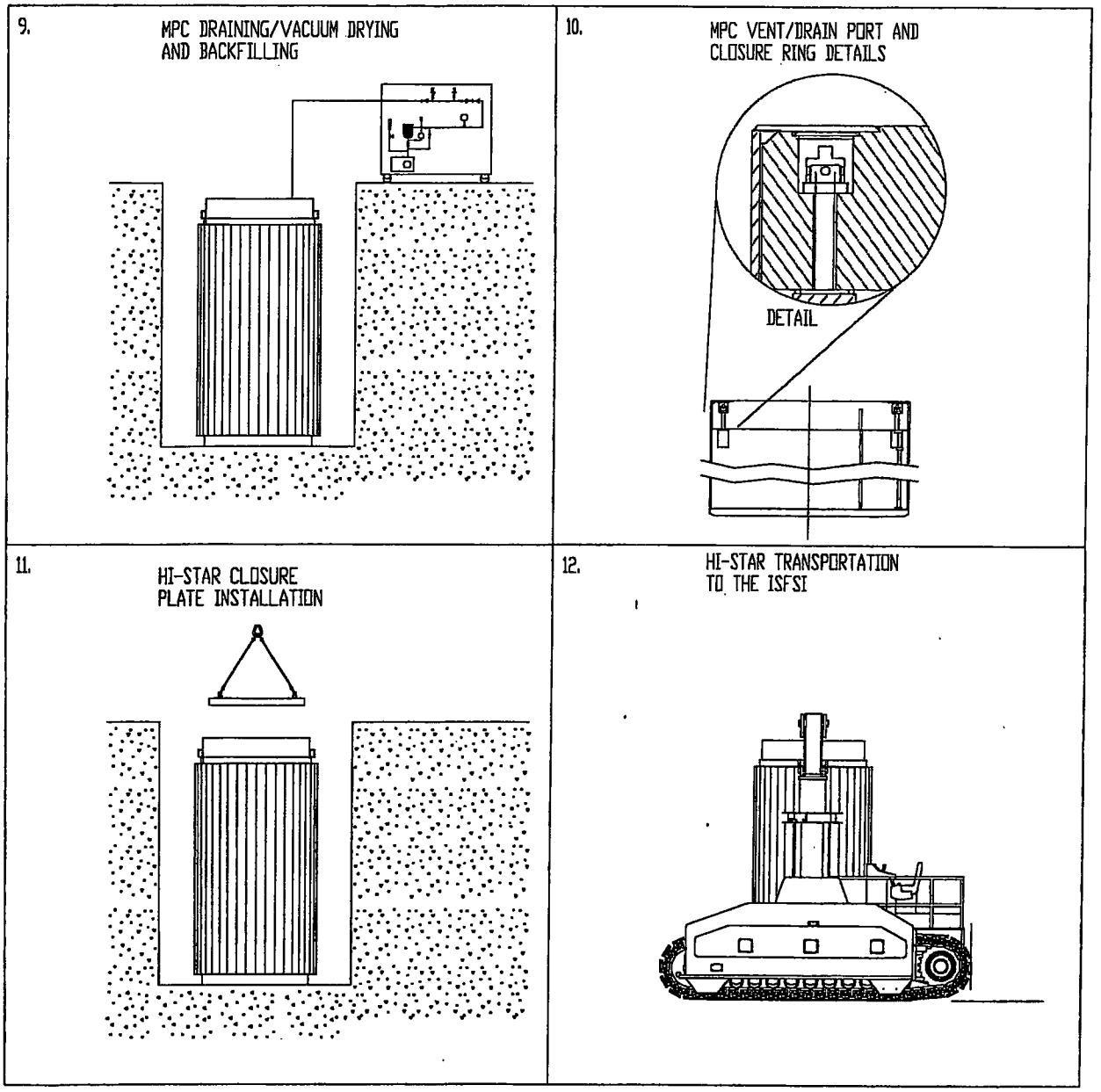

Figure 1.2.11c; Major HI-STAR 100 Loading Operations (Sheet 3 of 3)

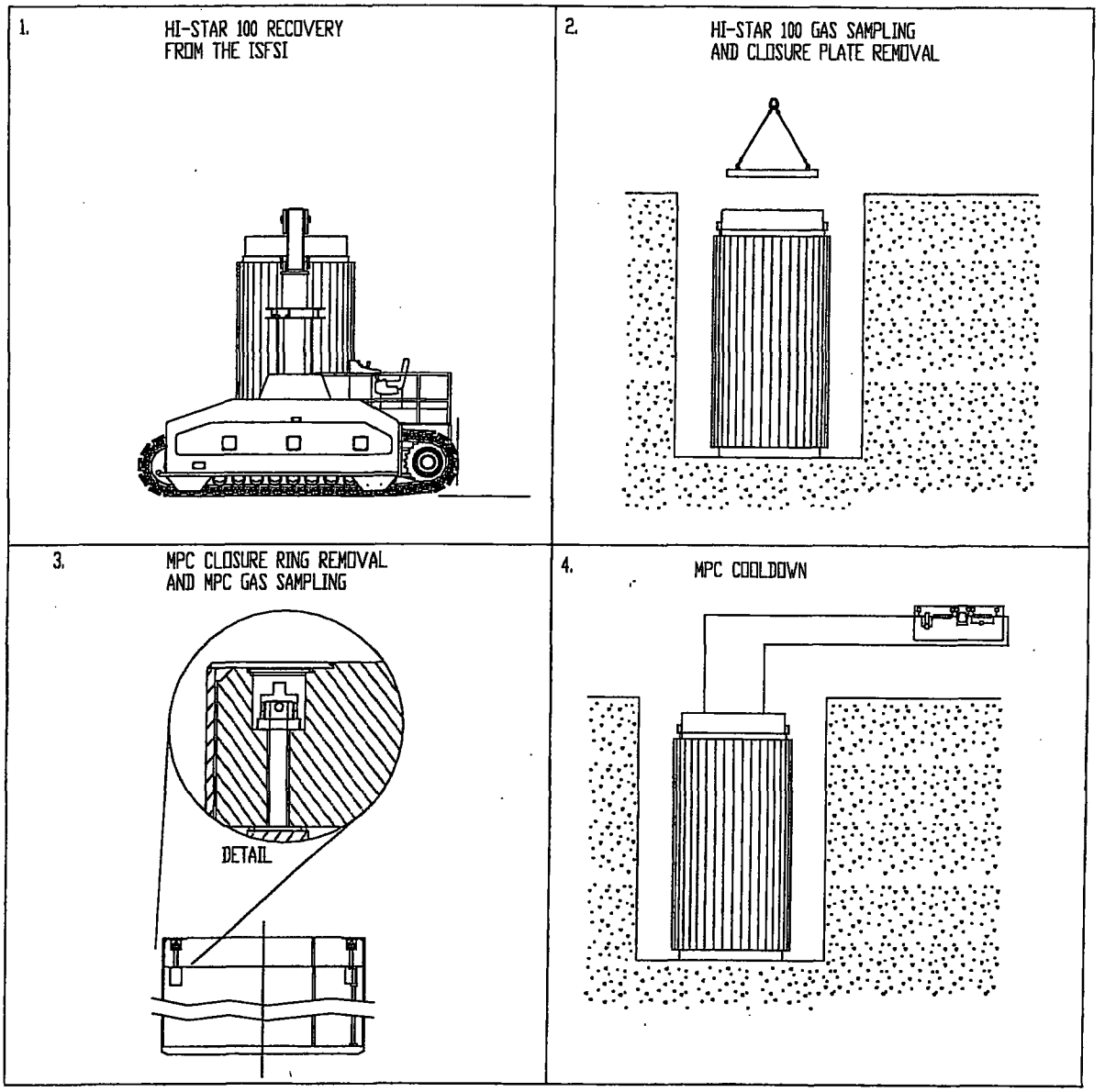

Figure 1.2.12a; Major HI-STAR 100 Unloading Operations (Sheet 1 of 3)

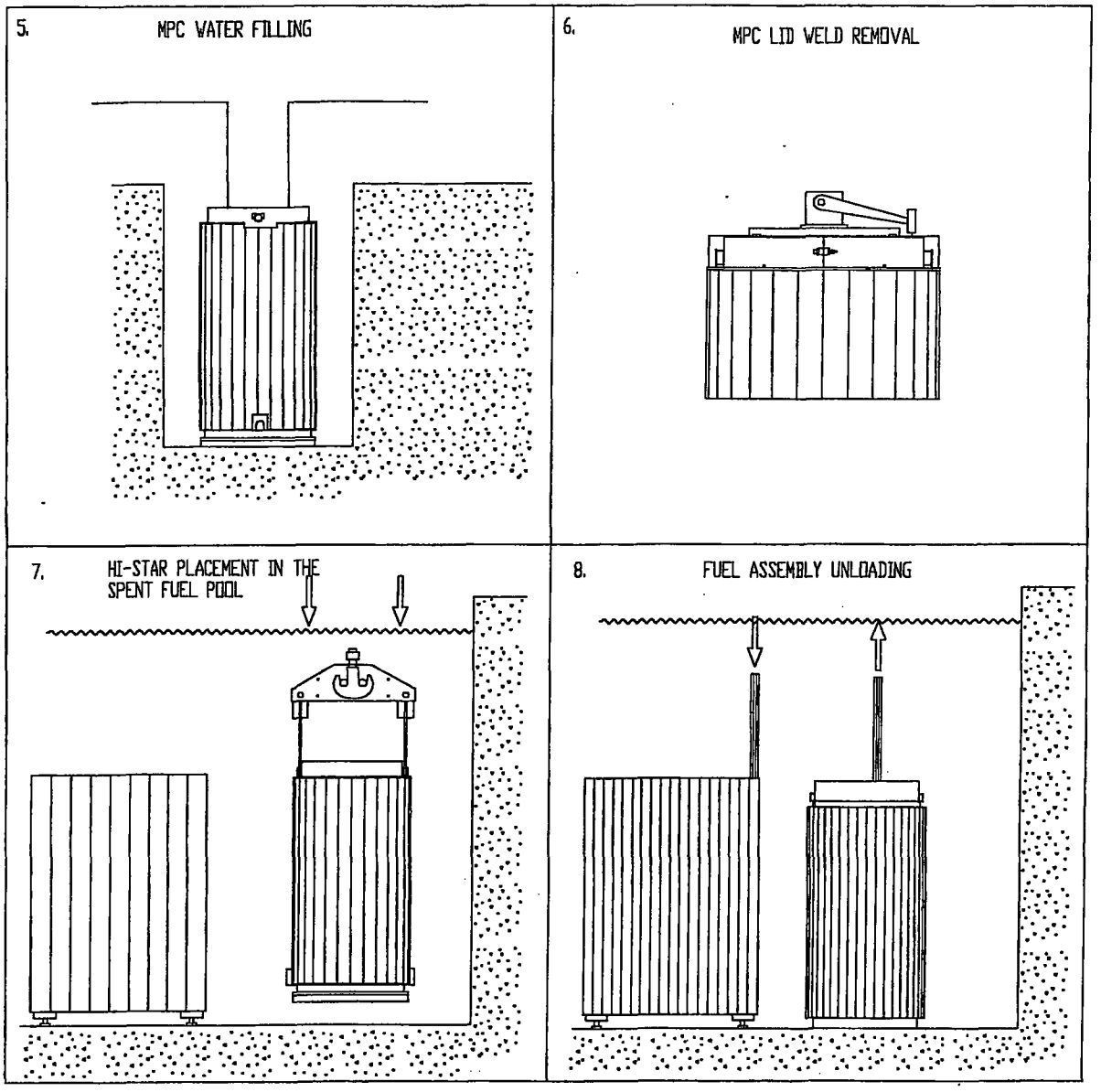

Figure 1.2.12b; Major HI-STAR 100 Unloading Operations (Sheet 2 of 3)

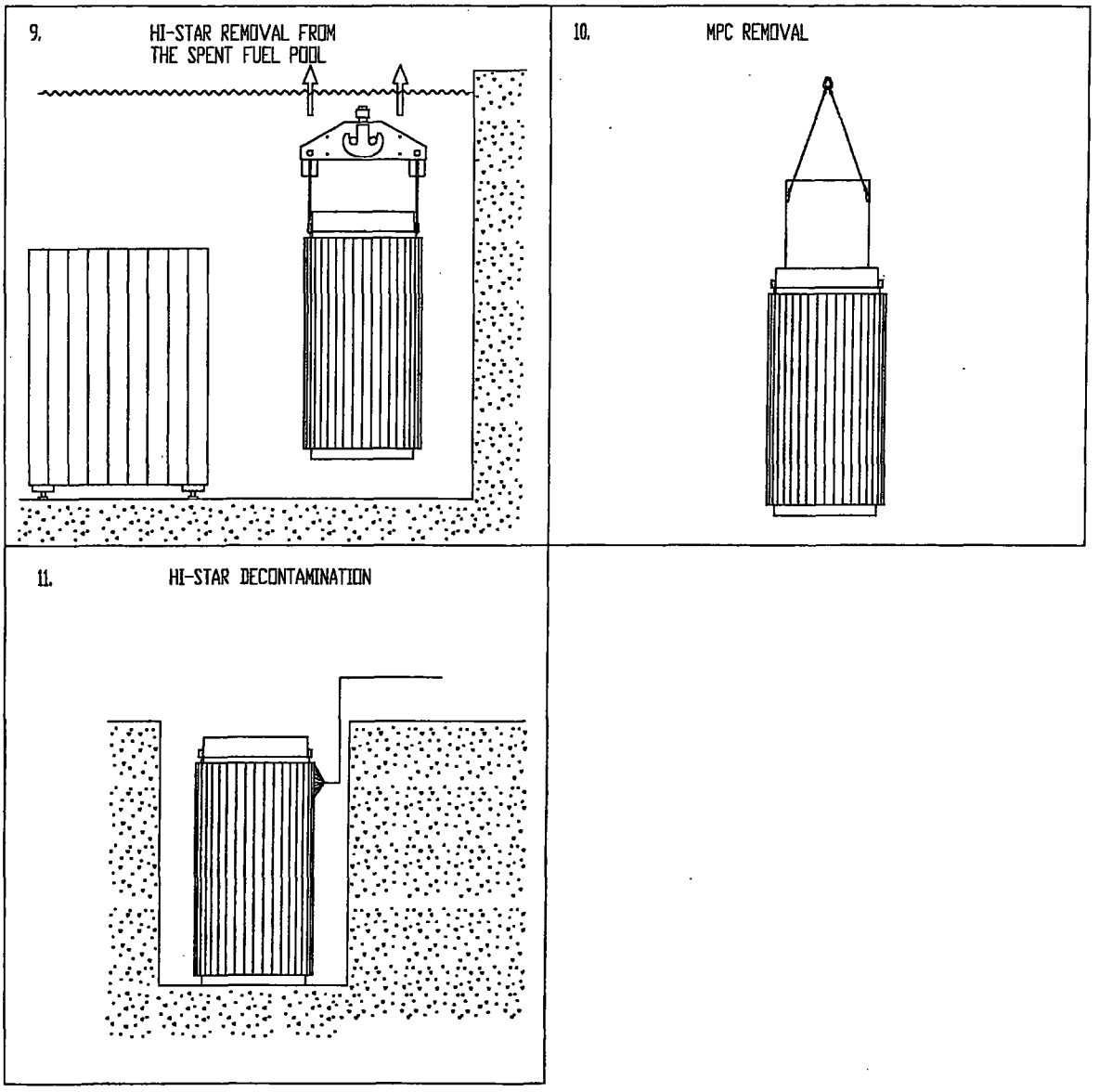

Figure 1.2.12c; Major HI-STAR 100 Unloading Operations (Sheet 3 of 3)

1.3 IDENTIFICATION OF AGENTS AND CONTRACTORS

Holtec International is a specialty engineering company with a principal focus on spent fuel storage technologies. Holtec has carried out turnkey wet storage capacity expansions (engineering, licensing, fabrication, removal of existing racks, performance of underwater modifications, volume reduction of the old racks and hardware, installation of new racks, and commissioning of the pool for increased storage capacity) in numerous plants around the world. Over 45 plants in the U.S., Britain, Brazil, Korea, and Taiwan have utilized Holtec's wet storage technology to extend their in-pool storage capacity.

Holtec's corporate engineering consists of experts with advanced degrees (Ph.D.'s) in every discipline germane to the fuel storage technologies, namely structural mechanics, heat transfer, computational fluid dynamics, and nuclear physics. All engineering analyses for Holtec's fuel storage projects (including HI-STAR 100) are carried out in-house.

Holtec International's quality assurance program was originally developed to meet NRC requirements delineated in 10CFR50, Appendix B, and was expanded to include provisions of 10CFR71, Subpart H, and 10CFR72, Subpart G, for structures, systems, and components designated as important to safety. A description of the quality assurance program and its method of satisfying all 18 criteria in 10CFR72, Subpart G, that apply to the design, fabrication, construction, testing, operation, modification, and decommissioning of structures, systems, and components important to safety is provided in Chapter 13.

It is currently planned that the HI-STAR 100 Systems will be fabricated by U.S. Tool & Die, Inc. (UST&D) of Pittsburgh, Pennsylvania. UST&D is an N-Stamp holder and a highly respected fabricator of nuclear components. UST&D is on Holtec's Approved Vendors List (AVL) and has a quality assurance program meeting 10CFR50 Appendix B criteria. Extensive prototypical fabrication of the MPCs has been carried out at the UST&D shop to resolve fixturing and tolerance issues. If another fabricator is to be used for fabrication of the HI-STAR 100 Systems, the proposed fabricator will be evaluated and audited in accordance with Holtec International's Quality Assurance Program described in Chapter 13.

Construction, assembly, and operations on-site may be performed by Holtec or a licensee as the prime contractor. A licensee shall be suitably qualified and experienced to perform selected activities. Typical licensees are technically qualified and experienced in commercial nuclear power plant construction and operation activities under a quality assurance program meeting 10CFR50 Appendix B criteria.

1.4 GENERIC CASK ARRAYS

The only system required for storage of the HI-STAR 100 System is the loaded overpack itself. The HI-STAR 100 System is stored in a vertical orientation. A typical ISFSI storage pattern is illustrated in Figure 1.4.1, which shows an array in a rectangular layout pattern. The required center-to-center spacing between the modules (layout pitch) is guided by heat transfer considerations. Table 1.4.1 provides the nominal pitch, determined by heat transfer calculations in Chapter 4. The pitch may be increased to suit facility considerations.

Table 1.4.1

CASK LAYOUT MINIMUM PITCH DATA BASED ON
THERMAL EVALUATION

MPC Type	Nominal Cask Pitch (ft.)
MPC-24	12
MPC-68	12

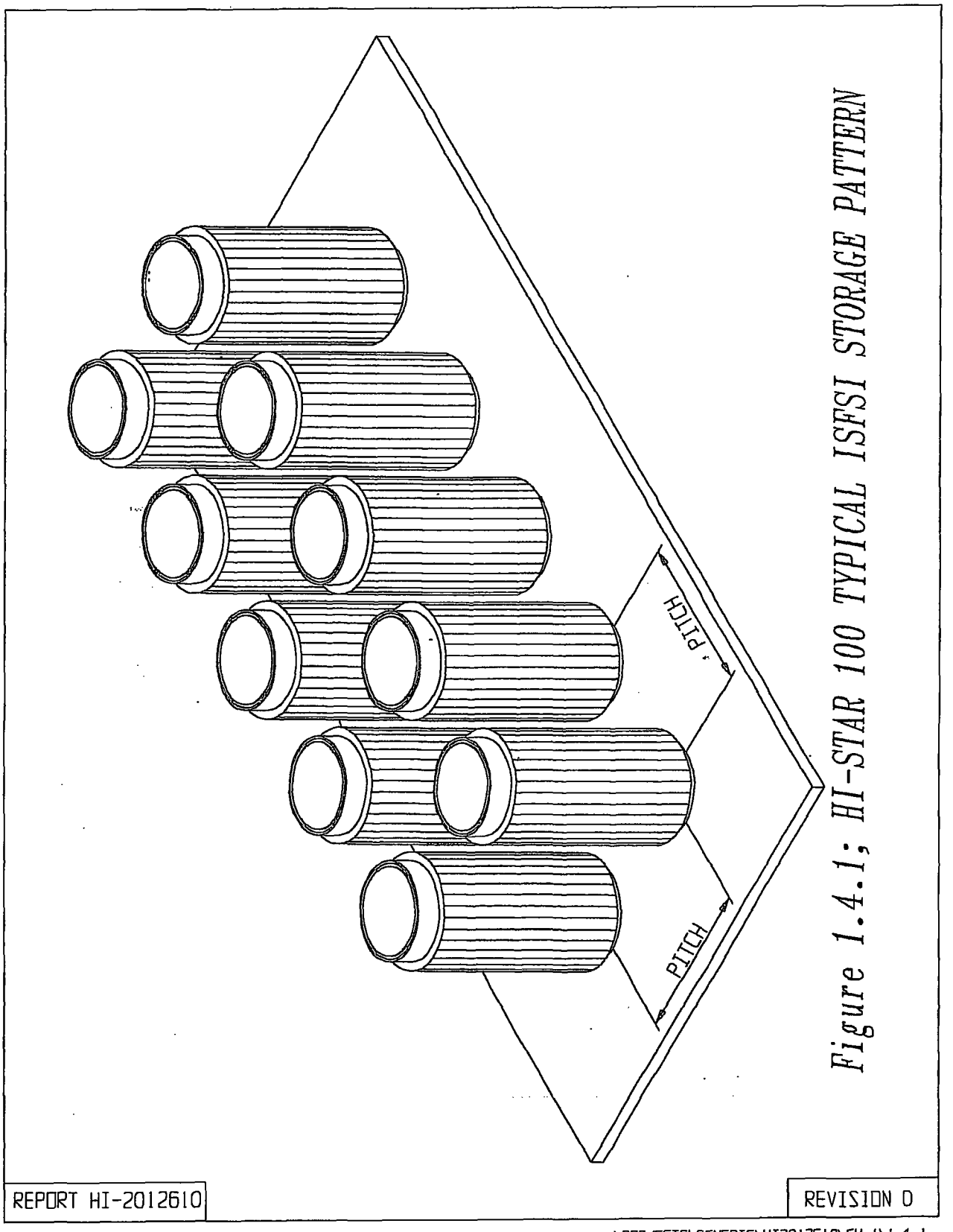

Figure 1.4.1; HI-STAR 100 TYPICAL ISFSI STORAGE PATTERN

1.5 GENERAL ARRANGEMENT DRAWINGS

The following HI-STAR 100 System drawings are provided in this section:

Drawing Number/Sheet	Description	Rev.
3913	HI-STAR 100 Overpack	5
3923	MPC Enclosure Vessel	10
3926	MPC-24 Fuel Basket Assembly	5
3928	MPC-68/68F/68FF Fuel Basket Assembly	5

Security-Related Information
Figure Withheld Under 10 CFR 2.390

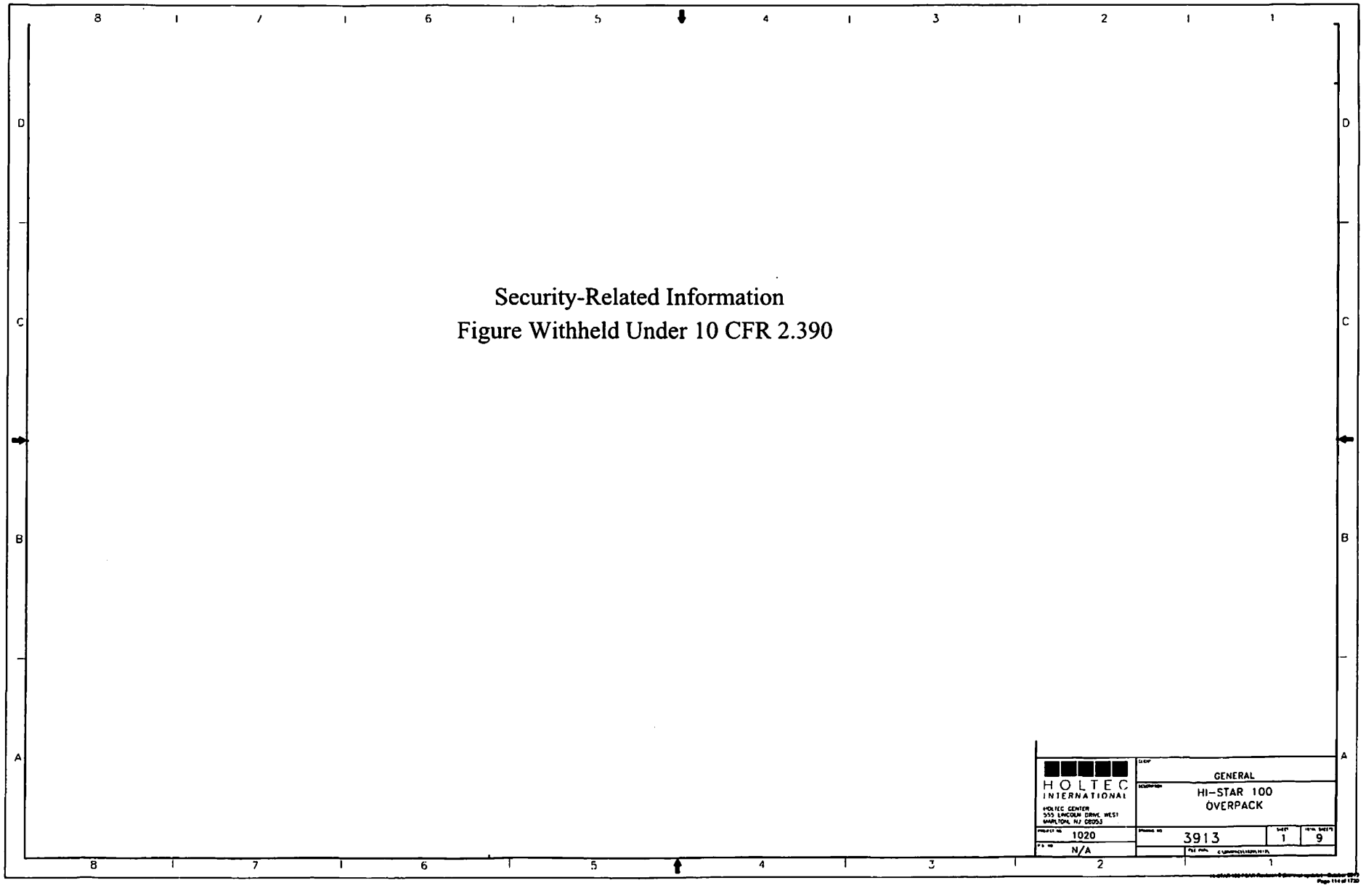

Security-Related Information
Figure Withheld Under 10 CFR 2.390

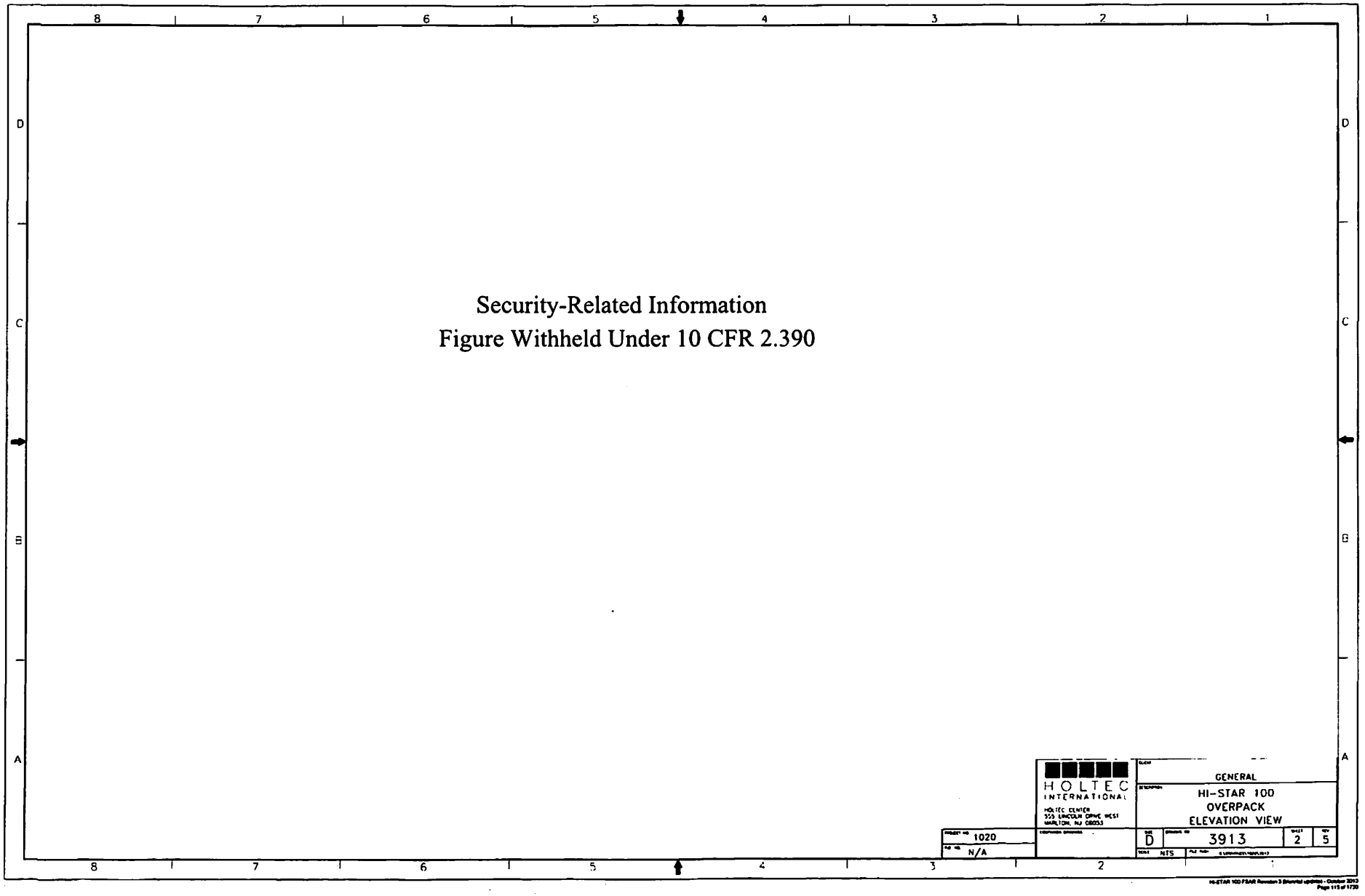

Security-Related Information
Figure Withheld Under 10 CFR 2.390

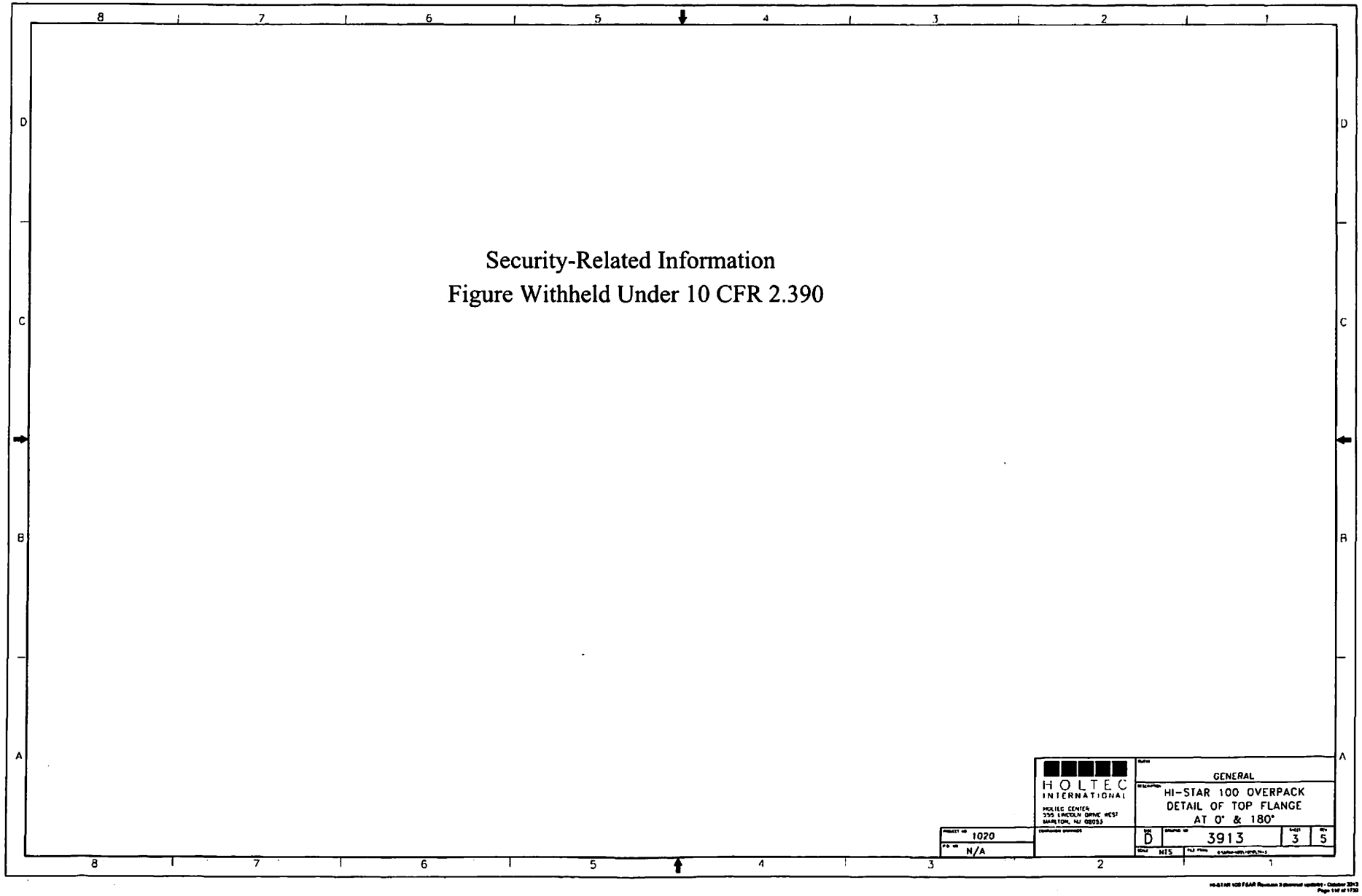

Security-Related Information
Figure Withheld Under 10 CFR 2.390

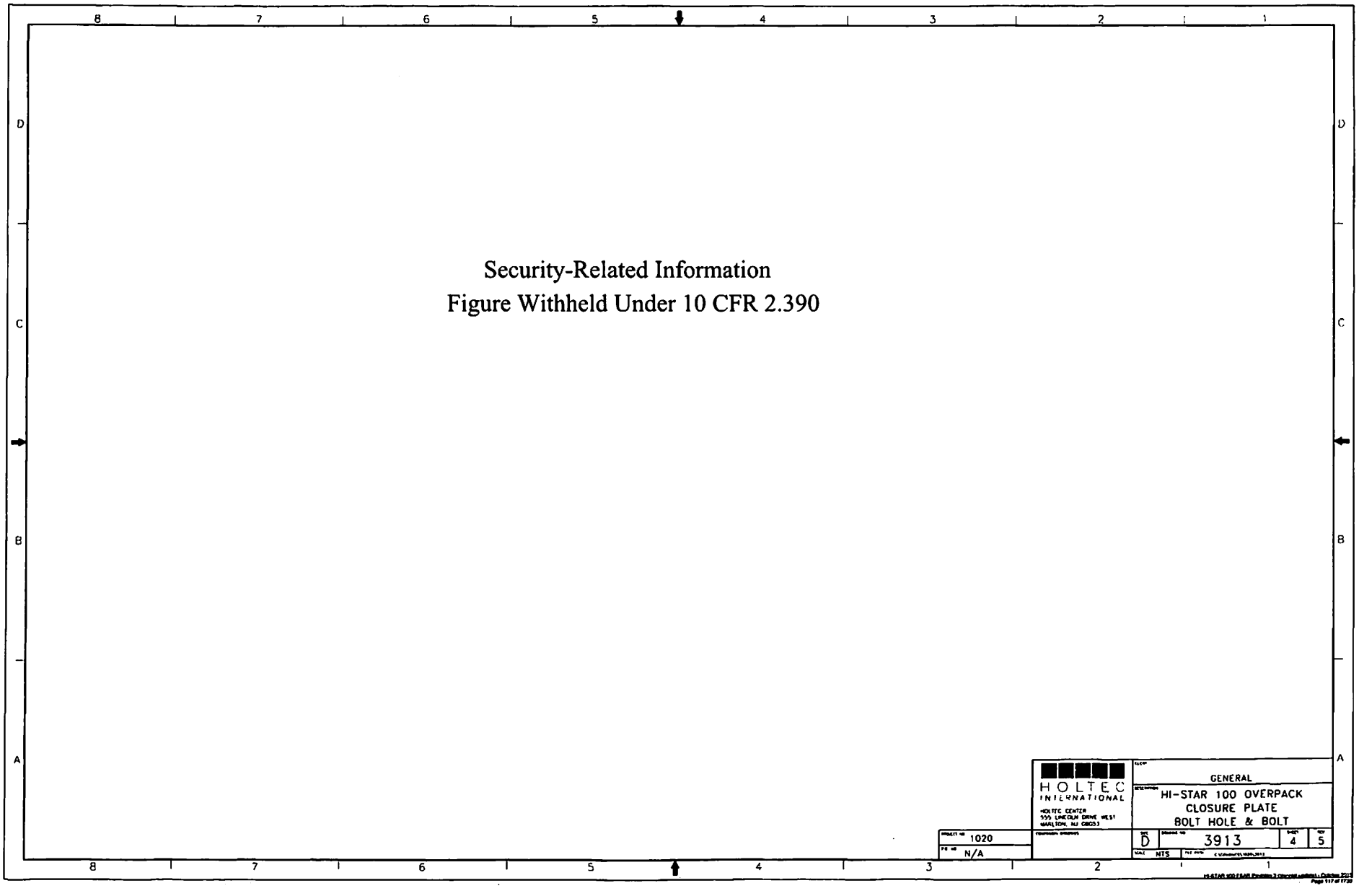

Security-Related Information
Figure Withheld Under 10 CFR 2.390

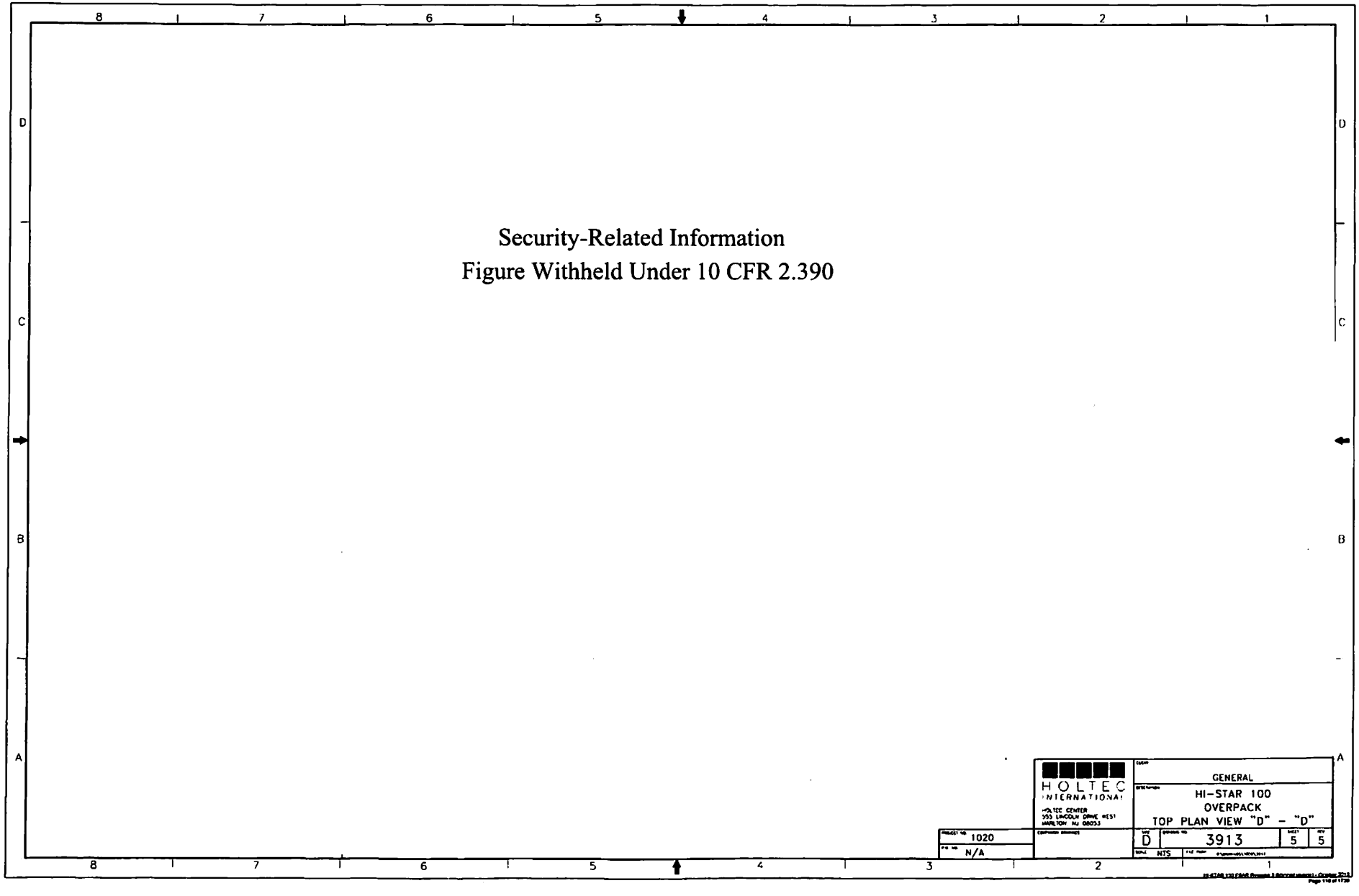

Security-Related Information
Figure Withheld Under 10 CFR 2.390

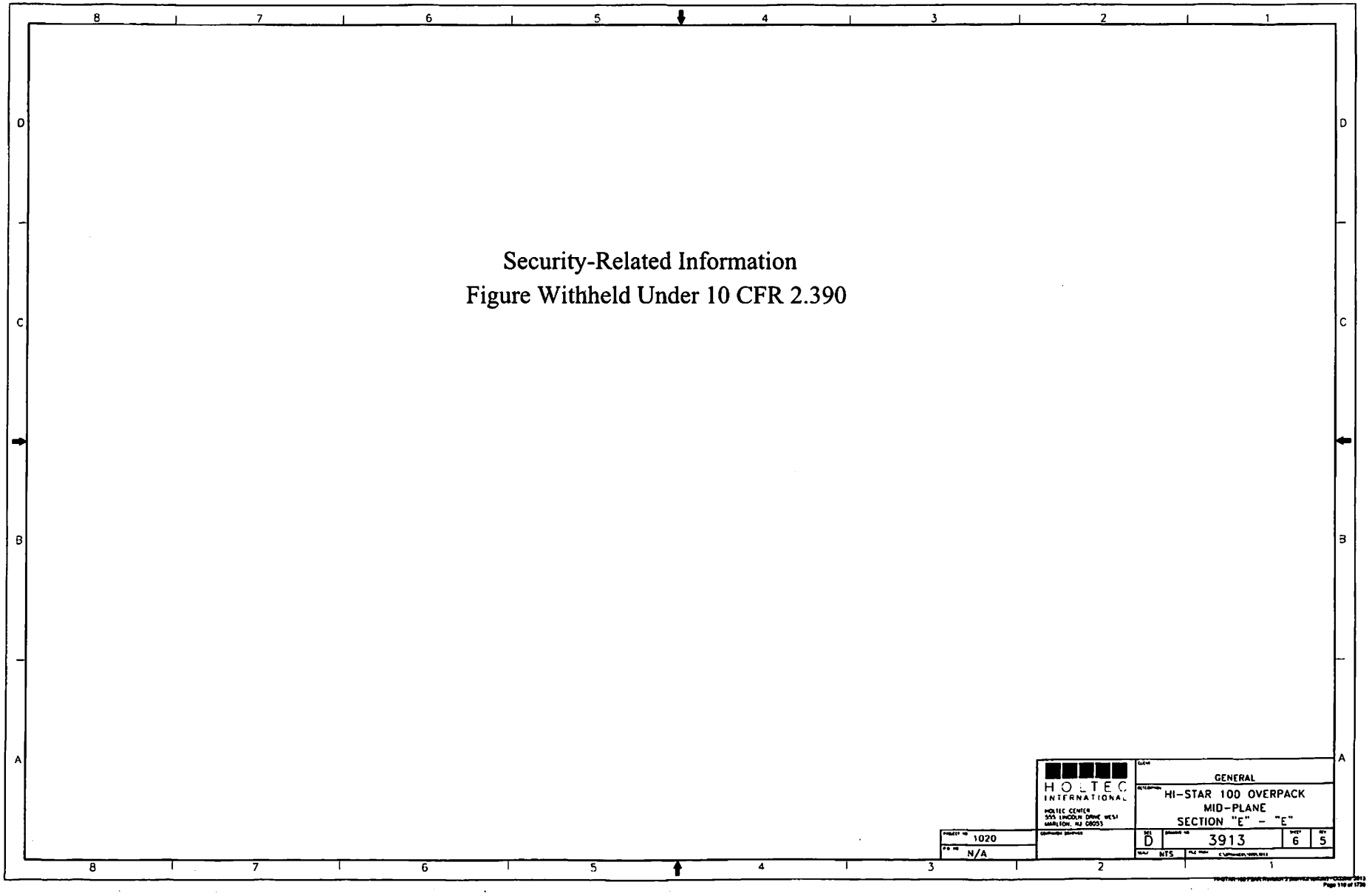

Security-Related Information
Figure Withheld Under 10 CFR 2.390

HOLTEC INTERNATIONAL
HOLTEC CENTER
555 LINCOLN DRIVE WEST
MARLTON, NJ 08053

GENERAL
HI-STAR 100 OVERPACK
TEST, VENT AND
DRAIN PORT DETAILS

PROJECT NO 1020
FIG NO N/A
SIZE D
DRAWING NO 3913
SHT 7
REV 5
SCALE NTS

Security-Related Information
Figure Withheld Under 10 CFR 2.390

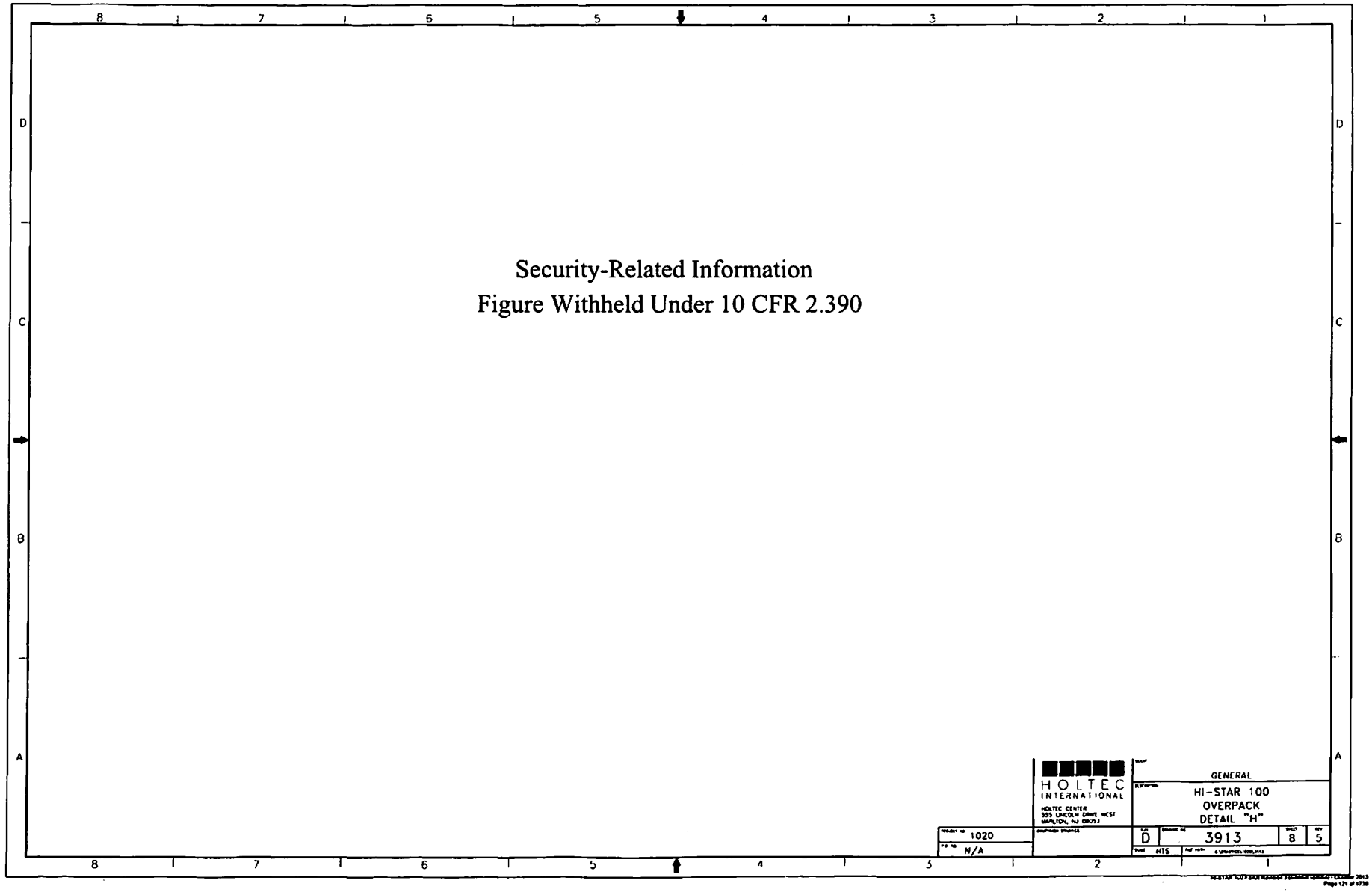

Security-Related Information
Figure Withheld Under 10 CFR 2.390

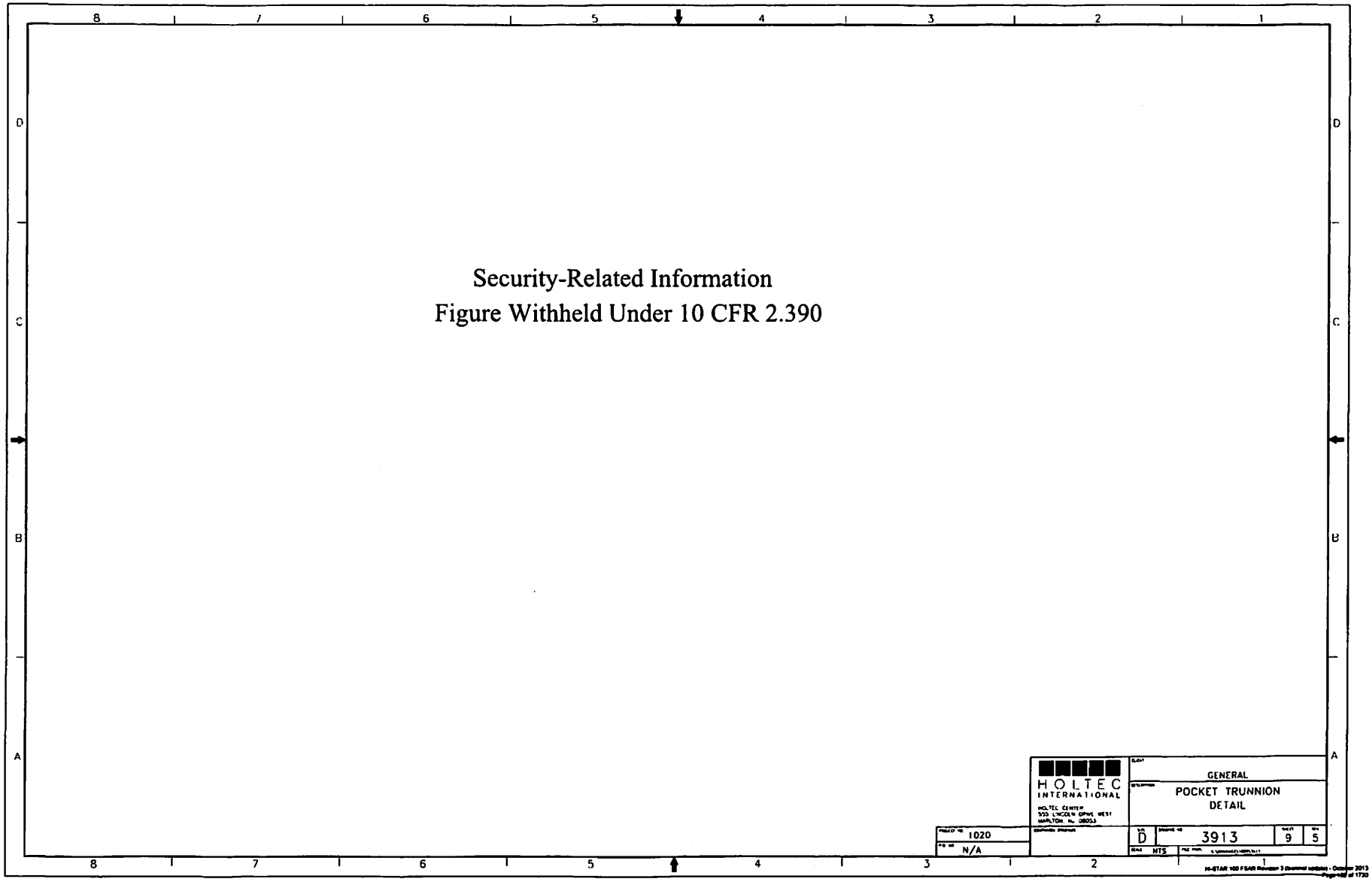

LICENSING DRAWING PACKAGE COVER SHEET

Security-Related Information
Figure Withheld Under 10 CFR 2.390

HOLTEC INTERNATIONAL	GENERAL
HOLTEC CENTER 555 LINCOLN DRIVE WEST MARLTON, NJ 08053	MPC ENCLOSURE VESSEL
PROJECT NO 5014	DRAWING NO 3923 SHEET 1 REV. 5
FCS NO N/A	

Security-Related Information
Figure Withheld Under 10 CFR 2.390

HOLTEC INTERNATIONAL		GENERAL	
		MPC ENCLOSURE VESSEL GENERAL ARRANGEMENT	
5014	3925, 3926, 3927, 3928	D	3923 2 10
N/A		NONE	

Security-Related Information
Figure Withheld Under 10 CFR 2.390

HOLTEC INTERNATIONAL			GENERAL		
			MPC ENCLOSURE ENCLOSURE VESSEL ELEVATION DETAILS		
5014	3925, 3926, 3927, 3928	D	3923	3	10
N/A		NONE			

Security-Related Information
Figure Withheld Under 10 CFR 2.390

HOLTEC INTERNATIONAL
HOLTEC CENTER
555 LINCOLN DRIVE WEST
MARLTON, NJ 08053

5014	GENERAL
N/A	MPC ENCLOSURE VESSEL LID DETAILS
3925, 3926, 3927, 3928	D 3923 4 10
	SCALE NONE

Security-Related Information
Figure Withheld Under 10 CFR 2.390

HOLTEC INTERNATIONAL			GENERAL		
			FUEL SPACER DETAILS		
5014	3923, 3925, 3927, 3929	D	3923	5	10
N/A		NONE			

LICENSING DRAWING PACKAGE COVER SHEET

Security-Related Information
Figure Withheld Under 10 CFR 2.390

HOLTEC INTERNATIONAL HOLTEC CENTER 359 LENCOLN DRIVE WEST MARLTON, NJ 08053	GENERAL MPC-24 FUEL BASKET ASSEMBLY
1022	3926 | 1 | 4
N/A	

Security-Related Information
Figure Withheld Under 10 CFR 2.390

HOLTEC INTERNATIONAL		GENERAL	
		MPC 24 FUEL BASKET ARRANGEMENT	
1022	3923	D	3926 2 5
N/A		NONE	

Security-Related Information
Figure Withheld Under 10 CFR 2.390

HOLTEC INTERNATIONAL
HOLTEC CENTER
555 LINCOLN DRIVE WEST
MARLTON, NJ 08053

PROJECT NO	1022
	N/A
DRAWING NO	3923

GENERAL

MPC-24
FUEL BASKET
LAYOUT AND WELD DETAILS

SIZE	DRAWING NO	SHEET	REV
D	3926	3	5
SCALE	NONE		

Security-Related Information
Figure Withheld Under 10 CFR 2.390

HOLTEC INTERNATIONAL
HOLTEC CENTER
555 LINCOLN DRIVE WEST
MARLTON, NJ 08053

PROJECT NO	1022
P.O. NO	N/A
DRAWING NO	3923

GENERAL

MPC 24
FUEL BASKET
SUPPORTS

D	3926	4	5

NONE

LICENSING DRAWING PACKAGE COVER SHEET

Security-Related Information
Figure Withheld Under 10 CFR 2.390

*MPC-68FF IS NOT CERTIFIED FOR TRANSPORTATION UNDER 10CFR71

HOLTEC INTERNATIONAL
HOLTEC CENTER
555 LINCOLN DRIVE WEST
MARLTON, NJ 08053

GENERAL

MPC-68/68F/68FF
FUEL BASKET

PROJECT NO 1021
P.O. NO N/A
DRAWING NO 3928
SHEET 1
TOTAL SHEETS 4
REV

Security-Related Information
Figure Withheld Under 10 CFR 2.390

HOLTEC INTERNATIONAL		GENERAL	
		MPC-68/68F/68FF FUEL BASKET	
1021	3923	D	3928 2 5
N/A		NONE	

Security-Related Information
Figure Withheld Under 10 CFR 2.390

HOLTEC INTERNATIONAL
HOLTEC CENTER
555 LINCOLN DRIVE WEST
MARLTON, NJ 08053

GENERAL

MPC-68/68F/68FF
FUEL BASKET
LAYOUT AND WELD DETAILS

PROJECT NO. 1021			
N/A	3923	D	3928	3	5
		NONE			

Security-Related Information
Figure Withheld Under 10 CFR 2.390

HOLTEC INTERNATIONAL
HOLTEC CENTER
555 LINCOLN DRIVE WEST
MARLTON, NJ 08053

GENERAL

MPC 68/68F/88FF
FUEL BASKET
SUPPORTS

1021	3923	D	3928	4 of 5
N/A			HDMS	

1.6 REGULATORY COMPLIANCE

Chapter 1 provides a general description of the HI-STAR 100 System which allows a reviewer to obtain a basic understanding of the system, its components, and the protection afforded for the health and safety of the public. The chapter has been written to provide the following pertinent information to allow verification of compliance with 10CFR72, NUREG-1536, and Regulatory Guide 3.61:

- A general description and discussion of the HI-STAR 100 System is presented in Sections 1.1 and 1.2 of the FSAR with special attention to design and operating characteristics, unusual or novel design features, and principal safety features.

- Drawings for structures, systems, and components (SSCs) important to safety are presented in Section 1.5 of the FSAR.

- Specifications for the spent fuel to be stored in the HI-STAR 100 System are provided in FSAR Subsection 1.2.3. Additional details concerning these specifications are provided in Section 2.1 of the FSAR.

- The technical qualifications of the Holtec International to engage in the proposed activities are identified in Section 1.3 of the FSAR.

- The quality assurance program and implementing procedures are described in Chapter 13 of the FSAR.

- The HI-STAR 100 System SAR has been submitted, Docket No. 71-9261, to request certification of the HI-STAR 100 System under 10CFR71 for use in transportation.

1.7 REFERENCES

[1.0.1] 10CFR Part 72, *Licensing Requirements for the Independent Storage of Spent Nuclear Fuel and High-Level Radioactive Waste.*

[1.0.2] Regulatory Guide 3.61 (Task CE306-4) "Standard Format for a Topical Safety Analysis Report for a Spent Fuel Storage Cask", USNRC, February 1989.

[1.0.3] NUREG-1536, "Standard Review Plan for Dry Cask Storage Systems", U.S. Nuclear Regulatory Commission, January 1997.

[1.0.4] 10CFR Part 71, "Packaging and Transportation of Radioactive Materials", Title 10 of the Code of Federal Regulations, 1998 Edition, Office of the Federal Register, Washington, D.C.

[1.1.1] U.S. Department of Energy, "Multi-Purpose Canister (MPC) Subsystem Design Procurement Specification", Document No. DBG000000-01717-6300-00001, Rev. 5, January 11, 1996.

[1.1.2] U.S. Department of Energy, "MPC Transportation Cask Subsystem Design Procurement Specification", Document No. DBF 000000-01717-6300-00001, Rev. 5, January 11, 1996.

[1.2.1] U.S. NRC Information Notice 96-34, "Hydrogen Gas Ignition During Closure Welding of a VSC-24 Multi-Assembly Scale Basket".

[1.2.2] *Directory of Nuclear Reactors, Vol. II, Research, Test & Experimental Reactors*, International Atomic Energy Agency, Vienna, 1959.

[1.2.3] V.L. McKinney and T. Rockwell III, Boral: A New Thermal-Neutron Shield, USAEC Report AECD-3625, August 29, 1949.

[1.2.4] *Reactor Shielding Design Manual*, USAEC Report TID-7004, March 1956.

[1.2.5] "Safety Analysis Report for the NAC Storable Transport Cask", Revision 8, August 1994, Nuclear Assurance Corporation (USNRC Docket No. 71-9235).

[1.2.6] HI-STAR 100 Safety Analysis Report, Holtec Report No. HI-951251, Current Revision.

APPENDIX 1.A: ALLOY X DESCRIPTION

1.A ALLOY X DESCRIPTION

1.A.1 Alloy X Introduction

Alloy X is used within this licensing application to designate a group of stainless steel alloys. Alloy X can be any one of the following alloys:

- Type 316
- Type 316LN
- Type 304
- Type 304LN

Qualification of structures made of Alloy X is accomplished by using the least favorable mechanical and thermal properties of the entire group for all MPC mechanical, structural, neutronic, radiological, and thermal conditions. The Alloy X approach is conservative because no matter which material is ultimately utilized, the Alloy X approach guarantees that the performance of the MPC will meet or exceed the analytical predictions.

This appendix defines the least favorable material properties of Alloy X.

1.A.2 Alloy X Common Material Properties

Several material properties do not vary significantly from one Alloy X constituent to the next. These common material properties are as follows:

- density
- specific heat
- Young's Modulus (Modulus of Elasticity)
- Poisson's Ratio

The values utilized for this licensing application are provided in their appropriate chapters.

1.A.3 Alloy X Least Favorable Material Properties

The following material properties vary between the Alloy X constituents:

- Design Stress Intensity (S_m)
- Tensile (Ultimate) Strength (S_u)
- Yield Strength (S_y)
- Coefficient of Thermal Expansion (α)
- Coefficient of Thermal Conductivity (k)

Each of these material properties are provided in the ASME Code Section II [1.A.1]. Tables 1.A.1 through 1.A.5 provide the ASME Code values for each constituent of Alloy X along with the least favorable value utilized in this licensing application. The ASME Code only provides values to -20°F. The design temperature of the MPC is -40 °F to 725 °F as stated in Table 1.2.2. Most of the above-mentioned properties become increasingly favorable as the temperature drops. Conservatively, the values at the lowest design temperature for the HI-STAR 100 System have been assumed to be equal to the lowest value stated in the ASME Code. The lone exception is the thermal conductivity. The thermal conductivity decreases with the decreasing temperature. The thermal conductivity value for -40 °F is linearly extrapolated from the 70 °F value using the difference from 70 °F to 100 °F.

The Alloy X material properties are the minimum values of the group for the design stress intensity, tensile strength, yield strength, and coefficient of thermal conductivity. Using minimum values of design stress intensity is conservative because lower design stress intensities lead to lower allowables that are based on design stress intensity. Similarly, using minimum values of tensile strength and yield strength is conservative because lower values of tensile strength and yield strength lead to lower allowables that are based on tensile strength and yield strength. When compared to calculated values, these lower allowables result in factors of safety that are conservative for any of the constituent materials of Alloy X. Further discussion of the justification for using the minimum values of coefficient of thermal conductivity is given in Chapter 4. The maximum and minimum values are used for the coefficient of thermal expansion of Alloy X. The maximum and minimum coefficients of thermal expansion are used as appropriate in this submittal. Figures 1.A.1-1.A.5 provide a graphical representation of the varying material properties with temperature for the Alloy X materials.

1.A.4 References

[1.A.1] ASME Boiler & Pressure Vessel Code Section II, 1995 ed. with Addenda.

Table 1.A.1

ALLOY X AND CONSTITUENT DESIGN STRESS INTENSITY (S_m) vs. TEMPERATURE

Temp. (°F)	Type 304	Type 304LN	Type 316	Type 316LN	Alloy X (minimum of constituent values)
-40	20.0	20.0	20.0	20.0	20.0
100	20.0	20.0	20.0	20.0	20.0
200	20.0	20.0	20.0	20.0	20.0
300	20.0	20.0	20.0	20.0	20.0
400	18.7	18.7	19.3	18.9	18.7
500	17.5	17.5	18.0	17.5	17.5
600	16.4	16.4	17.0	16.5	16.4
650	16.2	16.2	16.7	16.0	16.0
700	16.0	16.0	16.3	15.6	15.6
750	15.6	15.6	16.1	15.2	15.2
800	15.2	15.2	15.9	14.9	14.9

Notes:

1. Source: Table 2A on pages 314, 318, 326, and 330 of [1.A.1].

2. Units of design stress intensity values are ksi.

Table 1.A.2

ALLOY X AND CONSTITUENT TENSILE STRENGTH (S_u) vs. TEMPERATURE

Temp. (°F)	Type 304	Type 304LN	Type 316	Type 316LN	Alloy X (minimum of constituent values)
-40	75.0 (70.0)	75.0 (70.0)	75.0 (70.0)	75.0 (70.0)	75.0 (70.0)
100	75.0 (70.0)	75.0 (70.0)	75.0 (70.0)	75.0 (70.0)	75.0 (70.0)
200	71.0 (66.2)	71.0 (66.2)	75.0 (70.0)	75.0 (70.0)	71.0 (66.2)
300	66.0 (61.5)	66.0 (61.5)	73.4 (68.5)	70.9 (66.0)	66.0 (61.5)
400	64.4 (60.0)	64.4 (60.0)	71.8 (67.0)	67.1 (62.6)	64.4 (60.0)
500	63.5 (59.3)	63.5 (59.3)	71.8 (67.0)	64.6 (60.3)	63.5 (59.3)
600	63.5 (59.3)	63.5 (59.3)	71.8 (67.0)	63.1 (58.9)	63.1 (58.9)
650	63.5 (59.3)	63.5 (59.3)	71.8 (67.0)	62.8 (58.6)	62.8 (58.6)
700	63.5 (59.3)	63.5 (59.3)	71.8 (67.0)	62.5 (58.4)	62.5 (58.4)
750	63.1 (58.9)	63.1 (58.9)	71.4 (66.5)	62.2 (58.1)	62.2 (58.1)
800	62.7 (58.5)	62.7 (58.5)	70.9 (66.2)	61.7 (57.6)	61.7 (57.6)

Notes:

1. Source: Table U on pages 437, 439, 441, and 443 of [1.A.1].

2. Units of tensile strength are ksi.

3. The ultimate stress of Alloy X is dependent on the product form of the material (i.e., forging vs. plate). Values in parentheses are based on SA-336 forged materials (type F304, F304LN, F316, and F316LN), which are used solely for the one-piece construction MPC lids. All other values correspond to SA-240 plate material.

Table 1.A.3

ALLOY X AND CONSTITUENT YIELD STRESSES (S_y) vs. TEMPERATURE

Temp. (°F)	Type 304	Type 304LN	Type 316	Type 316LN	Alloy X (minimum of constituent values)
-40	30.0	30.0	30.0	30.0	30.0
100	30.0	30.0	30.0	30.0	30.0
200	25.0	25.0	25.8	25.5	25.0
300	22.5	22.5	23.3	22.9	22.5
400	20.7	20.7	21.4	21.0	20.7
500	19.4	19.4	19.9	19.4	19.4
600	18.2	18.2	18.8	18.3	18.2
650	17.9	17.9	18.5	17.8	17.8
700	17.7	17.7	18.1	17.3	17.3
750	17.3	17.3	17.8	16.9	16.9
800	16.8	16.8	17.6	16.6	16.6

Notes:

1. Source: Table Y-1 on pages 518, 519, 522, 523, 530, 531, 534, and 535 of [1.A.1].

2. Units of yield stress are ksi.

Table 1.A.4

ALLOY X AND CONSTITUENT COEFFICIENT OF THERMAL EXPANSION
vs. TEMPERATURE

Temp. (^{o}F)	Type 304 and Type 304LN	Type 316 and Type 316LN	Alloy X Maximum	Alloy X Minimum
-40	8.55	8.54	8.55	8.54
100	8.55	8.54	8.55	8.54
150	8.67	8.64	8.67	8.64
200	8.79	8.76	8.79	8.76
250	8.90	8.88	8.90	8.88
300	9.00	8.97	9.00	8.97
350	9.10	9.11	9.11	9.10
400	9.19	9.21	9.21	9.19
450	9.28	9.32	9.32	9.28
500	9.37	9.42	9.42	9.37
550	9.45	9.50	9.50	9.45
600	9.53	9.60	9.60	9.53
650	9.61	9.69	9.69	9.61
700	9.69	9.76	9.76	9.69
750	9.76	9.81	9.81	9.76
800	9.82	9.90	9.90	9.82

Notes:

1. Source: Table TE-1 on pages 590 and 591 of [1.A.1].
2. Units of coefficient of thermal expansion are in./in.- ^{o}F x 10^{-6}.

Table 1.A.5
ALLOY X AND CONSTITUENT THERMAL CONDUCTIVITY vs. TEMPERATURE

Temp. (°F)	Type 304 and Type 304LN	Type 316 and Type 316LN	Alloy X (minimum of constituent values)
-40	8.23	6.96	6.96
70	8.6	7.7	7.7
100	8.7	7.9	7.9
150	9.0	8.2	8.2
200	9.3	8.4	8.4
250	9.6	8.7	8.7
300	9.8	9.0	9.0
350	10.1	9.2	9.2
400	10.4	9.5	9.5
450	10.6	9.8	9.8
500	10.9	10.0	10.0
550	11.1	10.3	10.3
600	11.3	10.5	10.5
650	11.6	10.7	10.7
700	11.8	11.0	11.0
750	12.0	11.2	11.2
800	12.2	11.5	11.5

Notes:

1. Source: Table TCD on page 606 of [1.A.1].
2. Units of thermal conductivity are Btu/hr-ft-°F.

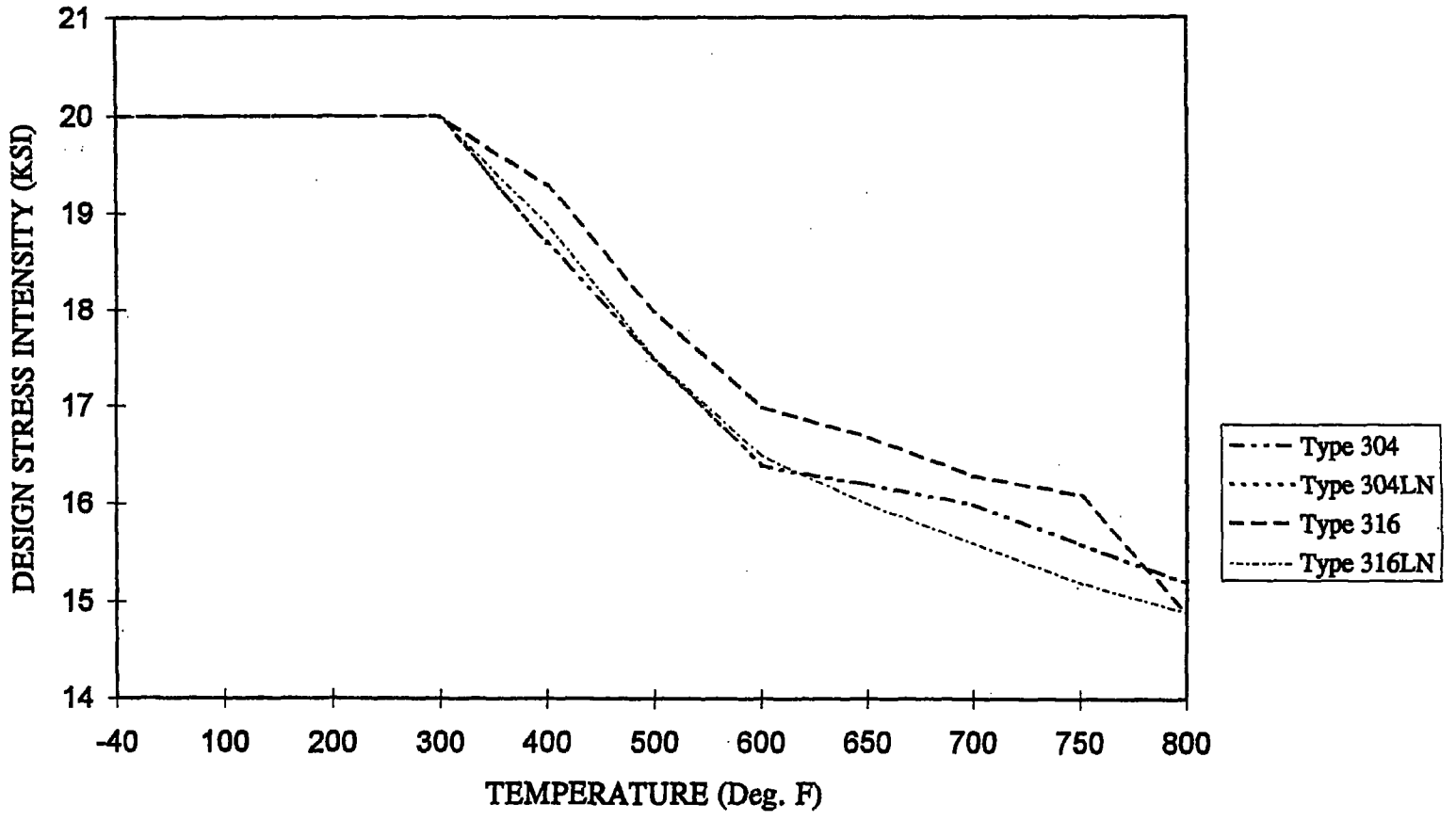

SOURCE: TABLE 1.A.1

FIGURE 1.A.1; DESIGN STRESS INTENSITY VS. TEMPERATURE

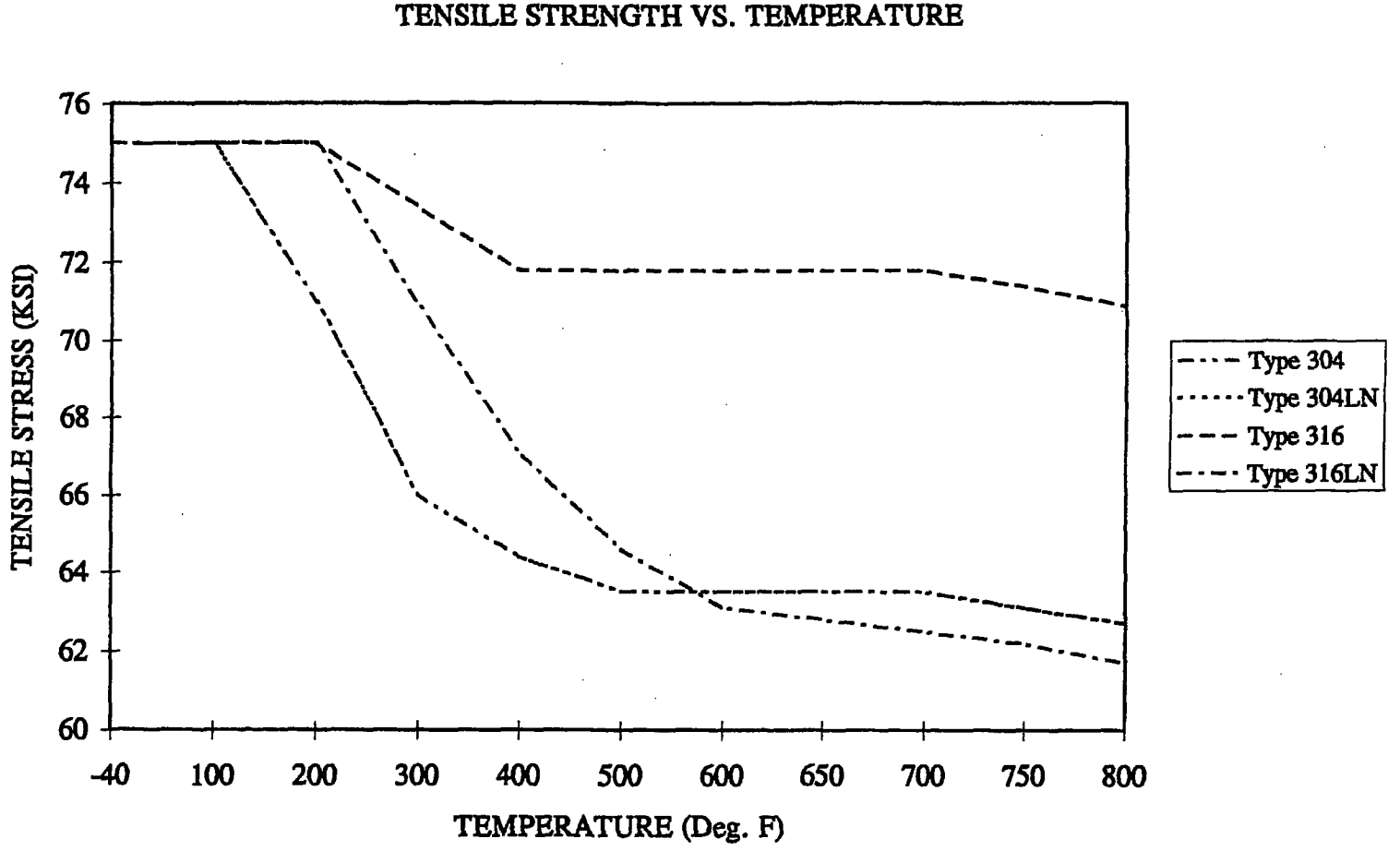

SOURCE: TABLE 1.A.2

FIGURE 1.A.2; TENSILE STRENGTH VS. TEMPERATURE

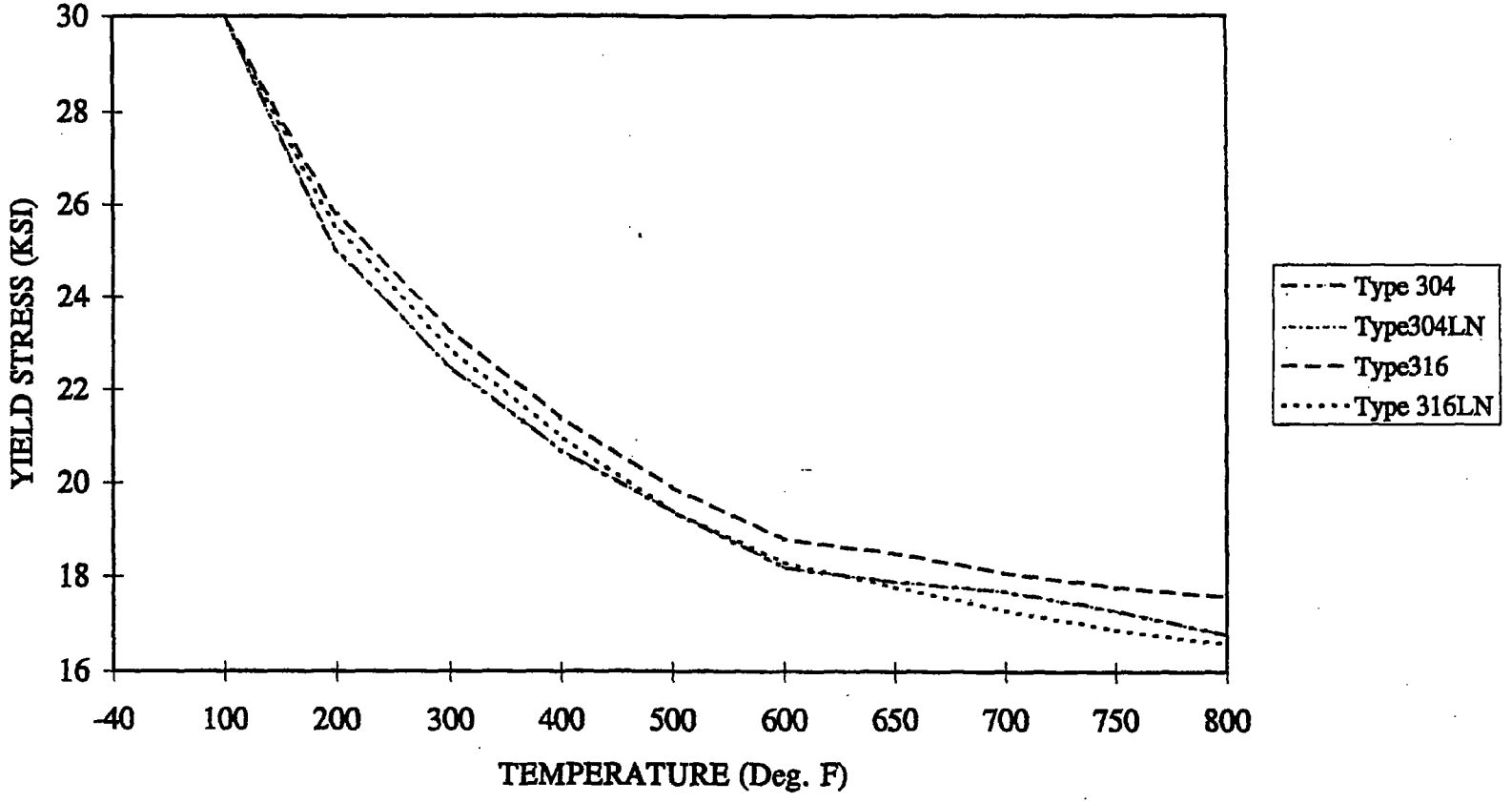

SOURCE: TABLE 1.A.3

FIGURE 1.A.3; YIELD STRESS VS. TEMPERATURE

SOURCE: TABLE 1.A.4 FIGURE 1.A.4; COEFFICIENT OF THERMAL EXPANSION VS. TEMPERATURE

REPORT HI-2012610

REVISION 0

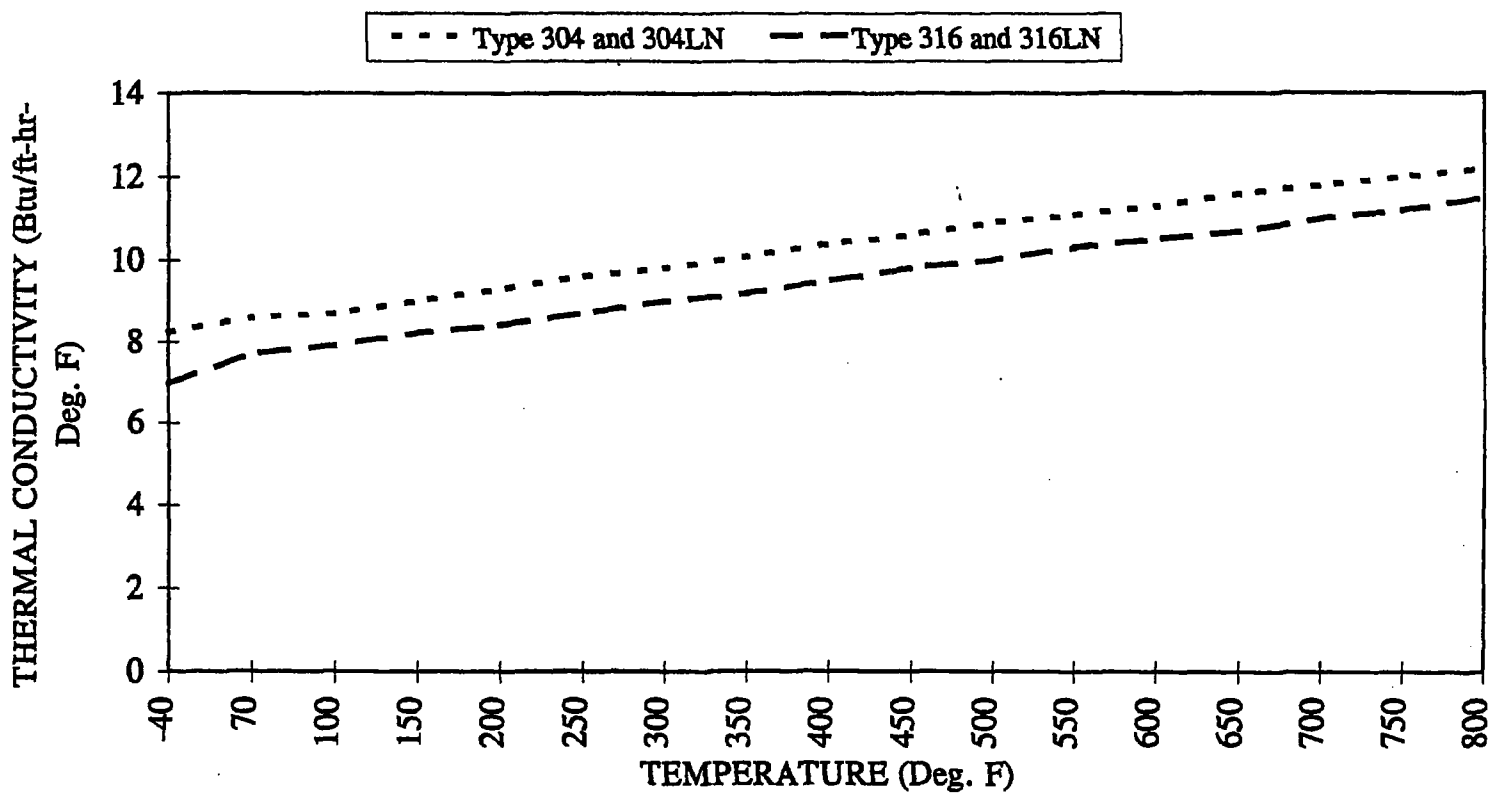

SOURCE: TABLE 1.A.5

FIGURE 1.A.5; THERMAL CONDUCTIVITY VS. TEMPERATURE

APPENDIX 1.B: HOLTITE-A ™ MATERIAL DATA
(Total of 4 Pages Including This Page)

The information provided in this appendix describes the neutron absorber material, Holtite-A for the purpose of confirming its suitability for use as a neutron shield material in spent fuel storage casks. Holtite-A is one of the family of Holtite neutron shield materials denoted by the generic name Holtite™. It is currently the only neutron shield material approved for installation in the HI-STAR 100 cask. It is chemically identical to NS-4-FR which was originally developed by Bisco Inc. and used for many years as a shield material with B_4C or Pb added.

Holtite-A contains aluminum hydroxide ($Al(OH)_3$) in an epoxy resin binder. Aluminum hydroxide is also known by the industrial trade name of aluminum tri-hydrate or ATH. ATH is often used commercially as a fire-retardant. Holtite-A contains approximately 62% ATH supported in a typical 2-part epoxy resin as a binder. Holtite-A contains 1% (nominal) by weight B_4C, a chemically inert material added to enhance the neutron absorption property. Pertinent properties of Holtite-A are listed in Table 1.B.1.

The essential properties of Holtite-A are:

1. the hydrogen density (needed to thermalize neutrons),
2. thermal stability of the hydrogen density, and
3. the uniformity in distribution of B_4C needed to absorb the thermalized neutrons.

ATH and the resin binder contain nearly the same hydrogen density so that the hydrogen density of the mixture is not sensitive to the proportion of ATH and resin in the Holtite-A mixture. B_4C is added as a finely divided powder and does not settle out during the resin curing process. Once the resin is cured (polymerized), the ATH and B_4C are physically retained in the hardened resin. Qualification testing for B_4C throughout a column of Holtite-A has confirmed that the B_4C is uniformly distributed with no evidence of settling or non-uniformity. Furthermore, an excess of B_4C is specified in the Holtite-A mixing and pouring procedure as a precaution to assure that the B_4C concentration is always adequate throughout the mixture.

The specific gravity specified in Table 1.B.1 does not include an allowance for weight loss. The specific gravity assumed in the shielding analysis includes a 4% reduction to conservatively account for potential weight loss at the design temperature of 300°F or an inability to reach theoretical density. Tests on the stability of Holtite-A were performed by Holtec International. The results of the tests are summarized in Holtec Reports HI-2002396, "Holtite-A Development History and Thermal Performance Data" and HI-2002420, "Results of Pre- and Post-Irradiation Test Measurements." The information provided in these reports demonstrates that Holtite-A™ possesses the necessary thermal and radiation stability characteristics to function as a reliable shielding material in the HI-STAR 100 overpack.

The Holtite-A is encapsulated in the HI-STAR 100 overpack and, therefore, should experience a very small weight reduction during the design life of the HI-STAR 100 System.

The data and test results confirm that Holtite-A remains stable under design thermal and radiation conditions, the material properties meet or exceed that assumed in the shielding analysis, and the B_4C remains uniformly distributed with no evidence of settling or non-uniformity.

Based on the information described above, Holtite-A meets all of the requirements for an acceptable neutron shield material.

Table 1.B.1

REFERENCE PROPERTIES OF HOLTITE-A NEUTRON SHIELD MATERIAL

PHYSICAL PROPERTIES	
% ATH	62 nominal
Specific Gravity	1.68 g/cc nominal
Max. Continuous Operating Temperature	300°F
Hydrogen Density	0.096 g/cc minimum
Radiation Resistance	Excellent
CHEMICAL PROPERTIES (Nominal)	
wt% Aluminum	21.5
wt% Hydrogen	6.0
wt% Carbon	27.7
wt% Oxygen	42.8
wt% Nitrogen	2.0
wt% B_4C	1.0

PAGES 1.B-4 THROUGH 1.B-20 INTENTIONALLY DELETED

APPENDIX 1.C: MISCELLANEOUS MATERIAL DATA
(Total of 8 Pages Including This Page)

The information provided in this appendix specifies the thermal expansion foam (silicone sponge), paint, and anti-seize lubricant properties and demonstrates their suitability for use in spent nuclear fuel storage casks. The following is a listing of the information provided.

- HT-800 Series, Silicone Sponge, Bisco Products Technical Data Sheet
- Thermaline 450, Carboline, Product Data Sheet and Application Instructions
- Carboline 890, Carboline, Product Data Sheet and Application Instructions
- FEL-PRO Technical Bulletin, N-5000 Nickel Based-Nuclear Grade Anti-Seize Lubricant

HT-870 silicone sponge is specified as a thermal expansion foam to be placed in the overpack outer enclosure with the neutron shield. Due to differing thermal expansion of the neutron shield and outer enclosure carbon steel, the silicone sponge is provided to compress and allow the neutron shield material to expand. The compression-deflection physical properties are provided for the silicone sponge.

Silicone has a long and proven history in the nuclear industry. Silicone is highly resistant to degradation as a result of radiation at the levels required for the HI-STAR 100 System. Silicone is inherently inert and stable and will not react with the metal surfaces or neutron shield material. Additionally, typical operating temperatures for silicone sponges range from -50°F to 400°F.

Thermaline 450 is specified to coat the inner cavity of the overpack and Carboline 890 is specified to coat the external surfaces of the overpack. As can be seen from the product data sheets, the paints are suitable for the design temperatures (see Table 2.2.3) and chemical environment.

Nuclear grade anti-seize lubricant, N-5000, from FEL-PRO is specified as the lubricant for the overpack closure bolts. The lubricant is formulated to have the lowest practical levels of halogens, sulfur, and heavy metals.

HT-800 SERIES

Specification Grade
Silicone Sponge

PHYSICAL PROPERTIES

PROPERTY	SPECIFICATION			TEST METHOD
	HT-870 (Soft)	HT-800 (Medium)	HT-820 (Firm)	
Density	12 - 24 pcf	16 - 28 pcf	20 - 32 pcf	ASTM D-3574
Compression Force @ 25% Deflection	2 - 7 psi	6 - 14 psi	12 - 20 psi	ASTM D-1056
Compression Set (Maximum)	10%	10%	10%	ASTM D-1056 (Compressed 50%for 22 hrs. @ 100°C)
Water Absorption (Maximum)	10%	5%	5%	ASTM D-1056

Available Industry Specifications: **AMS-3195 (HT-800)**
AMS-3196 (HT-820)
UL-94 (Limited to specific classes, densities, thicknesses and colors)

Data is based on laboratory tests and should not be used for writing specifications. Each user should run independent tests to confirm material suitability for each specific application.

Bisco Products and Dow Corning neither represent nor use this material for medical device applications or for pharmaceutical end-use.

2300 East Devon Avenue • Elk Grove Village, Illinois 60007-6120 • Toll Free 800/237-2068

carboline®

THERMALINE 450

VOC PLUS

SELECTION DATA

GENERIC TYPE: A glass flake filled, phenolic modified, amine cured epoxy novalac.

GENERAL PROPERTIES: A dense cross-linked polymer which exhibits outstanding barrier protection against a variety of chemical exposures. Excellent resistance to wet/dry cycling conditions at elevated temperatures. Designed to coat the exterior of insulated piping. It is also suitable for coating non-insulated piping and equipment exposed to chemical attack. The glass flakes help provide excellent abrasion resistance, permeation resistance and internal reinforcement.

- Temperature resistance to 450°F
- Excellent abrasion resistance
- Excellent overall chemical resistance
- Excellent thermal shock resistance

RECOMMENDED USES: Typically used as a one coat system to coat pipes and tanks that will be insulated. May also be used to coat non-insulated pipe, structural steel, equipment or concrete that may be subjected to severe chemical attack, abrasion or other abuse typical of a chemical plant environment.

TYPICAL CHEMICAL RESISTANCE:

Exposure	Splash & Spillage	Fumes
Acids	Excellent	Excellent
Alkalies	Excellent	Excellent
Solvents	Excellent	Excellent
Salt	Excellent	Excellent
Water	Excellent	Excellent

TEMPERATURE RESISTANCE (Under insulation):
Continuous: 425°F (218°C)
Excursions to: 450°F (232°C)

At 200°F (93°C) coating discoloration may be observed without loss of film integrity.

SUBSTRATES: Apply over properly prepared steel.

COMPATIBLE COATINGS: Normally applied directly to substrate. May be applied over epoxies and phenolics as recommended. May be topcoated with epoxies, polyurethanes or other finish coats as recommended.

July 96 Replaces September 95

SPECIFICATION DATA

0928

THEORETICAL SOLIDS CONTENT OF MIXED MATERIAL:

	By Volume
THERMALINE 450	70 ± 2%

VOLATILE ORGANIC CONTENT (VOC):
The following are nominal values:
As supplied: 2.13 lbs./gal. (255 gm./liter).

Thinner	Fluid Ounces/Gal.	Pounds/ Gallon	Grams/ Liter
213	13	2.56	307

RECOMMENDED DRY FILM THICKNESS:
8-10 mils (200-250 microns) to be achieved in 1 or 2 coats.

THEORETICAL COVERAGE PER MIXED GALLON:*
1,117 mil sq. ft. (27.9 sq.m/l at 25 microns)
139 sq. ft at 8 mils (3.5 sq. m/l at 200 microns)
111 sq. ft at 10 mils (2.8 sq.m/l at 250 microns)

*Mixing and application losses will vary and must be taken into consideration when estimating job requirements.

STORAGE CONDITIONS: Store indoors.
Temperature: 40-110°F (4-43°C) Humidity: 0-90%

SHELF LIFE: 24 months when stored indoors at 75°F (24°C)

COLOR: Red (0500) and Gray (5742)

GLOSS: Low (Epoxies lose gloss, discolor and eventually chalk in sunlight exposure.)

ORDERING INFORMATION

Prices may be obtained from your Carboline Sales Representative or Carboline Customer Service Department.

APPROXIMATE SHIPPING WEIGHT:

	1's	5's
THERMALINE 450	12 lbs. (5.5 kg)	58 lbs. (26.3 kg)
Thinner 213	8.4 lbs. (3.8 kg)	41 lbs. (18.6 kg)

FLASH POINT: (Setaflash)

THERMALINE 450 Part A:	53°F	(12°C)
THERMALINE 450 Part B:	>200°F	(>93°C)
Thinner 213	22°F	(-6°C)

APPLICATION INSTRUCTIONS

THERMALINE 450

These instructions are not intended to show product recommendations for specific service. They are issued as an aid in determining correct surface preparation, mixing instructions and application procedure. It is assumed that the proper product recommendations have been made. These instructions should be followed closely to obtain the maximum service from the materials.

0928

SURFACE PREPARATION: Remove all oil or grease from surface to be coated with Thinner 2 or Surface Cleaner 3 (refer to Surface Cleaner 3 instructions) in accordance with SSPC-SP 1.

STEEL:

Not Insulated: Abrasive blast to a Commercial Finish in accordance with SSPC-SP 6 and obtain a 2-3 mil (50-75 micron) blast profile.

Under Insulation: Abrasive blast to a Near White Finish in accordance with SSPC-SP 10 and obtain a 2-3 (50-75 micron) blast profile.

MIXING: Power mix each component separately, then combine and power mix in the following proportions.

Allow 30 minutes induction time at 75°F (24°C) prior to use.

	1 Gal. Kit	5 Gal. Kit
THERMALINE 450 Part A:	0.8 gals.	4.0 gals.
THERMALINE 450 Part B:	0.2 gals.	1.0 gals.

THINNING: May be thinned up to 13 oz/gal with Thinner 213.

Use of thinners other than those supplied or approved by Carboline may adversely affect product performance and void product warranty, whether express or implied.

POT LIFE: Three hours at 75°F (24°C) and less at higher temperatures. Pot life ends when coating loses body and begins to sag.

APPLICATION CONDITIONS:

	Material	Surfaces	Ambient	Humidity
Normal	65-85°F (18-29°C)	65-85°F (18-29°C)	65-85°F (18-29°C)	30-60%
Minimum	55°F (13°C)	50°F (10°C)	50°F (10°C)	0%
Maximum	90°F (32°C)	110°F (43°C)	100°F (38°C)	85%

Do not apply when the surface temperature is less than 5°F or 3°C above the dew point.

Special thinning and application techniques may be required above or below normal conditions.

SPRAY: The following spray equipment has been found suitable and is available from manufacturers such as Binks, DeVilbiss and Graco.

Conventional: Pressure pot equipped with dual regulators, 1/2" I.D. minimum material hose, .110" I.D. fluid tip and appropriate air cap.

July 96 Replaces September 95

Airless:

Pump Ratio:	30:1 (min)*
GPM Output:	3.0 (min)
Material Hose:	1/2" I.D. (min)
Tip Size:	.035"-.041"
Output psi:	2200-2500

*Teflon packings are recommended and are available from the pump manufacturer.

BRUSH: For striping of welds, touch-up of small areas only. Use a natural bristle brush, applying full strokes. Avoid rebrushing.

ROLLER: Not recommended.

DRYING TIMES: These times are based on a dry film thickness of 10 mils (250 microns). Higher film thickness, insufficient ventilation or cooler temperatures will require longer cure times and could result in solvent entrapment and premature failure.

Surface Temperature	Dry To Handle	Dry to Topcoat	Final Cure
50°F (10°C)	18 hours	48 hours	21 days
60°F (16°C)	12 hours	32 hours	14 days
75°F (24°C)	6 hours	16 hours	7 days
90°F (32°C)	3 hours	8 hours	4 days

If the final cure time has been exceeded, the surface must be abraded by sweep blasting prior to the application of any additional coats.

EXCESSIVE HUMIDITY OR CONDENSATION ON THE SURFACE DURING CURING MAY RESULT IN A SURFACE HAZE OR BLUSH; ANY HAZE OR BLUSH MUST BE REMOVED BY WATER WASHING BEFORE RECOATING.

VENTILATION & SAFETY: WARNING: VAPORS MAY CAUSE EXPLOSION. When used in enclosed areas, thorough air circulation must be used during and after application until the coating is cured. The ventilation system should be capable of preventing the solvent vapor concentration from reaching the lower explosion limit for the solvents used. In addition to insuring proper ventilation, fresh air respirators or fresh air hoods must be used by all application personnel. Where flammable solvents exist, explosion-proof lighting must be used. Hypersensitive persons should wear clean, protective clothing, gloves and/or protective cream on face, hands and all exposed areas.

CLEANUP: Use Thinner 2.

CAUTION: READ AND FOLLOW ALL CAUTION STATEMENTS ON THIS PRODUCT DATA SHEET AND ON THE MATERIAL SAFETY DATA SHEET FOR THIS PRODUCT.

CAUTION: CONTAINS FLAMMABLE SOLVENTS. KEEP AWAY FROM SPARKS AND OPEN FLAMES. WORKMEN IN CONFINED AREAS MUST WEAR FRESH AIRLINE RESPIRATORS. HYPERSENSITIVE PERSONS SHOULD WEAR GLOVES OR USE PROTECTIVE CREAM. ALL ELECTRICAL EQUIPMENT AND INSTALLATIONS SHOULD BE MADE IN ACCORDANCE WITH THE NATIONAL ELECTRICAL CODE. IN AREAS WHERE EXPLOSION HAZARDS EXIST, WORKMEN SHOULD BE REQUIRED TO USE NONFERROUS TOOLS AND TO WEAR CONDUCTIVE AND NONSPARKING SHOES.

carboline®

CARBOLINE® 890

VOC+ PLUS

SELECTION DATA

GENERIC TYPE: Cross-linked epoxy.

GENERAL PROPERTIES: CARBOLINE 890 is a self priming, high solids, high gloss, high build epoxy mastic. It can be applied by spray, brush, or roller over hand or power tool cleaned steel and is compatible with most existing coatings and tightly adhered rust. The cured film provides a tough, cleanable surface and is available in a wide variety of colors.

- Single coat corrosion protection.
- Excellent chemical resistance.
- Good flexibility and lower stress upon curing than most epoxy coatings.
- Excellent tolerance of damp (not wet) substrates.
- Very good abrasion resistance.
- Suitable replacement for Carbomastic 801.

RECOMMENDED USES: Recommended where a high performance, chemically resistant epoxy coating is desired. Offers outstanding protection for interior floors, walls, piping, equipment and structural steel or as an exterior coating for railcars, structural steel and equipment in various corrosive environments. Industrial environments include Chemical Processing, Offshore Oil and Gas, Food Processing, Pharmaceutical, Water and Waste Water Treatment, Pulp and Paper and Power Generation among others. May be used as a two coat system direct to metal or concrete for Water and Municipal Waste Water immersion. Acceptable for use in incidental food contact areas and as a lining for hopper cars carrying food grade plastic pellets when processed according to FDA criteria (ref: FDA 21 CFR 175.300). Consult Carboline Technical Service Department for other specific uses.

NOT RECOMMENDED FOR: Strong acid or solvent exposures, immersion service other than water, exterior weathering where color retention is desired, such as a finish for tank exteriors or over chlorinated rubber and latex coatings.

TYPICAL CHEMICAL RESISTANCE:

Exposure	Immersion	Splash & Spillage	Fumes
Acids	NR	Very Good	Very Good
Alkalies	NR	Excellent	Excellent
Solvents	NR	Very Good	Excellent
Salt Solutions	Excellent	Excellent	Excellent
Water	Excellent	Excellent	Excellent

TEMPERATURE RESISTANCE: (Non-Immersion)
Continuous: 250°F (121°C)
Non-continuous: 300°F (149°C)

At temperatures above 225°F, coating discoloration and loss of gloss can be observed, without loss of film integrity.

SUBSTRATES: Apply over suitably prepared metal, concrete, or other surfaces as recommended.

COMPATIBLE COATINGS: May be applied directly over inorganic zincs, weathered galvanizing, epoxies, phenolics or other coatings as recommended. A test patch is recommended before use over existing coatings. A mist coat of CARBOLINE 890 is required when applied over inorganic zincs to minimize bubbling. May be topcoated with polyurethanes or acrylics to upgrade weathering resistance. Not recommended over chlorinated rubber or latex coatings. Consult Carboline Technical Service Department for specific recommendations.

SPECIFICATION DATA

THEORETICAL SOLIDS CONTENT OF MIXED MATERIAL:*

	By Volume
CARBOLINE 890	75% ± 2%

VOLATILE ORGANIC CONTENT:*
As Supplied: 1.78 lbs./gal. (214 grams/liter)
Thinned:

Thinner	Fluid Ounces/Gal.	Pounds/ Gallon	Grams/ Liter
2	8	2.08	250
2	13	2.26	271
33	16	2.38	285

*Varies with color

RECOMMENDED DRY FILM THICKNESS PER COAT:
4-6 mils (100-150 microns).
6-8 mils (150-200 microns) DFT for a more uniform gloss over inorganic zincs, or for use over light rust.

In more severe environments a second coat of 4-6 mils (100-150 microns) is recommended.

Dry film thickness in excess of 10 mils (250 microns) per coat is not recommended. Excessive film thickness over inorganic zinc may increase damage during shipping or erection.

THEORETICAL COVERAGE PER MIXED GALLON:
1203 mil sq. ft. (30 sq. m/l at 25 microns)
241 sq. ft. at 5 mils (6.0 sq. m/l at 125 microns)

Mixing and application losses will vary and must be taken into consideration when estimating job requirements.

STORAGE CONDITIONS: Store Indoors
Temperature: 40-110°F (4-43°C) Humidity: 0-100%

SHELF LIFE: 36 months when stored at 75°F (24°C).

COLORS: Available in Carboline Color Chart colors. Some colors may require two coats for adequate hiding.

GLOSS: High gloss (Epoxies lose gloss, discolor and eventually chalk in sunlight exposure).

ORDERING INFORMATION

Prices may be obtained from your Carboline Sales Representative or Carboline Customer Service Department.

APPROXIMATE SHIPPING WEIGHT:

	2 Gal. Kit	10 Gal. Kit
CARBOLINE 890	29 lbs. (13 kg)	145 lbs. (66 kg)
	1's	5's
THINNER #2	8 lbs. (4 kg)	39 lbs. (18 kg)
THINNER #33	9 lbs. (4 kg)	45 lbs. (20 kg)

FLASH POINT: (Setaflash)

CARBOLINE 890 Part A	89°F (32°C)
CARBOLINE 890 Part B	71°F (22°C)
THINNER #2	24°F (-5°C)
THINNER #33	89°F (32°C)

0986

June 96 Replaces December 95

CARBOLINE® 890

These instructions are not intended to show product recommendations for specific service. They are issued as an aid in determining correct surface preparation, mixing instructions and application procedure. It is assumed that the proper product recommendations have been made. These instructions should be followed closely to obtain the maximum service from the materials.

0986

SURFACE PREPARATION: Remove all oil or grease from surface to be coated with Thinner #2 or Surface Cleaner #3 (refer to Surface Cleaner #3 instructions) in accordance with SSPC-SP 1.

Steel: For mild environments Hand Tool or Power Tool Clean in accordance with SSPC-SP 2, SSPC-SP 3 or SSPC-SP 11 to produce a rust-scale free surface.

For more severe environments, abrasive blast to a Commercial Finish in accordance with SSPC-SP 6 and obtain a 1½ - 3 mil (40-75 micron) blast profile.

For immersion service, abrasive blast to a Near White Metal Finish in accordance with SSPC-SP10 and obtain a 1½ - 3 mil (40-75 micron) blast profile.

Concrete: Must be cured at least 28 days at 70°F (21°C) and 50% R.H. or equivalent time. Remove fins and other protrusions by stoning, sanding or grinding. Abrasive blast to open all surface voids and remove all form oils, incompatible curing agents, hardeners, laitance and other foreign matter and produce a surface texture similar to that of a medium grit sandpaper. Voids in the concrete may require surfacing. Blow or vacuum off sand and dust.

MIXING: Power mix separately, then combine and power mix in the following proportions:

	2 Gal. Kit	10 Gal. Kit
CARBOLINE 890 Part A	1 gallon	5 gallons
CARBOLINE 890 Part B	1 gallon	5 gallons

THINNING: For spray applications, may be thinned up to 13 oz./gal. with Thinner #2. For hot and windy conditions, or for brush and roller application, may be thinned up to 16 oz./gal. with Thinner #33.

Use of thinners other than those supplied or approved by Carboline may adversely affect product performance and void product warranty, whether express or implied.

POT LIFE: Three hours at 75°F (24°C) and less at higher temperatures. Pot life ends when material loses film build.

APPLICATION CONDITIONS:

	Material	Surfaces	Ambient	Humidity
Normal	60-85°F (16-29°C)	60-85°F (16-29°C)	60-90°F (16-32°C)	0-80%
Minimum	50°F (10°C)	50°F (10°C)	50°F (10°C)	0%
Maximum	90°F (32°C)	125°F (52°C)	110°F (43°C)	90%

Do not apply or cure the material when the surface temperature is less than 5°F or 3°C above the dew point.

Special thinning and application techniques may be required above or below normal conditions.

SPRAY: This is a high solids coating and may require slight adjustments in spray techniques. Wet film thicknesses are easily and quickly achieved. The following spray equipment has been found suitable and is available from manufacturers such as Binks, DeVilbiss and Graco.

Conventional: Pressure pot equipped with dual regulators, 3/8" I.D. minimum material hose, .070" I.D. fluid tip and appropriate air cap.

June 96 Replaces December 95

Airless:

Pump Ratio:	30:1 (min.)*
GPM Output:	3.0 (min.)
Material Hose:	3/8" I.D. (min.)
Tip Size:	.017-.021"
Output psi:	2100-2300
Filter Size:	60 mesh

*Teflon packings are recommended and are available from the pump manufacturer.

BRUSH OR ROLLER: Use medium bristle brush, or good quality short nap roller. Avoid excessive rebrushing and rerolling. Two coats may be required to obtain desired appearance, hiding and recommended DFT. For best results, tie-in within 10 minutes at 75°F (24°C).

DRYING TIMES: These times are based on a 5 mils (125 microns) dry film thickness. Higher film thicknesses, insufficient ventilation or cooler temperatures will require longer cure times and could result in solvent entrapment and premature failure.

Dry to Touch 2 1/2 hours at 75°F (24°C)
Dry to Handle 6 1/2 hours at 75°F (24°C)

Surface Temperature	Recoating With Itself	Dry to Topcoat	Final Cure
50°F (10°C)	12 hours	24 hours	3 days
60°F (16°C)	8 hours	16 hours	2 days
75°F (24°C)	4 hours	8 hours	1 day
90°F (32°C)	2 hours	4 hours	16 hours

Excessive humidity or condensation on the surface during curing can interfere with the cure, can cause discoloration and may result in a surface haze or blush. Any haze or blush must be removed by water washing before recoating. During high humidity conditions, it is recommended that the application be done while temperatures are increasing. For best results over "damp" surfaces, apply by brush or roller.

Maximum Recoat or Topcoat Times at 75°F (24°C):

With Epoxies - 30 days
With Polyurethanes - 90 days

If the maximum recoat time has been exceeded, surface must be abraded by sweep blasting prior to the application of any additional coats.

Minimum cure time before immersion service is 5 days at 75°F (24°C) surface temperature. Cure at temperatures below 60°F (16°C) is not recommended for immersion service.

VENTILATION & SAFETY: WARNING: VAPORS MAY CAUSE EXPLOSION. When used as a tank lining or in enclosed areas, thorough air circulation must be used during and after application until the coating is cured. The ventilation system should be capable of preventing the solvent vapor concentration from reaching the lower explosion limit for the solvents used. In addition to ensuring proper ventilation, fresh air respirators or fresh air hoods must be used by all application personnel. Where flammable solvents exist, explosion-proof lighting must be used. Hypersensitive persons should wear clean, protective clothing, gloves and/or protective cream on face, hands and all exposed areas.

CLEANUP: Use Thinner # 2.

CAUTION: READ AND FOLLOW ALL CAUTION STATEMENTS ON THIS PRODUCT DATA SHEET AND ON THE MATERIAL SAFETY DATA SHEET FOR THIS PRODUCT.

CAUTION: CONTAINS FLAMMABLE SOLVENTS. KEEP AWAY FROM SPARKS AND OPEN FLAMES. IN CONFINED AREAS, WORKMEN MUST WEAR FRESH AIRLINE RESPIRATORS. HYPERSENSITIVE PERSONS SHOULD WEAR GLOVES OR USE PROTECTIVE CREAM. ALL ELECTRIC EQUIPMENT AND INSTALLATIONS SHOULD BE MADE AND GROUNDED IN ACCORDANCE WITH THE NATIONAL ELECTRICAL CODE. IN AREAS WHERE EXPLOSION HAZARDS EXIST, WORKMEN SHOULD BE REQUIRED TO USE NONFERROUS TOOLS AND TO WEAR CONDUCTIVE AND NONSPARKING SHOES.

FEL-PRO®
Technical Bulletin

N-5000 NICKEL BASED - NUCLEAR GRADE ANTI-SEIZE LUBRICANT

N-5000 is a nickel based nuclear grade anti-seize lubricant produced under 100% controlled conditions for highest purity and traceability. It is formulated to have the lowest practical levels of halogens, sulfur, and heavy metals, including copper. N-5000 has a general composition of nickel and graphite flake in petroleum carrier. All ingredients are selected for extreme purity. It meets or exceeds the following specifications, appendix A of NEDE-31295P, "BWR Operator's Manual for Materials and Processes", Westinghouse Material Specification 53701WQ, and 10CFR Ch1, Part 21, and Part 50, appendix B.

Special Features:

- High purity- made from highest purity ingredients.
- Traceability- each can marked.
- Free from copper- less than 50 ppm copper.
- Testing- each batch tested before packaging.
- Certifications- 3 copies with each case.

Recommended applications:

- Bolts, studs, valves, pipe fittings, slip fits and press fits in electric power generating plants, chemical plants, pharmaceutical plants, paper mills, and other locations where stainless steel fasteners are used.

Operational Benefits:

- Before assembly - certifications and traceability.
- During assembly - prevents high friction, galling,
- and seizing. Promotes uniform and predictable clamping.
- During operation - high purity prevents stress corrosion.
- Disassembly - prevents seizing, galling, destruction of threads.

Typical Physical Properties:

Composition	Nickel and Graphite in Petroleum Oil
Appearance	Silver-Gray paste
Specific gravity	1.2
Flash point (ASTM D 92-85)	424°F/218°C
Torque coefficient-K (Steel nuts and Bolts)	0.15
(Type 304 Stainless)	0.18
Maximum use temperature	1800°F/982°C

Quality Control Physical Properties:

Weight per gallon (ASTM D 1475-85)	Range 9.5 - 10.4
Penetration (ASTM D 217-88 unworked)	300 - 380

Purity:

Impurities - Elemental and Combined	Test Method Type	References ASTM OR (SM16)	Controlled Maximum	Average Values
Halogens: Chlorine, Bromine, Iodine	Parr Bomb, Turbidimetric	D808-87, C69979	50 ppm	18 ppm
Fluorine	Parr Bomb, Specific ION Electrode	D3761-84	200 ppm	7 ppm
Sulfur	Parr Bomb, Turbidimetric	D129-64, D1266-87	100 ppm	9 ppm
Lead	Wet Digestion, AAS	(302D), D3559-84	25 ppm	1ppm
Cadmium	Wet Digestion, AAS	(302D), D3557-84	2 ppm	0.2 ppm
Tin	Wet Digestion, AAS	(302D), E37-76	25 ppm	9 ppm
Zinc	Wet Digestion, AAS	(302D), D1691-84	25 ppm	1 ppm
Copper	Wet Digestion, AAS	(302D), D1688-84	50 ppm	12 ppm
Mercury	Wet Digestion, Cold Vapor AAS	(302D), D3223-80	2 ppm	0.04 ppm

Directions for use:

- Before or during assembly, wipe brush onto threads and other joint surfaces needing protection.
- Do not overuse, as excess will be pushed off.
- Use full strength, do not thin.

Packaging:

Part Number	Net Contents	Type Container	Units/Case	Shipping Wt/Case
51243	8 oz. (227 g)	Can-brush top	12	9 lb. (4. Kg.)
51245	8 lb. (3.6 kg)	Can	2	18 lb. (8. Kg.)
51246	2 lb. (908 g)	Can	12	29 lb. (13. Kg.)
51269	1 lb. (454 g)	Can-brush top	12	16 lb. (7. Kg.)
51346	1 oz. (28 g)	Tube	48	6 lb. (2.7 Kg.)

N-5000 has an unlimited shelf life when stored at room temperature in the original unopened container.

FOR INDUSTRIAL USE ONLY.
WASH THOROUGHLY AFTER HANDLING.
KEEP OUT OF REACH OF CHILDREN.
SEE MATERIAL SAFETY DATA For immediate answers to your technical questions, in the United States or Canada call the **Technical Support Line** at **1-800-992-9799.** International customers call (303) 289-5651, or fax (303) 289-5283

For a Material Safety Data Sheet or Technical Bulletin on this or any Fel-Pro product call our toll-free **FAX FOR THE INFO** line 24 hours a day, 7 days a week, in the United States or Canada call **800-583-3069.** International customers call (303) 289-5651, or fax (303) 289-5283.

Except as expressly stipulated, Fel-Pro's liability, expressed or implied, is limited to the stated selling price of any defective goods.

N-5000 8/97

FEL-PRO CHEMICAL PRODUCTS, L.P.

Fel-Pro
3412 W. Touhy Ave.
Lincolnwood, IL
60645 U.S.A.
847-568-2820
Fax 847-674-0019

Fel-Pro
6120 E. 58th Ave
Commerce City, CO
80022 U.S.A.
800-992-9799
Fax 303-289-5283

Fel-Pro of Canada, Ltd
6105 Kestrel Road
Mississauga, Ontario
L5T 1Y8 Canada
905-564-1530
Fax 905-564-1534

Fel-Pro Ltd.
4 Arkwright Way
North Newmoor, Irvine
KA11 4JU Scotland
44-1294-216094
Fax 44-1294-218157

Fel-Pro Chemical Products Latin America L.P.
Bodega No. 12, Zona Franca Palmaseca
Aeropuerto Internacional Bonilla Aragon
Cali, Colombia
57-2-651-1168
Fax 57-2-651-1179

Fel-Pro Chemical Products, Chile S.A.
Av. Pdte. Eduardo Frei M. 9231 Quilicura
Casilla (P.O. Box) 14325
Santiago, Chile
56-2-623-9216
Fax 56-2-623-2569

CHAPTER 2: PRINCIPAL DESIGN CRITERIA

This chapter contains a compilation of design criteria applicable to the HI-STAR 100 System. The loadings and conditions prescribed herein for the MPC, particularly those pertaining to mechanical accidents, are far more severe in most cases than those required for 10CFR72 compliance. The underlying reason for the more stringent design criteria selected in this submittal is the dual-purpose nature (storage and transport) of the HI-STAR 100 System and its concurrent application for 10CFR71 certification [2.0.1]. This chapter sets forth the loading conditions and relevant acceptance criteria; it does not provide results of any analyses. The analyses and results carried out to demonstrate compliance with the design criteria are presented in the subsequent chapters of this report.

This chapter is consistent with NUREG-1536, except for the exceptions and clarifications provided in Table 1.0.3. Table 1.0.3 provides the NUREG-1536 requirement, the justification for the exception or clarification, and the Holtec approach to meet the intent of the NUREG-1536 requirement.

2.0 PRINCIPAL DESIGN CRITERIA

The design criteria for the MPC and HI-STAR overpack are summarized in Tables 2.0.1 and 2.0.2, respectively, and described in the sections that follow.

2.0.1 MPC Design Criteria

General

The MPC is designed for 40 years of service, while satisfying the requirements of 10CFR72 [2.0.2]. The adequacy of the MPC design for the design life is discussed in Section 3.4.11.

Structural

The MPC is classified as important to safety. The MPC structural components include the internal fuel basket and the enclosure vessel. The fuel basket is designed and fabricated as a core support structure, in accordance with the applicable requirements of Section III, Subsection NG of the ASME Code [2.0.3], with certain NRC-approved alternatives, as discussed in Section 2.2.4. The enclosure vessel is designed and fabricated as a Class 1 component pressure vessel in accordance with Section III, Subsection NB of the ASME Code, to the maximum extent practicable, as discussed in Section 2.2.4. The principal exceptions are the MPC lid, vent and drain cover plates, and closure ring welds to the MPC lid and shell, as discussed in Section 2.2.4. In addition, the threaded holes in the MPC lid are designed in accordance with the requirements of ANSI N14.6 [2.0.4] for critical lifts to facilitate vertical MPC transfer.

The MPC closure welds are partial penetration welds that are structurally qualified by analysis, as presented in Chapter 3. The MPC lid and closure ring welds are inspected by performing a liquid penetrant examination of the root pass and final weld surface, in accordance with the drawings contained in Section 1.5. The integrity of the MPC lid weld is further verified by performing a

volumetric (or multi-layer liquid penetrant) examination, a hydrostatic pressure test and a helium leak test, in accordance with the Design Drawings and Technical Specification requirements.

The structural analysis of the MPC, in conjunction with the redundant closures and nondestructive examination, hydrostatic pressure testing, and helium leak testing performed during MPC fabrication and MPC closure, provides assurance of canister closure integrity in lieu of the specific weld joint requirements of the ASME Code, Section III, Subsection NB.

Compliance with the ASME Code as it is applied to the design and fabrication of the MPC, and the associated justification, are discussed in Section 2.2.4. Compliance with the ASME Code is fully consistent with that used by other canister-based dry storage systems previously approved by the NRC.

The MPC is designed for all design basis normal, off-normal, and postulated accident conditions, as defined in Section 2.2. These design loadings include the postulated drop accidents while in the cavity of the HI-STAR overpack. The load combinations for which the MPC is designed are defined in Section 2.2.7. In addition, the maximum allowable weight and dimensions of a fuel assembly to be stored in the MPC are limited in accordance with Section 2.1.4.

Thermal

The allowable fuel cladding temperatures imposed to prevent cladding degradation during long-term dry storage conditions for the MPC are based on the PNL Report [2.0.5], and LLNL Report [2.0.6]. The allowable cladding temperatures which correspond to varying cooling times for the SNF to be stored in the MPCs are provided in Table 2.2.3.

The short-term allowable cladding temperature that is applicable to off-normal and accident conditions of storage, as well as the fuel loading, canister closure, and transfer operations, is 570°C (1058°F) based on PNL-4835 [2.0.7]. Further, the MPC is backfilled with 99.995% pure helium at a pressure specified in Chapter 12 during canister sealing operations to promote heat transfer and prevent cladding degradation.

The design temperatures for the structural steel components of the MPC are based on the temperature limits provided in ASME Section II, Part D, tables referenced in ASME Section III, Subsection NB and NG, for those load conditions under which material properties are relied on for a structural load combination. The specific design temperatures for the components of the MPC are provided in Table 2.2.3.

The MPCs are designed for a bounding thermal source term, as described in Section 2.1.5. The maximum allowable fuel assembly heat load for each MPC is limited in accordance with the Technical Specifications.

Shielding

The allowable doses for an ISFSI using the HI-STAR 100 System are delineated in 10CFR72.104 and 72.106. Compliance with this criteria is necessarily site-specific and is to be demonstrated by the licensee, as discussed in Chapters 5 and 10.

The MPC provides axial gamma shielding at the top and bottom ends to maintain occupational exposures ALARA during canister closure and handling operations. The maximum allowable top axial dose rates for the MPC are controlled in accordance with plant-specific procedures and ALARA requirements (discussed in Chapter 10).

The MPCs are designed for the design basis fuel at the maximum burnup and minimum cooling times, as described in Sections 2.1.6 and 5.2. The radiological source term for the MPCs are limited based on the burnup and cooling times specified in the Technical Specifications. Calculated dose rates for each MPC are provided in Section 5.1. These dose rates are used to perform an occupational exposure evaluation in accordance with 10CFR20, as discussed in Chapter 10.

Criticality

The MPCs provide criticality control for all design basis normal, off-normal, and postulated accident conditions, as discussed in Section 6.1. The effective neutron multiplication factor is limited to $k_{eff} < 0.95$ for fresh unirradiated intact and damaged fuel assemblies with optimum unborated water moderation and close reflection, including all biases, uncertainties, and MPC manufacturing tolerances.

Criticality control is maintained by the geometric spacing of the fuel assemblies and fixed borated neutron absorbing materials incorporated into the fuel basket assembly. The minimum specified boron concentration verified during Boral manufacture is further reduced by 25% for criticality analysis. No credit is taken for burnup. The maximum allowable initial enrichment for fuel assemblies to be stored in each MPC are limited in accordance with the Technical Specifications.

Confinement

The MPC provides for confinement of all radioactive materials for all design basis normal, off-normal, and postulated accident conditions, as discussed in Section 7.1. A non-mechanistic postulated breach of the canister release of available fission products in accordance with specified release fractions is considered, as discussed in Section 7.3. The confinement function of the MPC is verified through hydrostatic testing, helium leak testing and weld examinations performed in accordance with the acceptance test program in Chapter 9 and the Technical Specifications.

Operations

There are no radioactive effluents that result from storage or transfer operations. Effluents generated during MPC loading and closure operations are handled by the plant's radwaste system and procedures under the licensee's 10CFR50 license.

Generic operating procedures for the HI-STAR 100 System are provided in Chapter 8. Detailed operating procedures will be developed by the licensee based on site-specific requirements that comply with the 10CFR50 Technical Specifications for the plant and the 10CFR72 Technical Specifications for the HI-STAR 100 System.

Acceptance Tests and Maintenance

The fabrication acceptance basis and maintenance program to be applied to the MPCs are described in Chapter 9. The operational controls and limits to be applied to the MPCs are contained in the Technical Specifications. Application of these requirements will assure that the MPC is fabricated, operated, and maintained in a manner that satisfies the design criteria defined in this chapter.

Decommissioning

The MPCs are designed to be transportable in the HI-STAR 100 overpack and are not required to be unloaded prior to shipment off-site. Decommissioning of the HI-STAR 100 System is addressed in Section 2.4.

2.0.2 HI-STAR Overpack

General

The HI-STAR overpack is designed for 40 years of service, while satisfying the requirements of 10CFR72. The adequacy of the overpack design for the design life is discussed in Section 3.4.10.

Structural

The HI-STAR overpack is classified as important to safety. The HI-STAR overpack top flange, closure plate, inner shell, and bottom plate are designed and fabricated in accordance with the requirements of ASME Code, Section III, Subsection NB, with certain NRC-approved alternatives (see Subsection 2.2.4). The remainder of the HI-STAR overpack steel structure is designed and fabricated in accordance with the requirements of ASME Code, Section III, Subsection NF, to the maximum extent practical (see Subsection 2.2.4). Compliance with the ASME Code is fully consistent with that used by other dry storage systems previously approved by the NRC.

The overpack is designed for all normal, off-normal, and design basis accident condition loadings, as defined in Section 2.2. These design loadings include a postulated drop accident from the maximum allowable handling height, consistent with Technical Specification requirements. The load combinations for which the overpack is designed are defined in Section 2.2.7. The physical characteristics of the MPCs for which the overpack is designed are defined in Chapter 1.

Thermal

The allowable temperatures for the structural steel components are based on the maximum temperature for which material properties and allowable stresses are provided in Section II of the ASME Code. The specific allowable temperatures for the structural steel components of the overpack are provided in Table 2.2.3. The allowable temperature for the Holtite-A neutron shield material specified in Table 2.2.3 is based on the data provided in Appendix 1.B.

The overpack is designed for extreme cold conditions, as discussed in Section 2.2.2.2. The structural steel materials used for the overpack that are susceptible to brittle fracture are discussed in Section 3.1.2.3.

The overpack is designed for the maximum allowable heat load for steady-state normal conditions, in accordance with Section 2.1.5. The thermal characteristics of the MPC for which the overpack is designed are defined in Chapter 4.

Shielding

The off-site dose for normal operating conditions and anticipated occurrences at the controlled area boundary to a real individual is limited by 10CFR72.104(a) to a maximum of 25 mrem/year whole body, 75 mrem/year thyroid, and 25 mrem/year for other critical organs, including contributions from all nuclear fuel cycle operations. Since these limits are dependent on plant operations as well as site-specific conditions (e.g., the ISFSI design and proximity to the controlled area boundary, and the number and arrangement of loaded storage casks), the determination and comparison of ISFSI doses to this limit are necessarily site-specific. Dose rates for a typical ISFSI using the HI-STAR 100 System are provided in Chapters 5 and 10. The determination of site-specific ISFSI dose rates at the controlled area boundary and demonstration of compliance with regulatory limits shall be performed by the licensee in accordance with 10CFR72.212.

The overpack is designed to limit the calculated surface dose rate at the cask midplane for all MPCs to 125 mrem/hr or less, as defined in Section 2.3.5. The overpack is also designed to maintain occupational exposures ALARA during MPC transfer operations, in accordance with 10CFR20. The calculated overpack dose rates are presented in Section 5.1. These dose rates are used to perform a generic occupational exposure estimate for MPC loading operations and a dose assessment for a typical ISFSI, as described in Chapter 10. In addition, overpack dose rates are limited in accordance with the Technical Specifications.

Confinement

The overpack is not defined as the confinement boundary for radioactive materials. Confinement during storage is provided by the MPC which is addressed in Chapter 7. The overpack provides physical protection and biological shielding for the MPC confinement boundary during MPC dry storage operations.

Operations

There are no radioactive effluents that result from MPC transfer or storage operations with the overpack. Effluents generated during MPC loading and closure operations are handled by the plant's radwaste system and procedures under the licensee's 10CFR50 license.

Generic operating procedures for the HI-STAR 100 System are provided in Chapter 8. The licensee is required to develop detailed operating procedures based on site-specific conditions and requirements that also comply with the applicable 10CFR50 Technical Specification requirements for the site and the HI-STAR 100 System Technical Specifications.

Acceptance Tests and Maintenance

The fabrication acceptance basis and maintenance program to be applied to the overpack are described in Chapter 9. The operational controls and limits to be applied to the overpack are contained in the Technical Specifications. Application of these requirements will assure that the overpack is fabricated, operated, and maintained in a manner that satisfies the design criteria defined in this chapter.

Decommissioning

Decommissioning considerations for the HI-STAR 100 System, including the overpack, are addressed in Section 2.4.

Table 2.0.1

MPC DESIGN CRITERIA SUMMARY

Type	Criteria	Basis	FSAR Reference
Design Life:			
Design	40 yrs.	-	Table 1.2.2
Regulatory	20 yrs.	10CFR72.42(a) and 10CFR72.236(g)	-
Structural:			
Design Codes:			
Enclosure Vessel	ASME Code, Section III, Subsection NB	10CFR72.24(c)(4)	Section 2.0.1
Fuel Basket	ASME Code, Section III, Subsection NG	10CFR72.24(c)(4)	Section 2.0.1
MPC Lifting Points	ANSI N14.6/NUREG-0612	10CFR72.24(c)(4)	Section 1.2.1.4
Design Dead Weights:			
Max. Loaded Canister (dry)	82,494 lb. (MPC-24) 87,171 lb. (MPC-68)	ANSI/ANS 57.9	Table 3.2.1
Empty Canister (dry)	40,868 lb. (MPC-24) 37,591 lb. (MPC-68)	ANSI/ANS 57.9	Table 3.2.1
Design Cavity Pressures:			
Normal:	100 psig	ANSI/ANS 57.9	Section 2.2.1.3

Table 2.0.1 (continued)

MPC DESIGN CRITERIA SUMMARY

Type	Criteria	Basis	FSAR Reference
Off-Normal:	100 psig	ANSI/ANS 57.9	Section 2.2.2.1
Accident (Internal)	125 psig	ANSI/ANS 57.9	Section 2.2.3.8
Accident (External)	60 psig	ANSI/ANS 57.9	Sections 2.2.3.6 and 2.2.3.10
Response and Degradation Limits	SNF assemblies confined in dry, inert environment	10CFR72.122(h)(l)	Section 2.0.1
Thermal:			
Maximum Design Temperatures:			
Structural Materials:			
Stainless Steel (Normal)	725°F	ASME Code Section II, Part D	Table 2.2.3
Stainless Steel (Accident)	950 °F	ASME Code Section II, Part D	Table 2.2.3
Neutron Poison:			
Boral (normal)	800 °F	See Section 4.3.1	Table 2.2.3
Boral (accident)	950 °F	See Section 4.3.1	Table 2.2.3
PWR Fuel Cladding:			
5-year cooled	720 °F	PNL-6189	Section 4.3
6-year cooled	698 °F	PNL-6189	Section 4.3
7-year cooled	657 °F	PNL-6189	Section 4.3
10-year cooled	647 °F	PNL-6189	Section 4.3
15-year cooled	633 °F	PNL-6189	Section 4.3

Table 2.0.1 (continued)

MPC DESIGN CRITERIA SUMMARY

Type	Criteria	Basis	FSAR Reference
BWR Fuel Cladding:			
5-year cooled	749 °F	PNL-6189	Section 4.3
6-year cooled	720 °F	PNL-6189	Section 4.3
7-year cooled	676 °F	PNL-6189	Section 4.3
10-year cooled	665 °F	PNL-6189	Section 4.3
15-year cooled	653 °F	PNL-6189	Section 4.3
Canister Backfill Gas	Helium	-	Chapter 12
Canister Backfill Pressure	Varies by MPC	-	Chapter 12
Short-Term Allowable Fuel Cladding Temperature	1058 °F	PNL-4835	Sections 2.0.1 & 4.3
Insolation	Protected by Overpack	10CFR71.71	-
Confinement:		10CFR72.128(a)(3) and 10CFR72.236(d) and (e)	
Closure Welds:			
Shell Seams and Shell-to-Baseplate	Full Penetration	-	Section 1.5 and Table 9.1.3
MPC Lid	Multi-pass Partial Penetration	10CFR72.236(e)	Section 1.5 and Table 9.1.3
MPC Closure Ring	Partial Penetration		
Port Covers	Partial Penetration		

Table 2.0.1 (continued)

MPC DESIGN CRITERIA SUMMARY

Type	Criteria	Basis	FSAR Reference
NDE:			
Shell Seams and Shell-to-Baseplate	100% RT or UT	NUREG-1536	Chapter 8 and Table 9.1.3
MPC Lid	Root Pass/Final Surface 100% PT and Volumetric or Multi-Layer PT	NUREG-1536	Chapter 8 and Table 9.1.3
Closure Ring	Root Pass/Final Surface 100% PT	NUREG-1536	Chapter 8 and Table 9.1.3
Port Covers	Root Pass/Final Surface 100% PT	NUREG-1536	Chapter 8 and Table 9.1.3
Leak Testing:			
Welds Tested	Shell seams, shell-to-baseplate, MPC lid-to-shell, and port covers-to-MPC lid	-	Section 7.1, Chapters 8, 9 and Technical Specifications
Medium	Helium	-	Section 7.2 and Technical Specifications
Max. Leak Rate	$5x10^{-6}$ atm cm^3/sec (helium)	-	Technical Specifications
Monitoring System	None	10CFR72.128(a)(1)	Section 2.3.2.1
Hydrostatic Testing:			
Test Pressure	125 psig (+5, -0 psig)	-	Chapters 8 and 9
Welds Tested	MPC Lid-to-Shell, MPC shell seams, MPC shell-to-baseplate	-	Section 8.1 and Table 9.1.1
Medium	Water	-	Section 8.1 and Chapter 9

Table 2.0.1 (continued)

MPC DESIGN CRITERIA SUMMARY

Type	Criteria	Basis	FSAR Reference
Retrievability:			
Normal and Off-normal: Post (design basis) Accident	No Encroachment on Fuel Assemblies or Exceeding Fuel Assembly Deceleration Limits	10CFR72.122(f),(h)(1), & (l)	Sections 3.4, 3.5, and 3.1.2
Criticality:		10CFR72.124 & 10CFR72.236(c)	
Method of Control	Fixed Borated Neutron Absorber & Geometry	-	Section 2.3.4
Min. Boron Loading	0.0267 g/cm^2 (MPC-24) 0.0372 g/cm^2 (MPC-68) 0.01 g/cm^2 (MPC-68F)	-	Section 2.1.7
Max. k_{eff}	0.95	-	Sections 6.1 and 2.3.4
Min. Burnup	0.0 GWd/MTU (fresh fuel)	-	Section 6.1
Radiation Protection/Shielding:		10CFR72.126, & 10CFR72.128(a)(2)	
MPC: (normal/off-normal/accident)			
MPC Closure	ALARA	10CFR20	Sections 10.1, 10.2, & 10.3
MPC Transfer	ALARA	10CFR20	Sections 10.1, 10.2, & 10.3
Exterior of Shielding: (normal/off-normal/accident)			
Storage Mode Position	See Table 2.0.2	10CFR20	Section 5.1.1
ISFSI Controlled Area Boundary	See Table 2.0.2	10CFR72.104 & 10CFR72.106	Section 5.1.1 and Chapter 10

Table 2.0.1 (continued)

MPC DESIGN CRITERIA SUMMARY

Type	Criteria	Basis	FSAR Reference
Design Bases:		10CFR72.236(a)	
Spent Fuel Specification:			
Assemblies/Canister	Up to 24 (MPC-24) Up to 68 (MPC-68)	-	Table 1.2.1
Type of Cladding	Zircaloy*	-	Table 2.1.6
Fuel Condition	Intact*	-	Section 2.1.2 & Table 2.1.6
* Also designed to accommodate failed fuel, stainless clad fuel, and MOX fuel (Tables 2.1.7 and 2.1.11 and Appendix B to CoC 72-1008)			
PWR Fuel Assemblies:			
Type/Configuration	Various	-	Table 2.1.3
Max. Burnup	42,100 MWD/MTU (MPC-24)	-	Figure 2.1.6
Max. Enrichment	Varies by fuel design	-	Table 2.1.3
Max. Decay Heat/Assembly:			
5-year cooled	791.6 W (MPC-24)	-	Figure 2.1.8
6-year cooled	773 W (MPC-24)	-	Figure 2.1.8
7-year cooled	703 W (MPC-24)	-	Figure 2.1.8
10-year cooled	687 W (MPC-24)	-	Figure 2.1.8
15-year cooled	665 W (MPC-24)	-	Figure 2.1.8
Minimum Cooling Time:	5 years (Intact Zr Clad Fuel) 9 years (Intact SS Clad Fuel)	-	Chapter 12
Max. Fuel Assembly Weights:	1,680 lb.	-	Table 2.1.6
Max. Fuel Assembly Length: (unirradiated nominal)	176.8 in.	-	Table 2.1.6
Max. Fuel Assembly Width (unirradiated nominal)	8.54 in.	-	Table 2.1.6
Fuel Rod Fill Gas:			
Pressure (max.)	500 psig	-	Section 4.3 & Table 4.3.2

Table 2.0.1 (continued)

MPC DESIGN CRITERIA SUMMARY

Type	Criteria	Basis	FSAR Reference
BWR Fuel Assemblies:			
Type	Various	-	Table 2.1.4
Max. Burnup	37,600 MWd/MTU	-	Figure 2.1.6 and Appendix B to CoC 72-1008
Max. Enrichment	Varies by fuel design	-	Section 6.1 and Appendix B to CoC 72-1008
Max. Decay Heat/Assy.:			
5-year cooled	272 W (MPC-68)	-	Figure 2.1.8
6-year cooled	261 W (MPC-68)	-	Figure 2.1.8
7-year cooled	238 W (MPC-68)		Figure 2.1.8
10-year cooled	232 W (MPC-68)	-	Figure 2.1.8
15-year cooled	226 W (MPC-68)	-	Figure 2.1.8
Minimum Cooling Time:	5 years (Intact Zr Clad Fuel) 18 years (Damaged Zr Clad Fuel) 18 years (Zr Clad Fuel Debris) 10 years (Intact SS Clad Fuel)	-	Appendix B to CoC 72-1008
Max. Fuel Assembly Weight:			
w/channels	700 lb.	-	Table 2.1.6
Max. Fuel Assembly Length (unirradiated nominal)	176.2 in.	-	Table 2.1.6
Max. Fuel Assembly Width (unirradiated nominal)	5.85 in.	-	Table 2.1.6
Fuel Rod Fill Gas:			
Pressure (max.)	147 psig	-	Table 4.3.5
Normal Design Event Conditions:		10CFR72.122(b)(1)	
Ambient Temperatures	See Table 2.0.2	ANSI/ANS 57.9	Section 2.2.1.4
Handling:			Section 2.2.1.2

Table 2.0.1 (continued)

MPC DESIGN CRITERIA SUMMARY

Type	Criteria	Basis	FSAR Reference
Handling Loads	115% of Dead Weight	CMAA #70	Section 2.2.1.2
Lifting Attachment Acceptance Criteria	1/10 Ultimate 1/6 Yield	NUREG-0612	Section 2.2.1.2
Attachment/Component Interface Acceptance Criteria	1/3 Yield	Regulatory Guide 3.61	Section 2.2.1.2
Away from Attachment Acceptance Criteria	ASME Code Level A	ASME Code	Section 2.2.1.2
Wet/Dry Loading	Wet or Dry	-	Section 1.2.2.2
Transfer Orientation	Vertical or Horizontal	-	Section 1.2.2.2
Storage Orientation	Vertical	-	Section 1.2.2.2
Fuel Rod Rupture Releases:			
Fuel Rod Failures	1%	NUREG-1536	Section 2.2.1.3
Fill Gases	100%	NUREG-1536	Section 2.2.1.3
Fission Gases	30%	NUREG-1536	Section 2.2.1.3
Snow and Ice	Protected by Overpack	ASCE 7-88	Section 2.2.1.6
Off-Normal Design Event Conditions:		10CFR72.122(b)(1)	
Ambient Temperature	See Table 2.0.2	ANSI/ANS 57.9	Section 2.2.2.2
Leakage of One Seal	No Loss of Confinement	ANSI/ANS 57.9	Section 2.2.2.4
Fuel Rod Rupture Releases:			
Fuel Rod Failures	10%	NUREG-1536	Section 2.2.2.1
Fill Gases	100%	NUREG-1536	Section 2.2.2.1
Fission Gases	30%	NUREG-1536	Section 2.2.2.1
Design-Basis (Postulated) Accident Design Events and Conditions:		10CFR72.24(d)(2) & 10CFR72.94	
Tip Over	See Table 2.0.2	-	Section 2.2.3.2
End Drop	See Table 2.0.2	-	Section 2.2.3.1
Side Drop	See Table 2.0.2	-	Section 2.2.3.1

Table 2.0.1 (continued)

MPC DESIGN CRITERIA SUMMARY

Type	Criteria	Basis	FSAR Reference
Fire	See Table 2.0.2	10CFR72.122(c)	Section 2.2.3.3
Fuel Rod Rupture Releases:			
Fuel Rod Failures	100%	NUREG-1536	Section 2.2.3.8
Fill Gases	100%	NUREG-1536	Section 2.2.3.8
Fission Gases	30%	NUREG-1536	Section 2.2.3.8
Particulates & Volatiles	See Table 7.3.1	-	Sections 2.2.3.9 and 7.3
Confinement Boundary Leakage	$5x10^{-6}$ atm cm^3/sec (helium)	-	Sections 2.2.3.9 and 7.3
Explosive Overpressure	Protected by Overpack	10CFR72.122(c)	Section 2.2.3.10
Design Basis Natural Phenomenon Design Events and Conditions:		10CFR72.92 & 10CFR72.122(b)(2)	
Flood Water Depth	125 ft.	ANSI/ANS 57.9	Section 2.2.3.6
Seismic	See Table 2.0.2	10CFR72.102(f)	Section 2.2.3.7
Wind	Protected by Overpack	ASCE-7-88	Section 2.2.3.5
Tornado & Missiles	Protected by Overpack	RG 1.76 & NUREG-0800	Section 2.2.3.5
Burial Under Debris	Adiabatic Heat-Up	-	Section 2.2.3.12
Lightning	See Table 2.0.2	NFPA 78	Section 2.2.3.11
Partial Blockage of MPC Basket Vent Holes	Crud Depth (Table 2.2.8)	ESEERCO Project EP91-29	Section 2.2.3.4
Extreme Environmental Temp.	See Table 2.0.2	-	Section 2.2.3.13

Table 2.0.2

OVERPACK DESIGN CRITERIA SUMMARY

Type	Criteria	Basis	FSAR Reference
Design Life:			
Design	40 yrs.	-	Section 2.0.2
Regulatory	20 yrs.	10CFR72.42(a) & 10CFR72.236(g)	
Structural:			
Design Codes:			
Inner Shell, Closure Plate, Top Flange, Bottom Plate, and Closure Plate Bolts			
Design	ASME Code Section III, Subsection NB	10CFR72.24(c)(4)	Section 2.0.2
Fabrication	ASME Code Section III, Subsection NB	10CFR72.24(c)(4)	Section 2.0.2
Remainder of Structural Steel			
Design	ASME Code Section III, Subsection NF	10CFR72.24(c)(4)	Section 2.0.2
Fabrication	ASME Code Section III, Subsection NF	10CFR72.24(c)(4)	Section 2.0.2
Design Weights:			
Max. Loaded MPC (Dry)	90,000 lb. (Bounding)	ANSI/ANS 57.9	Table 3.2.1
Max. Empty Overpack:			
Assembled with Closure Plate	153,710 lb.	ANSI/ANS 57.9	Table 3.2.1
Max. MPC/Overpack:	240,881 lb.	ANSI/ANS 57.9	Table 3.2.1

Table 2.0.2 (continued)

OVERPACK DESIGN CRITERIA SUMMARY

Type	Criteria	Basis	FSAR Reference
Design Cavity Pressures	40 psig (Normal) 40 psig (Off-Normal) 60 psig (Accident)	-	Table 2.2.1
Response and Degradation Limits	See Table 2.0.1	10CFR72.122(h)(1)	Section 2.0.1
Thermal:			
Maximum Design Temperatures:			
Inner Shell (SA203-E)			
Normal Condition Maximum	400 °F	ASME Code Section II, Part D	Table 2.2.3
Off-Normal/Accident Condition Maximum	500 °F	ASME Code Section II, Part D	Table 2.2.3
Top Flange & Closure Plate (SA350-LF3)			
Normal Condition Maximum	400 °F	ASME Code Section II, Part D	Table 2.2.3
Off-Normal/Accident Condition Maximum	700 °F	ASME Code Section II, Part D	Table 2.2.3
Bottom Plate (SA350-LF3)			
Normal Condition Maximum	350 °F	ASME Code Section II, Part D	Table 2.2.3
Off-Normal/Accident Condition Maximum	700 °F	ASME Code Section II, Part D	Table 2.2.3
Remainder of Steel Structure	350 °F	ASME Code Section II, Part D	Table 2.2.3
Neutron Shield	300 °F	Manufacturer's Test Data	Table 2.2.3

Table 2.0.2 (continued)

OVERPACK DESIGN CRITERIA SUMMARY

Type	Criteria	Basis	FSAR Reference
Insolation:	Averaged Over 24 Hours	10CFR71.71	Section 4.4.1.1.8
Confinement:	None	10CFR72.128(a)(3) & 10CFR72.236(d) & (e)	N/A
Retrievability:			
Normal and Off-normal	No damage which precludes Retrieval of MPC or Exceeding Fuel Assembly Deceleration Limits	10CFR72.122(f),(h)(1), & (l)	Sections 3.5 and 3.4
Accident			Sections 3.5 and 3.4
Criticality:	Protection of MPC and Fuel Assemblies	10CFR72.124 & 10CFR72.236(c)	Section 6.1
Radiation Protection/Shielding:		10CFR72.126 & 10CFR72.128(a)(2)	
Overpack (Normal/Off-normal/Accident)			
Surface	ALARA	10CFR20	Chapters 5 and 10
Position	ALARA	10CFR20	Chapters 5 and 10
Beyond Controlled Area During Normal Operation and Anticipated Occurrences	25 mrem/yr. to whole body 75 mrem/yr. to thyroid 25 mrem/yr. to any organ	10CFR72.104	Sections 5.1.1, 7.2, and 10.4
On Controlled Area Boundary from Design Basis Accident	5 rem to whole body or to any organ	10CFR72.106	Sections 5.1.2, 7.3, and 10.4
Design Bases:			
Spent Fuel Specification	See Table 2.0.1	10CFR72.236(a)	Section 2.1
Normal Design Event Conditions:		10CFR72.122(b)(1)	
Ambient Outside Temperatures:			

Table 2.0.2 (continued)

OVERPACK DESIGN CRITERIA SUMMARY

Type	Criteria	Basis	FSAR Reference
Lifetime Average	80 °F	ANSI/ANS 57.9	Section 2.2.1.4
Handling:			
Handling Loads	115% of Dead Weight	CMAA #70	Section 2.2.1.2
Lifting Attachment Acceptance Criteria	1/10 Ultimate 1/6 Yield	NUREG-0612	Section 2.2.1.2
Snow and Ice Load	100 lb./ft^2	ASCE 7-88	Section 2.2.1.6
Wet/Dry Loading	Wet/Dry	-	Section 1.2.2.2
Storage Orientation	Vertical	-	Section 1.2.2.2
Off-Normal Design Event Conditions:		10CFR72.122(b)(1)	
Ambient Temperature			
Minimum	-40 °F	ANSI/ANS 57.9	Section 2.2.2.2
Maximum	100 °F	ANSI/ANS 57.9	Section 2.2.2.2
Design-Basis (Postulated) Accident Design Events and Conditions:		10CFR72.94	
Drop Cases:			
End	21 in.	-	Section 2.2.3.1
Side	72 in.	-	Section 2.2.3.1
Tip-Over	Assumed (Non-mechanistic)	-	Section 2.2.3.2
Fire:			
Duration	305 seconds	10CFR72.122(c)	Section 2.2.3.3
Temperature	1,475 °F	10CFR72.122(c)	Section 2.2.3.3
Fuel Rod Rupture	See Table 2.0.1	-	Section 2.2.3.8
Flood			
Height	656 ft.	RG 1.59	Section 2.2.3.6
Velocity	13 ft/sec.	RG 1.59	Section 2.2.3.6
Seismic			
Max. ZPA Horizontal Ground	0.314g (w/1.0 vertical)	10CFR72.102(f)	Section 2.2.3.7

Table 2.0.2 (continued)

OVERPACK DESIGN CRITERIA SUMMARY

Type	Criteria	Basis	FSAR Reference
(Max. ZPA Vertical Ground)	0.332g (w/0.75 vertical) 0.339g (w/0.667 vertical) 0.354g (w/0.5 vertical)		
Tornado			
Wind			
Max. Wind Speed	360 mph	RG 1.76	Section 2.2.3.5
Pressure Drop	3.0 psi	RG 1.76	Section 2.2.3.5
Missiles			Section 2.2.3.5
Automobile			
Weight	1,800 kg	NUREG-0800	Table 2.2.5
Velocity	126 mph	NUREG-0800	Table 2.2.5
Rigid Solid Steel Cylinder (Artillery Shell)			
Weight	125 kg	NUREG-0800	Table 2.2.5
Velocity	126 mph	NUREG-0800	Table 2.2.5
Diameter	8 in.	NUREG-0800	Table 2.2.5
Steel Sphere			
Weight	0.22 kg	NUREG-0800	Table 2.2.5
Velocity	126 mph	NUREG-0800	Table 2.2.5
Diameter	1 in.	NUREG-0800	Table 2.2.5
Burial Under Debris	Adiabatic Heat-Up	-	Section 2.2.3.12
Lightning	Resistance Heat-Up	NFPA 70 & 78	Section 2.2.3.11
Extreme Environmental Temperature	125 °F	-	Section 2.2.3.13
Load Combinations:	See Table 2.2.14	ANSI/ANS 57.9 and NUREG-1536	Section 2.2.7

2.1 SPENT FUEL TO BE STORED

2.1.1 Determination of The Design Basis Fuel

The HI-STAR 100 System is designed to store most types of fuel assemblies generated in the commercial U.S. nuclear industry. Boiling-water reactor (BWR) fuel assemblies have been supplied by The General Electric Company (GE), Siemens (SPC), Exxon Nuclear, ANF, UNC, ABB Combustion Engineering, and Gulf Atomic. Pressurized-water reactor (PWR) fuel assemblies are generally supplied by Westinghouse, Babcock & Wilcox, ANF, and ABB Combustion Engineering. ANF, Exxon, and Siemens are historically the same manufacturing company under different ownership. Within this report, SPC is used to designate fuel manufactured by ANF, Exxon, or Siemens. Publications such as Refs. [2.1.1] and [2.1.2] provide a comprehensive description of fuel discharged from U.S. reactors. A central object in the design of the HI-STAR 100 System is to ensure that a majority of SNF discharged from the U.S. reactors can be loaded into one of the HI-STAR 100 MPCs.

The cell openings and lengths in the fuel basket have been sized to accommodate the BWR and PWR assemblies listed in Refs. [2.1.1] and [2.1.2] except as noted below. Similarly, the cavity length of the multi-purpose canisters has been set at a dimension which permits storing most types of PWR fuel assemblies and BWR fuel assemblies with or without fuel channels. The exceptions are as follows:

- The South Texas Units 1 & 2 SNF, and CE 16x16 System 80 SNF are too long to be accommodated in the available MPC cavity length.

In addition to satisfying the cross sectional and length compatibility, the active fuel region of the SNF must be enveloped in the axial direction by the neutron absorber located in the MPC fuel basket. Alignment of the neutron absorber with the active fuel region is ensured by the use of upper and lower fuel spacers suitably designed to support the bottom and restrain the top of the fuel assembly. The spacers axially position the SNF assembly such that its active fuel region is properly aligned with the neutron absorber in the fuel basket. Figure 2.1.5 provides a pictorial representation of the fuel spacers positioning the fuel assembly active fuel region. Both the upper and lower fuel spacers are designed to perform their function under normal, off-normal, and accident conditions of storage.

In summary, the geometric compatibility of the SNF with the MPC designs does not require the definition of a design basis fuel assembly. This, however, is not the case for structural, confinement, shielding, thermal-hydraulic, and criticality criteria. In fact, a particular fuel type in a category (PWR or BWR) may not control the cask design in all of the above-mentioned criteria. To ensure that no SNF listed in Refs. [2.1.1] and [2.1.2] which is geometrically admissible in the HI-STAR 100 MPC is precluded, it is necessary to determine the governing fuel specification for each analysis criteria. To make the necessary determinations, potential candidate fuel assemblies for each qualification criteria were considered. Table 2.1.1 lists the PWR fuel assemblies that were evaluated. These fuel assemblies were evaluated to define the governing design criteria for PWR fuel. The BWR fuel assembly designs evaluated are listed in Table 2.1.2. Tables 2.1.3 and 2.1.4 provide the fuel characteristics determined to be acceptable for storage in the HI-STAR 100 System

presented in groups of fuel assembly types defined as "array/classes" as described in further detail in Chapter 6. Table 2.1.5 lists the BWR and PWR fuel assembly designs which are found to govern for the three qualification criteria, namely reactivity, shielding, and decay heat generation. Substantiating results of analyses for the governing assembly types are presented in the respective chapters dealing with the specific qualification topic. Additional information on the design basis fuel definition is presented in the following subsections.

2.1.2 Intact SNF Specifications

Intact fuel assemblies are defined as fuel assemblies without known or suspected cladding defects greater than pinhole leaks and hairline cracks, and which can be handled by normal means. The design payload for the HI-STAR 100 System is intact zircaloy clad fuel assemblies with the characteristics listed in Table 2.1.6 or intact stainless steel clad fuel assemblies with the characteristics listed in Table 2.1.11. The placement of a single stainless steel clad fuel assembly in an MPC necessitates that all fuel assemblies (stainless steel clad or zircaloy clad) stored in that MPC meet the maximum heat generation requirements for stainless steel clad fuel specified in Table 2.1.11. Intact BWR MOX fuel assemblies shall meet the requirements of Table 2.1.7.

Intact fuel assemblies with missing pins cannot be loaded into the HI-STAR 100 System unless dummy fuel pins, which occupy a volume greater than or equal to the original fuel pins, replace the missing pins prior to loading. Any intact fuel assembly which falls within the geometric, thermal, and nuclear limits established for the design basis intact fuel assembly, as defined in Appendix B to Certificate of Compliance 72-1008 can be safely stored in the HI-STAR 100 System.

The fuel characteristics specified in Tables 2.1.3 and 2.1.4 have been evaluated in this FSAR and are acceptable for storage in the HI-STAR 100 System.

2.1.3 Damaged SNF and Fuel Debris Specifications

Damaged fuel assemblies are defined as fuel assemblies with known or suspected cladding defects greater than pinhole leaks and hairline cracks or missing fuel rods that are not replaced with dummy fuel rods, and which may have mechanical damage which would not allow it to be handled by normal means; however, there shall be no loose components. No loose fuel debris is allowed with the damaged fuel assembly.

Fuel debris is defined as fuel assemblies with known or suspected defects greater than pinhole leaks or hairline cracks such as ruptured fuel rods, severed fuel rods, or loose fuel pellets, and which cannot be handled by normal means.

To aid in loading and unloading, damaged fuel assemblies and fuel debris will be loaded into stainless steel damaged fuel containers (DFCs) provided with 250 micron fine mesh screens, prior to placement in the HI-STAR 100 System. This application requests approval of Dresden Unit 1 (UO_2 rods and MOX fuel rods) and Humboldt Bay fuel arrays (Assembly Classes 6x6A, 6x6B, 6x6C, 7x7A, and 8x8A) as damaged fuel assembly contents for storage in the MPC-68 and fuel debris as contents for storage in the MPC-68F. The design characteristics bounding Dresden Unit 1 and Humboldt Bay SNF are given in Table 2.1.7. The placement of a single damaged fuel assembly in an

MPC-68 or a single fuel debris damaged fuel container in an MPC-68F necessitates that all fuel assemblies (intact, damaged, or debris) stored in that MPC meet the maximum heat generation requirements specified in Table 2.1.7. The fuel characteristics specified in Table 2.1.4 for Dresden 1 and Humboldt Bay fuel arrays have been evaluated in this FSAR and are acceptable for storage as damaged fuel or fuel debris in the HI-STAR 100 System. The DFC design is illustrated in Figure 2.1.1. Because of the long cooling time, small size, and low weight of spent fuel assemblies qualified as damaged fuel or fuel debris, the DFC and its contents are bounded by the structural, thermal, and shielding analyses performed for the intact BWR design basis fuel. Separate criticality analysis of the bounding fuel assembly for the damaged fuel and fuel debris has been performed in Chapter 6.

2.1.4 Structural Parameters for Design Basis SNF

The main physical parameters of a SNF assembly applicable to the structural evaluation are the fuel assembly length, envelope (cross sectional dimensions), and weight. These parameters, which define the mechanical and structural design, are listed in Tables 2.1.6, 2.1.7, and 2.1.11. The centers of gravity reported in Section 3.2 are based on the maximum fuel assembly weight. Upper and lower fuel spacers (as appropriate) maintain the axial position of the fuel assembly within the MPC basket and, therefore, the location of the center of gravity. The upper and lower fuel spacers are designed to withstand normal, off-normal, and accident conditions of storage. An axial clearance of approximately 2 to 2-1/2 inches is provided to account for the irradiation and thermal growth of the fuel assemblies. The suggested upper and lower fuel spacer lengths are listed in Tables 2.1.9 and 2.1.10. In order to qualify for storage in the HI-STAR 100 MPC, the SNF must satisfy the physical parameters listed in Tables 2.1.6, 2.1.7, or 2.1.11.

2.1.5 Thermal Parameters for Design Basis SNF

The principal thermal design parameter for the stored fuel is the peak fuel cladding temperature, which is a function of the maximum heat generation rate per assembly, the allowable fuel cladding temperature based on cooling time, and the decay heat removal capabilities of the HI-STAR 100 System. The maximum heat generation rate per assembly for the design basis fuel assembly is based on the fuel assembly type with the highest decay heat for a given enrichment, burnup, and cooling time. This decay heat design basis fuel assembly is listed in Table 2.1.5. Section 5.2 describes the method used to determine the design basis fuel assembly type and calculate the decay heat load.

As can be seen in Table 2.2.3, the acceptable normal condition fuel cladding temperature limit decreases with increased cooling time. Therefore, the allowable decay heat load per fuel assembly must correspondingly decrease with increased fuel assembly cooling time. For example, the maximum decay heat load for 5-year cooled Zircaloy clad BWR fuel in the MPC-68 is 272W, but for 10-year cooled zircaloy clad BWR fuel, the decay heat load is limited to 232W. To ensure the allowable fuel cladding temperature limits are not exceeded, Figure 2.1.8 specifies the allowable decay heat per assembly versus cooling time for Zircaloy clad fuel in each MPC type. Tables 2.1.7 and 2.1.11 provide the maximum heat generation for damaged zircaloy clad fuel assemblies and stainless steel clad fuel assemblies, respectively. Due to the conservative thermal assessment and the long cooling time of the damaged and stainless steel clad fuel, a reduction in decay heat load is not required as the cooling time increases beyond the minimum specified.

The specified decay heat load can be attained by varying burnups and cooling times. Figure 2.1.6 provides illustrative burnup and cooling time characteristics for intact Zircaloy clad fuel to meet the thermal requirements for the MPC-24 and MPC-68. Any intact Zircaloy clad fuel assembly with a burnup and cooling time which lies on or below the curve of Figure 2.1.6 may be thermally acceptable for loading into the HI-STAR 100 System (MPC-24 or MPC-68). Each point on the curve produces a decay heat equal to or below the value specified in Figure 2.1.8 for the design basis fuel assembly type.

The fuel rod cladding temperature is also affected by other factors. A governing geometry which maximizes the impedance to the transmission of heat out of the fuel rods has been defined. The governing thermal parameters ensure that the range of SNF discussed previously are bounded by the thermal analysis is discussed in detail and specified in Chapter 4. By utilizing these bounding thermal parameters, the calculated peak fuel rod cladding temperatures are conservative for actual spent fuel assemblies which will have greater thermal conductivities.

Finally, the axial variation in the heat generation rate in the design basis fuel assembly is defined based on the axial burnup distribution. For this purpose, the data provided in Refs. [2.1.3] and [2.1.4] are utilized and summarized in Table 2.1.8 and Figures 2.1.3 and 2.1.4 for reference. These distributions are representative of fuel assemblies with the design basis burnup levels considered. These distributions are used for analyses only, and do not provide a criteria for fuel assembly acceptability for storage in the HI-STAR 100 System.

2.1.6 Radiological Parameters for Design Basis SNF

The principal radiological design criteria for the HI-STAR 100 System are the 10CFR72.104 site boundary dose rate limits and maintaining operational dose rates as low as reasonably achievable (ALARA). The radiation dose is directly affected by the gamma and neutron source terms of the SNF assembly.

The gamma and neutron sources are separate and are affected differently by enrichment, burnup, and cooling time. It is recognized that, at a given burnup, the radiological source terms increase monotonically as the initial enrichment is reduced. The shielding design basis fuel assembly, therefore, is evaluated at the maximum burnup, minimum cooling time, and a conservative enrichment corresponding to the burnup. The shielding design basis fuel assembly thus bounds all other fuel assemblies.

The design basis dose rates can be met by a variety of burnup levels and cooling times. Tables 2.1.7 and 2.1.11 provide the burnup and cooling time values which meet the radiological source term requirements for BWR damaged fuel/fuel debris and intact stainless steel clad fuel, respectively. Figure 2.1.6 provides illustrative burnup and cooling time values which meet the radiological source term requirements for intact zircaloy clad fuel in each MPC type.

Table 2.1.8 and Figures 2.1.3 and 2.1.4 provide the axial distribution for the radiological source terms for PWR and BWR fuel assemblies based on the axial burnup distribution. The axial burnup distributions are representative of fuel assemblies with the design basis burnup levels considered. These distributions are used for analyses only, and do not provide a criteria for fuel assembly

acceptability for storage in the HI-STAR 100 System.

Thoria rods placed in Dresden Unit 1 Thoria Rod Canisters meeting the requirements of Table 2.1.12 and Dresden Unit 1 fuel assemblies with one Antimony-Beryllium neutron source have been qualified for storage. Up to one Dresden Unit 1 Thoria Rod Canister plus any combination of damaged fuel assemblies in damaged fuel containers and intact fuel, up to a total of 68 may be stored.

Burnable Poison Rod Assemblies (BPRAs) and Thimble Plug Devices (TPDs) in PWR fuel have been qualified for storage in the MPC-24.

2.1.7 Criticality Parameters for Design Basis SNF

As discussed earlier, the MPC-68 features a basket without flux traps. In the MPC-68 basket, there is one panel of neutron absorber between two adjacent fuel assemblies. The MPC-24 employs a construction wherein two neighboring fuel assemblies are separated by two panels of neutron absorber with a water gap between them (flux trap construction).

The MPC-24 Boral ^{10}B areal density is specified at a minimum loading of 0.0267 g/cm^2. The MPC-68 Boral ^{10}B areal density is specified at a minimum loading of 0.0372 g/cm^2. The MPC-68F Boral ^{10}B areal density is specified at a minimum loading of 0.01 g/cm^2.

For all MPCs, the ^{10}B areal density used for analysis is conservatively established at 75% of the minimum ^{10}B areal density to demonstrate that the reactivity under the most adverse accumulation of tolerances and biases is less than 0.95. This satisfies NUREG-1536 [2.1.5], which requires a 25% reduction in ^{10}B areal density credit. A large body of sampling data accumulated by Holtec from thousands of manufactured Boral panels indicates the average ^{10}B areal densities to be approximately 15% greater than the specified minimum.

2.1.8 Summary of SNF Design Criteria

An intact zircaloy clad fuel assembly is acceptable for storage in a HI-STAR 100 System if it fulfills the following criteria:

a. It satisfies the physical characteristics listed in Tables 2.1.3 or 2.1.4, and 2.1.6.

b. Its initial enrichment is less than that indicated by Table 2.1.6 for the MPC it is intended to be stored in.

c. The period from discharge is greater than or equal to the minimum cooling time listed in Table 2.1.6, and the decay heat is equal to or less than the value stated in Figure 2.1.8 for a given cooling time.

d. The average burnup of the fuel assembly is equal to or less than the burnup specified in Figure 2.1.6 for a given cooling time.

A damaged fuel assembly shall meet the characteristics specified in Table 2.1.7 for storage in the MPC-68. Fuel debris shall meet the characteristics specified in Table 2.1.7 for storage in the MPC-68F.

Stainless steel clad fuel assemblies shall meet the characteristics specified in Table 2.1.11 for storage in the MPC-24 or MPC-68.

MOX BWR fuel assemblies shall meet the requirements of Tables 2.1.6 and 2.1.7 for intact and damaged fuel/fuel debris, respectively.

Only control components specifically authorized by the Technical Specifications for PWR fuel are to be included with the fuel assembly. Burnable Poison Rod Assemblies (BPRAs) and Thimble Plug Devices (TPDs) are authorized for storage in the MPC-24. Fuel assemblies with BPRAs shall satisfy the more restrictive burnup and cooling time requirements in Figure 2.1.6. BPRAs and TPDs shall meet the burnup and cooling time requirements specified in the Technical Specification.

Thoria rods placed in Dresden Unit 1 Thoria Rod Canisters meeting the requirements of Table 2.1.12 are authorized for storage. Up to one Dresden Unit 1 Thoria Rod Canister plus any combination of damaged fuel assemblies in damaged fuel containers and intact fuel, up to a total of 68 may be stored.

Dresden Unit 1 fuel assemblies with one Antimony-Beryllium neutron source are authorized for loading in the MPC-68 or MPC-68F.

Table 2.1.1

PWR FUEL ASSEMBLIES EVALUATED TO DETERMINE DESIGN BASIS SNF

Assembly Class	Array Type
B&W 15x15	All
B&W 17x17	All
CE 14x14	All
CE 16x16	All
WE 14x14	All
WE 15x15	All
WE 17x17	All
St. Lucie	All
Ft. Calhoun	All
Haddam Neck (Stainless Steel Clad)	All
San Onofre 1 (Stainless Steel Clad)	All

Table 2.1.2

BWR FUEL ASSEMBLIES EVALUATED TO DETERMINE DESIGN BASIS SNF

Assembly Class	**Array Type**			
GE BWR/2-3	All 7x7	All 8x8	All 9x9	All 10x10
GE BWR/4-6	All 7x7	All 8x8	All 9x9	All 10x10
Humboldt Bay	All 6x6	All 7x7 (Zircaloy Clad)		
Dresden-1	All 6x6	All 8x8		
LaCrosse (Stainless Steel Clad)	All			

Table 2.1.3
PWR FUEL ASSEMBLY CHARACTERISTICS (Note 1)

Fuel Assembly Array and Class	**14x14 A**	**14x14 B**	**14x14 C**	**14x14 D**	**15x15 A**
Clad Material (Note 2)	Zr	Zr	Zr	SS	Zr
Design Initial U (kg/assy.) (Note 3)	≤ 407	≤ 407	≤ 425	≤ 400	≤ 464
Initial Enrichment (wt % ^{235}U)	≤ 4.6	≤ 4.6	≤ 4.6	≤ 4.0	≤ 4.1
No. of Fuel Rods (Note 5)	179	179	176	180	204
Clad O.D. (in.)	≥ 0.400	≥ 0.417	≥ 0.440	≥ 0.422	≥ 0.418
Clad I.D. (in.)	≤ 0.3514	≤ 0.3734	≤ 0.3880	≤ 0.3890	≤ 0.3660
Pellet Dia. (in.)	≤ 0.3444	≤ 0.3659	≤ 0.3805	≤ 0.3835	≤ 0.3580
Fuel Rod Pitch (in.)	≤ 0.556	≤ 0.556	≤ 0.580	≤ 0.556	≤ 0.550
Active Fuel Length (in.)	≤ 150	≤ 150	≤ 150	≤ 144	≤ 150
No. of Guide Tubes	17	17	5 (Note 4)	16	21
Guide Tube Thickness (in.)	≥ 0.017	≥ 0.017	≥ 0.038	≥ 0.0145	≥ 0.0165

Table 2.1.3 (continued)
PWR FUEL ASSEMBLY CHARACTERISTICS (Note 1)

Fuel Assembly Array and Class	**15x15 B**	**15x15 C**	**15x15 D**	**15x15 E**	**15x15 F**
Clad Material (Note 2)	Zr	Zr	Zr	Zr	Zr
Design Initial U (kg/assy.) (Note 3)	≤ 464	≤ 464	≤ 475	≤ 475	≤ 475
Initial Enrichment (wt % ^{235}U)	≤ 4.1	≤ 4.1	≤ 4.1	≤ 4.1	≤ 4.1
No. of Fuel Rods (Note 5)	204	204	208	208	208
Clad O.D. (in.)	≥ 0.420	≥ 0.417	≥ 0.430	≥ 0.428	≥ 0.428
Clad I.D. (in.)	≤ 0.3736	≤ 0.3640	≤ 0.3800	≤ 0.3790	≤ 0.3820
Pellet Dia. (in.)	≤ 0.3671	≤ 0.3570	≤ 0.3735	≤ 0.3707	≤ 0.3742
Fuel Rod Pitch (in.)	≤ 0.563	≤ 0.563	≤ 0.568	≤ 0.568	≤ 0.568
Active Fuel Length (in.)	≤ 150	≤ 150	≤ 150	≤ 150	≤ 150
No. of Guide Tubes	21	21	17	17	17
Guide Tube Thickness (in.)	≥ 0.015	≥ 0.0165	≥ 0.0150	≥ 0.0140	≥ 0.0140

Table 2.1.3 (continued)
PWR FUEL ASSEMBLY CHARACTERISTICS (Note 1)

Fuel Assembly Array and Class	**15x15 G**	**15x15 H**	**16x16 A**	**17x17A**	**17x17 B**	**17x17 C**
Clad Material (Note 2)	SS	Zr	Zr	Zr	Zr	Zr
Design Initial U (kg/assy.) (Note 3)	≤ 420	≤ 475	≤ 443	≤ 467	≤ 467	≤ 474
Initial Enrichment (wt % ^{235}U)	≤ 4.0	≤ 3.8	≤ 4.6	≤ 4.0	≤ 4.0	≤ 4.0
No. of Fuel Rods (Note 5)	204	208	236	264	264	264
Clad O.D. (in.)	≥ 0.422	≥ 0.414	≥ 0.382	≥ 0.360	≥ 0.372	≥ 0.377
Clad I.D. (in.)	≤ 0.3890	≤ 0.3700	≤ 0.3320	≤ 0.3150	≤ 0.3310	≤ 0.3330
Pellet Dia. (in.)	≤ 0.3825	≤ 0.3622	≤ 0.3255	≤ 0.3088	≤ 0.3232	≤ 0.3252
Fuel Rod Pitch (in.)	≤ 0.563	≤ 0.568	≤ 0.506	≤ 0.496	≤ 0.496	≤ 0.502
Active Fuel Length (in.)	≤ 144	≤ 150	≤ 150	≤ 150	≤ 150	≤ 150
No. of Guide Tubes	21	17	5 (Note 4)	25	25	25
Guide Tube Thickness (in.)	≥ 0.0145	≥ 0.0140	≥ 0.0400	≥ 0.016	≥ 0.014	≥ 0.020

Table 2.1.3 (continued)
PWR FUEL ASSEMBLY CHARACTERISTICS

NOTES:

1. Fuel assembly array/classes are defined in Chapter 6. All dimensions are design nominal values. Maximum and minimum dimensions are specified to bound variations in design nominal values among fuel assemblies within a given array/class.

2. Zr designates cladding material made of zirconium or zirconium alloys.

3. Design initial uranium weight is the uranium weight specified for each fuel assembly by the fuel manufacturer or reactor user. For each PWR fuel assembly, the total uranium weight limit specified in this table may be increased up to 2.0 percent for comparison with users' fuel records to account for manufacturer tolerances.

4. Each guide tube replaces four fuel rods.

5. Missing fuel rods must be replaced with dummy fuel rods that displace an equal or greater amount of water as the original fuel rods.

Table 2.1.4
BWR FUEL ASSEMBLY CHARACTERISTICS (Note 1)

Fuel Assembly Array and Class	**6x6 A**	**6x6 B**	**6x6 C**	**7x7 A**	**7x7 B**	**8x8 A**
Clad Material (Note 2)	Zr	Zr	Zr	Zr	Zr	Zr
Design Initial U (kg/assy.) (Note 3)	≤ 110	≤ 110	≤ 110	≤ 100	≤ 195	≤ 120
Maximum Planar-Average Initial Enrichment (wt. % ^{235}U)	≤ 2.7	≤ 2.7 for the UO_2 rods. See Note 4 for MOX rods	≤ 2.7	≤ 2.7	≤ 4.2	≤ 2.7
Initial Maximum Rod Enrichment (wt. % ^{235}U)	≤ 4.0	≤ 4.0	≤ 4.0	≤ 5.5	≤ 5.0	≤ 4.0
No. of Fuel Rods (Note 14)	35 or 36	35 or 36 (up to 9 MOX rods)	36	49	49	63 or 64
Clad O.D. (in.)	≥ 0.5550	≥ 0.5625	≥ 0.5630	≥ 0.4860	≥ 0.5630	≥ 0.4120
Clad I.D. (in.)	≤ 0.5105	≤ 0.4945	≤ 0.4990	≤ .4204	≤ 0.4990	≤ 0.3620
Pellet Dia. (in.)	≤ 0.4980	≤ 0.4820	≤ 0.4880	≤ 0.4110	≤ 0.4910	≤ 0.3580
Fuel Rod Pitch (in.)	≤ 0.710	≤ 0.710	≤ 0.740	≤ 0.631	≤ 0.738	≤ 0.523
Active Fuel Length (in.)	≤ 120	≤ 120	≤ 77.5	≤ 80	≤ 150	≤ 120
No. of Water Rods (Note 11)	1 or 0	1 or 0	0	0	0	1 or 0
Water Rod Thickness (in.)	≥0	≥0	N/A	N/A	N/A	≥0
Channel Thickness (in.)	≤ 0.060	≤ 0.060	≤ 0.060	≤ 0.060	≤ 0.120	≤ 0.100

Table 2.1.4 (continued)
BWR FUEL ASSEMBLY CHARACTERISTICS (Note 1)

Fuel Assembly Array and Class	**8x8 B**	**8x8 C**	**8x8 D**	**8x8 E**	**8x8 F**	**9x9 A**	**9x9 B**
Clad Material (Note 2)	Zr	Zr	Zr	Zr	Zr	Zr	Zr
Design Initial U (kg/assy.) (Note 3)	≤ 185	≤ 185	≤ 185	≤ 185	≤ 185	≤ 177	≤ 177
Maximum Planar-Average Initial Enrichment (wt. % ^{235}U)	≤ 4.2	≤ 4.2	≤ 4.2	≤ 4.2	≤ 3.6	≤ 4.2	≤ 4.2
Initial Maximum Rod Enrichment (wt. % ^{235}U)	≤ 5.0	≤ 5.0	≤ 5.0	≤ 5.0	≤ 5.0	≤ 5.0	≤ 5.0
No. of Fuel Rods (Note 14)	63 or 64	62	60 or 61	59	64	74/66 (Note 5)	72
Clad O.D. (in.)	≥ 0.4840	≥ 0.4830	≥ 0.4830	≥ 0.4930	≥ 0.4576	≥ 0.4400	≥ 0.4330
Clad I.D. (in.)	≤ 0.4295	≤ 0.4250	≤ 0.4230	≤ 0.4250	≤ 0.3996	≤ 0.3840	≤ 0.3810
Pellet Dia. (in.)	≤ 0.4195	≤ 0.4160	≤ 0.4140	≤ 0.4160	≤ 0.3913	≤ 0.3760	≤ 0.3740
Fuel Rod Pitch (in.)	≤ 0.642	≤ 0.641	≤ 0.640	≤ 0.640	≤ 0.609	≤ 0.566	≤ 0.572
Design Active Fuel Length (in.)	≤ 150	≤ 150	≤ 150	≤ 150	≤ 150	≤ 150	≤ 150
No. of Water Rods (Note 11)	1 or 0	2	1 - 4 (Note 7)	5	N/A (Note 12)	2	1 (Note 6)
Water Rod Thickness (in.)	≥ 0.034	≥ 0.00	≥ 0.00	≥ 0.034	≥ 0.0315	≥ 0.00	≥ 0.00
Channel Thickness (in.)	≤ 0.120	≤ 0.120	≤ 0.120	≤ 0.100	≤ 0.055	≤ 0.120	≤ 0.120

Table 2.1.4 (continued)
BWR FUEL ASSEMBLY CHARACTERISTICS (Note 1)

Fuel Assembly Array and Class	**9x9 C**	**9x9 D**	**9x9 E (Note 13)**	**9x9 F (Note 13)**	**10x10A**
Clad Material (Note 2)	Zr	Zr	Zr	Zr	Zr
Design Initial U (kg/assy.) (Note 3)	≤ 177	≤ 177	≤ 177	≤ 177	≤ 186
Maximum Planar-Average Initial Enrichment (wt. % ^{235}U)	≤ 4.2	≤ 4.2	≤ 4.1	≤ 4.1	≤ 4.2
Initial Maximum Rod Enrichment (wt. % ^{235}U)	≤ 5.0	≤ 5.0	≤ 5.0	≤ 5.0	≤ 5.0
No. of Fuel Rods (Note 14)	80	79	76	76	92/78 (Note 8)
Clad O.D. (in.)	≥ 0.4230	≥ 0.4240	≥ 0.4170	≥ 0.4430	≥ 0.4040
Clad I.D. (in.)	≤ 0.3640	≤ 0.3640	≤ 0.3640	≤ 0.3860	≤ 0.3520
Pellet Dia. (in.)	≤ 0.3565	≤ 0.3565	≤ 0.3530	≤ 0.3745	≤ 0.3455
Fuel Rod Pitch (in.)	≤ 0.572	≤ 0.572	≤ 0.572	≤ 0.572	≤ 0.510
Design Active Fuel Length (in.)	≤ 150	≤ 150	≤ 150	≤ 150	≤ 150
No. of Water Rods (Note 11)	1	2	5	5	2
Water Rod Thickness (in.)	≥ 0.020	≥ 0.0300	≥ 0.0120	≥ 0.0120	≥ 0.030
Channel Thickness (in.)	≤ 0.100	≤ 0.100	≤ 0.120	≤ 0.120	≤ 0.120

Table 2.1.4 (continued)
BWR FUEL ASSEMBLY CHARACTERISTICS (Note 1)

Fuel Assembly Array and Class	**10x10 B**	**10x10 C**	**10x10 D**	**10x10 E**
Clad Material (Note 2)	Zr	Zr	SS	SS
Design Initial U (kg/assy.) (Note 3)	$\leq$ 186	$\leq$ 186	$\leq$ 125	$\leq$ 125
Maximum Planar-Average Initial Enrichment (wt. % ^{235}U)	$\leq$ 4.2	$\leq$ 4.2	$\leq$ 4.0	$\leq$ 4.0
Initial Maximum Rod Enrichment (wt. % ^{235}U)	$\leq$ 5.0	$\leq$ 5.0	$\leq$ 5.0	$\leq$ 5.0
No. of Fuel Rods (Note 14)	91/83 (Note 9)	96	100	96
Clad O.D. (in.)	$\geq$ 0.3957	$\geq$ 0.3780	$\geq$ 0.3960	$\geq$ 0.3940
Clad I.D. (in.)	$\leq$ 0.3480	$\leq$ 0.3294	$\leq$ 0.3560	$\leq$ 0.3500
Pellet Dia. (in.)	$\leq$ 0.3420	$\leq$ 0.3224	$\leq$ 0.3500	$\leq$ 0.3430
Fuel Rod Pitch (in.)	$\leq$ 0.510	$\leq$ 0.488	$\leq$ 0.565	$\leq$ 0.557
Design Active Fuel Length (in.)	$\leq$ 150	$\leq$ 150	$\leq$ 83	$\leq$ 83
No. of Water Rods (Note 11)	1 (Note 6)	5 (Note 10)	0	4
Water Rod Thickness (in.)	$\geq$ 0.00	$\geq$ 0.031	N/A	$\geq$ 0.022
Channel Thickness (in.)	$\leq$ 0.120	$\leq$ 0.055	$\leq$ 0.080	$\leq$ 0.080

Table 2.1.4 (continued)
BWR FUEL ASSEMBLY CHARACTERISTICS

NOTES:

1. Fuel assembly array/classes are defined in Chapter 6. All dimensions are design nominal values. Maximum and minimum dimensions are specified to bound variations in design nominal values among fuel assemblies within a given array/class.

2. Zr designates cladding material made from zirconium or zirconium alloys.

3. Design initial uranium weight is the uranium weight specified for each fuel assembly by the fuel manufacturer or reactor user. For each PWR fuel assembly, the total uranium weight limit specified in this table may be increased up to 1.5 percent for comparison with users' fuel records to account for manufacturer tolerances.

4. $\leq$ 0.635 wt. % ^{235}U and $\leq$ 1.578 wt. % total fissile plutonium (^{239}Pu and ^{241}Pu), (wt. % of total fuel weight, i.e., UO_2 plus PuO_2).

5. This assembly class contains 74 total fuel rods; 66 full length rods and 8 partial length rods.

6. Square, replacing nine fuel rods.

7. Variable.

8. This assembly class contains 92 total fuel rods; 78 full length rods and 14 partial length rods.

9. This assembly class contains 91 total fuel rods; 83 full length rods and 8 partial length rods.

10. One diamond-shaped water rod replacing the four center fuel rods and four rectangular water cross segments dividing the assembly into four quadrants.

11. These rods may be sealed at both ends and contain Zr material in lieu of water.

12. This assembly is known as "QUAD+" and has four rectangular water cross segments dividing the assembly into four quadrants.

13. For the SPC 9x9-5 fuel assembly, each fuel rod must meet either the 9x9E or the 9x9F set of limits for clad O.D., clad I.D., and pellet diameter.

14. Missing fuel rods must be replaced with dummy fuel rods that displace an equal or greater amount of water as the original fuel rods. Storage of 6x6A, 6x6B, 6x6C, 7x7A, and 8x8A fuel assemblies with missing fuel rods are permitted provided the fuel assemblies with missing fuel rods are stored as damaged fuel assemblies or fuel debris.

Table 2.1.5

DESIGN BASIS FUEL ASSEMBLY FOR EACH DESIGN CRITERION

Criterion	MPC-68	MPC-24
Reactivity (Criticality)	GE12/14 10x10 with Partial Length Rods (Class 10x10A)	B&W 15x15 (Class 15x15F)
Source Term (Shielding)	GE 7x7 (Class 7x7B)	B&W 15x15 (Class 15x15F)
Decay Heat (Thermal-Hydraulic)	GE 7x7 (Class 7x7B)	B&W 15x15 (Class 15x15F)

Table 2.1.6
CHARACTERISTICS FOR DESIGN BASIS INTACT ZIRCALOY CLAD FUEL ASSEMBLIES

	MPC-68	MPC-24
PHYSICAL PARAMETERS:		
Max. assembly width† (in.)	5.85	8.54
Max. assembly length† (in.)	176.2	176.8
Max. assembly weight†† (lb.)	700	1680
Max. active fuel length† (in.)	150	150
Fuel rod clad material	Zircaloy	Zircaloy
RADIOLOGICAL AND THERMAL CHARACTERISTICS:		
	MPC-68	**MPC-24**
Max. initial enrichment (wt% ^{235}U)	4.2 2.7 (Assembly Classes 6x6A, 6x6B†††, 6x6C, 7x7A, 8x8A)	See Table 2.1.3
Max. heat generation (W)	Figure 2.1.8 115 (Assembly Classes 6x6A, 6x6B, 6x6C, 7x7A, 8x8A) 183.5 (Assembly Class 8x8F)	Figure 2.1.8
Max. average burnup (MWD/MTU)	See Figure 2.1.6 30,000 (Assembly Classes 6x6A, 6x6B, 6x6C, 7x7A, 8x8A) 27,500 (Assembly Class 8x8F)	See Figure 2.1.6
Min. cooling time (years)	See Figure 2.1.6 18 (Assembly Classes 6x6A, 6x6B, 6x6C, 7x7A, 8x8A) 10 (Assembly Class 8x8F)	See Figure 2.1.6

† Unirradiated nominal design dimensions are shown.

Table 2.1.7

DESIGN CHARACTERISTICS FOR DAMAGED ZIRCALOY CLAD FUEL ASSEMBLIES AND BWR ZIRCALOY CLAD FUEL DEBRIS

	MPC-68 (Damaged Fuel)	MPC-68F (Fuel Debris)
PHYSICAL PARAMETERS:		
Max. assembly width† (in.)	4.7	4.7
Max. assembly length† (in.)	135	135
Max. assembly weight†† (lb.)	400	400
Max. active fuel length† (in.)	110	110
Fuel rod clad material	Zircaloy	Zircaloy
RADIOLOGICAL AND THERMAL CHARACTERISTICS:		
Max. heat generation (W)	115	115
Min. cooling time (yr)	18	18
Max. initial enrichment (w/o ^{235}U) for UO_2 rods	2.7	2.7
Max. initial enrichment for MOX rods	0.612 wt.% ^{235}U 1.578 wt. % Total Fissile Plutonium	0.612 wt.% ^{235}U 1.578 wt. % Total Fissile Plutonium
Max. average burnup (MWD/MTU)	30,000	30,000

Note:

1. A maximum of four (4) damaged fuel containers with BWR zircaloy clad fuel debris may be stored in the MPC-68F with the remaining locations filled with undamaged or damaged fuel assemblies meeting the maximum heat generation specifications of this table.

† Dimensions envelop unirradiated nominal dimensions of Array/Class 6x6A, 6x6B, 6x6C, 7x7A, and 8x8A (Dresden Unit 1 and Humboldt Bay SNF).

†† Fuel assembly weight including hardware based on DOE MPC DPS [2.1.6]. Weight does not include damaged fuel container.

Table 2.1.8

NORMALIZED DISTRIBUTION BASED ON BURNUP PROFILE

PWR DISTRIBUTION†		
Interval	**Axial Distance From Bottom of Active Fuel (% of Active Fuel Length)**	**Normalized Distribution**
1	0% to 4-1/6%	0.5485
2	4-1/6% to 8-1/3%	0.8477
3	8-1/3% to 16-2/3%	1.0770
4	16-2/3% to 33-1/3%	1.1050
5	33-1/3% to 50%	1.0980
6	50% to 66-2/3%	1.0790
7	66-2/3% to 83-1/3%	1.0501
8	83-1/3% to 91-2/3%	0.9604
9	91-2/3% to 95-5/6%	0.7338
10	95-5/6% to 100%	0.4670

BWR DISTRIBUTION††		
Interval	**Axial Distance From Bottom of Active Fuel (% of Active Fuel Length)**	**Normalized Distribution**
1	0% to 4-1/6%	0.2200
2	4-1/6% to 8-1/3%	0.7600
3	8-1/3% to 16-2/3%	1.0350
4	16-2/3% to 33-1/3%	1.1675
5	33-1/3% to 50%	1.1950
6	50% to 66-2/3%	1.1625
7	66-2/3% to 83-1/3%	1.0725
8	83-1/3% to 91-2/3%	0.8650
9	91-2/3% to 95-5/6%	0.6200
10	95-5/6% to 100%	0.2200

† Reference 2.1.3
†† Reference 2.1.4

Table 2.1.9

SUGGESTED PWR UPPER AND LOWER FUEL SPACER LENGTHS

Fuel Assembly Type	Assembly Length w/o C.C.† (in.)	Location of Active Fuel from Bottom (in.)	Max. Active Fuel Length (in.)	Upper Fuel Spacer Length (in.)	Lower Fuel Spacer Length (in.)
CE 14x14	157	4.1	137	9.5	10.0
CE 16x16	176.8	4.7	150	0	0
BW 15x15	165.7	8.4	141.8	6.7	4.1
W 17x17 OFA	159.8	3.7	144	8.2	8.5
W 17x17 Std	159.8	3.7	144	8.2	8.5
W 17x17 V5H	160.1	3.7	144	7.9	8.5
W 15x15	159.8	3.7	144	8.2	8.5
W 14x14 Std	159.8	3.7	145.2	9.2	7.5
W 14x14 OFA	159.8	3.7	144	8.2	8.5
Ft. Calhoun	146	6.6	128	10.25	20.25
St. Lucie 2	158.2	5.2	136.7	10.25	8.05
B&W 15x15 SS	137.1	3.873	120.5	19.25	19.25
W 15x15 SS	137.1	3.7	122	19.25	19.25
W 14x14 SS	137.1	3.7	120	19.25	19.25

Note: Each user shall specify the fuel spacer lengths based on their fuel length and allowing an approximate 2 to 2-1/2-inch gap.

† C.C. is an abbreviation for Control Components. Fuel assemblies with control components may require shorter fuel spacers. Each user shall specify the fuel spacer lengths based on their fuel length and any control components and allowing an approximate 2-inch gap.

Table 2.1.10

SUGGESTED BWR UPPER AND LOWER FUEL SPACER LENGTHS

Fuel Assembly Type	Assembly Length (in.)	Location of Active Fuel from Bottom (in.)	Max. Active Fuel Length (in.)	Upper Fuel Spacer Length (in.)	Lower Fuel Spacer Length (in.)
GE/2-3	171.2	7.3	150	4.8	0
GE/4-6	176.2	7.3	150	0	0
Dresden 1	134.4	11.2	110	18.0	28.0
Humboldt Bay	95.0	8.0	79.0	40.5	40.5
Dresden 1 Damaged Fuel or Fuel Debris	142.1†	11.2	110.0	17.0	16.9
Humboldt Bay Damaged Fuel or Fuel Debris	105.5†	8.0	79.0	35.25	35.25
LaCrosse	102.5	10.5	83.0	37.0	37.5

Note: Each user shall specify the fuel spacer lengths based on their fuel length and allowing an approximate 2 to 2-1/2-inch gap.

† Fuel assembly length includes the damaged fuel container.

Table 2.1.11

DESIGN CHARACTERISTICS FOR STAINLESS STEEL CLAD FUEL ASSEMBLIES

	BWR MPC-68	PWR MPC-24
PHYSICAL PARAMETERS:		
Max. assembly width† (in.)	5.62	8.42
Max. assembly length† (in.)	102.5	138.8
Max. assembly weight†† (lb.)	400	1421
Max. active fuel length† (in.)	83	122
RADIOLOGICAL AND THERMAL CHARACTERISTICS:		
Max. heat generation (W)	95	575 (MPC-24)
Min. cooling time (yr)	10	9 at 30,000 MWD/MTU (MPC-24) 15 at 40,000 MWD/MTU (MPC-24)
Max. initial enrichment (wt.% ^{235}U)	4.0	4.0
Max. average burnup (MWD/MTU)	22,500	40,000

† Dimensions are unirradiated nominal dimensions.
†† Fuel assembly weight including hardware based on DOE MPC DPS [2.1.6].

Table 2.1.12

DESIGN CHARACTERISTICS FOR THORIA RODS IN D1 THORIA ROD CANISTERS

PARAMETER	MPC-68 or MPC-68F
Cladding Type	Zircaloy (Zr)
Composition	98.2 wt.% ThO_2, 1.8 wt.% UO_2 with an enrichment of 93.5 wt. % ^{235}U
Number of Rods Per Thoria Canister	$\leq$ 18
Decay Heat Per Thoria Canister	$\leq$ 115 watts
Post-Irradiation Fuel Cooling Time and Average Burnup Per Thoria Canister	Cooling time $\geq$ 18 years and average burnup $\geq$ 16,000 MWD/MTIHM
Initial Heavy Metal Weight	$\leq$ 27 kg/canister
Fuel Cladding O.D.	$\geq$ 0.412 inches
Fuel Cladding I.D.	$\leq$ 0.362 inches
Fuel Pellet O.D.	$\leq$ 0.358 inches
Active Fuel Length	$\leq$ 111 inches
Canister Weight	$\leq$ 550 lbs., including Thoria Rods

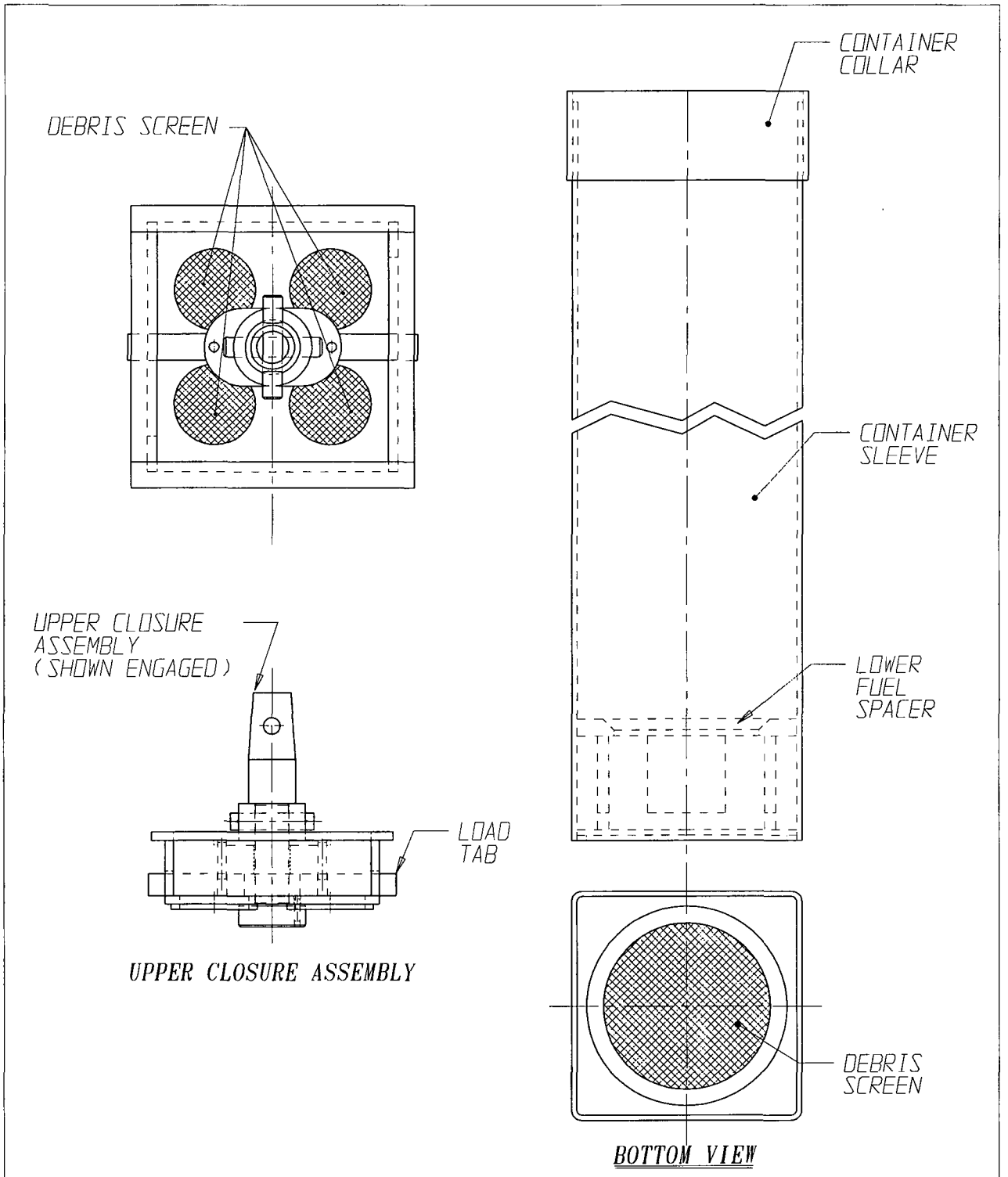

FIGURE 2.1.1; DAMAGED FUEL CONTAINER FOR DRESDEN UNIT-1/ HUMBOLDT BAY SNF

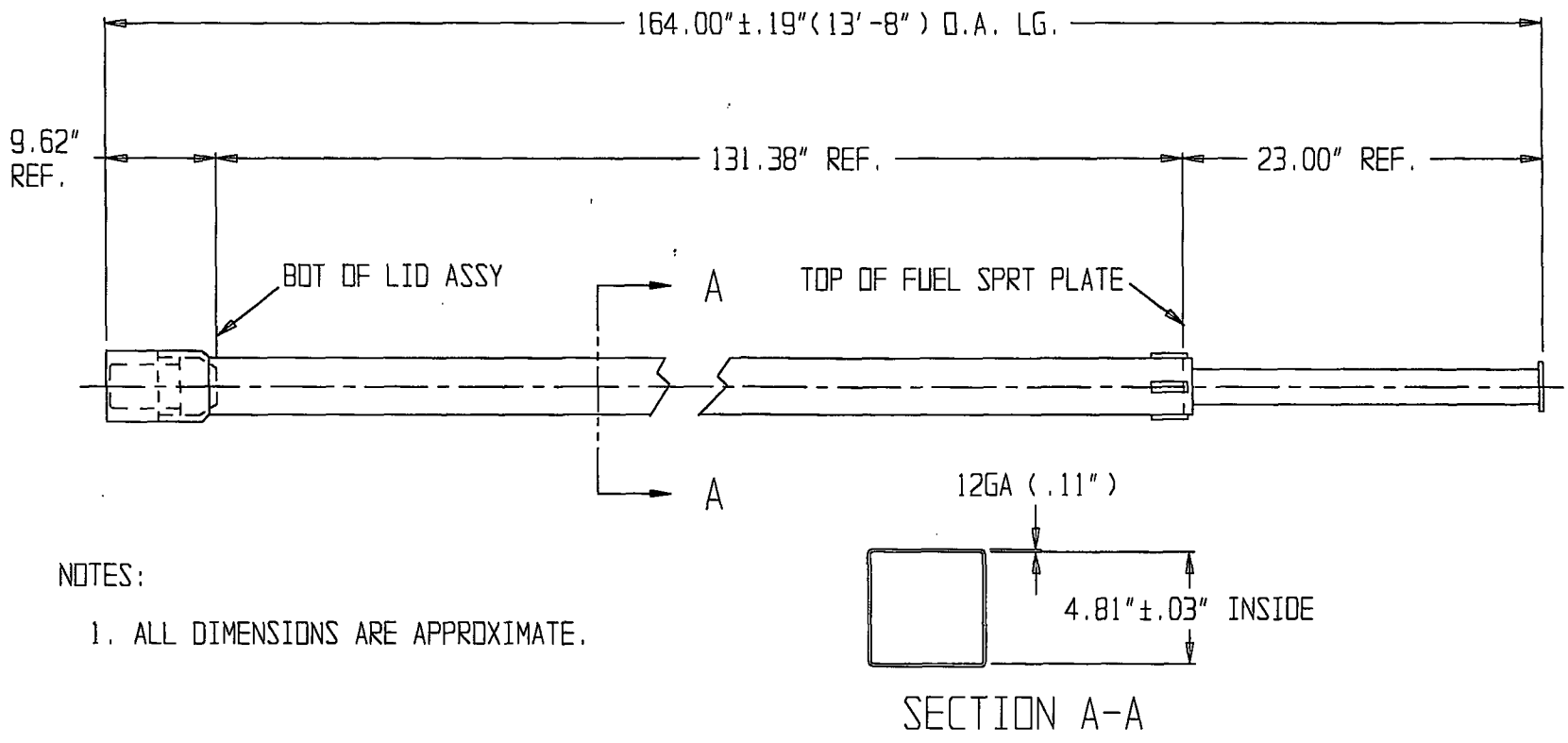

FIGURE 2.1.2; TN DAMAGED FUEL CANISTER FOR DRESDEN UNIT-1

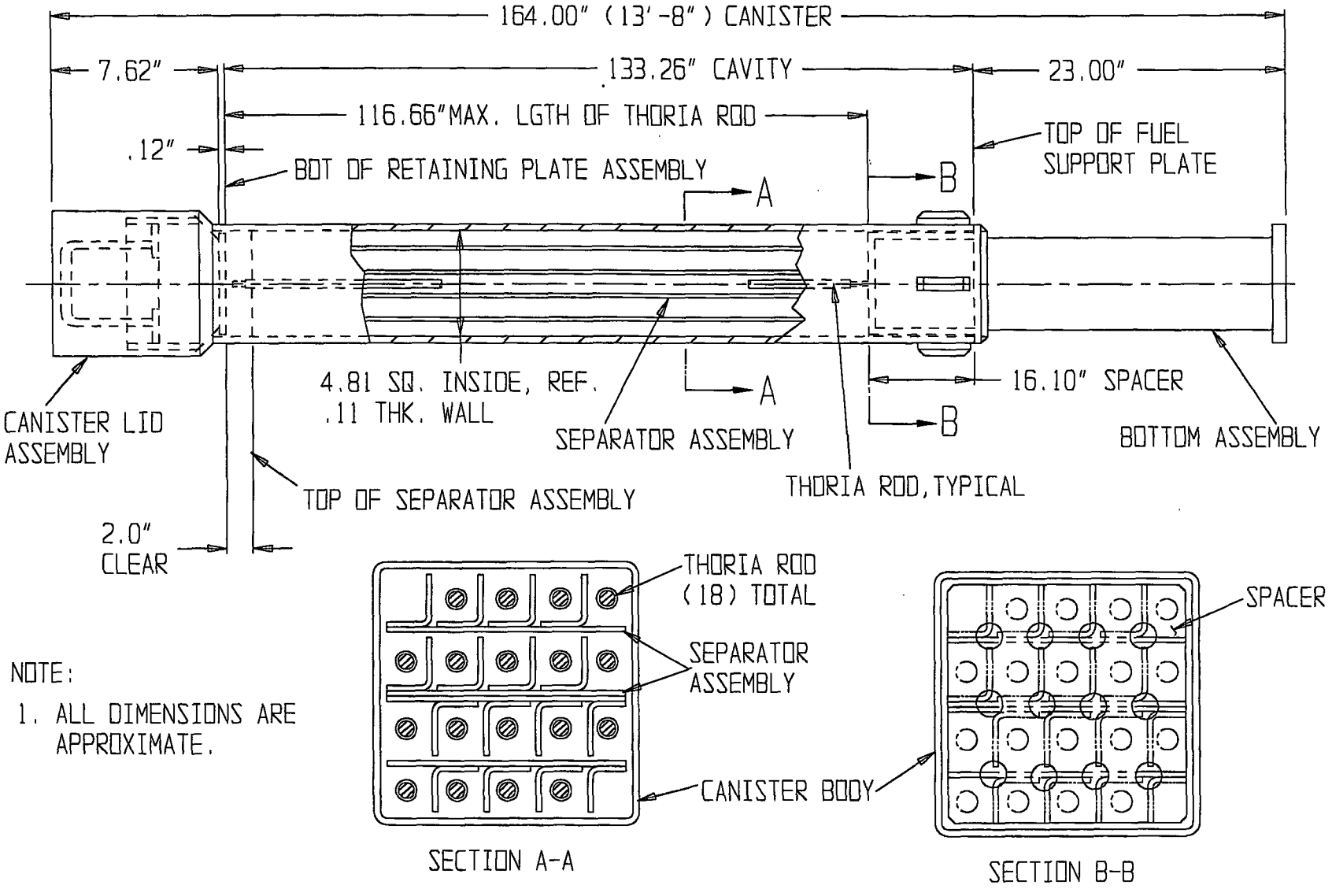

NOTE:

1. ALL DIMENSIONS ARE APPROXIMATE.

FIGURE 2.1.2A; TN THORIA ROD CANISTER FOR DRESDEN UNIT-1

REPORT HI-2012610

REVISION 0

F:\PROJECTS\GENERIC\HI2012610\CH_2\2_1_2A

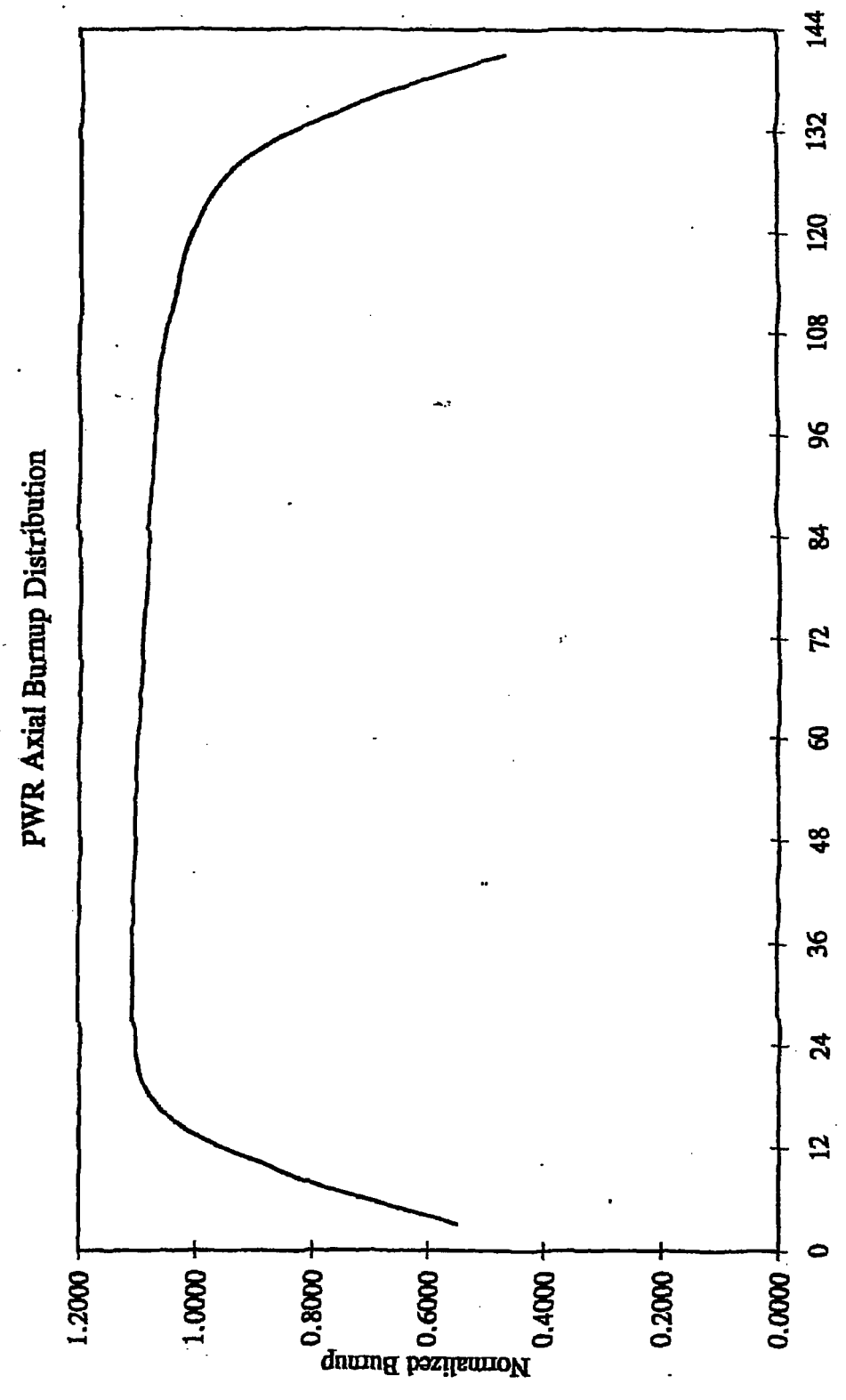

Figure 2.1.3; PWR Axial Burnup Profile with Normalized Distribution

REPORT HI-2012610

REVISION 0

\PROJECTS\GENERIC\HI2012610\CH. 2\2_1_3

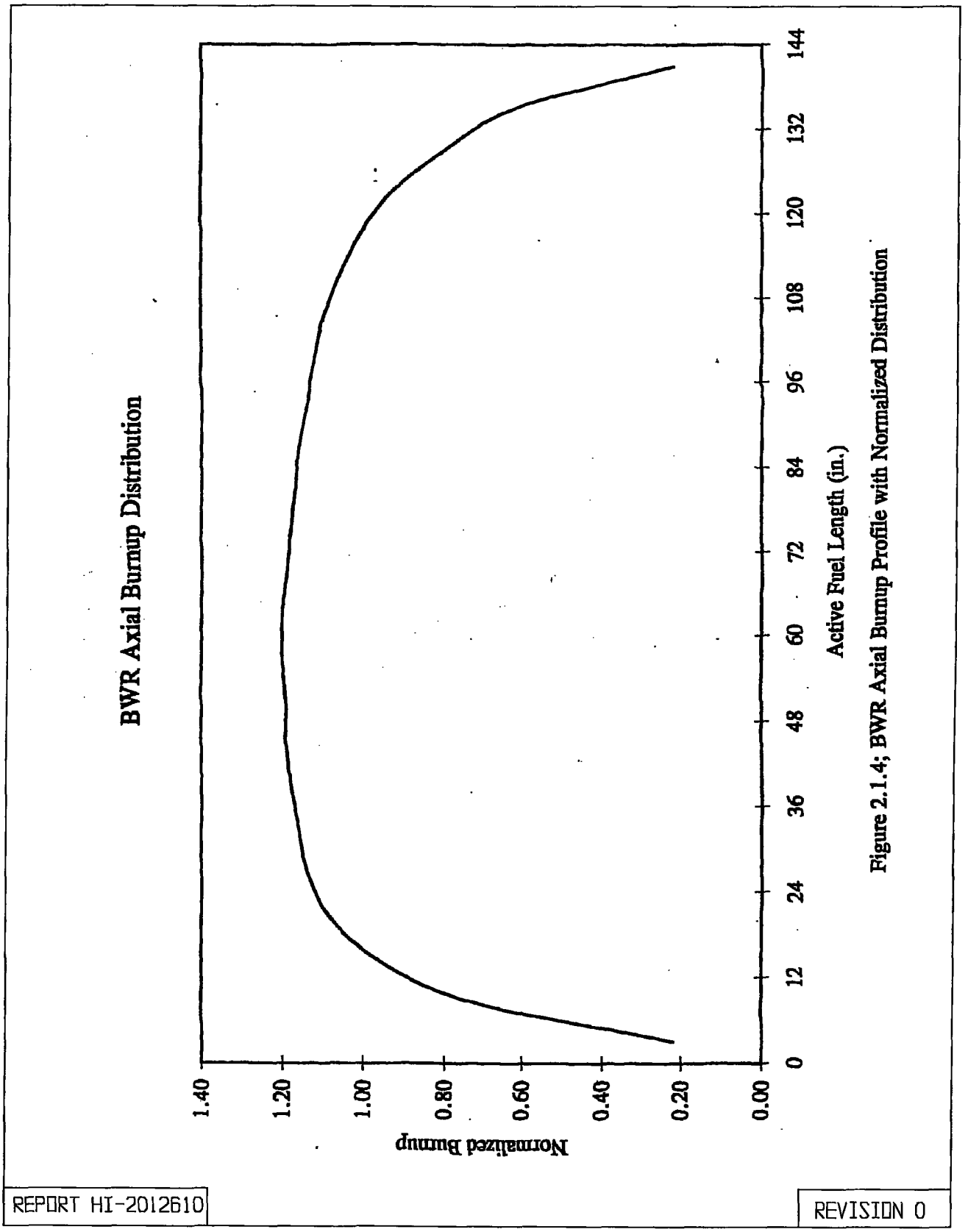

Figure 2.1.4; BWR Axial Burnup Profile with Normalized Distribution

\PROJECTS\GENERIC\HI2012610\CH. 2\2_1_4

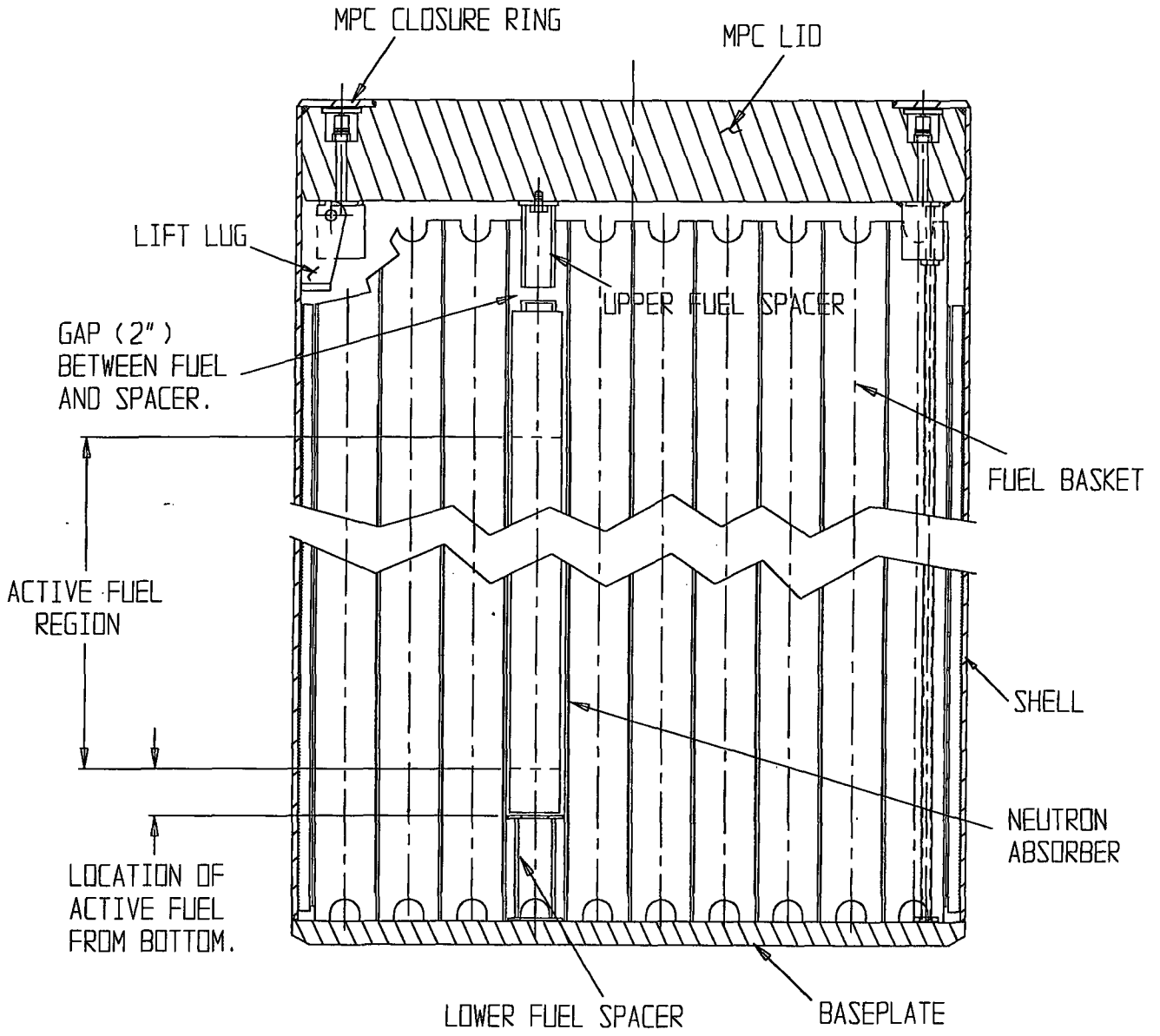

FIGURE 2.1.5; HI-STAR 100 MPC WITH UPPER AND LOWER FUEL SPACERS

REPORT HI-2012610

ILLUSTRATIVE BURNUP AND COOLING TIME FOR DECAY HEAT AND RADIATION SOURCE TERMS

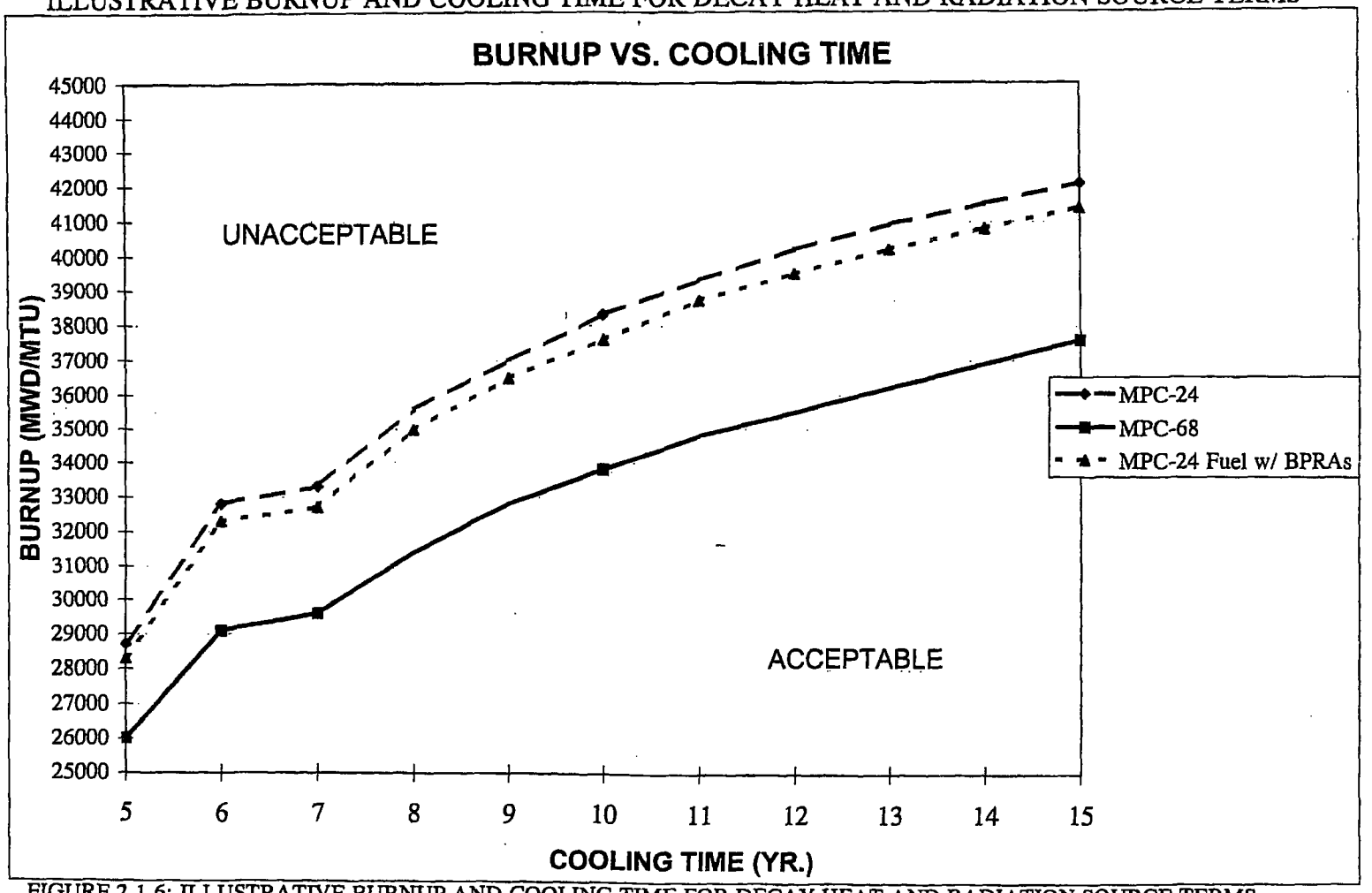

FIGURE 2.1.6; ILLUSTRATIVE BURNUP AND COOLING TIME FOR DECAY HEAT AND RADIATION SOURCE TERMS

REVISION 0

\PROJECTS\GENERIC\HI2012610\CH. 2\2_1_6

FIGURE 2.1.7; DELETED

Figure 2.1.8; Acceptable Decay Heat Load Per Assembly

2.2 HI-STAR 100 DESIGN CRITERIA

The HI-STAR 100 System is engineered for unprotected outside storage for the duration of its design life. Accordingly, the cask system is designed to withstand normal, off-normal, and environmental phenomena or accident conditions of storage. Normal conditions include the conditions that are expected to occur regularly or frequently in the course of normal operation. Off-normal conditions include those infrequent events that could reasonably be expected to occur during the lifetime of the cask system. Environmental phenomena or accident conditions includes events that are postulated because their consideration establishes a conservative design basis.

Normal condition loads act in combination with all other loads. Off-normal condition loads and environmental phenomena or accident condition loads are applied alone. However, loads which occur as a result of the same phenomena are applied simultaneously. For example, the tornado wind loads are applied in combination with the tornado missile loads.

Design criteria are satisfied if the specified allowable limits are not exceeded.

2.2.1 Normal Condition Design Criteria

2.2.1.1 Dead Weight

The HI-STAR 100 System must withstand the static loads due to the weight of each of its components.

2.2.1.2 Handling

The HI-STAR 100 System must withstand loads experienced during routine handling. Normal handling includes lifting, upending/downending, and transfer to the ISFSI of the loaded HI-STAR 100 System. The loads shall be increased by 15% to include any dynamic effects from the lifting operations as directed by CMAA #70 [2.2.1].

2.2.1.3 Pressure

Pressures on the HI-STAR 100 System components depend on the bulk temperature of the helium gas and any environmental or internal factor capable of causing a pressure change. The HI-STAR 100 System must be capable of withstanding normal condition pressures.

The MPC internal pressure is dependent on the initial volume of cover gas (helium), the volume of fill gas in the fuel rods, the fraction of fission gas released from the fuel matrix, the number of fuel rods assumed to have ruptured, and temperature. The normal condition MPC internal design pressure bounds the cumulative effects of the maximum fill gas volume, normal environmental ambient temperatures, the maximum MPC heat load, and an assumed 1% of the intact fuel rods ruptured with 100% of the rod fill gas and 30% of the significant radioactive gases (e.g., H^3, Kr, and Xe) released in accordance with NUREG-1536. The off-normal condition MPC internal design pressure bounds the cumulative effects of the maximum fill gas volume, off-normal environmental ambient temperatures, the maximum MPC heat load, and an assumed 10% of the intact fuel rods

ruptured with 100% of the rod fill gas and 30% of the significant radioactive gases (e.g., H^3, Kr, and Xe) released in accordance with NUREG-1536. For conservatism, the MPC normal internal design pressure bounds both normal and off-normal conditions. Therefore, the normal and off-normal condition MPC internal pressures are set equal for analysis purposes. Table 2.2.1 provides the design pressures for the HI-STAR 100 System.

For the storage of damaged Dresden Unit 1 or Humboldt Bay BWR fuel assemblies or fuel debris (Assembly Classes 6x6A, 6x6B, 6x6C, 7x7A, and 8x8A) in a damaged fuel container, it is conservatively assumed that 100% of the fuel rods are ruptured with 100% of the rod fill gas and 30% of the significant radioactive gases (e.g., H^3, Kr, and Xe) released for both normal and off-normal conditions. This condition is bounded by the pressure calculation for design basis intact fuel with 100% of the fuel rods ruptured in all 68 of the BWR fuel assemblies. It is shown in Chapter 4 that the normal condition design pressure is not exceeded with 100% of the fuel rods ruptured in all 68 of the design basis BWR fuel assemblies. Therefore, rupture of 100% of the fuel rods in the damaged fuel assemblies or fuel debris will not cause the MPC internal pressure to exceed the normal design pressure.

The MPC internal design pressure under accident conditions is discussed in Subsection 2.2.3, as a result of the fuel rod rupture and fire accident.

The MPC external pressure is equivalent to the overpack internal pressure, since this pressure exists in the annulus between the MPC and the overpack. During loading of the HI-STAR 100 System, the annulus is evacuated, dried, and pressurized with helium. The helium gas in the annulus is compressed due to the difference in the thermal expansion of the MPC and the overpack when the HI-STAR 100 System has a positive heat load (See Subsection 3.4.4.2.1). Therefore, the normal and off-normal pressure is specified in Table 2.2.1 above the initial fill pressure (10 psig). The ratio of the initial fill pressure to the normal design pressure is 1:4. Therefore, using the ideal gas law, the volume must decrease to 1/4 its initial size to reach the normal design pressure at a constant temperature. Subsection 3.4.4.2.1 provides the reduction in the annulus due to thermal expansion and it is demonstrated that the annulus does not decrease to 1/4 its initial size. The only other cause for a pressure increase is the fire accident conditions. The elevated accident condition pressure bounds the pressure developed as a result of the fire accident condition.

The overpack external pressure is a function of environmental conditions which may produce a pressure loading. The normal and off-normal condition external design pressure is set at ambient standard pressure (1 atmosphere).

The overpack neutron shield enclosure contains the neutron shield material Holtite-A. The enclosure is equipped with two rupture disks with a relief pressure at 30 psig. The design temperature of the neutron shield material is set sufficiently low to ensure that under normal and off-normal condition any potential off-gassing will be negligible. However, the overpack neutron shield enclosure is designed to withstand 30 psig under normal conditions. Under accident conditions, where the neutron shield material bulk temperature may exceed its design temperature, the redundant rupture disks will relieve ensuring that the pressure will not exceed the overpack neutron shield enclosure design pressure.

2.2.1.4 Environmental Temperatures

To evaluate the long-term effects of ambient temperatures on the HI-STAR 100 System, an upper bound value on the annual average ambient temperatures for the continental United States is used. The normal temperature specified in Table 2.2.2 is bounding for all reactor sites in the contiguous United States. The "normal" temperature set forth in Table 2.2.2 is intended to ensure that it is greater than the annual average of ambient temperatures at any location in the continental United States. In the northern region of the U.S., the design basis "normal" temperature used in this FSAR will be exceeded only for brief periods, whereas in the southern U.S., it may be straddled daily in summer months. Inasmuch as the sole effect of the "normal" temperature is on the computed fuel cladding temperature to establish long-term fuel integrity, it should not lie below the time averaged yearly mean for the ISFSI site. Previously licensed cask systems have employed lower "normal" temperatures (viz. 75 °F in Docket 72-1007) by utilizing national meteorological data.

Confirmation of the site-specific annual average ambient temperature is to be performed by the licensee, in accordance with 10CFR72.212. The annual average temperature is combined with insolation specified in 10CFR71.71 averaged over 24 hours in accordance with NUREG-1536 to establish the normal condition temperatures in the HI-STAR 100 System.

2.2.1.5 Design Temperatures

The ASME Boiler and Pressure Vessel Code (ASME Code) requires that the value of the vessel design temperature be established with appropriate consideration for the effect of heat generation internal or external to the vessel. The decay heat load from the spent nuclear fuel is the internal heat generation source for the HI-STAR 100 System. The ASME Code (Section III, Paragraph NCA-2142) requires the Design Temperature to be set at or above the maximum through thickness mean metal temperature of the pressure part under normal service (Level A) condition. Consistent with the terminology of NUREG-1536, this temperature is referred to as the "Design Temperature for Normal Conditions". Conservative calculations of the steady-state temperature field in the HI-STAR 100 System, under assumed environmental normal temperatures with the maximum decay heat load,
result in HI-STAR component temperatures below the normal condition design temperatures for the HI-STAR 100 System defined in Table 2.2.3.

Maintaining fuel rod cladding integrity is also a design consideration. The maximum fuel rod cladding temperature limits for normal conditions are, based on Pacific Northwest Laboratory Reports [2.0.5 and 2.0.7], summarized in Table 2.2.3. The PNL CSFM (Commercial Spent Fuel Management) methodology is shown to bound the DCCG (Diffusion Controlled Cavity Growth) methodology outlined in the LLNL report [2.0.6] in Section 4.3. Maximum stainless steel fuel rod cladding temperature limits recommended in EPRI report [2.2.2] are greater than allowable zircaloy fuel cladding temperature limits. However, in this FSAR the zircaloy fuel cladding temperature limits are conservatively applied to the stainless steel clad fuel. A detailed description of the maximum fuel rod cladding temperature limits determination is provided in Section 4.3.

2.2.1.6 Snow and Ice

The HI-STAR 100 System must be capable of withstanding pressure loads due to snow and ice. ASCE 7-88 (formerly ANSI A58.1) [2.2.3] provides empirical formulas and tables to compute the effective design pressure on the overpack due to the accumulation of snow for the contiguous U.S. and Alaska. Typical calculated values for heated structures such as the HI-STAR 100 System range from 50 to 70 pounds per square foot. For conservatism, the snow pressure loading is set at a level in Table 2.2.8, which bounds the ASCE 7-88 recommendation.

2.2.2 Off-Normal Conditions Design Criteria

As the HI-STAR 100 System is passive, loss of power and instrumentation failures are not defined as off-normal conditions. Off-normal condition design criteria are defined in the following subsections.

A discussion of the effects of each off-normal condition is provided in Section 11.1. Section 11.1 also provides the corrective action for each off-normal condition. The location of the detailed analysis for each event is referenced in Section 11.1.

2.2.2.1 Pressure

The HI-STAR 100 System must withstand loads due to off-normal pressure. The MPC and overpack off-normal pressure is bounded by the MPC and overpack normal condition design pressure specified in Table 2.2.1. For the MPC off-normal internal pressure, ten percent of the fuel rods are assumed to be ruptured with 100% of the fill gas and 30% of the significant radioactive gases (e.g., H^3, Kr, and Xe) released in accordance with NUREG-1536.

2.2.2.2 Environmental Temperatures

Limits on the peaks in the time-varying ambient temperature at an ISFSI site are recognized in the FSAR in the specification of the off-normal temperatures. The lower bound off-normal temperature is defined as the minimum of the 72-hour average of the ambient temperature at an ISFSI site. Likewise, the upper bound off-normal temperature is defined by the maximum of 72-hour average of the ambient temperature. The lower and upper bound off-normal temperatures listed in Table 2.2.2 are intended to cover all ISFSI sites in the continental U.S. The 72-hour average temperature used in the definition of the off-normal temperature recognizes the considerable thermal inertia of the HI-STAR 100 System which reduces the effect of undulations in instantaneous temperature on the internals of the MPC.

The HI-STAR 100 System must withstand off-normal environmental temperatures. The off-normal environmental temperatures are specified in Table 2.2.2. The lower bound temperature occurs with no solar loads and the upper bound temperature occurs with steady-state insolation. Each bounding temperature is assumed in the analysis to persist for a duration sufficient to allow the system to reach steady-state temperatures.

2.2.2.3 Design Temperatures

In addition to the normal design temperature, we also define an "off-normal/accident condition temperature" pursuant to the provisions of NUREG-1536 and Regulatory Guide 3.61. This is, in effect, the short-term temperature which may exist during a transition state or a transient event (examples of such instances are short-term temperature excursion during canister vacuum drying and backfilling operations (transition state) and fire (transient event)). The off-normal/accident design temperatures of Table 2.2.3 are set down to bound the maximax (maximum in time and space) value of the thru-thickness average temperature of the structural or non-structural part, as applicable, during a short-term event. These enveloping values, therefore, will bound the maximum temperature reached anywhere in the part, excluding skin effects during or immediately after, a short-term event.

2.2.2.4 Leakage of One Seal

The HI-STAR 100 System must withstand leakage of one seal in the radioactive material confinement boundary.

The HI-STAR 100 confinement boundary is defined by the MPC shell, baseplate, MPC lid, port cover plates, and closure ring. Most confinement boundary welds are inspected by radiography or ultrasonic examination. Field welds are examined by the liquid penetrant method on the root and final pass, if more than one weld pass is required. In addition to liquid penetrant examination of the root and final weld layers, the MPC lid-to-shell weld is leakage tested, hydrostatic tested, and volumetrically (or multi-layer liquid penetrant) examined. The vent and drain port cover plates are leakage tested in addition to the liquid penetrant examination. These inspection and testing techniques are performed to verify the integrity of the confinement boundary.

The helium retention boundary is defined by the overpack baseplate, inner shell, top flange, vent and drain port plugs, and bolted closure plate containing two concentric seals. All welds that form a part of the helium retention boundary are examined by radiography. The overpack welds and seals are helium leakage tested during fabrication to verify their integrity. Helium leakage tests of all overpack closure seals are performed following each loading sequence.

2.2.3 Environmental Phenomena and Accident Condition Design Criteria

Environmental phenomena and accident condition design criteria are defined in the following subsections.

The minimum acceptance criteria for the evaluation of the accident condition design criteria are that the MPC confinement boundary maintains radioactive material confinement, the MPC fuel basket structure maintains the fuel contents subcritical, and the stored SNF can be retrieved by normal means.

A discussion of the effects of each environmental phenomena and accident condition is provided in Section 11.2. The consequences of each accident or environmental phenomena are evaluated against the requirements of 10CFR72.106 and 10CFR20. Section 11.2 also provides the corrective action for each event. The location of the detailed analysis for each event is referenced in Section 11.2.

2.2.3.1 Handling Accident

The HI-STAR 100 System must withstand loads due to a handling accident. Even though the loaded HI-STAR 100 System will be handled in accordance with approved, written procedures and will use lifting equipment which complies with ANSI N14.6, certain drop events are considered herein to demonstrate the defense-in-depth features of the HI-STAR design.

The loaded overpack will be handled so that the bottom of the cask is at a height less than the calculated vertical handling limit above the floor. The horizontal handling limit is specified to limit the height the loaded overpack can be lifted while in the horizontal position. For conservatism, the postulated drop events assume that the loaded HI-STAR 100 System falls freely from the vertical or horizontal handling limit height before impacting a thick reinforced concrete pad. Table 2.2.17 provides the acceptable carry heights for the loaded HI-STAR 100 System.

The magnitude of loadings induced into the HI-STAR 100 System due to drop events is heavily influenced by the compliance characteristics of the impacted surface. The concrete pad for storing the HI-STAR 100 System shall comply with the requirements of Table 2.2.9 to ensure that impactive and impulsive loads under accident events such as cask drop and non-mechanistic tip-over are less than those calculated by the dynamic models used in the structural qualifications.

2.2.3.2 Tip-Over

The HI-STAR 100 System is demonstrated to remain kinematically stable under the design basis environmental phenomena (tornado, earthquake, etc.). However, the cask must also withstand impact due to a postulated tip-over event. The structural integrity of a loaded HI-STAR 100 System after a tip-over onto a reinforced concrete pad is demonstrated using a side drop bounding analysis. The cask tip-over is not postulated as an outcome of any environmental phenomenon or accident condition. The cask tip-over is a non-mechanistic event.

During original licensing for the HI-STAR 100 System, a single set of ISFSI pad and subgrade design parameters (now labeled Set A) was established. Experience has shown that achieving a maximum concrete compressive strength (at 28 days) of 4,200 psi can be difficult. Therefore, a second set of ISFSI pad and subgrade design parameters (labeled Set B) has been developed. The Set B ISFSI parameters include a thinner concrete pad and less stiff subgrade, which allow for a higher concrete compressive strength. Cask deceleration values for all design basis drop and tipover events have been verified to be less than or equal to the design limit of 60 g's at the top of the fuel basket for both sets of ISFSI pad and subgrade design parameters.

The original set and the new set (Set B) of acceptable ISFSI pad and subgrade design parameters are specified in Table 2.2.9. Users may design their ISFSI pads and subgrade in compliance with either parameter Set A or Set B. Alternatively, users may design their site-specific ISFSI pad and subgrade using any combination of design parameters that result in a structurally competent pad that meets the provisions of ACI 318 and also limits the deceleration of the cask to less than or equal to 60 g's for the design basis drop and tipover events. The structural analyses for site-specific ISFSI pad design shall be performed using methodologies consistent with those described in this FSAR, as applicable.

2.2.3.3 Fire

The possibility of a fire accident near an ISFSI site is considered to be extremely remote due to the absence of significant combustible materials. The only credible concern is related to a transport vehicle fuel tank fire engulfing a cask while it is being moved to the ISFSI.

The HI-STAR 100 System must withstand temperatures due to a fire event. The fire accident for storage is conservatively specified to be the result of the spillage and ignition of 50 gallons of combustible transporter fuel. The HI-STAR overpack surfaces are considered to receive an incident radiation and convection heat flux from the fire. Table 2.2.8 provides the fire duration based on the amount of flammable materials assumed. The temperature of the fire is assumed to be 1475 °F in accordance with 10CFR71.73.

The accident condition design temperatures for the HI-STAR 100 System, and the fuel rod cladding limits are specified in Table 2.2.3. The specified accident condition fuel cladding temperature limit is the short-term temperature limit based on a PNL report [2.0.7].

2.2.3.4 Partial Blockage of MPC Basket Vent Holes

The HI-STAR 100 System is designed to withstand reduction of flow area due to partial blockage of the MPC basket vent holes. As the MPC basket vent holes are internal to the confinement barrier, the only events that could partially block the vents are fuel cladding failure and debris associated with this failure, or crud. The HI-STAR 100 System maintains the SNF in an inert environment with fuel rod cladding temperatures below accepted values. Therefore, there is no credible mechanism for gross fuel cladding degradation during storage in the HI-STAR 100 System. For the storage of damaged BWR fuel assemblies or fuel debris, the assemblies and fuel debris will be placed in damaged fuel containers prior to placement in the MPC. The damaged fuel container is equipped with fine mesh screens which ensure that the damaged fuel and fuel debris will not be escape to block the MPC basket vent holes. In addition, each MPC will be loaded once for long-term storage and, therefore, buildup of crud in the MPC due to numerous loadings is precluded. Using crud quantities reported in an Empire State Electric Energy Research Corporation Report [2.2.4], a layer of crud of conservative depth is assumed to partially block the MPC basket vent holes. The crud depths for the different MPCs are listed in Table 2.2.8.

2.2.3.5 Tornado

The HI-STAR 100 System must withstand pressures, wind loads, and missiles generated by a tornado. The prescribed design basis tornado and wind loads for the HI-STAR 100 System are consistent with NRC Regulatory Guide 1.76 [2.2.5], ANSI 57.9 [2.2.6], and ASCE 7-88 [2.2.3]. Table 2.2.4 provides the wind speeds and pressure drop which the HI-STAR 100 System must withstand while maintaining kinematic stability. The small pressure drop is bounded by the accident condition overpack internal design pressure.

The stability of the HI-STAR 100 System must be demonstrated under impact from tornado-generated missiles in conjunction with the wind loadings. Standard Review Plan (SRP) 3.5.1.4 of NUREG-0800 [2.2.7] stipulates that the postulated missiles include at least three objects: a massive high kinetic energy missile which deforms on impact (large missile), a rigid missile to test

penetration resistance (penetrant missile), and a small rigid missile of a size sufficient to pass through any openings in the protective barriers (micro-missile). SRP 3.5.1.4 suggests an automobile for a large missile, an artillery shell for the penetrant missile, and a solid sphere for the small rigid missile, all impacting at 35% of the maximum horizontal wind speed of the design basis tornado. Table 2.2.5 provides the missile data used in the analysis, which is based on the above SRP guidelines.

The effects of a tornado missile are considered to bound the effects of a light general aviation airplane crashing on an ISFSI facility as specified in NUREG-1536.

2.2.3.6 Flood

The HI-STAR 100 System must withstand pressure and water forces associated with a flood. Resultant loads on the HI-STAR 100 System consist of buoyancy effects, static pressure loads, and pressure due to water velocity. The flood is assumed to deeply submerge the HI-STAR 100 System (see Table 2.2.8). The flood water depth is based on the submergence requirement of 10CFR71. This condition corresponds to a hydrostatic pressure which is bounded by the overpack external pressure stated in Table 2.2.1.

It must be shown that the overpack does not collapse, buckle, or allow water in-leakage under the hydrostatic pressure from the flood.

The flood water is assumed to be nonstagnant. The maximum allowable flood water velocity is determined by calculating the equivalent pressure loading required to slide or tip over the HI-STAR 100 System. The design basis flood water velocity is stated in Table 2.2.8. Site-specific safety reviews performed by the licensee must confirm that flood parameters do not exceed the flood depth, slide, or tip-over forces.

Most reactor sites are hydrologically characterized as required by Paragraph 100.10(c) of 10CFR100 [2.2.8] and further articulated in Reg. Guide 1.59, "Design Basis Floods for Nuclear Power Plants" [2.2.9] and Reg. Guide 1.102, "Flood Protection for Nuclear Power Plants" [2.2.10]. It is assumed that a complete characterization of the ISFSI's hydrosphere including the effects of hurricanes, floods, seiches and tsunamis is available to enable a site-specific evaluation of the HI-STAR 100 System for kinematic stability. An evaluation for tsunamis[†] for certain coastal sites should also be performed to demonstrate that sliding or tip-over will not occur and that the maximum flood depth will not be exceeded.

Analysis for each site for such transient hydrological loadings must be made for that site. It is expected that the plant licensee will perform this evaluation under the provisions of 10CFR Part 72.212.

2.2.3.7 Seismic Design Loadings

[†] A tsunami is an ocean wave from seismic or volcanic activity or from submarine landslides. A tsunami may be the result of nearby or distant events. A tsunami loading may exist in combination with wave splash and spray, storm surge and tides.

The HI-STAR 100 must withstand loads arising due to a seismic event and must be shown not to tip over during a seismic event. Section 3.4.7 contains calculations based on conservative static "incipient tipping" calculations which demonstrate static stability. The calculations in Section 3.4.7 result in the value specified in Table 2.2.8, which provide the maximum horizontal zero period acceleration (ZPA) versus vertical acceleration multiplier above which static incipient tipping would occur. This conservatively assumes the peak acceleration values of each of the two horizontal earthquake components occur simultaneously. The maximum horizontal ZPA provided in Table 2.2.8 is the vector sum of two horizontal earthquakes.

2.2.3.8 100% Fuel Rod Rupture

The HI-STAR 100 System must withstand loads due to 100% fuel rod rupture. For conservatism, 100 percent of the fuel rods are assumed to rupture with 100% of the rod fill gas and 30 percent of the significant radioactive gases (e.g., H^3, Kr, and Xe) released in accordance with NUREG-1536.

2.2.3.9 Confinement Boundary Leakage

No credible scenario has been identified that would cause failure of the confinement system. To demonstrate the overall safety of the HI-STAR 100 System, the largest test leakage rate for the confinement boundary plus the test sensitivity is assumed as the maximum credible confinement boundary leakage rate. No credit is taken for the overpack boundary and 100 percent of the fuel rods are assumed to have failed. Under this accident condition, doses to an individual located at the boundary of the controlled area are calculated.

2.2.3.10 Explosion

The HI-STAR 100 System must withstand loads due to an explosion. The accident condition overpack external pressure specified in Table 2.2.1 bounds all credible external explosion events. There are no credible internal explosion events since all materials are compatible with the various operating environments, as discussed in Section 3.4.1. The MPC is composed of stainless steel, Boral, and aluminum alloy 1100, all of which have a long proven history of use in fuel pool at nuclear power plants. For these materials there is no credible cause for an internal explosive event.

2.2.3.11 Lightning

The HI-STAR 100 System must withstand loads due to lightning. The effect of lightning on the HI-STAR 100 System is evaluated in Chapter 11.

2.2.3.12 Burial Under Debris

The HI-STAR 100 System must withstand burial under debris. Such debris may result from floods, wind storms, or mud slides. The thermal effects of burial under debris on the HI-STAR 100 System is evaluated in Chapter 11. Siting of the ISFSI pad shall ensure that the storage location is not located near shifting soil. Burial under debris is a highly unlikely accident, but is analyzed in this FSAR.

2.2.3.13 Extreme Environmental Temperature

The HI-STAR 100 System must withstand extreme environmental temperatures. The extreme accident level temperature is specified in Table 2.2.2. The extreme accident level temperature occurs with steady-state insolation. The environmental temperature is assumed to persist for a duration sufficient to allow the system to reach steady-state temperatures. The HI-STAR 100 System has a large thermal inertia. Therefore, this temperature is assumed to persist over three days (3-day average).

2.2.4 Applicability of Governing Documents

The ASME Boiler and Pressure Vessel Code (ASME Code), 1995 Edition with Addenda through 1997, is the governing code for the structural design of the HI-STAR 100 System. The ASME Code is applied to each component consistent with the function of the component. Table 2.2.6 lists each structure, system and component (SSC) of the HI-STAR 100 System which are labeled Important to Safety, along with its function and governing Code. Some components perform multiple functions and in those cases, the most restrictive Code is applied. In accordance with NUREG/CR-6407, "Classification of Transportation Packaging and Dry Spent Fuel Storage System Components" [2.2.11] and according to importance to safety, components of the HI-STAR 100 System are classified as A, B, C, or NITS (not important to safety) in Table 2.2.6. Section 13.1 provides the criteria used to classify each item.

Table 2.2.7 lists the applicable ASME Code section and paragraph for material procurement, design, fabrication and inspection of the components of the HI-STAR 100 System that are governed by the ASME Code. The ASME Code section listed in the design column is the section used to define allowable stresses for structural analyses.

Table 2.2.15 lists the alternatives to the ASME Code for the HI-STAR 100 System and the justification for those alternatives.

2.2.5 Service Limits

In the ASME Code, plant and system operating conditions are commonly referred to as normal, upset, emergency, and faulted. Consistent with the terminology in NRC documents, this FSAR utilizes the terms normal, off-normal, and accident conditions.

The ASME Code defines four service conditions in addition to the Design Limits for nuclear components. They are referred to as Level A, Level B, Level C, and Level D service limits, respectively. Their definitions are provided in Paragraph NCA-2142.4 of the ASME Code. The four levels are used in this FSAR as follows:

a. Level A Service Limits: Level A Service Limits are used to establish allowables for normal condition load combinations.

b. Level B Service Limits: Level B Service Limits are used to establish allowables for off-normal condition load combinations.

c. Level C Service Limits: Level C Service Limits are not used.

d. Level D Service Limits: Level D Service Limits are used to establish allowables for accident condition load combinations.

The ASME Code service limits are used in the structural analyses for definition of allowable stresses and allowable stress intensities. Allowable stresses and stress intensities for structural analyses are tabulated in Chapter 3. These service limits are matched with normal, off-normal, and accident condition loads combinations in the following subsections.

The MPC confinement boundary and the overpack helium retention boundary are required to meet Section III, Class 1 stress intensity limits. Table 2.2.10 lists the stress intensity limits for the Levels A, B, and D service limits for Class 1 structures extracted from the ASME Code (1995 Edition). The limits for the MPC fuel basket, required to meet the stress intensity limits of Subsection NG of the ASME Code, are listed in Table 2.2.11. Table 2.2.12 lists allowable stress limits for the external steel structures (intermediate shells, radial channels, and outer enclosure) which are analyzed to meet the stress limits of Subsection NF, Class 3.

2.2.6 Loads

Subsections 2.2.1, 2.2.2, and 2.2.3 describe the design criteria for normal, off-normal, and accident conditions, respectively. The individual loads listed in Table 2.2.13 are defined from the design criteria. Each load is assigned a symbol for subsequent use in the load combinations.

The loadings listed in Table 2.2.13 fall into two broad categories; namely, (i) those which affect kinematic stability, and (ii) those which produce significant stresses. The loadings in the former category are principally applicable to the overpack. Wind (W), earthquake (E), tornado (W'), and tornado-borne missile (M) are essentially loadings which can destabilize a cask. Analyses reported in Chapter 3 show that the HI-STAR 100 overpack structure will remain kinematically stable under

these loadings. Additionally, for the missile impact case (M), analyses must be performed to demonstrate that the overpack structure remains unbreached by the postulated missiles.

Loadings in the second category produce global stresses which must be shown to comply with the stress intensity or stress limits, as applicable. The relevant loading combinations for the fuel basket, the MPC, and the overpack are different because of differences in their function.

2.2.7 Load Combinations

Load combinations are created by summing the effects of individual loads. The purpose of the load combinations is to define analyses which demonstrate that the HI-STAR 100 System meets the design criteria. The loads present in each condition are listed in Table 2.2.14.

The number of loading combinations is reduced by defining the internal and external pressures (P_i and P_o) such that they bound other surface-intensive loads, namely snow (S), tornado wind (W'), flood (F), and explosion (E^*). Table 2.2.14 provides the loadings applicable to the MPC (with fuel basket), and the overpack for the design normal, off-normal, and accident conditions with the bounding pressures substituting for surface-intensive loads. Further discussion of the load combinations is provided in Chapter 3.

2.2.8 Allowable Stresses

The stress intensity limits for the MPC confinement boundary and the overpack helium retention boundary for the design condition and the four service conditions are provided in Table 2.2.10. The stress intensity limits for the MPC fuel basket are presented in Table 2.2.11 (governed by Subsection NG of Section III). The external structures in the overpack meet the stress limits of Subsection NF of ASME Code, Section III for plate and shell components. Limits for the Level D condition are obtained from Appendix F of ASME Code, Section III. The MPC confinement boundary stress intensity limits are obtained from ASME Code, Section III, Subsection NB. The following definitions of terms apply to the tables on stress intensity limits; these definitions are the same as those used throughout the ASME Code:

- S_m: Value of Design Stress Intensity listed in ASME Code Section II, Part D, Tables 2A, 2B and 4
- S_y: Minimum yield strength at temperature
- S_u: Minimum ultimate strength at temperature

The overpack closure bolts are designed in accordance with NUREG/CR-6007, "Stress Analysis of Closure Bolts for Shipping Casks" [2.2.12]. The overpack lifting trunnions and the assorted lifting bolts are designed according to NUREG-0612 [2.2.13] requirements. Table 2.2.16 provides the allowable stress criteria for the closure bolts, lifting trunnions, and lifting eye bolts.

Table 2.2.1

DESIGN PRESSURES

Pressure Location	Condition	Pressure (psig)
MPC Internal Pressure	Normal	100
	Off-Normal	100
	Accident	125
MPC External Pressure/Overpack Internal Pressure	Normal	40
	Off-Normal	40
	Accident	60
Overpack External Pressure	Normal	(0) Ambient
	Off-Normal	(0) Ambient
	Accident	300
Overpack Neutron Shield Enclosure Internal Pressure	Normal	30
	Off-Normal	30
	Accident	N/A[†]

[†] The overpack neutron shield enclosure is equipped with two rupture disks which are set a relief pressure of 30 psig. Therefore, the pressure cannot exceed 30 psig.

Table 2.2.2

ENVIRONMENTAL TEMPERATURES

Condition	Temperature (°F)	Comments
Normal (Bounding Annual Average)	80	
Off-Normal (3-Day Average)	-40 and 100	• -40 °F with no insolation • 100 °F with insolation
Extreme Accident Level (3-Day Average)	125	• 125 °F with maximum insolation

Table 2.2.3

DESIGN TEMPERATURES

HI-STAR 100 Component	Normal Condition Design Temp. (Long-Term Events) (°F)	Off-Normal and Accident Condition Design Temp. Limits (Short-Term Events) (°F)
MPC shell	450	775
MPC basket	725	950
MPC Boral	800	950
MPC lid	550	775
MPC closure ring	400	775
MPC baseplate	400	775
MPC heat conduction elements	725	950
Overpack inner shell	400	500
Overpack bottom plate	350	700
Overpack closure plate	400	700
Overpack top flange	400	700
Overpack closure plate seals	400	1200
Overpack closure plate bolts	350	1000
Overpack port plug seals (vent and drain)	400	1200
Overpack port cover seals (vent and drain)	400	1200
Neutron shielding	300	300
Overpack Neutron Shield Enclosure Shell	300	1350
Remainder of overpack	350	1000
Zircaloy fuel cladding (five-year cooled)	720 (PWR)749 (BWR)	1058
Zircaloy fuel cladding (six-year cooled)	698 (PWR)720 (BWR)	1058
Zircaloy fuel cladding (seven-year cooled)	657 (PWR)676 (BWR)	1058
Zircaloy fuel cladding (ten-year cooled)	647 (PWR)665 (BWR)	1058
Zircaloy fuel cladding (fifteen-year cooled)	633 (PWR)653 (BWR)	1058

Table 2.2.4

TORNADO CHARACTERISTICS

Condition	Value
Rotational wind speed (mph)	290
Translational speed (mph)	70
Maximum wind speed (mph)	360
Pressure drop (psi)	3.0

Table 2.2.5

TORNADO-GENERATED MISSILES

Missile Description	Mass (kg)	Velocity (mph)
Automobile	1800	126
Artillery shell (8 in. diameter)	125	126
Solid sphere (1 in. diameter)	0.22	126

TABLE 2.2.6

MATERIALS AND COMPONENTS OF THE HI-STAR 100 SYSTEM

MPC [1,2]

Primary Function	Component [3]	Safety Class [4]	Codes/Standards (as applicable to component)	Material	Strength (ksi)	Special Surface Finish/Coating	Contact Matl. (if dissimilar)
Confinement	Shell	A	ASME Section III; Subsection NB	Alloy X[5]	See Appendix 1.A	NA	NA
Confinement	Baseplate	A	ASME Section III; Subsection NB	Alloy X	See Appendix 1.A	NA	NA
Confinement	Lid (One-piece design and top portion of optional two-piece design)	A	ASME Section III; Subsection NB	Alloy X	See Appendix 1.A	NA	NA
Confinement	Closure Ring	A	ASME Section III; Subsection NB	Alloy X	See Appendix 1.A	NA	NA
Confinement	Port Cover Plates	A	ASME Section III; Subsection NB	Alloy X	See Appendix 1.A	NA	NA
Criticality Control	Basket Cell Plates	A	ASME Section III; Subsection NG	Alloy X	See Appendix 1.A	NA	NA
Criticality Control	Boral	A	Non-code	NA	NA	NA	Aluminum/SS
Shielding	Drain and Vent Shield Block	C	Non-code	Alloy X	See Appendix 1.A	NA	NA

Notes:
1) There are no known residuals on finished component surfaces.
2) All welding processes used in welding the components shall be qualified in accordance with the requirements of ASME Section IX. All welds shall be made using welders qualified in accordance with ASME Section IX. Weld material shall meet the requirements of ASME Section II and the applicable Subsection of ASME Section III.
3) Component nomenclature taken from Bill of Materials in Chapter 1.
4) A, B, and C denote important to safety classifications as described in Chapter 13. NITS stands for Not Important to Safety.
5) For details on Alloy X material, see Appendix 1.A .

TABLE 2.2.6

MATERIALS AND COMPONENTS OF THE HI-STAR 100 SYSTEM

MPC [1,2]

Primary Function	Component [3]	Safety Class [4]	Codes/Standards (as applicable to component)	Material	Strength (ksi)	Special Surface Finish/Coating	Contact Matl. (if dissimilar)
Shielding	Plugs for Drilled Holes	NITS	Non-code	Alloy X	See Appendix 1.A	NA	NA
Shielding	Bottom portion of optional two-piece MPC lid design	B	Non-code	Alloy X	See Appendix 1.A	NA	NA
Heat Transfer	Heat Conduction Elements	B	Non-code	Aluminum ; Alloy 1100	NA	Sandblast Specified Surfaces	Aluminum/SS
Structural Integrity	Upper Fuel Spacer Column	B	ASME Section III; Subsection NG (only for stress analysis)	Alloy X	See Appendix 1.A	NA	NA
Structural Integrity	Sheathing	A	Non-code	Alloy X	See Appendix 1.A	Aluminum/SS	NA
Structural Integrity	Shims	NITS	Non-code (shims welded directly to angle plate basket supports are ASME Section II)	Alloy X	See Appendix 1.A	NA	NA
Structural Integrity	Basket Supports (Angled Plates)	A	ASME Section III; Subsection NG	Alloy X	See Appendix 1.A	NA	NA

Notes:

1) There are no known residuals on finished component surfaces.
2) All welding processes used in welding the components shall be qualified in accordance with the requirements of ASME Section IX. All welds shall be made using welders qualified in accordance with ASME Section IX. Weld material shall meet the requirements of ASME Section II and the applicable Subsection of ASME Section III.
3) Component nomenclature taken from Bill of Materials in Chapter 1.
4) A, B, and C denote important to safety classifications as described in Chapter 13. NITS stands for Not Important to Safety.
5) For details on Alloy X material, see Appendix 1.A .

TABLE 2.2.6

MATERIALS AND COMPONENTS OF THE HI-STAR 100 SYSTEM

MPC [1,2]

Primary Function	Component [3]	Safety Class [4]	Codes/Standards (as applicable to component)	Material	Strength (ksi)	Special Surface Finish/Coating	Contact Matl. (if dissimilar)
Structural Form	Basket Supports (Flat Plates)	NITS	Non-Code	Alloy X	See Appendix 1.A	NA	NA
Structural Integrity	Lift Lug	C	NUREG-0612	Alloy X	See Appendix 1.A	NA	NA
Structural Integrity	Lift Lug Baseplate	C	Non-code	Alloy X	See Appendix 1.A	NA	NA
Structural Integrity	Upper Fuel Spacer Bolt	NITS	Non-code	A193-B8	Per ASME Section II	NA	NA
Structural Integrity	Upper Fuel Spacer End Plate	B	Non-code	Alloy X	See Appendix 1.A	NA	NA
Structural Integrity	Lower Fuel Spacer Column	B	ASME Section III; Subsection NG (only for stress analysis)	S/S	See Appendix 1.A	NA	NA
Structural Integrity	Lower Fuel Spacer End Plate	B	Non-code	Alloy X	See Appendix 1.A	NA	NA
Structural Integrity	Vent Shield Block Spacer	C	Non-code	Alloy X	See Appendix 1.A	NA	NA
Operations	Vent and Drain Tube	C	Non-code	S/S	Per ASME Section II	Thread area surface hardened	NA
Operations	Vent & Drain Cap	C	Non-code	S/S	Per ASME	NA	NA

Notes:
1) There are no known residuals on finished component surfaces.
2) All welding processes used in welding the components shall be qualified in accordance with the requirements of ASME Section IX. All welds shall be made using welders qualified in accordance with ASME Section IX. Weld material shall meet the requirements of ASME Section II and the applicable Subsection of ASME Section III.
3) Component nomenclature taken from Bill of Materials in Chapter 1.
4) A, B, and C denote important to safety classifications as described in Chapter 13. NITS stands for Not Important to Safety.
5) For details on Alloy X material, see Appendix 1.A .

TABLE 2.2.6

MATERIALS AND COMPONENTS OF THE HI-STAR 100 SYSTEM

MPC [1,2]

Primary Function	Component [3]	Safety Class [4]	Codes/Standards (as applicable to component)	Material	Strength (ksi)	Special Surface Finish/Coating	Contact Matl. (if dissimilar)
					Section II		
Operations	Vent & Drain Cap Seal Washer	NITS	Non-code	Aluminum	NA	NA	Aluminum/SS
Operations	Vent & Drain Cap Seal Washer Bolt	NITS	Non-code	Aluminum	NA	NA	NA
Operations	Reducer	NITS	Non-code	Alloy X	See Appendix 1.A	NA	NA
Operations	Drain Line	NITS	Non-code	Alloy X	See Appendix 1.A	NA	NA
Operations	Damaged Fuel Container	C	ASME Section III; Subsection NG	Primarily 304 S/S	See Appendix 1.A	NA	NA
Operations	Drain Line Guide Tube	NITS	Non-code	S/S	NA	NA	NA

Notes:

1) There are no known residuals on finished component surfaces.
2) All welding processes used in welding the components shall be qualified in accordance with the requirements of ASME Section IX. All welds shall be made using welders qualified in accordance with ASME Section IX. Weld material shall meet the requirements of ASME Section II and the applicable Subsection of ASME Section III.
3) Component nomenclature taken from Bill of Materials in Chapter 1.
4) A, B, and C denote important to safety classifications as described in Chapter 13. NITS stands for Not Important to Safety.
5) For details on Alloy X material, see Appendix 1.A .

TABLE 2.2.6

MATERIALS AND COMPONENTS OF THE HI-STAR 100 SYSTEM

OVERPACK [1,2]

Primary Function	Component [3]	Safety Class [4]	Codes/Standards (as applicable to component)	Material	Strength (ksi)	Special Surface Finish/Coating	Contact Matl. (if dissimilar)
Helium Retention	Inner Shell	A	ASME Section III; Subsection NB	SA203-E	Table 3.3.4	Paint inside surface with Thermaline 450	NA
Helium Retention	Bottom Plate	A	ASME Section III; Subsection NB	SA350-LF3	Table 3.3.4	Paint inside surface with Thermaline 450	NA
Helium Retention	Top Flange	A	ASME Section III; Subsection NB	SA350-LF3	Table 3.3.4	Paint inside surface with Thermaline 450. Paint outside surface with Carboline 890.	NA
Helium Retention	Closure Plate	A	ASME Section III; Subsection NB	SA350-LF3	Table 3.3.4	Paint inside surface with Thermaline 450. Paint outside surface with Carboline 890.	NA
Helium Retention	Closure Plate Bolts	A	ASME Section III; Subsection NB	SB637-N07718	Table 3.3.5	NA	NA
Helium Retention	Port Plug	A	Non-code	SA193-B8	Not required	NA	NA
Helium Retention	Port Plug Seal	A	Non-code	Alloy X750	Not required	NA	NA
Helium Retention	Closure Plate Seal	A	Non-code	Commercial	Not required	NA	NA
Helium Retention	Port Cover Seal	B	Non-code	Alloy X750	Not required	NA	NA

Notes:

1) There are no known residuals on finished component surfaces.
2) All welding processes used in welding the components shall be qualified in accordance with the requirements of ASME Section IX. All welds shall be made using welders qualified in accordance with ASME Section IX. Weld material shall meet the requirements of ASME Section II and the applicable Subsection of ASME Section III. For parts beyond the purview of ASME Section III, compliance with Section IX and Section II of the Code shall be observed to the extent practicable.(72. 48 No. 61)
3) Component nomenclature taken from Bill of Materials in Chapter 1.
4) A, B, and C denote important to safety classifications as described in Chapter 13. NITS stands for Not Important to Safety.

TABLE 2.2.6

MATERIALS AND COMPONENTS OF THE HI-STAR 100 SYSTEM

OVERPACK [1,2]

Primary Function	Component [3]	Safety Class [4]	Codes/Standards (as applicable to component)	Material	Strength (ksi)	Special Surface Finish/Coating	Contact Matl. (if dissimilar)
Shielding	Intermediate Shells	B	ASME Section III; Subsection NF	SA516-70	Table3.3.2	Exposed areas of fifth intermediate shell to be painted with Carboline 890.	NA
Shielding	Neutron Shield	B	Non-code	Holtite-A	Not required	NA	Holtite/CS
Shielding	Plugs for Drilled Holes	NITS	Non-code	SA193-B7	Not required	NA	NA
Shielding	Removable Shear Ring	B	ASME Section III; Subsection NF	SA203-E or SA 350 LF	Table 3.3.4	Paint external surface with Carboline 890.	NA
Shielding	Pocket Trunnion Plug Plate	C	Non-code	SA240-304	Not required	NA	NA
Heat Transfer	Radial Channels	B	ASME Section III; Subsection NF	SA515-70	Table 3.3.3	Paint outside surface with Carboline 890.	NA
Rotation Pivot and Shielding	Pocket Trunnion	B	Non-Code	SA705-630, 17-4 pH OR SA564-630, 17-4 pH	Table 3.3.5	NA	NA
Structural Integrity	Lifting Trunnion	A	ANSI N14.6	SB637-N07718	Table 3.3.5	NA	NA
Structural Integrity	Rupture Disk	C	Non-code	Commercial	Not required	NA	Brass-C/S

Notes:

1) There are no known residuals on finished component surfaces.
2) All welding processes used in welding the components shall be qualified in accordance with the requirements of ASME Section IX. All welds shall be made using welders qualified in accordance with ASME Section IX. Weld material shall meet the requirements of ASME Section II and the applicable Subsection of ASME Section III. For parts beyond the purview of ASME Section III, compliance with Section IX and Section II of the Code shall be observed to the extent practicable.(72. 48 No. 61)
3) Component nomenclature taken from Bill of Materials in Chapter 1.
4) A, B, and C denote important to safety classifications as described in Chapter 13. NITS stands for Not Important to Safety.

TABLE 2.2.6

MATERIALS AND COMPONENTS OF THE HI-STAR 100 SYSTEM

OVERPACK [1,2]

Primary Function	Component [3]	Safety Class [4]	Codes/Standards (as applicable to component)	Material	Strength (ksi)	Special Surface Finish/Coating	Contact Matl. (if dissimilar)
Structural Integrity	Rupture Disk Plate	C	Non-code	A569 or SA516 Gr. 70	Not required	NA	NA
Structural Integrity	Removable Shear Ring Bolt	C	Non-code	SA193-B7	Not required	NA	NA
Structural Integrity	Thermal Expansion Foam	NITS	Non-code	Silicone Foam	Not required	NA	Silicone with CS, brass, and Holtite
Structural Integrity	Closure Bolt Washer	NITS	Non-code	ASTM 564, 17-7 pH	Not required	NA	NA
Structural Integrity	Enclosure Shell Panels	B	ASME Section III; Subsection NF	SA515-70	Table 3.3.3	Paint outside surface with Carboline 890.	NA
Structural Integrity	Enclosure Shell Return	B	ASME Section III; Subsection NF	SA515-70	Table 3.3.3	Paint outside surface with Carboline 890.	NA
Structural Integrity	Port Cover	B	ASME Section III; Subsection NF	SA203E or SA 350 LF	Table 3.3.4	Paint outside surface with Carboline 890.	NA
Structural Integrity	Port Cover Bolt	C	Non-code	SA193-B7	Not required	NA	NA
Operations	Trunnion Locking Pad and End Cap Bolt	C	Non-code	SA193-B7	Not required	NA	NA

Notes:

1) There are no known residuals on finished component surfaces.
2) All welding processes used in welding the components shall be qualified in accordance with the requirements of ASME Section IX. All welds shall be made using welders qualified in accordance with ASME Section IX. Weld material shall meet the requirements of ASME Section II and the applicable Subsection of ASME Section III. For parts beyond the purview of ASME Section III, compliance with Section IX and Section II of the Code shall be observed to the extent practicable.(72. 48 No. 61)
3) Component nomenclature taken from Bill of Materials in Chapter 1.
4) A, B, and C denote important to safety classifications as described in Chapter 13. NITS stands for Not Important to Safety.

TABLE 2.2.6

MATERIALS AND COMPONENTS OF THE HI-STAR 100 SYSTEM

OVERPACK [1,2]

Primary Function	Component [3]	Safety Class [4]	Codes/Standards (as applicable to component)	Material	Strength (ksi)	Special Surface Finish/Coating	Contact Matl. (if dissimilar)
Operations	Lifting Trunnion End Cap	C	Non-code	SA516-70 or SA515 Gr. 70	Table 3.3.2	Paint exposed surfaces with Carboline 890.	NA
Operations	Lifting Trunnion Locking Pad	C	Non-code	SA516-70	Table 3.3.2	Paint exposed surfaces with Carboline 890.	NA
Operations	Nameplate	NITS	Non-code	S/S	Not required	NA	NA

Notes:

1) There are no known residuals on finished component surfaces.
2) All welding processes used in welding the components shall be qualified in accordance with the requirements of ASME Section IX. All welds shall be made using welders qualified in accordance with ASME Section IX. Weld material shall meet the requirements of ASME Section II and the applicable Subsection of ASME Section III. For parts beyond the purview of ASME Section III, compliance with Section IX and Section II of the Code shall be observed to the extent practicable.(72. 48 No. 61)
3) Component nomenclature taken from Bill of Materials in Chapter 1.
4) A, B, and C denote important to safety classifications as described in Chapter 13. NITS stands for Not Important to Safety.

Table 2.2.7

HI-STAR 100 ASME BOILER AND PRESSURE VESSEL CODE APPLICABILITY

HI-STAR 100 Component	Material Procurement	Design	Fabrication	Inspection
Overpack helium retention boundary	Section II, Section III, Subsection NB, NB-2000	Section III, Subsection NB, NB-3200	Section III, Subsection NB, NB-4000	Section III, Subsection NB, NB-5000 and Section V
Overpack intermediate shells, radial channels, outer enclosure	Section II, Section III, Subsection NF, NF-2000	Section III, Subsection NF, NF-3200	Section III, Subsection NF, NF-4000	Section III, Subsection NF, NF-5360 and Section V
MPC confinement boundary	Section II, Section III, Subsection NB, NB-2000	Section III, Subsection NB, NB-3200	Section III, Subsection NB, NB-4000	Section III, Subsection NB, NB-5000 and Section V
MPC fuel basket	Section II, Section III, Subsection NG, NG-2000	Section III, Subsection NG, NG-3300 and NG-3200	Section III, Subsection NG, NG-4000	Section III, Subsection NG, NG-5000 and Section V
Lifting Trunnions	Section II, Section III, Subsection NF, NF-2000	ANSI N14.6	Section III, Subsection NF, NF-4000	See Chapter 9
MPC basket supports	Section II, Section III, Subsection NG, NG-2000	Section III, Subsection NG, NG-3300 and NG-3200	Section III, Subsection NG, NG-4000	Section III, Subsection NG, NG-5000 and Section V
Damaged fuel Container	Section II, Section III, Subsection NG, NG-2000	Section III, Subsection NG, NG-3300 and NG-3200	Section III, Subsection NG, NG-4000	Section III, Subsection NG, NG-5000 and Section V

Table 2.2.8

ADDITIONAL DESIGN INPUT DATA FOR NORMAL, OFF-NORMAL, AND ACCIDENT CONDITIONS

Item	Condition	Value
Snow Pressure Loading (lb./ft^2)	Normal	100
Constriction of MPC Basket Vent Opening By Crud Settling (Depth of Crud, in.)	Accident	0.85 (MPC-68) 0.36 (MPC-24)
Cask Environment During the Postulated Fire Event (°F)	Accident	1475
Fire Duration (seconds)	Accident	305
Maximum submergence depth due to flood (ft)	Accident	656
Flood water velocity (ft/s)	Accident	13
Maximum Horizontal ZPA (Zero Period Acceleration) for HI-STAR† (g's)	Accident	0.314 (w/1.0 vertical) 0.332 (w/0.75 vertical) 0.339 (w/0.667 vertical) 0.354 (w/0.5 vertical)

† The maximum horizontal ZPA is specified as the vector sum of the g-loading in two orthogonal directions as a function of the vertical acceleration multiplier which is the maximum vertical ZPA divided by the maximum horizontal ZPA for a single orthogonal direction for the site.

Table 2.2.9

EXAMPLES OF ACCEPTABLE ISFSI PAD DESIGN PARAMETERS

PARAMETER	PARAMETER SET 'A'[†]	PARAMETER SET 'B'
Concrete thickness, t_p	$\leq$ 36 inches	$\leq$ 28 inches
Concrete Compressive Strength (at 28 days), f_c'	$\leq$ 4,200 psi	$\leq$ 6,000 psi
Reinforcement Top and Bottom (both directions)	Reinforcing bar shall be 60 ksi yield strength ASTM material	Reinforcing bar shall be 60 ksi yield strength ASTM material
Subgrade Effective Modulus of Elasticity[††] (measured prior to ISFSI pad installation), E	$\leq$ 28,000 psi	$\leq$ 16,000 psi

[††] An acceptable method of defining the soil effective modulus of elasticity applicable to the drop and tipover analysis is provided in Table 13 of NUREG/CR-6608 with soil classification in accordance with ASTM-D2487 Standard Classification of Soils for Engineering Purposes (Unified Soil Classification System USCS) and density determination in accordance with ASTM-D-1586 Standard Test Method for Penetration Test and Split/barrel Sampling of Soils.

Table 2.2.10
MPC CONFINEMENT BOUNDARY AND OVERPACK HELIUM RETENTION BOUNDARY
STRESS INTENSITY LIMITS
FOR DIFFERENT LOADING CONDITIONS (ELASTIC ANALYSIS PER NB-3220)†

STRESS CATEGORY	DESIGN	LEVELS A & B	LEVEL D††
Primary Membrane, P_m	S_m	N/A†††	AMIN ($2.4S_m$, $.7S_u$)
Local Membrane, P_L	$1.5S_m$	N/A	150% of P_m Limit
Membrane plus Primary Bending	$1.5S_m$	N/A	150% of P_m Limit
Primary Membrane plus Primary Bending	$1.5S_m$	N/A	150% of P_m Limit
Membrane plus Primary Bending plus Secondary	N/A	$3S_m$	N/A
Average Shear Stress†††† (Section in Pure Shear)	$0.6S_m$	$0.6S_m$	$0.42S_u$

† Stress combinations including F (peak stress) apply to fatigue evaluations only.

†† Governed by Appendix F, Paragraph F-1331 of the ASME Code, Section III.

††† No specific stress intensity limit applicable.

†††† Governed by NB-3227.2 or F-1331.1(d)

Table 2.2.11

MPC BASKET STRESS INTENSITY LIMITS
FOR DIFFERENT LOADING CONDITIONS (ELASTIC ANALYSIS PER NG-3220)

STRESS CATEGORY	DESIGN	LEVELS A & B	LEVEL D[†]
Primary Membrane, P_m	S_m	S_m	AMIN ($2.4S_m$, $.7S_u$)[††]
Primary Membrane plus Primary Bending	$1.5S_m$	$1.5S_m$	150% of P_m Limit
Primary Membrane plus Primary Bending plus Secondary	N/A[†††]	$3S_m$	N/A

† Governed by Appendix F, Paragraph F-1331 of the ASME Code, Section III.

†† Governed by NB-3227.2 or F-1331.1(d)

††† No specific stress intensity limit applicable.

Table 2.2.12

STRESS LIMITS FOR DIFFERENT
LOADING CONDITIONS FOR THE EXTERNAL STRUCTURES IN THE HI-STAR OVERPACK
(ELASTIC ANALYSIS PER NF-3260)

	SERVICE CONDITION[†]		
STRESS CATEGORY	**DESIGN + LEVEL A**	**LEVEL B**	**LEVEL D**[††]
Primary Membrane, P_m	S	1.33S	AMAX ($1.2S_y$, $1.5S_m$) but < $.7S_u$
Primary Membrane, P_m, plus Primary Bending, P_b	1.5S	1.995S	150% of P_m
Shear Stress (Average)	0.6S	0.6S	<$0.42S_u$

Definitions:

S = Allowable Stress Value for Table 1A, ASME Section II, Part D
S_m = Allowable Stress Intensity Value from Table 2A, ASME Section II, Part D
S_u = Ultimate Strength

---

† Limits for Design and Levels A and B are on maximum stress.
Limits for Level D are on maximum stress intensity.

†† Governed by Appendix F, Paragraph F-1332 of the ASME Code, Section III.

Table 2.2.13
NOTATION FOR DESIGN LOADINGS FOR NORMAL, OFF-NORMAL, AND ACCIDENT CONDITIONS

NORMAL CONDITION	
LOADING	**NOTATION**
Dead Weight	D
Handling Loads	H
Design Pressure (Internal)[†]	P_i
Design Pressure (External)[†]	P_o
Snow	S
Wind	W
Operating Temperature	T
OFF-NORMAL CONDITION	
LOADING	**NOTATION**
Off-Normal Pressure (Internal)[†]	P_i
Off-Normal Pressure (External)[†]	P_o
Off-Normal Temperature	T′

[†] Internal Design Pressure P_i bounds the normal and off-normal condition internal pressures. External Design Pressure P_o bounds off-normal external pressures. Similarly, accident pressures P_i^* and P_o^*, respectively, bound actual internal and external pressures under all postulated environment phenomena and accident events.

Table 2.2.13 (continued)

NOTATION FOR DESIGN LOADINGS FOR NORMAL, OFF-NORMAL, AND ACCIDENT CONDITIONS

ACCIDENT CONDITIONS	
LOADING	**NOTATION**
Handling Accident (Drop)	H′
Earthquake	E
Fire	T^*
Tornado Missile	M
Tornado Wind	W′
Flood	F
Explosion	E^*
Accident Pressure (Internal)	P_i^*
Accident Pressure (External)	P_o^*

Table 2.2.14

APPLICABLE LOAD CASES AND COMBINATIONS FOR EACH CONDITION AND COMPONENT[†, ††]

CONDITION	LOADING CASE	MPC	OVERPACK
Design (ASME Code Pressure Compliance)	1	P_i, P_o	P_i, P_o
Normal (Level A)	1	D , T , H , P_i	D , T , H , P_i
	2	D , T , H , P_o	N/A
Off-Normal (Level B)	1	D , T', H , P_i	D , T' , H , P_i
	2	D , T' , H , P_o	N/A
Accident (Level D)	1	D , T , P_i , H'	D , T , P_i , H'
	2	D, T^*, P_i^*	D , T^*, P_i^*
	3	D, T^*, P_i^*	D , T^* , $P_o^{*†††}$

† The loading notations are given in Table 2.2.13. Each symbol represents a loading type and may have different values for different components.

†† N/A stands for "Not Applicable".

††† P_o* bounds the external pressure due to explosion.

Table 2.2.15

LIST OF ASME CODE ALTERNATIVES FOR HI-STAR 100 SYSTEM

Component	Reference ASME Code Section/Article	Code Requirement	Alternative, Justification & Compensatory Measures
MPC	NB-1100	Statement of requirements for Code stamping of components.	MPC enclosure vessel is designed and will be fabricated in accordance with ASME Code, Section III, Subsection NB to the maximum practical extent, but Code stamping is not required.
MPC	NB-2000	Requires materials to be supplied by ASME-approved material supplier.	Materials will be supplied by Holtec approved suppliers with Certified Material Test Reports (CMTRs) in accordance with NB-2000 requirements.
MPC Lid and Closure Ring Welds	NB-4243	Full penetration welds required for Category C Joints (flat head to main shell per NB-3352.3)	MPC lid and closure ring are not full penetration welds. They are welded independently to provide a redundant seal. Additionally, a weld efficiency factor of 0.45 has been applied to the analyses of these welds.
MPC Lid to Shell Weld	NB-5230	Radiographic (RT) or ultrasonic (UT) examination required	Only UT or multi-layer liquid penetrant (PT) examination is permitted. If PT alone is used, at a minimum, it will include the root and final weld layers and each approximately 3/8 inch of weld depth.
MPC Closure Ring, Vent and Drain Cover Plate Welds	NB-5230	Radiographic (RT) or ultrasonic (UT) examination required.	Root (if more than one weld pass is required) and final liquid penetrant examination to be performed in accordance with NB-5245. The MPC vent and drain cover plate welds are leak tested. The closure ring provides independent redundant closure for vent and drain cover plates.

Table 2.2.15 (continued)

LIST OF ASME CODE ALTERNATIVES FOR HI-STAR 100 SYSTEM

Component	Reference ASME Code Section/Article	Code Requirement	Alternative, Justification & Compensatory Measures
MPC Enclosure Vessel and Lid	NB-6111	All completed pressure retaining systems shall be pressure tested.	The MPC enclosure vessel is seal welded in the field following fuel assembly loading. The MPC enclosure vessel shall then be hydrostatically tested as defined in Chapter 9. Accessibility for leakage inspections preclude a Code compliant hydrostatic test. All MPC enclosure vessel welds (except the closure ring and vent/drain cover plate welds) are inspected by volumetric examination, except the MPC lid-to shell weld shall be verified by volumetric or multi-layer PT examination. If PT alone is used, at a minimum, it must include the root and final layers and each approximately 3/8 inch of weld depth. For either UT or PT, the maximum undetectable flaw size must be demonstrated to be less than the critical flaw size. The critical flaw size must be determined in accordance with ASME XI methods. The critical flaw size shall not cause the primary stress limits of NB-3000 to be exceeded. examined. The vent/drain cover plate weld is confirmed by leakage testing and liquid penetrant examination and the closure ring weld is confirmed by liquid penetrant examination. The inspection process, including findings (indications) shall be made a permanent part of the certificate holder's records by video, photographic, or other means which provide an equivalent retrievable record of weld integrity. The video or photographic records should be taken during the final interpretation period described in ASME Section V, Article 6, T-676. The inspection of the weld must be performed by qualified personnel and shall meet the acceptance requirements of ASME Code Section III, NB-5350 for PT or NB-5332 for UT.

Table 2.2.15 (continued)

LIST OF ASME CODE ALTERNATIVES FOR HI-STAR 100 SYSTEM

Component	Reference ASME Code Section/Article	Code Requirement	Alternative, Justification & Compensatory Measures
MPC Enclosure Vessel	NB-7000	Vessels are required to have overpressure protection.	No overpressure protection is provided. Function of MPC enclosure vessel is to contain radioactive contents under normal, off-normal, and accident conditions of storage. MPC vessel is designed to withstand maximum internal pressure considering 100% fuel rod failure and maximum accident temperatures.
MPC Enclosure Vessel	NB-8000	States requirements for nameplates, stamping and reports per NCA-8000.	HI-STAR 100 System to be marked and identified in accordance with 10CFR71 and 10CFR72 requirements. Code stamping is not required. QA data package to be in accordance with Holtec approved QA program.
Overpack Helium Retention Boundary	NB-1100	Statement of requirements for Code stamping of components.	Overpack helium retention boundary is designed, and will be fabricated in accordance with ASME Code, Section III, Subsection NB to the maximum practical extent, but Code stamping is not required.
Overpack Helium Retention Boundary	NB-2000	Requires materials to be supplied by ASME approved Material Supplier.	Materials will be supplied by Holtec approved suppliers with CMTRs per NB-2000.
Overpack Helium Retention Boundary	NB-7000	Vessels are required to have overpressure protection.	No overpressure protection is provided. Function of overpack vessel is to contain helium contents under normal, off-normal, and accident conditions. Overpack vessel is designed to withstand maximum internal pressure and maximum accident temperatures.
Overpack Helium Retention Boundary	NB-8000	Statement of Requirements for nameplates, stamping and reports per NCA-8000.	HI-STAR 100 System to be marked and identified in accordance with 10CFR71 and 10CFR72 requirements. Code stamping is not required. QA data package to be in accordance with Holtec's approved QA program.
MPC Basket Assembly	NG-2000	Requires materials to be supplied by ASME approved Material Supplier.	Materials will be supplied by Holtec approved supplier with CMTRs in accordance with NG-2000 requirements.

Table 2.2.15 (continued)

LIST OF ASME CODE ALTERNATIVES FOR HI-STAR 100 SYSTEM

Component	Reference ASME Code Section/Article	Code Requirement	Alternative, Justification & Compensatory Measures
MPC Basket Assembly	NG-8000	States requirements for nameplates, stamping and reports per NCA-8000.	The HI-STAR 100 System will be marked and identified in accordance with 10CFR71 and 10CFR72 requirements. No Code stamping is required. The MPC basket data package will be in conformance with Holtec's QA program.
Overpack Intermediate Shells	NB-4622	All welds, including repair welds, shall be post-weld heat treated (PWHT).	PWHT of intermediate shell-to-top flange and intermediate shell-to-bottom plate welds do not require PWHT. These welds attach non-pressure retaining parts to pressure retaining parts. The pressure retaining parts are > 7 inches thick. Localized PWHT will cause material away from the weld to experience elevated temperatures which will have an adverse effect on the material properties.
Overpack Helium Retention Boundary	NG-2000	Perform radiographic examination after post-weld heat treatment (PWHT).	Radiography of the helium retention boundary welds after PWHT is not required. All welds (including repairs) will have passed radiographic examination prior to PWHT of the entire containment boundary. Confirmatory radiographic examination after PWHT is not necessary because PWHT is not known to introduce new weld defects in nickel steels.
Overpack Intermediate Shells	NF-2000	Requires materials to be supplied by ASME approved Material Supplier.	Materials will be supplied by Holtec approved supplier with CMTRs in accordance with NF-2000 requirements.
Overpack Helium Retention Boundary	NB-2330	Defines the methods for determining the T_{NDT} for impact testing of materials.	T_{NDT} shall be defined in accordance with Regulatory Guides 7.11 and 7.12 for the helium retention boundary components.

Table 2.2.16

NON-ASME CODE STRESS ALLOWABLE CRITERIA

OVERPACK CLOSURE BOLTS[†]:

STRESS CATEGORY	NORMAL AND OFF-NORMAL CONDITIONS	ACCIDENT CONDITIONS
Average Tensile Stress	$2/3\ S_y$	$AMIN(S_y, 0.7\ S_u)$
Average Shear Stress	$0.6\ (2/3\ S_y)$	$AMIN(0.6\ S_y, 0.42\ S_u)$
Combined Tensile and Shear Stress[††]	$R_t^2 + R_s^2 < 1.0$	$R_t^2 + R_s^2 < 1.0$

LIFTING TRUNNIONS AND LIFTING BOLTS:

The lifting trunnions and the lifting bolts, for the overpack closure plate and for the MPC lid, are designed in accordance with NUREG-0612 and ANSI N14.6. Specifically, the design must meet factors of safety of six based on the material yield stress and ten based on the material ultimate stress for non-redundant lifting devices.

[†] The overpack closure bolts are designed in accordance with NUREG/CR-6007, "Stress Analysis of Closure Bolts for Shipping Casks".

[††] R_t and R_s are the ratios of actual stress to allowable tensile and shear stress, respectively.

Table 2.2.17

ALLOWABLE CARRY HEIGHTS

Cask Orientation	Height (Inches)
Vertical	21
Horizontal	72

Note: The carry height is measured from the lowest surface of the overpack to the potential impact surface.

2.3 SAFETY PROTECTION SYSTEMS

2.3.1 General

The HI-STAR 100 System is a storage and transport cask engineered to provide safe long-term storage of spent nuclear fuel. The HI-STAR 100 System will withstand all normal, off-normal, and postulated accident conditions without any uncontrolled release of radioactive material or excessive radiation exposure to workers or members of the public. Special considerations in the design have been made to ensure long-term integrity and confinement of the stored SNF throughout all cask operating conditions. The design considerations which have been incorporated into the HI-STAR 100 System to ensure safe long-term fuel storage are:

1. The MPC confinement barrier is an enclosure vessel designed in accordance with the ASME Code, Subsection NB with most confinement welds inspected by radiography (RT) or ultrasonic testing (UT). Where RT or UT is not possible, a redundant closure system is provided. The MPC closure ring and vent and drain port cover plates are not inspected by UT or RT, but the closure ring provides an independent redundant closure for the vent and drain cover plates. The MPC lid-to-shell weld will be examined by PT (root and final weld layers) and UT or multi-layer PT.

2. The MPC confinement barrier is encapsulated by the overpack helium retention boundary.

3. The HI-STAR 100 System is designed to meet the requirements of storage while maintaining the safety of the spent nuclear fuel.

4. The spent nuclear fuel once initially loaded in the MPC and overpack does not require any further canister transfer or fuel handling operations for storage or transport.

5. The decay heat emitted by the spent nuclear fuel is rejected from HI-STAR 100 through passive means. No active cooling systems are employed.

It is recognized that a rugged design with large safety margins is essential, but not sufficient to ensure acceptable performance over the service life of any system. A carefully planned oversight and surveillance plan which does not diminish system integrity but provides reliable information on the effect of passage of time on the performance of the system is essential. Such a surveillance and performance assay program will be developed to be compatible with the specific conditions of the licensee's facility where the HI-STAR 100 System is installed. The general requirements for the acceptance testing and maintenance programs are provided in Chapter 9. Surveillance requirements are specified in Technical Specifications.

The structures, systems, and components of the HI-STAR 100 System designated as important to safety are identified in Table 2.2.6. Similar categorization of structures, systems, and components, which are part of the ISFSI, but not part of the HI-STAR 100 System, will be the responsibility of

the 10CFR72 licensee.

2.3.2 Protection by Multiple Confinement Barriers and Systems

2.3.2.1 Confinement Barriers and Systems

The radioactivity which the HI-STAR 100 must confine originates from the spent fuel assemblies and, to a lesser extent, the contaminated water in the fuel pool. This radioactivity is confined by multiple confinement barriers.

Radioactivity from the fuel pool water is minimized by preventing contact, removing the contaminated water, and decontamination.

An inflatable seal in the annular gap between the MPC and overpack prevents the fuel pool water from contacting the exterior of the MPC and interior of the overpack while submerged for fuel loading. The fuel pool water is drained from the interior of the MPC, and the MPC internals are dried. The exterior of the overpack has a painted surface which is decontaminated to acceptable levels. Any residual radioactivity deposited by the fuel pool water is confined by the MPC confinement boundary along with the spent nuclear fuel.

The HI-STAR 100 is designed with several confinement barriers for the radioactive fuel contents. Fuel assemblies classified as damaged fuel or fuel debris are placed within a damaged fuel container which restricts the release of fuel debris. Intact fuel assemblies have cladding which provides the first boundary preventing release of the fission products. The MPC is a seal welded enclosure which provides the confinement boundary. The MPC confinement boundary is defined by the MPC baseplate, shell, lid, closure ring, and port cover plates. An entirely redundant boundary is provided by the overpack helium retention boundary; however, no credit is taken for the overpack helium retention boundary other than its ability to retain a helium atmosphere.

The MPC confinement boundary has been designed to withstand any postulated off-normal operations, internal change, or external natural phenomena. The MPC is designed to endure normal, off-normal, and accident conditions of storage with the maximum decay heat loads without loss of confinement. Designed in accordance with the ASME Code, Section III, Subsection NB, the MPC confinement boundary provides assurance that there will be no release of radioactive materials from the cask under the specified loading conditions. Therefore, no monitoring system for the confinement boundary is required.

Confinement is discussed further in Chapter 7. MPC field weld examinations, hydrostatic testing, and helium leak testing are performed to verify the confinement function in accordance with the operating procedures in Chapter 8 and the testing and acceptance requirements in Chapter 9.

2.3.2.2 Cask Cooling

To facilitate the passive heat removal capability of the HI-STAR 100, several thermal design criteria are established for normal and off-normal conditions. They are as follows:

- A concentric set of metallic seals in the overpack closure plate contain the helium atmosphere between the exterior of the MPC and the interior of the overpack. A maximum steady-state temperature limit is conservatively set for the seals in Table 2.2.3 based on the manufacturer's specifications. The seals can also withstand the pressures specified in Table 2.2.1.

- The overpack helium retention boundary ensures that the helium atmosphere in the overpack annulus is maintained during normal, off-normal, and accident conditions.

- The MPC confinement boundary ensures that the helium atmosphere inside the MPC is maintained during normal and off-normal conditions. The MPC confinement boundary maintains the helium confinement atmosphere below the design temperatures and pressures stated in Table 2.2.3 and Table 2.2.1, respectively.

- The MPC thermal design maintains the fuel rod cladding temperatures below the values stated in Chapter 4 such that fuel cladding is not degraded during the normal storage period.

- The fabrication method used for layering of the intermediate shells will assure contact between layers. However, the thermal evaluation is conservatively based on small uniform gaps between each shell. During normal conditions, the internal heat source (decay heat from the fuel) acts to provide further assurance of inter-shell contact due to thermal expansion. Likewise, during the fire accident, the outermost intermediate shell would tend to expand more than the inner intermediate shells, possibly reducing the inter-surface contact between them. Such a reduction in contact would tend to insulate the cask during the fire accident. However, no credit is taken for this differential thermal expansion in the thermal analyses. Differential thermal expansion and the resultant stresses caused by restriction of free expansion are, however, accounted for in the structural analyses.

- The heat rejection capacity of the HI-STAR 100 is deliberately understated by conservatively determining the design basis fuel. The decay heat value in Table 2.1.6 is prepared by computing the decay heat from the design basis fuel assembly which produces the highest heat generation rate for a given burnup. Additional margin is built into the calculated cask cooling rate by using a fictitious fuel assembly which offers maximum resistance to the transmission of heat (minimum thermal conductivity).

2.3.3 Protection by Equipment and Instrumentation Selection

2.3.3.1 Equipment

Design criteria for the HI-STAR 100 System is described in Section 2.2. The HI-STAR 100 System may include support equipment. The lifting equipment used to handle the HI-STAR 100 System in and out of the pool is classified as Important to Safety. The lifting equipment is designed in accordance with ANSI N14.6. Other important to safety support equipment is listed in Table 8.1.4.

Auxiliary operational equipment (e.g., trailers, skids, portable cranes, transporters, or air pads) are Not Important to Safety, as the HI-STAR 100 is designed to withstand the failure of any of these components provided the requirements of this FSAR are met.

2.3.3.2 Instrumentation

As a consequence of the passive nature of the HI-STAR 100 System, instrumentation which is Important to Safety is not necessary. No instrumentation is required for HI-STAR 100 storage operations.

2.3.4 Nuclear Criticality Safety

The criticality safety criterion stipulates that the effective neutron multiplication factor, k_{eff}, including statistical uncertainties and biases, is less than 0.95 for all postulated arrangements of fuel within the cask under all credible conditions.

2.3.4.1 Control Methods for Prevention of Criticality

The control methods and design features used to prevent criticality for all MPC configurations are the following:

a. Incorporation of permanent neutron absorbing material (Boral) in the MPC fuel basket walls.

b. Favorable geometry provided by the MPC fuel basket

Administrative controls will be used to ensure that fuel placed in the HI-STAR 100 System meets the requirements of the Certificate of Compliance. All appropriate criticality analyses are presented in Chapter 6.

2.3.4.2 Error Contingency Criteria

Provision for error contingency is built into the criticality analyses performed in Chapter 6. Because biases and uncertainties are explicitly evaluated in the analysis, it is not necessary to introduce additional contingency for error.

2.3.4.3 Verification Analyses

In Chapter 6, critical experiments are selected which reflect the design configurations. These critical experiments are evaluated using the same calculation methods, and a suitable bias is incorporated in the reactivity calculation.

2.3.5 Radiological Protection

2.3.5.1 Access Control

As required by 10CFR72, uncontrolled access to the ISFSI will be prevented through physical means. A peripheral fence with an appropriate monitoring system is a standard approach to limit access. The details of the access control systems and procedures, including division of the site into radiation protection areas, will be developed by the licensee.

2.3.5.2 Shielding

The shielding design is governed by 10CFR72.104 and 10CFR72.106 which provide radiation dose limits for any real individual located at or beyond the nearest boundary of the controlled area. The individual must not receive an annual dose equivalent greater than the values stated in Table 2.3.1 for normal and off-normal conditions. Further, an individual located at the site boundary must not receive a dose to the whole body or any organ from any design basis accident greater than the values listed in Table 2.3.1.

The objective of shielding is to assure that radiation dose rates at key locations are below acceptable levels for those locations. Three locations are of particular interest in the storage mode:

- immediate vicinity of the cask
- restricted area boundary
- controlled area (site) boundary

Dose rates in the immediate vicinity of the cask are important in consideration of occupational exposure. A design objective for the radial neutron shield mid-height surface dose rate has been established as 125 mrem/hr. Dose rates above and below the neutron shield may be further reduced by temporary shielding as detailed in Chapter 10. Areas above and below the neutron shield in the radial direction are limited to 375 mrem/hr. Chapter 5 of this FSAR presents the analyses and evaluations to establish HI-STAR 100 compliance with these design objectives.

Because of the passive nature of the HI-STAR 100, human activity related to the system is infrequent and of short duration. Personnel exposures due to operational and maintenance activities are discussed in Chapter 10. Chapter 10 also provides information concerning temporary shielding which may be utilized to reduce the personnel dose during loading, unloading, and handling

operations. The estimated occupational doses for personnel must comply with the requirements of 10CFR20.

Dose rates at the restricted area and site boundaries shall be in accordance with applicable regulations. Licensees are required to demonstrate compliance with 10CFR72.104 and 10CFR72.106 for the actual fuel being stored, ISFSI storage array, and controlled area boundary.

The analyses presented in Chapters 5, 10 and 11 demonstrate that the HI-STAR 100 System meets the above radiation dose limits and design objectives.

2.3.5.3 Radiological Alarm System

There are no credible events which could result in release of radioactive materials or unacceptable increases in direct radiation. In addition, the releases postulated as the result of the hypothetical accidents described in Chapter 11 are of a very small magnitude. Therefore, radiological alarm systems are not necessary.

2.3.6 Fire and Explosion Protection

There are no combustible or explosive materials associated with the HI-STAR 100 System. No such materials would be stored within an ISFSI. However, for conservatism we have analyzed the fire accident as a bounding condition for HI-STAR 100 System. An evaluation of the HI-STAR 100 System in a fire accident is discussed in Chapter 11.

Small overpressures are the result of accidents involving explosive materials which are stored or transported near the site. Explosion is a load considered in Chapter 11.

Table 2.3.1

RADIOLOGICAL SITE BOUNDARY REQUIREMENTS

BOUNDARY OF CONTROLLED AREA (m) (minimum)	100
NORMAL AND OFF-NORMAL CONDITIONS: Whole Body (mrem/yr) Thyroid (mrem/yr) Any Other Critical Organ (mrem/yr)	 25 75 25
DESIGN BASIS ACCIDENT: TEDE (rem)	 5
DDE+CDE to any individual organ or tissue (other than lens of the eye) (rem)	50
Lens dose equivalent (rem)	15
Shallow dose equivalent to skin or any extremity (rem)	50

2.4 DECOMMISSIONING CONSIDERATIONS

Efficient decommissioning of the ISFSI is a paramount objective of the HI-STAR 100 System. The HI-STAR 100 System is ideally configured to facilitate rapid, safe, and economical decommissioning of the storage site.

The MPC which holds the SNF assemblies is engineered to be suitable as a waste package for permanent internment in a deep Mined Geological Disposal System (MGDS). The materials of construction permitted for the MPC are known to be highly resistant to severe environmental conditions. No carbon steel, paint, or coatings are used or permitted in the MPC. Therefore, the SNF assemblies stored in the MPC should not need to be removed. However, to ensure a practical, feasible method to defuel the HI-STAR 100 MPC, the top of the MPC is equipped with sufficient gamma shielding and markings locating the drain and vent locations to enable semiautomatic (or remotely actuated) boring of the MPC lid to provide access to the MPC vent and drain. The circumferential welds of the MPC lid and closure ring can be removed by semiautomatic or remotely actuated means, providing access to the SNF.

Likewise, the overpack consists of alloy materials rendering it suitable for permanent burial. Alternatively, the MPC can be removed from the overpack, and the latter reused for storage or transportation of other MPCs.

In either case, the overpack would be expected to have only minimal interior or exterior radioactive surface contamination. Any neutron activation of the metal cask walls and neutron shielding is expected to be extremely small, and the assembly would qualify as Class A waste in a stable form based on definitions and requirements in 10CFR61.55. As such, the material would be suitable for burial in a near-surface disposal site as Low Specific Activity (LSA) material.

If the HI-STAR 100 MPC needs to be opened and separated from the SNF before the fuel is placed into the MGDS, the MPC interior metal surfaces will be decontaminated using existing mechanical or chemical methods. This will be facilitated by the MPC fuel basket and interior structures' smooth metal surfaces designed to minimize crud traps. After the surface contamination is removed, the MPC radioactivity will be diminished significantly, allowing near-surface burial or secondary applications at the licensee's facility.

It is also likely that both the overpack and MPC, or extensive portions of both, can be further decontaminated to allow recycle or reuse options. After decontamination, the only radiological hazard the HI-STAR 100 System may pose is slight activation of the HI-STAR 100 materials caused by irradiation over a 40-year storage period. Table 2.4.1 provides the conservatively determined quantities of the major nuclides after 40 years of irradiation.

The calculation of the material activation is based on the following:

- Beyond design basis fuel assemblies (B&W 15x15, 3.7% enrichment, 47,500 MWD/MTU, and eight-year cooling time) stored for 40 years.
- Cask material quantities based on the design drawings.
- A constant flux equal to the initial loading condition is conservatively assumed.
- Material activation is based on MCNP-4A calculations.

As can be seen by the material activation results presented in Table 2.4.1, the HI-STAR 100 System total activation is very low.

Due to the design of the HI-STAR 100 System, no residual contamination is expected to be left behind on the concrete ISFSI pad. The base pad, fence, and peripheral utility structures will require no decontamination or special handling after the last cask is removed.

In any case, the HI-STAR 100 System would not impose any additional decommissioning requirements on the licensee of the ISFSI facility per 10CFR72.30, since the HI-STAR 100 System could eventually be shipped from the site as a complete assembly.

Table 2.4.1

HI-STAR 100 SYSTEM ACTIVATION

HI-STAR 100 Component	Nuclide	Curies After 40-Year Storage
MPC	^{54}Mn	1.434e-3
	^{55}Fe	2.30e-3
	^{59}Ni	1.89e-3
	^{60}Co	2.02e-3
	^{63}Ni	6.43e-3
	Total	1.41e-2
Overpack	^{54}Mn	1.788e-3
	^{55}Fe	8.887e-3
	^{59}Ni	N/A
	^{60}Co	N/A
	^{63}Ni	N/A
	Total	1.0675e-2
Total HI-STAR 100 System		2.48e-2

2.5 REGULATORY COMPLIANCE

Chapter 2 provides the principal design criteria related to structures, systems, and components important to safety. These criteria include specifications regarding the fuel, as well as, external conditions that may exist in the operating environment during normal and off-normal operations, accident conditions, and natural phenomena events. The chapter has been written to provide sufficient information to allow verification of compliance with 10CFR72, NUREG-1536, and Regulatory Guide 3.61. A more detailed evaluation of the design criteria and an assessment of compliance with those criteria is provided in Chapters 3 through 13.

2.6 REFERENCES

[2.0.1] HI-STAR Safety Analysis Report, Holtec Report HI-951251, current revision, Docket No. 71-9261.

[2.0.2] 10CFR72, "Licensing Requirements for the Storage of Spent Fuel in an Independent Spent Fuel Storage Installation", Title 10 of the Code of Federal Regulations.

[2.0.3] American Society of Mechanical Engineers, "Boiler and Pressure Vessel Code", 1995 with Addenda through 1997.

[2.0.4] ANSI N14.6-1993, "Special Lifting Devices for Shipping Containers Weighing 10,000 Pounds (4500 Kg) or More", June 1993.

[2.0.5] Levy, et al., "Recommended Temperature Limits for Dry Storage of Spent Light Water Reactor Zircaloy - Clad Fuel Rods in Inert Gas," Pacific Northwest Laboratory, PNL-6189, 1987.

[2.0.6] M.W. Schwartz and M.C. Witte, Lawrence Livermore National Laboratory, "Spent Fuel Cladding Integrity During Dry Storage", UCID-21181, September 1987.

[2.0.7] PNL-4835, "Technical Basis for Storage of Zircaloy-Clad Spent Fuel in Inert Gases", A.B. Johnson and E.R. Gilbert, Pacific Northwest Laboratories, September 1983.

[2.1.1] ORNL/TM-10902, "Physical Characteristics of GE BWR Fuel Assemblies", by R.S. Moore and K.J. Notz, Martin Marietta (1989).

[2.1.2] U.S. DOE SRC/CNEAF/96-01, Spent Nuclear Fuel Discharges from U.S. Reactors 1994, Feb. 1996.

[2.1.3] S.E. Turner, " Uncertainty Analysis - Axial Burnup Distribution Effects," presented in "Proceedings of a Workshop on the Use of Burnup Credit in Spent Fuel Transport Casks", SAND-89-0018, Sandia National Laboratory, Oct., 1989.

[2.1.4] Commonwealth Edison Company, Letter No. NFS-BND-95-083, Chicago, Illinois.

[2.1.5] NUREG-1536, SRP for Dry Cask Storage Systems, USNRC, Washington, DC, January 1997.

[2.1.6] DOE Multi-Purpose Canister Subsystem Design Procurement Specification.

[2.2.1] Crane Manufacturer's Association of America (CMAA), Specification #70, 1988, Section 3.3.

[2.2.2] Cunningham, et als., "Evaluation of Expected Behavior of LWR Stainless-Clad Fuel in Long-Term Dry Storage", EPRI TR-106440, April 1996.

[2.2.3] ASCE 7-88 (formerly ANSI A58.1), "Minimum Design Loads for Buildings and Other Structures", American Society of Civil Engineers, New York, NY, 1990.

[2.2.4] "Debris Collection System for Boiling Water Reactor Consolidation Equipment", EPRI Project 3100-02 and ESEERCO Project EP91-29, October 1995.

[2.2.5] Design Basis Tornado for Nuclear Power Plants, Regulatory Guide 1.76, U.S. Nuclear Regulatory Commission, April 1974.

[2.2.6] ANSI/ANS 57.9-1992, "Design Criteria for an Independent Spent Fuel Storage Installation (dry type)", American Nuclear Society, LaGrange Park, Illinois.

[2.2.7] NUREG-0800, SRP 3.5.1.4, USNRC, Washington, DC.

[2.2.8] 10CFR 100, "Reactor Site Criteria", Title 10 of the Code of Federal Regulations.

[2.2.9] Regulatory Guide 1.59, "Design Basis Floods for Nuclear Power Plants", U.S. Nuclear Regulatory Commission, Washington, D.C., August 1997.

[2.2.10] Regulatory Guide 1.102, "Flood Protection for Nuclear Power Plants", U.S. Nuclear Regulatory Commission, Washington, D.C.

[2.2.11] NUREG/CR-6407, "Classification of Transportation Packaging and Dry Spent Fuel Storage System Components According to Importance to Safety", U.S. Nuclear Regulatory Commission, Washington, D.C., February 1996.

[2.2.12] NUREG/CR-6007, "Stress Analysis of Closure Bolts for Shipping Casks", U.S. Nuclear Regulatory Commission, Washington, D.C., January 1993.

[2.2.13] NUREG-0612, "Control of Heavy Loads at Nuclear Power Plants", U.S. Nuclear Regulatory Commission, Washington, D.C., July 1980.

CHAPTER 3: STRUCTURAL EVALUATION

3.0 OVERVIEW

In this chapter, the structural components of the HI-STAR 100 System that are important to safety (ITS) are identified and all structural analyses to demonstrate their compliance with the provisions of 10CFR72 are presented. The objective of the structural analyses is to ensure that the integrity of the HI-STAR 100 System is maintained under all credible loads for normal and off-normal conditions, and design basis accident/natural phenomena. The results in this chapter support the conclusion that the confinement, criticality control, radiation shielding, and retrievability criteria set forth by 10CFR72.236(l), 10CFR72.124(a), 10CFR72.104, 10CFR72.106, and 10CFR72.122(l) are met. In particular, the design basis information contained in the previous two chapters and in this chapter provides sufficient data to permit the necessary structural evaluations to demonstrate compliance with the requirements of 10CFR72.24. To facilitate regulatory review, the assumptions and conservatism inherent in the analyses are identified along with a complete description of the analytical methods, models, and acceptance criteria. A summary of other considerations germane to satisfactory structural performance, such as corrosion and material fracture toughness, is also provided.

Detailed numerical computations supporting the conclusions in the main body of this chapter are presented in a series of appendices. Where appropriate, the subsections make reference to results in the appendices. Section 3.6.3 contains the complete list of appendices that support this chapter.

The organization of technical information in this chapter follows the format and content guidelines of USNRC Regulatory Guide 3.61 (February 1989). This revision of this FSAR ensures that the responses to the review requirements listed in NUREG-1536[2.1.5] are complete and comprehensive. It is noted that the areas of NRC staff technical inquiries, with respect to structural evaluation in NUREG-1536, span a wide array of technical topics within and beyond the material in this chapter. To facilitate staff review to ascertain compliance with the stipulations of NUREG-1536, Table 3.0.1 "Matrix of NUREG-1536 Compliance - Structural Evaluation", is included in this chapter. A comprehensive cross-reference of the topical areas set forth in NUREG-1536 and the location of the required compliance information is contained in Table 3.0.1.

Sections 3.1 through 3.6 provide technical information in the formatting sequence set forth in Regulatory Guide 3.61. Section 3.7 describes in detail HI-STAR 100 System's compliance to NUREG-1536 Structural Evaluation Requirements.

Table 3.0.1 MATRIX OF NUREG-1536 COMPLIANCE ITEMS – STRUCTURAL EVALUATION †

PARAGRAPH IN NUREG-1536	NUREG-1536 COMPLIANCE ITEM	LOCATION IN FSAR CHAPTER 3	LOCATION OUTSIDE OF FSAR CHAPTER 3
IV.1.a	ASME B&PV Compliance		
	NB	3.1.1	Tables 2.2.6,2.2.7
	NG	3.1.1	Tables 2.2.6,2.2.7
V.	Identification of SSC that are ITS		Table 2.2.6
"	Applicable Codes/Standards	3.6.1	Table 2.2.6
"	Loads	3.1.2.1.1	Table 2.2.13
"	Load Combinations	3.1.2.1.2; Table 3.1.1, Tables 3.1.3-3.1.5	Table 2.2.14
"	Summary of Safety Factors	3.4.3; 3.4.4.3.1-2; 3.4.6-3.4.8; Tables 3.4.3-3.4.19	
"	Design/Analysis Procedures	Chapter 3 plus Appendices	
"	Structural Acceptance Criteria		Tables 2.2.10-2.2.12
"	Material/QC/Fabrication	Table 3.4.2	Chap. 9; Chap. 13
"	Testing/In-Service Surveillance		Chap. 9; Chap. 12

Table 3.0.1 MATRIX OF NUREG-1536 COMPLIANCE ITEMS – STRUCTURAL EVALUATION † (Continued)

PARAGRAPH IN NUREG-1536	NUREG-1536 COMPLIANCE ITEM	LOCATION IN FSAR CHAPTER 3	LOCATION OUTSIDE OF FSAR CHAPTER 3
"	Conditions for Use		Table 1.2.6; Chaps. 8,9,12
V.1.a	Description of SSC	3.1.1	1.2; Table 2.2.6
V.1.b.i.(2)	Identification of Codes & Standards		Tables 2.2.6, 2.2.7
V.1.b.ii	Drawings/Figures		1.5
"	Identification of Confinement Boundary		1.5; 2.3.2; 7.1; Table 7.1.1
"	Boundary Weld Specifications	3.3.1.4	1.5; Table 7.1.2
"	Boundary Bolt Torque	NA	
"	Weights and C.G. Location	Tables 3.2.1-3.2.4	
"	Chemical/Galvanic Reactions	3.4.1; Table 3.4.2	
V.1.c	Material Properties	3.3; Tables 3.3.1-3.3.5	1.A; Figures 1.A.1-1.A-5; 1.C
"	Allowable Strengths	3.1.2.2; Tables 3.1.6-3.1.17	Tables 2.2.10-2.2.12
"	Suitability of Materials	3.3; Table 3.4.2	1.A; 1.B
"	Corrosion	3.4.1; Table 3.4.2	
"	Material Examination before Fabrication		9.1.1

Table 3.0.1 MATRIX OF NUREG-1536 COMPLIANCE ITEMS – STRUCTURAL EVALUATION [†] (Continued)

PARAGRAPH IN NUREG-1536	NUREG-1536 COMPLIANCE ITEM	LOCATION IN FSAR CHAPTER 3	LOCATION OUTSIDE OF FSAR CHAPTER 3
"	Material Testing and Analysis		9.1; Table 9.1.1; Table 9.1.2
"	Material Traceability		9.1.1
"	Material Long Term Performance	3.4.10; 3.4.11	9.2
"	Materials Appropriate to Load Conditions		Chap. 1
"	Restrictions on Use		Chap. 12
"	Temperature Limits	Table 3.1.17	Table 2.2.3
"	Creep/Slump	NA	
"	Brittle Fracture Considerations	3.1.2.3; Table 3.1.18-19	
"	Low Temperature Handling	NA	NA
V.1.d.i.(1)	Normal Load Conditions		2.2.1; Tables 2.2.13,2.2.14
"	Fatigue	3.1.2.4	
"	Internal Pressures/Temperatures for Hot and Cold Conditions	3.4.4.1	Tables 2.2.1,2.2.3
"	Required Evaluations		

Table 3.0.1 MATRIX OF NUREG-1536 COMPLIANCE ITEMS – STRUCTURAL EVALUATION † (Continued)

PARAGRAPH IN NUREG-1536	NUREG-1536 COMPLIANCE ITEM	LOCATION IN FSAR CHAPTER 3	LOCATION OUTSIDE OF FSAR CHAPTER 3
"	Weight+Pressure	3.4.4.3.1.2; Table 3.4.7	
"	Weight+Pressure+Temp.	3.4.4.3.1.2; Table 3.4.8	
"	Free Thermal Expansion	3.4.4.2; 3.U; 3.W; 3.AD	Tables 4.4.16, 4.4.22; Table 11.2.5
V.1.d.i.(2)	Off-Normal Conditions		2.2.2; Tables 2.2.13, 2.2.14; 11.1
V.1.d.i.(3)	Accident Level Events and Conditions	Table 3.1.2	2.2.3; Tables 2.2.13, 2.2.14; 11.2
V.1.d.i.(3).(a)	Storage Cask Vertical Drop	3.1.2.1.1.2; 3.4.9; 3.A	
"	Storage Cask Tipover	3.1.2.1.1.1; 3.4.9; 3.A	2.2.3.2
"	Storage Horizontal Drop	3.1.2.1.1.2; 3.A	
V.1.d.i.(3).(b)	Explosive Overpressure	3.1.2.1.1.4	2.2.3.10
V.1.d.i.(3).(c)	Fire		
"	Structural Evaluations	3.4.4.2.2	2.2.3.3
"	Material Properties	3.4.4.2.2	
"	Material Suitability	3.3.1.1; 3.4.4.2.2	Table 2.2.3
V.1.d.i.(3).(d)	Flood		

Table 3.0.1 MATRIX OF NUREG-1536 COMPLIANCE ITEMS – STRUCTURAL EVALUATION † (Continued)

PARAGRAPH IN NUREG-1536	NUREG-1536 COMPLIANCE ITEM	LOCATION IN FSAR CHAPTER 3	LOCATION OUTSIDE OF FSAR CHAPTER 3
"	Identification	3.1.2.1.1.3; 3.4.6	2.2.3.6
"	Cask Tipover	3.4.6	
"	Cask Sliding	3.4.6	
"	Hydrostatic Loading	3.1.2.1.1.3; 3.4.6; 3.H	
"	Consequences	3.4.6	11.2
V.1.d.i.(3).(e)	Tornado Winds		
"	Specification	3.1.2.1.1.5	2.2.3.5; Table 2.2.4
"	Drag Coefficients	3.4.8; 3.C	
"	Load Combination	3.4.8; 3.C	
"	Overturning	3.4.8; 3.C	
"	Overturning –Transfer Cask	NA	
V.1.d.i.(3).(f)	Tornado Missiles		
"	Missile Parameters	3.1.2.1.1.5	Table 2.2.5
"	Tipover	3.4.8; 3.C	
"	Damage	3.G; 3.H	

Table 3.0.1 MATRIX OF NUREG-1536 COMPLIANCE ITEMS – STRUCTURAL EVALUATION † (Continued)

PARAGRAPH IN NUREG-1536	NUREG-1536 COMPLIANCE ITEM	LOCATION IN FSAR CHAPTER 3	LOCATION OUTSIDE OF FSAR CHAPTER 3
"	Consequences	3.4.8	11.2
V.1.d.i.(3).(g)	Earthquakes		
"	Definition of DBE	3.1.2.1.1.6; 3.4.7	2.2.3.7; Table 2.2.8
"	Sliding	3.4.7.1	
"	Overturning	3.4.7.1	
"	Structural Evaluations	3.4.7.2	
V.1.d.i.(4).(a)	Lifting Analyses		
"	Trunnions		
"	Requirements	3.1.1; 3.4.3.1	
"	Analyses	3.4.3.1; 3.D	
"	Other Lift Analyses	3.4.3.2-3.4.3.4; 3.D; 3.E; 3.I; 3.K; 3.Y; 3.AH	
V.1.d.i.(4).(b)	Fuel Basket		
"	Requirements	3.1.2.1.2; Table 3.1.3	

Table 3.0.1 MATRIX OF NUREG-1536 COMPLIANCE ITEMS – STRUCTURAL EVALUATION † (Continued)

PARAGRAPH IN NUREG-1536	NUREG-1536 COMPLIANCE ITEM	LOCATION IN FSAR CHAPTER 3	LOCATION OUTSIDE OF FSAR CHAPTER 3
"	Specific Analyses	3.4.4.2; 3.4.4.3.1; 3.4.4.4.1; 3.B; 3.M; 3.U; 3.W; 3.AD; 3.AI; Table 3.4.3; Table 3.4.9; Table 3.4.11	
"	Dynamic Amplifiers	3.X	
"	Stability	3.4.4.3.1.3; Figures 3.4.27-32	
V.1.d.i.(4).(c)	Confinement Closure Lid Bolts		
"	Pre-Torque	NA	
"	Analyses	NA	
"	Engagement Length	NA	
"	Miscellaneous Bolting		
"	Pre-Torque	3.F; 3.K	Table 8.1.3
"	Analyses	3.4.4.3.2.3; 3.F; 3.K; 3.Z; Tables 3.4.17, 3.4.18; 3.AE; 3.AF	
"	Engagement Length	3.K	

Table 3.0.1 MATRIX OF NUREG-1536 COMPLIANCE ITEMS – STRUCTURAL EVALUATION † (Continued)

PARAGRAPH IN NUREG-1536	NUREG-1536 COMPLIANCE ITEM	LOCATION IN FSAR CHAPTER 3	LOCATION OUTSIDE OF FSAR CHAPTER 3
V.1.d.i.(4)	Confinement		
"	Requirements	3.1.2.1.2; Table 3.1.4	Chap. 7
"	Specific Analyses	3.4.4.2; 3.4.4.3.1; 3.4.4.4.1; 3.E; 3.H; 3.I; 3.U; 3.W; 3.Y; ; 3.AD; Tables 3.4.4, 3.4.7-3.4.9,3.4.11-3.4.15	Chap. 7
"	Dynamic Amplifiers	3.X	
"	Stability	3.4.4.3.1.7; 3.H	

Table 3.0.1 MATRIX OF NUREG-1536 COMPLIANCE ITEMS – STRUCTURAL EVALUATION † (Continued)

PARAGRAPH IN NUREG-1536	NUREG-1536 COMPLIANCE ITEM	LOCATION IN FSAR CHAPTER 3	LOCATION OUTSIDE OF FSAR CHAPTER 3
"	Overpack		
"	Requirements	3.1.2.1.2; Tables 3.1.1, 3.1.5	
"	Specific Analyses	3.4.4.3.2; 3.4.4.4.2; 3.L; 3.Y; 3.AG; Tables 3.4.5, 3.4.6, 3.4.10, 3.4.16	
"	Dynamic Amplifiers	3.X	
"	Stability	3.4.4.3.2.5; 3.H	

† Legend for Table 3.0.1

Per the nomenclature defined in Chapter 1, the first digit refers to the chapter number, the second digit is the section number within the chapter; an alphabetic character in the second place means it is an appendix to the chapter.

NA Not Applicable for this item

3.1 STRUCTURAL DESIGN

3.1.1 Discussion

The HI-STAR 100 System consists of two principal components: the Multi-Purpose Canister (MPC), and the overpack. The MPC is a hermetically sealed, welded structure of cylindrical profile with flat ends and a honeycomb fuel basket. A complete description is provided in Section 1.2.1.1 wherein the anatomy of the MPC and its fabrication details are presented with the aid of figures. A detailed discussion of the HI-STAR 100 overpack geometry is presented in Section 1.2. Drawings for the HI-STAR 100 System are provided in Section 1.5. In this section, the discussion is confined to characterizing and establishing the structural features of the MPC and the storage overpack.

The design of the MPC seeks to attain three objectives which are central to its functional adequacy, namely;

- Ability to Dissipate Heat: The thermal energy produced by the stored spent fuel must be transported to the outside surface of the MPC such that the prescribed temperature limits for the fuel cladding and for the fuel basket metal walls are not exceeded.

- Ability to Withstand Large Impact Loads: The MPC, with its payload of nuclear fuel, must be sufficiently robust to withstand large impact loads associated with the postulated handling accident events. Furthermore, the strength of the MPC must be sufficiently isotropic to meet structural requirements under a variety of handling and tip-over accidents.

- Restraint of Free End Expansion: The membrane and bending stresses produced by restraint of free-end expansion of the fuel basket are conservatively categorized as primary stresses. In view of the concentration of heat generation in the fuel basket, it is necessary to ensure that structural constraints to its external expansion do not exist.

Where the first two criteria call for extensive inter-cell connections, the last criterion requires the opposite. The design of the MPC seeks to realize all of the above three criteria in an optimal manner.

As the description presented in Chapter 1 indicates, the MPC enclosure vessel is the confinement vessel designed to meet ASME Code, Section III, Subsection NB stress limits. The enveloping canister shell, the baseplate, and the lid system form a complete confinement boundary for the stored fuel which is referred to as the "enclosure vessel". Within this cylindrical shell confinement vessel is an integrally welded assemblage of cells comprised of square cross sectional openings for fuel storage, referred to herein as the "fuel basket". The fuel basket is analyzed under the provisions of Subsection NG of Section III of the ASME Code. There are two different multi-purpose canisters which are exactly alike in their external dimensions. The essential difference between the MPCs lies in the fuel baskets. Each fuel storage MPC is designed to house fuel assemblies with different characteristics. Although all fuel baskets are configured to maximize structural ruggedness through extensive inter-cell connectivity, they are

sufficiently dissimilar in structural details to warrant separate evaluations. Therefore, analyses for each of the two MPC types are presented, as appropriate, throughout this chapter.

Components of the HI-STAR 100 System that are important to safety and their applicable design codes are defined in Chapter 2.

The structural function of the MPC in the storage mode is:

1. To maintain position of the fuel in a subcritical configuration, and

2. To provide a radiological confinement boundary.

The structural function of the overpack in the storage mode is:

1. To serve as a missile barrier for the MPC

2. To ensure stability of the HI-STAR 100 System, and

3. To provide a structurally robust support for the radiation shielding, and

4. To provide a helium retention boundary

Some structural features of the MPCs which allow the system to perform these functions are summarized below:

- There are no gasketed ports or openings in the MPC. The MPC does not rely on any sealing arrangement except welding. The absence of any gasketed or flanged joints precludes joint leaks. The confinement boundary contains no valves or other pressure relief devices.

- The closure system for the MPCs consists of two components, namely, the MPC lid and closure ring. The MPC lid can be either a single thick lid or two dual lids welded around their common periphery. The MPC closure system is shown in the drawings in Section 1.5. The MPC lid-to-MPC shell weld is a J-groove weld which is subject to root and final pass liquid penetrant examinations and finally, a volumetric examination to ensure the absence of unacceptable flaws and indications. The MPC lid is equipped with vent and drain ports which are utilized for evacuating moisture and air from the MPC following fuel loading, and subsequent backfilling with an inert gas (helium) in a specified quantity. The vent and drain ports are covered by a cover plate and welded before the closure ring is installed. The closure ring is a circular annular plate edge-welded to the MPC shell. The two closure members are interconnected by welding around the inner diameter of the ring. Lift points for the MPC are provided in the MPC lid.

- The MPC fuel baskets consist of an array of interconnecting plates (Figure 3.1.1). The number of storage cells formed by this interconnection process varies depending on the type of fuel being stored. Basket designs containing 24 (PWR), and 68 (BWR) cell configurations have been designed and are explained in detail in Section 1.2. Both baskets are designed to fit into the same MPC shell. Welding of the basket plates along their edges essentially renders the fuel basket into a multiflange beam. Figure 3.1.1 provides an isometric illustration of a fuel basket for the MPC-68 design.

- The MPC basket is separated from the longitudinal supports installed in the enclosure vessel shell by a small gap. The gap size decreases as a result of thermal expansion (depending on the magnitude of internal heat generation from the stored spent fuel). The provision of a small gap between the basket and the basket support structure is consistent with the natural thermal characteristics of the MPC. The planar temperature distribution across the basket, as shown in Section 4.4, approximates a shallow parabolic profile. This profile will create high thermal stresses unless structural constraints at the interface between the basket and the basket support structure are removed.

The MPCs will be loaded with fuel with widely varying heat generation rates. The basket/basket support structure gap tends to be reduced due to thermal expansion from decay heat generation. Gaps between the fuel basket and the basket support structure are specified to be sufficiently large such that a gap will exist around the periphery under any normal or off-normal operating or accident conditions (such as the postulated fire event).

A small number of flexible thermal conduction elements (thin aluminum tubes) are interposed between the basket and the MPC shell. The elements are designed to be resilient. They do not provide structural support for the basket, and thus their resistance to thermal growth is negligible. It is quite evident from the geometry of the MPC that a critical loading event pertains to the drop condition, when the MPC is postulated to undergo a handling side drop (the longitudinal axis of the MPC is horizontal) or tip-over. Under the side drop or tip-over condition the flat panels of the fuel basket are subject to an equivalent pressure loading that simulates the deceleration magnified inertia load from the stored fuel and the MPC's own metal mass.

The MPC fuel basket maintains the spent nuclear fuel in a subcritical arrangement. Its safe operation is assured by maintaining the physical configuration of the storage cell cavities intact in the aftermath of a drop event. This requirement is considered to be satisfied if the MPC fuel basket meets the stress intensity criteria set forth in the ASME Code, Section III, Subsection NG. Therefore, the demonstration that the fuel basket meets Subsection NG limits ensures that there is no impairment of ready retrievability (as required by NUREG-1536), that there is no unacceptable release of radioactive materials, and that there is no unacceptable radiation level.

The MPC confinement boundary contains no valves or other pressure relief devices. The MPC enclosure vessel will be shown to meet the stress intensity criteria of the ASME Code, Section III, Subsection NB for all service conditions.

Structural features of the overpack that allow the system to perform its structural function are summarized below:

- The HI-STAR 100 overpack is a missile barrier, radiation shield, and helium retention boundary in the storage mode. The overpack provides kinematic stability to the system, and acts as a cushion for the MPC in the event of a postulated tip-over accident. The overpack features a thick inner shell welded to a bottom plate which forms the load bearing surface (foundation interface) for the HI-STAR 100 System. A solid metal top flange welded at the top of the inner shell provides the attachment location for lifting trunnions. The top flange is also designed to provide a recessed ledge for the closure plate to protect the bolts from direct shear loadings resulting from an impulsive load at the top edge of the overpack. The helium retention boundary of the HI-STAR 100 overpack is subject to the stress limits of the ASME Code, Section III, Subsection NB.

- The inner shell is reinforced by multilayered intermediate shells. The multi layer approach eliminates the potential for a crack in any one layer, developed by any postulated mechanical loading or material flaw, to travel uninterrupted through the vessel wall. The intermediate shells also buttress the overpack inner shell against buckling. The intermediate shells of the HI-STAR 100 overpack are subject to the stress limits of the ASME Code, Section III, Subsection NF, Class 3.

- To facilitate handling of the loaded system, the HI-STAR 100 overpack is equipped with lifting trunnions and pocket trunnions. The pocket trunnions are located on the overpack intermediate shells just above the bottom plate. The centerline through the pocket trunnion recess is offset from a vertical plane containing the overpack's center of gravity to ensure a stable rotation direction during upending and down ending operations. Lifting trunnions are conservatively designed to meet the design safety factor requirements of NUREG-0612 [3.1.1] and ANSI N14.6-1993 [3.1.2] for single failure proof lifting equipment.

Table 2.2.6 provides a listing of the applicable design codes for all structures, systems, and components which are designated as "Important to Safety"(ITS). Since no structural credit is required for the weld between the adjustable basket support pieces (i.e., shims and basket support flat plates), the adjustable basket supports are classified as NITS.

3.1.2 Design Criteria

This subsection provides information requested in Subsection 3.1.2 of Regulatory Guide 3.61. Principal design criteria for normal, off-normal, and accident/environmental events are discussed in Section 2.2 in Chapter 2. In this section, the loads, load combinations, and allowable stresses used in the structural evaluation of the HI-STAR 100 System are presented.

Consistent with the provisions of NUREG-1536, the central objective of the structural analysis presented in this chapter is to ensure that the HI-STAR 100 System possesses sufficient structural capability to withstand normal and off-normal loads and the worst case loads under natural phenomenon events. Withstanding such loadings enables the HI-STAR 100 System to successfully preclude the following negative consequences:

- risk of criticality
- release of radioactive materials
- unacceptable radiation levels
- impairment of ready retrievability of the SNF

The design objectives for the HI-STAR 100 are particularized for individual components as follows:

- The objective of the structural analysis of the MPC is to demonstrate that:

  1. Confinement of radioactive material is maintained under normal, off-normal, accident conditions, and natural phenomenon events.

  2. The MPC basket does not deform under credible loading conditions such that the sub-criticality or retrievability of the SNF is jeopardized.

- The objective of the structural analysis of the storage overpack is to demonstrate that:

  1. Tornado-generated missiles do not compromise integrity of the MPC confinement boundary.

  2. The integrity of the helium retention boundary is not compromised.

  3. The radiation shielding remains properly positioned in the case of a natural phenomenon or accident event.

The aforementioned objectives are deemed to be satisfied for the MPC, and the overpack, if stresses (or stress intensities, as applicable) calculated by the appropriate structural analyses are less than the allowables defined in Subsection 3.1.2.2.

Stresses arise in the components of the HI-STAR 100 System due to various loads which originate under normal, off-normal, or accident conditions. These individual loads are combined to form load combinations. Stresses and stress intensities resulting from the load combinations are compared to allowable stresses and stress intensities. The following subsections present loads, load combinations, and allowable strengths for use in the structural analyses of the MPC and the HI-STAR 100 overpack.

3.1.2.1 Loads and Load Combinations

The individual loads are defined in Section 2.2 of this report (Table 2.2.13). Load combinations are developed by appropriately combining the individual loads (Table 2.2.14). Load combinations are applied to the mathematical models of the MPCs, and the overpack. Results of the analyses carried out under bounding load combinations are compared to allowable stresses or stress intensities, as applicable.

3.1.2.1.1 Individual Load Cases

The individual load cases which address each design criterion applicable to the structural design of the HI-STAR 100 System are catalogued in Table 2.2.13. Each load is given a symbol for subsequent use in the load combination listed in Table 2.2.14.

Accident condition and natural phenomena-induced events, collectively referred to as the "Level D" condition in Section III of the ASME Boiler & Pressure Vessel Codes, *in general* do not have a universally prescribed limit. For example, the impact load from a tornado borne missile, or the overturning load under flood or tsunami, cannot be prescribed as design basis values with absolute certainty that all ISFSI sites will be covered. Therefore, as applicable, allowable magnitudes of such loadings are postulated for the HI-STAR system. The allowable values are drawn from ANSI documents (such as for tornado and wind) or from an intrinsic limitation in the system (such as the permissible "drop height" under a postulated handling accident). In the following, the essential characteristic of each "Level D" type loading is explained.

3.1.2.1.1.1 Tip-Over

It is required to demonstrate that the HI-STAR 100 System will not tip over as a result of a postulated natural phenomenon event, including tornado wind, a tornado-generated missile, a seismic or a hydrological event (flood). However, to demonstrate the defense-in-depth features of the design, a non-mechanistic tip-over scenario per NUREG-1536 (page 3-11) is analyzed. Table 3.1.2 lists the design basis deceleration limit.

3.1.2.1.1.2 Handling Accident

The design basis handling accident during transport of a loaded HI-STAR 100 storage overpack results in either a vertical or horizontal drop. Table 3.1.2 lists the design basis deceleration limit.

3.1.2.1.1.3 Flood

The postulated flood event results into two discrete scenarios which must be considered; namely,

1. Stability of the HI-STAR 100 System due to flood water velocity, and

2. Structural effects of hydrostatic pressure and water velocity induced lateral pressure.

The maximum design external pressure for the overpack is 300 psi (Table 2.2.1). The maximum design flood water depth of 656 ft. (Table 2.2.8) corresponds to an external pressure that is bounded by the design external pressure in Table 2.2.1.

3.1.2.1.1.4 Explosion

Explosive materials are not permitted within the protective boundary of an ISFSI where a loaded HI-STAR 100 System is maintained in normal storage. The accident condition overpack external pressure specified in Table 2.2.1 is also set as the overall external pressure that bounds all credible external explosion events. There are no credible internal explosion events.

3.1.2.1.1.5 Tornado

The three components of a tornado load are:

1. Pressure changes,
2. Wind loads, and
3. Tornado-generated missiles.

Wind speeds and tornado-induced pressure drop are specified in Table 2.2.4. Tornado missiles are listed in Table 2.2.5. Potential consequences of a tornado on the cask system are:

- Instability (tip-over) due to tornado missile impact plus either steady wind or impulse from sudden pressure drop.

- Stress in the overpack induced by the lateral force caused by the steady wind or missile impact.

3.1.2.1.1.6 Earthquake

Subsections 2.2.3.7 and 3.4.7 contain the detailed specification of the seismic inputs applied to the HI-STAR 100 System. The design basis earthquake is assumed to be applied at the top of the ISFSI pad. Potential consequences of a seismic event are sliding/overturning of the loaded overpack, and stresses in the overpack arising from the inertia forces on the system.

3.1.2.1.1.7 Lightning

The HI-STAR 100 overpack contains many thousands of pounds of highly conductive carbon steel with over 400 square feet of external surface area. Such a large surface area and metal mass is adequate to dissipate any lightning which may strike the HI-STAR 100 System. There are no combustible materials on the HI-STAR 100 surface. Therefore, lightning will not impair the structural performance of components of the HI-STAR 100 System that are important to safety.

3.1.2.1.2 Load Combinations

Load combinations are created by summing the effects of all applicable individual loads which can act concurrently. The load combinations are selected for the normal, off-normal, and accident conditions. The loadings appropriate for HI-STAR 100 under the various conditions are presented in Table 2.2.14. These loadings are combined into meaningful combinations for the various HI-STAR 100 System components in Tables 3.1.1, and 3.1.3-3.1.5. Table 3.1.1 lists the load combinations that address overpack stability. Tables 3.1.3 through 3.1.5 list the applicable load combinations for the fuel basket, the enclosure vessel, and the overpack, respectively.

As discussed in Section 2.2.7, the number of discrete load combinations for each situational condition (i.e., normal, off-normal, etc.) is consolidated by defining bounding loads for certain groups of loadings. Thus, the accident condition pressure P_o^* bounds the surface loadings arising from accident and extreme natural phenomenon events, namely tornado wind W', flood F, and explosion E^*.

As noted previously, certain loads, namely earthquake E, flowing water under flood condition F, and tornado missile M, act to destabilize a cask. Additionally, these loads act on the overpack and produce localized stresses at the HI-STAR 100 System to ISFSI interface. Table 3.1.1 provides the load combinations which are relevant to the stability analyses. The site ISFSI DBE zero period acceleration (ZPA) must be bounded by the design basis seismic ZPA defined by the Load Case C of Table 3.1.1 to demonstrate that the margins against tip-over and inter-cask collision during a seismic event are maintained.

As noted at the beginning of this section, there are two principal components to the HI-STAR 100 System: the multi-purpose canister (MPC) and the overpack. The MPC is made up of the fuel basket and the enclosure vessel. A complete account of analyses and results for all load cases for all three constituent parts: (i) the fuel basket, (ii) the enclosure vessel, and (iii) the overpack is provided in Section 3.4, as required by Regulatory Guide 3.61.

In the following, the loadings listed as applicable for each situational condition in Table 2.2.14 are addressed in meaningful load combinations for the fuel basket, enclosure vessel, and the overpack. Each component is considered separately. It is noted that off-normal condition pressure temperatures for structural analyses are conservatively bounded by the specified design pressures and temperatures. Therefore, load combinations for normal and off-normal condition are subsumed into a consolidated set of bounding load combinations.

Fuel Basket

Table 3.1.3 summarizes all loading cases (derived from Table 2.2.14) which are germane to demonstrating compliance of the fuel baskets to Subsection NG when these baskets are housed within the HI-STAR 100 overpack.

Normal Condition

- The fuel basket is not a pressure vessel; therefore, the pressure loadings are not meaningful loads for the basket. Further, the basket is structurally decoupled from the enclosure vessel. The gap between the basket and the enclosure vessel is sized to ensure that no constraint of free-end thermal expansion of the basket occurs. The demonstration of the adequacy of the basket to the enclosure vessel (EV) gap to ensure absence of interference is a physical problem which must be analyzed. Temperature, like pressure, is not a source of loading for the fuel basket. All loadings on the fuel basket, therefore, arise from handling and postulated handling accident conditions.
- Normal handling encompasses both vertical and horizontal orientation. When the cask is being handled in the vertical orientation, the vertical load produces a strictly axial compressive stress. When the cask is being lifted from the horizontal orientation, the amplified dead load may cause flexing of the fuel basket panels.

Off-Normal Conditions

- The off-normal condition handling loads are identical to the normal condition, and therefore, a separate analysis is not required.

Accident Condition

- Three accident condition scenarios must be considered: (i) drop with the storage overpack axis vertical; (ii) drop with the storage overpack axis horizontal; and (iii) storage overpack tip-over.

- The vertical drop scenario induces compression in the longitudinal panel of the fuel basket.

- The horizontal drop and tip-over must consider multiple orientations of the fuel basket as the fuel basket is not radially symmetric. Heretofore, two horizontal drop orientations are considered which are referred to as the 0-degree drop and 45-degree drop, respectively. In the 0-degree drop, the basket drops with its panels oriented parallel and normal to the vertical (see Figure 3.1.2). The 45-degree drop implies that the basket's honeycomb section is rotated meridionally by 45 degrees (Figure 3.1.3).

Enclosure Vessel

Table 3.1.4 summarizes all load cases that are applicable to structural analysis of the enclosure vessel to ensure integrity of the confinement boundary.

Normal Conditions

- The enclosure vessel is a pressure vessel consisting of a cylindrical shell, a thick circular baseplate at the bottom, and a thick circular lid at the top. This pressure vessel must be shown to meet the primary stress intensity limits for ASME Section III Class 1 at the design temperature and primary plus secondary stress intensity limits under the combined action of pressure plus thermal loads.

- The MPC lid system of the enclosure vessel is equipped with tapped holes for lifting operations. A normal handling operation is defined to encompass a vertical lift where the MPC is supported by threaded inserts in the MPC lid. Stress intensities in the MPC lid, must satisfy Level A limits for Class 1 components. The threaded inserts (i.e., the lifting eye bolts) and the internal threads in the tapped holes must meet NUREG-0612 stress limits. Further discussion on design criteria applicable to lifting operations is presented in Subsection 3.4.3 herein, as required by Regulatory Guide 3.61.

Off-Normal Conditions

- The off-normal condition loads are identical to the normal condition, and therefore, a separate analysis is not required.

Accident Conditions

- The design basis deceleration for the MPC in the HI-STAR 100 System is 60g's. The deceleration loading developed in the enclosure vessel during a horizontal drop event must be combined with those due to P_i (internal pressure) acting alone. The accident condition pressure is bounded by P_i^*. During a vertical drop scenario, the axial buckling of the enclosure vessel shell is the item of principal concern. To render the loading combination most adverse, the vertical deceleration load is assumed to act in the absence of P_i, which produces tensile stresses (and thus counteracts the loads which produce buckling).

- The fire event (T^* loading) is considered for ensuring absence of interference between the enclosure vessel and the fuel basket and between the enclosure vessel and the overpack. The metal temperatures of the "NB pressure parts" (defined by the ASME Code, loc. cit.) are required to remain in the range of temperatures permitted by the ASME Code.

Storage Overpack

Table 3.1.5 identifies the load cases to be considered for the overpack. These are in addition to the kinematic criteria listed in Table 3.1.1. Within these load cases and kinematic criteria, the following items must be addressed:

Normal Conditions

- The inner shell, the bottom plate, the top flange, and the closure plate of the overpack constitute a pressure vessel and must be engineered to meet ASME Code requirements for helium pressure retention.

- In the normal handling condition, the most adverse configuration is the vertical lift. The top flange/closure plate region and the bottom plate are most affected by the handling loads acting in concert with design internal or external pressure. The specific stress limits which must be satisfied under normal handling are discussed in depth in Subsection 3.4.3, as required by Regulatory Guide 3.61.

Off-Normal Conditions

- The off-normal condition loads are identical to the normal condition, and therefore, a separate analysis is not required.

Accident Conditions

- Maximum flood water velocity for the overpack with an empty MPC (to minimize system weight and thus maximize the potential for kinematic instability) must be specified to ensure that no sliding or tip-over occurs.

- Tornado missile plus wind on an overpack with an empty MPC must be specified to demonstrate that no cask tip-over occurs.

- Tornado missile penetration analysis must demonstrate that the postulated penetrant missiles cannot reach the MPC stored inside the HI-STAR 100 overpack.

- Under seismic conditions, a fully loaded HI-STAR 100 overpack must not tip over under the maximum ZPA event. The maximum sliding of the overpack must demonstrate that casks will not impact each other.

- Under a non-mechanistic postulated tip-over or a drop accident with a full HI-STAR 100 overpack, the overpack structure must meet faulted (Level D) requirements of the ASME Code.

3.1.2.2 Allowables

The important to safety components of the HI-STAR 100 System are listed in Table 2.2.6. Allowable stresses, as appropriate, are tabulated for these components for all service conditions in Tables 3.1.6 through 3.1.16.

In Subsection 2.2.5, the applicable service level from the ASME Code for determination of allowables is listed. Table 2.2.14 provides a tabulation of normal, off-normal, and accident conditions and the service levels defined in the ASME Code, along with the applicable loadings for each service condition.

Allowable stresses and stress intensities are calculated using the data provided in the ASME Code and Tables 2.2.10 through 2.2.12. Tables 3.1.6 through 3.1.16 contain numerical values of the stresses/stress intensities for all MPC and overpack load bearing materials as a function of temperature.

In all tables the terms S, S_m, S_y, and S_u, respectively, denote the design stress, design stress intensity, minimum yield strength, and the ultimate strength. Property values at intermediate temperatures which are not reported in the ASME Code are obtained by linear interpolation. Property values are not extrapolated beyond the limits of the Code in any structural calculation. Additional terms relevant to the analyses are extracted from the ASME Code (Figure NB-3222-1, for example) as follows:

Symbol	Description	Notes
P_m	Average primary stress across a solid section.	Excludes effects of discontinuities and concentrations. Produced by pressure and mechanical loads.
P_L	Average stress across any solid section.	Considers effects of discontinuities but not concentrations. Produced by pressure and mechanical loads, including inertia earthquake effects.
P_b	Primary bending stress.	Component of primary stress proportional to the distance from the centroid of a solid section. Excludes the effects of discontinuities and concentrations. Produced by pressure and mechanical loads, including inertia earthquake effects.
P_e	Secondary expansion stress.	Stresses which result from the constraint of free-end displacement. Considers effects of discontinuities but not local stress concentration. (Not applicable to vessels.)
Q	Secondary membrane plus bending stress.	Self-equilibrating stress necessary to satisfy continuity of structure. Occurs at structural discontinuities. Can be caused by pressure, mechanical loads, or differential thermal expansion.

Symbol	Description	Notes
F	Peak stress.	Increment added to primary or secondary stress by a concentration (notch), or, certain thermal stresses which may cause fatigue but not distortion. This value is not used in the tables.

It is shown that there is no interference between component parts due to free thermal expansion. Therefore, P_e does not develop within any HI-STAR 100 component.

It is recognized that the planar temperature distribution in the fuel basket and the overpack under the maximum heat load condition is the highest at the cask center and drops monotonically, reaching its lowest value at the outside surface. Strictly speaking, the allowable stresses/stress intensities at any location in the basket, the enclosure vessel, or the overpack should be based on the coincident metal temperature under the specific operating condition. However, in the interest of conservatism, reference temperatures are established for each component which are upper bound on the metal temperature for each situational condition. Table 3.1.17 provides the reference temperatures for the fuel basket and the MPC canister and, utilizing Tables 3.1.6 through 3.1.16, provides conservative numerical limits for the stresses and stress intensities for all loading cases. Reference temperatures for the MPC baseplate and the MPC lid are 400°F and 550°F, respectively, as specified in Table 2.2.3.

Finally, the lift devices in the HI-STAR 100 overpack and the multi-purpose canisters, collectively referred to as "trunnions", are subject to specific limits set forth by NUREG-0612: the primary stresses in a trunnion must be less than the smaller of 1/10 of the material ultimate strength and 1/6 of the material yield strength under a normal handling condition (Load Cases F2, E2, and 03 in Tables 3.1.3 through 3.1.5, respectively. The load combination D+H in Table 3.1.5 is equivalent to 1.15D. This is further explained in Subsection 3.4.3.

The region around the trunnions is part of the NF structure in HI-STAR 100 and an NB pressure boundary in the MPC, and as such, must satisfy the applicable stress (or stress intensity) limits for the load combination. In addition to meeting the applicable Code limits, it is further required that the local primary stresses at the trunnion/mother structure interface must not exceed the material yield stress at three times the handling condition load (1.15D). This criterion, mandated by Regulatory Guide 3.61, Section 3.4.3, eliminates the potential of local yielding at the trunnion/structure interface.

3.1.2.3 Brittle Fracture

The MPC canister and basket are constructed from a series of stainless steels termed Alloy X. These stainless steel materials do not undergo a ductile-to-brittle transition in the minimum temperature range of the HI-STAR 100 System. Therefore, brittle fracture is not a concern for the MPC components. However, the HI-STAR 100 overpack is composed of ferritic steel materials which will be subject to impact loading in a cold environment and, therefore, must be evaluated and/or subjected to impact testing in accordance with the ASME Code to ensure protection against brittle fracture.

Tables 3.1.18 and 3.1.19 provide the fracture toughness test criteria for the HI-STAR 100 components in accordance with the applicable ASME Code and Regulatory Guide requirements for prevention of brittle fracture. Regulatory Guides 7.11 [3.1.3] and 7.12 [3.1.4] are used to determine drop test requirements for the helium retention boundary components, as discussed below.

All helium retention boundary materials subject to impact loading in a cold environment must be evaluated and/or tested for their propensity for brittle fracture. The overpack baseplate, top flange, and closure plate have thicknesses greater than four inches. Table 1 of Regulatory Guide 7.12 requires that the Nil Ductility Transition temperature, T_{NDT}, (for the lowest service temperature of -20°F) be -129°F for 6-in. thick material, and linear interpolation of the table shows that for 7-inch thick material, the T_{NDT} is -132°F. SA350-LF3 has been selected as the material for these overpack components based on the material's capability to perform at low temperatures with excellent ductility properties

The overpack inner shell has a thickness of 2.5 inches. SA203-E has been selected as the material for this item due to its capability to perform at low temperatures (see Table A1.15 of ASME Section IIA). Regulatory Guide 7.11 requires that the T_{NDT} for this material be less than -70°F.

The overpack closure plate bolts are fabricated from SB-637 Grade N07718, a high strength nickel alloy material. Section 5 of NUREG/CR-1815 [3.1.5] indicates that bolts are generally not considered a fracture critical component. Nevertheless, this material has a high resistance to fracture at low temperatures, as can be shown by calculating the transition temperature of the material and assessing its performance as indicated in NUREG/CR-1815.

The Aerospace Structural Metals Handbook [Ref. 3.1.6] shows that a minimum impact absorption energy for SB-637 Grade N07718 at -320°F is 18.5 ft-lb. This may be transferred into a fracture toughness value by using the relationship (presented in Section 4.2 of NUREG/CR-1815) between Charpy impact measurement, C_v (ft-lb), and dynamic fracture toughness, K_{ID} (psi $\sqrt{in.}$)

$$K_{ID} = (5\ E\ C_v)^{1/2}$$

where $E \approx 31 \times 10^6$ psi at -320°F and C_v (minimum) = 18.5 ft-lb. Therefore,

$$K_{ID} = 53.5 \text{ ksi } \sqrt{in.}$$

Using Figure 2 of NUREG/CR-1815 yields

$$(T - T_{NDT}) \approx 32°F$$

Since the data used is for T = -320°F, then T_{NDT} = -320° - 32° = -352°F

Using Figure 3 of NUREG/CR-1815 where thickness is defined as the bolt diameter (1.5 inch), and $\sigma/\sigma_{yd} = 1$ per Regulatory Guide 7.11, A (°F) is found to be 60°F. Therefore, the required maximum nil ductility transition temperature per NUREG/CR-1815 for the closure bolts is

$$T_{NDT} = T_{LT} - A$$

$$= -40°F - 60°F = -100°F$$

where $T_{LT} = -40°F$.

The large margin between the calculated T_{NDT} and the required maximum nil ductility transition temperature leads to the conclusion that SB-637 Grade N07718 possesses appropriate fracture toughness for use as closure lid bolting.

ASME Code Section III, Subsection NF requires Charpy V-notch tests for materials of certain non-helium retention boundary components of the overpack. The intermediate shells used for gamma shielding are fabricated from normalized SA516-70. Table A1.15 of ASME Section IIA shows that normalized SA516-70 should have a minimum energy absorption of 12 ft-lb at -40°F for a Charpy V-notch test. The lowest service temperature for the overpack is -40°F. Therefore, these tests on the normalized SA516-70 materials of the intermediate shells will confirm the minimum energy absorption of 12 ft-lb at -40°F and the ability of the intermediate shells to perform their intended function at the lowest service temperature.

The pocket trunnions are fabricated from 17-4PH material that is precipitation hardened to condition H1150. ARMCO Product Data Bulletin S-22 [Ref. 3.1.7] shows that Charpy V-notch testing of 17-4PH H1150 material at -110°F gives energy absorption values of approximately 48 ft-lb. Using the same methodology as used for the closure plate bolts,

$$K_{ID} = 83 \text{ ksi } \sqrt{\text{in.}}$$

where $E = 28.7 \times 10^6$ psi and $C_v = 48$ ft-lbs.

Using Figure 2 of NUREG/CR-1815 yields

$$T - T_{NDT} = 65°F$$

and therefore

$$T_{NDT} = -110°F - 65°F = -175°F$$

While the pocket trunnions are not part of the helium retention boundary for the overpack, Regulatory Guide 7.12 is used to define the required T_{NDT} for the trunnion pocket thickness ($T_{NDT} = -140°F$). The 35°F margin between the calculated T_{NDT} and the T_{NDT} defined in Regulatory Guide 7.12 provides assurance that brittle fracture failure of the 17-4PH material will not occur at the lowest service temperature.

3.1.2.4 Fatigue

In storage, the HI-STAR 100 System is not subject to significant cyclic loads. Failure due to fatigue is not a concern for the HI-STAR 100 System.

The system is subject to cyclic temperature fluctuations. These fluctuations result in small changes of thermal expansions and pressures in the MPC. The loads resulting from these changes are small and do not significantly contribute to the "usage factor" of the cask.

The closure plate bolts will be installed with a specified pre-load and, therefore, will be subject to little fluctuation in their state of stress due to small variations in overpack internal pressure.

Inspection of the trunnions specified in Chapter 9 will preclude use of a trunnion which exhibits visual damage.

3.1.2.5 Buckling

Certain load combinations subject structural sections with relatively large slenderness ratios (such as the enclosure vessel shell) to compressive stresses which may actuate buckling instability before the allowable stress is reached. Tables 3.1.4 and 3.1.5 list load combinations for the enclosure vessel and the HI-STAR 100 structure; the cases which warrant stability (buckling) check are listed therein.

Table 3.1.1

LOAD COMBINATIONS SIGNIFICANT TO HI-STAR 100 OVERPACK
KINEMATIC STABILITY ANALYSIS

Load Case	Combinations[†]	Comment	Analysis of this Load Case Presented in:
A	D + F	This case establishes flood water flow velocity with a minimum safety factor of 1.1 against overturning and sliding.	Subsection 3.4.6
B	D + M + W'	Demonstrate that the HI-STAR 100 overpack with minimum SNF stored (minimum D) will not tip over.	Appendix 3.C
C	D + E	Establish the value of ZPA[††] which will not cause the overpack to tip over.	Subsection 3.4.7

† Loading symbols are defined in Table 2.2.13.
†† ZPA is zero period acceleration.

Table 3.1.2

DESIGN BASIS DECELERATIONS FOR THE DROP AND TIP-OVER EVENTS

Case	Value (in multiples of acceleration due to gravity)
Vertical axis drop	60
Horizontal axis (side) drop and tip-over	60

Table 3.1.3
LOADING CASES FOR THE FUEL BASKET

Load Case I.D.	Loading[†]	Notes	Location Where this Case is Evaluated
F1	T, T'	Demonstrate that the most adverse of the temperature distributions in the basket will not cause fuel basket to expand and contact the enclosure vessel wall.	Appendices 3.AD, 3.U, 3.W; Subsection 3.4.4.2
F2	D + H	For a lateral handling load, a 2g deceleration is imposed on the stored fuel.	Subsections 3.4.4.3.1.1, 3.4.4.4.1
F3			
F3.a	D + H'	Vertical axis drop event	Subsections 3.4.4.3.1.6, 3.4.4.3.1.3
F3.b	D + H'	Side Drop, 0^{o} orientation (Figure 3.1.2)	Subsections 3.4.4.3.1.1, 3.4.4.4.1
F3.c	D + H'	Side Drop, 45^{o} orientation (Figure 3.1.3)	Subsections 3.4.4.3.1.1, 3.4.4.4.1

[†] The symbols used for the loadings are defined in Table 2.2.13.

Table 3.1.4

LOADING CASES FOR THE ENCLOSURE VESSEL (CONFINEMENT BOUNDARY)

Load Case I.D.	Load Combination†	Notes	Comments and Location in FSAR Where this Case is Analyzed
E1.a	Design internal pressure, P_i	Primary stress intensity limits in the shell, baseplate, and closure ring	Lid 3.E.8.1.1 Baseplate 3.I.8.1 Shell 3.4.4.3.1.2 Supports N/A
E1.b	Design external pressure, P_o	Primary stress intensity limits, buckling stability	Lid P_i bounds Baseplate P_i bounds Shell 3.H (Case 7) Supports N/A
E1.c	Design internal pressure, P_i, plus Temperature, T	Primary plus secondary stress intensity under Level A condition	Subsection 3.4.4.3.1.2
E2	D + H + (P_i, P_o)†† For elastic stability, only D+H is considered.	Vertical lift, internal operating pressure conservatively assumed to be equal to the normal design pressure.	Lid 3.E.8.1.2 Baseplate 3.I.8.2 Shell 3.4.4.3.1.1, 3.4.4.4.1 (stress) 3.H (Case 4) (buckling) Supports 3.4.4.3.1.1, 3.4.4.4.1

† The symbols used for the loadings are defined in Table 2.2.13.

†† The notation (P_i, P_o) means that both cases are checked for stresses with either P_o or P_i applied.

Table 3.1.4 (continued)

LOADING CASES FOR THE ENCLOSURE VESSEL (CONFINEMENT BOUNDARY)

Load Case I.D.	Load Combination†	Notes	Comments and Location in FSAR Where this Case is Analyzed
E3			
E3.a	D + H' + (P_o, P_i) For elastic stability, only D+H' is considered.	Vertical axis drop event	Lid 3.E.8.2.1 Baseplate 3.I.8.3 Shell 3.H (Case 5) (Buckling) Supports N/A
E3.b	D + H' + (P_i, P_o)	Side drop, 0° orientation (Figure 3.1.2)	Lid End drop bounds Baseplate End drop bounds Shell 3.4.4.3.1.1, 3.4.4.4.1 Supports 3.4.4.3.1.1, 3.4.4.4.1, 3.M
E3.c	D + H' + (P_i, P_o)	Side drop, 45° orientation (Figure 3.1.3)	Lid End drop bounds Baseplate End drop bounds Shell 3.4.4.3.1.1, 3.4.4.4.1 Supports 3.4.4.3.1.1, 3.4.4.4.1, 3.M
E4	T	Demonstrate that interference with the overpack will not develop for T.	Subsection 3.4.4.2 Appendices 3.U; 3.V; 3.W; 3.AD

Table 3.1.4 (continued)

LOADING CASES FOR THE ENCLOSURE VESSEL (CONFINEMENT BOUNDARY)

Load Case I.D.	**Load Combination†**	**Notes**	**Comments and Location in FSAR Where this Case is Analyzed**
E5	P_i^* or P_o^* + D + T^*	Demonstrate compliance with Level D stress limits - buckling stability.	Lid 3.E.8.2.1.3 Baseplate 3.I.8.4 Shell 3.H (Case 6) (buckling) 3.4.4.3.1.5 (thermal stress) Supports N/A

Table 3.1.5
LOAD CASES FOR THE HI-STAR 100 OVERPACK

Load Case I.D.	Loading†	Notes	Location in FSAR Where this Case is Analyzed
01	(P_i, P_o)	Compliance with NB stress intensity limits	3.4.4.3.2.1, 3.4.4.4.2
02	$(P_i^*, P_o^*) + D + T^*$	Compliance with NB Level D stress intensity limits	3.4.4.3.2.1, 3.4.4.4.2
03	$D + H + T + (P_o, P_i)$	Vertical load handling of HI-STAR 100 Overpack	3.4.4.3.2.1, 3.4.4.4.2; 3.D
04			
04.a	$D + H' + (P_o, P_i)$	End drop; primary stress intensities must meet Level D limits.	3.4.4.3.2.1, 3.4.4.4.2
04.b	$D + H' + (P_o, P_i)$	Horizontal (side) drop; meet Level D limits for NF components away from the impacted zone	3.4.4.3.2.1, 3.4.4.4.2
05	T	Satisfy primary membrane plus bending stress limits for NB components	3.4.4.3.2.1, 3.4.4.4.2
06	M (small and medium penetrant missiles)	Demonstrate that no thru-wall breach of the overpack occurs, no loss of helium retention boundary occurs, and that primary stress levels are not exceeded.	3.G

Notes:

1. Under each of these load cases, different regions of the structure are analyzed to demonstrate compliance.

† The symbols used for the loadings are defined in Table 2.2.13.

Table 3.1.6

DESIGN, LEVELS A AND B: STRESS INTENSITY

Code: ASME NB
Material: SA203-E
Service Conditions: Design, Levels A and B
Item: Stress Intensity

Temp. (°F)	Classification and Value (ksi)					
	S_m	P_m†	P_L†	$P_L + P_b$†	$P_L + P_b + Q$††	P_e††
-20 to 100	23.3	23.3	35.0	35.0	69.9	69.9
200	23.3	23.3	35.0	35.0	69.9	69.9
300	23.3	23.3	35.0	35.0	69.9	69.9
400	22.9	22.9	34.4	34.4	68.7	68.7
500	21.6	21.6	32.4	32.4	64.8	64.8

Definitions:

S_m = Stress intensity values per ASME Code
P_m = Primary membrane stress intensity
P_L = Local membrane stress intensity
P_b = Primary bending stress intensity
P_e = Expansion stress
Q = Secondary stress
P_L+P_b = Either primary or local membrane plus primary bending

Definitions for Table 3.1.6 apply to all following tables unless modified.

Notes:

1. Limits on values are presented in Table 2.2.10.

† Evaluation required for Design condition only.
†† Evaluation required for Levels A and B conditions only. P_e not applicable to vessels.

Table 3.1.7

LEVEL D: STRESS INTENSITY

Code: ASME NB
Material: SA203-E
Service Condition: Level D
Item: Stress Intensity

Temp. (°F)	Classification and Value (ksi)		
	P_m	P_L	$P_L + P_b$
-20 to 100	49.0	70.0	70.0
200	49.0	70.0	70.0
300	49.0	70.0	70.0
400	48.2	68.8	68.8
500	45.4	64.9	64.9

Notes:

1. Level D allowables per NB-3225 and Appendix F, Paragraph F-1331.
2. Average primary shear stress across a section loaded in pure shear may not exceed 0.42 S_u.
3. Limits on values are presented in Table 2.2.10.
4. P_m, P_L, and P_b are defined in Table 3.1.6.

Table 3.1.8

DESIGN, LEVELS A AND B: STRESS INTENSITY

Code: ASME NB
Material: SA350-LF3
Service Conditions: Design, Levels A and B
Item: Stress Intensity

Temp. (°F)	Classification and Value (ksi)					
	S_m	P_m†	P_L†	$P_L + P_b$†	$P_L + P_b + Q$††	P_e††
-20 to 100	23.3	23.3	35.0	35.0	69.9	69.9
200	22.8	22.8	34.2	34.2	68.4	68.4
300	22.2	22.2	33.3	33.3	66.6	66.6
400	21.5	21.5	32.3	32.3	64.5	64.5
500	20.2	20.2	30.3	30.3	60.6	60.6
600	18.5	18.5	27.75	27.75	55.5	55.5
700	16.8	16.8	25.2	25.2	50.4	50.4

Notes:

1. Source for S_m is ASME Code.

2. Limits on values are presented in Table 2.2.10.

3. S_m, P_m, P_L, P_b, Q, and P_e are defined in Table 3.1.6.

† Evaluation required for Design condition only.
†† Evaluation required for Levels A and B conditions only. P_e not applicable to vessels.

Table 3.1.9

LEVEL D, STRESS INTENSITY

Code: ASME NB
Material: SA350-LF3
Service Conditions: Level D
Item: Stress Intensity

Temp. (°F)	Classification and Value (ksi)		
	P_m	P_L	$P_L + P_b$
-20 to 100	49.0	70.0	70.0
200	48.0	68.5	68.5
300	46.7	66.7	66.7
400	45.2	64.6	64.6
500	42.5	60.7	60.7
600	38.9	58.4	58.4
700	35.3	53.1	53.1

Notes:

1. Level D allowables per NB-3225 and Appendix F, Paragraph F-1331.
2. Average primary shear stress across a section loaded in pure shear may not exceed 0.42 S_u.
3. Limits on values are presented in Table 2.2.10.
4. P_m, P_L, and P_b are defined in Table 3.1.6.

Table 3.1.10

DESIGN AND LEVEL A: STRESS

Code: ASME NF
Material: SA516, Grade 70, SA515, Grade 70
Service Conditions: Design and Level A
Item: Stress

Temp. (^{O}F)	Classification and Value (ksi)		
	S	Membrane Stress	Membrane plus Bending Stress
-20 to 650	17.5	17.5	26.3
700	16.6	16.6	24.9

Notes:

1. S = Maximum allowable stress values from Table 1A of ASME Code, Section II, Part D.

2. Stress classification per Paragraph NF-3260.

3. Limits on values are presented in Table 2.2.12.

Table 3.1.11

LEVEL B: STRESS

Code: ASME NF
Material: SA516, Grade 70, SA515, Grade 70
Service Conditions: Level B
Item: Stress

Temp. (^{O}F)	Classification and Value (ksi)	
	Membrane Stress	Membrane plus Bending Stress
-20 to 650	23.3	34.9
700	22.1	33.1

Notes:

1. Limits on values are presented in Table 2.2.12 with allowables from Table 3.1.10.

Table 3.1.12

LEVEL D: STRESS INTENSITY

Code: ASME NF
Material: SA516, Grade 70, SA515, Grade 70
Service Conditions: Level D
Item: Stress Intensity

Temp. (^{O}F)	Classification and Value (ksi)		
	S_m	P_m	$P_m + P_b$
-20 to 100	23.3	45.6	68.4
200	23.1	41.5	62.3
300	22.5	40.4	60.6
400	21.7	39.1	58.7
500	20.5	36.8	55.3
600	18.7	33.7	50.6
650	18.4	33.1	49.7
700	18.3	32.9	49.3

Notes:

1. Level D allowable stress intensities per Appendix F, Paragraph F-1332.

2. S_m = Stress intensity values per Table 2A of ASME, Section II, Part D.

3. Limits on values are presented in Table 2.2.12.

4. P_m and P_b are defined in Table 3.1.6.

Table 3.1.13

DESIGN, LEVELS A AND B: STRESS INTENSITY

Code: ASME NB
Material: Alloy X
Service Conditions: Design, Levels A and B
Item: Stress Intensity

Temp. (^{O}F)	Classification and Numerical Value					
	S_m	P_m†	P_L†	$P_L + P_b$†	P_L+P_b+Q††	P_e††
-20 to 100	20.0	20.0	30.0	30.0	60.0	60.0
200	20.0	20.0	30.0	30.0	60.0	60.0
300	20.0	20.0	30.0	30.0	60.0	60.0
400	18.7	18.7	28.1	28.1	56.1	56.1
500	17.5	17.5	26.3	26.3	52.5	52.5
600	16.4	16.4	24.6	24.6	49.2	49.2
650	16.0	16.0	24.0	24.0	48.0	48.0
700	15.6	15.6	23.4	23.4	46.8	46.8
750	15.2	15.2	22.8	22.8	45.6	45.6
800	14.9	14.9	22.4	22.4	44.7	44.7

Notes:

1. S_m = Stress intensity values per Table 2A of ASME II, Part D.
2. Alloy X S_m values are the lowest values for each of the candidate materials at temperature.
3. Stress classification per NB-3220.
4. Limits on values are presented in Table 2.2.10.
5. P_m, P_L, P_b, Q, and P_e are defined in Table 3.1.6.

† Evaluation required for Design condition only.
†† Evaluation required for Levels A, B conditions only. P_e not applicable to vessels.

Table 3.1.14

LEVEL D: STRESS INTENSITY

Code: ASME NB
Material: Alloy X
Service Conditions: Level D
Item: Stress Intensity

Temp. (^{O}F)	Classification and Value (ksi)		
	P_m	P_L	$P_L + P_b$
-20 to 100	48.0	72.0	72.0
200	48.0	72.0	72.0
300	46.2	69.3	69.3
400	44.9	67.4	67.4
500	42.0	63.0	63.0
600	39.4	59.1	59.1
650	38.4	57.6	57.6
700	37.4	56.1	56.1
750	36.5	54.8	54.8
800	35.8	53.7	53.7

Notes:

1. Level D stress intensities per ASME NB-3225 and Appendix F, Paragraph F-1331.

2. The average primary shear strength across a section loaded in pure shear may not exceed 0.42 S_u.

3. Limits on values are presented in Table 2.2.10.

4. P_m, P_L, and P_b are defined in Table 3.1.6.

Table 3.1.15

DESIGN, LEVELS A AND B: STRESS INTENSITY

Code: ASME NG
Material: Alloy X
Service Conditions: Design, Levels A and B
Item: Stress Intensity

Temp. (^{O}F)	Classification and Value (ksi)				
	S_m	P_m	P_m+P_b	P_m+P_b+Q	P_e
-20 to 100	20.0	20.0	30.0	60.0	60.0
200	20.0	20.0	30.0	60.0	60.0
300	20.0	20.0	30.0	60.0	60.0
400	18.7	18.7	28.1	56.1	56.1
500	17.5	17.5	26.3	52.5	52.5
600	16.4	16.4	24.6	49.2	49.2
650	16.0	16.0	24.0	48.0	48.0
700	15.6	15.6	23.4	46.8	46.8
750	15.2	15.2	22.8	45.6	45.6
800	14.9	14.9	22.4	44.7	44.7

Notes:

1. S_m = Stress intensity values per Table 2A of ASME, Section II, Part D.

2. Alloy X S_m values are the lowest values for each of the candidate materials at temperature.

3. Classifications per NG-3220.

4. Limits on values are presented in Table 2.2.11.

5. P_m, P_b, Q, and P_e are defined in Table 3.1.6.

Table 3.1.16

LEVEL D: STRESS INTENSITY

Code: ASME NG
Material: Alloy X
Service Conditions: Level D
Item: Stress Intensity

Temp. (°F)	Classification and Value (ksi)		
	P_m	P_L	$P_L + P_b$
-20 to 100	48.0	72.0	72.0
200	48.0	72.0	72.0
300	46.2	69.3	69.3
400	44.9	67.4	67.4
500	42.0	63.0	63.0
600	39.4	59.1	59.1
650	38.4	57.6	57.6
700	37.4	56.1	56.1
750	36.5	54.8	54.8
800	35.8	53.7	53.7

Notes:

1. Level D stress intensities per ASME NG-3225 and Appendix F, Paragraph F-1331.

2. The average primary shear strength across a section loaded in pure shear may not exceed 0.42 S_u.

3. Limits on values are presented in Table 2.2.11.

4. P_m, P_L, and P_b are defined in Table 3.1.6.

Table 3.1.17

REFERENCE TEMPERATURES AND STRESS LIMITS
FOR THE VARIOUS LOAD CASES

Load Case I.D.	Material	Reference Temperature†, °F	Stress Intensity Allowables, ksi		
			P_m	$P_L + P_b$	$P_L + P_b + Q$
F1	Alloy X	725	15.4	23.1	46.2
F2	Alloy X	725	15.4	23.1	46.2
F3	Alloy X	725	36.9	55.4	NL††
E1	Alloy X	450	18.1	27.2	54.3
E2	Alloy X	450	18.1	27.2	54.3
E3	Alloy X	450	43.4	65.2	NL
E4	Alloy X	450	18.1	27.2	54.3
E5	Alloy X	775	36.15	54.25	NL

Note:

1. Q, P_m, P_L, and P_b are defined in Table 3.1.6.

† Values for reference temperatures are taken as the design temperatures (Table 2.2.3).
†† NL: No specified limit in the Code.

Table 3.1.17 (continued):
REFERENCE TEMPERATURES AND STRESS LIMITS
FOR THE VARIOUS LOAD CASES

Load Case I.D.	Material	Reference Temperature,[†, ††] °F	Stress Intensity Allowables, ksi		
			P_m	$P_L + P_b$	$P_L + P_b + Q$
O1	SA203-E	400	22.9	34.4	68.7
	SA350-LF3	400	21.5	32.3	64.5
	SA516 Gr. 70 SA515 Gr. 70	400	17.5	26.3	NL[†††]
O2	SA203-E	400	48.2	68.8	NL
	SA350-LF3	400	45.2	64.6	NL
	SA516 Gr. 70 SA515 Gr. 70	400	39.1	58.7	NL
O3	SA203-E	400	22.9	34.4	68.7
	SA350-LF3	400	21.5	32.3	64.5
	SA516 Gr. 70 SA515 Gr. 70	400	17.5	26.3	NL
O4	SA203-E	400	48.2	68.8	NL
	SA350-LF3	400	45.2	64.6	NL
	SA516 Gr. 70 SA515 Gr. 70	400	39.1	58.7	NL
O5	SA203-E	400	22.9	34.4	68.7
	SA350-LF3	400	21.5	32.3	64.5
	SA516 Gr. 70 SA515 Gr. 70	400	17.5	26.3	NL
O6	SA203-E	400	48.2	68.8	NL
	SA350-LF3	400	45.2	64.6	NL
	SA516 Gr. 70 SA515 Gr. 70	400	39.1	58.7	NL

Note: 1. P_m, P_L, P_b, and Q are defined in Table 3.1.6.

† Values for reference temperatures are taken as the design temperatures (Table 2.2.3).
†† For storage fire analysis, temperatures are defined by thermal solution.
††† NL: No specified limit in the Code.

Table 3.1.18
FRACTURE TOUGHNESS TEST CRITERIA: HELIUM RETENTION BOUNDARY

Item	Material	Thickness (in.)	Charpy V-Notch Temperature†	Drop Test Temperature††
Weld Metal for NB Welds	As required	NA	As required per ASME Section III, Subsection NB, Article NB-2430 and Article NB-2330 Min. test temperature = -40°F	As required per ASME Section III, Subsection NB, Articles NB-2430 and Article NB-2330
Shell	SA203E	2-1/2	$T_{NDT} \leq -70°F$ with testing and acceptance criteria per ASME Section III, Subsection NB, Article NB-2330	$T_{NDT} \leq -70°F$ per Reg. Guide 7.11
Top Flange	SA350-LF3	8-3/4	$T_{NDT} \leq -136°F$ with testing and acceptance criteria per ASME Section III, Subsection NB, Article NB-2330	$T_{NDT} \leq -136°F$ per Reg. Guide 7.12
Bottom Plate	SA350-LF3	6	$T_{NDT} \leq -129°F$ with testing and acceptance criteria per ASME Section III, Subsection NB, Article NB-2330	$T_{NDT} \leq -129°F$ per Reg. Guide 7.12

† Temperature is T_{NDT} unless noted.
†† Materials to be tested in accordance with ASTM E208-87a.

Table 3.1.19
FRACTURE TOUGHNESS TEST CRITERIA
MISCELLANEOUS ITEMS

Item	Material	Thickness (in.)	Charpy V-Notch Temperature†	Drop Test Temperature
Closure Plate	SA350-LF3	6	$T_{NDT} \leq -129°F$ with testing and acceptance criteria per ASME Section III, Subsection NB, Article NB-2330	$T_{NDT} \leq -129°F$ per Reg. Guide 7.12
Intermediate Shells	SA516 Grade 70	1-1/4 and 1	Test temperature = -40°F with acceptance criteria per ASME Section III, Subsection NF, Table NF-2331(a)-3 and Figure NF-2331(a)-2	Not Required
Port Cover Plates	SA203-E	1-1/2	Test temperature = -40°F with acceptance criteria per ASME Section III, Subsection NF, Table NF--2331(a)-3 and Figure NF-2331(a)-2	Not Required
Weld Metal for NF Welds	As required	NA	As required per ASME Section III, Subsection NF, Article NF-2430 and Article NF-2330 Test temperature = -40°F	Not Required

† Temperature is T_{NDT} unless noted.

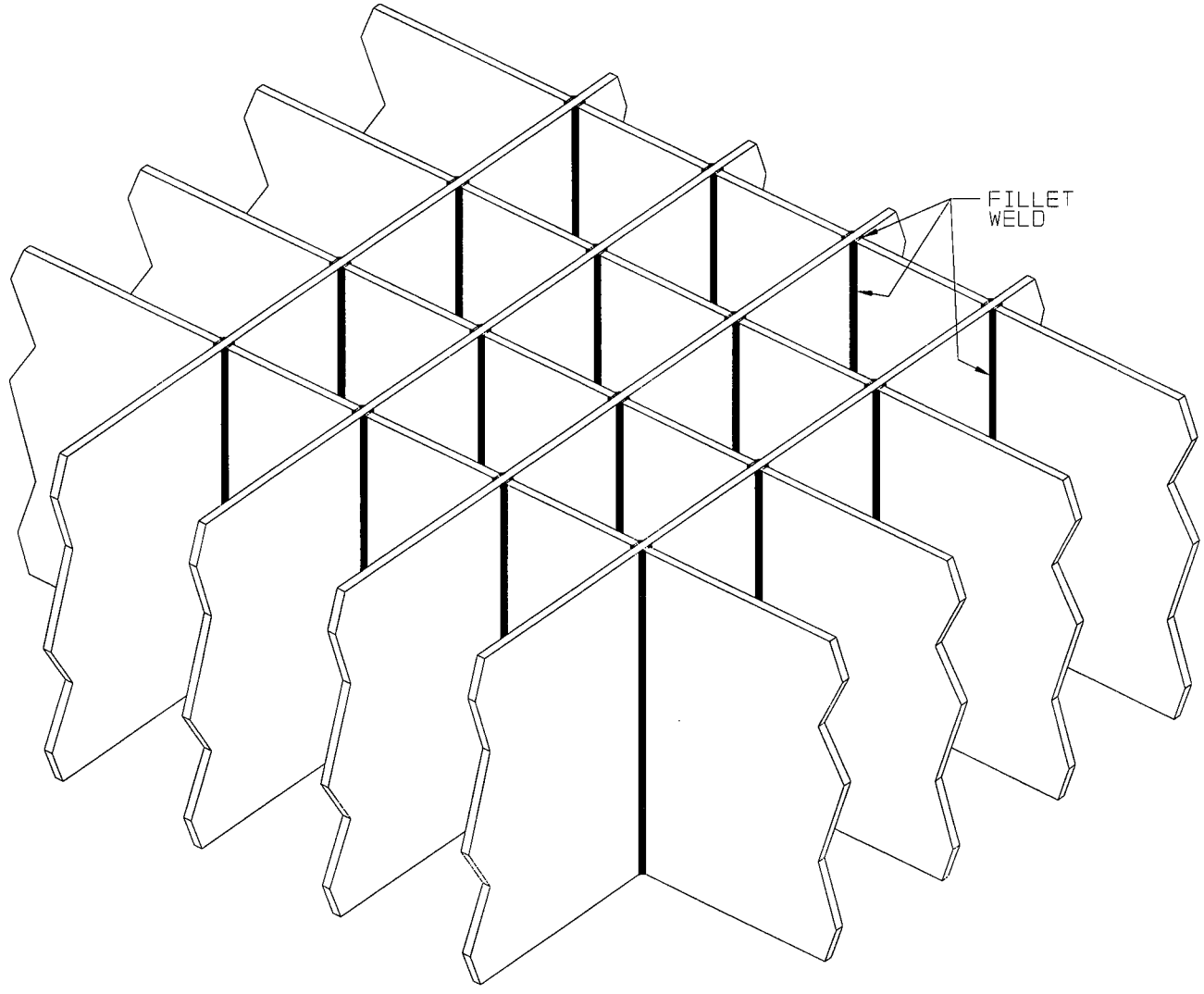

FIGURE 3.1.1; MPC FUEL BASKET GEOMETRY

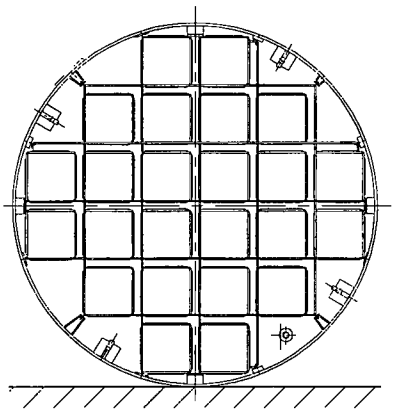

GRAVITY

MPC-24

DELETED

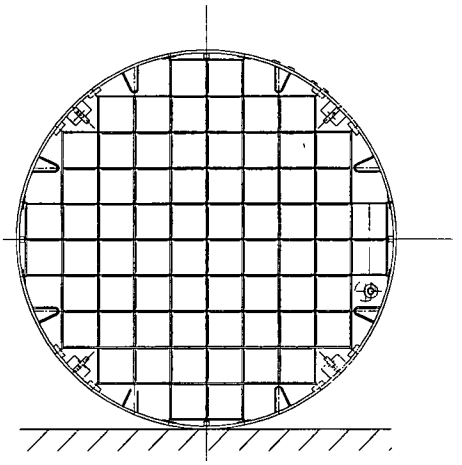

GRAVITY

MPC-68

FIGURE 3.1.2; 0° DROP ORIENTATIONS FOR THE MPCs

REPORT HI-2012610 | REVISION 0

\PROJECTS\GENERIC\HI2012610\CH. 3\3_1_2

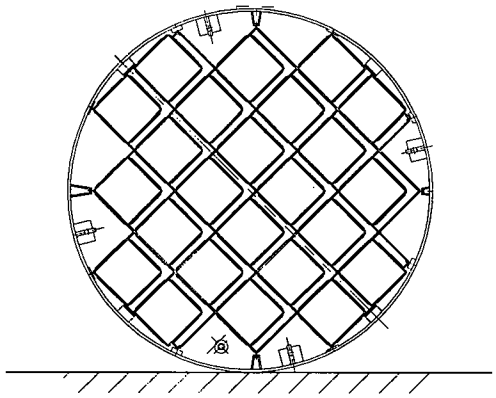

GRAVITY

MPC-24

DELETED

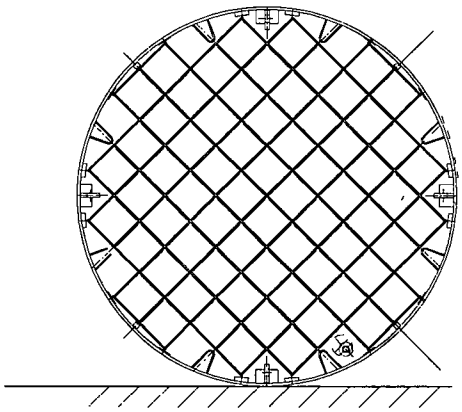

GRAVITY

MPC-68

FIGURE 3.1.3; 45° DROP ORIENTATIONS FOR THE MPCs

REPORT HI-2012610 REVISION 0

\PROJECTS\GENERIC\HI2012610\CH. 3\3_1_3

3.2 WEIGHTS AND CENTERS OF GRAVITY

Table 3.2.1 provides the weights of the individual HI-STAR 100 components as well as the total system weights. Contained water during loading is not included in this table.

The locations of the calculated centers of gravity (CGs) are presented in Table 3.2.2. All centers of gravity are located on the cask centerline, since the non-axisymmetry effects of the cask system plus contents are negligible.

Table 3.2.3 provides the lift weight when the HI-STAR 100 System with the heaviest fully loaded MPC is being lifted from the fuel pool. The effect of buoyancy is neglected, and the weight of rigging is set at a conservative value.

Table 3.2.4 provides a set of bounding weights that may be used in analytical calculations.

Table 3.2.1

HI-STAR 100 WEIGHT DATA†

Item	CALCULATED WEIGHT (lb)	
	Component	**Assembly**
• Overpack		
• Overpack closure plate	7,984	153,710
• MPC-24		
• Fuel basket	20,842	
• Without SNF		40,868
• Fully loaded with SNF		82,494
• Overpack with loaded MPC-24		236,204
• MPC-68		
• Fuel basket	16,240	
• Without SNF		37,591
• Fully loaded with SNF		87,171
• Overpack with fully loaded MPC-68		240,881
• Overpack with minimum weight MPC without SNF (Value listed is lower bound to actual minimum weight of 191,301 lb)		189,000

† All calculated weights are rounded to the nearest pound

Table 3.2.2

CENTERS OF GRAVITY OF HI-STAR 100 CONFIGURATIONS

Component	Height of CG Above Datum†, inches
Overpack empty	99.7
MPC-24 empty	109.0
MPC-68 empty	111.5
MPC-24 with fuel in overpack	102.9
MPC-68 with fuel in overpack	103.2

† The datum used for calculations involving the overpack is the bottom of the overpack bottom plate. The datum used for calculations involving the MPC only is the bottom of MPC baseplate (see Figure 3.2.1).

Table 3.2.3

LIFT WEIGHT ABOVE POOL

Item	Calculated Weight (lb.)[†]
Total weight of overpack	153,710
Total weight of an MPC (Upper Bound) + fuel	89,057[††]
Overpack closure plate	-7,984
Water in MPC and overpack	16,384
Lift yoke	3,600
Inflatable annulus seal	50
TOTAL	254,816[†††]

[†] The actual weight of some of these items may vary in the field due to differences in client procedures for performing loading/unloading operations.

[††] Includes MPC closure ring.

[†††] Trunnion rating and crane limits at certain sites may require temporary water removal from the HI-STAR 100 System during removal from the pool (See Chapter 8).

Table 3.2.4
COMPONENT WEIGHTS AND DIMENSIONS FOR
ANALYTIC CALCULATIONS†

Component	Weight (lbs)
MPC baseplate	3,000
MPC closure lid	10,400
MPC shell	5,900
MPC basket supports and fuel spacers	3,700
Fuel basket	13,000
Fuel	54,000
Total MPC package	90,000
Overpack bottom plate	10,000
Overpack closure plate	8,000
Overpack shell	137,000
Total overpack bounding weight	158,000
Total HI-STAR 100 bounding lift weight	250,000
Item	**Dimension (inch)**
Overpack Outer Diameter	96
Overpack Length	203.125††
MPC Outer Diameter	68.375
MPC Length	190.5
Overpack Inner Diameter	68.75

† Analytic calculations may use the weights and dimensions in Table 3.2.4 or actual weights and dimensions for conservatism in calculation of safety factors. Finite element analyses use other bounding weights or weights calculated based on input weight densities.

†† Overpack length is measured from the bottom surface of the bottom plate to the top surface of the closure plate. The maximum overall length of the overpack is 203.25 inches, as measured from the bottom of the bottom plate to the top of the top flange. The difference in length has a negligible effect on the calculations.

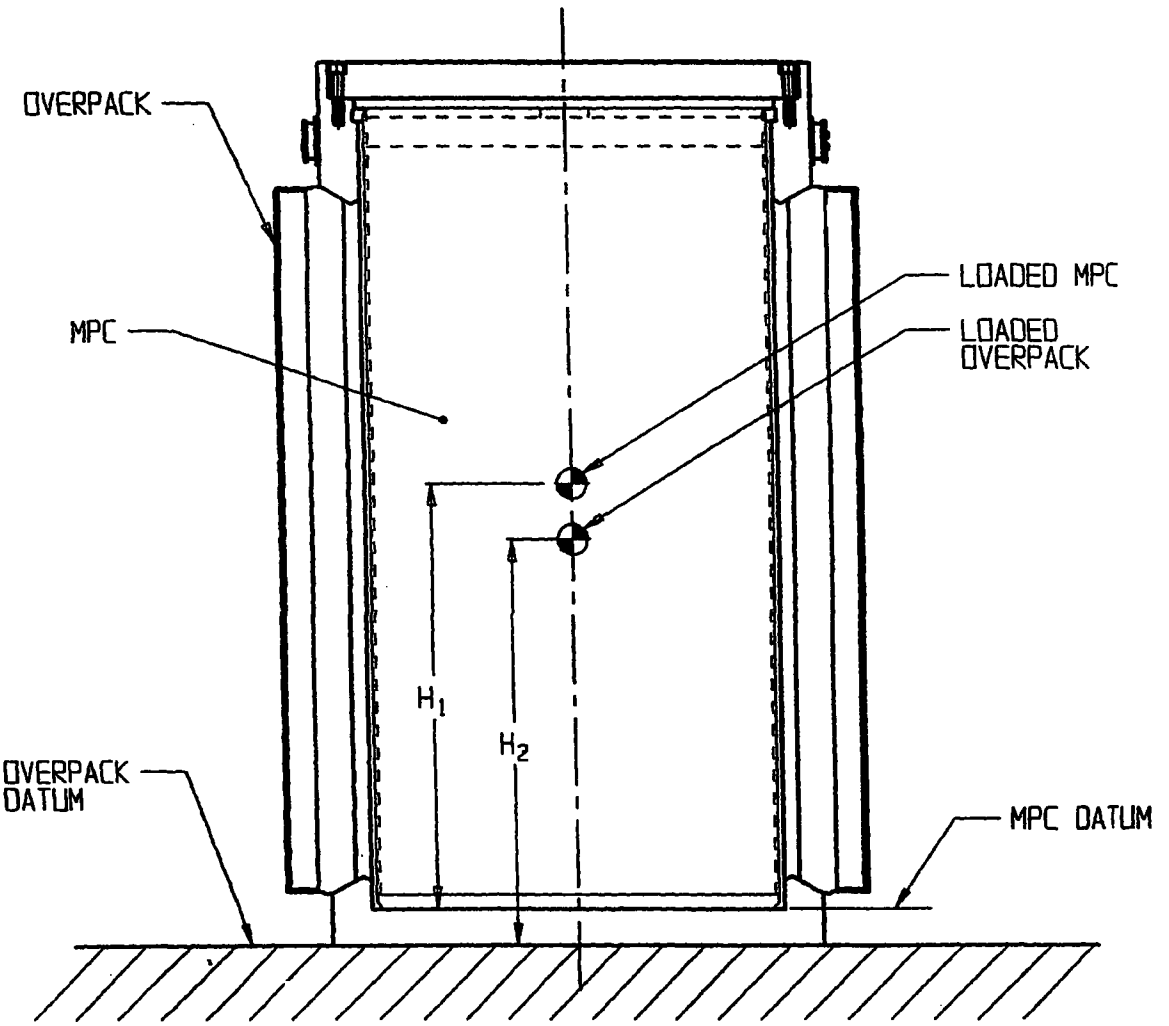

FIGURE 3.2.1; HI-STAR 100 DATUM DEFINITION FOR TABLE 3.2.2

3.3 MECHANICAL PROPERTIES OF MATERIALS

This section provides the mechanical properties used in the structural evaluation. The properties include yield stress, ultimate stress, modulus of elasticity, Poisson's ratio, weight density, and coefficient of thermal expansion. Values are presented for a range of temperatures; the limits of which are below the off-normal environmental temperature and above the off-normal design temperature.

The materials selected for use in the HI-STAR 100 MPC and overpack are presented on the Bills-of-Material. In this chapter, the materials are divided into two categories, structural and nonstructural. Structural materials are materials that act as load bearing members in the analysis. Materials that do not support mechanical loads are considered nonstructural. For example, while the overpack inner shell is a structural material, Holtite-A (neutron shield) is a nonstructural material.

3.3.1 Structural Materials

3.3.1.1 Alloy X

A hypothetical material termed Alloy X is defined for all MPC structural components. The material properties of Alloy X are the least favorable values from the set of candidate stainless alloys. The purpose of a least favorable material definition is to ensure that all structural analyses are conservative, regardless of the actual MPC material. For example, when evaluating the stresses in the MPC, it is conservative to work with the minimum values for yield strength and ultimate strength. This guarantees that the material used for fabrication of the MPC is of equal or greater strength than the hypothetical material used in the analysis. In the structural evaluation, the only property for which it is not always conservative to use the set of minimum values is the coefficient of thermal expansion. Two sets of values for the coefficient of thermal expansion are specified, a minimum set and a maximum set. For each analysis, the set of coefficients, minimum or maximum, that causes the most adverse result for the cask system is used. Table 3.3.1 lists the numerical values for the material properties of Alloy X versus temperature. These values, taken from the ASME Code, Section II, Part D [3.3.1], are used to complete all structural analyses. The maximum temperatures in some MPC components may exceed the allowable limits of temperature during short time duration loading operations, off-normal transfer operations, or storage accident events. However, under no scenario does the maximum temperature of Alloy X material used in the confinement boundary exceed 1000°F. As shown in ASME Code Case N-47-33 (Class 1 Components in Elevated Temperature Service, 1995 Code Cases, Nuclear Components), the strength properties of austenitic stainless steels do not change due to exposure to 1000°F temperature for up to 10,000 hours. Therefore, there is no significant effect on mechanical properties of the confinement or basket material during the short time duration loading. A further description of Alloy X, including the materials from which it is derived, is provided in Appendix 1.A.

Two properties of Alloy X which are not included in Table 3.3.1 are weight density and Poisson*s ratio. These properties are assumed constant for all structural analyses because there is no significant variation with temperature. The values used are shown in the table below.

PROPERTY	VALUE
Weight Density (lb/in^3)	0.290
Poisson's Ratio	0.30

3.3.1.2 Carbon Steel, Low-Alloy and Nickel Alloy Steel

The carbon steels in the HI-STAR 100 System are SA516 Grade 70 and SA515 Grade 70. The nickel alloy and low alloy steels are SA203-E and SA350-LF3, respectively. These steels are not constituents of Alloy X. The material properties of SA516 Grade 70 and SA515 Grade 70 are presented in Tables 3.3.2 and 3.3.3, respectively. The material properties of SA203-E and SA350-LF3 are given in Table 3.3.4.

Two properties of these steels which are not included in Tables 3.3.2, 3.3.3, and 3.3.4 are weight density and Poisson*s ratio. These properties are assumed constant for all structural analyses because there is no significant variation with temperature. The values used are shown in the table below.

PROPERTY	VALUE
Weight Density (lb/in^3)	0.283
Poisson's Ratio	0.30

3.3.1.3 Bolting Materials

Material properties of the bolting materials used in the HI-STAR 100 System are given in Table 3.3.5.

3.3.1.4 Weld Material

All weld materials utilized in the welding of the Code components will comply with the provisions of the appropriate ASME subsection (e.g., Subsection NB for the enclosure vessel) and Section IX. All non-code welds shall also be made using weld procedures which meet Section IX of the ASME Code, as practicable. The minimum tensile strength of the weld wire and filler material (where applicable) will be equal to or greater than the tensile strength of the base metal listed in the ASME Code.

3.3.2 Nonstructural Materials

3.3.2.1 Neutron Shield

The neutron shield in the overpack is not considered as a structural member of the HI-STAR 100 System. Its load carrying capacity is neglected in all structural analyses except where such omission would be nonconservative. The only material property of the neutron shield which is important to the structural evaluation is its weight density ($1.63 g/cm^3$).

3.3.2.2 Boral Neutron Absorber

Boral is not a structural member of the HI-STAR 100 System. Its load carrying capacity is neglected in all structural analyses. The only material property of Boral which is important to the structural evaluation is its weight density. As the MPC fuel baskets can be constructed with Boral panels of variable areal density, the weight that produces the most severe cask load is assumed in each analysis (density $2.644 g/cm^3$).

3.3.2.3 Aluminum Conduction Inserts

Aluminum conduction inserts are located between the fuel basket and MPC vessel. They are thin, flexible elements whose sole function is to transmit heat. They are not credited with any structural load capacity, and are shaped to provide negligible resistance to basket thermal expansion. The total weight of the aluminum inserts is less than 1,000 lb. per MPC.

Table 3.3.1
ALLOY X MATERIAL PROPERTIES

Temp. (°F)	Alloy X				
	S_y	S_u†	α_{min}	α_{max}	E
-40	30.0	75.0 *(70.0)*	8.54	8.55	28.82
100	30.0	75.0 *(70.0)*	8.54	8.55	28.14
150	27.5	73.0 *(68.1)*	8.64	8.67	27.87
200	25.0	71.0 *(66.2)*	8.76	8.79	27.6
250	23.75	68.5 *(63.85)*	8.88	8.9	27.3
300	22.5	66.0 *(61.5)*	8.97	9.0	27.0
350	21.6	65.2 *(60.75)*	9.10	9.11	26.75
400	20.7	64.4 *(60.0)*	9.19	9.21	26.5
450	20.05	64.0 *(59.65)*	9.28	9.32	26.15
500	19.4	63.5 *(59.3)*	9.37	9.42	25.8
550	18.8	63.3 *(59.1)*	9.45	9.50	25.55
600	18.2	63.1 *(58.9)*	9.53	9.6	25.3
650	17.8	62.8 *(58.6)*	9.61	9.69	25.05
700	17.3	62.5 *(58.4)*	9.69	9.76	24.8
750	16.9	62.2 *(58.1)*	9.76	9.81	24.45
800	16.6	61.7 *(57.6)*	9.82	9.90	24.1

Definitions:

S_y = Yield Stress (ksi)
α = Mean Coefficient of thermal expansion (in./in. per degree F x 10^{-6})
S_u = Ultimate Stress (ksi)
E = Young's Modulus (psi x 10^6)

Notes:

1. Source for S_y values is Table Y-1 of [3.3.1].
2. Source for S_u values is Table U of [3.3.1].
3. Source for α_{min} and α_{max} values is Table TE-1 of [3.3.1].
4. Source for E values is material group G in Table TM-1 of [3.3.1].

† The ultimate stress of Alloy X is dependent on the product form of the material (i.e., forging vs. plate). Values in parentheses are based on SA-336 forged materials (type F304, F304LN, F316, and F316LN), which are used solely for the one-piece construction MPC lids. All other values correspond to SA-240 plate material.

Table 3.3.2
SA516, GRADE 70 MATERIAL PROPERTIES

Temp. (°F)	SA516, Grade 70			
	S_y	S_u	α	E
-40	38.0	70.0	5.53	29.95
100	38.0	70.0	5.53	29.34
150	36.3	70.0	5.71	29.1
200	34.6	70.0	5.89	28.8
250	34.15	70.0	6.09	28.6
300	33.7	70.0	6.26	28.3
350	33.15	70.0	6.43	28.0
400	32.6	70.0	6.61	27.7
450	31.65	70.0	6.77	27.5
500	30.7	70.0	6.91	27.3
550	29.4	70.0	7.06	27.0
600	28.1	70.0	7.17	26.7
650	27.6	70.0	7.30	26.1
700	27.4	70.0	7.41	25.5
750	26.5	69.3	7.50	24.85

Definitions:

S_y = Yield Stress (ksi)
α = Mean Coefficient of thermal expansion (in./in. per degree F x 10^{-6})
S_u = Ultimate Stress (ksi)
E = Young's Modulus (psi x 10^6)

Notes:
1. Source for S_y values is Table Y-1 of [3.3.1].
2. Source for S_u values is Table U of [3.3.1].
3. Source for α values is material group C in Table TE-1 of [3.3.1].
4. Source for E values is "Carbon steels with C ≤ 0.30%" in Table TM-1 of [3.3.1].

Table 3.3.3
SA515, GRADE 70 MATERIAL PROPERTIES

Temp. (°F)	SA515, Grade 70			
	S_y	S_u	α	E
-40	38.0	70.0	5.53	29.95
100	38.0	70.0	5.53	29.34
150	36.3	70.0	5.71	29.1
200	34.6	70.0	5.89	28.8
250	34.15	70.0	6.09	28.6
300	33.7	70.0	6.26	28.3
350	33.15	70.0	6.43	28.0
400	32.6	70.0	6.61	27.7
450	31.65	70.0	6.77	27.5
500	30.7	70.0	6.91	27.3
550	29.4	70.0	7.06	27.0
600	28.1	70.0	7.17	26.7
650	27.6	70.0	7.30	26.1
700	27.4	70.0	7.41	25.5
750	26.5	69.3	7.50	24.85

Definitions:

S_y = Yield Stress (ksi)
α = Mean Coefficient of thermal expansion (in./in. per degree F x 10^{-6})
S_u = Ultimate Stress (ksi)
E = Young's Modulus (psi x 10^6)

Notes:
1. Source for S_y values is Table Y-1 of [3.3.1].
2. Source for S_u values is Table U of [3.3.1].
3. Source for α values is material group C in Table TE-1 of [3.3.1].
4. Source for E values is "Carbon steels with C ≤ 0.30%" in Table TM-1 of [3.3.1].

Table 3.3.4

SA350-LF3 AND SA203-E MATERIAL PROPERTIES

Temp. (°F)	SA350-LF3			SA350-LF3/SA203-E		SA203-E		
	S_m	S_y	S_u	E	α	S_m	S_y	S_u
-20	23.3	37.5	70.0	28.2	---	23.3	40.0	70.0
100	23.3	37.5	70.0	27.6	6.27	23.3	40.0	70.0
200	22.8	34.2	68.5	27.1	6.54	23.3	36.5	70.0
300	22.2	33.2	66.7	26.7	6.78	23.3	35.4	70.0
400	21.5	32.2	64.6	26.1	6.98	22.9	34.3	68.8
500	20.2	30.3	60.7	25.7	7.16	21.6	32.4	64.9
600	18.5	-	-	-	-	-	-	-
700	16.8	-	-	-	-	-	-	-

Definitions:

S_m = Design Stress Intensity (ksi)
S_y = Yield Stress (ksi)
S_u = Ultimate Stress (ksi)
α = Coefficient of Thermal Expansion (in./in. per degree F x 10^{-6})
E = Young's Modulus (psi x 10^6)

Notes:

1. Source for S_m values is ASME Code, Table 2A of [3.3.1].
2. Source for S_y values is ASME Code, Table Y-1 of [3.3.1].
3. Source for S_u values is ratioing S_m values.
4. Source for α values is material group E in Table TE-1 of [3.3.1].
5. Source for E values is material group B in Table TM-1 of [3.3.1]

Table 3.3.5
SB637-N07718, SA564-630, AND SA705-630 MATERIAL PROPERTIES

Temp. (°F)	SB637-N07718				
	S_y	S_u	E	α	S_m
-100	150.0	185.0	29.9	---	50.0
-20	150.0	185.0	---	---	50.0
70	150.0	185.0	29.0	7.05	50.0
100	150.0	185.0	---	7.08	50.0
200	144.0	177.6	28.3	7.22	48.0
300	140.7	173.5	27.8	7.33	46.9
400	138.3	170.6	27.6	7.45	46.1
500	136.8	168.7	27.1	7.57	45.6
600	135.3	166.9	26.8	7.67	45.1
SA705-630/SA564-630 (Age Hardened at 1075°F)					
Temp. (°F)	S_y	S_u	E	α	-
200	115.6	145.0	28.5	5.9	-
300	110.7	145.0	27.9	5.9	-
SA705-630/SA564-630 (Age Hardened at 1150°F)					
200	97.1	135.0	28.5	5.9	-
300	93.0	135.0	27.9	5.9	-

Definitions:

S_m = Design stress intensity (ksi)
S_y = Yield Stress (ksi)
α = Mean Coefficient of thermal expansion (in./in. per degree F x 10^{-6})
S_u = Ultimate Stress (ksi)
E = Young's Modulus (psi x 10^6)

Notes:

1. Source for S_m values is Table 4 of [3.3.1].
2. Source for S_y values is ratioing design stress intensity values.
3. Source for S_u values is ratioing design stress intensity values.
4. Source for α values is Tables TE-1 and TE-4 of [3.3.1], as applicable.
5. Source for E values is Table TM-1 of [3.3.1].

3.4 GENERAL STANDARDS FOR CASKS

3.4.1 Chemical and Galvanic Reactions

In this subsection, it is shown that there is no credible mechanism for significant chemical or galvanic reactions in the HI-STAR 100 System during long-term storage operations.

The MPC, which is filled with helium, provides a nonaqueous and inert environment. Insofar as corrosion is a long-term time-dependent phenomenon, the inert gas environment in the MPC precludes the incidence of corrosion during storage on the ISFSI. Furthermore, the only dissimilar material groups in the MPC are: (1) Boral and stainless steel and (2) aluminum and stainless steel. Boral and stainless steel have been used in close proximity in wet storage for over 30 years. Many spent fuel pools at nuclear plants contain fuel racks, which are fabricated from Boral and stainless steel materials, with geometries similar to the HI-STAR 100 MPC. Not one case of chemical or galvanic degradation has been found in fuel racks built by Holtec. This experience provides a sound basis to conclude that corrosion will not occur in these materials. Additionally, the aluminum conduction inserts and stainless steel basket are very close on the galvanic series chart. Aluminum, like other metals of its genre (e.g., titanium and magnesium) rapidly passivates in an aqueous environment, leading to a thin ceramic (Al_2O_3) barrier which renders the material essentially inert and corrosion-free over long periods of application. The physical properties of the material, e.g., thermal expansion coefficient, diffusivity, and thermal conductivity, are essentially unaltered by the exposure of the aluminum metal stock to an aqueous environment.

In order to minimize the incidence of aluminum water reaction inside the MPC during fuel loading operation (when the MPC is flooded with pool water) all aluminum surfaces are pre-passivated or anodized before installation of Boral or conduction inserts in the MPC. The aluminum in the optional heat conduction elements will quickly passivate in air and in water to form a protective oxide layer that prevents any significant hydrogen production during MPC cask loading and unloading operations. The aluminum in the Boral, particularly in the core area, will also react with water to generate hydrogen gas. The exact rate of generation and total amount of hydrogen generated is a function of a number of variables (see Section 1.2.1.3.1) and cannot be predicted with any certainty. Therefore, to preclude the potential for hydrogen ignition during lid welding or cutting, the operating procedures in Chapter 8 require monitoring for combustible gas and either exhausting or purging the space beneath the MPC lid with an inert gas during these activities. Once the MPC cavity is drained, dried, and backfilled with helium, the source of hydrogen gas (the aluminum-water reaction) is eliminated.

The HI-STAR 100 overpack combines low alloy and nickel alloy steels, carbon steels, neutron and gamma shielding materials, thermal expansion foam, and bolting materials. All of these materials have a long history of nongalvanic behavior within close proximity of each other. The internal and external steel surfaces of each of the overpacks are sandblasted and coated to preclude surface oxidation. Therefore, chemical or galvanic reactions involving the overpack materials are highly unlikely and are not expected.

In accordance with NRC Bulletin 96-04 [3.4.7], a review of the potential for chemical, galvanic, or other reactions among the materials of the HI-STAR 100 System, its contents and the operating environments which may produce adverse reactions has been performed. Table 3.4.2 provides a listing of the materials of fabrication for the HI-STAR 100 System and evaluates the performance of the material in the expected operating environments during short-term loading/unloading operations and long-term storage operations. As a result of this review, no operations were identified which could produce adverse reactions beyond those conditions already analyzed in this FSAR.

3.4.2 Positive Closure

There are no quick-connect/disconnect ports in the confinement boundary of the HI-STAR 100 System. The all welded design of the MPC enclosure vessel precludes access to the stored nuclear fuel without use of special equipment for disconnecting Alloy X pressure vessel parts. The only access to the MPC is through the closure plate, which weighs over 7,000 pounds. The closure plate is fastened to the overpack with an array of large bolts. Inadvertent opening of the overpack is not feasible; opening an overpack requires mobilization of special tools and heavy-load lifting equipment.

3.4.3 Lifting Devices

As required by Reg. Guide 3.61, in this subsection, analyses for all lifting operations applicable to the deployment of a HI-STAR 100 System are presented to demonstrate compliance with applicable codes and standards.

The HI-STAR 100 System has the following types of lifting devices: lifting trunnions located on the overpack top flange; threaded holes for eyebolts to lift the overpack closure plate; lifting lugs for the MPC enclosure vessel; and threaded holes for eyebolts for lifting a loaded MPC or the MPC top lid.

The evaluation of the adequacy of the lifting devices entails careful consideration of the applied loading and associated stress limits. The load combination D+H, where H is the "handling load", is the generic case for all lifting adequacy assessments. The term D denotes the dead load. Quite obviously, D must be taken as the bounding value of the dead load of the component being lifted. Table 3.2.4 gives bounding weights. In all lifting analyses considered in this document, the handling load H is assumed to be 0.15D. In other words, the inertia amplifier during the lifting operation is assumed to be equal to 0.15g. This value is consistent with the guidelines of the Crane Manufacturer's Association of America (CMAA), Specification No. 70, 1988, Section 3.3, which stipulates a dynamic factor equal to 0.15 for slowly executed lifts. Thus, the "apparent dead load" of the component for stress analysis purposes is $D^* = 1.15D$. Unless otherwise stated, all lifting analyses in this report use the "apparent dead load", D^*, in the lifting analysis.

Analysis methodology to evaluate the adequacy of the lifting device may be analytical or numerical. For the analysis of the trunnion, an accepted conservative technique for computing the bending stress is to assume that the lifting force is applied at the tip of the trunnion "cantilever" and that the stress state is fully developed at the base of the cantilever. This conservative technique, recommended in NUREG-1536, is applied to all trunnion analyses presented in this FSAR.

In general, the stress analysis to establish safety pursuant to NUREG-0612, Regulatory Guide 3.61, and the ASME Code requires evaluation of three discrete zones which may be referred to as (i) the trunnion, (ii) the trunnion/component interface, hereinafter referred to as Region A, and (iii) the rest of the component, specifically the stressed metal zone adjacent to Region A, herein referred to as Region B.

Stress limits germane to each of the above three areas are discussed below:

i. Trunnion: NUREG-0612 requires that under the "apparent dead load", D^*, the maximum primary stress in the trunnion be less than 10% of the trunnion material ultimate strength *and* less than 1/6th of the trunnion material yield strength. In otherwords, the maximum moment and shear force developed in the trunnion cantilever is less than 1/6 of the moment and shear force corresponding to incipient plasticity, and less than 1/10 of the flexural collapse moment or ultimate shear force for the section.

ii. Region A: Trunnion/Component Interface: Stresses in Region A must meet ASME Code Level A limits under applied load D*. Additionally, Regulatory Guide 3.61 requires that the maximum primary stress under $3D^*$ be less than the yield strength of the weaker of the two materials at the trunnion/component interface. In cases involving section bending, the developed section moment must be compared against the plastic moment at yield. Typically, the stresses in the component in the vicinity of the trunnion/component interface are higher than elsewhere. However, exceptional situations exist. For example, when lifting a loaded MPC, the MPC baseplate, which supports the entire weight of the fuel and the fuel basket, is a candidate location for high stress even though it is far removed from the lifting location (which is located in the top lid).

iii. Region B: This region constitutes the remainder of the component where the stress limits under the concurrent action of the apparent dead load D* and other mechanical loads that may be present during handling (e.g. internal pressure) are required to meet Level A Service Limits.

In summary, both Region A and Region B are required to meet the stress limits corresponding to ASME Level A under the load D*. Additionally, portions of the component that may experience high stress during the lift are subject to the stress criterion of Regulatory Guide 3.61, which requires satisfaction of yield strength as the limit when the sole applied load is 3D*. In general, all locations of high stress in the component under D* must also be checked for compliance with ASME Code Level A stress limits.

Unless explicitly stated otherwise, all analyses of lifting operations presented in this report follow the load definition and allowable stress provisions of the foregoing. Consistent with the practice adopted throughout this chapter, results are presented in dimensionless form, as safety factors, defined as

$$\text{Safety Factor, } SF = \frac{\text{Allowable Stress in the Region Considered}}{\text{Computed Maximum Stress in the Region}}$$

It should be emphasized that the safety factor, SF, defined in the foregoing, represents the *additional margin* that is over any beyond the margin built into NUREG 0612 (e.g. a factor of 10 on ultimate strength or 6 on yield strength).

In the following subsections, we briefly describe each of the lifting analyses performed to demonstrate compliance with regulations. Summary results are presented for each of the analyses.

It is recognized from the discussion in the foregoing that stresses in Region A are subject to two distinct criteria, namely Level A stress limits under D* and other loading that may be present (such as pressure) and yield strength at 3D*. We will use the "3D*" identifier whenever the Regulatory Guide 3.61 load case (the stresses must be bounded by the yield point at 3D*) is the applied loading.

All of the lifting analyses for the overpack reported in this subsection are designated as Load Case 03 in Table 3.1.5. All of the lifting analyses for the MPC reported in this subsection are designated as Load Case E2 in Table 3.1.4. In Subsection 3.4.4, a finite element analysis of the entire overpack is undertaken and results for Load Case 03 (Vertical Handling) in Table 3.1.5 obtained. The results for safety factors from the general finite element model are presented in a later subsection.

3.4.3.1 Overpack Lifting Trunnion Analysis

The lifting trunnion for the HI-STAR 100 overpack is presented in Holtec Drawing 3913 (Section 1.5 herein).

The two lifting trunnions for HI-STAR 100 are circumferentially spaced at 180 degrees. The trunnions are designed for a two-point lift and are sized to satisfy the aforementioned NUREG-0612 criteria. Figure 3.4.43 shows the overall lifting configuration. Appendix 3.D contains details of the lifting trunnion stress analysis. It is demonstrated in Appendix 3.D that the stresses in the trunnions, computed in the manner of the foregoing, comply with NUREG-0612 and Regulatory Guide 3.61 provisions.

Specifically, the following results are obtained:

Safety Factors from HI-STAR 100 Lifting Trunnion Stress Analysis†			
Item	Value (ksi) or (lb) or (lb-in)	Allowable (ksi) or (lb) or (lb.-in.)	Safety Factor
Bending stress (Comparison with Yield Stress/6)	17.3	24.5	1.41
Shear stress (Comparison with Yield Stress/6)	7.4	14.7	1.99
Bending Moment (Comparison with Ultimate Moment/10)	323,000	574,600	1.78
Shear Force (Comparison with Ultimate Force/10)	144,000	282,000	1.97

† The bounding lifted load is 250000 lb. (per Table 3.2.4).

We note from the above that all safety factors are greater than 1.0. A factor of safety of exactly 1.0 means that the maximum stress is equal to the yield stress in tension or shear divided by 6, or that the section moment or shear force is equal to the ultimate section moment capacity or section force capacity divided by 10.

3.4.3.2 HI-STAR 100 Overpack Lifting (Load Case 03 in Table 3.1.5)

3.4.3.2.1 Top Flange Under D*

During lifting of a loaded HI-STAR 100, the top flange of the overpack (in which the lift trunnions are located) is identified as a potential location for high stress levels.

Appendix 3.D contains calculations that analyze the top flange interface with the trunnion under the lifted load D*. The top flange is considered an NB component subject to the lifted load and internal pressure. The membrane stress intensity is computed at the interface and compared to the allowable local membrane stress intensity. The interface region is also conservatively considered as subject to the provisions of NUREG-0612 and the thread shear stress and bearing stress are compared to 1/6 of the top forging yield stress. The following table summarizes the results:

Top Flange – Minimum Safety Factors (Interface with Trunnion)			
Item	Value (ksi)	Allowable (ksi)	Safety Factor
Bearing Stress (NUREG-0612 Comparison)	3.808	5.975	1.57
Thread Shear Stress (NUREG-0612 Comparison)	3.376	3.585	1.06
Stress Intensity (NB Comparison)	7.857	34.6	4.4

It is noted from the above that all safety factors are greater than 1.0 and that the safety factors for bearing stress and thread shear stress represent the *additional* margin over the factor of safety of 6 on material yielding. A factor of safety of exactly 1.0 means that the maximum stress is equal to the yield stress in tension or shear divided by 6.

3.4.3.2.2 Overpack Top Flange and Baseplate under 3D*

Appendix 3.Y contains finite element analysis and results for the components of the HI-STAR 100 structure that are considered as Region A (namely, the top flange region and baseplate) and evaluated for safety under three times the apparent lifted load (3D*). Figure 3.Y.1 shows details of the finite element model for the top flange region. The overpack baseplate is analyzed using classical plate theory and conservatively assumes that the allowable strengths are determined at the component design temperature rather than at the lower normal operating conditions. The results from Appendix 3.Y for both regions are summarized in the table below.

Overpack Top Flange and Baseplate Minimum Safety Factors (Reg. Guide 3.61 Loading)			
Item	Value (ksi)	Allowable (ksi)	Safety Factor
Top Flange Membrane Stress Intensity (3D*)	27.44	32.2	1.17
Top Flange Membrane plus Bending Stress Intensity (3D*)	30.0	48.3	1.61
Baseplate Membrane plus Bending Stress Intensity (3D*)	1.452	32.2	22.2

It is noted from the above table that all safety factors of safety are greater than 1.0.

3.4.3.3 MPC Lifting Analysis (Load Case E2 in Table 3.1.4)

The MPC can be inserted or removed from an overpack by lifting bolts that are designed for installation into threaded holes in the top lid. The strength requirements of the bolts and base metal are examined in Appendix 3.K based on the requirements of NUREG 0612. Sufficiency of thread engagement length and bolt pre-load are also considered in Appendix 3.K. The MPC top closure is examined in Appendix 3.E, considering the top lid as "Region B", where satisfaction of ASME Code Level A requirements is demonstrated. The same appendix also considers highly stressed regions of the top closure as "Region A" where applied load is 3D*. Appendix 3.I includes structural analysis of the baseplate under normal handling and subject to the allowable strengths appropriate to a component considered in "Region B". Finally, Appendix 3.Y contains analysis and results for the same baseplate region where the loading is 3D* consistent with the baseplate of the MPC being considered as a "Region A". The definitions of "Region A", "Region B", and "3D*" as they apply to lifting analyses have been introduced at the beginning of this Subsection.

The following table summarizes the results from all of these analyses. As stated earlier, safety factors tabulated in this section represent margins that are over and beyond those implied by the loading magnification mandated in NUREG 0612 or Regulatory Guide 3.61, as appropriate.

Summary of MPC Lifting Analyses-Minimum Safety Factors			
Item	Value of Stress (ksi) or Load (lb.)	Allowable (ksi) or Capacity (lb.)	Safety Factor = Allowable/Value or Capacity/Load
Lifting Bolt Load – NUREG 0612 (Note 1)	103,500	111,300	1.08
Top Lid Peripheral Weld Load – (3D*) (Note 2)	310,500	1,055,000	3.40
Top Lid Peripheral Weld Load– "Region B" (Note 2)	460,023	1,055,000	2.29
Baseplate Bending Stress – (3D*) (Note 3)	13.26	20.7	1.56
Baseplate Bending Stress – "Region B" (Note 4)	25.78	28.05	1.09

Notes:
1. Detailed analysis presented in Appendix 3.K
2. Detailed analysis presented in Appendix 3.E
3. Detailed analysis presented in Appendix 3.Y
4. Detailed analysis presented in Appendix 3.I

We note that all factors of safety are greater than 1.0 as required. We also note that the baseplate bending stress calculation in Appendix 3.I is conservative in that the load from the fuel basket is applied as a uniform pressure over the entire baseplate; in reality, the load is applied as a ring load located near the periphery of the basket. Applying the load in this manner would increase the reported safety factor.

3.4.3.4 Miscellaneous Lifting Analyses

The closure plate of the HI-STAR 100 overpack is lifted using four eyebolt lugs that are threaded into tapped holes in the closure plate. The MPC top lid is lifted using the same tapped holes that are used for lifting a loaded MPC. Figure 8.1.2 identifies the typical lid lifting operation that is indicated as one of the steps in the cask deployment operation.

Appendix 3.K contains details of the strength qualification of the overpack top closure lifting holes. Qualification is based on the previously discussed NUREG-0612 requirement. Minimum safety factors are summarized in the table below where we note that a safety factor of 1.0 means that the stress is the lesser of yield stress/6 or ultimate stress/10.

Miscellaneous Lid Lifting – Minimum Safety Factors			
Item	Value (lb.)	Capacity (lb.)	Minimum Safety Factor
Overpack Top Closure Lifting Bolt Shear	9,200	12,010	1.31
Overpack Top Closure Lifting Bolt Tension	9,200	13,250	1.44

Synopses of lifting device, device/component interface, and component stresses, under all contemplated lifting operations for the HI-STAR 100 System have been presented in the foregoing. The results show that all factors of safety are greater than 1.0.

3.4.3.5 Miscellaneous Handling Considerations

Reg. Guide 3.61 and NUREG-1536 do not provide any guidance on the structural requirements for upending or downending operations wherein a location within the body of the cask is used as a pivot or rotational fulcrum. Rotation of the HI-STAR 100 overpack can, however, be carried out using the pocket trunnions as the pivot axis. Under such a scenario, where each pocket trunnion is conservatively assumed to support 50% of the loaded HI-STAR 100 weight (125,000 lbs), the pocket is subject to a modest state of stress which can be readily calculated using standard methods.

Because the pocket trunnions are inserts in the ASME Section III, Subsection NF, Class 3 structure, they do not carry any primary mechanical or inertial loading required of an "NF" part. Therefore, in the storage mode (under 10 CFR 72), the pocket trunnion can be designated as a non-Code part. The pocket trunnions do, however, perform an important-to-safety function, namely shielding. By virtue of their structural strength, the pocket trunnions will maintain their shielding integrity design function under all normal, abnormal, and accident loadings. A detailed discussion of the structural capacity of the pocket trunnions is provided below.

If the stress limit corresponding to ASME Section III Subsection NF, Level A (normal conditions) is conservatively assumed to be applied, then the factors of safety (as shown in the table below) are quite large. Even larger factors of safety are shown to exist if the structural capacity of the trunnion and welded region are computed using the material ultimate strength diminished by a lower bound value of weld quality factor (0.5 per "NG" of the Code for groove welds).

Factors-of-Safety in the Pocket Trunnion		
Reference for Permissible Stress Limit Values	Location	
	Pocket Trunnion Material	Pocket Trunnion to Cask Body Weld
NF	12.63	8.71
NG	20.48	13.56

It can be seen from the above table that regardless of the ASME Code reference used for the permissible stress level, the relevant factors-of-safety exceed the minimum required value of 1.0 by large margins.

Finally, it can be readily shown that the pocket trunnions will maintain their shielding function under the most limiting handling accident scenario. Under a design basis drop event, the pocket trunnions (300 lbs each) may experience a vertical load from their self-inertia of up to:

$$300 \text{ lbs} \times 60 \text{ g} = 18{,}000 \text{ lbs}$$

This load is reacted by the surrounding weld and by direct bearing on the overpack body. The geometry of the pocket trunnion is shown on Drawing 3913; the pocket trunnion insert is completely encapsulated by the surrounding intermediate shells and radial channels and cannot separate from the overpack. The 18,000 pound load on the pocket trunnion is much less than the 125,000 pound load applied during pocket trunnion use as a pivot point and, therefore, is bounded by the pivot point analysis above. The encapsulation, together with support from the peripheral welding, ensures that the shielding function of the pocket trunnion is maintained.

3.4.4 Heat

Subsection 3.4.4, labeled "Heat" in Regulatory Guide 3.61 is required to contain information on all structural (including thermoelastic) analyses performed in the cask to demonstrate positive safety margins, except for lifting operations that are covered in Subsection 3.4.3 in the preceding. Accordingly, this subsection contains all necessary information on the applied loadings, differential thermal expansion considerations, stress analysis models, and results for all normal and off-normal operations, and for natural phenomena/accident events. Assessment of potential malfunction under "Cold" conditions is required to be presented in Subsection 3.4.5.

As instructed by Regulatory Guide 3.61, the thermal evaluation of the HI-STAR 100 System is reported in Chapter 4.

3.4.4.1 Summary of Pressures and Temperatures

Design pressures and design temperatures for all conditions of storage are listed in Tables 2.2.1 and 2.2.3, respectively. Load Cases F1 (Table 3.1.3) and E4 (Table 3.1.4) are defined to study the effect of differential thermal expansion among the constituent components in the HI-STAR 100 System. Figures 3.4.1 and 3.4.2 provide the defining bounding temperature distributions used for the MPC and overpack finite element thermal stress calculations so as to maximize stresses that develop due to such radial gradients. The distribution T is applied conservatively to analyze its effect on the fuel basket, the enclosure vessel, and the overpack.

3.4.4.2 Differential Thermal Expansion

Consistent with the requirements of Reg. Guide 3.61, Load Cases F1 (Table 3.1.3) and E4 (Table 3.1.4) are defined to study the effect of differential thermal expansion among the constituent components in the HI-STAR 100 System. Tables 4.4.9 to 4.4.11 provide the temperatures necessary to perform the differential thermal expansion analyses for the MPC in the HI-STAR 100 System. The material presented in the remainder of this paragraph demonstrates that a physical interference between discrete components of the HI-STAR 100 System (e.g. overpack and enclosure vessel) will not develop due to differential thermal expansion during any operating condition.

3.4.4.2.1 Normal Hot Environment

Closed form calculations are performed to demonstrate that initial gaps between the HI-STAR 100 overpack and the MPC canister, and between the MPC canister and the fuel basket, will not close due to thermal expansion of the system components under normal, off-normal, and accident cases, defined as F1 and E4 in Tables 3.1.3 and 3.1.4, respectively. To assess this in the most conservative manner, the thermal solutions computed in Chapter 4 are surveyed for the following information.

- The radial temperature distribution in each of the fuel baskets at the location of peak center metal temperature.

- The highest and lowest mean temperatures of the canister shell for the hot environment condition.

- The inner and outer surface temperature of the overpack shell (inner shell, intermediate shells, neutron shield, and outer enclosure shell) at the location of highest and lowest surface temperature (which will produce the lowest mean temperature).

Table 4.4.16 presents the resulting temperatures used in the evaluation of the MPC expansion in the HI-STAR 100 overpack.

Using the temperature information in the above-mentioned tables, simplified thermoelastic solutions of equivalent axisymmetric problems are used to obtain conservative estimates of gap closures. The following procedure, which conservatively neglects axial variations in temperature distribution, is utilized.

1. Use the surface temperature information for the fuel basket to define a parabolic distribution in the fuel basket that bounds (from above) the actual temperature distribution. Using this result, generate a conservatively high estimate of the radial and axial growth of the different fuel baskets using classical closed form solutions for thermoelastic deformation in cylindrical bodies.

2. Use the temperatures obtained for the canister to predict an estimate of the radial and axial growth of the canister to check the canister-to-basket gaps.

3. Use the temperatures obtained for the canister to predict an estimate of the radial and axial growth of the canister to check the canister-to-overpack gaps.

4. Use the overpack surface temperatures to construct a logarithmic temperature distribution (characteristic of a thick walled cylinder) at the location used for canister thermal growth calculations; and use this distribution to predict an estimate of overpack radial and axial growth.

5. For given initial clearances, compute the operating clearances.

The calculation procedure outlined above is used in Appendices 3.U and 3.W (HI-STAR 100 overpack with MPC-24 and MPC-68, respectively). The results are summarized in the tables given below for normal storage conditions.

THERMOELASTIC DISPLACEMENTS IN THE MPC AND OVERPACK UNDER HOT TEMPERATURE ENVIRONMENT CONDITION				
CANISTER – FUEL BASKET				
	Radial Direction (in.)		Axial Direction (in.)	
Unit	Initial Clearance	Final Gap	Initial Clearance	Final Gap
MPC-24	0.1875	0.140	2.0	1.77
MPC-68	0.1875	0.144	2.0	1.79
CANISTER – OVERPACK				
	Radial Direction (in.)		Axial Direction (in.)	
Unit	Initial Clearance	Final Gap	Initial Clearance	Final Gap
MPC-24	0.09375	0.068	0.625	0.482
MPC-68	0.09375	0.069	0.625	0.482

It can be verified by referring to the design drawings and the foregoing table, that the clearances between the MPC basket and canister structure, as well as that between the MPC shell and storage overpack, are sufficient to preclude a temperature induced interference from differential thermal expansions under normal operating conditions.

3.4.4.2.2 Fire Accident

Appendix 3.AD evaluates the growth of the fuel basket during and after the fire accident. It is shown that under the most conservative set of assumptions the fuel basket does not contact either the canister or the MPC lid due to free thermal growth. Therefore, restraint of free end expansion leading to fuel basket distortion will not occur. Hence, ready retrievability of the fuel will be maintained and the fuel will remain in a subcritical configuration. The table below summarizes the results from Appendix 3.AD

THERMOELASTIC DISPLACEMENTS IN THE MPC AND OVERPACK UNDER FIRE ACCIDENT TEMPERATURE ENVIRONMENT				
CANISTER – FUEL BASKET				
	Radial Direction (in.)		Axial Direction (in.)	
Unit	Initial Clearance	Final Gap	Initial Clearance	Final Gap
Bounding MPC	0.1875	0.106	2.0	1.604
CANISTER – OVERPACK				
	Radial Direction (in.)		Axial Direction (in.)	
Unit	Initial Clearance	Final Gap	Initial Clearance	Final Gap
Bounding MPC	0.09375	0.052	0.625	0.383

Chapter 11 shows that the fire accident has little effect on the MPC temperatures because of the short duration of the fire and the large thermal inertia of the storage overpack. Therefore, structural evaluation of the MPC under the postulated fire event is not required. The external surfaces of the HI-STAR 100 overpack that are directly exposed to the fire event experience maximum rise in temperature. The outer shell and top closure plate are the external surfaces that are in direct contact with heated air from fire. The table below, extracted from data provided in Chapter 11 (Table 11.2.2), provides maximum bulk temperatures attained.

Component Peak Temperatures due to Storage Fire Event	
Component	Maximum Fire Condition Section Temperature (°F)
Overpack Inner Shell	328
Overpack Top Flange	524
Overpack Outer Shell (external skin)	854
Overpack Baseplate	496
Overpack Closure Plate	384
Neutron Shield Inner Surface	314
Neutron Shield Outer Surface	551
MPC Shell	364

The following conclusions are readily reached from the above table.

- The maximum temperature of the ferritic steel material in the body of the HI-STAR 100 overpack is well below 50% of the material melting point. (The melting point of carbon and low alloy steels is approximately 2750°F, per Mark's Standard Handbook, Ninth Edition, pp 6-11.)

- The temperature of the neutron shielding material experiences a gradient across the thickness of the shielding. The shielding material adjacent to the hot outer enclosure shell experiences a local temperature of 551 degrees F. This means that a limited loss of shielding effectiveness may occur.

- Data published by the Oak Ridge National Laboratories indicates that low stresses from the self-weight of the most heated steel members of HI-STAR 100 (the external skin) ensures that no material rupture will occur. According to the Nuclear System Materials Handbook, TID-2666, ORNL, the time-to-rupture for carbon steels at 1250°F and 4821 psi tensile stress is 520 hours. According to the analyses summarized in Chapter 11, the duration of high temperature in the most heated portion of HI-STAR 100 is well under 1 hour, and the temperature never reaches 900°F.

3.4.4.3 Stress Calculations

This subsection presents calculations of the stresses in the different components of the HI-STAR 100 System from the effects of mechanical load case assembled in Section 3.1. Loading cases for the MPC fuel basket, the MPC enclosure vessel, and the HI-STAR 100 storage overpack are listed in Tables 3.1.3 through 3.1.5, respectively. Detailed analyses for the load cases are presented in labeled appendices that are listed in the load case tables (Tables 3.1.3, 3.1.4, and 3.1.5). An abbreviated description of each of the analyses is presented in the body of the chapter.

In general, as required by Regulatory Guide 3.61, the comparison of the calculated stresses with their corresponding allowables is presented in Subsection 3.4.4.4. However, for clarity in the narrative in this subsection (3.4.4.3), unnumbered summary tables are presented within the text. However, the key stress comparisons are subsequently reproduced in numbered tables associated with Subsection 3.4.4.4 to provide strict compliance with Regulatory Guide 3.61.

The purpose of the analyses is to provide the necessary assurance that there will be no unacceptable risk of criticality, unacceptable release of radioactive material, unacceptable radiation levels, or impairment of ready retrievability.

For all stress evaluations, the allowable stresses and stress intensities for the various HI-STAR 100 System components are based on bounding high metal temperatures to provide additional conservatism (Table 3.1.17 for the MPC basket and shell, for example). Elastic behavior is assumed for all stress analyses. Elastic analysis is based on the assumption of a linear relationship between stress and strain.

In addition to the loading cases germane to stress evaluations mentioned above, three cases pertaining to the stability of HI-STAR 100 are also considered (Table 3.1.1).

The results of various stress calculations on components are reported in this subsection. The calculations are either performed directly as part of the text, or summarized in an appendix (see the list of all supporting appendices provided in Section 3.6.3) that provides details of strength of materials evaluations or finite element numerical analysis. The specific calculations reported in this subsection are:

1. MPC stress and stability calculations
2. HI-STAR 100 overpack stress and stability calculations

The MPC fuel basket and enclosure vessel have been evaluated for the load combinations in Tables 3.1.3 and 3.1.4. The HI-STAR 100 overpack has also been evaluated for certain limiting load conditions that are germane to the storage and operational modes specified for the system in Tables 3.1.1 and 3.1.5.

MPC stress and stability analyses are considered in Subsection 3.4.4.3.1. Within this subsection, the following analyses are performed:

a. Finite element analysis of the MPC fuel basket and enclosure shell under lateral loads
b. Finite element and analytical analysis of the enclosure vessel as an ASME Code pressure vessel.
c. Elastic stability and yielding analysis of the MPC fuel basket under lateral and axial compression.
d. Analysis of the MPC baseplate under lateral loads.
e. Analysis of the MPC closure lid under lateral load.
f. Analysis of the fuel support spacers under compression load.
g. Elastic stability and yielding of the MPC enclosure shell under axial and lateral loads

Overpack stress and stability analyses are considered in Subsection 3.4.4.3.2. Within this subsection, the following analyses are performed:

a. Three-dimensional finite element analysis of the overpack subjected to load cases listed in Table 3.1.5.
b. Consideration of fabrication stresses
c. Structural analysis of closure bolting for normal operation, top closure puncture, and a postulated accident drop condition.
d. Stress analysis of the overpack closure plate under lateral loads.
e. Elastic stability and yielding of the overpack inner shell.
f. Stress analysis of the enclosure shell and enclosure return under internal pressure.

3.4.4.3.1 MPC Stress and Stability Calculations

The structural function of the MPC in the storage mode is stated in Section 3.1. The calculations presented here demonstrate the ability of the MPC to perform its structural function. Analyses are performed for each of the two MPC designs. The purpose of the analyses is to provide the necessary assurance that there will be no unacceptable risk of criticality, unacceptable release of radioactive material, or impairment of ready retrievability. The following subsections describe the model, individual loads, load combinations, and analysis procedures applicable to the MPC.

3.4.4.3.1.1 Analysis of Load Cases E.3.b, E.3.c (Table 3.1.4) and F2, F.3.b, F.3.c (Table 3.1.3)

The load cases considered herein pertain to lateral loading on the MPC components, namely the fuel basket and the enclosure vessel. For this purpose, a finite element model of the MPC is necessary.

- Description of Finite Element Models of the MPCs under Lateral Loading

A finite element model of each MPC is used to assess the effects of the normal, off normal, and accident loads. The models are constructed using ANSYS [3.4.1], and they are identical to the models used in Holtec's HI-STAR 100 10CFR71 submittal under Docket Number 71-9261. The following model description is common to all MPCs.

The MPC structural model is two-dimensional. It represents a one-inch long cross section of the MPC fuel basket and MPC canister.

The MPC model includes the fuel basket, the basket support structures, and the MPC shell. A basket support is defined as any structural member that is welded to the inside surface of the MPC shell. A portion of the overpack inner surface is modeled to provide the correct restraint conditions for the MPC. Figures 3.4.3 through 3.4.11 show the two MPC models.

The fuel basket support structure shown in the figures and in the drawings in Section 1.5 is a multi-plate structure consisting of solid shims or support members having two separate compressive load supporting members. For conservatism in the finite element model some dual path compression members (i.e., "V" angles) are simulated as single columns. Therefore, the calculated stress intensities in the fuel basket angle supports are conservatively overestimated in some locations.

The ANSYS model is not intended to resolve the detailed stress distributions in weld areas. Individual welds are not included in the finite element model. A separate analysis for basket welds and for the basket support "V" angles is contained in Appendix 3.M.

No credit is taken for any load support offered by the Boral panels, sheathing, and the aluminum heat conduction elements. Therefore, these so-called non-structural members are not represented in the model. The bounding MPC weight used, however, does include the mass contributions of these non-structural components.

The model is built using five ANSYS element types: BEAM3, PLANE82, CONTAC12, CONTAC26, and COMBIN14. The fuel basket and MPC shell are modeled entirely with two-dimensional beam elements (BEAM3). Plate-type basket supports are also modeled with BEAM3 elements. Eight-node plane elements (PLANE82) are used for the solid-type basket supports. The gaps between the fuel basket and the basket supports are represented by two-dimensional point-to-point contact elements (CONTAC12). Contact between the MPC shell and the overpack is modeled using two-dimensional point-to-ground contact elements (CONTAC26) with an appropriate clearance gap.

For each MPC type, three variations of the finite element model were prepared. The basic model includes only the fuel basket and the enclosure shell (Figures 3.4.3 through 3.4.5) and is used only to study the free thermal expansion due to the temperature field developed in the system. The other two models include a representation of the overpack and are used for the two drop cases considered. Two orientations of the deceleration vector are considered. The 0-degree drop model includes the overpack-MPC interface in the basket orientation illustrated in Figure 3.1.2. The 45-degree drop model represents the overpack-MPC interface with the basket oriented in the manner of Figure 3.1.3. The 0-degree and the 45-degree drop models are shown in Figures 3.4.6 through 3.4.11. Table 3.4.1 lists the element types and number of elements for all models for all fuel storage MPC types.

A contact surface is provided in the models used for drop analyses to represent the overpack inner shell. As the MPC makes contact with the overpack, the MPC shell deforms to mate with the inside surface of the inner shell. The nodes that define the elements representing the fuel basket and the MPC shell are located along the centerline of the plate material. As a result, the line of nodes that

forms the perimeter of the MPC shell is inset from the real boundary by a distance that is equal to half of the shell thickness. In order to maintain the specified MPC shell/overpack gap dimension, the radius of the overpack inner shell is decreased by an equal amount in the model.

Contact is simulated using two-dimensional point-to-ground elements (CONTAC26). The surface is tangent to the MPC shell at the initial point of impact and extends 135 degrees on both sides. This is sufficient to capture the full extent of contact between the MPC and the overpack.

The three discrete components of the HI-STAR 100 System, namely the fuel basket, the MPC shell, and the storage overpack are engineered with small diametral clearances which are large enough to permit unconstrained thermal expansion of the three components under the rated (maximum) heat duty condition. A small diametral gap under ambient conditions is also necessary to assemble the system without physical interference between the contiguous surfaces of the three components. The required gap to ensure unrestricted thermal expansion between the basket and the MPC shell is less than 0.1 inch. This gap, too, will decrease under maximum heat load conditions, but will introduce a physical nonlinearity in the structural events involving lateral loading (such as side drop of the system) under ambient conditions. It is evident from the system design drawings that the fuel basket, which is non-radially symmetric, is in proximate contact with the MPC shell at a discrete number of locations along the circumference. At these locations, the MPC shell, backed by the massive overpack weldment, provides a virtually rigid support line to the fuel basket during lateral drop events. Because the fuel basket, the MPC shell, and the overpack are all three-dimensional structural weldments, their inter-body clearances may be somewhat uneven at different azimuthal locations. As the lateral loading is increased, clearances close at the support locations, resulting in the activation of the support from the overpack.

The bending stresses in the basket and the MPC shell at low lateral loading levels which are too small to close the support location clearances are secondary stresses since further increase in the loading will activate the overpack's support action, mitigating further increase in the stress. Therefore, to compute primary stresses in the basket and the MPC shell under lateral drop events, the gaps should be assumed to be closed. However, in the analysis, we have conservatively assumed that an initial gap of 0.1875" exists, in the direction of the applied deceleration, at all support locations between the basket and the shell and the radial gap between the shell and the overpack at the support locations is 3/32". In the evaluation of safety factors for the MPC-68, the total stress state produced by the applied loading on this configuration is conservatively compared with primary stress levels, even though the self-limiting stresses should be considered secondary in the strict definition of the Code. To illustrate the conservatism, we have eliminated the secondary stress (that develops to close the clearances) in the comparison with primary stress allowable values and report safety factors for the MPC-24 that are based only on primary stresses necessary to maintain equilibrium with the inertia forces.

- Description of Individual Loads and Boundary Conditions Applied to the MPCs

The method of applying each individual load to the MPC model is described in this subsection. The individual loads are listed in Table 2.2.14. A free-body diagram of the MPC corresponding to each individual load is given in Figures 3.4.12-3.4.15. In the following discussion, references to vertical

and horizontal orientations are made. Vertical refers to the direction along the cask axis, and horizontal refers to a radial direction.

Quasi-static structural analysis methods are used. The effects of any dynamic load factors (DLFs) are included in the final evaluation of safety margins. All analyses are carried out using the design basis decelerations in Table 3.1.2

The MPC models used for side drop evaluations are shown in Figures 3.4.6 through 3.4.11. In each model, the fuel basket and the enclosure vessel are constrained to move only in the direction that is parallel to the acceleration vector. The overpack inner shell, which is defined by three nodes needed to represent the contact surface, is fixed in all degrees of freedom. The fuel basket, enclosure vessel, and overpack inner shell are all connected at one location by linear springs (see Figure 3.4.6, for example).

(a) Accelerations

During a side impact event, the stored fuel is directly supported by the cell walls in the fuel basket. Depending on the orientation of the drop, 0 or 45 degrees (see Figures 3.4.14 and 3.4.15), either one or two walls support the fuel. The effect of deceleration on the fuel basket and canister metal structure is accounted for by amplifying the gravity field in the appropriate direction. In the finite element model this load is effected by applying a uniformly distributed pressure over the full span of the supporting walls. The magnitude of the pressure is determined by the weight of the fuel assembly (Table 2.1.6), the axial length of the fuel basket support structure, the width of the cell wall, and the impact acceleration. It is assumed that the load is evenly distributed along an axial length of basket equal to the fuel basket support structure. For example, the pressure applied to an impacted cell wall during a 0-degree side drop event is calculated as follows:

$$p = \frac{a_n W}{L \ell}$$

where:

p = pressure

a_n = ratio of the impact acceleration to the gravitational acceleration

W = weight of a stored fuel assembly

L = axial length of the fuel basket support structure

ℓ = width of a cell wall

For the case of a 45-degree side drop the pressure on any cell wall equals p (defined above) divided by the square root of 2. Figure 3.4.12 shows the details of the fuel assembly pressure load on the fuel basket.

(b) Internal Pressure

Design internal pressure in the MPC model is applied by specifying pressure on the inside surface of the enclosure vessel. The magnitude of the internal pressure applied to the model is taken from Table 2.2.1.

For this load condition, the center of the fuel basket is fixed in all degrees of freedom.

(c) Temperature

Temperature distributions are developed in Chapter 4 and applied as nodal temperatures to the finite element model of the MPC enclosure vessel (confinement boundary). Maximum design heat load has been used to develop the temperature distribution used to demonstrate compliance with ASME Code stress intensity levels. A plot of the applied temperature distribution as a function of radius is shown in Figure 3.4.1. Figure 3.4.13 shows the MPC-68 with the typical boundary conditions for all thermal and pressure load cases.

(d) Handling (Lateral Loading)

As discusses in Subsection 3.1.2.1.2, loads arise on the HI-STAR 100 System from normal handling of the cask (e.g., lateral loads while moving the system to the ISFSI). A 2g lateral acceleration, imposed on the fuel basket/enclosure shell finite element model, is assumed to bound lateral handling loads on the MPC under normal handling conditions (Level A Service Conditions).

- Analysis Procedure

The analysis procedure for this set of load cases is as follows:

1. The stress intensity and deformation field due to the combined loads is determined by the finite element solution.

2. The results for each load combination are compared to allowables. The comparison with allowable values is made in Subsection 3.4.4.4.

3.4.4.3.1.2 Analysis of Load Cases E1.a and E1.c (Table 3.1.4)

Load Cases E1.a and E1.c pertain to the performance of the enclosure vessel as a pressure vessel.

Since the MPC shell is a pressure vessel, the classical Lame's calculations should be performed to demonstrate the shell's performance as a pressure vessel. We note that dead load has an insignificant effect on this stress state. We first perform calculations for the shell under internal pressure. Subsequently, we perform a finite element analysis on the entire confinement boundary as a pressure vessel subject to both internal pressure and temperature gradients. Finally, we perform confirmatory hand calculations to gain confidence in the finite element predictions,

- Lame's Solution for the MPC Shell

The stress from internal pressure is found for normal and accident pressures conditions using classical formulas:

We define the following quantities:

P = pressure, r = MPC radius, and t = shell thickness.

Using classical thin shell theory, the circumferential stress, $\sigma_1 = Pr/t$, the axial stress $\sigma_2 = Pr/2t$, and the radial stress $\sigma_3 = -P$ are computed for both normal and accident internal pressures. The results are given in the following table:

Classical Shell Theory Results for Normal and Accident Internal Pressures				
Item	σ_1 (psi)	σ_2 (psi)	σ_3 (psi)	$\sigma_1 - \sigma_3$ (psi)
P= 100 psi	6,838	3,419	-100	6,938
P= 125 psi	8,548	4,274	-123	8,673

Table 3.1.17 provides the allowable membrane strength for Load Case E1 for Alloy X. We see that a safety factor greater than 1.0 exists for the case of normal and accident pressures.

- Finite Element Analysis (Load Case E1.a and E1.c of Table 3.1.4)

Having performed the classical "thin shell under pressure" evaluation, we now proceed to perform a finite element analysis where the interaction between the end closures and the MPC shell is rigorously modeled.

The MPC shell, the top lid, and the baseplate together form the confinement boundary (enclosure vessel) for storage of spent nuclear fuel. In this section, we evaluate the operating condition consisting of dead weight, internal pressure, and thermal effects for the normal heat condition of storage. The top and bottom plates of the MPC enclosure vessel (EV) are modeled using plane axisymmetric elements, while the shell is modeled using the axisymmetric thin shell element. The

thickness of the top lid varies in the two MPC types and can be either a single thick lid, or two dual lids welded around their common periphery; the minimum thickness top lid is modeled in the finite element analysis. As applicable, the results for the MPC top lid are modified to account for the fact that in the dual lid configuration, the two lids act independently under mechanical loading. The temperature distributions for all MPC constructions are nearly identical in magnitude and gradient. Temperature differences across the thickness of both the baseplate and the top lid exist during HI-STAR 100's operations. There is also a thermal gradient from the center of the top lid and baseplate out to the shell wall. The metal temperature profile is essentially parabolic from the centerline of the MPC out to the MPC shell. There is also a parabolic temperature profile along the length of the MPC canister. Figure 3.4.44 shows a sketch of the confinement boundary structure `with identifiers A-I (also called locating points) where temperature input data is used to represent a continuous temperature distribution for analysis purposes. The overall dimensions of the confinement boundary are also shown in the figure.

Table 4.4.22 provides the desired temperatures for confinement thermal stress analysis. From the tables, we see that the distribution for the MPC-24 provides the largest temperature gradients in the baseplate (from centerline to outer edge) and in the shell (from the joint at the baseplate to the half-height of the cask). It will be shown later than stress intensities are greatest in these components of the confinement vessel. Therefore, detailed stress analyses are performed only for the MPC-24. Because of the intimate contact between the two lid plates when the MPC lid is a two piece unit, there is no significant thermal discontinuity through the thickness; thermal stresses arising in the MPC top lid will be bounding when there is only a single lid. Therefore, for thermal stresses, results from the analysis that considers the lid as a one-piece unit are used and are amplified to reflect the increase in stress in the dual lid configuration.

Figure 3.4.45 shows details of the finite element model of the top lid (considered as a single piece), canister shell, and baseplate. The top lid is modeled with 40 axisymmetric quadrilateral elements; the weld connecting the lid to the shell is modeled by a single element solely to capture the effect of the top lid attachment to the canister offset from the middle surface of the top lid. The MPC canister is modeled by 50 axisymmetric shell elements, with 20 elements concentrated in a short length of shell appropriate to capture the so-called "bending boundary layer" at both the top and bottom ends of the canister. The remaining 10 shell elements model the MPC canister structure away from the shell ends in the region where stress gradients are lower (from the physics of the problem). The baseplate is modeled by 20 axisymmetric quadrilateral elements. Deformation compatibility at the connections is enforced at the top by the single weld element, and deformation and rotation compatibility at the bottom by additional shell elements between nodes 106-107 and 107-108.

The geometry of the model is listed below (terms are defined in Figure 3.4.45):

H_t = 9.5" (the minimum total thickness lid is assumed)

R_L = 0.5 x 67.25" (Bill of Materials for Top Lid, Section 1.5)

L_{MPC} = 190.5" (Table 3.2.4)

t_s = 0.5"

R_S = 0.5 x 68.375"

t_{BP} = 2.5"

βL = $2\sqrt{R_s t_s} \approx 12$" (the "bending boundary layer")

Stress analyses are carried out for two cases as follows:

a. internal pressure = 100 psi

b. internal pressure = 100 psi, plus applied temperatures for the MPC-24

We note that dead weight of the top lid reduces the stresses due to pressure. For example, the equivalent pressure simulating the effect of the weight of the top lid is an external pressure of 3 psi, which reduces the pressure difference across the top lid to 97 psi. Thus, for conservatism, dead weight of the top lid is neglected to provide additional conservatism in the results. The dead weight of the baseplate, however, adds approximately 0.73 psi to the effective internal pressure acting on the base. The effect of dead weight is still insignificant compared to the 100 psi design pressure, and is therefore neglected. The thermal loading in the confinement vessel is obtained by developing a parabolic temperature profile to the entire length of the MPC canister and to the top lid and baseplate. The temperature data provided at locations A-I in Figures 3.4.44 and 3.4.45 are sufficient to establish the profiles. Through-thickness temperatures are assumed linearly interpolated between top and bottom surfaces of the top lid and baseplate. All material properties and expansion coefficients are considered to be temperature-dependent in the model.

Results for stress intensity are reported for the case of internal pressure alone and for the combined loading of pressure plus temperature (Load Case E1.c in Table 3.1.4). Tables 3.4.7 and 3.4.8 report results at the inside and outside surfaces of the top lid and baseplate at the centerline and at the extreme radius. Canister results are reported in the "bending boundary layer" and at a location near mid-length of the MPC canister. In the tables, the calculated value is the value from the finite element analysis, the categories are P_m = primary membrane; $P_L + P_b$ = local membrane plus primary bending; and $P_L + P_b + Q$ = primary plus secondary stress intensity. The allowable stress intensity value is obtained from the appropriate table in Section 3.1 for Level A conditions, and the safety factor SF is defined as the allowable strength divided by the calculated value. Allowable stresses for Alloy X are taken at 300°F, which bounds the temperatures everywhere except at the mid-length position of the MPC shell (Location I in Figure 3.4.44) during the normal operation. At Location I, the allowable strength is taken at 400°F. The results given in Tables 3.4.7 and 3.4.8 demonstrate the ruggedness of the MPC as a confinement boundary. Since mechanically induced stresses in the top lid are increased when a dual lid configuration is considered, the stress results obtained from an analysis of a single top lid must be corrected to reflect the maximum stress state when a dual lid configuration is considered. The modifications required are based on the following logic:

Consider the case of a simply supported circular plate of thickness h under uniform lateral pressure "q". Classical strength of materials provides the solution for the maximum stress, which occurs at the center of the plate, in the form:

$\sigma_s = 1.225q(a/h)^2$ where a is the radius of the plate and h is the plate thickness.

Now consider the MPC simply supported top lid as fabricated from two plates "1" and "2", of thickness h_1 and h_2, respectively, where the lower surface of plate 2 is subjected to the internal pressure "q", the upper surface of plate 1 is the outer surface of the helium retention boundary, and the lower surface of plate 1 and the upper surface of plate 2 are in contact. The following sketch shows the dual lid configuration for the purposes of this discussion:

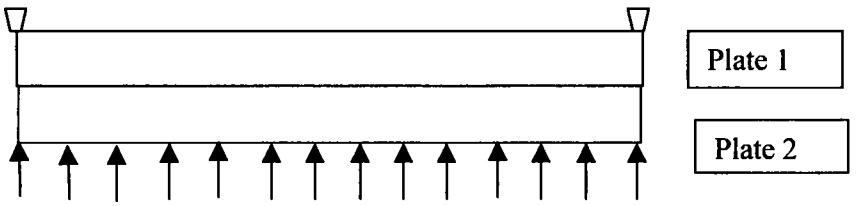

From classical plate theory, if it is assumed that the interface pressure between the two plates is uniform and that both plates deform to the same central deflection, then if

$h_1+h_2 = h$, and if $h_2/h_1 = r$

the following relations exist between the maximum stress in the two individual plates, σ_1, σ_2 and the maximum stress σ_s in the single plate of thickness "h":

$$\frac{\sigma_1}{\sigma_s} = \frac{(1+r)^2}{(1+r^3)} \qquad \frac{\sigma_2}{\sigma_s} = \frac{(1+r)^2}{(1+r^3)}r$$

Since the two lid thicknesses are the same in the dual lid configuration, r = 1.0 so that the stresses in plates 1 and 2 are both two times larger than the maximum stress computed for the single plate lid having the same total thickness. In Tables 3.4.7 and 3.4.8, bounding results for the dual lid configuration are reported by using these ratios at all locations in the top lid.

- Confirmatory Closed Form Solution

The results in Table 3.4.7 and 3.4.8 also show that the baseplate and the shell connection to the baseplate are the most highly stressed regions under the action of internal pressure. To confirm the finite element results, we perform an alternate closed form solution using classical plate and shell theory equations that are listed in or developed from the reference Timoshenko and Woinowsky-Krieger, Theory of Plate and Shells, McGraw Hill, Third Edition.

Assuming that the thick baseplate receives little support against rotation from the thin shell, the bending stress at the centerline is evaluated by considering a simply supported plate of radius a and thickness h, subjected to lateral pressure p. The maximum bending stress is given by

$$\sigma = \frac{3(3+\nu)}{8} p \left(\frac{a}{h}\right)^2$$

where:

a = .5 x 68.375"

h = 2.5"

ν = 0.3 (Poisson's Ratio)

p = 100 psi

Calculating the stress in the plate gives σ = 23,142 psi.

Now consider the thin MPC shell (t = 0.5") and first assume that the baseplate provides a clamped support to the shell. Under this condition, the bending stress in the thin shell at the connection to the plate is given as

$$\sigma_{Bp} = 3p\frac{a}{t}\frac{(1-\nu/2)}{\sqrt{3}(1-\nu^2)^{1/2}} = 10{,}553 \text{ psi}$$

In addition to this stress, there is a component of stress in the shell due to the baseplate rotation that causes the shell to rotate. The joint rotation is essentially driven by the behavior of the baseplate as a simply supported plate; the shell offers little resistance because of the disparity in thickness and will essentially follow the rotation of the thick plate.

Using formulas from thin shell theory, the additional axial bending stress in the shell due to this rotation θ can be written in the form

$$\sigma_{B\theta} = 12\ \beta\ D_s \frac{\theta}{t^2}$$

where

$$\theta = pa^3/8D(1+\nu) * \left(1/1+\alpha\right)$$

and

$$D = \frac{Eh^3}{12(1-\nu^2)} \qquad E = \text{plate Young's Modulus}$$

$$\alpha = \frac{2\beta a t^3}{h^3(1+\nu)}$$

$$D_s = \frac{Et^3}{12(1-\nu^2)}$$

$$\beta^2 = \sqrt{3(1-\nu^2)}/at$$

Substituting the numerical values gives

$$\sigma_{B\theta} = 40{,}563 \text{ psi}$$

We note that the approximate solution is independent of the value chosen for Young's Modulus as long as the material properties for the plate and shell are the same.

Combining the two contributions to the shell bending stress gives the total extreme fiber stress in the longitudinal direction as 51,116 psi.

The baseplate stress value, 23,142 psi, compares well with the finite element result 20,528 psi (Table 3.4.7). The shell joint stress, 51,116 psi, is greater than the finite element result (43,986 psi in Table 3.4.7). This is due to the local effects of the shell-to-baseplate connection offset. That is, the connection between shell and baseplate in the finite element model is at the surface of the baseplate, not at the middle surface of the baseplate. This offset will cause an additional bending moment that will reduce the rotation of the plate and hence, reduce the stress in the shell due to the rotation of the baseplate.

In summary, the approximate closed form solution confirms the accuracy of the finite element analysis in the baseplate region.

3.4.4.3.1.3 Elastic Stability and Yielding of the MPC Basket under Compression Loads (Load Case F3 in Table 3.1.3)

This load case corresponds to the scenario wherein the loaded MPC is postulated to drop causing a compression state in the fuel basket panels.

a. Elastic Stability

Following the provisions of Appendix F of the ASME Code [3.4.3] for stability analysis of Subsection NG structures, (F1331.5(a)(1)), a comprehensive buckling analysis is performed using ANSYS. For this analysis, ANSYS's large deformation capabilities are used. This feature allows ANSYS to account for large nodal rotations in the fuel basket, which are characteristic of column buckling. The interaction between compressive and lateral loading, caused by the deformation, is included in a rigorous manner. The finite element model used for the large deflection analysis of the basket is identical to the model described in Subsection 3.4.4.3.1.1 used for the fuel basket stress analysis. The large deflection option is "turned on" so that equilibrium equations for each load increment are computed based on the current deformed shape. Subsequent to the large deformation analysis, the individual basket panel that is most susceptible to buckling failure is identified by a review of the results. The lateral displacement of a node located at the mid-span of the panel is measured for the range of impact decelerations. The buckling or collapse load is defined as the impact deceleration for which a slight increase in its magnitude results in a disproportionate increase in the lateral displacement. The most critical element is a vertically oriented panel that is subject to a compressive load together with bending moments from adjacent connected lateral basket panels.

The stability requirement for the MPC fuel basket under lateral loading is satisfied if two-thirds of the collapse deceleration load is greater than the design basis horizontal acceleration (Table 3.1.2). Figures 3.4.27 through 3.4.32 are plots of the local lateral displacement versus impact deceleration for the most limiting basket panel. It should be noted that the displacements in Figures 3.4.27 through 3.4.31 are expressed in $1x10^{-1}$ inch and Figure 3.4.32 is expressed in $1x10^{-2}$ inch. The plots clearly show that the large deflection collapse load of the MPC fuel basket is greater than 1.5 times the inertia load corresponding to the design basis deceleration for all baskets in all orientations. Thus, the requirements of Appendix F are met for lateral deceleration loading under Subsection NG stress limit s for faulted conditions.

An alternative solution for the stability of the fuel basket panel is obtained using the methodology espoused in NUREG/CR-6322 [3.4.12]. In particular, we consider the fuel basket panels as wide plates in accordance with Section 5 of NUREG/CR-6322. We use eq.(19) in that section with the "K" factor set to the value appropriate to a clamped panel. Material properties are selected corresponding to a metal temperature of 500 degrees F which bounds computed metal temperatures at the periphery of the basket. The critical buckling stress is

$$\sigma_{cr} = \left(\pi/K\right)^2 \frac{E}{12\left(1-\nu^2\right)}\left(\frac{h}{a}\right)^2$$

where h is the panel thickness, a is the unsupported panel length, E is the Young's Modulus of Alloy X at 500 degrees F, ν is Poisson's Ratio, and K=0.65 (per Figure 6 of NUREG/CR-6322).

The MPC-24 has the smallest h/a ratio; the results of the finite element stress analyses under design basis deceleration load show that this basket is subject to the highest compressive load in the panel. Therefore, the critical buckling load is computed using the geometry of the MPC-24. The following table shows the results from the finite element stress analysis and from the stability calculation.

Panel Buckling Results From NUREG/CR-6322			
Item	Finite Element Stress (ksi)	Critical Buckling Stress (ksi)	Factor of Safety
Stress	13.717	49.22	3.588

For a stainless steel member under an accident condition load, the recommended safety factor is 2.12. We see that the calculated safety factor exceeds this value; therefore, we have independently confirmed the stability predictions of the large deflection analysis based on classical plate stability analysis by employing a simplified method.

Stability of the basket panels, under longitudinal deceleration loading (Load Cases F3.a in Table 3.1.3), is demonstrated in the following manner. From Table 3.2.1 we have the weight of each fuel basket (including sheathing and Boral). The metal areas of the basket bearing on the MPC baseplate can be computed from the drawings in Section 1.5. Dividing weight by area and multiplying by the design basis deceleration from Table 3.1.2 gives the following results.

Fuel Basket Compressive Stress For End Drop (Load Case F3.a)			
Item	Weight (lb)	Area (sq. inch)	Stress (psi)
MPC-68	16,240	250.3	3,893
MPC-24	20,842	357.1	3,502

To demonstrate that elastic instability in the basket panels is not credible, we compute the flat panel buckling stress, σ_{cr}, (critical stress level at which elastic buckling may occur) using the formula in reference [3.4.8].

For elastic stability, Reference [3.4.8] provides the formula for critical axial stress as

$$\sigma_{cr} = \frac{4\pi^2 E}{12(1-\nu^2)}\left(\frac{T}{W}\right)^2$$

where T is the panel thickness and W is the width of the panel, E is the Young's Modulus at the metal temperature and ν is the metal Poisson's Ratio. The following table summarizes the calculation for the critical buckling stress using the formula given above:

Elastic Stability Result for a Flat Panel	
Reference Temperature	725 degrees F
T (MPC-24)	5/16 inch
W	10.777 inch
E	24,600,000 psi
Critical Axial Stress	74,781 psi

It is noted the critical axial stress is an order of magnitude greater than the computed basket axial stress reported in the foregoing and demonstrates that elastic stability under longitudinal deceleration load is not a concern.

b. Yielding

The safety factor against yielding of the basket under longitudinal compressive stress from a design basis inertial loading is given by

SF = 17,100/3,739 = 4.57

Therefore, plastic deformation of the fuel basket under design basis deceleration is not credible.

3.4.4.3.1.4 MPC Baseplate Analysis (Load Cases E2, E3, E5)

These load cases from Table 3.1.4 consider normal handling, accidental drop, and storage fire.

Minimum safety factors have been reported for Load Case E2 in Subsection 3.4.3 where an evaluation has been performed for stresses under three times the "apparent" load D*. Load Case E3.a provides the limiting accident loading on the baseplate wherein the combined effect of a 60g deceleration plus accident internal pressure is considered. The analysis conservatively neglects support from the overpack during the storage drop accident. During a fire (Load Case E5), the MPC baseplate is subjected to the accident pressure plus dead load, and the fire temperature (which serves only to lower the allowable strengths). All of these analyses are detailed in Appendix 3.I; the results are summarized below:

MPC Baseplate Minimum Safety Factors – Load Cases E3, E5			
Item	Value (ksi)	Allowable (ksi)	Safety Factor
Center of Baseplate – Primary Bending (Load Case E3)	35.93	67.32	1.87
Center of Baseplate – Primary Bending (Load Case E5)	30.46	54.23	1.78

We note from the above that all safety factors are greater than 1.0.

3.4.4.3.1.5 Analysis of the MPC Closure Lid (Load Cases E3, E5)

The closure lid, the closure lid peripheral weld, and the closure ring are examined for maximum stresses developed during the accident drop event and the storage fire.

Analysis of the closure lid for Load Case E1 has been performed previously as part of the finite element analysis of the confinement boundary. Similarly, results for Load Case E2 have been discussed in Subsection 3.4.3 as part of a lifting device. Appendix 3.E contains stress analysis of the MPC top closure lid for Load Cases E3 and E5. The closure lid is modeled as a single simply supported plate and is subject to deceleration from an end drop plus appropriate design pressures. Figure 3.E.1 shows the configuration considered. Results are presented for both the single and dual lid configuration (in parentheses). For the dual lid configuration, the two plates each support their own amplified weight as simply supported plates under a bottom end drop. The results for minimum safety factor are reported in the table below:

MPC Top Closure Lid – Minimum Safety Factors – Load Cases E3, E5			
Item	Stress (ksi) or Load (lb.)	Allowable Stress (ksi) or Load Capacity (lb.)	Safety Factor
Lid Bending Stress – Load Case E3.a	3.35/(7.94)	61.05	18.2/(7.69)
Lid-to-Shell Peripheral Weld Load – Load Case E3.a	624,000	1,477,000††	2.37
Lid Bending Stress – Load Case E5	1.991/(3.982)	54.225	27.24/(13.6)
Lid-to-Lid Peripheral Weld Load – Load Case E3.a	312,000	443,200†††	1.42
Closure Ring Bending Stress – Load Case E1.a†	20.0	28.1	1.41
Closure Ring Weld Load – Load Case E1.a	140,956	316,400	2.24

† The closure ring is only subject to load subsequent to a postulated loss of integrity in the "NB" pressure boundary (such as a leak in the MPC lid that is joined to the shell using a volumetrically examined groove weld). Nevertheless, the stress results are compared to Level A allowables for conservatism. The pressure loading is assumed to correspond to the Design Pressure, which as stated before, bounds both normal and off-normal conditions of storage.

†† Based on 0.625" single groove weld and conservatively includes a quality factor of 0.45.

††† This is a non-Code weld; limit is based on a 0.1875 inch groove weld and includes a quality factor of 0.45 for additional conservatism.

3.4.4.3.1.6 Structural Analysis of the Fuel Support Spacers (Load Cases F2 and F3.a)

Upper and lower fuel support spacers are utilized to position the active fuel region of the spent nuclear fuel within the poisoned region of the fuel basket. It is necessary to ensure that the spacers will continue to maintain their structural integrity after an accident event. Ensuring structural integrity implies that the spacer will not buckle under the maximum compressive load, and that the maximum compressive stress will not exceed the compressive strength of the spacer material (Alloy X). Detailed calculations in Appendix 3.J demonstrate that large structural margins in the fuel spacers are available for the entire range of spacer lengths that may be used in HI-STAR 100 applications (for the various acceptable fuel types). For normal and off-normal operation (Level A Service Condition), a 10g deceleration load is applied (to cover the case of transport wherein the railroad longitudinal design basis g level is 10 (see the HI-STAR 100 SAR, Docket 71-9261)). For accident conditions, a 60g deceleration is the applied loading (Level D Service Condition). The following table summarizes the results:

Fuel Spacers – Minimum Safety Factors (Load Cases F2 and F3.a)			
Item	Load (lb.)	Capacity (lb.)	Safety Factor
Axial Load – Level A	16,800	46,446	2.76
Elastic Stability – Level D – Lower Spacer	100,800	1,300,000	12.9
Elastic Stability – Level D – Upper Spacer	100,800	577,000	5.72

3.4.4.3.1.7 Enclosure Vessel Stability (Load Case E1.b, E2, E3, and E5 Table 3.1.4)

The MPC shell is examined for elastic/plastic instability due to external pressure or compressive loads introduced as part of these load cases (design external pressure, normal handling, accident vertical drop, and storage fire). Each load component is examined separately. Design external pressure is applied to the outer surface of the EV shell in the MPC model. The magnitude of the external pressure applied to the model is taken from Table 2.2.1. Analysis of the MPC under the external pressure is provided in Appendix 3.H Analyses are performed using the methodology of ASME Code Case N-284 [3.4.6]. The following stability evaluations are performed in Appendix 3.H for the MPC shell:

a. A 1.15g compressive handling load.

b. Design basis deceleration inertia load.

c. Accident external pressure plus a 1g compressive dead load.

d. Design external pressure plus a 1g compressive dead load.

The interaction equations for the ASME Code Case N-284 are evaluated and shown to give results less than 1.0 for all of the above conditions. The following table summarizes the limiting result from all of the calculations performed.

MPC Shell - Elastic/Plastic Stability (ASME Code Case N-284) – Minimum Safety Factors			
Item	Value	Allowable†	Safety Factor
Load Case E3.a (Yield)	0.698	1.34	1.92
Load Case E5 (Stability Interaction Equation)	0.847	1.0	1.18
Load Case E1.b (Stability Interaction Curve)	0.832	1.0	1.20

† We note that for Load Case E3.a, the yield strength criteria in the Code Case N-284 method govern. In this event, we include the safety factor 1.34, built into the Code Case, in the tabular result in order to obtain the actual safety factor with respect to the yield strength of the material.

The results demonstrate that the MPC shell meets the requirements of Code Case N-284. We note that the stability results presented above are very conservative. The stability analyses in Appendix 3.H carried out for the MPC shell assumed no axial stiffening from the fuel basket supports that run the full length of the shell. An analysis that included the effect of the stiffening (and therefore, recognized the fact that instability will most likely occur between stiffeners) will give increased safety factors for Load Cases E5 and E1.b.

3.4.4.3.2 Overpack Stress Calculations

The structural functions of the overpack are stated in Section 3.1. The analyses presented here demonstrate the ability of components of the HI-STAR 100 overpack to perform their structural functions in the storage mode. Load cases applicable to the structural evaluation of the HI-STAR 100 overpack are compiled in Table 3.1.5.

The purpose of the analyses is to provide the necessary assurance that the design of the HI-STAR 100 overpack precludes unacceptable release of radioactive material, unacceptable radiation levels, or impairment of ready retrievability of the MPC during system deployment and throughout its service life.

In this subsection, stresses and stress intensities in the HI-STAR 100 overpack due to the combined effects of thermal gradients, pressure, and mechanical loads are presented. The results are obtained from a series of finite element analyses on the complete overpack and separate analyses on overpack components.

3.4.4.3.2.1 Finite Element Analysis – Load Cases 01 to 05 in Table 3.1.5

Load Cases 01 and 05 pertain to demonstration of the overpack helium retention boundary as an ASME "NB" component under Design Pressure and Level A Service Condition thermal loading. Other cases pertain to handling, handling accident, and natural phenomena events. To analyze these load cases, a suitable finite element model of the complete overpack is required.

- Description of Finite Element Model

The purpose of the HI-STAR 100 overpack model is to calculate stresses and stress intensities resulting from the loadings defined in Chapter 2 and compiled into load cases in Table 3.1.5 (including Load Cases 01 and 05).

A three-dimensional finite element model of the HI-STAR 100 overpack is used to assess the effects of normal, off normal, and accident condition loads. The overpack is a large structure subject to a variety of complex loads and boundary conditions. The finite element model developed for this analysis allows efficient determination of the stresses in this complex structure.

The finite element model of the overpack is constructed using ANSYS [3.4.1]. This model is duplicated in the HI-STAR 100 SAR (10CFR71) submittal for transport.

For structural analysis purposes, the overpack is assumed to be symmetric about a diametral mid-plane. This assumption is reasonable because the purpose of the model is to investigate global stresses in the model. The model is not intended to resolve effects due to small penetrations that produce peak stresses (which are significant only in cyclic fatigue conditions).

Element plots of the model are shown in four figures (Figures 3.4.17 through 3.4.20). The basic building blocks of the finite element model are 20-node brick (SOLID95), 8-node brick (SOLID45), and 6-node tetrahedron elements (SOLID45). These are 3-D solid elements with 3 degrees of freedom at each node (three linear displacement degrees of freedom). Element densities are increased towards the top and bottom of the model in order to provide increased resolution of the stress fields in those regions.

The top flange/closure plate interface is modeled using linear spring elements (COMBIN14). The concentric seals are not modeled explicitly. The model is not intended to resolve the stress field around the grooves for the seals. The status of joint seal is ascertained by "compression springs" which simulate the O-ring gaskets. Contact between the overpack top flange and closure plate is verified by checking the status of these spring elements. If contact between the closure plate and top flange is maintained (indicated by a compressive load in the "compression springs"), then the integrity of the seal is determined to have been maintained.

The overpack closure bolts are modeled with beam elements (BEAM4). The top of the beam elements represents the bolt head and is connected to the overpack closure plate. The bottom of the elements represents the threaded region of the bolt and is connected to nodes of elements representing the top flange.

The inner shell of the overpack is modeled with two element layers through the thickness of the shell.

Each of the lifting trunnions is modeled as three rigid beam elements (BEAM4) connected to the top flange. The beams extend from the flange and meet at a single node location. Trunnion stress analysis is carried out in Appendix 3.D; the inclusion of the trunnion herein is solely to provide the appropriate offset for handling loads.

The neutron shield material is not a load bearing or supporting component in the finite element model. However, the weight of the neutron shield material must be included in the model in order to obtain the proper inertia loads. The neutron shield material is modeled with SOLID45 elements having a weight density that is specified in Subsection 3.3.2.1. In the model herein, we include the neutron shield material as an element set to ensure that proper accounting of total weight (and accompanying deceleration loads) occurs. Therefore, the neutron shield material must be assigned a Young's Modulus in the model. A value approximately equal to 1% of the Modulus of the steel load carrying components is assigned to the neutron shield material to insure that the neutron shield material serves as a load rather than a structural member in the model.

It is recognized that the layered shells of the overpack are connected to each other and to innermost shell only at their top and bottom extremities. The finite element model must incorporate the potential for separation between the intermediate shells in certain regions under certain loading. Likewise, the intermediate shells cannot interpenetrate each other or the inner shell structure. This is accomplished by radially coupling adjacent intermediate shell nodes over two 60-degree spans. Figure 3.4.33 illustrates the nodal coupling pattern. The intermediate shell nodes that lie in the 60-degree sector between the top and bottom portions of the model remain uncoupled. The intermediate shells, in the uncoupled region, are free to separate from one another as the overpack cross section ovalizes during side impact. This modeling approach ensures that load transfer in a side drop is modeled correctly. With respect to the overpack model, "bottom portion" refers to the 60-degree segment of the model closest to the point of impact. Conversely, "top portion" refers to the 60-degree sector farthest from the point of impact. This nodal coupling arrangement conservatively represents the structural contribution of the intermediate shells. In addition, no axial or circumferential nodal coupling has been used between adjacent intermediate shells. Thus, axial bending stiffness of the composite shell structure is conservatively underestimated.

The two pocket trunnions at the base of the HI-STAR 100 overpack may be used for rotating the overpack from horizontal to vertical orientation (upending) or downending. In its role as a rotation pivot, the pocket trunnion is subject to minor stress levels as described in Subsection 3.4.3.5. Because the pocket trunnions are essentially local inserts in the form of a machined block in the layered shell structure, they do not provide a primary load transmission path within the HI-STAR 100 overpack. Therefore, the pocket trunnion is categorized as a non-Code part and in the finite element analysis of the overpack for storage; the pocket trunnions are not included in the structural representation of the overpack.

A one-dimensional force equilibrium evaluation has been performed to demonstrate that, even under the limiting accident condition of vertical drop leading to an inertial design basis deceleration of 60 g's, the structural joints between the outer layers of the overpack multi-shell structure and the cask body will maintain their structural integrity.

The overpack outer (5^{th} layer) intermediate shell, radial channels, enclosure panels, and the Holtite-A neutron shielding material (total weight approximately 38,000 lbs.) are joined by a full-penetration circumferential weld to the top flange and a circumferential partial penetration groove weld to the fourth intermediate shell just above the bottom forging. The total axial load capacity of this weld configuration is greater than 22,000,000 lbs. In the most limiting design basis scenario for storage (an end-drop handling accident), the amplified load on these welds is 2.28 million pounds (38,000 lb weight amplified by 60 g's). Sixty g's is the design basis deceleration limit for the HI-STAR 100 storage system. A comparison of weld load capacity against the amplified load indicates a safety factor greater than 9.9 for the weld. This provides assurance that the outer intermediate shell layer, the radial channels, and the neutron shield material will remain in place and perform their design function under all conditions of storage.

Elements at locations of welds in the modeled components are assumed to have complete connectivity in all directions. Material in the model located at positions where welds exist is assumed to have material properties identical to the base material.

To summarize, the total number of nodes and elements in the overpack model are 11265 and 8642, respectively. The elements used are SOLID45, SOLID95, BEAM4, SHELL63, and COMBIN14.

For all structural analyses, material properties are obtained from the appropriate tables in Section 3.3. Property data for temperatures that are not listed in the material property tables are obtained by linear interpolation. Property values are not extrapolated beyond the limits of the code for any structural analysis.

- Description of Individual Loads and Boundary Conditions

The method of applying each individual load to the overpack model is described in this subsection. The individual loads are listed in Table 2.2.14. A free-body diagram of the overpack corresponding to each individual load is given in Figures 3.4.21 through 3.4.26. In the following discussion, references to vertical and horizontal orientations are made. Vertical refers to the direction along the cask axis, and horizontal refers to a radial direction.

Quasi-static methods of structural analysis are used. The effects of any dynamic load factors (DLF) are discussed in the final evaluation of safety factors.

(a) Accelerations (Used to Form Load Cases 04.a and 04.b in Table 3.1.5)

Table 3.1.2 provides the bounding values of the accelerations used for design basis structural evaluation. The loading is imposed by amplifying the gravity vector by the design basis deceleration.

Boundary conditions for the model are as follows:

i. End drop - In an end drop, displacement fixities are applied to the model on a cross-section through the top flange that is normal to the drop direction. Figure 3.4.21 shows the free-body diagram for this load event. No reactions or internal body forces are shown.

ii. Side drop - In a side drop, the impacted region of the enclosure shell, radial channels, enclosure panels, and neutron shield located between the overpack and the impacting surface may sustain plastic deformation. Using a linear elastic overpack model, we cannot account for this behavior. For conservatism, the displacement constraints are placed directly at the outermost intermediate shell. That is, it is assumed that the outer radial plates and the outer enclosure have been rendered ineffective. The constraints are applied over an arc of 9 degrees. Figure 3.4.22 shows the free-body diagram. No reaction forces or internal body forces are shown.

(b) Loads on the Overpack from the MPC

Pressures are applied on the inner surfaces of the overpack model to represent loads from the MPC for the drop loads.

i. End drop - For a bottom end drop (Load Case 04.a in Table 3.1.5), the pressure load on the inside surface of the overpack bottom plate is assumed to be uniform and represents the load from the heaviest MPC (Figure 3.4.21). Note that this analysis conservatively assumes that the drop angle is not exactly 90° from the horizontal; attention is focussed on the overpack baseplate subject to the deceleration load from the heaviest MPC (applied as a uniform pressure) without the ameliorating effect of opposing distributed reaction from the impacted surface.

The magnitude of the pressure is the weight of the heaviest fully loaded MPC divided by the area of the faces of the elements over which the pressure is applied. The weight of the heaviest fully loaded MPC is taken from the tables in Section 3.2, and is amplified by the design basis deceleration.

ii. Side drop - The shape and extent of the pressure distribution is determined from the results of the structural analysis of the MPC presented in Subsection 3.4.4.3.1. In the MPC structural analysis, the extent of the support conditions of the MPC shell is determined with contact elements. The overpack is assumed to be a rigid circular surface. Based on the results of the MPC evaluations, the loaded region is taken as 81 degrees (measured from the vertical) and is applied as a sinusoid with maximum value at the line of symmetry.

The MPC load on the overpack model is applied uniformly along the axial length of the inner surface of the model. Figure 3.4.22 shows the overpack loading for the side drop event.

(c) Temperature (Used to Form Load Case 05 in Table 3.1.5)

Based on the results of the thermal evaluation for normal hot environment presented in Chapter 4, a temperature distribution with a bounding gradient is applied to the overpack model. The purpose is to determine the stress intensities that develop in the overpack under the applied thermal load. A plot of the applied temperature distribution as a function of radius is shown in Figure 3.4.2.
The temperature distribution is applied to the ANSYS finite element model at discrete nodes using a parabolic curve fit of the computed distribution. Figure 3.4.23 shows the displacement constraints for the thermal load case.

(d) Internal Pressure (Used to Form Load Cases 01 to 04 in Table 3.1.5)

Design internal pressure is applied to the overpack model. All interior overpack surfaces, including the inner shell, the bottom of the closure plate, and the top of the bottom plate are loaded with pressure. The magnitude of the internal pressure applied to the model is taken from Table 2.2.1. Figure 3.4.24 shows the displacement constraints for this load case.

(e) External Pressure (Used to Form Load Cases 01 to 04 in Table 3.1.5)

Design external pressure is applied to the overpack model. External pressure is applied to the model as a uniform pressure on the outer surface of the model. The magnitude of the external pressure applied to the model is taken from Table 2.2.1. Figure 3.4.25 shows the displacement constraints for this load case.

(f) Dead Weight in Vertical Orientation (Used in Load Cases 02 to 04 in Table 3.1.5)

A pressure load is applied on the top surface of the overpack bottom plate to represent the weight of the MPC. The magnitude of the pressure is the weight of the heaviest fully loaded MPC divided by the area of the faces of the elements over which the pressure is applied. The weight of the heaviest fully loaded MPC is taken from the tables in Section 3.2. The dead weight of the overpack itself is simulated by a 1g acceleration load in the appropriate direction. Figure 3.4.26 shows the displacement constraints for this load case.

(g) Handling Load (Used in Load Case 03 in Table 3.1.5)

As discussed in Section 3.1.2.1.2, a fully loaded HI-STAR 100 System using the lifting trunnions is a governing normal handling event. This load case is performed to determine the effects of normal condition handling loads on the overall overpack structure. This load case is intended to resolve the detailed stress distribution in the top flange in the region of the trunnion, to demonstrate that the ASME Code requirements (Level A Condition limits) are met.

Nodes in the region of the trunnions are fixed in all translational degrees-of- freedom. For additional conservatism, a vertical load amplifier of 2.0 is applied in this case (even though, as discussed in Subsection 3.4.3, the appropriate multiplier for a heavy load lift condition is 1.15).

A pressure load, applied on the top surface of the overpack bottom plate, represents the weight of the MPC. The magnitude of the pressure is the weight of the heaviest fully loaded MPC, amplified by 2.0, divided by the area of the faces of the elements over which the pressure is applied. Figure 3.4.26 shows the displacement constraints for this load case.

(h) Bolt Pre-load (Used in Load Cases 01-05 in Table 3.1.5)

The overpack closure bolts are torqued to values given in Chapter 8. This torque generates a pre-load in the bolts and stresses in the closure plate and top flange in the region adjacent to the bolts. This load is applied to the overpack model by applying an initial strain to the beam elements representing the bolts.

- Finite Element Analysis Solution Procedure

The analysis procedure is as follows:

1. The stress and deformation field due to each individual load is determined.

2. The results for each individual load are combined in a postprocessor to create each load case. The load cases analyzed are listed in Table 3.1.5.

3. The results for each load case are compared to allowables. The calculated values are compared with allowable values in Subsection 3.4.4.4.

3.4.4.3.2.2 Fabrication Stress

The fabrication stresses originate from welding operations to affix the intermediate shells in position. As the molten weld metal solidifies, it shrinks pulling the two parts of the shells together. Adjacent points at the weld location will close together after welding by an amount δ which is a complex function of the root opening, shape of the bevel, type of weld process, etc. The residual stresses generated by the welding process are largely confined to the weld metal and the "heat affected zone". The ASME Code recognizes the presence of residual stresses in the welds, but does not require their calculation. The Code also seeks to minimize fabrication stresses in the welds through controlled weld procedures. Nevertheless, fabrication stresses cannot be eliminated completely. Similarly, Regulatory Guide 3.61 does not require computation of stresses arising from the manufacturing operations

The computation of fabrication stresses, however, is carried out to comply with the provisions of Regulatory Guide 7.8, Article C-15 when the HI-STAR 100 is functioning as a transport cask. The Regulatory Guide requires that "Fabrication and installation stresses in evaluating transportation loadings should be consistent with the joining, forming, fitting, and aligning processes employed during the construction of casks...the phrase fabrication stresses includes the stresses caused by

interference fits and the shrinkage of bonded lead shielding during solidification but does not include the residual stresses due to plate formation, welding, etc."

A literal interpretation of the above-cited Regulatory Guide text exempts the HI-STAR 100 designer from computing the stresses in the containment shell due to welding. However, in the interest of conservatism, it was decided to compute and establish an upper bound on the stresses induced in the containment shell ("helium retention boundary" in the storage mode) and in the intermediate shells due to welding of the intermediate shell layers. Detailed calculations are presented in Appendix 3.L

To calculate the so-called fabrication stresses, we recall that in affixing the intermediate shells to the cask body, the design objective does not call for a definite radial surface pressure between the layers. Rather, the objective is to ensure that the shells are not loosely installed. Fortunately, extensive experience in fabricating multi-layer shells has been acquired by the industry over the past half-century. The technology that was developed and has matured for fabrication in older industries (such as oil and chemical) will be used in HI-STAR 100 fabrication of the multi-layered shells. Mock-up tests on carbon steel coupons indicate that the total shrinkage after welding can range from 0.010" to 0.0625" for the bevel and fit-up geometry in the HI-STAR 100 design drawings. Therefore, the calculations in Appendix 3.L are carried out using the upper bound gap of 0.0625". To bound the computed stresses even further, the inter-layer friction coefficient is set equal to zero. It is intuitively apparent that increasing the friction increases the localized stresses near the "point of pull" (i.e., the weld) while mitigating the stresses elsewhere. Since our object is to maximize the distributed (membrane) stress, the friction coefficient is set equal to zero in the analysis of Appendix 3.L.

The results from the analyses in Appendix 3.L are summarized in the table below:

Fabrication Stresses in Overpack Shells –Minimum Safety Factors (Level A Service Condition at Assembly Temperature)			
Item	Value (ksi)	Allowable (ksi) (Note 3)	Safety Factor
First Intermediate Shell (Note 1)	11.22	52.5	4.68
Fourth Intermediate Shell (Note 1)	7.79	52.5	6.74
Inner Shell Mid Plane (Note 2)	10.6	69.9	6.59
Inner Shell Outer Surface (Note 2)	16.27	69.9	4.30

Notes:

1. The fabrication stress is a tensile circumferential stress.
2. The fabrication stress is a compressive circumferential stress
3. Fabrication stresses are self-limiting and are therefore classified as "secondary" and are compared to 3 times the membrane stress or stress intensity.

The above table leads to the conclusion that the maximum possible values for stresses resulting from the HI-STAR 100 fabrication process are only a fraction of the relevant ASME Code limit.

3.4.4.3.2.3 Structural Analysis of Overpack Closure Bolting (Load Cases 01, 06 and 04.a - Table 3.1.5)

Stresses are developed in the closure bolts due to pre-load, pressure loads, temperature loads, and accident loads. Closure bolts are explored in detail in Reference [3.4.5] that was prepared for analysis of shipping casks. The method presented is equally valid for storage casks and is considered as an acceptable analysis method by NUREG-1536. The analysis of the overpack closure bolts under normal and accident conditions appropriate for storage is carried out in Appendix 3.F and follows the procedures defined in Reference [3.4.5]. The allowable stresses used for the closure bolts follow that reference.

The following combined load cases are analyzed in Appendix 3.F.

Normal: pressure, temperature, and pre-load loads are included. (Load Case 01 in Table 3.1.5).

Top Closure Puncture: pressure, temperature, pre-load, and 8-in. diameter missile loads are included. (Load Case 06 in Table 3.1.5)

Drop: pressure, temperature, pre-load, and impact loads from a top end drop are included. We note that reference [3.4.5] is for shipping casks and therefore allows for a top end drop. There is no such credible event defined for a storage cask but it provides a bounding case for the HI-STAR 100 closure bolts (Load Case 04.a in Table 3.1.5).

Reference [3.4.5] reports safety factors defined as the calculated stress combination divided by the allowable stress for the load combination. This definition of safety factor is the inverse of the definition consistently used in this FSAR. In summarizing the closure bolt analyses performed in Appendix 3.F, we report results using the safety factor definition of allowable stress divided by calculated stress. The following results for closure lid bolting are obtained from Appendix 3.F.

Overpack Closure Bolt - Minimum Safety Factors	
Combined Load Case	Safety Factor on Bolt Tension
Normal (Load Case 01 in Table 3.1.5)	1.44
Top Closure Puncture (Load Case 06 in Table 3.1.5)	1.86
Drop (Load Case 04.a in Table 3.1.5)	1.30

It is seen from the above table that all safety factors are greater than 1.0.

3.4.4.3.2.4 Structural Analysis of the Overpack Closure Plate (Load Case 04.a in Table 3.5.1)

The simplified analysis given here complements the result from the finite element analysis of the overpack for calculation of stresses in the overpack closure plate.

The loading condition considered here is a bottom end drop where the overpack bottom plate impacts the supporting surface (Load Case 04.a in Table 3.1.5).

The following assumptions apply:

1. Stresses in the closure plate due to bolt pre-load will counteract the downward inertia load; the pre-load is conservatively ignored.
2. The closure plate is assumed to be a simply supported plate, i.e., the rotational fixity projected by the flanged joint is conservatively ignored.
3. The plate is assumed to be loaded with its own weight multiplied by the design basis deceleration from Table 3.1.2.
4. The pressure within the overpack counteracts the amplified self-weight load in a bottom end drop. Internal overpack pressure is conservatively neglected.

The geometry of the model is the same as shown in Figure 3.4.16 for the MPC lid except for the dimension change appropriate to the overpack closure plate. Using Table 24, Case 10 of reference [3.G.1], page 429 (reference is listed in Appendix 3.G), the maximum radial bending stress (σ) in the closure plate due to bending is

$$\sigma = \frac{3qa^2(3+\nu)}{8t^2}$$

where

q = load per unit area $= \frac{a_v W}{\pi a^2}$

W = weight of the plate = 8,000 lb.

a_v = design basis deceleration in an end drop = 60g's

a = radius of the simply supported plate = 38.6875 in.

υ = Poisson's ratio

t = thickness of the closure plate = 6 in.

Therefore,

$$\sigma = \frac{3(3+\nu)W\,a_v}{8\pi t^2}$$

The result is summarized in the table below:

Bending Stress in Overpack Closure Plate – Closed Form Solution (Load Case 04.a)			
Item	Value (ksi)	Allowable (ksi)	Safety Factor
Stress at Center of Plate	5.25	70.0	13.3

The safety factor is much greater than 1.0.

3.4.4.3.2.5 Elastic/Plastic Stability Considerations for the Overpack Inner Shell (Load Cases 02, 03 and 04.a in Table 3.1.5)

Appendix 3.H contains a complete stability analysis of the HI-STAR 100 System. The case of normal handling (Load Case 03 in Table 3.1.5), the accident end drop (Load Case 04.a in Table 3.1.5), and the accident external pressure plus dead load case (Load Case 02 in Table 3.1.5) are evaluated for elastic and plastic stability in accordance with the ASME Code Case N-284 [3.4.6]. All required interaction equation requirements set by [3.4.6] are met. It is shown in Appendix 3.H that yield strength limits rather than instability limits governs the minimum safety factor. Minimum safety factors from Appendix 3.H are summarized in Table 3.4.19.

3.4.4.3.2.6 Stress Analysis of Enclosure Shell

The overpack enclosure shell and the overpack enclosure return are examined for structural integrity under a bounding internal pressure in Appendix 3.AG. It is shown there that large safety factors exist against overstress due to an internal pressure developing from off-gassing of the neutron absorber material.

In HI-STAR 100 serial numbers 1 through 4, the enclosure shell is lined with a thin layer of thermal expansion foam. The purpose of the foam is to mitigate the pressure on the enclosure shell caused by radial expansion of the neutron absorber material at high temperatures.

As of July 2000, the radially oriented foam was removed from the HI-STAR 100 design. A finite element analysis has been performed to demonstrate that the removal of this foam material does not lead to excessive stress levels in the enclosure shell. Figure 3.4.46 shows a picture of the 2-D finite element model, which was created using ANSYS Version 5.4. Two-dimensional plate elements are used to model the steel channels and the neutron absorber material. The interface between the two materials is simulated by contact elements. The maximum stress in the radial channel under the worst-case thermal loading is 46,251 psi, which is less than the ultimate stress of the material at 300°F (70,000 psi). Therefore, the removal of the radially directed expansion foam is justified.

3.4.4.4 Comparison with Allowable Stresses

Consistent with the formatting guidelines of Reg. Guide 3.61, calculated stresses and stress intensities from the finite element and classical elasticity evaluations are compared with the allowable stresses and stress intensities defined in Subsection 3.1.2.2 per the applicable service conditions and the ASME Code relevant for the component. Safety factors for those components that are identified as lifting devices have been reported in Subsection 3.4.3.

3.4.4.4.1 MPC Fuel Basket and Enclosure Vessel

It is recalled that the stress analyses for the load cases applicable to the fuel basket and the enclosure vessel (EV) (that together constitute the Multi-Purpose Canister) are stated in Tables 3.1.3 and 3.1.4, respectively. All detailed analyses, including finite element model details and the necessary explanations to collate and interpret the voluminous numerical results are contained in a series of appendices to this chapter. These appendices are identified in Subsection 3.6.3 and in Tables 3.1.3 and 3.1.4 for ease of reference. Summaries of results for the load cases pertinent to the fuel basket and the enclosure vessel (EV) are provided in Tables 3.4.7-3.4.9 wherein the source appendices containing detailed results are also identified. To further facilitate perusal of results, another level of summarization is performed in Tables 3.4.3-3.4.4 where the global minima of safety factor for each load case are presented. The following elements of information are relevant in ascertaining the safety factors under the various load cases presented in the tables.

- In the interest of simplification of presentation and conservatism, the total stress intensities under mechanical loading are considered to be of the primary genre' even though, strictly speaking, a portion can be categorized as secondary (that have much higher stress limits).
- In load cases involving accident events, the deceleration loads also produce internal dynamic effects, qualified as dynamic load factors (DLF). These DLF's, which depend on the duration of impact and the fundamental frequency of the internal component (e.g. the fuel basket panel) are computed in Appendix 3.X using input data from Appendix 3.A.The factors of safety presented in the above mentioned summary tables do not include the DLF's. Therefore, the tabulated factors of safety should be compared against the applicable DLF to insure that a positive design margin exists for a given load case.

The MPC stress distributions that correspond to the worst case for each MPC are provided in Figures 3.4.34 and 3.4.36. The stresses appear as colored bars where the height is proportional to the magnitude of the stress and the width equals the element length. The figures also include the design temperature of the component and the allowable stress intensity taken from Table 3.1.17 for the Level D condition of primary membrane plus bending stress. We note that for the MPC-68, the worst case is in the basket support structure.

A perusal of the results for Tables 3.4.3 and 3.4.4 under different load combinations for the fuel basket and the enclosure vessel reveals that all factors of safety are above 1.0 even if we use the most conservative value for dynamic amplification factor. The relatively modest factor of safety in the fuel basket under side drop events (Load Case F3.b and F3.c) in Table 3.4.3 warrants further explanation.

The wall thickness of the storage cells, which is by far the most significant variable in the fuel basket's structural strength, is significantly greater in the HI-STAR 100 MPCs than in comparable fuel baskets licensed in the past. For example, the cell wall thickness in the TN-32 basket (Docket No. 72-1021, M-56) is 0.1 inch and that in the NAC-STC basket (Docket No. 71-7235) is 0.048 inch. In contrast, the cell wall thickness in the MPC-24 is 0.3125 inch. In spite of their relatively high flexural rigidities, computed margins in the HI-STAR 100 fuel baskets are rather modest. This is because of some assumptions in the analysis which lead to an overstatement of the state of stress in the fuel basket. For example:

i. The section properties of longitudinal fillet welds that attach contiguous cell walls to each other are completely neglected in the finite element model (Figure 3.4.7). The fillet welds strengthen the cell wall section modulus at the very locations where maximum stresses develop.

ii. The radial gaps at the fuel basket-MPC shell and at the MPC shell-overpack interface are explicitly modeled. As the applied loading is incrementally increased, the MPC shell and fuel basket deform until a "rigid" backing surface of the overpack is contacted, making further unlimited deformation under lateral loading impossible. Therefore, some portion of the fuel basket and enclosure vessel (EV) stress has the characteristics of secondary stresses (which by definition, are self-limited by deformation in the structure to achieve compatibility). For conservativeness in the incremental analysis, we make no distinction between deformation controlled (secondary) stress and load controlled (primary) stress in the stress categorization of the MPC-68 fuel basket. We treat all stresses, regardless of their origin, as primary stresses. Such a conservative interpretation of the Code has a direct (adverse) effect on the computed safety factors. As noted earlier, the results for the MPC-24 are properly based on primary stresses to illustrate the conservatism in the reporting of results for the MPC-68 basket.

iii. The SNF inertia loading on the cell panels is simulated by a uniform pressure, which is a most conservative approach for incorporating the SNF/cell wall structure interaction.

The above assumptions act to depress the computed values of factors of safety in the fuel basket finite element analysis and render conservative results.

As stated earlier, the reported values do not include the effect of dynamic load amplifiers. As noted in Appendices 3.A and 3.X, the duration of impact and the predominant natural frequency of the basket panels under lateral drop events, result in dynamic load factors (DLF) below 1.1. Therefore, since all reported factors of safety for the fuel basket panels (based on stress analysis) are greater

than the DLF, the MPC fuel basket is structurally adequate for its intended functions during and after a lateral drop event.

Tables 3.4.7 and 3.4.8 report stress intensities and safety factors for the confinement boundary subject to internal pressure alone and internal pressure plus the normal operating condition temperature with the most severe thermal gradient. The final values for safety factors in the various locations of the confinement boundary provide assurance that the MPC enclosure vessel is a robust pressure vessel.

3.4.4.4.2 Overpack

3.4.4.4.2.1 Discussion

The overpack is subject to the load cases listed in Table 3.1.5. Results from the series of finite element analyses are summarized in Table 3.4.10. In order to identify and to locate appropriate regions with limiting safety factors, we note that safety factors are calculated for each load case at a select set of nodes identified as "stress report locations".

Figures 3.4.37 through 3.4.42 identify the locations of minimum safety margin for all overpack load combinations.

For any load case associated with a Level D Service Condition (accident event), the results are provided only at locations where primary stresses predominate. However, in the interest of conservatism, the stress intensity reported at these locations does not separate out any secondary components. Every value is placed in the primary membrane or primary bending category, even though many locations clearly involve non-primary bending components. This simplification in stress intensity tabulation imputes considerable additional safety margin to the processed results, which is not explicitly recognized in the results presented herein.

The following text is a brief description of how the results are presented for evaluation:

- The extensive body of results is summarized in Table 3.10 wherein the minimum safety factor for different components of the overpack for each of the load cases is presented.

- Table 3.4.6 presents results of calculation of the safety factors to include "fabrication stresses" where appropriate. Table 3.4.6 summarizes safety factors, based on limits for primary plus secondary stresses, and reports the limiting safety factors for the overpack shells for events subject to Level A Service Conditions. Fabrication stresses are not included for any load case involving accident conditions since secondary stresses need not be considered for Level D Service Conditions. Fabrication stress, reported in Subsection 3.4.4.3.2.2, is "added" in absolute value to finite element stress intensity or stress results. This conservatively produces modified stress intensity or stress that is used to compute modified safety factors.

- Finally, Table 3.4.5 summarizes the minimum values of safety factors (global minima) for the overpack components.

The modifications summarized in Table 3.4.6 are briefly discussed below:

Case 01 (Pressure) –Safety factors are summarized in Table.3.4.10 prior to inclusion of fabrication stress. Table 3.4.6 shows modified safety factors that include fabrication stress. The pressure stresses result in tensile longitudinal and circumferential stresses in the inner shell and in the intermediate shells. The fabrication stress dominates the stress state in the inner and intermediate shells but comparison with the allowable values is considers a primary plus secondary stress state.

Case 03 (Normal Handling): Safety factors are summarized in Table.3.4.10 prior to inclusion of fabrication stress. Table 3.4.6 shows modified safety factors that conservatively include fabrication stress but compute safety factors considering primary plus secondary stress allowables.

Case 05 (Thermal Load) - Safety factors are summarized in Table.3.4.10 prior to inclusion of fabrication stress. Table 3.4.6 shows modified safety factors that include the effect of fabrication stress in a conservative manner. Safety factors are based on allowable strengths for primary plus secondary stresses since thermal stress is a secondary stress.

3.4.4.4.3 Result Summary for the Heat Condition

- Stress Results from Overall Finite Element Models of the MPC and Overpack

Tables 3.4.7 to 3.4.10 summarize minimum safety factors from load cases analyzed using the finite element models of the MPC fuel basket plus canister and the overpack described in Subsections 3.4.4.3.1.1 and 3.4.4.3.2. All safety factors are greater than 1.0 and are greater than any credible dynamic amplifier for the location. Table 3.4.6 provides a summary table that includes the effect of fabrication stress on safety factors for the intermediate and inner shells of the overpack. Table 3.4.6 reports safety factors based on primary plus secondary allowable strengths.

- Status of Lid Bolts and Seals on the Overpack

The finite element analysis for the overpack provides results at the lid-to top flange interface. The output results for each load combination indicate that all seal springs remain closed under load indicating that the sealworthiness of the bolted joint will not be breached.

For each load combination, the total compressive force on the closure plate-overpack interface as well as the total tangential force (labeled as "friction force" in the tables) is computed. If the ratio "total friction force/total compressive force" is formed for each set of results, the maximum value of the ratio is 0.268. There will be no slip of the closure plate relative to the overpack if the interface coefficient of friction is greater than the value given above. Note that Mark's Handbook for Mechanical Engineers [3.4.9] in Table 3.2.1 shows $\mu = 0.74\text{-}0.79$ for clean and dry steel on steel surfaces. It is concluded that there is no propensity for relative movement.

Based on the results of the finite element analysis, the following conclusions are made.

No bolt overstress is indicated under any loading event. Note that this confirms the results of closure bolt analyses performed in Appendix 3.F.

The closure plate seals do not unload under any load combination; therefore, the seals continue to perform their function.

- Stress and Stability Results from Miscellaneous Component Analyses in Subsection 3.4.4.3

Tables 3.4.11 to 3.4.19 repeats summary results from additional analyses described and reported on in Subsection 3.4.4.3 for components of the MPC and the overpack. The tables have been listed within the text of Subsection 3.4.4.3 and are reproduced in this subsection in accordance with the requirements of Regulatory Guide 3.61. The tables report comparisons of calculated values with allowable values for both stress and stability and represent a compilation of analyses detailed in appendices that form an integral part of this chapter.

- Summary of Minimum Safety Factors

Tables 3.4.3 through 3.4.5 present a concise summary of safety factors for the fuel basket, the enclosure vessel, and the overpack, respectively. Locations in this FSAR where detailed information on each summary value exists is also identified in these tables.

Based on the results of all analyses, with results presented or summarized in the text, in tabular form, and in appendices, we close by concluding that:

i. All safety factors reported in the text, summary tables, and in appendices are greater than 1.0.

ii. There is no restraint of free thermal expansion between component parts of the HI-STAR 100 System.

3.4.5 Cold

A discussion of the resistance to failure due to brittle fracture is provided in Subsection 3.1.2.3.

The value of the ambient temperature has two principal effects on the HI-STAR 100 storage system, namely:

i. The steady-state temperature of all material points in the cask system will go up or down by the amount of change in the ambient temperature.

ii. As the ambient temperature drops, the absolute temperature of the contained helium will drop accordingly, producing a proportional reduction in the internal pressure in accordance with the Ideal Gas Law.

In other words, the temperature gradients in the cask system under steady-state conditions will remain the same regardless of the value of the ambient temperature. The internal pressure, on the other hand, will decline with the lowering of the ambient temperature. Since the stresses under normal storage condition arise principally from pressure and thermal gradients, it follows that the stress field in the MPC under -40°F ambient would be smaller than the "heat" condition of storage, treated in the preceding subsection. Therefore, the stress margins computed in Section 3.4.4 can be conservatively assumed to apply to the "cold" condition as well. Appendix 3.AE demonstrates that the overpack closure bolts will retain the helium seal under the cold ambient conditions.

Under the 80°F ambient temperature and the maximum fuel decay heat load (normal heat condition of storage), the thermal analysis in Chapter 4 reports the resultant component temperatures. These temperatures were than used in Appendices 3.U and 3.W to demonstrate that there was no restraint of free thermal expansion for the MPC-24 and MPC-68 in the HI-STAR overpack. The results from these appendices have been presented in Subsection 3.4.4.2.1. Under the postulated cold ambient temperature of -40°F the component temperatures will decrease by 80°F minus -40°F or 120°F. Thermal expansion is calculated from the product of the coefficient of thermal expansion, α, and the change in temperature, ΔT. Since the changes in temperature in each component would decrease by 120°F, the resultant thermal expansion would also decrease. This is coupled with the fact that the coefficient of thermal expansion for carbon steel and stainless steel decreases as the temperatures are decreased. Therefore, if the analysis performed in Appendices 3.U and 3.W demonstrate that there is no restraint of thermal expansion, analysis performed at component temperatures 120°F less (to account for the cold ambient temperature, -40°F) would also show that there is no constraint of thermal expansion. That is, the operational clearances predicted in Appendices 3.U and 3.W are a conservative lower bound on the clearances with the ambient temperature corresponding to extreme cold conditions.

Finally, the HI-STAR 100 System is engineered to withstand "cold" temperatures (-40°F) without impairment of its storage function.

The structural material used in the MPC (Alloy X) and the Helium Retention Boundary is recognized to be completely immune from brittle fracture in the ASME Codes. As no liquids are included in the HI-STAR 100 overpack design, loads due to expansion of freezing liquids are not considered.

3.4.6 HI-STAR 100 Kinematic Stability under Flood Condition (Load Case A in Table 3.1.1)

The flood condition subjects the HI-STAR 100 System to external pressure, together with a horizontal load due to water velocity.

The design external pressure bounds any credible pressure due to complete submergence during flooding (see Subsection 3.1.2.1.1.3 and Appendix 3.H). The use of such a large external design pressure is mandated by 10CFR71 considerations.

Horizontal loads on the HI-STAR 100 System may, however, cause sliding (translation), or rotation (tipping); this is addressed below, where it is shown that the maximum permitted flood water velocity is limited by sliding of the cask.

Rotation of the HI-STAR 100 System due to motion of the floodwater is analyzed by assuming that the overpack is pinned at the outer edge of the baseplate opposite the water flow. The pinned edge does not permit sliding.

The water velocity associated with flood produces a horizontal drag force, which may act to cause sliding or tip-over. In accordance with the provisions of ANSI/ANS 57.9, the acceptable upper bound flood velocity, V, must provide a minimum factor of safety of 1.1 against overturning and sliding. For HI-STAR 100, the design basis flood velocity is 13 feet/sec.

The overturning horizontal force, F, due to hydraulic drag, is given by the classical formula:

$$F = Cd\ A\ V^*$$

where:

V^* is the velocity head = $\frac{\rho V^2}{2g}$; (ρ is water weight density, g is acceleration due to gravity, and V is the crossflow water velocity).

A: projected area of the HI-STAR 100 cylinder perpendicular to the fluid velocity vector.

Cd: drag coefficient

The value of Cd for flow past a cylinder at Reynolds number above 5E+05 is given as 0.5 in the literature (viz. Hoerner, Fluid Dynamics, 1965).

The drag force tending to cause HI-STAR 100's sliding is opposed by the friction force, which is given by

$$F_f = \mu\ K\ W$$

where:

μ = limiting value of the friction coefficient at the HI-STAR 100/ISFSI pad interface (conservatively taken as 0.25, although literature citations give somewhat higher values).

K = buoyancy coefficient

W= Minimum weight of HI-STAR 100 with an empty MPC

Sliding Factor of Safety

The factor of safety against sliding, SF_1, is given by

$$SF_1 = \frac{F_f}{F} = \frac{\mu KW}{Cd\ A\ V^*}$$

It is apparent from the above equation that SF_1 will be minimized if the lower bound weight of HI-STAR 100 is used in the above equation.

As stated previously, $\mu = 0.25$, $Cd = 0.5$.

V^* corresponding to 13 ft./sec. water velocity (see Chapter 2 Design Criterion) is 163.75 lb. per sq. ft.

A = length x diameter of HI-STAR 100 = 96" x 203"/144 sq. in./sq.ft. = 135.33 sq. ft.

W = 189,000 lbs. (Table 3.2.1)

K = buoyancy factor = (1-weight of water displaced by HI-STAR 100/W) =0.719

Therefore, the drag force is

$F_f = \mu\ K\ W = 33{,}973$ lb.

Substituting in the above formula for SF_1, we have

$SF_1 = 3.07 > 1.1$ (required)

Overturning Factor of Safety

For determining the margin of safety against overturning SF_2, the cask is assumed to pivot about a fixed point located at the outer edge of the contact circle at the interface between HI-STAR 100 and the ISFSI. The overturning moment due to a force F_T applied at height H^* is balanced by a restoring moment from the reaction to the cask buoyant force KW acting at radius D/2.

$$F_T H^* = KW\frac{D}{2}$$

or

$$F_T = \frac{K\ W\ D}{2\ H^*}$$

W is the minimum weight of the storage overpack with an empty MPC.

We have,

W = 189,000 lb. (Table 3.2.1)

H^* = 102" (maximum height of mass center per Table 3.2.2)

D = 83.25" (Holtec Drawing 3913, Sheet 1)

K = 0.719 (calculated)

so that

F_T = 55,456 lb.

F_T is the horizontal drag force at incipient tip-over.

F = Cd A V^* = 11,080 lbs. (drag force at 13 feet/sec)

The safety factor against overturning, SF_2, is given by

$$SF_2 = \frac{F_T}{F} = 5.01 > 1.1 \text{ (required)}$$

3.4.7 Seismic Event on HI-STAR 100 (Load Case C in Table 3.1.1

3.4.7.1 Stability

The HI-STAR 100 System plus its contents are subject to the design basis seismic event consisting of three orthogonal statistically independent acceleration time-histories (orthogonal components). The HI-STAR 100 System can be considered as a rigid body subject to a net horizontal inertia force and a vertical inertia force for the purpose of performing a conservative analysis to determine the maximum ZPA that will not cause incipient tipping. The vertical seismic loading is conservatively assumed to act in the most unfavorable direction (upwards) at the same instant. The vertical seismic load is assumed to be equal to or less than the net horizontal load with $\tilde{\varepsilon}$ being the ratio of vertical component to one of the horizontal components. Define D as the contact patch diameter, and H_{CG} as the height of the centroid of an empty HI-STAR 100 System (no fuel).

D = 83.25" (Drawing 3913, Sheet 2)

Tables 3.2.1 and 3.2.2 give HI-STAR 100 weight data and center-of-gravity heights.

The weights and center-of-gravity heights are reproduced here for calculation of the composite center of gravity height of the overpack together with an empty MPC.

Weight (pounds)	H of C.G. Height (Inches)
Overpack - W_o = 153,710	99.7
MPC-24 - W_{24} = 40,868	109.0 + 6 = 115.0†
MPC-68 - W_{68} = 37,591	111.5 + 6 = 117.5†

† MPC centroids reported in Section 3.2 are measured from the base of the MPC.

The composite centroid, H_{CG}, is determined from the equation

$$H_{cg} = \frac{W_o \times 99.7 + W_{MPC} \times H}{W_o + W_{MPC}}$$

Performing the calculations for all of the MPC's gives the following results:

	H_{CG} (inches)
MPC-24 with overpack	102.9
MPC-68 with overpack	103.2

A conservative stability limit is achieved by using the largest value of H_{CG} (call it H) from above or from Table 3.2.2. Because the HI-STAR 100 System is a radially symmetric structure, the two horizontal seismic accelerations can be combined vectorially and applied as an overturning force at the C.G. of the cask. The overturning static moment in each of the two horizontal directions is "WGH_{CG}" where W is the total system weight, G is the zero period acceleration seismic amplifier so that WG is the inertia load due to horizontal seismic loading. The overturning moment is balanced by a vertical reaction force, acting at the outermost contact patch radial location r = D/2. At many sites, the vertical seismic acceleration is specified as a fraction of the horizontal acceleration. Let us assume that the vertical acceleration is ε times G. The resistive moment is minimized when the vertical acceleration tends to reduce the apparent weight of the cask. At that instant, the moment that resists "incipient tipping" is:

$$W (1- \varepsilon G) r$$

where the vertical seismic amplifier is εG ($|\varepsilon| \leq 1$).

Equating the two moments to ensure equilibrium of moments yields

$$\sqrt{(WG)^2+(WG)^2}\,H = W(1-\varepsilon G)\,r$$

$$\sqrt{2}\,WGH = W(1-\varepsilon G)\,r$$

or, after canceling W and solving for G

$$G = \frac{1}{\sqrt{2}\,\frac{H}{r}+\varepsilon}$$

The values of r and H for the HI-STAR 100 are r = 41.625", H = 103", which yields the following results for different values of ε

Acceptable Horizontal g-Level in Each of Two Orthogonal Directions	Vertical Acceleration Multiplier (ε)	Vectorial Sum of Acceptable Horizontal Accelerations (g)
0.222	1.0	0.314
0.235	0.75	0.332
0.240	0.667	0.339
0.250	0.50	0.354

The tabular results above define the envelope g-levels from the resultant inertia load from two horizontal seismic events to ensure against incipient tipping. The acceptable g-level is increased as the ratio of vertical zero period accelerations to net horizontal g-level decreases. Additionally, in case of a 2-D earthquake plant, i.e., one horizontal and one vertical seismic acceleration, the acceptable g-level will correspond to the last two columns in the above table.

3.4.7.2 Primary Stresses in the HI-STAR 100 Structure

A simplified calculation to assess the flexural bending stress in the HI-STAR 100 structure under the limiting seismic event (at which tipping is incipient) is presented in the following:

From the acceptable acceleration table presented above, the maximum horizontal acceleration is 0.354g. The corresponding lateral seismic load, F, is given by F = 0.354 W. This load will be maximized if the upper bound HI-STAR 100 weight (W = 245,000 lbs., from Table 3.2.4) is used. Accordingly, F = (0.354) (245,000) = 86,730 lbs.

The moment, M, at the base of the HI-STAR 100 due to this lateral force is given by

$$M = \frac{F H}{2}$$

where H = height of HI-STAR 100 (taken conservatively as 204 inches)

The flexural stress, σ, is conservatively given by the ratio of the moment M to the section modulus of the inner steel shell structure, z, which is computed to be 9,644 $in.^3$.

Therefore,

$$\sigma = \frac{(86{,}730)(204)}{(9{,}644)(2)} = 917 \text{ psi}$$

We note that the contribution from any of the intermediate shells has been neglected in the above calculation.

The maximum axial stress in the overpack shell will be reached in the "compressive" side where the flexural bending stress algebraically sums with the direct compression stress τ from vertical compression.

From the acceleration table the vertical seismic accelerations corresponding to the net 0.354g horizontal acceleration is 0.125g.

Therefore, using the maximum overpack weight

$$\tau = \frac{(245{,}000)(1.125)}{560} = 492 \text{ psi}$$

where 560 sq. inch is the metal area (cross section) of the inner shell in the HI-STAR 100 overpack.

The total axial stress, therefore, is

$$\sigma_T = 917 + 492 = 1{,}409 \text{ psi}$$

Per Table 3.1.7, the allowable membrane stress intensity for a Level D event is 48,200 psi at 400°F. Therefore, a factor of safety is calculated as

$$SF = \frac{48{,}200}{1{,}409} = 34.2$$

Sliding Analysis

An assessment of sliding of the HI-STAR 100 System on the ISFSI pad during a postulated limiting seismic event is performed using a one-dimensional "slider block on friction supported surface" model. The HI-STAR 100 is simulated as a rigid block of mass *m* placed on a surface which is subject to a sinusoidal acceleration of amplitude *a*. The apparent mass of the block is assumed to be reduced by a factor α to recognize the contribution of vertical acceleration in the most adverse manner (vertical acceleration acts to reduce the downward force on the friction interface). The equation of motion for such a "slider block" is given by

$$m\ddot{x} = R - m\,a\,\sin\omega t$$

where:

$\ddot{x}$: relative acceleration of the slider block (double dot denotes second derivative of displacement x in time)

a: amplitude of the sinusoidal acceleration input

ω: frequency of the seismic input motion (radians/sec)

t: time coordinate

R is the resistive Coulomb friction force which can reach a maximum value of μ (αmg) (μ = coefficient of friction) and which always acts in the direction of opposite to $\dot{x}(t)$.

Solution of the above equation can be obtained by standard numerical integration for specified values of m, a, ω and α. The following input values are used.

a = 0.354g

α = 0.875 = 1 - vertical acceleration - (vertical acceleration is 0.125g for net horizontal acceleration equal to 0.354 from the acceleration table provided in the foregoing)

m = 245,000 lbs/g

μ = 0.25

For establishing the appropriate value of ω, reference is made to the USAEC publication TID-7024, "Nuclear Reactor and Earthquakes", page 35, 1963, which states that the significant energy of all seismic events in the U.S. essentially lies in the range of 0.4 to 10 Hz. Taking the mid-point value

$$\omega = (2\pi)\ (0.5)\ (0.4+10) = 32.7 \text{ rad/sec.}$$

The numerical solution of the above equation yields the maximum displacement of the slider block x_{max} as 0.047 inches, which is negligible compared to the spacing between casks.

Calculations performed at lower values of ω show an increase in x_{max} with reducing ω. At 1 Hz, for example, x_{max} = 1.236 inches. It is apparent from the above that there is a large margin of safety against inter-module collision within the HI-STAR 100 arrays at an ISFSI, where the minimum installed spacing is approximately 4 feet (Table 1.4.1).

3.4.8 Tornado Wind and Missile Impact (Load Case B in Table 3.1.1 and Load Case 06 in Table 3.1.5

During a tornado event, the HI-STAR 100 System is conservatively assumed to be subjected to a constant wind force. It is also subject to impacts by postulated missiles. The maximum wind speed is specified in Table 2.2.4 and the three missiles, designated as large, intermediate, and small, are described in Table 2.2.5.

The post impact response of the HI-STAR 100 System is required to assess stability.

Appendix 3.C contains results for the post-impact response of the HI-STAR 100 where it is demonstrated there that the combination of tornado missile plus either steady tornado wind or instantaneous tornado pressure drop causes a rotation of the HI-STAR 100 to a maximum angle of inclination 18.23 degrees from vertical. This is less than the angle required to overturn the cask. The appropriate value for the drag coefficient used in the computation of the lateral force on the overpack from tornado wind is justified in Appendix 3.C

Appendix 3.C computes the maximum force acting on the projected area of the cask to be

$$F = 26{,}380 \text{ lbs.}$$

This is bounded by the seismic overturning force computed in Section 3.4.7. Therefore, the overpack stress analysis performed in Section 3.4.7 remains governing.

The penetration potential of the missile strikes (Load Case 06 in Table 3.1.5) is examined in Appendix 3.G. It is shown in Appendix 3.G that there will be no penetration of the intermediate shells surrounding the inner shell of the overpack or penetration of the top closure plate. Therefore, there will be no radiological release associated with any missile strikes during a tornado. The following results summarize the work in Appendix 3.G.

a. The small missile will dent any surface it impacts, but no significant puncture force is generated.

b. The following table summarizes the denting and penetration analysis performed for the intermediate missile in Appendix 3.G. Denting is used to connote a local deformation mode encompassing material beyond the impacting missile envelope, while penetration is used to indicate a plug type penetration mechanism involving only the target material immediately under the impacting missile.

Intermediate Missile Strike – Denting and Penetration		
Location	Denting (in.)	Penetration
Outer Enclosure Shell	2.77	Yes (> 0.5 in.)
Intermediate shells	2.81	No (< 8.5 in.)
Closure plate	3.00	No (< 6 in.)

Since the intermediate missile generates a large puncture force for a short duration, the effect of this puncture force on the overpack closure bolts is examined in Appendix 3.F.

The primary stresses that arise due to an intermediate missile strike on the side of the overpack and in the center of the overpack top lid are also determined in Appendix 3.G. It is demonstrated there that Level D stress limits are not exceeded in either the side shell or the top lid. The safety factor in the overpack inner shell, considered as a cantilever beam under tip load, is computed, as is the safety factor in the top lid, considered as a centrally loaded plate. The applied load, in each case, is the missile impact load. A summary of the results is given in the table below:

HI-STAR 100 Missile Impact - Global Stress Results (Load Case 06 in Table 3.1.5)			
Item	Value (ksi)	Allowable (ksi)	Safety Factor
Inner Shell - Side Strike	12.6	48.2	3.83
Intermediate Shell – Side Strike -	14.3	39.1	2.73
Top Lid - (End Strike)	48.45	64.6.	1.33

The above summary table does not include the circumferential fabrication stress since these have been designated as self-limiting, and therefore fall into the category of a secondary stress which need not be included in a Level D stress evaluation.

3.4.9 Non-Mechanistic Tip-over, Side and Vertical Drop Events

Pursuant to the provision in NUREG-1536, a non-mechanistic tip-over of a loaded HI-STAR 100 System on to the ISFSI pad is considered. Analyses are also performed to determine the maximum deceleration sustained by a side or vertical free fall of a loaded HI-STAR 100 System onto the ISFSI pad. The object of the analyses is to demonstrate that the plastic deformation in the fuel basket is sufficiently limited to permit the stored SNF to be retrieved by normal means and that there is no significant loss of radiation shielding in the system.

Ready retrievability of the fuel is presumed to be ensured if stress levels in the MPC structure remain below Level D limits during the postulated drop events.

Subsequent to the accident events, the overpack must be shown to contain the shielding so that unacceptable radiation levels do not result from the accident.

Appendix 3.A provides a description of the dynamic finite element analyses undertaken to establish the decelerations resulting from the postulated event. A non-mechanistic tip-over is considered together with a side and end drop of a loaded HI-STAR 100 System. A dynamic finite element analysis of each event is performed using a commercial finite element code well suited for such dynamic analyses with interface impact and non-linear material behavior. This code and methodology have been fully benchmarked against Lawrence Livermore Laboratories test data and correlation [3.4.12].

It is shown in Appendix 3.A that the peak deceleration is less than 60g's for tip-over. Table 3.A.3 shows that the maximum deceleration level at the top of the cask is 52.8 g's, while the corresponding deceleration level at the top of the fuel basket is 47.8 g's. For the case of a vertical drop from a height of 21", the bounding longitudinal deceleration is 51.9 g's. Finally, for a side drop from a height of 72", the maximum deceleration is 49.2 g's.

Based on the above results, it is concluded that the design basis deceleration limit of 60g's (Table 3.1.2) provides a conservative input for Level D stress calculations to demonstrate retrievability of stored fuel.

3.4.10 Overpack Service Life

The term of the 10CFR72, Subpart L C of C, granted by the NRC is 20 years. Nonetheless, the HI-STAR 100 Overpack is designed for 40 years of service life, while satisfying the conservative design requirements defined in Chapter 2, including the regulatory requirements of 10CFR72. In addition, the overpack is designed, fabricated, and inspected under the comprehensive Quality Assurance Program discussed in Chapter 13 and in accordance with the applicable requirements of the ASME Codes. The pressure boundary (helium retention boundary) of the overpack is engineered to meet ASME Section III, Subsection NB (Class 1) stress intensity limits. Even though compliance to a less rigorous standard (such as the AISC Manual for Steel Construction) would be acceptable, all structural members of the HI-STAR 100 overpack located outside of the pressure boundary meet ASME Section III, Subsection NF stress limits. The aforementioned design and manufacturing measures assure high design margins, high quality fabrication, and verification of compliance

through rigorous inspection and testing, as describe in Chapter 9. Technical Specifications defined in Chapter 12 assure that the integrity of the cask and the contained MPC are maintained throughout the components' service life.

The principal design considerations which bear on the adequacy of the overpack for the design basis service life are addressed as follows:

Exposure to Environmental Effects

All exposed surfaces of HI-STAR 100 are made from ferritic steels that are readily painted. Therefore, the potential of environmental vagaries are ruled out for HI-STAR 100. Under normal storage conditions, the bulk temperature of the HI-STAR 100 overpack will, because of its large thermal inertia, change very gradually with time. Therefore, material degradation from rapid thermal ramping conditions is not credible for the HI-STAR 100 overpack. The configuration of the overpack assures resistance to freeze-thaw degradation. In addition, the overpack is specifically designed for a full range of enveloping design basis natural phenomena which could occur over the 40-year service life of the overpack as defined in Section 2.2.3 and evaluated in Chapter 11.

Material Degradation

The relatively low neutron flux to which the overpack is subjected cannot produce measurable degradation of the cask's material properties and impair its intended safety function. Exposed carbon steel components are coated to prevent corrosion. The controlled environment of the ISFSI storage pad mitigates damage due to direct exposure to corrosive chemicals that may be present in other industrial applications.

Maintenance and Inspection Provisions

The requirements for periodic inspection and maintenance of the overpack throughout the 40-year service life are defined in Chapter 9. These requirements include provisions for routine inspection of the overpack exterior. ISFSIs located in areas subject to atmospheric conditions which may degrade the storage cask or canister should be evaluated by the licensee on a site-specific basis to determine the frequency for such inspections to assure long-term performance. In addition, the HI-STAR 100 System is designed for easy retrieval of the MPC from the overpack should it become necessary to perform more detailed inspections and repairs on the overpack.

The above findings are consistent with those of the NRC's Waste Confidence Decision Review [3.4.11], which concluded that dry storage systems designed, fabricated, inspected, and operate in accordance with such requirements are adequate for a 100-year service life while satisfying the requirements of 10CFR72.

3.4.11 MPC Service Life

The term of the 10CFR72, Subpart L C of C, granted by the NRC is 20 years. Nonetheless, the HI-STAR 100 MPC is designed for 40 years of service, while satisfying the conservative design requirements defined in Chapter 2, including the regulatory requirements of 10CFR72. Additional assurance of the integrity of the MPC and the contained SNF assemblies throughout the 40-year service life of the MPC is provided through the following:

- Design, fabrication, and inspection in accordance with the applicable requirements of the ASME Code as described in Chapter 2 assures high design margins.
- Fabrication and inspection performed in accordance with the comprehensive Quality Assurance program discussed in Chapter 13 assures competent compliance with the fabrication requirements.
- Use of materials with known characteristics, verified through rigorous inspection and testing, as described in Chapter 9, assures component compliance with design requirements.
- Use of welding procedures in full compliance with Sections III and IX of the ASME Code ensures high quality weld joints.

Technical Specifications, as defined in Chapter 12, have been developed and imposed on the MPC which assure that the integrity of the MPC and the contained SNF assemblies are maintained throughout the 40-year service life of the MPC.

The principal design considerations bearing on the adequacy of the MPC for the design basis service life are summarized below.

Corrosion

All MPC materials are fabricated from corrosion-resistant austenitic stainless steel and passivated aluminum. The corrosion-resistant characteristics of such materials for dry SNF storage canister applications, as well as the protection offered by these materials against other material degradation effects, are well established in the nuclear industry. The MPC is vacuum dried to remove all oxidizing liquids and gases and backfilled with dry inert helium at the time of closure to maintain an atmosphere in the MPC that provides corrosion protection for the SNF cladding throughout the dry storage period. The preservation of this non-corrosive atmosphere is assured by the inherent sealworthiness of the MPC confinement boundary integrity (there are no gasketed joints in the MPC).

Structural Fatigue

The passive non-cyclic nature of dry storage conditions does not subject the MPC to conditions that might lead to structural fatigue failure. Ambient temperature and insolation cycling during normal dry storage conditions and the resulting fluctuations in MPC thermal gradients and internal pressure is the only mechanism for fatigue. These low stress, high-cycle conditions cannot lead to a fatigue

failure of the MPC which is made from stainless alloy stock (endurance limit well in excess of 20,000 psi). All other off-normal or postulated accident conditions are infrequent or one-time occurrences which cannot produce fatigue failures. Finally, the MPC uses materials that are not susceptible to brittle fracture.

Maintenance of Helium Atmosphere

The inert helium atmosphere in the MPC provides a non-oxidizing environment for the SNF cladding to assure its integrity during long-term storage. The preservation of the helium atmosphere in the MPC is assured by the robust design of the MPC confinement boundary described in Section 7.1. Maintaining an inert environment in the MPC mitigates conditions that might otherwise lead to SNF cladding failures. The required mass quantity of helium backfilled into the canister at the time of closure as defined in the Technical Specification contained in Chapter 12, and the associated leak tightness requirements for the canister defined in the Technical Specification contained in Chapter 12, are specifically set down to assure that an inert helium atmosphere is maintained in the canister throughout a 40-year service life.

Allowable Fuel Cladding Temperatures

The helium atmosphere in the MPC promotes heat removal and thus reduces SNF cladding temperatures during dry storage. In addition, the SNF decay heat will substantially attenuate over a 40-year dry storage period. Maintaining the fuel cladding temperatures below allowable levels during long-term dry storage mitigates the damage mechanism that might otherwise lead to SNF cladding failures. The allowable long-term SNF cladding temperatures used for thermal acceptance of the MPC design are conservatively determined, as discussed in Section 4.3.

Neutron Absorber Boron Depletion

The effectiveness of the fixed borated neutron absorbing material used in the MPC fuel basket design requires that sufficient concentrations of boron be present to assure criticality safety during worst case design basis conditions over the 40-year service life of the MPC. Information on the characteristics of the borated neutron absorbing material used in the MPC fuel basket is provided in Section 1.2.1.3.1. The low neutron flux, which will continue to decay over time, to which this borated material is subjected, does not result in depletion of the material's available boron to prevent performing its intended safety function. In addition, the boron content of the material used in the criticality safety analysis is conservatively based on the minimum specified boron areal density (rather than the nominal), which is further reduced by 25% for analysis purposes, as described in Section 6.1. Analysis discussed in Section 6.3.2 demonstrates that the boron depletion in the Boral is negligible over a 50-year duration. Thus, sufficient levels of boron are present in the fuel basket neutron absorbing material to maintain criticality safety functions over the 40-year service life of the MPC.

The above findings are consistent with those of the NRC's Waste Confidence Decision Review, which concluded that dry storage systems designed, fabricated, inspected, and operated in the manner of the requirements set down in this document are adequate for a 100-year service life, while satisfying the requirements of 10CFR72.

Table 3.4.1

FINITE ELEMENTS IN THE MPC STRUCTURAL MODELS

MPC Type	Model Type		
Element Type	Basic	0 Degree Drop	45 Degree Drop
MPC-24	1068	1179	1178
BEAM3	1028	1028	1028
PLANE82	0	0	0
CONTAC12	40	38	38
CONTAC26	0	110	110
COMBIN14	0	3	2
MPC-68	1234	1347	1344
BEAM3	1174	1174	1174
PLANE82	16	16	16
CONTAC12	44	43	40
CONTAC26	0	112	111
COMBIN14	0	2	3

Table 3.4.2

HI-STAR 100 SYSTEM MATERIAL COMPATIBILITY
WITH OPERATING ENVIRONMENTS

Material/Component	Fuel Pool (Borated and Unborated Water†)	ISFSI Pad (Open to Environment)
Alloy X: - MPC Fuel Basket - MPC Baseplate - MPC Shell - MPC Lid - MPC Fuel Spacers	Stainless steels have been extensively used in spent fuel storage pools with both borated and unborated water with no adverse reactions or interactions with spent fuel.	The MPC internal and external environment will be inert (helium) atmosphere. No adverse interactions identified.
Aluminum: - Conduction Elements	Aluminum and stainless steels form a galvanic couple. However, they are very close in the galvanic series chart and aluminum rapidly passivates in an aqueous environment forming a thin ceramic (Al_2O_3) barrier. Therefore, during the short time they are exposed to fuel pool water, significant corrosion or production of hydrogen is not expected (see operational requirements under "Boral" below).	In a non-aqueous atmosphere galvanic corrosion is not expected.
Boral: - Neutron Absorber	The Boral will be passivated before installation in the fuel basket to minimize the amount of hydrogen released from the aluminum-water reaction to a non-combustible concentration during MPC lid welding or cutting operations. See Chapter 8 for additional requirements for combustible gas monitoring and required actions for control of combustible gas accumulation under the MPC lid.	The Boral will be in a helium environment. No adverse reactions identified.

† HI-STAR 100 System short-term operating environment during loading and unloading.

Table 3.4.2 (continued)

HI-STAR 100 SYSTEM MATERIAL COMPATABILITY WITH OPERATING ENVIRONMENT

Material/Component	Fuel Pool (Borated and Unborated Water) †	ISFSI Pad (Open to Environment)
Steels: - SA350-LF3 - SA203-E - SA515 Grade 70 - SA516 Grade 70 - SA750 630 17-4 PH - SA564 630 17-4 PH - SA106 - SA193-B7 Overpack Body	All exposed steel surfaces (except seal areas, pocket trunnions, and bolt locations) will be coated with paint specifically selected for performance in the operating environments. Even without coating, no adverse reactions (other than nominal corrosion) have been identified.	Internal surfaces of the overpack will be painted and maintained in an inert atmosphere. Exposed external surfaces (except those listed in fuel pool column) will be painted and will be maintained with a fully painted surface. No adverse reactions identified.

† HI-STAR 100 System short-term operating environment during loading and unloading.

Table 3.4.2 (continued)

HI-STAR 100 SYSTEM MATERIAL COMPATABILITY WITH OPERATING ENVIRONMENT

Material/Component	Fuel Pool (Borated and Unborated Water) †	ISFSI Pad (Open to Environment)
Stainless Steels: - SA240 304 - SA193 Grade B8 - 18-8 S/S Miscellaneous Components	Stainless steels have been extensively used in spent fuel storage pools with both borated and unborated water with no adverse reactions.	Stainless steel has a long proven history of corrosion resistance when exposed to the atmosphere. These materials are used for bolts and threaded inserts. No adverse reactions with steel have been identified. No impact on performance.
Nickel Alloy: - SB637-NO7718 Bolting	Bolts are not used in pool.	Exposed to weathering effects. No adverse reactions with overpack closure plate. No impact on performance.
Brass: - Rupture Disk	Small surface of rupture disk will be exposed. No significant adverse impact identified.	Exposed to external weathering. No loss of function expected. Disks inspected prior to transport.
Holtite-A: - Neutron Shield	The neutron shield is fully enclosed by the outer enclosure. No adverse reaction identified. No adverse reactions with thermal expansion foam or steel.	The neutron shield is fully enclosed in the outer enclosure. No adverse reaction identified. No adverse reactions with thermal expansion foam or steel.

† HI-STAR 100 System short-term operating environment during loading and unloading.

Table 3.4.2 (continued)

HI-STAR 100 SYSTEM MATERIAL COMPATABILITY WITH OPERATING ENVIRONMENT

Material/Component	Fuel Pool (Borated and Unborated Water) †	ISFSI Pad (Open to Environment)
Silicone Foam: - Thermal Expansion Foam	Fully enclosed in the outer enclosure. No adverse reaction identified. No adverse reactions with neutron shield or steel.	Foam is fully enclosed in outer enclosure. No adverse reaction identified. No adverse reactions with neutron shield or steel.
Paint: - Carboline 890 - Thermaline 450	Carboline 890 used for exterior surfaces. Acceptable performance for short-term exposure in mild borated pool water. Thermaline 450 selected for excellent high temperature resistance properties. Will only be exposed to demineralized water during in-pool operations as annulus is filled prior to placement in the spent fuel pool and the inflatable seal prevents fuel pool water in-leakage. No adverse interaction identified which could affect MPC/fuel assembly performance.	Good performance on exterior surfaces. Discoloration is not a concern. During storage, internal overpack surfaces will operate in an inert (helium) atmosphere. No adverse reaction identified.
Metallic Seals: - Alloy X750 - 304 S/S	Not installed or exposed during in-pool handling.	Seals enclosed by closure plate or port coverplates. Closure plate seals seat against stainless steel overlay surfaces. No degradation of seal integrity due to corrosion is expected.

† HI-STAR 100 System short-term operating environment during loading and unloading.

Table 3.4.3

FUEL BASKET RESULTS- GLOBAL MINIMUM OF SAFETY FACTORS

Load Case I.D.	**Loading†**	**Safety Factor**	**Location in FSAR where Results or Detailed Calculations are Presented††**
F1	T, T'	No Interference	3.4.4.2.1
F2	D + H	2.87	Table 3.4.9
F3			
F3.a	D + H' (end drop)	4.27	3.4.4.3.1.3
F3.b	D + H' (side drop 0°)	1.19	
F3.c	D + H' (side drop 45°)	1.29	

† The symbols used for the loading are defined in Table 2.2.13.

†† All Safety Factors for the Fuel Basket are conservatively evaluated using allowable stresses evaluated at 725 degrees F.

Table 3.4.4

ENCLOSURE VESSEL RESULTS – GLOBAL MINIMUM OF SAFETY FACTORS

Load Case I.D.	Load Combination†	Safety Factor	Component ID and Location in FSAR where Results or Detailed Calculations are Presented†††	
E1				
E1.a	Design internal pressure, P_i	5.06††††† 1.33 1.27	Lid Baseplate Shell	Table 3.4.7 3.I.8.1 3.4.4.3.1.2
E1.b	Design external pressure, P_o	7.5††††† 1.2 1.2	Lid Baseplate Shell	3.E.8.1.1 Table 3.4.7†††† Table 3.4.15
E1.c	Design internal pressure, P_i, plus Temperature T	16.4 2.7 1.5	Lid Baseplate Shell	Table 3.4.8 Table 3.4.8 Table 3.4.8
E2	(P_i, P_o)†† + D + H	1.8††††† 1.09 2.64 5.85	Lid Baseplate Shell Supports	3.E.8.1.2 3.I.8.2 Table 3.4.9 Table 3.4.9

† The symbols used for the loadings are defined in Table 2.2.13.

†† The notation (P_i,P_o) means that one or the other pressure is applied to determine the governing condition.

††† Safety Factors computed in Table 3.4.9 are conservatively based on the design temperature given in Table 3.1.17.

†††† Safety Factor obtained by multiplication of result for internal pressure by external pressure/internal pressure ratio.

††††† Minimum safety factor is based on dual lid configuration.

Table 3.4.4 (Continued)

ENCLOSURE VESSEL RESULTS – GLOBAL MINIMUM OF SAFETY FACTORS

Load Case I.D.	Load Combination†	Safety Factor	Component ID and Location in FSAR where Detailed Calculations are Presented††	
E3				
E3.a	$(P_i, P_o) + D + H'$, end drop	7.69†††	Lid	Table 3.4.13
		1.87	Baseplate	Table 3.4.12
		1.92	Shell	Table 3.4.15
E3.b	$(P_i, P_o) + D + H'$, side drop 0°	NA	Lid	
		NA	Baseplate	
		3.07	Shell	Table 3.4.9
		1.16	Supports	Table 3.4.9
E3.c	$(P_i, P_o) + D + H'$, side drop 45°	NA	Lid	
		NA	Baseplate	
		2.74	Shell	Table 3.4.9
		1.51	Supports	Table 3.4.9

† Symbols used in the loading are defined in Table 2.2.13

†† Safety Factors computed in Table 3.4.9 conservatively use allowable stresses at the design temperature of 450 degrees F (Table 3.1.17)

††† Minimum safety factor is based on dual lid configuration.

Table 3.4.4 (Continued)

ENCLOSURE VESSEL RESULTS – GLOBAL MINIMUM OF SAFETY FACTORS

Load Case I.D.	Load Combination†	Safety Factor	Component ID and Location in FSAR where Detailed Calculations are Presented
E4	T	No restraint of free thermal expansion under normal heat or fire accident	3.U; 3.W; 3.AD
E5	$(P_I^*, P_o^*) + D + T^*$	13.6†† 1.78 1.18	Lid Table 3.4.13 Baseplate Table 3.4.12 Shell Table 3.5.15

† The symbols used for the loading are defined in Table 2.2.13

†† Minimum safety factor is based on the dual lid configuration.

Table 3.4.5

OVERPACK – GLOBAL MINIMUM SAFETY FACTORS

Load Case I.D.	Load Combination†	Safety Factor	Location in FSAR
01	(P_i, P_o)	2.86	Table 3.4.10
02	$(P_i^*, P_o^*) + D + T^*$	3.56	Table 3.4.6
03	$(P_i, P_o) + D + T + H$	4.45	Table 3.4.10
04			
04.a	$(P_i, P_o) + D + H$ (end drop)	1.27	Table 3.4.10
04.b	$(P_i, P_o) + D + H$ (side drop)	1.48	Table 3.4.10
05	T	1.93	Table 3.4.6
06	M (small and medium penetrant missiles)	No effect on confinement boundary	3.G

† The symbols used for the loadings are defined in Table 2.2.13.

Table 3.4.6

OVERPACK SAFETY FACTORS TO INCORPORATE FABRICATION STRESS AND ACCIDENT TEMPERATURE†

Load Case	Inner Shell (Exterior Surface)			Inner Shell (Middle Surface)			Intermediate Shell		
	Value (ksi)	Allowable (ksi)	Safety Factor	Value (ksi)	Allowable (ksi)	Safety Factor	Value (ksi)	Allowable (ksi)	Safety Factor
01	19.1	68.7	3.60	12.19	68.7	5.33	12.74	52.5	4.12
03	19.28	68.7	3.56	12.30	68.7	5.59	14.61	52.5	3.59
05	35.68	68.7	1.93	26.65	68.7	2.58	NA	NA	NA

† The Value is obtained by adding the fabrication stress from Subsection 3.4.4.3.2.2 (absolute value) to the stress intensity from the finite element solution to compute a conservative modified stress intensity and then re-computing the safety factor based on allowable values for primary plus secondary stresses.

Table 3.4.7
STRESS INTENSITY RESULTS FOR CONFINEMENT BOUNDARY -
INTERNAL PRESSURE ONLY (Load Case E1.a in Table 3.1.4)

Component Locations (Per Fig.3.4.44)	Calculated Value of Stress Intensity (psi)	Category	Table 3.1.13 Allowable Value (psi)†	Safety Factor (Allowable/Calculated)
Top Lid††				
A	3,282	$P_L + P_b$	30,000	9.14
Neutral Axis	40.4	P_m	20,000	495
B	3,210	$P_L + P_b$	30,000	9.34
C	1,374	$P_L + P_b$	30,000	21.8
Neutral Axis	1,462	P_m	20,000	13.6
D	5,920	$P_L + P_b$	30,000	5.06
Baseplate				
E	19,683	$P_L + P_b$	30,000	1.5
Neutral Axis	412	P_m	20,000	48.5
F	20,528	$P_L + P_b$	30,000	1.5
G	9,695	$P_L + P_b$	30,000	3.1
Neutral Axis	2,278	P_m	20,000	8.8
H	8,340	$P_L + P_b$	30,000	3.5

† Allowable stress intensity conservatively taken at 300 degrees F.

†† The stresses in the top lid are reported for the dual lid configuration. The stresses for the single lid configuration are 50% less (see Subsection 3.4.4.3.1.2 for further details).

Table 3.4.7 (Continued)

STRESS INTENSITY RESULTS FOR CONFINEMENT BOUNDARY -
INTERNAL PRESSURE ONLY (Load Case E1.a in Table 3.1.4)

Component Locations (Per Fig. 3.4.44)	Calculated Value of Stress Intensity (psi)	Category	Table 3.1.13 Allowable Value (psi)†	Safety Factor (Allowable/Calculated)
Canister				
I	6,860	P_m	18,700	2.72
Upper Bending	7,189	$P_L + P_b + Q$	30,000	4.2
Boundary Layer Region	7,044	$P_L + P_b$	20,000	2.8
Lower Bending	43,986	$P_L + P_b + Q$	60,000	1.36
Boundary Layer Region	10,621	$P_L + P_b$	30,000	2.82

† Allowable stress intensity conservatively based at 300 degrees F except for Location I where allowable stress intensity values are based on 400 degree F.

Table 3.4.8

PRIMARY AND SECONDARY STRESS INTENSITY RESULTS FOR
CONFINEMENT BOUNDARY - PRESSURE PLUS THERMAL LOADING (Load Case E1.c in Table 3.1.4)

Locations (Per Fig. 3.4.44)	Calculated Value of Stress Intensity (psi)	Category	Allowable Stress Intensity (psi)†	Safety Factor (Allowable/Calculated)
Top Lid††				
A	4,750	$P_L + P_b + Q$	60,000	12.6
Neutral Axis	1,530	P_L	30,000	19.6
B	2,140	$P_L + P_b + Q$	60,000	28.0
C	2,200	$P_L + P_b + Q$	60,000	27.2
Neutral Axis	3,650	P_L	30,000	8.21
D	7,034	$P_L + P_b + Q$	60,000	8.52
Baseplate				
E	21,921	$P_L + P_b + Q$	60,000	2.7
Neutral Axis	1,287	P_L	30,000	23.3
F	19,386	$P_L + P_b + Q$	60,000	3.1
G	6,152	$P_m + P_L$	60,000	9.8
Neutral Axis	4,564	P_L	30,000	6.6
H	11,306	$P_L + P_b + Q$	60,000	5.3

† Allowable stresses based on temperature of 300 degrees F

†† The stresses in the top lid are reported for the dual lid configuration. The stresses for the single lid configuration are 50% less (see Subsection 3.4.4.3.1.2 for further details).

Table 3.4.8 (Continued)

PRIMARY AND SECONDARY STRESS INTENSITY RESULTS FOR
CONFINEMENT BOUNDARY - PRESSURE PLUS THERMAL LOADING (Load Case E1.c in Table 3.1.4)

Locations (Per Fig. 3.4.44)	Calculated Value of Stress Intensity (psi)	Category	Allowable Stress Intensity (psi)†	Safety Factor (Allowable/Calculated)
Canister				
I	6,900	P_L	28,100	4.07
Upper Bending	6,490	$P_L + P_b + Q$	60,000	9.2
Boundary Layer Region	4,834	P_L	30,000	6.2
Lower Bending	39,929	$P_L + P_b + Q$	60,000	1.5
Boundary Layer Region	7,480	P_L	30,000	4.0

†Allowable stresses based on temperature of 300 degree F except at Location I where the temperatures are based on 400 degrees F.

Table 3.4.9

FINITE ELEMENT ANALYSIS RESULTS
MINIMUM SAFETY FACTORS FOR MPC COMPONENTS (Load Cases from Tables 3.1.3 and 3.1.4)

Component – Stress Result	MPC-24		
	Handling Load Load Cases F2 or E2	0 Degree Side Drop Load Cases F3.b or E3.b	45 Degree Side Drop Load Cases F3.c or E3.c
Fuel Basket – Primary Membrane (P_m)	45.5(396)	2.80(1134)	3.85(396)
Fuel Basket – Local Membrane Plus Primary Bending ($P_L + P_b$)	11.9(75)	1.19(1065)	1.29(433)
Enclosure Vessel - Primary Membrane (P_m)	2.67(1370)	6.43(1277)	6.88(1370)
Enclosure Vessel – Local Membrane Plus Primary Bending ($P_L + P_b$)	3.56(1343)	4.24(1276)	4.28(1295)
Basket Supports – Primary Membrane (P_m)	N/A	N/A	N/A
Basket Supports – Local Membrane Plus Primary Bending ($P_L + P_b$)	N/A	N/A	N/A

Notes:
1. Corresponding ANSYS element number shown in parentheses.

Table 3.4.9 (continued)

FINITE ELEMENT ANALYSIS RESULTS
MINIMUM SAFETY FACTORS FOR MPC COMPONENTS (Load Cases from Tables 3.1.3 and 3.1.4)

Component - Stress Result	MPC-68		
	Handling Load Load Cases F2 or E2	0 Degree Side Drop Load Cases F3.b or E3.b	45 Degree Side Drop Load Cases F3.c or E3.c
Fuel Basket - Primary Membrane (P_m)	40.0 (798)	3.07 (1603)	4.30 (1603)
Fuel Basket - Local Membrane Plus Primary Bending ($P_L + P_b$)	2.87 (438)	2.64 (1033)	1.56 (774)
Enclosure Vessel - Primary Membrane (P_m)	2.64 (1747)	5.64~~5~~ (1770)	7.12~~3~~ (1864)
Enclosure Vessel - Local Membrane Plus Primary Bending ($P_L + P_b$)	2.96 (1864)	3.07 (1770)	2.74 (1866)
Basket Supports - Primary Membrane (P_m)	5.84~~5~~ (1714)	6.67~~8~~ (1699)	8.67~~8~~ (1644)
Basket Supports - Local Membrane Plus Primary Bending ($P_L + P_b$)	9.01~~2~~ (1713)	1.16 (1704)	1.51 (1649)

Notes:

1. Corresponding ANSYS element number shown in parentheses.

Table 3.4.10

FINITE ELEMENT RESULTS
MINIMUM SAFETY FACTORS FOR OVERPACK COMPONENTS UNDER VARIOUS LOADS (Load Case from Table 3.1.5)

Component - Stress Result	Internal Pressure – Load Case 01	Accident Internal Pressure – Load Case 02	Accident External Pressure - Load Case 02	Handling Load – Load Case 03	End Drop Load Case 04.a	Side Drop – Load Case 04.b	Thermal Load – Load Case 05
Lid – Local Membrane Plus Primary Bending ($P_L + P_b$)	2.86 (501)	5.50 (501)	14.3 (501)	4.45 (501)	9.2 (501)	3.68 (501)	2.55 (479)
Inner Shell - Local Membrane Plus Primary Bending ($P_L + P_b$)	12.1 (11023)	24.6 (11023)	13.6 (47)	11.3 (8338)	2.20 (10790)	1.70 (47)	3.72 (10925)
Inner Shell - Primary Membrane (P_m)	13.7 (281)	27.7 (281)	17.4 (10791)	12.7 (2969)	2.37 (48)	2.65 (2969)	2.98 (11024)
Intermediate Shells – Local Membrane Plus Primary Bending ($P_L + P_b$)	17.2 (11025)	36.6 (11025)	24.3 (49)	7.76 (285)	3.47 (10792)	1.48 (51)	2.42 (10796)
Baseplate - Local Membrane Plus Primary Bending ($P_L + P_b$)	10.6 (1)	17.9 (1)	7.77 (1)	18.8 (1)	1.27 (1)	4.98 (1)	2.07 (27)
Enclosure Shell - Primary Membrane (P_m)	35.1 (288)	72.7 (288)	41.4 (55)	13.2 (288)	8.47 (55)	1.55 (288)	2.03 (5428)

Notes:

1. Corresponding ANSYS node number shown in parentheses.

Table 3.4.11

SAFETY FACTORS FROM MISCELLANEOUS CALCULATIONS

Item	Loading	Safety Factor	FSAR Text or Appendix Location Where Details are Provided
MPC Closure Ring	Internal Pressure	1.41	3.E
Fuel Basket Panels	Elastic Stability	15.9	3.4.4.3.1.3
MPC Top Lid Weld	Lifting	2.29	3.E
Fuel Support Spacers	Compression	2.76	3.J
MPC Cover Plates in MPC Lid	Accident Condition Internal Pressure	1.44	3.M
MPC Top Closure	10CFR71 Top End Drop (Transport) (Provided for Information Only)	2.8/(1.4)†	3.E
MPC Cover Plate Weld	Accident Condition Internal Pressure	4.03	3.M

† Results are presented for both the single and dual lid configurations (in parentheses). Refer to Subsection 3.4.4.3.1.2 for further information.

Table 3.4.12

MPC BASEPLATE MINIMUM SAFETY FACTORS FOR LOAD CASES E3 AND E5MPC Baseplate Minimum Safety Factors – Load Cases E3, E5

Item	Value (ksi)	Allowable (ksi)	Safety Factor
Center of Baseplate – Primary Bending (Load Case E3)	35.93	67.32	1.87
Center of Baseplate – Primary Bending (Load Case E5)	30.46	54.23	1.78

Details of calculation are in Subsection 3.4.4.3.1.4.

Table 3.4.13

MPC TOP CLOSURE LID MINIMUM SAFETY FACTORS FOR LOAD CASES E3 AND E5

MPC Top Closure Lid – Minimum Safety Factors – Load Cases E3, E5			
Item	Stress (ksi) or Load (lb.)	Allowable Stress (ksi) or Load Capacity (lb.)	Safety Factor
Lid Bending Stress – Load Case E3.a	3.35/(7.94)	61.05	18.2/(7.69)
Lid Peripheral Weld Load – Load Case E3.a	624,000	1,477,000[††]	2.37
Lid Bending Stress – Load Case E5	1.991/(3.982)	54.225	27.24/(13.6)
Lid-to-Lid Peripheral Weld Load – Load Case E3.a	312,000	443,200[†††]	1.42
Closure Ring Bending Stress – Load Case E1.a[†]	20.0	28.1	1.41
Closure Ring Weld Load – Load Case E1.a	140,956	316,400	2.24

Details of calculation are in Subsection 3.4.4.3.1.5

[†] The closure ring is only subject to load subsequent to a postulated loss of integrity in the "NB" pressure boundary. Nevertheless, the stress results are compared to Level A allowables for conservatism. The pressure loading is assumed to correspond to the Design Pressure.

[††] Based on 0.625" single groove weld and conservatively includes a quality factor of 0.45.

[†††] This is a non-Code weld; limit is based on a 0.1875 inch groove weld and includes a quality factor of 0.45 for additional conservatism.

Table 3.4.14

MPC FUEL SPACERS – MINIMUM SAFETY FACTORS FOR LOAD CASES F2 AND F3.a

Fuel Spacers – Minimum Safety Factors (Load Cases F2 and F3.a)			
Item	Load (lb.)	Capacity (lb.)	Safety Factor
Axial Load – Level A	16,800	46,446	2.76
Elastic Stability – Level D – Lower Spacer	100,800	1,300,000	12.9
Elastic Stability – Level D – Upper Spacer	100,800	577,000	5.72

Details of calculation are in Subsection 3.4.4.3.1.6

Table 3.4.15

MPC SHELL STABILITY SAFETY FACTORS FROM ASME CODE CASE N-284

MPC Shell – Elastic/Plastic Stability (ASME Code Case N-284) – Minimum Safety Factors			
Item	Value	Allowable†	Safety Factor
Load Case E3.a (Yield)	0.698	1.34	1.92
Load Case E5 (Stability Interaction Equation)	0.847	1.0	1.18
Load Case E1.b (Stability Interaction Curve)	0.832	1.0	1.20

† We note that for Load Case E3.a, the yield strength criteria in the Code Case N-284 method governs. In this event, we include the safety factor 1.34, built into the Code Case, in the tabular result in order to obtain the actual safety factor with respect to the yield strength of the material.

Details of calculation are in Subsection 3.4.4.3.1.7

Table 3.4.16

OVERPACK FABRICATION STRESS – MINIMUM SAFETY FACTORS

Fabrication Stresses in Overpack Shells –Minimum Safety Factors (Level A Service Condition at Assembly Temperature)			
Item	Value (ksi)	Allowable (ksi) - (Note 3)	Safety Factor
First Intermediate Shell (Note 1)	11.22	52.5	4.68
Fourth Intermediate Shell (Note 1)	7.79	52.5	6.74
Inner Shell Mid Plane (Note 2)	10.6	69.9	6.59
Inner Shell Outer Surface (Note 2)	16.27	69.9	4.30

Notes:

1. The fabrication stress is a tensile circumferential stress.
2. The fabrication stress is a compressive circumferential stress
3. Fabrication stresses are self-limiting and are therefore classified as "secondary" and are compared to 3 times the membrane stress or stress intensity.

Details of calculation are in Subsection 3.4.4.3.2.2

Table 3.4.17

OVERPACK CLOSURE BOLT MINIMUM SAFETY FACTORS

Overpack Closure Bolt - Minimum Safety Factors	
Combined Load Case	Safety Factor on Bolt Tension
Normal (Load Case 01 in Table 3.1.5)	1.44
Top Closure Puncture (Load Case 06 in Table 3.1.5)	1.86
Drop (Load Case 04.a in Table 3.1.5)	1.30

Details of calculations are in Subsection 3.4.4.3.2.3

Table 3.4.18

OVERPACK CLOSURE PLATE – SAFETY FACTOR FOR LOAD CASE 04.a

Bending Stress in Overpack Closure Plate – Closed Form Solution (Load Case 04.a)			
Item	Value (ksi)	Allowable (ksi)	Safety Factor
Stress at Center of Plate	5.25	70.0	13.3

Details of calculations are in Subsection 3.4.4.3.2.4

Table 3.4.19

OVERPACK INNER SHELL SAFETY FACTORS FROM ASME CODE CASE N-284

Code Case N-284 Minimum Safety Factors – (Load Cases 02, 03 and 04.a in Table 3.1.5)			
Item	Calculated Interaction Value	Allowable Interaction Value†	Safety Factor against Yield†
Load Case 02 in Table 3.1.5	0.577	1.34	2.32
Load Case 03 in Table 3.1.5	0.613	2.0	3.26
Load Case 04 in Table 3.1.5	0.62	1.34	2.21

† We note that in computing the safety factor against yield for this table, we have included the safety factor implicit in the Code Case N-284 allowable interaction equation. We note also that the safety factors given above from the Code Case analysis are all safety factors against the circumferential or longitudinal stresses reaching the material yield stress. The actual safety factors against instability are larger than the factors reported in the table as can be seen by a perusal of Appendix 3.H. Finally, we note that fabrication stresses have been included in the stability calculations even though these stresses are self-limiting. Therefore, all results corresponding to the calculated stability interaction equations in Appendix 3.H are conservatively high.

Details of calculations are in Subsection 3.4.4.3.2.5

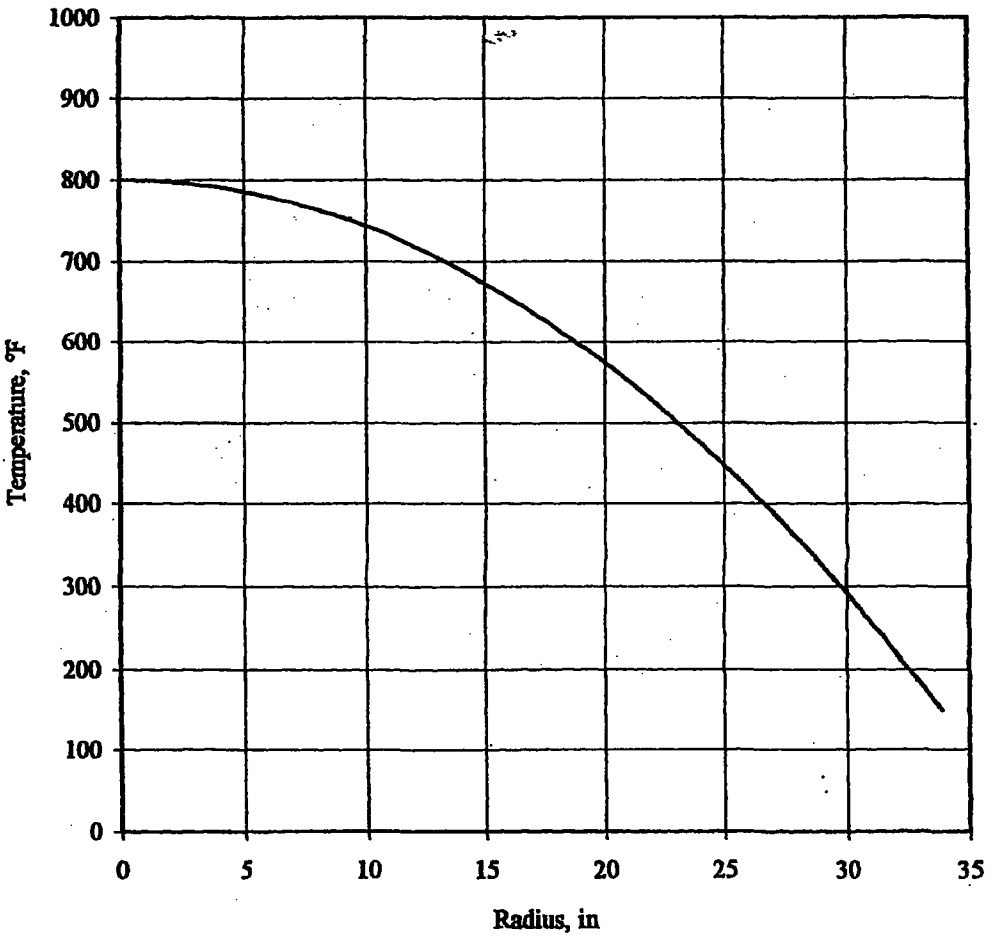

FIGURE 3.4.1; TEMPERATURE DISTRIBUTION FOR MPC THERMAL STRESS ANALYSIS

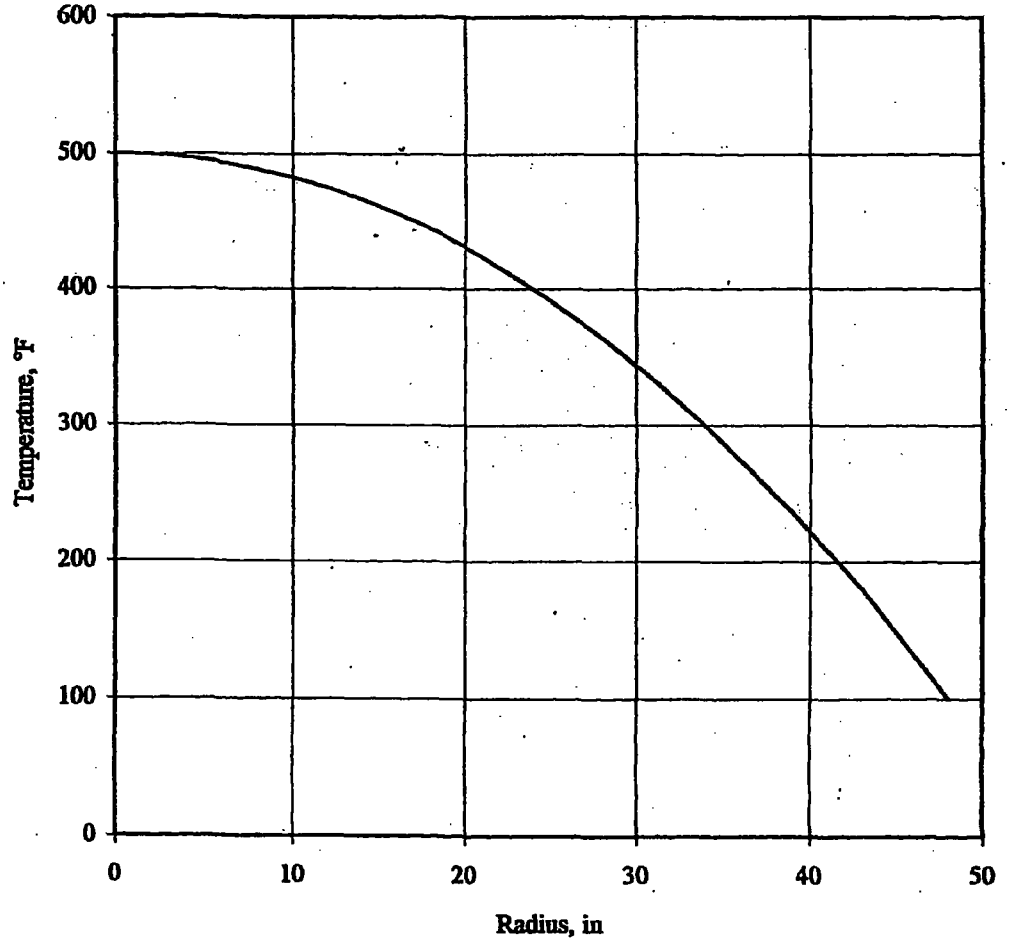

FIGURE 3.4.2; TEMPERATURE DISTRIBUTION FOR OVERPACK THERMAL STRESS ANALYSIS

REPORT HI-2012610

REVISION 0

\\PROJECTS\5014\HI1941184\CH_3\3_4_2

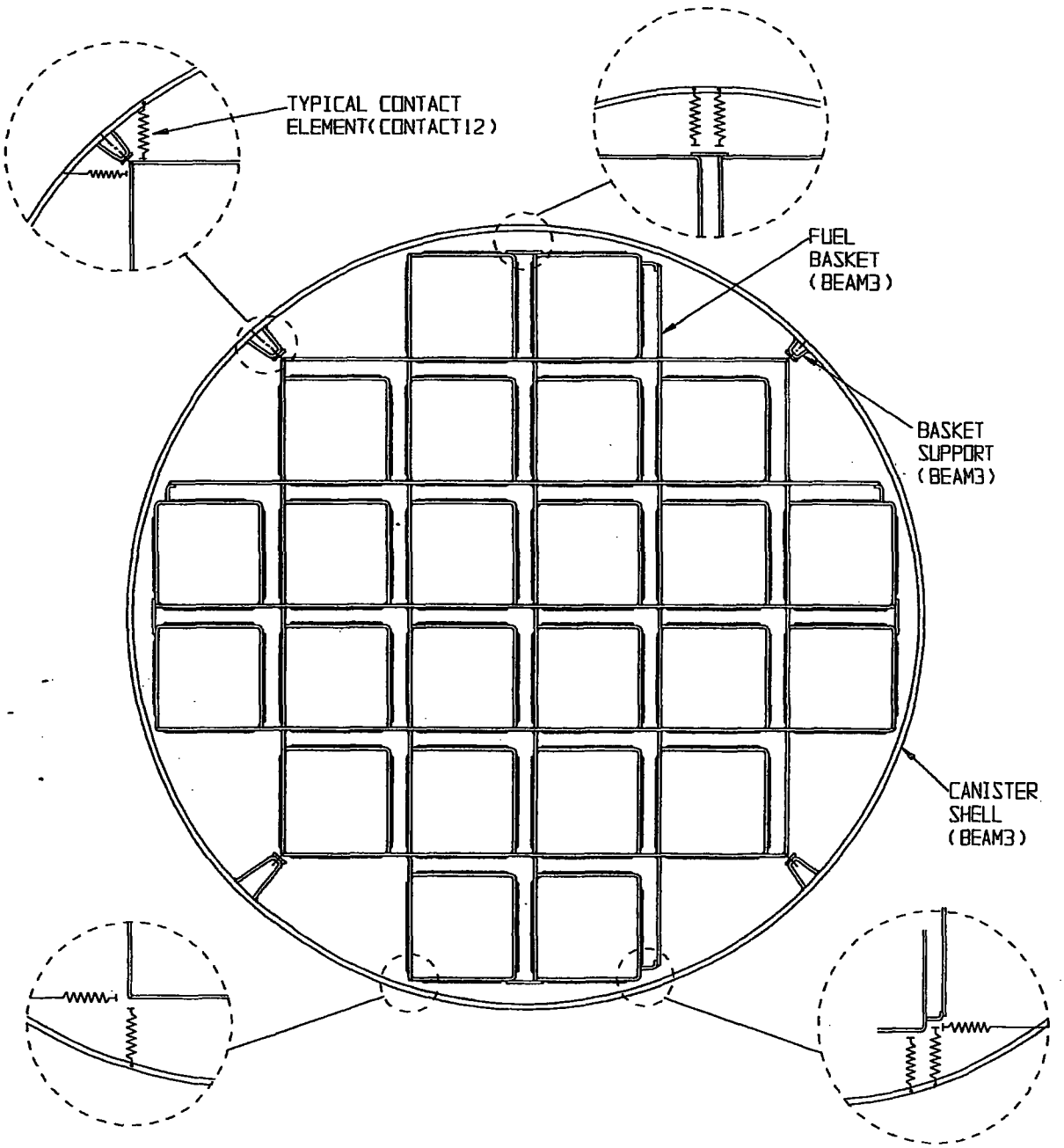

FIGURE 3.4.3: FINITE ELEMENT MODEL OF MPC-24
(BASIC MODEL)

REPORT HI-2012610 | REVISION 0

e\PROJECTS\GENERIC\HI2012610\CH_3\3_4_3

DELETED

FIGURE 3.4.4;

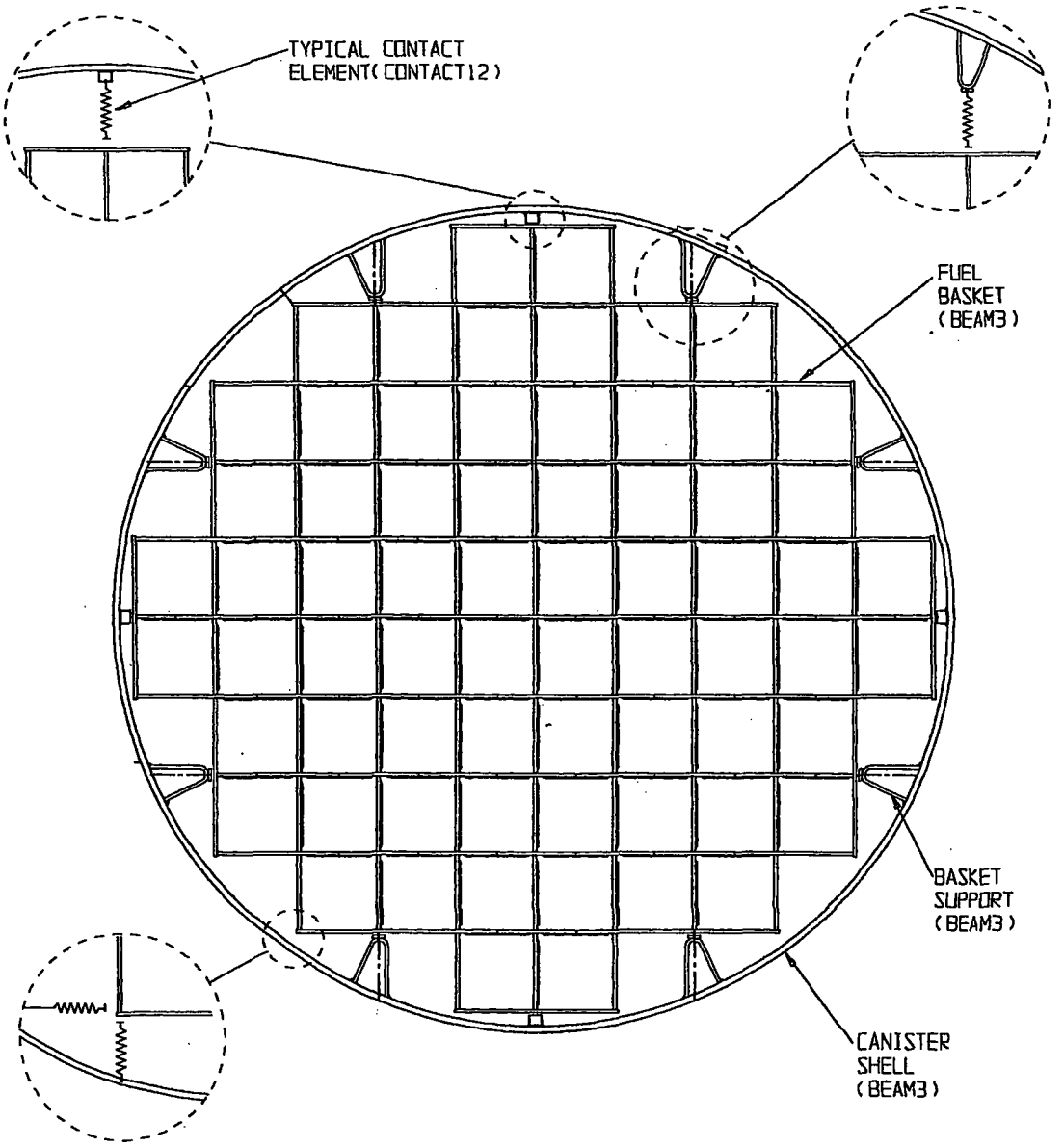

FIGURE 3.4.5: FINITE ELEMENT MODEL OF MPC-68

(BASIC MODEL)

REPORT HI-2012610

REVISION 0

e\PROJECTS\GENERIC\HI2012610\CH_3\3_4_5

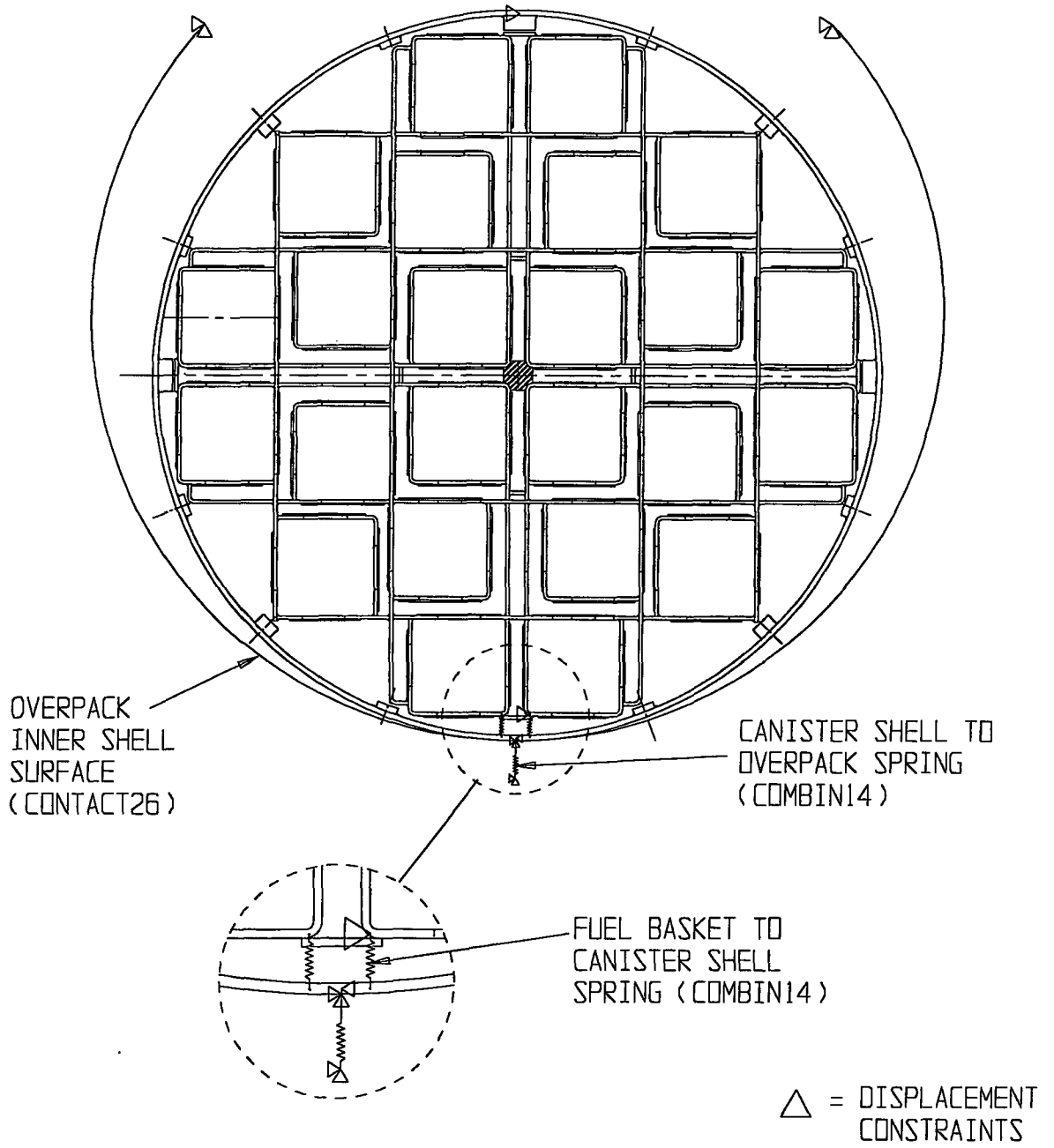

FIGURE 3.4.6: FINITE ELEMENT MODEL OF MPC-24

(0 DEGREE DROP MODEL)

DELETED

FIGURE 3.4.7;

REPORT HI-2012610

REVISION 0

\PROJECTS\GENERIC\HI2012610\CH. 3\3_4_7

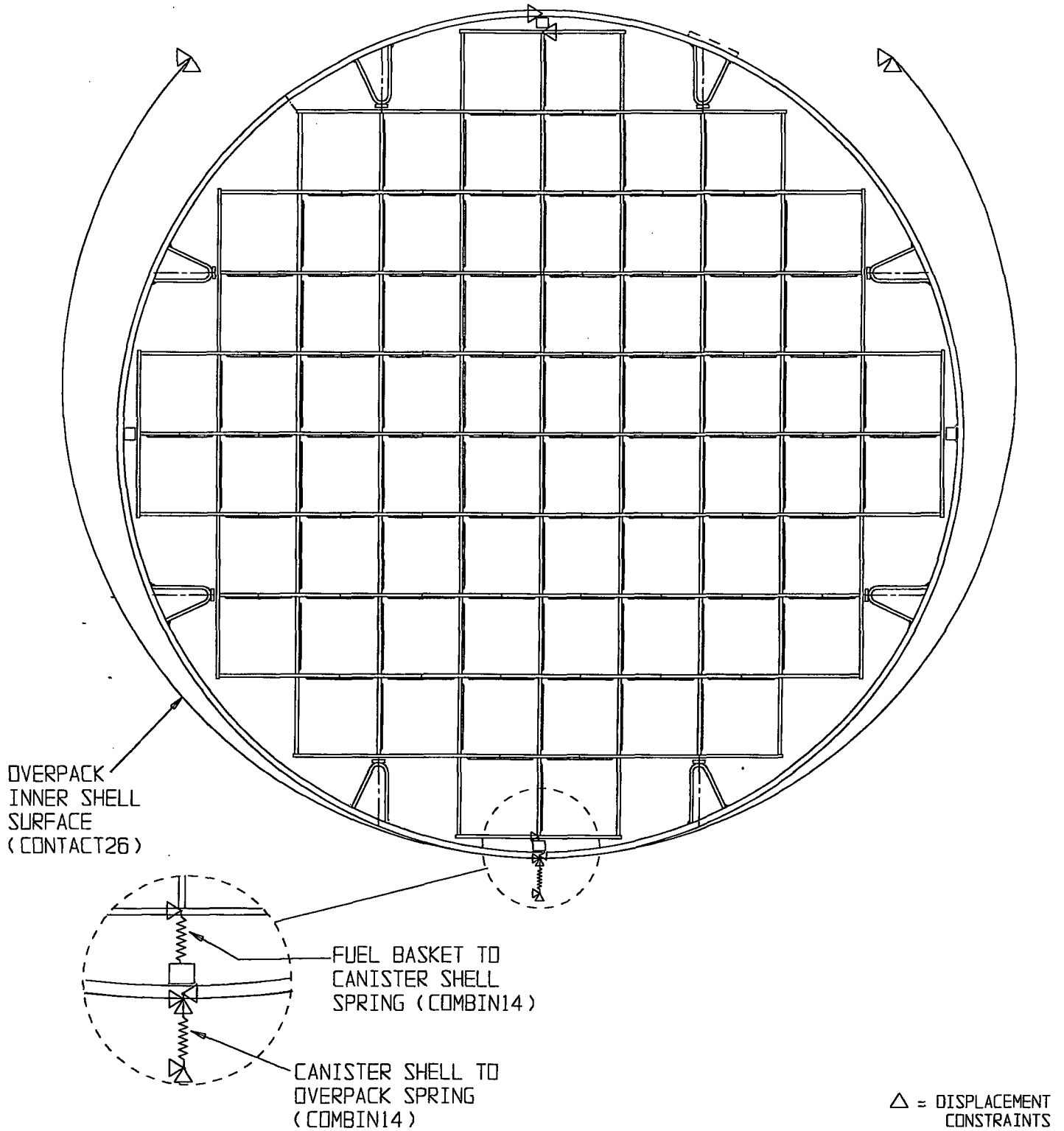

FIGURE 3.4.8; FINITE ELEMENT MODEL OF MPC-68

(0 DEGREE DROP MODEL)

REPORT HI-2012610

REVISION 0

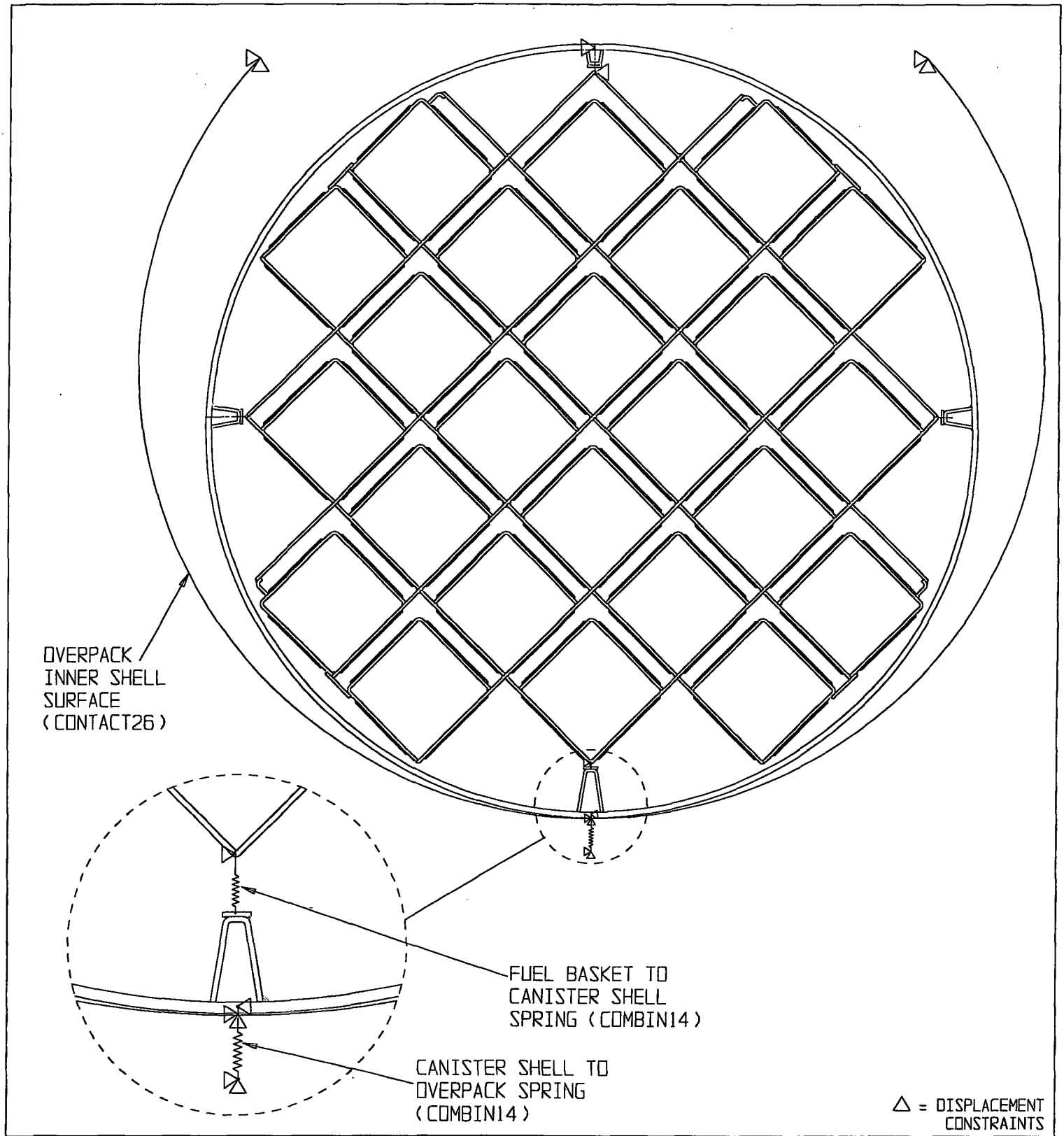

FIGURE 3.4.9; FINITE ELEMENT MODEL OF MPC-24

(45 DEGREE DROP MODEL)

REPORT HI-2012610

REVISION 0

DELETED

FIGURE 3.4.10; DELETED

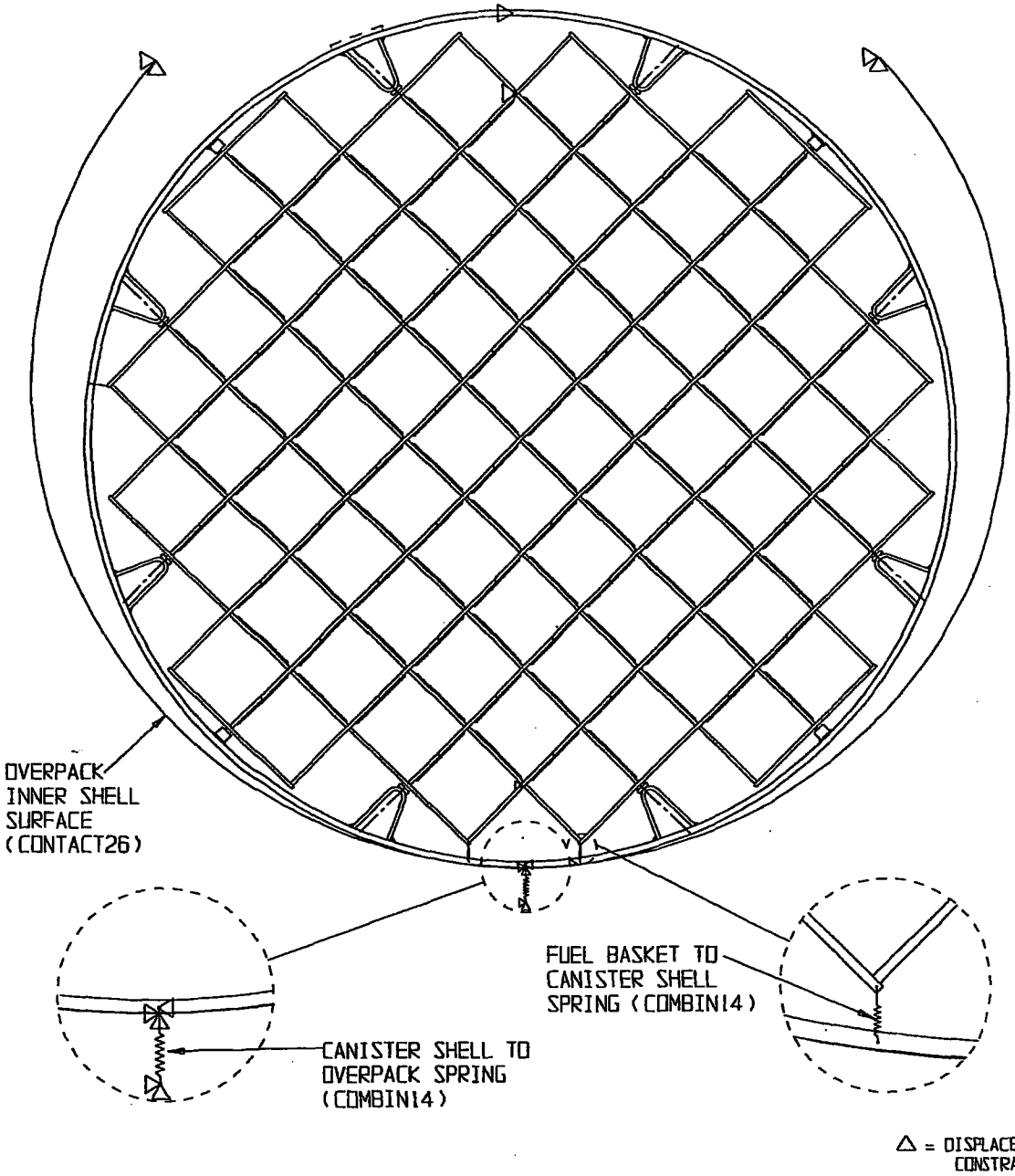

FIGURE 3.4.11: FINITE ELEMENT MODEL OF MPC-68

(45 DEGREE DROP MODEL)

REPORT HI-2012610

REVISION 0

e\PROJECTS\GENERIC\HI2012610\CH_3\3_4_11

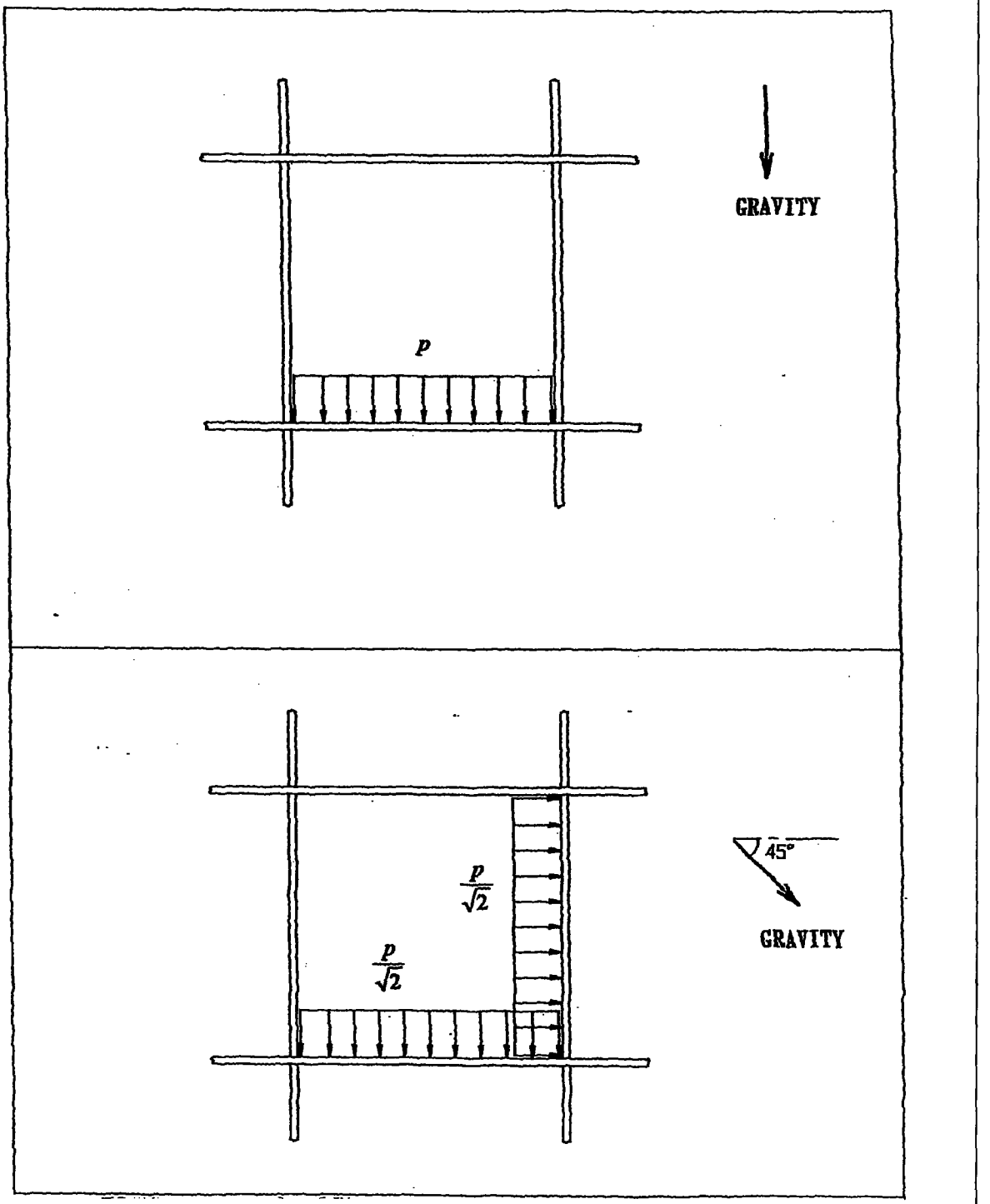

FIGURE 3.4.12: DETAIL OF FUEL ASSEMBLY PRESSURE LOAD ON MPC BASKET

REPORT HI-2012610

REVISION 0

e:\PROJECTS\GENERIC\HI2012610\CH_3\3_4_12

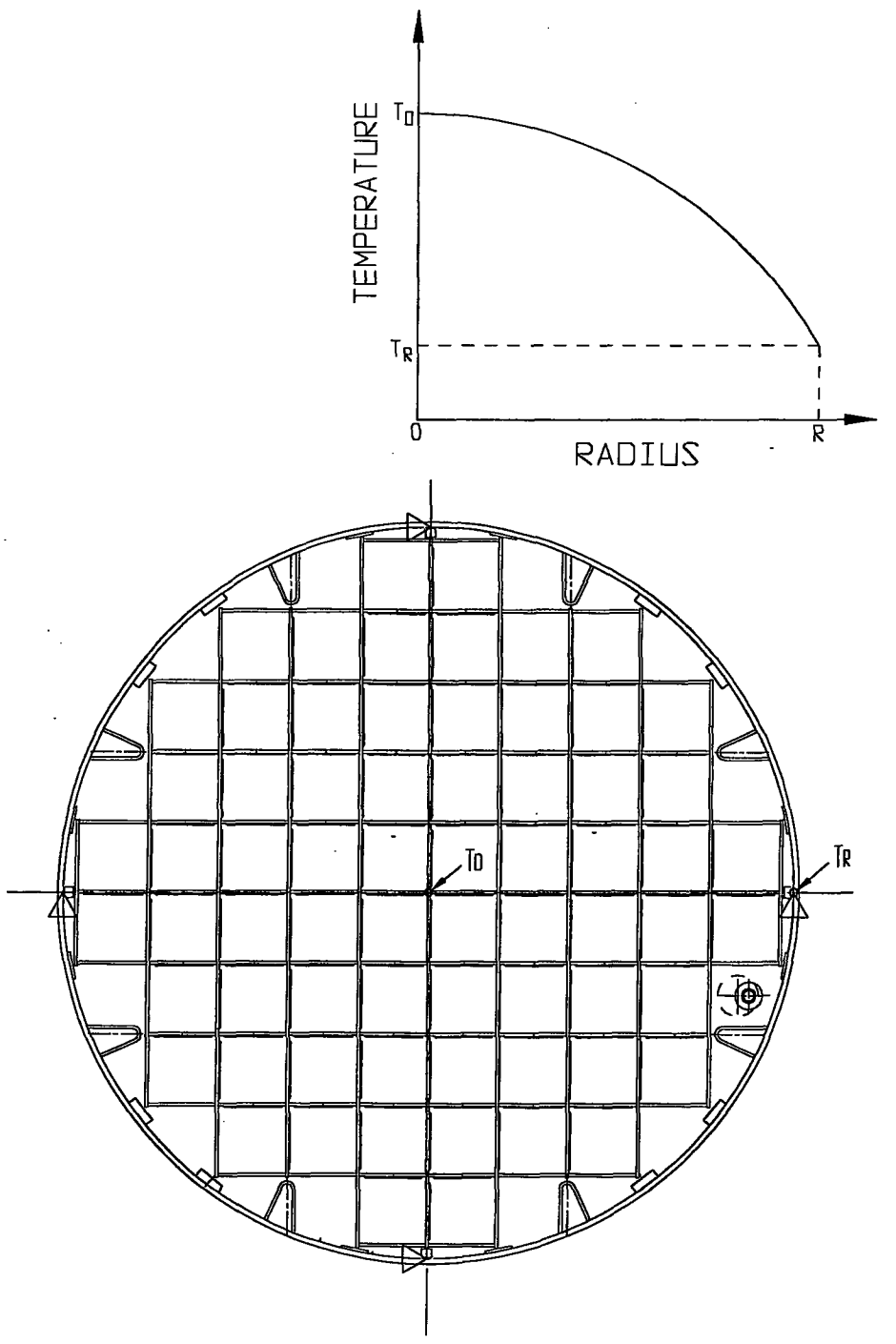

FIGURE 3.4.13; MPC THERMAL LOAD

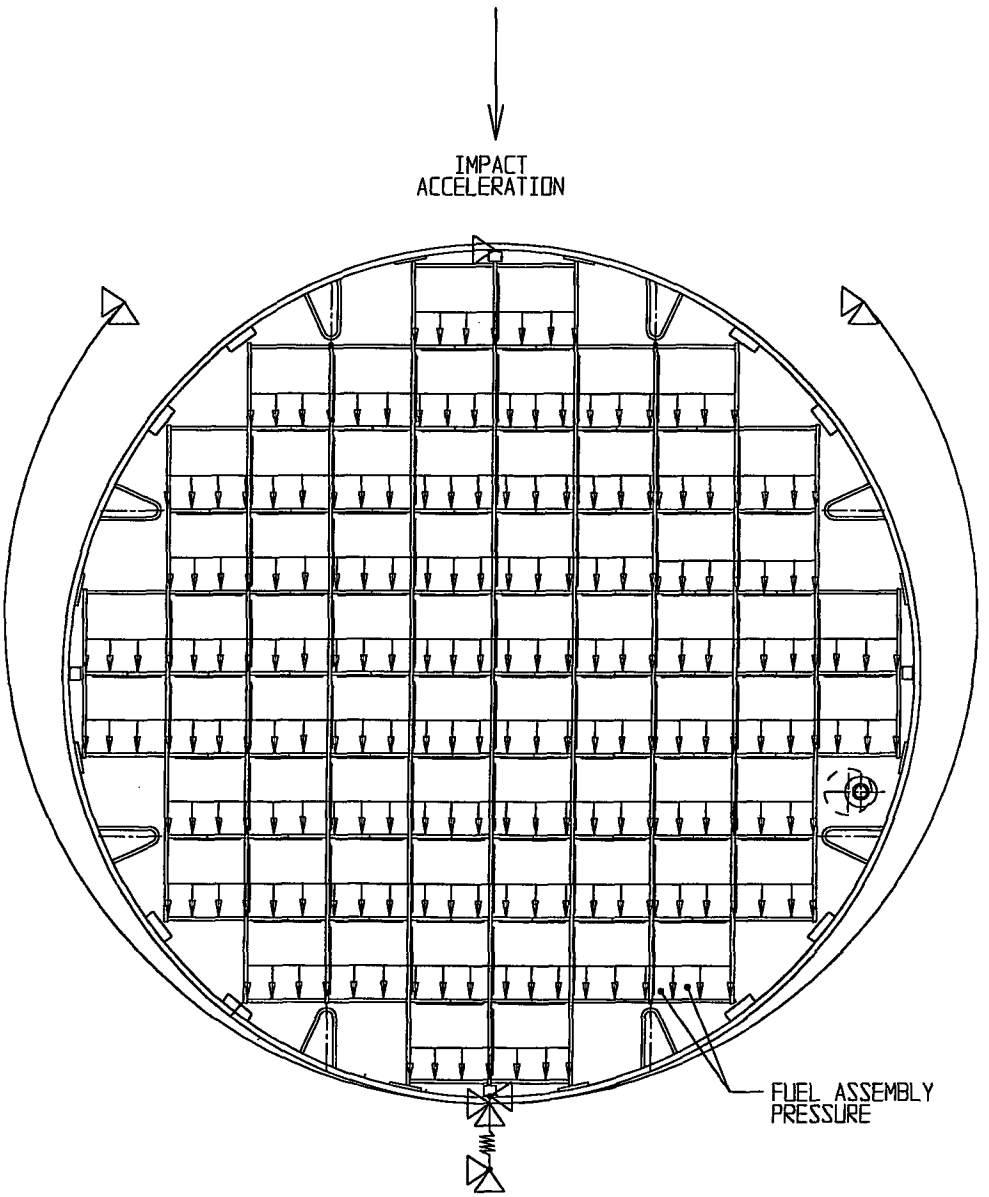

FIGURE 3.4.14; 0 DEGREE SIDE DROP OF MPC

REPORT HI-2012610 | REVISION 0

\PROJECTS\GENERIC\HI2012610\CH. 3\3_4_14

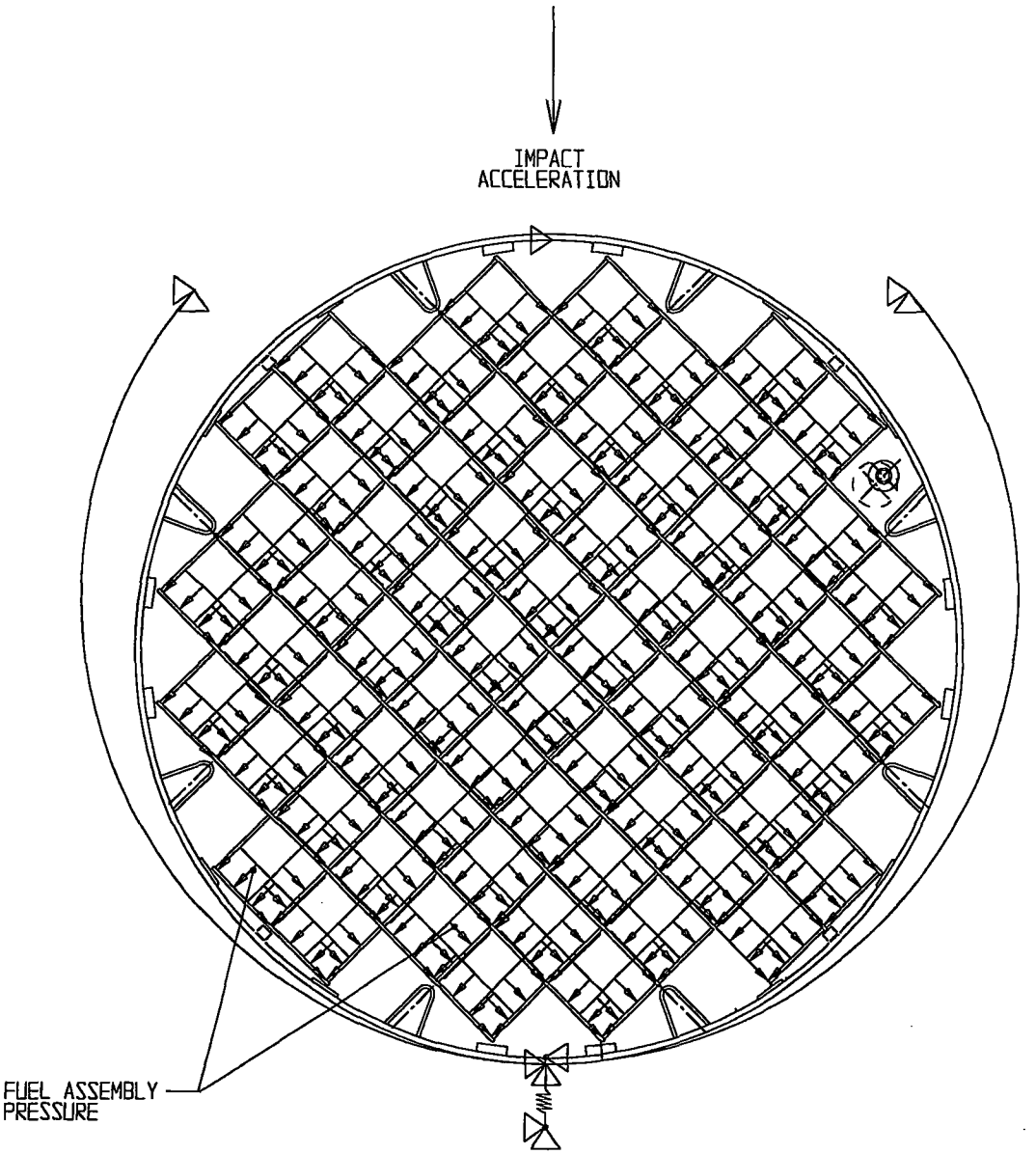

FIGURE 3.4.15; 45 DEGREE SIDE DROP OF MPC

REPORT HI-2012610 | REVISION 0

\PROJECTS\GENERIC\HI2012610\CH. 3\3_4_15

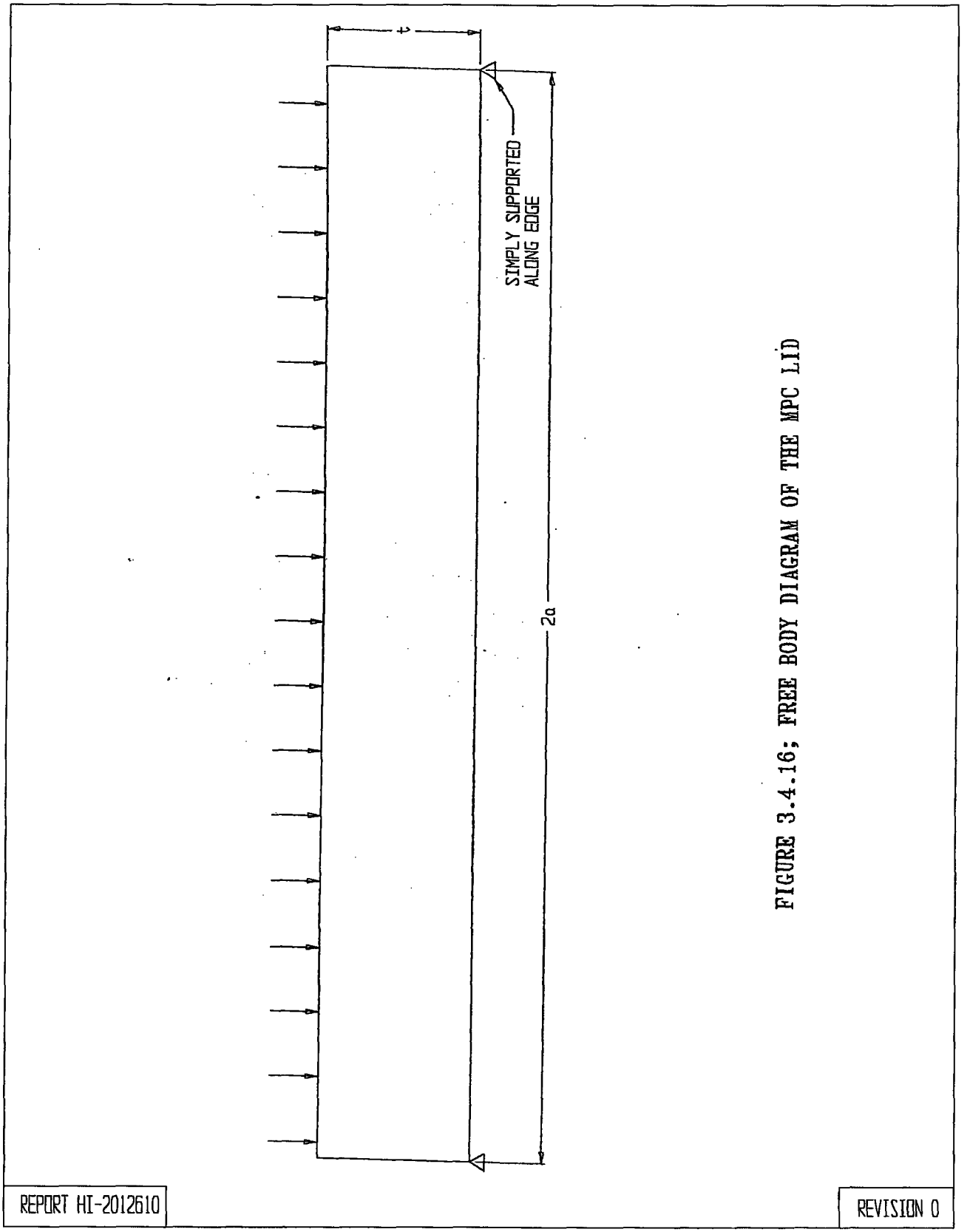

FIGURE 3.4.16; FREE BODY DIAGRAM OF THE MPC LID

e\PROJECTS\GENERIC\HI2012610\CH_3\3_4_16

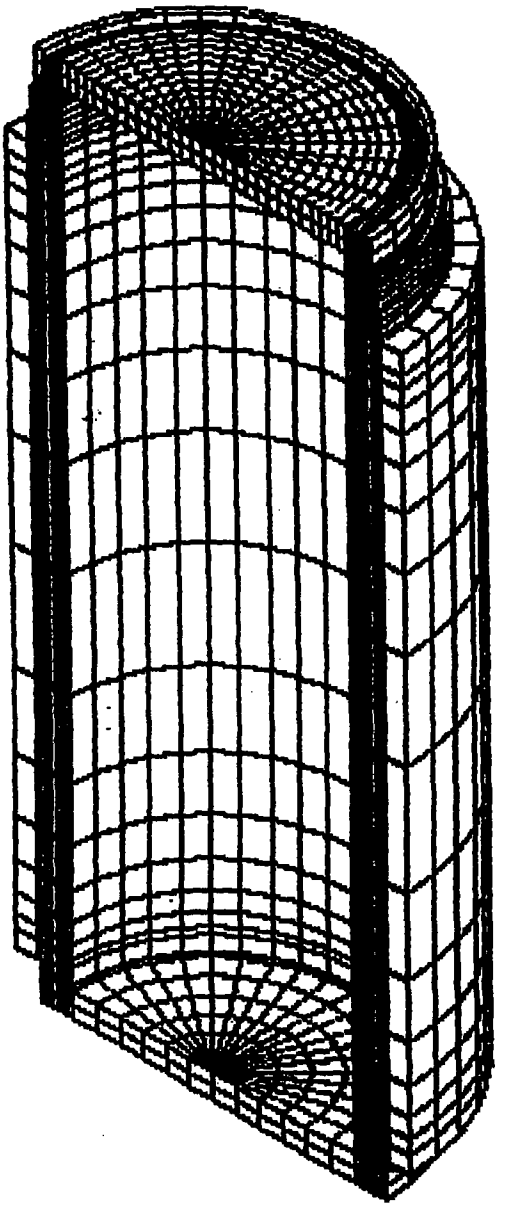

FIGURE 3.4.17; OVERPACK FINITE ELEMENT MODEL

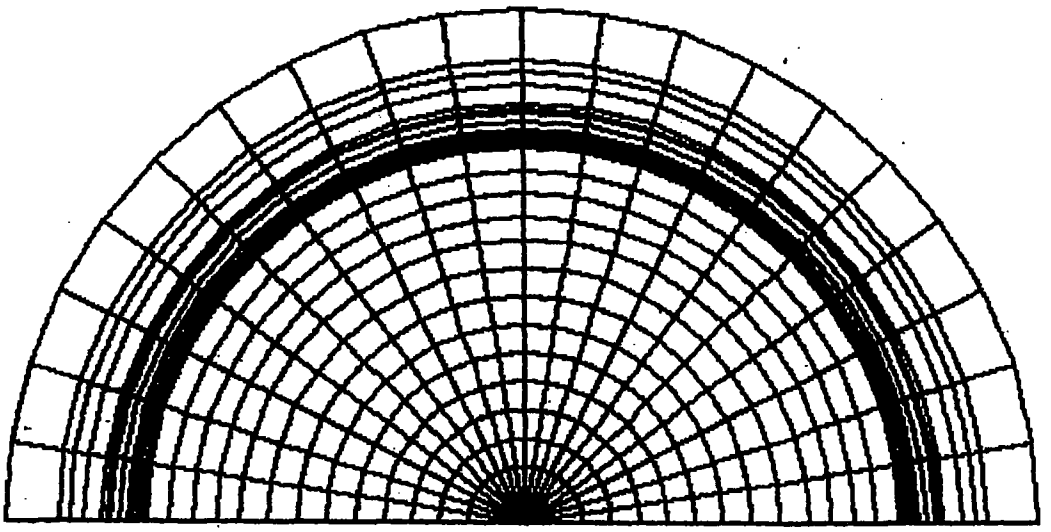

FIGURE 3.4.18; OVERPACK FINITE ELEMENT MODEL

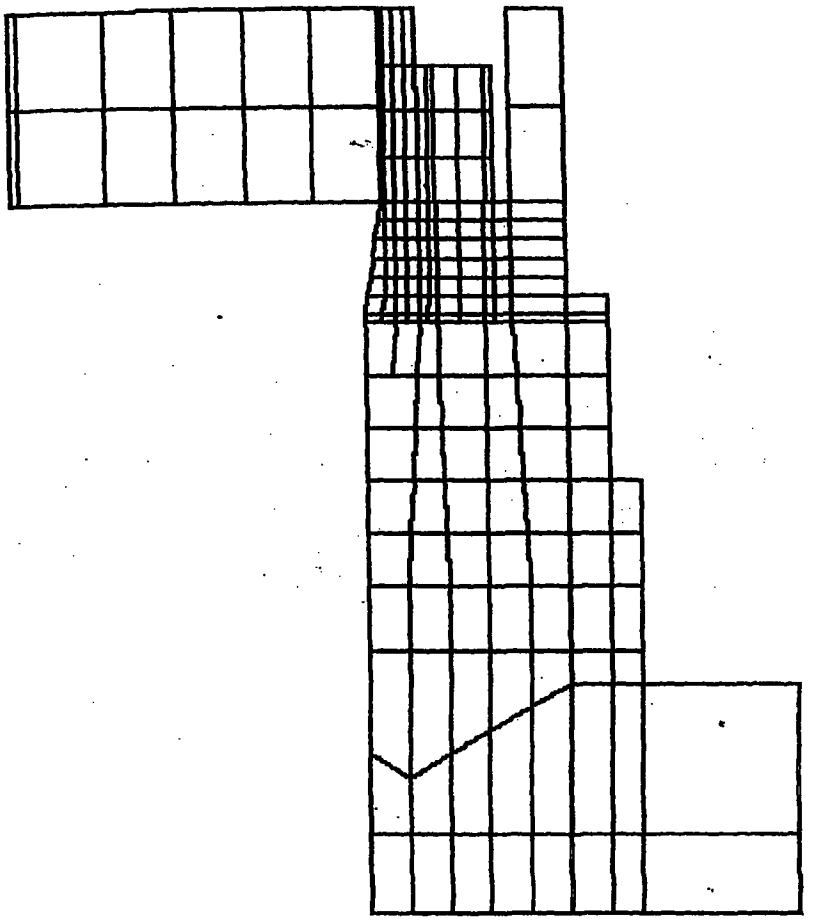

FIGURE 3.4.19; OVERPACK FINITE ELEMENT MODEL

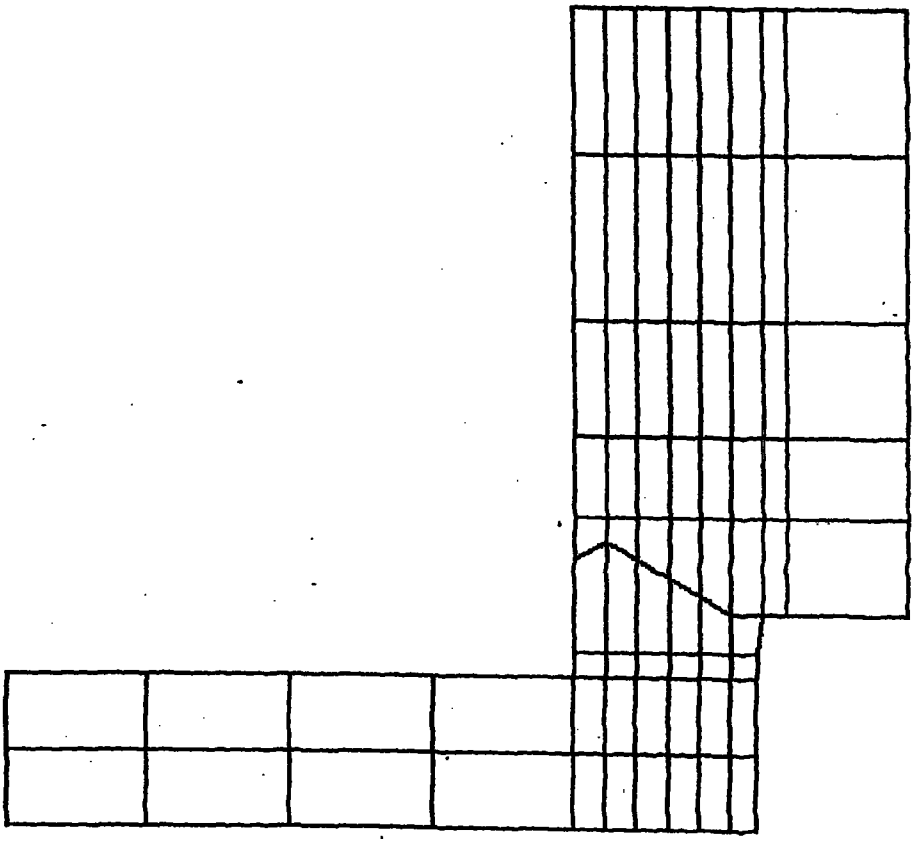

FIGURE 3.4.20; OVERPACK FINITE ELEMENT MODEL

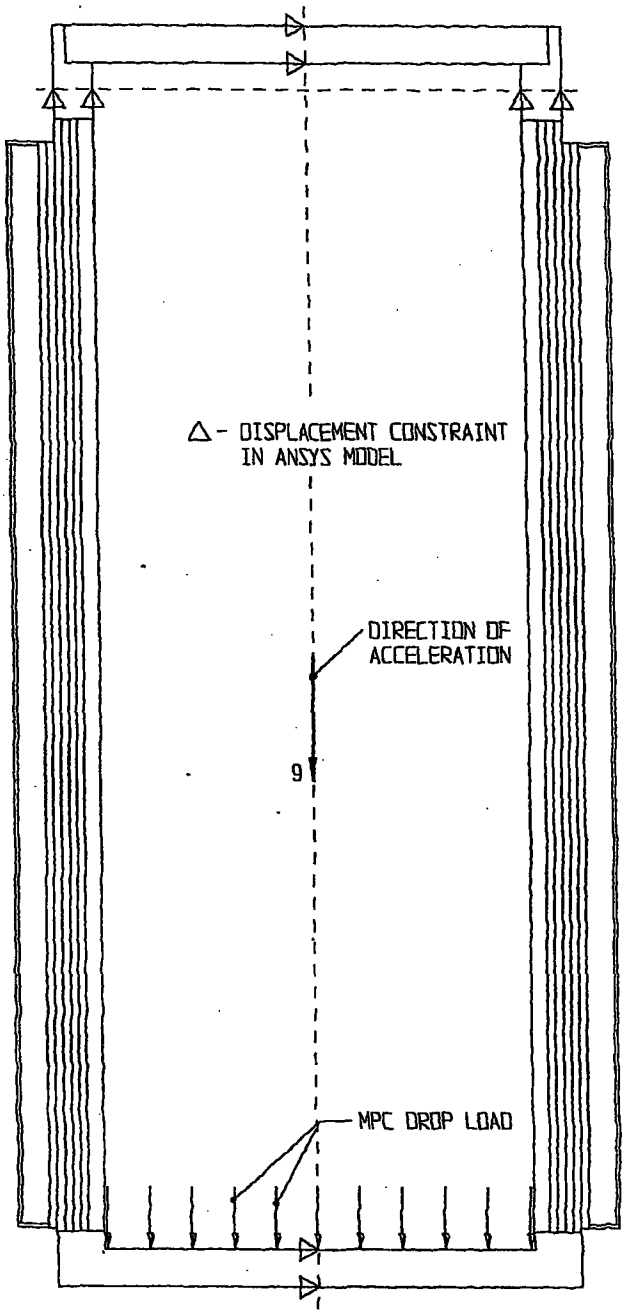

FIGURE 3.4.21; FREE BODY DIAGRAM OF OVERPACK - BOTTOM END DROP

REPORT HI-2012610 REVISION 0

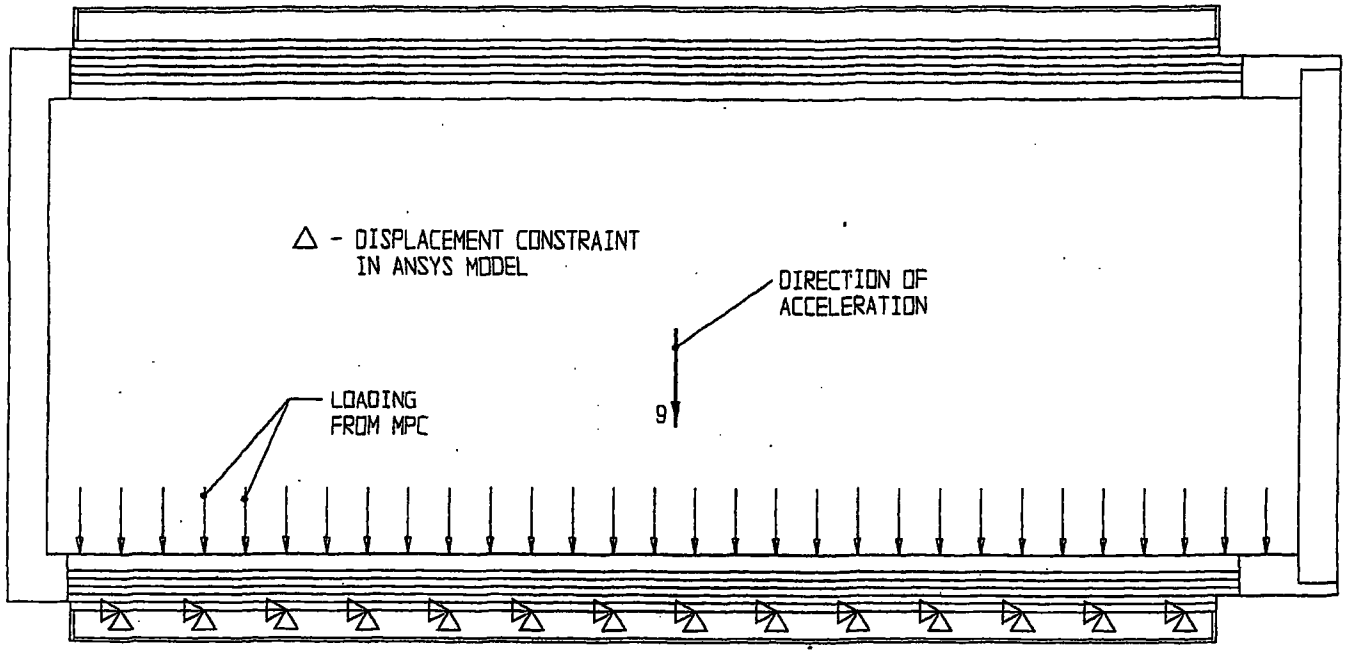

FIGURE 3.4.22; FREE BODY DIAGRAM OF OVERPACK - SIDE DROP

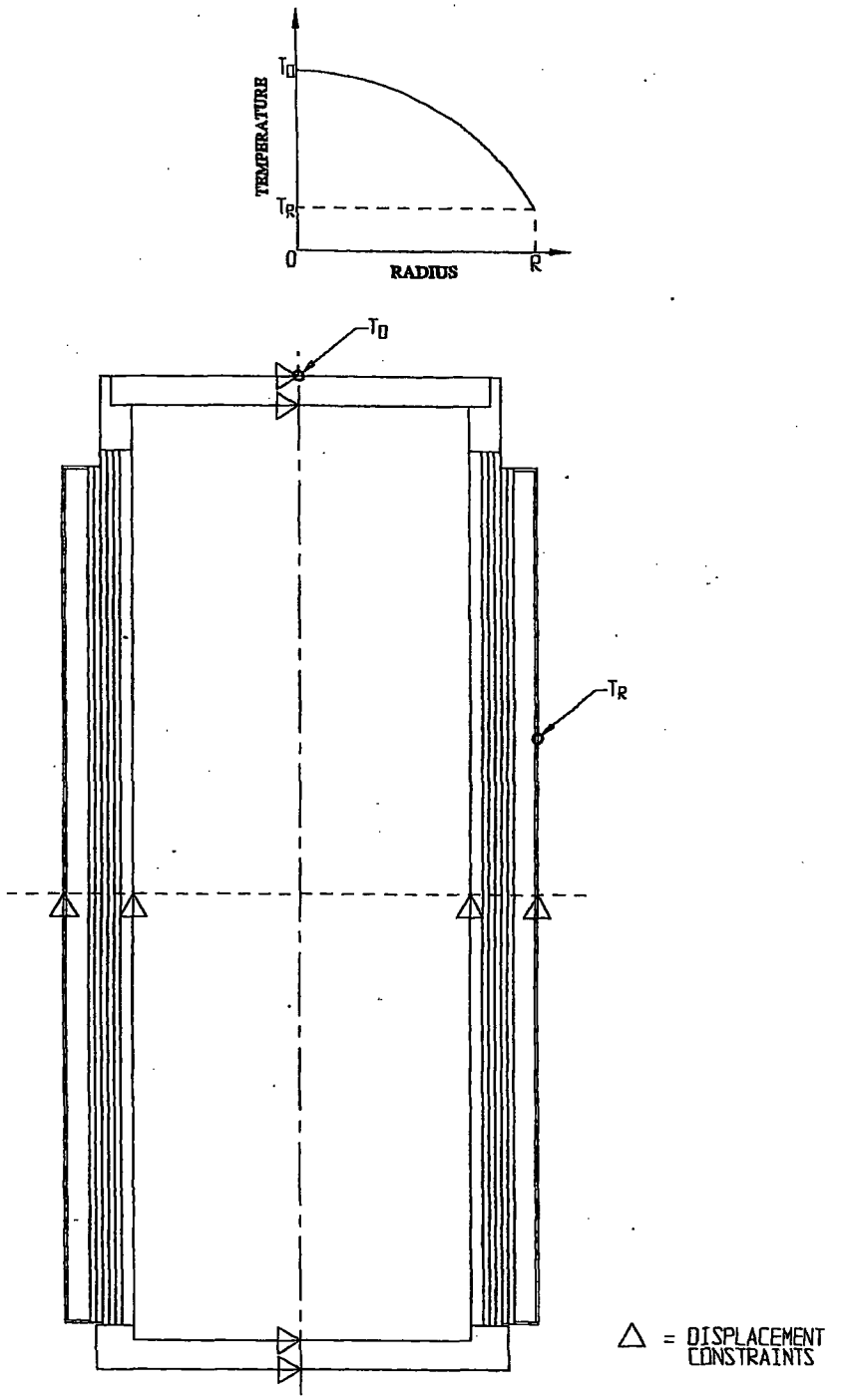

FIGURE 3.4.23; FREE BODY DIAGRAM OF OVERPACK - THERMAL LOAD

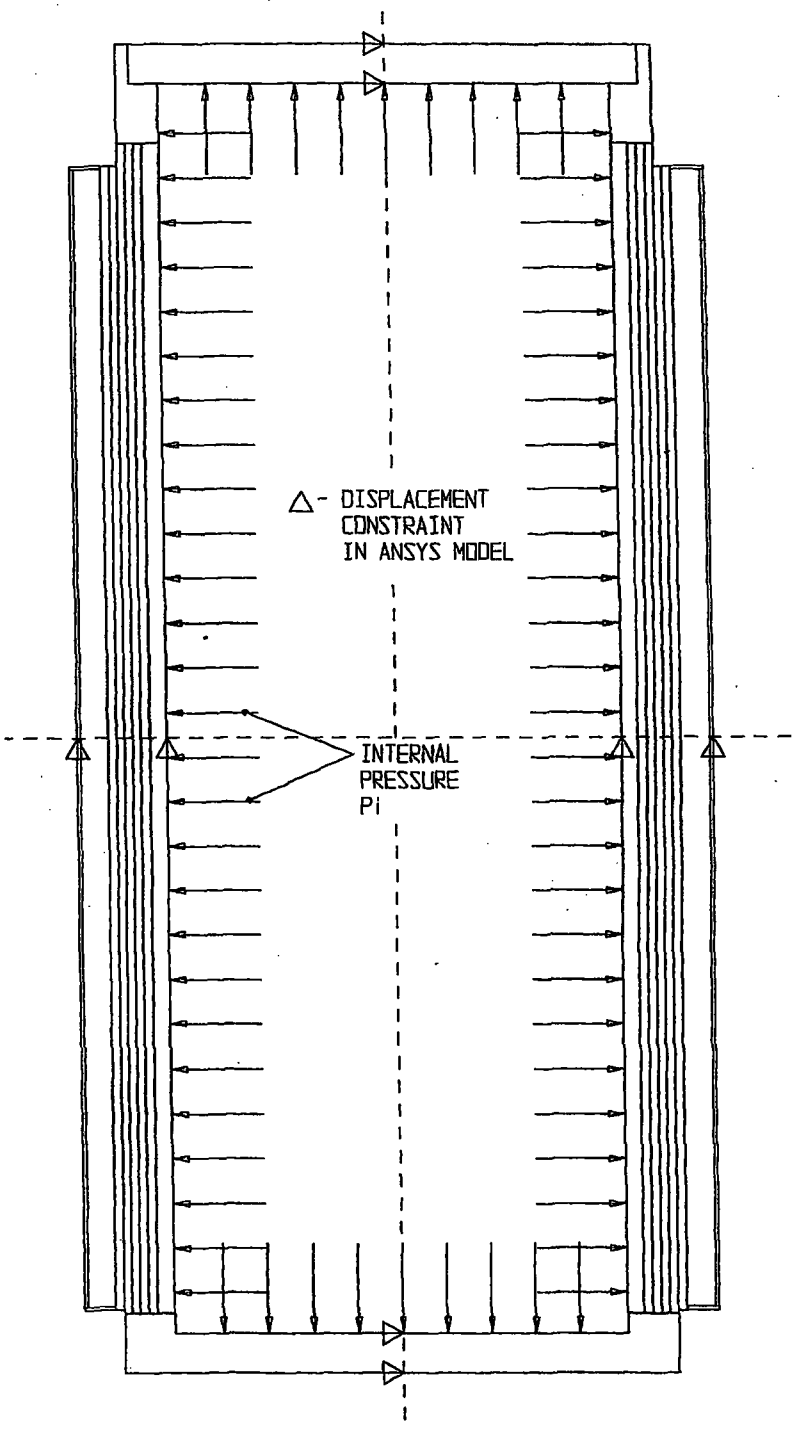

FIGURE 3.4.24; FREE BODY DIAGRAM OF OVERPACK - INTERNAL PRESSURE

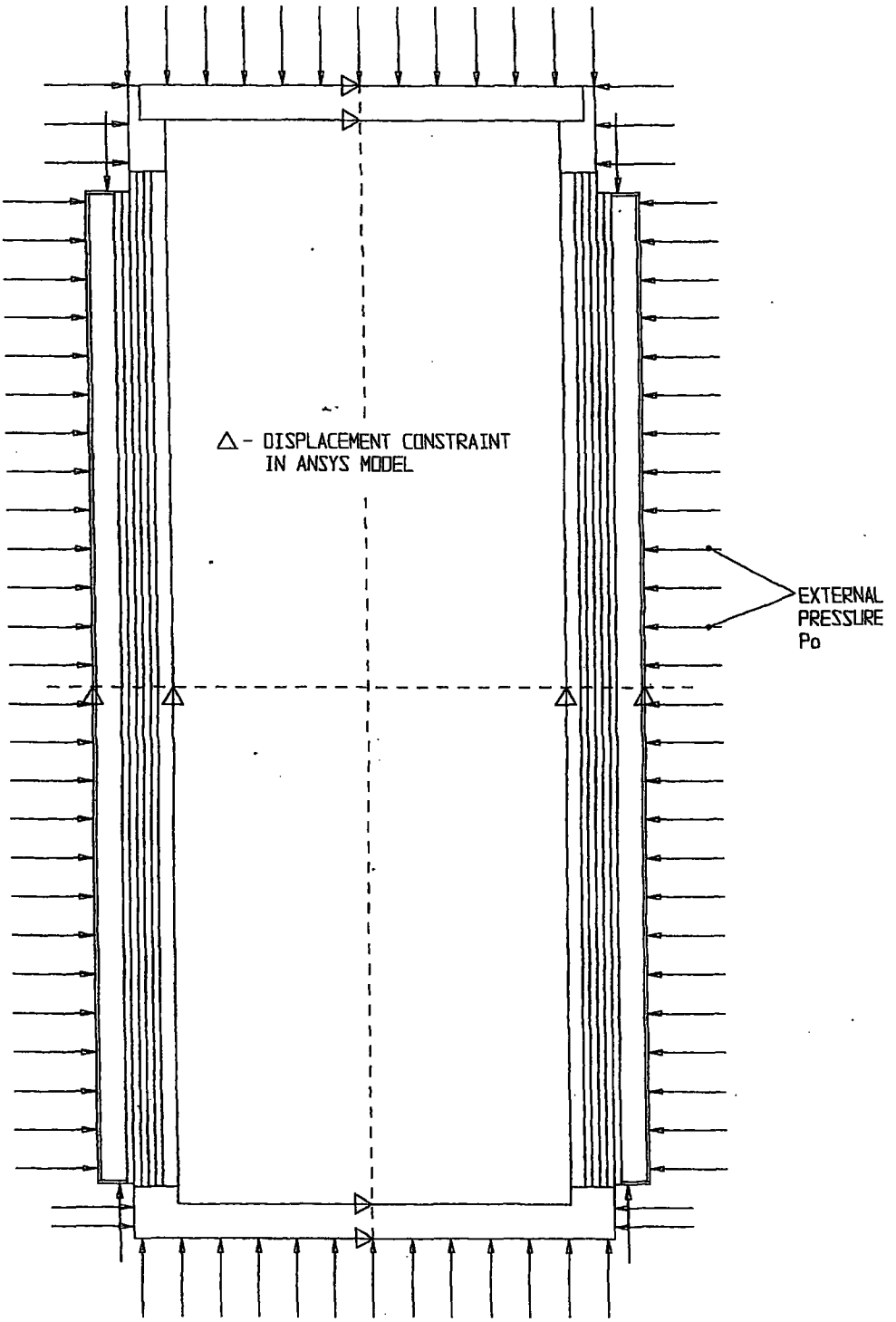

FIGURE 3.4.25: FREE BODY DIAGRAM OF OVERPACK - EXTERNAL PRESSURE

REPORT HI-2012610 REVISION 0

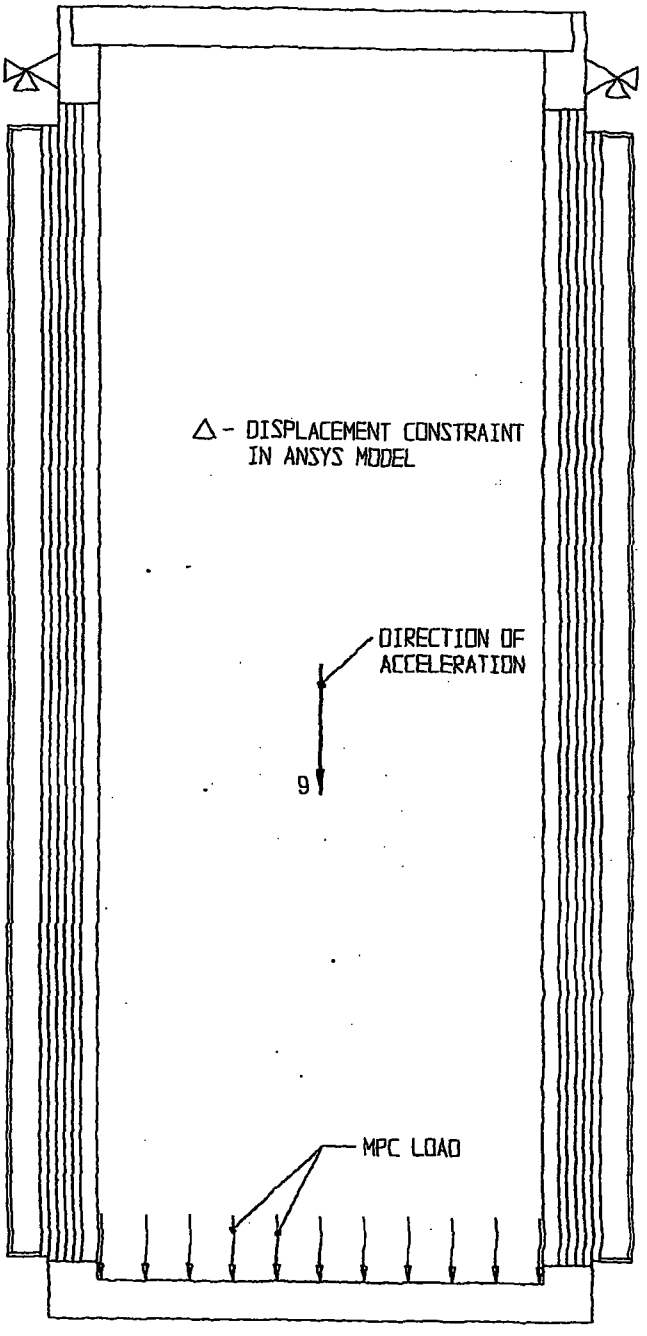

FIGURE 3.4.26; FREE BODY DIAGRAM OF OVERPACK - HANDLING LOAD

REPORT HI-2012610

REVISION 0

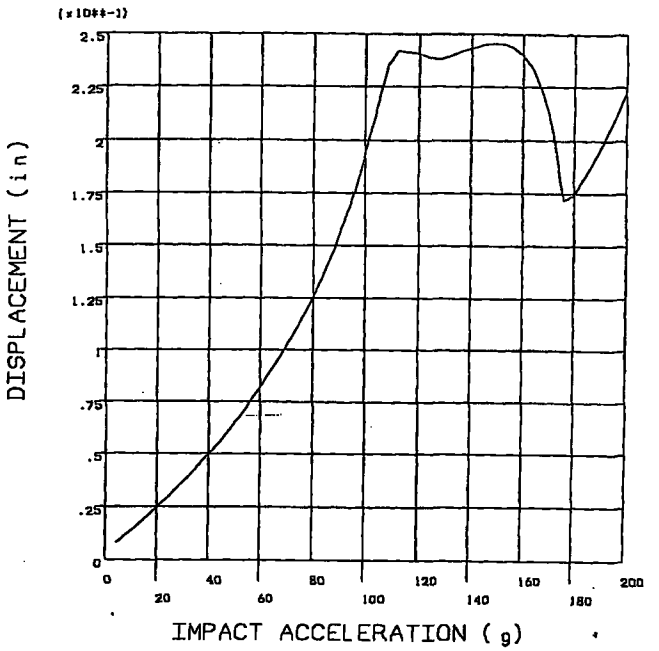

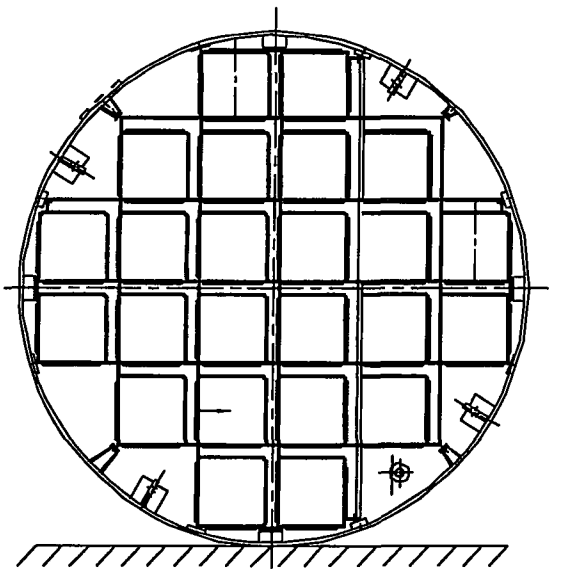

FIGURE 3.4.27; NON-LINEAR BUCKLING ANALYSIS FOR MPC-24 DISPLACEMENT Vs. IMPACT ACCELERATION (0° DROP)

REPORT HI-2012610 REVISION 0

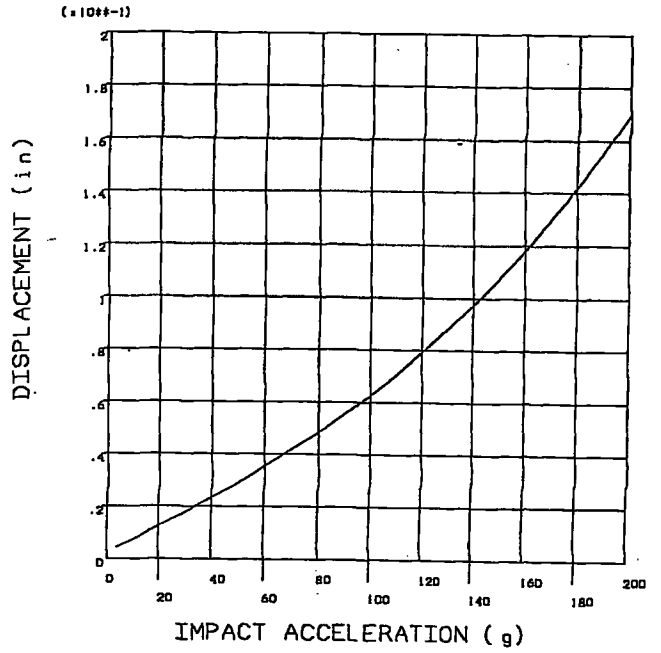

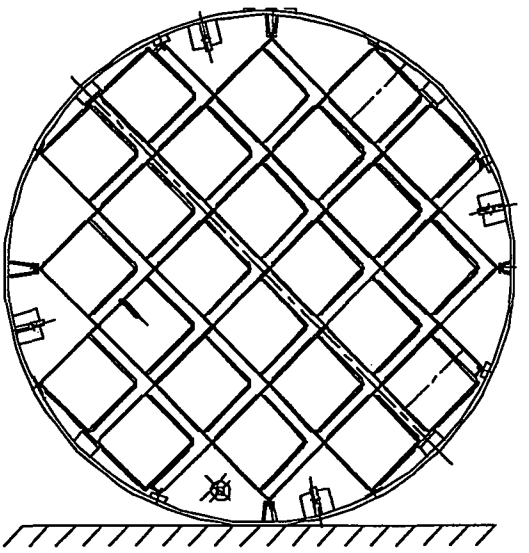

FIGURE 3.4.28; NON-LINEAR BUCKLING ANALYSIS FOR MPC-24
DISPLACEMENT Vs. IMPACT ACCELERATION (45° DROP)

REPORT HI-2012610 REVISION 0

DELETED

FIGURE 3.4.29;

DELETED

FIGURE 3.4.30;

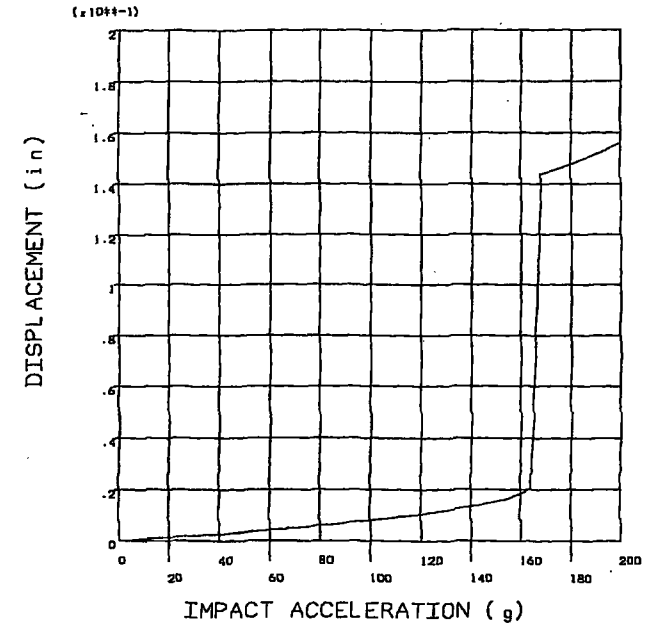

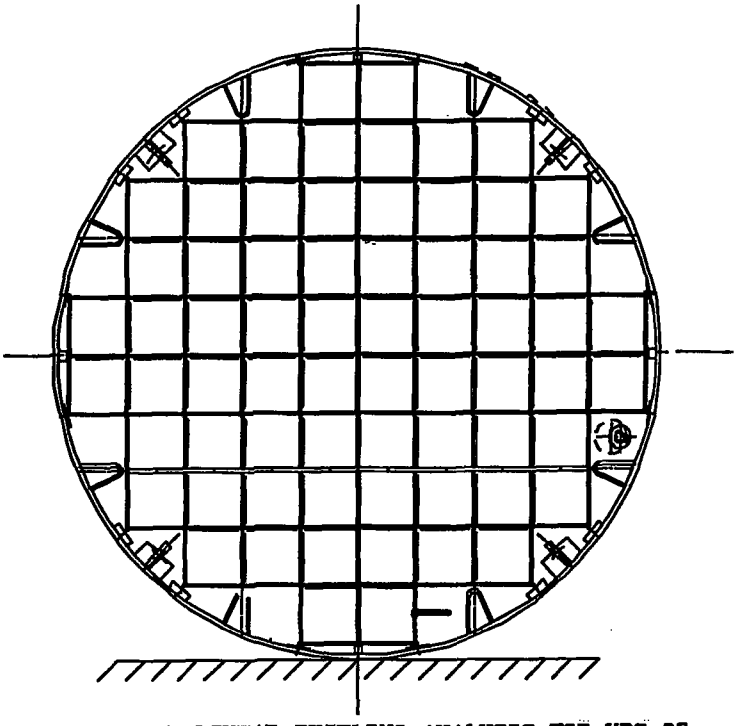

FIGURE 3.4.31; NON-LINEAR BUCKLING ANALYSIS FOR MPC-68 DISPLACEMENT Vs. IMPACT ACCELERATION (0° DROP)

REPORT HI-2012610 REVISION 0

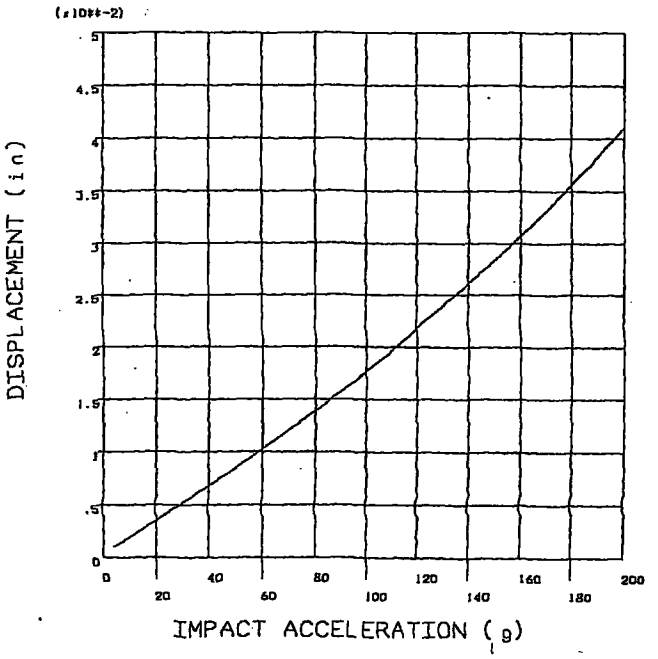

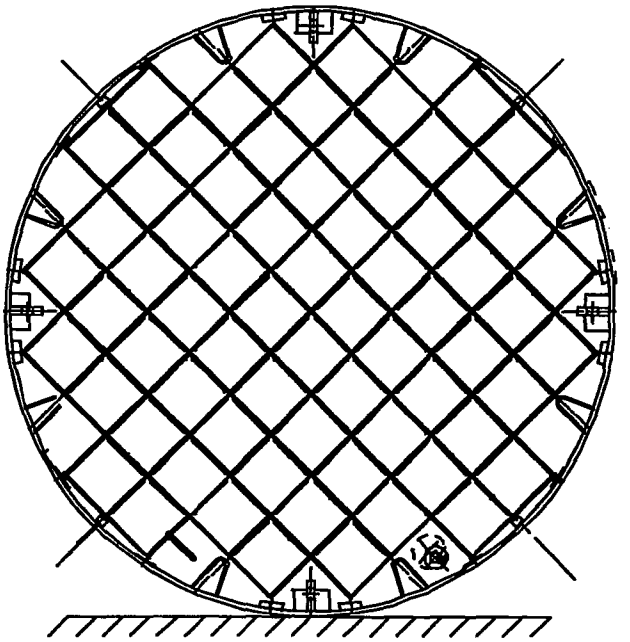

FIGURE 3.4.32; NON-LINEAR BUCKLING ANALYSIS FOR MPC-68 DISPLACEMENT Vs. IMPACT ACCELERATION (45° DROP)

REPORT HI-2012610 REVISION 0

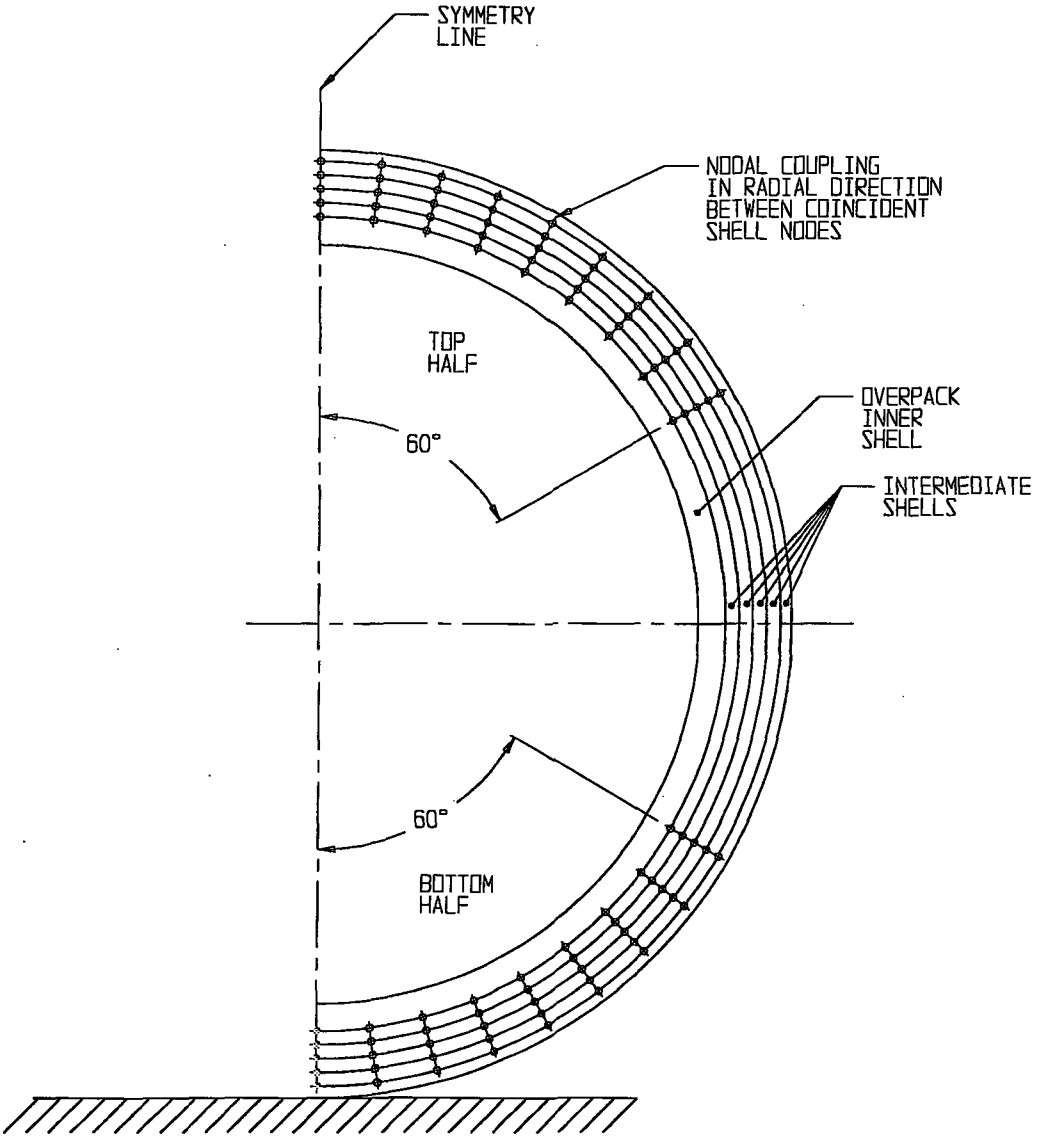

FIGURE 3.4.33; NODAL COUPLING IN OVERPACK
FINITE ELEMENT MODEL

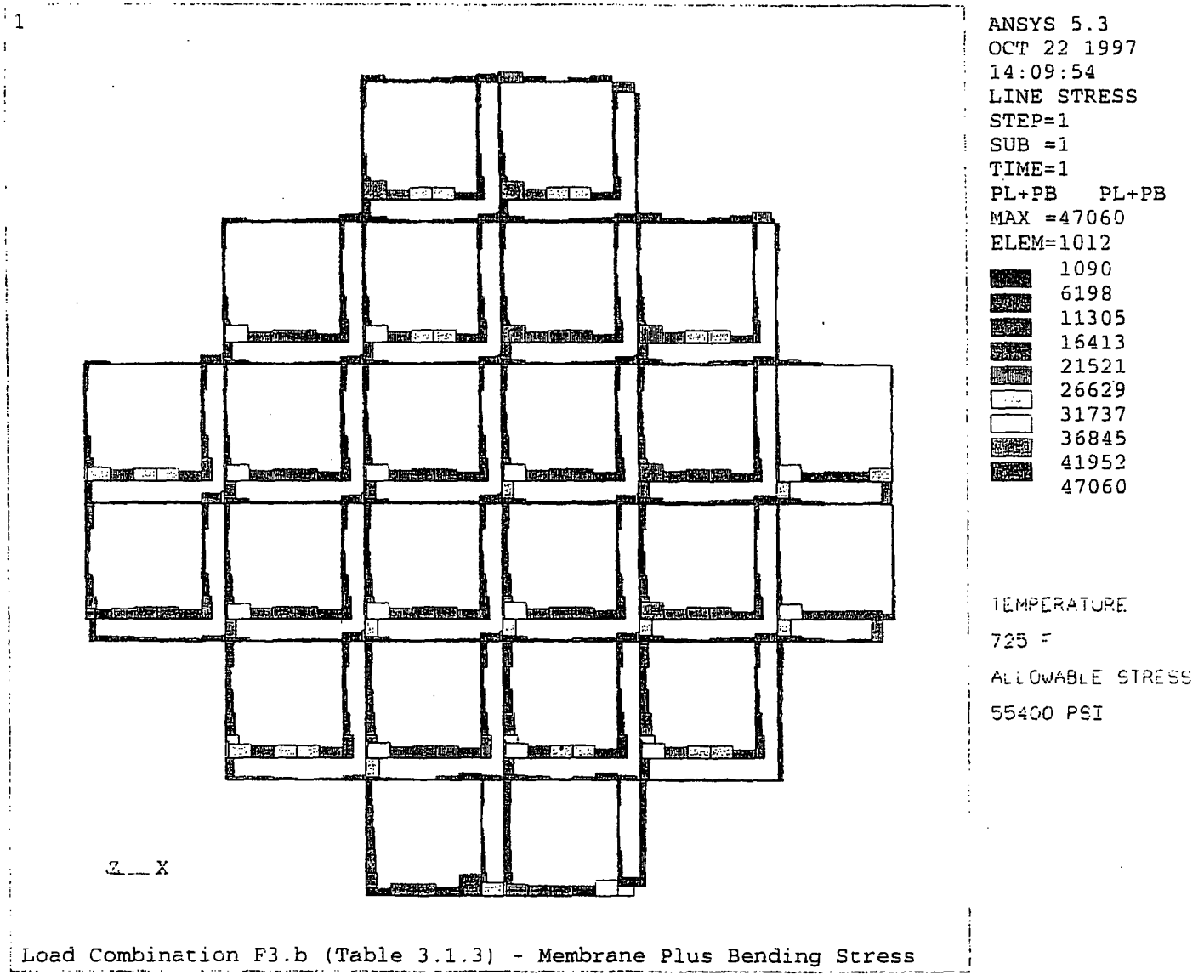

FIGURE 3.4.34: CRITICAL STRESS RESULTS FOR THE MPC-24

DELETED

FIGURE 3.4.35;

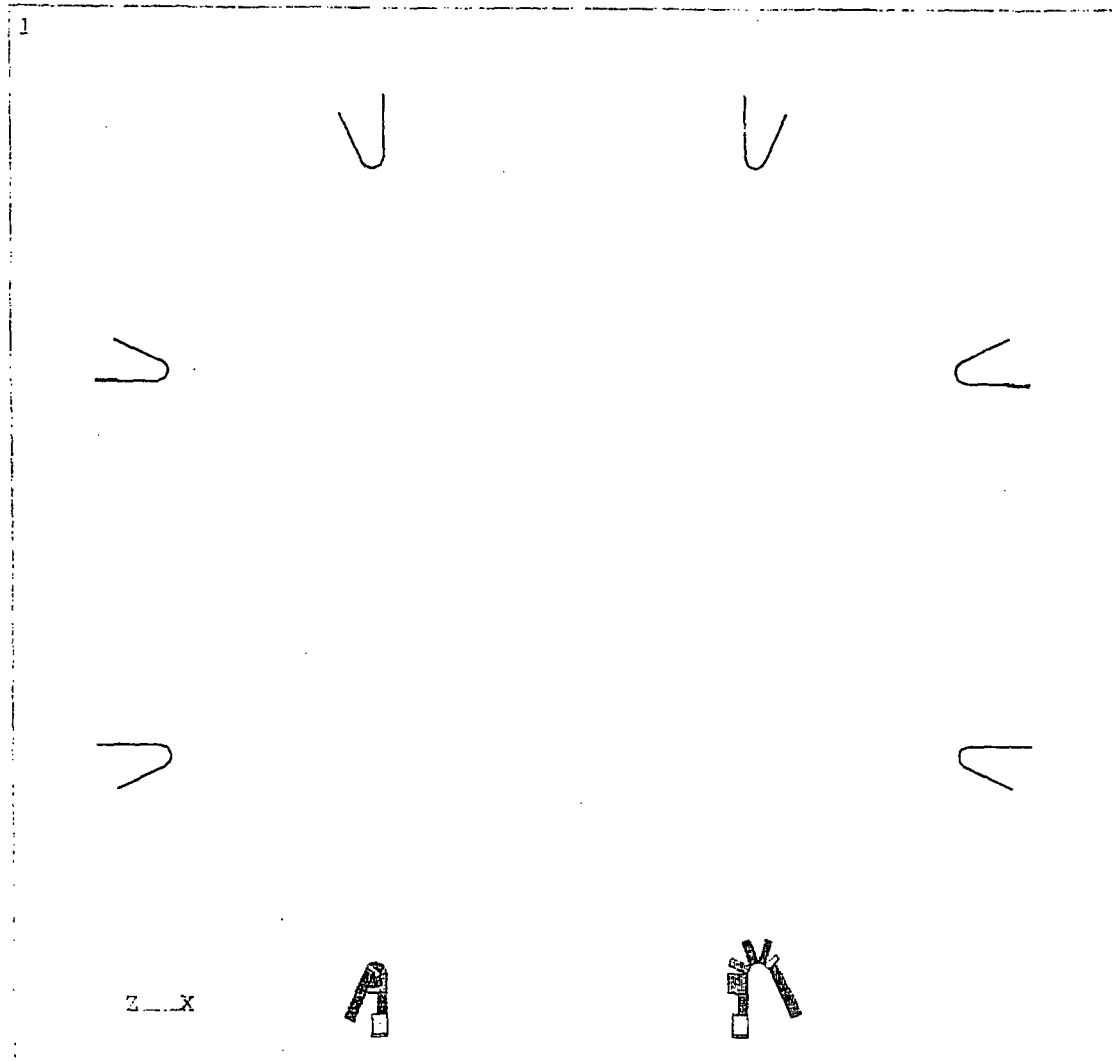

Load Combination E3.b (Table 3.1.3) - Membrane Plus Bending Stress

FIGURE 3.4.36; CRITICAL STRESS RESULTS FOR THE MPC-68

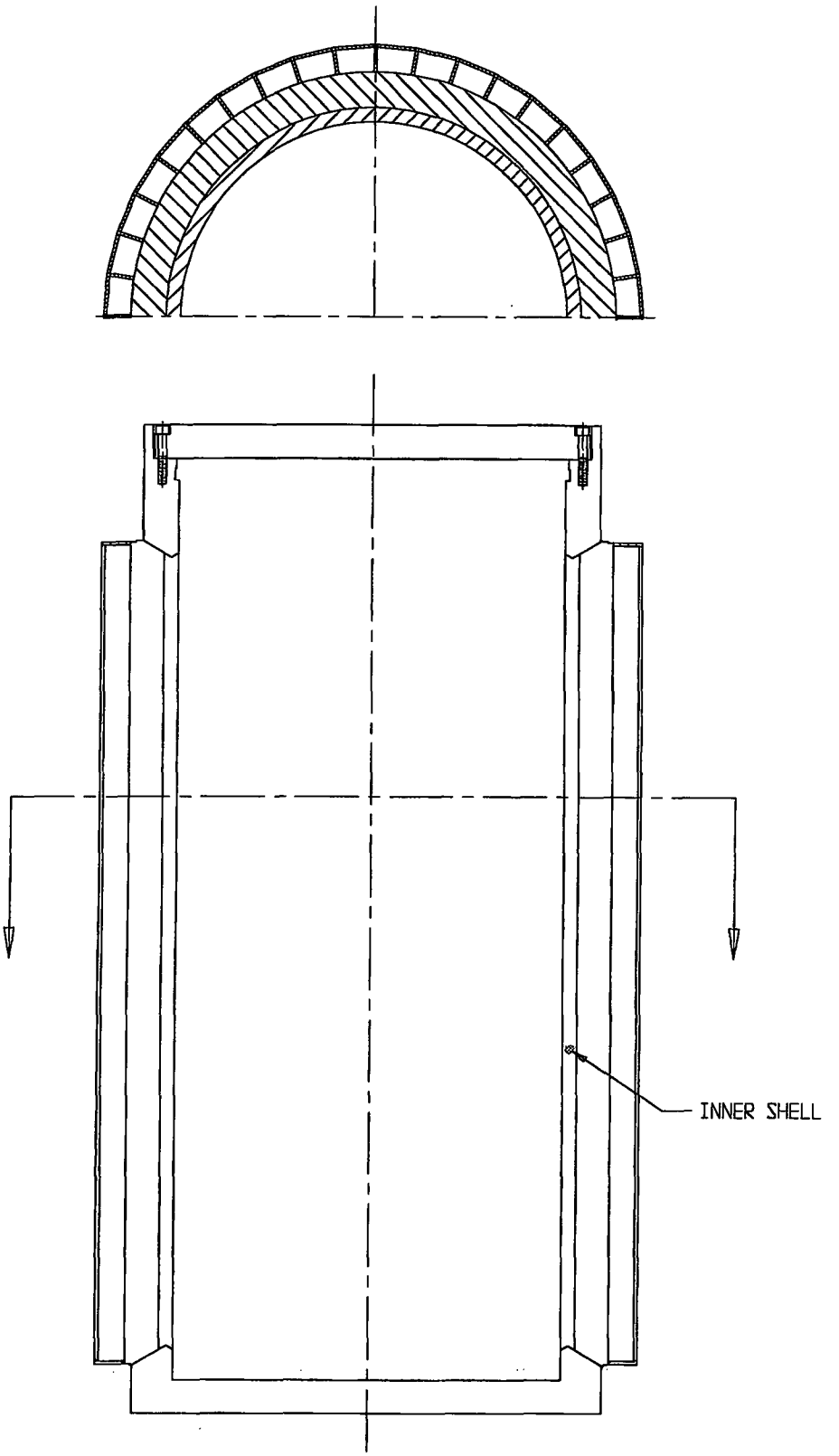

FIGURE 3.4.37; LOCATION OF MINIMUM SAFETY FACTOR FOR LOAD CASE 01

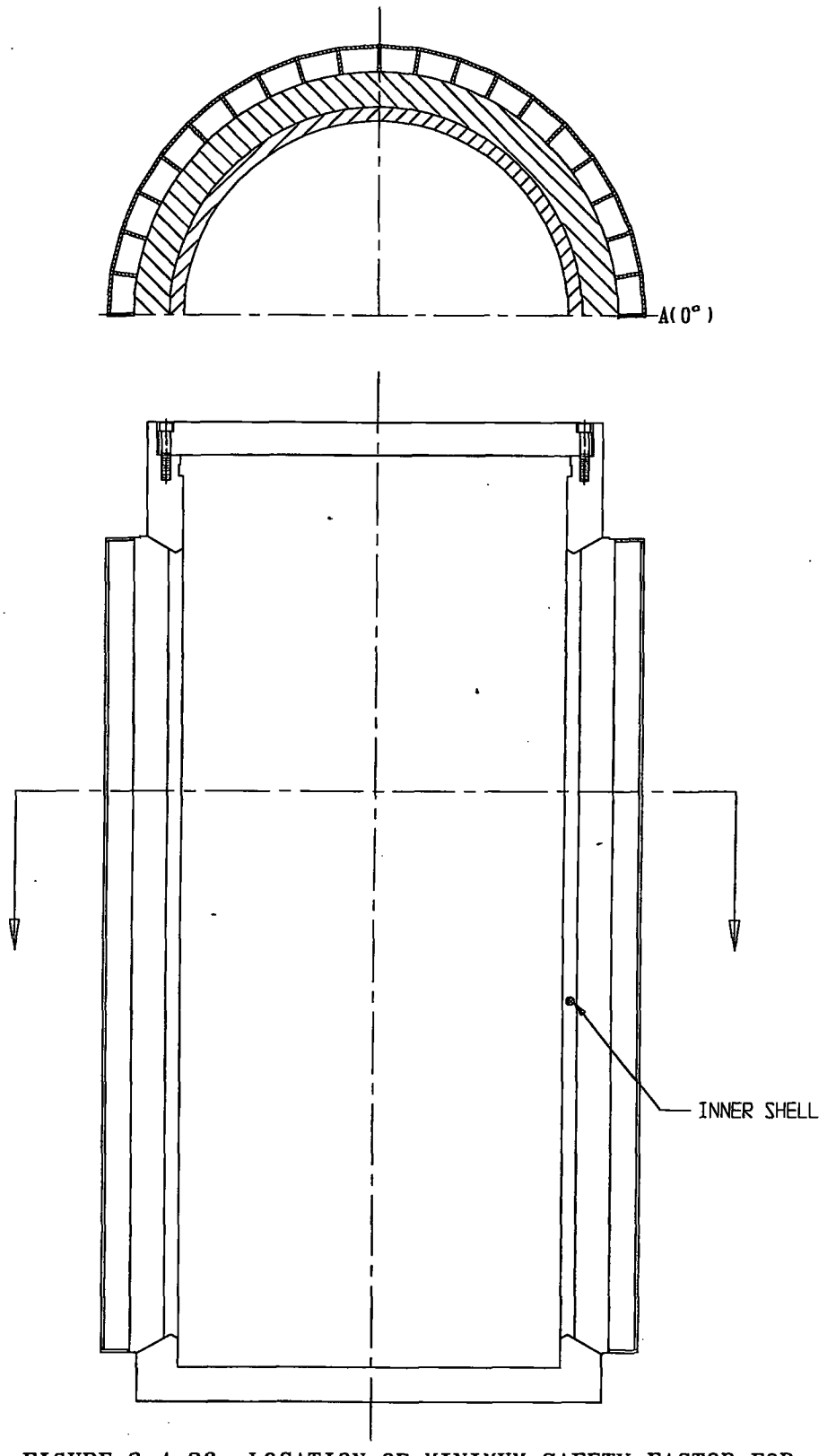

FIGURE 3.4.38; LOCATION OF MINIMUM SAFETY FACTOR FOR LOAD CASE 02

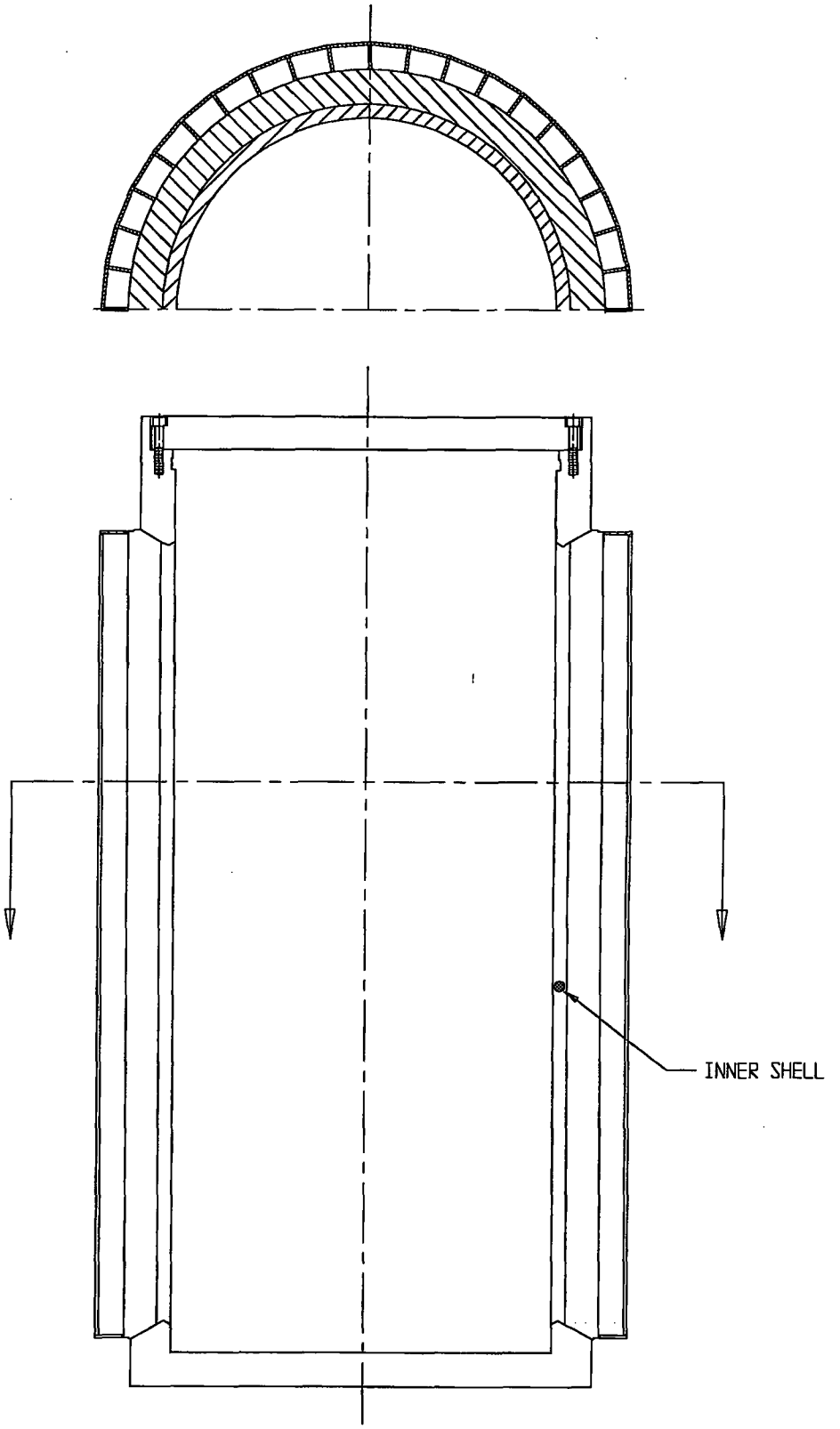

FIGURE 3.4.39; LOCATION OF MINIMUM SAFETY FACTOR FOR LOAD CASE 03

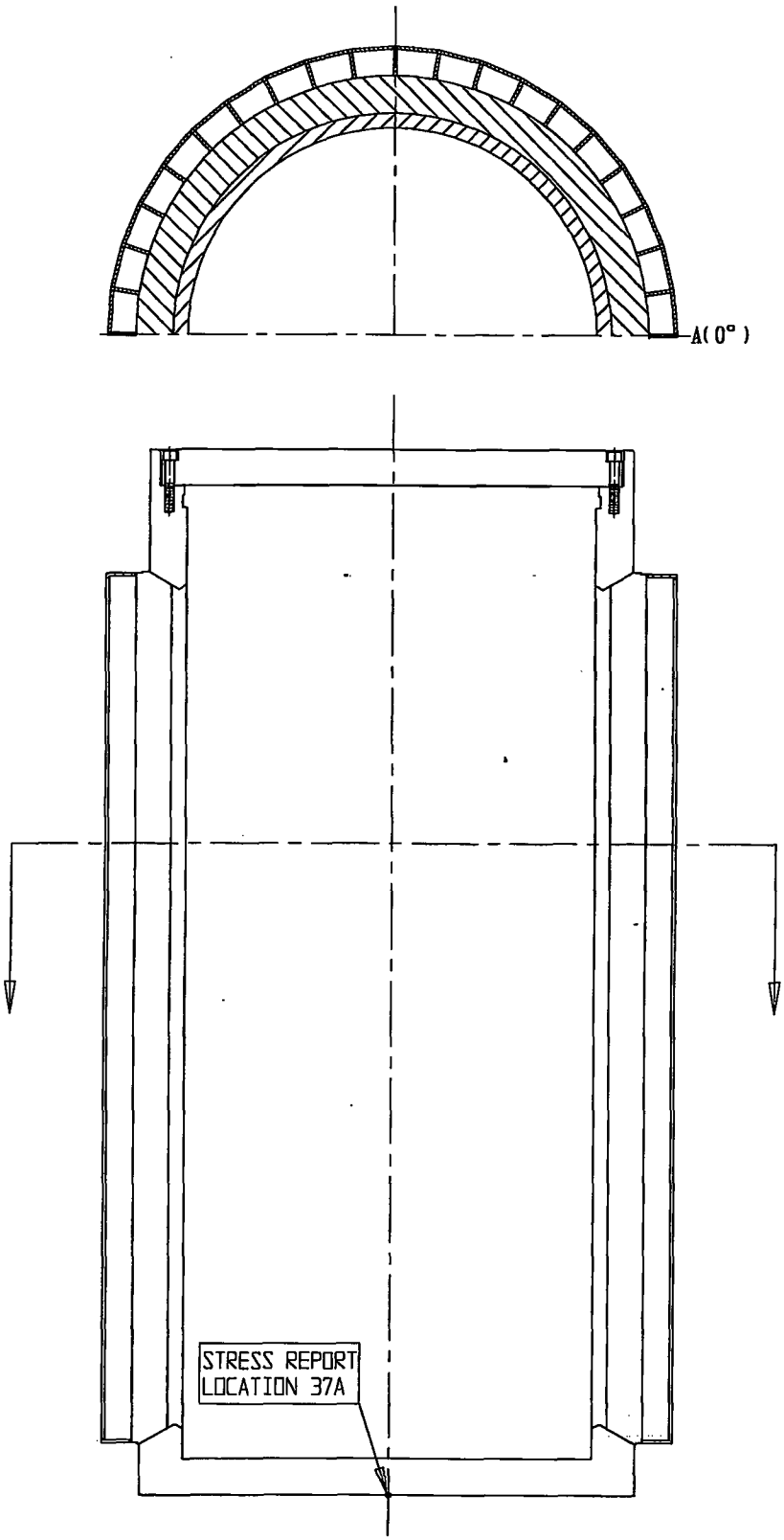

FIGURE 3.4.40; LOCATION OF MINIMUM SAFETY FACTOR FOR LOAD CASE 04.a

REPORT HI-2012610

REVISION 0

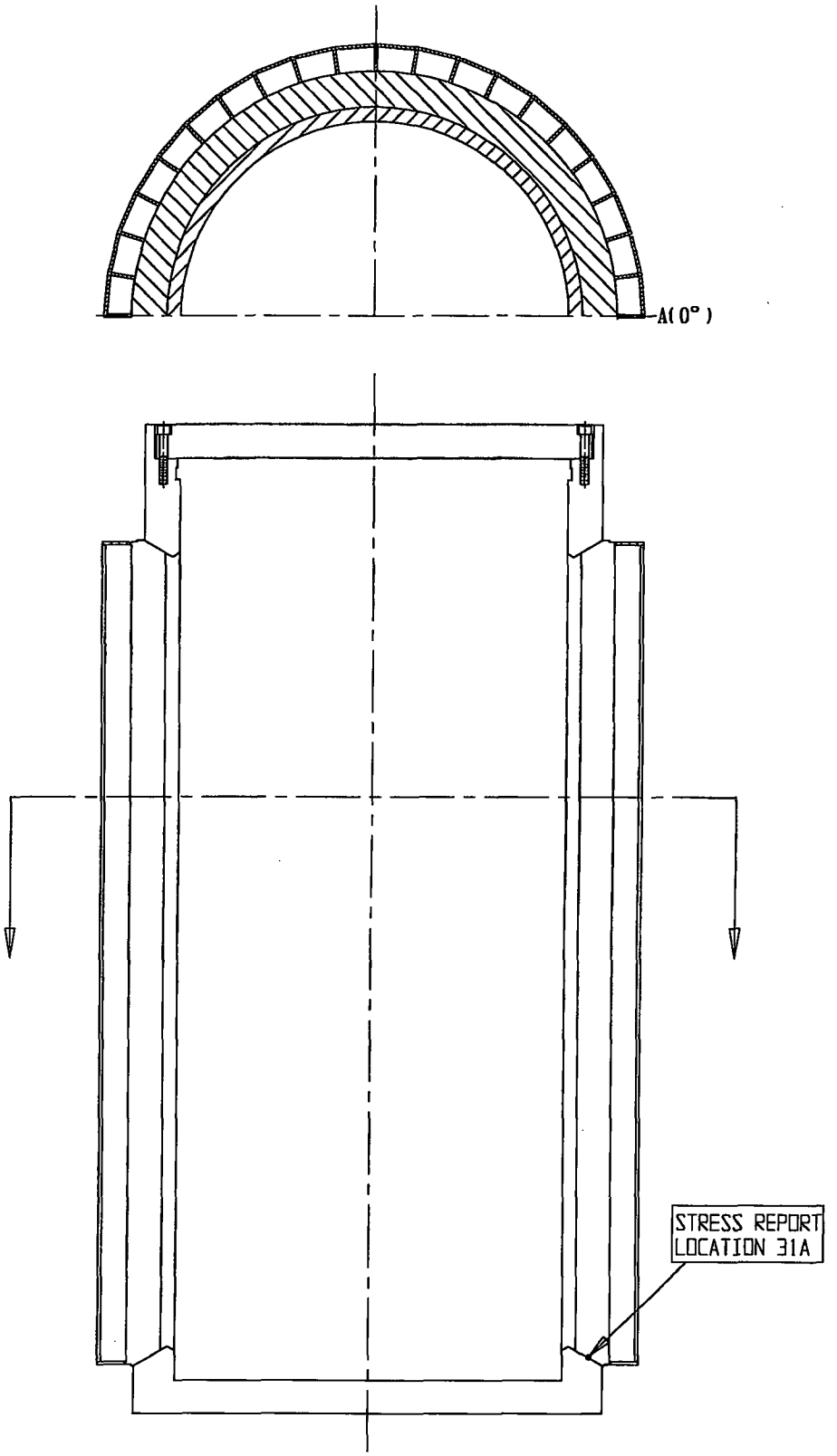

FIGURE 3.4.41; LOCATION OF MINIMUM SAFETY FACTOR FOR LOAD CASE 04.b

REPORT HI-2012610 REVISION 0

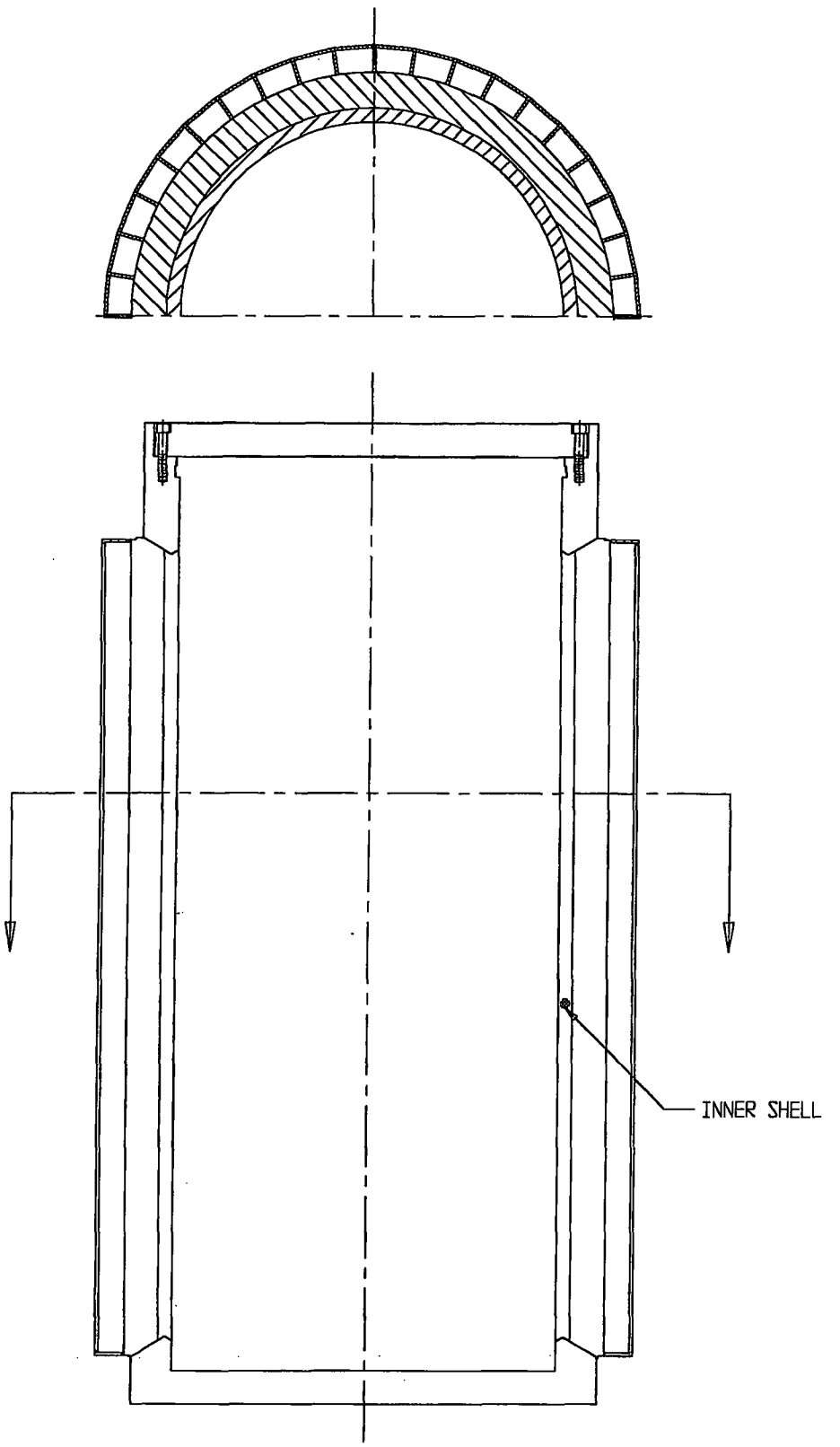

FIGURE 3.4.42; LOCATION OF MINIMUM SAFETY FACTOR FOR LOAD CASE 05

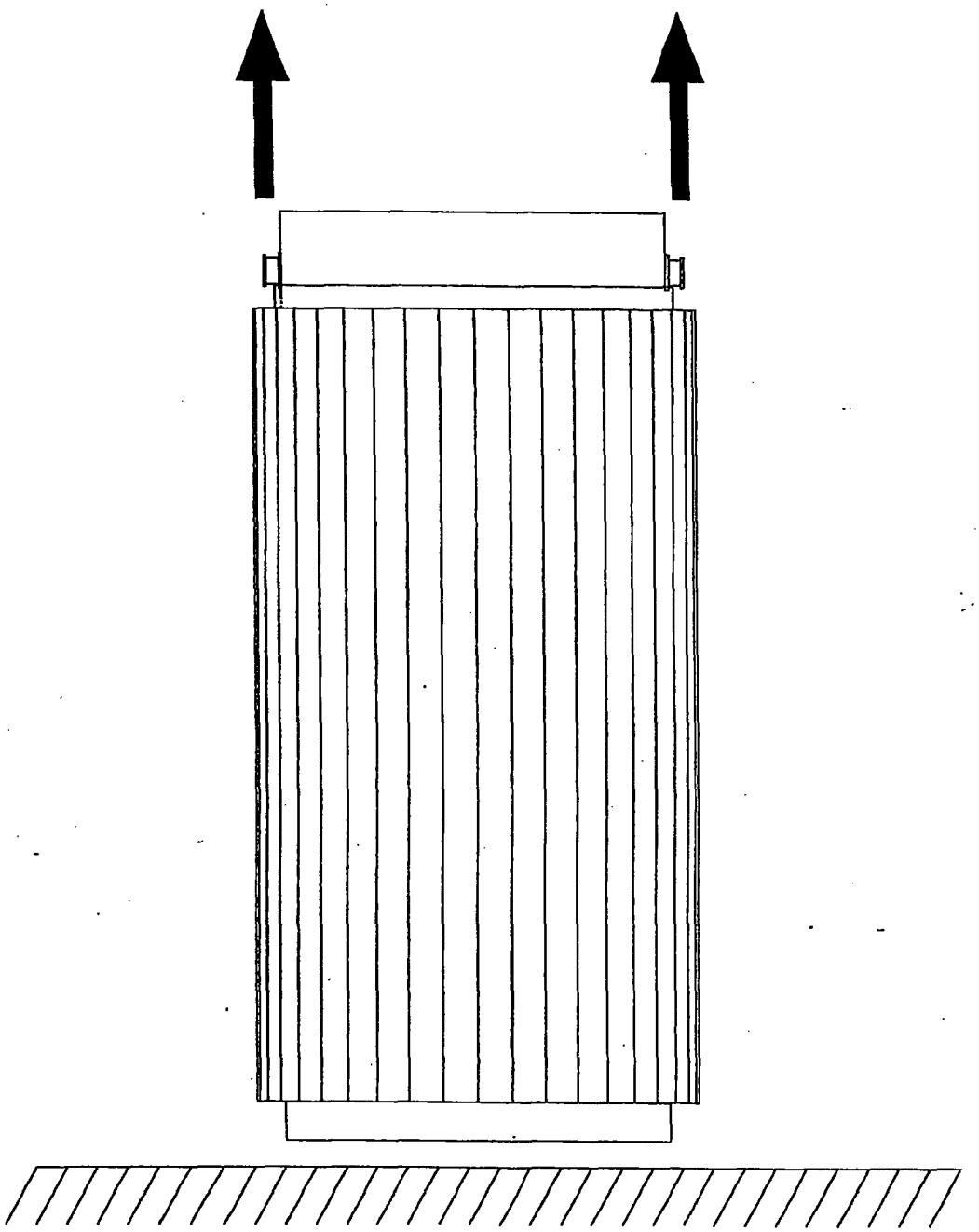

Figure 3.4.43; HI-STAR 100 Vertical Lifting

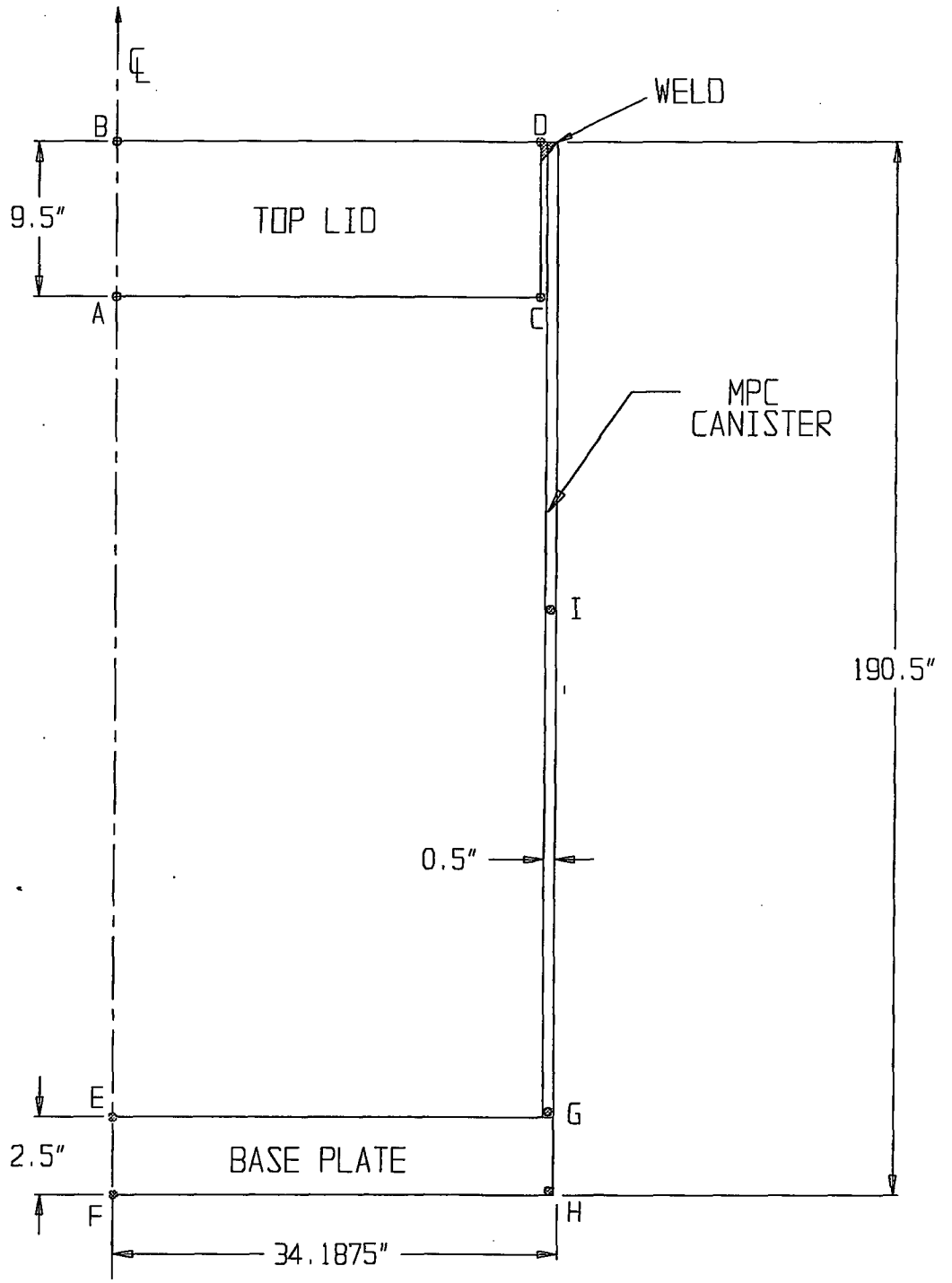

FIGURE 3.4.44 CONFINEMENT BOUNDARY MODEL SHOWING TEMPERATURE DATA POINTS

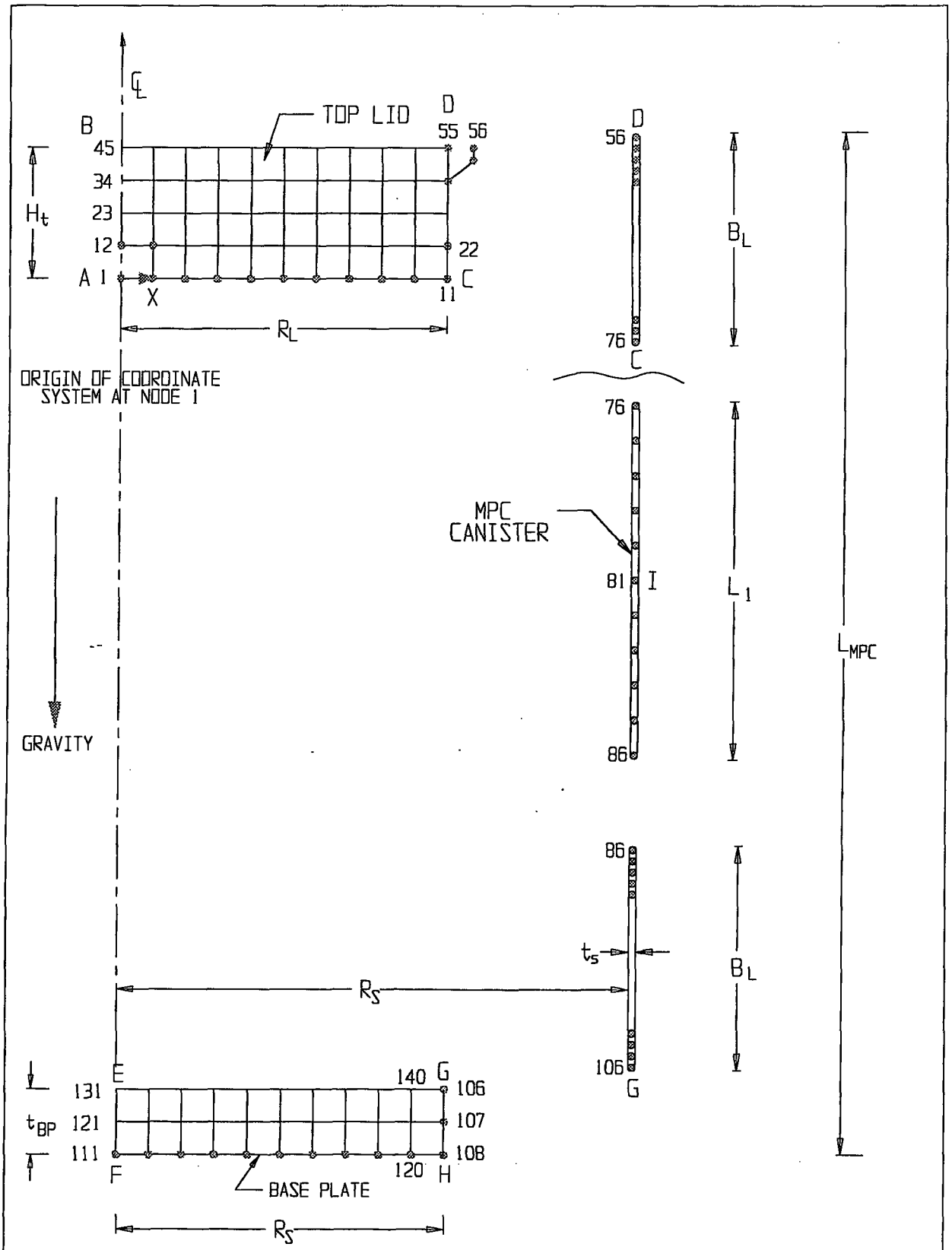

FIGURE 3.4.45 MPC - CONFINEMENT BOUNDARY FINITE ELEMENT GRID (EXPLODED VIEW)

REPORT HI-2012610

REVISION 0

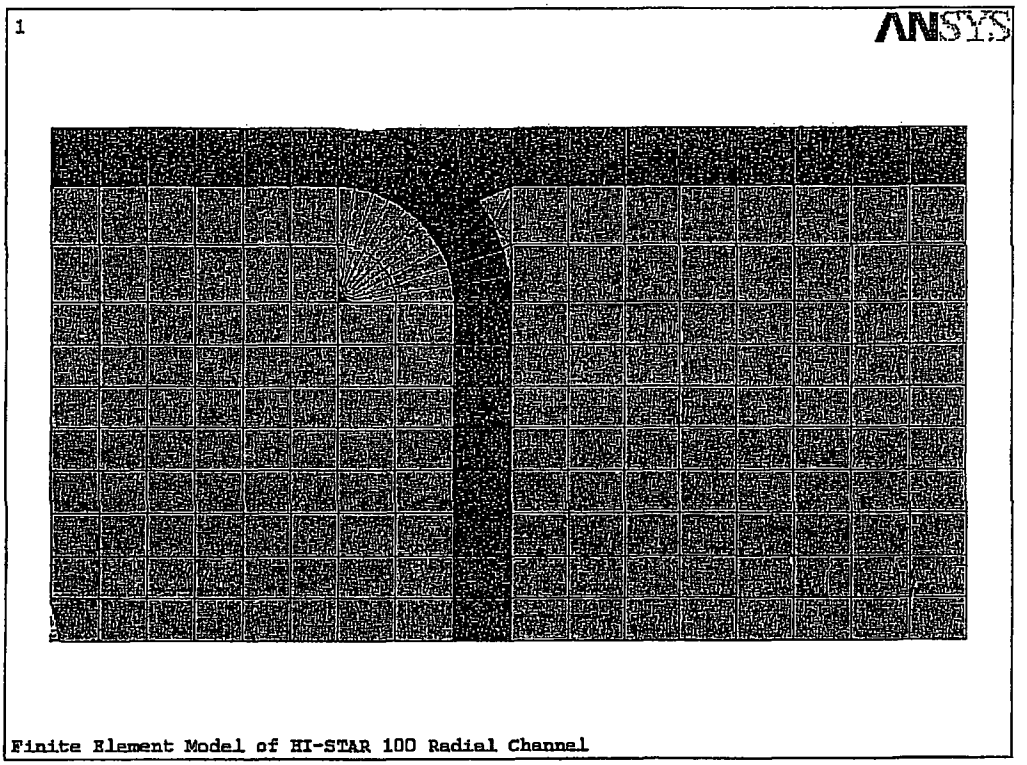

FIGURE 3.4.46; FINITE ELEMENT MODEL OF THERMAL EXPANSION FOAM

3.5 FUEL RODS

The cladding of the fuel rods is the initial confinement boundary in the HI-STAR 100 System. Analyses have been performed in Chapter 4 to ensure that the maximum temperature of the fuel cladding is below the Pacific Northwest Laboratory's threshold values for various cooling times. These temperature limits ensure that the fuel cladding will not degrade in an inert helium environment. Additional details on the fuel rod cladding temperature analyses for the spent fuel to be loaded into the HI-STAR 100 System are provided in Chapter 4.

The dimensions of the storage cell openings in the MPC are equal to or greater than those used in spent fuel racks supplied by Holtec International. Thousands of fuel assemblies have been shuffled in and out of these cells over the years without a single instance of cladding failure. The vast body of physical evidence provides confirmation that the fuel handling and loading operations with the HI-STAR 100 MPC will not endanger or compromise the integrity of the cladding or the structural integrity of the assembly.

The HI-STAR 100 System is designed and evaluated for a maximum deceleration of 60g's. Studies of the capability of spent fuel rods to resist impact loads [3.5.1] indicate that the most vulnerable fuel can withstand 63 g's in the most adverse orientation. Therefore, designing the HI-STAR 100 System to a maximum deceleration of 60 g's will ensure that fuel rod cladding integrity is maintained during all normal, off-normal, and accident conditions.

3.6 SUPPLEMENTAL DATA

3.6.1 Additional Codes and Standards Referenced in HI-STAR 100 System Design and Fabrication

The following additional codes, standards and practices were used as aids in developing the design, manufacturing, quality control and testing methods for HI-STAR 100 System:

a. Design Codes

(1) AISC Manual of Steel Construction, 1964 Edition and later.

(2) ANSI N210-1976, "Design Requirements for Light Water Reactor Spent Fuel Storage Facilities at Nuclear Power Stations".

(3) American Concrete Institute Building Code Requirements for Reinforced Concrete, ACI-318.

(4) Code Requirements for Nuclear Safety Related Concrete Structures, ACI349-85/ACI349R-85, and ACI349.1R-80.

(5) ASME NQA-1, Quality Assurance Program Requirements for Nuclear Facilities.

(6) ASME NQA-2-1989, Quality Assurance Requirements for Nuclear Facility Applications.

(7) ANSI Y14.5M, Dimensioning and Tolerancing for Engineering Drawings and Related Documentation Practices.

(8) ACI Detailing Manual - 1980.

(9) Crane Manufacturer's Association of America, Inc., CMAA Specification #70, Specifications for Electric Overhead Traveling Cranes, Revised 1988.

b. Material Codes - Standards of ASTM

(1) E165 - Standard Methods for Liquid Penetrant Inspection.

(2) A240 - Standard Specification for Heat-Resisting Chromium and Chromium-Nickel Stainless Steel Plate, Sheet and Strip for Fusion-Welded Unfired Pressure Vessels.

(3) A262 - Detecting Susceptibility to Intergranular Attack in Austenitic Stainless Steel.

(4) A276 - Standard Specification for Stainless and Heat-Resisting Steel Bars and Shapes.

(5) A479 - Steel Bars for Boilers & Pressure Vessels.

(6) ASTM A564, Standard Specification for Hot-Rolled and Cold-Finished Age-Hardening Stainless and Heat-Resisting Steel Bars and Shapes.

(7) C750 - Standard Specification for Nuclear-Grade Boron Carbide Powder.

(8) A380 - Recommended Practice for Descaling, Cleaning and Marking Stainless Steel Parts and Equipment.

(9) C992 - Standard Specification for Boron-Based Neutron Absorbing Material Systems for Use in Nuclear Spent Fuel Storage Racks.

(10) ASTM E3, Preparation of Metallographic Specimens.

(11) ASTM E190, Guided Bend Test for Ductility of Welds.

(12) NCA3800 - Metallic Material Manufacturer's and Material Supplier's Quality System Program.

c. Welding Codes: ASME Boiler and Pressure Vessel Code, Section IX - Welding and Brazing Qualifications, 1995 Edition.

d. Quality Assurance, Cleanliness, Packaging, Shipping, Receiving, Storage, and Handling Requirements

(1) ANSI 45.2.1 - Cleaning of Fluid Systems and Associated Components during Construction Phase of Nuclear Power Plants.

(2) ANSI N45.2.2 - Packaging, Shipping, Receiving, Storage and Handling of Items for Nuclear Power Plants (During the Construction Phase).

(3) ANSI - N45.2.6 - Qualifications of Inspection, Examination, and Testing Personnel for Nuclear Power Plants (Regulatory Guide 1.58).

(4) ANSI-N45.2.8, Supplementary Quality Assurance Requirements for Installation, Inspection and Testing of Mechanical Equipment and Systems for the Construction Phase of Nuclear Power Plants.

(5) ANSI - N45.2.11, Quality Assurance Requirements for the Design of Nuclear Power Plants.

(6) ANSI-N45.2.12, Requirements for Auditing of Quality Assurance Programs for Nuclear Power Plants.

(7) ANSI N45.2.13 - Quality Assurance Requirements for Control of Procurement of Equipment Materials and Services for Nuclear Power Plants (Regulatory Guide 1.123).

(8) ANSI N45.2.15-18 - Hoisting, Rigging, and Transporting of Items for Nuclear Power Plants.

(9) ANSI N45.2.23 - Qualification of Quality Assurance Program Audit Personnel for Nuclear Power Plants (Regulatory Guide 1.146).

(10) ASME Boiler and Pressure Vessel, Section V, Nondestructive Examination, 1995 Edition.

(11) ANSI - N16.9-75 Validation of Calculation Methods for Nuclear Criticality Safety.

e. Reference NRC Design Documents

(1) NUREG-0800, Radiological Consequences of Fuel Handling Accidents.

(2) NUREG 0612, "Control of Heavy Loads at Nuclear Power Plants", USNRC, Washington, D.C., July, 1980.

(3) NUREG-1536, "Standard Review Plan for Dry Cask Storage Systems", USNRC, January 1997, Final Report.

f. Other ANSI Standards (not listed in the preceding)

(1) ANSI/ANS 8.1 (N16.1) - Nuclear Criticality Safety in Operations with Fissionable Materials Outside Reactors.

(2) ANSI/ANS 8.17, Criticality Safety Criteria for the Handling, Storage, and Transportation of LWR Fuel Outside Reactors.

(3) N45.2 - Quality Assurance Program Requirements for Nuclear Facilities - 1971.

(4) N45.2.9 - Requirements for Collection, Storage and Maintenance of Quality Assurance Records for Nuclear Power Plants - 1974.

(5) N45.2.10 - Quality Assurance Terms and Definitions - 1973.

(6) ANSI/ANS 57.2 (N210) - Design Requirements for Light Water Reactor Spent Fuel Storage Facilities at Nuclear Power Plants.

(7) N14.6 (1993) - American National Standard for Special Lifting Devices for Shipping Containers Weighing 10,000 pounds (4500 kg) or more for Nuclear Materials.

(8) ANSI/ASME N626-3, Qualification and Duties of Personnel Engaged in ASME Boiler and Pressure Vessel Code Section III, Div. 1, Certifying Activities.

g. Code of Federal Regulations

(1) 10CFR20 - Standards for Protection Against Radiation.

(2) 10CFR21 - Reporting of Defects and Non-compliance.

(3) 10CFR50 - Appendix A - General Design Criteria for Nuclear Power Plants.

(4) 10CFR50 - Appendix B - Quality Assurance Criteria for Nuclear Power Plants and Fuel Reprocessing Plants.

(5) 10CFR61 - Licensing Requirements for Land Disposal of Radioactive Material.

(6) 10CFR71 - Packaging and Transportation of Radioactive Material.

h. Regulatory Guides

(1) RG 1.13 - Spent Fuel Storage Facility Design Basis (Revision 2 Proposed).

(2) RG 1.25 - Assumptions Used for Evaluating the Potential Radiological Consequences of a Fuel Handling Accident in the Fuel Handling and Storage Facility of Boiling and Pressurized Water Reactors.

(3) RG 1.28 - (ANSI N45.2) - Quality Assurance Program Requirements.

(4) RG 1.29 - Seismic Design Classification (Rev. 3).

(5) RG 1.31 - Control of Ferrite Content in Stainless Steel Weld Material.

(6) RG 1.38 - (ANSI N45.2.2) Quality Assurance Requirements for Packaging, Shipping, Receiving, Storage and Handling of Items for Water-Cooled Nuclear Power Plants.

(7) RG 1.44 - Control of the Use of Sensitized Stainless Steel.

(8) RG 1.58 - (ANSI N45.2.6) Qualification of Nuclear Power Plant Inspection, Examination, and Testing Personnel.

(9) RG 1.61 - Damping Values for Seismic Design of Nuclear Power Plants, Rev. 0, 1973.

(10) RG 1.64 - (ANSI N45.2.11) Quality Assurance Requirements for the Design of Nuclear Power Plants.

(11) RG 1.71 - Welder Qualifications for Areas of Limited Accessibility.

(12) RG 1.74 - (ANSI N45.2.10) Quality Assurance Terms and Definitions.

(13) RG 1.85 - Materials Code Case Acceptability - ASME Section 3, Div. 1.

(14) RG 1.88 - (ANSI N45.2.9) Collection, Storage and Maintenance of Nuclear Power Plant Quality Assurance Records.

(15) RG 1.92 - Combining Modal Responses and Spatial Components in Seismic Response Analysis.

(16) RG 1.122 - Development of Floor Design Response Spectra for Seismic Design of Floor-Supported Equipment or Components.

(17) RG 1.123 - (ANSI N45.2.13) Quality Assurance Requirements for Control of Procurement of Items and Services for Nuclear Power Plants.

(18) RG 1.124 - Service Limits and Loading Combinations for Class 1 Linear-Type Component Supports, Revision 1, 1978.

(19) Reg. Guide 3.4 - Nuclear Criticality Safety in Operations with Fissionable Materials at Fuels and Materials Facilities.

(20) RG 3.41 - Validation of Calculational Methods for Nuclear Criticality Safety, Revision 1, 1977.

(21) Reg. Guide 8.8 - Information Relative to Ensuring that Occupational Radiation Exposure at Nuclear Power Plants will be as Low as Reasonably Achievable (ALARA).

(22) DG-8006, "Control of Access to High and Very High Radiation Areas in Nuclear Power Plants".

i. Branch Technical Position

(1) CPB 9.1-1 - Criticality in Fuel Storage Facilities.

(2) ASB 9-2 - Residual Decay Energy for Light-Water Reactors for Long-Term Cooling.

j. Standard Review Plan (NUREG-0800)

(1) SRP 3.2.1 - Seismic Classification.

(2) SRP 3.2.2 - System Quality Group Classification.

(3) SRP 3.7.1 - Seismic Design Parameters.

(4) SRP 3.7.2 - Seismic System Analysis.

(5) SRP 3.7.3 - Seismic Subsystem Analysis.

(6) SRP 3.8.4 - Other Seismic Category I Structures (including Appendix D), Technical Position on Spent Fuel Rack.

(7) SRP 3.8.5 - Foundations

(8) SRP 9.1.2 - Spent Fuel Storage, Revision 3, 1981.

(9) SRP 9.1.3 - Spent Fuel Pool Cooling and Cleanup System.

(10) SRP 9.1.4 - Light Load Handling System.

(11) SRP 9.1.5 - Overhead Heavy Load Handling System.

(12) SRP 15.7.4 - Radiological Consequences of Fuel Handling Accidents.

k. AWS Standards

(1) AWS D1.1 - Structural Welding Code, Steel.

(2) AWS A2.4 - Standard Symbols for Welding, Brazing and Nondestructive Examination.

(3) AWS A3.0 - Standard Welding Terms and Definitions.

(4) AWS A5.12 - Tungsten Arc-welding Electrodes.

(5) AWS QC1 - Standards and Guide for Qualification and Certification of Welding Inspectors.

l. Others

(1) ASNT-TC-1A - Recommended Practice for Nondestructive Personnel Qualification and Certification.

(2) SSPC SP-2 - Surface Preparation Specification No. 2 Hand Tool Cleaning.

(3) SSPC SP-3 - Surface Preparation Specification No. 3 Power Tool Cleaning.

(4) SSPC SP-10 - Near-White Blast Cleaning.

3.6.2 Computer Programs

Three computer programs, all with a well established history of usage in the nuclear industry, have been utilized to perform structural and mechanical analyses documented in this report. These codes are ANSYS, DYNA3D, and WORKING MODEL. ANSYS is a public domain code which utilizes the finite element method for structural analyses.

WORKING MODEL, Version V.3.0

This code is primarily used in the analysis of cask drop events for the 10CFR71 submittal. It is also used in this 10CFR72 submittal to verify the results reported in Appendix 3.A for tip-over and to compute the dynamic load resulting from intermediate missile impact on the overpack closure in Appendix 3.G.

"WORKING MODEL" (V3.0) is a Computer Aided Engineering (CAE) tool with an integrated user interface that merges modeling, simulation, viewing, and measuring. The program includes a dynamics algorithm that provides automatic collision and contact handling, including detection, response, restitution, and friction.

Numerical integration is performed using the Kutta-Merson integrator which offers options for variable or fixed time-step and error bounding.

The Working Model Code is commercially available. Holtec has performed independent QA validation of the code by comparing the solution of several classical dynamics problems with the numerical results predicted by Working Model. Agreement in all cases is excellent.

Additional theoretical material is available in the manual: "Users Manual, Working Model, Version 3", Knowledge Revolution, 66 Bovet Road, Suite 200, San Mateo, CA, 94402.

DYNA3D

"DYNA3D" is a nonlinear, explicit, three-dimensional finite element code for solid and structural mechanics. It was originally developed at Lawrence Livermore Laboratories and is ideally suited for study of short-time duration, highly nonlinear impact problems in solid mechanics. DYNA3D is commercially available for both UNIX work stations and Pentium class PCs running Windows 95 or Windows NT. The PC version has been fully validated at Holtec following Holtec's QA procedures for commercial computer codes. This code is used to analyze the drop accidents and the tip-over scenario for the HI-STAR 100. Benchmarking of DYNA3D for these storage analyses is discussed and documented in Appendix 3.A.

3.6.3 Appendices Included in Chapter 3

3.A HI-STAR Deceleration Under Postulated Drop Events and Tipover
3.B Damaged Fuel Container
3.C Response of Cask to Tornado Wind Load and Large Missile Impact
3.D Lifting Trunnion Stress Analysis
3.E Analysis of MPC Top Closure
3.F Stress Analysis of Overpack Closure Bolts
3.G Missile Penetration Analysis
3.H Code Case N-284 Stability Calculations
3.I Structural Qualification of MPC Baseplate
3.J Fuel Support Spacer Strength Evaluations
3.K Lifting Bolts - MPC Lid and Overpack Top Closure
3.L Fabrication Stresses
3.M Miscellaneous Calculations
3.N Deleted
3.O Deleted
3.P Deleted
3.Q Deleted
3.R Deleted
3.S Deleted
3.T Deleted
3.U HI-STAR 100 Component Thermal Expansion - MPC-24
3.V Deleted
3.W HI-STAR 100 Component Thermal Expansion - MPC-68
3.X Calculation of Dynamic Load Factors
3.Y Cask Under Three Times Dead Load
3.Z Top Flange Bolt Hole Analysis
3.AA Deleted
3.AB Deleted
3.AC Deleted
3.AD Thermal Expansion During Fire Accident
3.AE Stress Analysis of Overpack Closure Bolts Under Cold Conditions of Storage
3.AF Stress Analysis of Overpack Closure Bolts for the Storage Fire Accident
3.AG Stress Analysis of the HI-STAR 100 Enclosure Shell Under 30 psi Internal Pressure
3.AH MPC-Lift Lugs
3.AI Analysis of Transnuclear Damaged Fuel Canister and Thoria Rod Canister

3.7 COMPLIANCE TO NUREG-1536

Supporting information to provide reasonable assurance with respect to the adequacy of the HI-STAR 100 System to store spent nuclear fuel in accordance with the stipulations of the Technical Specifications (Chapter 12) is provided throughout this Final Safety Analysis Report. An itemized table (Table 3.0.1 at the beginning of this chapter) has been provided to locate and collate the substantiating material to support the technical evaluation findings listed in NUREG-1536 Chapter 3, Article VI.

The following statements are germane to the finding of an affirmative safety evaluation for HI-STAR 100 spent fuel storage system:

- The design and structural analysis of the HI-STAR 100 System is in full compliance with the provisions of Chapter 3 of NUREG-1536. No exceptions are taken.

- The list of Regulatory Guides, Codes, and standards presented in Section 3.6 herein is in full compliance with the provisions of NUREG-1536.

- All HI-STAR 100 structures, systems, and components (SSC) that are important to safety (ITS) are identified in Table 2.2.6. Section 1.5 contains the design drawings which describe the HI-STAR 100 SSCs in complete detail. Explanatory narrations in Subsections 3.4.3, 3.4.4, and appendices to this chapter provide sufficient textual details to allow an independent evaluation of their structural adequacy.

- The requirements of 10CFR72.24 with regard to information pertinent to structural evaluation is provided in Chapters 2, 3, and 11.

- Technical Specifications pertaining to the structures of the HI-STAR 100 System have been provided in Section 12.3 herein pursuant to the requirements of 10CFR72.26.

- A series of analyses to demonstrate compliance with the requirements of 10CFR72.122(b) and (c), and 10CFR72.24(c)(3) have been performed which show that SSCs designated as ITS possess an adequate margin of safety with respect to all load combinations applicable to normal, off-normal, accident, and natural phenomenon events. In particular, the following information is provided:

  i. Load combinations for the fuel basket, enclosure vessel, and the HI-STAR 100 overpack for normal, off-normal, accident, and natural phenomenon events are compiled in Tables 2.2.14, 3.1.1, and 3.1.3 through 3.1.5, respectively.

  ii. Stress limits applicable to the materials are provided in Subsection 3.3.

  iii. Stresses at various locations in the fuel basket, the enclosure vessel, and the HI-STAR 100 overpack have been computed by analysis. Descriptions of stress analyses are presented in Sections 3.4.3 and 3.4.4, which are further elaborated in a series of appendices listed at the end of this chapter.

iv. Factors of safety in the components of the HI-STAR 100 System are reported as below:

a.	Fuel basket	Tables 3.4.3, 3.4.9, and 3.4.11
b.	Enclosure vessel	Tables 3.4.4, 3.4.7, 3.4.8, 3.4.9, 3.4.11, 3.4.12, 3.4.13, 3.4.15
c.	HI-STAR 100 overpack	Tables 3.4.5, 3.4.6, 3.4.10, and 3.4.16-3.4.19
d.	Miscellaneous components	Tables 3.4.11 and 3.4.14
e.	Lifting devices	Subsection 3.4.3

- The structural design and fabrication details of the fuel baskets whose safety function in the HI-STAR 100 System is to maintain nuclear criticality safety, have been carried out to comply with the provisions of Subsection NG of the ASME Code (loc. cit.) Section III. The structural factors of safety, summarized in Tables 3.4.3 and 3.4.6 for all credible load combinations under normal, off-normal, accident, and natural phenomenon events demonstrate that the Code limits are satisfied in all cases. As the stress analyses have been performed using linear elastic methods and the computed stresses are well within the respective ASME Code limits, it follows that the physical geometry of the fuel basket will not be altered under any load combination to create a condition adverse to criticality safety. This conclusion satisfies the requirement of 10CFR72.124(a), with respect to structural margins of safety for SSCs important to nuclear criticality safety.

  Structural margins of safety during handling, packaging, and transfer operations, mandated by the provisions of 10CFR Part 72.236(b), require that the lifting and handling devices are engineered to comply with the stipulations of ANSI N14.6, NUREG-0612, Regulatory Guide 3.61, and NUREG-1536, and that the components being handled meet the applicable ASME Code service condition stress limits. The requirements of the governing codes for handling operations are summarized in Subsection 3.4.3 herein. A summary table of factors of safety for all ITS components under lifting and handling operations, presented in Subsection 3.4.3, shows that adequate structural margins exist in all cases.

- Consistent with the requirements of 10CFR72.236(i), the confinement boundary for the HI-STAR 100 System has been engineered to maintain confinement of radioactive materials under normal, off-normal, and postulated accident conditions. This assertion of confinement integrity is made principally on the strength of the following information provided in this FSAR.

  i. The MPC Enclosure Vessel which constitutes the confinement boundary is designed and fabricated in accordance with Section III, Subsection NB (Class 1 nuclear components) of the ASME Code to the maximum extent practicable.

ii. The MPC lid of the MPC Enclosure Vessel is welded using a strength groove weld and is subjected to volumetric examination, hydrostatic testing, liquid penetrant (root and final), and leakage testing to establish maximum confidence in weld joint integrity.

iii. The closure of the MPC Enclosure Vessel consists of *two* independent isolation barriers.

iv. The confinement boundary is constructed from stainless steel alloys with a proven history of material integrity under environmental conditions encountered in terrestrial applications.

v. The load combinations for normal, off-normal, accident, and natural phenomena events have been compiled (Table 2.2.14) and applied on the HI-STAR 100 MPC Enclosure Vessel (confinement boundary) and on the HI-STAR 100 overpack. The results, summarized in Tables 3.4.4 through 3.4.19, show that the factor of safety (with respect to the appropriate ASME Code limits) is greater than one in all cases. Design Basis natural phenomena events such as tornado-borne missiles (large, intermediate, or small) have also been analyzed to evaluate their potential for breaching the helium retention boundary and the confinement boundary. Analyses presented in Subsection 3.4.8 (summarized in unnumbered tables in Subsection 3.4.8 and in the appendices to this chapter), show that the integrity of the helium retention boundary and the confinement boundary is preserved under all design basis projectile impact scenarios.

- The information on structural design included in this FSAR complies with the requirements of 10CFR72.120 and 10CFR72.122, and can be ascertained from the information contained in Table 3.7.1.

- The provisions of features in the HI-STAR 100 structural design, listed in Table 3.7.2, demonstrate compliance with the specific requirements of 10CFR72.236(e), (f), (g), (h), (i), (j), (k), and (m).

Table 3.7.1

COMPLIANCE OF HI-STAR 100 SYSTEM WITH 10CFR72.236(e), ET AL.

Item		Compliance	Location of Supporting Information in This Document
i.	Design and fabrication to acceptable quality standards	All ITS components designed and fabricated to recognized Codes and Standards:	Subsections 2.0.1 and 3.1.1 Tables 2.2.6 and 2.2.7
		• Basket: Subsection NG, Section III	Subsections 2.0.1 and 3.1.1 Tables 2.2.6 and 2.2.7
		• Enclosure Vessel: Subsection NB, loc. cit.	
		• HI-STAR 100 Structure: Subsection NF, loc. cit.	Subsections 2.0.2 and 3.1.1
ii.	Erection to acceptable quality standards	HI-STAR 100 will be installed in a vertical orientation using proven deployment procedures which are in full compliance with established construction practices at nuclear power plants.	Section 8.1
iii.	Testing to acceptable quality standards	• All non-destructive examination of ASME Code components for provisions in the Code (see exceptions in Table 2.2.15).	Section 9.1
		• Hydrotest of pressure vessel per the Code (see Table 12.3.18).	Section 9.1
		• Testing for radiation containment per provisions of NUREG-1536 (see Tables 12.3.8 and 12.3.9).	Sections 7.1 and 9.1
iv.	Adequate structural protection against environmental conditions and natural phenomena.	Analyses presented in Chapter 3 demonstrate that the confinement boundary will preserve its integrity under all postulated off-normal and natural phenomena events listed in Chapter 2.	Section 2.2 Chapter 11

Table 3.7.1 (continued)

COMPLIANCE MATRIX FOR 10CFR72.120 AND 10CFR72.122

Item	Compliance	Location of Supporting Information in This Document
v. Adequate protection against fires and explosions	• The extent of combustible (exothermic) material in the vicinity of the cask system is procedurally controlled (the sole source of hydrocarbon energy is diesel in the tow vehicle).	Chapter 8
	• Analyses show that the heat energy released from the postulated fire accident condition surrounding the cask will not result in impairment of the confinement boundary and will not lead to structural failure of the overpack. The effect on shielding will be localized to the external surfaces directly exposed to the fire which will cause no significant change in the HI-STAR 100 overpack.	Subsection 11.2.4
	• Explosion effects are shown to be bounded by the Code external pressure design basis. Pressure pulse from explosion will act on the HI-STAR 100 overpack; the MPC (confinement boundary) is completely protected.	Subsection 11.2.11 and Subsection 3.1.2.1.1.4
vi. Appropriate inspection, maintenance, and testing	Inspection, maintenance, and testing requirements set forth in this FSAR are in full compliance with the governing regulations and established industry practice.	Sections 9.1 and 9.2 Chapter 12
vii. Adequate accessibility in emergencies	The HI-STAR 100 overpack lid can be removed to gain access to the multi-purpose canister.	Chapter 8

Table 3.7.1 (continued)

COMPLIANCE MATRIX FOR 10CFR72.120 AND 10CFR72.122

Item		Compliance	Location of Supporting Information in This Document
viii.	A confinement barrier that acceptably protects the spent fuel cladding during storage	• The peak temperature of the fuel cladding at design basis heat duty of each MPC has been demonstrated to be maintained below the limits recommended in the reports of national laboratories.	Subsection 4.4.2
		• The confinement barriers consist of highly ductile stainless steel alloys. The multi-purpose canister is housed in the overpack, built from a steel structure whose materials are selected and examined to maintain protection against brittle fracture under off-normal ambient (cold) temperatures (minimum of -40°F).	Subsection 3.1.1 Subsection 3.1.2.3
ix.	The structures are compatible with the appropriate monitoring systems.	The HI-STAR 100 overpack	Section 1.5 Subsection 2.3.3.2
x.	Structural designs that are compatible with ready retrievability of fuel.	• The fuel basket is designed to be an extremely stiff honeycomb structure such that the storage cavity dimensions will remain unchanged under all postulated normal and accident events. Therefore, the retrievablity of the spent nuclear fuel from the basket will not be jeopardized.	Subsection 3.1.1
		• The MPC canister lid is attached to the shell with a groove weld which is made using an automated welding device. A similar device is available to remove the weld. Thus, access to the fuel basket can be realized.	Sections 8.1 and 8.3

Table 3.7.2

COMPLIANCE OF HI-STAR 100 SYSTEM WITH 10CFR72.236(e), ET AL.

Item	Compliance	Location of Supporting Information in This Document
i. Redundant sealing of confinement systems	Two physically independent lids, each separately welded to the MPC shell (Enclosure Vessel shell) provide a redundant confinement system.	Section 1.5 Drawing Nos. 1392, 1395, and 1401; Figure 7.1.2 Section 7.1.
ii. Adequate heat removal without active cooling systems.	Thermal analyses presented in Chapter 4 show that the HI-STAR 100 System will remove the decay heat generated from the stored spent fuel by strictly passive means and maintain the system temperature within prescribed limits.	Sections 4.4 and Sections 9.1 and 9.2
iii. Storage of spent fuel for a minimum of 20 years.	The service life of the overpack and MPC are engineered to be in excess of 20 years.	Subsections 3.4.10 and 3.4.11
iv. Compatibility with wet or dry spent fuel loading and unloading facilities	The system is designed to eliminate any significant material interactions in the wet (spent fuel pool) environment.	Subsection 3.4.1
v. Ease of decontamination	The external surface of the multi-purpose canister is protected from contamination during fuel loading through a custom designed sealing device.	Figures 8.1.13 and 8.1.14
vi. Inspections of defects that might reduce confinement effectiveness.	Post-fabrication inspection of the shielding materials will be performed to ensure that no HI-STAR 100 Systems containing unacceptable voids are deployed at the ISFSI for long-term storage.	Section 9.1 and Chapter 12
vii. Conspicuous and durable marking.	The stainless steel lid of each MPC will have model number and serial number engraved for ready identification.	Section 1.5,

Table 3.7.2 (continued)

COMPLIANCE MATRIX FOR 10CFR72.120 AND 10CFR72.122

Item	Compliance	Location of Supporting Information in This Document
viii. Compatibility with removal of the stored fuel from the site, transportation, and ultimate disposal by the U.S. Department of Energy.	The MPC is designed to be in full compliance with the DOE's draft specification for transportability and disposal published under the now dormant "MPC" program.	Section 2.4 Subsection 1.2.1.1

3.8 REFERENCES

[3.1.1] NUREG-0612, "Control of Heavy Loads at Nuclear Power Plants," United States Nuclear Regulatory Commission.

[3.1.2] ANSI N14.6-1993, "American National Standard for Special Lifting Devices for Shipping Containers Weighing 10000 Pounds (4500 kg) or More for Nuclear Materials," American National Standards Institute, Inc.

[3.1.3] Regulatory Guide 7.11, "Fracture Toughness Criteria of Base Material for Ferritic Steel Shipping Cask Containment Vessels with a Maximum Wall Thickness of 4 Inches."

[3.1.4] Regulatory Guide 7.12, "Fracture Toughness Criteria of Base Material for Ferritic Steel Shipping Cask Containment Vessels with a Wall Thickness Greater Than 4 Inches but Not Exceeding 12 Inches."

[3.1.5] NUREG/CR-1815, "Recommendations for Protecting Against Failure by Brittle Fracture in Ferritic Steel Shipping Containers Up to Four Inches Thick."

[3.1.6] Aerospace Structural Metals Handbook, Manson.

[3.1.7] Armco Product Data Bulletin S-22.

[3.3.1] ASME Boiler & Pressure Vessel Code, Section II, Part D, 1995.

[3.4.1] ANSYS 5.2, ANSYS, Inc., 1995.

[3.4.2] ASME Boiler & Pressure Vessel Code, Section III, Subsection NF, 1995.

[3.4.3] ASME Boiler & Pressure Vessel Code, Section III, Appendices, 1995.

[3.4.4] ASME Boiler & Pressure Vessel Code, Section III, Subsection NB, 1995.

[3.4.5] Mok, Fischer, Hsu, "Stress Analysis of Closure Bolts for Shipping Casks" (NUREG/CR 6007 UCRL-ID-110637), Lawrence Livermore National Laboratory/Kaiser Engineering, 1993.

[3.4.6] Code Case N-284, "Metal Containment Shell Buckling Design Methods", Section III, Division 1, Class MC, Approval Date 8/25/80.

[3.4.7] NRC Bulletin 96-04: Chemical, Galvanic or Other Reactions in Spent Fuel Storage and Transportation Casks, July 5, 1996.

[3.4.8] Theory of Elastic Stability, S.P. Timoshenko and J. Gere, McGraw Hill, 2nd Edition.

[3.4.9] Marks Standard Handbook for Mechanical Engineering, 9th ed.

[3.4.10] ASME Boiler and Pressure Vessel Code, Section III, Subsection NG, 1995.

[3.4.11] 10CFR71, Waste Confidence Decision Review, USNRC, September 11, 1990.

[3.4.12] NUREG/CR-6322, Buckling Analysis of Spent Fuel Basket, Lawrence Livermore National Laboratory, May, 1995.

[3.5.1] Chun, Witte, Schwartz, "Dynamic Impact Effects on Spent Fuel Assemblies", UCID-21246, Lawrence Livermore National Laboratory, October 20, 1987.

APPENDIX 3.A: HI-STAR DECELERATION UNDER POSTULATED DROP EVENTS AND TIPOVER

3.A.1 INTRODUCTION

Handling accidents with a HI-STAR overpack containing a loaded MPC are credible events (Section 2.2.3). The stress analyses carried out in Chapter 3 of this safety analysis report assume that the inertial loading on the load bearing members of the MPC, fuel basket, and the overpack due to a handling accident are limited by the Table 3.1.2 decelerations. The maximum deceleration experienced by a structural component is the product of the rigid body deceleration sustained by the structure and the dynamic load factor (DLF) applicable to that structural component. The dynamic load factor (DLF) is a function of the contact impulse and the structural characteristics of the component. A solution for dynamic load factors is provided in Appendix 3.X.

The rigid body deceleration is a strong function of the load-deformation characteristics of the impact interface, weight of the cask, and the drop height. For the HI-STAR 100 System, the weight of the structure and its surface compliance characteristics are known. However, the contact stiffness of the ISFSI pad (and other surfaces over which the HI-STAR 100 may be carried during its movement to the ISFSI) is site-dependent. The contact resistance of the collision interface, which is composed of the HI-STAR 100 and the impacted surface compliances, therefore, is not known a priori for a site. For conservatism, the HI-STAR 100 cask is simulated as a rigid body (infinite surface stiffness) which has the effect of maximizing the stiffness of the contact interface. Analyses for the rigid body decelerations are presented here for a reference ISFSI pad (which is the pad used in a recent Lawrence Livermore National Laboratory report). The surface compliance of the pad, therefore, is the only source of interface deformation in the dynamic simulations considered in this appendix.

An in-depth investigation by the Lawrence Livermore Laboratory (LLNL) into the mechanics of impact between a cask-like impactor on a reinforced concrete slab founded on a soil-like subgrade has identified three key parameters, namely, the thickness of the concrete slab, t_p, compressive strength of the concrete, f_c' and equivalent Young's Modulus of the subgrade, E. These three parameters are key variables in establishing the stiffness of the pad under impact scenarios. The LLNL reference pad parameters, which we hereafter denote as Set A, provide one set of values of t_p, f_c' , and E which are found to satisfy the deceleration criteria applicable to the HI-STAR 100 cask. Another set of parameters, referred to as Set B herein, are also shown to satisfy the g-load limit requirements. In fact, an infinite number of combinations of t_p, f_c' , and E can be compiled which would meet the g-load limit qualification. However, in addition to satisfying the g-limit criterion, the pad must be demonstrated to possess sufficient flexural and shear stiffness to meet the ACI 318 strength limits under factored load combinations. The minimum strength requirement to comply with ACI 318 provisions places a restriction on the lower bound values of t_p, f_c' , and E which must be met in an ISFSI pad design.

Our focus in this appendix, however, is to quantify the peak decelerations that would be experienced by a loaded HI-STAR 100 cask under the postulated impact scenarios for two pad designs defined by parameter Sets A and B, respectively. The information presented in this appendix also serves to further authenticate the veracity of the Holtec DYNA3D model described in the 1997 benchmark report [3.A.4.].

3.A.2 Purpose

The purpose of this appendix is to demonstrate that the rigid body decelerations are sufficiently low so that the design basis deceleration of 60g is not exceeded. Three scenarios of accidental drop of a loaded HI-STAR 100 cask on the ISFSI pad are considered in this appendix. They are:

i. Side drop: A loaded HI-STAR 100 free-falls in a horizontal orientation (cask's axis is horizontal) from a height "h" before impacting the ISFSI pad.

ii. Tipover: A loaded HI-STAR 100 is assumed to undergo a non-mechanistic tipover event at an ISFSI pad resulting in an impact with a pre-incipient impact angular velocity of ω which is readily calculated from elementary dynamics.

iii. End drop: The loaded cask is assumed to drop with its longitudinal axis in the vertical orientation such that its bottom plate hits the pad after free-falling from a height, h.

It is shown in Appendix 3.X that dynamic load factors are a function of the dominant natural frequency of vibration of the component for a given input load pulse shape. Therefore, for the purposes of this Appendix 3.A, it is desired to demonstrate that the rigid body deceleration experienced in each of the drop scenarios is below the 60g HI-STAR 100 design basis.

3.A.3 Background and Methodology

An earlier TSAR revision of this FSAR contained an analytical treatment of the three cask drop scenarios. In the earlier submittal, the cask/ISFSI interface was simulated by a linear spring with the spring stiffeners calculated using the Bousinesq elastic half-space solution. All three scenarios reduced to the solution of a simple mass-spring system. The need for such an idealized solution was eliminated when the Lawrence Livermore National Laboratory (LLNL) published results of the so-called fourth series billet tests [3.A.1] with a companion report [3.A.2] documenting a numerical solution based methodology which simulated the drop test results with reasonable accuracy. Subsequently, USNRC personnel published a paper [3.A.3] affirming the NRC's endorsement of the LLNL methodology. The LLNL simulation used modeling and simulation algorithms contained within the commercial computer code DYNA3D [3.A.6].

The LLNL cask drop model is not completely set forth in the above-mentioned LLNL reports. Using the essential information provided by the LLNL [3.A.2] report, however, Holtec is able to develop a finite element model for implementation on DYNA3D which is fully consistent with LLNL's (including the use of the Butterworth filter for discerning rigid body deceleration from "noisy" impact data). The details of the DYNA3D dynamic model, henceforth referred to as the

Holtec model, are contained in the proprietary benchmark report [3.A.4] wherein it is shown that the peak deceleration in every case of billet drop analyzed by LLNL is replicated within a small tolerance by the Holtec model. The case of the so-called "generic" cask for which LLNL provided predicted response under side drop and tipover events is also bounded by the Holtec model. In summary, the benchmarking effort documented in [3.A.4] is in full compliance with the guidance of the Commission [3.A.3].

Having developed and benchmarked an LLNL-consistent cask impact model, this model is applied to prognosticate the HI-STAR drop scenarios.

In the tipover scenario, the angular velocity of approach is readily calculated using planar rigid body dynamics and is used as an initial condition in the DYNA3D simulation.

For the side drop and end drop scenarios, considering the reference target (pad) elasto-plastic-damage characteristics, the object is to determine the maximum allowable drop height "h" such that the rigid body deceleration is below the design basis.

It is recognized, from the elementary analogy of the spring-mass impact, that the maximum deceleration increases monotonically as the rigidity of the cask is increased. Therefore, an upper bound on the deceleration of HI-STAR is obtained by replacing the polymeric zone in HI-STAR also by a rigid medium, making the entire cask a rigid body. Simulations for side drop and tipover conditions under the complete rigid body assumption provide an upper bound on the cask response. For the case of vertical drop, the impacting region is bottom plate forging which, without excessive conservatism, can be also modeled as a rigid body. Thus, all drop simulations presented in this appendix assume the HI-STAR 100 cask to simulate a rigid body for conservatism.

A description of the work effort and a summary of the results are presented in the following sections. In all cases, the reported decelerations are below the design basis limit of 60 g's at the top of the MPC fuel basket.

3.A.4 Assumptions and Input Data

3.A.4.1 Assumptions

The assumptions used to create the model are completely described in Reference [3.A.4] and are shown there to be consistent with the LLNL simulation. There are two key aspects which are restated here:

The maximum deceleration experienced by the cask during a collision event is a direct function of the structural rigidity (or conversely, compliance) of the impact surface. The compliance of the ISFSI pad is quite obviously dependent on the thickness of the pad, t_p, the compressive strength of the concrete, f_c' and stiffness of the subgrade (expressed by its effective Young's modulus, E). The structural rigidity of the ISFSI pad will increase if any of the three above-mentioned parameters, t_p, f_c' or E is increased. For the reference pad, the governing parameters

(i.e., t_p, f_c' and E) are assumed to be identical to the pad defined by LLNL [3.A.2] which is also the same as the pad utilized in the benchmark report [3.A.4]. We refer to the LLNL ISFSI pad parameters as Set A. (Table 3.A.1).

As can be seen from Table 3.A.1, the nominal compressive strength f_c' in Set A is limited to 4200 psi. However, experience has shown that ISFSI owners have considerable practical difficulty in limiting the 28 day strength of poured concrete to 4200 psi, chiefly because a principal element of progress in reinforced concrete materials technology has been in realizing ever increasing concrete nominal strength. Inasmuch as a key objective of the ISFSI pad is to limit its structural rigidity (and not f_c' per se), and limiting f_c' to 4200 psi may be problematic in certain cases, an alternative set of reference pad parameters is defined (Set B in Table 3.A.1) which permits a higher value of f_c' but much smaller values of pad thickness, t_p and sub-grade Young's modulus, E.

The ISFSI owner has the option of constructing the pad to comply with the limits of Set A or Set B without performing site-specific cask impact analyses. It is recognized that, for a specific ISFSI site, the reinforced concrete, as well as the underlying engineered fill properties, may be different at different locations on the pad or may be uniform, but non-compliant with either Set A or Set B. In that case, the site-specific conditions must be performed to demonstrate compliance with the design limits of the HI-STAR system (e.g., maximum rigid body g-load less than or equal to 60g's). The essential data which define the pad (Set A and Set B) used to qualify the HI-STAR 100 are provided in Table 3.A.1.

As the results presented in this appendix show, Set B parameters lead to a lower g-loads than the LLNL Set (Set A).

3.A.4.2 Input Data

Table 3.A.1 characterizes the properties of the reference target pad (Set A and Set B) used in the analysis.

The principal strength parameters that define the stiffness of the pad, namely t_p, E and f_c' are input in the manner described in [3.A.2] and [3.A.4].

Table 3.A.2 details the geometry of the HI-STAR 100 used in the drop simulations. This data is taken from applicable HI-STAR 100 drawings.

3.A.5 Finite Element Model

The finite-element model of the Holtec HI-STAR 100 cask (bottom plate, shells, forging, lid, Holtite polymer and its connectors), concrete pad and a portion of the subgrade soil is constructed using the pre-processor integrated with the LS-DYNA3D software [3.A.5]. The deformation field for all postulated drop events, the end-drop, the side-drop and the tipover, exhibits symmetry with the vertical plane passing through the vertical diameter of the cask and the concrete pad length. Using this symmetry condition of the deformation field a half finite-

element model is constructed. The finite-element model is organized into five independent parts (the cask, the MPC steel plates, the basket fuel zone, the concrete pad and the soil). The final model contains 35431 nodes, 29944 solid type finite-elements, five (5) materials, one (1) property and four (4) interfaces. The finite-element model used for the side-drop and tipover-drop events is depicted in Figures 3.A.1 through 3.A.4. Figures 3.A.5 through 3.A.8 show the end-drop finite-element model.

The half portion of the cylindrical cask contains 7,320 solid finite-elements. Figure 3.A.11 depicts details of the cask finite-element mesh.

The elasto-plastic behavior characteristics of all HI-STAR components (shells, lids, Holtite, outer skin, connectors, etc.) are simulated as rigid materials using a DYNA3D built-in command.

The soil grid, shown in Figure 3.A.9, is a rectangular prism (800 inches long, 375 inches wide and 470 inches deep), is constructed from 13294 solid type finite-elements. The material defining this part is an elastic orthotropic material. The central portion of the soil (400 inches long, 150 inches wide and 170 inches deep) where the stress concentration is expected to appear is discretized with a finer mesh.

The concrete pad is 320 inches long, 100 inches wide and is 36 inches thick. This part contains 8208 solid finite-elements. A uniform sized finite-element mesh, shown in Figure 3.A.10, is used to model the concrete pad. The concrete behavior is described using a special constitutive law and yielding surface contained within DYNA3D. The geometry, the material properties, and the material behavior are identical to the LLNL reference pad.

The MPC and the contained fuel is modeled in two parts which represent the lid and baseplate, and the fuel area. An elastic material is used for both parts. The finite-element mesh pertinent to the MPC contains 1122 solid finite-elements and is shown in Figure 3.A.14. The mass density is appropriate to match a representative weight of 241,937 lb which is an approximate mean of the upper and lower weight estimates for a loaded HI-STAR 100. The total weight used in the analysis is approximately 8,000 lb heavier than the HI-STAR 100 containing the lightest weight MPC.

Analysis of a single mass impacting a spring with a given initial velocity shows that both the maximum deceleration "a_M" of the mass and the time duration of contact with the spring "t_c" are related to the dropped weight "w" and drop height "h" as follows:

$$a_M \sim \frac{\sqrt{h}}{\sqrt{w}}; t_c \sim \sqrt{w}$$

Therefore, the most conservatism is introduced into the results by using the minimum weight. However, since the difference between the heaviest and the lightest HI-STAR 100 is only 9,500 lb, a small percentage of the total weight, the results using the minimum weight will yield a 2%

increase in the maximum deceleration and a 2% decrease in the duration of the impact. This small difference is neglected in the presentation of results.

It is emphasized that the finite element model described in the foregoing is identical in its approach to the "Holtec model" described in the benchmark report [3.A.4]. Gaps between the MPC and the overpack are included in the model.

3.A.6 Impact Velocity

a. Linear Velocity: Vertical Drops

For the side drop and vertical drop events, the impact velocity, υ, is readily calculated from the Newtonian formula:

$$\upsilon = \sqrt{(2gh)}$$

where

g = acceleration due to gravity
h = free-fall height

b. Angular velocity: Tipover

The tipover event is an artificial construct wherein the HI-STAR 100 overpack is assumed to be perched on its edge with its C.G. directly over the pivot point A (Figure 3.A.15). In this orientation, the overpack begins its downward rotation with zero initial velocity. At angle ψ_1 (Figure 3.A.17), the pivot point shifts to point B; but otherwise the downward rotation of the overpack continues with increasing angular velocity. Towards the end of the tipover, the overpack is horizontal with its downward velocity ranging from zero at the pivot point to a maximum at the farthest point of impact (point E in Figure 3.A.18). The angular velocity at the instant of impact defines the downward velocity distribution along the contact line.

In the following, we derive an explicit expression for calculating the angular velocity of the cask at the instant when it impacts on the ISFSI pad.

Referring to Figure 3.A.15, let r be the length AC where C is the cask centroid. Therefore,

$$r = \left(\frac{d^2}{4} + (h+a)^2 \right)^{1/2} \qquad \textbf{(3.A.1)}$$

The mass moment of inertia of the HI-STAR 100 System, considered as a rigid body, can be written about an axis through point A, as

$$I_A = I_c + \frac{W}{g} r^2 \qquad \textbf{(3.A.2)}$$

where I_c is the mass moment of inertia about a parallel axis through the cask centroid C, and W is the weight of the cask (W = Mg).

Let $\theta_1(t)$ be the rotation angle between a vertical line and the line AC. The equation of motion for rotation of the cask around point A, during the time interval prior to contact with point B (Figure 3.A.15), is

$$I_A \frac{d^2\theta_1}{dt^2} = \text{Mgr} \sin\theta_1 \qquad \textbf{(3.A.3)}$$

This equation can be rewritten in the form

$$\frac{I_A}{2} \frac{d\left(\dot{\theta}_1\right)^2}{d\theta_1} = \text{Mgr} \sin\theta_1 \qquad \textbf{(3.A.4)}$$

which can be integrated over the limits $\theta_1 = 0$ to $\theta_1 = \psi_1$. (See Figure 3.A.17).

The final angular velocity $(d\theta_1/dt)_B$ at the time instant just prior to contact at point B is given by the expression

$$\dot{\theta}_1(t_B) = \sqrt{\frac{2Mgr}{I_A}}\left(1 - \cos\psi_1\right) \qquad \textbf{(3.A.5)}$$

The angle ψ_1 between AC and the vertical, at the time just prior to contact, is given by geometry as

$$\psi_1 = \psi_A - \psi_B \qquad \textbf{(3.A.6)}$$

where

$$\psi_A = \tan^{-1}\left(\frac{a}{b}\right)$$

$$\psi_B = \tan^{-1}\left(\frac{d}{2h}\right)$$

and a and b are shown in Figure 3.A.17. At contact with point B at time t_B (Figure 3.A.16), the angular impulse momentum equation can be used to determine a new initial angular velocity for subsequent determination of the angular motion about point B. Ignoring the small impulsive moment from the cask weight due to the instantaneous change in moment arm, the angular momentum balance gives

$$I_A\dot{\theta}_1(t_B) = I_B\dot{\theta}_2(0) \tag{3.A.7}$$

where $I_B = I_C + Mr_1^2$ is the mass moment of inertia of the cask about point B. Solving for $\dot{\theta}_2$ (0) and eliminating $\dot{\theta}_1$ (t_b) using Eq. (3.A.5) gives

$$\dot{\theta}_2(0) = \sqrt{\frac{2Mgr_1}{I_B}\frac{I_A}{I_B}(1-\cos\psi_1)\left(\frac{r}{r_1}\right)} \tag{3.A.8}$$

The angle $\theta_2(0)$, which is the starting point for the rotational motion around point B, is easily obtained from the cask geometry. With X defined in Figure 3.A.16.

$$\sin\theta_2(0) = \frac{X(0)}{r_1} \tag{3.A.9}$$

where X(0) can be determined from Figure 3.A.17 as

$$X(0) = r\sin\psi_1 - (a^2+b^2)^{1/2}$$

so that

$$\sin\theta_2(0) = \frac{r}{r_1}\sin\psi_1 - \frac{(a^2+b^2)^{1/2}}{r_1} \tag{3.A.10}$$

where

$$r_1 = \left[\left(\frac{D}{2}\right)^2 + h^2\right]^{1/2}$$

With the initial conditions determined by Eq. (3.A.9) and (3.A.10), the solution for the motion is easily obtained.

The angular velocity $(d\theta_2/dt)_f$ at the instant of ground contact is

$$\dot{\theta}_{2f}^2 - \dot{\theta}_2^2(0) = \frac{2Mgr_1}{I_B}\left(\cos\theta_2(0) - \cos\theta_{2f}\right) \qquad \textbf{(3.A.11)}$$

where, from Figure 3.A.18

$$\theta_{2f} = \cos^{-1}\left(\frac{D}{2r_1}\right) \qquad \textbf{(3.A.12)}$$

Using Eq. (3.A.8) to eliminate $(d\theta_2/dt)_0$ from Eq. (3.A.11) leads to a solution for the angular velocity $(d\theta_2/dt)_f$ when interface contact occurs, in the form

$$\dot{\theta}_{2f} = \sqrt{\frac{2Mgr_1}{I_B}\beta} = \omega \qquad \textbf{(3.A.13)}$$

$$\text{where, } \beta = \frac{I_A r}{I_B r_1}\left(1 - \cos\psi_1\right) + \cos\theta_2(0) - \cos\theta_{2f} \qquad \textbf{(3.A.14)}$$

Equations (3.A.13) and (3.A.14) establish the initial conditions for the final phase of the tipover analysis; namely, the portion of the motion when the cask is decelerated by the resistive force at the ISFSI pad interface.

Using the data germane to HI-STAR 100 (Table 3.A.2), and the above equations, the angular velocity of impact is calculated as 1.79 rad/sec.

3.A.7 Results

3.A.7.1 Set A Pad Parameters:

The LS-DYNA3D time-history results are processed using the Butterworth filter (in conformance with the LLNL methodology) to establish the time-history rigid body motion of the cask. The material points on the cask where the acceleration displacement and velocity are computed for each of the three drop scenarios are shown in Figure 3.A.19.

Node 2901 (Channel A2), which is located midway on the outermost shell generator at the top in side drop events serves as the reference point.

Node 5151 (Channel A1), which is located at the center of the outer surface of the bottom forging, serves as the reference point for end-drop scenarios.

Node 6000 (Channel A3), which is located at the center of the cask top lid outer surface, serves as the reference point for the tipover scenario with the pivot point indicated as Point 0 in Figure 3.A.19.

The results reported below for maximum cask-ISFSI contact force have been multiplied by 2.0 to reflect the fact that only 50% of the dropped mass is included in the model due to the symmetry assumption.

i. Side Drop:

The time-histories of the impact force and displacement, velocity, and deceleration at the reference node point (Channel A2) have been determined for a drop height, h, of 72". The peak cask/pad impact force is 9.636E+06 lbs and the contact duration associated with the initial peak is 9.5 milli-seconds.

The maximum rigid body deceleration (filtered at 350 Hz cut-off frequency) is 49.67 g's, which is below the design basis limit of 60 g's. The time duration of the peak deceleration pulse is 4.4 milli-seconds.

ii. Tipover:

The time-histories of the impact force and displacement, velocity and vertical deceleration of Channel A3 (in Figure 3.A.19) for this event have been determined [3.A.7].

The deceleration at the tip of the fuel basket is obtained by ratioing the filtered deceleration of Node 6000. The maximum filtered deceleration at the tip of the fuel basket is 66.02 x 0.906 = 59.81 g's which is below the design basis limit. The 0.906 multiplier is based on the geometry of the loaded HI-STAR 100 (further explained in Table 3.A.3). The maximum contact force in this event is 6.43E+06 lbs and the contact duration associated with the initial peak is approximately 8.8 milli-seconds. It should be emphasized that the calculated deceleration for Node 6000 was filtered at 350 Hz cut-off frequency.

The duration of the initial deceleration pulse is 4.4 milli-seconds.

iii. End Drop:

As in all other impact cases analyzed in this appendix, the overpack is treated as a completely rigid body in the end drop scenario. One drop height is considered: h = 21". The results are summarized in Table 3.A.3 and the contact force, displacement, velocity, and acceleration time-histories at Channel A1 (Figure 3.A.19) for the 21" end drop are documented in the calculation package [3.A.7]. The duration of the contact force initial pulse is approximately 2.7 milli-seconds, and the filtered cask deceleration pulse is 2.1 milli-seconds.

A carry height of 21" gives peak filtered deceleration in the event of an end drop of approximately 53 g's.

Decelerations obtained from the DYNA3D numerical solutions are filtered through a Butterworth type filter identical to the filter used by LLNL to investigate the "generic" cask [3.A.2]. The filter has the following characteristics: 350 Hz passband frequency, 10,000 Hz stopband frequency, 0.15 maximum passband ripple, and 10 minimum stopband attenuation.

The computer code utilized in this analysis is LS-DYNA3D [3.A.5] validated under Holtec's QA system. Table 3.A.3 summarizes the key results for all impact simulations for the Set A parameters discussed in the foregoing.

3.A.7.2 Set B Pad Parameters:

As stated previously, Set B parameters produce a much more compliant pad than the LLNL reference pad (Set A). This fact is borne out by the side drop, tipover and end drop analyses performed on the pad defined by the Set B parameters. Table 3.A.4 provides the filtered results for the three impact scenarios. In every case, the peak decelerations corresponding to Set B parameters are less than those for Set A (provided in Table 3.A.3).

Impact force and acceleration time history curves for Set B have the same general shape as those for Set A and are contained in the calculation package. All significant results are summarized in Table 3.A.4.

3.A.8 Computer Codes and Archival Information

The input and output files created to perform the analyses reported in this appendix are archived in the Holtec International calculation package.

3.A.9 Conclusion

The DYNA3D analysis of HI-STAR 100 reported in this appendix leads to the following conclusion:

a. If a loaded HI-STAR undergoes a free fall for a height of 21 inches in a vertical orientation, the maximum rigid body deceleration is limited to 52.26 g's and 50.25 g's for Set A and Set B pad parameters, respectively.

b. If a loaded HI-STAR 100 undergoes a free fall in a horizontal orientation (side drop) for a height 72", the maximum rigid body deceleration is limited to 49.67 and 46.77g's for Set A and Set B pad parameters, respectively.

c. If a loaded HI-STAR 100 overpack pivots about its bottom edge and tips over then the maximum rigid body deceleration of the cask centerline at the plane of the top of the fuel basket cellular region is 59.81 and 50.64 g's respectively for pad parameter Set A and Set B.

Tables 3.A.3 and 3.A.4 provides the key results for all drop cases studied herein for pad parameter Set A and B respectively.

Recalling that the design basis g-load is 60 g's, the above impact scenarios are comfortably enveloped by the level D design limit and allow ample margin for the introduction of appropriate dynamic load factors into the component stress analyses.

If the pad designer maintains each of the three significant parameters (t_p, f_c' and E) below the limit for the specific set selected (Set A or Set B), then the stiffness of the pad at the ISFSI site will be lower and the computed decelerations at the ISFSI site will also be expected to be lower. Furthermore, because the mathematical model for the cask assumes infinite rigidity (which is not a requirement for the LLNL methodology (3.A.2) or Holtec's benchmark work effort (3.A.4), refinement of the cask dynamic model will accrue further reduction in the computed peak deceleration. Likewise, incorporation of the structure flexibility in the MPC enclosure vessel, fuel basket, etc., would lead to additional reductions in the computed values of the peak deceleration. These refinements, however, add to the computational complexity. Because g-limits are met without the above-mentioned and other refinements in the cask dynamic model, the rigid body model for HI-STAR 100 was retained to preserve simplicity.

3.A.10 References

[3.A.1] Witte, M., et al., "Evaluation of Low-Velocity Impacts Tests of Solid Steel Billet onto Concrete Pads.", Lawrence Livermore National Laboratory, UCRL-ID-126274, Livermore, California, March 1997.

[3.A.2] Witte, M., et al., "Evaluation of Low-Velocity Impacts Tests of Solid Steel Billet onto Concrete Pads, and Application to Generic ISFSI Storage Cask for Tipover and Side Drop.", Lawrence Livermore National Laboratory, UCRL-ID-126295, Livermore, California, March 1997.

[3.A.3] Tang, D.T., Raddatz, M.G., and Sturz, F.C., "NRC Staff Technical Approach for Spent Fuel Cask Drop and Tipover Accident Analysis", SFPO, USNRC (1997).

[3.A.4] Simulescu, I., "Benchmarking of the Holtec LS-DYNA3D Model for Cask Drop Events", Holtec Report HI-971779, September 1997.

[3.A.5] LS-DYNA3D, Version 936-03, Livermore Software Technology Corporation, September 1996.

[3.A.6] Whirley, R.G., "DYNA3D, A Nonlinear, Explicit, Three-Dimensional Finite element Code for Solid and Structural Mechanics - User Manual.", Lawrence Livermore National Laboratory, UCRL-MA-107254, Revision 1, 1993.

[3.A.7] Zhai, J., "Analysis of the Loaded HI-STAR 100 System Under Drop and Tip-Over Scenarios," Holtec Report HI-2002466.

Table 3.A.1
Essential Variables to Characterize the ISFSI Pad (Set A and Set B)

Item	Parameter Set A	Parameter Set B
Thickness of concrete (inches)	36	28
Nominal compressive strength of concrete at 28 days (psi)	4,200	6,000
Max. modulus of elasticity of the subgrade (psi)	28,000	16,000

Notes:

1. The concrete Young's Modulus is derived from the American Concrete Institute recommended formula where f is the nominal compressive strength of the concrete (psi).

2. The effective modulus of elasticity of the subgrade shall be measured by the classical "plate test" or other appropriate means before pouring of the concrete to construct the ISFSI pad.

Table 3.A.2
Key Input Data in Drop Analyses

Cask weight	128,275 lb
Holtite weight	12,926 lb
Holtite connectors weight	11,879 lb
Length of the cask	203.125 inches
Length of the Holtite	173.125 inches
Diameter of the bottom plate	83.25 inches
Inside diameter of the cask	68.75 inches
Outside diameter of the cask shells	85.75 inches
Outside diameter of the enclosure plate	96.00 inches
Outside diameter of the Holtite	95.00 inches
MPC weight (including fuel)	88,857 lb
MPC height	190.5 inches
MPC diameter	68.375 inches
MPC bottom plate thickness	2.5 inches
MPC top plate thickness	9.5 inches

Table 3.A.3
FILTERED RESULTS FOR DROP AND TIPOVER SCENARIOS (SET A)

Drop Event	Rigid Cask Model†			
	Max. Displ (in)	**Impact Velocity (in/sec)**	**Max. Acc. (g's)**	**Acc. Pulse Duration (msec.)**
End-21"	1.144	127.4	52.26	2.1
Side-72"	2.674	235.9	49.67	4.4
Tipover Top of Cask††	4.231	348.4	66.02	4.4
Tipover Top of Basket Elevation	--	--	59.81	--

† The passband frequency of the Butterworth filter is 350 Hz.

†† The distance of the top of the fuel basket is 176.25" from the pivot point. The distance of the top of the cask is 194.375" from the pivot point. Therefore, all displacements, velocities, and accelerations of the top of the fuel basket are 90.6% of the cask top (176.25/194.4).

Table 3.A.4
FILTERED RESULTS FOR DROP AND TIPOVER SCENARIOS (SET B)

Drop Event	Rigid Cask Model[†]			
	Max. Displ (in)	**Impact Velocity (in/sec)**	**Max. Acc. (g's)**	**Acc. Pulse Duration (msec.)**
End-21"	1.335	127.4	50.25	2.0
Side-72	4.533	235.9	46.77	4.0
Tipover Top of Cask[††]	6.620	348.4	55.89	4.0
Tipover Top of Basket Elevation	--	--	50.64	--

[†] The passband frequency of the Butterworth filter is 350 Hz.

[††] The distance of the top of the fuel basket is 176.25" from the pivot point. The distance of the top of the cask is 194.375" from the pivot point. Therefore, all displacements, velocities, and accelerations of the top of the fuel basket are 90.6% of the cask top (176.25/194.4).

"MISCELLANEOUS NUMERICAL CALCULATIONS SUPPORTING APPENDIX 3.A"
INTENTIONALLY DELETED

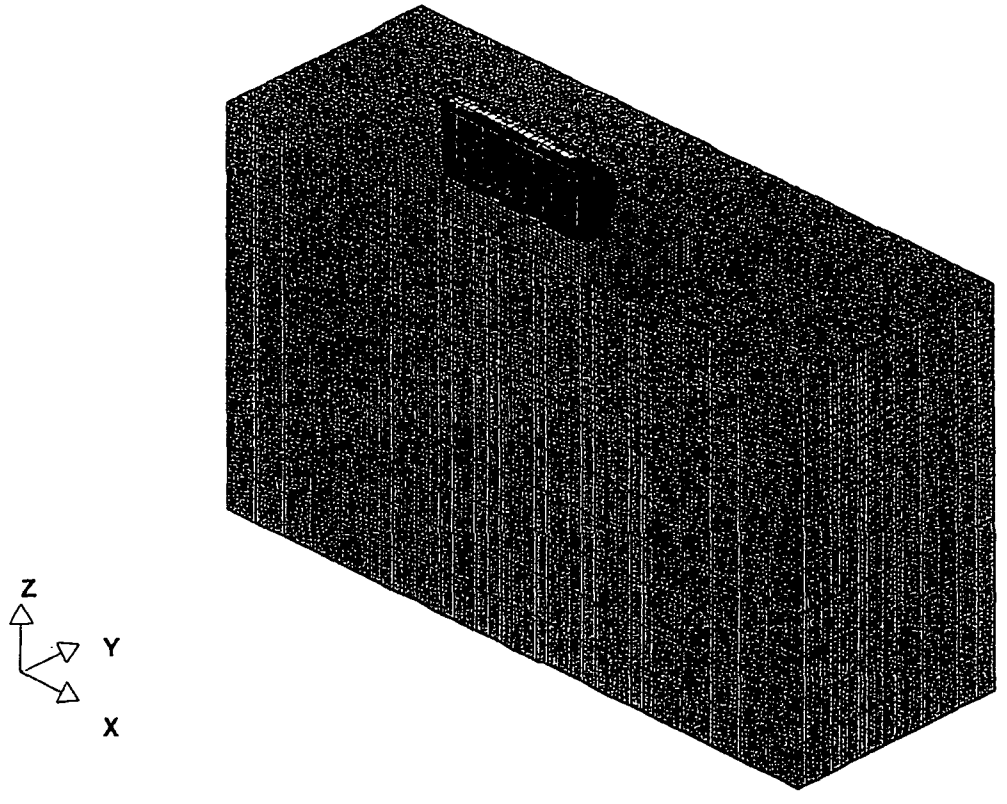

Fig. 3.A.1 Side-Drop and Tipover Finite-Element Model (3-D View)

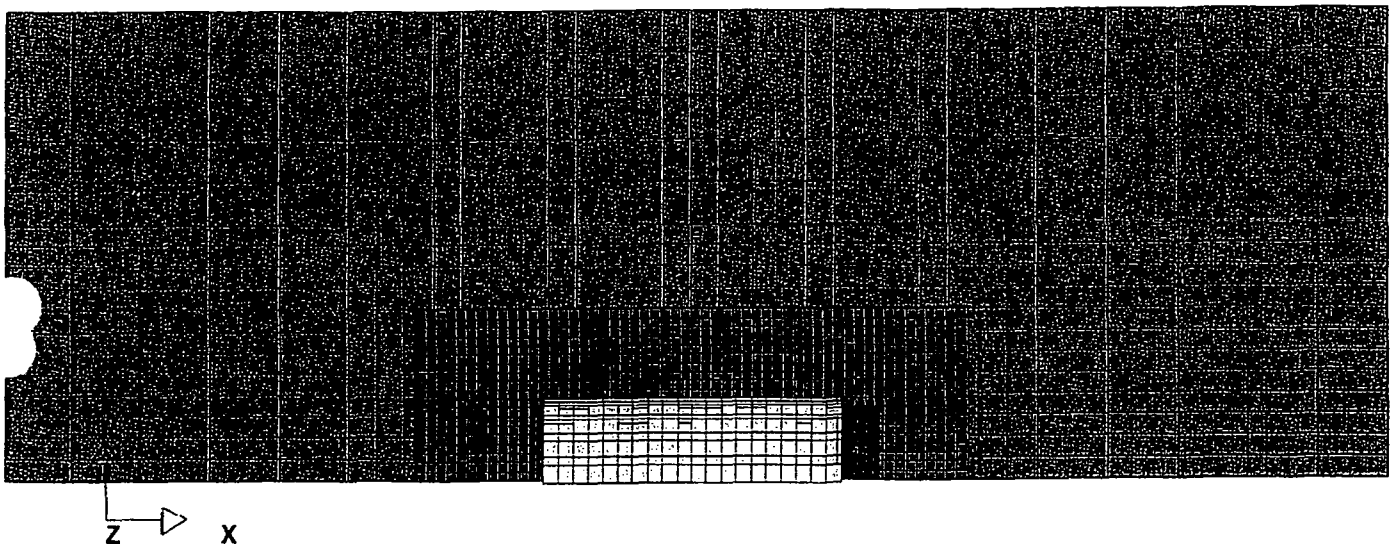

Fig. 3.A.2 Side-Drop and Tipover Finite-Element Model (Plan View)

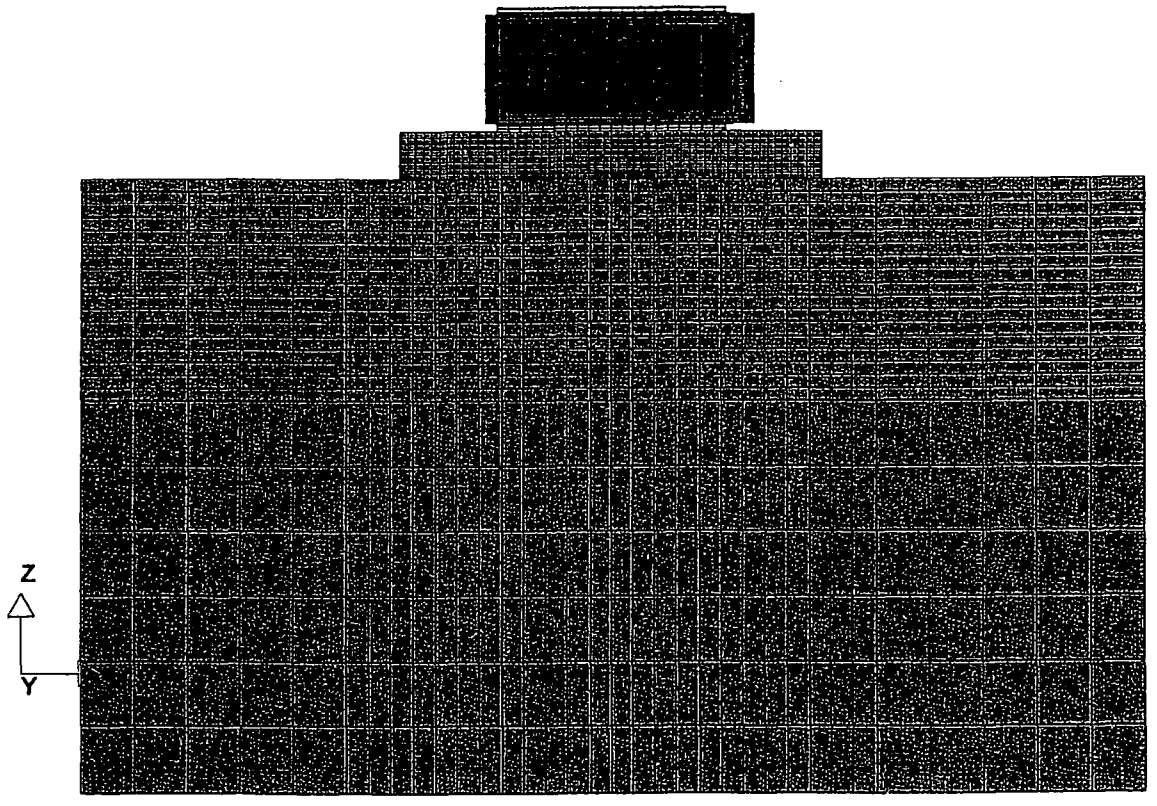

Fig. 3.A.3 Side-Drop and Tipover Finite-Element Model (XZ View)

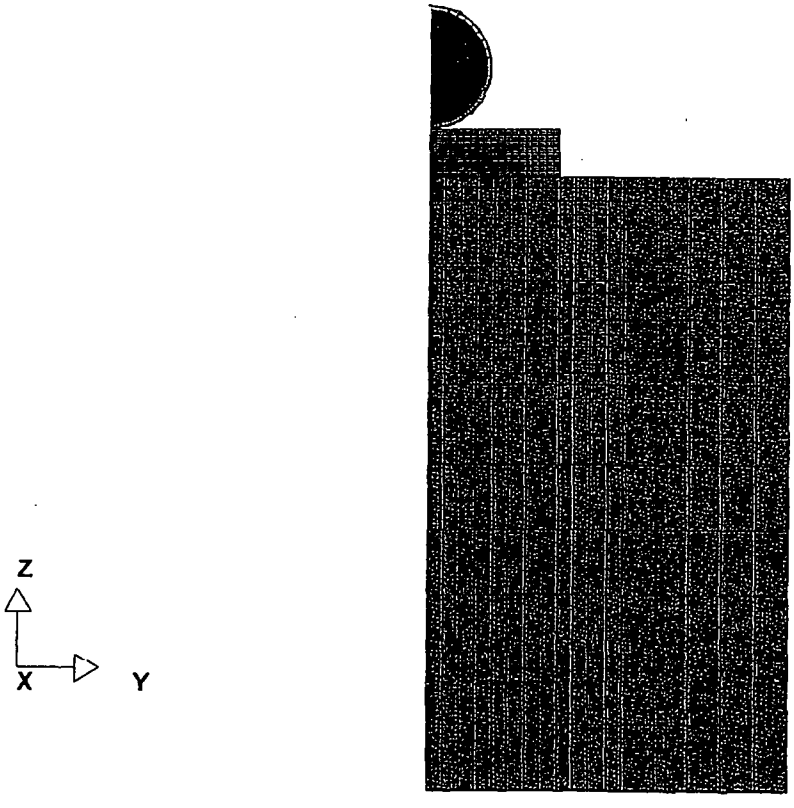

Fig. 3.A.4 Side-Drop and Tipover Finite-Element Model (YZ View)

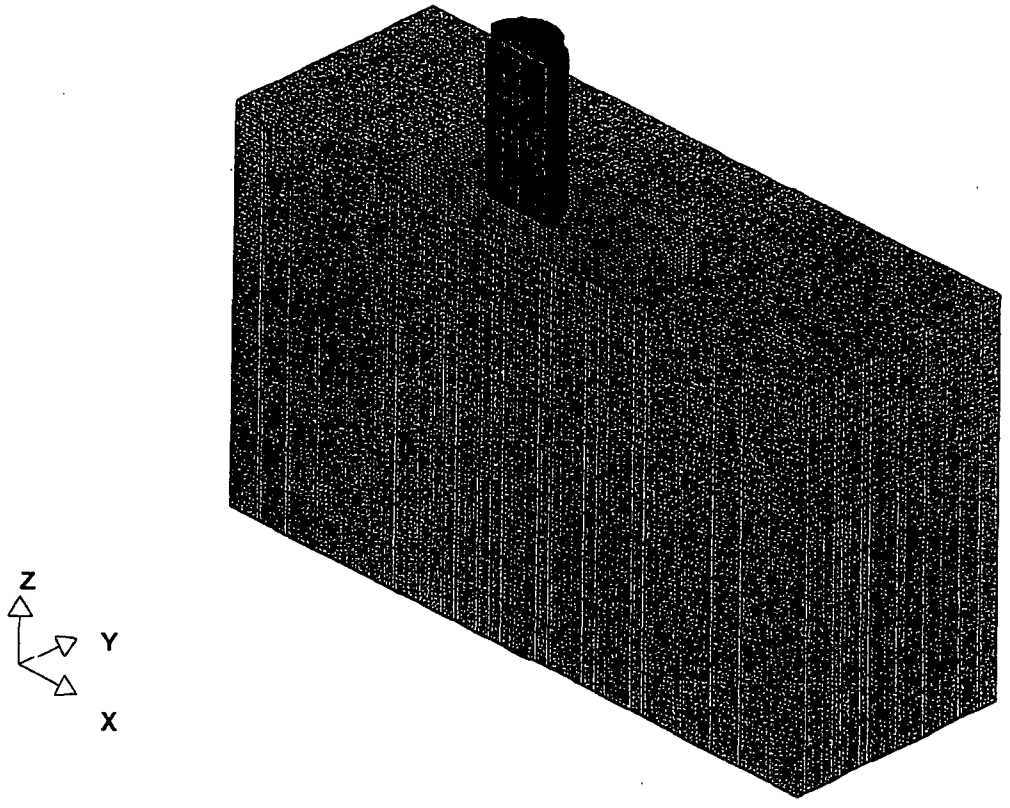

Fig. 3.A.5 End-Drop Finite-Element Model (3-D View)

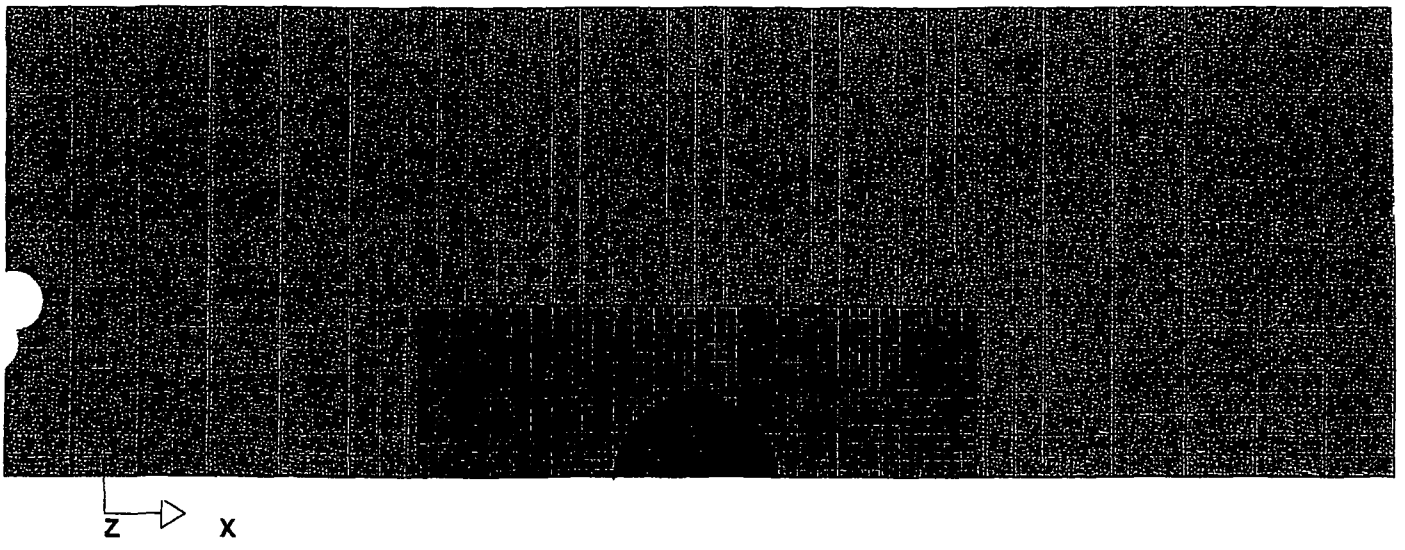

Fig. 3.A.6 End-Drop Finite-Element Model (Plan View)

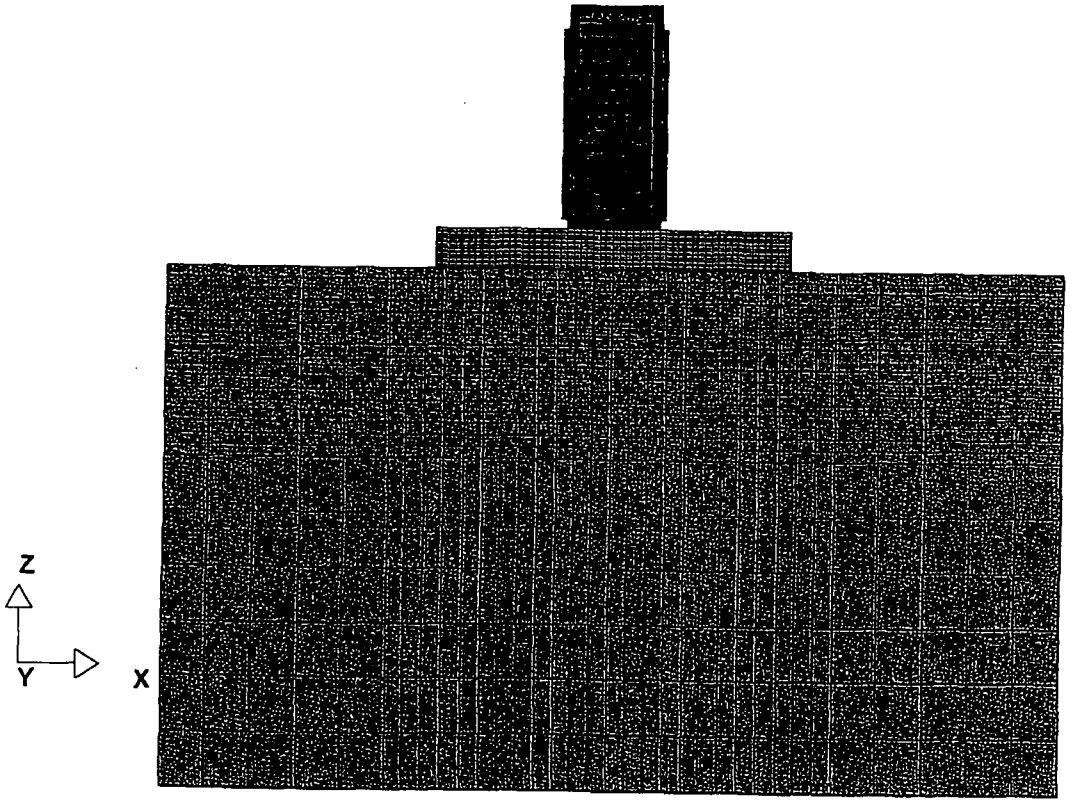

Fig. 3.A.7 End-Drop Finite-Element Model (XZ View)

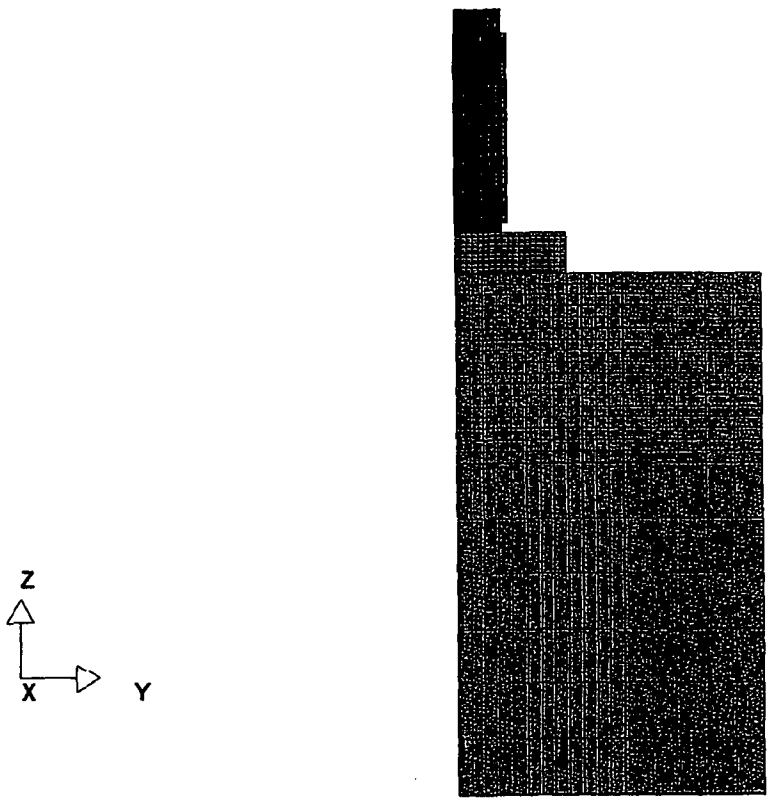

Fig. 3.A.8 End-Drop Finite-Element Model (YZ View)

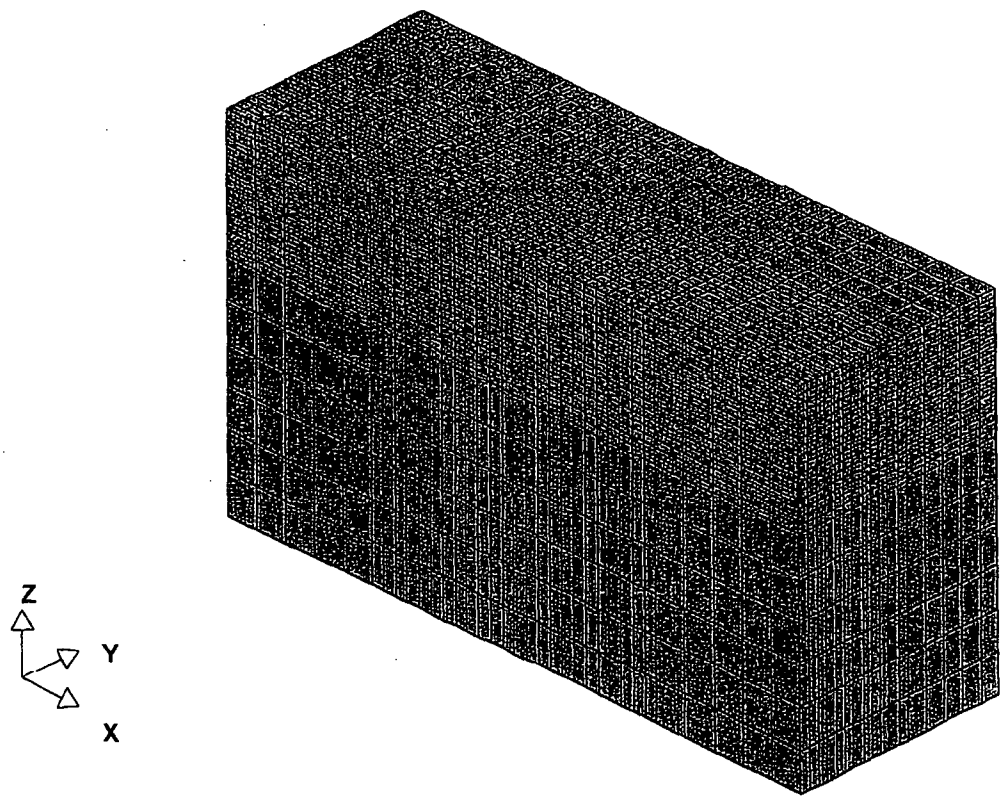

Fig. 3.A.9 Soil Finite-Element Model (3-D View)

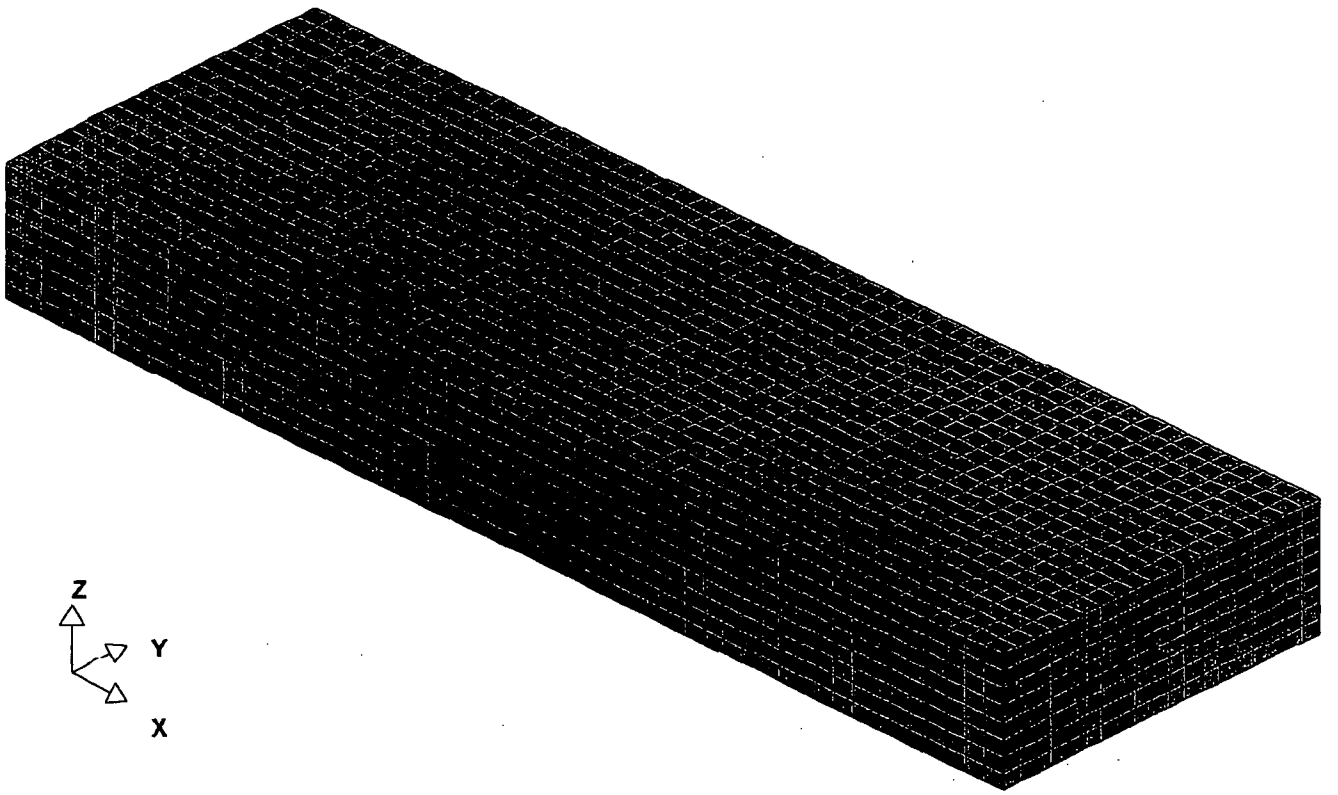

Fig. 3.A.10 Concrete Pad Finite-Element Model (3-D View)

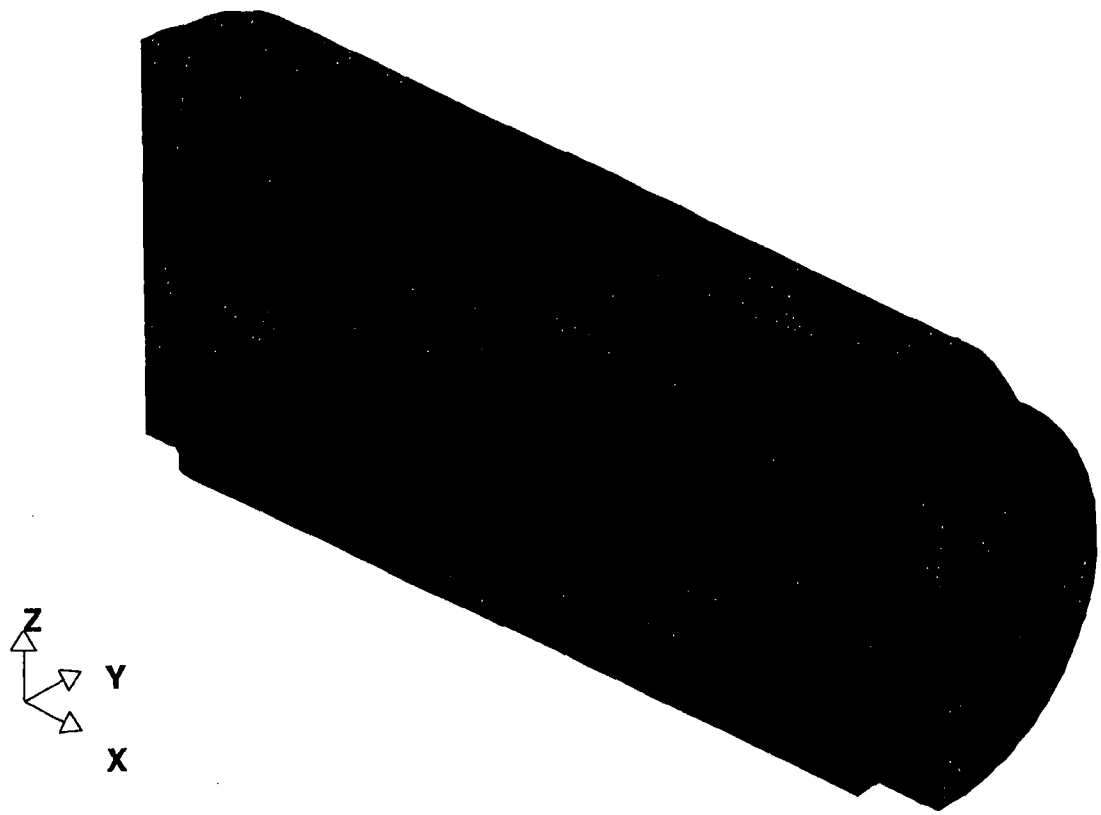

Figure 3.A.11 Cask Finite-Element Model (3-D View)

FIGURE 3.A.12 DELETED

FIGURE 3.A.13 DELETED

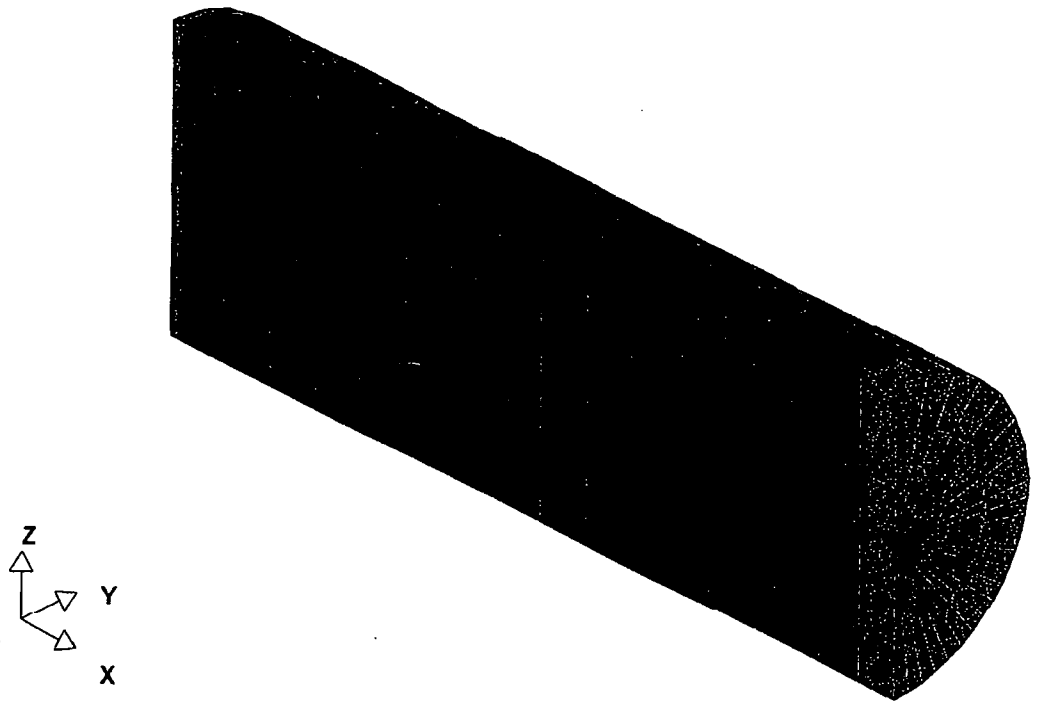

Fig. 3.A.14 MPC Finite-Element Model (3-D View)

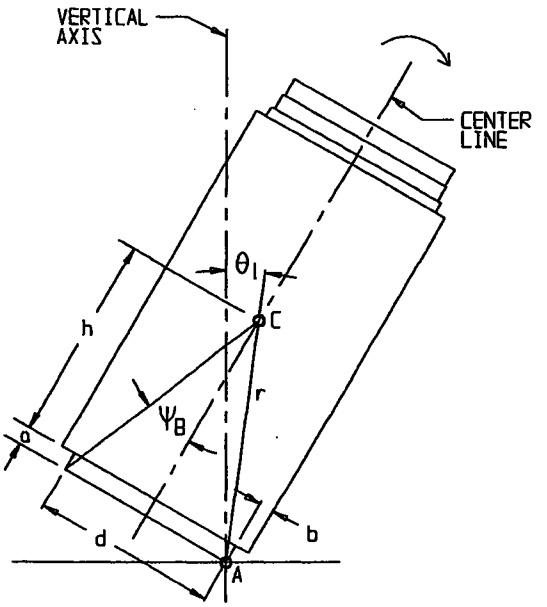

FIGURE 3.A.15; PIVOT POINT SHIFT DURING TIP-OVER
INITIAL CONDITION

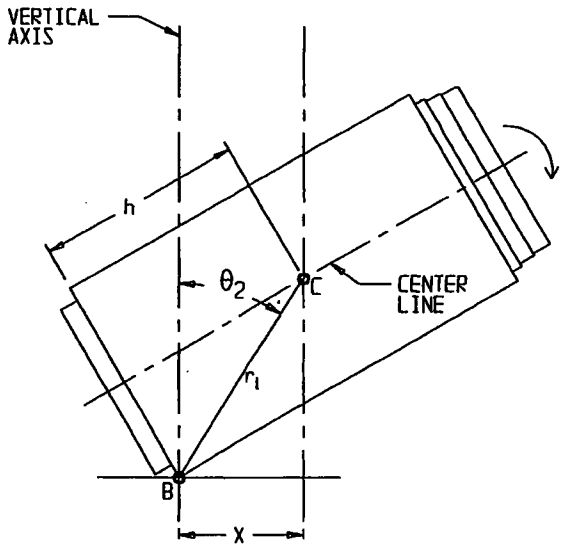

FIGURE 3.A.16; PIVOT POINT SHIFT DURING TIP-OVER
INTERMEDIATE CONDITION

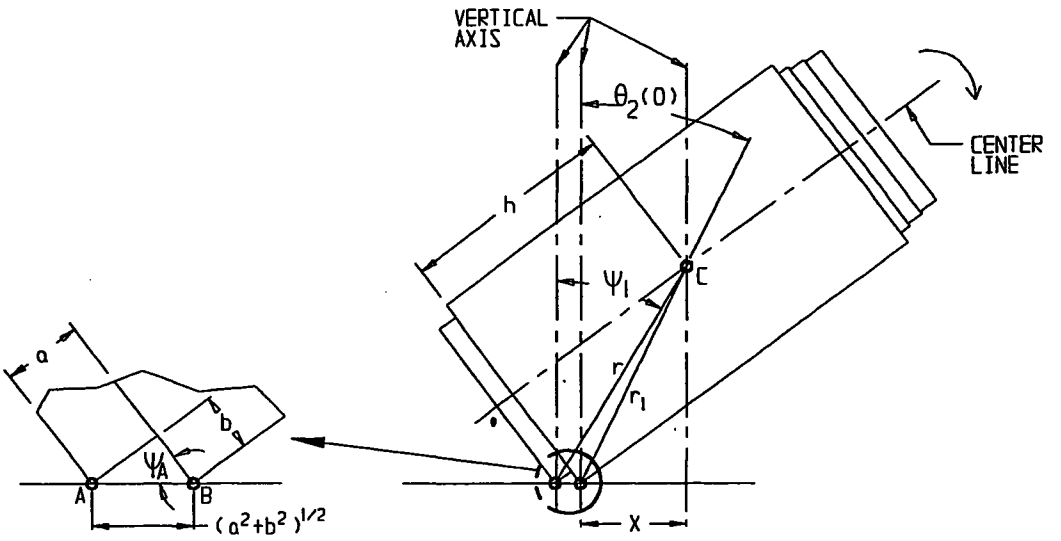

FIGURE 3.A.17; TIP-OVER EVENT AT THE INSTANT WHEN POINTS A AND B ARE BOTH IN CONTACT WITH THE GROUND

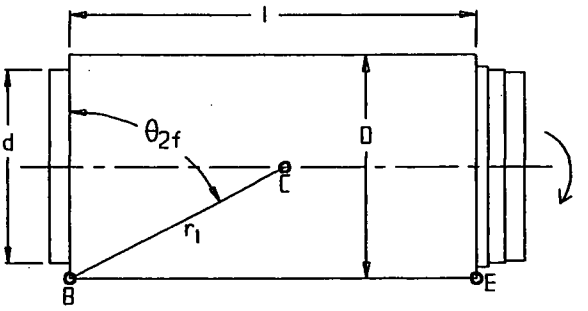

FIGURE 3.A.18; TIP-OVER EVENT OVERPACK SLAMS AGAINST THE FOUNDATION DEVELOPING A RESISTIVE FORCE

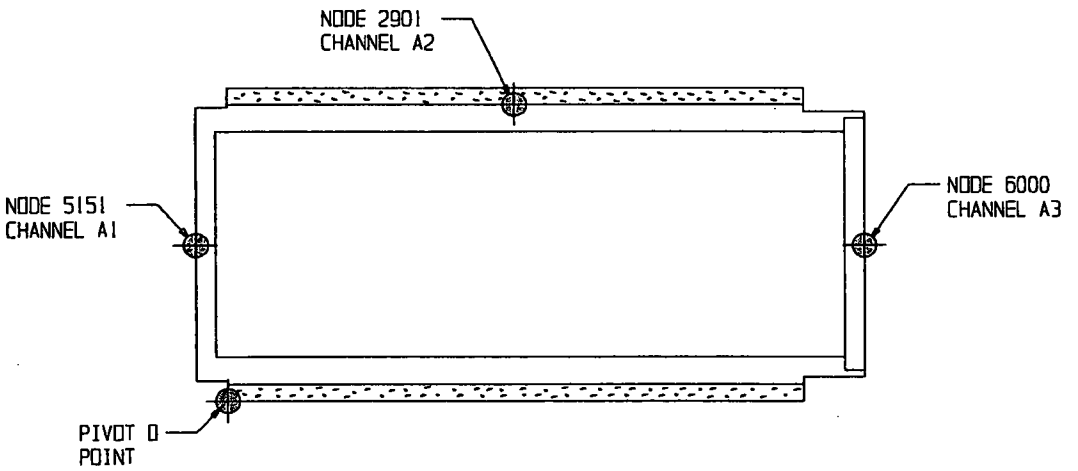

FIGURE 3.A.19; MEASUREMENT POINTS AND CORRESPONDING FINITE-ELEMENT MODEL NODES

APPENDIX 3.B - ANALYSIS OF DAMAGED FUEL CONTAINER

3.B.1 Introduction

This appendix contains an analysis of the damaged fuel container that is used for the HI-STAR 100 MPC. The objective of the analysis is to demonstrate that the storage container is structurally adequate to support the loads that develop during normal lifting operations and during an end drop.

The upper closure assembly is designed to meet the requirements set forth for Special Lifting Devices in Nuclear Plants [2]. The remaining components of the damaged fuel container are governed by ASME Code Section III, Subsection NG.

3.B.2 Composition

This appendix was created using the Mathcad (version 6.0+) software package. Mathcad uses the symbol ':=' as an assignment operator, and the equals symbol '=' retrieves values for constants or variables.

3.B.3 References

1. Crane Manufacture's of America Association, Specifications for Electric Overhead Traveling Cranes #70.

2. ANSI N14-6, Special Lifting Devices for Loads Greater than 10000 lbs. in Nuclear Plants.

3. ASME Boiler and Pressure Vessel Code, Section III Subsection NG, July 1995

3.B.4 Assumptions

1. Buckling is not a concern during an accident since during a drop the canister will be supported by the walls of the fuel basket.

2. The strength of the weld is assumed to decrease the same as the base metal as the temperature is increased.

3.B.5 Method

Three cases are considered: 1) normal handling of container, 2) evaluation of lifting attachment to ANSI N14-6 criteria, and 3) accident drop event.

3.B.6 Acceptance Criteria

1) Normal Handling -

a) Container governed by ASME NG[3] allowables:
shear stress allowable is 60% of membrane stress intensity

b)Welds are governed by NG Code allowables with appropriate quality factors;
stress limit =60% of tensile stress intensity(per Section III, Subsection NG-3227.2).

2) Drop Accident -

a) Container governed by ASME Section III, Appendix F allowables:
(allowable shear stress = 0.42 Su)

3.B.7 Input Data

The damaged fuel container is only handled while still in the spent fuel pool. Therefore, its design temperature for lifting considerations is the temperature of the fuel pool water (150°F). The design temperature for accident conditions is 725°F. All dimensions are taken from the design drawings and bill of materials in Chapter 1. The basic input parameters used to perform the calculations are:

Design stress intensity of SA240-304 (150°F)	$S_{m1} := 20000 \cdot psi$	Table 1.A.1
Design stress intensity of SA240-304 (725°F)	$S_{m2} := 15800 \cdot psi$	
Yield stress of SA240-304 (150°F)	$S_{y1} := 27500 \cdot psi$	Table 1.A.3
Yield stress of SA240-304 (725°F)	$S_{y2} := 17500 \cdot psi$	
Ultimate strength of SA240-304 (150°F)	$S_{u1} := 73000 \cdot psi$	Table 1.A.2
Ultimate strength of SA240-304 (725°F)	$S_{u2} := 63300 \cdot psi$	
Ultimate strength of weld material (150°F)	$Su_w := 70000 \cdot psi$	
Ultimate strength of weld material (725°F)	$Su_{wacc} := Su_w \cdot \frac{S_{u2}}{S_{u1}}$	
Weight of a BWR fuel assembly	$W_{fuel} := 400 \cdot lbf$	
Weight of the damaged fuel container	$W_{container} := 150 \cdot lbf$	

Wall thickness of the container sleeve	$t_{sleeve} := 0.12 \cdot in$
Thickness of the base	$t_{base} := 0.12 \cdot in$
Inner dimension of the container sleeve	$id_{sleeve} := 4.93 \cdot in$
Wall thickness of container collar	$t_{collar} := 0.12 \cdot in$
Distance from end of sleeve to top of engagement slot	$d_{slot} := 0.44 \cdot in$
Diameter of the shear pin	$D_{pin} := 0.375 \cdot in$
Diameter of the lead-in	$D_{leadin} := 1.00 \cdot in$
Diameter of the lead-in at tapered end	$D_{taper} := 0.63 \cdot in$
Thickness of weld between lead-in and lead-in collar	$t_{weld1} := 0.12 \cdot in$
Length of the load tab	$l_{tab} := 2.15 \cdot in$
Height of the load tab	$h_{tab} := 0.5 \cdot in$
Width of the load tab	$w_{tab} := 0.5 \cdot in$
Thickness of weld between locking shaft and load tab	$t_{weld2} := 0.1875 \cdot in$
Thickness of fuel spacer tubing	$t_{tube} := 0.25 \cdot in$
Size of fuel spacer (square) tubing	$s_{tube} := 4.0 \cdot in$
Size of square cutout in fuel spacer tubing	$s_{cutout} := 2.00 \cdot in$
Quality factor for full penetration weld (visual inspection)	$n := 0.5$ Table NG-3352-1
Quality factor for single fillet weld (visual inspection)	$nf := 0.35$
Dynamic load factor for lifting [1]	$DLF := 1.15$

3.B.8 Calculations

3.B.8.1 Lifting Operation (Normal Condition)

The critical load case under normal conditions is the lifting operation. The key areas of concern are the container sleeve, the weld between the sleeve and the base of the container, the container collar, and the upper closure assembly. All calculations performed for the lifting operation assume a dynamic load factor of 1.15.

3.B.8.1.1 Container Sleeve

During a lift, the container sleeve is loaded axially, and the stress state is pure tensile membrane. For the subsequent stress calculation, it is assumed that the full weight of the damaged fuel container and the fuel assembly are supported by the sleeve. The magnitude of the load is

$$F := DLF \cdot (W_{container} + W_{fuel}) \qquad F = 632\,lbf$$

The cross sectional area of the sleeve is

$$A_{sleeve} := (id_{sleeve} + 2 \cdot t_{sleeve})^2 - id_{sleeve}^2 \qquad A_{sleeve} = 2.42\,in^2$$

Therefore, the tensile stress in the sleeve is

$$\sigma := \frac{F}{A_{sleeve}} \qquad \sigma = 261\,psi$$

The allowable stress intensity for the primary membrane category is S_m per Subsection NG of the ASME Code. The corresponding safety factor is

$$SF := \frac{S_{m1}}{\sigma} \qquad SF = 76.6$$

3.B.8.1.2 Base Weld

The base of the container must support the amplified weight of the fuel assembly. This load is carried directly by the full penetration weld which connects the base to the container sleeve. The magnitude of the load is

$$F := DLF \cdot W_{fuel} \qquad F = 460\,lbf$$

The area of the weld, with proper consideration of quality factors, is

$$A_{weld} := n \cdot 4 \cdot id_{sleeve} \cdot t_{base} \qquad A_{weld} = 1.18\,in^2$$

Therefore, the amplified shear stress in the weld, including the quality factor, is

$$\sigma := \frac{F}{A_{weld}} \qquad \sigma = 389\,psi$$

From the ASME Code the allowable weld shear stress, under normal conditions (Level A), is 60% of the membrane strength of the base metal. The corresponding safety factor is

$$SF := \frac{0.6 \cdot S_{m1}}{\sigma} \qquad SF = 30.9$$

3.B.8.1.3 Container Collar

The load tabs of the upper closure assembly engage the container collar during a lift. The load transferred to the engagement slot, by a single tab, is

$$F := \frac{DLF \cdot (W_{container} + W_{fuel})}{2} \qquad F = 316.25\,lbf$$

The shear area of the container collar is

$$A_{collar} := 2 \cdot d_{slot} \cdot (t_{sleeve} + t_{collar}) \qquad A_{collar} = 0.211\,in^2$$

The shear stress in the collar is

$$\sigma := \frac{F}{A_{collar}} \qquad \sigma = 1497\,psi$$

The allowable shear stress from Subsection NG, under normal conditions, is

$$\sigma_{allowable} := 0.6 \cdot S_{m1} \qquad \sigma_{allowable} = 12000\,psi$$

Therefore, the safety factor is

$$SF := \frac{\sigma_{allowable}}{\sigma} \qquad SF = 8$$

3.B.8.1.4 Upper Closure Assembly

The upper closure assembly is classified as a special lifting device [2]. As such the allowable tensile stress for design is the lesser of one-third of the yield stress and one-fifth of the ultimate strength.

$$\sigma_1 := \frac{S_{y1}}{3} \qquad \sigma_2 := \frac{S_{u1}}{5}$$

$$\sigma_1 = 9167\,\text{psi} \qquad \sigma_2 = 14600\,\text{psi}$$

For SA240-304 material the yield stress governs at the lifting temperature.

$$\sigma_{allowable} := \sigma_1$$

The total lifted load is

$$F := DLF \cdot \left(W_{container} + W_{fuel}\right) \qquad F = 632\,\text{lbf}$$

The shear stress in the shear pin under this load is calculated as

$$A_{pin} := \frac{\pi}{4} \cdot D_{pin}^{\ 2} \qquad A_{pin} = 0.11\,\text{in}^2$$

$$\sigma := \frac{F}{2 \cdot A_{pin}} \qquad \sigma = 2863\,\text{psi}$$

The safety factor is

$$SF := \frac{0.6\sigma_{allowable}}{\sigma} \qquad SF = 1.92$$

The bearing stress in the lead-in and the corresponding safety factor are

$$\sigma := \frac{F}{D_{pin} \cdot D_{taper}} \qquad \sigma = 2677\,\text{psi}$$

$$SF := \frac{\sigma_{allowable}}{\sigma} \qquad SF = 3.42$$

The stress in the fillet weld between the lead-in and the lead-in collar is (quality factor is 0.35) is computed from the available weld area and the force F

$$A_{weld} := \pi \cdot D_{leadin} \cdot \frac{t_{weld1}}{\sqrt{2}} \qquad A_{weld} = 0.267\,in^2$$

The shear stress in the weld is

$$\sigma := \frac{F}{A_{weld}} \qquad \sigma = 2373\,psi$$

The safety factor is

$$SF := \frac{nf \cdot \sigma_{allowable}}{\sigma} \qquad SF = 1.35$$

The shear stress in the load tabs due to the lifted weight is computed as follows:

$$A_{tab} := h_{tab} \cdot w_{tab} \qquad A_{tab} = 0.25\,in^2$$

$$\sigma := \frac{F}{2 \cdot A_{tab}} \qquad \sigma = 1265\,psi$$

The safety factor is

$$SF := \frac{.6 \cdot \sigma_{allowable}}{\sigma} \qquad SF = 4.35$$

If the full weight of the lift is supported by the fillet welds between the locking shaft and the load tabs, the shear stress in the welds is

$$A_{weld} := 2 \cdot h_{tab} \cdot t_{weld2} \qquad A_{weld} = 0.187\,in^2 \qquad \sigma := \frac{F}{2 \cdot A_{weld}} \qquad \sigma = 1687\,psi$$

The safety factor is

$$SF := \frac{nf \cdot .6 \cdot \sigma_{allowable}}{\sigma} \qquad SF = 1.14$$

3.B.8.2 60g End Drop (Accident Condition)

The critical member of the damaged fuel container during the drop scenario is the lower fuel spacer. It is subjected to direct compression due to the amplified weight of the fuel assembly. The lower fuel spacer has four leg members at the corners of the tube. The load per leg due to a 60g end drop is

$$F := \frac{60 \cdot W_{fuel}}{4} \qquad F = 6000\,lbf$$

The cross sectional area of each leg is

$$A_{leg} := (s_{tube} - s_{cutout}) \cdot t_{tube} \qquad A_{leg} = 0.5\,in^2$$

The stress in the member is

$$\sigma := \frac{F}{A_{leg}} \qquad \sigma = 12000\,psi$$

The allowable primary membrane stress from Subsection NG of the ASME Code, for accident conditions (Level D), is

$$\sigma_{allowable} := 2.4 \cdot S_{m2}$$

$$\sigma_{allowable} = 37920\,psi$$

The safety factor is

$$SF := \frac{\sigma_{allowable}}{\sigma}$$

$$SF = 3.2$$

3.B.9 Conclusion

The damaged fuel container and the upper closure assembly are structurally adequate to withstand the specified normal and accident condition loads. All calculated safety factors are greater than one, which demonstrates that all acceptance criteria have been met or exceeded.

APPENDIX 3.C - RESPONSE OF CASK TO TORNADO WIND LOAD AND LARGE MISSILE IMPACT

3.C.1 Introduction

The objective of this analysis is to determine the response of the cask to the combined load of the wind due to the design basis tornado and the large missile impact (loading case B) specified in Section 2.2.3. It is demonstrated that under this loading condition, the cask will not tip over. The case of large missile impact plus the instantaneous pressure drop due to the tornado passing the cask is also considered. The two cases need not be combined.

Impacts from two types of smaller missiles are considered in Appendix 3.G.

3.C.2 Method

In this analysis, the cask is simultaneously subjected to a missile impact at the top of the cask and either a constant wind force or an instantaneous pressure drop leading to an impulsive adder to the initial angular velocity imparted by a missile strike. The configuration of the system just prior to impact by the missile is shown in Figure 3.C.1.

The first step of the analysis is to determine the post-strike angular velocity of the cask, which is the relevant initial condition for the solution of the post-impact cask equation of motion. There are certain limiting assumptions that we can make to compute the post-impact angular velocity of the cask. There are three potential limiting options available.

a. Assume a coefficient of restitution (ratio of velocity of separation to velocity of approach) = 1. This assumption results in independent post impact motion of both the cask and the missile with the change in kinetic energy of the missile being entirely transmitted to the cask.

b. Assume a coefficient of restitution =0. This assumption results in the missile and the cask moving together after the impact with a certain portion of the kinetic energy lost by the missile being dissipated during the collision so that the post impact kinetic energy is less than the energy change in the missile.

c. Assume a coefficient of restitution = mass of missile/mass of cask. This assumption brings the missile to rest after the impact. There is kinetic energy dissipated during the impact process but the kinetic energy acquired by the cask is larger than in case b.

Missile impact tests conducted under the auspices of the Electric Power Research Institute (see EPRI NP-440, Full Scale Tornado Missile Impact Tests", 1977) have demonstrated that case c above matches the results of testing.

Determination of the force on the cask due to the steady tornado wind is the next step. The primary tornado load is assumed to be a constant force due to the wind, acting on the projected area of the cask and acting in the direction that tends to cause maximum propensity for overturning.

The equation of motion of the cask under the wind loading is developed, and using the initial angular velocity of the cask due to the missile strike, the time-dependent solution for the post-impact position of the cask centroid is obtained.

In the second scenario, the missile impact occurs at the same instant that the cask sees the pressure drop due to the passing of the tornado.

3.C.3 Assumptions

The assumptions for the analysis are stated here; further explanation is provided in the subsequent text.

1. The cask is assumed to be a rigid solid cylinder, with uniform mass distribution. This assumption implies that the cask sustains no plastic deformation (i.e. no absorption of energy through plastic deformation of the cask occurs).

2. The angle of incidence of the missile is assumed to be such that its overturning effect on the cask is maximized.

3. The missile is assumed to strike at the highest point of the cask, again maximizing the overturning effect.

4. The cask is assumed to pivot about a point at the bottom of the baseplate opposite the location of missile impact and application of wind force in order to conservatively maximize the propensity for overturning.

5. Inelastic impact is assumed, indicating that the missile velocity is reduced to zero after impact. This assumption conservatively lets the missile impart the maximum amount of momentum to the cask.

6. The missile does not adhere to the cask, even though the coefficient of restitution is assumed to be zero.

7. The analysis is performed for a cask without fuel. A lighter cask will tend to rotate further after the missile strike. The weight of the missile is not included in the total post-impact weight. A lower bound weight of 189,000 lbs is used in this analysis.

8. Planar motion of the cask is assumed; any loads from out-of-plane wind forces are neglected. In typical impacts, a portion of the energy will be expended in rotating the cask. No such energy dissipation is assumed.

9. The drag coefficient for a cylinder in turbulent crossflow is conservatively taken as 0.6. Per Mark's Standard Handbook for Mechanical Engineers [3.C.1], the drag coefficient (C_d) for a cylinder in crossflow at the calculated Reynold's number is less than 0.5. The use of a higher drag coefficient results in a greater overturning force.

10. The missile and wind loads are assumed to be perfectly aligned in direction.

11. The instantaneous pressure drop is converted to an initial angular motion of the cask by an impulse-momentum relation.

12. The coefficient of friction between the cask and the foundation is assumed to be infinite. In other words, there is no conversion of the missile kinetic energy into translational motion of the cask.

It is recognized that the above assumptions taken together impose a large measure of conservatism in the dynamic model, but render the analysis highly simplified. In a similar spirit of simplification, the calculations are performed by neglecting the geometry changes which occur due to the dynamic motion of the cask. This linearity assumption is consistent with the spirit of the simplified model used herein.

Certain overseas and domestic sites may have different missile and wind load requirements. The evaluation for the specific site shall consider its design basis loads, but shall utilize the methodology presented in this appendix.

3.C.4 Input Data

The following input data is used to perform the analysis. All dimensions are obtained from the Design Drawings in Section 1.5.

The weight of the cask plus contents, $W_c := 189000 \cdot lbf$

The cask total height, $L := 203.125 \cdot in$

The diameter of the cask base in contact with the supporting surface, $a := 83.25 \cdot in$

The maximum diameter of the overpack, $D := 96.0 \cdot in$

Gravitational acceleration, $g := 386.4 \cdot \frac{in}{sec^2}$

The weight of the large missile (1800 kg, from Table 2.2.5), $W_m := 3960 \cdot lbf$

The maximum tornado wind speed (from Table 2.2.4), $v_t := 360 \cdot mph$

The pre-impact missile velocity (from Table 2.2.5), $v_m := 126 \cdot mph$

The translation speed of the tornado (from Table 2.2.4), $V_{tr} := 70 \cdot mph$

The drag coefficient for cylinder in turbulent crossflow, $Cd := 0.6$

The density of air, $\rho_{air} := 0.075 \cdot \frac{lbf}{ft^3}$ ("lbf" indicates pounds "force")

The viscosity of air, $\mu_{air} := 4.18 \cdot 10^{-7} \cdot \frac{lbf}{ft \cdot sec}$

Maximum instantaneous pressure drop (from Table 2.2.4), $dp := 3 \cdot psi$

The total mass of the cask and its contents (M_c) can be calculated from the total weight and gravitational acceleration as:

$$M_c := \frac{W_c}{g}$$

Similarly, the mass of the large missile (M_m) can be calculated from its weight and gravitational acceleration as:

$$M_m := \frac{W_m}{g}$$

3.C.5 Solution for Post-Missile Strike Motion of Cask

The missile imparts the maximum angular momentum to the cask when the initial angle of the strike is defined by the relation:

$$\phi_0 := \operatorname{atan}\left(\frac{a}{L}\right)$$

Substituting the values of a and L defined above, the missile strike angle $\phi_0 = 22.286\,deg$

The distance between the missile impact location and the cask pivot point, as shown on Figure 3.C.1, is calculated as:

$$d := \left(a^2 + L^2\right)^{0.5}$$

The centroidal mass moment of inertia of a cylindrical object about an axis parallel to and intersecting its axial midplane (I_z), for rotation about z, is given by:

$$I_z := \frac{1}{12} \cdot M_c \cdot \left[3 \cdot \left(\frac{D}{2} \right)^2 + L^2 \right]$$

Using the parallel axis theorem, the moment of inertia of the cask after the missile strike about the rotation point can be determined as:

$$I_r := I_z + M_c \cdot \left(\frac{d}{2} \right)^2$$

$$I_r = 3.033 \times 10^9 \, lb \cdot in^2 \qquad \text{("lb" indicates pounds "mass")}$$

As stated in Section 3.C.3, it is conservatively assumed that the missile does not remain attached to the cask after impact. Using balance of angular momentum, the post-impact initial angular velocity of the cask can be determined using:

$$\omega := \frac{M_m \cdot v_m \cdot d}{I_r}$$

Thus, the post-impact initial angular velocity, $\omega = 0.635 \frac{1}{sec}$

For subsequent dynamic analysis, this angular velocity is used as the initial condition on the equation for the angular rotation of the cask as a function of time.

3.C.6 Calculation of Pressure due to Tornado Wind

The drag coefficient of a cylinder in turbulent crossflow is a function of the Reynold's Number, which can be calculated using the relation:

$$Re := \frac{\rho_{air} \cdot v_t \cdot D}{\mu_{air}} \qquad Re = 7.579 \times 10^8$$

The drag coefficient (C_d) for a cylinder in crossflow for this Reynold's Number is less than 0.5 [3.C.1], so a conservatively higher value of 0.6 is used.

$$Cd := 0.6$$

The pressure on the side of the cask (p_{max}), due to wind loading, is determined using:

$$p_{max} := \frac{1}{2} \cdot Cd \cdot \frac{\rho_{air}}{g} \cdot v_t^2$$

and the resulting force on the projected area of the cask is therefore given by:

$$F_{max} := p_{max} \cdot D \cdot L$$

Thus, the force due to tornado wind, $F_{max} = 2.638 \times 10^4$ lbf

3.C.7 Post Impact Plus Steady Wind Solution

The solution of the post-impact dynamics problem for the period of time when the horizontal displacement of the cask mass center is greater than or equal to zero is obtained by solving the following equation of motion:

$$I_r \cdot \alpha := \left(-W_c \cdot \frac{a}{2}\right) + F_{max} \cdot \left(\frac{L}{2}\right)$$

where I_r is the cask moment of inertia about the rotation point and α is the angular acceleration of the cask. The above equation arises from summation of dynamic moments about the cask pivot point. The steady wind enters into the above equation through F_{max}, and the impacting missile enters into the equation through the initial angular velocity.

The angular position of the cask is examined through 250 time steps of 0.005 sec duration.

Let $i := 1 .. 250$

$$t_i := \frac{i}{200} \cdot sec$$

Let θ = the angular rotation variable of the cask subsequent to the impact. The analytical solution of the above equation is therefore:

$$\theta_i := \omega \cdot t_i + \frac{(t_i)^2}{2 \cdot I_r} \cdot \left(-W_c \cdot \frac{a}{2} + F_{max} \cdot \frac{L}{2}\right)$$

3.C.8 Results

Once the angular rotation with respect to time is known, the horizontal displacement of the cask center of gravity can be calculated as:

$$x_i := \frac{D}{2} - \frac{d}{2}\cdot\cos\left(\operatorname{acos}\left(\frac{D}{d}\right) + \theta_i\right)$$

Figure 3.C.2 shows a plot of the motion of the cask center versus time.

3.C.9 Missile Impact Plus Pressure Drop

The case of instantaneous pressure drop plus impact by a missile is studied by finding the increment of initial angular speed imparted to the cask by the pressure wave. Using a balance of angular momentum relation, the increment of angular speed is determined and added to that of the missile strike.

Time of pressure wave to cross cask body $\quad dt := \frac{D}{V_{tr}} \qquad dt = 0.078\,\text{sec}$

Increment of angular velocity imparted to cask in time dt

$$d\omega := \frac{(dp\cdot D\cdot L)\cdot\left(\frac{L}{2}\right)\cdot dt}{I_r} \qquad d\omega = 0.059\,\text{sec}^{-1}$$

Therefore, for this case the initial angular speed is

$$\omega_1 := \omega + d\omega \qquad \omega_1 = 0.694\,\text{sec}^{-1}$$

The angular position of the cask is examined through 250 time steps of 0.005 sec duration.

Let $i := 1..250$

$$t_i := \frac{i}{200}\cdot\text{sec}$$

Let $\theta 1$ = the angular rotation variable of the cask subsequent to the impact. The analytical solution of the above equation is therefore:

$$\theta 1_i := \omega_1 \cdot t_i + \frac{(t_i)^2}{2 \cdot I_r} \cdot \left(-W_c \cdot \frac{a}{2}\right)$$

3.C.8 Results

Once the angular rotation with respect to time is known, the horizontal displacement of the cask center of gravity can be calculated as:

$$x1_i := \frac{D}{2} - \frac{d}{2} \cdot \cos\left(\operatorname{acos}\left(\frac{D}{d}\right) + \theta 1_i\right)$$

Figure 3.C.3 shows a plot of the motion of the cask center versus time.

3.C.9 Conclusion

As is shown in Figure 3.C.2, the maximum horizontal excursion of the cask centroid under the given loading is less than 2.8 feet. In order for a cask tipover accident to occur, the centroid must undergo a horizontal displacement of 3.3 feet. Therefore, the combined tornado wind and missile strike events will not result in cask tipover. The case of missile strike plus tornado passing the cask is not a bounding case.

3.C.10 References

[3.C.1] E. Avallone and T. Baumeister, Marks' Standard Handbook for Mechanical Engineers, McGraw-Hill, Inc., Ninth Edition, 1987, p. 11-77.

REPORT HI-2012610

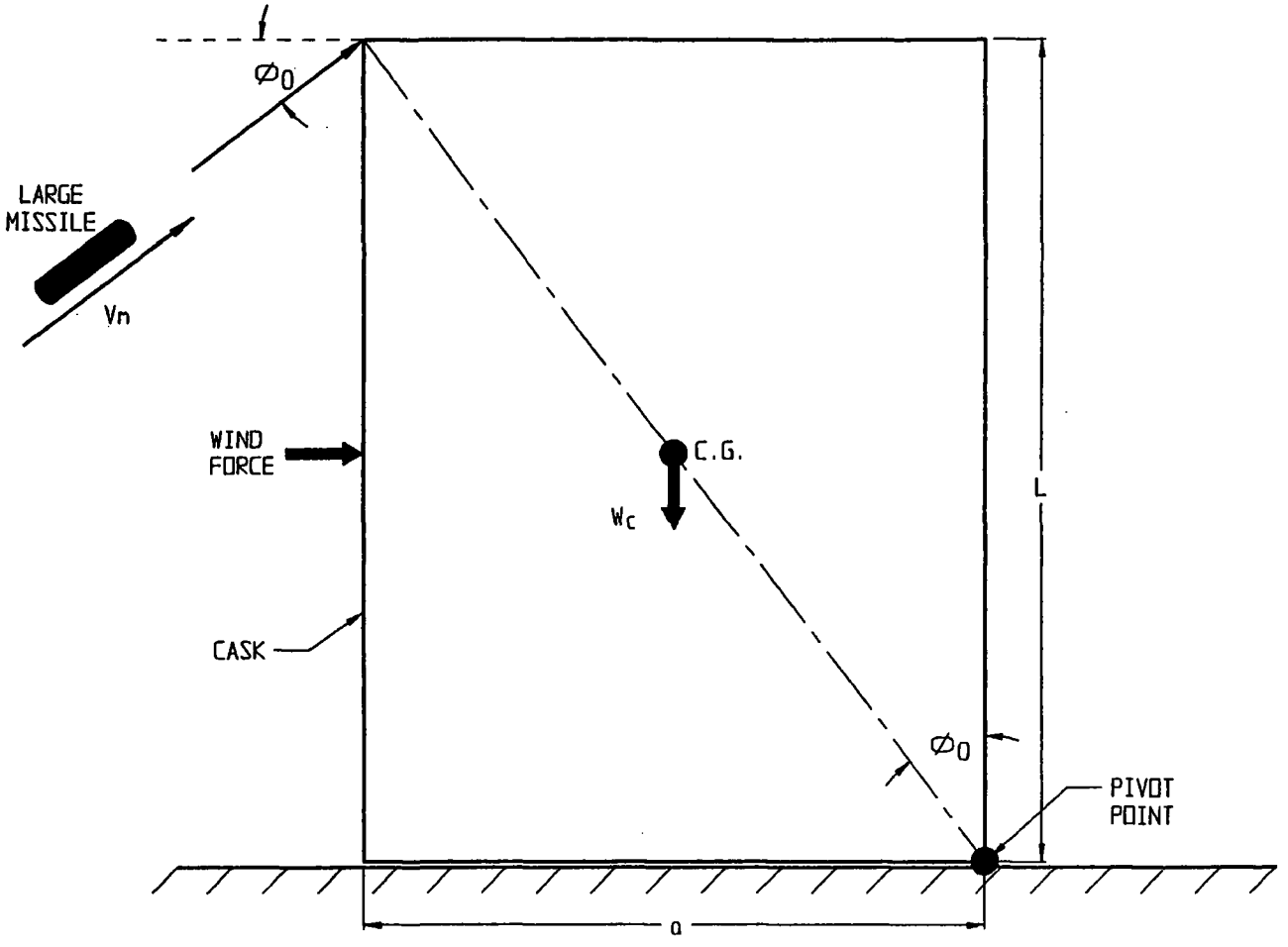

FIGURE 3.C.1; FREE BODY DIAGRAM OF CASK FOR LARGE MISSILE STRIKE/TORNADO EVENT

REVISION 0

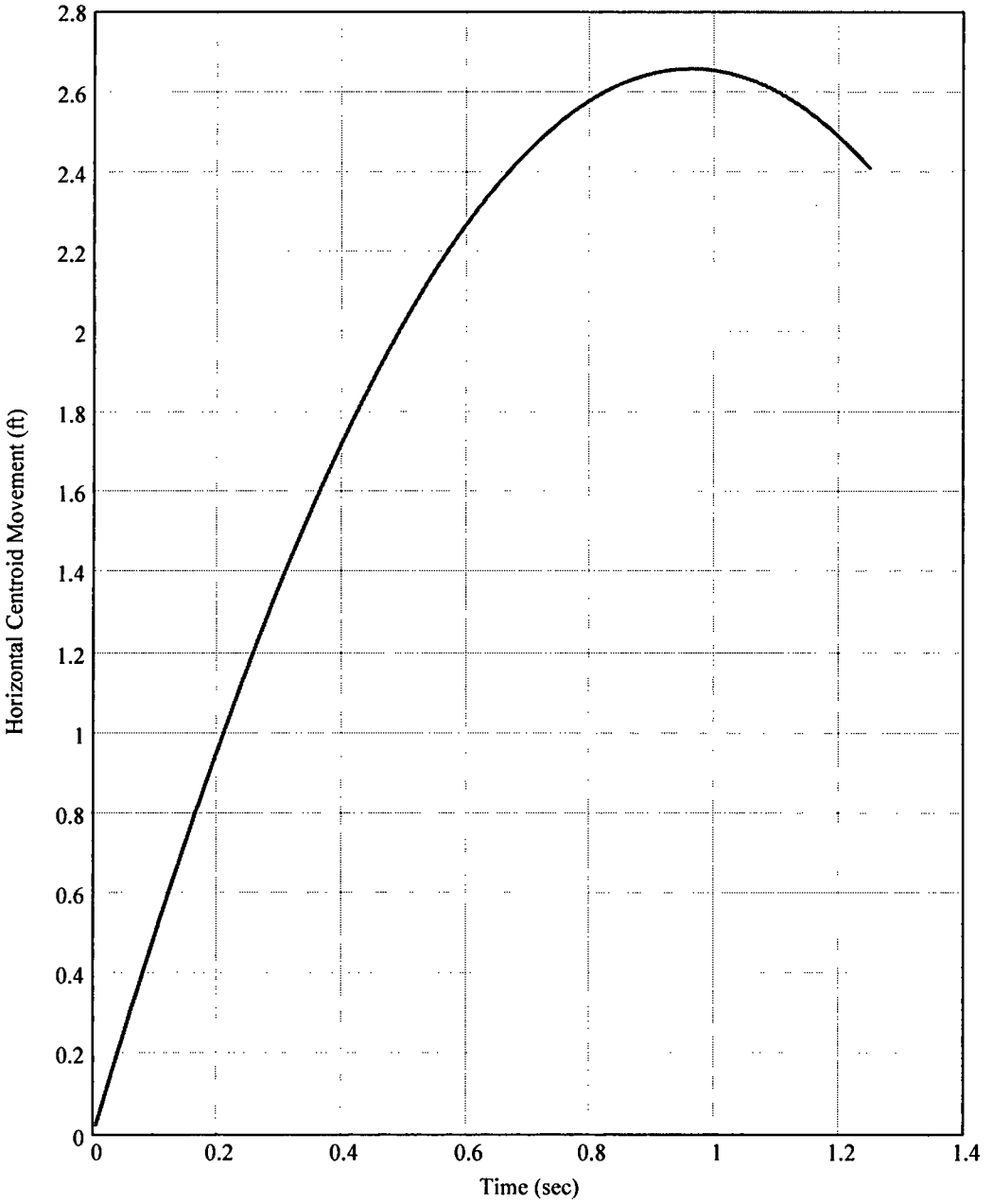

Fig. 3.C.2 Horizontal Motion of Centroid

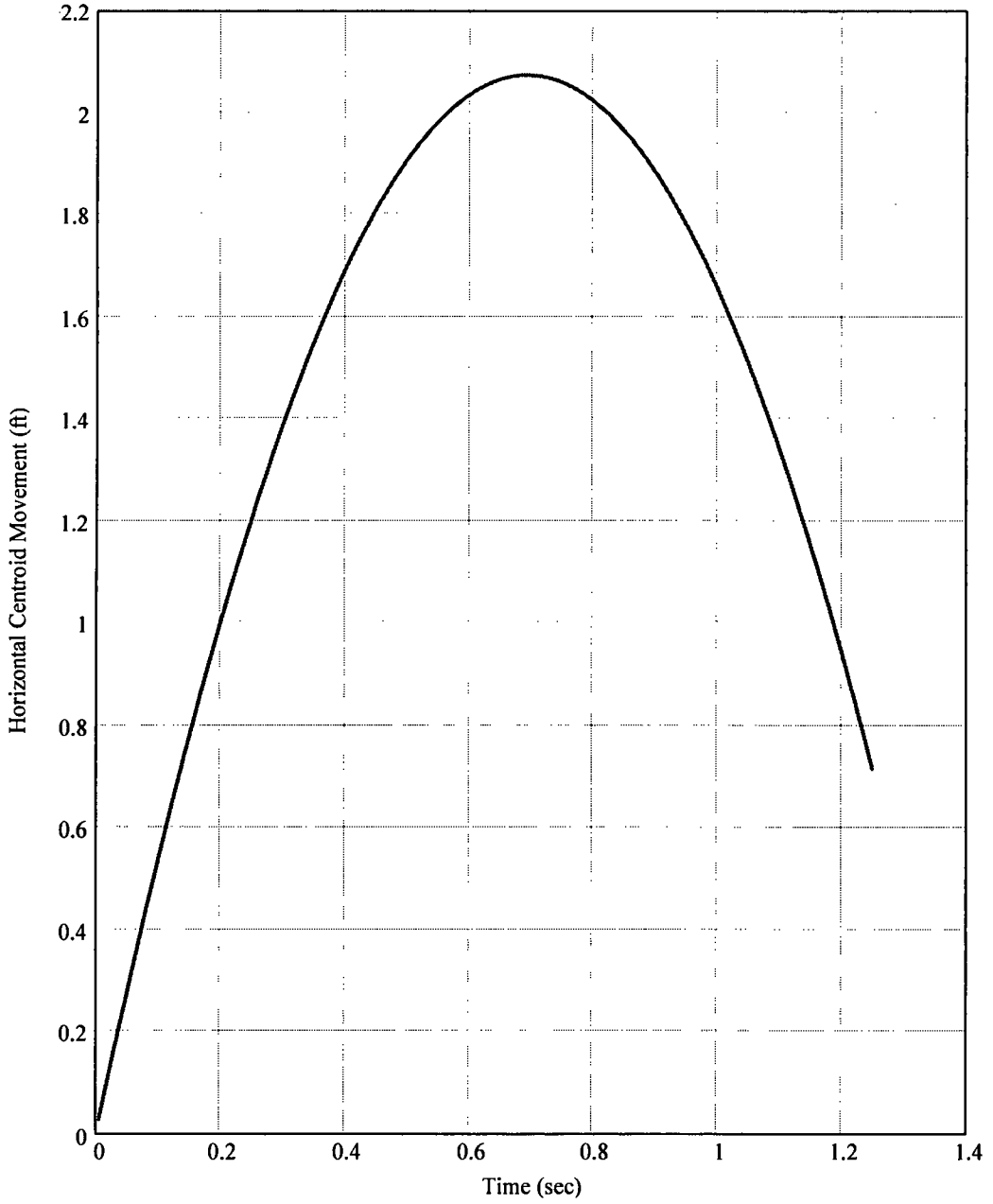

Fig. 3.C.3 Horizontal Motion of Centroid

APPENDIX 3.D - LIFTING TRUNNION STRESS ANALYSIS

3.D.1 Introduction and Description

This appendix contains a stress analysis of the upper lifting trunnions on the HI-STAR 100 Overpack. The objective of this analysis is to show that under any cask lifting condition, the stress in the trunnions and in the surrounding overpack forging do not exceed allowable limits. Note that, to further demonstrate the robust nature of the cask, Appendix 3.Y, describes a lift at three times deadweight.

The appendix is self contained in that all references cited are listed in the appendix, and the necessary "free body" diagrams are shown by figures at the conclusion of the appendix. This Appendix is written using the Mathcad electronic scratchpad computer code [3.D.1]. The notation ":=" represents the equal sign for a defined calculation. The notation "=" represents a computed response or answer.

3.D.2 Methodology and Acceptance Criteria

Methodology

The lifting trunnions are threaded into the forging. A locking plate, secured with attachment bolts, prevents the trunnions from backing out.

The lifting trunnions are analyzed using a mechanics of materials method with the trunnions considered as short beams. Stresses in both the trunnions and in the overpack top forging are calculated under the specified load. Sketches at the end of the appendix show the appropriate free body diagrams.

In this analyses, primary bending moments and shear forces in the trunnions are determined first. Then, local bearing stress, thread shear stress and stress due to internal pressure are calculated.

The global effects of the trunnion loading are considered as a load case in the finite element analysis of the HI-STAR 100 Overpack and are reported elsewhere.

Acceptance Criteria

The HI-STAR 100 Overpack trunnions are part of a non-redundant lifting system. NUREG-0612 [3.D.2], section 5.1.6(3), requires that the lifting trunnions be able to support a load of 10 times the actual lifted load without exceeding the material ultimate strength and 6 times the actual lifted load without exceeding yield. The ultimate strength criterion governs the trunnion and forging materials.

The lifted load should include a dynamic load factor to account for inertia effects. CMAA Specification #70 (1988) [3.D.3], recommends an appropriate minimum hoist load factor for lifted loads. Since cask lifting is a low speed operation the use of a minimum hoist load factor for dynamic effects is conservative.

Where the trunnions and the top forging interface, the top forging allowable strengths are used in the determination of structural margins; the limits on strength are those of the ASME Code, Section III, Subsection NB for the appropriate load combination.

3.D.3 Materials and Material Properties

Trunnions are SB-637-N07718 steel. The overpack top forging is SA-350-LF3 steel. Based on thermal analyses in Chapter 4 (see Table 4.4.16), the maximum normal operating temperature on the inside surface of the top forging in the vicinity of the lifting trunnion will not exceed 163 degrees F. The outer surface temperature of the top forging will be higher than the ambient environment temperature. In the calculations, a bulk metal temperature of 150 degrees F is assumed for determination of material properties. Material properties are extracted from the appropriate tables in Section 3.3.

The trunnion material yield strength,	$S_y := 147000 \cdot psi$	Table 3.3.5
The trunnion material ultimate strength,	$S_u := 181300 \cdot psi$	Table 3.3.5
The forging material yield strength,	$S_{yf} := 35850 \cdot psi$	Table 3.3.4
The forging material local membrane stress intensity,	$SI_f := 34600 \cdot psi$	Table 3.1.8

3.D.4 Assumptions

1. The trunnions are analyzed for strength as beam members.

2. The weight of the extended portion of the trunnion is conservatively neglected since it opposes the lifted load.

3. Any load carrying capacity of the locking plate is conservatively neglected in the analysis of the trunnion as a beam.

4. Trunnions are loaded equally.

5. The lifting yoke is conservatively set at the outer end of the trunnion so as to maximize the moment arm for the analysis of the trunnion as a beam member. The minimum thickness of the lifting yoke is specified. Therefore, the maximum value of the moment arm can be established

6. In the determination of local shear stress in the trunnion thread, the actual location of the lift point is used based on a conservative "worst case" analysis of the tolerance stack-up.

7. Trunnion stress analysis is based only on mechanical loads applied laterally to the trunnion axis.

3.D.5 References

[3.D.1] MATHCAD 7.02, Mathsoft, 1998.

[3.D.2] NUREG-0612, Control of Heavy Loads at Nuclear Power Plants Resolution of Generic Technical Activity A-36, Section 5.1.6(3), 1980.

[3.D.3] Crane Manufacturers Association of America (CMAA), Specification #70, 1988, Section 3.3.

[3.D.4] J.Shigley and C. Mischke, Mechanical Engineering Design, McGraw-Hill, 5th Edition, 1989, p.328.

3.D.6 Analysis

In this section, moments, forces, and stresses in the trunnion and the top forging material are determined. Moments and forces in the trunnions are compared to allowable strengths per NUREG-0612, and local stresses in the top forging are compared with appropriate allowable stress intensities.

3.D.6.1 Moments and Forces in the Trunnion

In this subsection, the geometry of the system is defined, and bending moments and shear forces in the lifting trunnions are determined.

3.D.6.1.1 Input Data

The trunnion outer diameter, $d := 5.75 \cdot in$

The minimum lift yoke connecting link yoke width $t_f := 2.25 \cdot in$

The maximum lifted weight of the cask and contents, $W := 250000 \cdot lbf$ Table 3.2.4

The number of lifting trunnions, $n := 2$

The dynamic load factor (from Reference 3.D.3), $DLF := 0.15$

The exposed trunnion length (including locking plate), $L := 3.375 \cdot in$

The minimum clearance between lifting link and trunnion end $c := 0.25 \cdot in$

This minimum lift yoke connecting link width conservatively defines the contact patch on the trunnion and establishes the location of the concentrated lifting load. for the purpose of determining the bending moment at the root of the trunnion beam member. The maximum lifted weight bounds the actual maximum weights of the HI-STAR 100 systems.

The trunnion cross sectional area (Area), moment of inertia (I) and applied per trunnion load (P) can be determined using the following formulae:

$$\text{Area} := \frac{\pi}{4}\cdot d^2 \qquad I := \frac{\pi}{4}\cdot\left(\frac{d}{2}\right)^4 \qquad P := \frac{W\cdot(1+DLF)}{n}$$

Substituting the input values defined above into these three equations yields the following values:

$$\text{Area} = 25.97\,\text{in}^2 \qquad I = 53.65884\,\text{in}^4 \qquad P = 1.44\times 10^5\,\text{lbf}$$

3.D.6.1.2 Bending Stress at the Root of the Trunnion

The lifting yoke arm is conservatively set at the outer end of the trunnion to maximize the moment arm. The applied moment arm (L_{arm}) is defined as the distance from the root of the trunnion to the centerline of the lifting yoke connecting link (see Figure 3.D.1).

$L_{arm} := L - .5\cdot t_f$ Conservatively neglect the clearance "c"

$L_{arm} = 2.25\,\text{in}$

The applied moment (M) at the root of the trunnion is therefore determined as:

$$M := P\cdot L_{arm} \qquad M = 3.23\times 10^5\,\text{in}\cdot\text{lbf}$$

From beam theory, the maximum tensile stress occurs in an outer fiber at the root of the trunnion. The distance from the neutral axis to an outer fiber (y) is one-half of the trunnion diameter:

$$y := \frac{d}{2}$$

and the maximum bending stress due to the applied moment is therefore determined as:

$$\sigma := \frac{M\cdot y}{I} \qquad \sigma = 17329.51\,\text{psi}$$

Comparing the value of the bending stress with the yield strength of the material results in a safety factor of:

$$S_1 := \frac{S_y}{\sigma} \qquad S_1 = 8.48$$

This safety factor is greater than 6, which is the factor of safety on yield required by [3.D.2]. Note that the safety factor calculated above, and used elsewhere in this appendix, is defined as the allowable yield strength divided by the calculated stress (or stress intensity).

3.D.6.1.3 Shear Stress in the Trunnion

The maximum shear stress in the trunnion, which occurs at the neutral axis, is determined using beam theory. The first moment of the area above the neutral axis is determined as:

$$Q := \int_0^{\pi} \int_{0\cdot in}^{\frac{d}{2}} r^2 \cdot \sin(\theta)\, dr\, d\theta \qquad \text{or} \qquad Q := \frac{1}{12}\cdot d^3$$

$$Q = 15.84\,in^3$$

The shear load (V) is equal to the applied per trunnion load (P) and the "thickness" of the beam (t) at the neutral axis is equal to the trunnion diameter (d).

$$V := P$$

$$t := d$$

From beam theory, the maximum shear stress is determined as:

$$\tau := \frac{V\cdot Q}{I\cdot t} \qquad \tau = 7381.09\,psi$$

The shear yield strength is defined as 60% of the tensile yield strength. This definition of yield strength in shear is consistent with formulas given in ASME Section III, Subsection NG, NG-3227.2 and NG-3232.1(b) where the ratio of allowable shear strength to allowable tensile strength is 0.6. It is also consistent (and conservative) when compared to the same ratio given in ASME Section III, Subsection NF where the ratio of allowable shear/allowable average tension is 0.4/0.6 = 0.667. Comparing the calculated shear stress value with the yield shear strength, result in a safety factor of:

$$S_2 := \frac{0.6\cdot S_y}{\tau} \qquad S_2 = 11.95$$

This safety factor is greater than 6, as required by [3.D.2].

In addition to a check based on yield strength, the calculated moment and shear force must be checked against the ultimate carrying capacity in bending and in shear. We calculate the ultimate moment dfrom the following formula (which is easily derived from the classical principles of Limit Analysis applied to a circular section).

$$M_u := S_u \cdot \left[\frac{4}{3} \cdot \left(\frac{d}{2} \right)^3 \right] \qquad M_u = 5.74 \times 10^6 \, lbf \cdot in$$

Comparing the ultimate capacity with the applied moment gives

$$S_3 := \frac{M_u}{M} \qquad S_3 = 17.76$$

Similarly, the ultimate shear force capacity is

$$V_u := .6 \cdot S_u \cdot Area \qquad V_u = 2.82 \times 10^6 \, lbf$$

Therefore the ultimate carrying capacity in shear is

$$S_4 := \frac{V_u}{V} \qquad S_4 = 19.65$$

3.D.6.2 Local Stresses in the Top Forging

In the following subsection, stresses in the top forging due to bearing loads, thread shear loads, and internal pressure are determined.

3.D.6.2.1 Input Data

The number of threads per inch, $NTI := 4$

The trunnion length inserted into the top forging, $L_w := 5.875 \cdot in$

The design internal pressure under normal handling, $p := 40 \cdot psi$ Table 2.2.1

The overpack forging outer diameter, $D_o := 83.25 \cdot in$

The overpack forging inner diameter, $D_i := 68.75 \cdot in$

The mean diameter in thread region $d_m := d + 1.0 \cdot in$

3.D.6.2.2 Bearing Stress

A longitudinal local bearing stress is developed in the base material, during cask handling, at the contact surface between the embedded portion of the trunnion and the cavity in the top forging. The effective diameter (for stress evaluation purposes) of the portion of the trunnion that is threaded into the top forging is determined as per [3.D.4] as:

$$dd := d_m - \frac{1.299038}{NTI}\cdot in \qquad dd = 6.43\,in$$

The projected area supporting the bearing load is determined as:

$$A := L_w \cdot dd \qquad A = 37.75\,in^2$$

and the average bearing stress on the top forging material is therefore determined as:

$$\sigma_d := \frac{V}{A} \qquad \sigma_d = 3808.11\,psi$$

3.D.6.2.3 Thread Shear Stress Due to Trunnion Bending

The bending moment that is transferred from the trunnion to the top forging is reacted by a shear stress distribution on the threads. (see Figure 3.D.2, a free body of the portion of the trunnion inserted into the forging). We recalculate the bending moment using a bounding value for the actual location of the applied load. This bounding value considers that the maximum position of the lifting link on the trunnion will leave a clearance "c" between the edge of the link and the end of the trunnion.

$c = 0.25\,in$

The total bending moment applied to the trunnion threads is therefore defined by:

$$Moment := M\cdot\frac{(L_{arm} - c)}{L_{arm}} + V\cdot\left(\frac{L_w}{2}\right) \qquad \frac{(L_{arm} - c)}{L_{arm}} = 0.89$$

The average shear stress in the threaded region is assumed to be a sinusoidal distribution around the periphery. Therefore, moment equilibrium yields:

$$Moment := \int_0^{2\cdot\pi} \tau\cdot R\cdot\sin(theta)\cdot R\cdot(L_w)\,dtheta$$

where the average shear stress along the threaded length, $\tau := \tau_{max}\cdot\sin(theta)$

Integrating the moment expression above, over the required interval, yields the following expression for the total bending moment:

$$\text{Moment} := \tau_{max} \cdot \pi \cdot dd^2 \cdot \frac{(L_w)}{4}$$

Solving for the maximum shear stress existing around the circumference of the trunnion (averaged along the length of the insert) gives the stress at the root of the trunnion thread.

$$\tau_{max} := 4 \cdot \frac{\text{Moment}}{\pi \cdot dd^2 \cdot (L_w)} \qquad \tau_{max} = 3725.96\,\text{psi}$$

Similarly, the shear stress at the external root of the thread in the top forging is:

$$\tau_{froot} := 4 \cdot \frac{\text{Moment}}{\pi \cdot d_m^2 \cdot L_w} \qquad \tau_{froot} = 3376.05\,\text{psi}$$

3.D.6.2.4 Local Stress in Forging Due to Internal Pressure

The stress in the top forging due to the design internal pressure is calculated using shell theory. This stress is approximated as a circumferential stress using a mean diameter and thickness of the top forging. The mean radius of the overpack forging is determined as:

$$r := \frac{D_o + D_i}{2} \qquad r = 76\,\text{in}$$

and the thickness of the overpack forging is determined as:

$$t := \frac{D_o - D_i}{2} \qquad t = 7.25\,\text{in}$$

From shell theory, the circumferential stress in the forging due to internal pressure is determined as:

$$\sigma_{pres} := p \cdot \frac{r}{t} \qquad \sigma_{pres} = 419.31\,\text{psi}$$

3.D.6.2.5 Comparison with Allowable Stress Intensity Per ASME Subsection NB

The allowable local membrane stress intensity of the top forging material in the region supporting the lifting trunnions is set forth in Section 3.D.3 of this appendix as:

$$SI_f = 34600\,\text{psi}$$

The safety factor on membrane stress intensity in the top forging is calculated at the location of maximum shear stress and bearing stress, and uses the classical formula for stress intensity [3.D.4]. The three normal stresses acting on the point are defined as:

A longitudinal minimum normal stress, $\sigma_1 := -\sigma_d + .5\cdot\sigma_{pres}$

A normal stress estimate on a surface perpendicular to a radial line, $\sigma_2 := -.5\cdot p$

The normal "hoop" stress, $\sigma_3 := \sigma_{pres}$

Substituting the appropriate values of σ_d, σ_{pres} and p, the three normal stresses are:

$\sigma_1 = -3598.46\,psi$ $\sigma_2 = -20\,psi$ $\sigma_3 = 419.31\,psi$

The formula for maximum stress intensity in the plane of the shear stress involves σ_1 and σ_2. For a bounding estimate of the safety factor, we use σ_1 and σ_3 instead since σ_3 adds to σ_1. The maximum in-plane stress intensity is therefore calculated as:

$$SI_{calc} := \left[\left(\sigma_1 - \sigma_3\right)^2 + 4\cdot\tau_{froot}^2\right]^{0.5} \qquad SI_{calc} = 7857.06\,psi$$

and the safety factor (must be > 1.0) is determined as:

$$SF_m := \frac{SI_f}{SI_{calc}} \qquad SF_m = 4.4$$

Note that this calculation does not consider the global effect of the trunnion load on the top forging. The global analysis is considered as a load combination for the overpack finite element analysis, reported elsewhere.

The calculation above demonstrates that the local membrane stress intensity in the forging section, adjacent to the lifting trunnion, is within the limit required by the ASME Code, Section III, Subsection NB. Appendix 3.Y contains a finite element analysis of the top forging subject to a trunnion load equal to three times the dead weight of the cask.

3.D.6.2.5 Comparison with Yield Strength Per NUREG-0612

The allowable yield stress of the top forging material in the region supporting the lifting trunnions is set forth in Section 3.D.3 of this appendix as:

$$S_{yf} = 35850\,psi$$

The safety factor against yield in the top forging is calculated for bearing stress and for thread shear stress separately. The same calulation is also performed for the trunnion material at the interface.

We note that Regulatory Guide 3.61 only requires that the material anywhere in the cask not exceed 1/3 of the yield stress. Nevertheless, at the thread interface between the trunnion and and the top forging, we conservatively apply the more stringent requirements of NUREG-0612.

Safety Factor Against Yielding for Bearing Stress in Forging at Interface

$$SF_{bearing} := \frac{S_{yf}}{\sigma_d} \qquad SF_{bearing} = 9.41$$

Safety Factor Against Yielding for Thread Shear Stress in Forging at interface.

$$SF_{thread\_shear} := .6 \cdot \frac{S_{yf}}{\tau_{froot}} \qquad SF_{thread\_shear} = 6.37$$

Safety Factor Against Yielding for Bearing Stress in Trunnion

$$SF_{bearing} := \frac{S_y}{\sigma_d} \qquad SF_{bearing} = 38.6$$

Safety Factor Against Yielding for Thread Shear Stress in Trunnion

$$SF_{thread\_shear} := .6 \cdot \frac{S_y}{\tau_{max}} \qquad SF_{thread\_shear} = 23.67$$

The above calculations demonstrate that the local bearing stress and the thread shear stress at the trunnion-forging interface satisfy NUREG-0612 requirements on trunnion safety factors against material yield.

3.D.7 Conclusion

The lifting trunnions meet the requirements of NUREG 0612 for lifting heavy loads in a nuclear power plant.

The local membrane stress intensity limits in the top forging satisfy the required ASME Section III, Subsection NB limits.

The bearing stress and the thread shear stress satisfy NUREG-0612 requirements at the trunnion-forging interface. During the lift, these stresses are less than 1/6 the respective yield stress.

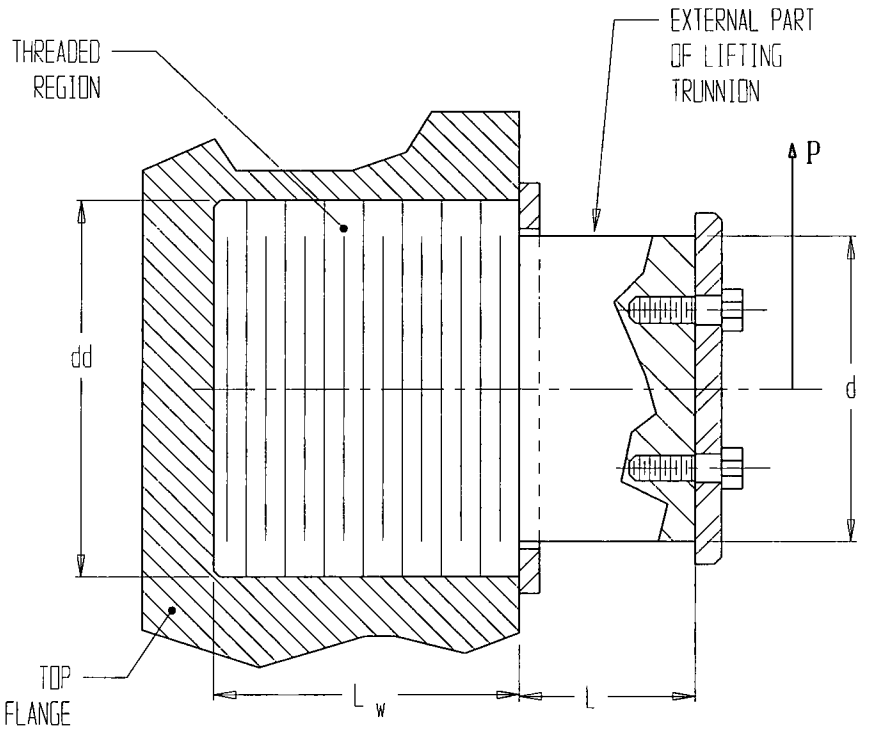

FIGURE 3.D.1; SKETCH OF LIFTING TRUNNION GEOMETRY SHOWING APPLIED LOAD

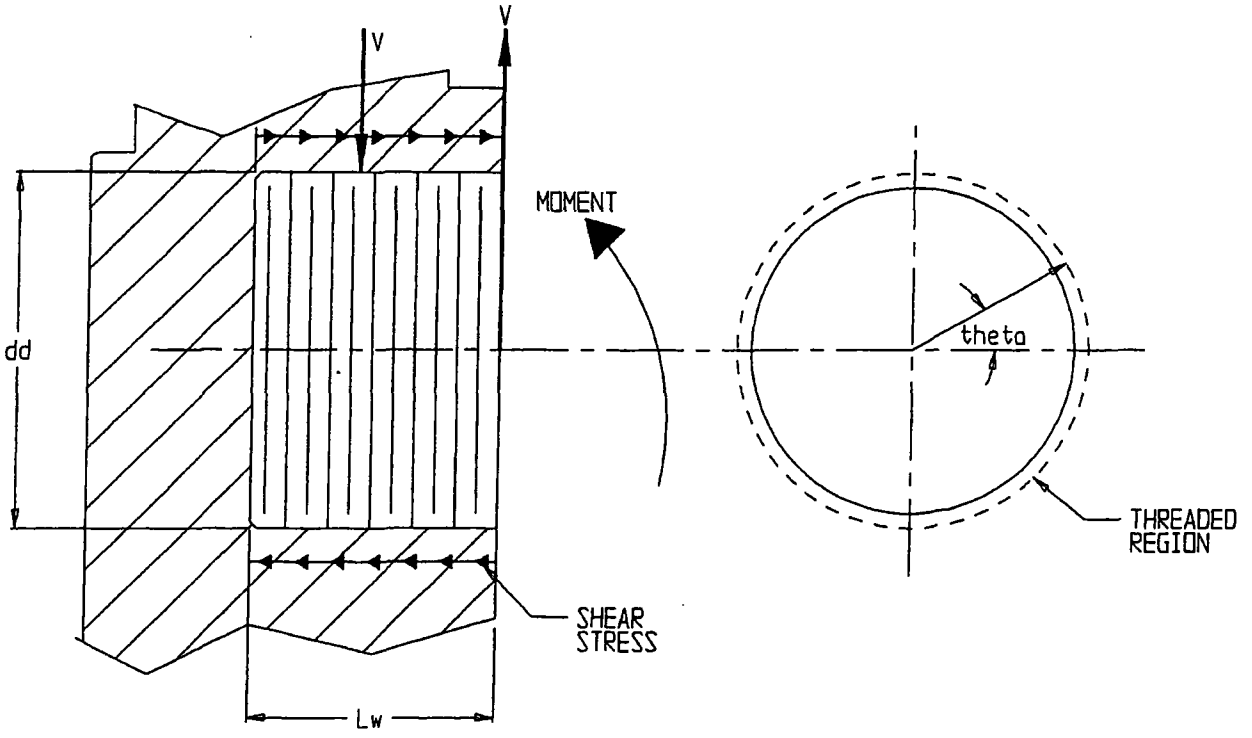

FIGURE 3.D.2; FREE BODY SKETCH OF LIFTING TRUNNION THREADED REGION SHOWING MOMENT BALANCE BY SHEAR STRESSES

APPENDIX 3.E: ANALYSIS OF MPC TOP CLOSURE

3.E.1 Scope

This appendix provides the stress analysis of the MPC top closure plate under bounding load cases for both storage and transport scenarios.

3.E.2 Methodology

Conservative values for stresses on the closure plate are obtained by using classical strength of materials formulations, which are sufficient for determining primary stresses in the component. The peripheral weld to the MPC shell is protected by a thin closure ring. The analysis of this ring is performed using a finite element model.

3.E.3 References

[3.E.1] S.P. Timoshenko, Strength of Materials, Vol. 2, Third Edition, Van Nostrand, 1956.

[3.E.2] ANSYS Finite Element Code, 5.0, Ansys, Inc., 1994.

3.E.4 Configuration, Geometry, and Input Weight Data

3.E.4.1 Configuration and Geometry

Figure 3.E.1 shows a sketch of the top closure lid with the the closure ring attached. The configuration is the same for all MPC types. The following dimensions are obtained from drawing no. 1393.

The outer radius of the lid, $R_{lid} := \frac{67.375}{2} \cdot in$

The inner radius of the closure ring, $R_i := \frac{53.03125}{2} \cdot in$

The outer radius of the closure ring, $R_o := \frac{67.875}{2} \cdot in$

The minimum thickness of the lid, $h := 9.5 \cdot in$

Note that the MPC lid can be fabricated from a single plate of thickness h or from two plates, each of thickness h/2, welded together around their circumference. The calculations in this appendix consider both options.

The closure ring thickness, $t := 0.375 \cdot in$

3.E.4.2 Input Weight Data

The bounding weight of the closure lid (MPC-68), $W_{lid} := 10400 \cdot lbf$ Table 3.2.4

The bounding weight per square inch of lid, $P_{lid} := \frac{W_{lid}}{\pi \cdot R_{lid}^2}$ $P_{lid} = 2.917 psi$

The bounding weight of the fuel basket plus fuel,

$W_{fuel} := 13000 \cdot lbf + 54000 \cdot lbf$ Table 3.2.4

The maximum total package weight of the MPC (including dynamic load factor),

$W_{lift} := 1.15 \cdot 90000 \cdot lbf$ Table 3.2.4

The maximum lifted weight is the bounding MPC weight with an applied 0.15 inertia load factor to bound loads during an MPC transfer operation.

3.E.5 Acceptance Criteria

Level A or Level D primary stress intensity levels must not be exceeded under the defined load conditions. Load cases considered are set to bound all requirements for either storage or transport.

3.E.6 Allowable Strengths

Allowable strengths at the design temperature of 550°F and at the accident temperature of 775°F are used. The material used is Alloy X. The relevant allowable stress intensities for primary membrane stress and for combined primary bending and primary membrane stress, for ASME Section III, Subsection NB components, are therefore:

The Level A allowable stress intensity for combined stress (550°F), $S_{ac} := 25450 \cdot psi$

The Level A allowable stress intensity for membrane stress (550°F), $S_{am} := 16950 \cdot psi$

The Level D allowable stress intensity for combined stress (550°F), $S_{dc} := 61050 \cdot psi$

The Level D allowable stress intensity for membrane stress (550°F), $S_{dm} := 40700 \cdot psi$

The Level D allowable stress intensity for combined (775°F), $S_{firec} := 54225 \cdot psi$

The Level D allowable stress intensity for membrane (775°F), $S_{firem} := 36150 \cdot psi$

The closure ring, which functions as the secondary seal for the MPC, is located on the upper surface of the lid. The appropriate design temperature at this location is 400°F, which bounds all non-accident metal temperatures obtained at that location in the analyses of Chapter 4. The Level A membrane and membrane plus bending allowable stress intensities at this temperature are:

$$S_{amr} := 18700 \cdot psi$$

$$S_{acr} := 28100 \cdot psi$$

3.E.7 Load Cases

The following bounding loads are considered as potential limiting loads for the top closure plate structural qualification. Only the most limiting combinations are used for the qualification. For calculation purposes, the applied loads are considered as equivalent surface pressures.

The external pressure, $P_{ext} := 40 \cdot psi$

The internal pressure, $P_{int} := 100 \cdot psi$

The fire pressure, $P_{fire} := 125 \cdot psi$

A bottom end drop on the overpack baseplate gives a pressure of,

$$P_{sd} := \frac{60 \cdot W_{lid}}{\pi \cdot R_{lid}^2} \qquad P_{sd} = 175.0\,psi$$

A top end drop on the overpack closure plate gives a pressure,

$$P_{td} := \frac{60 \cdot W_{fuel}}{\pi \cdot R_{lid}^2} \qquad P_{td} = 1128\,psi$$

The center lift weight, $P_{lift} := W_{lift}$

Note that external pressure never governs because internal pressure adds a membrane stress component. The center lift weight load is included to incorporate a future fully-loaded lifting operation.

For the qualification of the closure ring, only a single load case need be considered. If the primary, load carrying MPC cover plate-to-MPC shell peripheral weld leaks, then the closure ring will be subjected to the internal pressure load, and behaves as an annular plate supported at its inner and outer periphery. While this case is amenable to manual calculations, the case is analyzed using the finite element method for simplicity.

3.E.8 Calculations

The stress analysis of the closure plate is performed by conservatively assuming that the closure plate acts as a simply supported plate. This will conservatively predict a higher stress at the center of the plate. In the plate analysis, it is assumed that the thickness is constant. This is slightly nonconservative at the outer periphery of the plate since the closure ring is a separate component; however, as will be seen from the results, the safety margins are large so that the effect is negligible.

In all of the following analyses, since the circumferential stress has the same sign as the radial stress, stress intensities differ from stresses only by the surface pressure, where applicable.

3.E.8.1 Level A Bounding Calculations

The design load is the internal pressure case, since there is a direct stress as well as a bending stress because of the peripheral weld. However, for a transfer operation, there exists the potential for a bounding Level A condition to be internal pressure plus a central lifted load.

3.E.8.1.1 Load Case E1.a, Table 3.1.4

This load case consists of internal pressure only. Reference [3.E.1] provides a formula for the maximum bending stress at the center of a simply supported circular plate of uniform thickness h. For the case of internal pressure alone, the stress intensity SI_1 and resultant margin of safety are determined as:

The Poisson's ratio of the material, $\nu := 0.3$

The bending stress due to internal pressure, $\sigma_b := \frac{3\cdot(3+\nu)}{8}\cdot(P_{int}+P_{lid})\cdot\left(\frac{R_{lid}}{h}\right)^2$

$\sigma_b = 1601\,psi$

The direct stress due to internal pressure, $\sigma_d := -P_{int}$ $\sigma_d = -100\,psi$

The combined stress intensity, $SI_1 := (\sigma_b + |\sigma_d|)$ $SI_1 = 1701\,psi$

The margin of safety, $MS_1 := \frac{S_{ac}}{SI_1} - 1$ $MS_1 = 14.0$

From the discussion of the dual lid configuration in Subsection 3.4.4.3.1.2, the maximum bending stress in the two piece lid is two times the stress computed for the solid (one-piece) lid having the same total thickness. Thus, the margin of safety for the dual lid configuration is

The margin of safety, $MS_{1\_dual} := \frac{S_{ac}}{2SI_1} - 1$ $MS_{1\_dual} = 6.5$

3.E.8.1.2 Load Case E2, Table 3.1.4

This load case consists of the combined internal pressure and lifting loads. From pp.106-107 of [3.E.1], the following stress result is conservative since it assumes the lifting load is applied at the center of the plate. In reality, the lifting load acts on the plate at some radial distance from the center point. Therefore, the value computed here overestimates the maximum stress.

$$\sigma_{lift} := \frac{P_{lift}}{h^2}\cdot(1+\nu)\cdot\left(.485\cdot\ln\left(\frac{R_{lid}}{h}\right)+0.52\right)+1.5\cdot\frac{P_{lift}}{\pi\cdot h^2} \qquad \sigma_{lift} = 2238\,psi$$

This stress must be added to the stress intensity due to internal pressure to determine the total combined stress intensity SI_2. The limiting stress intensity and resultant margin of safety are therefore determined as:

The limiting combined stress intensity, $SI_2 := \sigma_{lift} + SI_1$ $SI_2 = 3940\,psi$

The limiting margin of safety, $MS_2 := \frac{S_{ac}}{SI_2} - 1$ $MS_2 = 5.5$

Next the calculations above are repeated for the dual lid configuration. In this case, the bending stress in the lid is computed based on a simply supported plate of thickness h/2.

$$\sigma_{lift\_dual} := \frac{P_{lift}}{(0.5\cdot h)^2}\cdot(1+\nu)\cdot\left(.485\cdot\ln\left(\frac{R_{lid}}{0.5\cdot h}\right)+0.52\right)+1.5\cdot\frac{P_{lift}}{\pi\cdot(0.5\cdot h)^2}$$

$\sigma_{lift\_dual} = 10957\,psi$

The limiting stress intensity and resultant safety margin for the dual lid configuration are therefore determined as:

The limiting combined stress intensity, $SI_{2\_dual} := \sigma_{lift\_dual} + 2SI_{1\,2\_dual} = 14360\,psi$

The limiting margin of safety, $MS_{2\_dual} := \frac{S_{ac}}{SI_{2\_dual}} - 1 \quad MS_{2\_dual} = 0.8$

3.E.8.2 Level D Bounding Calculations

3.E.8.2.1 Load Case E3.a, Table 3.1.4

3.E.8.2.1.1 Bounding 10CFR72 (Storage) Bottom End Drop

This load case corresponds to the 10CFR72 (storage) end drop on the overpack baseplate. The amplified weight of the lid, plus the external design pressure, give rise to a bending stress. This bending stress and the resultant margin of safety are determined as:

The bending stress due to the loading, $\sigma_b := \frac{3\cdot(3+\nu)}{8}\cdot(P_{sd}+P_{ext})\cdot\left(\frac{R_{lid}}{h}\right)^2$

$\sigma_b = 3346\,psi$

The margin of safety, $MS_3 := \frac{S_{dc}}{\sigma_b} - 1 \qquad MS_3 = 17.2$

For the dual lid configuration, the bending stress in the lower plate (assuming that its weight equals 50% of W_{lid}) is computed as follows:

The bounding weight per square inch, $P_{plate} := \frac{0.5W_{lid}}{\pi\cdot R_{lid}^2} \qquad P_{plate} = 1.459\,psi$

The bending stress due to the loading, $\sigma_{b\_lower} := \frac{3\cdot(3+\nu)}{8}\cdot(60\cdot P_{plate})\cdot\left(\frac{R_{lid}}{0.5\cdot h}\right)^2$

$\sigma_{b\_lower} = 5447\,psi$

The margin of safety, $MS_{3\_lower} := \frac{S_{dc}}{\sigma_{b\_lower}} - 1$ $MS_{3\_lower} = 10.2$

Since the upper plate is exposed to the MPC external pressure during transport, the stress in the upper plate is

The bending stress due to the loading, $\sigma_{b\_upper} := \frac{3\cdot(3+\nu)}{8}\cdot(60\cdot P_{plate} + P_{ext})\cdot\left(\frac{R_{lid}}{0.5\cdot h}\right)^2$

$\sigma_{b\_upper} = 7937\,psi$

The margin of safety, $MS_{3\_upper} := \frac{S_{dc}}{\sigma_{b\_upper}} - 1$ $MS_{3\_upper} = 6.69$

3.E.8.2.1.2 Bounding 10CFR71 (Transport) Top End Drop

For this case, the MPC closure plate is supported by the overpack closure plate over a peripheral band of support. It is conservative for the MPC qualification to assume that all support is at the outer edge. Therefore, the bending stress and resultant margin of safety due to the equivalent pressure of the fuel basket and fuel, the applied weight of the closure plate and the internal pressure is determined as:

The bending stress due to the loading, $\sigma_b := \frac{3\cdot(3+\nu)}{8}\cdot(P_{int} + P_{sd} + P_{td})\cdot\left(\frac{R_{lid}}{h}\right)^2$

$\sigma_b = 21825\,psi$

The margin of safety, $MS_4 := \frac{S_{dc}}{(\sigma_b + P_{int})} - 1$ $MS_4 = 1.8$

The margin of safety for the dual lid configuration is computed per Subsection 3.4.4.3.1.2 by multiplying the bending stress by a factor of 2.

The margin of safety, $MS_{4\_dual} := \frac{S_{dc}}{(2\cdot\sigma_b + P_{int})} - 1$ $MS_{4\_dual} = 0.4$

3.E.8.2.1.3 Load Case E5, Table 3.1.4

This load case considers dead load, fire pressure, and fire temperature material properties.

The bending stress is, $\sigma_b := \frac{3\cdot(3+\nu)}{8}\cdot(P_{fire}+P_{lid})\cdot\left(\frac{R_{lid}}{h}\right)^2$

$\sigma_b = 1.991\times 10^3\,psi$

The margin of safety is, $MS_5 := \frac{S_{firec}}{\sigma_b} - 1$ $MS_5 = 26.2$

The margin of safety for the dual lid configuration is computed per Subsection 3.4.4.3.1.2 by multiplying the bending stress by a factor of 2.

The margin of safety, $MS_{5\_dual} := \frac{S_{firec}}{2\cdot\sigma_b} - 1$ $MS_{5\_dual} = 12.6$

3.E.8.3 Peripheral Weld Stress

The area of the weld is computed by multiplying the total length of the weld (at radius R_{lid}) by the weld thickness. The weld capacity is found by multiplying this area by a quality factor (defined in ASME Subsection NG) and by the appropriate weld stress allowable from ASME Subsection NF. The weld between the MPC lid and the shell is a 3/4 inch(minimum) J-groove weld. For conservatism, a smaller weld size (i.e., 5/8 inch) is considered in the following stress evaluations.

The thickness of the weld, $t_{weld} := 0.625\cdot in$

The quality factor for a single groove weld that is examined by root and final PT is
$n := 0.45$
The allowable weld stresses for Level A and Level D conditions are Sa and Sd, respectively. The weld metal strength is assumed to decrease with temperature in the same manner as does the base metal (Alloy X)

$Sa := 0.3\cdot 70000\cdot\left[1-\left(\frac{75-63.3}{75}\right)\right]\cdot psi$ $Sa = 1.772\times 10^4\,psi$

$Sd := .42\cdot 70000\cdot\left[1-\left(\frac{75-63.3}{75}\right)\right]\cdot psi$ $Sd = 2.481\times 10^4\,psi$

The maximum load capacity of the weld, $LC_{weld} := n \cdot 2 \cdot \pi \cdot R_{lid} \cdot t_{weld} \cdot Sa$

$$LC_{weld} = 1.055 \times 10^{6}\,lbf$$

The margin of safety of this load capacity, for the Level A center lift loading case (Load Case E2, Table 3.1.4), is determined as:

$$MS_6 := \frac{LC_{weld}}{W_{lift} + \pi \cdot P_{int} \cdot R_{lid}^{2}} - 1 \qquad MS_6 = 1.29$$

The bounding weld load for Level D conditions is determined by multiplying the equivalent pressure load for the load case by the area of the closure plate. The bottom end drop is taken by the welds, and the top end drop is taken by bearing on the overpack closure plate.

$$L_{weld} := P_{sd} \cdot \pi \cdot \left(R_{lid}\right)^2 \qquad L_{weld} = 624000\,lbf$$

$$MS_7 := \frac{Sd}{Sa} \cdot \frac{LC_{weld}}{L_{weld}} - 1 \qquad MS_7 = 1.37$$

To further demonstrate the adequacy of the weld, its capacity is compared to a weld load that equals three times the total lifted weight. The margin of safety is

$$MS_8 := \frac{LC_{weld}}{3 \cdot W_{lift}} - 1 \qquad MS_8 = 2.40$$

For the dual lid configuration, the two plates are joined by a 3/16 inch groove weld around the periphery. This weld must support the amplified weight of the lower plate in the event of a bottom end drop. The capacity of the weld and its margin of safety are

The thickness of the weld, $t_{weld2} := 0.1875 \cdot in$

The maximum load capacity of the weld, $LC_{weld} := n \cdot 2 \cdot \pi \cdot R_{lid} \cdot t_{weld2} \cdot Sd$

$$LC_{weld} = 4.432 \times 10^{5}\,lbf$$

The load due to a bottom end drop, $L_{weld} := 60 \cdot \pi \cdot R_{lid}^2 \cdot P_{plate}$

$L_{weld} = 3.12 \times 10^5 \, lbf$

The margin of safety, $MS_9 := \frac{LC_{weld}}{L_{weld}} - 1$ $MS_9 = 0.42$

3.E.8.4 Fatigue Analysis of Weld

The welds will be subjected to cyclic stress each time the cask is lifted. The force difference is equal to W_{lift}. Pressure loads are not a fatigue consideration since they remain relatively constant during normal operation. Therefore, the effective fatigue stress can be determined as follows

The fatigue factor for a single groove weld that is examined by root and final PT is $f := 4$ and the alternating stress is

$$\sigma := \frac{\left(f \cdot \frac{W_{lift}}{2}\right)}{2 \cdot \pi \cdot R_{lid} \cdot t_{weld}} \qquad \sigma = 1565 \, psi$$

This stress is compared to curve B in Figure I-9.2.2 of the ASME Division I Appendices per Subsection NG. This curve shows that the welds have unlimited life at this stress level.

3.E.8.5 Closure Ring Analysis

The closure ring must be capable of withstanding the application of the full MPC internal pressure, to ensure that a leak in the primary closure plate weld will be contained. This condition is modeled as an annular ring subject to the design internal pressure. A finite element analysis of a thin ring with an applied pressure is performed using the ANSYS finite element code. The thin ring is simulated by four layers of PLANE42 axisymmetric quadrilateral elements (see Figure 3.E.2). The boundary condition is conservatively set as zero displacement at node locations 1 and 2 (see Figure 3.E.2). The bottom surface is subjected to a 100 psi pressure to simulate leakage of the primary MPC weld. The maximum stress intensity in the ring (occurring at the top center point) and the resultant margin of safety for Level A conditions are determined as:

The maximum stress intensity in the ring, $SI_{ring} := 20001 \cdot psi$

The margin of safety, $MS_{10} := \frac{S_{acr}}{SI_{ring}} - 1$ $MS_{10} = 0.405$

Since the actual support condition provides some clamped support, this result is very conservative.

The total load capacity of the closure ring weld is determined by calculating the total area of the two weld lines at radii R_i and R_o, multiplying by the allowable weld stress, and conservatively applying the specified weld efficiency.

The closure ring weld thickness, $t_{crw} := 0.125 \cdot in$ (this allows for fit-up)

The quality factor for a single groove or a single fillet weld that is examined by root and final PT is $n := 0.45$

The load capacity of the ring welds, $LC_{crw} := n \cdot 2 \cdot \pi \cdot \left(R_i + \frac{R_o}{\sqrt{2}} \right) \cdot t_{crw} \cdot Sa$

$LC_{crw} = 3.164 \times 10^5 \, lbf$

The margin of safety of these welds for the applied loading condition (internal pressure only) is determined as:

$$MS_{11} := \frac{LC_{crw}}{\pi \cdot P_{int} \cdot \left(R_o^2 - R_i^2 \right)} - 1 \qquad MS_{11} = 1.24$$

3.E.9 Conclusions

The results of the evaluations presented in this appendix demonstrate the adequacy of the MPC closure plate, closure ring and associated weldments to maintain their structural integrity during applied bounding load cases considered. Positive safety margins exist for all components examined for all load cases considered.

The bending stress evaluation of the closure ring conservatively assumes a simple support condition at the peripheral welds. Therefore, any seal welds in the closure ring configuration need be sized based on positive margins on shear stress.

The seal weld size (0.125") adequately supports the expected shear load. Note that a closure ring peripheral weld thickness as small as 0.056" provides a small positive margin of safety.

REPORT HI-2012610

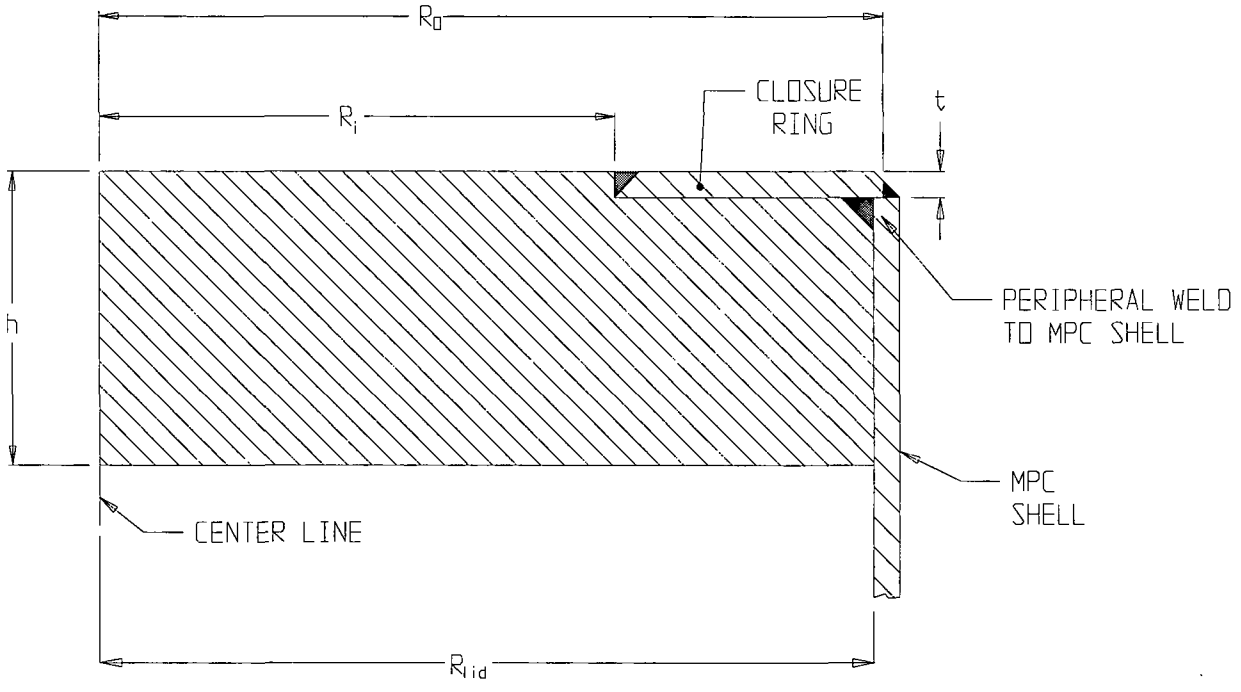

FIGURE 3.E.1; TOP CLOSURE LID WITH CLOSURE RING ATTACHED

REVISION 0

REPORT HI-2012610

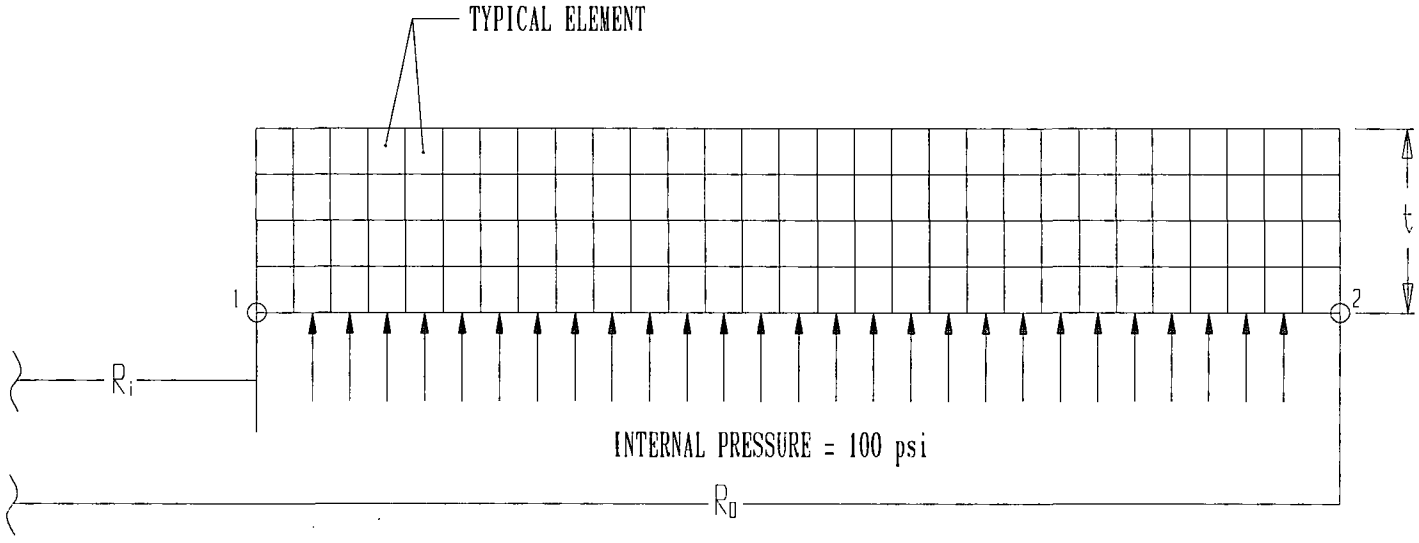

FIGURE 3.E.2; FINITE ELEMENT MODEL - CLOSURE RING

REVISION 0

APPENDIX 3.F - STRESS ANALYSIS OF OVERPACK CLOSURE BOLTS

3.F.1 Introduction

This appendix contains a stress analysis of the HI-STAR 100 Overpack closure bolts. The purpose of the analysis is to demonstrate that stresses in the closure bolts do not exceed allowable maximums.

The HI-STAR 100 package can be used for both transportation and storage of spent nuclear fuel. Loadings from the normal and hypothetical accident conditions of transport as specified in Federal Regulation 10 CFR part 71 are more severe than the loadings placed on the bolts in the storage condition.

The complex interaction of forces and moments in bolted joints of shipping casks has been investigated in Reference 3.F.1, resulting in a comprehensive method of closure bolt stress analysis. That method is employed here. The analysis is presented in a step-by-step form for each loading combination considered. For each set of formulas or calculations used, reference to the appropriate table in [3.F.1] is given. Tables 4.3, 4.4, 4.5, and 4.7 are reproduced directly from [3.F.1] and placed at the end of this appendix to assist the reader. Where necessary, the formulas are modified to reflect the particulars of the HI-STAR system. For example, the loads due to impact from the MPC are applied as a pressure band near the bolt circle rather than as a uniform pressure load since the MPC contacts the overpack closure plate only around the periphery. Further, since the HI-STAR 100 closure lid has a raised face outside of the bolt circle, no prying forces can develop from loads directed outward (such as internal pressure or impact loads on the lid from the internals).

3.F.2 References

[3.F.1] Mok, Fischer, Hsu, *Stress Analysis of Closure Bolts for Shipping Casks* (NUREG/CR-6007 UCRL-ID-110637), Lawrence Livermore National Laboratory/Kaiser Engineering, 1993.

[3.F.2] Horton, H. (Ed.), *Machinery's Handbook*, 15th Ed., The Industrial Press, 1957.

[3.F.3] FEL-PRO Technical Bulletin, N-5000 Nickel Based - Nuclear Grade Anti-Seize Lubricant, 8/97.

[3.F.4] K.P. Singh and A.I. Soler, *Mechanical Design of Heat Exchangers and Pressure Vessel Components*, First Edition, Arcturus Publishers, Inc., 1984.

3.F.3 Assumptions

The assumptions used in the analysis are given as a part of Reference 3.F.1. The assumptions in that reference are considered valid for this analysis except where noted below.

1. No bolt prying can occur from outward directed loads since the closure lid has a raised face outside of the bolt circle which eliminates the potential for prying due to positive bending moments.

2. The forces and moments in the bolts due to the gasket load are included in the preload imposed.

3. Puncture forces are calculated using pressure equal to 3 times the lid yield strength. This is conservative since a dynamic analysis of the impact would demonstrate lower contact loads .

4. The forces and moments in the bolts due to vibration loads are small relative to the forces and moments generated by all other loads, and are considered negligible.

5. A recess is provided in the overpack closure plate that causes the MPC to contact the bottom face of the overpack closure plate over an annular region at the outer periphery of the closure plate. The formulas for plates under uniform pressure used in the reference are replaced here by formulas for plates loaded uniformly over an annular region at the outer periphery.

6. As the HI-STAR 100 Overpack includes a protected lid, shear bolt forces are defined to be zero.

7. The temperatures used in the analyses are taken from the thermal analysis of the HI-STAR.

8. The actual weight of the overpack closure plate is replaced by a somewhat larger weight in this analysis. This is conservative because loads on the bolts are increased with a heavier closure plate.

9. The impact load in this analysis is assumed to be 60 g. This is conservative because actual accelerations of the cask are less than 60 g. An impact angle of 80 degrees is assumed since the impact limiter will load the closure plate in the near top drop condition.

3.F.4 Terminology

Some terminology in Reference 3.F.1 differs from Holtec's terminology. In this analysis, the 'cask wall' is Holtec's 'main flange'. The 'cask' is Holtec's 'Overpack'. 'Closure lid' and 'closure plate' are used interchangeably.

Wherever possible, parameter names are consistent with Reference 3.F.1.

3.F.5 Composition

This appendix was created with the Mathcad (version 6.0+) software package. Mathcad uses the symbol ':=' as an assignment operator, and the equals symbol '=' retrieves values for constants or variables. Inequalities are also employed. Mathcad returns 0 for a false inequality, and 1 for a true inequality.

Units are also carried with Mathcad variables.

3.F.6 Analysis Procedure

The analysis procedure is taken from Section 6.4 of Reference 3.F.1. The following general steps are taken:

1. Identification of individual loadings.

2. Identification of critical combined load cases. Three critical combined load cases are considered in the HI-STAR bolt analysis.

3. Identification and evaluation of load parameters.

4. Determination of the forces and moments acting on the bolts due to each of individual loading.

5. Determination of the forces and moments acting on the bolts for the combined load case under analysis.

6. Evaluation of the stresses in the bolts for the combined load case.

7. Comparison with acceptance criteria.

3.F.7 Identification of Individual Loadings

The individual loadings acting on the cask closure are the following:

a. Bolt preload. Bolt preload is present in all loadings and includes any gasket sealing loads.

b. Pressure. Design internal pressure is applied to the overpack wall and lid for all load combinations.

c. Temperature. Temperatures from an appropriate thermal analysis are used.

d. Impact. An impact angle and g-level are specified. A near top end drop resulting in an 80 degree impact angle is consistent with the assumption that the impact limiter does not load the closure plate.

e. Puncture. The cask is subjected to a puncture load from an 6 inch diameter mild steel punch. A punch angle of 90 degrees is used. This simulates the hypothetical puncture condition.

3.F.8 Identification of Critical Combined Load Cases

The critical combined load cases that apply to the HI-STAR 100 system in the transport mode are as follows:

1. Normal condition maximum stress analysis: Preload + pressure + temperature

2. Accident condition maximum stress analysis: Preload + pressure + temperature + puncture
3. Accident condition maximum stress analysis: Preload + pressure + temperature + impact

These three cases are examined below.

3.F.9 Geometry Parameters

The parameters which define the HI-STAR 100 closure geometry are given in this section. The following information is obtained from the design drawings in Section 1.5 unless otherwise noted.

The nominal closure bolt diameter, $Db := 1.625 \cdot in$

The total number of closure bolts, $Nb := 54$

The stress area of a closure bolt (from [3.F.4], p. 100), $A_b := 1.680 \cdot in^2$

The closure lid diameter at the bolt circle, $Dlb := 74.75 \cdot in$

Closure lid diameter at the location of the gasket load reaction, $Dlg := 71.565 \cdot in$

The HI-STAR overpack gasket system includes two concentric seals. The value for Dlg above locates the gasket load reaction between the two seal diameters.

The thickness of the cask wall, $tc := 6.25 \cdot in$

The minimum thickness of the closure lid, $tl := \left(6 - \frac{1}{16}\right) \cdot in$

This value for the closure lid thickness accounts for the thickness reduction (recess) in the bottom face of the lid.

The effective thickness of the closure lid flange, $tlf := 4.25 \cdot in$

The closure plate diameter at the inner edge, $Dli := 69.75 \cdot in$

The closure plate diameter at the inner edge is overpack inner diameter plus twice the width of the cut-out in the top flange which accommodates the inflatable annulus seal.

The closure plate diameter at the outer edge, $Dlo := 77.375 \cdot in$

The bolt length, $Lb := 4.25 \cdot in$

The bolt length is the length between the top and bottom surfaces of the closure plate, at the bolt circle location.

The number of bolt threads per inch, $n := 8 \cdot \frac{1}{in}$

The bolt thread pitch, $p := \frac{1}{n}$

The upper bound MPC weight (from Table 3.2.4), $Wc := 90000 \cdot lb$

The bounding weight used for closure plate (from Table 3.2.4), $Wl := 8000 \cdot lb$

The overpack closure lid recess inner diameter, $d_l := 52.75 \cdot in$

3.F.10 Material Properties

The overpack closure bolts are SB-637-N07718 steel, and the closure plate and top flange are SA-350-LF3 steel. The following material properties are used in the analysis based on a design temperature of 400 degrees F. The property values are obtained from Sections 3.1 and 3.3.

The Young's modulus of the cask wall material, $Ec := 26100000 \cdot psi$

The Young's modulus of the closure plate material, $El := 26100000 \cdot psi$

The Poisson's ratio of the closure plate material, $NUl := 0.3$

The closure bolt material coefficient of thermal expansion, $ab := 7.45 \cdot 10^{-6} \cdot R^{-1}$

The cask wall material coefficient of thermal expansion, $ac := 6.98 \cdot 10^{-6} \cdot R^{-1}$

The closure plate material coefficient of thermal expansion, $al := 6.98 \cdot 10^{-6} \cdot R^{-1}$

The zero points of the Fahrenheit and Rankine scales differ by a constant (1 °F = 1 R), therefore the above numbers are accurate with either unit.

Young's modulus of the closure bolt material, $Eb := 27600000 \cdot psi$

Yield strength of closure plate material, $Syl := 32200 \cdot psi$

Tensile strength of closure plate material, $Sul := 64600 \cdot psi$

Young's modulus of top flange material, $Elf := 26100000 \cdot psi$

Bolt material minimum yield stress or strength (room temperature), $Sy1 := 150000 \cdot psi$

Bolt material minimum yield stress or strength (design temperature), $Sy2 := 138300 \cdot psi$

Bolt material minimum ultimate stress or strength (design temperature), $Su := 170600 \cdot psi$

3.F.11 Combined Load Case 1

Normal Condition maximum stress analysis: Preload + pressure + temperature

3.F.11.1 Identification and Evaluation of Load Parameters, Combined Load Case 1

For each individual loading in this combined load case, the load parameters must be defined. The load parameters for the first individual load case in load combination 1 are as follows:

Loading parameters for preload (nominal bolt torque = 2000 ft lbf):

The nominal value of the nut factor is 0.15 from Reference 3.F.3.
The minimum nut factor, based on a tolerance of +/- 5%, is $K := 0.1425$

The maximum bolt preload torque per bolt (Table 8.1.3), $Q := 2000 \cdot ft \cdot lbf + 250 \cdot ft \cdot lbf$

Loading parameters for pressure load:

The pressure inside the cask wall, $Pci := 100 \cdot psi$

The pressure outside the cask wall, $Pco := 14.7 \cdot psi$

The pressure inside the closure lid, $Pli := 100 \cdot psi$

The pressure outside the closure lid, $Plo := 14.7 \cdot psi$

Loading parameters for the normal condition temperature load: (bolt installation at 70 deg. F)

The maximum temperature rise of the main flange, $Tc := (155 - 70) \cdot R$

The maximum temperature rise of the closure lid inner surface, $Tli := (155 - 70) \cdot R$

The maximum temperature rise of the closure lid outer surface, $Tlo := (150 - 70) \cdot R$

The maximum temperature change of the closure lid, $Tl := \frac{Tli + Tlo}{2}$ $Tl = 82.5\,R$

The maximum temperature change of the closure bolts, $Tb := \frac{Tl + Tc}{2}$ $Tb = 83.75\,R$

As these parameters are all temperature differences, the Fahrenheit-to-Rankine conversion factor of 460° can be omitted. The temperature values are obtained from the normal steady state analysis of a bounding MPC (highest heat load and temperatures).

3.F.11.2 Determination of Bolt Forces and Moments for the Individual Loadings

Array parameters are used to account for the multiple individual loadings within one combined load case. In combined load case 1, there are three individual loadings, so let i include the range from 1 to 3 as follows:

Let $i := 1..3$

The forces and moments generated by each individual load case are represented by the following symbols:

The non-prying tensile bolt force per bolt = Fa_i

The shear bolt force per bolt = Fs_i

The fixed-edge closure lid force = Ff_i

Fixed-edge closure lid moment = Mf_i

The subscript i is used only to keep track of each individual load case within a load combination.

The first individual loading in this load combination is the residual load after the preload operation. The forces and moments generated by this load are defined as [3.F.1, Table 4.1]:

The non-prying tensile bolt force per bolt, $Fa_1 := \frac{Q}{K \cdot Db}$

The maximum residual tensile bolt force (preload) per bolt, $Far_1 := Fa_1$

The maximum residual torsional bolt moment per bolt, $Mtr := 0.5 \cdot Q$

The preload stress in each bolt (based on stress area), $Preload := \frac{Fa_1}{A_b}$

Substituting the appropriate input data, the values of these parameters are determined as:

$Fa_1 = 116599\,lbf$

$Far_1 = 116599\,lbf$

$Mtr = 13500\,in \cdot lbf$

$Preload = 69404\,psi$

The second individual loading in this load combination is the pressure load. The forces and moments generated by this load are defined as follows [3.F.1, Table 4.3]:

The non-prying tensile force per bolt, $Fa_2 := \frac{\pi \cdot Dlg^2 \cdot (Pli - Plo)}{4 \cdot Nb}$

The shear bolt force per bolt, $Fs_2 := \frac{\pi \cdot El \cdot tl \cdot (Pci - Pco) \cdot Dlb^2}{2 \cdot Nb \cdot Ec \cdot tc \cdot (1 - NUl)}$

The fixed-edge closure lid force, $Ff_2 := \frac{Dlb \cdot (Pli - Plo)}{4}$

The fixed-edge closure lid moment, $Mf_2 := \frac{(Pli - Plo) \cdot Dlb^2}{32}$

Substituting the appropriate input data, the values of these parameters are determined as:

$$Fa_2 = 6354\,lbf$$

$$Fs_2 = 18816\,lbf$$

$$Ff_2 = 1594\,\frac{lbf}{in}$$

$$Mf_2 = 14894\,lbf$$

The third individual loading in this load combination is the temperature load. The forces and moments generated by this load are defined as [3.F.1, Table 4.4]:

The non-prying tensile bolt force per bolt, $Fa_3 := 0.25 \cdot \pi \cdot Db^2 \cdot Eb \cdot (al \cdot Tl - ab \cdot Tb)$

The shear bolt force per bolt, $Fs_3 := \frac{\pi \cdot El \cdot tl \cdot Dlb \cdot (al \cdot Tl - ac \cdot Tc)}{Nb \cdot (1 - NUl)}$

The fixed-edge closure lid force, $Ff_3 := 0 \cdot \frac{lbf}{in}$

The fixed-edge closure lid moment, $Mf_3 := \frac{El \cdot al \cdot tl^2 \cdot (Tlo - Tli)}{12 \cdot (1 - NUl)}$

Substituting the appropriate input data, the values of these parameters are determined as:

$$Fa_3 = -2753\,lbf$$

$$Fs_3 = -16800\,lbf$$

$$Ff_3 = 0\,\frac{lbf}{in}$$

$$Mf_3 = -3823\,lbf$$

3.F.11.3 Determination of Combined Bolt Forces and Combined Bolt Moments

The calculations in the following subsections are performed in accordance with Tables 4.9, 2.1 and 2.2 of Reference 3.F.1.

3.F.11.3.1 Tensile Bolt Force

First, combine the non-prying tensile bolt forces (Fa_i):

The total preload and temperature load, $Fa\_pt := Fa_1 + Fa_3$

$$Fa\_pt = 113847\,lbf$$

The sum of the remaining forces (pressure), $Fa\_al := Fa_2$

$$Fa\_al = 6354\,lbf$$

The combined non-prying tensile bolt force, $Fa\_c := Fa\_al \cdot (Fa\_al > Fa\_pt) + Fa\_pt \cdot (Fa\_pt > Fa\_al)$

$$Fa\_c = 113847\,lbf$$

If the combined non-prying tensile bolt force (Fa_c) is negative, set it equal to zero. Per Appendix 3 of Reference [3.F.1], inward directed loads are not reacted by the bolts, but the developed formulations are still valid if the spurious bolt forces < 0.0 are removed from the calculation.

$$Fa\_c := Fa\_c \cdot (Fa\_c > 0 \cdot lbf)$$

$$Fa\_c = 113847\,lbf$$

Next, combine the prying tensile bolt forces and moments (these bolt forces develop due to Ff_i and Mf_i):

The sum of the fixed edge forces, $Ff\_c := Ff_1 + Ff_2 + Ff_3$

$$Ff\_c = 1594\,\frac{lbf}{in}$$

If the combined fixed-edged force (Ff_c) is negative, set it equal to zero.

$$Ff\_c := Ff\_c \cdot \left(Ff\_c > 0 \cdot \frac{lbf}{in}\right) + 0 \cdot \frac{lbf}{in} \cdot \left(Ff\_c < 0 \cdot \frac{lbf}{in}\right)$$

$$Ff\_c = 1.594 \times 10^3\,\frac{lbf}{in}$$

The sum of fixed-edge moments, $Mf\_c := Mf_1 + Mf_2 + Mf_3$

$$Mf\_c = 11071\,\frac{lbf \cdot in}{in}$$

Define the appropriate prying force moment arm depending on the direction of Mf_c. For inward directed loading, prying moments are developed by the lid rotating about the flange inner edge; for outward directed loading, prying moments are developed by the lid rotating about its outer edge. Thus, the moment arms are different in the two cases.

$$Arm := (Dlo - Dlb)\cdot(Mf\_c > 0\cdot lbf) + (Dlb - Dli)\cdot(Mf\_c < 0\cdot lbf)$$

$$Arm = 2.625\,in$$

The prying tensile bolt force for the combined loading can therefore be determined as:

The constants C_1 and C_2 are: $C_1 := 1$

$$C_2 := \left[\frac{8}{3\cdot(Arm)^2}\right]\cdot\left[\frac{El\cdot tl^3}{1 - NUl} + \frac{(Dlo - Dli)\cdot Elf\cdot tlf^3}{Dlb}\right]\cdot\left(\frac{Lb}{Nb\cdot Db^2\cdot Eb}\right)$$

$$C_2 = 3.347$$

The bolt preload per unit length of bolt circle, $P := Fa\_pt\cdot\left(\frac{Nb}{\pi\cdot Dlb}\right)$

$$P = 26179\,\frac{lbf}{in}$$

The parameter P is the pressure/temperature force which is multiplied to determine preload per unit length of bolt circle (see Tables 2.1 and 4.9 in Section II.3 of Reference 3.F.1).

The non-prying tensile bolt force, $B := Ff\_c\cdot(Ff\_c > P) + P\cdot(P > Ff\_c)$

$$B = 26179\,\frac{lbf}{in}$$

The additional tensile bolt force per bolt caused by prying action of the closure lid, $Fap := \left(\frac{\pi\cdot Dlb}{Nb}\right)\cdot\left[\frac{\frac{2\cdot Mf\_c}{Arm} - C_1\cdot(B - Ff\_c) - C_2\cdot(B - P)}{C_1 + C_2}\right]$

$$Fap = -16156\,lbf$$

The prying force must be tensile. If the result is negative, set it equal to zero.

$$Fab\_c := Fap\cdot(Fap > 0\cdot lbf) + 0\cdot lbf\cdot(Fap < 0\cdot lbf)$$

$$Fab\_c = 0\,lbf$$

The total tensile bolt force for stress analysis, $FA := Fa\_c + Fab\_c$

$$FA = 113847\,lbf$$

3.F.11.3.2 Bolt Shear Force

The sum of the shear forces, $Fs\_c := Fs_1 + Fs_2 + Fs_3$

$$Fs\_c = 2016\,lbf$$

$Fs := 0 \cdot lbf$ (protected cask lid)

3.F.11.3.3 Bolt Bending Moment

The calculations in this section are performed in accordance with Table 2.2 of Reference 3.F.1. The following relations are defined:

$$Kb := \left(\frac{Nb}{Lb}\right)\cdot\left(\frac{Eb}{Dlb}\right)\cdot\left(\frac{Db^4}{64}\right)$$

$$Kl := \frac{El\cdot tl^3}{3\cdot\left[\left(1-NUl^2\right)+(1-NUl)^2\cdot\left(\frac{Dlb}{Dlo}\right)^2\right]\cdot Dlb}$$

$$Mbb\_c := \left(\frac{\pi\cdot Dlb}{Nb}\right)\cdot\left(\frac{Kb}{Kb+Kl}\right)\cdot Mf\_c$$

$$Mbb := Mbb\_c$$

where Mbb is the bolt bending moment. Substituting the appropriate values, these parameters are calculated as:

$$Kb = 511136\,lbf$$

$$Kl = 17817619\,lbf$$

$$Mbb\_c = 1.343 \times 10^3\,lbf\cdot in$$

$$Mbb = 1.343 \times 10^3\,lbf\cdot in$$

3.F.11.3.4 Bolt Torsional Moment

The torsional bolt moment is generated only by the preloading operation, therefore no combination is necessary.

3.F.11.4 Evaluation of Bolt Stresses

Per Table 5.1 of Reference 3.F.1, the average and maximum bolt stresses for comparison with the acceptance criteria are obtained. Inch-series threads are used and the maximum shear and bending are in the bolt thread.

The bolt diameter for tensile stress calculation [3.F.1, Table 5.1], $Dba := Db - 0.9743 \cdot p$

$$Dba = 1.503\,in$$

The bolt diameter for shear stress calculation, $Dbs := Dba$

$$Dbs = 1.503\,in$$

The bolt diameter for bending stress calculation, $Dbb := Dba$

$$Dbb = 1.503\,in$$

The bolt diameter for torsional stress calculation, $Dbt := Dba$

$$Dbt = 1.503\,in$$

The average tensile stress caused by the tensile bolt force FA, $Sba := 1.2732 \cdot \frac{FA}{Dba^2}$

$$Sba = 64147\,psi$$

The average shear stress caused by the shear bolt force Fs, $Sbs := 1.2732 \cdot \frac{Fs}{Dbs^2}$

$$Sbs = 0\,psi$$

The maximum bending stress caused by the bending bolt moment Mb, $Sbb := 10.186 \cdot \frac{Mbb}{Dbb^3}$

$$Sbb = 4026\,psi$$

The maximum shear stress caused by the torsional bolt moment Mt, $Sbt := 5.093 \cdot \frac{Mtr}{Dbt^3}$

$$Sbt = 20242\,psi$$

The maximum stress intensity caused by the combined loading of tension, shear, bending and torsion can therefore be determined as:

$$Sbi := \left[(Sba + Sbb)^2 + 4 \cdot (Sbs + Sbt)^2\right]^{0.5}$$

$Sbi = 79288\,psi$

3.F.11.5 Comparison with Acceptance Criteria: Normal Conditions, Maximum Stress Analysis

These comparisons are performed in accordance with Table 6.1 of Reference 3.F.1.

The basic allowable stress limit for the bolt material, $Sm := \frac{2}{3}\cdot Sy1\cdot(Sy1 \le Sy2) + \frac{2}{3}\cdot Sy2\cdot(Sy2 < Sy1)$

$Sm = 9.22 \times 10^4\,psi$

The average tensile stress (must be < Sm), $Sba = 64147\,psi$

The average shear stress (must be < 0.6Sm), $Sbs = 0\,psi$

For combined tensile and shear stress, the sum of the squares of the stress-to-allowable ratios (R_t and R_s) must be less than 1.0.

The tensile stress-to-allowable ratio, $R_t := \frac{Sba}{Sm}$ $R_t = 0.696$

The shear stress-to-allowable ratio, $R_s := \frac{Sbs}{0.6\cdot Sm}$

The sum of the squares of the ratios (must be < 1.0), $R_t^2 + R_s^2 = 0.484$

For combined tension, shear, bending and torsion loadings, the maximum stress intensity must be less than 1.35 times the allowable stress limit of the bolt material (Sm).

$1.35\cdot Sm = 124470\,psi$

$Sbi = 79288\,psi$

3.F.11.6 Conclusion

For the first loading combination, allowable stress limits are not exceeded.

3.F.12 Critical Combined Load Case 2

Accident Condition maximum stress analysis: Preload + pressure + temperature + puncture

3.F.12.1 Identification and Evaluation of Load Parameters, Combined Load Case 2

The first three individual loadings in this combined load case are the same as the individual loadings in the previous load case. Therefore, only the puncture load parameters must be defined for this load combination. The load parameters for the puncture individual load case in load combination 2 are as follows:

The diameter of the puncture bar, $D_{pb} := 6 \cdot in$

The impact angle between the cask axis and the ground, $xi := 90 \cdot deg$

3.F.12.2 Determination of Bolt Forces and Moments of Individual Loadings

Four individual loadings exist, so we define a range from 1 to 4 as follows:

Let $i := 0..4$

Bolt forces and moments for the preload, pressure, and temperature loads have already been calculated in the previous section. Determination of bolt forces and moments for the puncture load (the fourth individual load in this load combination) are required here [3.F.1, Table 4.7].

First, calculate the maximum puncture load generated by the puncture bar. The puncture force is assumed to be based on a dynamic flow stress S_y at the circular contact area between the bar and the lid surface. The dynamic flow stress is taken as the average of the yield strength and the ultimate strength of the lid material. Therefore, for this puncture analysis:

The dynamic flow stress, $Sy := .5 \cdot (Syl + Sul)$

$$Sy = 4.84 \times 10^4 \, psi$$

The puncture contact area, $Pun := 0.75 \cdot \pi \cdot D_{pb}^2 \cdot Syl$

$$Pun = 2.731 \times 10^6 \, lbf$$

The bolt forces and moments due to the puncture load can now be determined as:

The non-prying tensile bolt force per bolt, $Fa_4 := \frac{-\sin(xi) \cdot Pun}{Nb}$

$$Fa_4 = -50580 \, lbf$$

The shear bolt force per bolt, $Fs_4 := \frac{\cos(xi) \cdot Pun}{Nb}$

$$Fs_4 = -1.936 \times 10^{-11} \, lbf$$

The fixed-edge closure lid force, $Ff_4 := \frac{-\sin(xi) \cdot Pun}{\pi \cdot Dlb}$

$$Ff_4 = -11631 \frac{lbf}{in}$$

The fixed-edge closure lid moment, $Mf_4 := \frac{-\sin(xi) \cdot Pun}{4 \cdot \pi}$

$$Mf_4 = -217350\,\frac{lbf \cdot in}{in}$$

3.F.12.3 Determination of Combined Bolt Forces and Combined Bolt Moments

3.F.12.3.1 Bolt Tensile Force

Combine the non-prying tensile bolt forces.

The total preload and temperature load, $Fa\_pt := Fa_1 + Fa_3$

$$Fa\_pt = 113847\,lbf$$

The sum of the remaining loads (pressure and puncture), $Fa\_al := Fa_2 + Fa_4$

$$Fa\_al = -44226\,lbf$$

The combined non-prying tensile bolt force, $Fa\_c := Fa\_al \cdot (Fa\_al > Fa\_pt) + Fa\_pt \cdot (Fa\_pt > Fa\_al)$

$$Fa\_c = 113847\,lbf$$

If Fa_c is negative, set it equal to zero: $Fa\_c := Fa\_c \cdot (Fa\_c > 0 \cdot lbf)$

$$Fa\_c = 113847\,lbf$$

Combine the prying tensile bolt forces.

The sum of the fixed-edge forces, $Ff\_c := Ff_1 + Ff_2 + Ff_3 + Ff_4$

$$Ff\_c = -10037\,\frac{lbf}{in}$$

If Ff_c is negative, set it equal to zero: $Ff\_c := Ff\_c \cdot \left(Ff\_c > 0 \cdot \frac{lbf}{in}\right) + 0 \cdot \frac{lbf}{in} \cdot \left(Ff\_c < 0 \cdot \frac{lbf}{in}\right)$

$$Ff\_c = 0\,\frac{lbf}{in}$$

The sum of the fixed-edge moments, $Mf\_c := Mf_1 + Mf_2 + Mf_3 + Mf_4$

$$Mf\_c = -206279\,\frac{lbf \cdot in}{in}$$

Determine the appropriate prying force moment arm depending on the direction of Mf_c.

$$Arm := (Dlo - Dlb) \cdot (Mf\_c > 0 \cdot lbf) + (Dlb - Dli) \cdot (Mf\_c < 0 \cdot lbf)$$

$$Arm = 5\,in$$

Determine the prying tensile bolt force for the combined loading.

The non-prying tensile bolt force, $B := Ff\_c \cdot (Ff\_c > P) + P \cdot (P > Ff\_c)$

$$B = 26179 \frac{lbf}{in}$$

The additional tensile force per bolt caused by prying action of the lid can now be determined as:

The constants C_1 and C_2 are: $C_1 := 1$

$$C_2 := \left[\frac{8}{3 \cdot (Arm)^2}\right] \cdot \left[\frac{El \cdot tl^3}{1 - NUl} + \frac{(Dlo - Dli) \cdot Elf \cdot tlf^3}{Dlb}\right] \cdot \left(\frac{Lb}{Nb \cdot Db^2 \cdot Eb}\right)$$

$$C_2 = 0.923$$

The additional tensile force per bolt caused by prying action of the closure lid, $Fap := \left(\frac{\pi \cdot Dlb}{Nb}\right) \cdot \left[\frac{\frac{2 \cdot Mf\_c}{Arm} - C_1 \cdot (B - Ff\_c) - C_2 \cdot (B - P)}{C_1 + C_2}\right]$

$$Fap = -245857\,lbf$$

If the prying force is negative, set it equal to zero: $Fab\_c := Fap \cdot (Fap > 0 \cdot lbf) + 0 \cdot lbf \cdot (Fap < 0 \cdot lbf)$

$$Fab\_c = 0\,lbf$$

The total tensile bolt force for stress analysis, $FA := Fa\_c + Fab\_c$

$$FA = 113847\,lbf$$

3.F.12.3.2 Bolt Shear Force

The sum of the shear forces, $Fs\_c := Fs_1 + Fs_2 + Fs_3 + Fs_4$

$$Fs\_c = -1.936 \times 10^{-11}\,lbf$$

$Fs := 0 \cdot lbf$ (protected cask lid)

3.F.12.3.3 Bolt Bending Moment

The bolt bending moment can be determined as:

$$Mbb\_c := \left(\frac{\pi \cdot Dlb}{Nb}\right) \cdot \left(\frac{Kb}{Kb + Kl}\right) \cdot Mf\_c$$

$$Mbb\_c = -25016\,in \cdot lbf$$

$$Mbb := Mbb\_c$$

$Mbb = -25016\,in\cdot lbf$

3.F.12.3.4 Bolt Torsional Moment

The torsional bolt moment is generated only by the preloading operation. No combination is necessary.

3.F.12.4 Evaluation of Bolt Stresses

Per Table 5.1 of Reference 3.F.1, the average and maximum bolt stresses are obtained for comparison to the acceptance criteria.

The average tensile stress caused by the bolt tensile force FA, $Sba := 1.2732 \cdot \frac{FA}{Dba^2}$

$Sba = 64147\,psi$

The average shear stress caused by the bolt shear force Fs, $Sbs := 1.2732 \cdot \frac{Fs}{Dbs^2}$

$Sbs = 0\,psi$

The maximum bending stress caused by the bolt bending moment Mb, $Sbb := 10.186 \cdot \frac{Mbb}{Dbb^3}$

$Sbb = -75018\,psi$

The maximum shear stress caused by the bolt torsional moment Mt, $Sbt := 5.093 \cdot \frac{Mtr}{Dbt^3}$

$Sbt = 20242\,psi$

3.F.12.5 Comparison with Acceptance Criteria: Accident Conditions, Maximum Stress Analysis

the comparison with acceptance criteria is performed as per Table 6.3 of Reference 3.F.1.

Compute $0.7 \cdot Su = 119420\,psi$

$Sy2 = 1.383 \times 10^5\,psi$

The average tensile stress (must be < the smaller of 0.7Su and Sy2), $Sba = 64147\,psi$

Compute $0.42 \cdot Su = 71652\,psi$

$0.6 \cdot Sy2 = 82980\,psi$

The average shear stress (must be < the smaller of 0.42Su and 0.6Sy), $Sbs = 0\,psi$

For combined tensile and shear stress, the sum of the squares of the stress-to-allowable ratios (R_t and R_s) must be less than 1.0.

The tensile stress-to-allowable ratio, $R_t := \frac{Sba}{0.7 \cdot Su \cdot (0.7 \cdot Su \le Sy2) + Sy2 \cdot (Sy2 \le 0.7 \cdot Su)}$ $R_t = 0.537$

The shear stress-to-allowable ratio, $R_s := \frac{Sbs}{0.42 \cdot Su \cdot (0.42 \cdot Su \le 0.6 \cdot Sy2) + 0.6 \cdot Sy2 \cdot (0.6 \cdot Sy2 \le 0.42 \cdot Su)}$

The sum of the squares of the ratios (must be < 1.0), $R_t^2 + R_s^2 = 0.289$

3.F.12.6 Conclusion

For the second loading combination, allowable stress limits are not exceeded.

3.F.13 Critical Combined Load Case 3

Accident condition maximum stress analysis: Preload + pressure + temperature + impact

The preload, pressure, and temperature individual loadings in this combined load case are the same as in the two previous load cases. Therefore, only the impact load parameters must be defined for this load combination.

3.F.13.1 Identification and Evaluation of Impact Load Parameters

Impact load parameters are defined in Table 4.5 of Reference 3.F.1. Impact decelerations have been accurately computed elsewhere using a dynamic analysis. Nevertheless, an additional dynamic load factor is applied for conservatism in the results.

The applied dynamic load factor, $DLF := 1.05$

Impact angle between the cask axis and the target surface, $xi := 80 \cdot deg$

Maximum rigid-body impact acceleration (g) of the cask, $ai := 60 \cdot g$

We conservatively assume that if an impact limiter is in place, it will provide a reacting load at a location r_p, relative to the pivot point assumed in [3.F.1]. The distance from the pivot point to the center of pressure on an impact limiter r_p must therefore be specified. The following formula is used to ensure, for any given case, that r_p is underestimated.

$$r_p := \left(\frac{Dlo}{2}\right) \cdot \sin(xi)^8$$

$r_p = 34.228\,in$

For conservatism, this offset is neglected since it will reduce the tensile load in the bolts.

$$r_p := 0 \cdot in$$

3.F.13.3 Determination of Bolt Forces and Moments of Individual Loadings

The fourth and final individual loading in this load combination is the impact load. The forces and moments generated by this load are determined (per Reference 3.F.1, Table 4.5) as:

The non-prying force per bolt, $Fa_4 := \frac{1.34 \cdot \sin(xi) \cdot DLF \cdot ai \cdot (Wl + Wc)}{Nb} \cdot \frac{\frac{Dlo}{2} - r_p}{\left(\frac{Dlb}{2}\right)}$

$$Fa_4 = 156178\,lbf$$

This formula has been modified by addition of the correct location of the load from the impact limiter (non zero r_p), although for storage, r_p is zero.

The shear bolt force per bolt, $Fs_4 := \frac{\cos(xi) \cdot ai \cdot Wl}{Nb}$

$$Fs_4 = 1544\,lbf$$

The fixed-edge closure lid force, $Ff_4 := \frac{1.34 \cdot \sin(xi) \cdot DLF \cdot ai \cdot (Wl + Wc)}{\pi \cdot Dlb}$

$$Ff_4 = 34695 \frac{lbf}{in}$$

The fixed-edge closure lid moment, $Mf_4 := \frac{1.34 \cdot \sin(xi) \cdot DLF \cdot ai \cdot (Wl + Wc)}{8 \cdot \pi} \cdot \left[1 - \left(\frac{d_l}{Dlb}\right)^2\right]$

$$Mf_4 = 162740 \frac{in \cdot lbf}{in}$$

The above formula has been modified to reflect the physical fact that in the HI-STAR 100 system the MPC transfers load to the overpack closure plate only around the periphery, because of the recess at the center of the closure plate. Therefore, the formula for a fixed edge plate with a pressure load applied only around the surface greater than $r=d_l/2$ has been used.

3.F.13.4 Determination of Combined Bolt Forces and Combined Bolt Moments

3.F.13.4.1 Bolt Tensile Force

First, combine the non-prying bolt tensile forces.

The total preload and temperature load, $Fa\_pt := Fa_1 + Fa_3$

$$Fa\_pt = 113847\,lbf$$

The sum of the remaining loads (pressure and impact), $Fa\_al := Fa_2 + Fa_4$

$$Fa\_al = 162531\,lbf$$

The combined non-prying tensile bolt force, $Fa\_c := Fa\_al \cdot (Fa\_al > Fa\_pt) + Fa\_pt \cdot (Fa\_pt > Fa\_al)$

$$Fa\_c = 162531\,lbf$$

If Fa_c is negative, set it equal to zero: $Fa\_c := Fa\_c \cdot (Fa\_c > 0 \cdot lbf)$

$$Fa\_c = 162531\,lbf$$

Next, combine the prying bolt tensile forces.

The sum of the fixed-edge forces, $Ff\_c := Ff_1 + Ff_2 + Ff_3 + Ff_4$

$$Ff\_c = 36289\,\frac{lbf}{in}$$

The sum of the fixed-edge moments, $Mf\_c := Mf_1 + Mf_2 + Mf_3 + Mf_4$

$$Mf\_c = 173811\,\frac{in \cdot lbf}{in}$$

Define the appropriate prying force moment arm depending on the direction of Mf_c.

$$Arm := (Dlo - Dlb) \cdot (Mf\_c > 0 \cdot lbf) + (Dlb - Dli) \cdot (Mf\_c < 0 \cdot lbf)$$

$$Arm = 2.625\,in$$

Determine the prying bolt tensile force for the combined loading.

The non-prying tensile bolt force, $B := Ff\_c \cdot (Ff\_c > P) + P \cdot (P > Ff\_c)$

$$B = 3.629 \times 10^4\,\frac{lbf}{in}$$

The additional tensile force per bolt caused by prying action of the closure lid can be determined as:

The constants C_1 and C_2 are: $C_1 := 1$

$$C_2 := \left[\frac{8}{3 \cdot (Arm)^2}\right] \cdot \left[\frac{Elf \cdot tl^3}{1 - NUl} + \frac{(Dlo - Dli) \cdot Elf \cdot tlf^3}{Dlb}\right] \cdot \left(\frac{Lb}{Nb \cdot Db^2 \cdot Eb}\right)$$

$$C_2 = 3.347$$

The additional tensile force per bolt caused by prying action of the closure lid, $Fap := \left(\frac{\pi \cdot Dlb}{Nb}\right) \cdot \left[\frac{\frac{2 \cdot Mf\_c}{Arm} - C_1 \cdot (B - Ff\_c) - C_2 \cdot (B - P)}{C_1 + C_2}\right]$

$$Fap = 98627\,lbf$$

If the prying bolt force is negative, set it equal to zero: $Fab\_c := Fap \cdot (Fap > 0 \cdot lbf) + 0 \cdot lbf \cdot (Fap < 0 \cdot lbf)$

$$Fab\_c = 98627\,lbf$$

For a raised face flange outboard of the bolt circle, no prying force can be developed.

$$Fab\_c := 0 \cdot lbf$$

The total tensile bolt force for stress analysis, $FA := Fa\_c + Fab\_c$

$$FA = 162531\,lbf$$

3.F.13.4.2 Bolt Shear Force

The sum of the shear forces, $Fs\_c := Fs_1 + Fs_2 + Fs_3 + Fs_4$

$$Fs\_c = 1544\,lbf$$

$Fs := 0 \cdot lbf$ (protected cask lid)

3.F.13.4.3 Bolt Bending Moment

The bolt bending moment can now be determined as:

$$Mbb\_c := \left(\frac{\pi \cdot Dlb}{Nb}\right) \cdot \left(\frac{Kb}{Kb + Kl}\right) \cdot Mf\_c$$

$$Mbb\_c = 21079\,in \cdot lbf$$

$$Mbb := Mbb\_c$$

$$Mbb = 21079\,in \cdot lbf$$

3.F.13.4.4 Bolt Torsional Moment

The torsional bolt moment is generated only by the preloading operation. No combination is necessary.

3.F.13.5 Evaluation of Bolt Stresses

Per Table 5.1 of Reference 3.F.1, obtain the average and maximum bolt stresses for comparison to the acceptance criteria.

The average tensile stress caused by the bolt tensile force FA, $Sba := 1.2732 \cdot \frac{FA}{Dba^2}$

$Sba = 91578\,psi$

The average shear stress caused by the bolt shear force Fs, $Sbs := 1.2732 \cdot \frac{Fs}{Dbs^2}$

$Sbs = 0\,psi$

The maximum bending stress caused by the bolt bending moment Mb, $Sbb := 10.186 \cdot \frac{Mbb}{Dbb^3}$

$Sbb = 63211\,psi$

The maximum shear stress caused by the bolt torsional moment Mt, $Sbt := 5.093 \cdot \frac{Mtr}{Dbt^3}$

$Sbt = 20242\,psi$

3.F.13.5 Comparison with Acceptance Criteria: Accident Conditions, Maximum Stress Analysis

The comparison with acceptance criteria is performed as per Table 6.3 of Reference 3.F.1.

$0.7 \cdot Su = 119420\,psi$

$Sy2 = 1.383 \times 10^5\,psi$

The average tensile stress (must be <0.7Su and Sy2), $Sba = 91578\,psi$

$0.42 \cdot Su = 71652\,psi$

$0.6 \cdot Sy2 = 82980\,psi$

The average shear stress (must be < 0.42Su and 0.6Sy), $Sbs = 0\,psi$

For combined tensile and shear stress, the sum of the squares of the stress-to-allowable ratios (R_t and R_s) must be less than 1.0.

The tensile stress-to-allowable ratio, $R_t := \frac{Sba}{0.7 \cdot Su \cdot (0.7 \cdot Su \le Sy2) + Sy2 \cdot (Sy2 \le 0.7 \cdot Su)}$ $R_t = 0.767$

The shear stress-to-allowable ratio, $R_s := \frac{Sbs}{0.42 \cdot Su \cdot (0.42 \cdot Su \le 0.6 \cdot Sy2) + 0.6 \cdot Sy2 \cdot (0.6 \cdot Sy2 \le 0.42 \cdot Su)}$

The sum of the squares of the ratios (must be < 1.0), $R_t^2 + R_s^2 = 0.588$

3.F.13.6 Conclusion

For the third loading combination, allowable stress limits are not exceeded.

3.F.14 Bolt Analysis Conclusion

Using the standard method presented in Reference 3.F.1, the above analysis demonstrates that stresses closure bolts for the HI-STAR 100 Overpack will not exceed allowable limits.

APPENDIX 3.G - MISSILE PENETRATION ANALYSES

3.G.1 Introduction

In this appendix, deformations and stresses in the HI-STAR 100 Overpack due to two missile strikes are investigated. The objective of the analysis is to show that deformations in the HI-STAR 100 system due to the missile strike events do not compromise the containment boundary of the system, and that global stresses that arise from the missile strikes do not exceed the appropriate limits.

The two missiles considered are a 1-in. diameter steel sphere and an 8-in. diameter rigid cylinder, both traveling at 126 miles per hour. The two missile impacts are separate events. No metal thinner than 0.25-in. is exposed to impact.

3.G.2 References

[3.G.1] Young, Warren C., Roark's Formulas for Stress and Strain, 6th Edition, McGraw-Hill,1989.

[3.G.2] Rothbart, H., Mechanical Design and Systems Handbook, 2nd Edition, McGraw Hill, 1985.

[3.G.3] Working Model, v.3.0, Knowledge Revolution, 1995.

3.G.3 Composition

This appendix was created using the Mathcad (version 6.0+) software package. Mathcad uses the symbol ':=' as an assignment operator, and the equals symbol '=' retrieves values for constants or variables. Mathcad's built-in equation solver is also used.

3.G.4 General Assumptions

General assumptions that apply to all analyses in this appendix are stated here. Further assumptions are stated in the subsequent text.

1. Formulae taken from Reference 3.G.1 are based on assumptions that are delineated in that reference.

2. The missiles are assumed to strike the cask at the most vulnerable location, in a manner that imparts the largest amount of energy to the cask surface.

3. In missile strikes on the side of the overpack, no structural resistance is offered by the neutron absorber material.

4. All material property data are specified at the design temperature of the particular component. For components with multiple materials (i.e. the overpack), the properties for the material with the lowest strength are used.

3.G.5 1-in. Diameter Steel Sphere Impact

3.G.5.1 Method

The first step in the 1-in. diameter sphere missile impact analysis is an investigation of the elastic behavior of the cask component being impacted. By balancing the kinetic energy of the missile with the work done deforming the impacted surface, it is shown that the missile's energy will not be entirely absorbed by elastic deformation. Therefore, the small missile will dent the cask. The elastic impact of the sphere is treated as a contact problem. The geometry is shown in Figure 3.G.1.

Following the elastic investigation of the impact, a plastic analysis is performed to determine the depth of the dent.

3.G.5.2 Elastic Analysis

The input data is specified as follows:

The diameter of the sphere (from Table 2.2.5), $D := 1 \cdot in$

The mass of the sphere (from Table 2.2.5) $M := 0.22 \cdot kg \cdot 2.204 \cdot \frac{lb}{kg}$

The velocity of sphere before impact (from Table 2.2.5), $V_0 := 126 \cdot mph$

The density of steel (from Section 3.3), $\rho := 0.283 \cdot \frac{lbf}{in^3}$

The modulus of elasticity of the material (from Table 3.3.4), $E := 26.1 \cdot 10^6 \cdot psi$

The Poisson's ratio of steel (from Section 3.3), $\nu := 0.3$

The yield stress of the material (from Table 3.3.4), $S_y := 32600 \cdot psi$

In the 1-in. diameter sphere impact problem, the final velocity at which elastic deformation ends is assumed. This velocity is assumed to be 99.96% of the pre-impact velocity of the missile. Thus, the velocity at which the average surface stress reaches the yield stress of the material (V_f) is:

$$V_f := 125.95 \cdot mph$$

Using Table 33, case 1 (p. 650) of reference 3.G.1 for a sphere penetrating a flat plate, the spring constant K_2 relating the contact load to the local target deformation (raised to the power 1.5) is defined as:

$$K_2 := \left(\frac{E^2 \cdot D}{1.55^3}\right)^{0.5}$$

Balancing the kinetic energy with the work done deforming the bodies, we obtain the relation:

$$\frac{1}{2} \cdot M(dV)^2 := Fdx$$

where:

$$F := K_2 \cdot x^{\frac{3}{2}}$$

and x is the depth of penetration.

Integrating and applying the condition that x = 0 at time t = 0 gives:

$$\frac{M}{2} \cdot \left(V^2 - V_o^2\right) := \frac{2}{5} \cdot K_2 \cdot x^{2.5}$$

Solving this equation for x, the depth of penetration $x := \left[\frac{M \cdot \left(V_0^2 - V_f^2\right)}{0.4 \cdot K_2}\right]^{0.4}$

and the peak impact force $F := K_2 \cdot x^{1.5}$ Thus, the depth of penetration $x = 0.003\,\text{in}$

and the peak impact force $F = 2112.312\,\text{lbf}$

The surface area of the cask/missile contact patch is determined as:

$$\text{Area} := \pi \cdot \left(D \cdot x - x^2\right) \qquad \text{Area} = 0.009\,\text{in}^2$$

and the average pressure on the patch to elastically support the load is approximately given as:

$$p_{avg} := \frac{F}{\text{Area}}$$

$$p_{avg} = 232519\,\text{psi}$$

This average pressure is greater than the yield stress of the impacted material. Therefore, the
impact produces an inelastic deformation at the missile/cask contact location and local yielding occurs almost immediately after impact. From this conclusion, the change in kinetic energy of the missile is assumed to be entirely absorbed by plastic deformation.

3.G.5.3 Plastic Analysis

Disregarding the small amount of energy absorbed in elastic deformation, the kinetic energy of the missile is entirely balanced by the plastic work done in forming a spherically shaped dent in the surface. Perfectly plastic behavior of the impacted material is assumed. The kinetic energy of the missile just before impact is determined as:

$$KE := \frac{1}{2}\cdot M\cdot V_0^{\,2}$$

$$KE = 257.338\,ft\cdot lbf$$

Using Mathcad's built-in solver, determination of the depth of penetration begins with an estimate:

Assume $d := 0.18\cdot in$

Given $$KE = S_y\cdot\pi\cdot\left(D\cdot\frac{d^2}{2}-\frac{d^3}{3}\right)$$

where the right hand side is the plastic work. The final deformation is characterized by the depth (d1) of the spherical dent in the cask surface, which is obtained as the value d (which solves the energy balance equation):

$$d1 := Find(d) \qquad d1 = 0.271\,in$$

Note that the solution to the equation, d1, that is obtained by using the "Find(d)" command, can be checked by direct substitution of d1 for d in the equation. The maximum load, assuming that a constant stress is maintained until all of the impact energy is absorbed, is therefore:

$$P_{max} := S_y\cdot\pi\cdot\left(D\cdot d1 - d1^2\right)$$

$$P_{max} = 20249\,lbf$$

3.G.5.4 Conclusion: 1-in. Diameter Sphere Missile Impact

The 0.271 in. depth of penetration of the small missile, which is required to absorb all of the impact energy, is less than the thinnest section of material on the exterior surface of the cask. Therefore, the small missile will dent, but not penetrate, the cask. Global stresses in the overpack that arise from the 1-in. missile strike are assumed to be negligible.

3.G.6 Impact of an 8-in. Diameter Rigid Cylinder

3.G.6.1 Method

An 8-in. diameter cylindrical missile is postulated to impact the cask at the most vulnerable location, as shown in Figure 3.G.2.

Assuming the impacted material yields at the surface and then gross deformation occurs, the maximum force that can develop is the limit stress of the target material multiplied by the impact area. This limit stress is assumed to be the impacted material's "flow" stress, which is assumed to be the average of yield and ultimate strength.

This force is of sufficient magnitude to cause local denting of the immediate surface under the contact patch, and form a conical shaped region of gross deformation away from the contact patch. The large impact force occurs only for a short instant of time and will not cause a cask instability. The post-impact deformed shape is shown in Figure 3.G.3. The deformation is exaggerated for clarity.

The cylindrical punch may impact any exposed surface of the cask. The following three impact locations are investigated:

a. Impact on outer overpack shell (no support from underlying neutron absorber is assumed),
b. Impact on overpack closure plate, and
c. Impact on the outside of the 8.5" overpack wall. For this strike location, the neutron absorber and outer shell are conservatively assumed not to slow the missile.

Penetration is examined by balancing the kinetic energy of the missile with the work required to punch out a slug of the target material.

Finally, global stresses in the overpack due to the 8-in. cylindrical missile impact are considered. Two impact locations are investigated, a side strike and an end strike.

3.G.6.2 Determination of Input Kinetic Energy and Applied Impact Force

The input data are specified as follows:

The diameter of the missile (from Table 2.2.5), $D := 8 \cdot in$

The weight of the missile (125 kg, from Table 2.2.5), $Weight := 125 \cdot kg \cdot 2.204 \cdot \frac{lb}{kg} \cdot g$

The velocity of the missile before impact (from Table 2.2.5), $V_0 := 126 \cdot mph$

The yield stress of the material at 400°F (from Table 3.3.4), $S_y := 32200 \cdot psi$

The ultimate stress of the material at 400°F (from Table 3.3.4), $S_u := 64600 \cdot psi$

The design stress intensity of the material at 400°F (from Table 3.3.4), $S_m := 21500 \cdot psi$

The flow stress is defined as the average of the yield stress and the ultimate stress.
The flow stress (S_{flow}) is therefore determined as:

$$S_{flow} := 0.5 \cdot (S_u + S_y)$$

$$S_{flow} = 48400\,psi$$

The force required to reach the flow stress of the material is determined by multiplying the flow stress by the impact area of the missile as:

$$Force := S_{flow} \cdot \pi \cdot \frac{D^2}{4}$$

$$Force = 2.433 \times 10^6\,lbf$$

3.G.6.3 Local Penetration

Local penetration is examined by requiring that the impact force developed be balanced by only the resistance force developed in shear along the side area of a plug that would be punched out from an otherwise rigid material. That is, a "shear plug" type failure mechanism is assumed. Figure 3.G.5 shows this type of failure pictorially. The failure mode is based on achievement of the ultimate stress in shear. The following three impact locations are examined:

a. Penetration of the overpack outer shell,
b. Penetration of the overpack inner shell plus five intermediate shells, and
c. Penetration of the overpack closure plate.

a. Penetration of the overpack outer shell:

The thickness of overpack outer shell, $t := 0.5 \cdot in$

The ultimate stress of the overpack outer shell (from Table 3.3.3), $S_u := 70000 \cdot psi$

Given $\pi \cdot D \cdot t \cdot \left(\frac{S_u}{2}\right) = Force$ the maximum depth of penetration can be determined.

$$h := Find(t)$$

$$h = 2.766\,in$$

Because the maximum depth of penetration (h) is greater than the shell thickness (t), the outer shell is penetrated if no resistance from the the neutron absorber is considered.

b. Penetration of overpack inner shell plus five intermediate shells:

The overpack outer shell and neutron absorber are assumed to offer no resistance to penetration.

The total thickness of the section (from BM-1476), $t := 8.5 \cdot in$

The ultimate stress of the section at 400°F (from Table 3.3.4), $S_u := 68800 \cdot psi$

The applied force (Force) is a known value. Therefore, the maximum penetration can be determined as:

$$\text{Given} \quad \pi \cdot D \cdot t \cdot \left(\frac{S_u}{2}\right) = \text{Force} \qquad h := \text{Find}(t) \qquad h = 2.814\,in$$

Because the depth of penetration (h) is less than the total section thickness, the overpack inner shell is not penetrated.

c. Penetration of closure plate:

The closure plate thickness (from BM-1476), $t := 6 \cdot in$

The ultimate stress of closure plate (from Table 3.3.4), $S_u := 64600 \cdot psi$

The applied force (Force) is a known value. Therefore, the maximum penetration can be determined as:

$$\text{Given} \quad \pi \cdot D \cdot t \cdot \left(\frac{S_u}{2}\right) = \text{Force} \qquad h := \text{Find}(t) \qquad h = 2.997\,in$$

Because the depth of penetration (h) is less than the closure plate thickness, the closure plate is not penetrated.

The results of the investigation of penetration at these three locations demonstrate that the HI- STAR 100 Overpack adequately protects the MPC from a direct missile strike. The following section demonstrates that the global stresses in the overpack remain below allowable limits in the missile strike event.

3.G.6.4 Stresses in the Overpack Due to 8-in. Diameter Missile Strike

Global stresses in the overpack due to missile strikes at two locations are examined in this subsection. The first location is a side strike at the level of the cask center of gravity (approximately 100 inches from the bottom of the baseplate), where the entire force is supported by the overpack inner shell acting as a simply supported beam (see Figure 3.G.4). The actual overpack wall consists of metal that is a minimum of 8.5 inches in thickness, but this analysis conservatively considers only the inner 2.5 inches.

The second location is an end strike at the center of the overpack closure plate.

a. First Location: Side Strike on Overpack

The length of the inner shell (assumed equal to the full cavity length), $L := 191.125 \cdot in$

The inside diameter of the overpack (from Drawing 1397), $ID := 68.75 \cdot in$

The thickness of the inner shell (from BM-1476), $t := 2.5 \cdot in$

The applied force, $Force = 2.433 \times 10^6 lbf$

We have previously shown that the missile will not penetrate through all of the intermediate shells. Therefore, in the computation of the global stress state induced by the missile strike, we include in the moment of inertia calculation of the overpack shells, the inner shell and the four intermediate shells that are welded to the baseplate.

The thickness of the intermediate shell (from BM-1476) is $t_i := 1.25 \cdot in$

The outer diameter of the inner shell (D), and subsequently the area moment of inertia (I), are determined as:

$$D := 2 \cdot t + ID \qquad D_{inner} := D$$

Then the metal moment of inertia is computed as follows:

$$I := \frac{1}{4} \cdot \pi \cdot \left[\left(\frac{D}{2} \right)^4 - \left(\frac{D}{2} - t \right)^4 \right]$$

$$I = 3.555 \times 10^5 in^4$$

The outer diameter of the innermost intermediate shell (Di), and subsequently the area moment of inertia (Ii), are determined as:

$$D := 2 \cdot t_i + D \qquad D = 76.25\,in$$

Then the metal moment of inertia is computed as follows:

$$Ii := \frac{1}{4} \cdot \pi \cdot \left[\left(\frac{D}{2} \right)^4 - \left(\frac{D}{2} - t_i \right)^4 \right]$$

$$Ii = 2.071 \times 10^5 in^4$$

The total area moment of inertia is obtained by summing the results from the two cylinders.

$$I := I + Ii \qquad I = 5.627 \times 10^5 \, in^4$$

The outer diameter of the next intermediate shell (Di), and subsequently the area moment of inertia (Ii), are determined as:

$$D := 2 \cdot t_i + D \qquad D = 78.75 \, in$$

Then the metal moment of inertia is computed as follows:

$$Ii := \frac{1}{4} \cdot \pi \cdot \left[\left(\frac{D}{2} \right)^4 - \left(\frac{D}{2} - t_i \right)^4 \right]$$

$$Ii = 2.286 \times 10^5 \, in^4$$

The total area moment of inertia is obtained by summing the results from the three cylinders.

$$I := I + Ii \qquad I = 7.912 \times 10^5 \, in^4$$

The outer diameter of the next intermediate shell (Di), and subsequently the area moment of inertia (Ii), are determined as:

$$D := 2 \cdot t_i + D \qquad D = 81.25 \, in$$

Then the metal moment of inertia is computed as follows:

$$Ii := \frac{1}{4} \cdot \pi \cdot \left[\left(\frac{D}{2} \right)^4 - \left(\frac{D}{2} - t_i \right)^4 \right]$$

$$Ii = 2.514 \times 10^5 \, in^4$$

The total area moment of inertia is obtained by summing the results from the four cylinders.

$$I := I + Ii \qquad I = 1.043 \times 10^6 \, in^4$$

The outer diameter of the final intermediate shell (Di), and subsequently the area moment of inertia (Ii), are determined as:

$$D := 2 \cdot t_i + D \qquad D = 83.75\,in \qquad D_{outer} := D$$

Then the metal moment of inertia is computed as follows:

$$Ii := \frac{1}{4} \cdot \pi \cdot \left[\left(\frac{D}{2} \right)^4 - \left(\frac{D}{2} - t_i \right)^4 \right]$$

$$Ii = 2.757 \times 10^5\,in^4$$

The total area moment of inertia is obtained by summing the results from the five cylinders.

$$I := I + Ii \qquad I = 1.318 \times 10^6\,in^4$$

We assume the missile strike is at height L above the base of the shells. Then, assuming that the shells behave as a cantilever beam, the bending moment at the base is

$$Moment := Force \cdot L$$

The resultant stress in the inner shell can then be determined as:

$$Stress := Moment \cdot \frac{D_{inner} - t}{2 \cdot I} \qquad Stress = 12565\,psi$$

The allowable strength for this Level D condition is obtained by using the membrane stress intensity for SA203 at 400 degrees F from Table 3.1.7,

$$S_a := 48200 \cdot psi$$

Therefore the safety factor for the membrane stress in the helium retention boundary inner shell is

$$SF := \frac{S_a}{Stress} \qquad SF = 3.836$$

This is conservative since the load will spread out into a pressure band at the smaller radius after the strike at the outside perimeter.

The resultant stress in the outermost intermediate shell can then be determined as:

$$\text{Stress} := \text{Moment} \cdot \frac{D_{outer} - t}{2 \cdot I} \qquad \text{Stress} = 14329\,\text{psi}$$

The allowable strength for this Level D condition is obtained by using the membrane stress intensity for SA516 Grade 70 at 400 degrees F from Table 3.1.17,

$$S_a := 39100 \cdot \text{psi}$$

Therefore the safety factor for the membrane stress in the helium retention boundary inner shell is

$$SF := \frac{S_a}{\text{Stress}} \qquad SF = 2.729$$

This is conservative since the load will spread out into a pressure band at the smaller radius after the strike at the outside perimeter.

b. Second Location: End Strike on Overpack Closure Plate

The effect of a normal missile impact has been studied in Appendix 3.F where a conservative methodology used for shipping cask puncture has been applied assuming that the so called "puncture pin" is replaced by the "impacting missile". It is shown that the bolt stress remains within the required margins. For the analysis of the bolt stress, it is conservatively assumed that the closure plate develops a full clamping moment inboard of the bolt circle. Continuing with this conservatism, the stress at the edge of the outer closure plate section is determined using the conservative estimate of maximum impact force developed above. Stresses at the bolt circle can be determined using the calculated limiting impact load as a uniform pressure applied over an 8" circle at the center of the overpack closure plate. Assuming that the closure plate has a fixed edge at the bolt circle, and using case 17 from Reference [3.G.1] (Table 24, p.433), the stress at the bolt circle is determined as follows:

The closure plate thickness (from BM-1476), $t := 6 \cdot \text{in}$

The applied moment, $M_r := \frac{\text{Force}}{4 \cdot \pi}$

The radial stress at bolt circle (from [3.G.1], p.398), $\sigma_r := 6 \cdot \frac{M_r}{t^2}$

The closure plate thickness is reduced inboard of the bolt circle; bending stress will increase here if the section is assumed clamped. However, this would not be classified as a primary bending stress. The stress intensity in the closure plate under an impact load is required to be less than 3.6 times the material design stress intensity (S_m, from Table 3.3.4) and less than the material ultimate stress.

$$S_m := 21500 \cdot psi$$

$$3.6 \cdot S_m = 77400\,psi$$

$$S_u = 64600\,psi$$

$$\frac{3.6 \cdot S_m}{\sigma_r} = 2.399 \qquad \frac{S_u}{\sigma_r} = 2.002$$

These results indicate that the bolt stress and the minimum plate primary bending stress near the bolt circle remain below allowable strength values for the Level D impact condition investigated.

The stress state near the center of the closure plate is investigated by performing a dynamic analysis to ascertain the maximum load applied to the closure plate as it undergoes a global mode of deflection. It is assumed that the plate deforms like a simply supported plate for this analysis. The initial striking velocity and the striking weight of the missile is known. It is determined from [3.G.2], p.5-55, that 50% of the plate weight acts during the subsequent deformation. It remains to establish an appropriate spring constant to represent the plate elastic behavior in order to establish all of the necessary input for solving the dynamic problem representing the post-strike behavior of the plate-missile system. To determine the spring rate, apply Case 16 of Table 24 in [3.G.1] which is the static solution for a circular plate, simply supported at the edge, and subject to a load applied over a small circular region. Using the notation of [3.G.1] for the case in question, and assuming deformation only inboard of the top flange:

The diameter of contact (from Drawing 1397), $d_{con} := 8 \cdot in$

The radius of simple support (from Drawing 1397), $a := \frac{72 \cdot in}{2}$ $a = 36\,in$

The minimum closure plate thickness (from Drawing 1397), $h := 5.9375 \cdot in$

The plate stiffness, $D := \frac{E \cdot h^3}{12 \cdot \left(1 - \nu^2\right)}$ $D = 5.003 \times 10^8\,lbf \cdot in$

The global stiffness of the plate (K) is simply the total load divided by the corresponding displacement at the plate center:

$$K := \frac{16 \cdot \pi \cdot D \cdot (1 + \nu)}{(3 + \nu) \cdot a^2}$$

$$K = 7.644 \times 10^6 \frac{lbf}{in}$$

To establish the appropriate structural damping value, a post-impact natural frequency is determined as follows:

The weight of the closure plate (7,984 lbf, from Table 3.3.3) that participates in the analysis,

$$W_{clp} := 0.5 \cdot 7984 \cdot lbf \qquad W_{clp} = 3992\,lbf$$

Using the appropriate expression from [3.G.2], the natural frequency can be determined as:

$$f := \frac{1}{2 \cdot \pi} \cdot \sqrt{K \cdot \frac{g}{(Weight + W_{clp})}}$$

$$f = 132.354\,Hz$$

It is conservatively assumed that 4% structural damping is conservative for an impact scenario.

$$c := \left(\frac{.04}{\pi \cdot f}\right) \cdot K$$

$$c = 735.352\,lbf \cdot \frac{sec}{in}$$

The dynamics problem is solved using the Working Model program [3.G.3], with the impacting missile striking a target mass which is supported by the spring k to ground. The system is constrained to move vertically, and gravitational forces are included in the solution. Figure 3.G.6 shows a schematic of the model and a trace of the total force in the spring-damper element. The maximum force developed, $W := 1212000 \cdot lbf$.

The stress near the center of the closure plate is obtained by computing the bending moment due to W. For Level D conditions, only primary bending stress intensities are required to be compared to the allowable strength value. The stress directly under the loaded region, by the very nature of the form of solution (ln(a/r)), should not be considered as a primary stress. Employing St.Venant's Principle of classical elasticity, the primary stress intensity state is considered to be established at the plate cross section at a radius 150% of the load patch radius. Therefore, the bending moment and the stress are computed at:

$$r := 1.5 \cdot \left(\frac{d_{con}}{2} \right)$$

$$r = 6\,in$$

The tangential moment exceeds the radial moment at this location, so the maximum moment and corresponding stress are:

$$M_t := \frac{W}{16 \cdot \pi} \cdot \left[(1+\nu) \cdot \ln\left(\frac{a}{r} \right) \cdot 4 + (1-\nu) \cdot \left[4 - \left(\frac{d_{con}}{2 \cdot r} \right)^2 \right] \right]$$

$$M_t = 2.847 \times 10^5\,lbf \cdot \frac{in}{in}$$

$$\sigma_t := 6 \cdot \frac{M_t}{h^2} \qquad \sigma_t = 4.845 \times 10^4\,psi$$

This stress represents a stress intensity and when compared with the allowable strength for combined membrane plus bending for a Level D condition, yields a stress ratio of:

$$\frac{S_u}{\sigma_t} = 1.333$$

c. 8" Missile strike at other surface locations

If the 8" missile impacts at other locations, the global stress state will be less than the values computed here. A strike near a bolt location will impart additional compression on the lid surface near the bolt (since the bolt is protected. This additional compressive load cannot unload the seals. A direct strike on any of the small cover plates the protect various quick disconnects will not damage the quick disconnects since the unbacked diameter of the protective cover plate is less than 4"; therefore, all impact load will be directly onto the surrounding lid surface.

3.G.7 Conclusion

The above calculations demonstrate that the HI-STAR 100 Overpack provides an effective containment barrier for the HI-STAR 100 MPC after being subjected to various missile strikes. No missile strike compromises the integrity of the containment boundary; further, global stress intensities arising from the missile strikes satisfy ASME Code Level D allowable strengths away from the immediate vicinity of the loaded region.

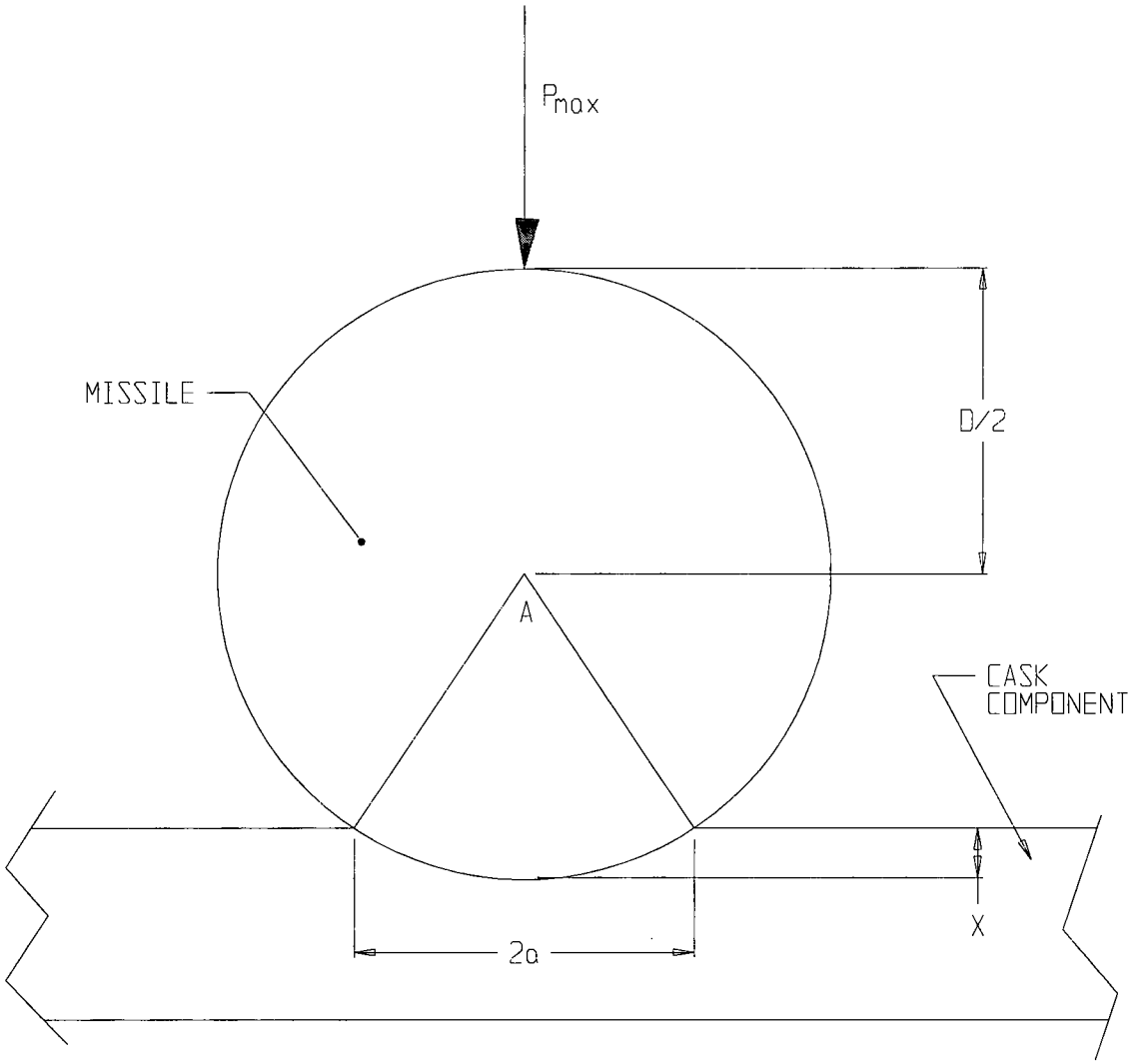

FIGURE 3.G.1; SMALL MISSILE IMPACT

REPORT HI-2012610 REVISION 0

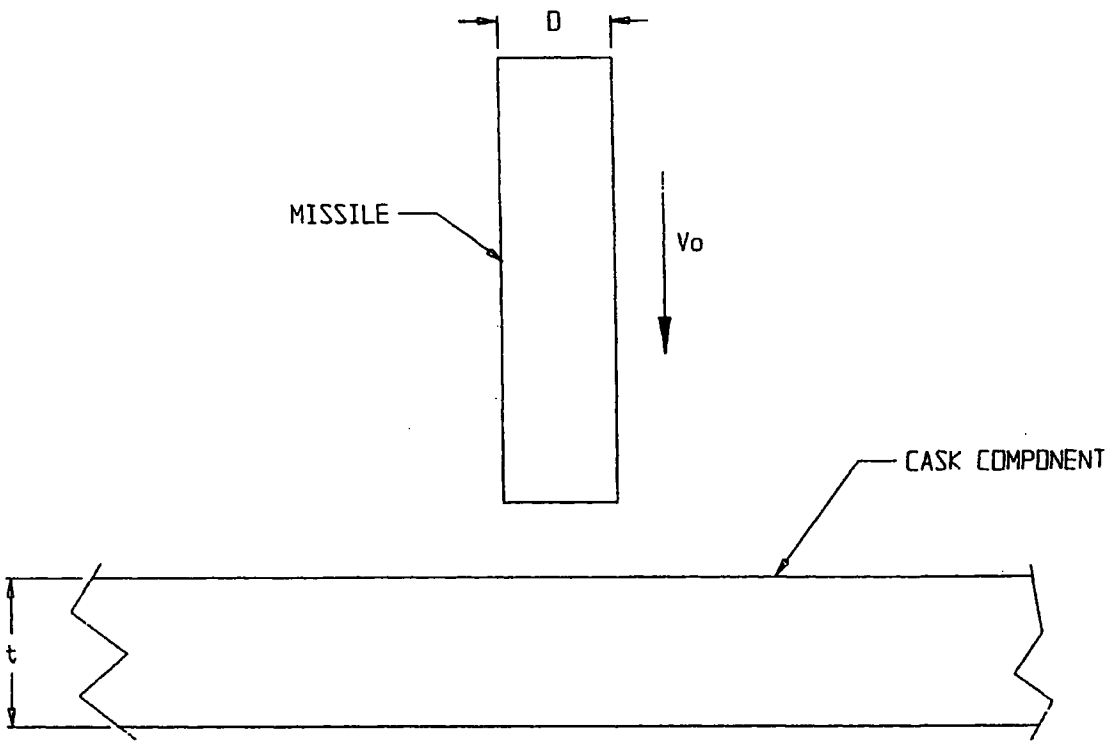

FIGURE 3.G.2; 8-inch DIAMETER MISSILE IMPACT

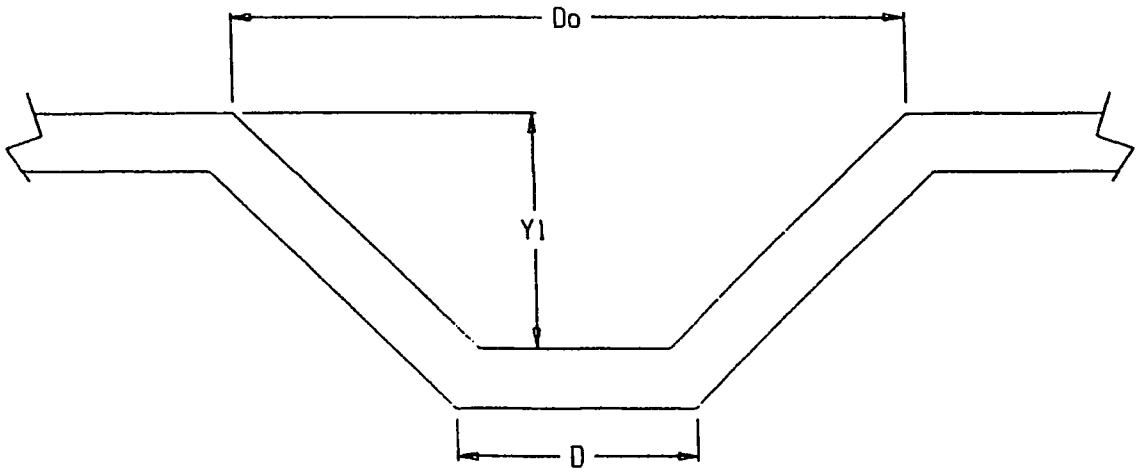

FIGURE 3.G.3; ASSUMED POST-IMPACT DEFORMED SHAPE

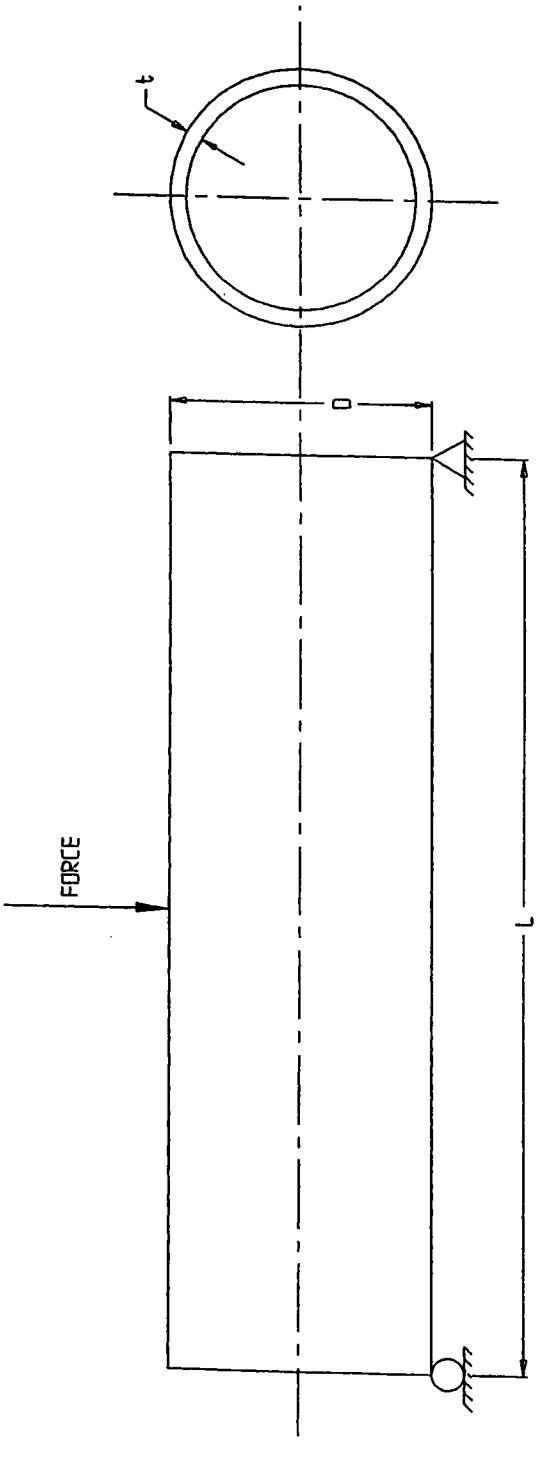

FIGURE 3.G.4; SIDE STRIKE GEOMETRY

REPORT HI-2012610

REVISION 0

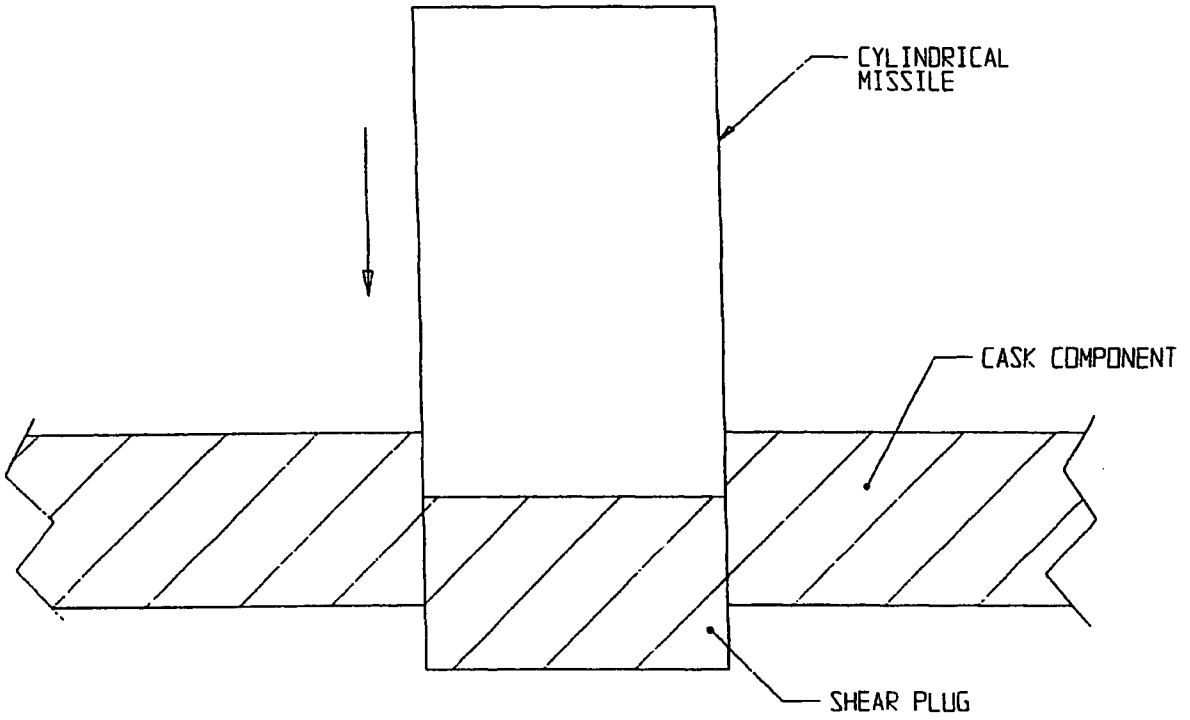

FIGURE 3.G.5; SHEAR PLUG FAILURE

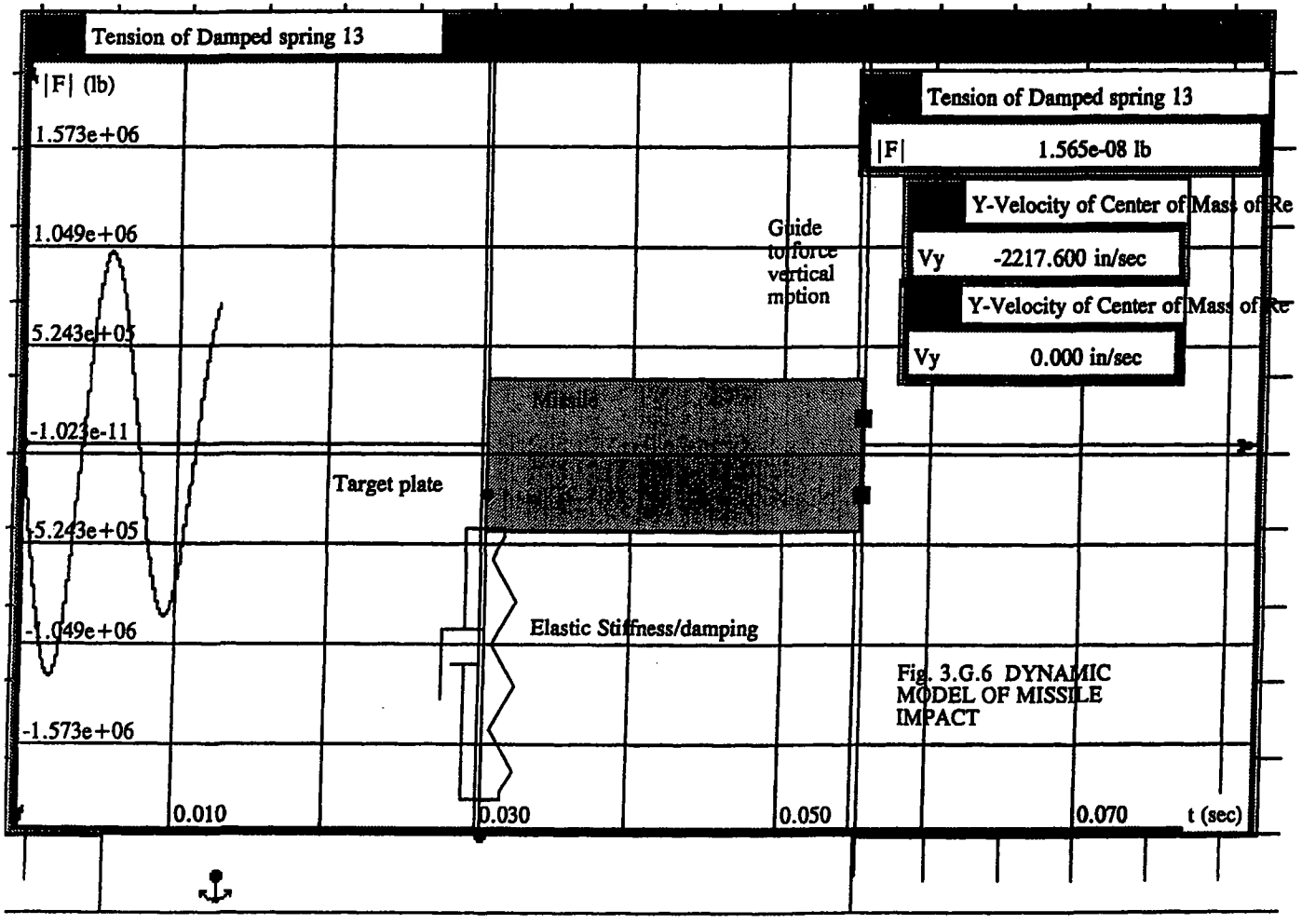

Fig. 3.G.6 DYNAMIC MODEL OF MISSILE IMPACT

FIGURE 3.G.6: DYNAMIC MODEL OF MISSILE IMPACT

APPENDIX 3.H - CODE CASE N-284 STABILITY CALCULATIONS

3.H.1 Scope

The purpose of this analysis is to determine the buckling capacity of the HI-STAR 100 System under the load combinations specified in Section 3. It is shown that both the overpack and the MPC meet the buckling requirements of USNRC Regulatory Guide 7.6 (C.5).

The most probable locations of failure due to buckling are the overpack inner shell, and the the MPC confinement shell. In this appendix, the stability of each shell is evaluated using the criteria set forth in ASME Code Case N-284, Metal Containment Shell Buckling Design Methods, Section III, Division 1, Class MC. In addition to axial loading, the Overpack is subject to a compressive circumferential stress due to external pressure and fabrication. The MPC confinement shell is also subject to a compressive circumferential stress due to a defined external pressure (although the net pressure across the shell will always lead to a tensile circumferential stress).

The symbols used in this appendix, where possible, are consistent with those used in ASME Code. Material properties for Alloy X and SA-203-E are taken from Tables in Section 3.

This appendix was created using the Mathcad (version 6.0+) software package. Mathcad uses the symbol ':=' as an assignment operator, and the equals symbol '=' retrieves values for constants or variables. The logical 'if' construction is also used in this appendix. The 'if' statement format is as follows:

...if(expression,true value,false value)

3.H.2 References

[3.H.1] ASME Boiler & Pressure Vessel Code, Code Case N-284, Metal Containment Shell Buckling Design Methods.

[3.H.2] MATHCAD, V7.0, Mathsoft, 1996.

3.H.3 Load Cases Considered

3.H.3.1 Overpack

Case 1 Fabrication Stress + 1.15G End Loading Due to Handling. This is a Level A event.

Case 2 Fabrication Stress + 60G End Drop. This is a Level D event.

Case 3 Fabrication Stress + Deep Submergence. This is a Level D event

3.H.3.2 MPC

Case 4 Design Internal Pressure + 1.15G End Loading Due to Handling. This is a Level A event.

Case 5 Design Internal Pressure + 60G End Drop. This is a Level D event.

Case 6 Accident External Pressure + 1G Dead Load. This is a Level D event.

Case 7 Design External Pressure + 1G Dead Load. This is a Level A event.

3.H.4 Stability of the Overpack Inner Shell

3.H.4.1 Method - ASME Code Case N-284

Code Case N-284 provides guidelines for determining the stability of metal confinement shells. This method applies to shells with radius-to-thickness ratios of up to 1000 and shell thicknesses greater than 0.25 in..

The buckling characteristics of any confinement shell are governed by the longitudinal membrane, circumferential membrane, and in-plane shear stresses which develop under loading. Only these three stress components are considered in the analysis.

The factors of safety against buckling required by the Code are the following

$FS_{LA} := 2.0$ Level A Service Limit

$FS_{LD} := 1.34$ Level D Service Limit

The analysis method provided by Case N-284 for treatment of confinement shells is further outlined below:

1. The stress components which cause buckling are identified, and each is multiplied by the appropriate factor of safety. As a minimum, the amplified longitudinal and circumferential membrane stresses must be less than the material yield stress, and the in-plane shear stress must be less than 60% of the yield stress. Failure to meet this condition requires a redesign of the system.

2. Capacity reduction factors are calculated in order to account for the difference between classical theory and actual predictions of instability stress.

3. The theoretical elastic buckling stresses are calculated. The stresses correspond to the minimum theoretical values for shells with simple support boundary conditions under uniform stress fields.

4. The amplified stress components are compared to the elastic limits of the material. In the event that any stress exceeds the proportional limit, plasticity reduction factors are introduced in order to account for any material nonlinearities.

5. The interaction equations for elastic and inelastic buckling set forth in the Code Case are used to calculate safety factors.

3.H.4.2 Assumptions

1. Under the postulated end drop, the weight of the overpack (minus the weight of the bottom plate) is supported vertically by the 2.5 in. thick inner shell. This assumption conservatively neglects the intermediate shells and enclosure shell as load bearing members.

2. By employing the method of Case N-284, the inner shell is assumed to be simply supported. The welded base of the inner shell more closely represents a clamped boundary. Therefore, elastic buckling stress limits are actually higher.

3. All material properties are choosen at the overpack design temperature (400 deg. F). The Young's modulus and the yield stress decrease with increasing temperature, therefore, the analysis is conservative.

4. Fabrication stresses are included in the calculation. This is very conservative since fabrication stress is secondary in nature (self-limiting). Therefore, these stress components are relieved as the shell begins to buckle.

3.H.4.3 Input Data

The following is a list of input parameters for the overpack inner shell that are common to each case. The dimensions are obtained from the design drawings in Section 1.5.

$R_i := \frac{68.75}{2} \cdot in$ Inner radius of shell

$R_o := \frac{73.75}{2} \cdot in$ Outer radius of shell

$L := 173.625 \cdot in$ Axial length of shell (conservative)

$t := 2.5 \cdot in$ Shell thickness

$W := 158000 \cdot lbf - 10000 \cdot lbf$ Bounding Weight of overpack (minus the bottom plate) Table 3.2.4

$g := 386.4 \cdot \frac{in}{sec^2}$ Gravitational acceleration

$E := 26.1 \cdot 10^6 \cdot psi$ Young's modulus (400° F) SA203-E Table 3.3.4

$\sigma_y := 34300 \cdot psi$ Yield strength (400° F) SA203-E Table 3.3.4

3.H.4.4 Analysis of Overpack Load Cases

3.H.4.4.1 Load Case 1 (Load Case 03 in Table 3.1.5)

The G level for Longitudinal Load is $G := 1.15 \cdot g$

The Factor of Safety for Design is $FS_D := FS_{LA}$ $FS_D = 2$

Stress components

The longitudinal membrane stress is the impact weight supported by the inner shell divided by the cross sectional area of the shell.

$P := G \cdot \frac{W}{g}$ $P = 1.702 \times 10^5\,lbf$

$A := \pi \cdot \left(R_o^2 - R_i^2\right)$ $A = 559.596\,in^2$

$\sigma_\phi := \frac{P}{A}$ $\sigma_\phi = 304.147\,psi$ Longitudinal stress

The circumferential membrane stress is equal to the mean fabrication stress (from Appendix 3.I.)

$\sigma_\theta := 10506 \cdot psi$ Bounding circumferential mean stress from fabrication analysis

$\sigma_{\phi\theta} := 0 \cdot psi$ In-plane shear stress

As an initial check, the amplified stress components must meet the allowable limits stated in Section 3.H.4.1 of the appendix.

$\frac{\sigma_\phi \cdot FS_D}{\sigma_y} = 0.018 < 1.0$ $\frac{|\sigma_\theta| \cdot FS_D}{\sigma_y} = 0.613 < 1.0$ $\frac{\sigma_{\phi\theta} \cdot FS_D}{\sigma_y} = 0 < 0.6$

Capacity reduction factors

The first step towards defining the capacity reduction factors is to calculate the following geometric parameters.

$R := \frac{R_i + R_o}{2}$ $R = 35.625\,in$ Mean radius

The unsupported longitudinal and circumferential lengths are

$l_\phi := L$ $l_\phi = 173.625\,in$

$l_\theta := 2 \cdot \pi \cdot R$ $l_\theta = 223.838\,in$

M_i is a dimensionless factor defined as follows

$M_\phi := \frac{l_\phi}{(R \cdot t)^{0.5}}$ $M_\phi = 18.398$ $M_\theta := \frac{l_\theta}{(R \cdot t)^{0.5}}$ $M_\theta = 23.719$

$M := if(M_\phi < M_\theta, M_\phi, M_\theta)$ $M = 18.398$ M equals smaller of two values

The radius-to-thickness ratio is $\frac{R}{t} = 14.25$

Next, the capacity reduction factors are computed per Sec. 1511(a), (b), and (c) of Code Case N-284.

Axial Compression

Effect of R/t (R/t < 600)

$\alpha_1 := 1.52 - 0.473 \cdot \log\left(\frac{R}{t}\right)$ $\alpha_1 = 0.974$

$\alpha_2 := 1.0 \cdot 10^{-5} \cdot \frac{\sigma_y}{psi} - 0.033$ $\alpha_2 = 0.31$

$\alpha_{\phi L1} := if(\alpha_1 < \alpha_2, \alpha_1, \alpha_2)$ $\alpha_{\phi L1} = 0.31$ $\alpha_{\phi L1}$ equals smaller of two values

Effect of Length (M > 10)

$\alpha_{\phi L2} := 0.207$

$\alpha_{\phi L} := if(\alpha_{\phi L1} > \alpha_{\phi L2}, \alpha_{\phi L1}, \alpha_{\phi L2})$ $\alpha_{\phi L} = 0.31$ $\alpha_{\phi L}$ equals larger of two values

Hoop Compression

$\alpha_{\theta L} := 0.8$

Shear (R/t < 250)

$\alpha_{\phi\theta L} := 0.8$

Theoretical elastic buckling stresses

The basic equations used are given in Sec. 1712.1.1 of Code Case N-284.

Axial Compression ($M_\phi > 1.73$) $C_\phi := 0.605$

$\sigma_{\phi eL} := C_\phi \cdot \frac{E \cdot t}{R}$ $\sigma_{\phi eL} = 1.108 \times 10^6$ psi

External Pressure

No End Pressure ($3.0 < M_\phi < 1.65\ R/t$)

$C_{\theta r} := \frac{0.92}{M_\phi - 1.17}$ $C_{\theta r} = 0.053$

$\sigma_{reL} := C_{\theta r} \cdot \frac{E \cdot t}{R}$ $\sigma_{reL} = 9.781 \times 10^4$ psi

End Pressure Included ($3.5 < M_\phi < 1.65\ R/t$)

$C_{\theta h} := \frac{0.92}{M_\phi - 0.636}$ $C_{\theta h} = 0.052$

$\sigma_{heL} := C_{\theta h} \cdot \frac{E \cdot t}{R}$ $\sigma_{heL} = 9.487 \times 10^4$ psi

Shear ($1.5 < M_\phi < 26$)

$C_{\phi\theta} := \frac{4.82}{M_\phi^{\,2}} \cdot \left(1 + 0.0239 \cdot M_\phi^{\,3}\right)^{0.5}$ $C_{\phi\theta} = 0.174$

$\sigma_{\phi\theta eL} := C_{\phi\theta} \cdot \frac{E \cdot t}{R}$ $\sigma_{\phi\theta eL} = 3.193 \times 10^5$ psi

Plasticity reduction factors

The plasticity reduction factors are calculated according to the equations provided by Sec. 1610(a), (b), and (c) of the Code Case.

Axial Compression

$\eta_\phi := 1.0$ $\qquad \frac{\sigma_\phi \cdot FS_D}{\sigma_y} = 0.018 \quad < .55$

Hoop Compression

$\eta_\theta := 1.0$ $\qquad \left(\frac{|\sigma_\theta| \cdot FS_D}{\sigma_y} < 0.67 \right)$

Shear

$\eta_{\phi\theta} := 1.0$ $\qquad \left(\frac{\sigma_{\phi\theta} \cdot FS_D}{\sigma_y} < 0.48 \right)$

Interaction equations

The interaction equations for local buckling are supplied in Sec. 1713 of Code Case N-284.

Elastic Buckling

$\sigma_{\phi s} := \frac{\sigma_\phi \cdot FS_D}{\alpha_{\phi L}}$ $\qquad \sigma_{\phi s} = 1.962 \times 10^3 \text{ psi}$

$\sigma_{\theta s} := \frac{\sigma_\theta \cdot FS_D}{\alpha_{\theta L}}$ $\qquad \sigma_{\theta s} = 2.626 \times 10^4 \text{ psi} \quad < \quad \sigma_{heL} = 9.487 \times 10^4 \text{ psi}$

$\sigma_{\phi\theta s} := \frac{\sigma_{\phi\theta} \cdot FS_D}{\alpha_{\phi\theta L}}$ $\qquad \sigma_{\phi\theta s} = 0 \text{ psi}$

Axial Compression Plus Hoop Compression

$$\frac{\sigma_{\phi s} - 0.5 \cdot \sigma_{heL}}{\sigma_{\phi eL} - 0.5 \cdot \sigma_{heL}} + \left(\frac{\sigma_{\theta s}}{\sigma_{heL}} \right)^2 = 0.034 \qquad < 1.0$$

Axial Compression Plus Shear

$$\frac{\sigma_{\phi s}}{\sigma_{\phi eL}} + \left(\frac{\sigma_{\phi\theta s}}{\sigma_{\phi\theta eL}} \right)^2 = 1.771 \times 10^{-3} \qquad < 1.0$$

Hoop Compression Plus Shear

$$\frac{|\sigma_{\theta s}|}{\sigma_{reL}} + \left(\frac{\sigma_{\phi\theta s}}{\sigma_{\phi\theta eL}}\right)^2 = 0.269 \qquad < 1.0$$

Axial Compression Plus Hoop Compression Plus Shear

The shear constant, K, is computed as follows

$$K := 1 - \left(\frac{\sigma_{\phi\theta s}}{\sigma_{\phi\theta eL}}\right)^2 \qquad K = 1$$

As a result of the shear stress equaling zero, the value of K equals one. Therefore, no further interaction checks are required for this combination of stresses.

Inelastic Buckling

$$\sigma_{\phi p} := \frac{\sigma_{\phi s}}{\eta_\phi} \qquad \sigma_{\phi p} = 1.962 \times 10^3 \text{ psi}$$

$$\sigma_{\theta p} := \frac{\sigma_{\theta s}}{\eta_\theta} \qquad \sigma_{\theta p} = 2.626 \times 10^4 \text{ psi}$$

$$\sigma_{\phi\theta p} := \frac{\sigma_{\phi\theta s}}{\eta_{\phi\theta}} \qquad \sigma_{\phi\theta p} = 0 \text{ psi}$$

Axial Compression Plus Shear

$$\left(\frac{\sigma_{\phi p}}{\sigma_{\phi eL}}\right)^2 + \left(\frac{\sigma_{\phi\theta p}}{\sigma_{\phi\theta eL}}\right)^2 = 3.136 \times 10^{-6} \qquad < 1.0$$

Hoop Compression Plus Shear

$$\left(\frac{\sigma_{\theta p}}{\sigma_{reL}}\right)^2 + \left(\frac{\sigma_{\phi\theta p}}{\sigma_{\phi\theta eL}}\right)^2 = 0.072 \qquad < 1.0$$

Analysis of the overpack inner shell shows that under this load case, the interaction equations for elastic and inelastic buckling are satisfied (less than 1.0). Therefore, stability of the inner shell is assured.

3.H.4.4.2 Load Case 2 (Load Case 04.a in Table 3.1.5)

The G level for Drop Load is	$G := 60 \cdot g$	Table 3.1.2
The Factor of Safety for Design is	$FS_D := FS_{LD}$	$FS_D = 1.34$

Stress components

The longitudinal membrane stress is the impact weight supported by the inner shell divided by the cross sectional area of the shell.

$P := G \cdot \frac{W}{g}$ $P = 8.88 \times 10^6 \, lbf$ $A := \pi \cdot \left(R_o^2 - R_i^2\right)$ $A = 559.596 \, in^2$

$\sigma_\phi := \frac{P}{A}$ $\sigma_\phi = 1.587 \times 10^4 \, psi$ Longitudinal stress

The circumferential membrane stress is equal to the mean fabrication stress (from Appendix 3.I.).

$\sigma_\theta := 10506 \cdot psi$ Bounding circumferential mean stress from fabrication analysis

$\sigma_{\phi\theta} := 0 \cdot psi$ In-plane shear stress

The amplified stress components must meet the allowable limits in Section 3.H.4.1 of the appendix.

$\frac{\sigma_\phi \cdot FS_D}{\sigma_y} = 0.62 < 1.0$ $\frac{|\sigma_\theta| \cdot FS_D}{\sigma_y} = 0.41 < 1.0$ $\frac{\sigma_{\phi\theta} \cdot FS_D}{\sigma_y} = 0 < 0.6$

Capacity reduction factors

The factors are as calculated previously for load case 1 since the geometry is the same

Theoretical elastic buckling stresses

The basic equations used are given in Sec. 1712.1.1 of Code Case N-284 and are functions of geometry; therefore, there is no change from the load case 1 calculation..

Plasticity reduction factors

The plasticity reduction factors are calculated according to the equations provided by Sec. 1610(a), (b), and (c) of the Code Case. Since these are a function of the current load state, they need to be recomputed.

Axial Compression

$\eta_\phi := \frac{0.18}{\left(1 - \frac{0.45 \cdot \sigma_y}{\sigma_\phi \cdot FS_D}\right)}$ $\eta_\phi = 0.657$ $\left(0.55 < \frac{\sigma_\phi \cdot FS_D}{\sigma_y} < 0.738\right)$

Hoop Compression

$\eta_\theta := 1.0$ $\left(\frac{|\sigma_\theta| \cdot FS_D}{\sigma_y} < 0.67\right)$

Shear

$\eta_{\phi\theta} := 1.0$ $\left(\frac{\sigma_{\phi\theta} \cdot FS_D}{\sigma_y} < 0.48\right)$

Interaction equations

The interaction equations for local buckling are supplied in Sec. 1713 of Code Case N-284.

Elastic Buckling

$\sigma_{\phi s} := \frac{\sigma_\phi \cdot FS_D}{\alpha_{\phi L}}$ $\sigma_{\phi s} = 6.859 \times 10^4$ psi

$\sigma_{\theta s} := \frac{\sigma_\theta \cdot FS_D}{\alpha_{\theta L}}$ $\sigma_{\theta s} = 1.76 \times 10^4$ psi $<$ $\sigma_{heL} = 9.487 \times 10^4$ psi

$\sigma_{\phi\theta s} := \frac{\sigma_{\phi\theta} \cdot FS_D}{\alpha_{\phi\theta L}}$ $\sigma_{\phi\theta s} = 0$ psi

Axial Compression Plus Hoop Compression ($\sigma_{\phi s} > 0.5\ \sigma_{\theta s}$)

$\frac{\sigma_{\phi s} - 0.5 \cdot \sigma_{heL}}{\sigma_{\phi eL} - 0.5 \cdot \sigma_{heL}} + \left(\frac{\sigma_{\theta s}}{\sigma_{heL}}\right)^2 = 0.054$ < 1.0

Axial Compression Plus Shear

$\frac{\sigma_{\phi s}}{\sigma_{\phi eL}} + \left(\frac{\sigma_{\phi\theta s}}{\sigma_{\phi\theta eL}}\right)^2 = 0.062$ < 1.0

Hoop Compression Plus Shear

$\frac{|\sigma_{\theta s}|}{\sigma_{reL}} + \left(\frac{\sigma_{\phi\theta s}}{\sigma_{\phi\theta eL}}\right)^2 = 0.18$ < 1.0

Axial Compression Plus Hoop Compression Plus Shear

The shear constant, K, is computed as follows

$$K := 1 - \left(\frac{\sigma_{\phi\theta s}}{\sigma_{\phi\theta eL}}\right)^2 \qquad K = 1$$

As a result of the shear stress equaling zero, the value of K equals one. Therefore, no further interaction checks are required for this combination of stresses.

Inelastic Buckling

$$\sigma_{\phi p} := \frac{\sigma_{\phi s}}{\eta_\phi} \qquad \sigma_{\phi p} = 1.045 \times 10^5 \text{ psi}$$

$$\sigma_{\theta p} := \frac{\sigma_{\theta s}}{\eta_\theta} \qquad \sigma_{\theta p} = 1.76 \times 10^4 \text{ psi}$$

$$\sigma_{\phi\theta p} := \frac{\sigma_{\phi\theta s}}{\eta_{\phi\theta}} \qquad \sigma_{\phi\theta p} = 0 \text{ psi}$$

Axial Compression Plus Shear

$$\left(\frac{\sigma_{\phi p}}{\sigma_{\phi eL}}\right)^2 + \left(\frac{\sigma_{\phi\theta p}}{\sigma_{\phi\theta eL}}\right)^2 = 8.887 \times 10^{-3} \qquad < 1.0$$

Hoop Compression Plus Shear

$$\left(\frac{\sigma_{\theta p}}{\sigma_{reL}}\right)^2 + \left(\frac{\sigma_{\phi\theta p}}{\sigma_{\phi\theta eL}}\right)^2 = 0.032 \qquad < 1.0$$

Analysis of the overpack inner shell shows that under this load case, the interaction equations for elastic and inelastic buckling are satisfied (less than 1.0). Therefore, stability of the inner shell is assured.

3.H.4.4.3 Load Case3 (Load Case 02 in Table 3.1.5)

The external pressure is	$p_{ext} := 300 \cdot psi$	Table 2.2.1
The G level for Longitudinal Load is	$G := 1 \cdot g$	
The Factor of Safety for Design is	$FS_D := FS_{LD}$	$FS_D = 1.34$

Stress components

The longitudinal membrane stress is the impact weight supported by the inner shell divided by the cross sectional area of the shell plus the effects of the submergence pressure..

$P := G \cdot \frac{W}{g}$ $P = 1.48 \times 10^5\,lbf$ $A := \pi \cdot \left(R_o^2 - R_i^2\right)$ $A = 559.596\,in^2$

$\sigma_\phi := \frac{P}{A} + p_{ext} \cdot \frac{R_o^2}{2 \cdot t \cdot R}$ $\sigma_\phi = 2.555 \times 10^3\,psi$ Longitudinal stress

The circumferential membrane stress is equal to the mean fabrication stress (from Appendix 3.L) plus the submergence pressure.

$\sigma_\theta := 10506 \cdot psi + p_{ext} \cdot \frac{R}{t}$ $\sigma_\theta = 1.478 \times 10^4\,psi$

$\sigma_{\phi\theta} := 0 \cdot psi$ In-plane shear stress

As an initial check, the amplified stress components must meet the allowable limits stated in Section 3.H.4.1 of the appendix.

$\frac{\sigma_\phi \cdot FS_D}{\sigma_y} = 0.1 < 1.0$ $\frac{|\sigma_\theta| \cdot FS_D}{\sigma_y} = 0.577 < 1.0$ $\frac{\sigma_{\phi\theta} \cdot FS_D}{\sigma_y} = 0 < 0.6$

Capacity reduction factors

The factors are as calculated in load case 1 since the geometry is the same

Theoretical elastic buckling stresses

The basic equations used are given in Sec. 1712.1.1 of Code Case N-284 and are functions of geometry; therefore, there is no change from the load case 1 calculation..

Plasticity reduction factors

The plasticity reduction factors are calculated according to the equations provided by Sec. 1610(a), (b), and (c) of the Code Case. Since these are a function of the current load state, they need to be recomputed.

Axial Compression

$\eta_\phi := 1.0$ $\frac{\sigma_\phi \cdot FS_D}{\sigma_y} = 0.1 < .55$

Hoop Compression

$\eta_\theta := 1.0$ $\left(\frac{|\sigma_\theta| \cdot FS_D}{\sigma_y} < 0.67\right)$

Shear

$\eta_{\phi\theta} := 1.0$ $\left(\frac{\sigma_{\phi\theta} \cdot FS_D}{\sigma_y} < 0.48\right)$

Interaction equations

The interaction equations for local buckling are supplied in Sec. 1713 of Code Case N-284.

Elastic Buckling

$\sigma_{\phi s} := \frac{\sigma_\phi \cdot FS_D}{\alpha_{\phi L}}$ $\sigma_{\phi s} = 1.104 \times 10^4 \text{ psi}$

$\sigma_{\theta s} := \frac{\sigma_\theta \cdot FS_D}{\alpha_{\theta L}}$ $\sigma_{\theta s} = 2.476 \times 10^4 \text{ psi} \quad < \quad \sigma_{heL} = 9.487 \times 10^4 \text{ psi}$

$\sigma_{\phi\theta s} := \frac{\sigma_{\phi\theta} \cdot FS_D}{\alpha_{\phi\theta L}}$ $\sigma_{\phi\theta s} = 0 \text{ psi}$

Axial Compression Plus Hoop Compression ($\sigma_\phi > 0.5\ \sigma_\theta$)

$\frac{\sigma_{\phi s} - 0.5 \cdot \sigma_{heL}}{\sigma_{\phi eL} - 0.5 \cdot \sigma_{heL}} + \left(\frac{\sigma_{\theta s}}{\sigma_{heL}}\right)^2 = 0.034 \qquad < 1.0$

Axial Compression Plus Shear

$\frac{\sigma_{\phi s}}{\sigma_{\phi eL}} + \left(\frac{\sigma_{\phi\theta s}}{\sigma_{\phi\theta eL}}\right)^2 = 9.965 \times 10^{-3} \qquad < 1.0$

Hoop Compression Plus Shear

$\frac{|\sigma_{\theta s}|}{\sigma_{reL}} + \left(\frac{\sigma_{\phi\theta s}}{\sigma_{\phi\theta eL}}\right)^2 = 0.253 \qquad < 1.0$

Axial Compression Plus Hoop Compression Plus Shear

The shear constant, K, is computed as follows

$$K := 1 - \left(\frac{\sigma_{\phi\theta s}}{\sigma_{\phi\theta eL}} \right)^2 \qquad K = 1$$

As a result of the shear stress equaling zero, the value of K equals one. Therefore, no further interaction checks are required for this combination of stresses.

Inelastic Buckling

$$\sigma_{\phi p} := \frac{\sigma_{\phi s}}{\eta_{\phi}} \qquad \sigma_{\phi p} = 1.104 \times 10^4 \text{ psi}$$

$$\sigma_{\theta p} := \frac{\sigma_{\theta s}}{\eta_{\theta}} \qquad \sigma_{\theta p} = 2.476 \times 10^4 \text{ psi}$$

$$\sigma_{\phi\theta p} := \frac{\sigma_{\phi\theta s}}{\eta_{\phi\theta}} \qquad \sigma_{\phi\theta p} = 0 \text{ psi}$$

Axial Compression Plus Shear

$$\left(\frac{\sigma_{\phi p}}{\sigma_{\phi eL}} \right)^2 + \left(\frac{\sigma_{\phi\theta p}}{\sigma_{\phi\theta eL}} \right)^2 = 9.931 \times 10^{-5} \qquad < 1.0$$

Hoop Compression Plus Shear

$$\left(\frac{\sigma_{\theta p}}{\sigma_{reL}} \right)^2 + \left(\frac{\sigma_{\phi\theta p}}{\sigma_{\phi\theta eL}} \right)^2 = 0.064 \qquad < 1.0$$

Analysis of the overpack inner shell shows that under this load case, the interaction equations for elastic and inelastic buckling are satisfied (less than 1.0). Therefore, stability of the inner shell is assured.

3.H.5 Stability of the MPC Containment Shell

3.H.5.1 Method - ASME Code Case N-284

A description is provided in the previous section.

3.H.5.2 Assumptions

1. Under the postulated end drop, the appropriate weight of the MPC confinement vessel (minus the weight of the baseplate) is supported vertically by the 0.5 in. thick shell. Lateral pressure is neglected since design internal pressure exceeds design external pressure.

2. By employing the method of Case N-284, the confinement shell is assumed to be simply supported. The welded base of the shell more closely represents a clamped boundary. Therefore, elastic buckling stress limits are actually higher.

3. The channels and other shims welded axially to the inside surface of the confinement shell act as stiffeners. The effect of these axial stiffeners is neglected. This is a conservative and a simplifying assumption.

4. Material properties are choosen at the bounding temperature for normal heat condition or for the fire condition of the MPC confinement boundary. The Young's modulus and the yield stress decrease with increasing temperature, therefore, the analysis is conservative.

3.H.5.3 Input Data

The following is a list of input parameters for the MPC confinement shell. The dimensions are obtained from the design drawings in Section 1.5.

$R_i := \frac{67.375}{2}\cdot in$	Inner radius of shell
$R_o := \frac{68.375}{2}\cdot in$	Outer radius of shell
$L := 188\cdot in$	Axial length of shell
$t := 0.5\cdot in$	Shell thickness
$W := 10400\cdot lbf + 5900\cdot lbf \ldots + 3700\cdot lbf$	Bounding weight of MPC components. This weight excludes the fuel basket and the baseplate but includes the closure lid and all of the basket support structure. The values are obtained from Table 3.2.4.
$g := 386.4\cdot\frac{in}{sec^2}$	Gravitational acceleration

$p_{ext} := 40 \cdot psi$ Design basis external pressure Table 2.2.1

Multiplier on external design pressure to define accident pressure $mp := 1.5$

$E := 26.75 \cdot 10^6 \cdot psi$ Young's modulus (350 deg. F), Alloy X Table 3.3.1

$\sigma_y := 21600 \cdot psi$ Yield strength (350 deg. F) Alloy X Table 3.3.1

3.H.5.4 Analysis

3.H.5.4.1 Load Case 4 (Load Case E2 in Table 3.1.4)

The external pressure is $p_{ext} = 40\,psi$

The G level for Longitudinal Load is $G := 1.15 \cdot g$

The Factor of Safety for Design is $FS_D := FS_{LA}$ $FS_D = 2$

Stress components

The longitudinal membrane stress is the impact weight supported by the confinement shell divided by the cross sectional area of the shell.

$P := G \cdot \frac{W}{g}$ $P = 2.3 \times 10^4\,lbf$

$A := \pi \cdot \left(R_o^2 - R_i^2\right)$ $A = 106.618\,in^2$

$\sigma_\phi := \frac{P}{A} + p_{ext} \cdot \frac{R_i + R_o}{4 \cdot t} \cdot 0.0$ $\sigma_\phi = 215.724\,psi$ Longitudinal stress

No lateral pressure is assumed since use of actual internal pressure is not conservative.

$\sigma_\theta := \frac{p_{ext} \cdot \left(R_i + R_o\right) \cdot 0.0}{2 \cdot t}$ $\sigma_\theta = 0\,psi$ Circumferential stress

The shear stresses on the gross section of the inner shell are equal to zero.

$\sigma_{\phi\theta} := 0 \cdot psi$ In-plane shear stress

As an initial check, the amplified stress components must meet the allowable limits stated in Section 3.H.4.1 of the appendix.

$\frac{\sigma_\phi \cdot FS_D}{\sigma_y} = 0.02 < 1.0$ $\frac{|\sigma_\theta| \cdot FS_D}{\sigma_y} = 0 < 1.0$ $\frac{\sigma_{\phi\theta} \cdot FS_D}{\sigma_y} = 0 < 0.6$

Capacity reduction factors

$R := \frac{R_i + R_o}{2}$ $R = 33.938\,in$ Mean radius

The unsupported longitudinal and circumferential lengths are

$l_\phi := L$ $l_\phi = 188\,in$

$l_\theta := 2 \cdot \pi \cdot R$ $l_\theta = 213.236\,in$ Neglect stiffeners

M_i is a dimensionless factor defined as follows

$M_\phi := \frac{l_\phi}{(R \cdot t)^{0.5}}$ $M_\phi = 45.639$

$M_\theta := \frac{l_\theta}{(R \cdot t)^{0.5}}$ $M_\theta = 51.765$

$M := if(M_\phi < M_\theta, M_\phi, M_\theta)$ $M = 45.639$ M equals smaller of two values

The radius-to-thickness ratio is $\frac{R}{t} = 67.875$

Next, the capacity reduction factors are computed per Sec. 1511(a), (b), and (c) of Code Case N-284.

Axial Compression

Effect of R/t (R/t < 600)

$\alpha_1 := 1.52 - 0.473 \cdot \log\left(\frac{R}{t}\right)$ $\alpha_1 = 0.654$

$\alpha_2 := 1.0 \cdot 10^{-5} \cdot \frac{\sigma_y}{psi} - 0.033$ $\alpha_2 = 0.183$

$\alpha_{\phi L1} := if(\alpha_1 < \alpha_2, \alpha_1, \alpha_2)$ $\alpha_{\phi L1} = 0.183$ $\alpha_{\phi L1}$ equals smaller of two values

Effect of Length (M > 10)

$$\alpha_{\phi L2} := \frac{0.826}{M^{0.6}} \qquad \alpha_{\phi L2} = 0.083$$

$$\alpha_{\phi L} := \text{if}\left(\alpha_{\phi L1} > \alpha_{\phi L2}, \alpha_{\phi L1}, \alpha_{\phi L2}\right) \qquad \alpha_{\phi L} = 0.183$$

$\alpha_{\phi L}$ equals larger of two values

Hoop Compression

$$\alpha_{\theta L} := 0.8$$

Shear (R/t < 250)

$$\alpha_{\phi\theta L} := 0.8$$

Theoretical elastic buckling stresses

The basic equations used are given in Sec. 1712.1.1 of Code Case N-284.

Axial Compression $\qquad M_\phi = 45.639$

$$C_\phi := .605 \qquad C_\phi = 0.605$$

$$\sigma_{\phi eL} := C_\phi \cdot \frac{E \cdot t}{R} \qquad \sigma_{\phi eL} = 2.384 \times 10^5 \text{ psi}$$

External Pressure $\qquad 1.65 \cdot \frac{R}{t} = 111.994$

No End Pressure

$$C_{\theta r} := \frac{.92}{M_\phi - 1.17} \qquad C_{\theta r} = 0.021$$

$$\sigma_{reL} := C_{\theta r} \cdot \frac{E \cdot t}{R} \qquad \sigma_{reL} = 8.154 \times 10^3 \text{ psi}$$

End Pressure Included

$$C_{\theta r} := \frac{.92}{M_\phi - .636} \qquad C_{\theta h} = 0.052$$

$$\sigma_{heL} := C_{\theta h} \cdot \frac{E \cdot t}{R} \qquad \sigma_{heL} = 2.041 \times 10^4 \text{ psi}$$

Shear (26 < M_ϕ < 8.69 R/t)

$$C_{\phi\theta} := \frac{0.746}{M_\phi^{0.5}} \qquad C_{\phi\theta} = 0.11$$

$$\sigma_{\phi\theta eL} := C_{\phi\theta} \cdot \frac{E \cdot t}{R} \qquad \sigma_{\phi\theta eL} = 4.352 \times 10^4 \text{ psi}$$

Plasticity reduction factors

The plasticity reduction factors are calculated according to the equations provided by Sec. 1610(a), (b), and (c) of the Code Case.

Axial Compression

$$\eta_\phi := 1 \qquad \frac{\sigma_\phi \cdot FS_D}{\sigma_y} = 0.02$$

Hoop Compression

$$\eta_\theta := 1.0 \qquad \left(\frac{|\sigma_\theta| \cdot FS_D}{\sigma_y} < 0.67 \right)$$

Shear

$$\eta_{\phi\theta} := 1.0 \qquad \left(\frac{\sigma_{\phi\theta} \cdot FS_D}{\sigma_y} < 0.48 \right)$$

Interaction equations

The interaction equations for local buckling are supplied in Sec. 1713 of Code Case N-284.

Elastic Buckling

$$\sigma_{\phi s} := \frac{\sigma_\phi \cdot FS_D}{\alpha_{\phi L}} \qquad \sigma_{\phi s} = 2.358 \times 10^3 \text{ psi}$$

$$\sigma_{\theta s} := \frac{\sigma_\theta \cdot FS_D}{\alpha_{\theta L}} \qquad \sigma_{\theta s} = 0 \text{ psi} \qquad < \qquad \sigma_{heL} = 2.041 \times 10^4 \text{ psi}$$

$$\sigma_{\phi\theta s} := \frac{\sigma_{\phi\theta} \cdot FS_D}{\alpha_{\phi\theta L}} \qquad \sigma_{\phi\theta s} = 0\,\text{psi}$$

Axial Compression Plus Hoop Compression ($\sigma_{\phi} > 0.5\ \sigma_{\theta}$)

$$\frac{\sigma_{\phi s} - 0.5 \cdot \sigma_{heL}}{\sigma_{\phi eL} - 0.5 \cdot \sigma_{heL}} + \left(\frac{\sigma_{\theta s}}{\sigma_{heL}}\right)^2 = -0.034 \qquad < 1.0$$

No need to check this per Code Case.

Axial Compression Plus Shear

$$\frac{\sigma_{\phi s}}{\sigma_{\phi eL}} + \left(\frac{\sigma_{\phi\theta s}}{\sigma_{\phi\theta eL}}\right)^2 = 9.888 \times 10^{-3} \qquad < 1.0$$

Hoop Compression Plus Shear

$$\frac{|\sigma_{\theta s}|}{\sigma_{reL}} + \left(\frac{\sigma_{\phi\theta s}}{\sigma_{\phi\theta eL}}\right)^2 = 0 \qquad < 1.0$$

Axial Compression Plus Hoop Compression Plus Shear

The shear constant, K, is computed as follows

$$K := 1 - \left(\frac{\sigma_{\phi\theta s}}{\sigma_{\phi\theta eL}}\right)^2 \qquad K = 1$$

As a result of the shear stress equaling zero, the value of K equals one. Therefore, no further interaction checks are required for this combination of stresses.

Inelastic Buckling

$$\sigma_{\phi p} := \frac{\sigma_{\phi s}}{\eta_{\phi}} \qquad \sigma_{\phi p} = 2.358 \times 10^3\,\text{psi}$$

$$\sigma_{\theta p} := \frac{\sigma_{\theta s}}{\eta_{\theta}} \qquad \sigma_{\theta p} = 0\,\text{psi}$$

$$\sigma_{\phi\theta p} := \frac{\sigma_{\phi\theta s}}{\eta_{\phi\theta}} \qquad \sigma_{\phi\theta p} = 0\,\text{psi}$$

Axial Compression Plus Shear

$$\left(\frac{\sigma_{\phi p}}{\sigma_{\phi eL}}\right)^2 + \left(\frac{\sigma_{\phi\theta p}}{\sigma_{\phi\theta eL}}\right)^2 = 9.777 \times 10^{-5} \qquad < 1.0$$

Hoop Compression Plus Shear

$$\left(\frac{\sigma_{\theta p}}{\sigma_{reL}}\right)^2 + \left(\frac{\sigma_{\phi\theta p}}{\sigma_{\phi\theta eL}}\right)^2 = 0 \qquad < 1.0$$

Conclusion

Analysis of the MPC confinement shell shows that the interaction equations for elastic and inelastic buckling are satisfied (less than 1.0). Therefore, stability of the inner shell is assured for load case 4.

3.H.5.4.2 Load Case 5 (Load Case E3.a in Table 3.1.4)

The external pressure is $p_{ext} = 40\,psi$

The G level for Drop Load is $G := 60 \cdot g$

The Factor of Safety for Design is $FS_D := FS_{LD}$ $FS_D = 1.34$

Stress components

The longitudinal membrane stress is the impact weight supported by the confinement shell divided by the cross sectional area of the shell.

$P := G \cdot \frac{W}{g}$ $P = 1.2 \times 10^6\,lbf$ $A := \pi \cdot \left(R_o^2 - R_i^2\right)$ $A = 106.618\,in^2$

$\sigma_\phi := \frac{P}{A} + p_{ext} \cdot \frac{R_i + R_o}{4 \cdot t} \cdot 0.0$ $\sigma_\phi = 1.126 \times 10^4\,psi$ Longitudinal stress

We neglect stresses due to pressure since the normal operation will have tensile circumferentailstress in the shell.

$\sigma_\theta := \frac{p_{ext} \cdot \left(R_i + R_o\right) \cdot 0.0}{2 \cdot t}$ $\sigma_\theta = 0\,psi$ Circumferential stress

The shear stresses on the gross section of the inner shell are equal to zero.

$\sigma_{\phi\theta} := 0 \cdot psi$ In-plane shear stress

As an initial check, the amplified stress components must meet the allowable limits stated in Section 3.H.4.1 of the appendix.

$$\frac{\sigma_\phi \cdot FS_D}{\sigma_y} = 0.698 \quad < 1.0 \qquad \frac{|\sigma_\theta| \cdot FS_D}{\sigma_y} = 0 \quad < 1.0 \qquad \frac{\sigma_{\phi\theta} \cdot FS_D}{\sigma_y} = 0 \quad < 0.6$$

Plasticity reduction factors

The plasticity reduction factors are calculated according to the equations provided by Sec. 1610(a), (b), and (c) of the Code Case.

Axial Compression

$$\eta_\phi := 1.31 - 1.15 \cdot \sigma_\phi \cdot \frac{FS_D}{\sigma_y} \qquad \eta_\phi = 0.507$$

Hoop Compression

$$\eta_\theta := 1.0 \qquad \left(\frac{|\sigma_\theta| \cdot FS_D}{\sigma_y} < 0.67 \right)$$

Shear

$$\eta_{\phi\theta} := 1.0 \qquad \left(\frac{\sigma_{\phi\theta} \cdot FS_D}{\sigma_y} < 0.48 \right)$$

Interaction equations

The interaction equations for local buckling are supplied in Sec. 1713 of Code Case N-284.

Elastic Buckling

$$\sigma_{\phi s} := \frac{\sigma_\phi \cdot FS_D}{\alpha_{\phi L}} \qquad \sigma_{\phi s} = 8.241 \times 10^4 \text{ psi}$$

$$\sigma_{\theta s} := \frac{\sigma_\theta \cdot FS_D}{\alpha_{\theta L}} \qquad \sigma_{\theta s} = 0 \text{ psi} \qquad < \qquad \sigma_{heL} = 2.041 \times 10^4 \text{ psi}$$

$$\sigma_{\phi\theta s} := \frac{\sigma_{\phi\theta} \cdot FS_D}{\alpha_{\phi\theta L}} \qquad \sigma_{\phi\theta s} = 0 \text{ psi}$$

Axial Compression Plus Hoop Compression ($\sigma_\phi > 0.5\ \sigma_\theta$)

$$\frac{\sigma_{\phi s} - 0.5\cdot\sigma_{heL}}{\sigma_{\phi eL} - 0.5\cdot\sigma_{heL}} + \left(\frac{\sigma_{\theta s}}{\sigma_{heL}}\right)^2 = 0.316 \qquad < 1.0$$

Axial Compression Plus Shear

$$\frac{\sigma_{\phi s}}{\sigma_{\phi eL}} + \left(\frac{\sigma_{\phi\theta s}}{\sigma_{\phi\theta eL}}\right)^2 = 0.346 \qquad < 1.0$$

Hoop Compression Plus Shear

$$\frac{|\sigma_{\theta s}|}{\sigma_{reL}} + \left(\frac{\sigma_{\phi\theta s}}{\sigma_{\phi\theta eL}}\right)^2 = 0 \qquad < 1.0$$

Axial Compression Plus Hoop Compression Plus Shear

The shear constant, K, is computed as follows

$$K := 1 - \left(\frac{\sigma_{\phi\theta s}}{\sigma_{\phi\theta eL}}\right)^2 \qquad K = 1$$

As a result of the shear stress equaling zero, the value of K equals one. Therefore, no further interaction checks are required for this combination of stresses.

Inelastic Buckling

$$\sigma_{\phi p} := \frac{\sigma_{\phi s}}{\eta_\phi} \qquad \sigma_{\phi p} = 1.625 \times 10^5\ \text{psi} \qquad \sigma_{\phi eL} = 2.384 \times 10^5\ \text{psi}$$

$$\sigma_{\theta p} := \frac{\sigma_{\theta s}}{\eta_\theta} \qquad \sigma_{\theta p} = 0\ \text{psi}$$

$$\sigma_{\phi\theta p} := \frac{\sigma_{\phi\theta s}}{\eta_{\phi\theta}} \qquad \sigma_{\phi\theta p} = 0\ \text{psi}$$

Axial Compression Plus Shear

$$\left(\frac{\sigma_{\phi p}}{\sigma_{\phi eL}}\right)^2 + \left(\frac{\sigma_{\phi\theta p}}{\sigma_{\phi\theta eL}}\right)^2 = 0.465 \qquad < 1.0$$

Hoop Compression Plus Shear

$$\left(\frac{\sigma_{\theta p}}{\sigma_{reL}}\right)^2 + \left(\frac{\sigma_{\phi\theta p}}{\sigma_{\phi\theta eL}}\right)^2 = 0 \qquad < 1.0$$

Conclusion

Analysis of the MPC confinement shell shows that the interaction equations for elastic and inelastic buckling are satisfied (less than 1.0). Therefore, stability of the inner shell is assured for load case 5.

3.H.5.4.3 Load Case 6 (Load Case E5 in Table 3.1.4)

The external pressure is	$p_{ext} := mp \cdot p_{ext}$	$p_{ext} = 60\,psi$
The G level for Longitudinal Load is	$G := 1 \cdot g$	
The Factor of Safety for Design is	$FS_D := FS_{LD}$	$FS_D = 1.34$

The Young's modulus and the yield strength are evaluated at (400°F), which bounds the MPC shell temperature during a fire accident (see Subsection 3.4.4.2.2).

$E := 26.5 \cdot 10^6 \cdot psi$	Young's modulus (400 deg. F), Alloy X	Table 3.3.1
$\sigma_y := 20700 \cdot psi$	Yield strength (400 deg. F) Alloy X	Table 3.3.1

Stress components

The longitudinal membrane stress is the impact weight supported by the confinement shell divided by the cross sectional area of the shell.

$P := G \cdot \frac{W}{g}$ $\qquad P = 2 \times 10^4\,lbf$

$A := \pi \cdot \left(R_o^2 - R_i^2\right)$ $\qquad A = 106.618\,in^2$

$\sigma_\phi := \frac{P}{A} + p_{ext} \cdot \frac{R_i + R_o}{4 \cdot t}$ $\qquad \sigma_\phi = 2.224 \times 10^3\,psi$ $\qquad$ Longitudinal stress

A circumferential membrane stress develops in the MPC confinement shell due to external pressure.

$\sigma_\theta := \frac{p_{ext}\cdot(R_i + R_o)}{2\cdot t}$ $\sigma_\theta = 4.073 \times 10^3\,psi$ Circumferential stress

The shear stresses on the gross section of the inner shell are equal to zero.

$\sigma_{\phi\theta} := 0\cdot psi$ In-plane shear stress

As an initial check, the amplified stress components must meet the allowable limits stated in Section 3.H.4.1 of the appendix.

$\frac{\sigma_\phi\cdot FS_D}{\sigma_y} = 0.144 < 1.0$ $\frac{|\sigma_\theta|\cdot FS_D}{\sigma_y} = 0.264 < 1.0$ $\frac{\sigma_{\phi\theta}\cdot FS_D}{\sigma_y} = 0 < 0.6$

Capacity reduction factors

$R := \frac{R_i + R_o}{2}$ $R = 33.938\,in$ Mean radius

The unsupported longitudinal and circumferential lengths are

$l_\phi := L$ $l_\phi = 188\,in$

$l_\theta := 2\cdot\pi\cdot R$ $l_\theta = 213.236\,in$ No credit for stiffeners

M_i is a dimensionless factor defined as follows

$M_\phi := \frac{l_\phi}{(R\cdot t)^{0.5}}$ $M_\phi = 45.639$

$M_\theta := \frac{l_\theta}{(R\cdot t)^{0.5}}$ $M_\theta = 51.765$

$M := if(M_\phi < M_\theta, M_\phi, M_\theta)$ $M = 45.639$ M equals smaller of two values

The radius-to-thickness ratio is $\frac{R}{t} = 67.875$

Next, the capacity reduction factors are computed per Sec. 1511(a), (b), and (c) of Code Case N-284.

Axial Compression

Effect of R/t (R/t < 600)

$$\alpha_1 := 1.52 - 0.473 \cdot \log\left(\frac{R}{t}\right) \qquad \alpha_1 = 0.654$$

$$\alpha_2 := 1.0 \cdot 10^{-5} \cdot \frac{\sigma_y}{psi} - 0.033 \qquad \alpha_2 = 0.174$$

$$\alpha_{\phi L1} := if(\alpha_1 < \alpha_2, \alpha_1, \alpha_2) \qquad \alpha_{\phi L1} = 0.174$$

$\alpha_{\phi L1}$ equals smaller of two values

Effect of Length (M > 10)

$$\alpha_{\phi L2} := .207 \qquad \alpha_{\phi L2} = 0.207$$

$$\alpha_{\phi L} := if(\alpha_{\phi L1} > \alpha_{\phi L2}, \alpha_{\phi L1}, \alpha_{\phi L2}) \qquad \alpha_{\phi L} = 0.207$$

$\alpha_{\phi L}$ equals larger of two values

Hoop Compression

$$\alpha_{\theta L} := 0.8$$

Shear (R/t < 250)

$$\alpha_{\phi\theta L} := 0.8$$

Theoretical elastic buckling stresses

The basic equations used are given in Sec. 1712.1.1 of Code Case N-284.

Axial Compression $\qquad M_\phi = 45.639$

$$C_\phi := .605 \qquad C_\phi = 0.605$$

$$\sigma_{\phi eL} := C_\phi \cdot \frac{E \cdot t}{R} \qquad \sigma_{\phi eL} = 2.362 \times 10^5 \, psi$$

External Pressure $1.65 \cdot \frac{R}{t} = 111.994$

No End Pressure

$$C_{\theta r} := \frac{.92}{M_\phi - 1.17} \qquad C_{\theta r} = 0.021$$

$$\sigma_{reL} := C_{\theta r} \cdot \frac{E \cdot t}{R} \qquad \sigma_{reL} = 8.077 \times 10^3 \text{ psi}$$

End Pressure Included

$$C_{\theta r} := \frac{.92}{M_\phi - .636} \qquad C_{\theta h} = 0.052$$

$$\sigma_{heL} := C_{\theta h} \cdot \frac{E \cdot t}{R} \qquad \sigma_{heL} = 2.022 \times 10^4 \text{ psi}$$

Shear ($26 < M_\phi < 8.69\ R/t$)

$$C_{\phi\theta} := \frac{0.746}{M_\phi^{0.5}} \qquad C_{\phi\theta} = 0.11$$

$$\sigma_{\phi\theta eL} := C_{\phi\theta} \cdot \frac{E \cdot t}{R} \qquad \sigma_{\phi\theta eL} = 4.311 \times 10^4 \text{ psi}$$

Plasticity reduction factors

The plasticity reduction factors are calculated according to the equations provided by Sec. 1610(a), (b), and (c) of the Code Case.

Axial Compression

$$\eta_\phi := 1 \qquad \frac{\sigma_\phi \cdot FS_D}{\sigma_y} = 0.144 \quad < .55$$

Hoop Compression

$$\eta_\theta := 1.0 \qquad \left(\frac{|\sigma_\theta| \cdot FS_D}{\sigma_y} < 0.67 \right)$$

Shear

$$\eta_{\phi\theta} := 1.0 \qquad \left(\frac{\sigma_{\phi\theta}\cdot FS_D}{\sigma_y} < 0.48\right)$$

Interaction equations

The interaction equations for local buckling are supplied in Sec. 1713 of Code Case N-284.
Elastic Buckling

$$\sigma_{\phi s} := \frac{\sigma_\phi \cdot FS_D}{\alpha_{\phi L}} \qquad \sigma_{\phi s} = 1.44 \times 10^4 \text{ psi}$$

$$\sigma_{\theta s} := \frac{\sigma_\theta \cdot FS_D}{\alpha_{\theta L}} \qquad \sigma_{\theta s} = 6.821 \times 10^3 \text{ psi} \quad < \quad \sigma_{heL} = 2.022 \times 10^4 \text{ psi}$$

$$\sigma_{\phi\theta s} := \frac{\sigma_{\phi\theta} \cdot FS_D}{\alpha_{\phi\theta L}} \qquad \sigma_{\phi\theta s} = 0 \text{ psi}$$

Axial Compression Plus Hoop Compression ($\sigma_\phi > 0.5\ \sigma_\theta$)

$$\frac{\sigma_{\phi s} - 0.5\cdot\sigma_{heL}}{\sigma_{\phi eL} - 0.5\cdot\sigma_{heL}} + \left(\frac{\sigma_{\theta s}}{\sigma_{heL}}\right)^2 = 0.133 \qquad < 1.0$$

Axial Compression Plus Shear

$$\frac{\sigma_{\phi s}}{\sigma_{\phi eL}} + \left(\frac{\sigma_{\phi\theta s}}{\sigma_{\phi\theta eL}}\right)^2 = 0.061 \qquad < 1.0$$

Hoop Compression Plus Shear

$$\frac{|\sigma_{\theta s}|}{\sigma_{reL}} + \left(\frac{\sigma_{\phi\theta s}}{\sigma_{\phi\theta eL}}\right)^2 = 0.845 \qquad < 1.0$$

Axial Compression Plus Hoop Compression Plus Shear

The shear constant, K, is computed as follows

$$K := 1 - \left(\frac{\sigma_{\phi\theta s}}{\sigma_{\phi\theta eL}}\right)^2 \qquad K = 1$$

As a result of the shear stress equaling zero, the value of K equals one. Therefore, no further interaction checks are required for this combination of stresses.

Inelastic Buckling

$$\sigma_{\phi p} := \frac{\sigma_{\phi s}}{\eta_\phi} \qquad \sigma_{\phi p} = 1.44 \times 10^4 \text{ psi} \qquad \sigma_{\phi eL} = 2.362 \times 10^5 \text{ psi}$$

$$\sigma_{\theta p} := \frac{\sigma_{\theta s}}{\eta_\theta} \qquad \sigma_{\theta p} = 6.821 \times 10^3 \text{ psi}$$

$$\sigma_{\phi\theta p} := \frac{\sigma_{\phi\theta s}}{\eta_{\phi\theta}} \qquad \sigma_{\phi\theta p} = 0 \text{ psi}$$

Axial Compression Plus Shear

$$\left(\frac{\sigma_{\phi p}}{\sigma_{\phi eL}}\right)^2 + \left(\frac{\sigma_{\phi\theta p}}{\sigma_{\phi\theta eL}}\right)^2 = 3.714 \times 10^{-3} \qquad < 1.0$$

Hoop Compression Plus Shear

$$\left(\frac{\sigma_{\theta p}}{\sigma_{reL}}\right)^2 + \left(\frac{\sigma_{\phi\theta p}}{\sigma_{\phi\theta eL}}\right)^2 = 0.713 \qquad < 1.0$$

Conclusion

Analysis of the MPC confinement shell shows that the interaction equations for elastic and inelastic buckling are satisfied (less than 1.0). Therefore, stability of the inner shell is assured for load case 6.

3.H.5.4.4 Load Case 7 (Load Case E1.b in Table 3.1.4)

The external pressure is $p_{ext} := 40 \cdot psi$ $p_{ext} = 40\,psi$

The G level for Longitudinal Load is $G := 1 \cdot g$

The Factor of Safety for Design is $FS_D := FS_{LA}$ $FS_D = 2$

The Young's modulus and the yield strength are evaluated at (300°F), which bounds all MPC temperatures during the normal heat condition.

$E := 26.75 \cdot 10^6 \cdot psi$ Young's modulus (350 deg. F), Alloy X Table 3.3.1

$\sigma_y := 21600 \cdot psi$ Yield strength (350 deg. F) Alloy X Table 3.3.1

Stress components

The longitudinal membrane stress is the impact weight supported by the confinement shell divided by the cross sectional area of the shell.

$P := G \cdot \frac{W}{g}$ $P = 2 \times 10^4\,lbf$

$A := \pi \cdot \left(R_o^2 - R_i^2\right)$ $A = 106.618\,in^2$

$\sigma_\phi := \frac{P}{A} + p_{ext} \cdot \frac{R_i + R_o}{4 \cdot t}$ $\sigma_\phi = 1.545 \times 10^3\,psi$ Longitudinal stress

A circumferential membrane stress develops in the MPC confinement shell due to external pressure.

$\sigma_\theta := \frac{p_{ext} \cdot \left(R_i + R_o\right)}{2 \cdot t}$ $\sigma_\theta = 2.715 \times 10^3\,psi$ Circumferential stress

The shear stresses on the gross section of the inner shell are equal to zero.

$\sigma_{\phi\theta} := 0 \cdot psi$ In-plane shear stress

As an initial check, the amplified stress components must meet the allowable limits stated in Section 3.H.4.1 of the appendix.

$\frac{\sigma_\phi \cdot FS_D}{\sigma_y} = 0.143 < 1.0$ $\frac{|\sigma_\theta| \cdot FS_D}{\sigma_y} = 0.251 < 1.0$ $\frac{\sigma_{\phi\theta} \cdot FS_D}{\sigma_y} = 0 < 0.6$

Capacity reduction factors

$R := \frac{R_i + R_o}{2}$ $R = 33.938\,in$ Mean radius

The unsupported longitudinal and circumferential lengths are

$l_\phi := L$ $l_\phi = 188\,in$

$l_\theta := 2 \cdot \pi \cdot R$ $l_\theta = 213.236\,in$ No credit for stiffeners

M_i is a dimensionless factor defined as follows

$M_\phi := \frac{l_\phi}{(R \cdot t)^{0.5}}$ $M_\phi = 45.639$

$M_\theta := \frac{l_\theta}{(R \cdot t)^{0.5}}$ $M_\theta = 51.765$

$M := if(M_\phi < M_\theta, M_\phi, M_\theta)$ $M = 45.639$ M equals smaller of two values

The radius-to-thickness ratio is $\frac{R}{t} = 67.875$

Next, the capacity reduction factors are computed per Sec. 1511(a), (b), and (c) of Code Case N-284.

Axial Compression

Effect of R/t (R/t < 600)

$\alpha_1 := 1.52 - 0.473 \cdot \log\left(\frac{R}{t}\right)$ $\alpha_1 = 0.654$

$\alpha_2 := 1.0 \cdot 10^{-5} \cdot \frac{\sigma_y}{psi} - 0.033$ $\alpha_2 = 0.183$

$\alpha_{\phi L1} := if(\alpha_1 < \alpha_2, \alpha_1, \alpha_2)$ $\alpha_{\phi L1} = 0.183$ $\alpha_{\phi L1}$ equals smaller of two values

Effect of Length (M > 10)

$\alpha_{\phi L2} := .207$ $\alpha_{\phi L2} = 0.207$

$\alpha_{\phi L} := \text{if}(\alpha_{\phi L1} > \alpha_{\phi L2}, \alpha_{\phi L1}, \alpha_{\phi L2})$ $\alpha_{\phi L} = 0.207$ $\alpha_{\phi L}$ equals larger of two values

Hoop Compression

$\alpha_{\theta L} := 0.8$

Shear (R/t < 250)

$\alpha_{\phi\theta L} := 0.8$

Theoretical elastic buckling stresses

The basic equations used are given in Sec. 1712.1.1 of Code Case N-284.

Axial Compression $M_\phi = 45.639$

$C_\phi := .605$ $C_\phi = 0.605$

$\sigma_{\phi eL} := C_\phi \cdot \frac{E \cdot t}{R}$ $\sigma_{\phi eL} = 2.384 \times 10^5 \text{ psi}$

External Pressure $1.65 \cdot \frac{R}{t} = 111.994$

No End Pressure

$C_{\theta r} := \frac{.92}{M_\phi - 1.17}$ $C_{\theta r} = 0.021$

$\sigma_{reL} := C_{\theta r} \cdot \frac{E \cdot t}{R}$ $\sigma_{reL} = 8.154 \times 10^3 \text{ psi}$

End Pressure Included

$C_{\theta r} := \frac{.92}{M_\phi - .636}$ $C_{\theta h} = 0.052$

$\sigma_{heL} := C_{\theta h} \cdot \frac{E \cdot t}{R}$ $\sigma_{heL} = 2.041 \times 10^4 \text{ psi}$

Shear (26 < M_ϕ < 8.69 R/t)

$$C_{\phi\theta} := \frac{0.746}{M_\phi^{0.5}} \qquad C_{\phi\theta} = 0.11$$

$$\sigma_{\phi\theta eL} := C_{\phi\theta} \cdot \frac{E \cdot t}{R} \qquad \sigma_{\phi\theta eL} = 4.352 \times 10^4 \text{ psi}$$

Plasticity reduction factors

The plasticity reduction factors are calculated according to the equations provided by Sec. 1610(a), (b), and (c) of the Code Case.

Axial Compression

$$\eta_\phi := 1 \qquad \frac{\sigma_\phi \cdot FS_D}{\sigma_y} = 0.143 \quad < .55$$

Hoop Compression

$$\eta_\theta := 1.0 \qquad \left(\frac{|\sigma_\theta| \cdot FS_D}{\sigma_y} < 0.67 \right)$$

Shear

$$\eta_{\phi\theta} := 1.0 \qquad \left(\frac{\sigma_{\phi\theta} \cdot FS_D}{\sigma_y} < 0.48 \right)$$

Interaction equations

The interaction equations for local buckling are supplied in Sec. 1713 of Code Case N-284.

Elastic Buckling

$$\sigma_{\phi s} := \frac{\sigma_\phi \cdot FS_D}{\alpha_{\phi L}} \qquad \sigma_{\phi s} = 1.493 \times 10^4 \text{ psi}$$

$$\sigma_{\theta s} := \frac{\sigma_\theta \cdot FS_D}{\alpha_{\theta L}} \qquad \sigma_{\theta s} = 6.787 \times 10^3 \text{ psi} \quad < \quad \sigma_{heL} = 2.041 \times 10^4 \text{ psi}$$

$$\sigma_{\phi\theta s} := \frac{\sigma_{\phi\theta} \cdot FS_D}{\alpha_{\phi\theta L}} \qquad \sigma_{\phi\theta s} = 0 \text{ psi}$$

Axial Compression Plus Hoop Compression ($\sigma_{\phi s} > 0.5\ \sigma_{\theta s}$)

$$\frac{\sigma_{\phi s} - 0.5\cdot\sigma_{heL}}{\sigma_{\phi eL} - 0.5\cdot\sigma_{heL}} + \left(\frac{\sigma_{\theta s}}{\sigma_{heL}}\right)^2 = 0.131 \qquad < 1.0$$

Axial Compression Plus Shear

$$\frac{\sigma_{\phi s}}{\sigma_{\phi eL}} + \left(\frac{\sigma_{\phi\theta s}}{\sigma_{\phi\theta eL}}\right)^2 = 0.063 \qquad < 1.0$$

Hoop Compression Plus Shear

$$\frac{|\sigma_{\theta s}|}{\sigma_{reL}} + \left(\frac{\sigma_{\phi\theta s}}{\sigma_{\phi\theta eL}}\right)^2 = 0.832 \qquad < 1.0$$

Axial Compression Plus Hoop Compression Plus Shear

The shear constant, K, is computed as follows

$$K := 1 - \left(\frac{\sigma_{\phi\theta s}}{\sigma_{\phi\theta eL}}\right)^2 \qquad K = 1$$

As a result of the shear stress equaling zero, the value of K equals one. Therefore, no further interaction checks are required for this combination of stresses.

Inelastic Buckling

$\sigma_{\phi p} := \dfrac{\sigma_{\phi s}}{\eta_\phi}$ $\quad \sigma_{\phi p} = 1.493 \times 10^4\ \text{psi}$ $\quad \sigma_{\phi eL} = 2.384 \times 10^5\ \text{psi}$

$\sigma_{\theta p} := \dfrac{\sigma_{\theta s}}{\eta_\theta}$ $\quad \sigma_{\theta p} = 6.787 \times 10^3\ \text{psi}$

$\sigma_{\phi\theta p} := \dfrac{\sigma_{\phi\theta s}}{\eta_{\phi\theta}}$ $\quad \sigma_{\phi\theta p} = 0\ \text{psi}$

Axial Compression Plus Shear

$$\left(\frac{\sigma_{\phi p}}{\sigma_{\phi eL}}\right)^2 + \left(\frac{\sigma_{\phi\theta p}}{\sigma_{\phi\theta eL}}\right)^2 = 3.92 \times 10^{-3} \qquad < 1.0$$

Hoop Compression Plus Shear

$$\left(\frac{\sigma_{\theta p}}{\sigma_{reL}}\right)^2 + \left(\frac{\sigma_{\phi\theta p}}{\sigma_{\phi\theta eL}}\right)^2 = 0.693 \qquad < 1.0$$

Conclusion

Analysis of the MPC confinement shell shows that the interaction equations for elastic and inelastic buckling are satisfied (less than 1.0). Therefore, stability of the inner shell is assured for load case 7.

3.H.6 Conclusions

Three bounding load cases have been defined for the Overpack, and a corresponding set of four cases defined for the MPC. The characteristics of the load cases are that they combine a large mean axial stress with a high circumferential stress both of which extend over the entire vessel both axially and circumferentially.

Although some stiffening effect is expected from the basket support ribs, the effect of such stiffening on the MPC buckling is conservatively neglected.

All required safety margins are met for the load cases considered.

APPENDIX 3.I: STRUCTURAL QUALIFICATION OF MPC BASEPLATE

3.I.1 SCOPE

This appendix provides the structural qualification of the MPC baseplate for a bounding set of loadings. The results demonstrate that the baseplate thickness is adequately sized to insure satisfaction of stress intensity allowables.

3.I.2 Methodology

A stress analysis of the MPC baseplate and adjoining local regions of the MPC canister is carried out using a finite element model and the finite element code ANSYS [3.I.1]. The configuration is shown in Figure 3.I.1. Values extracted from the "raw" results of this finite element analysis are then used to form the final combined stresses.

3.I.3 References

[3.I.1] ANSYS 5.2, Ansys, Inc., 1995.

3.I.4 Acceptance Criteria

Loads are identified for Level A analyses and for Level D analyses. It is required that the following stress combinations be examined:

1. Primary Membrane Stress Intensity plus Primary Bending Stress Intensity

2. Primary Membrane Stress Intensity plus Primary Bending Stress Intensity plus Secondary Stress Intensity

The following allowable stress intensity values are used to calculate the margin of safety resulting from each loading condition. The values are obtained from Tables 3.1.15 and 3.1.16 for Levels A and D, respectively.

Level A

Primary Membrane Allowable, Sm_{am} = 18,700 psi

Primary Membrane and Bending Allowable, $Sm_{amb} = 1.5 \times Sm_{am}$ = 28,050 psi

Primary Membrane and Bending and Secondary Allowable, $Sm_{as} = 2 \times Sm_{amb}$ = 56,100 psi

Level D

Primary Membrane Allowable, $S_{dm} = 2.4\ S_{am} = 44{,}880$ psi

Primary Membrane and Bending Allowable, $Sm_{dmb} = 2.4 \times Sm_{amb} = 67{,}320$ psi

Primary Membrane and Bending Allowable (775F), S_m fire = 54,225 psi

3.I.5 Assumptions

1. The baseplate and the lower portion of the canister are modeled as plate and shell structures. The SHELL51 axisymmetric shell element is used.

2. All loadings are assumed to be applied in an axisymmetric manner.

3. Allowable strength values for Alloy X at 400 degrees F are used except for the fire evaluation.

4. The canister is included in the model only to the extent necessary to adequately capture secondary bending stress intensities in the analysis.

3.I.6 Input Load Data

3.I.6.1 Level A Loads

For the Level A condition, the following loadings must be accounted for:

Accident Pressure = (P_{ACC}) = 125 psi	Table 2.2.1
Design Internal Pressure (P) = 100 psi	Table 2.2.1
MPC Basket Weight (W_{basket}) = 13,000 lb	Table 3.2.4
MPC Baseplate Weight (W_{base}) = 3,000 lb	Table 3.2.4
Fuel Weight = 54,000 lb	Table 3.2.4

The total bounding lifted load is determined by summing the weights of the fuel, the basket, and the baseplate. Note that this value anticipates the potential scenario where a fully loaded MPC is lifted from the threaded connections on top of the MPC lid.

3.I.6.2 Level D Load

The only identified Level D load condition that could lead to significant stress in the MPC baseplate is a 60-g top end drop of a HI-STAR 100. The drop loading on the baseplate is the weight of the baseplate multiplied by 60.

Top End Drop Load (L_{drop}) = $W_{base} \times 60$ = 180,000 lb

3.I.7 Input Geometry

The pertinent geometric input values are obtained from the Design Drawings in Section 1.5.

Baseplate Thickness (t_{base}) = 2.5 in

Canister Thickness (t_{can}) = 0.5 in

Mean Radius to Canister Mid-Plane (R_{mean}) = $1/2 \times 68.375 - t_{can}/2$ = 33.9375 in

3.I.8 Analysis and Results

An axisymmetric finite element analysis is performed for three load cases. From the results of these evaluations, the stresses from all loads listed above can be either evaluated or bounded. The first evaluated load case applies a 60-g gravitational load to the baseplate. This gravitational load is not applied to the canister. The second load case applies a 125 psi external pressure to both the baseplate and the canister. The final load case applies a 1,000 lb ring load to the baseplate at a radius of 23 inches. This represents a "unit load" case which describes the basket-induced load on the baseplate. The results of these three finite element solutions are examined and are either amplified or attenuated to form (or bound) the required combinations.

3.I.8.1 Load Case E1 (Design Internal Pressure)

Based on the finite element analysis of the 125 psi external pressure load case, the stress intensity and corresponding margin of safety of the baseplate under the design internal pressure loading (P) can be determined. The maximum value of the combined membrane and bending stress intensities in the baseplate, obtained from the finite element analysis, is 26,427 psi. The corresponding combined stress intensity for the design internal pressure case can be determined by multiplying the calculated value by the ratio of the pressures.

$\sigma_{E1mb} = 26,427 \times P \div 125$ psi = 21,141.6 psi

The corresponding margin of safety is:

$$MS_{E1mb} = (Sm_{amb} \div \sigma_{E1mb}) - 1 = 0.326$$

The maximum value of the combined primary membrane, primary bending and secondary bending stress intensities in the canister, obtained from the finite element analysis, is 39,948 psi. This maximum value occurs near the baseplate-to-canister connection. Using the same method of multiplying the stress intensity by the pressure ratio, the stress intensity and margin of safety for this canister under design internal pressure can be determined as:

$$\sigma_{E1S} = 39{,}948 \times P \div 125 \text{ psi} = 31{,}958.4 \text{ psi}$$

$$MS_{E1S} = (Sm_{aS} \div \sigma_{E1S}) - 1 = 0.755$$

The primary membrane stress intensity in the canister under design internal pressure must be calculated if it is to be considered individually. This value is determined as:

$$\sigma_{E1m} = (P \times R_{mean} \div t_{can}) + P = 6{,}887.5 \text{ psi}$$

and the corresponding margin of safety is:

$$MS_{E1m} = (Sm_{am} \div \sigma_{E1m}) - 1 = 1.715$$

It should be noted that the margin of safety for all three of these stress intensities is greater than zero, as required.

3.I.8.2 Load Case E2 (Normal Handling)

This load condition consists of the design internal pressure combined with an effective pressure due to the weight of the fuel and baseplate and a ring load due to the MPC basket. Once again, the results of the three finite element evaluations are combined, with the use of appropriate multipliers, to obtain the desired stress results.

The load supported by the baseplate as a distributed load is the weight of the fuel plus the weight of the baseplate. If a dynamic load factor of 1.15 (based on the Crane Manufacturer's Association of America Standard (CMAA #70) for a low-speed lift) is applied to this value, it then increases to:

$$W_{dyn} = (W_{fuel} + W_{base}) \times 1.15 = 65{,}550 \text{ lb}$$

The finite element solution for the first load case (60-g gravitational loading on a baseplate of weight of 2,662 lb) gives a total support reaction load of 157,394 lb from the amplified gravitational load. An effective gravitational multiplier can be determined by calculating the ratio of W_{dyn} to the support reaction load.

$g_{eff} = W_{dyn} \div 157{,}394 \text{ lb} = 0.416$ (geff allows finite element results to be ratioed for the case considered here)

The maximum stress intensity produced by the 1,000 lb ring load is 49.5 psi (this can be used with the proper multiplier to evaluate the case here). From the results of the finite element analyses we again determine the stress intensity and resulting margin of safety in the baseplate using the attenuation method. The maximum combined baseplate membrane and bending stress intensity is determined from the finite element analysis of the 60-g gravitational load as 9,375 psi. The corresponding maximum stress intensity from the finite element analysis of the external pressure case is 26,552 psi. The maximum combined primary membrane and primary bending stress intensity and the resultant margin of safety of the baseplate, under the design internal pressure and dynamic lift weight, are determined as:

$$\sigma_{E2mb} = 9{,}375\text{psi} \times g_{eff} + 26{,}427\text{psi} \times P \div 125\text{psi} + 49.5\text{psi} \times \frac{1.15 W_{basket}}{1{,}000\text{lb}} = 25{,}781\text{psi}$$

$MS_{E2mb} = (Sm_{amb} \div \sigma_{E2mb}) - 1 = 0.088$

Similarly, the finite-element analysis results give the maximum stress intensities in the canister, for the combination of primary membrane and primary bending, for the 60-g load, the external pressure load and the ring load, as 12,299 psi, 39,948 psi, and 84 psi, respectively. Again using the appropriate attenuation factors, the maximum canister stress intensity and resultant margin of safety are:

$$\sigma_{E2S} = 12{,}299\text{psi} \times g_{eff} + 39{,}948\text{psi} \times P \div 125\text{psi} + 84\text{psi} \times \frac{1.15 W_{basket}}{1{,}000\text{lb}} = 38{,}331\text{psi}$$

$MS_{E2S} = (Sm_{as} \div \sigma_{E2S}) - 1 = 0.46$

3.I.8.3 Load Case E3 (drop events)

The limiting Level D loading condition for the baseplate is a postulated end drop condition. In the storage mode the MPC baseplate will not experience loadings in a credible end drop because the MPC baseplate will be supported by the overpack baseplate. In the transport mode, however, a top end drop of the HI-STAR 100 System is a credible postulated accident. For this case, the baseplate must meet Level D structural design requirements under the amplified g loading acting on the baseplate weight together with the mandated surface pressure.

The two finite element solutions correspond to the 60-g drop loading and the accident design internal pressure of 125 psi, respectively. Therefore, no attenuation multipliers are used to form the desired stress intensity combinations.

Using the results of the finite element analyses, the combined stress intensity at the center of the baseplate from the applied g-loading and pressure is:

$$\sigma_{E3mb} = 9{,}375 \text{ psi} + 26{,}552 \text{ psi} = 35{,}927 \text{ psi}$$

and the resultant margin of safety is therefore:

$$MS_{E3mb} = (Sm_{dmb} \div \sigma_{E3mb}) - 1 = 0.874$$

The combined stress intensity in the canister from the applied g-loading and pressure is:

$$\sigma_{E3S} = 12{,}299 \text{ psi} + 39{,}948 \text{ psi} = 52{,}247 \text{ psi}$$

Note that the secondary stress intensity due to the discontinuity at the baseplate-to-canister joint has been included in this combination, even though such inclusion is not required for a Level D condition. Therefore, the margin of safety is conservatively computed at this location as:

$$MS_{E3S} = (Sm_{Edmb} \div \sigma_{E3S}) - 1 = 0.288$$

3.I.8.4 Load Case E5 (Fire Accident)

During a fire the MPC baseplate is assumed to be subjected to the fire pressure, dead load, and fire temperature. The stress results reported for normal handling can be used to find the stress by eliminating the 1.15 load factor.

$$\sigma_{E5} = \frac{9{,}375\text{psi} \times g_{eff}}{1.15} + 26{,}427\text{psi} \times \frac{P_{ACC}}{125\text{psi}} + 49.5\text{psi} \times \frac{W_{basket}}{1{,}000\text{lb}} = 30{,}461\text{psi}$$

$$MS_{E5} = \left(\frac{Sm_{fire}}{\sigma_{E5}}\right) - 1 = 0.78$$

3.I.9 Conclusion

Safety margins for all defined Design, limiting Level A and limiting Level D loading conditions have safety margins greater than zero, as required.

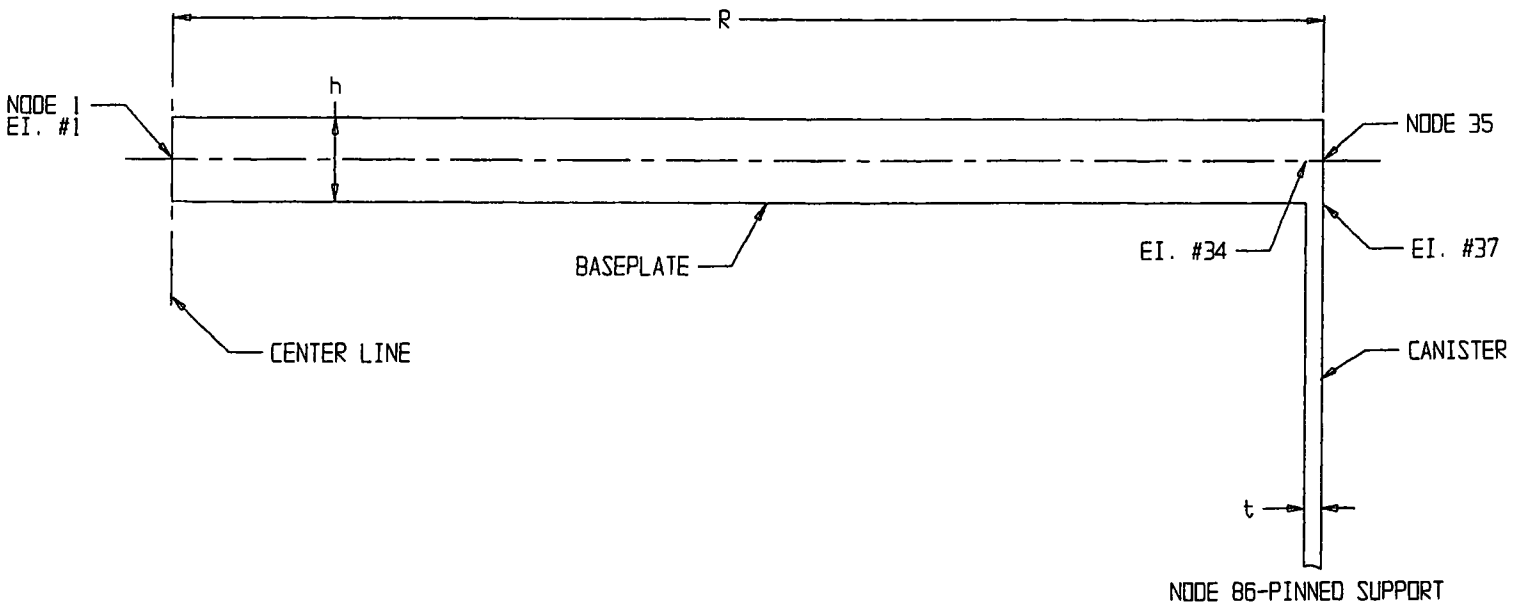

FIGURE 3.I.1; FINITE ELEMENT MODEL

APPENDIX 3.J

FUEL SUPPORT SPACER STRENGTH EVALUATIONS

3.J.1 Fuel Spacer Strength Analysis

The upper and lower fuel spacers are illustrated in the design drawings with lengths specified in Tables 2.1.9 and 2.1.10. The following calculations are presented to show that the spacer designs are structurally adequate for their intended function under the design loadings. The spacers are not required to be designed in accordance with ASME Code, Section III, Subsection NG; however, the Subsection NG stress limits are conservatively applied.

The fuel spacers must maintain the axial position of the fuel assembly during normal, off-normal, and accident loading conditions. The maximum fuel assembly weights are taken from Table 2.1.6 as:

PWR assembly	1680 lbs.
BWR assembly	700 lbs.

The fuel spacers are manufactured from Alloy X. The normal, off-normal, and accident design temperature is 725°F. The normal and off-normal loading condition is simply the maximum weight of the fuel assembly multiplied by a deceleration factor of 10g's. The accident loading is the inertia loading corresponding to an axial fuel assembly deceleration of 60g's, which would accompany the design basis cask drop.

The fuel spacers are shown to meet ASME Code Subsection NG stress limits for normal and off-normal loads. For the accident condition loading, it is necessary to show that:

a. The maximum axial load induced in the spacer is less than the elastic buckling load.

b. The axial stress in the smallest section under the maximum axial load in the spacer is less than the Subsection NG stress limit for accident loads.

The above criteria, (a) and (b), shall be referred to as the "stability" and "strength" compliance, respectively.

3.J.2 Normal and Off-Normal Loading Condition

ASME Code Subsection NG, Article NG-3133.6 lists the maximum allowable compressive stress for cylinders as the lesser of the values for the stress intensity, S_m, at the design temperature or the factor B.

The normal and off-normal loads are the following, where W_{PWR} = 1680 lb., H (deceleration factor) = 10, and W_{BWR} = 700 lb.

$F_{PWR} = W_{PWR} H$ and $F_{BWR} = W_{BWR} H$

F_{PWR} = 16,800 lb. F_{BWR} = 7,000 lb.

The MPC fuel spacers are depicted in the Design Drawings of Section 1.5. The cross sectional area of the PWR and BWR fuel spacers are as follows:

$^{\dagger}AL_{p\ell} = 6^2 - 5.5^2 - 4(2.75)(1/4) = 3.0 \text{ in}^2$

$AL_{b\ell} = 4^2 - 3.5^2 - 4(2.5)(1/4) = 1.25 \text{ in}^2$

$AL_{pu} = AL_{bu} = \pi (1.75^2 - 1.45^2) = 3.016 \text{ in}^2$

Using the fuel spacer with the smallest area, the maximum axial load which a spacer can withstand without exceeding the NG Level A limit, listed in Table 2.1.18, for axial stress is

BWR or PWR: $F_{max} = AL_{b\ell} S_m = (1.25 \text{ in}^2)(15.4 \text{ ksi}) = 19{,}250$ lb.

Comparison of the load with the allowable follows:

PWR	BWR
F_{PWR} = 16,800 lb.	F_{BWR} = 7,000 lb.
F_{max} = 19,250 lb.	F_{max} = 19,250 lb.
$F_{PWR} < F_{max}$	$F_{BWR} < F_{max}$

Therefore, the normal and off-normal loads do not exceed the values for S_m at design temperatures.

---

† Subscripts p and b refer to PWR and BWR cases, respectively. Second subscript u or ℓ indicates upper and lower fuel spacer, respectively.

The factor B is determined in accordance with Article NG-3133.6, as follows.

An equivalent thin walled cylinder is determined for the lower fuel spacer by using equivalent moments of inertia. S_o equals the outer side length, S_i equals the inner side length of the lower fuel spacer square tube, t is the wall thickness, and c is the width of the flow hole at the bottom of the fuel spacer.

$$I_{p\ell} = \frac{1}{12}(S_o^4 - S_i^4) - 2[\frac{1}{12}tc^3 + \frac{1}{12}ct^3 + ct(\frac{S_o - t}{2})^2]$$

$$I_{p\ell} = \frac{1}{12}(6^4 - 5.5^4) - 2[\frac{1}{12}(0.25)(2.75)^3 + \frac{1}{12}(2.75)(0.25)^3 + (2.75)(0.25)(2.875)^2]$$

$$I_{p\ell} = 19.50\ in^4$$

$$I_{b\ell} = \frac{1}{12}(S_o^4 - S_i^4) - 2[\frac{1}{12}tc^3 + \frac{1}{12}ct^3 + ct(\frac{S_o - t}{2})^2]$$

$$I_{b\ell} = \frac{1}{12}(4^4 - 3.5^4) - 2[\frac{1}{12}(0.25)(2.5)^3 + \frac{1}{12}(2.5)(0.25)^3 + 2.5(0.25)(1.875)^2]$$

$$I_{b\ell} = 3.8\ in^4$$

Equivalent Thin Walled Cylinder

$$Equiv.\ I_{p\ell} = \frac{\pi}{4}(R_o^4 - R_i^4) = 19.50\ in^4$$

$$Equiv.\ I_{b\ell} = \frac{\pi}{4}(R_o^4 - R_i^4) = 3.8\ in^4$$

Assume t = 0.25, the thickness of the square tube in the PWR and BWR lower fuel spacer, yields

$$R_o = R_i + 0.25 \ in.$$

$$Equiv.\ R_{p\ell} = R_o = 3.041 \ in.$$

$$Equiv.\ R_{b\ell} = R_o = 1.813 \ in.$$

$$R_{pu} = R_{bu} = 1.75 \ in.$$

Article NG-3133.6 states the following, where T = the thickness and R = the inner radius (R_i).

$$A1 = \frac{0.125}{(R/T)}$$

Using the inner radius for the equivalent thin walled cylinder and the inner radius of the upper fuel spacer, yields

$A1_{p\ell} = 0.0112$ $A1_{pu} = A_{bu} = 0.0259$
$A1_{b\ell} = 0.0200$

Using the value A with Figures HA-1 and HA-2 on page 628 of Part D, ASME Section II, the value B is determined to be the following (the lower value from the two figures is utilized):

$B_{p\ell} = 8{,}100$ $B_{pu} = B_{bu} = 8{,}500$
$B_{b\ell} = 8{,}400$

The area as calculated earlier is:

$AL_{P\ell} = 3.0\ in^2$
$AL_{b\ell} = 1.25\ in^2$
$AL_{pu} = AL_{bu} = 3.016\ in^2$

The compressive stress is the following:

$S_{p\ell} = F_{PWR}/AL_{p\ell} = 16{,}800/3.0 = 5{,}600$ psi
$S_{b\ell} = F_{BWR}/AL_{b\ell} = 7{,}000/1.25 = 5{,}600$ psi
$S_{pu} = F_{PWR}/AL_{pu} = 16{,}800/3.016 = 5{,}570$ psi
$S_{bu} = F_{BWR}/AL_{bu} = 7{,}000/3.016 = 2{,}321$ psi

The maximum compressive stress of the fuel spacers, S_{pu}, is less than the minimum B value, $B_{p\ell}$. Therefore, the fuel spacers meet the B value allowables of Article NG-3133.6 for the normal and off-normal conditions.

3.J.3 Accident Loading Condition

Table 3.3.1 provides the following properties for the Alloy X material, required for our computations.

Young's Modulus, E @ 725°F = 24.625 x 10^6 psi
Ultimate Strength, S_u @ 725°F = 62,350 psi

Other properties, namely net minimum cross sectional area and moment of inertia, are calculated as follows:

$AL_{p\ell} = 6^2 - 5.5^2 - 4(2.75)(1/4) = 3.0$ in^2

$$\text{Moment of Inertia, } I_p = \frac{1}{12}(h_o^4 - h_i^4) - 2[\frac{1}{12}tc^3 + \frac{1}{12}ct^3 + ct(\frac{h_o - t}{2})^2]$$

where h_o and h_i are outside and inside side dimensions of the square tubes, t is the wall thickness, and c is the width of the flow hole at the bottom of the fuel spacer.

or
$$I_{p\ell} = \frac{1}{12}(6^4 - 5.5^4) - 2[\frac{1}{12}(0.25)(2.75)^3 + \ldots \frac{1}{12}(2.75)(0.25)^3 + (2.75)(0.25)(2.875)^2]$$

or
$$I_{p\ell} = 19.50\ in^4$$

The corresponding data for the BWR lower fuel spacer is 4 inch square tube, 1/4 inch wall with a 2.5 inch wide cutout, $I_{b\ell} = 3.8$ in^4, $AL_{b\ell} = 1.25$ in^2

The upper spacer for both PWRs and BWRs is 3 inch Sch. 80 pipe (3.5 inch O.D. x 0.3 inch wall):

$AL_{pu} = AL_{bu} = 3.016$ in^2

Moment of inertia, $I_{pu} = I_{bu} = 3.9$ in^4

Strength Compliance

The minimum area, A_{min}, for the spacers is 1.25 in^2 for the BWR lower fuel spacer. The maximum axial load which a spacer of this net area can withstand without exceeding the NG Level D limit for axial stress is

BWR: $F_{max} = (1.25 \text{ in}^2)\ (36{,}950 \text{ psi})$
$F_{max} = 46{,}188$ lb.

PWR: $F_{max} = (3.00 \text{ in}^2)\ (36{,}950 \text{ psi})$
$F_{max} = 110{,}850$ lb.

Let W_{max} be the maximum fuel assembly weight, then at 60 g's

$$W_{max} = \frac{F_{max}}{60}$$

BWR: $W_{max} = 46{,}188/60 = 770$

PWR: $W_{max} = 110{,}850/60 = 1848$

As can be seen from Table 2.1.6, all fuel assemblies weigh less than the W_{max}.

Stability Compliance

The critical buckling load for the spacers is computed using the classical Euler formula for slender columns (see, for example, Seely F.B. and Smith J.D., "Advanced Mechanics of Materials", Wiley (1965), p. 587).

$$F_{cr} = \frac{\pi^2 E I}{\ell^2}$$

where

E: Young's Modulus of the spacer material at temperature (725°F)
I: Planar moment of inertia

Referring to Tables 2.1.9 and 2.1.10, the maximum upper fuel spacer length is 40.5 inches. Therefore, using the longest spacer length to obtain the lowest critical load, we have

$$F_{cr} = \frac{(\pi^2)\ (24.625 \times 10^6)\ (3.9)}{40.5^2}$$

or

$$F_{cr} = 5.77 \times 10^5\ lb.$$

Allowable fuel weight W_{max} is again given by (for 60g axial inertial deceleration)

$$W_{max} = \frac{F_{cr}}{60}$$

or

$$W_{max} = 9{,}616\ lb.$$

This weight bounds all PWR and BWR assemblies, even allowing for a factor of safety of 1.5.

Referring to Table 2.1.9, the maximum length of the lower spacer for PWR fuel is 20.25" (ℓ = 20.25").

The critical load is given by

$$F_{cr} = \frac{\pi^2\ E\ I_{P\ell}}{\ell^2} = \frac{(\pi^2)\ (24.625 \times 10^6)\ (19.50)}{20.25^2}$$
$$= 1.16 \times 10^7$$

The maximum allowable fuel assembly weight for 60g deceleration is, therefore,

$$W_{max} = 1.16 \times 10^7/60$$
$$= 193{,}333\ lb.$$

W_{max} bounds all PWR fuel assemblies, even allowing for a large safety margin.

Finally, the critical load for lower fuel spacer is computed using the Euler formula, ℓ = 40.5" (maximum length from Table 2.1.10)

$$F_{cr} = \frac{(\pi^2)\ (24.625 \times 10^6)\ (3.8)}{40.5^2}$$
$$= 5.63 \times 10^5\ lb.$$

Therefore

$$W_{max} = \frac{5.63 \times 10^5}{60} = 9{,}383\ lb.$$

W_{max} bounds all BWR fuel assembly weights.

Therefore, it is concluded that the upper and lower fuel spacers have sufficient axial strength to withstand the axial inertia loads without suffering plastic collapse or elastic instability.

3.J.4 Analysis of Upper Spacer End Plate for PWR Spacers

Some PWR fuel types are not supportable by the current upper spacer design having a simple pipe extension. To insure that all PWR fuel types are captured, an end plate having sufficient diameter is welded to the end of the pipe to extend the contact area. This section of the appendix addresses the stress analysis of the end plate to insure that it performs as desired under a handling accident that results in a direct impact of the fuel assembly onto the end plate. The configuration is shown below:

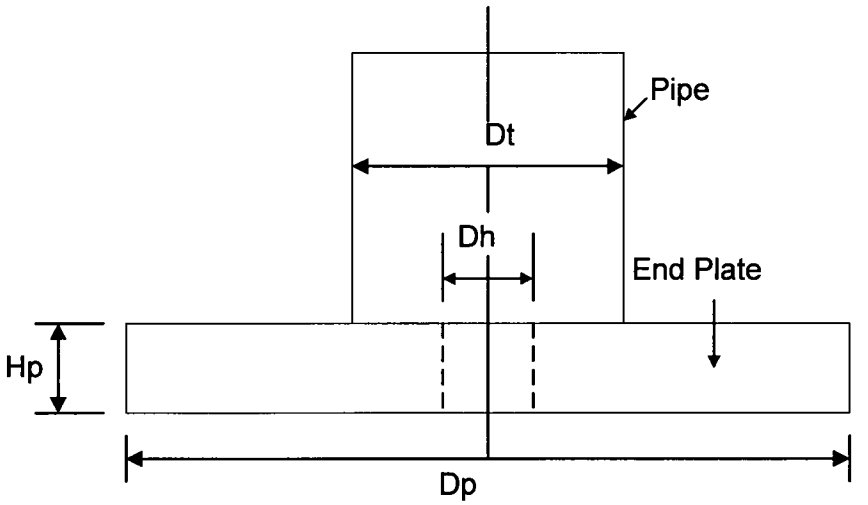

The dimensions are:(note that outer adius is taken equal to inside radius of limiting fuel assembly contact circle

$Hp := 0.75 \cdot in$ $Dp := 4.1 \cdot in$ $Dt := 3.5 \cdot in$ $Dh := 1 \cdot in$

Under the postulated handling accident, the total applied load is (design basis deceleration of 60 g's):

$P := 60 \cdot 1680 \cdot lbf$ $P = 1.008 \times 10^5\ lbf$

This load may be applied as a line load around the outer periphery

$$q_o := \frac{P}{\pi \cdot Dp} \qquad q_o = 7.826 \times 10^3 \frac{lbf}{in}$$

or it may be applied as a line load at a diameter of 1.8" (from a survey of fuel assembly types)

$$q_i := \frac{P}{\pi \cdot 1.8 \cdot in} \qquad q_i = 1.783 \times 10^4 \frac{lbf}{in}$$

In either case, the shear load at the pipe connection is approximately

$$q_p := \frac{P}{\pi \cdot Dt} \qquad q_p = 9.167 \times 10^3 \frac{lbf}{in}$$

At the design temperature, the ultimate strength is, (conservatively neglect any increase in ultimate strength due to strain rate effects

$$S_u := 62350 \cdot psi$$

The spacer pipe has been designed to NG, Level D requirements for axial strength and to the appropriate ASME Code requirements for gross stability. The function of the end plate is to insure that the fuel assembly impacts the spacer; the only requirement is that under an accident condition, no permanent deformation of this end plate occurs to the extent that the positioning limits of the fuel assembly is compromised. This is insured if we demonstrate that the ultimate shear capacity of the added end plate and the ultimate moment capacity of the end plate is not exceeded during the impact. Satisfaction of these stress limits will insure that no large axial movement of the assembly can occur because of the impact.

The ultimate shear capacity of the section is taken as 0.577Su, and the ultimate moment capacity is calculated assuming perfectly plastic behavior at the ultimate stress. Therefore, at any section of the plate the shear capacity is:

$$q_{cap} := .577 \cdot S_u \cdot Hp \qquad q_{cap} = 2.698 \times 10^4 \frac{lbf}{in}$$

Comparison of this limit with the peripheral shear loads computed previously demonstrates that the end plate will not experience a gross shear failure at any section. The minimum safety factor "SF" is

$$\frac{q_{cap}}{q_i} = 1.514$$

The ultimate moment capacity is (assume rectangular distribution throuh the thickness):

$$M_u := S_u \cdot \frac{Hp^2}{4} \qquad M_u = 8.768 \times 10^3 \, in \cdot \frac{lbf}{in}$$

The weight of the added end plate is:

$$Weight := 0.29 \cdot \frac{lbf}{in^3} \cdot \frac{\pi}{4} \cdot Hp \cdot \left(Dp^2 - Dh^2\right) \qquad Weight = 2.701 \, lbf$$

The following calculations are performed to establish the maximum bending moment in the end plate based on the two extreme locations of impact load. The electronic version of Roark's Handbook (6th Edition) that is a Mathcad add-on, is used for this computation. Mathcad 2000 is used for this section of Appendix 3.J.

Table 24 Formulas for shear, moment and deflection of flat circular plates of constant thickness

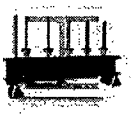

Cases 1a - 1d Annular Plate With Uniform Annular Line Load w at Radius r_0; Outer Edge Simply Supported

---

This file corresponds to Cases 1a - 1d in *Roark's Formulas for Stress and Strain.*

Annular plate with a uniform annular line load w at a radius r_o

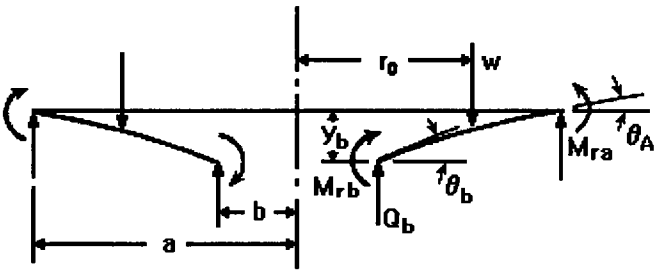

Outer edge simply supported, inner edge free

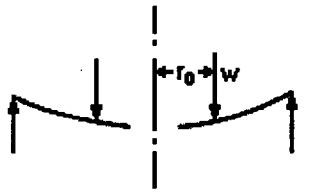

Outer edge simply supported, inner edge guided

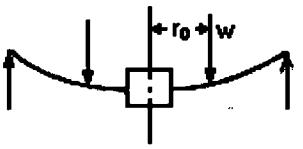

Outer edge simply supported, inner edge simply supported

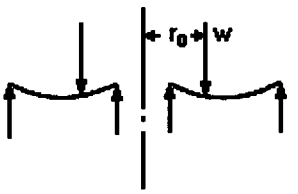

Outer edge simply supported, inner edge fixed

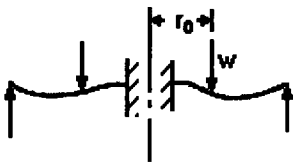

CASE 1A applies to the impact load at the outer periphery. The pipe diameter is the applied load location

Enter dimensions, properties and loading

Plate dimensions:

thickness: $t \equiv 0.75 \cdot in$

outer radius: $a \equiv 2.05 \cdot in$

inner radius: $b \equiv 0.5 \cdot in$

Applied unit load: $w \equiv 9167. \cdot \frac{lbf}{in}$

Modulus of elasticity: $E \equiv 24.625 \cdot 10^6 \cdot \frac{lbf}{in^2}$

Poisson's ratio: $\nu \equiv 0.3$

Radial location of applied load: $r_o \equiv .5 \cdot 3.5 \cdot in$

Constants

Shear modulus: $G \equiv \frac{E}{2 \cdot (1 + \nu)}$

D is a plate constant used in determining boundary values; it is also used in the general equations for deflection, slope, moment and shear. K_{sb} and K_{sro} are tangential shear constants used in determining the deflection due to shear:

$$D \equiv \frac{E \cdot t^3}{12 \cdot (1 - \nu^2)} \qquad D = 9.513 \times 10^5 \, lbf \cdot in$$

$$K_{sro} \equiv -1.2 \cdot \frac{r_o}{a} \cdot \ln\left(\frac{a}{r_o}\right) \qquad K_{sb} \equiv K_{sro}$$

General formulas and graphs for deflection, slope, moment, shear and stress as a function of r

Define r, the range of the radius and i, the vector index:

$r \equiv b, 1.1 \cdot b .. a$ $\quad$ $i \equiv 0 .. 3$

Deflection

$$y(r,i) := y_{b_i} + \theta_{b_i} \cdot r \cdot F_1(r) + M_{rb_i} \cdot \frac{r^2}{D} \cdot F_2(r) + Q_{b_i} \cdot \frac{r^3}{D} \cdot F_3(r) - w \cdot \frac{r^3}{D} \cdot G_3(r)$$

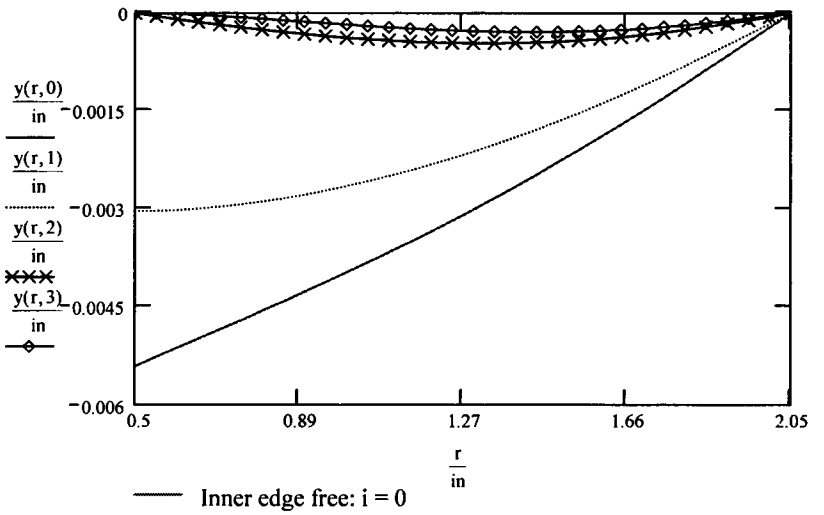

Slope

$$\theta(r,i) := \theta_{b_i}\cdot F_4(r) + M_{rb_i}\cdot\frac{r}{D}\cdot F_5(r) + Q_{b_i}\cdot\frac{r^2}{D}\cdot F_6(r) - w\cdot\frac{r^2}{D}\cdot G_6(r)$$

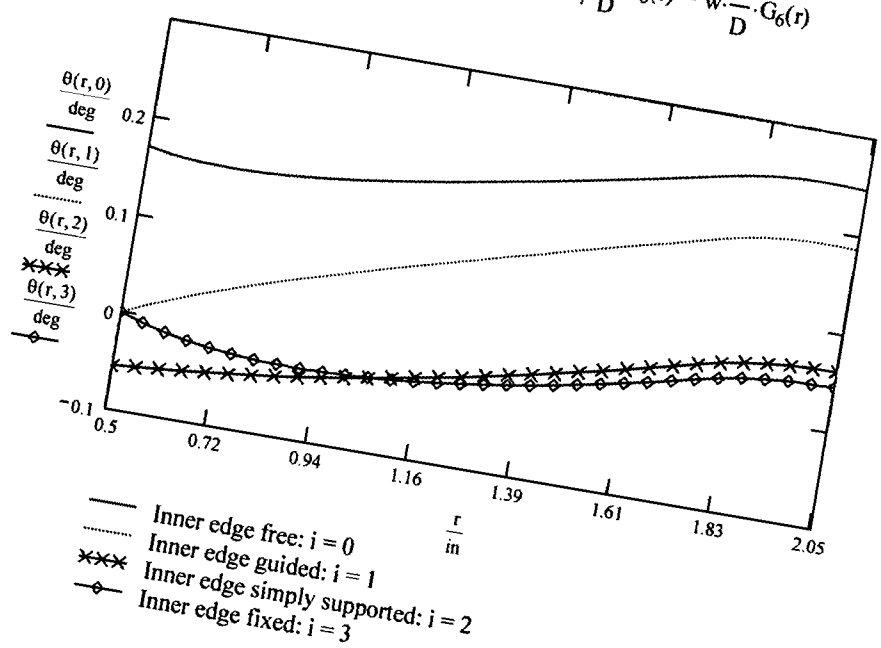

Radial moment $M_r(r,i) := \theta_{b_i} \cdot \frac{D}{r} \cdot F_7(r) + M_{rb_i} \cdot F_8(r) + Q_{b_i} \cdot r \cdot F_9(r) - w \cdot r \cdot G_9(r)$

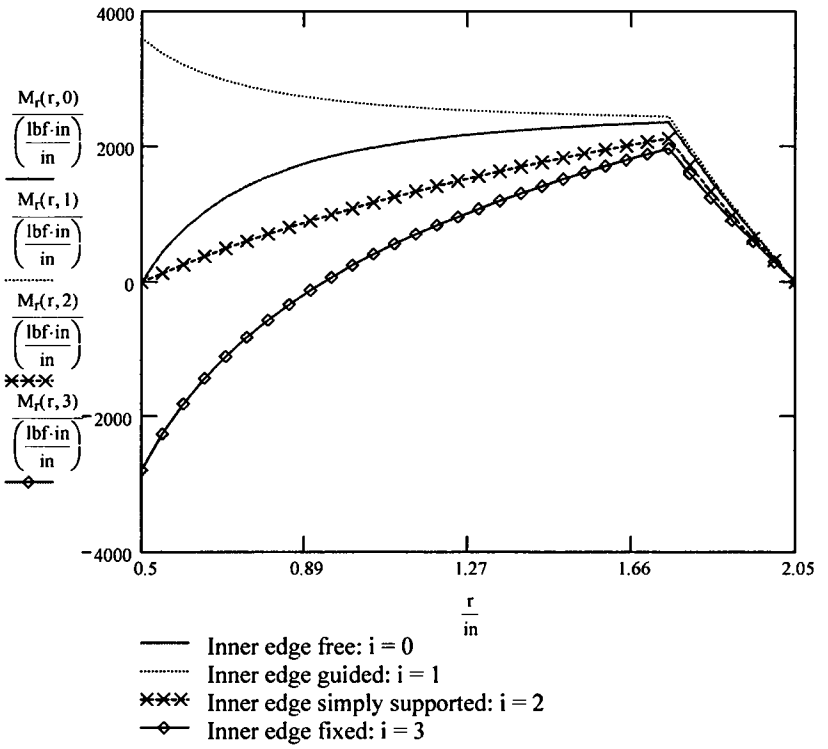

The following values are listed in order of inner edge:

- **free (i = 0)**
- **guided (i = 1)**
- **simply supported (i = 2)**
- **fixed (i = 3)**

Moment at points b and a (inner and outer radius):

$$\frac{M_{rb}}{\left(\frac{lbf \cdot in}{in}\right)} = \begin{pmatrix} 0 \\ 3.595 \times 10^3 \\ 0 \\ -2.798 \times 10^3 \end{pmatrix} \quad \frac{M_{ra}}{\left(\frac{lbf \cdot in}{in}\right)} = \begin{pmatrix} 0 \\ 0 \\ 0 \\ 0 \end{pmatrix}$$

Maximum radial moment (magnitude):

$$Mr_{(r-b)\cdot\frac{100}{in},i} := M_r(r,i) \qquad A_{mr_i} := \max\left(Mr^{\langle i \rangle}\right) \qquad B_{mr_i} := \min\left(Mr^{\langle i \rangle}\right)$$

$$Mr_{max_i} := \left(A_{mr_i} > -B_{mr_i}\right)\cdot A_{mr_i} + \left(A_{mr_i} \le -B_{mr_i}\right)\cdot B_{mr_i}$$

$$\frac{Mr_{max}}{\left(\frac{lbf \cdot in}{in}\right)} = \begin{pmatrix} 2.355 \times 10^3 \\ 3.595 \times 10^3 \\ 2.115 \times 10^3 \\ -2.798 \times 10^3 \end{pmatrix}$$

Transverse moment

$$M_t(r,i) := \frac{\theta(r,i)\cdot D\cdot\left(1-\nu^2\right)}{r} + \nu\cdot M_r(r,i)$$

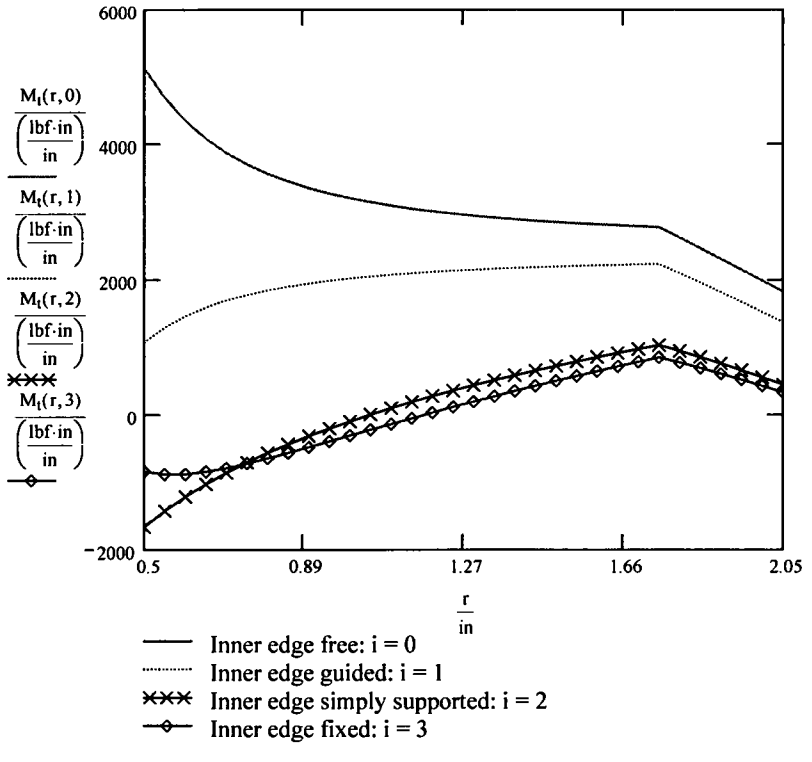

The following values are listed in order of inner edge:

- **free (i = 0)**
- **guided (i = 1)**
- **simply supported (i = 2)**
- **fixed (i = 3)**

Transverse moment at points b and a (inner and outer radius) due to bending:

$$\frac{M_t(b,i)}{\left(\frac{lbf\cdot in}{in}\right)} =$$

$5.128\cdot10^3$
$1.078\cdot10^3$
$-1.661\cdot10^3$
-839.265

$$\frac{M_t(a,i)}{\left(\frac{lbf\cdot in}{in}\right)} =$$

$1.828\cdot10^3$
$1.373\cdot10^3$
452.798
334.706

Maximum tangential moment (magnitude):

$$Mt_{(r-b)\cdot\frac{100}{in},i} := M_t(r,i) \qquad A_{mt_i} := \max\left(Mt^{\langle i\rangle}\right) \qquad B_{mt_i} := \min\left(Mt^{\langle i\rangle}\right)$$

$$Mt_{max_i} := \left(A_{mt_i} > -B_{mt_i}\right)\cdot A_{mt_i} + \left(A_{mt_i} \le -B_{mt_i}\right)\cdot B_{mt_i}$$

$$\frac{Mt_{max}}{\frac{lbf\cdot in}{in}} = \begin{pmatrix} 5.128\times10^3 \\ 2.234\times10^3 \\ -1.661\times10^3 \\ -884.013 \end{pmatrix} \qquad SF := \frac{M_u}{5128\cdot lbf} \qquad SF = 1.71$$

The remainder of the document displays the general plate functions and constants used in the equations above.

$$C_1 \equiv \frac{1+\nu}{2}\cdot\frac{b}{a}\cdot\ln\left(\frac{a}{b}\right)+\frac{1-\nu}{4}\cdot\left(\frac{a}{b}-\frac{b}{a}\right)$$

$$C_2 \equiv \frac{1}{4}\cdot\left[1-\left(\frac{b}{a}\right)^2\cdot\left(1+2\cdot\ln\left(\frac{a}{b}\right)\right)\right]$$

$$C_3 \equiv \frac{b}{4\cdot a}\cdot\left[\left[\left(\frac{b}{a}\right)^2+1\right]\cdot\ln\left(\frac{a}{b}\right)+\left(\frac{b}{a}\right)^2-1\right]$$

$$C_4 \equiv \frac{1}{2}\cdot\left[(1+\nu)\cdot\frac{b}{a}+(1-\nu)\cdot\frac{a}{b}\right]$$

$$C_5 \equiv \frac{1}{2}\cdot\left[1-\left(\frac{b}{a}\right)^2\right]$$

$$C_6 \equiv \frac{b}{4\cdot a}\cdot\left[\left(\frac{b}{a}\right)^2-1+2\cdot\ln\left(\frac{a}{b}\right)\right]$$

$$C_7 \equiv \frac{1}{2}\cdot\left(1-\nu^2\right)\cdot\left(\frac{a}{b}-\frac{b}{a}\right)$$

$$C_8 \equiv \frac{1}{2}\cdot\left[1+\nu+(1-\nu)\cdot\left(\frac{b}{a}\right)^2\right]$$

$$C_9 \equiv \frac{b}{a}\cdot\left[\frac{1+\nu}{2}\cdot\ln\left(\frac{a}{b}\right)+\left(\frac{1-\nu}{4}\right)\cdot\left[1-\left(\frac{b}{a}\right)^2\right]\right]$$

$$L_3 \equiv \frac{r_o}{4\cdot a}\cdot\left[\left[\left(\frac{r_o}{a}\right)^2+1\right]\cdot\ln\left(\frac{a}{r_o}\right)+\left(\frac{r_o}{a}\right)^2-1\right]$$

$$L_6 \equiv \frac{r_o}{4\cdot a}\cdot\left[\left(\frac{r_o}{a}\right)^2-1+2\cdot\ln\left(\frac{a}{r_o}\right)\right]$$

$$L_9 \equiv \frac{r_o}{a}\cdot\left[\frac{1+\nu}{2}\cdot\ln\left(\frac{a}{r_o}\right)+\frac{1-\nu}{4}\cdot\left[1-\left(\frac{r_o}{a}\right)^2\right]\right]$$

Boundary values due to bending:

At the inner edge of the plate:

$$Q_b \equiv \begin{bmatrix} 0 \cdot \frac{lbf}{in} \\ 0 \cdot \frac{lbf}{in} \\ w \cdot \left(\frac{C_1 \cdot L_9 - C_7 \cdot L_3}{C_1 \cdot C_9 - C_3 \cdot C_7} \right) \\ w \cdot \left(\frac{C_2 \cdot L_9 - C_8 \cdot L_3}{C_2 \cdot C_9 - C_3 \cdot C_8} \right) \end{bmatrix} \qquad M_{rb} \equiv \begin{bmatrix} 0 \cdot \frac{lbf \cdot in}{in} \\ \frac{w \cdot a}{C_8} \cdot L_9 \\ 0 \cdot \frac{lbf \cdot in}{in} \\ -w \cdot a \cdot \left(\frac{C_3 \cdot L_9 - C_9 \cdot L_3}{C_2 \cdot C_9 - C_3 \cdot C_8} \right) \end{bmatrix}$$

$$y_b \equiv \begin{bmatrix} \frac{-w \cdot a^3}{D} \cdot \left(\frac{C_1 \cdot L_9}{C_7} - L_3 \right) \\ \frac{-w \cdot a^3}{D} \cdot \left(\frac{C_2 \cdot L_9}{C_8} - L_3 \right) \\ 0 \cdot in \\ 0 \cdot in \end{bmatrix} \qquad \theta_b \equiv \begin{bmatrix} \frac{w \cdot a^2}{D \cdot C_7} \cdot L_9 \\ 0 \cdot deg \\ \frac{-w \cdot a^2}{D} \cdot \left(\frac{C_3 \cdot L_9 - C_9 \cdot L_3}{C_1 \cdot C_9 - C_3 \cdot C_7} \right) \\ 0 \cdot deg \end{bmatrix}$$

At the outer edge of the plate:

$$y_a \equiv \begin{pmatrix} 0\cdot in \\ 0\cdot in \\ 0\cdot in \\ 0\cdot in \end{pmatrix}$$

$$\theta_a \equiv \begin{bmatrix} \frac{w\cdot a^2}{D}\cdot\left(\frac{C_4\cdot L_9}{C_7} - L_6\right) \\ \frac{w\cdot a^2}{D}\cdot\left(\frac{C_5\cdot L_9}{C_8} - L_6\right) \\ \theta_{b_2}\cdot C_4 + Q_{b_2}\cdot\frac{a^2}{D}\cdot C_6 - \frac{w\cdot a^2}{D}\cdot L_6 \\ M_{rb_3}\cdot\frac{a}{D}\cdot C_5 + Q_{b_3}\cdot\frac{a^2}{D}\cdot C_6 - \frac{w\cdot a^2}{D}\cdot L_6 \end{bmatrix} \qquad Q_a \equiv \begin{pmatrix} -w\cdot\frac{r_o}{a} \\ -w\cdot\frac{r_o}{a} \\ Q_{b_2}\cdot\frac{b}{a} - \frac{w\cdot r_o}{a} \\ Q_{b_3}\cdot\frac{b}{a} - \frac{w\cdot r_o}{a} \end{pmatrix} \qquad M_{ra} \equiv \begin{pmatrix} 0\cdot\frac{lbf\cdot in}{in} \\ 0\cdot\frac{lbf\cdot in}{in} \\ 0\cdot\frac{lbf\cdot in}{in} \\ 0\cdot\frac{lbf\cdot in}{in} \end{pmatrix}$$

Due to tangential shear stresses:

$$y_{sb} \equiv \begin{pmatrix} \frac{K_{sb}\cdot w\cdot a}{t\cdot G} \\ \frac{K_{sb}\cdot w\cdot a}{t\cdot G} \\ 0\cdot in \\ 0\cdot in \end{pmatrix} \qquad y_{sro} \equiv \begin{pmatrix} \frac{K_{sro}\cdot w\cdot r_o}{t\cdot G} \\ \frac{K_{sro}\cdot w\cdot r_o}{t\cdot G} \\ 0\cdot in \\ 0\cdot in \end{pmatrix}$$

$$F_1(r) \equiv \frac{1+\nu}{2}\cdot\frac{b}{r}\cdot\ln\left(\frac{r}{b}\right) + \frac{1-\nu}{4}\cdot\left(\frac{r}{b} - \frac{b}{r}\right) \qquad F_6(r) \equiv \frac{b}{4\cdot r}\cdot\left[\left(\frac{b}{r}\right)^2 - 1 + 2\cdot\ln\left(\frac{r}{b}\right)\right]$$

$$F_2(r) \equiv \frac{1}{4}\cdot\left[1 - \left(\frac{b}{r}\right)^2\cdot\left(1 + 2\cdot\ln\left(\frac{r}{b}\right)\right)\right] \qquad F_7(r) \equiv \frac{1}{2}\cdot\left(1-\nu^2\right)\cdot\left(\frac{r}{b} - \frac{b}{r}\right)$$

$$F_3(r) \equiv \frac{b}{4\cdot r}\cdot\left[\left[\left(\frac{b}{r}\right)^2 + 1\right]\cdot\ln\left(\frac{r}{b}\right) + \left(\frac{b}{r}\right)^2 - 1\right] \qquad F_8(r) \equiv \frac{1}{2}\cdot\left[1 + \nu + (1-\nu)\cdot\left(\frac{b}{r}\right)^2\right]$$

$$F_4(r) \equiv \frac{1}{2}\cdot\left[(1+\nu)\cdot\frac{b}{r} + (1-\nu)\cdot\frac{r}{b}\right] \qquad F_9(r) \equiv \frac{b}{r}\cdot\left[\frac{1+\nu}{2}\cdot\ln\left(\frac{r}{b}\right) + \frac{1-\nu}{4}\cdot\left[1 - \left(\frac{b}{r}\right)^2\right]\right]$$

$$F_5(r) \equiv \frac{1}{2}\cdot\left[1 - \left(\frac{b}{r}\right)^2\right]$$

$$G_3(r) \equiv \frac{r_o}{4\cdot r}\cdot\left[\left[\left(\frac{r_o}{r}\right)^2 + 1\right]\cdot\ln\left(\frac{r}{r_o}\right) + \left(\frac{r_o}{r}\right)^2 - 1\right]\cdot(r > r_o)$$

$$G_6(r) \equiv \frac{r_o}{4\cdot r}\cdot\left[\left(\frac{r_o}{r}\right)^2 - 1 + 2\cdot\ln\left(\frac{r}{r_o}\right)\right]\cdot(r > r_o)$$

$$G_9(r) \equiv \frac{r_o}{r}\cdot\left[\frac{1+\nu}{2}\cdot\ln\left(\frac{r}{r_o}\right) + \frac{1-\nu}{4}\cdot\left[1 - \left(\frac{r_o}{r}\right)^2\right]\right]\cdot(r > r_o)$$

The actual safety factor against a complete collapse of the ring like plate is much larger since unlimited large rotations will only occur when a substantial region of the plate has the circumferential moment reach capacity (this can be shown by a limit analysis solution of the plate equations).

The second impact scenario has the loading applied over a region inside the outer diameter of the pipe. To qualify this load case, we consider the plate as simply supported at the pipe diameter and conservatively neglect the overhanging portion of the pipe. Further, we assume the loading is conservatively applied as a uniform pressure over an area equal to the minimum impact diameter of 1.8". For simplicity, we neglect the inner hole in this calculation. Therefore, the limit analysis model for the second impact scenario is shown below:

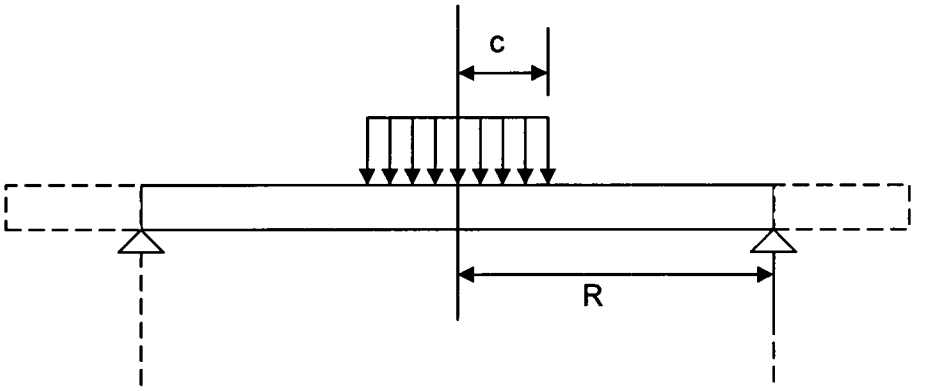

Calculate effective load area at middle surface assuming a 45 degree spread of load patch

$Hp = 0.75\,in$

$R := 0.5\cdot[(3.5 - 2\cdot 0.226)\cdot in]$

$P = 1.008 \times 10^5\,lbf$

$c := 0.5\cdot(1.8\cdot in + Hp)$

Use inside radius of pipe for this calc.

$M_u = 8.768 \times 10^3\,lbf\cdot\frac{in}{in}$

Using a solution in the text "Introduction to Plasticity"by W. Prager, Addison Wesley, 1959, p. 61, the limit load is

$$P_{lim} := 6\cdot\pi\cdot\frac{M_u}{\left(3 - 2\cdot\frac{c}{R}\right)}$$

Therefore, the safety factor for this case is

$$\frac{P_{lim}}{P} = 1.236$$

Therefore it is concluded that an end plate of diameter and thickness equal to

$Dp = 4.1\,in$ $Hp = 0.75\,in$

will perform the intended load transfer and limit the movement of the fuel assembly.

APPENDIX 3.K - LIFTING BOLTS - MPC LID and OVERPACK TOP CLOSURE

3.K.1 Scope of Appendix

In this Appendix, the bolts on the MPC top lid that are used for lifting a fully loaded MPC are analyzed for strength and engagement length. The required number of bolts are set at a specific radius of the MPC lid. Only the bolts are considered; the mating lifting device is not a part of this submittal. Bolt sizes required for lifting of the overpack top closure alone (during the fuel loading operation) are also determined.

3.K.2 Configuration

The required data for analysis is 1) the number of bolts NB; 2) the bolt diameter db; 3) the lifted weight; and 4), the details of the individual bolts.

3.K.3 Acceptance Criteria

The lifting bolts are considered as part of a special lifting device; therefore, NUREG-0612 applies. The acceptance criteria is that the bolts and the adjacent lid threads must have stresses less than 1/6 x material yield strength and 1/10 x material ultimate strength.

3.K.4 Composition of Appendix

This appendix is created using the Mathcad (version 6.0+) software package. Mathcad uses the symbol ':=' as an assignment operator, and the equals symbol '=' retrieves values for constants or variables.

3.K.5 References

[3.K.1] E. Oberg and F.D. Jones, *Machinery's Handbook*, Fifteenth Edition, Industrial Press, 1957, pp987-990.

[3.K.2] FED-STD-H28/2A, *Federal Standard Screw-Thread Standards for Federal Services*, United States Government Printing Office, April, 1984.

3.K.6 Input Data for Lifting of a Fully Loaded MPC

Lifted Weight: (use a value that bounds all MPC's per Table 3.2.4 - this is the only load)

$W_{lift} := 1.15 \cdot 90000 \cdot lbf$ includes any anticipated inertia load factor

Bolt diameter $db := 1.75 \cdot in$

Number of Bolts $NB := 4$

It is anticipated that the eventual lifting device will enable a straight (90 deg) lift. For conservatism the minimum lift angle (from the horizontal) is assumed to be 75 deg.

$$ang := 75 \cdot deg$$

Therefore, the load inducing direct shear in the unthreaded bolt region is:

$$T_h := \frac{W_{lift}}{\tan(ang)} \qquad T_h = 2.773 \times 10^4 \text{ lbf}$$

$A_d := \pi \cdot \frac{db^2}{4} = 2.405 \text{ in}^2$ is the area of the unthreaded portion of the bolt

$A_{stress} := 1.8983 \cdot in^2$ is the stress area of the bolt

$d_{pitch} := 1.6201 \cdot in$ is the pitch diameter of the bolt

$dm_{ext} := 1.5046 \cdot in$ is the minor diameter of the bolt

$dm_{int} := 1.5335 \cdot in$ is the minor diameter of the hole

The design temperature of the MPC closure ring, located atop the MPC lid, is 400 deg. F. The lifting bolts, however, penetrate several inches into the lid. Therefore, for conservatism, the material properties and allowable stresses for the MPC lid and bolt materials used in the qualification are taken at 450 deg F.

The yield and ultimate strengths of the MPC lid and bolt materials are reduced by factors of 6 and 10, respectively.

$$S_{ulid} := \frac{64000}{10} \cdot psi \qquad S_{ubolt} := \frac{169650}{10} \cdot psi \qquad S_{mbolt} := 46100 \cdot psi$$

$$S_{ylid} := \frac{20050}{6} \cdot psi \qquad S_{ybolt} := \frac{137550}{6} \cdot psi$$

Since this is an analysis using allowable strengths based on fractions of yield or ultimate strengths, the allowable strength in shear is taken as 57.7% of the postulated tensile allowable strengths.

3.K.7 Calculations

3.K.7.1 Length of Engagement/Strength Calculations

In this section, it is shown that the length of thread engagement is adequate The method and terminology of Reference 3.K.2 is followed.

$N := 5 \cdot \frac{1}{in}$ is the number of threads per inch (UNC)

$p := \frac{1}{N}$ is the thread pitch

$H := 4 \cdot 0.21651 \cdot p$ $H = 0.173\,in$

$Depth_{ext} := \frac{17}{24} \cdot H$ $Depth_{ext} = 0.123\,in$

$Depth_{int} := \frac{5}{8} \cdot H$ $Depth_{int} = 0.108\,in$

$dmaj_{ext} := dm_{ext} + 2 \cdot Depth_{ext}$ $dmaj_{ext} = 1.75\,in$

$L_{eng} := 3.0 \cdot in$ is the length of engagement

Using page 103 of reference 3.K.2,

$$Bolt\_thrd\_shr\_A := \pi \cdot N \cdot L_{eng} \cdot dm_{int} \cdot \left[\frac{1}{2 \cdot N} + .57735 \cdot (d_{pitch} - dm_{int}) \right]$$

$Bolt\_thrd\_shr\_A = 10.84\,in^2$

$$Ext\_thrd\_shr\_A := \pi \cdot N \cdot L_{eng} \cdot dmaj_{ext} \cdot \left[\frac{1}{2 \cdot N} + 0.57735 \cdot (dmaj_{ext} - d_{pitch}) \right]$$

$Ext\_thrd\_shr\_A = 14.43\,in^2$

The load capacities of the bolt and the lid material based on yield strength are:

$Load\_Capacity_{bolt} := S_{ybolt} \cdot A_{stress}$ $\quad Load\_Capacity_{bolt} = 4.352 \times 10^4 \text{ lbf}$

$Load\_Capacity_{boltshear} := .577 \cdot S_{ybolt} \cdot A_d$

$Load\_Capacity_{boltshear} = 3.182 \times 10^4 \text{ lbf}$

$Load\_Capacity_{boltthrd} := (0.577 \cdot S_{ybolt}) \cdot Bolt\_thrd\_shr\_A$

$Load\_Capacity_{boltthrd} = 1.434 \times 10^5 \text{ lbf}$

$Load\_Capacity_{lid} := (0.577 \cdot S_{ylid}) \cdot Ext\_thrd\_shr\_A$

$Load\_Capacity_{lid} = 2.782 \times 10^4 \text{ lbf}$

Therefore, the lifting capacity of the configuration is based on thread shear in the lid material.

$Max\_Lift\_Load := NB \cdot Load\_Capacity_{lid}$ $\quad Max\_Lift\_Load = 1.113 \times 10^5 \text{ lbf}$

$MS := \frac{Max\_Lift\_Load}{W_{lift}} - 1$ $\quad MS = 0.075$

> 0

The load capacities of the bolt and the lid material based on ultimate strength are:

$Load\_Capacity_{bolt} := S_{ubolt} \cdot A_{stress}$ $\quad Load\_Capacity_{bolt} = 3.22 \times 10^4 \text{ lbf}$

$Load\_Capacity_{boltthrd} := (0.577 \cdot S_{ubolt}) \cdot Bolt\_thrd\_shr\_A$

$Load\_Capacity_{boltthrd} = 1.061 \times 10^5 \text{ lbf}$

$Load\_Capacity_{boltshear} := .577 \cdot S_{ubolt} \cdot A_d$

$Load\_Capacity_{boltshear} = 2.354 \times 10^4 \text{ lbf}$

$Load\_Capacity_{lid} := (0.577 \cdot S_{ulid}) \cdot Ext\_thrd\_shr\_A$

$Load\_Capacity_{lid} = 5.329 \times 10^4 \text{ lbf}$

Therefore, the load capacity is based on bolt tensile strength or bolt shear due to the lift angle.

$$Max\_Lift\_Load := NB \cdot Load\_Capacity_{bolt} \qquad Max\_Lift\_Load = 1.288 \times 10^5\ lbf$$

$$Max\_Lift\_Load_{boltshear} := NB \cdot Load\_Capacity_{boltshear}$$

$$Max\_Lift\_Load_{boltshear} = 9.418 \times 10^4\ lbf$$

$$MS := \frac{Max\_Lift\_Load}{W_{lift}} - 1 \qquad MS = 0.245$$

or

$$MS := \frac{Max\_Lift\_Load_{boltshear}}{T_h} - 1 \qquad MS = 2.396$$

The previous calculations indicate that external thread shear stresses govern the design when yield strength is used as the criteria and bolt tension governs the design when ultimate strength is used as the criteria.

3.K.7.2 Preload Stress

$$Bolt_{pl} := \frac{W_{lift}}{NB} \qquad Bolt_{pl} = 25875\ lbf$$

The minimum preload stress required is:

$$\sigma := \frac{Bolt_{pl}}{A_{stress}} \qquad \sigma = 13630.6\ psi$$

If preload of the bolt is specified, using an unlubricated joint, the preload torque is:

$$T_{pre} := .2 \cdot \left(\frac{W_{lift}}{NB}\right) \cdot db \qquad T_{pre} = 754.687\ ft \cdot lbf$$

3.K.8 Input Data for Lifting of an Overpack Top Closure Alone

diameter_lid := 77.375·in

thickness_of_lid := 6·in Bill of Materials BM-1476

ang := 45·deg Minimum Lift Angle from Horizontal

inertia_load_factor := 0.15 appropriate for slow speed operation of lifting equipment

Weight := 8000·lbf Table 3.2.4

W_{lift} := Weight·(1.0 + inertia_load_factor)

$W_{lift} = 9.2 \times 10^3$ lbf includes any anticipated inertia load factor

$T_h := \frac{W_{lift}}{\tan(ang)}$ $T_h = 9.2 \times 10^3$ lbf

Bolt diameter db := .625·in

Number of Bolts NB := 4

$A_d := \pi \cdot \frac{db^2}{4} = 0.307\ in^2$ is the area of the unthreaded portion of the bolt

$A_{stress} := .2256 \cdot in^2$ is the stress area of the bolt

$d_{pitch} := .5660 \cdot in$ is the pitch diameter of the bolt

$dm_{ext} := .5135 \cdot in$ is the major diameter of the bolt

$dm_{int} := .5266 \cdot in$ is the minor diameter of the threaded hole

3.K.9 Calculations

3.K.9.1 Length of Engagement/Strength Calculations

In this section, it is shown that the length of thread engagement is adequate The method and terminology of reference 3.K.2 is followed.

$N := 11 \cdot \frac{1}{in}$ is the number of threads per inch

$p := \frac{1}{N}$ is the thread pitch

$H := 4 \cdot 0.21651 \cdot p$ $H = 0.079\,in$

$Depth_{ext} := \frac{17}{24} \cdot H$ $Depth_{ext} = 0.056\,in$

$Depth_{int} := \frac{5}{8} \cdot H$ $Depth_{int} = 0.049\,in$

$dmaj_{ext} := dm_{ext} + 2 \cdot Depth_{ext}$ $dmaj_{ext} = 0.625\,in$

$L_{eng} := 1.00 \cdot in$ is the length of engagement

Using page 103 of reference 3.K.2,

$$Bolt\_thrd\_shr\_A := \pi \cdot N \cdot L_{eng} \cdot dm_{int} \left[\frac{1}{2 \cdot N} + .57735 \cdot (d_{pitch} - dm_{int}) \right]$$

$Bolt\_thrd\_shr\_A = 1.241\,in^2$

$$Ext\_thrd\_shr\_A := \pi \cdot N \cdot L_{eng} \cdot dmaj_{ext} \left[\frac{1}{2 \cdot N} + 0.57735 \cdot (dmaj_{ext} - d_{pitch}) \right]$$

$Ext\_thrd\_shr\_A = 1.718\,in^2$

The load capacities of the bolt and the lid material based on yield strength are:

$Load\_Capacity_{bolt} := S_{ybolt} \cdot A_{stress}$ $\quad Load\_Capacity_{bolt} = 5.172 \times 10^3\ lbf$

$Load\_Capacity_{boltshear} := .577 \cdot S_{ybolt} \cdot A_d$

$Load\_Capacity_{boltshear} = 4.058 \times 10^3\ lbf$

$Load\_Capacity_{boltthrd} := (0.577 \cdot S_{ybolt}) \cdot Bolt\_thrd\_shr\_A$

$Load\_Capacity_{boltthrd} = 1.642 \times 10^4\ lbf$

$Load\_Capacity_{lid} := (0.577 \cdot S_{ylid}) \cdot Ext\_thrd\_shr\_A$

$Load\_Capacity_{lid} = 3.313 \times 10^3\ lbf$

Therefore, the lifting capacity of the configuration is based on thread shear in the lid.

$Max\_Lift\_Load := NB \cdot Load\_Capacity_{lid}$ $\quad Max\_Lift\_Load = 1.325 \times 10^4\ lbf$

$Max\_Lift\_Load_{boltshear} := NB \cdot Load\_Capacity_{boltshear}$

$Max\_Lift\_Load_{boltshear} = 1.623 \times 10^4\ lbf$

$MS := \frac{Max\_Lift\_Load}{W_{lift}} - 1$ $\quad MS = 0.44 \quad > 0$

The load capacities of the bolt and the lid material based on ultimate strength are:

$Load\_Capacity_{bolt} := S_{ubolt} \cdot A_{stress}$

$Load\_Capacity_{bolt} = 3.827 \times 10^3\ lbf$

$Load\_Capacity_{boltshear} := .577 \cdot S_{ubolt} \cdot A_d$

$Load\_Capacity_{boltshear} = 3.003 \times 10^3\ lbf$

$Load\_Capacity_{boltthrd} := (0.577 \cdot S_{ubolt}) \cdot Bolt\_thrd\_shr\_A$

$Load\_Capacity_{boltthrd} = 1.215 \times 10^4\ lbf$

$Load\_Capacity_{lid} := (0.577 \cdot S_{ulid}) \cdot Ext\_thrd\_shr\_A$

$Load\_Capacity_{lid} = 6.344 \times 10^3\ lbf$

Therefore, the load capacity is based on bolt tensile strength or bolt shear strength due to inclined lift cable.

$Max\_Lift\_Load := NB \cdot Load\_Capacity_{bolt}$ $Max\_Lift\_Load = 1.531 \times 10^4\ lbf$

$Max\_Lift\_Load_{boltshear} := NB \cdot Load\_Capacity_{boltshear}$

$Max\_Lift\_Load_{boltshear} = 1.201 \times 10^4\ lbf$

$$MS := \frac{Max\_Lift\_Load}{W_{lift}} - 1 \qquad MS = 0.664 \qquad > 0$$

or

$$MS := \frac{Max\_Lift\_Load_{boltshear}}{T_h} - 1 \qquad MS = 0.306$$

3.K.9.2 Preload Stress

$$Bolt_{pl} := \frac{W_{lift}}{NB} \qquad Bolt_{pl} = 2300\ lbf$$

The minimum preload stress required is:

$$\sigma := \frac{Bolt_{pl}}{A_{stress}} \qquad \sigma = 10195\ psi$$

If preload of the bolt is specified, using an unlubricated joint, the minimum preload torque is:

$$T_{pre} := .2 \cdot \left(\frac{W_{lift}}{NB}\right) \cdot db \qquad T_{pre} = 23.958\ ft \cdot lbf$$

3.K.10 Conclusion

The preceding analysis demonstrates that the length of thread engagement at the lifting locations is conservatively set. In addition, the minimum bolt preload requirements based on the lifted load are set. When lifting of a loaded MPC is not part of the operating procedure, plugs of a non-galling material with properties equal to or better than Alloy X shall be in-place to provide a filler material.

APPENDIX 3.L: FABRICATION STRESSES

3.L.1 INTRODUCTION

The HI-STAR 100 System overpack intermediate shells are constructed by layering circular shell sections around the inner confinement shell. The shell longitudinal welding process pulls each shell together and establishes a radial contact pressure between each layer and circumferential stresses in each layer. Girth welds at each end of the intermediate shells (top and bottom) further connect the layers to each other and to the top flange and to the bottom plate. In accordance with NRC requirements, fabrication stresses arising in the intermediate shells must be included in load combinations when performing structural evaluation of the overpack. This appendix documents the stress analysis. The results from this evaluation are included as added stresses in the overpack finite element analysis and the results of the overpack stress analysis includes the fabrication stresses in the final safety margins.

3.L.2 Methodology

A two-dimensional finite element analysis of the inner confinement shell and the five intermediate shells is performed to establish the level of fabrication circumferential stress developing during the assembly process. Figure 3.L.1 shows a 180 degree section through the overpack consisting of six layers of metal. The ANSYS finite element code is used to model the fabrication process; each layer is modeled using PLANE42 four node

quadrilateral elements. Contact (or lack of contact) is modeled by CONTAC48 point-to-surface elements. Symmetry boundary conditions apply at 90°, and radial movement of the inner nodepoint of the confinement layer is restrained. At -90°, the inner confinement layer is restrained while the remaining layers are subject to a prescribed circumferential displacement d to stretch the layer and to simulate the shrinkage caused by the weld process. Although the actual fabrication process locates the longitudinal weld in each layer at different circumferential orientation, in the analytical simulations all layer welds are located together. This is acceptable for analysis since the stress of interest is the primary membrane component. Figure 3.L.2 shows a partial free body of a small section of one of the layers. Normal pressures p develop between each layer due to the welding process; shear stresses due to friction between the layers also develop since there is relative circumferential movement between the layers. The free body also shows the section forces and moment that develop within the layer.

3.L.3 Analysis and Results

The fabrication stress distribution is a function of the coefficient-of-friction between the layers. For a large enough coefficient-of-friction the effects of the assembly process are localized near the weld. Localized stresses are not considered as primary stresses. For a coefficient-of-friction = 0.0, the membrane hoop stress in the component shells is non-local in nature. Therefore, the fabrication stress computation conservatively considers only

the case coefficient of friction (COF) = 0.0 since this will develop the largest in-plane primary membrane stress in each layer. The simulation is nonlinear in that each of the contact elements is checked for closure during increments of applied loading (the weld displacement).

Results for maximum primary membrane stress S_m in each layer are presented in Table 3.L.1 for circumferential locations -90°, -80°, 0°, 90°. There is no significant variation through the layer thickness except near the actual weld location. For the purposes of load combination with other mandated load cases, the maximum circumferential stress at the middle surface in each layer is designated as the fabrication membrane stress level for the layer and is used in the load combination process in the overpack finite element post-processor. The fabrication stresses generated here are also included in the appropriate Code Case N-284 evaluations since a compressive stress state is developed. The notations "inner, outer, and middle" used in the tables refer to inner surface, outer surface, and mid-plane stress locations for the respective layers.

3.L.4 Conclusions

The finite element solution has identified appropriate circumferential stresses in the various shells of the overpack due to the fabrication process. These stresses are required to be added to the stress components obtained from the finite element analysis of other load cases, and the safety margins on stress intensity reported include the

fabrication stress effect.

Where appropriate, the fabrication stresses reported herein need to be included in the Code Case N-284 evaluations of the overpack confinement shell.

Table 3.L.1

FABRICATION STRESS S_m (psi) IN THE
OVERPACK CONFINEMENT AND INTERMEDIATE SHELLS
(COF = 0.0)

Location (degrees)	Confinement Shell	Intermediate Shells				
		1	2	3	4	Outer
-90	Inner-16266	11219	9369	8539	7787	6189
	Outer-4569	172	-351	-165.0	-115	294
	Middle-10418	5695	4509	4187	3836	3241
-80	Inner-14256	8218	7300	6776	6068	5048
	Outer-6756	3895	1606	1496	1506	1358
	Middle-10506	6057	4453	4136	3787	3203
0	Inner-8716	3063	4571	3932	4229	2583
	Outer-11185	6133	4678	3858	3823	4295
	Middle-9951	4598	4625	3895	4026	3439
90	Inner-11399	1597	5371	4693	4694	4637
	Outer-7416	5171	4295	3489	2445	2738
	Middle-9408	3384	4833	4091	3570	3687

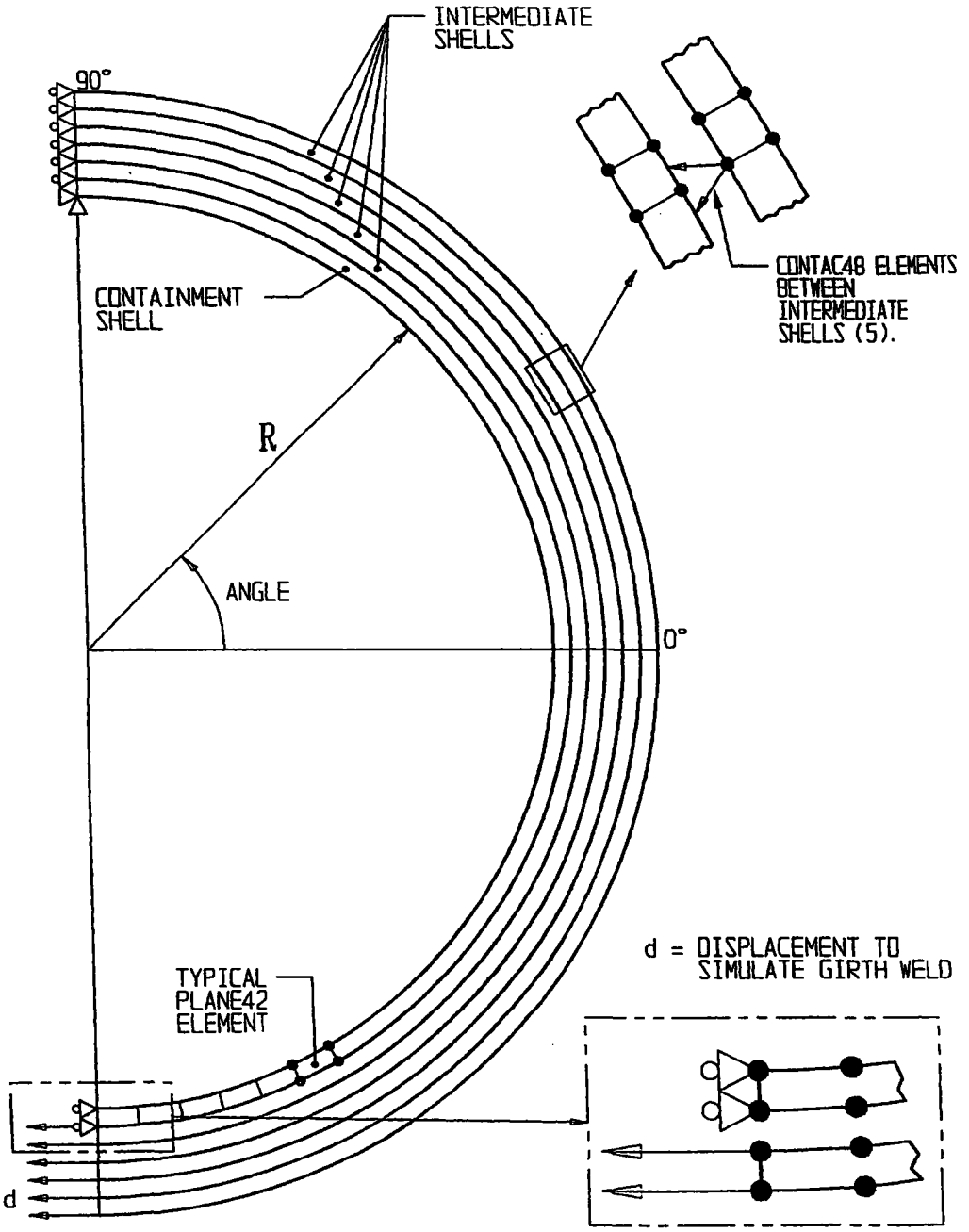

FIGURE 3.L.1; SIMULATION MODEL FOR FABRICATION STRESSES IN THE OVERPACK

REPORT HI-2012610 REVISION 0

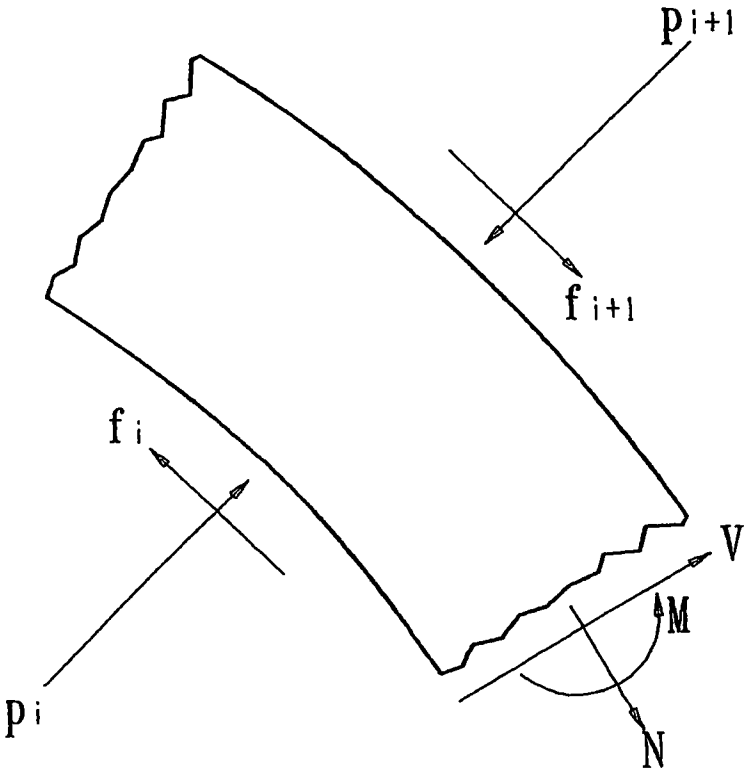

$$|f_i| \leq COF * |p_i|$$

COF = COEFFICIENT OF FRICTION

FIGURE 3.L.2; PARTIAL FREE BODY DIAGRAM OF A SHELL SECTION

APPENDIX 3.M: MISCELLANEOUS CALCULATIONS

3.M.1 CALCULATION FOR THE FILLET WELDS IN THE FUEL BASKET

The fillet welds in the fuel basket honeycomb are made by an autogenous operation that has shown to produce highly consistent and porosity free weld lines. However, Subsection NG of the ASME Code permits only 40% quality credit on double fillet welds that can be only visually examined. Subsection NG, however, fails to provide specific stress limit on such fillet welds. In the absence of a Code mandated limit, Holtec International's standard design procedure requires that the weld section possess as much load resistance capability as the parent metal section. Since the loading on the honeycomb panels is essentially that of section bending, it is possible to develop a closed form expression for the required weld throat t corresponding to panel thickness h.

We refer to Figure 3.M.1 that shows a unit depth of panel-to-panel joint subjected to moment M.

The stress distribution in the panel is given by the classical Kirchoff beam formula

$$S_p = \frac{6M}{h^2}$$

or

$$M = \frac{S_p h^2}{6}$$

S_p is the extreme fiber stress in the panel.

Assuming that the panel edge-to-panel contact region develops no resistive pressure, Figure 3.M.1(c) shows the free body of the dual fillet welds. F is the net compressive or tensile force acting on the surface of the leg of the weld.

From moment equilibrium

$$M = F(h + t)$$

Following standard weld design practice, we assume that the shear stress on the throat of the weld is equal to the force F divided by the weld throat area. If we assume 40% weld efficiency, minimum weld throat, and define S_W as the average shear stress on the weld throat, then for a unit depth of weld,

$$F = S_w (0.707)(0.4)\, t$$

$$F = 0.283\, S_w\, t$$

Then, since M is given in terms of F, we can write M in terms of S_w. Also, a relation exists between M and S_p. Between these two expressions for M, we can eliminate M and arrive at a relationship between S_w, S_p, the weld size t, and the basket panel thickness h:

$$M = 0.283\, S_w\, t\,(h+t)$$

$$0.283\, S_w\,(ht + t^2) = \frac{S_p\, h^2}{6}$$

This is to be solved for the weld by thickness t that is required for a panel thickness h. The relationship between S_p and S_W is evaluated using the most limiting hypothetical accident condition. The allowable base metal membrane plus bending stress intensity is (Table 3.1.16):

$$S_p = 55{,}450 \text{ psi at } 725^\circ F$$

The appropriate limit for the weld stress S_w is set at

$$S_w = 0.42\, S_u$$

Table 3.3.1 gives a value for the ultimate strength of the base metal as 62,350 psi at 725°F. The weld metal used at the panel connections is one grade higher in ultimate tensile stress than the adjacent base metal (80,000 psi at room temperature compared with 75,000 for the base metal at room temperature).

The strength of the weld is assumed to decrease with temperature the same as the base metal.

$$S_W = .42x80{,}000\left(\frac{62{,}350}{75{,}000}\right) = 27{,}930 \text{ psi}$$

Therefore, the corresponding limit stress on the weld throat is

$$h^2 = (0.283)(6)\frac{S_w}{S_p}(ht + t^2)$$

$$h^2 = 1.698\frac{S_w}{S_p}(ht + t^2)$$

The equation given above establishes the relationship between the weld size "t", the fuel basket panel wall thickness "h", and the ratio of allowable weld strength "S_W" to base metal allowable strength "S_p". We now apply this formula to establish the *minimum* fillet weld size to be specified on the design drawings to insure a factor of safety of 1.0 subsequent to incorporation of the appropriate dynamic load amplifier. Table 3.4.9 gives fuel basket safety factors "SF" for primary membrane plus bending stress intensities corresponding to the base metal allowable strength S_p at 725 degrees F. Similarly, Appendix 3.X provides dynamic amplification factors "DAF" for each fuel basket type. To establish the minimum permissible weld size, Sp is replaced in the above formula by (S_px(DAF/SF)), and t/h computed for each basket. The following results are obtained:

MINIMUM WELD SIZE FOR FUEL BASKETS					
Item	SF (Table 3.4.9)	DAF (Appendix 3.X)	t/h	h (inch)	t (inch)
MPC-24	1.19	1.03	0.623	10/32	0.194
MPC-68	1.56	1.08	0.529	8/32	0.132

Sheathing Weld Capacity

Simple force equilibrium relationships are used to demonstrate that the sheathing weld is adequate to support a 60g deceleration load applied vertically and horizontally to the sheathing and to the confined Boral.

Definitions

h = height of weld line (in.)

w = width of weld line (in.)

t_w = weld size

e = 0.3 = quality factor for single fillet weld

W_b = weight of a Boral panel (lbf)

W_s = weight of sheathing confining a Boral panel (lbf)

G = 60

S_w = weld shear stress (psi)

Equations

Weld area = $2\ (0.707\ t_w\ e)\ (h)$ (Neglect the top and bottom of the sheathing)

Load on weld = $(W_b + W_s)\ G$

Weld stress from combined action of vertical plus horizontal load in each of the two directions

$$S_w = \sqrt{(3)}\,\frac{G\,(W_b + W_s)}{2\,(.707)\,e\,t_w\,(h)}$$

For a PWR panel, the weights are calculated as

W_b = 11.35 lb.

W_s = 28.0 lb.

The weld size is conservatively assumed as a 0.024" fillet weld, and the length and width of the weld line is

$$h = 156 \text{ in.} \qquad w = 7.5 \text{ in.}$$

Therefore,

$$S_w = \frac{60 \text{ x } (11.35 + 28) \text{ x } 1.732}{1.414 \text{ x } 0.3 \text{ x } (0.024)\,(156)} = 2575 \text{ psi}$$

For an MPC-68 panel, the corresponding values are

$W_b =$ 7.56 lb.

$W_s =$ 20.0 lb.

$h =$ 156 in. (use h = 139 in. for conservatism)

$W =$ 5 in.

$$S_W = \frac{60\,x\,(7.56 + 20.0) \text{ x } 1.732}{1.414\,x\,0.3\,x\,(0.024)\,(139)} = 2024 \text{ psi}$$

The actual welding specified along the length of a sheathing panel is 2" weld on 8" pitch (or any other stitch weld pattern that provides 25% coverage). The effect of the intermittent weld is to raise the average weld shear stress by a factor of 4. From the above results, it is concluded that the sheathing weld stress is negligible during the most severe drop accident.

3.M.2 Calculation for MPC Cover Plates in MPC Lid

The MPC cover plates are welded to the MPC lid during loading operations. The cover plates are part of the confinement boundary for the MPC. No credit is taken for the pressure retaining abilities of the quick disconnect couplings for the MPC vent and drain. Therefore, the MPC cover plates must meet ASME Code, Section III, Subsection NB limits for normal, off-normal, and accident conditions.

The normal and off-normal condition design basis MPC internal pressure is 100 psi. The accident condition design basis MPC internal pressure is 125 psi. Conservatively, the accident condition pressure loading is applied and it is demonstrated that the Level A limits for Subsection NB are met. The MPC cover plate is depicted in the Design Drawings. The cover plate is stepped and has a maximum and minimum thickness of 0.38 inches and 0.1875 inches, respectively. Conservatively, the minimum thickness is utilized for these calculations.

To verify the MPC cover plate maintains the MPC internal pressure while meeting the ASME Code, Subsection NB limits, the cover plate bending stress and shear stress, and weld stress are calculated and compared to allowables.

Definitions

P = accident condition MPC internal pressure (psi) = 125 psi

r = cover plate radius (in.) = 2 in.

t = cover plate minimum thickness (in.) = 0.1875 in.

t_w = weld size (in.) = 0.125 in.

The design temperature of the MPC cover plate is conservatively taken as equal to the MPC lid, 550°F. The peak temperature of the MPC lid is experience on the internal portion of the MPC lid, and the actual operating temperature of the top surface is less than 400°F.

For the design temperature of 550°F, the Alloy X allowable membrane stress intensity is

$$S_m = 16{,}950 \text{ psi}$$

The allowable weld shear stress is 0.3 S_u per Subsection NF of the ASME Code for Level A conditions.

Calculations

Using Timoshenko, Strength of Materials, Part II, Advanced Theory and Problems, Third Edition, page 99, the formula for the bending stress in the cover plate is:

$$S_b = \frac{(9.9)(P)(r^2)}{(8)(t^2)} \qquad (\nu = 0.3)$$

$$S_b = \frac{(9.9)(125 \text{ psi})(2 \text{ in})^2}{(8)(0.1875 \text{ in})^2}$$

$$S_b = 17{,}600 \text{psi}$$

The allowable bending stress is $1.5S_m$; therefore, $S_b < 1.5S_m$ (i.e., 17,600 psi < 25,425 psi).

The shear stress in the cover plate due to the accident MPC internal pressure is calculated as follows

$$\tau = \frac{P \pi r^2}{2 \pi r t}$$

$$\tau = \frac{(125\ \text{psi})(\pi)(2\ \text{in})^2}{(2)(\pi)(2\ \text{in})(0.1875\ \text{in})^2}$$

$$\tau = 667\ \text{psi}$$

This shear stress is less than the Level A limit of $0.4S_m = 6{,}780$ psi.

The stress in the weld is calculated by multiplying the shear stress in the cover plate by $\sqrt{2} \cdot t/t_w$ and applying a quality factor of 0.3.

$$S_w = \frac{\sqrt{2}\,(0.1875\ \text{in})(667\ \text{psi})}{0.3\,(0.125\ \text{in})}$$

$$S_w = 4{,}716\ \text{psi}$$

$$S_w < 0.3S_u = 0.3 \times 63{,}300\ \text{psi} = 18{,}990\ \text{psi}$$

The Level A weld stress limit of 30% of the ultimate strength (at 550°F) has been taken from Section NF of the ASME Code, the only section that specifically addresses stress limits for welds.

The stress developed as a result of the accident condition MPC internal pressure has been conservatively shown to be below the Level A, Subsection NB, ASME Code limits. The MPC cover plates meet the stress limits for normal, off-normal, and accident conditions at design temperature.

PAGE 3.M-8 IS INTENTIONALLY LEFT BLANK

3.M.3 Fuel Basket Angle Support Stress Calculations

The fuel basket internal to the MPC canister is supported by a combination of angle fuel basket supports and flat plate or solid bar fuel basket supports. These fuel basket supports are subject to significant load only when a lateral acceleration is applied to the fuel basket and the contained fuel. The quasi-static finite element analyses of the MPC's, under lateral inertia loading, focused on the structural details of the fuel basket and the MPC shell. Basket supports were modeled in less detail which served only to properly model the load transfer path between fuel basket and canister. Safety factors reported for the fuel basket supports from the finite element analyses, are overly conservative, and do not reflect available capacity of the fuel basket angle support. A more detailed stress analysis of the fuel basket angle supports is performed herein. We perform a strength of materials analysis of the fuel basket angle supports that complements the finite element results. We compute weld stresses at the support-to-shell interface, and membrane and bending stresses in the basket support angle plate itself. Using this strength of materials approach, we demonstrate that the safety factors for the fuel basket angle supports are larger than indicated by the finite element analysis.

The fuel basket supports of interest are angled plate components that are welded to the MPC shell using continuous single fillet welds. The design drawings and bill of materials in Section 1.5 of this submittal define the location of these supports for all MPC constructions. These basket supports experience no loading except when the fuel assembly basket and contained fuel is subject to lateral deceleration loads either from normal handling or accident events.

In this section, the analysis proceeds in the following manner. The fuel basket support loading is obtained by first computing the fuel basket weight (cell walls plus Boral plus sheathing) and adding to it the fuel weight. To maximize the support load, the MPC is assumed to be fully populated with fuel assemblies. This total calculated weight is then amplified by the design basis deceleration load and divided by the length of the fuel basket support. The resulting value is the load per unit length that must be resisted by all of the fuel basket supports. We next conservatively estimate, from the drawings for each MPC, the number of cells in a direct line (in the direction of the deceleration) that is resisted by the most highly loaded fuel basket angle support. We then compute the resisting load on the particular support induced by the inertia load from this number of cells. Force equilibrium on a simplified model of the fuel basket angle support then provides the weld load and the axial force and bending moment in the fuel basket support.

The computation of safety factors is performed for a 60G load that bounds the non-mechanistic tip-over accident in the HI-STAR 100.

This entire section of Appendix 3.M has been written using Mathcad; all computations are performed directly within the document. The notation ":=" represents an equality.

We first establish as input data common to all three MPC's, the allowable weld shear stress. In section 3.M.1, the allowable weld stress for a Level D accident event defined. We further reduce this allowable stress by an appropriate weld efficiency obtained from the ASME Code, Section III, Subsection NG, Table NG-3352-1.

Weld efficiency $e := 0.35$ (single fillet weld, visual inspection only)

The fuel support brackets are constructed from Alloy "X". At the canister interface,

Ultimate Strength $S_u := 64000 \cdot psi$ Alloy X @ 450 degrees F (Table 3.3.1)

Note that here we use the design temperature for the MPC shell under normal conditions (Table 2.2.3) since the fire accident temperature is not applicable during the tip-over. The allowable weld shear stress, incorporating the weld efficiency is (use the base metal ultimate strength for additional conservatism) determined as:

$\tau_{all} := .42 \cdot S_u \cdot e$ $\tau_{all} = 9.408 \times 10^3 psi$

For the non-mechanistic tip-over, the design basis deceleration in "g's" is

$G := 60$ (Table 3.1.2)

The total load to be resisted by the fuel basket supports is obtained by first computing the moving weight, relative to the MPC canister, for each MPC.

The weights of the fuel baskets and total fuel load are (the notation "lbf" = "pound force")

Fuel Basket	Fuel	
$W_{mpc68} := 16240 \cdot lbf$	$W_{f68} := 47600 \cdot lbf$	MPC-68
$W_{mpc24} := 20842 \cdot lbf$	$W_{f24} := 40320 \cdot lbf$	MPC-24

The minimum length of the fuel basket support is $L := 168 \cdot in$

Dwg. 1396, sheet 1 Note that for the MPC-68, the support length is increased by 1/2"

Therefore, the load per unit length that acts along the line of action of the deceleration, and is resisted by the total of all supports, is computed as

$$Q_{68} := \frac{(W_{mpc68} + W_{f68}) \cdot G}{(L + 0.5 \cdot in)} \qquad Q_{68} = 2.273 \times 10^4 \frac{lbf}{in}$$

$$Q_{24} := \frac{(W_{mpc24} + W_{f24}) \cdot G}{L} \qquad Q_{24} = 2.184 \times 10^4 \frac{lbf}{in}$$

The subscript associated with the above items is used as the identifier for the particular MPC.

An examination of the MPC construction drawings 1395, 1401, (sheet 1 of each drawing) indicates that the deceleration load is supported by shims and by fuel basket angle supports. By inspection of the relevant drawing, we can determine that the most highly loaded fuel basket angle support will resist the deceleration load from "NC" cells where NC for each basket type is obtained by counting the cells and portions of cells "above" the support in the direction of the deceleration. The following values for NC are used in the subsequent computation of fuel basket angle support stress:

$$NC_{68} := 8 \qquad NC_{24} := 7$$

The total normal load per unit length on the fuel basket support for each MPC type is therefore computed as:

$$P_{68} := Q_{68} \cdot \frac{NC_{68}}{68} \qquad P_{68} = 2.674 \times 10^3 \frac{lbf}{in}$$

$$P_{24} := Q_{24} \cdot \frac{NC_{24}}{24} \qquad P_{24} = 6.371 \times 10^3 \frac{lbf}{in}$$

Here again, the subscript notation identifies the particular MPC.

Figure 3.M.2 shows a typical fuel basket support with the support reactions at the base of the leg. The applied load and the loads necessary to put the support in equilibrium is not subscripted since the figure is meant to be typical of any MPC fuel basket angle support. The free body is drawn in a conservative manner by assuming that the load P is applied at the quarter point of the top flat portion. In reality, as the load is applied, the top flat portion deforms and the load shifts completely to the outer edges of the top flat section of the support. From the design drawings, we use the appropriate dimensions and perform the following analyses (subscripts are introduced as necessary as MPC identifiers):

The free body diagram shows the bending moment that will arise at the location where the idealized top flat section and the angled support are assumed to meet. Compatibility of joint rotation at the connection between the top flat and the angled portion of the support plus force and moment equilibrium equations from classical beam theory provide sufficient equations to solve for the bending moment at the connection (point O in Figure 3.M.2), the load R at the weld, and the bending moment under the load P/2.

$$M_o := \frac{9}{16}\cdot\frac{Pw^2}{(S+3\cdot w)}$$

Note that the small block after the equation indicates that this is a text equation rather than an evaluated equation. This is a Mathcad identifier.

The load in the weld, R, is expressed in the form

$$R := \frac{P\cdot H}{2\cdot L} + \frac{M_o}{L}$$

Finally, the bending moment under the load, on the top flat portion, is given as

$$M_p := \frac{P}{2}\cdot\frac{w}{2} - M_o$$

Performing the indicated computations and evaluations for each of the MPC's gives:

MPC-24 (Dwg.1395 sheet 4)

$\theta_{24} := 9\cdot deg$ $\quad L_{24} := 4\cdot in$ $\quad w_{24} := \left(0.25 + .125 + .5\cdot\frac{5}{16}\right)\cdot in$

Therefore

$H_{24} := L_{24}\cdot\tan(\theta_{24})$ $\quad H_{24} = 0.634\,in$ $\quad w_{24} = 0.531\,in$

$S := \sqrt{L_{24}^2 + H_{24}^2}$ $\quad S = 4.05\,in$

$$M_o := \frac{9}{16}\cdot\frac{\left(P_{24}\cdot w_{24}^2\right)}{\left(S+3\cdot w_{24}\right)}* \qquad M_o = 179.215\,lbf\cdot\frac{in}{in}$$

$$R_{24} := \frac{P_{24}\cdot H_{24}}{2\cdot L_{24}} + \frac{M_o}{L_{24}}* \qquad R_{24} = 549.341\,\frac{lbf}{in}$$

$$M_p := \frac{P_{24}}{2}\cdot\frac{w_{24}}{2} - M_{o*} \qquad M_p = 666.939\,\text{lbf}\cdot\frac{\text{in}}{\text{in}}$$

The fillet weld throat thickness is $t_w := 0.125\cdot\text{in}\cdot 0.7071$

The weld stress is

$$\tau_{weld} := \frac{R_{24}}{t_w} \qquad \tau_{weld} = 6.215\times 10^3\,\text{psi}$$

For this event, the safety factor on the weld is

$$SF_{weld} := \frac{\tau_{all}}{\tau_{weld}} \qquad SF_{weld} = 1.514$$

For computation of member stresses, the wall thickness is $t_{wall} := \frac{5}{16}\cdot\text{in}$

The maximum bending stress in the angled member is

$$\sigma_{bending} := 6\cdot\frac{M_o}{t_{wall}^2} \qquad \sigma_{bending} = 1.101\times 10^4\,\text{psi}$$

The direct stress in the basket support angled section is

$$\sigma_{direct} := \frac{\left(R_{24}\cdot\sin\left(\theta_{24}\right) + .5\cdot P_{24}\cdot\cos\left(\theta_{24}\right)\right)}{t_{wall}} \qquad \sigma_{direct} = 1.034\times 10^4\,\text{psi}$$

From Table 3.1.16, the allowable membrane stress intensity for this condition is

$S_{membrane} := 39400\cdot\text{psi}$ (use the value at 600 degree F to conservatively bound the Safety Factor)

$$SF_{membrane} := \frac{S_{membrane}}{\sigma_{direct}} \qquad SF_{membrane} = 3.809$$

From Table 3.1.16, the allowable combined stress intensity for this accident condition is

$S_{combined} := 59100 \cdot psi$ (use the value at 600 degree F to conservatively bound the Safety Factor)

$$SF_{combined} := \frac{S_{combined}}{\sigma_{direct} + \sigma_{bending}} \qquad SF_{combined} = 2.768$$

Note that for this model, it is appropriate to compare the computed stress with allowable stress intensities since we are dealing with beams and there are no surface pressure stresses.

$$SF_{membrane} := \frac{S_{membrane}}{\sigma_{direct}} \qquad SF_{membrane} = 3.809$$

$$SF_{combined} := \frac{S_{combined}}{\sigma_{direct} + \sigma_{bending}} \qquad SF_{combined} = 2.768$$

The maximum bending stress in the top flat section is

$$\sigma_{bending} := 6 \cdot \frac{M_p}{t_{wall}^2} \qquad \sigma_{bending} = 4.098 \times 10^4 \, psi$$

The direct stress in the basket support top flat section is

$$\sigma_{direct} := \frac{R_{24}}{t_{wall}} \qquad \sigma_{direct} = 1.758 \times 10^3 \, psi$$

Computing the safety factors gives:

$$SF_{membrane} := \frac{S_{membrane}}{\sigma_{direct}} \qquad SF_{membrane} = 22.413$$

$$SF_{combined} := \frac{S_{combined}}{\sigma_{direct} + \sigma_{bending}} \qquad SF_{combined} = 1.383$$

All safety factors are greater than 1.0; therefore, the design is acceptable

MPC-68 (Dwg 1401 sheet 4)

$\theta_{68} := 12.5 \cdot deg$ $L_{68} := 4.75 \cdot in$ (estimated) $w_{68} := \left(0.75 - .5 \cdot \frac{5}{16}\right) \cdot in$

Note that in the MPC-68, there is no real top flat portion to the angle support. "w" is computed as the radius of the bend less 50% of the wall thickness. However, in the remaining calculations, the applied load is assumed a distance w/2 from the center on each side of the support centerline in Figure 3.M.2.

Therefore

$H_{68} := L_{68} \cdot \tan(\theta_{68})$ $H_{68} = 1.053\,in$ $w_{68} = 0.594\,in$

$S := \sqrt{L_{68}^2 + H_{68}^2}$ $S = 4.865\,in$

$M_o := \frac{9}{16} \cdot \frac{P_{68} \cdot w_{68}^2}{(S + 3 \cdot w_{68})}$ $M_o = 79.792\,lbf \cdot \frac{in}{in}$

$R_{68} := \frac{P_{68} \cdot H_{68}}{2 \cdot L_{68}} + \frac{M_o}{L_{68}}$* $R_{68} = 313.248 \frac{lbf}{in}$

$M_p := \frac{P_{68}}{2} \cdot \frac{w_{68}}{2} - M_o$* $M_p = 317.189\,lbf \cdot \frac{in}{in}$

The weld stress is

$\tau_{weld} := \frac{R_{68}}{t_w}$ $\tau_{weld} = 3.544 \times 10^3\,psi$

The safety factor on the weld is

$SF_{weld} := \frac{\tau_{all}}{\tau_{weld}}$ $SF_{weld} = 2.655$

The maximum bending stress in the angled member is

$$\sigma_{bending} := 6 \cdot \frac{M_o}{t_{wall}^2} \qquad \sigma_{bending} = 4.902 \times 10^3 \text{ psi}$$

The direct stress in the basket support angled section is

$$\sigma_{direct} := \frac{\left(R_{68} \cdot \sin\left(\theta_{68}\right) + .5 \cdot P_{68} \cdot \cos\left(\theta_{68}\right)\right)}{t_{wall}} \qquad \sigma_{direct} = 4.395 \times 10^3 \text{ psi}$$

$$SF_{membrane} := \frac{S_{membrane}}{\sigma_{direct}} \qquad SF_{membrane} = 8.966$$

$$SF_{combined} := \frac{S_{combined}}{\sigma_{direct} + \sigma_{bending}} \qquad SF_{combined} = 6.357$$

The maximum bending stress in the idealized top flat section is

$$\sigma_{bending} := 6 \cdot \frac{M_p}{t_{wall}^2} \qquad \sigma_{bending} = 1.949 \times 10^4 \text{ psi}$$

The direct stress in the basket support top flat section is

$$\sigma_{direct} := \frac{R_{68}}{t_{wall}} \qquad \sigma_{direct} = 1.002 \times 10^3 \text{ psi}$$

$$SF_{membrane} := \frac{S_{membrane}}{\sigma_{direct}} \qquad SF_{membrane} = 39.306$$

$$SF_{combined} := \frac{S_{combined}}{\sigma_{direct} + \sigma_{bending}} \qquad SF_{combined} = 2.884$$

All safety factors are greater than 1.0; therefore, the design is acceptable

SUMMARY OF RESULTS

The above calculations demonstrate that for all MPC fuel basket angle supports, the minimum safety margin is 1.38 (MPC-24 combined membrane plus bending in the top flat section). This is a larger safety factor than predicted from the finite element solution. The reason for this increase is attributed to the fact that the finite element analysis used a less robust structural model of the supports for stress analysis purposes since the emphasis there was on analysis of the fuel basket itself and the MPC canister. Therefore, in reporting safety factors, or safety margins, the minimum safety factor of 1.38 can be used for this component in any summary table.

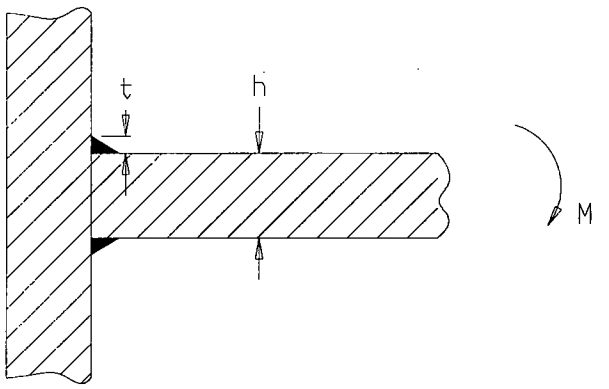

(a) Loading Configuration

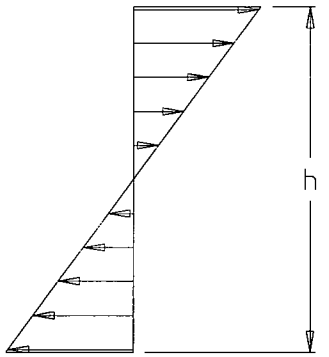

(b) Bending Stress in the Panel

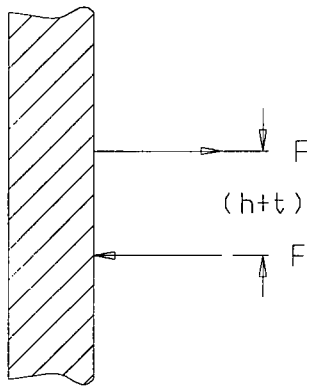

(c) Reaction in the Welds

FIGURE 3.M.1; FREEBODY OF STRESS DISTRIBUTION IN THE WELD AND THE HONEYCOMB PANEL

REPORT HI-2012610 REVISION 0

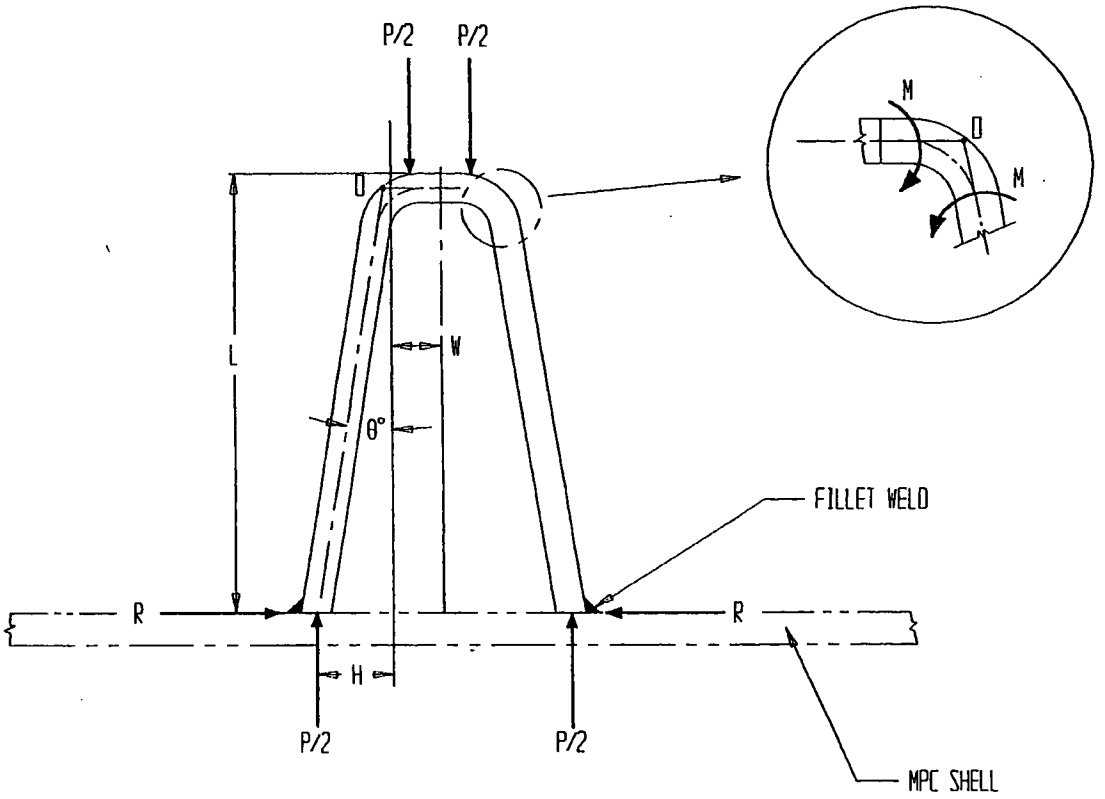

$$S^2 = L^2 + H^2$$

WHERE
S = LENGTH OF ANGLED SECTION

FIGURE 3.M.2: FREEBODY OF IDEALIZED FUEL BASKET SUPPORT

Appendix 3.N -

DELETED

Appendix 3.O -

DELETED

Appendix 3.P -

DELETED

Appendix 3.Q -

DELETED

Appendix 3.R -

DELETED

Appendix 3.S -

DELETED

Appendix 3.T -

DELETED

APPENDIX 3.U: HI-STAR 100 COMPONENT THERMAL EXPANSIONS; MPC-24

3.U.1 Scope

In this calculation, estimates of operating gaps, both radially and axially, are computed for the fuel basket-to-MPC shell, and for the MPC shell-to-overpack. This calculation is in support of the results presented in Section 3.4.4.2. Two sets of results are presented based on nominal gaps.

3.U.2 Methodology

Bounding temperatures are used to construct temperature distributions that will permit calculation of differential thermal expansions both radially and axially for the basket-to-MPC gaps, and for the MPC-to-overpack gaps. Reference temperatures are set at 70 °F for all components. Temperature distributions are computed at the middle of the HI-STAR 100 System where the temperatures are highest, and also at the top of the system where the temperatures are lowest along the entire length. Subsequent to these calculations and the prediction of radial and axial growths, the average values of the gaps are used to estimate an overall realistic "most probable" growth. A comprehensive nomenclature listing is provided in Section 3.U.7.

3.U.3 References

[3.U.1] Boley and Weiner, Theory of Thermal Stresses, John Wiley, 1960, Sec. 9.10, pp. 288-291.

[3.U.2] Burgreen, Elements of Thermal Stress Analysis, Arcturus Publishers, Cherry Hill, NJ, 1988.

3.U.4 Calculations for Hot Components (Middle of System)

3.U.4.1 Input Data

Based on thermal calculations in Chapter 4, the following temperatures are appropriate at the mid-height of the cask (see Figure 3.U.1).

The temperature change at the inside surface of the overpack, $\Delta T_{1h} := 292 - 70$

The temperature change at the outside neutron absorber enclosure, $\Delta T_{2h} := 229 - 70$

The temperature change at the mean radius of the MPC shell, $\Delta T_{3h} := 332 - 70$

The temperature change at the outside of the MPC basket, $\Delta T_{4h} := (451 - 70) \cdot 1.1$

The temperature change at the center of the basket, $\Delta T_{5h} := 709 - 70$

Note that the outer basket temperature is conservatively amplified by 10% to insure a bounding parabolic distribution. This conservatism serves to maximize the growth of the basket.

The geometry of the components are as follows (referring to Figure 3.U.1)

The outer radius of the overpack, $b := 48 \cdot in$

The inner radius of the overpack, $a := 34.375 \cdot in$

The mean radius of the MPC shell, $R_{mpc} := \frac{68.375 \cdot in - 0.5 \cdot in}{2}$

$$R_{mpc} = 33.938\,in$$

The initial MPC-to-overpack nominal radial clearance at shim locations, $RC_{mo} := 0.09375 \cdot in$

This initial radial clearance value, used to perform a radial growth check, is conservatively based on the MPC outer diameter of 68.5625 in. (see Dwg. 1395, Sh. 4, Note 5). For axial growth calculations for the MPC-to-overpack lid clearance, the axial length of the overpack is defined as the distance from the top of the overpack baseplate to the bottom of the overpack closure lid and the axial length of the MPC is defined as the overall MPC height.

The axial length of the overpack, $L_{ovp} := 191.125 \cdot in$

The axial length of the MPC, $L_{mpc} := 190.5 \cdot in$

The initial MPC-to-overpack nominal axial clearance, $AC_{mo} := L_{ovp} - L_{mpc}$

$$AC_{mo} = 0.625\,in$$

For growth calculations for the fuel basket-to-MPC shell clearances, the axial length of the basket is defined as the total length of the basket and the outer radius of the basket is defined as the mean radius of the MPC shell minus one-half of the shell thickness minus the initial basket-to-shell radial clearance.

The axial length of the basket, $L_{bas} := 176.5 \cdot in$

The initial basket-to-MPC lid nominal axial clearance, $AC_{bm} := 2 \cdot in$

The initial basket-to-MPC shell nominal radial clearance, $RC_{bm} := 0.1875 \cdot in$

The outer radius of the basket, $R_b := R_{mpc} - \frac{0.5}{2} \cdot in - RC_{bm}$

$$R_b = 33.5\,in$$

The coefficients of thermal expansion used in the subsequent calculations are based on the mean temperature of the MPC shell and the peak temperature of the basket.

The coefficient of thermal expansion for the MPC shell, $\alpha_{mpc} := 9.0704 \cdot 10^{-6}$

The coefficient of thermal expansion for the basket, $\alpha_{bas} := 9.769 \cdot 10^{-6}$

3.U.4.2 Thermal Growth of the Overpack

Results for thermal expansion deformation and stress in the overpack are obtained here. The system is replaced by a equivalent uniform hollow cylinder with approximated average properties.

Based on the given inside and outside surface temperatures, the temperature solution in the cylinder is given in the form:

$$C_a + C_b \cdot \ln\left(\frac{r}{a}\right)$$

where,

$C_a := \Delta T_{1h}$ $\quad C_a = 222$

$C_b := \dfrac{\Delta T_{2h} - \Delta T_{1h}}{\ln\left(\frac{b}{a}\right)}$ $\quad C_b = -188.695$

Next, form the integral relationship:

$$Int := \int_a^b \left[C_a + C_b \cdot \left(\ln\left(\frac{r}{a}\right)\right)\right] \cdot r \, dr$$

The Mathcad program, which was used to create this appendix, is capable of evaluating the integral "Int" either numerically or symbolically. To demonstrate that the results are equivalent, the integral is evaluated both ways in order to qualify the accuracy of any additional integrations that are needed.

The result obtained through numerical integration, $Int = 1.05 \times 10^5 \, in^2$

To perform a symbolic evaluation of the solution the integral "Ints" is defined. This integral is then evaluated using the Maple symbolic math engine built into the Mathcad program as:

$$Int_s := \int_a^b \left[C_a + C_b \cdot \left(\ln\left(\frac{r}{a}\right) \right) \right] \cdot r \, dr$$

$$Int_s := \frac{1}{2} \cdot C_b \cdot \ln\left(\frac{b}{a}\right) \cdot b^2 + \frac{1}{2} \cdot C_a \cdot b^2 - \frac{1}{4} \cdot C_b \cdot b^2 + \frac{1}{4} \cdot C_b \cdot a^2 - \frac{1}{2} \cdot C_a \cdot a^2$$

$$Int_s = 1.05 \times 10^5 \, in^2$$

We note that the values of Int and Ints are identical. The average temperature in the overpack cylinder (T_{bar}) is therefore determined as:

$$T_{bar} := \frac{2}{(b^2 - a^2)} \cdot Int$$

$$T_{bar} = 187.02$$

We estimate the average coefficient of thermal expansion for the overpack by weighting the volume of the various layers. A total of four layers are identified for this calculation. They are:

1) the overpack inner shell
2) the total of the 5 intermediate shells
3) the neutron absorber
4) the outer enclosure shell

Thermal properties are based on estimated temperatures in the component and coefficient of thermal expansion values taken from the tables in Chapter 3. The following averaging calculation involves the thicknesses (t) of the various components, and the estimated coefficients of thermal expansion at the components' mean radial positions. The results of the weighted average process yields an effective coefficient of linear thermal expansion for use in computing radial growth of a solid cylinder (the overpack).

The thicknesses of each component are defined as:

$$t_1 := 2.5 \cdot in$$

$$t_2 := 6 \cdot in$$

$$t_3 := 4.625 \cdot in$$

$$t_4 := 0.5 \cdot in$$

and the corresponding mean radii can therefore be defined as:

$$r_1 := a + .5 \cdot t_1$$

$$r_2 := r_1 + .5 \cdot t_1 + .5 \cdot t_2$$

$$r_3 := r_2 + .5 \cdot t_2 + .5 \cdot t_3$$

$$r_4 := r_3 + .5 \cdot t_3 + .5 \cdot t_4$$

To check the accuracy of these calculations, the outer radius of the overpack is calculated from r_4 and t_4, and the result is compared with the previously defined value (b).

$$b_1 := r_4 + 0.5 \cdot t_4$$

$$b_1 = 48\,\text{in}$$

$$b = 48\,\text{in}$$

We note that the the calculated value b_1 is identical to the previously defined value b. The coefficient of thermal expansion for each component, estimated based on the temperature gradient, are defined as:

$$\alpha_1 := 6.7608 \cdot 10^{-6}$$

$$\alpha_2 := 6.243 \cdot 10^{-6}$$

$$\alpha_3 := 6.125 \cdot 10^{-6}$$

$$\alpha_4 := 6.006 \cdot 10^{-6}$$

Thus, the average coefficient of thermal expansion of the overpack is determined as:

$$\alpha_{avg} := \frac{r_1 \cdot t_1 \cdot \alpha_1 + r_2 \cdot t_2 \cdot \alpha_2 + r_3 \cdot t_3 \cdot \alpha_3 + r_4 \cdot t_4 \cdot \alpha_4}{\frac{a + b}{2} \cdot (t_1 + t_2 + t_3 + t_4)}$$

$$\alpha_{avg} = 6.271 \times 10^{-6}$$

Reference 3.U.1 gives an expression for the radial deformation due to thermal growth. At the inner radius of the overpack (r = a), the radial growth is determined as:

$$\Delta R_{ah} := \alpha_{avg} \cdot a \cdot T_{bar}$$

$$\Delta R_{ah} = 0.04\,\text{in}$$

Similarly, an overestimate of the axial growth of the overpack can be determined by applying the average temperature (T_{bar}) over the entire length of the overpack as:

$$\Delta L_{ovph} := L_{ovp} \cdot \alpha_{avg} \cdot T_{bar}$$

$$\Delta L_{ovph} = 0.224\,in$$

Estimates of the secondary thermal stresses that develop in the overpack due to the radial temperature variation are determined using a conservatively high value of E as based on the temperature of the steel. The circumferential stress at the inner and outer surfaces (σ_{ca} and σ_{cb}, respectively) are determined as:

The Young's Modulus of the material, $E := 28600000 \cdot psi$

$$\sigma_{ca} := \alpha_{avg} \cdot \frac{E}{a^2} \cdot \left[2 \cdot \frac{a^2}{(b^2 - a^2)} \cdot Int - (C_a) \cdot a^2 \right]$$

$$\sigma_{ca} = -6274\,psi$$

$$\sigma_{cb} := \alpha_{avg} \cdot \frac{E}{b^2} \cdot \left[2 \cdot \frac{b^2}{(b^2 - a^2)} \cdot Int - \left[C_a + C_b \cdot \left(\ln\left(\frac{b}{a} \right) \right) \right] \cdot b^2 \right]$$

$$\sigma_{cb} = 5026\,psi$$

The radial stress due to the temperature gradient is zero at both the inner and outer surfaces of the overpack. The radius where a maximum radial stress is expected, and the corresponding radial stress, are determined by trial and error as:

$$N := 0.43$$

$$r := a \cdot (1 - N) + N \cdot b$$

$$r = 40.234\,in$$

$$\sigma_r := \alpha_{avg} \cdot \frac{E}{r^2} \cdot \left[\frac{r^2 - a^2}{2} \cdot T_{bar} - \int_a^r \left[C_a + C_b \cdot \left(\ln\left(\frac{y}{a} \right) \right) \right] \cdot y \, dy \right]$$

$$\sigma_r = -468.673\,psi$$

The axial stress developed due to the temperature gradient is equal to the sum of the radial and tangential stresses at any radial location (see Eq. 9.10.7 of [3.U.1]). Therefore, the axial stresses are available from the above calculations. The stress intensities in the overpack due to the temperature distribution are below the Level A membrane stress.

3.U.4.3 Thermal Growth of the MPC Shell

The radial and axial growth of the MPC shell (ΔR_{mpch} and ΔL_{mpch}, respectively) are determined as:

$$\Delta R_{mpch} := \alpha_{mpc} \cdot R_{mpc} \cdot \Delta T_{3h}$$

$$\Delta R_{mpch} = 0.081\,in$$

$$\Delta L_{mpch} := \alpha_{mpc} \cdot L_{mpc} \cdot \Delta T_{3h}$$

$$\Delta L_{mpch} = 0.453\,in$$

3.U.4.4 Clearances Between the MPC Shell and Overpack

The final radial and axial MPC shell-to-overpack clearances (RG_{moh} and AG_{moh}, respectively) are determined as:

$$RG_{moh} := RC_{mo} + \Delta R_{ah} - \Delta R_{mpch}$$

$$RG_{moh} = 0.053\,in$$

$$AG_{moh} := AC_{mo} + \Delta L_{ovph} - \Delta L_{mpch}$$

$$AG_{moh} = 0.396\,in$$

Note that this axial clearance (AG_{moh}) is based on the temperature distribution at mid-height.

3.U.4.5 Thermal Growth of the MPC-24 Basket

Using formulas given in [3.U.2] for a solid body of revolution, and assuming a parabolic temperature distribution in the radial direction with the center and outer temperatures given previously, the following relationships can be developed for free thermal growth.

Define $\Delta T_{bas} := \Delta T_{5h} - \Delta T_{4h}$ $\Delta T_{bas} = 219.9$

Then the mean temperature can be defined as $T_{bar} := \frac{2}{R_b^2} \cdot \int_0^{R_b} \left(\Delta T_{5h} - \Delta T_{bas} \cdot \frac{r^2}{R_b^2} \right) \cdot r \, dr$

Using the Maple symbolic engine again, the closed form solution of the integral is:

$$T_{bar} := \frac{2}{R_b^2} \cdot \left(\frac{-1}{4} \cdot \Delta T_{bas} \cdot R_b^2 + \frac{1}{2} \cdot \Delta T_{5h} \cdot R_b^2 \right)$$

$$T_{bar} = 529.05$$

The corresponding radial growth at the periphery (ΔR_{bh}) is therefore determined as:

$$\Delta R_{bh} := \alpha_{bas} \cdot R_b \cdot T_{bar}$$

$$\Delta R_{bh} = 0.173 \text{ in}$$

and the corresponding axial growth (ΔL_{bas}) is determined from [3.U.2] as:

$$\Delta L_{bh} := \Delta R_{bh} \cdot \frac{L_{bas}}{R_b}$$

$$\Delta L_{bh} = 0.912 \text{ in}$$

Note that the coefficient of thermal expansion for the hottest basket temperature has been used, and the results are therefore conservative.

3.U.4.6 Clearances Between the Fuel Basket and MPC Shell

The final radial and axial fuel basket-to-MPC shell and lid clearances (RG_{bmh} and AG_{bmh}, respectively) are determined as:

$$RG_{bmh} := RC_{bm} - \Delta R_{bh} + \Delta R_{mpch}$$

$$RG_{bmh} = 0.095 \text{ in}$$

$$AG_{bmh} := AC_{bm} - \Delta L_{bh} + \Delta L_{mpch}$$

$$AG_{bmh} = 1.541 \text{ in}$$

3.U.5 Calculations for Cold Components (Top of System)

3.U.5.1 Input Data

Based on thermal calculations in Chapter 4, the following temperatures are appropriate at the top end of the cask.

The temperature change at the inside surface of the overpack, $\Delta T_{1c} := 162 - 70$

The temperature change at the outside surface of the overpack, $\Delta T_{2c} := 159 - 70$

The temperature change at the mean radius of the MPC shell, $\Delta T_{3c} := 166 - 70$

The temperature at the center of the MPC basket, $\Delta T_{4c} := 180 - 70$

The temperature at the outside of the MPC basket, $\Delta T_{5c} := 168 - 70$

The coefficient of thermal expansion for the MPC shell is based on the average shell temperature. The coefficient of linear expansion for the basket is based on the highest basket temperature.

The coefficient of thermal expansion for the MPC shell, $\alpha_{mpc} := 8.708 \cdot 10^{-6}$

The coefficient of thermal expansion for the basket, $\alpha_{bas} := 8.742 \cdot 10^{-6}$

3.U.5.2 Thermal Growth of the Overpack

The overpack is replaced by an equivalent uniform hollow cylinder with approximated average properties.

Based on the given inside and outside surface temperatures, the temperature solution in the cylinder is given in the form:

$$C_a + C_b \cdot \ln\left(\frac{r}{a}\right)$$

where,

$C_a := \Delta T_{1c}$ $\quad C_a = 92$

$C_b := \dfrac{\Delta T_{2c} - \Delta T_{1c}}{\ln\left(\frac{b}{a}\right)}$ $\quad C_b = -8.985$

Next, form the integral relationship:

$$Int_s := \int_a^b \left[C_a + C_b \cdot \left(\ln\left(\frac{r}{a} \right) \right) \right] \cdot r \, dr$$

and solve symbolically as:

$$Int_s := \frac{1}{2} \cdot C_b \cdot \ln\left(\frac{b}{a} \right) \cdot b^2 + \frac{1}{2} \cdot C_a \cdot b^2 - \frac{1}{4} \cdot C_b \cdot b^2 + \frac{1}{4} \cdot C_b \cdot a^2 - \frac{1}{2} \cdot C_a \cdot a^2$$

$$Int_s = 5.069 \times 10^4 \, in^2$$

The average temperature in the overpack cylinder is therefore determined as:

$$T_{bar} := \frac{2}{(b^2 - a^2)} \cdot Int_s$$

$$T_{bar} = 90.334$$

The average coefficient of thermal expansion for the overpack was previously determined in Section 3.U.4.2. The overpack geometry is unchanged, and the thicknesses and radii of each component are therefore also unchanged. The temperature and corresponding coefficient of thermal expansion for each material, however, are different. The coefficient of thermal expansion for each component, estimated from the temperature gradient, are defined as:

$$\alpha_1 := 6.4374 \cdot 10^{-6}$$

$$\alpha_2 := 5.7532 \cdot 10^{-6}$$

$$\alpha_3 := 5.75 \cdot 10^{-6}$$

$$\alpha_4 := 5.74 \cdot 10^{-6}$$

and the average coefficient of thermal expansion of the overpack is therefore determined as:

$$\alpha := \frac{r_1 \cdot t_1 \cdot \alpha_1 + r_2 \cdot t_2 \cdot \alpha_2 + r_3 \cdot t_3 \cdot \alpha_3 + r_4 \cdot t_4 \cdot \alpha_4}{\frac{a + b}{2} \cdot (t_1 + t_2 + t_3 + t_4)}$$

$$\alpha = 5.86 \times 10^{-6}$$

Once again using the expression from [3.U.1], the radial growth at the inner radius of the overpack is determined as:

$$\Delta R_{ac} := \alpha \cdot a \cdot T_{bar}$$

$$\Delta R_{ac} = 0.018\,in$$

and the axial growth of the overpack, with uniform temperature T_{bar}, can be determined as:

$$\Delta L_{ovpc} := L_{ovp} \cdot \alpha \cdot T_{bar}$$

$$\Delta L_{ovpc} = 0.101\,in$$

Estimates of the non-linear thermal stresses due to the radial temperature gradient can also be determined, for a Young's Modulus based on the mean steel temperature. The circumferential stress at the inner and outer surfaces (σ_{ca} and σ_{cb}, respectively) are determined as:

The Young's Modulus of the material, $E := 29000000 \cdot psi$

$$\sigma_{ca} := \alpha \cdot \frac{E}{a^2} \cdot \left[2 \cdot \frac{a^2}{\left(b^2 - a^2\right)} \cdot Int_s - (C_a) \cdot a^2 \right]$$

$$\sigma_{ca} = -283.072\,psi$$

$$\sigma_{cb} := \alpha \cdot \frac{E}{b^2} \cdot \left[2 \cdot \frac{b^2}{\left(b^2 - a^2\right)} \cdot Int_s - \left[C_a + C_b \cdot \left(\ln\left(\frac{b}{a} \right) \right) \right] \cdot b^2 \right]$$

$$\sigma_{cb} = 226.751\,psi$$

As before, the radial stress due to the temperature gradient is zero at the inner and outer surfaces. The maximum stress will occur at the same radial location as previously calculated, and the corresponding maximum stress is determined as:

$$\sigma_r := \alpha \cdot \frac{E}{r^2} \cdot \left[\frac{r^2 - a^2}{2} \cdot T_{bar} - \int_a^r \left[C_a + C_b \cdot \left(\ln\left(\frac{y}{a} \right) \right) \right] \cdot y \, dy \right]$$

$$\sigma_r = -21.146\,psi$$

The axial stress developed due to the temperature gradient is equal to the sum of the radial and tangential stresses at any radial location (see Eq. 9.10.7 of [3.U.1]). Therefore, the axial stresses are available from the above calculations. The stress intensities in the overpack due to the temperature distribution are below the Level A membrane stress.

3.U.5.3 Thermal Growth of the MPC Shell

The radial and axial growth of the MPC shell (ΔR_{mpcc} and ΔL_{mpcc}, respectively) are determined as:

$$\Delta R_{mpcc} := \alpha_{mpc} \cdot R_{mpc} \cdot \Delta T_{3c}$$

$$\Delta R_{mpcc} = 0.028\,in$$

$$\Delta L_{mpcc} := \alpha_{mpc} \cdot L_{mpc} \cdot \Delta T_{3c}$$

$$\Delta L_{mpcc} = 0.159\,in$$

3.U.5.4 Clearance Between the MPC Shell and Overpack

The final radial and axial MPC shell-to-overpack clearances (RG_{moc} and AG_{moc}, respectively) are determined as:

$$RG_{moc} := (RC_{mo} + \Delta R_{ac}) - \Delta R_{mpcc}$$

$$RG_{moc} = 0.084\,in$$

$$AG_{moc} := AC_{mo} + \Delta L_{ovpc} - \Delta L_{mpcc}$$

$$AG_{moc} = 0.567\,in$$

Note that this axial clearance (AG_{moc}) is based on the temperature distribution at the top end of the system.

3.U.5.5 Thermal Growth of the MPC-24 Basket

Using formulas given in [3.U.2] for a solid body of revolution, and assuming a parabolic temperature in the radial direction with the center and outer temperatures given previously, the following relationships can be developed for free thermal growth.

Define $\Delta T_{bas} := \Delta T_{4c} - \Delta T_{5c}$ $\Delta T_{bas} = 12$

Then the mean temperature can be defined as $T_{bar} := \frac{2}{R_b^2} \cdot \int_0^{R_b} \left(\Delta T_{4c} - \Delta T_{bas} \cdot \frac{r^2}{R_b^2} \right) \cdot r \, dr$

Solving symbolically, the closed form solution for this integral is determined as:

$$T_{bar} := \frac{2}{R_b^2} \cdot \left(\frac{-1}{4} \cdot \Delta T_{bas} \cdot R_b^2 + \frac{1}{2} \cdot \Delta T_{4c} \cdot R_b^2 \right)$$

$$T_{bar} = 104$$

The corresponding radial growth at the periphery (ΔR_{bc}) is determined as:

$$\Delta R_{bc} := \alpha_{bas} \cdot R_b \cdot T_{bar}$$

$$\Delta R_{bc} = 0.03 \text{ in}$$

and the corresponding axial growth (ΔL_{bas}) is determined from [3.U.2] as:

$$\Delta L_{bc} := \Delta R_{bc} \cdot \frac{L_{bas}}{R_b}$$

$$\Delta L_{bc} = 0.16 \text{ in}$$

3.U.5.6 Clearances Between Fuel Basket and MPC Shell

The final radial and axial fuel basket-to-MPC shell clearances (RG_{bmc} and AG_{bmc}, respectively) are determined as:

$$RG_{bmc} := RC_{bm} - \Delta R_{bc} + \Delta R_{mpcc}$$

$$RG_{bmc} = 0.185 \text{ in}$$

$$AG_{bmc} := AC_{bm} - \Delta L_{bc} + \Delta L_{mpcc}$$

$$AG_{bmc} = 1.999 \text{ in}$$

3.U.6 Summary of Results and Computations of Averaged Final Clearances

The previous results are summarized here and used to predict results based on an average thermal distribution over the length of the unit.

Mid-Height of HI-STAR 100

MPC Shell-to-Overpack	Fuel Basket-to-MPC Shell
$RG_{moh} = 0.053\,in$	$RG_{bmh} = 0.095\,in$
$AG_{moh} = 0.396\,in$	$AG_{bmh} = 1.541\,in$

Top of HI-STAR 100

MPC Shell-to-Overpack	Fuel Basket-ti-MPC Shell
$RG_{moc} = 0.084\,in$	$RG_{bmc} = 0.185\,in$
$AG_{moc} = 0.567\,in$	$AG_{bmc} = 1.999\,in$

The final MPC shell-to-overpack and fuel basket-to-MPC shell clearances are now determined. The final radial and axial MPC shell-to-overpack clearances are determined as:

$$RG_{mo} := \frac{1}{2}\cdot(RG_{moh} + RG_{moc})$$

$$RG_{mo} = 0.068\,in$$

$$AG_{mo} := \frac{1}{2}\cdot(AG_{moh} + AG_{moc})$$

$$AG_{mo} = 0.482\,in$$

and the final radial and axial fuel basket-to-MPC shell clearances are determined as:

$$RG_{bm} := \frac{1}{2}\cdot(RG_{bmh} + RG_{bmc})$$

$$RG_{bm} = 0.14\,in$$

$$AG_{bm} := \frac{1}{2}\cdot(AG_{bmh} + AG_{bmc})$$

$$AG_{bm} = 1.77\,in$$

3.U.7 Nomenclature

a is the inner radius of the overpack
AC_{bm} is the initial fuel basket-to-MPC axial clearance.
AC_{mo} is the initial MPC-to-overpack axial clearance.
AG_{bm} is the average final fuel basket-to-MPC shell gap.
AG_{bmh} (AG_{bmc}) is the final fuel basket-to-MPC shell axial gap for the hot (cold) components.
AG_{mo} is the average final MPC shell-to-overpack axial gap.
AG_{moh} (AG_{moc}) is the final MPC shell-to-overpack axial gap for the hot (cold) components.
b is the outer radius of the overpack.
L_{bas} is the axial length of the fuel basket.
L_{mpc} is the axial length of the MPC.
L_{ovp} is the axial length of the overpack.
r_1 (r_2,r_3,r_4) is mean radius of the overpack inner shell (intermed. shells, neutron absorber, outer shell).
R_b is the outer radius of the fuel basket.
R_{mpc} is the mean radius of the MPC shell.
RC_{bm} is the initial fuel basket-to-MPC radial clearance.
RC_{mo} is the initial MPC shell-to-overpack radial clearance.
RG_{bm} is the average final fuel basket-to-MPC shell gap.
RG_{bmh} (RG_{bmc}) is the final fuel basket-to-MPC shell radial gap for the hot (cold) components.
RG_{mo} is the average final MPC shell-to-overpack radial gap.
RG_{moh} (RG_{moc}) is the final MPC shell-to-overpack radial gap for the hot (cold) components.
t_1 (t_2,t_3,t_4) is the thickness of the overpack inner shell (intermed. shells, neutron absorber, outer shell).
T_{bar} is the average temperature of the overpack cylinder.
α_1 (α_2,α_3,α_4) is the coefficient of thermal expansion of the overpack inner shell (intermed. shells, neutron absorber, outer shell).
α_{avg} is the average coefficient of thermal expansion of the overpack.
α_{bas} is the coefficient of thermal expansion of the overpack.
α_{mpc} is the coefficient of thermal expansion of the MPC.
ΔL_{bh} (ΔL_{bc}) is the axial growth of the fuel basket for the hot components.
ΔL_{mpch} (ΔL_{mpcc}) the the axial growth of the MPC for the hot (cold) components.
ΔL_{ovph} (ΔL_{ovpc}) is the axial growth of the overpack for the hot (cold) components.
ΔR_{ah} (ΔR_{ac}) is the radial growth of the overpack inner radius for the hot (cold) components.
ΔR_{bh} (ΔR_{bc}) is the radial growth of the fuel basket for the hot components.

ΔR_{mpch} (ΔR_{mpcc}) is the radial growth of the MPC shell for the hot (cold) components.
ΔT_{1h} (ΔT_{1c}) is the temperature change at the overpack inside surface for hot (cold) components.
ΔT_{2h} (ΔT_{2c}) is the temperature change at the outside enclosure shell surface for hot (cold) components.
ΔT_{3h} (ΔT_{3c}) is the temperature change at the MPC shell mean radius for hot (cold) components.
ΔT_{4h} (ΔT_{4c}) is the temperature change at the MPC basket periphery for hot (cold) components.
ΔT_{5h} (ΔT_{5c}) is the temperature change at the MPC basket centerline for hot (cold) components.
ΔT_{bas} is the fuel basket centerline-to-periphery temperature gradient.
σ_{ca} is the circumferential stress at the overpack inner surface.
σ_{cb} is the circumferential stress at the overpack outer surface.
σ_r is the maximum radial stress of the overpack.

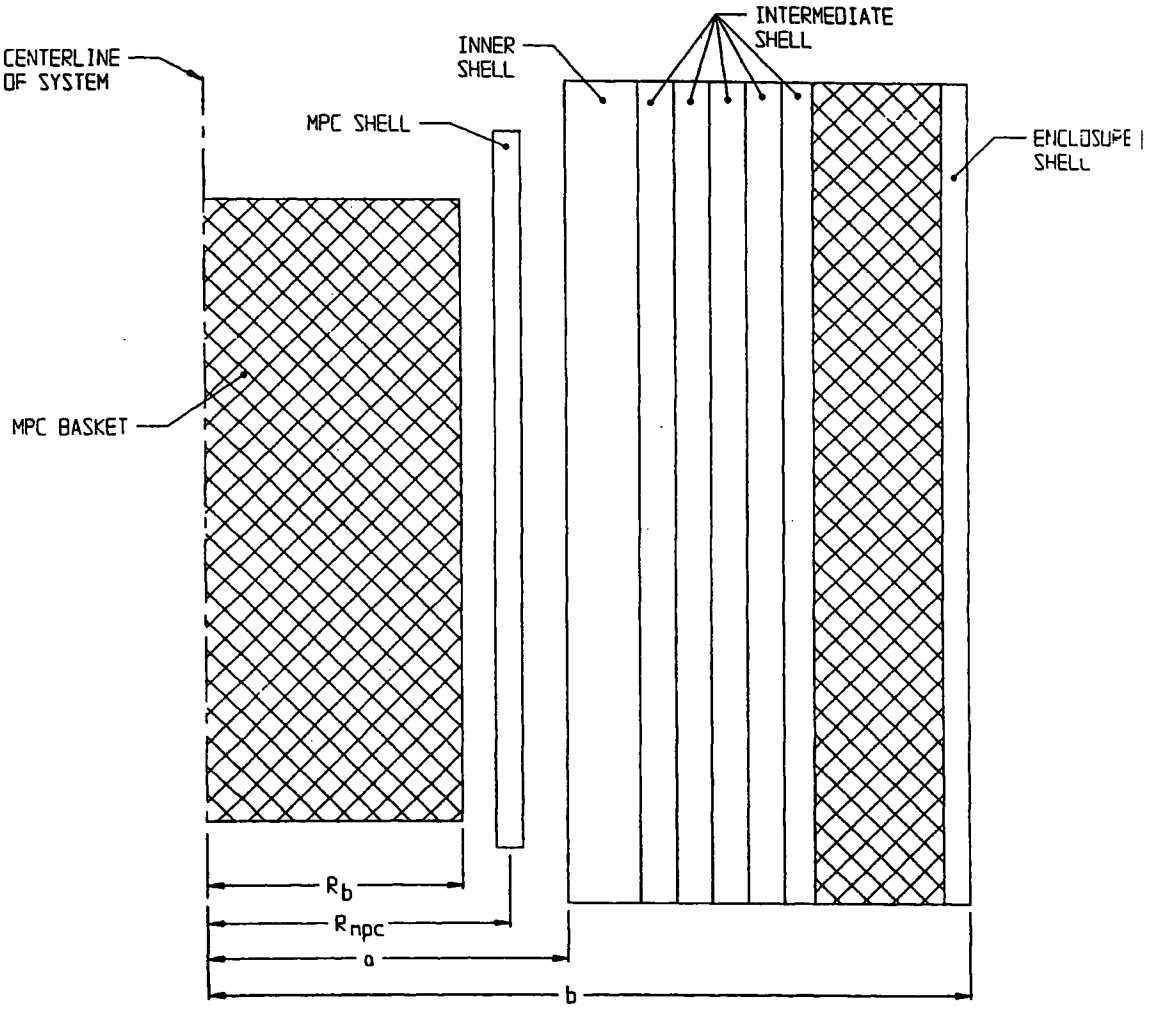

FIGURE 3.U.1; GEOMETRY OF SECTION FOR THERMAL EXPANSION CALCULATIONS

Appendix 3.V -

DELETED

APPENDIX 3.W: HI-STAR 100 COMPONENT THERMAL EXPANSIONS; MPC-68

3.W.1 Scope

In this calculation, estimates of operating gaps, both radially and axially, are computed for the fuel basket-to-MPC shell, and for the MPC shell-to-overpack. This calculation is in support of the results presented in Section 3.4.4.2. Two sets of results are presented based on nominal gaps.

3.W.2 Methodology

Bounding temperatures are used to construct temperature distributions that will permit calculation of differential thermal expansions both radially and axially for the basket-to-MPC gaps, and for the MPC-to-overpack gaps. Reference temperatures are set at 70 °F for all components. Temperature distributions are computed at the middle of the HI-STAR 100 System where the temperatures are highest, and also at the top of the system where the temperatures are lowest along the entire length. Subsequent to these calculations and the prediction of radial and axial growths, the average values of the gaps are used to estimate an overall realistic "most probable" growth. A comprehensive nomenclature listing is provided in Section 3.W.7.

3.W.3 References

[3.W.1] Boley and Weiner, Theory of Thermal Stresses, John Wiley, 1960, Sec. 9.10, pp. 288-291.

[3.W.2] Burgreen, Elements of Thermal Stress Analysis, Arcturus Publishers, Cherry Hill, NJ, 1988.

3.W.4 Calculations for Hot Components (Middle of System)

3.W.4.1 Input Data

Based on thermal calculations in Chapter 4, the following temperatures are appropriate at the mid-height of the cask (see Figure 3.W.1).

The temperature change at the inside surface of the overpack, $\Delta T_{1h} := 292 - 70$

The temperature change at the outside neutron absorber enclosure, $\Delta T_{2h} := 228 - 70$

The temperature change at the mean radius of the MPC shell, $\Delta T_{3h} := 331 - 70$

The temperature change at the outside of the MPC basket, $\Delta T_{4h} := (393 - 70) \cdot 1.1$

The temperature change at the center of the basket, $\Delta T_{5h} := 725 - 70$

Note that the outer basket temperature is conservatively amplified by 10% to insure a bounding parabolic distribution. This conservatism serves to maximize the growth of the basket.

The geometry of the components are as follows (referring to Figure 3.W.1)

The outer radius of the overpack, $b := 48 \cdot in$

The inner radius of the overpack, $a := 34.375 \cdot in$

The mean radius of the MPC shell, $R_{mpc} := \frac{68.375 \cdot in - 0.5 \cdot in}{2}$

$$R_{mpc} = 33.938\,in$$

The initial MPC-to-overpack nominal radial clearance at shim locations, $RC_{mo} := 0.09375 \cdot in$

This initial radial clearance value, used to perform a radial growth check, is conservatively based on the MPC outer diameter of 68.5625 in. (see Dwg. 1395, Sh. 4, Note 5). For axial growth calculations for the MPC-to-overpack lid clearance, the axial length of the overpack is defined as the distance from the top of the overpack baseplate to the bottom of the overpack closure lid and the axial length of the MPC is defined as the overall MPC height.

The axial length of the overpack, $L_{ovp} := 191.125 \cdot in$

The axial length of the MPC, $L_{mpc} := 190.5 \cdot in$

The initial MPC-to-overpack nominal axial clearance, $AC_{mo} := L_{ovp} - L_{mpc}$

$$AC_{mo} = 0.625\,in$$

For growth calculations for the fuel basket-to-MPC shell clearances, the axial length of the basket is defined as the total length of the basket and the outer radius of the basket is defined as the mean radius of the MPC shell minus one-half of the shell thickness minus the initial basket-to-shell radial clearance.

The axial length of the basket, $L_{bas} := 176.5 \cdot in$

The initial basket-to-MPC lid nominal axial clearance, $AC_{bm} := 2 \cdot in$

The initial basket-to-MPC shell nominal radial clearance, $RC_{bm} := 0.1875 \cdot in$

The outer radius of the basket, $R_b := R_{mpc} - \frac{0.5}{2} \cdot in - RC_{bm}$

$$R_b = 33.5\,in$$

The coefficients of thermal expansion used in the subsequent calculations are based on the mean temperature of the MPC shell and the peak temperature of the basket.

The coefficient of thermal expansion for the MPC shell, $\alpha_{mpc} := 9.0682 \cdot 10^{-6}$

The coefficient of thermal expansion for the basket, $\alpha_{bas} := 9.785 \cdot 10^{-6}$

3.W.4.2 Thermal Growth of the Overpack

Results for thermal expansion deformation and stress in the overpack are obtained here. The system is replaced by a equivalent uniform hollow cylinder with approximated average properties.

Based on the given inside and outside surface temperatures, the temperature solution in the cylinder is given in the form:

$$C_a + C_b \cdot \ln\left(\frac{r}{a}\right)$$

where,

$$C_a := \Delta T_{1h} \qquad C_a = 222$$

$$C_b := \frac{\Delta T_{2h} - \Delta T_{1h}}{\ln\left(\frac{b}{a}\right)} \qquad C_b = -191.691$$

Next, form the integral relationship:

$$Int := \int_a^b \left[C_a + C_b \cdot \left(\ln\left(\frac{r}{a}\right)\right)\right] \cdot r \, dr$$

The Mathcad program, which was used to create this appendix, is capable of evaluating the integral "Int" either numerically or symbolically. To demonstrate that the results are equivalent, the integral is evaluated both ways in order to qualify the accuracy of any additional integrations that are needed.

The result obtained through numerical integration, $Int = 1.046 \times 10^5 \, in^2$

To perform a symbolic evaluation of the solution the integral "Ints" is defined. This integral is then evaluated using the Maple symbolic math engine built into the Mathcad program as:

$$Int_s := \int_a^b \left[C_a + C_b \cdot \left(\ln\left(\frac{r}{a}\right) \right) \right] \cdot r \, dr$$

$$Int_s := \frac{1}{2} \cdot C_b \cdot \ln\left(\frac{b}{a}\right) \cdot b^2 + \frac{1}{2} \cdot C_a \cdot b^2 - \frac{1}{4} \cdot C_b \cdot b^2 + \frac{1}{4} \cdot C_b \cdot a^2 - \frac{1}{2} \cdot C_a \cdot a^2$$

$$Int_s = 1.046 \times 10^5 \, in^2$$

We note that the values of Int and Ints are identical. The average temperature in the overpack cylinder (T_{bar}) is therefore determined as:

$$T_{bar} := \frac{2}{\left(b^2 - a^2\right)} \cdot Int$$

$$T_{bar} = 186.465$$

We estimate the average coefficient of thermal expansion for the overpack by weighting the volume of the various layers. A total of four layers are identified for this calculation. They are:

1) the overpack inner shell
2) the total of the 5 intermediate shells
3) the neutron absorber
4) the outer enclosure shell

Thermal properties are based on estimated temperatures in the component and coefficient of thermal expansion values taken from the tables in Chapter 3. The following averaging calculation involves the thicknesses (t) of the various components, and the estimated coefficients of thermal expansion at the components' mean radial positions. The results of the weighted average process yields an effective coefficient of linear thermal expansion for use in computing radial growth of a solid cylinder (the overpack).

The thicknesses of each component are defined as:

$$t_1 := 2.5 \cdot in$$

$$t_2 := 6 \cdot in$$

$$t_3 := 4.625 \cdot in$$

$$t_4 := 0.5 \cdot in$$

and the corresponding mean radii can therefore be defined as:

$$r_1 := a + .5 \cdot t_1$$

$$r_2 := r_1 + .5 \cdot t_1 + .5 \cdot t_2$$

$$r_3 := r_2 + .5 \cdot t_2 + .5 \cdot t_3$$

$$r_4 := r_3 + .5 \cdot t_3 + .5 \cdot t_4$$

To check the accuracy of these calculations, the outer radius of the overpack is calculated from r_4 and t_4, and the result is compared with the previously defined value (b).

$$b_1 := r_4 + 0.5 \cdot t_4$$

$$b_1 = 48\,\text{in}$$

$$b = 48\,\text{in}$$

We note that the the calculated value b_1 is identical to the previously defined value b. The coefficient of thermal expansion for each component, estimated based on the temperature gradient, are defined as:

$$\alpha_1 := 6.7608 \cdot 10^{-6}$$

$$\alpha_2 := 6.2328 \cdot 10^{-6}$$

$$\alpha_3 := 6.12 \cdot 10^{-6}$$

$$\alpha_4 := 6.002 \cdot 10^{-6}$$

Thus, the average coefficient of thermal expansion of the overpack is determined as:

$$\alpha_{avg} := \frac{r_1 \cdot t_1 \cdot \alpha_1 + r_2 \cdot t_2 \cdot \alpha_2 + r_3 \cdot t_3 \cdot \alpha_3 + r_4 \cdot t_4 \cdot \alpha_4}{\frac{a + b}{2} \cdot (t_1 + t_2 + t_3 + t_4)}$$

$$\alpha_{avg} = 6.265 \times 10^{-6}$$

Reference 3.W.1 gives an expression for the radial deformation due to thermal growth. At the inner radius of the overpack (r = a), the radial growth is determined as:

$$\Delta R_{ah} := \alpha_{avg} \cdot a \cdot T_{bar}$$

$$\Delta R_{ah} = 0.04\,\text{in}$$

Similarly, an overestimate of the axial growth of the overpack can be determined by applying the average temperature (T_{bar}) over the entire length of the overpack as:

$$\Delta L_{ovph} := L_{ovp} \cdot \alpha_{avg} \cdot T_{bar}$$

$$\Delta L_{ovph} = 0.223\,in$$

Estimates of the secondary thermal stresses that develop in the overpack due to the radial temperature variation are determined using a conservatively high value of E as based on the temperature of the steel. The circumferential stress at the inner and outer surfaces (σ_{ca} and σ_{cb}, respectively) are determined as:

The Young's Modulus of the material, $E := 28600000 \cdot psi$

$$\sigma_{ca} := \alpha_{avg} \cdot \frac{E}{a^2} \cdot \left[2 \cdot \frac{a^2}{\left(b^2 - a^2\right)} \cdot Int - \left(C_a\right) \cdot a^2 \right]$$

$$\sigma_{ca} = -6367\,psi$$

$$\sigma_{cb} := \alpha_{avg} \cdot \frac{E}{b^2} \cdot \left[2 \cdot \frac{b^2}{\left(b^2 - a^2\right)} \cdot Int - \left[C_a + C_b \cdot \left(\ln\left(\frac{b}{a}\right) \right) \right] \cdot b^2 \right]$$

$$\sigma_{cb} = 5100\,psi$$

The radial stress due to the temperature gradient is zero at both the inner and outer surfaces of the overpack. The radius where a maximum radial stress is expected, and the corresponding radial stress, are determined by trial and error as:

$$N := 0.43$$

$$r := a \cdot (1 - N) + N \cdot b$$

$$r = 40.234\,in$$

$$\sigma_r := \alpha_{avg} \cdot \frac{E}{r^2} \cdot \left[\frac{r^2 - a^2}{2} \cdot T_{bar} - \int_a^r \left[C_a + C_b \cdot \left(\ln\left(\frac{y}{a}\right) \right) \right] \cdot y \, dy \right]$$

$$\sigma_r = -475.628\,psi$$

The axial stress developed due to the temperature gradient is equal to the sum of the radial and tangential stresses at any radial location (see Eq. 9.10.7 of [3.W.1]). Therefore, the axial stresses are available from the above calculations. The stress intensities in the overpack due to the temperature distribution are below the Level A membrane stress.

3.W.4.3 Thermal Growth of the MPC Shell

The radial and axial growth of the MPC shell (ΔR_{mpch} and ΔL_{mpch}, respectively) are determined as:

$$\Delta R_{mpch} := \alpha_{mpc} \cdot R_{mpc} \cdot \Delta T_{3h}$$

$$\Delta R_{mpch} = 0.08\,in$$

$$\Delta L_{mpch} := \alpha_{mpc} \cdot L_{mpc} \cdot \Delta T_{3h}$$

$$\Delta L_{mpch} = 0.451\,in$$

3.W.4.4 Clearances Between the MPC Shell and Overpack

The final radial and axial MPC shell-to-overpack clearances (RG_{moh} and AG_{moh}, respectively) are determined as:

$$RG_{moh} := RC_{mo} + \Delta R_{ah} - \Delta R_{mpch}$$

$$RG_{moh} = 0.054\,in$$

$$AG_{moh} := AC_{mo} + \Delta L_{ovph} - \Delta L_{mpch}$$

$$AG_{moh} = 0.397\,in$$

Note that this axial clearance (AG_{moh}) is based on the temperature distribution at mid-height.

3.W.4.5 Thermal Growth of the MPC-68 Basket

Using formulas given in [3.W.2] for a solid body of revolution, and assuming a parabolic temperature distribution in the radial direction with the center and outer temperatures given previously, the following relationships can be developed for free thermal growth.

Define $\Delta T_{bas} := \Delta T_{5h} - \Delta T_{4h}$ $\Delta T_{bas} = 299.7$

Then the mean temperature can be defined as $T_{bar} := \frac{2}{R_b^2} \cdot \int_0^{R_b} \left(\Delta T_{5h} - \Delta T_{bas} \cdot \frac{r^2}{R_b^2} \right) \cdot r \, dr$

Using the Maple symbolic engine again, the closed form solution of the integral is:

$$T_{bar} := \frac{2}{R_b^2} \cdot \left(\frac{-1}{4} \cdot \Delta T_{bas} \cdot R_b^2 + \frac{1}{2} \cdot \Delta T_{5h} \cdot R_b^2 \right)$$

$$T_{bar} = 505.15$$

The corresponding radial growth at the periphery (ΔR_{bh}) is therefore determined as:

$$\Delta R_{bh} := \alpha_{bas} \cdot R_b \cdot T_{bar}$$

$$\Delta R_{bh} = 0.166\,in$$

and the corresponding axial growth (ΔL_{bas}) is determined from [3.W.2] as:

$$\Delta L_{bh} := \Delta R_{bh} \cdot \frac{L_{bas}}{R_b}$$

$$\Delta L_{bh} = 0.872\,in$$

Note that the coefficient of thermal expansion for the hottest basket temperature has been used, and the results are therefore conservative.

3.W.4.6 Clearances Between the Fuel Basket and MPC Shell

The final radial and axial fuel basket-to-MPC shell and lid clearances (RG_{bmh} and AG_{bmh}, respectively) are determined as:

$$RG_{bmh} := RC_{bm} - \Delta R_{bh} + \Delta R_{mpch}$$

$$RG_{bmh} = 0.102\,in$$

$$AG_{bmh} := AC_{bm} - \Delta L_{bh} + \Delta L_{mpch}$$

$$AG_{bmh} = 1.578\,in$$

3.W.5 Calculations for Cold Components (Top of System)

3.W.5.1 Input Data

Based on thermal calculations in Chapter 4, the following temperatures are appropriate at the top end of the cask.

The temperature change at the inside surface of the overpack, $\Delta T_{1c} := 163 - 70$

The temperature change at the outside surface of the overpack, $\Delta T_{2c} := 160 - 70$

The temperature change at the mean radius of the MPC shell, $\Delta T_{3c} := 167 - 70$

The temperature at the center of the MPC basket, $\Delta T_{4c} := 179 - 70$

The temperature at the outside of the MPC basket, $\Delta T_{5c} := 168 - 70$

The coefficient of thermal expansion for the MPC shell is based on the average shell temperature. The coefficient of linear expansion for the basket is based on the highest basket temperature.

The coefficient of thermal expansion for the MPC shell, $\alpha_{mpc} := 8.7108 \cdot 10^{-6}$

The coefficient of thermal expansion for the basket, $\alpha_{bas} := 8.766 \cdot 10^{-6}$

3.W.5.2 Thermal Growth of the Overpack

The overpack is replaced by an equivalent uniform hollow cylinder with approximated average properties.

Based on the given inside and outside surface temperatures, the temperature solution in the cylinder is given in the form:

$$C_a + C_b \cdot \ln\left(\frac{r}{a}\right)$$

where,

$C_a := \Delta T_{1c}$ $\quad C_a = 93$

$C_b := \dfrac{\Delta T_{2c} - \Delta T_{1c}}{\ln\left(\frac{b}{a}\right)}$ $\quad C_b = -8.985$

Next, form the integral relationship:

$$Int_s := \int_a^b \left[C_a + C_b \cdot \left(\ln\left(\frac{r}{a} \right) \right) \right] \cdot r \, dr$$

and solve symbolically as:

$$Int_s := \frac{1}{2} \cdot C_b \cdot \ln\left(\frac{b}{a} \right) \cdot b^2 + \frac{1}{2} \cdot C_a \cdot b^2 - \frac{1}{4} \cdot C_b \cdot b^2 + \frac{1}{4} \cdot C_b \cdot a^2 - \frac{1}{2} \cdot C_a \cdot a^2$$

$$Int_s = 5.125 \times 10^4 \, in^2$$

The average temperature in the overpack cylinder is therefore determined as:

$$T_{bar} := \frac{2}{\left(b^2 - a^2 \right)} \cdot Int_s$$

$$T_{bar} = 91.334$$

The average coefficient of thermal expansion for the overpack was previously determined in Section 3.W.4.2. The overpack geometry is unchanged, and the thicknesses and radii of each component are therefore also unchanged. The temperature and corresponding coefficient of thermal expansion for each material, however, are different. The coefficient of thermal expansion for each component, estimated from the temperature gradient, are defined as:

$$\alpha_1 := 6.4401 \cdot 10^{-6}$$

$$\alpha_2 := 5.7568 \cdot 10^{-6}$$

$$\alpha_3 := 5.796 \cdot 10^{-6}$$

$$\alpha_4 := 5.746 \cdot 10^{-6}$$

and the average coefficient of thermal expansion of the overpack is therefore determined as:

$$\alpha := \frac{r_1 \cdot t_1 \cdot \alpha_1 + r_2 \cdot t_2 \cdot \alpha_2 + r_3 \cdot t_3 \cdot \alpha_3 + r_4 \cdot t_4 \cdot \alpha_4}{\frac{a + b}{2} \cdot \left(t_1 + t_2 + t_3 + t_4 \right)}$$

$$\alpha = 5.879 \times 10^{-6}$$

Once again using the expression from [3.W.1], the radial growth at the inner radius of the overpack is determined as:

$$\Delta R_{ac} := \alpha \cdot a \cdot T_{bar}$$

$$\Delta R_{ac} = 0.018\,in$$

and the axial growth of the overpack, with uniform temperature T_{bar}, can be determined as:

$$\Delta L_{ovpc} := L_{ovp} \cdot \alpha \cdot T_{bar}$$

$$\Delta L_{ovpc} = 0.103\,in$$

Estimates of the non-linear thermal stresses due to the radial temperature gradient can also be determined, for a Young's Modulus based on the mean steel temperature. The circumferential stress at the inner and outer surfaces (σ_{ca} and σ_{cb}, respectively) are determined as:

The Young's Modulus of the material, $E := 29000000 \cdot psi$

$$\sigma_{ca} := \alpha \cdot \frac{E}{a^2} \cdot \left[2 \cdot \frac{a^2}{\left(b^2 - a^2\right)} \cdot Int_s - \left(C_a\right) \cdot a^2 \right]$$

$$\sigma_{ca} = -284.007\,psi$$

$$\sigma_{cb} := \alpha \cdot \frac{E}{b^2} \cdot \left[2 \cdot \frac{b^2}{\left(b^2 - a^2\right)} \cdot Int_s - \left[C_a + C_b \cdot \left(\ln\left(\frac{b}{a}\right) \right) \right] \cdot b^2 \right]$$

$$\sigma_{cb} = 227.5\,psi$$

As before, the radial stress due to the temperature gradient is zero at the inner and outer surfaces. The maximum stress will occur at the same radial location as previously calculated, and the corresponding maximum stress is determined as:

$$\sigma_r := \alpha \cdot \frac{E}{r^2} \cdot \left[\frac{r^2 - a^2}{2} \cdot T_{bar} - \int_a^r \left[C_a + C_b \cdot \left(\ln\left(\frac{y}{a}\right) \right) \right] \cdot y \, dy \right]$$

$$\sigma_r = -21.216\,psi$$

The axial stress developed due to the temperature gradient is equal to the sum of the radial and tangential stresses at any radial location (see Eq. 9.10.7 of [3.W.1]). Therefore, the axial stresses are available from the above calculations. The stress intensities in the overpack due to the temperature distribution are below the Level A membrane stress.

3.W.5.3 Thermal Growth of the MPC Shell

The radial and axial growth of the MPC shell (ΔR_{mpcc} and ΔL_{mpcc}, respectively) are determined as:

$$\Delta R_{mpcc} := \alpha_{mpc} \cdot R_{mpc} \cdot \Delta T_{3c}$$

$$\Delta R_{mpcc} = 0.029\,in$$

$$\Delta L_{mpcc} := \alpha_{mpc} \cdot L_{mpc} \cdot \Delta T_{3c}$$

$$\Delta L_{mpcc} = 0.161\,in$$

3.W.5.4 Clearance Between the MPC Shell and Overpack

The final radial and axial MPC shell-to-overpack clearances (RG_{moc} and AG_{moc}, respectively) are determined as:

$$RG_{moc} := \left(RC_{mo} + \Delta R_{ac}\right) - \Delta R_{mpcc}$$

$$RG_{moc} = 0.084\,in$$

$$AG_{moc} := AC_{mo} + \Delta L_{ovpc} - \Delta L_{mpcc}$$

$$AG_{moc} = 0.567\,in$$

Note that this axial clearance (AG_{moc}) is based on the temperature distribution at the top end of the system.

3.W.5.5 Thermal Growth of the MPC-68 Basket

Using formulas given in [3.W.2] for a solid body of revolution, and assuming a parabolic temperature in the radial direction with the center and outer temperatures given previously, the following relationships can be developed for free thermal growth.

Define $\Delta T_{bas} := \Delta T_{4c} - \Delta T_{5c}$ $\Delta T_{bas} = 11$

Then the mean temperature can be defined as $T_{bar} := \frac{2}{R_b^2} \cdot \int_0^{R_b} \left(\Delta T_{4c} - \Delta T_{bas} \cdot \frac{r^2}{R_b^2} \right) \cdot r \, dr$

Solving symbolically, the closed form solution for this integral is determined as:

$$T_{bar} := \frac{2}{R_b^2} \cdot \left(\frac{-1}{4} \cdot \Delta T_{bas} \cdot R_b^2 + \frac{1}{2} \cdot \Delta T_{4c} \cdot R_b^2 \right)$$

$$T_{bar} = 103.5$$

The corresponding radial growth at the periphery (ΔR_{bc}) is determined as:

$$\Delta R_{bc} := \alpha_{bas} \cdot R_b \cdot T_{bar}$$

$$\Delta R_{bc} = 0.03 \text{ in}$$

and the corresponding axial growth (ΔL_{bas}) is determined from [3.W.2] as:

$$\Delta L_{bc} := \Delta R_{bc} \cdot \frac{L_{bas}}{R_b}$$

$$\Delta L_{bc} = 0.16 \text{ in}$$

3.W.5.6 Clearances Between Fuel Basket and MPC Shell

The final radial and axial fuel basket-to-MPC shell clearances (RG_{bmc} and AG_{bmc}, respectively) are determined as:

$$RG_{bmc} := RC_{bm} - \Delta R_{bc} + \Delta R_{mpcc}$$

$$RG_{bmc} = 0.186 \text{ in}$$

$$AG_{bmc} := AC_{bm} - \Delta L_{bc} + \Delta L_{mpcc}$$

$$AG_{bmc} = 2.001 \text{ in}$$

3.W.6 Summary of Results and Computations of Averaged Final Clearances

The previous results are summarized here and used to predict results based on an average thermal distribution over the length of the unit.

Mid-Height of HI-STAR 100

MPC Shell-to-Overpack	Fuel Basket-to-MPC Shell
$RG_{moh} = 0.054\,in$	$RG_{bmh} = 0.102\,in$
$AG_{moh} = 0.397\,in$	$AG_{bmh} = 1.578\,in$

Top of HI-STAR 100

MPC Shell-to-Overpack	Fuel Basket-to-MPC Shell
$RG_{moc} = 0.084\,in$	$RG_{bmc} = 0.186\,in$
$AG_{moc} = 0.567\,in$	$AG_{bmc} = 2.001\,in$

The final MPC shell-to-overpack and fuel basket-to-MPC shell clearances are now determined. The final radial and axial MPC shell-to-overpack clearances are determined as:

$$RG_{mo} := \frac{1}{2}\cdot\left(RG_{moh} + RG_{moc}\right)$$

$$RG_{mo} = 0.069\,in$$

$$AG_{mo} := \frac{1}{2}\cdot\left(AG_{moh} + AG_{moc}\right)$$

$$AG_{mo} = 0.482\,in$$

and the final radial and axial fuel basket-to-MPC shell clearances are determined as:

$$RG_{bm} := \frac{1}{2}\cdot\left(RG_{bmh} + RG_{bmc}\right)$$

$$RG_{bm} = 0.144\,in$$

$$AG_{bm} := \frac{1}{2}\cdot\left(AG_{bmh} + AG_{bmc}\right)$$

$$AG_{bm} = 1.79\,in$$

3.W.7 Nomenclature

a is the inner radius of the overpack

AC_{bm} is the initial fuel basket-to-MPC axial clearance.

AC_{mo} is the initial MPC-to-overpack axial clearance.

AG_{bm} is the average final fuel basket-to-MPC shell gap.

AG_{bmh} (AG_{bmc}) is the final fuel basket-to-MPC shell axial gap for the hot (cold) components.

AG_{mo} is the average final MPC shell-to-overpack axial gap.

AG_{moh} (AG_{moc}) is the final MPC shell-to-overpack axial gap for the hot (cold) components.

b is the outer radius of the overpack.

L_{bas} is the axial length of the fuel basket.

L_{mpc} is the axial length of the MPC.

L_{ovp} is the axial length of the overpack.

r_1 (r_2,r_3,r_4) is mean radius of the overpack inner shell (intermed. shells, neutron absorber, outer shell).

R_b is the outer radius of the fuel basket.

R_{mpc} is the mean radius of the MPC shell.

RC_{bm} is the initial fuel basket-to-MPC radial clearance.

RC_{mo} is the initial MPC shell-to-overpack radial clearance.

RG_{bm} is the average final fuel basket-to-MPC shell gap.

RG_{bmh} (RG_{bmc}) is the final fuel basket-to-MPC shell radial gap for the hot (cold) components.

RG_{mo} is the average final MPC shell-to-overpack radial gap.

RG_{moh} (RG_{moc}) is the final MPC shell-to-overpack radial gap for the hot (cold) components.

t_1 (t_2,t_3,t_4) is the thickness of the overpack inner shell (intermed. shells, neutron absorber, outer shell).

T_{bar} is the average temperature of the overpack cylinder.

α_1 (α_2,α_3,α_4) is the coefficient of thermal expansion of the overpack inner shell (intermed. shells, neutron absorber, outer shell).

α_{avg} is the average coefficient of thermal expansion of the overpack.

α_{bas} is the coefficient of thermal expansion of the overpack.

α_{mpc} is the coefficient of thermal expansion of the MPC.

ΔL_{bh} (ΔL_{bc}) is the axial growth of the fuel basket for the hot components.

ΔL_{mpch} (ΔL_{mpcc}) the the axial growth of the MPC for the hot (cold) components.

ΔL_{ovph} (ΔL_{ovpc}) is the axial growth of the overpack for the hot (cold) components.

ΔR_{ah} (ΔR_{ac}) is the radial growth of the overpack inner radius for the hot (cold) components.

ΔR_{bh} (ΔR_{bc}) is the radial growth of the fuel basket for the hot components.

ΔR_{mpch} (ΔR_{mpcc}) is the radial growth of the MPC shell for the hot (cold) components.

ΔT_{1h} (ΔT_{1c}) is the temperature change at the overpack inside surface for hot (cold) components.

ΔT_{2h} (ΔT_{2c}) is the temperature change at the outside enclosure shell surface for hot (cold) components.

ΔT_{3h} (ΔT_{3c}) is the temperature change at the MPC shell mean radius for hot (cold) components.

ΔT_{4h} (ΔT_{4c}) is the temperature change at the MPC basket periphery for hot (cold) components.

ΔT_{5h} (ΔT_{5c}) is the temperature change at the MPC basket centerline for hot (cold) components.

ΔT_{bas} is the fuel basket centerline-to-periphery temperature gradient.

σ_{ca} is the circumferential stress at the overpack inner surface.

σ_{cb} is the circumferential stress at the overpack outer surface.

σ_r is the maximum radial stress of the overpack.

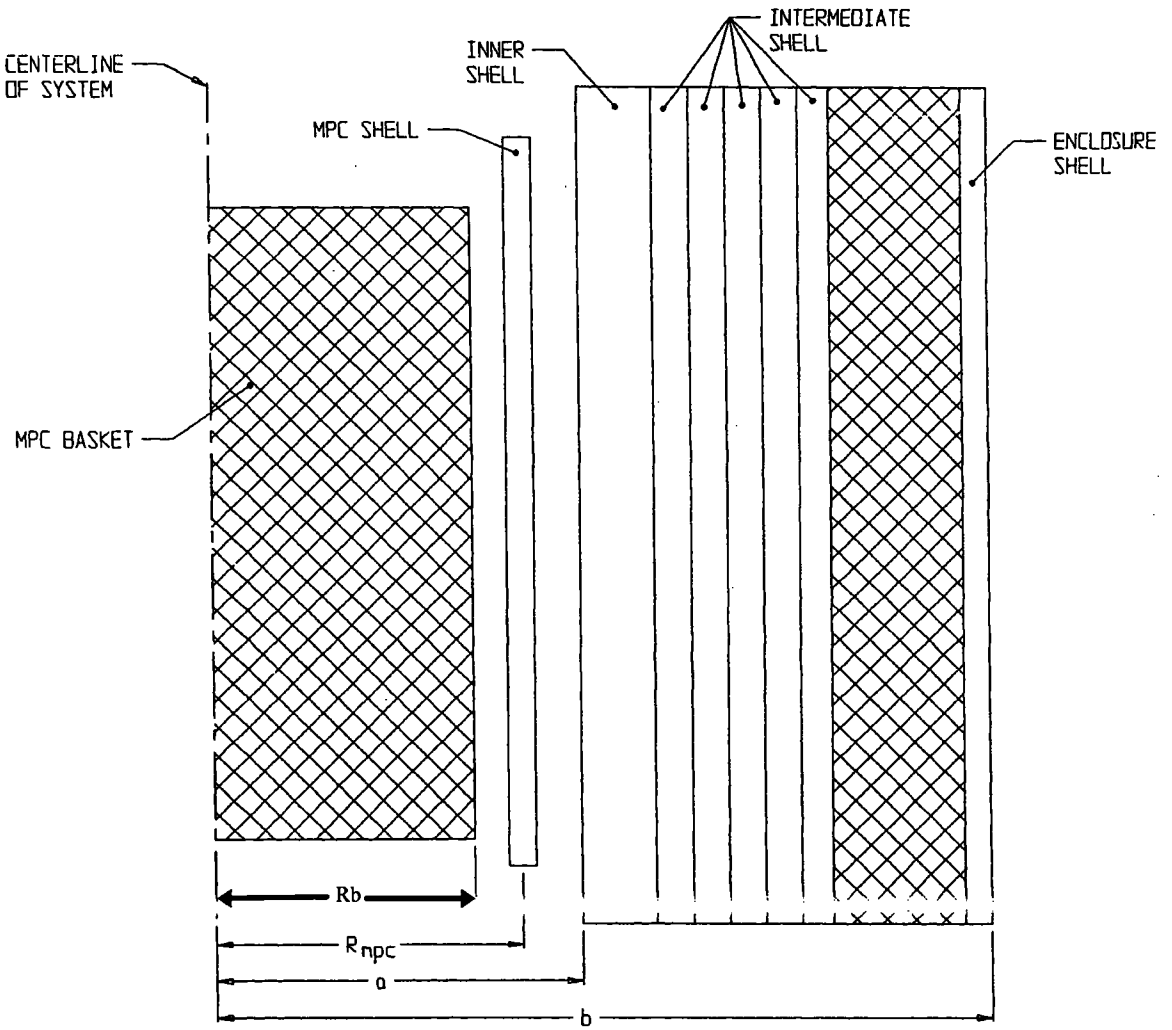

FIGURE 3.W.1; GEOMETRY OF SECTION FOR THERMAL EXPANSION CALCULATIONS

APPENDIX 3.X CALCULATION OF DYNAMIC LOAD FACTORS

3.X.1 Introduction

In Appendix 3.A, the rigid body deceleration sustained by a loaded HI-STAR 100 system under postulated drop events has been calculated. The deceleration profile encompassed by the first half cycle is found to be approximated by a triangular half-wave. It is recognized that the local structural flexibility of the structural members within the cask would modify the net equivalent inertia load for which the member is subjected.

In classical elastic stress analysis, a dynamic load factor (DLF) is determined to reflect the local dynamic effects due to local flexibilities. The DLF is a function of the frequency content of the component being analyzed, the postulated level of structural damping, and the shape and duration of the input load pulse. For most structural elements, it is adequate to compute the fundamental frequency of the element and utilize the classical DLF charts to establish the DLF for the specified impulse. However, in more complicated situations, it is necessary to determine the DLF using a direct numerical formulation. For example, the DLF of the cask bolted cover under a lateral excitation can be readily established from a structural dynamics textbook chart for a wide variety of pulse shapes. On the other hand, the case of lateral excitation of a fuel basket, which involves simultaneous deceleration of the self mass of the panel along with a much heavier fuel assembly mass, requires a direct time integration solution. The fuel assembly is modeled as a lumped compliant mass "riding" the fuel basket panel mass during the impulsive deceleration event. Thus, the fuel basket DLF problem is modeled as a two-degree of freedom system with the basket panel represented by a single degree of freedom mass-spring-damper system (consistent with its fundamental mode) with the added spent nuclear fuel (SNF) mass appended to it, but not permanently affixed. The SNF should be assumed to be plastically connected; i.e., the coefficient of restitution set equal to zero to simulate the absence of springback and to render the dynamic analysis consistent with the "lumped uniform load" modeling of the SNF effect in the static stress analysis of the fuel basket.

Therefore, to cover all structural cases within the cask, both a single-degree of freedom spring-mass-damper system and a multi-mass system with contacting compliant surface, are subject to a pulse load of duration and shape consistent with the dynamic drop analyses to determine the appropriate DLF.

The DLF is defined as the ratio of the peak dynamic displacement of the structural mass when subject to a time dependent pulse force with peak amplitude F, to the corresponding static displacement of the structural mass when subject to the constant force amplitude F. Since the displacement in the dynamic models is related to the elastic internal energy imparted to the component, the calculation of the DLF in this manner properly reflects any increase in the stress levels in a corresponding static analysis.

3.X.2 Analysis Models

3.X.2.1 Components Modeled by Single Degree of Freedom Systems

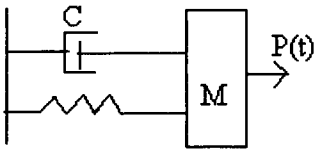

The following items are defined:
c = damping coefficient
M=mass contributing to dynamic motion
k = spring constant
P(t) = pulse loading with peak value F
x(t) = displacement of mass M

If the pulse force is defined as P(t) = F * f(t) where the maximum value of f(t) is 1.0, then F is the peak force magnitude and the static solution x_s may be defined as

$x_s = F/k$

For the determination of the DLF for the cask system, it is appropriate to use a half triangular wave as a pulse, with duration of the pulse equal to t_p. The dynamic load factor (DLF) is the maximum value of the ratio x/x_s that occurs for a total event time >> t_p.

The input triangular pulse shape is defined in Figure 3.X.1.

F is the peak value of the pulse shape and tp is the duration of the half-pulse. The solution for the single degree of freedom undamped system is given in [3.X.3,(Section 4, p125,128)]. The results are reproduced in Figure 3.X.2. The graph plots the ratio of the maximum dynamic response x to the static response F/k (i.e., the DLF) versus the ratio of the triangular pulse duration divided by the period associated with the natural frequency of the single degree of freedom system.

3.X.2.2 Components Modeled by Multiple Degree of Freedom Systems

The MPC fuel basket has been stress analyzed using finite element analysis methods assuming that the applied load is a design basis constant deceleration. The spent fuel mass, which is heavier than a fuel basket panel, is conservatively assumed to be a very compliant component with no structural stiffness and to transfer load to the panel element as a uniform pressure acting on the panel surface. In the actual dynamic environment, the fuel assembly mass is confined, during a drop event, by the surrounding walls of the basket, but is not physically attached to the fuel basket. To derive an appropriate dynamic load factor, the configuration consisting of the confining panels and the fuel mass must be modeled and the assemblage subjected to the appropriate triangular pulse shape and time duration. The peak displacement response of the panel mass is then compared to the static response under a static deceleration having the same peak to define the appropriate DLF. The specific configuration analyzed for determination of dynamic load factors is shown in Figure 3.X.3. The solution to this problem is obtained using the commercial computer code "Working Model" which has been subject to independent Quality Assurance verification and validation at Holtec International. Working Model is ideally suited to the solution of dynamics problems involving multiple masses in contact with each other and is also utilized in the HI-STAR 100 Part 71 SAR submittal for a transport license to analyze impact limiter performance under hypothetical accident conditions. Specific results are reported in a subsequent section of this appendix.

In Figure 3.X.3, the SNF assembly is confined by the basket wall panels; the inertia load resulting from the deceleration pulse is applied to the SNF and to the panels. The structural configuration is simulated by a mass-spring system representing the lower supporting panel, by a compliant lumped mass representing the SNF assembly, and by a second mass-spring system representing the confining panel above the SNF mass The two linear springs represent the structural flexibility of the basket panels. The applied time varying inertia force which is applied to each of the masses is equal to the respective mass multiplied by a triangular shaped pulse with peak value equal to the specified drop deceleration. The compliant spent fuel assembly contact is simulated by using a coefficient of restitution value near zero which is consistent with the assumption in the static stress analysis that the fuel loading is a uniform load over the panel surface because the SNF assembly follows the panel deformation.

In subsequent sections, an evaluation of potential DLF magnitudes is carried out for representative components of HI-STAR. While a number of cask components are examined to determine the fundamental frequency, DLF's are projected only for those components most affected by the storage handling events.

3.X 3 References

[3.X.1] H.A. Rothbart, Mechanical Design and Systems Handbook, 2nd Edition, McGraw Hill, 1985.

[3.X.2] Working Model 3.0, Knowledge Revolution, San Mateo, CA., 1995.

[3.X.3] W.T. Thomson, Theory of Vibration With Applications, 2nd Edition, Prentice Hall, 1981, Section 7.4, p. 220.

[3.X.4] Dynamic Characteristics of an MPC Fuel Basket Panel Subject to Lateral Drops-Preliminary Calculations

The most significant loading level applied to a HI-STAR 100 component occurs during drop conditions. In particular, the fuel basket, under side drop or tipover, may have individual panels subjected to high levels of lateral load. Since the stress analyses of the basket is based on static methods, the results must be amplified by a DLF prior to performing a structural integrity evaluation involving comparison against specified stress or stress intensity levels. As described previously, the DLF depends on the product of component natural frequency and impulse time duration. Appendix 3.A presents the analysis of the postulated drop events appropriate for a 10CFR72 submittal and computes impulse durations. Here we compute appropriate dynamic load factors using the multi-mass model described previously, with deceleration pulse durations and strengths determined in Appendix 3.A. Calculations are made and results obtained for both PWR and BWR fuel baskets.

For the dynamic simulation, the panel flexibilities, the panel fundamental frequency (or period), and the effective panel mass participating in the dynamics of the configuration must be established. The panel section perpendicular to the applied deceleration pulse is modeled by a beam clamped at both ends (to the adjacent perpendicular panel). Figure 3.X.4 defines the configuration and the variables.

From Table 7.1 of [3.X.1], the spring constant of a clamped-clamped beam is given as

$$K := 384 \cdot \frac{E \cdot I}{L^3}$$

Input data for the Holtec MPC-24 basket is(L is the largest panel width, t is the panel metal thickness, and b is equal to the total length of the panel along the axis of HI-STAR).Use of a smaller L, representing only the panel confining the fuel, leads to a higher K and results in a lower dynamic amplification factor. To be conservative, we use the large L associated with the pitch.

$L := 10.777 \cdot in$ $\quad t := \frac{10}{32} \cdot in$ $\quad b := 176.5 \cdot in$

At 725 deg. F the Young's Modulus is $E := 24600000 \cdot psi$ (FSAR Table 3.3.1)

The actual weight of the modeled stainless steel panel is

$$W_{actual} := 0.29 \cdot \frac{lbf}{in^3} \cdot b \cdot L \cdot t \qquad W_{actual} = 172.3815\,lbf$$

Compute the moment of inertia "I" and the cross section area "A" perpendicular to the bending axis.

$$I := b \cdot \frac{t^3}{12} \qquad A := b \cdot t$$

Therefore, the spring constant K is given, for the PWR panel, as (use the entire length "b")

$$K := 384 \cdot \frac{E \cdot I}{L^3} \qquad K = 3.3876 \times 10^6 \frac{lbf}{in}$$

Compute the natural frequency of the panel considered as a clamped-clamped beam.

The natural frequency is computed from a formula and tables given in [3.X.1] (Chap. 5 and Tables 5.8(c) and 5.10). The nomenclature that used in the reference.

$K_m := 0.9$ $C_n := 71.95$

Therefore the lowest natural frequency of the panel is

$$f_n := C_n \cdot \frac{\sqrt{\frac{I}{A}}}{L^2} \cdot 10^4 \cdot K_m \cdot \frac{in}{sec} \qquad f_n = 502.964\,sec^{-1} \qquad \tau_{pwr} := \frac{1}{f_n}$$

$\omega_n := 2 \cdot \pi \cdot f_n$ $\omega_n = 3.1602 \times 10^3\,sec^{-1}$ $\tau_{pwr} = 1.9882 \times 10^{-3}\,sec$

The effective panel mass participating in the dynamic motion is computed as

$$m_e := \frac{K}{\omega_n^2}$$

The effective participating weight of the panel is

$W_{PWR} := m_e \cdot g$ $W_{PWR} = 130.9603\,lbf$

which is, as expected, less than the actual weight.

The calculations are now repeated for a BWR panel

$L := 6.24 \cdot in$ $t := \frac{8}{32} \cdot in$ $b := 176 \cdot in$

The actual weight of the stainless steel panel is

$$W_{actual} := 0.29 \cdot \frac{lbf}{in^3} \cdot b \cdot L \cdot t \qquad W_{actual} = 79.6224\,lbf$$

Compute the moment of inertia "I" and the cross section area "A" perpendicular to the bending axis.

$$I := b \cdot \frac{t^3}{12} \qquad A := b \cdot t$$

Therefore, the spring constant K is given as

$$K := 384 \cdot \frac{E \cdot I}{L^3} \qquad K = 8.9097 \times 10^6\,\frac{lbf}{in}$$

Compute natural frequency of the panel considered as a clamped-clamped beam

$K_m := 0.9$ $C_n := 71.95$

$$f_n := C_n \cdot \frac{\sqrt{\frac{I}{A}}}{L^2} \cdot 10^4 \cdot K_m \cdot \frac{in}{sec} \qquad f_n = 1.2002 \times 10^3\, sec^{-1}$$

$$\tau_{bwr} := \frac{1}{f_n} \qquad \tau_{bwr} = 8.3319 \times 10^{-4}\, sec$$

$\omega_n := 2 \cdot \pi \cdot f_n$ $\omega_n = 7.5411 \times 10^3\, sec^{-1}$

The effective mass participating in the dynamic motion is computed as

$$m_e := \frac{K}{\omega_n^2}$$

The effective participating weight of the panel is

$W_{BWR} := m_e \cdot g$ $W_{BWR} = 60.4901\, lbf$

3.X.5 Analysis for Dynamic Load Factors for the HI-STAR Fuel Basket Subject to Handling Accidents Resulting in a Lateral Deceleration Pulse - Multi-Degree of Freedom System

The data developed in Section 3.X.4 is used as input data in Working Model to determine dynamic amplification factors. The description of the model is provided in Section 3.X.2.2. Fuel weights used in the multi-mass model are the design basis fuel weights (Table 2.1.6). To determine the DLF, the peak deflection of the panel needs to be established. The DLF is obtained as the maximum ratio of the spring force resisting the dynamic deceleration load, divided by the static spring force obtained if the peak value of the deceleration was applied statically. In this simulation, only drop orientations causing lateral panel bending are significant. From Appendix 3.A, g loads for the side drop and for the non-mechanistic tipover are used to establish the DLF. The tipover g load is obtained by scaling the calculated g load at the top end of the overpack by the ratio of the MPC basket height to the overpack height. The maximum resulting load for the MPC basket is 59.81g. The design basis value of 60g is used in this appendix for calculations

$$G_{to} := 60$$

with a triangular pulse duration of 4.5 milliseconds. The quasi-static force in the spring induced by dead load plus drop inertia load is easily computed for the two basket types as

$$Force\_PWR_{to} := \left(1680 \cdot lbf + W_{PWR}\right) \cdot \left(G_{to} + 1\right) \qquad Force\_PWR_{to} = 1.1047 \times 10^{5}\, lbf$$

$$Force\_BWR_{to} := \left(700 \cdot lbf + W_{BWR}\right) \cdot \left(G_{to} + 1\right) \qquad Force\_BWR_{to} = 4.639 \times 10^{4}\, lbf$$

The Working Model analyses are performed for both types of fuel baskets with deceleration pulses of triangular shape and with a time duration of 0.0045 seconds. In all simulations, the coefficient of restitution between the SNF mass and the panel masses is set to 0.2 to bound the actual fully compliant case. As is noted above, the use of a zero coefficient of restitution is consistent with the completely compliant SNF mass assumption which permeates all of the basket stress analyses. Figures 3.X.5-3.X.6 provide the time history of the force in the loaded lower panel spring for the PWR, BWR baskets, respectively. For each case, the DLF is obtained by dividing the peak dynamic spring force by the static spring forces computed above (note that since the spring forces are linear functions of the panel central deflection, the DLF is directly calculated from the spring force results).

From the results obtained from the multi-degree of freedom dynamic analyses, the DLF's are approximately 1.1 for both the PWR basket and for the BWR basket for the pulse duration considered. The peak value for the dynamic force is achieved at approximately the time when the actual applied force pulse returns to a zero value. The DLF of 1.1 should be applied to all of the static stress results from stress analysis of the basket under lateral loads arising from a handling accident when assessing structural safety factors.

3.X.6 Overpack Top Closure Lid Considered as a Simply Supported Circular Plate

3.X.6.1 Input Data

Outer bolt circle radius $R := \frac{74.75 \cdot in}{2}$ From Holtec Drawings

Lid thickness $h := 6 \cdot in$

3.X.6.2 Calculations

Compute the natural frequency of the lid.

The natural frequency is computed from a formula and tables given in [3.X.1] (Chap. 5 and Tables 5.8(g) and 5.10). The nomenclature that used in the reference.

$K_m := 0.92$ $C_n := 4.84$

Therefore the lowest natural frequency of the lid is

$f_l := C_n \cdot \frac{h}{R^2} \cdot 10^4 \cdot K_m \cdot \frac{in}{sec}$ $f_l = 191.2591\,sec^{-1}$ $\tau_l := \frac{1}{f_l}$

$\tau_l = 5.2285 \times 10^{-3}\,sec$

3.X.7 MPC Bottom Plate - Clamped at Edge

3.X.7.1 Input Data

Mean radius $R := \frac{(68.375 - .5) \cdot in}{2}$ $R = 33.9375\,in$

Thickness $h := 2.5 \cdot in$

3.X.7.2 Calculations

The natural frequency is computed from a formula and tables given in [3.X.1] (Chap. 5 and Tables 5.8(g) and 5.10). The nomenclature that used in the reference.

$K_m := 0.9$ $C_n := 9.94$

Therefore the lowest natural frequency of the bottom plate is

$f_p := C_n \cdot \frac{h}{R^2} \cdot 10^4 \cdot K_m \cdot \frac{in}{sec}$ $f_p = 194.1821\,sec^{-1}$ $\tau_p := \frac{1}{f_p}$

$\tau_p = 5.1498 \times 10^{-3}\,sec$

3.X.8 Dynamic Load Factor Upper Bound Estimates for End Drop Event

The impact deceleration pulse duration is obtained from Appendix 3.A as

$$t_p := 0.002 \cdot sec$$

The DLF for the Overpack Top Lid is based on a bottom end drop

$$\frac{t_p}{\tau_1} = 0.3825$$

From Figure 3.X.2, the DLF associated with this ratio is approximately 1.05.

There is no credible dynamic impact event while in storage that would affect the MPC base plate; however, in transport, the MPC base plate would require a DLF in the evaluation of a so called "top end drop".

3.X.9 Conclusions

Dynamic Load Factor Equations have been obtained in this appendix. All stress calculations and safety margins use these dynamic load amplifiers to evaluate the adequacy of final safety margins. For the MPC fuel baskets, modeled by multi-degree of freedom simulations, the DLF is approximately 1.1 for both the MPC-24 and the MPC-68 using an impact duration simulating a handling accident that leads to lateral loading of the fuel basket panels. For other components affected by handling or other dynamic events, and modeled by single degree of freedom systems, the DLF is bounded by the value 1.1.

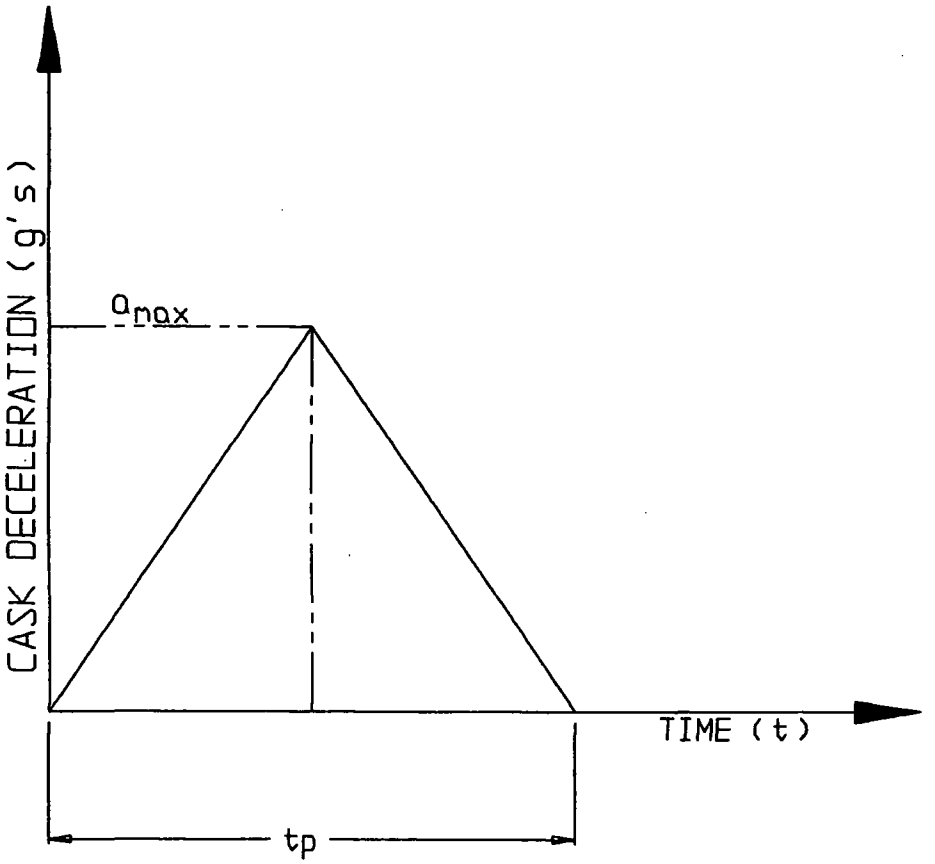

a_{max}	:	PEAK g LEVEL (FILTERED DATA)
tp	:	PULSE DURATION (sec)

FIGURE 3.X.1 : TRIANGULAR DECELERATION PULSE SHAPE

REPORT HI-2012610 | REVISION 0

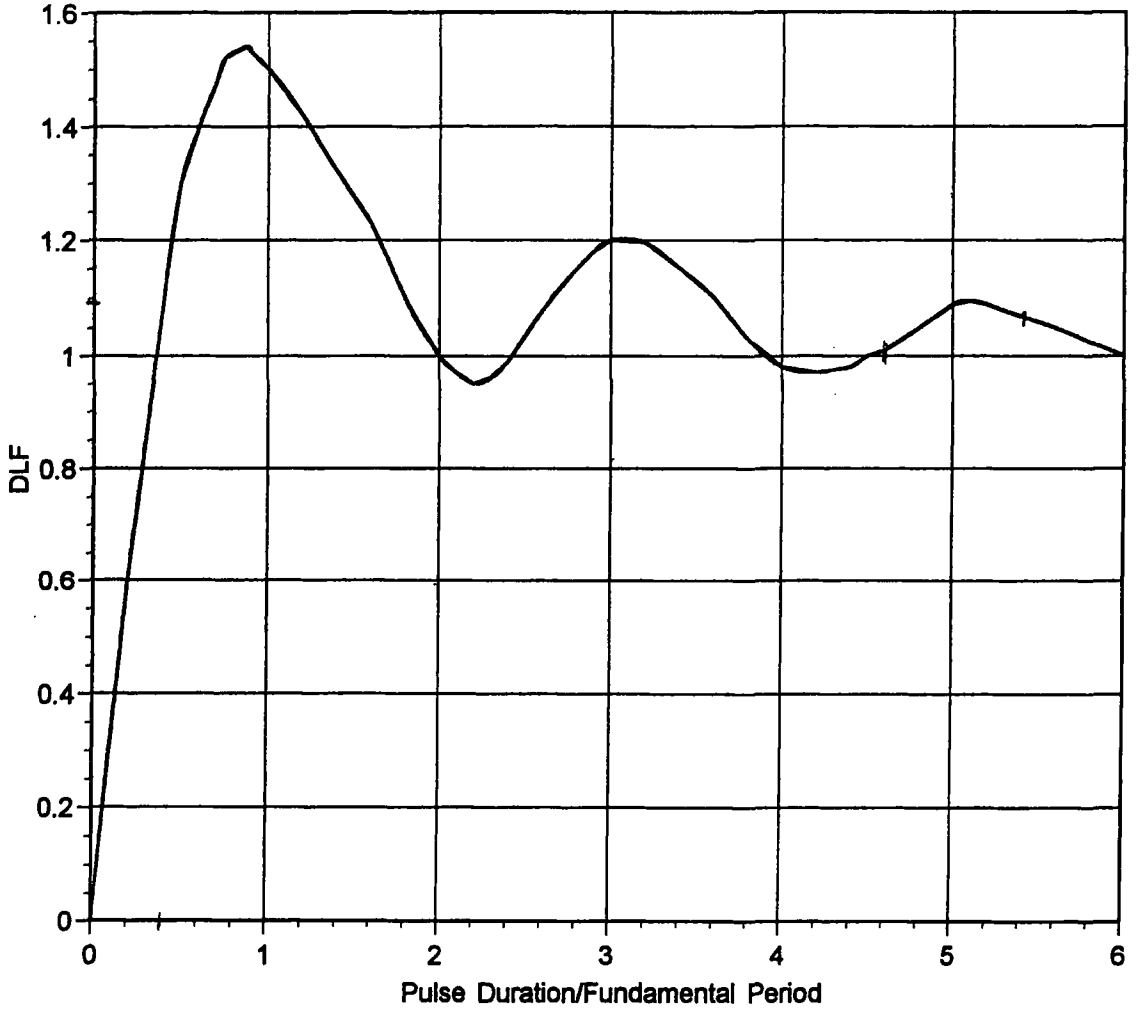

FIGURE 3.X.2 - Dynamic Load Factor for Single Degree of Freedom System - Triangular Pulse Shape, No Damping

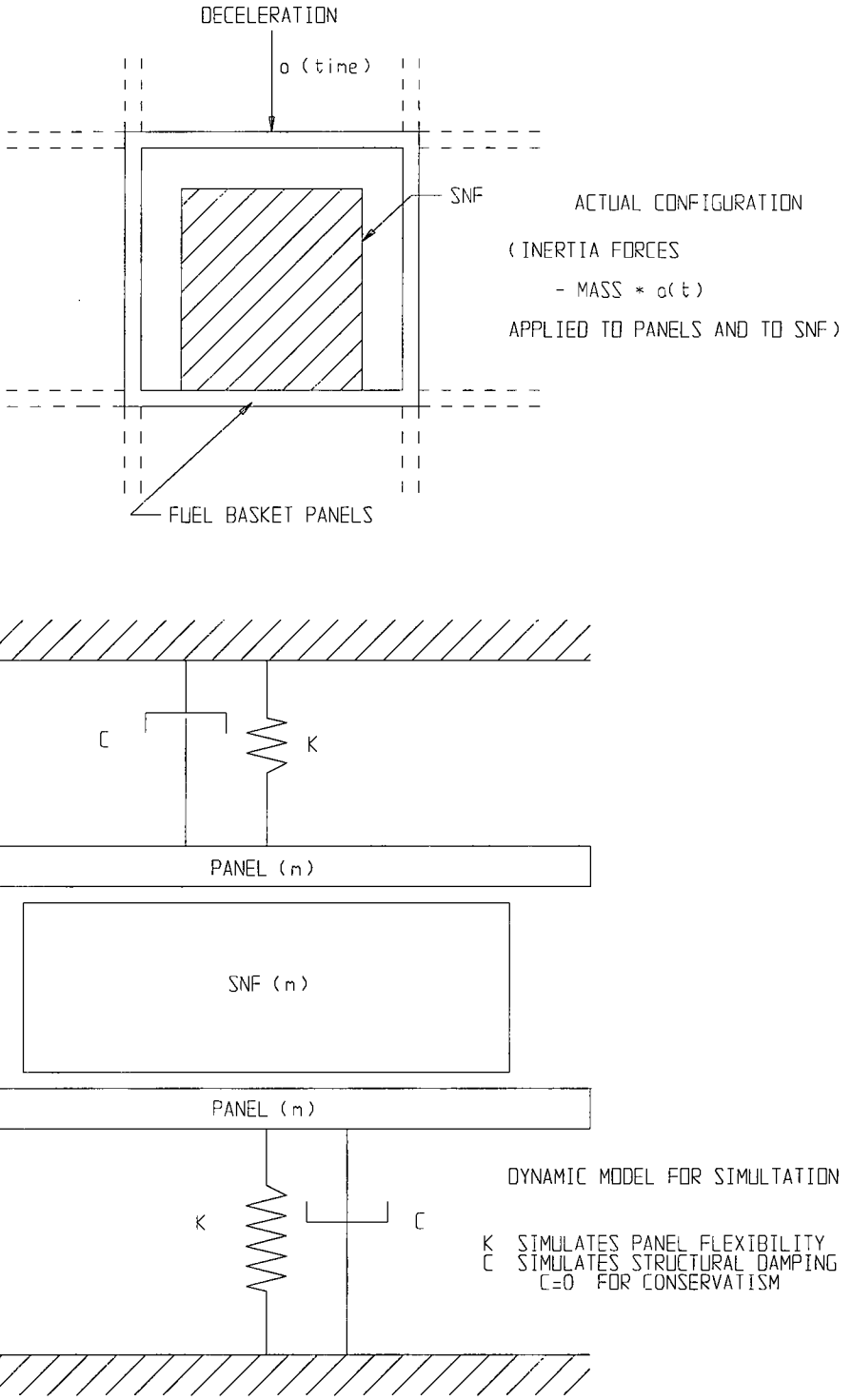

FIGURE 3.X.3; DYNAMIC MODEL FOR MULTI-DEGREE OF FREEDOM ANALYSIS FOR DLF DETERMINATION

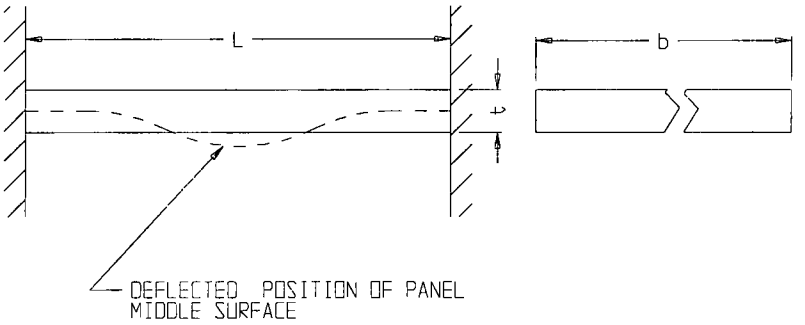

FIGURE 3.X.4; CLAMPED BEAM MODEL FOR FUEL BASKET PANEL

REPORT HI-2012610

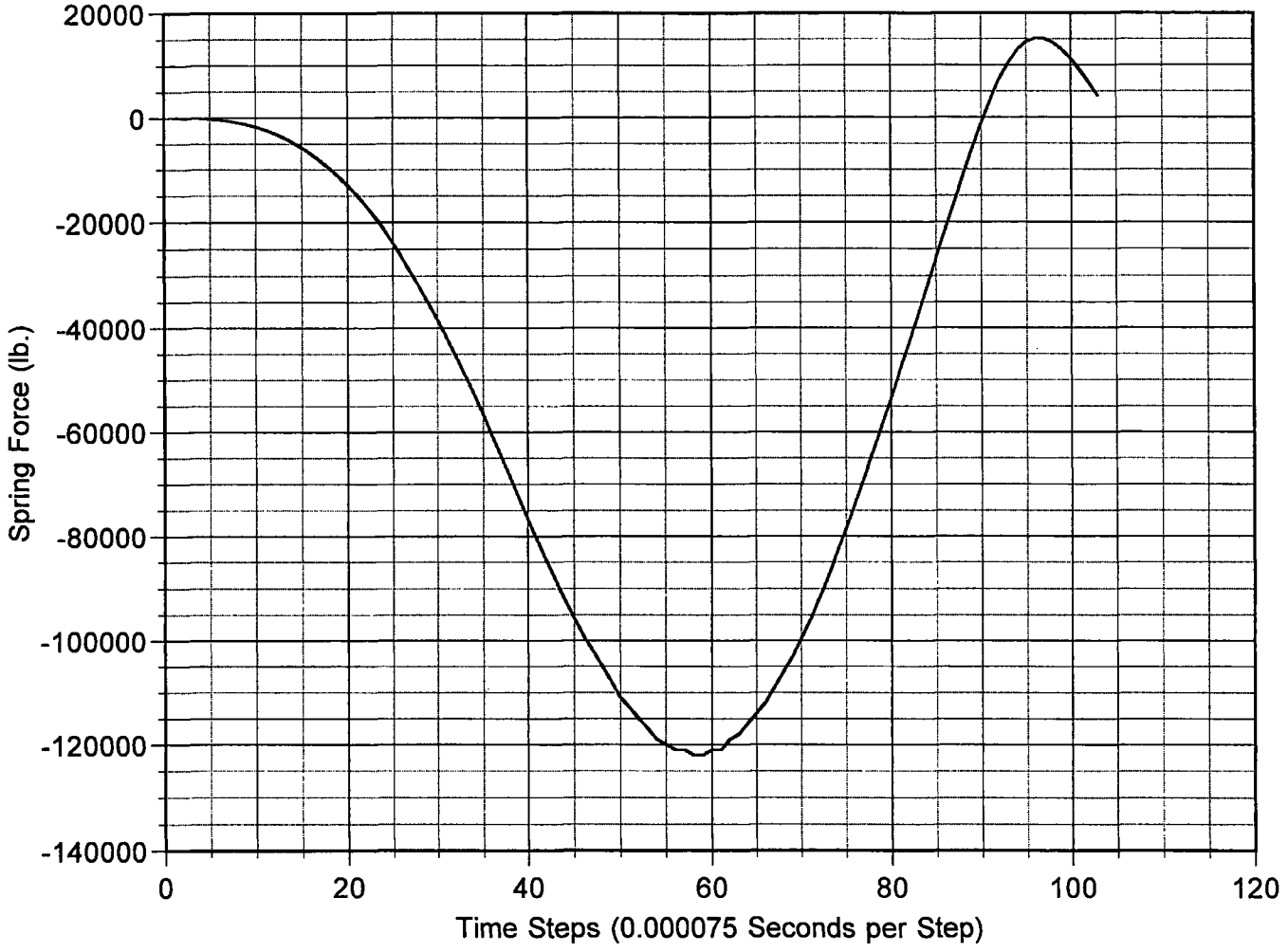

FIGURE 3.X.5 Dynamic Force in Lower Panel Spring vs. Time - PWR Basket, 60g Peak Value of Deceleration, Triangular Pulse, Duration 0.0045 Seconds

REVISION 0

REPORT HI-2012610

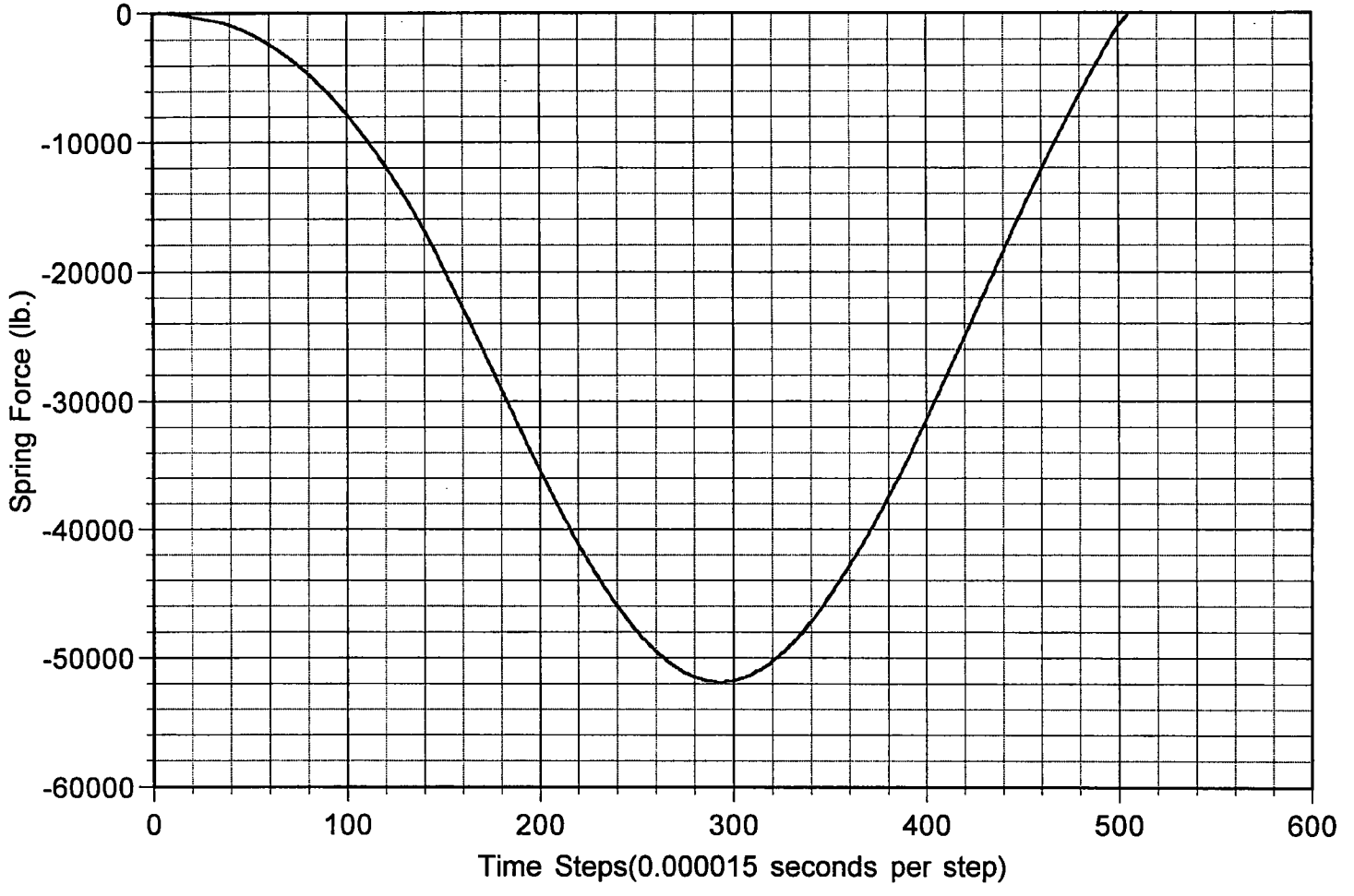

FIGURE 3.X.6 Dynamic Force in Lower Panel Spring vs. Time - BWR Basket, 60g Peak Value of Deceleration, Triangular Pulse, Duration 0.0045 Seconds

REVISION 0

Appendix 3.Y - Cask Under Three Times Dead-load

3.Y.1 Purpose

Regulatory Guide 3.61 requires that the maximum primary stress near the trunnion/cask interface must be limited to the yield stress when three times the lifted load is applied. In other words, there must be a safety factor of three on yield when subject to the lifted load. Safety factor is defined in this section as the allowable strength divided by the calculated stress.

This requirement is applied to portions of the cask body in this analysis. The critical areas of concern during a lift are the top flange near the lifting trunnions and the MPC and Overpack baseplates.

It is shown that the stresses in the cask body are less than the acceptance limit when the structure is subjected to three times dead load.

3.Y.2 Top-Flange Analysis

In order for the trunnion stress to fully develop, the top flange must be able to accommodate stresses during a lift. This section determines the primary membrane and bending stresses in the HI-STAR 100 top flange when the trunnions are subject to a load equal to three times the cask weight.

3.Y.2.1 Assumptions

The assumptions in the finite element analysis are as follows:

1. The analysis does not take any credit for the thread engagement between the trunnion and the top flange. The interface between the top flange and the trunnion is assumed smooth and frictionless.

2. The weight of the cask is conservatively applied to a single point at the axis of the trunnion as show in the finite element plot in Figure 3.Y.1.
3. The finite element model that represents the cask is truncated approximately 36 inches below the top of the cask and all points there are fixed against translational movement along the axis of the cask.
4. The analysis model conservatively does not include the cask lid and the lid connections since there is a lifting operation when the lid is absent.

3.Y.2.2 Methodology

A one-quarter symmetry finite element model of the top section of the HI-STAR, without the lid, has been constructed using ANSYS[Ref. 1] 3-D isoparametric elements, SOLID45. The interface between the top flange and the trunnion is modeled with 3-D, compression only, interface elements, CONTACT49, with interface contact stiffness set at the large value of 1.0E+09 pounds-per-inch. A concentrated force F, equal to 25% of the amplified load, is vertically applied to the trunnion at the node located on the outer edge of its axis as shown in Figure 3.Y.1.

$$F = 3W/4 = 187{,}500 \text{ pounds} \quad (¼ \text{ symmetry})$$

where, W, the total weight of HI-STAR equals 250,000 pounds. The truncated end of the finite element model is fixed against vertical translation. The details of the finite element model are shown in Figure 3.Y.1.

The contact region between the trunnion and flange is expected to experience localized plasticity. Thus, a non-linear material property is defined for the top flange. The yield stress, at 400 °F, and the tangent modulus that defines the bilinear elastic-plastic material property are respectively taken as 32.20 ksi and 264.0 ksi. The plot of the bilinear stress-strain curve is shown in Figure 3.Y.2. The Young's modulus and the Poisson's ratio are respectively taken as 2.76E+04 ksi and 0.3

3.Y.2.3 Input Data

The top flange is constructed from steel material, Type SA350-LF3. The temperature dependent material properties of SA350-LF3 are listed in Table 3.3.4 of this FSAR. The material yield strength is taken as 32.2 ksi at the design temperature of 400 °F.

Cask dimensions are taken from applicable drawings in this submittal.

3.Y.2.4 Acceptance Criteria

Lifting attachments on casks are traditionally analyzed in accordance with NUREG-0612 and ANSI 14.6. These documents require a factor of safety during lifts based on six times yield for non-redundant lifts and based on three times yield for redundant lifts. Regulatory Guide 3.61 requires regions adjacent to the trunnion to have stresses below yield when lifted at 3 times deadweight.

In this case, the appropriate criterion for a pressure vessel is that the maximum membrane stress across any section must be below yield and that membrane plus bending stresses do not exceed 1.5 times yield when the applied loading is set at three times the lifted load. This is consistent with the design philosophy of the ASME code.

3.Y.2.5 Analysis

The stress intensity classifications (i.e., *membrane*, and *membrane* plus *bending*) at five critical locations in the top flange are presented in Figures 3.Y.4(a) through 3.Y.4(e). The location and path of each of the five sections in the top flange is identified by a set of nodes shown on the top right side of the stress classification plots [Figures 3.Y.4(a) through 3.Y.4(e)]. The two nodes in each of these figures define the beginning and the end of the path for which the maximum stress is classified. Furthermore, Figure 3.Y.3 displays the physical locations of these nodal points. The maximum *membrane* stress of

27.44 ksi and the maximum membrane plus bending stress of 30 ksi are respectively reported in Figure 3.Y.4(e).

3.Y.2.6 Results

The safety factors in the top flange, based on the results of the finite element analysis calculated using three times the cask weight as the applied trunnion load, are as follows:

Stress Class	Maximum(ksi)	Allowable(ksi)	S.F.
Membrane	27.44	32.2	1.17 [Figure 3.Y.4(e)]
Mem. + Bending	30.00	48.3	1.61 [Figure 3.Y.4(e)]

It is seen from the above table that the safety factors are greater than 1.0 when subjected to a vertical lift through the lifting trunnions, at three times the weight of the cask.

3.Y.2.7 Top-Flange Conclusion

It is concluded that the top flange can accommodate the stress from a lift at three times the cask weight and therefore the intent of Regulatory Guide 3.61 with regard to stress limits in the cask is satisfied.

3.Y.2.8 References

[1] ANSYS 5.3, ANSYS Inc. 1996

3.Y.3 Baseplate Analysis

In this section, the MPC baseplate and the HI-STAR overpack baseplate are considered as simply supported plates subject to bending action under lateral loads equivalent to three times the actual loads when these components are subject to a vertical lift. The object of the calculation is to demonstrate that the intent of 10CFR71, Section 45 with regards to safety factors (or safety margins) is met during a lifting operation

3.Y.3.1 Input Data

Bounding weights are used in this calculation per Table 3.2.4.

Weight of Cask = 250,000 lbs.
Weight of MPC = 90,000 lbs.
Weight of Fuel = 54,000 lbs.
Weight of Fuel Basket = 13,000 lbs.
Weight of MPC baseplate = 3000 lbs.
Weight of Overpack baseplate = 10,000 lbs.

The geometry of the configuration is taken from applicable drawing submitted with this document.

Thickness of MPC baseplate = 2.5 inches
Thickness of Overpack baseplate = 6.0 inches
Diameter of MPC = 68.375 in
Diameter of Overpack = 83.25 in
Weld thickness of MPC = treat as ½" fillet weld
Weld thickness on Overpack = treat as four fillet welds with thickness of tan (30)(1-1/4")= 0.72 in and a length of 1-1/4" in each.

Allowable strengths at design temperatures are used.

Yield stress of Overpack = 32,200 psi (SA350-LF3 at 400 F)
Yield stress of MPC= 20,700 psi (Alloy X at 400 F)
Ultimate stress of weld material (E70xx) = 59,400 psi (400 F)
(weld strength is assumed to decrease with temperature the same as base metal, thus ultimate strength= 70- (300 F)[75 ksi -64.4 ksi /300 F] = 59,400 ksi)

3.Y.3.2 Acceptance Criteria

Consistent with the discussion in 3.Y.2.4, the stresses must be less than yield in the baseplate. Additionally, weld stress is limited to 30% of ultimate based on the weld stress limits set in ASME Section III, Subsection NF, the only section of the Code, which specifically addresses limits for welds of different configurations.

3.Y.3.3 Method

The MPC baseplate is modeled as simply supported circular plate subject to a uniform pressure load. The Overpack baseplate is modeled as a simply supported circular plate subject to a ring load.

3.Y.3.4 Assumptions

1. The baseplates are simply supported (conservative).

3.Y.3.5 References

1. Young, Roark's Formulas of Stress and Strain, 6th edition.

3.Y.3.6 Calculation

A. MPC Evaluation

The MPC baseplate is modeled as a simply supported plate with a uniform pressure load. The maximum stress is given in reference 1 (Table 24, case 10a),

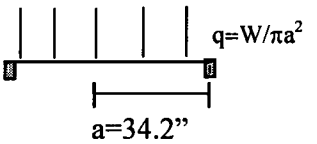

b=0,ro=b=0

$$\sigma = \frac{0.375}{\pi}\frac{W(3+\nu)}{t^2}$$

$$\boxed{\sigma = \frac{1.24}{\pi}\frac{W}{t^2}}$$

Thus, the stress in the MPC baseplate is,

$$\sigma = \frac{1.24}{\pi}\frac{(3\times(54{,}000lbs + 13{,}000lbs + 3{,}000lbs))}{(2.5in)^2} = 13{,}262psi < S_y \text{ O.K.}$$

Therefore, the MPC baseplate meets the acceptance criteria with a margin of safety of:

$$M\arg in = \frac{20{,}700 psi}{13{,}262 psi} - 1 = 0.56$$

The margin of safety on the weld is,

$$\tau = \frac{3W}{A_{weld}} = \frac{3(54{,}000 + 3{,}000 lbs + 13000 lbs)}{2\pi(0.707 in)(34.2 in)(0.5 in)} = 2{,}765 psi$$

$$\text{Margin} = \frac{17{,}820\text{psi}}{2{,}765\text{psi}} - 1 = 5.4$$

B. Overpack

The overpack is modeled as a simply supported circular plate with a ring load. The ring load has the radius of the MPC. Using Reference 1(table 24, case 9a), the stress is:

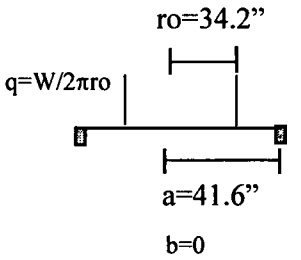

$$\sigma = L9\frac{6qa}{t^2}$$

$$L9 = \frac{ro}{a}\left\{\frac{1+\nu}{2}\ln\frac{a}{ro} + \frac{1-\nu}{4}\left[1-\left(\frac{ro}{a}\right)^2\right]\right\}$$

$$L9 = \frac{34.2}{41.6}\left\{\frac{1+\nu}{2}\ln\frac{41.6}{34.2} + \frac{1-\nu}{4}\left[1-\left(\frac{34.2}{41.6}\right)^2\right]\right\} = 0.15$$

$$\sigma = \frac{0.45}{\pi}\frac{a}{ro}\frac{W}{t^2}$$

$$\therefore \sigma = \frac{0.45}{\pi}\frac{a}{ro}\frac{W}{t^2}$$

$$\sigma = \frac{0.45}{\pi}\frac{(41.6")}{(34.2")}\frac{(3\times(90{,}000+10{,}000lbs)}{(6in)^2} = 1452psi << S_y \text{ O.K.}$$

Therefore the overpack has a margin of safety for bending of,

$$M \arg in = \frac{32{,}200psi}{1452psi} - 1 = 21.2$$

3.Y.3.7 Baseplate Conclusion

The MPC and Overpack baseplates meet the yield criteria when subjected to three times dead load.

3.Y.4 Overall Conclusion

The cask body meets appropriate acceptance criteria when subjected to a lift of three times dead load.

REPORT HI-2012610

FIGURE 3.Y.1 FINITE ELEMENT PLOT

REVISION 0

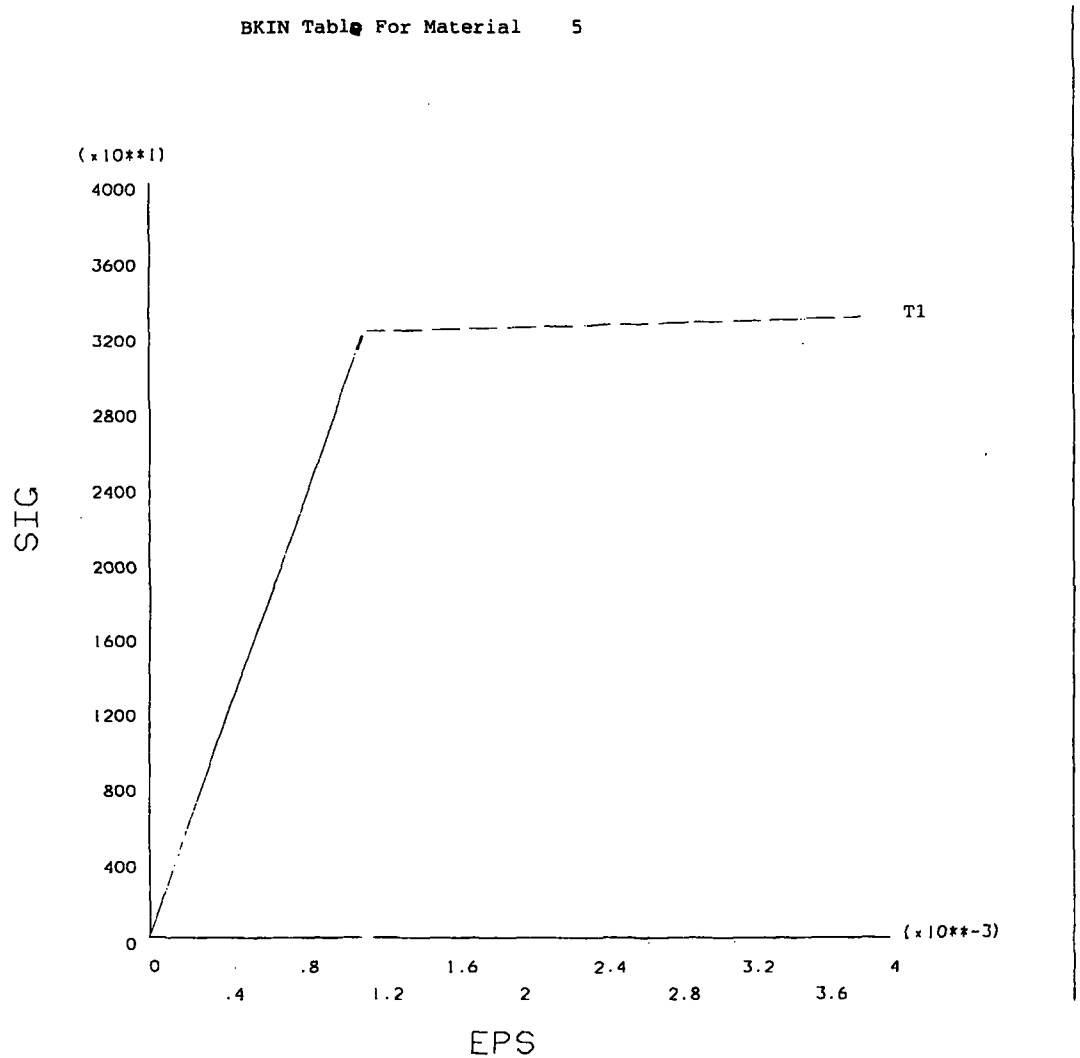

FIGURE 3.Y.2 MATERIAL STRESS-STRAIN CURVE.

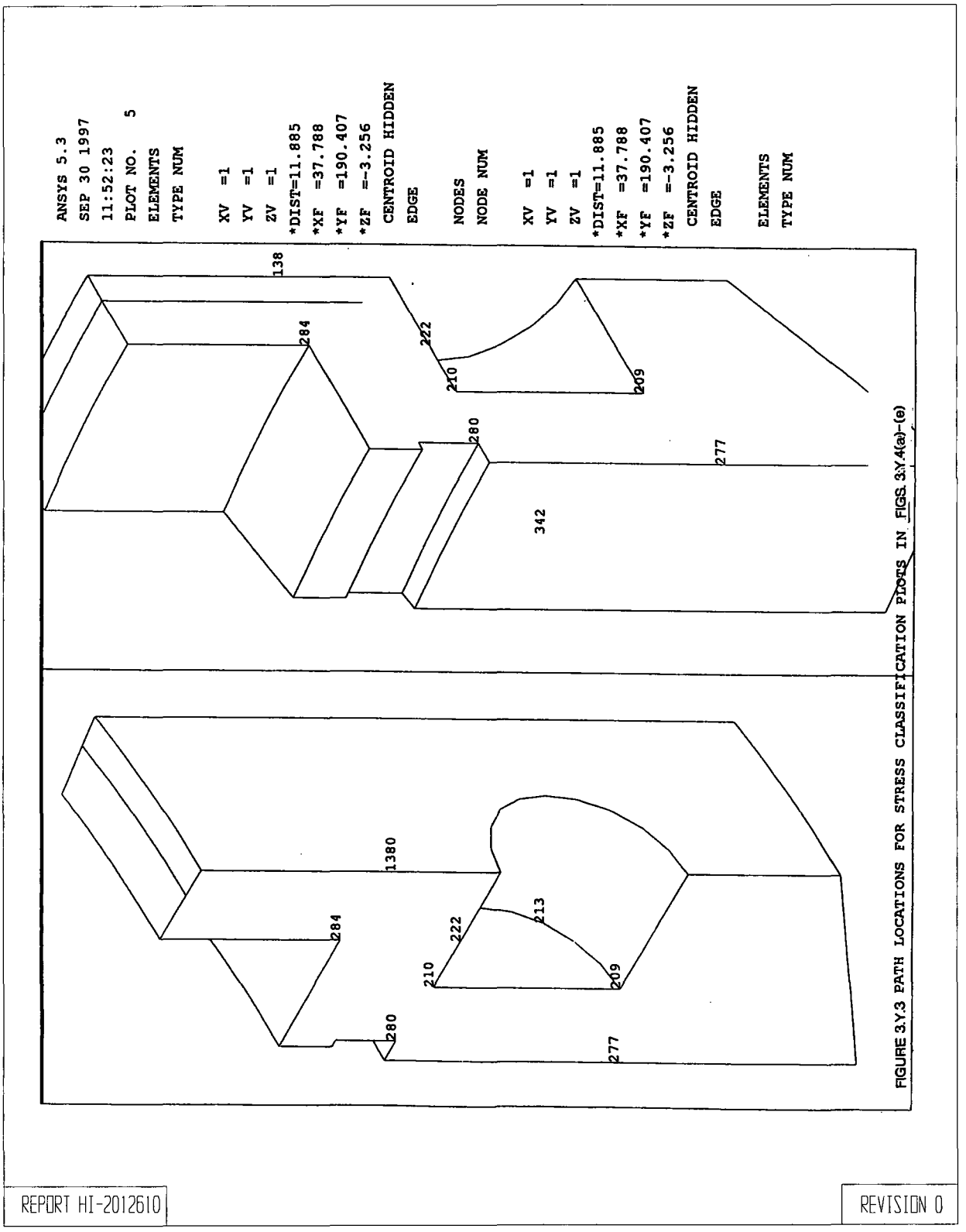

FIGURE 3.Y.3 PATH LOCATIONS FOR STRESS CLASSIFICATION PLOTS IN FIGS 3.Y.4(a)-(e)

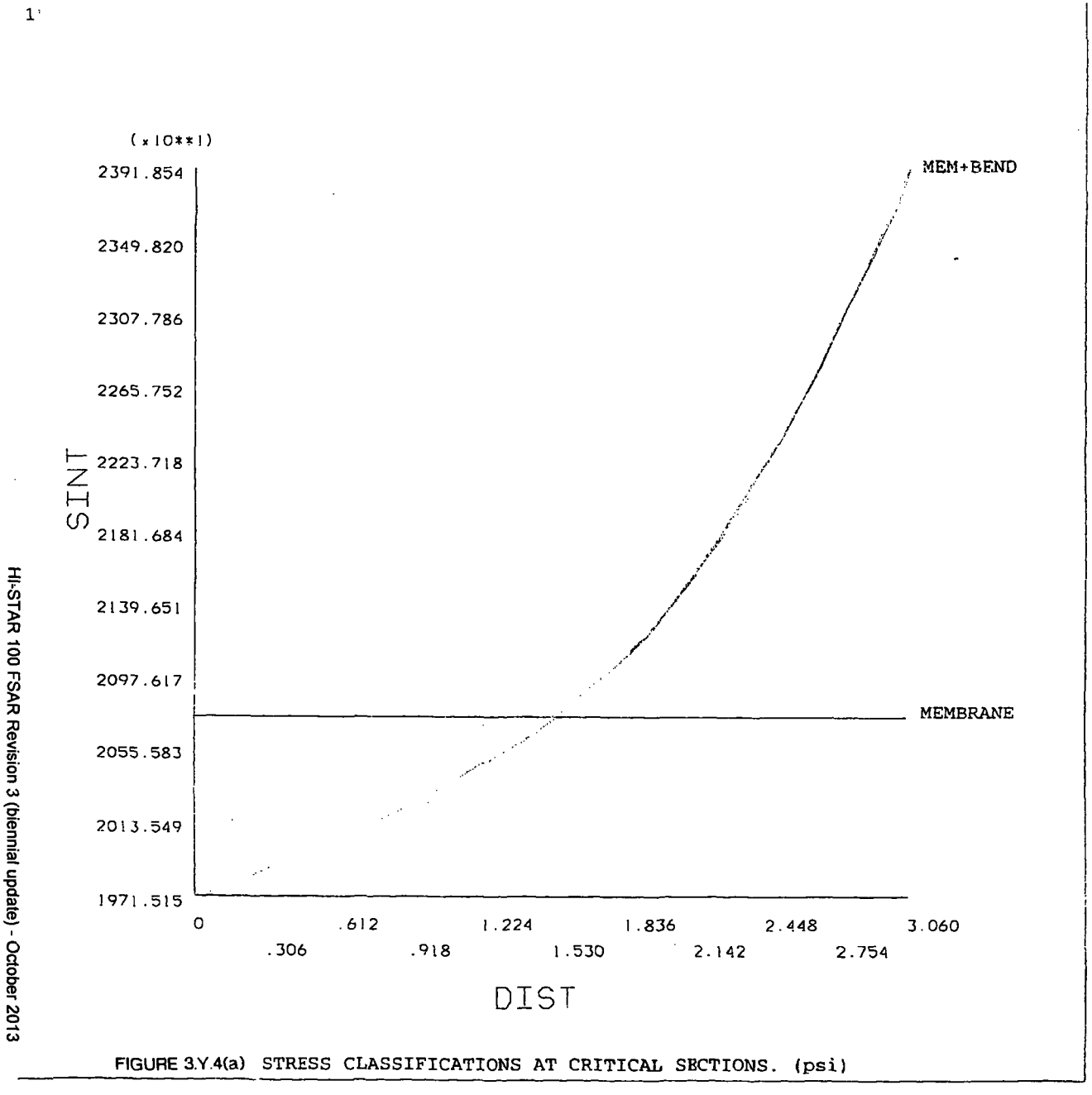

FIGURE 3.Y.4(a) STRESS CLASSIFICATIONS AT CRITICAL SECTIONS. (psi)

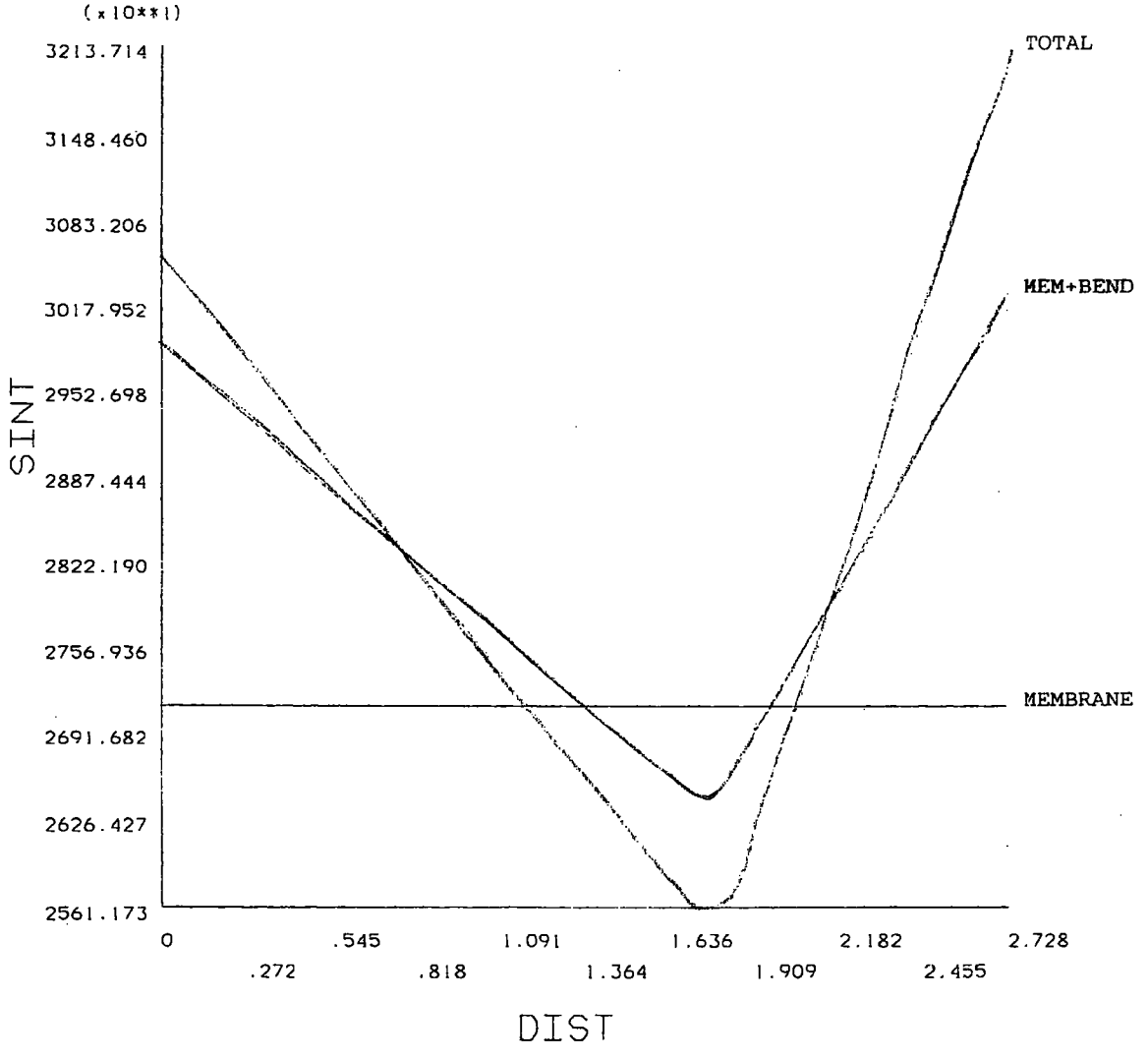

ANSYS 5.3
SEP 30 1997
10:44:25
PLOT NO. 5
POST1
STEP=1
SUB =10
TIME=1
SECTION PLOT
NOD1=284
NOD2=1380
SINT

ZV =1.732
*DIST=.75
*XF =.5
*YF =.5
*ZF =.5
CENTROID HIDDEN

FIGURE 3Y.4(b) STRESS CLASSIFICATIONS AT CRITICAL SECTIONS. (psi)

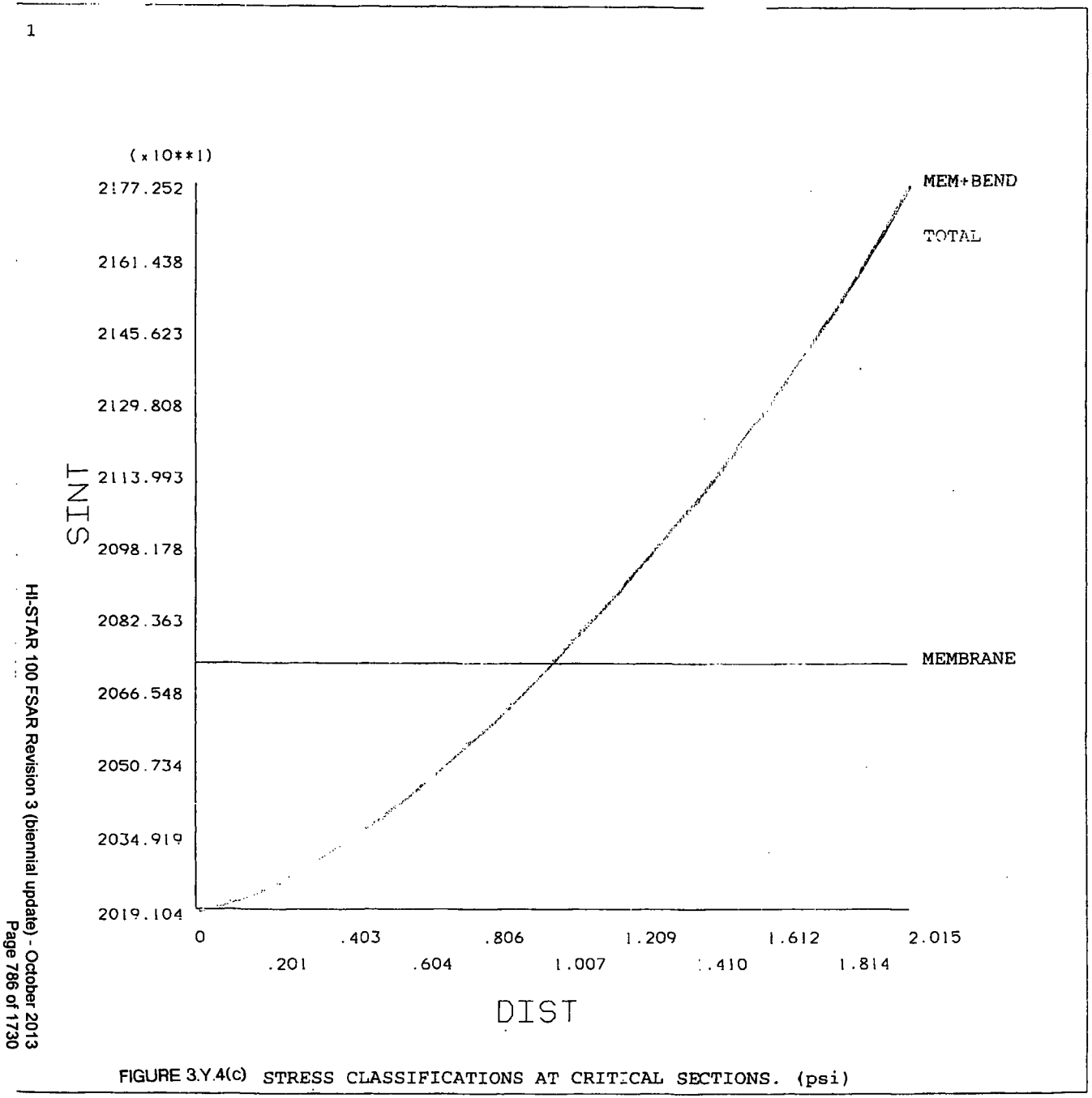

FIGURE 3.Y.4(c) STRESS CLASSIFICATIONS AT CRITICAL SECTIONS. (psi)

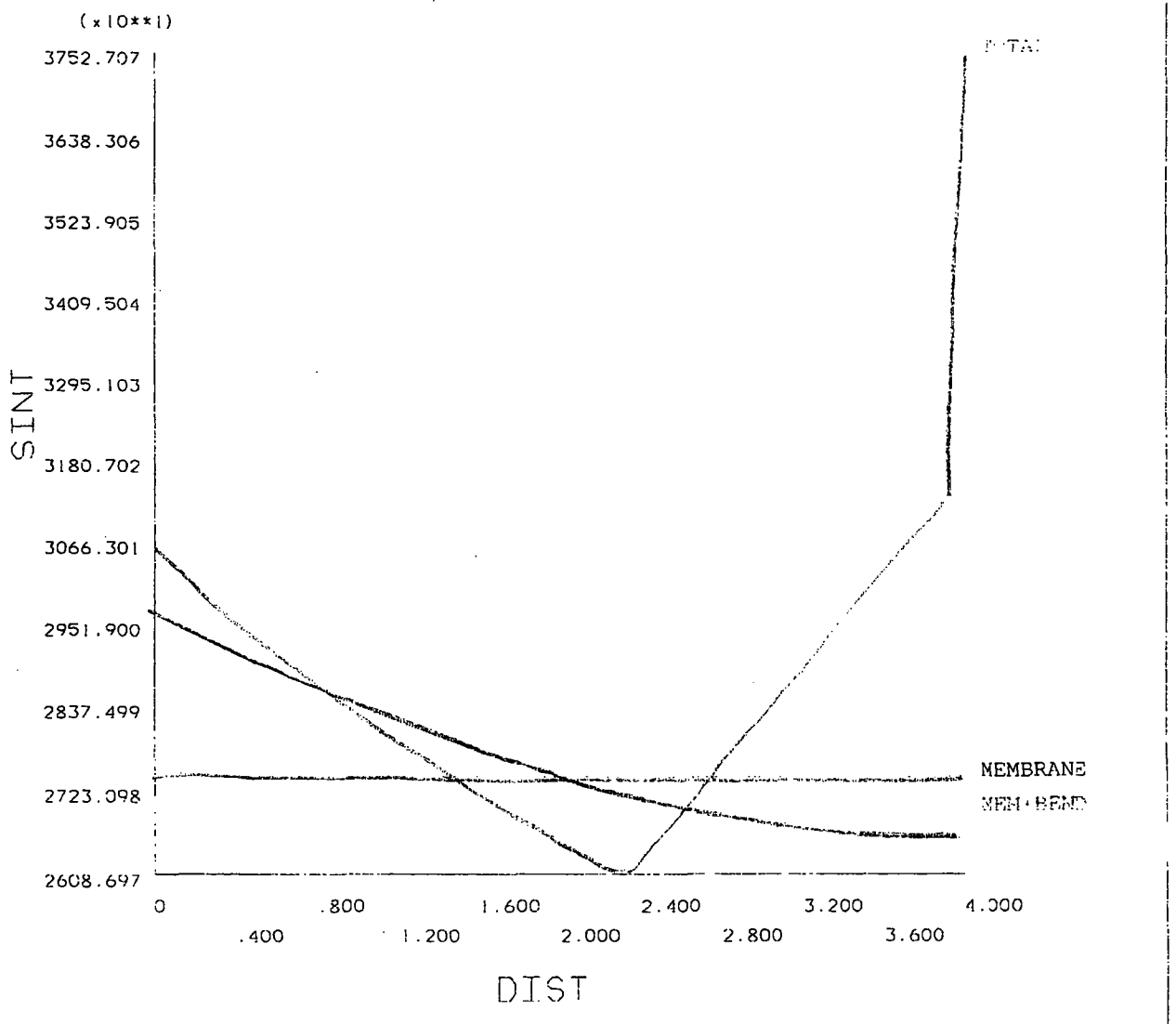

ANSYS 5.3
SEP 22 1997
10:15:25
PLOT NO. 6
POST1
STEP=1
SUB =10
TIME=1
SECTION PLOT
NOD1=284
NOD2=222
SINT

FIGURE 3.Y.4(d) STRESS CLASSIFICATIONS AT CRITICAL SECTIONS. (psi)

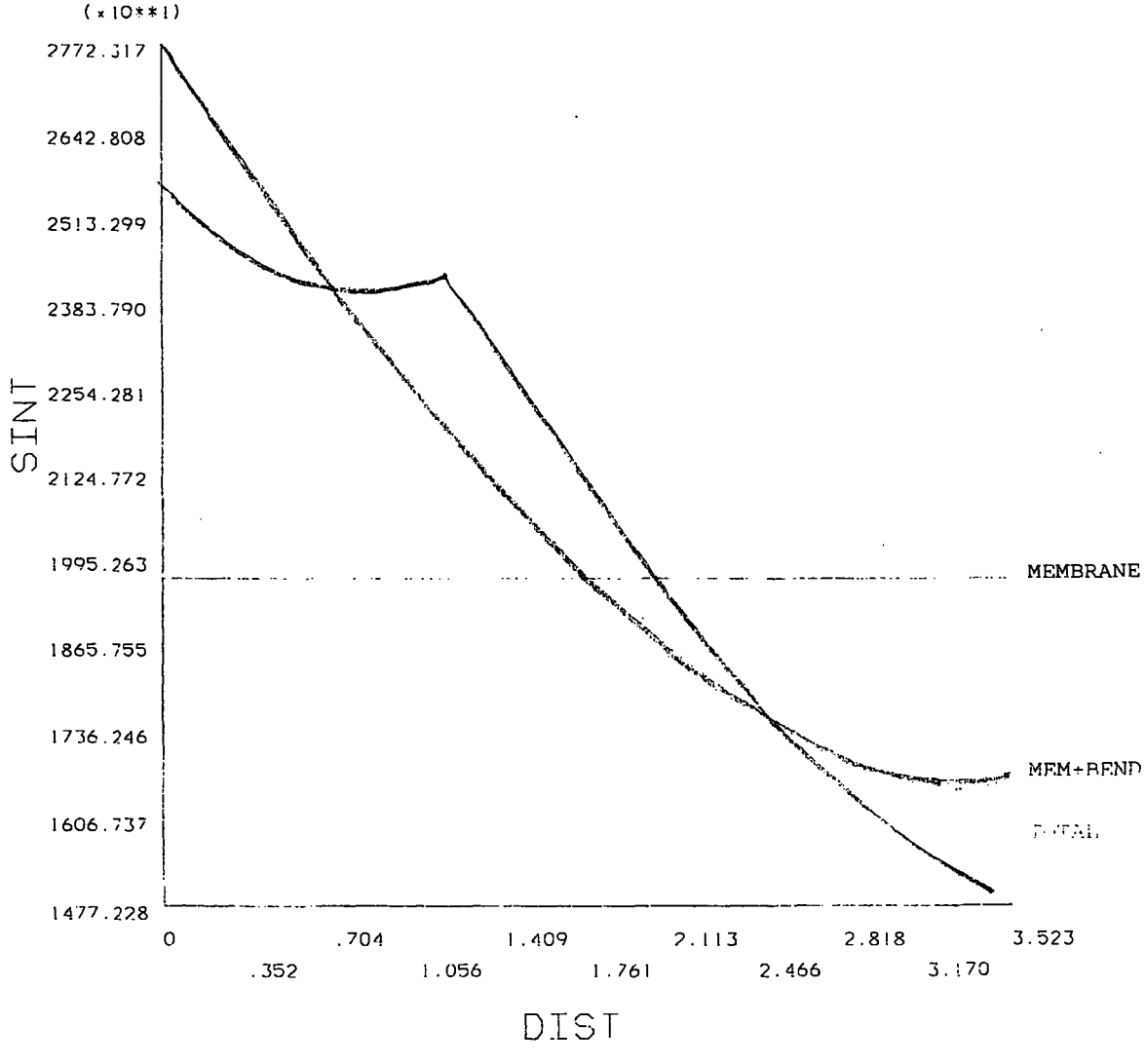

ANSYS 5.3
SEP 22 1997
10:15:26
PLOT NO. 7
POST1
STEP=1
SUB =10
TIME=1
SECTION PLOT
NOD1=213
NOD2=342
SINT

FIGURE 3.Y.4(e) STRESS CLASSIFICATIONS AT CRITICAL SECTIONS. (psi)

APPENDIX 3.Z - TOP FLANGE BOLT HOLE ANALYSIS

3.Z.1 Introduction

This appendix contains an analysis of the threaded holes for the closure bolts in the top flange of the HI-STAR 100 Overpack. The objective of the analysis is to demonstrate that the design of the threaded region is conservative and that the limiting region for structural integrity evaluation is the bolt shaft in tension rather than the threaded region in shear.

The following steps are performed in this analysis:

1. It is shown that the depth of engagement of the closure bolts in the top flange is adequate.

2. It is demonstrated that the limiting section for evaluating the design is the bolt shaft, as opposed to thread shear in either the bolt or in the flange.

3. A lower bound on the preload required to ensure that the hypothetical accident load can be supported without closure plate/top flange separation is determined.

3.Z.2 Composition

This appendix was created using the Mathcad (version 6.0+) software package. Mathcad uses the symbol ':=' as an assignment operator, and the equals symbol '=' retrieves values for constants or variables.

3.Z.3 References

[3.Z.1] E. Oberg and F.D. Jones, *Machinery's Handbook*, Fifteenth Edition, Industrial Press, 1957.

[3.Z.2] FED-STD-H28/2A, *Federal Standard Screw-Thread Standards for Federal Services*, United States Government Printing Office, April, 1984.

[3.Z.3] K.P. Singh and A.I. Soler, *Mechanical Design of Heat Exchangers and Pressure Vessel Components*, First Edition, Arcturus Publishers, Inc., 1984.

[3.Z.4] Letter from Mr. Joe Kedves of American Seal & Engineering Co., Inc. to Mr. Steve Agace of Holtec International, dated September 6, 1996.

[3.Z.5] FEL-PRO Technical Bulletin, N-5000 Nickel Based - Nuclear Grade Anti-Seize Lubricant, 8/97.

3.Z.4 Assumptions

1. Thermal effects are neglected in this analysis, but material properties are taken at design temperatures.

2. In determining the minimum preload required for the closure bolts, the overpack closure plate is assumed to be rigid.

3. In determining the most stress limiting area, the capacity of each section is based on ASME Code Section III, Subsection NB stress limits.

4. The design temperature for the closure bolts is set as 350°F.

3.Z.5 Input Data

Figure 3.Z.1 shows the HI-STAR 100 Overpack closure plate/top flange interface schematically. A free-body diagram of the system used to determine the minimum preload is given in Figure 3.Z.2. The following is a list of the basic input parameters required to perform the calculations. All dimensions are obtained from the Design Drawings in Section 1.5.

The number of closure plate bolts (including two short bolts over the lifting trunnions),

$$NB := 54$$

The nominal radius of the closure bolt shaft, $a := 0.8125 \cdot in$

The major diameter of the bolt, $d_b := 2 \cdot a$

The cross-sectional area of the bolt unthreaded section, $A_d := \pi \cdot \frac{d_b^2}{4}$

The thread engagement length of the closure plate short bolts, $L_{eng} := 2.75 \cdot in$

The diameter of the sealing gasket compression load, $D_{seal} := 71.565 \cdot in$

The gasket seating load (from Reference 3.Z.4), $f_{seal} := 4400 \cdot \frac{lbf}{in}$ (2 gaskets)

The internal pressure of the overpack, $P_{int} := 100 \cdot psi$

For conservatism the internal pressure of the overpack is set equal to the design internal pressure of the MPC under normal conditions (see Table 2.2.1). This accounts for the unlikely failure of the MPC pressure boundary.

The upper bound MPC weight (from Table 3.2.4), $W_{mpc} := 90000 \cdot lbf$

The upper bound closure plate weight (from Table 3.2.4), $W_{lid} := 8000 \cdot lbf$

The design maximum drop acceleration (from Table 3.1.2), $GLoad_{des} := 60$

The root area of the bolt is the area derived from the minor diameter of the bolt. The following values are obtained from page 100 of Reference 3.Z.3 and page 987 of Reference 3.Z.1.

The root area of the bolt, $A_{root} := 1.680 \cdot in^2$

The pitch diameter of the bolt, $d_{pitch} := 1.542 \cdot in$

The minor diameter of the bolt, $dm_{ext} := 1.472 \cdot in$

The minor diameter of the threaded hole, $dm_{int} := 1.490 \cdot in$

The number of threads per inch, $N := 8 \cdot in^{-1}$

From the tables in Section 3.3, the yield and ultimate strengths of the closure plate/top flange material (at the design temperature of 400 °F) and the bolt material (at the bolt design temperature of 350 °F) are:

The forging material ultimate strength, $Su_{forg} := 64600 \cdot psi$

The forging material yield strength, $Sy_{forg} := 32200 \cdot psi$

The forging material design stress intensity, $Sm_{forg} := 21500 \cdot psi$

The bolt material ultimate strength, $Su_{bolt} := 172050 \cdot psi$

The bolt material yield strength, $Sy_{bolt} := 139500 \cdot psi$

The bolt material design stress intensity, $Sm_{bolt} := 46500 \cdot psi$

3.Z.6 Length of Engagement/Strength Calculations

In this section, it is shown that the length of thread engagement is adequate, and that tensile stress in the bolt governs the analysis. The method and terminology of Reference 3.Z.2 are adhered to.

The thread pitch, $p := \frac{1}{N}$

On page 987 of Reference 3.Z.1, the height of a sharp V-thread (H) is defined as:

$$H := 0.86603 \cdot p$$

$$H = 0.108\,in$$

The thread depth of an internal thread (i.e. the forging top flange bolt hole) is determined as:

$$D_{int} := \frac{5}{8} \cdot H \qquad D_{int} = 0.068\,in$$

and the thread depth of an external thread (i.e. the bolt) is determined as:

$$D_{ext} := \frac{17}{24} \cdot H$$

$$D_{ext} = 0.077\,in$$

The major diameter of the bolt can be determined from the minor diameter and the thread depth of an external thread as:

$$dmaj_{ext} := dm_{ext} + 2 \cdot D_{ext}$$

$$dmaj_{ext} = 1.625\,in$$

As defined on page 103 of Reference 3.Z.2, the bolt thread shear area is determined as:

$$A_{bolt} := \pi \cdot N \cdot L_{eng} \cdot dm_{int} \cdot \left[\frac{1}{2 \cdot N} + .57735 \cdot \left(d_{pitch} - dm_{int} \right) \right]$$

$$A_{bolt} = 9.528\,in^2$$

and the forging thread shear area is determined as:

$$A_{frg} := \pi \cdot N \cdot L_{eng} \cdot dmaj_{ext} \cdot \left[\frac{1}{2 \cdot N} + 0.57735 \cdot \left(dmaj_{ext} - d_{pitch} \right) \right]$$

$$A_{frg} = 12.428\,in^2$$

The load capacities of the bolt, bolt thread and the top flange thread, based on the appropriate Subsection NB stress limits under normal conditions, are:

$$LC_{bolt} := 2 \cdot Sm_{bolt} \cdot A_{root}$$

$$LC_{bolt} = 156240\,lbf$$

$$LC_{thrd} := 0.6 \cdot Sm_{bolt} \cdot A_{bolt}$$

$$LC_{thrd} = 265833\,lbf$$

$$LC_{forg} := 0.6 \cdot Sm_{forg} \cdot A_{frg}$$

$$LC_{forg} = 160316\,lbf$$

If the load capacity of the forging thread is greater than the load capacity of the bolt, then the bolt tension will govern. If the margin of safety calculated below is greater than 0.0, then the bolt tension will govern in this analysis.

$$MS := \frac{LC_{forg}}{LC_{bolt}} - 1 \qquad MS = 0.03$$

These calculations confirm that all strength checks can be based on the bolt tensile capacity, and that the depth of engagement is adequate to support the loads.

3.Z.7 Determination of Minimum Preload

In this section, a lower bound estimate of preload requirements for the overpack closure bolts is obtained. The load on the closure plate due to design internal pressure is determined as:

$$L_{press} := \pi \cdot \frac{D_{seal}^{2}}{4} \cdot P_{int} \qquad L_{press} = 402246\,lbf$$

The required gasket seating load (f_{seal}), in pounds per unit circumferential length, is specified by the gasket manufacturer as:

$$f_{seal} = 4400 \frac{lbf}{in}$$

and the total gasket load can therefore be determined as: $L_{gask} := f_{seal} \cdot \pi \cdot D_{seal}$

$$L_{gask} = 989244\,lbf$$

The force applied to the closure plate by quasi-static impact loads is therefore determined as:

$$G_{load} := GLoad_{des} \cdot (W_{mpc} + W_{lid}) \qquad G_{load} = 5880000\,lbf$$

The preload torque needs only to be set to seal the joint under steady state loads or to insure gasket seating, whichever governs. Under an accident, the only criteria is that the bolt meets the allowable stress under accident conditions (i.e., momentary joint decompression is permitted as long as the bolt does not yield). Appendix 3.F demonstrates that allowable stress conditions are met using the preload set herein under normal and accident loads. However, to provide additional conservatism to the joint by minimizing the potential for gross joint unloading, the preload is increased to a value that also maintains compression under normal loading plus 80% of the peak impact load. This insures an adequate safety factor for bolt stress under normal conditions and minimizes the potential for a gross unloading of all bolts during a handling accident (i.e., a short duration non-uniform loading around the bolt circle).

The total preload force required to seat the gasket or seal under steady state loads plus 80% of impact load isovercome these combined loads is determined as:

$$\text{Preload} := L_{press} + .80 \cdot G_{load}$$

$$\text{Preload} = 5106246\,\text{lbf}$$

and the preload per bolt is therefore:

$$\text{Bolt}_{pl} := \frac{\text{Preload}}{NB} \qquad \text{Bolt}_{pl} = 94560\,\text{lbf}$$

The nominal nut factor is 0.15 [3.Z.5] with an allowable tolerance of +/- 5%. The maximum torque corresponds to a nut factor of 0.1575, and the value is:

$$T_{pl} := 0.1575 \cdot \text{Bolt}_{pl} \cdot dm_{ext} \qquad T_{pl} = 1826.9\,\text{lbf} \cdot \text{ft}$$

Therefore, the minimum bolt torque, which equals the nominal value minus an acceptable tolerance, must exceed the value of T_{pl} which is calculated above. For the HI-STAR 100 System, where the final torque for the closure bolts is specified as 2,000 +250/-0 ft-lb in Table 8.1.3, the minimum bolt torque is 2,000 ft-lb.

The bolt preload force becomes a maximum when the maximum bolt torque is combined with the minimum nut factor. This combination leads to the maximum preload stress in the bolt. For a minimum nut factor of 0.1425, which is five percent less than the torque coefficient in Appendix 1.C, the preload force is calculated as:

$$T_{max} := 2000 \cdot \text{ft} \cdot \text{lbf} + 250 \cdot \text{ft} \cdot \text{lbf}$$

$$\text{Bolt}_{pl} := \frac{T_{max}}{0.1425 \cdot dm_{ext}} \qquad \text{Bolt}_{pl} = 128719\,\text{lbf}$$

and the corresponding preload stress is determined as:

$$\sigma := \frac{\text{Bolt}_{pl}}{A_{root}} \qquad \sigma = 76618\,\text{psi}$$

The average stress in the closure bolts, according to Subsection NB, must not exceed twice the design stress intensity. Thus, the ratio of the allowable stress to the closure bolt stress must be greater than 1.0. This ratio, under the loadings examined in this appendix, is determined as:

$$\frac{2 \cdot Sm_{bolt}}{\sigma} = 1.21$$

which is greater than 1.0.

3.Z.8 Conclusion

The analyses presented in this appendix demonstrate that the length of thread engagement is sufficient and conservative, and that the load capacity of the bolts is less than the load capacity of the threaded region in the top flange. In addition, the minimum bolt preload (and corresponding bolt torque) required to maintain compression on the seals during normal operation is established. The preload torque is set to insure a large safety margin on bolt stress during normal operation.

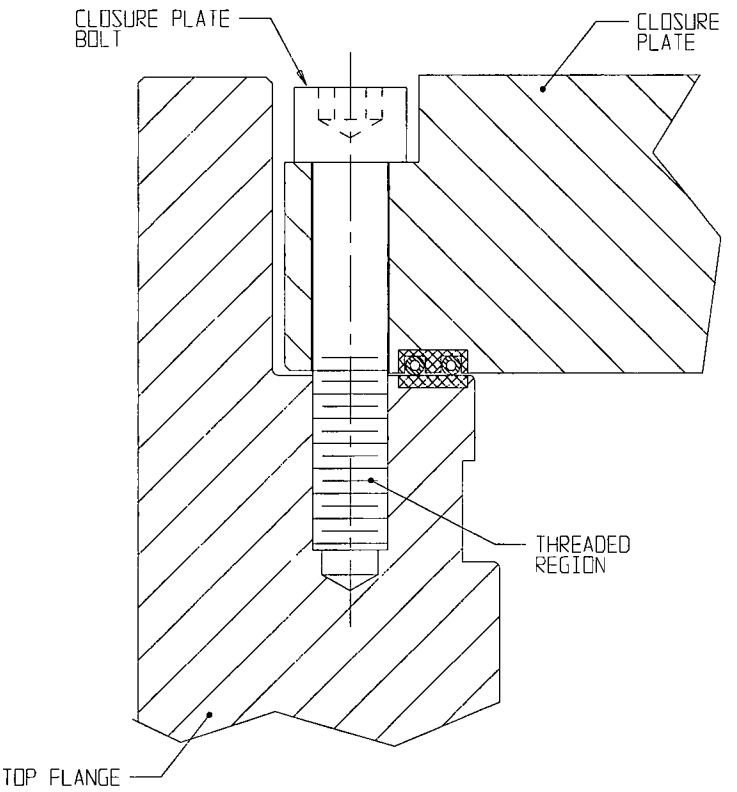

FIGURE 3.Z.1; SCHEMATIC OF CLOSURE PLATE/TOP FLANGE INTERFACE

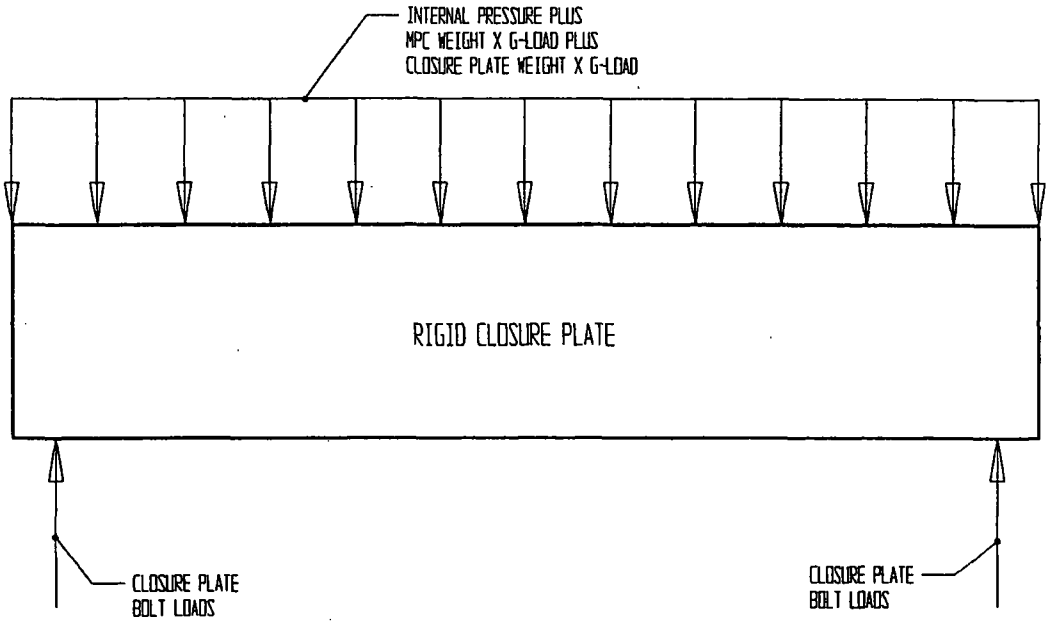

FIGURE 3.Z.2; FREE BODY DIAGRAM FOR THE DETERMINATION OF MINIMUM CLOSURE PLATE BOLT PRELOAD

Appendix 3.AA -

DELETED

Appendix 3.AB -

DELETED

Appendix 3.AC

Deleted

APPENDIX 3.AD: THERMAL EXPANSION DURING FIRE ACCIDENT

3.AD.1 Scope

In this appendix, bounding calculations are performed to demonstrate that the fuel basket-to-MPC shell gap is not closed during the postulated fire accident. This calculation is in support of the results presented in Section 3.4.4.2.2 and utilizes fire temperatures given or inferred from Table 11.2.5.

3.AD.2 Methodology

Bounding temperatures calculated during analyses for the postulated fire accident conditions are used to construct temperature distributions in the HI-STAR 100 cask. This imposed temperature distribution is used to evaluate the thermal expansion effects. The clearances in both the fuel basket-to-MPC shell radial gap and the MPC lid-to-overpack cover plate will be examined. Reference temperatures are set at 70 deg. F for all components. A comprehensive nomenclature listing is provided in Section 3.AD.7.

The analysis is based on temperature data from Chapter 11.

3.AD.3 References

[3.AD.1] Boley and Weiner, Theory of Thermal Stresses, John Wiley, 1960, Sec. 9.10, pp. 288-291.

[3.AD.2] Burgreen, Elements of Thermal Stress Analysis, Arcturus Publishers, Cherry Hill NJ, 1988.

3.AD.4 Fuel Basket-to-MPC Shell Radial Clearance

3.AD.4.1 Input Data

Based on thermal calculations detailed in Chapter 11 with results summarized in Table 11.2.5 , temperature changes are assigned to various locations as appropriate (see Figure 3.AD.1). The interference calculation is performed using the post-fire cooldown temperatures where the basket reaches its highest temperature.

The temperature change at the inside surface of the overpack, $\Delta T_{1h} := 317 - 70$

The temperature change of the outside enclosure shell, $\Delta T_{2h} := 249 - 70$

The temperature change of the MPC shell, $\Delta T_{3h} := 358 - 70$

The temperature change at the outside of the MPC basket, $\Delta T_{4h} := 419 - 70$

The temperature change of the center of the fuel basket, $\Delta T_{5h} := 755 - 70$

The geometry of the components are as follows (referring to Figure 3.AD.1)

The inner radius of the overpack, $a := 34.375 \cdot in$

The outer radius of the overpack, $b := 48 \cdot in$

The inner radius of the MPC shell, $R_{mpc} := 33.6875 \cdot in$

The initial minimum basket-to-MPC shell radial clearance, $RC_{bm} := 0.1875 \cdot in$

The outer radius of the basket, $R_b := R_{mpc} - RC_{bm}$

$$R_b = 33.5\,in$$

The initial nominal MPC-to-overpack radial clearance, $RC_{mo} := 0.09375 \cdot in$

$$RC_{mo} = 0.0938\,in$$

This initial minimum radial clearance value is conservatively based on the MPC outer diameter of 68.5625 in. (see Dwg. 1395, Sh. 4, Note 5). The coefficient of thermal expansion of the fuel basket used in subsequent calculations is based on the hottest fuel basket temperature.

The coefficient of thermal expansion for the fuel basket, $\alpha_{bh} := 9.82 \cdot 10^{-6}$

The minimum coefficient of thermal expansion is used for the shell.

The coefficient of thermal expansion for the MPC shell, $\alpha_{mh} := 9.11 \cdot 10^{-6}$

3.AD.4.2 Radial Thermal Growth of the Overpack

The diameter of the overpack will increase as a result of the temperature increase above the reference temperature of 70 deg. F. The overpack is evaluated as an equivalent uniform hollow cylinder with approximated average properties.

Based on the given inside and outside surface temperatures, the temperature solution in the cylinder is given in the form:

$$C_a + C_b \cdot \ln\left(\frac{r}{a}\right)$$

where, $C_a := \Delta T_{1h}$ $C_a = 247$

$$C_b := \frac{\Delta T_{2h} - \Delta T_{1h}}{\ln\left(\frac{b}{a}\right)} \qquad C_b = -203.671$$

Next, form the integral relationship:

$$Int := \int_a^b \left[C_a + C_b \cdot \left(\ln\left(\frac{r}{a}\right) \right) \right] \cdot r \, dr$$

This integral is evaluated using the Maple symbolic math engine built into the Mathcad program as:

$$Int := \frac{1}{2} \cdot C_b \cdot \ln\left(\frac{b}{a}\right) \cdot b^2 + \frac{1}{2} \cdot C_a \cdot b^2 - \frac{1}{4} \cdot C_b \cdot b^2 + \frac{1}{4} \cdot C_b \cdot a^2 - \frac{1}{2} \cdot C_a \cdot a^2$$

$$Int = 1.174 \times 10^5 \, in^2$$

The average temperature change in the overpack cylinder (T_{bo}) is therefore determined as:

$$T_{bo} := \frac{2}{\left(b^2 - a^2\right)} \cdot Int \qquad T_{bo} = 209.244$$

We estimate the average coefficient of thermal expansion for the overpack by weighting the volume of the various layers. A total of four layers are identified for this calculation. They are:

1) the overpack inner shell
2) the total of the 5 intermediate shells
3) the neutron absorber
4) the outer enclosure shell

Thermal properties are based on estimated temperatures in the component and coefficient of thermal expansion values taken from the tables in Chapter 3. The following averaging calculation involves the thicknesses (t) of the various components, and the estimated coefficients of thermal expansion at the components' mean radial positions. The results of the weighted average process yields an effective coefficient of linear thermal expansion for use in computing radial growth of a solid cylinder (the overpack).

The thicknesses of each component are defined as:

$$t_1 := 2.5 \cdot in$$

$$t_2 := 6 \cdot in$$

$$t_3 := 4.625 \cdot in$$

$$t_4 := 0.5 \cdot in$$

and the corresponding mean radii can therefore be defined as:

$$r_1 := a + .5 \cdot t_1$$

$$r_2 := r_1 + .5 \cdot t_1 + .5 \cdot t_2$$

$$r_3 := r_2 + .5 \cdot t_2 + .5 \cdot t_3$$

$$r_4 := r_3 + .5 \cdot t_3 + .5 \cdot t_4$$

To check the accuracy of these calculations, the outer radius of the overpack is calculated from r_4 and t_4, and the result is compared with the previously defined value (b).

$$b_1 := r_4 + 0.5 \cdot t_4$$

$$b_1 = 48\,in$$

$$b = 48\,in$$

We note that the the calculated value b_1 is identical to the previously defined value b. The coefficient of thermal expansion for each component, estimated based on the temperature gradient, are defined as:

$$\alpha_1 := 6.814 \cdot 10^{-6} \qquad \alpha_2 := 6.26 \cdot 10^{-6} \qquad @\ 300 \text{ degrees F}$$

$$\alpha_3 := 6.46 \cdot 10^{-6} \qquad \alpha_4 := 6.66 \cdot 10^{-6}$$

Thus, the average coefficient of thermal expansion of the overpack is determined as:

$$\alpha_{avg} := \frac{r_1 \cdot t_1 \cdot \alpha_1 + r_2 \cdot t_2 \cdot \alpha_2 + r_3 \cdot t_3 \cdot \alpha_3 + r_4 \cdot t_4 \cdot \alpha_4}{\frac{a+b}{2} \cdot (t_1 + t_2 + t_3 + t_4)}$$

$$\alpha_{avg} = 6.439 \times 10^{-6}$$

Reference 3.AD.1 gives an expression for the radial deformation due to thermal growth. At the inner radius of the overpack (r = a), the radial growth is determined as:

$$\Delta R_{ah} := \alpha_{avg} \cdot a \cdot T_{bo}$$

$$\Delta R_{ah} = 0.046\,in$$

3.AD.4.3 Radial Thermal Growth of the MPC Shell

Using the same expression for radial growth used above (from Reference 3.AD.1), the radial growth of the MPC shell is determined as:

$$\Delta R_{mh} := \alpha_{mh} \cdot R_{mpc} \cdot \Delta T_{3h} \qquad \Delta R_{mh} = 0.088\,in$$

This value is conservatively based on the inner radius of the MPC shell. This assumption will lessen the expansion of the MPC shell, thereby minimizing the available fuel basket-to-MPC shell gap. If the initial MPC shell-to-overpack clearance plus the overpack radial growth minus the MPC shell radial thermal growth is negative, then the MPC shell will contact and conform to the inner surface of the overpack.

$$RC_{moh} := RC_{mo} + \Delta R_{ah} - \Delta R_{mh} \qquad RC_{moh} = 0.052\,in$$

The result is positive, indicating no contact.

3.AD.4.4 Radial Thermal Growth of the Fuel Basket

Using formulas given in [3.AD.2] for a solid body of revolution, and assuming a parabolic temperature distribution in the radial direction with the center and outer temperatures given previously, the following relationships can be developed for free thermal growth.

Define $\Delta T_{bas} := \Delta T_{5h} - \Delta T_{4h}$

$$\Delta T_{bas} = 336$$

Then the mean temperature change can be defined as $T_{bb} := \frac{2}{R_b^2} \cdot \int_0^{R_b} \left(\Delta T_{5h} - \Delta T_{bas} \cdot \frac{r^2}{R_b^2} \right) \cdot r\,dr$

Using the Maple symbolic engine again, the closed form solution of the integral is:

$$T_{bb} := \frac{2}{R_b^2}\cdot\left(\frac{-1}{4}\cdot\Delta T_{bas}\cdot R_b^2 + \frac{1}{2}\cdot\Delta T_{5h}\cdot R_b^2\right) \qquad T_{bb} = 517$$

and the corresponding radial growth at the periphery (ΔR_{bh}) is therefore determined as:

$$\Delta R_{bh} := \alpha_{bh}\cdot R_b\cdot T_{bb} \qquad \Delta R_{bh} = 0.17\,in$$

Note that the coefficient of thermal expansion for the hottest basket temperature has been used, and the results are therefore conservative.

3.AD.4.5 Final Fuel Basket-to-MPC Shell Radial Clearance

The initial minimum fuel basket-to-MPC shell gap plus the MPC shell radial thermal growth minus the maximum fuel basket radial growth of the fuel basket must be greater than zero.

$$RG_{bmh} := RC_{bm} + \Delta R_{mh} - \Delta R_{bh} \qquad RG_{bmh} = 0.106\,in$$

This value is greater than zero, and the no contact condition for the fuel basket is therefore met.

3.AD.5 MPC Lid -to-Overpack Closure Plate Axial Clearance

3.AD.5.1 Input Data

The same temperatures, previously input, are assumed for this calculation.

The following geometric dimensions are needed to determine the axial thermal growth of the cask components. The axial length of the overpack is defined as the distance from the top of the overpack baseplate to the bottom of the overpack closure plate.

The axial length of the MPC, $L_{mpc} := 190.5\cdot in$

The axial length of the basket, $L_{bas} := 176.5\cdot in$

The axial length of the overpack, $L_{ovp} := 191.125\cdot in$

The initial minimum fuel basket-to-MPC lid axial clearance, $AC_{bm} := 2 \cdot in$

The initial minimum MPC-to-overpack nominal axial clearance, $AC_{mo} := L_{ovp} - L_{mpc}$

$$AC_{mo} = 0.625\,in$$

3.AD.5.2 Axial Growth Based on Specified Temperatures

The axial thermal growth of the overpack, based on the temperature distribution specified for the cask, can be calculated using the previously calculated average coefficient of thermal expansion and overpack cylinder average temperature as:

$$\Delta L_{ovph} := L_{ovp} \cdot \alpha_{avg} \cdot T_{bo}$$

$$\Delta L_{ovph} = 0.258\,in$$

The axial growth of the MPC shell is determined as:

$$\Delta L_{mpch} := \alpha_{mh} \cdot L_{mpc} \cdot \Delta T_{3h}$$

$$\Delta L_{mpch} = 0.5\,in$$

And the axial growth of the fuel basket is determined from [3.AD.2] as:

$$\Delta L_{bh} := \Delta R_{bh} \cdot \frac{L_{bas}}{R_b} \qquad \Delta L_{bh} = 0.896\,in$$

3.AD.5.3 Final MPC Lid-to-Overpack Closure Plate Axial Clearance

In order to prevent the overpack cover plate bolts from experiencing extreme axial stresses, the MPC lid must not contact the closure plate bottom. Therefore, the initial minimim axial clearance plus the overpack axial growth minus the MPC axial growth must be greater than zero.

$$\Delta L_{mpc} := (\Delta L_{mpch}) \qquad \Delta L_{mpc} = 0.5\,in$$

$$\Delta L_{ovp} := \Delta L_{ovph} \qquad \Delta L_{ovp} = 0.258\,in$$

$$AG_{mo} := AC_{mo} + \Delta L_{ovp} - \Delta L_{mpc} \qquad AG_{mo} = 0.383\,in$$

This value is greater than zero, and the no contact condition for the closure plate is therefore met.

3.AD.5.4 Final Fuel Basket-to-MPC Lid Axial Clearance

The final axial growth of the fuel basket is the average of the hot (top of cask) and cold (bottom of cask) axial thermal growth values. In order to ensure that the fuel assemblies will be removable, by normal means, from the fuel basket, the fuel basket must not be allowed to contact the underside of the MPC lid. Therefore, the initial minimim axial clearance plus the MPC axial growth minus the fuel basket axial growth must be greater than zero.

$$\Delta L_{bas} := (\Delta L_{bh}) \qquad \Delta L_{bas} = 0.896\,in$$

$$AG_{bm} := (AC_{bm} + \Delta L_{mpc}) - \Delta L_{bas}$$

$$AG_{bm} = 1.604\,in$$

This value is greater than zero, and the no-contact condition for the fuel basket is met.

3.AD.6 Conclusions

The results of calculations performed in this appendix demonstrate that a postulated fire accident does not result in restraint of free-end expansion in the fuel basket. Therefore, large stresses will not occur as a result of this mechanism and the retrievability of the fuel assemblies is not compromised.

3.AD.7 Nomenclature

a is the inner radius of the overpack
AC_{bm} is the initial fuel basket-to-MPC axial clearance.
AC_{mo} is the initial MPC-to-overpack axial clearance.
AG_{bm} is the average final fuel basket-to-MPC shell gap.
AG_{mo} is the average final MPC shell-to-overpack axial gap.
b is the outer radius of the overpack.
L_{bas} is the axial length of the fuel basket.
L_{mpc} is the axial length of the MPC.
L_{ovp} is the axial length of the overpack.
r_1 (r_2,r_3,r_4) is mean radius of the overpack inner shell (intermed. shells, neutron absorber, outer shell).
R_b is the outer radius of the fuel basket.

R_{mpc} is the mean radius of the MPC shell.

RC_{bm} is the initial fuel basket-to-MPC radial clearance.

RC_{mo} is the initial MPC shell-to-overpack radial clearance.

RC_{moh} is the final MPC shell-to-overpack radial gap for the hot components.

RG_{bmh} is the final fuel basket-to-MPC shell radial gap for the hot components.

t_1 (t_2,t_3,t_4) is the thickness of the overpack inner shell (intermed. shells, neutron absorber, outer shell).

T_{bb} is the average temperature of the fuel basket.

T_{bo} is the average temperature of the overpack cylinder.

α_1 (α_2,α_3,α_4) is the coefficient of thermal expansion of the overpack inner shell (intermediate shells, neutron absorber, outer shell).

α_{avg} is the average coefficient of thermal expansion of the overpack.

α_{bh} is the coefficient of thermal expansion of the fuel basket for the hot components.

α_{mh} is the coefficient of thermal expansion of the MPC shell for the hot components.

ΔL_{bas} is the total axial thermal growth of the fuel basket.

ΔL_{bh} is the axial growth of the fuel basket for the hot components.

ΔL_{mpc} is the total axial thermal growth of the MPC shell.

ΔL_{mpch} the the axial growth of the MPC for the hot components.

ΔL_{ovp} is the total axial thermal growth of the overpack.

ΔL_{ovph} is the axial growth of the overpack for the hot components.

ΔR_{ah} is the radial growth of the overpack inner radius for the hot components.

ΔR_{bh} is the radial growth of the fuel basket for the hot components.

ΔR_{mh} is the radial growth of the MPC shell for the hot components.

ΔR_{mpch} is the radial growth of the MPC shell for the hot components.

ΔT_{1h} is the temperature change at the overpack inside surface for hot components.

ΔT_{2h} is the temperature change at the outside enclosure shell surface for hot components.

ΔT_{3h} is the temperature change at the MPC shell mean radius for hot components.

ΔT_{4h} is the temperature change at the MPC basket periphery for hot components.

ΔT_{5h} is the temperature change at the MPC basket centerline for hot components.

ΔT_{bas} is the fuel basket centerline-to-periphery temperature gradient.

APPENDIX 3.AE - STRESS ANALYSIS OF OVERPACK CLOSURE BOLTS DURING COLD CONDITION OF STORAGE

3.AE.1 Introduction

This appendix contains a stress analysis of the HI-STAR 100 Overpack closure bolts under the temperature conditions which exist during the cold condition of storage. The purpose of the analysis is to demonstrate that the closure bolts do not "unload" during this condition.

The complex interaction of forces and moments in bolted joints of shipping casks has been investigated in Reference 3.AE.1, resulting in a comprehensive method of closure bolt stress analysis. That method is employed here. For each set of formulas or calculations used, reference to the appropriate table in [3.AE.1] is given. Where necessary, the formulas are modified to reflect the particulars of the HI-STAR system. For example, since the HI-STAR 100 closure lid has a raised face outside of the bolt circle, no prying forces can develop from loads directed outward (such as internal pressure).

3.AE.2 References

[3.AE.1] Mok, Fischer, Hsu, *Stress Analysis of Closure Bolts for Shipping Casks* (NUREG/CR-6007 UCRL-ID-110637), Lawrence Livermore National Laboratory/Kaiser Engineering, 1993.

[3.AE.2] Horton, H. (Ed.), *Machinery's Handbook*, 15th Ed., The Industrial Press, 1957.

[3.AE.3] FEL-PRO Technical Bulletin, N-5000 Nickel Based - Nuclear Grade Anti-Seize Lubricant, 8/97.

[3.AE.4] K.P. Singh and A.I. Soler, *Mechanical Design of Heat Exchangers and Pressure Vessel Components*, First Edition, Arcturus Publishers, Inc., 1984.

3.AE.3 Assumptions

The assumptions used in the analysis are given as a part of Reference 3.AE.1. The assumptions in that reference are considered valid for this analysis except where noted below.

1. The temperature conditions of the bolt circle area for the extreme cold ambient condition of storage are used here.

2. Bolt forces due to prying action can only develop from inward directed loads because of the raised face on the closure lid which precludes metal-to-metal contact outside of the bolt circle.

3. The forces and moments in the bolts due to the gasket load are included in the preload imposed.

4. The forces and moments in the bolts due to vibration loads are small relative to the forces and moments generated by all other loads, and are considered negligible.

5. A recess is provided in the overpack closure plate that causes the MPC to contact the bottom face of the overpack closure plate over an annular region at the outer periphery of the closure plate. The formulas for plates under uniform pressure used in the reference are replaced here by formulas for plates loaded uniformly over an annular region at the outer periphery.

6. As the HI-STAR 100 Overpack includes a protected lid, shear bolt forces are defined to be zero.

7. The actual weight of the overpack closure plate is replaced by a somewhat larger weight in this analysis. This is conservative because loads on the bolts are increased with a heavier closure plate.

8. No prying action can occur from outward directed loads since the closure lid has a raised face outside of the bolt circle which eliminates the potential for prying action from positive bending moments.

3.AE.4 Terminology

Some terminology in Reference 3.AE.1 differs from Holtec's terminology. In this analysis, the 'cask wall' is Holtec's 'main flange'. The 'cask' is Holtec's 'Overpack'. 'Closure lid' and 'closure plate' are used interchangeably.

Wherever possible, parameter names are consistent with Reference 3.AE.1.

3.AE.5 Composition

This appendix was created with the Mathcad (version 7.0) software package. Mathcad uses the symbol ':=' as an assignment operator, and the equals symbol '=' retrieves values for constants or variables. Inequalities are also employed. Mathcad returns 0 for a false inequality, and 1 for a true inequality.

Units are also carried with Mathcad variables.

3.AE.6 Analysis Procedure

The analysis procedure is taken from Section 6.4 of Reference 3.AE.1. The following general steps are taken:

1. Identification of individual loadings.

2. Identification and evaluation of load parameters.

3. Determination of the forces and moments acting on the bolts due to each of individual loading.

4. Determination of the forces and moments acting on the bolts for the combined load case under analysis.

5. Evaluation of the stresses in the bolts for the combined load case.

6. Comparison with acceptance criteria.

3.AE.7 Identification of Individual Loadings

The individual loadings acting on the cask closure are the following:

a. Bolt preload. Bolt preload is present in all loadings and includes any gasket sealing loads.

b. Pressure. Design internal pressure is applied to the overpack wall and lid for all load combinations.

c. Temperature. Temperatures assumed equal to the cold ambient environment to provide a bounding result.

3.AE.8 Geometry Parameters

The parameters which define the HI-STAR 100 closure geometry are given in this section.

The nominal closure bolt diameter, $Db := 1.625 \cdot in$

The total number of closure bolts, $Nb := 54$

The stress area of a closure bolt (from [3.AE.4], p. 100), $A_b := 1.680 \cdot in^2$

The closure lid diameter at the bolt circle, $Dlb := 74.75 \cdot in$

Closure lid diameter at the location of the gasket load reaction, $Dlg := 71.565 \cdot in$

The HI-STAR overpack gasket system includes two concentric seals. The value for Dlg above locates the gasket load reaction between the two seal diameters.

The thickness of the cask wall, $tc := 6.25 \cdot in$

The minimum thickness of the closure lid, $tl := \left(6 - \frac{1}{16}\right) \cdot in$

This value for the closure lid thickness accounts for the thickness reduction (recess) in the bottom face of the lid.

The effective thickness of the closure lid flange, $tlf := 4.25 \cdot in$

The closure plate diameter at the inner edge, $Dli := 69.75 \cdot in$

The closure plate diameter at the inner edge is overpack inner diameter plus twice the width of the cut-out in the top flange which accommodates the inflatable annulus seal.

The closure plate diameter at the outer edge, $Dlo := 77.375 \cdot in$

The bolt length, $Lb := 4.25 \cdot in$

The bolt length is the length between the top and bottom surfaces of the closure plate, at the bolt circle location.

The number of bolt threads per inch, $n := 8 \cdot \frac{1}{in}$

The bolt thread pitch, $p := \frac{1}{n}$

The upper bound MPC weight (Table 3.2.4), $Wc := 90000 \cdot lb$

The bounding weight used for closure plate,(Table 3.2.4) $Wl := 8000 \cdot lb$

The overpack closure lid recess inner diameter, $d_l := 52.75 \cdot in$

3.AE.9 Material Properties

The overpack closure bolts are SB-637-N07718 steel, and the closure plate and top flange are SA-350-LF3 steel. The following material properties are used in the analysis based on a cold temperature of -40 degrees F. Extrapolation of table data is carried out where necessary.

The Young's modulus of the cask wall material, $Ec := 28170000 \cdot psi$

The Young's modulus of the closure plate material, $El := 28170000 \cdot psi$

The Poisson's ratio of the closure plate material, $NUl := 0.3$

The closure bolt material coefficient of thermal expansion, $ab := 6.60 \cdot 10^{-6} \cdot R^{-1}$

The cask wall material coefficient of thermal expansion, $ac := 6.23 \cdot 10^{-6} \cdot R^{-1}$

The closure plate material coefficient of thermal expansion, $al := 6.23 \cdot 10^{-6} \cdot R^{-1}$

The zero points of the Fahrenheit and Rankine scales differ by a constant (1 °F = 1 R), therefore the above numbers are accurate with either unit.

Young's modulus of the closure bolt material, $Eb := 29580000 \cdot psi$

Young's modulus of top flange material, $Elf := 28170000 \cdot psi$

3.AE.10 Bolt Stress Calculations

3.AE.10.1 Identification and Evaluation of Load Parameters, Combined Load Case 1

The load parameters for each individual loading are defined as follows.

Loading parameters for preload:

The nominal value of the nut factor is 0.15 from Reference 3.AE.3.
The minimum nut factor, based on a tolerance of +/- 5%, is $K := 0.1425$

Per Table 8.1.3, the maximum bolt preload torque is 2,000 +250/-0 ft-lb. For conseravtism, the following preload torque is used in the calculations:

$Q := 2895 \cdot ft \cdot lbf + 90 \cdot ft \cdot lbf$

Loading parameters for pressure load:

The pressure inside the cask wall, $Pci := 100 \cdot psi$

The pressure outside the cask wall, $Pco := 14.7 \cdot psi$

The pressure inside the closure lid, $Pli := 100 \cdot psi$

The pressure outside the closure lid, $Plo := 14.7 \cdot psi$

Loading parameters for the cold condition temperature load: (bolt installation at 70 deg. F)

The maximum temperature change of the main flange, $Tc := (-40 - 70) \cdot R$

The maximum temperature change of the closure lid inner surface, $Tli := (-40 - 70) \cdot R$

The maximum temperature change of the closure lid outer surface, $Tlo := (-40 - 70) \cdot R$

The maximum temperature change of the closure lid, $Tl := \frac{Tli + Tlo}{2}$ $Tl = -110\,R$

The maximum temperature change of the closure bolts, $Tb := (-40 - 70)\cdot R$ $Tb = -110\,R$

As these parameters are all temperature differences, the Fahrenheit-to-Rankine conversion factor of 460° can be omitted.

3.AE.10.2 Determination of Bolt Forces and Moments for the Individual Loadings

Array parameters are used to account for the multiple individual loadings within the combined load case. There are three individual loadings, so let i include the range from 1 to 3 as follows:

Let $i := 1..3$

The forces and moments generated by each individual load case are represented by the following symbols:

The non-prying tensile bolt force per bolt = Fa_i

The shear bolt force per bolt = Fs_i

The fixed-edge closure lid force = Ff_i

Fixed-edge closure lid moment = Mf_i

The subscript i is used only to keep track of each individual load case within a load combination.

The first individual loading in this load combination is the residual load after the preload operation. The forces and moments generated by this load are defined as [3.AE.1, Table 4.1]:

The non-prying tensile bolt force per bolt, $Fa_1 := \frac{Q}{K\cdot Db}$

The maximum residual tensile bolt force (preload) per bolt, $Far_1 := Fa_1$

The maximum residual torsional bolt moment per bolt, $Mtr := 0.5\cdot Q$

The preload stress in each bolt (based on stress area), $Preload := \frac{Fa_1}{A_b}$

Substituting the appropriate input data, the values of these parameters are determined as:

$$Fa_1 = 154688\,lbf$$

$$Far_1 = 154688\,lbf$$

$$Mtr = 17910\,in{\cdot}lbf$$

$$Preload = 92076\,psi$$

The second individual loading in this load combination is the pressure load. The forces and moments generated by this load are defined as follows [3.AE.1, Table 4.3]:

The non-prying tensile force per bolt, $Fa_2 := \frac{\pi \cdot Dlg^2 \cdot (Pli - Plo)}{4 \cdot Nb}$

The shear bolt force per bolt, $Fs_2 := \frac{\pi \cdot El \cdot tl \cdot (Pci - Pco) \cdot Dlb^2}{2 \cdot Nb \cdot Ec \cdot tc \cdot (1 - NUl)}$

The fixed-edge closure lid force, $Ff_2 := \frac{Dlb \cdot (Pli - Plo)}{4}$

The fixed-edge closure lid moment, $Mf_2 := \frac{(Pli - Plo) \cdot Dlb^2}{32}$

Substituting the appropriate input data, the values of these parameters are determined as:

$$Fa_2 = 6354\,lbf$$

$$Fs_2 = 18816\,lbf$$

$$Ff_2 = 1594\,\frac{lbf}{in}$$

$$Mf_2 = 14894\,lbf$$

The third individual loading in this load combination is the temperature load. The forces and moment generated by this load are defined as [3.AE.1, Table 4.4]:

The non-prying tensile bolt force per bolt, $Fa_3 := 0.25 \cdot \pi \cdot Db^2 \cdot Eb \cdot (al \cdot Tl - ab \cdot Tb)$

The shear bolt force per bolt, $Fs_3 := \frac{\pi \cdot El \cdot tl \cdot Dlb \cdot (al \cdot Tl - ac \cdot Tc)}{Nb \cdot (1 - NUl)}$

The fixed-edge closure lid force, $Ff_3 := 0 \cdot \frac{lbf}{in}$

The fixed-edge closure lid moment, $Mf_3 := \frac{El \cdot al \cdot tl^2 \cdot (Tlo - Tli)}{12 \cdot (1 - NUl)}$

Substituting the appropriate input data, the values of these parameters are determined as:

$$Fa_3 = 2497\,lbf$$

$$Fs_3 = 0\,lbf$$

$$Ff_3 = 0\,\frac{lbf}{in}$$

$$Mf_3 = 0\,lbf$$

3.AE.10.3 Determination of Combined Bolt Forces and Combined Bolt Moments

The calculations in the following subsections are performed in accordance with Tables 4.9, 2.1 and 2.2 of Reference 3.AE.1.

3.AE.10.3.1 Tensile Bolt Force

First, combine the non-prying tensile bolt forces (Fa_i):

The total preload and temperature load, $Fa\_pt := Fa_1 + Fa_3$

$$Fa\_pt = 157185\,lbf$$

The sum of the remaining forces (pressure), $Fa\_al := Fa_2$

$$Fa\_al = 6354\,lbf$$

The combined non-prying tensile bolt force, $Fa\_c := Fa\_al \cdot (Fa\_al > Fa\_pt) + Fa\_pt \cdot (Fa\_pt > Fa\_al)$

$$Fa\_c = 157185\,lbf$$

If the combined non-prying tensile bolt force (Fa_c) is negative, set it equal to zero. Per Appendix 3 of Reference [3.AE.1], inward directed loads are not reacted by the bolts, but the developed formulations are still valid if the spurious bolt forces < 0.0 are removed from the calculation.

$$Fa\_c := Fa\_c \cdot (Fa\_c > 0 \cdot lbf)$$

$$Fa\_c = 157185\,lbf$$

Next, combine the prying tensile bolt forces and moments (these bolt forces develop due to Ff_i and Mf_i):

The sum of the fixed edge forces, $Ff\_c := Ff_1 + Ff_2 + Ff_3$

$$Ff\_c = 1594 \frac{lbf}{in}$$

If the combined fixed-edged force (Ff_c) is negative, set it equal to zero.

$$Ff\_c := Ff\_c \cdot \left(Ff\_c > 0 \cdot \frac{lbf}{in}\right) + 0 \cdot \frac{lbf}{in} \cdot \left(Ff\_c < 0 \cdot \frac{lbf}{in}\right)$$

$$Ff\_c = 1.594 \times 10^3 \frac{lbf}{in}$$

The sum of fixed-edge moments, $Mf\_c := Mf_1 + Mf_2 + Mf_3$

$$Mf\_c = 14894 \frac{lbf \cdot in}{in}$$

Define the appropriate prying force moment arm depending on the direction of Mf_c. For inward directed loading, prying moments are developed by the lid rotating about the flange inner edge; for outward directed loading, prying moments are developed by the lid rotating about its outer edge. Thus, the moment arms are different in the two cases.

$$Arm := (Dlo - Dlb) \cdot (Mf\_c > 0 \cdot lbf) + (Dlb - Dli) \cdot (Mf\_c < 0 \cdot lbf)$$

$$Arm = 2.625 \text{ in}$$

The prying tensile bolt force for the combined loading can therefore be determined as:

The constants C_1 and C_2 are: $C_1 := 1$

$$C_2 := \left[\frac{8}{3 \cdot (Arm)^2}\right] \cdot \left[\frac{El \cdot tl^3}{1 - NUl} + \frac{(Dlo - Dli) \cdot Elf \cdot tlf^3}{Dlb}\right] \cdot \left(\frac{Lb}{Nb \cdot Db^2 \cdot Eb}\right)$$

$$C_2 = 3.371$$

The bolt preload per unit length of bolt circle, $P := Fa\_pt \cdot \left(\frac{Nb}{\pi \cdot Dlb}\right)$

$$P = 36145 \frac{lbf}{in}$$

The parameter P is the pressure/temperature force which is multiplied to determine preload per unit length of bolt circle (see Tables 2.1 and 4.9 in Section II.3 of Reference 3.AE.1).

The non-prying tensile bolt force, $B := Ff\_c \cdot (Ff\_c > P) + P \cdot (P > Ff\_c)$

$$B = 36145 \frac{lbf}{in}$$

The additional tensile bolt force per bolt caused by prying action of the closure lid, $Fap := \left(\frac{\pi \cdot Dlb}{Nb}\right) \cdot \left[\frac{\frac{2 \cdot Mf\_c}{Arm} - C_1 \cdot (B - Ff\_c) - C_2 \cdot (B - P)}{C_1 + C_2}\right]$

$$Fap = -23086\,lbf$$

The prying force must be tensile. If the result is negative, set it equal to zero.

$$Fab\_c := Fap \cdot (Fap > 0 \cdot lbf) + 0 \cdot lbf \cdot (Fap < 0 \cdot lbf)$$

$$Fab\_c = 0\,lbf$$

The total tensile bolt force for stress analysis, $FA := Fa\_c + Fab\_c$

$$FA = 157185\,lbf$$

3.AE.10.3.2 Bolt Shear Force

The sum of the shear forces, $Fs\_c := Fs_1 + Fs_2 + Fs_3$

$$Fs\_c = 18816\,lbf$$

$Fs := 0 \cdot lbf$ (protected cask lid)

3.AE.10.3.3 Bolt Bending Moment

The calculations in this section are performed in accordance with Table 2.2 of Reference 3.AE.1. The following relations are defined:

$$Kb := \left(\frac{Nb}{Lb}\right) \cdot \left(\frac{Eb}{Dlb}\right) \cdot \left(\frac{Db^4}{64}\right)$$

$$Kl := \frac{El \cdot tl^3}{3 \cdot \left[\left(1 - NUl^2\right) + (1 - NUl)^2 \cdot \left(\frac{Dlb}{Dlo}\right)^2\right] \cdot Dlb}$$

$$Mbb\_c := \left(\frac{\pi \cdot Dlb}{Nb}\right) \cdot \left(\frac{Kb}{Kb + Kl}\right) \cdot Mf\_c$$

$$Mbb := Mbb\_c$$

where Mbb is the bolt bending moment. Substituting the appropriate values, these parameters are calculated as:

$$Kb = 547804\ lbf$$

$$Kl = 19230745\ lbf$$

$$Mbb\_c = 1.794 \times 10^3\ lbf \cdot in$$

$$Mbb = 1.794 \times 10^3\ lbf \cdot in$$

3.AE.10.3.4 Bolt Torsional Moment

The torsional bolt moment is generated only by the preloading operation, therefore no combination is necessary.

3.AE.10.4 Evaluation of Bolt Stresses

Per Table 5.1 of Reference 3.AE.1, the average and maximum bolt stresses for comparison with the acceptance criteria are obtained. Inch-series threads are used and the maximum shear and bending are in the bolt thread.

The bolt diameter for tensile stress calculation [3.AE.1, Table 5.1], $Dba := Db - 0.9743 \cdot p$

$$Dba = 1.503\ in$$

The bolt diameter for shear stress calculation, $Dbs := Dba$

$$Dbs = 1.503\ in$$

The bolt diameter for bending stress calculation, $Dbb := Dba$

$$Dbb = 1.503\ in$$

The bolt diameter for torsional stress calculation, $Dbt := Dba$

$$Dbt = 1.503\ in$$

The average tensile stress caused by the tensile bolt force FA, $Sba := 1.2732 \cdot \frac{FA}{Dba^2}$

$$Sba = 88566\,psi$$

The average shear stress caused by the shear bolt force Fs, $Sbs := 1.2732 \cdot \frac{Fs}{Dbs^2}$

$$Sbs = 0\,psi$$

The maximum bending stress caused by the bending bolt moment Mb, $Sbb := 10.186 \cdot \frac{Mbb}{Dbb^3}$

$$Sbb = 5380\,psi$$

The maximum shear stress caused by the torsional bolt moment Mt, $Sbt := 5.093 \cdot \frac{Mtr}{Dbt^3}$

$$Sbt = 26854\,psi$$

The maximum stress intensity caused by the combined loading of tension, shear, bending and torsion can therefore be determined as:

$$Sbi := \left[(Sba + Sbb)^2 + 4 \cdot (Sbs + Sbt)^2 \right]^{0.5}$$

$$Sbi = 108214\,psi$$

3.AE.10.5 Comparison with Acceptance Criteria

The final bolt stress is less than the preload stress $Preload = 9.208 \times 10^4\,psi$

$$\frac{Sba}{Preload} = 0.962$$

The average tensile stress under the imposed condition is close to the corresponding stress under the preload condition. There is a 3.8% decrease in average bolt tensile stress. Therefore, the sealing will be maintained.

3.AE.11 Conclusion

Using the standard method presented in Reference 3.AE.1, the above analysis demonstrates that the tensile stress in the closure bolts remains positive under the imposed preload, pressure and temperature conditions under the extreme cold storage environment where the metal in the vicinity of the bolts is -40 degrees. The closure bolts for the HI-STAR 100 Overpack will therefore not unload.

APPENDIX 3.AF - STRESS ANALYSIS OF OVERPACK CLOSURE BOLTS FOR THE STORAGE FIRE ACCIDENT

3.AF.1 Introduction

This appendix contains a stress analysis of the HI-STAR 100 Overpack closure bolts under the temperature conditions which exist during the storage fire accident. The purpose of the analysis is to demonstrate that the closure bolts do not "unload" during this condition.

The complex interaction of forces and moments in bolted joints of shipping casks has been investigated in Reference 3.AF.1, resulting in a comprehensive method of closure bolt stress analysis. That method is employed here. For each set of formulas or calculations used, reference to the appropriate table in [3.AF.1] is given. Where necessary, the formulas are modified to reflect the particulars of the HI-STAR system. For example, since the HI-STAR 100 closure lid has a raised face outside of the bolt circle, no prying forces can develop from loads directed outward (such as internal pressure).

3.AF.2 References

[3.AF.1] Mok, Fischer, Hsu, *Stress Analysis of Closure Bolts for Shipping Casks* (NUREG/CR-6007 UCRL-ID-110637), Lawrence Livermore National Laboratory/Kaiser Engineering, 1993.

[3.AF.2] Horton, H. (Ed.), *Machinery's Handbook*, 15th Ed., The Industrial Press, 1957.

[3.AF.3] FEL-PRO Technical Bulletin, N-5000 Nickel Based - Nuclear Grade Anti-Seize Lubricant, 8/97.

[3.AF.4] K.P. Singh and A.I. Soler, *Mechanical Design of Heat Exchangers and Pressure Vessel Components*, First Edition, Arcturus Publishers, Inc., 1984.

3.AF.3 Assumptions

The assumptions used in the analysis are given as a part of Reference 3.AF.1. The assumptions in that reference are considered valid for this analysis except where noted below.

1. The temperature conditions of the bolt circle area for the storage fire accident are used here.

2. Bolt forces due to prying action can only develop from inward directed loads because of the raised face on the closure lid which precludes metal-to-metal contact outside of the bolt circle.

3. The forces and moments in the bolts due to the gasket load are included in the preload imposed.

4. The forces and moments in the bolts due to vibration loads are small relative to the forces and moments generated by all other loads, and are considered negligible.

5. A recess is provided in the overpack closure plate that causes the MPC to contact the bottom face of the overpack closure plate over an annular region at the outer periphery of the closure plate. The formulas for plates under uniform pressure used in the reference are replaced here by formulas for plates loaded uniformly over an annular region at the outer periphery.

6. As the HI-STAR 100 Overpack includes a protected lid, shear bolt forces are defined to be zero.

7. The actual weight of the overpack closure plate is replaced by a somewhat larger weight in this analysis. This is conservative because loads on the bolts are increased with a heavier closure plate.

8. No prying action can occur from outward directed loads since the closure lid has a raised face outside of the bolt circle which eliminates the potential for prying action from positive bending moments.

3.AF.4 Terminology

Some terminology in Reference 3.AF.1 differs from Holtec's terminology. In this analysis, the 'cask wall' is Holtec's 'main flange'. The 'cask' is Holtec's 'Overpack'. 'Closure lid' and 'closure plate' are used interchangeably.

Wherever possible, parameter names are consistent with Reference 3.AF.1.

3.AF.5 Composition

This appendix was created with the Mathcad (version 7.0) software package. Mathcad uses the symbol ':=' as an assignment operator, and the equals symbol '=' retrieves values for constants or variables. Inequalities are also employed. Mathcad returns 0 for a false inequality, and 1 for a true inequality.

Units are also carried with Mathcad variables.

3.AF.6 Analysis Procedure

The analysis procedure is taken from Section 6.4 of Reference 3.AF.1. The following general steps are taken:

1. Identification of individual loadings.

2. Identification and evaluation of load parameters.

3. Determination of the forces and moments acting on the bolts due to each of individual loading.

4. Determination of the forces and moments acting on the bolts for the combined load case under analysis.

5. Evaluation of the stresses in the bolts for the combined load case.

6. Comparison with acceptance criteria.

3.AF.7 Identification of Individual Loadings

The individual loadings acting on the cask closure are the following:

a. Bolt preload. Bolt preload is present in all loadings and includes any gasket sealing loads.

b. Pressure. Design internal pressure is applied to the overpack wall and lid for all load combinations.

c. Temperature. Temperatures are taken from Table 11.2.2.

3.AF.8 Geometry Parameters

The parameters which define the HI-STAR 100 closure geometry are given in this section.

The nominal closure bolt diameter, $Db := 1.625 \cdot in$

The total number of closure bolts, $Nb := 54$

The stress area of a closure bolt (from [3.AF.4], p. 100), $A_b := 1.680 \cdot in^2$

The closure lid diameter at the bolt circle, $Dlb := 74.75 \cdot in$

Closure lid diameter at the location of the gasket load reaction, $Dlg := 71.565 \cdot in$

The HI-STAR overpack gasket system includes two concentric seals. The value for Dlg above locates the gasket load reaction between the two seal diameters.

The thickness of the cask wall, $tc := 6.25 \cdot in$

The minimum thickness of the closure lid, $t_l := \left(6 - \frac{1}{16}\right) \cdot in$

This value for the closure lid thickness accounts for the thickness reduction (recess) in the bottom face of the lid.

The effective thickness of the closure lid flange, $t_{lf} := 4.25 \cdot in$

The closure plate diameter at the inner edge, $D_{li} := 69.75 \cdot in$

The closure plate diameter at the inner edge is overpack inner diameter plus twice the width of the cut-out in the top flange which accommodates the inflatable annulus seal.

The closure plate diameter at the outer edge, $D_{lo} := 77.375 \cdot in$

The bolt length, $L_b := 4.25 \cdot in$

The bolt length is the length between the top and bottom surfaces of the closure plate, at the bolt circle location.

The number of bolt threads per inch, $n := 8 \cdot \frac{1}{in}$

The bolt thread pitch, $p := \frac{1}{n}$

The upper bound MPC weight (Table 3.2.4), $W_c := 90000 \cdot lb$

The bounding weight used for closure plate,(Table 3.2.4) $W_l := 8000 \cdot lb$

The overpack closure lid recess inner diameter, $d_l := 52.75 \cdot in$

3.AF.9 Material Properties

The overpack closure bolts are SB-637-N07718 steel, and the closure plate and top flange are SA-350-LF3 steel. The following material properties are used in the analysis based on a storage fire temperature of 524 degrees F (near the bolts). Interpolation of of table data from the appropriate ASME Code table (between 500 and 600 deg. F) in Part D of Section II of the Code is carried out where necessary to obtain appropriate Young's Modulus and Coefficient of Thermal Expansion.

The Young's modulus of the cask wall material, $E_c := 25580000 \cdot psi$

The Young's modulus of the closure plate material, $E_l := 25580000 \cdot psi$

The Poisson's ratio of the closure plate material, $NU_l := 0.3$

The closure bolt material coefficient of thermal expansion, $ab := 7.594 \cdot 10^{-6} \cdot R^{-1}$

The cask wall material coefficient of thermal expansion, $ac := 7.198 \cdot 10^{-6} \cdot R^{-1}$

The closure plate material coefficient of thermal expansion, $al := 7.198 \cdot 10^{-6} \cdot R^{-1}$

The zero points of the Fahrenheit and Rankine scales differ by a constant (1 °F = 1 R), therefore the above numbers are accurate with either unit.

Young's modulus of the closure bolt material, $Eb := 27028000 \cdot psi$

Young's modulus of top flange material, $Elf := 25580000 \cdot psi$

3.AF.10 Bolt Stress Calculations

3.AF.10.1 Identification and Evaluation of Load Parameters, Combined Load Case 1

The load parameters for each individual loading are defined as follows.

Loading parameters for preload:

The nominal value of the nut factor is 0.15 from Reference 3.AF.3.
The minimum nut factor, based on a tolerance of +/- 5%, is $K := 0.1425$

Per Table 8.1.3, the maximum bolt preload torque is 2,000 +250/-0 ft-lb. For conservatism, the following preload torque is used in the calculations:

$$Q := 2895 \cdot ft \cdot lbf + 90 \cdot ft \cdot lbf$$

Loading parameters for pressure load:

The pressure inside the cask wall, $Pci := 100 \cdot psi$

The pressure outside the cask wall, $Pco := 14.7 \cdot psi$

The pressure inside the closure lid, $Pli := 100 \cdot psi$

The pressure outside the closure lid, $Plo := 14.7 \cdot psi$

Loading parameters for the cold condition temperature load: (bolt installation at 70 deg. F)

The maximum temperature change of the main flange, $Tc := (524 - 70) \cdot R$

The maximum temperature change of the closure lid inner surface, $Tli := (524 - 70) \cdot R$

The maximum temperature change of the closure lid outer surface, $Tlo := (524 - 70) \cdot R$

The maximum temperature change of the closure lid, $Tl := \frac{Tli + Tlo}{2}$ $Tl = 454\,R$

The maximum temperature change of the closure bolts, $Tb := (524 - 70) \cdot R$ $Tb = 454\,R$

As these parameters are all temperature differences, the Fahrenheit-to-Rankine conversion factor of 460° can be omitted.

3.AF.10.2 Determination of Bolt Forces and Moments for the Individual Loadings

Array parameters are used to account for the multiple individual loadings within the combined load case. There are three individual loadings, so let i include the range from 1 to 3 as follows:

Let $i := 1 .. 3$

The forces and moments generated by each individual load case are represented by the following symbols:

The non-prying tensile bolt force per bolt = Fa_i

The shear bolt force per bolt = Fs_i

The fixed-edge closure lid force = Ff_i

Fixed-edge closure lid moment = Mf_i

The subscript i is used only to keep track of each individual load case within a load combination.

The first individual loading in this load combination is the residual load after the preload operation. The forces and moments generated by this load are defined as [3.AF.1, Table 4.1]:

The non-prying tensile bolt force per bolt, $Fa_1 := \frac{Q}{K \cdot Db}$

The maximum residual tensile bolt force (preload) per bolt, $Far_1 := Fa_1$

The maximum residual torsional bolt moment per bolt, $Mtr := 0.5 \cdot Q$

The preload stress in each bolt (based on stress area), $\text{Preload} := \frac{Fa_1}{A_b}$

Substituting the appropriate input data, the values of these parameters are determined as:

$Fa_1 = 154688\,\text{lbf}$

$Far_1 = 154688\,\text{lbf}$

$Mtr = 17910\,\text{in}\cdot\text{lbf}$

$\text{Preload} = 92076\,\text{psi}$

The second individual loading in this load combination is the pressure load. The forces and moments generated by this load are defined as follows [3.AF.1, Table 4.3]:

The non-prying tensile force per bolt, $Fa_2 := \frac{\pi \cdot Dlg^2 \cdot (Pli - Plo)}{4 \cdot Nb}$

The shear bolt force per bolt, $Fs_2 := \frac{\pi \cdot El \cdot tl \cdot (Pci - Pco) \cdot Dlb^2}{2 \cdot Nb \cdot Ec \cdot tc \cdot (1 - NUl)}$

The fixed-edge closure lid force, $Ff_2 := \frac{Dlb \cdot (Pli - Plo)}{4}$

The fixed-edge closure lid moment, $Mf_2 := \frac{(Pli - Plo) \cdot Dlb^2}{32}$

Substituting the appropriate input data, the values of these parameters are determined as:

$Fa_2 = 6354\,\text{lbf}$

$Fs_2 = 18816\,\text{lbf}$

$Ff_2 = 1594\,\frac{\text{lbf}}{\text{in}}$

$Mf_2 = 14894\,\text{lbf}$

The third individual loading in this load combination is the temperature load. The forces and moment generated by this load are defined as [3.AF.1, Table 4.4]:

The non-prying tensile bolt force per bolt, $Fa_3 := 0.25 \cdot \pi \cdot Db^2 \cdot Eb \cdot (al \cdot Tl - ab \cdot Tb)$

The shear bolt force per bolt, $Fs_3 := \frac{\pi \cdot El \cdot tl \cdot Dlb \cdot (al \cdot Tl - ac \cdot Tc)}{Nb \cdot (1 - NUl)}$

The fixed-edge closure lid force, $Ff_3 := 0 \cdot \frac{lbf}{in}$

The fixed-edge closure lid moment, $Mf_3 := \frac{El \cdot al \cdot tl^2 \cdot (Tlo - Tli)}{12 \cdot (1 - NUl)}$

Substituting the appropriate input data, the values of these parameters are determined as:

$$Fa_3 = -10078\ lbf$$

$$Fs_3 = 0\ lbf$$

$$Ff_3 = 0 \frac{lbf}{in}$$

$$Mf_3 = 0\ lbf$$

3.AF.10.3 Determination of Combined Bolt Forces and Combined Bolt Moments

The calculations in the following subsections are performed in accordance with Tables 4.9, 2.1 and 2.2 of Reference 3.AF.1.

3.AF.10.3.1 Tensile Bolt Force

First, combine the non-prying tensile bolt forces (Fa_i):

The total preload and temperature load, $Fa\_pt := Fa_1 + Fa_3$

$$Fa\_pt = 144611\ lbf$$

The sum of the remaining forces (pressure),

$$Fa\_al := Fa_2$$

$$Fa\_al = 6354\ lbf$$

The combined non-prying tensile bolt force,

$$Fa\_c := Fa\_al \cdot (Fa\_al > Fa\_pt) + Fa\_pt \cdot (Fa\_pt > Fa\_al)$$

$$Fa\_c = 144611\ lbf$$

If the combined non-prying tensile bolt force (Fa_c) is negative, set it equal to zero. Per Appendix 3 of Reference [3.AF.1], inward directed loads are not reacted by the bolts, but the developed formulations are still valid if the spurious bolt forces < 0.0 are removed from the calculation.

$$Fa\_c := Fa\_c \cdot (Fa\_c > 0 \cdot lbf)$$

$$Fa\_c = 144611\ lbf$$

Next, combine the prying tensile bolt forces and moments (these bolt forces develop due to Ff_i and Mf_i):

The sum of the fixed edge forces, $Ff\_c := Ff_1 + Ff_2 + Ff_3$

$$Ff\_c = 1594 \frac{lbf}{in}$$

If the combined fixed-edged force (Ff_c) is negative, set it equal to zero.

$$Ff\_c := Ff\_c \cdot \left(Ff\_c > 0 \cdot \frac{lbf}{in}\right) + 0 \cdot \frac{lbf}{in} \cdot \left(Ff\_c < 0 \cdot \frac{lbf}{in}\right) \qquad Ff\_c = 1.594 \times 10^3 \frac{lbf}{in}$$

The sum of fixed-edge moments, $Mf\_c := Mf_1 + Mf_2 + Mf_3$

$$Mf\_c = 14894 \frac{lbf \cdot in}{in}$$

Define the appropriate prying force moment arm depending on the direction of Mf_c. For inward directed loading, prying moments are developed by the lid rotating about the flange inner edge; for outward directed loading, prying moments are developed by the lid rotating about its outer edge. Thus, the moment arms are different in the two cases.

$$Arm := (Dlo - Dlb) \cdot (Mf\_c > 0 \cdot lbf) + (Dlb - Dli) \cdot (Mf\_c < 0 \cdot lbf)$$

$$Arm = 2.625\ in$$

The prying tensile bolt force for the combined loading can therefore be determined as:

The constants C_1 and C_2 are: $C_1 := 1$

$$C_2 := \left[\frac{8}{3 \cdot (Arm)^2}\right] \cdot \left[\frac{El \cdot tl^3}{1 - NUl} + \frac{(Dlo - Dli) \cdot Elf \cdot tlf^3}{Dlb}\right] \cdot \left(\frac{Lb}{Nb \cdot Db^2 \cdot Eb}\right)$$

$$C_2 = 3.35$$

The bolt preload per unit length of bolt circle, $P := Fa\_pt \cdot \left(\frac{Nb}{\pi \cdot Dlb}\right)$

$$P = 33253 \frac{lbf}{in}$$

The parameter P is the pressure/temperature force which is multiplied to determine preload per unit length of bolt circle (see Tables 2.1 and 4.9 in Section II.3 of Reference 3.AF.1).

The non-prying tensile bolt force, $B := Ff\_c \cdot (Ff\_c > P) + P \cdot (P > Ff\_c)$

$$B = 33253 \frac{lbf}{in}$$

The additional tensile bolt force per bolt caused by prying action of the closure lid,

$$Fap := \left(\frac{\pi \cdot Dlb}{Nb}\right) \cdot \left[\frac{\frac{2 \cdot Mf\_c}{Arm} - C_1 \cdot (B - Ff\_c) - C_2 \cdot (B - P)}{C_1 + C_2}\right]$$

$$Fap = -20306\ lbf$$

The prying force must be tensile. If the result is negative, set it equal to zero.

$$Fab\_c := Fap \cdot (Fap > 0 \cdot lbf) + 0 \cdot lbf \cdot (Fap < 0 \cdot lbf)$$

$$Fab\_c = 0\ lbf$$

The total tensile bolt force for stress analysis, $FA := Fa\_c + Fab\_c$

$$FA = 144611\ lbf$$

3.AF.10.3.2 Bolt Shear Force

The sum of the shear forces, $Fs\_c := Fs_1 + Fs_2 + Fs_3$

$$Fs\_c = 18816\ lbf$$

$Fs := 0 \cdot lbf$ (protected cask lid)

3.AF.10.3.3 Bolt Bending Moment

The calculations in this section are performed in accordance with Table 2.2 of Reference 3.AF.1. The following relations are defined:

$$Kb := \left(\frac{Nb}{Lb}\right)\cdot\left(\frac{Eb}{Dlb}\right)\cdot\left(\frac{Db^4}{64}\right)$$

$$Kl := \frac{El\cdot tl^3}{3\cdot\left[\left(1 - NUl^2\right) + (1 - NUl)^2\cdot\left(\frac{Dlb}{Dlo}\right)^2\right]\cdot Dlb}$$

$$Mbb\_c := \left(\frac{\pi\cdot Dlb}{Nb}\right)\cdot\left(\frac{Kb}{Kb + Kl}\right)\cdot Mf\_c$$

$$Mbb := Mbb\_c$$

where Mbb is the bolt bending moment. Substituting the appropriate values, these parameters are calculated as:

$Kb = 500543\ lbf$

$Kl = 17462636\ lbf$

$Mbb\_c = 1.805 \times 10^3\ lbf\cdot in$

$Mbb = 1.805 \times 10^3\ lbf\cdot in$

3.AF.10.3.4 Bolt Torsional Moment

The torsional bolt moment is generated only by the preloading operation, therefore no combination is necessary.

3.AF.10.4 Evaluation of Bolt Stresses

Per Table 5.1 of Reference 3.AF.1, the average and maximum bolt stresses for comparison with the acceptance criteria are obtained. Inch-series threads are used and the maximum shear and bending are in the bolt thread.

The bolt diameter for tensile stress calculation [3.AF.1, Table 5.1], $Dba := Db - 0.9743\cdot p$

$Dba = 1.503\ in$

The bolt diameter for shear stress calculation, $Dbs := Dba$

$$Dbs = 1.503\ in$$

The bolt diameter for bending stress calculation, $Dbb := Dba$

$$Dbb = 1.503\ in$$

The bolt diameter for torsional stress calculation,

$$Dbt := Dba$$

$$Dbt = 1.503\ in$$

The average tensile stress caused by the tensile bolt force FA, $Sba := 1.2732 \cdot \frac{FA}{Dba^2}$

$$Sba = 81481\ psi$$

The average shear stress caused by the shear bolt force Fs, $Sbs := 1.2732 \cdot \frac{Fs}{Dbs^2}$

$$Sbs = 0\ psi$$

The maximum bending stress caused by the bending bolt moment Mb, $Sbb := 10.186 \cdot \frac{Mbb}{Dbb^3}$

$$Sbb = 5412\ psi$$

The maximum shear stress caused by the torsional bolt moment Mt, $Sbt := 5.093 \cdot \frac{Mtr}{Dbt^3}$

$$Sbt = 26854\ psi$$

The maximum stress intensity caused by the combined loading of tension, shear, bending and torsion can therefore be determined as:

$$Sbi := \left[(Sba + Sbb)^2 + 4 \cdot (Sbs + Sbt)^2 \right]^{0.5}$$

$$Sbi = 102152\ psi$$

3.AF.10.5 Comparison with Acceptance Criteria

The final bolt stress is less than the preload stress $\text{Preload} = 9.208 \times 10^4 \text{ psi}$

$$\frac{\text{Sba}}{\text{Preload}} = 0.885$$

The average tensile stress under the imposed condition is close to the corresponding stress under the preload condition. There is only a 11.5% decrease in average bolt tensile stress. Therefore, the sealing will be maintained.

3.AF.11 Conclusion

Using the standard method presented in Reference 3.AF.1, the above analysis demonstrates that the tensile stress in the closure bolts remains positive under the imposed preload, pressure and temperature conditions under the postulated storage fire accident where the metal in the vicinity of the bolts is 524 degrees F. The closure bolts for the HI-STAR 100 Overpack will therefore not unload.

APPENDIX 3.AG - STRESS ANALYSIS OF THE HI-STAR 100 ENCLOSURE SHELL UNDER 30psi INTERNAL PRESSURE

3.AG.1 Introduction:

The outer region of the HI-STAR 100 overpack consists of radial sector shells made of stabilized carbon steel plate stock with annular ring closures at the top and bottom. These closed "sector shaped" cylindrical spaces are referred to as "enclosure shells" because they enclose the neutron absorber material (Holtite-A). Experimental data by Holtec and others conclusively suggests that Holtite-A is a stable material under the environmental and thermal conditions corresponding to the normal operation modes of the HI-STAR 100 overpack. However, under an extreme environmental event (notably, a fire), the temperature in the enclosure shell cavity may rise, leading to the generation of water vapor. This occurs because neutron absorbers in use in contemporary cask designs utilize materials with water molecules in intermolecular bond with metal alloys to maximize their hydrogen content; the molecular bond weakens at high temperature leading to the liberation of water droplets. To protect the enclosure shell from overpressure, two design measures are incorporated:

(i) The inside surfaces of the top and bottom enclosure shell returns are lined with a layer of foam to allow for expansion of the Holtite-A material.

(ii) Two rupture disks (for redundancy) with a relatively low set pressure (30 psig) are installed to relieve water vapor if the temperature rise in the cask, for whatever reason, is rapid and excessive.

In addition to the built-in pressure protection, the structural design of the enclosure shell is configured to insure that at 30 psi internal pressure, the stresses in the enclosure shell structure are well below the "Level A" stress limits for a ASME Section III, Subsection NF structure. Furthermore, information necessary to demonstrate that Holtite-A will not off-gas under the design basis heat load and maximum normal ambient condition is also compiled herein from the main body of the report.

Finally, the geometric details of the enclosure shell may be found in drawings 1397, 1399 and BM-1476 wherein the top and bottom annular plates are denoted as "shell returns". Stress analysis presented in this appendix uses data from the above mentioned design documents (placed in Section 1.5 of this FSAR).

3.AG.2 Stability of Holtite-A in Normal Operating Condition Mode

A paper by Asano and Niomura ("Experimental Studies on Long-term Thermal Degradation of Enclosed Neutron Shielding Resin"), which experimentally evaluates the weight loss of Holtite-A, is included in Appendix 1.B of this FSAR. For long-term exposure of an enclosed Holtite-A sample to a temperature of 125°C, the paper shows that the water loss rate is insignificant.

The maximum calculated temperature of Holtite, for the design basis decay heat load and maximum normal ambient temperature conditions, is presented in Table 4.4.10 for the MPC-24 and Table 4.4.11 for the MPC-68 (MPC-24 governs). This calculated maximum normal temperature occurs at the inner surface of the Holtite near the cask mid-height. The maximum overpack enclosure surface temperature, also presented in Table 4.4.10, is approximately equal to the maximum outer Holtite surface temperature. As the Holtite temperature decreases with distance from the cask mid-height, a conservative estimate of the maximum bulk average Holtite temperature can be obtained by averaging these two maximum temperatures.

$T_i := 274$ Inner Holtite Surface Maximum Temperature, F

$T_o := 229$ Outer Holtite Surface Maximum Temperature, F

$T_b := \frac{T_i + T_o}{2}$ $T_b = 251.5$ Conservative Holtite Bulk Average Temperature, F

$T_{bc} := (T_b - 32) \cdot \frac{5}{9}$ $T_b = 121.9$ Conservative Holtite Bulk Average Temperature, C

This temperature is less than the 125°C temperature which has been shown by experiment to have no significant water loss. It is further noted that the Holtite bulk average temperature is not constant over the 20 year cask design life, but will reduce monotonically with the decay heat load.

As the decay heat load of the stored fuel assemblies attenuates over time, the Holtite bulk average temperature will approach the ambient temperature of 80°F (approximately 27°C). For example, a Holtite bulk average temperature of 100°C would require a temperature reduction of:

$\Delta T_b := \frac{T_b - 100}{T_b - 27}$ $\Delta T_b = 23.1\%$ Required Temperature Reduction

This reduction in temperature will require an equivalent reduction in decay heat load. The reduction in decay heat load is not linear with time, but is governed by the exponential nature of radioactive decay. For the design basis BWR and PWR fuel assemblies, the assembly decay heat load is determined as a function of time in Holtec Report HI-951322, Revision 6 (pages 24-3 and 25-3). For both BWR and PWR fuel assemblies, a decay heat reduction equal to the required temperature reduction is achieved in less than 2 years. The temperature margin to 125 degrees C will, therefore, increase rapidly as the design basis fuel cools.

It can therefore be concluded that there will be no significant water loss from the Holtite during the entire HI-STAR 100 System storage life. Therefore, the production of water vapor in the Holtite-filled cavities during normal storage conditions, resulting in the rise of pressure in the enclosure shell cavity, is ruled out as a credible possibility.

3.AG.3 Stress Analysis for Internal Pressure

The stress analysis of the flat panels in the enclosure shell and the flat annular ring making up the enclosure shell return are analyzed by considering a representative beam strip of unit width. This approach is conservative as it neglects any additional support from the flat plate and annular ring effects.

(i) References:

[3.1] Mathcad 7.0, Mathsoft, 1997.

(ii) Input Data:

All dimensions taken from Holtec drawings 1397, 1399, and from BM 1476 for HI-STAR 100.

Thickness of enclosure shell panels: $t_v := 0.5 \cdot in$

Thickness of enclosure shell return: $t_p := 0.5 \cdot in$

Enclosure shell return unsupported outer diameter: $OD := 96 \cdot in - t_v$

Enclosure shell return inner diameter: $ID := 85.75 \cdot in$

Enclosure shell panel unsupported width: $b_s := 7.875 \cdot in$ Bounding reference value

Bottom panel unsupported length: $L := .5 \cdot (OD - ID)$ $L = 4.875 in$

The allowable primary bending stress is (SA-515,Gr.70 allowable stresses are listed in Table 3.1.10 of the HI-STAR FSAR):

$S_a := 26300 \cdot psi$

(iii) Calculations

(a) Internal pressure for stress analysis

For the purpose of this calculation, 30 psi is used as the internal pressure to bound the effects of off-gassing of the neutron absorber material. We denote this input pressure as q. Table 2.2.1 lists 30 psi as the design pressure.

$q := 30 \cdot psi$

(b) Bottom annular plate (enclosure shell return):

The plate is conservatively considered to be simply supported at both the inside and at the outside diameter. Because of the small unsupported annulus, the solution for a beam strip 1" wide is considered since the plate effects are negligible.

w = strip width $\qquad w := 1 \cdot in$

The bending moment at the center of the strip is

$$M_c := w \cdot \frac{q \cdot L^2}{8} \qquad M_c = 89.121\,lbf \cdot in$$

The maximum bending stress for a simply supported beam strip is

$$\sigma := M_c \cdot \frac{(.5 \cdot t_p)}{\left(\frac{w \cdot t_p^{\,3}}{12}\right)} \qquad \text{or} \qquad \sigma := .75 \cdot q \cdot \left(\frac{L}{t_p}\right)^2$$

$$\sigma = 2.139 \times 10^3\,psi$$

The calculated stress in the plate is less than the allowable limit. The safety factor for primary bending is

$$SF := \frac{S_a}{\sigma} \qquad SF = 12.296$$

(c) Enclosure Shell Flat Side Panels

These flat panels are treated as 1 inch wide beams. The actual end boundary condition is considered as an average of the simply supported and clamped conditions. This is reasonable since the groove welds most likely provide a support condition that is essentially clamped; the use of an average between pinned and clamped conditions will be conservative. The stress at the center of the panel is computed as follows:

The maximum bending moment is computed as the average of the moment for the two limiting end conditions:

$$M_{max} := 0.5 \cdot \left(\frac{q \cdot w \cdot b_s^{\,2}}{8} + \frac{q \cdot w \cdot b_s^{\,2}}{24} \right) \qquad M_{max} = 155.039\,lbf \cdot in$$

The beam section modulus is:

$$S := \frac{w \cdot t_v^{\,2}}{6} \qquad S = 0.042\,in^3$$

The maximum calculated bending stress is:

$$\sigma_{maxv} := \frac{M_{max}}{S} \qquad \sigma_{maxv} = 3.721 \times 10^3\,psi$$

$$SF := \frac{S_a}{\sigma_{maxv}} \qquad SF = 7.068$$

(d) Calculation of Weld Shear Stress

We consider the vertical weld between enclosure shell flat panels and the radial sectors and the circumferential weld between the enclosure shell and the enclosure shell return as representative welds for analysis. Table NF-3324.5(a)-1 in Subsection NF of the Code, requires that the allowable stress for the weld be equal to the allowable stress in the base metal. For the allowable weld stress in shear, we apply the limit given in NF-3252.2 for pure shear, namely, 60% of the tensile limit.

Model the weld as a 3/16" groove weld for calculation purposes.

$$t_{weld} := \frac{3}{16} \cdot in$$

The shear stress due to the internal pressure in the vertical flat panel weld is

$$\tau_{weld} := \frac{q \cdot .5 \cdot b_s}{t_{weld}} \qquad \tau_{weld} = 630\,psi$$

Since the allowable base metal stress for primary bending has been input earlier, we divide this value by 1.5 to obtain an allowable primary membrane stress.

$$SF := \frac{.6 \cdot \left(\frac{S_a}{1.5}\right)}{\tau_{weld}} \qquad SF = 16.698$$

For the weld around the annular ring, we note that since the unsupported strip width is less than the value used above, the weld shear stress will be even lower. Thus, the flat panel weld controls the design.

3.AG.4 Conclusion

For a 30 psi internal pressure, all safety factors are well in excess of 1.0 demonstrating that the 30 psig internal pressure is safely supported by the enclosure shell and the enclosure shell return.

Although the effect of dead weight of the neutron absorber material has not been included as an additional loading in the analysis of the enclosure shell return, it is clear from the large safety factors that structural integrity will not be compromised.

There is no credible mechanism for the pressure to exceed 30 psi under normal operating conditions in the enclosure shell sectors.

APPENDIX 3.AH MPC-LIFT LUGS

AH.1.0 SCOPE:

During fabrication and transport to the site, an MPC with fuel basket may be lifted vertically using four lift lugs, which are welded to the inside of the MPC shell. This analysis considers the four MPC Lift Lugs. The lifted load is equal to the MPC empty weight without top lid plus the fuel basket. No fuel is carried when these lugs are used for lifting. The four lift lugs each consist of a vertical lug stiffened by a horizontal plate. The lift lug is shown in Drawings 1395 Sheet 4 and 1402, Sheet 5.

AH.2.0 METHODOLOGY:

Strength of Materials beam formulas are used to compute the stress in the lug assuming that the shell plate acts as a fixed base for the lift lug. The applied load is the weight of the heaviest MPC without fuel (MPC-24E). The geometry for the lift lug, however, is that of the smallest lift lug.

AH.3.0 ACCEPTANCE CRITERIA:

NUREG 0612 is applied with a factor of safety of 6 on yield strength or 10 on ultimate strength, whichever governs. Each unit has four (4) lift lugs.

AH.4.0 INPUT DATA

AH.4.1 Allowable Strength

Per Table 3.3.1, FSAR @ 100 degrees F, the yield and ultimate strengths for Alloy "X" are

$S_y := 30000 \cdot psi$

$S_u := 75000 \cdot psi$

Therefore, in accordance with NUREG 0612 and ANSI N14-6, the allowable strength under the actual lifted load is

$$\sigma_a := \frac{S_y}{6} \qquad \sigma_a = 5 \times 10^3 \, psi$$

The actual lifted load is

$W_{empty\_MPC} := 43561 \cdot lbf$ Ref. Holtec drawing 3471

$W_{lid} := 9822 \cdot lbf$ From detailed weight calculation

Therefore

$$W := W_{empty\_MPC} - W_{lid} \qquad W = 3.374 \times 10^4 \, lbf$$

In accordance with Holtec's accepted practice for Cask lifts, we apply a 15% dynamic amplification factor appropriate to a low speed lift (Per CMAA, #70). Therefore, the apparent lifted load, per lift lug, is

$W_{lift} := W \cdot \frac{1.15}{4}$ $\quad W_{lift} = 9.7 \times 10^3\ lbf$

If the minimum rigging angle is assumed to be 70 degrees (measured from the horizontal), the tension in the rigging is

$\theta_{rigging} := 70 \cdot deg$

$P := \frac{W_{lift}}{\sin(\theta_{rigging})}$ $\quad P = 1.032 \times 10^4\ lbf$

Thus the horizontal and vertical forces acting on each lift lug are

$P_h := P \cdot \cos(\theta_{rigging})$ $\quad P_h = 3.53 \times 10^3\ lbf$

$P_v := P \cdot \sin(\theta_{rigging})$ $\quad P_v = 9.7 \times 10^3\ lbf$

AH.4.2 Geometry

From the MPC drawing 1402, Sheet 5, we use the following data

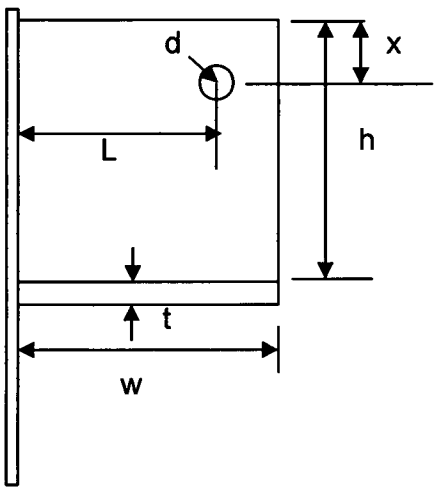

$t := 1.0 \cdot in$ $\quad x := 1.75 \cdot in$

$h := 9.375 \cdot in$ width of flange $wf := 4 \cdot in$

$L := 1.75 \cdot in$ Weld sizes

$w := 3.5 \cdot in$ $t_{weld\_web} := 0.25 \cdot in$

$d := 1.3125 \cdot in$ $t_{weld\_flange} := 0.25 \cdot in$

AH.5.0 CALCULATIONS

AH.5.1 Bearing Stress in Lift Hole

$$\sigma_{bearing} := \frac{P}{t \cdot d} \qquad \sigma_{bearing} = 7.865 \times 10^3 \, psi$$

Note that there is no requirement per ANSI N14.6 that local bearing stresses are subject to the same allowable stress as the primary stresses (see section 3.2.1.2 of ANSI N14.6). If load testing is performed, the bearing stress will not exceed yield even under three times the lifted load.

AH.5.2 Shear Pullout

$$\tau_{shear} := \frac{P}{2 \cdot x \cdot t} \qquad \tau_{shear} = 2.949 \times 10^3 \, psi$$

$$SF := \frac{.6 \cdot \sigma_a}{\tau_{shear}} \qquad SF = 1.017$$

AH.5.3 Net Shear Stress on Root of Lug (Beam)

$$\tau_{net} := \frac{P_v}{h \cdot t} \qquad \tau_{net} = 1.035 \times 10^3 \, psi$$

$$SF_{shear} := \frac{.6 \cdot \sigma_a}{\tau_{net}} \qquad SF_{shear} = 2.899$$

AH.5.4 Net Bending Stress at Root of Lug

AH.5.4.1 Determine moment of inertia of inverted "T" section

The lug plate plus the stiffener form a "T" section. For stress determination, we need to compute the section properties of the lug, considered as a composite member.

GEOMETRY OF BUILT UP TEE SECTION

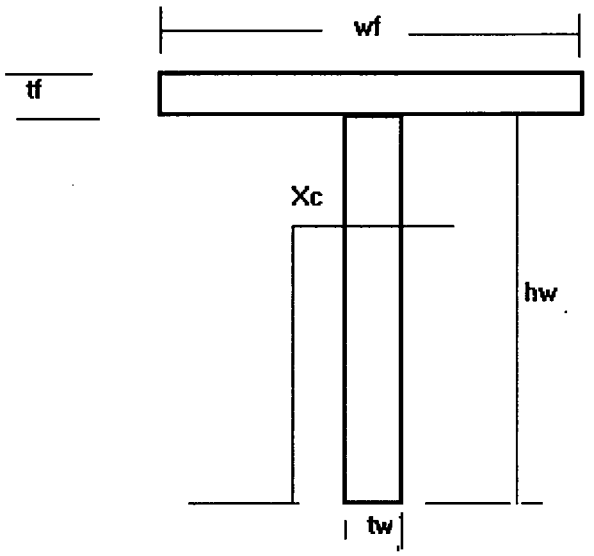

$hw := h$ $tw := t$

$wf = 4\,in$ $tf := t$

Guess value for centroid

$$X_c := \frac{hw}{2}$$

Measurement of centroid is relative to free end of web

Given

$$(hw \cdot tw + wf \cdot tf) \cdot X_c = hw \cdot tw \cdot \frac{hw}{2} + (wf \cdot tf) \cdot \left(hw + \frac{tf}{2}\right) \qquad X_{cent} := \text{Find}(X_c) \qquad X_{cent} = 6.239\,in$$

$$I_e := tw \cdot \frac{hw^3}{12} + wf \cdot \frac{tf^3}{12} + (hw \cdot tw) \cdot \left(X_{cent} - \frac{hw}{2}\right)^2 + (wf \cdot tf) \cdot \left[X_{cent} - (hw + .5 \cdot tf)\right]^2 \qquad I_e = 144.447\,in^4$$

AH.5.4.2 Bending Stress

$$Moment := P_v \cdot L - P_h \cdot (X_{cent} - x) \qquad Moment = 1.127 \times 10^3\,lbf \cdot in$$

$$\sigma_{web} := \frac{Moment \cdot X_{cent}}{I_e} \qquad \sigma_{web} = 48.672\,psi$$

$$\sigma_{flange} := \frac{Moment \cdot (h + t - X_{cent})}{I_e} \qquad \sigma_{flange} = 32.267\,psi$$

$$SF_{bending} := \frac{\sigma_a}{\sigma_{web}} \qquad SF_{bending} = 102.729$$

AH.5.4.3 Weld Stress

Weld Area of web plus flange

$$A_{weld} := 2 \cdot t_{weld\_web} \cdot .7071 \cdot hw + (2wf - tw) \cdot t_{weld\_flange} \cdot .7071 \qquad A_{weld} = 4.552\,in^2$$

Weld Centroid

$$x_c := \frac{(wf - tw) \cdot (.7071 \cdot t_{weld\_flange}) \cdot tf + 2 \cdot hw \cdot (.7071 \cdot t_{weld\_web}) \cdot \left(tf + \frac{hw}{2}\right)}{A_{weld}} \qquad x_c = 4.258\,in$$

Weld Moment of Inertia

$$I_{weld} := \frac{1}{6} \cdot (.7071 \cdot t_{weld\_web}) \cdot hw^3 + 2 \cdot hw \cdot (.7071 \cdot t_{weld\_web}) \cdot \left(tf + \frac{hw}{2} - x_c\right)^2 \ldots$$
$$+ wf \cdot (.7071 \cdot t_{weld\_flange}) \cdot x_c^2 + (wf - tw) \cdot (.7071 \cdot t_{weld\_flange}) \cdot (x_c - tf)^2$$

$$I_{weld} = 49.499\,in^4$$

The shear stresses in the weld due to the horizontal and vertical rigging forces are

$$\tau_{weldh} := \frac{P_h}{A_{weld}} \qquad \tau_{weldh} = 775.6\,psi$$

$$\tau_{weldv} := \frac{P_v}{A_{weld}} \qquad \tau_{weldv} = 2.131 \times 10^3\,psi$$

The weld stress due to bending is

$$Moment_{weld} := P_v \cdot L - P_h \cdot (hw + tf - x - x_c) \qquad Moment_{weld} = 1.557 \times 10^3\,lbf \cdot in$$

$$\tau_{weldb} := \frac{Moment_{weld} \cdot (hw + tf - x_c)}{I_{weld}} \qquad \tau_{weldb} = 192.398\,psi$$

The maximum combined shear stress in the weld is

$$\tau := \sqrt{\tau_{weldv}^{2} + (\tau_{weldh} + \tau_{weldb})^{2}} \qquad \tau = 2.341 \times 10^{3}\,psi$$

For this lifting calculation, we do not apply any weld efficiency factors since NG is not the applicable code for this calculation.

$$SF := 0.6 \cdot \frac{\sigma_a}{\tau} \qquad SF = 1.282$$

AH.5.4.4 Vertical Stress in Web at Minimum Section (plane through hole)

The area of the minimum section is

$$w_{min} := w - d \qquad w_{min} = 2.188\,in \qquad A_{min} := t \cdot w_{min} \qquad A_{min} = 2.187\,in^{2}$$

$$\sigma_{avg} := \frac{P_v}{A_{min}} \qquad \sigma_{avg} = 4.434 \times 10^{3}\,psi$$

$$SF_{avg} := \frac{\sigma_a}{\sigma_{avg}} \qquad SF_{avg} = 1.128$$

AH.6.0 CONCLUSION

Stresses are compared with NUREG-0612 requirements of 6 on yield strength and 10 on ultimate strength. All primary stress computations show safety factors greater than 1.0 in the lug and in the lug to shell weld. The bearing stress in the lifting hole exceeds the 1/6 yield stress limit. However, this stress is not a primary stress and there will be no tests to increased load levels. Should a test be imposed, the test level should not cause yielding in the base metal at the hole due to excessive bearing stress.

AH.7.0 REFERENCES

7.1 NUREG 0612

7.2 ANSI N14.6 (1993) Special Lifting Devices for Loads in Nuclear Plants Over 10000 lb.

7.3 Holtec Drawing 1402, Sheet 5 for MPC-68.

7.4 HI-2012610 (HI-STAR FSAR), Tables in Chapter 3

7.5 ASME Code, Section III, Subsection NG, 1995.

7.6 Crane Manufacturers Association of America, CMAA #70.

APPENDIX 3.AI - ANALYSIS OF TRANSNUCLEAR DAMAGED FUEL CANISTER AND THORIA ROD CANISTER

3.AI.1 Introduction

Some of the items at the Dresden Station that have been considered for storage in the HI-STAR 100 System are damaged fuel stored in Transnuclear damaged fuel canisters and Thoria rods that are also stored in a special canister designed by Transnuclear. Both of these canisters have been designed and have been used by ComEd to transport the damaged fuel and the Thoria rods. Despite the previous usage of these canisters, it is prudent and appropriate to provide an independent structural analysis of the major load path of these canisters prior to accepting them for inclusion as permitted items in the HI-STAR 100 MPC's. This appendix contains the necessary structural analysis of the Transnuclear damaged fuel canister and Thoria rod canister. The objective of the analysis is to demonstrate that the canisters are structurally adequate to support the loads that develop during normal lifting operations and during postulated accident conditions.

The upper closure assembly is designed to meet the requirements of NUREG-0612 [2]. The remaining components of the canisters are governed by ASME Code Section III, Subsection NG [3]. These are the same criteria used in Appendix 3.B to analyze the Holtec damaged fuel container for Dresden damaged fuel.

3.AI.2 Composition

This appendix was created using the Mathcad (version 8.02) software package. Mathcad uses the symbol ':=' as an assignment operator, and the equals symbol '=' retrieves values for constants or variables.

3.AI.3 References

1. Crane Manufacture's of America Association, Specifications for Electric Overhead Traveling Cranes #70.

2. NUREG-0612, Control of Heavy Loads at Nuclear Power Plants

3. ASME Boiler and Pressure Vessel Code, Section III, July 1995

3.AI.4 Assumptions

1. Buckling is not a concern during an accident since during a drop the canister will be confined by the fuel basket.

2. The strength of the weld is assumed to decrease the same as the base metal as the temperature increases.

3.AI.5 Method

Two are considered: 1) normal lifting and handling of canister, and 2) accident drop event.

3.AI.6 Acceptance Criteria

1) Normal Handling -

a) Canister governed by ASME NG allowables:

b)Welds governed by NG and NF allowables;
quality factors taken from NG
stress limit = 0.3 Su

c) Lifting governed by NUREG-0612 allowables.

2) Drop Accident -

a) canister governed by ASME NG allowables:
shear = 0.42 Su (conservative)

b)Welds governed by NG and NF allowables;
quality factors taken from NG
stress limit = 0.42 Su

3.AI.7 Input Stress Data

The canisters is handled while still in the spent fuel pool. Therefore, its design temperature for lifting considerations is the temperature of the fuel pool water (150°F). The design temperature for accident conditions is 725°F. All dimensions are taken from the Transnuclear design drawings listed at the end of this appendix. The basic input parameters used to perform the calculations are:

Design stress intensity of SA240-304 (150°F)	$S_{m1} := 20000 \cdot psi$
Design stress intensity of SA240-304 (775°F)	$S_{m2} := 15800 \cdot psi$
Yield stress of SA240-304 (150°F)	$S_{y1} := 27500 \cdot psi$
Yield stress of SA240-304 (775°F)	$S_{y2} := 17500 \cdot psi$
Ultimate strength of SA240-304 (150°F)	$S_{u1} := 73000 \cdot psi$
Ultimate strength of SA240-304 (775°F)	$S_{u2} := 63300 \cdot psi$

Ultimate strength of weld material (150°F) $Su_w := 70000 \cdot psi$

Ultimate strength of weld material (775°F) $Su_{wacc} := Su_w - (S_{u1} - S_{u2})$

Weight of a BWR fuel assembly (D-1) $W_{fuel} := 400 \cdot lbf$

Weight of 18 Thoria Rods (Calculated by Holtec) $W_{thoria} := 90 \cdot lbf$

Bounding Weight of the damaged fuel canister (Estimated by Holtec) $W_{container} := 150 \cdot lbf$

Bounding Weight of the Thoria Rod Canister (Estimated) $W_{rodcan} := 300 \cdot lbf$

Quality factor for full penetration weld (visual inspection) $n := 0.5$

Dynamic load factor for lifting $DLF := 1.15$

The remaining input data is provided as needed in the calculation section

3.AI.8 Calculations for Transnuclear Damaged Fuel Canister

3.AI.8.1 Lifting Operation (Normal Condition)

The critical load case under normal conditions is the lifting operation. The key areas of concern for ASME NG analysis are the canister sleeve, the sleeve to lid frame weld, and the lid frame. All calculations performed for the lifting operation assume a dynamic load factor of 1.15 [1].

3.AI.8.1.1 Canister Sleeve

During a lift, the canister sleeve is loaded axially, and the stress state is pure tensile membrane. For the subsequent stress calculation, it is assumed that the full weight of the damaged fuel canister and the fuel assembly are supported by the sleeve. The magnitude of the load is

$$F := DLF \cdot (W_{container} + W_{fuel}) \qquad F = 632\,lbf$$

From TN drawing 9317.1-120-4, the canister sleeve geometry is

$id_{sleeve} := 4.81 \cdot in$ $t_{sleeve} := 0.11 \cdot in$

The cross sectional area of the sleeve is

$$A_{sleeve} := (id_{sleeve} + 2 \cdot t_{sleeve})^2 - id_{sleeve}^2 \qquad A_{sleeve} = 2.16\,in^2$$

Therefore, the tensile stress in the sleeve is $\sigma := \frac{F}{A_{sleeve}}$ $\sigma = 292\,psi$

The allowable stress intensity for the primary membrane category is S_m per Subsection NG of the ASME Code. The corresponding safety margin is

$$SM := \frac{S_{m1}}{\sigma} - 1 \qquad SM = 67.5$$

3.AI.8.1.2 Sleeve Welds

The top of the canister must support the amplified weight. This load is carried directly by the fillet weld that connects the lid frame to the canister sleeve. The magnitude of the load is conservatively taken a the entire amplified weight of canister plus fuel.

$$F = 632\,lbf$$

The weld thickness is $t_{base} := 0.09 \cdot in$

The area of the weld, with proper consideration of quality factors, is

$$A_{weld} := n \cdot 4 \cdot (id_{sleeve} + 2 \cdot t_{sleeve}) \cdot .7071 \cdot t_{base} \qquad A_{weld} = 0.64\,in^2$$

Therefore, the shear stress in the weld is $\tau := \frac{F}{A_{weld}}$ $\tau = 988\,psi$

From the ASME Code the allowable weld shear stress, under normal conditions (Level A), is 30% of the ultimate strength of the base metal. The corresponding safety margin is

$$SM := \frac{0.3 \cdot S_{u1}}{\tau} - 1 \qquad SM = 21.2$$

3.AI.8.1.3 Lid Frame Assembly

The Lid Frame assembly is classified as a NUREG-0612 lifting device. As such the allowable stress for design is the lesser of one-sixth of the yield stress and one-tenth of the ultimate strength.

$$\sigma_1 := \frac{S_{y1}}{6} \qquad \sigma_2 := \frac{S_{u1}}{10}$$

$$\sigma_1 = 4583\,psi \qquad \sigma_2 = 7300\,psi$$

For SA240-304 material the yield stress governs. $\sigma_{allowable} := \sigma_1$

The total lifted load is $F := DLF \cdot (W_{container} + W_{fuel})$ $F = 632\,lbf$

The frame thickness is obtained from Transnuclear drawing 9317.1-120-11

$t_{frame} := 0.395 \cdot in$

The inside span is the same as the canister sleeve $id_{sleeve} = 4.81\,in$

The area available for direct load is

$A_{frame} := (id_{sleeve} + 2 \cdot t_{frame})^2 - id_{sleeve}^2$ $A_{frame} = 8.224\,in^2$

The direct stress in the frame is

$$\sigma := \frac{F}{A_{frame}} \qquad \sigma = 77\,psi$$

The safety margin is

$$SM := \frac{\sigma_{allowable}}{\sigma} - 1 \qquad SM = 58.59$$

The bearing stress at the four lift locations is computed from the same drawing

$A_{bearing} := 4 \cdot t_{frame} \cdot (2 \cdot 0.38 \cdot in)$ $A_{bearing} = 1.201\,in^2$

$$\sigma_{bearing} := \frac{F}{A_{bearing}} \qquad \sigma_{bearing} = 526.732\,psi \qquad SM := \frac{\sigma_{allowable}}{\sigma_{bearing}} - 1 \qquad SM = 7.7$$

3.AI.8.2 60g End Drop (Accident Condition)

The critical member of the damaged fuel canister during the drop scenario is the bottom assembly (see Transnuclear drawing 9317.1-120-5). It is subjected to direct compression due to the amplified weight of the fuel assembly and the canister. The bottom assembly is a 3.5" Schedule 40S pipe. The load due to the 60g end drop is

$F := 60 \cdot (W_{fuel} + W_{container})$ $F = 33000\,lbf$

The properties of the pipe are obtained from the Ryerson Stock Catalog as

$od := 4 \cdot in$ $id := 3.548 \cdot in$ $t_{pipe} := \frac{(od - id)}{2}$ $t_{pipe} = 0.226\,in$

The pipe area is

$$A_{pipe} := \frac{\pi}{4}\cdot\left(od^2 - id^2\right) \qquad A_{pipe} = 2.68\,in^2$$

The stress in the member is

$$\sigma := \frac{F}{A_{pipe}} \qquad \sigma = 12316\,psi$$

The allowable primary membrane stress from Subsection NG of the ASME Code, for accident conditions (Level D), is

$$\sigma_{allowable} := 2.4\cdot S_{m2} \qquad \sigma_{allowable} = 37920\,psi$$

The safety margin is

$$SM := \frac{\sigma_{allowable}}{\sigma} - 1 \qquad SM = 2.1$$

To check the stability of the pipe, we conservatively compute the Euler Buckling load for a simply supported beam.

The Young's Modulus is

$$E := 27600000\cdot psi$$

Compute the moment of inertia as

$$I := \frac{\pi}{64}\cdot\left(od^4 - id^4\right) \qquad I = 4.788\,in^4$$

$$L := 22\cdot in \qquad P_{crit} := \pi^2\cdot\frac{E\cdot I}{L^2} \qquad P_{crit} = 2.695\times 10^6\,lbf$$

The safety margin is

$$SM := \frac{P_{crit}}{F} - 1 \qquad SM = 80.654$$

3.AI.8.3 Conclusion for TN Damaged Fuel Canister

The damaged fuel canister and the upper closure assembly are structurally adequate to withstand the specified normal and accident condition loads. All calculated safety margins are greater than zero.

3.AI.9 Calculations for Transnuclear Thoria Rod Canister

3.AI.9.1 Lifting Operation (Normal Condition)

The critical load case under normal conditions is the lifting operation. The key areas of concern for ASME NG analysis are the canister sleeve, the sleeve to lid frame weld, and the lid frame. All calculations performed for the lifting operation assume a dynamic load factor of 1.15.

3.AI.9.1.1 Canister Sleeve

During a lift, the canister sleeve is loaded axially, and the stress state is pure tensile membrane. For the subsequent stress calculation, it is assumed that the full weight of the Thoria rod canister and the Thoria rods are supported by the sleeve. The magnitude of the load is

$F := DLF \cdot (W_{rodcan} + W_{thoria})$ $F = 449\,lbf$

From TN drawing 9317.1-182-1, the canister sleeve geometry is

$id_{sleeve} := 4.81 \cdot in$ $t_{sleeve} := 0.11 \cdot in$

The cross sectional area of the sleeve is

$A_{sleeve} := (id_{sleeve} + 2 \cdot t_{sleeve})^2 - id_{sleeve}^2$ $A_{sleeve} = 2.16\,in^2$

Therefore, the tensile stress in the sleeve is $\sigma := \frac{F}{A_{sleeve}}$ $\sigma = 207\,psi$

The allowable stress intensity for the primary membrane category is S_m per Subsection NG of the ASME Code. The corresponding safety margin is

$SM := \frac{S_{m1}}{\sigma} - 1$ $SM = 95.5$

3.AI.9.1.2 Sleeve Welds

The top of the canister must support the amplified weight. This load is carried directly by the fillet weld that connects the lid frame to the canister sleeve. The magnitude of the load is conservatively taken a the entire amplified weight of canister plus Thoria rod.

$F = 449\,lbf$

The weld thickness is $t_{base} := 0.09 \cdot in$ (assumed equal to the same weld for the damaged fuel canister

The area of the weld, with proper consideration of quality factors, is

$A_{weld} := n \cdot 4 \cdot (id_{sleeve} + 2 \cdot t_{sleeve}) \cdot .7071 \cdot t_{base}$ $A_{weld} = 0.64\,in^2$

Therefore, the shear stress in the weld is $\tau := \frac{F}{A_{weld}}$ $\tau = 701\,psi$

From the ASME Code the allowable weld shear stress, under normal conditions (Level A), is 30% of the ultimate strength of the base metal. The corresponding safety margin is

$SM := \frac{0.3 \cdot S_{u1}}{\tau} - 1$ $SM = 30.3$

3.AI.9.1.3 Lid Frame Assembly

The Lid Frame assembly is classified as a NUREG-0612 lifting device. As such the allowable stress for design is the lesser of one-sixth of the yield stress and one-tenth of the ultimate strength.

$$\sigma_1 := \frac{S_{y1}}{6} \qquad \sigma_2 := \frac{S_{u1}}{10}$$

$$\sigma_1 = 4583\,\text{psi} \qquad \sigma_2 = 7300\,\text{psi}$$

For SA240-304 material the yield stress governs. $\sigma_{allowable} := \sigma_1$

The total lifted load is $F := DLF \cdot (W_{rodcan} + W_{thoria})$ $F = 449\,\text{lbf}$

The frame thickness is obtained from Transnuclear drawing 9317.1-182-8. This drawing was not available, but the TN drawing 9317.1-182-4 that included a view of the lid assembly suggests that it is identical in its structural aspects to the lid frame in the damaged fuel canister.

$t_{frame} := 0.395 \cdot \text{in}$

The inside span is the same as the canister sleeve $id_{sleeve} = 4.81\,\text{in}$

The area available for direct load is

$$A_{frame} := (id_{sleeve} + 2 \cdot t_{frame})^2 - id_{sleeve}^2 \qquad A_{frame} = 8.224\,\text{in}^2$$

The direct stress in the frame is

$$\sigma := \frac{F}{A_{frame}} \qquad \sigma = 55\,\text{psi}$$

The safety margin is

$$SM := \frac{\sigma_{allowable}}{\sigma} - 1 \qquad SM = 83.04$$

The bearing stress at the four lift locations is computed from the same drawing

$$A_{bearing} := 4 \cdot t_{frame} \cdot (2 \cdot 0.38 \cdot \text{in}) \qquad A_{bearing} = 1.201\,\text{in}^2$$

$$\sigma_{bearing} := \frac{F}{A_{bearing}} \qquad \sigma_{bearing} = 373.501\,\text{psi} \qquad SM := \frac{\sigma_{allowable}}{\sigma_{bearing}} - 1 \qquad SM = 11.27$$

3.AI.9.2 60g End Drop (Accident Condition)

The critical member of the damaged fuel canister during the drop scenario is the bottom assembly. Transnuclear drawing 9317.1-120-5). It is subjected to direct compression due to the amplified weight of the Thoria rods and the canister.

$F := 60 \cdot (W_{thoria} + W_{rodcan})$ $F = 23400\,lbf$

The properties of the pipe are obtained from the Ryerson Stock Catalog as

$od := 4 \cdot in$ $id := 3.548 \cdot in$ $t_{pipe} := \frac{(od - id)}{2}$ $t_{pipe} = 0.226\,in$

The pipe area is

$A_{pipe} := \frac{\pi}{4} \cdot (od^2 - id^2)$ $A_{pipe} = 2.68\,in^2$

The stress in the member is

$\sigma := \frac{F}{A_{pipe}}$ $\sigma = 8733\,psi$

The allowable primary membrane stress from Subsection NG of the ASME Code, for accident conditions (Level D), is

$\sigma_{allowable} := 2.4 \cdot S_{m2}$ $\sigma_{allowable} = 37920\,psi$

The safety margin is

$SM := \frac{\sigma_{allowable}}{\sigma} - 1$ $SM = 3.3$

To check the stability of the pipe, we compute the Euler Buckling load for a simply supported beam.

The Young's Modulus is

$E := 27600000 \cdot psi$

Compute the moment of inertia as

$I := \frac{\pi}{64} \cdot (od^4 - id^4)$ $I = 4.788\,in^4$

$L := 22 \cdot in$

$P_{crit} := \pi^2 \cdot \frac{E \cdot I}{L^2}$ $P_{crit} = 2.695 \times 10^6\,lbf$

The safety margin is

$SM := \frac{P_{crit}}{F} - 1$ $SM = 114.153$

3.AI.9.4 60g Side Drop (Accident Condition)

The Thoria Rod Separator Assembly is shown in TN drawings 9317.1-182-1 and 9317.1-182-3. under the design basis side drop or tipover accident, we examine the consequences to one of the rod support strips acting as a cantilever strip acted upon by self-weight and the weight of one Thoria rod.

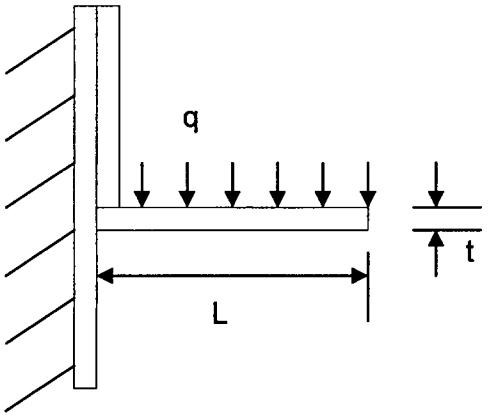

Weight of 1 rod per unit length

length := 113.16·in

$w_{rod} := 90 \cdot \frac{lbf}{18} \cdot \frac{1}{length}$ $\quad w_{rod} = 0.044 \frac{lbf}{in}$

Weight of support per unit length (per drawing 9317.1-182-3

L := 1.06·in $\quad$ t := 0.11·in

$w_{sup} := .29 \cdot \frac{lbf}{in^3} \cdot L \cdot t$ $\quad w_{sup} = 0.034 \frac{lbf}{in}$

Amplified load (assumed as a uniform distribution)

$q := 60 \cdot (w_{rod} + w_{sup})$ $\quad q = 4.68 \frac{lbf}{in}$

$Moment := \frac{q \cdot L^2}{2}$ $\quad Moment = 2.629\,in \cdot lbf$

Bending stress at the root of the cantilever beam is

$\sigma := 6 \cdot \frac{Moment}{1 \cdot in \cdot t^2}$ $\quad \sigma = 1.304 \times 10^3\,psi$

Shear stress at the root of the cantilever $\quad \tau := q \cdot \frac{L}{t \cdot 1 \cdot in}$ $\quad \tau = 45.098\,psi$

Large margins of safety are indicated by these stress results.

3.AI.9.5 Conclusion for TN Thoria Rod Canister

The Thoria rod canister is structurally adequate to withstand the specified normal and accident condition loads. All calculated safety margins are greater than zero.

3.AI.10 General Conclusion

The analysis of the TN damaged fuel canister and the TN Thoria rod canister have demonstrated that all structural safety margins are large. We have confirmed that the TN canisters have positive safety margins for the HI-STAR 100 govening design basis loads. Therefore, the loaded TN canisters from ComEd Dresden Unit#1 can safely be carried in the HI-STAR 100 System.

3.AI.11 List of Transnuclear Drawing Numbers

9317.1-120 - 2,3,4,5,6,7,8,9,10,11,13,14,15,17,18,19,20,21,22,23

9317.1-182- 1,2,3,4,5,6

CHAPTER 4 THERMAL EVALUATION

4.0 INTRODUCTION

The HI-STAR 100 System is designed for the long-term storage of spent nuclear fuel (SNF) in a vertical position. An array of HI-STAR 100 Systems regularly spaced on a square pitch will be stored on a concrete ISFSI pad in an open environment. In this section, compliance of the HI-STAR 100 thermal performance to 10CFR72 requirements for storage under normal conditions is established. The analysis considers passive rejection of decay heat from the stored SNF assemblies to the environment under the most severe design basis ambient conditions. Effects due to incident solar radiation as well as partial radiation blockage due to the presence of neighboring casks at an ISFSI site are included in the analyses.

The guidelines presented in NUREG-1536 [4.1.3] include eight specific acceptance criteria that should be fulfilled by the cask thermal design. These eight criteria are summarized here as follows:

1. The fuel cladding temperature at the beginning of dry cask storage should generally be below the anticipated damage-threshold temperatures for normal conditions and a minimum of 20 years of cask storage.

2. The fuel cladding temperature should generally be maintained below 570°C (1058°F) for short-term accident, short-term off-normal, and fuel transfer conditions.

3. The maximum internal pressure of the cask should remain within its design pressures for normal (1% rod rupture), off-normal (10% rod rupture), and accident (100% rod rupture) conditions.

4. The cask and fuel materials should be maintained within their minimum and maximum temperature criteria for normal, off-normal, and accident conditions.

5. For fuel assemblies proposed for storage, the cask system should ensure a very low probability of cladding breach during long-term storage.

6. Fuel cladding damage resulting from creep cavitation should be limited to 15% of the original cladding cross sectional area.

7. The cask system should be passively cooled.

8. The thermal performance of the cask should be within the allowable design criteria specified in FSAR Chapters 2 and 3 for normal, off-normal, and accident conditions.

As demonstrated in this chapter (see Section 4.5), the HI-STAR 100 System is designed to comply with all eight criteria listed above. All thermal analyses to evaluate the normal condition performance of a HI-STAR 100 System are described in Section 4.4. All analyses for off-normal conditions are described in Section 11.1. All analyses for accident conditions are described in Section 11.2. Section 4.2 lists the material properties data required to perform the thermal analyses and Section 4.3 provides the applicable temperature limits criteria required to demonstrate the adequacy of the HI-STAR 100 System design under all conditions. This FSAR chapter is in full compliance with NUREG-1536 requirements, subject to the exceptions and clarifications discussed in Chapter 1, Table 1.0.3.

4.1 DISCUSSION

A sectional view of the HI-STAR 100 dry storage system has been presented earlier (see Figure 1.2.1). The system consists of an MPC loaded into an overpack with a bolted closure plate. The fuel assemblies reside inside the MPC which is sealed with a welded lid to form the confinement boundary. The MPC contains a stainless steel honeycomb basket structure which provides square-shaped fuel compartments (called boxes) of appropriate dimensions to facilitate insertion of fuel assemblies prior to welding of the lid. Each box panel (except the periphery panels of the MPC-68) is provided with Boral thermal neutron absorber sandwiched between a sheathing plate and the box panel along the entire length of the active fuel region. Prior to sealing the lid, the MPC is backfilled with helium up to the design basis initial loading (Table 1.2.2). This provides a stable and inert environment for long-term storage of the SNF. Additionally, the annular gap formed between the MPC and the overpack is backfilled with helium of the same quality before the overpack vent and drain port plugs are installed. Heat is transferred from the SNF in a HI-STAR 100 System to the environment by passive heat transport mechanisms only.

The helium backfill gas is an integral part of the MPC and overpack thermal designs. The helium fills all the spaces between solid components and provides an improved conduction medium (compared to air) for dissipating decay heat in the MPC. Additionally, helium in the spaces between the fuel basket and the MPC shell is heated differentially and, therefore, subject to the "Rayleigh" effect which is discussed in detail later. To ensure that the helium gas is retained and is not diluted by lower conductivity air, the MPC confinement boundary is designed to comply with the provisions of the ASME B&PV Code Section III, Subsection NB, as an all-seal-welded pressure vessel with redundant closures. Similarly, the overpack helium retention boundary is designed as an ASME B&PV Code Section III, Subsection NB pressure vessel. Both the MPC confinement boundary and the overpack helium retention boundary are required to meet maximum leakage rate Technical Specifications included in Chapter 12 of this FSAR. These leakage rate criteria are selected to ensure the presence of helium during the entire storage life. It is additionally demonstrated in Section 11.1.3 that the failure of one confinement boundary seal, a severe off-normal event, will not result in a breach of the confinement boundary. The helium gas is therefore retained and undiluted, and may be credited in the thermal analyses.

An important thermal design criterion imposed on the HI-STAR 100 System is to limit the maximum fuel cladding temperature to within design basis limits (Table 2.2.3) for long-term storage of design basis fuel assemblies. An equally important design criterion is to reduce temperature gradients within the MPC to minimize thermal stresses. In order to meet these design objectives, the HI-STAR 100 MPC basket is designed to possess certain distinctive characteristics, which are summarized in the following.

The MPC design minimizes resistance to heat transfer within the basket and basket periphery regions. This is ensured by an uninterrupted panel-to-panel connectivity realized in the all-welded honeycomb basket structure. Furthermore, the MPC design incorporates top and bottom plena with interconnected downcomer paths. The top plenum is formed by the gap between the bottom of the MPC lid and the top of the honeycomb fuel basket, and by elongated semicircular holes in each basket cell wall. The bottom plenum is formed by large elongated semicircular holes at the base of all cell walls. The MPC basket is designed to eliminate structural

discontinuities (i.e., gaps) which introduce large thermal resistances to heat flow. Consequently, temperature gradients are minimized in the design, which results in lower thermal stresses within the basket. Low thermal stresses are also ensured by an MPC design which permits unrestrained axial and radial growth of the basket to eliminate the possibility of thermally induced stresses due to restraint of free-end expansion.

Finally, it is heuristically apparent from the geometry of the MPC that the basket metal, the fuel assemblies, and the contained helium mass will be at their peak temperatures at or near the longitudinal axis of the MPC. The temperatures will attenuate with increasing radial distance from this axis, reaching their lowest values at the outer surface of the MPC shell. Conduction along the metal walls and radiant heat exchange from the fuel assemblies to the MPC metal mass would therefore result in substantial differences in the bulk temperatures of helium columns in different fuel storage cells. Since two fluid columns at different temperatures in communicative contact cannot remain in static equilibrium, the non-isotropic temperature field in the MPC internal space due to conduction and radiation heat transfer mechanisms guarantee the incipience of the third mode of heat transfer: natural convection.

The helium columns traverse the vertical storage cavity spaces, redistributing heat within the MPC. Elongated holes in the bottom of the cell walls, liberal flow space and elongated holes at the top, and wide open downcomers along the outer periphery of the basket ensure a smooth helium flow regime. The most conspicuous beneficial effect of the helium thermosiphon circulation, as discussed above, is the mitigation of internal thermal stresses in the MPC. Another beneficial effect is reduction of the peak fuel cladding temperatures of the fuel assemblies located in the interior of the basket. However, in the interest of conservatism, *no credit* for the thermosiphon action is taken in the thermal analysis reported in this chapter. To partially compensate for the reduction in the *computed* heat rejection capability due to the complete neglect of the global thermosiphon action within the MPC, flexible heat conduction elements made of aluminum are interposed in the large peripheral spaces between the MPC shell and the fuel basket. These heat conduction elements, shown in the MPC Drawings in Section 1.5, are engineered to possess lateral flexibility such that they can be installed in the peripheral spaces to create a nonstructural thermal connection between the basket and the MPC shell. In their installed condition, the heat conduction elements will conform to and contact the MPC shell and the basket walls. MPC manufacturing procedures have been established to ensure that the thermal design objectives for the conduction elements set forth in this document are realized in the actual hardware.

Two distinct MPC basket geometries are included in the HI-STAR 100 System for storage of PWR and BWR SNF assemblies. For intact PWR fuel storage, a 24-assembly design is depicted in Figure 1.2.4. A 68-assembly design for storage of intact or damaged BWR fuel is shown in Figure 1.2.2. Damaged BWR fuel and fuel debris must comply with design basis characteristics listed in Table 2.1.7 to allow storage in the MPC-68 and MPC-68F, respectively. Each basket design must comply with the applicable temperature limits for normal, off-normal and accident conditions under the imposed heat generation loads from stored fuel assemblies.

The design basis intact PWR and BWR decay heat per assembly and the MPC total decay heat load for the two basket configurations (i.e., MPC-24, and MPC-68) are stated in Tables 2.1.6 and

1.2.2, respectively. Table 2.1.7 lists the design basis thermal requirements for damaged fuel assemblies. Table 2.1.11 lists the design basis thermal requirements for stainless steel clad fuel assemblies for storage in the MPC-24 or MPC-68. The HI-STAR 100 System consisting of the overpack and MPCs under normal storage conditions at an ISFSI pad is conservatively analyzed for the limiting design basis heat loads.

Thermal analysis of the HI-STAR 100 System is based on including all three fundamental modes of heat transfer: conduction, natural convection and radiation. Different combinations of these modes are active in different regions of the system. These modes are properly identified and conservatively analyzed within each region of the MPC and overpack to enable bounding calculations of the temperature distribution within the HI-STAR 100 System.

On the outside surface of the overpack, heat is dissipated to the environment by buoyancy induced convective air flow (natural convection) and thermal radiation. In the overpack internal metal structure, only conductive heat transport is possible. Between metal surfaces (e.g., between neighboring fuel rod surfaces) heat transport is due to a combination of conduction through a gaseous medium (helium) and thermal radiation. The heat transfer between the fuel basket external surface and the MPC shell's inner surface is further influenced by the so-called "Rayleigh" effect. However, in the interest of conservatism, the most potent heat transport mechanism, the buoyancy induced thermosiphon which occurs within the MPC basket (aided by the MPC design which provides low pressure drop helium flow recirculation loops formed by the fuel cells, top plenum, downcomers and bottom plenum) is neglected.

The total heat generation in each assembly is non-uniformly distributed over the active fuel length to account for the design basis fuel burnup distribution listed in Chapter 2 (Table 2.1.8). As discussed later in this chapter (Subsection 4.4.6), an array of conservative assumptions bias the results of the thermal analysis towards much reduced computed margins than would be obtained by a rigorous analysis of the problem.

The complete thermal analysis is performed using the industry standard ANSYS finite element modeling package [4.1.1] and the finite volume Computational Fluid Dynamics (CFD) code FLUENT [4.1.2]. ANSYS has been previously used and accepted by the NRC on numerous dockets [4.1.3,4.V.5.a]. The FLUENT CFD program is independently benchmarked and validated with a wide class of theoretical and experimental studies reported in the technical journals. Additionally, Holtec has confirmed the code's capability to reliably predict temperature fields in dry storage applications using independent full-scale test data from a loaded cask [4.1.4]. This study concluded that FLUENT can be used to model all modes of heat transfer, namely, conduction, convection, and radiation in dry cask systems.

4.2 SUMMARY OF THERMAL PROPERTIES OF MATERIALS

Materials used in the HI-STAR 100 System include stainless steels (Alloy X), carbon steels, Holtite-A neutron shield, Boral neutron absorber, aluminum alloy 1100 heat conduction elements, and helium. In Table 4.2.1, a summary of references used to obtain cask material properties for performing all thermal analyses is presented.

Thermal conductivities of the constituent Alloy X steels and the bounding Alloy X thermal conductivity are reported in Appendix 1.A of this report. Tables 4.2.2, 4.2.3 and 4.2.9 provide numerical thermal conductivity data of materials at several representative temperatures. Table 4.2.8 lists the thermal properties of Boral components (i.e., B_4C core and aluminum cladding materials). Surface emissivity data for key materials of construction is provided in Table 4.2.4.

The emissivity properties of painted external cask surfaces are generally excellent. Kern [4.2.5] reports an emissivity range of 0.8 to 0.98 for a wide variety of paints. In the HI-STAR 100 thermal analysis, an emissivity of 0.85[†] is applied to external painted surfaces. A conservative solar absorptivity coefficient of 1.0 is applied to all exposed cask surfaces.

In Table 4.2.5, the heat capacity and density of different cask materials are presented. These properties are used in performing transient (i.e., hypothetical fire accident condition) analyses. Table 4.2.6 provides viscosity data on the helium gas.

The overpack outside surface heat transfer coefficient is calculated by accounting for both natural convection heat transfer and radiation. The natural convection coefficient depends upon the product of Grashof (Gr) and Prandtl (Pr) numbers. Following the approach developed by Jakob and Hawkins [4.2.9], the product Gr×Pr is expressed as $L^3\Delta TZ$, where L is the height of the cask, ΔT is the overpack surface-to-ambient temperature differential and Z is a parameter which depends upon air properties (which are known functions of temperature) evaluated at the average film temperature. The temperature dependence of Z for air is provided in Table 4.2.7.

[†] This is conservative with respect to prior cask industry practice, which has historically accepted higher emissivities. For example, a higher emissivity for painted surfaces (ε = 0.95) is used in the TN-32 cask TSAR (Docket 72-1021).

Table 4.2.1

SUMMARY OF HI-STAR 100 SYSTEM MATERIALS
THERMAL PROPERTY REFERENCES

Material	Emissivity	Conductivity	Density	Heat Capacity
Helium	N/A	Handbook [4.2.2]	Ideal Gas Law	Handbook [4.2.2]
Air	N/A	Handbook [4.2.2]	Ideal Gas Law	Handbook [4.2.2]
Zircaloy	EPRI [4.2.3]	NUREG [4.2.6], [4.2.7]	Rust [4.2.4]	Rust [4.2.4]
UO_2	Not Used	NUREG [4.2.6], [4.2.7]	Rust [4.2.4]	Rust [4.2.4]
Stainless steel	Kern [4.2.5]	ASME [4.2.8]	Marks [4.2.1]	Marks [4.2.1]
Carbon steel	Kern [4.2.5]	ASME [4.2.8]	Marks [4.2.1]	Marks [4.2.1]
Aluminum Alloy 1100 (Heat Conduction Elements)	Handbook [4.2.2]	ASME [4.2.8]	ASME [4.2.8]	ASME [4.2.8]
Boral†	Not Used	Test Data	Test Data	Test Data
Holtite-A††	Not Used	Conservative Bounding Values	See Footnote	See Footnote

† AAR Structures Boral thermophysical test data.

†† The Holtite-A thermophysical properties (density, ρ, and heat capacity, c_p) were selected to conservatively understate the neutron shield thermal inertia (product of ρ and c_p) in the fire accident evaluation (see Table 4.2.5).

Table 4.2.2

SUMMARY OF HI-STAR 100 SYSTEM MATERIALS THERMAL CONDUCTIVITY DATA

Material	**@ 200°F (Btu/ft-hr-°F)**	**@ 450°F (Btu/ft-hr-°F)**	**@ 700°F (Btu/ft-hr-°F)**
Helium	0.0976	0.1289	0.1575
Air	0.0173	0.0225	0.0272
Alloy X	8.4	9.8	11.0
Carbon Steel Radial Connectors	29.2	27.1	24.6
Carbon Steel Gamma Shield Layers	24.4	23.9	22.4
Holtite-A[†]	See Footnote	See Footnote	See Footnote
Cryogenic Steel	23.8	23.7	22.3

[†] No credit taken for conduction through Holtite-A for the steady-state analysis. Before and after fire conditions for fire accident analysis (i.e., the conductivity is conservatively set equal to zero). A conductivity of 1.0 Btu/ft-hr-°F is conservatively applied during fire condition.

Table 4.2.3

SUMMARY OF FUEL ELEMENT COMPONENTS THERMAL CONDUCTIVITY DATA

Zircaloy Cladding		Fuel (UO_2)	
Temperature (°F)	**Conductivity (Btu/ft-hr-°F)**	**Temperature (°F)**	**Conductivity (Btu/ft-hr-°F)**
392	8.28†	100	3.48
572	8.76	448	3.48
752	9.60	570	3.24
932	10.44	793	2.28†

† Lowest value of conductivity is used in the thermal analysis for conservatism.

Table 4.2.4

SUMMARY OF MATERIALS SURFACE EMISSIVITY DATA

Material	Emissivity
Zircaloy cladding	0.80
Painted surfaces	0.85
Rolled carbon steel	0.66
Stainless steel	0.36
Sandblasted aluminum	0.40

Table 4.2.5

MATERIALS DENSITY AND HEAT CAPACITY PROPERTIES SUMMARY

Material	Density (lbm/ft^3)	Heat Capacity ($Btu/lbm-^oF$)
Helium	(Ideal Gas Law)	1.24
Zircaloy cladding	409	0.0728
Fuel (UO_2)	684	0.056
Carbon steel	489	0.1
Stainless steel	501	0.12
Boral	154.7	0.13
Aluminum Alloy 1100	169.9	0.23
Holtite-A	105.0	0.39

Table 4.2.6

HELIUM GAS VISCOSITY[†] VARIATION WITH TEMPERATURE

Temperature (^{o}F)	Viscosity (Micropoise)
167.4	220.5
200.3	228.2
297.4	250.6
346.9	261.8
463.0	288.7
537.8	299.8
737.6	338.8

[†] Obtained from Rohsenow and Hartnett [4.2.2].

Table 4.2.7

VARIATION OF NATURAL CONVECTION PROPERTIES
PARAMETER "Z" FOR AIR WITH TEMPERATURE†

Temperature, (^{o}F)	Z ($ft^{-3o}F^{-1}$)
40	$2.1x10^{6}$
140	$9.0x10^{5}$
240	$4.6x10^{5}$
340	$2.6x10^{5}$
440	$1.5x10^{5}$

† Obtained from Jakob and Hawkins [4.2.9]

Table 4.2.8

BORAL COMPONENT MATERIALS[†]
THERMAL CONDUCTIVITY DATA

Temperature (°F)	B_4C Core Conductivity (Btu/ft-hr-°F)	Aluminum Cladding Conductivity (Btu/ft-hr-°F)
212	48.09	100.00
392	48.03	104.51
572	47.28	108.04
752	46.35	109.43

[†] Both B_4C and aluminum cladding thermal conductivity values are obtained from AAR Structures Boral thermophysical test data.

Table 4.2.9

HEAT CONDUCTION ELEMENTS (ALUMINUM ALLOY 1100)
THERMAL CONDUCTIVITY DATA

Temperature (°F)	**Conductivity (Btu/ft-hr-°F)**
100	131.8
200	128.5
300	126.2
400	124.5

4.3 SPECIFICATIONS FOR COMPONENTS

HI-STAR 100 System materials and components designated as "Important to Safety" (i.e., required to be maintained within their safe operating temperature ranges to ensure their intended function) which warrant special attention are summarized in Table 4.3.1. Long-term stability and continued neutron shielding ability of Holtite-A neutron shield material under normal storage conditions are ensured when material exposure temperatures are maintained below the maximum allowable limit. The integrity of the overpack helium retention boundary is assured by maintaining the temperature of the mechanical seals within the manufacturer's recommended operating temperature limits. Long-term integrity of SNF is ensured by the HI-STAR 100 System thermal performance, which demonstrates that fuel cladding temperatures are maintained below design basis limits. Boral used in MPC baskets for criticality control (a composite material composed of B_4C and aluminum) is stable up to 1000°F for short-term and 850°F for long-term dry storage[†]. However, for conservatism, a significantly lower maximum temperature limit is imposed.

Compliance to 10CFR72 requires, in part, identification and evaluation of short-term off-normal and severe hypothetical accident conditions. The inherent mechanical stability characteristics of cask materials and components ensure that no significant functional degradation is possible due to exposure to short-term temperature excursions outside the normal long-term temperature limits. For evaluation of HI-STAR 100 System thermal performance under off-normal or hypothetical accident conditions, material temperature limits for short-duration events are provided in Table 4.3.1.

Demonstration of fuel cladding integrity against the potential for degradation and gross rupture throughout the entire dry cask storage period is mandated by the Code of Federal Regulations (Part 72, Section 72.72(h)). The specific criteria required to demonstrate fuel cladding integrity is set forth in the NUREG-1536 document as listed below.

A. The dry cask storage system shall ensure a less than 0.5 percent probability of cladding failure during long-term storage.

B. Fuel cladding damage shall be limited to 15% of the original cladding cross section.

Several potential damage mechanisms for Zircaloy clad fuel have been discussed by Schwartz and Witte [4.3.6] and Levy et al. [4.3.1]. These mechanisms are listed below:

i. stress corrosion cracking
ii. hydriding
iii. creep induced stress rupture
iv. Diffusion Controlled Cavity Growth (DCCG)

Out of the four potential damage mechanisms listed above, two mechanisms, namely creep-

[†] AAR Structures Boral thermophysical test data.

induced stress rupture [4.3.1] and DCCG [4.3.6], are the controlling mechanisms established for Zircaloy cladding life prediction during dry storage of spent nuclear fuel. Pacific Northwest Laboratory (PNL) has established a Commercial Spent Fuel Management (CSFM) model based on creep rupture data for Zircaloy [4.3.1]. The CSFM model enables a cask designer to determine fuel-specific maximum initial peak cladding temperature limits. The Zircaloy cladding temperature limit established using the generic CSFM Inerted Dry Storage (IDS) temperature limit curves [4.3.1] meets the NUREG-1536 Criterion (A) discussed earlier in this section. This requires a less than 0.5% probability of rods rupture during the entire storage life (assumed to equal 40 years) against creep rupture mode of local cladding damage, which may result in pinhole or through-cladding cracks during dry storage.

The DCCG mode of cladding damage is concluded in the above-mentioned Schwarz et al., report to be the only mechanism which may result in gross cladding damage [4.3.6]. This mode of cladding damage manifests itself as a sudden non-ductile type of fracture. NUREG-1536 (Criterion (B), discussed earlier in this section), requires that the total damage from the DCCG mode of degradation be limited to 15% of the original cladding cross sectional area during the entire dry storage period.

In accordance with the NUREG-1536 criteria, the HI-STAR 100 storage system is designed to preclude both local and gross fuel cladding failures during the entire duration of storage. Initial maximum peak cladding temperature limits are determined using the CSFM IDS temperature limit curves to preclude local cladding failure [4.3.1] and the LLNL methodology to preclude gross cladding failure [4.3.6]. A discussion on the application of the PNL and LLNL methodologies in establishing the HI-STAR system specific fuel types cladding temperature limits criteria is provided in the balance of this section.

The generic CSFM IDS temperature limit curves [4.3.1] define the maximum allowable initial storage temperature at initial cladding stresses as a function of fuel age. Therefore, for SNF of a given age (decay time), the permissible peak cladding temperature is a direct function of the cladding hoop stress, which in turn depends on the radius-to-thickness ratio of the fuel rod and its internal pressure. The rod internal pressure P_i is calculated based upon the maximum initial fill pressures (Tables 4.3.2 and 4.3.5) with fission gas release at a conservatively bounding maximum burnup under HI-STAR 100 System storage conditions (40,000 MWD/MTU for BWR fuel and 42,500 MWD/MTU for PWR fuel). The free rod volumes in the third column of Tables 4.3.2 and 4.3.5 are defined as free rod volumes, in each fuel rod, available for pressurization with fill gas. The free rod volume is the cumulative sum of the open top plenum space, the pellet-to-cladding annular space and the inter-pellet junction space. As a lower bound value of the free rod volume will lead to a conservative estimate of the cladding stress at operating temperatures, the nominal gas plenum space is included in the free rod volume. The plenum length for miscellaneous BWR fuel assemblies is set to 12 inches. The fission gas release fraction data is based on Regulatory Guide 1.25 (Table 4.3.4). The radius-to-thickness ratio r^* is determined based on rod nominal dimension values (Tables 4.3.3 and 4.3.6) including the maximum cladding thickness loss due to in-reactor oxidation, as reported in the PNL study [4.3.4].

By utilizing P_i and r^*, the cladding stress for various PWR fuel types is calculated from Lame's formula and summarized in Table 4.3.3. It can be seen from Figure 4.4.21 that the average temperature of the gas in the fuel rods, a great bulk of which is located in the top region of the SNF, is well below 300°C for the PWR fuel array types. Therefore, to compute the cladding hoop stress in a conservative manner, the ideal gas law is used to obtain the value of the in-rod gas pressure at 300°C. An inspection of cladding stress data summarized in Table 4.3.3 indicates 96.7 MPa is the bounding value of cladding stress (σ_{max}) for the PWR SNF. Corresponding fill gas data and calculations of cladding stress for the various BWR SNF types are summarized in Tables 4.3.5 and 4.3.6, respectively. It can be seen from Figure 4.4.22 that the average temperature of gas in the fuel rods, a great bulk of which is located in the top region of the SNF, is well below 300°C for all BWR fuel array types considered in this topical report. Therefore, to compute the cladding hoop stress in a conservative manner, the ideal gas law is used to obtain the value of the in-rod gas pressure at 300°C. An inspection of the cladding stress data in Table 4.3.6 indicates that the bounding value of the cladding hoop stress for all SNF types is 53.3 MPa (except for 8x8 GE Dresden-1 and 6x6 GE Humboldt Bay fuel types). A conservative cladding stress of 54.7 MPa is used in determining BWR fuel peak cladding temperature limits.

The bounding values of σ_{max} for the array of PWR and BWR SNF types are thus 96.7 MPa and 54.7 MPa, respectively (except for 8x8 GE Dresden-1 and 6x6 GE Humboldt Bay fuel assembly types for which the bounding value of σ_{max} is 59.1 MPa).

Several implicit assumptions in the calculation of σ_{max}, such as neglect of the rod cavity growth due to thermal expansion, internal fill pressure, and in-core irradiation, ensure that the hoop stress value (which is the sole determinant in the establishment of permissible cladding temperature for a given cooling time) is indeed a bounding number.

The generic CSFM IDS temperature limit curves developed in the PNL study [4.3.1] are used to determine Zircaloy cladding temperature limits at the conservative 300°C average rod temperature. The fuel cladding temperature limits obtained from these PNL curves ensure a low failure probability for rods (less than 0.5% over the 40-year dry storage life).

The value of σ_{max} is also required to establish the peak cladding temperature limit using the DCCG method, which we discuss in the following. The DCCG model-based Zircaloy cladding temperature limit computation, in accordance with the LLNL procedure [4.3.6], requires a solution to the following equation expressed in terms of the area fraction of de-cohesion (A):

$$\int_{A_i}^{A_f} \frac{dA}{f(A)} = \int_{t_o}^{t_o + t_s} G(t)\, dt$$

where:

A_i = initial area fraction of de-cohesion

A_f = end of storage life area fraction of de-cohesion (limited to 0.15)

t_o = age of fuel prior to dry cask storage

t_s = dry cask storage period (40 years)

f(A) = area fraction of de-cohesion function

$$= \frac{[1-(\frac{A_i}{A})^{1/2}](1-A)}{A^{1/2}[\frac{1}{2}\ell n\frac{1}{A}-\frac{3}{4}+A(1-\frac{A}{4})]}$$

$$G(t) = \frac{32}{3\pi^{1/2}} \frac{F_b^{3/2}(\alpha)}{F_v(\alpha)} \frac{\Omega\delta\ \sigma_\infty(t)}{K\lambda^3} \frac{D_{GB}[T(t)]}{T(t)}$$

$$F_b(\alpha) = \pi\ \sin^2(\alpha)$$

$$F_v(\alpha) = \frac{2\pi}{3}(2-3\cos\alpha+\cos^3\alpha)$$

T = time-dependent peak cladding temperature

K = Boltzmann constant (1.38053×10^{-23} J/K)

A discussion on the balance of parameters in the G(t) damage function is provided below.

Cladding Hoop Stress ($\sigma_\infty(t)$)

The cladding hoop stress is principally dependent upon the specific fuel rod dimensions, initial fill rod pressure, time-dependent storage temperature, and fuel burnup dependent fission gas release from the fuel pellets into the rod plenum space. The peak fuel rod pressure for various PWR and BWR fuel types at the start of the dry storage period are summarized in Tables 4.3.3 and 4.3.6. The highest peak rod stress among the various PWR fuel types and a bounding peak rod stress for BWR fuel are applied as constant (time-independent) cladding hoop stresses in the DCCG model-based damage function.

Grain Boundary Cavity Dihedral Angle (α)

The LLNL report [4.3.6] has determined the dihedral angle (α) for pure metals to be 75°. To account for possible non-ideal conditions, a conservatively lower α equal to 60° is applied to the DCCG model.

Zirconium Atomic Volume (Ω)

The zirconium atomic volume estimated from several literature sources as documented in the LLNL report [4.3.6] is in the range of 2.31×10^{-29} m^3 to 3.37×10^{-29} m^3. In the interest of conservatism, the maximum estimated atomic volume equal to 3.37×10^{-29} m^3 is used for the analysis.

Grain Boundary Thickness (δ)

The LLNL report [4.3.6] has recommended a grain boundary thickness of three Burgers vectors to be adequate for the analysis. Thus, $\delta = 3\ (3.23\times10^{-10}) = 9.69\times10^{-10}$ m is used in the analysis.

Average Cavity Spacing (λ)

Cavity spacing is controlled by the type of nucleation mechanism and the density of nucleation sites. The LLNL report [4.3.6] references an experimental study which found that the cavity spacing is in the range of 10×10^{-6} to 20×10^{-6} m. In the interest of conservatism, the minimum reported cavity spacing equal to 10×10^{-6} m is used in the analysis.

Grain Boundary Diffusion Rate (D_{GB})

Two grain boundary diffusion rate correlations for zirconium are reported in the LLNL report [4.3.6]. The two correlations provide diffusion rate estimates which are approximately two orders of magnitude apart from each other. Consequently, the more conservative correlation (i.e., $D_{gb} = 5.9\times10^{-6}$ exp [-131,000/RT] m^2/s) which provides a higher estimate of the grain boundary diffusion rate is used in the analysis.

Time-Dependent Peak Cladding Temperature (T)

The steady state peak cladding temperature during long-term storage is principally dependent upon the thermal heat load from the stored fuel assemblies which is imposed on the cask. It is well established that the rate of radioactive decay in a fuel assembly exponentially attenuates with the age of fuel. Consequently, the peak cladding temperature during long-term storage will also attenuate rapidly as a direct consequence of the heat load reduction with time. In recognition of this anticipated decaying cask temperature response, the PNL report [4.3.1] recommends a uni-modal power law type decaying temperature model of the form $T = T_o\ t^{\gamma}$. In the DCCG analysis, an improved multi-modal exponentially attenuating decay heat model based on the Branch Technical Position Paper ASB 9-2 is used. Thus, the form of the decaying temperature model is expressed as:

$$T = \frac{\sum_{K=0}^{10} A_K \exp(-a_k\ t)}{\sum_{K=0}^{10} A_K \exp(-a_k\ t_o)} [(T_o - T_a)] + T_a$$

where:

$A_0 =$	0.5980	$a_o =$	1.772
$A_1 =$	1.65	$a_1 =$	5.774×10^{-1}
$A_2 =$	3.1	$a_2 =$	6.743×10^{-2}
$A_3 =$	3.87	$a_3 =$	6.214×10^{-3}
$A_4 =$	2.33	$a_4 =$	4.739×10^{-4}
$A_5 =$	1.29	$a_5 =$	4.810×10^{-5}
$A_6 =$	0.462	$a_6 =$	5.344×10^{-6}
$A_7 =$	0.328	$a_7 =$	5.716×10^{-7}
$A_8 =$	0.17	$a_8 =$	1.036×10^{-7}
$A_9 =$	0.0865	$a_9 =$	2.959×10^{-8}
$A_{10} =$	0.1140	$a_{10} =$	7.585×10^{-10}

$t =$ time after reactor discharge (s)

$t_o =$ initial age of fuel at start of storage (s)

$T_o =$ initial peak cladding temperature limit (°K)

$T_a =$ ambient temperature (°K)

It should be noted that the area fraction of de-cohesion function f(A) approaches zero in the limit as $A \rightarrow A_i$. Consequently, the mathematical singularity in the integral $\int_{A_i}^{A} \frac{dA}{f(A)}$ is numerically accommodated by using an alternate form given below:

$$\int_{A_i}^{A} \frac{dA}{f(A)} = \text{Limit } \varepsilon \rightarrow 0 \int_{A_i \rightarrow \varepsilon}^{A_f} \frac{A^{1/2}[\frac{1}{2}\ell n \frac{1}{A} - \frac{3}{4} + A(1-\frac{A}{4})]\,dA}{[1-(\frac{A_i}{A})]^{1/2}(1-A)}$$

The allowable area fraction of de-cohesion using $A_i = 0.05$, $\varepsilon = 0.0001$, and $A_f = 0.15$ is determined to be equal to 0.15211. This is consistent with an alternate form of the DCCG model reported in the PNL study [4.3.1, Appendix D] as reproduced below:

$$A_f = \int_0^{t_f} G(t)\,dt \leq 0.15$$

All parameters in the G(t) function (except for the initial peak cladding temperature limit T_o), have been defined as discussed previously in this section. The cumulative cladding damage experienced during the proposed 40-year dry cask storage period is determined by integrating the G(t) function. The initial peak cladding temperature limit parameter T_o is iteratively adjusted to limit the cumulative damage to 15% as required by the NUREG-1536 Criterion (B) discussed earlier in this section. The initial peak cladding temperature limit for 5-year old fuel is determined to be 388.5°C (731°F) and 405.4°C (762°F) for the bounding PWR and BWR fuel

assemblies (except for 8×8 GE Dresden-1, 6x6 Dresden 1, 6×6 Humboldt Bay, and Quad+ fuel types), respectively. The temperature limits are slightly higher than the respective temperature limits determined from the generic CSFM IDS temperature limit curves [4.3.1]. Consequently, the more conservative peak cladding temperature limits obtained from the generic CSFM IDS temperature limit curves are applied to the HI-STAR 100 System thermal analysis for long-term storage.

4.3.1 Evaluation of Stainless Steel Clad Fuel

Approximately 2,200 PWR and BWR fuel assemblies stored in the United States employ stainless steel cladding. All stainless steel cladding materials are of the austenitic genre with the ASTM alloy compositions being principally type 304 and 348H. The long-term storage condition peak allowable temperature applicable to stainless steel fuel is significantly higher than that applicable to Zircaloy clad fuel. A recent EPRI/PNL study [4.3.5] recommends a 430°C (806°F) peak stainless steel cladding temperature limit versus a typical 380°C (716°F) [4.3.1] peak Zircaloy cladding temperature limit. Since the peak cladding temperature limits applied to the thermal analysis herein for both Zircaloy clad and stainless steel clad fuel are based on the Zircaloy clad limit, it is readily apparent that the PNL criteria [4.3.1] is overly restrictive for stainless steel clad fuel. The peak cladding temperature limits applied to both Zircaloy and stainless steel clad fuel assemblies are provided in Table 4.3.1.

It is recognized that the peak cladding temperature of stainless fuel will differ from Zircaloy clad fuel principally due to the following differences:

i. Differences in decay heat levels
ii. Differences in cladding emissivity
iii. Differences in cladding conductivity
iv. Differences in fuel rod array dimensions

The net planar thermal resistance of the equivalent homogenized axisymmetric MPC basket containing stainless steel clad fuel is greater than that with Zircaloy clad fuel. The higher resistance arises principally from the significantly lower emissivity of the stainless steel cladding. This factor is, however, offset by significantly lower design basis heat loads prescribed for a HI-STAR 100 System containing stainless steel clad fuel. A 20% reduction in the design basis heat duty for stainless steel fuel (20% lower than Zircaloy clad fuel) bounds the nominal percentage decrease in MPC basket effective thermal conductivity† (stainless steel fueled baskets are between 9% (MPC-68) to 13% (MPC-24) less conducting, as shown in Table 4.4.7). As can be seen by comparing the design basis maximum allowable decay heat loads for Zircaloy clad (Tables 4.4.18 and 4.4.19) and stainless steel clad (Table 2.1.11) fuel assemblies, the allowable assembly decay heat load for stainless steel clad fuel is approximately 73% of the PWR Zircaloy clad fuel heat load and 35% of the BWR Zircaloy clad fuel heat load. Therefore, it is concluded that the peak cladding temperature for stainless steel clad fuel will be bounded by Zircaloy clad fuel results. Consequently, in view of significantly higher peak stainless steel cladding

† The term "effective conductivity" of the fuel basket is defined in Section 4.4.1.

temperature limits recommended by the EPRI study [4.3.5] and the conservative heat loads prescribed for stainless steel clad fuel, a separate thermal analysis to demonstrate the adequacy of stainless steel clad integrity for storage in the HI-STAR 100 System is not necessary.

4.3.2 Short-Term Cladding Temperature Limit

For short-term durations, relatively high fuel cladding temperature limits have been historically accepted by the USNRC. For example, the Safety Analysis Report of the STC transport cask (Docket No. 71-9235), recently certified by the USNRC, permits 1200°F (approximately 649°C) as the maximum value of the peak cladding temperature (T_{max}) for transport of SNF with up to 45,000 MWD/MTU burnup. NUREG-1536 and PNL test data [4.3.4], limiting themselves to medium burnup levels (28,800 MWD/MTU), endorse a somewhat lower T_{max} value (T_{max} = 570°C or 1058°F). Based on the published industry test data, guidance in the literature, and analytical reasoning, we herein prescribe 570°C as the admissible value of T_{max} for the SNF for the relatively lower burnup levels in the HI-STAR 100 System for storage[††].

A Brookhaven report written for EPRI [4.3.7] asserts that fuel cladding rupture becomes "virtually absent at stresses below about 200 MPa". It can be readily deduced that the peak cladding stress for the limiting condition of 570°C cladding temperature will be below 200 MPa for the SNF burnup levels considered in this FSAR. Recalling σ_{max} at 96.7 MPa (Table 4.3.3) at 300°C gas temperature, the cladding circumferential stress (σ_{peak}) at 570°C is obtained by direct proportionality in absolute gas temperature:

$$\sigma_{peak} = \sigma_{max} (570 + 273)/(300 + 273) = 142.3 \text{ MPa (approximately 20,600 psi)}$$

Therefore, short-term temperature values (T_{max}) of 570°C are considered safe to preclude fuel cladding failure.

The EPRI report cites experiments on fourteen irradiated Turkey Point Unit 3 rods carried out by Einziger et al.[†] in 1982 which showed no breach in cladding even after as much as 7% strain was accumulated in elevated temperatures lasting for 740-1,000 hours. Einziger's test data corroborates our selection of T_{max} = 570°C as the short duration limiting temperature.

---

†† 40,000 MWD/MTU for BWR fuel and 42,500 MWD/MTU for PWR fuel bounds permissible maximum burnups.

† "High Temperature Post Irradiation Materials Performance of Spent Pressurized Water Reactor Fuel Rods under Dry Storage Conditions," by R.E. Einziger, S.D. Atkin, D.E. Stallrecht, and V.S. Pasupathi, Nuclear Technology, 57:65-80 (1982).

Table 4.3.1

HI-STAR 100 SYSTEM MATERIAL TEMPERATURE [°F] LIMITS

Material	Normal Long-Term Temperature Limits	Short-Term Temperature Limits
Fuel cladding (Zircaloy and stainless steel)	See Table 4.3.7	1058
Boral†	800	950
Overpack closure plate mechanical seal, vent and drain port plug seals	See Table 2.2.3	See Table 2.2.3
Holtite-A††	300	300

† Based on AAR Structures Boral thermophysical test data.

†† See Appendix 1.B.

Table 4.3.2

SUMMARY OF PWR ASSEMBLY RODS INITIAL GAS FILL DATA

Assembly Type	Rods Per Assembly	Free Rod Volume ($in.^3$)	Fill Pressure (psig) at 70°F	Fill Gas Volume at STP†	
				(Liters) Per Rod	(Liters) Per Assembly
W-14x14 Std.	179	1.72	0-460	0.845	151.2
W-15x15 Std.	204	1.25	0-475	0.633	129.1
W-17x17 Std.	264	1.05-1.25	275-500	0.666	175.8
B&W-15x15 Mark B	208	1.308	415	0.582	121.1
B&W-17x17 Mark C	264	0.819	435	0.381	100.6
CE-14x14 Std.	164	1.693	300-450	0.814	133.5
CE-16x16 Std.	220	1.411	300-450	0.678	149.2
B&W-15x15 Mark B-11	208	1.260	415	0.560	116.5
CE-14x14 (MP2)	176	1.728	300-450	0.831	146.2

† STP stands for standard temperature (°C) and pressure (1 atmosphere).

Table 4.3.3
BOUNDING VALUES OF FUEL CLADDING STRESS FOR PWR SNF

	W-14X14 Std	W-15x15 Std	W-17x17 Std	B&W-15x15 Mark B	B&W-17x17 Mark C	CE-14x14 Std	CE-16x16 Sys 80	B&W-15x15 Mark B-11	CE-14x14 (MP2)
Fresh Fuel Rods O.D. (inch)	0.4220	0.422	0.374	0.430	0.379	0.440	0.382	0.414	0.440
End of Life Oxidation Thickness (inch)†	0.0027	0.0027	0.0027	0.0027	0.0027	0.0027	0.0027	0.0027	0.0027
End of Life Rods O.D. (inch)	0.4166	0.4166	0.3686	0.4246	0.3736	0.4346	0.3766	0.4086	0.4346
Rods I.D. (inch)	0.3734	0.373	0.329	0.377	0.331	0.384	0.332	0.370	0.388
Average tube Diameter (inch)	0.3950	0.3948	0.3488	0.4008	0.3523	0.4093	0.3493	0.3893	0.4113
Wall Thickness (inch)	0.0216	0.0218	0.0198	0.0238	0.0213	0.0253	0.0223	0.0193	0.0233
Hot Volume Pressure at 300°C (MPa)††	9.77	10.67	10.08	9.62	10.87	10.01	9.61	9.76	9.67
Cladding Stress (MPa)	89.3	96.7	88.8	81.0	90.0	81.0	75.2	98.4	85.3

† PNL-4835 [4.3.4] reported maximum cladding thickness loss due to in-reactor oxidation.

†† This average rod gas temperature conservatively bounds the plenum gas temperature, which, as can be seen from Figure 4.4.21, is approximately 225°C. The cladding stresses reported in the bottom row of this table will be accordingly reduced by the factor (225+273)/(300+273) = 0.87. However, 96.7 MPa cladding stress for PWR SNF is used as the upper bound value in this FSAR.

Table 4.3.4

SUMMARY OF FISSION GASES RELEASE PER ASSEMBLY†

Component	Release†† Fraction	Release Amount (g-moles/ PWR assembly)	Release Amount (g-moles/ BWR assembly)
Tritium	0.3	0.004	0.003
^{85}Kr	0.3	0.805	0.297
^{129}I	0.12	0.137	0.050
^{131}Xe	0.10	2.664	0.985

† Bounding for 42,500 MWD/MTU burnup PWR assemblies and 40,000 MWD/MTU burnup BWR assemblies.

†† From Regulatory Guide 1.25.

Table 4.3.5
SUMMARY OF BWR ASSEMBLY RODS INITIAL GAS FILL DATA

Assembly Type	Rods/ Assembly	Free Rod Volume (in^3)	Fill Pressure (psig) at 70°F	Fill Gas Volume at STP	
				(liters) Per Rod	(liters) Per Assembly
GE-7x7 (1966)	49	2.073	0-44.1†	0.126	6.17
GE-7x7 (1968)	49	2.073	0-44.1	0.126	6.17
GE-7x7R	49	1.991	0-44.1	0.121	5.93
GE-8x8	60	1.504	0-44.1	0.0915	5.49
GE-8x8R	62	1.433	0-147††	0.240	14.88
EXXON-9x9	79	1.323	58.8-88.2†††	0.141	11.1
6x6 GE Dresden-1	36	2.304	58.8-88.2	0.245	8.82
6x6 Dresden-1 MOX	36	2.286	58.8-88.2	0.243	8.75
6x6 GE Humboldt Bay	36	2.346	58.8-88.2	0.250	9.0
7x7 GE Humboldt Bay	49	1.666	58.8-88.2	0.177	8.67
8x8 GE Dresden-1	64	1.235	58.8-88.2	0.131	8.38
8x8 SPC	63	1.615	58.8-88.2	0.172	10.8
9x9 SPC-2 wtr. Rods	79	1.248	58.8-88.2	0.133	10.5
9x9 SPC-1 wtr. Rod	80	1.248	58.8-88.2	0.133	10.6
9x9 GE11/GE13	74	1.389	58.8-88.2	0.150	11.1
9x9 Atrium 9B SPC	72	1.366	58.8-88.2	0.145	10.4
10x10 SVEA-96	96	1.022	58.8-88.2	0.109	10.5
10x10 GE12	92	1.167	58.8-88.2	0.124	11.4
6x6 Dresden Thin Clad	36	2.455	58.8-88.2	0.261	9.4
7x7 Oyster Creek	49	2.346	58.8-88.2	0.250	12.2
8x8 Oyster Creek	64	1.739	58.8-88.2	0.185	11.8
8x8 Quad+ Westinghouse	64	1.201	58.8-88.2	0.128	8.2
8x8 TVA Browns Ferry	61	1.686	58.8-88.2	0.179	10.9
9x9 SPC-5	76	1.249	58.8-88.2	0.133	10.1

† Conservatively bounding for GE-7x7 (1966), GE-7x7 (1968), GE-7x7R and GE-8x8 (ORNL/TM-9591/V1-R1).

†† Conservatively bounding initial fill pressure. ORNL/TM-9591/V1-R1 reports GE-8x8R prepressurized to 3 atm.

††† BWR fuel rods internal pressurization between 4 to 6 atm (PNL-4835).

Table 4.3.6

BOUNDING VALUES OF FUEL CLADDING STRESS FOR BWR SNF

Fuel Type	Fresh Fuel Rod O.D. (inch)	End of Life Oxidation Thickness (inch)	End of Life Rods O.D. (inch)	Rods I.D. (inch)	Average Tube Diameter (inch)	Wall Thickness (inch)	Hot Volume Pressure at 300°C (MPa)	Cladding Stress (MPa)
GE-7x7 (1966)	0.563	0.0047	0.5536	0.499	0.5263	0.0273	4.61	44.4
GE-7x7 (1968)	0.570	0.0047	0.5606	0.499	0.5298	0.0308	4.61	39.6
GE-7x7R	0.563	0.0047	0.5536	0.489	0.5213	0.0323	4.76	38.4
GE-8x8	0.493	0.0047	0.4836	0.425	0.4543	0.0293	5.08	39.4
GE-8x8R	0.483	0.0047	0.4736	0.419	0.4463	0.0273	6.52	53.3
EXXON-9x9	0.42	0.0047	0.4106	0.36	0.3853	0.0253	5.08	38.7
6x6 GE Dresden-1	0.5645	0.0047	0.5551	0.4945	0.5248	0.0303	6.1	52.8
6x6 Dresden-1 MOX	0.5625	0.0047	0.5531	0.4925	0.5228	0.0303	6.1	52.8
6x6 GE Humboldt Bay	0.563	0.0047	0.5536	0.499	0.5263	0.0273	5.98	57.6†
7x7 GE Humboldt Bay	0.486	0.0047	0.4766	0.4204	0.4485	0.0281	6.13	48.9
8x8 GE Dresden-1	0.412	0.0047	0.4026	0.362	0.3813	0.0203	6.29	59.1†
8x8 SPC	0.484	0.0047	0.4746	0.414	0.4443	0.0303	5.19	38.0
9x9 SPC-2 wtr. Rods	0.424	0.0047	0.4146	0.364	0.3893	0.0253	5.32	40.9
9x9 SPC-1 wtr. Rod	0.423	0.0047	0.4136	0.364	0.3888	0.0248	5.25	41.1
9x9 GE11/GE 13	0.44	0.0047	0.4306	0.384	0.4073	0.0233	5.17	45.2
9x9 Atrium 9B SPC	0.433	0.0047	0.4236	0.3808	0.4022	0.0214	5.32	50.0

† These two fuel types are separately analyzed for peak fuel cladding temperature limits.

Table 4.3.6 (continued)

BOUNDING VALUES OF FUEL CLADDING STRESS FOR BWR SNF

Fuel Type	Fresh Fuel Rod O.D. (inch)	End of Life Oxidation Thickness (inch)	End of Life Rods O.D. (inch)	Rods I.D. (inch)	Average Tube Diameter (inch)	Wall Thickness (inch)	Hot Volume Pressure at 300°C (MPa)	Cladding Stress (MPa)
10x10 SVEA-96	0.379	0.0047	0.3696	0.3294	0.3495	0.0201	4.38	38.1
10x10 GE12	0.404	0.0047	0.3946	0.352	0.3733	0.0213	4.99	43.7
6x6 Dresden Thin Clad	0.5625	0.0047	0.5531	0.5105	0.5318	0.0213	5.77	72.5†
7x7 Oyster Creek	0.5700	0.0047	0.5606	0.499	0.5298	0.0308	4.74	40.7
8x8 Oyster Creek	0.5015	0.0047	0.4921	0.4295	0.4608	0.0313	4.87	35.9
8x8 Quad+ Westinghouse	0.4576	0.0047	0.4482	0.3996	0.4239	0.0243	6.42	56.0†
8x8 TVA Browns Ferry	0.483	0.0047	0.4736	0.423	0.4483	0.0253	5.14	45.5
9x9 SPC-5	0.417	0.0047	0.4076	0.364	0.3858	0.0218	5.46	48.3

† These fuel types are separately analyzed for peak fuel cladding temperature limits.

Table 4.3.7

INITIAL PEAK ZIRCALOY[†] CLADDING TEMPERATURE LIMITS FOR STORAGE

Fuel Age (years)	Temperature Limits for PWR SNF (°C) [°F]	Temperature Limits for Design Basis BWR SNF (except 8x8 GE Dresden-1, 6x6 Dresden 1, 6x6 GE Humboldt Bay, and Quad+) (°C) [°F]	Temperature Limits for 8x8 GE Dresden-1, 6x6 Dresden-1, 6x6 GE Humboldt Bay, and 8x8 Quad+ SNF[††] (°C) [°F]
5	382.3 [720]	398.2 [749]	391.2 [736]
6	370.2 [698]	382.3 [720]	376.2 [709]
7	347.0 [657]	357.9 [676]	352.2 [666]
10	341.6 [647]	351.4 [665]	346.6 [656]
15	334.1 [633]	344.9 [653]	339.5 [643]

[†] The listed limits are conservatively applied to stainless steel clad fuel assemblies, which actually have substantially higher limits.

[††] The 8x8 GE Dresden-1, 6x6 Dresden-1, Quad+ and 6x6 Humboldt Bay fuel types are low heat emitting assemblies. The Technical Specifications limit the heat load for these assemblies to 115 watts per assembly (approximately 58% lower than the design basis maximum heat load for BWR fuel (Table 4.4.19) (183.5 watts/assembly for Quad+). Consequently, these assembly types are not deemed to be limiting.

4.4 THERMAL EVALUATION FOR NORMAL CONDITIONS OF STORAGE

4.4.1 Thermal Model

The HI-STAR 100 MPC basket designs consist of two distinct geometries to hold 24 PWR or 68 BWR fuel assemblies. The basket is a matrix of square compartments (called boxes) to hold the fuel assemblies in a vertical position. The basket is a honeycomb structure of Alloy X plates with full-length edge-welded intersections to form an integral basket configuration. Individual cell walls (except outer periphery MPC-68 cell walls) are provided with Boral neutron absorber sandwiched between the box wall and a sheathing plate over the full length of the active fuel region.

The design basis decay heat generation (per PWR or BWR assembly) for long-term normal storage is specified in Table 2.1.6. The decay heat is conservatively considered to be non-uniformly distributed over the active fuel length based on the design basis axial burnup distribution provided in Chapter 2 (Table 2.1.8).

Transport of heat from the interior of the MPC basket to its outer periphery is accomplished by a combination of conduction through the MPC basket metal grid structure, conduction and radiation heat transfer in the relatively small helium gaps between the fuel assemblies and basket cell walls, and radiation and conduction from the fuel basket periphery to the MPC shell. Heat dissipation across the gap between the MPC basket periphery and the MPC shell is by a combination of helium conduction, natural convection (by means of the "Rayleigh" effect), radiation across the gap, and conduction in the aluminum alloy 1100 heat conduction elements. Between the MPC exterior and the overpack interior is a small clearance region which is evacuated and backfilled with helium. Helium, besides being inert, is a better heat conduction medium than air. Thus, heat conduction through the MPC/overpack helium gap will minimize temperature differentials across this region.

The overpack, under normal storage conditions, passively rejects heat to the outside environment. Cooling of the outside overpack vertical and horizontal (top) surfaces is by natural convection and thermal radiation. The bottom surface conducts heat through the ISFSI concrete pad to the ground. Analytical modeling details of the various thermal transport mechanisms are provided in the following.

4.4.1.1 Analytical Model - General Remarks

Transport of heat from the heat generation region (fuel assemblies) to the outside environment (ambient air or ground) is analyzed broadly in terms of three interdependent thermal models. The first model considers transport of heat from the fuel assembly to the basket cell walls. This model recognizes the combined effects of conduction (through helium) and radiation, and is essentially a finite element technology based update of the classical Wooton & Epstein [4.4.1] (which considered radiative heat exchange between fuel rod surfaces) formulation. The second model considers heat transport within an MPC cross section by conduction and radiation. The effective cross sectional thermal conductivity of the basket and basket periphery regions, obtained from a combined fuel assembly/basket heat conduction-radiation model developed on

ANSYS, are applied to an axisymmetric thermal model of the HI-STAR 100 System on the FLUENT [4.1.2] code. The third model deals with the transmission of heat from the MPC exterior surface to the external environment (heat sink). From the MPC shell to the overpack exterior surface, heat is conducted through an array of concentric shells representing the MPC-to-overpack helium gap, overpack inner shell, intermediate shells, Holtite-A and overpack outer shell. Heat rejection from the outside cask surfaces to ambient air is considered by accounting for natural convection and thermal radiation heat transfer mechanisms from the vertical (cylindrical shell) and top cover (flat) surfaces. The bottom overpack face, in contact with the ISFSI pad, rejects a small quantity of heat by conduction through the pad to the ground. The reduction in radiative heat exchange between cask outside vertical surfaces and ambient air because of blockage from the neighboring casks arranged for normal storage in a regular square array on the ISFSI pad is recognized in the analysis. The overpack closure plate is modeled as a heated surface in convective and radiative heat exchange with air and as a recipient of heat input through insolation. Insolation on the cask surfaces is based on 12-hour levels prescribed in 10CFR71, averaged over a 24-hour period, after accounting for partial blockage conditions.

Subsections 4.4.1.1.1 through 4.4.1.1.11 contain a systematic description of the mathematical models devised to articulate the temperature field in the HI-STAR 100 System. Table 4.4.2 shows the relationship between the mathematical models and the corresponding regions (i.e., fuel, MPC, overpack, etc.) of the HI-STAR 100 System. The description begins with the method to characterize the heat transfer behavior of the prismatic (square) opening referred to as the "fuel space" with a heat emitting fuel assembly situated in it. The methodology utilizes a finite element procedure to replace the heterogeneous SNF/fuel space region with an equivalent solid body having a well-defined temperature-dependent conductivity. In the following subsection, the method to replace the "composite" walls of the fuel basket cells with an equivalent "solid" wall is presented. Having created the mathematical equivalents for the SNF/fuel spaces and the fuel basket walls, the method to represent the MPC cylinder containing the fuel basket by an equivalent cylinder whose thermal conductivity is a function of the spatial location and coincident temperature is presented.

Following the approach of presenting descriptions starting from the inside and moving to the outer region of a cask, the next subsections present the mathematical model to simulate the overpack. Subsection 4.4.1.1.11 concludes the presentation with a description of how the different models for the specific regions within the HI-STAR 100 System are assembled into the final FLUENT model. Finally, a subsection to describe the solution for the special case of vacuum in the MPC space (no helium) is presented.

4.4.1.1.1 Overview of the Thermal Model

Thermal analysis of the HI-STAR 100 System is performed by assuming that the system is subject to its maximum heat duty with each storage location occupied and with the heat generation rate in each stored fuel assembly equal to design basis maximum value. While the assumption of equal heat generation imputes a certain symmetry to the cask thermal problem, the

thermal model must incorporate three attributes of the physical problem to perform a rigorous analysis of a fully loaded cask:

i. While the rate of heat conduction through metals is a relatively weak function of temperature, radiation heat exchange is a nonlinear function of surface temperatures.

ii. Heat generation in the MPC is axially non-uniform due to non-uniform axial burnup profile in the fuel assemblies.

iii. Inasmuch as the transfer of heat occurs from inside the basket region to the outside, the temperature field in the MPC is spatially distributed with the maximum values reached in the central core region.

It is clearly impractical to model every fuel rod in every stored fuel assembly explicitly. Instead, the cross section bounded by the inside of the storage cell, which surrounds the assemblage of fuel rods and the interstitial helium gas, is replaced with an "equivalent" square (solid) section characterized by an effective thermal conductivity. Figure 4.4.1 pictorially illustrates the homogenization concept. Further details of this procedure for determining the effective conductivity are presented in Subsection 4.4.1.1.2; it suffices to state here that the effective conductivity of the cell space will be a function of temperature because the radiation heat transfer (a major component of the heat transport between the fuel rods and the surrounding basket cell metal) is a strong function of the temperatures of the participating bodies. Therefore, in effect, every storage cell location will have a different value of effective conductivity (depending on the coincident temperature) in the homogenized model. The temperature-dependent fuel assembly region effective conductivity is determined by a finite volume procedure, as described in Subsection 4.4.1.1.2.

In the next step of homogenization, a planar section of MPC is considered. With each storage cell inside space replaced with an equivalent solid square, the MPC cross section consists of a metallic gridwork (basket cell walls with each square cell space containing a solid fuel cell square of effective thermal conductivity, which is a function of temperature) circumscribed by a circular ring (MPC shell). There are five distinct materials in this section, namely the homogenized fuel cell squares, the Alloy X structural materials in the MPC (including Boral sheathing), Boral, alloy 1100 aluminum heat conduction elements, and helium gas. Each of the five constituent materials in this section has a different conductivity. It is emphasized that the conductivity of the homogenized fuel cells is a strong function of temperature.

In order to replace this thermally heterogeneous MPC section with an equivalent conduction-only region, resort to the finite element procedure is necessary. Because the rate of transport of heat within the MPC is influenced by radiation, which is a temperature-dependent effect, the equivalent conductivity of the MPC region must also be computed as a function of temperature. Finally, it is recognized that the MPC section consists of two discrete regions, namely, the basket region and the peripheral region. The peripheral region is the space between the peripheral storage cells and the MPC shell. This space is essentially full of helium surrounded by Alloy X plates and alloy 1100 aluminum heat conduction elements. Accordingly, as illustrated in Figure 4.4.2 for MPC-68, the MPC cross section is replaced with two homogenized regions with temperature-dependent conductivities. In particular, the effective conductivity of the fuel cells is

subsumed into the equivalent conductivity of the basket cross section. The finite element procedure used to accomplish this is described in Subsection 4.4.1.1.4. The ANSYS finite element code is the vehicle for all modeling efforts described in the foregoing.

In summary, appropriate finite element models are used to replace the MPC cross section with an equivalent two region homogeneous conduction lamina whose local conductivity is a known function of coincident absolute temperature. Thus, the MPC cylinder containing discrete fuel assemblies, helium, Boral and Alloy X, is replaced with a right circular cylinder whose material conductivity will vary with the radial and axial position as a function of the coincident temperature.

The MPC-to-overpack gap is simply an annular space which is readily modeled with an equivalent conductivity which reflects conduction and radiation modes of heat transfer. The overpack is a radially symmetric structure except for the neutron absorber region which is built from radial connectors and Holtite-A (see Figure 4.4.7). Using the classical equivalence procedure described in Subsection 4.4.1.1.9, this region is replaced with an equivalent radially symmetric annular cylinder.

The thermal analysis procedure described above makes frequent use of equivalent thermal properties to ease the geometric modeling of the cask components. These equivalent properties are rigorously calculated values based on detailed evaluations of actual cask system geometries. All these calculations are performed conservatively to ensure a bounding representation of the cask system. This process, commonly referred to as submodeling, yields accurate (not approximate) results. Given the detailed nature of the submodeling process, experimental validation of the individual submodels is not necessary.

In this manner, a HI-STAR 100 System overpack containing a loaded MPC standing upright on the ISFSI pad is replaced with a right circular cylinder with spatially varying temperature-dependent conductivity. Heat is generated within the basket space in this cylinder in the manner of the prescribed axial burnup distribution. In addition, heat is deposited from insolation on the external surface of the overpack. Under steady state conditions the total heat due to internal generation and insolation is dissipated from the outer cask surfaces by natural convection and thermal radiation to the ambient environment. Details of the elements of mathematical modeling are provided in the following.

4.4.1.1.2 Fuel Region Effective Thermal Conductivity Calculation

Thermal properties of a large number of PWR and BWR fuel assembly configurations manufactured by the major fuel suppliers (i.e., Westinghouse, CE, B&W, and GE) have been evaluated for inclusion in the HI-STAR 100 System thermal analysis. It is noted that PWR fuel assemblies are equipped with removable non-fuel hardware, in particular, control rods which are inserted in guide tube locations for in-core usage. In dry cask storage, PWR fuel is optionally stored with the control rods. The control rods, when inserted in the fuel assemblies, displace gas in the guide tubes replacing it with solid materials (neutron absorbers and metals) which conduct heat much more readily. As a result, dissipation of heat in the fuel assemblies is enhanced by the presence of these control rods. For conservatism, credit for presence of control rods in fuel

assemblies is neglected. Bounding PWR and BWR fuel assembly configurations are determined using the simplified procedure described below. This is followed by the determination of temperature-dependent properties of the bounding PWR and BWR fuel assembly configurations to be used for cask thermal analysis using a finite volume (FLUENT) approach.

To determine which of the numerous PWR assembly types listed in Table 4.4.5 should be used in the thermal model for the MPC-24 fuel basket, we must establish which assembly has the maximum thermal resistance. The same determination must be made for the MPC-68, out of the menu of SNF types listed in Table 4.4.6. For this purpose, we utilize a simplified procedure which we describe below.

Each fuel assembly consists of a large array of fuel rods typically arranged on a square layout. Every fuel rod in this array is generating heat due to radioactive decay in the enclosed fuel pellets. There is a finite temperature difference required to transport heat from the innermost fuel rods to the storage cell walls. Heat transport within the fuel assembly is based on principles of conduction heat transfer combined with the highly conservative analytical model proposed by Wooton and Epstein [4.4.1]. The Wooton-Epstein model considers radiative heat exchange between individual fuel rod surfaces as a means to bound the hottest fuel rod cladding temperature.

Transport of heat energy within any cross section of a fuel assembly is due to a combination of radiative energy exchange and conduction through the helium gas which fills the interstices between the fuel rods in the array. With the assumption of uniform heat generation within any given horizontal cross section of a fuel assembly, the combined radiation and conductive heat transport effects result in the following heat flow equation:

$$Q = \sigma\ C_o\ F_\varepsilon\ A\ [T_C^4 - T_B^4] + 13.5740\ L\ K_{cs}\ [T_C - T_B]$$

where:

F_ε = Emissivity Factor

$$= \frac{1}{\left(\frac{1}{\varepsilon_C} + \frac{1}{\varepsilon_B} - 1\right)}$$

$\varepsilon_C, \varepsilon_B$ = emissivities of fuel cladding, fuel basket (see Table 4.2.4)

C_o = Assembly Geometry Factor

$$= \frac{4N}{(N+1)^2} \text{ (when N is odd)}$$

$$= \frac{4}{N+2} \text{ (when N is even)}$$

N	=	Number of rows or columns of rods arranged in a square array
A	=	fuel assembly "box" heat transfer area
	=	4 × width × length
L	=	fuel assembly length
K_{cs}	=	fuel assembly constituent materials volume fraction weighted mixture conductivity
T_C	=	hottest fuel cladding temperature (^oR)
T_B	=	box temperature (^oR)
Q	=	net radial heat transport from the assembly interior
σ	=	Stefan-Boltzmann Constant (0.1714×10^{-8} Btu/ft^2-hr-$^oR^4$)

In the above heat flow equation, the first term is the Wooten-Epstein radiative heat flow contribution while the second term is the conduction heat transport contribution based on the classical solution to the temperature distribution problem inside a square shaped block with uniform heat generation [4.4.5]. The 13.574 factor in the conduction term of the equation is the shape factor for two-dimensional heat transfer in a square section. Planar fuel assembly heat transport by conduction occurs through a series of resistances formed by the interstitial helium fill gas, fuel cladding and enclosed fuel. An effective planar mixture conductivity is determined by a volume fraction weighted sum of the individual constituent material resistances. For BWR assemblies, this formulation is applied to the region inside the fuel channel. A second conduction and radiation model is applied between the channel and the fuel basket gap. These two models are combined, in series, to yield a total effective conductivity.

The effective conductivity of the fuel for several representative PWR and commonly used BWR assemblies is presented in Tables 4.4.5 and 4.4.6. At higher temperatures (approximately 450°F and above), the zircaloy clad fuel assemblies with the lowest effective thermal conductivities are the W-17×17 OFA (PWR) and the GE11-9×9 (BWR). A discussion of fuel assembly conductivities for some of the newer 10×10 array and plant specific BWR fuel designs is presented near the end of this subsection. As noted in Table 4.4.6, the Dresden 1 (intact and damaged) fuel assemblies are excluded from consideration. The design basis decay heat load for Dresden-1 intact and damaged fuel (Table 2.1.7) is approximately 58% lower than the MPC-68 design basis maximum heat load (Table 4.4.19). Examining Table 4.4.6, the effective conductivity of the damaged Dresden-1 fuel assembly in a damaged fuel container is approximately 40% lower than the bounding (GE-11 9×9) fuel assembly. Consequently, the fuel cladding temperatures in the HI-STAR 100 System with Dresden-1 intact of damaged fuel assemblies will be bounded by design basis fuel cladding temperatures. This is demonstrated in Subsection 4.4.1.1.16. Based on this simplified analysis, the W-17×17 OFA PWR and GE11-9×9 BWR fuel assemblies are determined to be the bounding configurations for analysis of zircaloy

clad fuel at design basis maximum heat loads. As discussed in Section 4.3.1, stainless clad fuel assemblies with significantly lower decay heat emission characteristics are not deemed to be bounding.

Having established the governing (most resistive) PWR and BWR SNF types, we use a finite volume code to determine the effective conductivities in a conservative manner. Detailed conduction-radiation finite volume models of the bounding PWR and BWR fuel assemblies are developed in the FLUENT code as shown in Figures 4.4.8 and 4.4.9, respectively. The PWR model was originally developed on the ANSYS code which enables individual rod-to-rod and rod-to-basket wall view factor calculations to be performed by the AUX12 procedure for the special case of black body radiation (surfaces emissivity = 1). Limitations of radiation modeling techniques implemented in ANSYS do not permit taking advantage of quarter symmetry of the fuel assembly geometry. Unacceptably long CPU time and large workspace requirements necessary for performing gray body radiation calculations for a complete fuel assembly geometry on ANSYS prompted the development of an alternate simplified model on the FLUENT code. The FLUENT model is benchmarked with the ANSYS model results for a Westinghouse 17×17 fuel assembly geometry for the case of black body radiation (emissivities = 1). The FLUENT model is found to yield conservative results in comparison to the ANSYS model for the "black" surface case. The FLUENT model benchmarked in this manner is used to solve the gray body radiation problem to provide the necessary results for determining the effective thermal conductivity of the governing PWR fuel assembly. The same modeling approach using FLUENT is then applied to the governing BWR fuel assembly, and the effective conductivity of GE11-9×9 fuel determined.

The combined fuel rods-helium matrix is replaced by an equivalent homogeneous material which fills the basket opening by the following two-step procedure. In the first step, the FLUENT-based fuel assembly model is solved by applying equal heat generation per unit length to the individual fuel rods and a uniform boundary temperature along the basket cell opening inside periphery. The temperature difference between the peak cladding and boundary temperatures is used to determine an effective conductivity as described in the next step. For this purpose, we consider a two-dimensional cross section of a square shaped block of size equal to 2L and a uniform volumetric heat source (q_g) cooled at the periphery with a uniform boundary temperature. Under the assumption of constant material thermal conductivity (K), the temperature difference (ΔT) from the center of the cross section to the periphery is analytically given by [4.4.5]:

$$\Delta T = 0.29468 \frac{q_g L^2}{K}$$

This analytical formula is applied to determine the effective material conductivity from a known quantity of heat generation applied in the FLUENT model (smeared as a uniform heat source, q_g) basket opening size and ΔT calculated in the first step.

As discussed earlier, the effective fuel space conductivity is a function of the temperature coordinate. The above two step analysis is carried out for a number of reference temperatures. In

this manner, the effective conductivity as a function of temperature is established.

In Table 4.4.23, 10×10 array type BWR fuel assembly conductivity results from a simplified analysis are presented to determine the most resistive fuel assembly in this class. From the data in Table 4.4.23, the Atrium-10 fuel type is determined to be the most resistive in this class of fuel assemblies. A detailed finite element model of this assembly type was developed to rigorously quantify the heat dissipation characteristics. The results of this study are presented in Table 4.4.24 and compared to the BWR bounding fuel assembly conductivity depicted in Figure 4.4.14. The results of this study demonstrate that the bounding fuel assembly conductivity is conservative with respect to the 10x10 class of BWR fuel assemblies.

Table 4.4.25 summarizes plant specific fuel types effective conductivities. From these analytical results, the SPC-5 is determined to be the most resistive fuel assembly in this group of fuel types. A rigorous finite element model of SPC-5 fuel assembly was developed to confirm that its in-plane heat dissipation characteristics are bounded from below by the Design Basis BWR fuel conductivities used in the HI-STAR thermal analysis.

Temperature-dependent effective conductivities of PWR and BWR design basis fuel assemblies (most resistive SNF types) are shown in Figure 4.4.14. The finite volume computational results are also compared to results reported from independent technical sources. From this comparison, it is readily apparent that FLUENT-based fuel assembly conductivities are conservative. The FLUENT computed values (not the published literature data) are used in the MPC thermal analysis presented in this document.

4.4.1.1.3 Effective Thermal Conductivity of Boral/Sheathing/Box Wall Sandwich

Each MPC basket cell wall (except the MPC-68 outer periphery cell walls) is manufactured with a Boral neutron absorbing plate for criticality control. Each Boral plate is sandwiched in a sheathing-to-basket wall pocket. A schematic of the "Box Wall-Boral-Sheathing" sandwich geometry of an MPC basket is illustrated in Figure 4.4.3. During fabrication, a uniformly normal pressure is applied to each "Box Wall-Boral-Sheathing" sandwich in the assembly fixture during stitch-welding of the sheathing periphery on the box wall. This ensures adequate surface-to-surface contact for elimination of any macroscopic air gaps. The mean coefficient of linear expansion of the Boral is higher than the thermal expansion coefficients of the basket and sheathing materials. Consequently, basket heat-up from the stored SNF will further ensure a tight fit of the Boral plate in the sheathing-to-box pocket. The presence of small microscopic gaps due to less than perfect surface finish characteristics requires consideration of an interfacial contact resistance between the Boral and box-sheathing surfaces. A conservative contact resistance resulting from a 2 mil Boral to pocket gap is applied in the analysis. In other words, no credit is taken for the interfacial pressure between Boral and stainless plate/sheet stock produced by the fixturing and welding process.

Heat conduction properties of a composite "Box Wall-Boral-Sheathing" sandwich in the two principal basket cross sectional directions as illustrated in Figure 4.4.3 (i.e., lateral "out-of-plane" and longitudinal "in-plane") are unequal. In the lateral direction, heat is transported across

layers of sheathing, air-gap, Boral (B_4C and cladding layers) and box wall resistances which are essentially in series (except for the small helium filled end regions shown in Figure 4.4.4). Heat conduction in the longitudinal direction, in contrast, is through an array of essentially parallel resistances comprised of these several layers listed above. For the ANSYS based MPC basket thermal model, corresponding non-isotropic effective thermal conductivities in the two orthogonal sandwich directions are determined and applied in the analysis.

These non-isotropic conductivities are determined by constructing two-dimensional finite-element models of the composite "Box Wall-Boral-Sheathing" sandwich in ANSYS. A fixed temperature is applied to one edge of the model and a fixed heat flux is applied to the other edge, and the model is solved to obtain the average temperature of the fixed-flux edge. The equivalent thermal conductivity is obtained using the computed temperature difference across the sandwich as input to a one-dimensional Fourier equation for conduction heat transfer as follows:

$$K_{eff} = \frac{q \times L}{T_h - T_c}$$

where:

Keff = effective thermal conductivity
q = heat flux applied in the ANSYS model
L = ANSYS model heat transfer path length
T_h = ANSYS calculated average edge temperature
T_c = specified edge temperature

The heat transfer path length is the width or thickness of the sandwich, respectively, depending on the direction of transfer (i.e., in-plane or out-of-plane).

4.4.1.1.4 Finite Element Modeling of Basket In-Plane Conductive Heat Transport

The heat rejection capability of each MPC basket design (i.e., MPC-24, and MPC-68) is evaluated by developing a thermal model of the combined fuel assemblies and composite basket walls geometry on the ANSYS finite element code. The ANSYS model includes a geometric layout of the basket structure in which the basket "Box Wall-Boral-Sheathing" sandwich is replaced by a "homogeneous wall" with an equivalent thermal conductivity. Since the thermal conductivity of the Alloy X material is a weakly varying function of temperature, the equivalent "homogeneous wall" must have a temperature-dependent effective conductivity. Similarly, as illustrated in Figure 4.4.4, the conductivities in the "in-plane" and "out-of-plane" directions of the equivalent "homogeneous wall" are different. Finally, as discussed earlier, the fuel assemblies and the surrounding basket cell openings are modeled as homogeneous heat generating regions with effective temperature dependent in-plane conductivity. The methodology used to reduce the
heterogeneous MPC basket - fuel assemblage to an equivalent homogeneous region with effective thermal properties is discussed in the following.

Consider a cylinder of height, L, and radius, r_o, with a uniform volumetric heat source term, q_g, insulated top and bottom faces, and its cylindrical boundary maintained at a uniform

temperature, T_c. The maximum centerline temperature (T_h) to boundary temperature difference is readily obtained from classical one-dimensional conduction relationships (for the case of a conducting region with uniform heat generation and a constant thermal conductivity K_s):

$$(T_h - T_c) = q_g r_o^2/(4 K_s)$$

Noting that the total heat generated in the cylinder (Q_t) is $\pi r_o^2 L q_g$, the above temperature rise formula can be reduced to the following simplified form in terms of total heat generation per unit length (Q_t/L):

$$(T_h - T_c) = (Q_t / L)/ (4 \pi K_s)$$

This simple analytical approach is employed to determine an effective basket cross-sectional conductivity by applying an equivalence between the ANSYS finite element model of the basket and the analytical case. The equivalence principle employed in the HI-STAR 100 System thermal analysis is depicted in Figure 4.4.2. The 2-dimensional ANSYS finite element model of each MPC basket is solved by applying a uniform heat generation per unit length in each basket cell region and a constant basket periphery boundary temperature, T_c'. Noting that the basket region with uniformly distributed heat sources and a constant boundary temperature is equivalent to the analytical case of a cylinder with uniform volumetric heat source discussed earlier, an effective MPC basket conductivity (K_{eff}) is readily derived from the analytical formula and ANSYS solution leading to the following relationship:

$$K_{eff} = N (Q_f'/L) / (4 \pi [T_h' - T_c'])$$

where:

N = number of fuel assemblies

(Q_f'/L) = per fuel assembly heat generation per unit length applied in ANSYS model

T_h' = peak basket cross-section temperature from ANSYS model

Cross sectional views of MPC basket ANSYS models are depicted in Figures 4.4.11 and 4.4.12. Notice that many of the basket supports and all shims have been conservatively neglected in the models. This conservative geometry simplification, coupled with the conservative neglect of thermal expansion which would minimize the gaps, yields conservative gap thermal resistances. Temperature-dependent equivalent thermal conductivities of fuel region and composite basket walls, as determined from analysis procedures described earlier, are applied to the ANSYS model. The planar ANSYS conduction model is solved by applying a constant basket periphery temperature with uniform heat generation in the fuel region. Table 4.4.7 summarizes effective thermal conductivityvalues used in subsequent cask thermal modeling. It should be noted that the planar conductivities calculated as described above are actually higher than those reported in Table 4.4.7, imparting additional conservatism to the subsequent calculations. The effective calculated basket cross sectional conductivity and the effective axial direction effective conductivity is conservatively assumed to be equal in the comprehensive HI-STAR 100 System

thermal model (see Section 4.4.1.1.11). It is recalled that the equivalent thermal conductivity values presented in Table 4.4.7 are lower bound values because, among other elements of conservatism, the effective conductivity of most resistive SNF types (Tables 4.4.5 and 4.4.6) are used in the MPC finite element simulations.

4.4.1.1.5 Heat Transfer in MPC Basket Peripheral Region

Each of the two MPC designs for storing PWR or BWR fuel are provided with relatively large regions, formed between the relatively cooler MPC shell and hot basket peripheral panels, filled with helium gas. Heat transfer in these helium-filled regions corresponds to the classical case of heat transfer in a differentially heated closed cavity. Experimental studies of this arrangement have been performed by many investigators, including Eckert and Carlson (Int. J. Heat Mass Transfer, vol. 2, p. 106, 1961) and Elder (J. Fluid Mech., vol. 23, p. 77, 1965). The peripheral region between the basket and MPC inner surface is simulated as a tall fluid-filled cavity of height H formed between two differentially heated surfaces (ΔT) separated by a small distance L. In a closed cavity, an exchange of hot and cold fluids occurs near the top and bottom ends of the cavity, resulting in a net transport of heat across the gap. The rate of heat transfer across the cavity is characterized by a Rayleigh number, Ra_L, defined as:

$$Ra_L = \frac{C_p \rho^2 g \beta \Delta T L^3}{\mu K}$$

where:

C_p	=	fluid heat capacity
ρ	=	fluid density
g	=	acceleration due to gravity
β	=	coefficient of thermal expansion (equal to reciprocal of absolute temperature for gases)
ΔT	=	temperature difference between the hot and cold surfaces
L	=	spacing between the hot and cold surfaces
μ	=	fluid viscosity
K	=	fluid conductivity

Hewitt et al. [4.4.6] recommends the following Nusselt number correlation for heat transport in tall cavities:

$$Nu_L = 0.42\ Ra_L^{1/4}\ Pr^{0.012}\ \left(\frac{H}{L}\right)^{-0.3}$$

where Pr is the Prandtl number of the cavity fill gas.

A Nusselt number of unity implies heat transfer by fluid conduction only, while a higher than unity Nusselt number is due to the so-called "Rayleigh" effect which monotonically increases with increasing Rayleigh number. Nusselt numbers applicable to helium-filled PWR and BWR fueled HI-STAR 100 MPCs in the peripheral voids are provided in Table 4.4.1.

4.4.1.1.6 Effective Conductivity of Multilayered Intermediate Shell Region

Fabrication of the multi-layered overpack shell is discussed in Section 1.2 which explains how an interfacial contact between successive layers from the fabrication process is ensured. In the thermal analysis, each intermediate shell metal-to-metal interface presents an additional resistance to heat transport. The contact resistance arises from microscopic pockets of air entrapped between surface irregularities of the contacting surfaces. Since air is a relatively poor conductor of heat, this results in a reduction in the ability to transport heat across the interface compared to that of the base metal. Interfacial contact conductance depends upon three principal factors, namely: (i) base material conductivity, (ii) interfacial contact pressure, and (iii) surface finish. Rohsenow and Hartnett [4.2.2] have reported results from experimental studies of contact conductance across air entrapped stainless steel surfaces with a typical 100 μ-inch surface finish. A minimum contact conductance of 350 Btu/ft^2-hr-°F is determined from extrapolation of Rohsenow, et al. data to zero contact pressure.

Thermal conductivity of carbon steel is about three times that of stainless steel. Thus, the choice of carbon steel as base material in a multi-layered construction significantly improves heat transport across interfaces. The fabrication process, as discussed in Section 1.2, guarantees significant interfacial contact. Contact conductance values extrapolated to zero contact pressure are therefore conservative. The surface finish of the hot-rolled carbon steel plate stock is generally in the range of 250-1000 μ-inch [4.2.1]. The process of forming hot-rolled flat plate stock to cylindrical shapes to form the intermediate shells will result in additional smoothening of the surfaces (from the large surface pressures exerted by the hardened roller faces which flatten out any surface irregularities).

In the HI-STAR 100 thermal analysis, a conservatively bounding interfacial contact conductance value is determined using the following assumptions:

1. No credit is taken for higher base metal conductivity (carbon versus stainless steel).

2. No credit is taken for interfacial contact pressure.

3. No credit is taken for a smooth surface finish resulting from rolling of hot-rolled plate stock to cylindrical shapes.

4. Contact conductance is based on a uniform 2000 μ-inch (1000 μ-inch for each surface condition) interfacial air gap at all interfaces.

5. No credit for radiation heat exchange across this hypothetical inter-surface air gap.

6. Bounding low thermal conductivity at 200°F.

These assumptions guarantee a conservative assessment of heat dissipation characteristics of the multi-layered intermediate shell region. The resistance of the five carbon steel layers along with the associated interfacial resistances are combined as resistances in series to determine an effective conductivity of this region leading to the following relationship:

$$K_i = r_o \ell n\left(\frac{r_5}{r_o}\right)\left[\sum_{i=1}^{5} \frac{\delta}{K_{air}} \frac{r_o}{r_i} + \frac{r_o \ell n \frac{r_5}{r_o}}{K_{cst}}\right]^{-1}$$

where (in conventional U.S. units):

K_i	=	effective intermediate shell region thermal conductivity
r_o	=	inside radius of inner intermediate shell
r_i	=	outer radius of i^{th} intermediate shell
δ	=	interfacial air gap (2000 μ-inch)
K_{air}	=	air thermal conductivity
K_{cst}	=	carbon steel thermal conductivity

4.4.1.1.7 Heat Rejection from Overpack Exterior Surfaces

Jacob and Hawkins [4.2.9] recommend the following correlations for natural convection heat transfer to air from heated vertical or horizontal surfaces:

Turbulent range:

$$h = 0.19(\Delta T)^{1/3} \quad (Vertical, GrPr > 10^9)$$

$$h = 0.22(\Delta T)^{1/3} \quad (Horizontal, GrPr > 10^7)$$

(in conventional U.S. units)

Laminar Range:

$$h = 0.29\left(\frac{\Delta T}{L}\right)^{1/4} \text{ (Vertical } GrPr < 10^9\text{)}$$

$$h = 0.27\left(\frac{\Delta T}{L}\right)^{1/4} \text{ (Horizontal } GrPr < 2x10^7\text{)}$$

(in conventional U.S. units)

where ΔT is the temperature differential between the overpack surface and ambient air. The length scale L is the overpack height for vertical surfaces or the overpack diameter for the top horizontal surface. Noting that GrPr is expressed as $L^3\Delta TZ$, where Z (from Table 4.2.7) is at least $2.6x10^5$ at a conservatively high upper bound overpack exterior air film temperature of 340°F, it is apparent that the turbulent condition is always satisfied for ΔT in excess of a small fraction of 1°F. Under turbulent conditions, the more conservative heat transfer correlation for vertical surfaces (i.e., $h = 0.19\ \Delta T^{1/3}$) is applied for thermal analysis to all exposed overpack surfaces.

Including both natural convection and thermal radiation heat loss from the overpack outer surfaces, the following relationship for surface heat flux is developed:

$$q_s = 0.19\ (T_s - T_A)^{4/3} + \sigma\ \varepsilon\ F_{1,A}\ [(T_s + 460)^4 - (T_A + 460)^4]$$

where:

T_s, T_A = surface, ambient temperatures (°F)

q_s = surface heat flux (Btu/ft^2-hr)

ε = surface emissivity

$F_{1,A}$ = view factor between surface and air

σ = Stefan Boltzman constant ($0.1714x10^{-8}$ Btu/ft^2-hr-°R^4)

In order to determine the view factor for vertical overpack outside surfaces, an ANSYS [4.1.1] finite-element based radiation heat transfer model is developed. The model geometry is based on a HI-STAR 100 System array layout depicted schematically in Figure 1.4.1. The design basis HI-STAR 100 System ISFSI storage square layout pitch is provided in Section 1.4. The ANSYS model developed is shown in Figure 4.4.5. In this figure, a center HI-STAR 100 System cask is shown surrounded by two rows of casks on all sides. The ANSYS solution determines view factors between this most adversely located system in the middle with all other neighboring casks. A sum of all these individual blockages gives the total blockage factor. Thus, the view factor $F_{1,A}$ between this most adversely affected HI-STAR 100 System and outside air is determined by the following relationship:

$$F_{1,A} = 1 - \sum_{K} F_{1,K}$$

where $F_{1,K}$ is the view factor between HI-STAR 100 System 1 and a neighboring system K. This factor is determined by a series of ANSYS solutions as a function of ISFSI cask array pitch, and the results are shown in Figure 4.4.6.

4.4.1.1.8 Determination of Solar Heat Input

The intensity of solar radiation incident on an exposed surface depends on a number of time varying terms. The solar heat flux strongly depends upon the time of the day as well as on latitude and day of the year. Also, the presence of clouds and other atmospheric conditions (dust, haze, etc.) can significantly attenuate solar intensity levels. Rapp [4.4.2] has discussed the influence of such factors in considerable detail.

Consistent with the guidelines in NUREG-1536 [4.1.3], solar input to the exposed surfaces of the overpack is determined based on 12-hour insolation levels recommended in 10CFR71 (averaged over a 24-hour period) and applied to the most adversely located cask after accounting for partial blockage of incident solar radiation on the lateral surfaces of the cask by surrounding casks. The blocking factor is identical to the radiative blocking considered for cooling of outside surfaces to the ambient environment. This is conservative compared to the case of an isolated cask with significantly improved radiative cooling and higher insolation levels because the cask is emitting much more heat than the insolation heat input. The imposed steady insolation level for the exposed top lid is based on a view factor equal to unity. The solar absorptivity of all exposed cask surfaces is assumed to be a conservatively bounding value of unity.

4.4.1.1.9 Effective Thermal Conductivity of Holtite Neutron Shielding Region

In order to minimize heat transfer resistance limitations due to the poor thermal conductivity of the Holtite-A neutron shield material, a large number of thick radial channels of high strength and conductivity carbon steel material are embedded in the neutron shield region. The legs of the radial channels form highly conducting heat transfer paths for efficient heat removal. Each channel leg is welded to the outside surface of the outermost intermediate shell. Enclosure shell panels are welded to the radial channels to form the external wall of the overpack, and thus provide a continuous path for heat removal to the ambient environment.

The effective thermal conductivity of the composite neutron shield and the network of radial channel legs is determined by combining the heat transfer resistance of individual components in a parallel network. In determining the heat transfer capability of this region to the outside ambient environment for normal long-term storage conditions, no credit is taken for conduction through the neutron shielding material. Thus, heat transport from the outer intermediate shell surface to the overpack outer shell is conservatively based on heat transfer through the carbon steel radial connectors alone. Thermal conductivity of the parallel neutron shield and radial channel leg region is given by the following formula:

$$K_{ne} = \frac{K_r N_r t_r \ell n\left(\frac{r_B}{r_A}\right)}{2\pi \ell_R} + \frac{K_{ns} N_r t_{ns} \ell n\left(\frac{r_B}{r_A}\right)}{2\pi \ell_R}$$

where (in consistent U.S. units):

K_{ne} = effective thermal conductivity of Holtite region

r_A = inner radius of neutron shielding

r_B = outer radius of neutron shielding

K_r = effective thermal conductivity of carbon steel radial channel leg

N_r = total number of radial channel legs (also equal to number of neutron shield sections)

t_r = minimum (nominal) thickness of each radial channel leg

ℓ_R = effective radial heat transport length through radial channel leg

K_{ns} = neutron shield thermal conductivity

t_{ns} = neutron shield thickness (between two radial channel legs)

The radial channel-to-outer intermediate shell surface weld thickness is equal to half the plate thickness. The additional weld resistance is accounted for by reducing the plate thickness in the weld region for a short radial span equal to the weld size. As a result, the conductivity of the radial carbon steel connectors based on full thickness for the entire radial span is reduced. Figure 4.4.7 depicts a resistance network developed to combine the neutron shield and radial connectors resistances to determine an effective conductivity of the neutron shield region. Note that in the resistance network analogy, only the annulus region between overpack outer enclosure inner surface and intermediate shells outer surface is considered in this analysis. The effective thermal conductivity of the neutron shield/radial channel leg region is provided in Table 4.4.8.

4.4.1.1.10 Effective Thermal Conductivity of Flexible MPC Basket-to-Shell Aluminum Heat Conduction Elements

As shown in HI-STAR 100 System MPC drawings in Section 1.5, flexible full-length heat conduction elements fabricated from thin aluminum alloy 1100 sheet metal are inserted in the large MPC basket-to-shell gaps to provide uninterrupted metal pathways to transport heat from the basket to the MPC shell. Due to the high thermal conductivity of aluminum alloy 1100 (about 15 times that of Alloy X), a significant rate of heat transfer is possible along thin flexible plates. Flexibility of the heat conduction elements is an important asset to enable a snug fit in the confined spaces and for ease of installation. Figure 4.4.13 shows the mathematical idealization of

a typical conduction element inserted in a basket periphery panel-to-MPC shell space. The aluminum heat conduction element is shown to cover the MPC basket Alloy X peripheral panel and MPC shells (Regions I and III depicted in Figure 4.4.13) surfaces along the full-length of the basket except for isolated locations where fitup or interference with other parts precludes complete basket coverage. Heat transport to and from the aluminum heat conduction element is conservatively postulated to occur across a thin helium gap as shown in the figure (i.e., no credit is taken for aluminum heat conduction element to Alloy X metal-to-metal contact). Aluminum surfaces inside the hollow region are sandblasted prior to fabrication to result in a rough surface finish which has a significantly higher emissivity compared to smooth surfaces of rolled aluminum. The untreated aluminum surfaces directly facing Alloy X panels have a smooth finish to minimize contact resistance.

Net heat transfer resistance from the hot basket periphery panel to the relatively cooler MPC shell along the aluminum heat conduction element pathway is a sum of three individual resistances in regions labeled I, II, and III as shown in Figure 4.4.13. In Region I, heat is transported from the basket to the aluminum heat conduction element surface directly facing the basket panel across a thin helium resistance gap. Longitudinal transport of heat (in the z direction) in the aluminum plate (in Region I) will result in an axially non-uniform temperature distribution. Longitudinal one-dimensional heat transfer in the Region I aluminum plate was analytically formulated to result in the following ordinary differential equation for the non-uniform temperature distribution:

$$t\, K_{A\ell}\, \frac{\partial^2 T}{\partial z^2} = -\frac{K_{He}}{h}\,(T_h - T) \qquad \text{(Equation a)}$$

Boundary Conditions

$$\frac{\partial T}{\partial z} = 0 \text{ at } z = 0$$

$$T = T_h' \text{ at } z = P \qquad \text{(Equation b)}$$

where (see Figure 4.4.13):

$T(z)$ = non-uniform aluminum metal temperature distribution

t = heat conduction element thickness

K_{Al} = heat conduction element conductivity

K_{He} = helium conductivity

h = helium gap thickness

T_h = hot basket temperature

T_h' = heat conduction element Region I boundary temperature at $z = P$

P = heat conduction element Region I length

W = conduction element Region II length

Solution of this ordinary differential equation subject to the imposed boundary condition is:

$$(T_h - T) = (T_h - T_h') \left[\frac{e^{\frac{z}{\sqrt{\alpha}}} + e^{-\frac{z}{\sqrt{\alpha}}}}{e^{\frac{P}{\sqrt{\alpha}}} + e^{-\frac{P}{\sqrt{\alpha}}}} \right] \qquad \text{(Equation c)}$$

where α is a dimensional parameter equal to $(h \times t \times K_{Al}/K_{he})$. The net heat transfer (Q_I) across the Region I helium gap can be determined by the following integrated heat flux to a heat conduction element of length L as:

$$Q_I = \int_0^P \frac{K_{He}}{h} (T_h - T) (L) \, dz \qquad \text{(Equation d)}$$

Substituting the analytical temperature distribution result obtained in Equation c, the following expression for net heat transfer is obtained:

$$Q_I = \frac{K_{He} L \sqrt{\alpha}}{h} \left(1 - \frac{1}{e^{\frac{P}{\sqrt{\alpha}}} + e^{-\frac{P}{\sqrt{\alpha}}}} \right) (T_h - T_h') \qquad \text{(Equation e)}$$

Based on this result, an expression for Region I resistance is obtained as shown below:

$$R_I = \frac{T_h - T_{h'}}{Q_I} = \frac{h}{K_{He} L \sqrt{\alpha}} \left(1 - \frac{1}{e^{\frac{P}{\sqrt{\alpha}}} + e^{-\frac{P}{\sqrt{\alpha}}}} \right)^{-1} \qquad \text{(Equation f)}$$

The Region II resistance expression can be developed from the following net heat transfer equation in the vertical leg of the conduction element as shown below:

$$Q_{II} = \frac{K_{Al} L t}{W} (T_h' - T_c') \qquad \text{(Equation g)}$$

$$R_{II} = \frac{T_h' - T_c'}{Q_{II}} = \frac{W}{K_{Al} L t} \qquad \text{(Equation h)}$$

Similarly, a Region III resistance expression can be analytically determined as shown below:

$$R_{III} = \frac{(T_c' - T_c)}{Q_{III}} = \frac{h}{K_{He} L \sqrt{\alpha}} \left(1 - \frac{1}{e^{\frac{P}{\sqrt{\alpha}}} + e^{-\frac{P}{\sqrt{\alpha}}}} \right)^{-1} \qquad \text{(Equation i)}$$

This completes the analysis for the total thermal resistance attributable to the heat conduction elements, equal to the sum of the three individual resistances. The total heat conduction element

resistance is smeared across the basket-to-MPC shell region as an effective uniform annular gap conductivity (see Figure 4.4.2). We note that heat transport along the conduction elements is an independent conduction path in parallel with conduction and radiation mechanisms in the large helium gaps. Helium conduction and radiation in the MPC basket-to-MPC shell peripheral gaps is accounted for separately in the ANSYS models for the MPCs, described earlier. Therefore, the total MPC basket-to-MPC shell peripheral gaps conductivity will be the sum of the heat conduction elements effective conductivity and the helium gap conduction-radiation effective conductivity.

4.4.1.1.11 FLUENT Model for HI-STAR 100 Temperature Field Computation

In the preceding subsection, a series of analytical and numerical models to define the thermal characteristics of the various elements of the HI-STAR 100 System are presented. The thermal modeling begins with the replacement of the SNF cross section and surrounding fuel cell space with a solid region with an equivalent conductivity. Since radiation is an important constituent of the heat transfer process in the SNF/storage cell space, and the rate of radiation heat transfer is a strong function of the surface temperatures, it is necessary to treat the equivalent region conductivity as a function of temperature. Because of the relatively large range of temperatures in a loaded HI-STAR 100 System under the design basis heat loads, the effects of variation in the thermal conductivity of materials with temperature throughout the system model are included. The presence of significant radiation effects in the storage cell spaces adds to the imperative to treat the equivalent storage cell lamina conductivity as temperature-dependent.

FLUENT finite volume simulations have been performed to establish the equivalent thermal conductivity as a function of temperature for the limiting (thermally most resistive) BWR and PWR spent fuel types. Utilizing the limiting SNF (established through a simplified analytical process for comparing conductivities) ensures that the numerical idealization for the fuel space effective conductivity is conservative for all non-limiting fuel types.

Having replaced the fuel spaces by solid square blocks with temperature-dependent conductivity essentially renders the basket into a non-homogeneous three-dimensional solid where the non-homogeneity is introduced by the honeycomb basket structure. The basket panels themselves are a composite of Alloy X cell wall, Boral neutron absorber, and Alloy X sheathing metal. A conservative approach to replace this composite section with an equivalent "solid wall" was described earlier.

In the next step, a planar section of the MPC is considered. The MPC contains a non-symmetric basket lamina wherein the equivalent fuel spaces are separated by the "equivalent" solid metal walls. The space between the basket and the MPC, called the peripheral gap, is filled with helium gas and aluminum heat conduction elements (shown in the MPC drawings in Section 1.5). The equivalent thermal conductivity of the MPC section is computed using a finite element procedure on ANSYS. To the "helium conduction-radiation" based peripheral gap conductivity, the effective conductivity of the aluminum conduction elements is added to obtain a combined peripheral gap effective conductivity. At this stage in the thermal analysis, the SNF/basket/MPC assemblage has been replaced with a two-zone (Figure 4.4.2) cylindrical solid whose thermal conductivity is a strong function of temperature.

The idealization for the overpack is considerably more straightforward. The overpack is radially symmetric except for the neutron absorber (Holtite-A) region (Figure 4.4.7). The procedure to replace the multiple shell layers, Holtite-A and radial connectors with an equivalent solid utilizes classical heat conduction analogies, as discussed in Sections 4.4.1.1.6 and 4.4.1.1.9.

In the final step of the analysis, the equivalent two-zone MPC cylinder, equivalent overpack shell, top and bottom plates, and ISFSI pad are assembled into a comprehensive finite volume model. A cross section of this axisymmetric model implemented on FLUENT is shown in Figure 4.4.15. A summary of the essential features of this model is presented in the following:

- The overpack shell is represented by 840 axisymmetric elements.
- The overpack bottom plate and bolted closure plate are modeled by 312 axisymmetric elements.
- The two-zone MPC "solid" (including the baseplate, lid and shell) is represented by 1188 axisymmetric elements.
- The ISFSI pad is conservatively modeled as a thermal resistance from a 36" thick concrete cylinder whose bottom surface is at 60°F. The portion of the concrete outside the footprint of the cask is conservatively omitted from the model.
- The space between the MPC and the overpack interior inner surface contains helium.
- Heat input due to insolation is applied to the top surface and the cylindrical surface of the overpack.
- The heat generation in the MPC is assumed to be uniform in each horizontal plane, but to vary in the axial direction to correspond to the axial power distribution listed in Table 2.1.8.
- The most disadvantageously placed cask in a HI-STAR cask array (i.e., the one subjected to maximum radiative blockage (see Subsection 4.4.1.1.7), is modeled.

The emissivity applied to the external surfaces of the HI-STAR model accounts for radiation-blockage of the outer enclosure surface and no blockage for the overpack closure plate top surface.

The finite element model constructed in this manner will produce an axisymmetric temperature distribution. The peak temperature will occur at the centerline and is expected to occur at the axial location of peak heat generation. As we will see later, the results from the finite volume solution bear out these observations.

4.4.1.1.12 MPC Temperature Distribution Under Vacuum Conditions

The initial loading of SNF in the MPC requires that the water within the MPC be drained and replaced with helium. This operation on the HI-STAR MPCs will be carried out using a conventional vacuum drying approach. In this method, removal of the last traces of residual moisture from the MPC cavity is accomplished by evacuating the MPC for a short time after draining the MPC.

Prior to the start of the MPC draining operation, both the overpack annulus and the MPC are full of water. The presence of water in the MPC ensures that the fuel cladding temperatures are lower than design basis limits by large margins. As the heat generating active fuel length is uncovered during the draining operation, the fuel and basket mass will undergo a gradual heat up from the initially cold conditions when the heated surfaces were submerged under water.

Thermal analysis of the MPC basket for bounding design basis decay heat loads is performed on the ANSYS finite element code. The ANSYS model is constructed to evaluate the heat rejection ability of the basket under evacuated conditions. The vacuum condition effective fuel assembly conductivity is determined by procedures discussed earlier (Subsection 4.4.1.1.2) after setting the thermal conductivity of the gaseous medium to a small fraction (one part in one thousand) of helium conductivity in the fuel assembly finite element model. Basket periphery-to-MPC shell heat transfer occurs through conduction and radiation. During draining and vacuum drying operations, the overpack annulus is required to be kept filled with water. Thus, the MPC thermal analysis problem is formulated with cooling of the MPC shell with water, which under worst case conditions would be slightly higher than its normal boiling temperature at the bottom of the overpack annulus. Results of vacuum condition analyses are provided in Subsection 4.4.2.2.

4.4.1.1.13 Effect of Fuel Cladding Crud Resistance

In this subsection, a conservatively bounding estimate of temperature drop across a crud film adhering to a fuel rod during dry storage conditions is determined. The evaluation is performed for a BWR fuel assembly based on an upper bound crud thickness obtained from the PNL-4835 report ([4.3.4], Table 3). The crud present on the fuel assemblies is predominately iron oxide mixed with small quantities of other metals such as cobalt, nickel, chromium, etc. Consequently, the effective conductivity of the crud mixture is expected to be in the range of typical metal alloys. However, in the interest of extreme conservatism, the crud layer thickness is replaced by a film of helium. The calculation is performed in two steps. In the first step, a crud film resistance is determined based on bounding maximum film on the fuel rod surfaces. This is followed by a peak local cladding heat flux calculation for the GE 7×7 array fuel assembly postulated to emit a conservatively bounding decay heat equal to 0.5kW. The temperature drop across the crud film obtained as a product of the heat flux and crud resistance terms is determined to be less than 0.1°F. The calculations are presented below.

Bounding Crud Thickness(s) (PNL-4835)	=	130μm (4.26×10^{-4} ft)
Crud Conductivity (K) (Conservative Assumption)	=	0.1 Btu/ft-hr-°F

GE 7×7 Fuel Assembly:

Rod O.D.	=	0.563"
Active Fuel Length	=	150"
Heat Transfer Area	=	$(7\times7)\ (\pi\times0.563)\times 150/144$
	=	$90.3\ ft^2$
Axial Peaking Factor	=	1.195 (Burnup distribution Table 2.1.8)
Decay Heat (Conservative Assumption)	=	500W

$$\text{Crud Resistance} = \frac{\delta}{K} = \frac{4.26\times10^{-4}}{0.1} = 4.26\times10^{-3}\ \frac{ft^2\text{-}hr\text{-}^\circ F}{Btu}$$

$$\text{Peak Heat Flux} = \frac{(500\times3.417)\ Btu/hr}{90.3\ ft^2}\times 1.195 = 22.6\ \frac{Btu}{ft^2\ hr}$$

$\therefore$ Temperature drop (ΔT_c) across crud film

$$= 4.26\times10^{-3}\ \frac{ft^2\text{-}hr\text{-}^\circ F}{Btu}\times 22.6\ \frac{Btu}{ft^2\text{-}hr} = 0.096^\circ F$$

(i.e., less than $0.1^\circ F$)

Therefore, it is concluded that deposition of crud does not materially change the SNF cladding temperature.

4.4.1.1.14 Maximum Time Limit During Wet Transfer

In accordance with NUREG-1536, water inside the MPC cavity during wet transfer operations is not permitted to boil in the HI-STAR 100 System. Consequently, uncontrolled pressures in the de-watering, purging, and recharging system which may result from two-phase condition, are completely avoided. This requirement is accomplished by imposing a limit on the maximum allowable time duration for fuel to be submerged in water after a loaded HI-STAR cask is removed from the pool and prior to the start of vacuum drying operations.

When the HI-STAR overpack and the loaded MPC under water-flooded conditions are removed from the pool, the combined mass of the water, the fuel, the MPC, and the HI-STAR will absorb the decay heat emitted by the fuel assemblies. This results in a slow temperature rise of the entire system with time, starting from an initial temperature of the contents. The rate of temperature rise is limited by the thermal inertia of the HI-STAR system. To enable a bounding heat-up rate determination for the HI-STAR system, the following conservative assumptions are imposed:

i. Heat loss by natural convection and radiation from the exposed HI-STAR

surfaces to the pool building ambient air is neglected (i.e., an adiabatic temperature rise calculation is performed).

ii. Design Basis maximum decay heat input from the loaded fuel assemblies is imposed on the HI-STAR system.

iii. The smallest of the minimum MPC cavity-free volumes among the two MPC types is considered for flooded water mass determination.

iv. Fifty percent of the water mass in the MPC cavity is credited towards water thermal inertia evaluation.

Table 4.4.20 summarizes the weights and thermal inertias of several components in the loaded HI-STAR system. The rate of temperature rise of the HI-STAR and its contents during an adiabatic heat-up is governed by the following equation:

$$\frac{dT}{dt} = \frac{Q}{C_h}$$

where:

Q = decay heat load (Btu/hr)
[equal to Design Basis maximum (among the two MPC types) 19.0 kW (i.e., 64,847 Btu/hr)]

C_h = combined thermal inertia of the loaded HI-STAR system (Btu/°F)

T = temperature of the contents (°F)

t = time after HI-STAR system is removed from the pool (hr)

A bounding heat-up rate for the HI-STAR system contents is determined to be equal to 2.08°F/hr. From this adiabatic rate of temperature rise estimate, the maximum allowable time duration (t_{max}) for fuel to be submerged in water is determined as follows:

$$t_{max} = \frac{T_{boil} - T_{initial}}{(dT/dt)}$$

where:

T_{boil} = boiling temperature of water
(equal to 212°F at the water surface in the MPC cavity)

$T_{initial}$ =initial temperature of the HI-STAR contents when removed from the pool

Table 4.4.21 provides a summary of t_{max} at several initial HI-STAR contents temperatures.

As set forth in the HI-STAR 100 operating procedures, in the unlikely event where the maximum allowable time provided in Table 4.4.21 is found to be insufficient to complete all wet transfer operations, a forced water circulation shall be initiated and maintained to remove the decay heat from the MPC cavity. In this case, relatively cooler water will enter via the MPC lid drain port connection and heated water will exit from the vent port. The minimum water flow rate required to maintain the MPC cavity water temperature below boiling with an adequate subcooling margin is determined as follows:

$$M_W = \frac{Q}{C_{pw}\,(T_{max} - T_{in})}$$

where:

M_W = minimum water flow rate (lb/hr)

C_{pw} = water heat capacity (Btu/lb-°F)

T_{max} = maximum MPC cavity water mass temperature

T_{in} = temperature of water supply to MPC

With the MPC cavity water temperature limited to 150°F, MPC inlet water maximum temperature equal to 125°F and at the design basis maximum heat load, the water flow rate is determined to be 2,594 lb/hr (5.3 gpm).

4.4.1.1.15 Cask Cooldown and Reflood Analysis During Fuel Unloading Operation

NUREG-1536 requires an evaluation of cask cooldown and reflood procedures to support fuel unloading from a dry condition. Past industry experience generally supports cooldown of cask internals and fuel from hot storage conditions by direct water quenching. However, the extremely rapid cooldown rates that are typical during water injection, to which the hot cask internals and fuel cladding are subjected to, may result in uncontrolled thermal stresses and failure in the structural members. Moreover, water injection results in large amounts of steam generation and unpredictable transient two-phase flow conditions inside the MPC cavity, which may result in over-pressurization of the confinement boundary and a potentially unacceptable reduction in the safety margins to prevent criticality. To avoid potential safety concerns related

to rapid cask cooldown by direct water quenching, the HI-STAR MPCs are designed to be cooled in a gradual manner, thereby eliminating thermal shock loads on the cask internals and fuel cladding.

In the unlikely event that a HI-STAR system is required to be unloaded, it will be transported back to the fuel handling building. Prior to reflooding the MPC cavity with water, a forced flow helium recirculation system with adequate flow capacity shall be operated to remove the decay heat and initiate a slow cask cooldown lasting for several days. The operating procedures in Chapter 8 (Section 8.3) provide a detailed description of the steps involved in the cask unloading. In this section, an analytical evaluation is presented to provide the basis for helium flow rates and time of forced cooling to meet the objective of eliminating thermal shock when the MPC cavity is eventually flooded with water.

Under a closed loop forced helium circulation condition, the helium gas is cooled via an external chiller, down to 100°F, and then introduced inside the MPC cavity from the drain line near the bottom baseplate. The helium gas enters the MPC basket from the bottom oversized flow holes and moves upwards through the hot fuel assemblies, removing heat and cooling the MPC internals. The heated helium gas exits from the basket top and collects in the top plenum, from where it is expelled through the MPC lid vent connection to the helium recirculation and cooling system. The MPC contents bulk average temperature reduction as a function of time is principally dependent upon the rate of helium circulation. The temperature transient is governed by the following heat balance equation

$$C_h \frac{dT}{dt} = Q_D - m\, C_p\, (T - T_i) - Q_c$$

Initial Condition: $T = T_o$ at $t = 0$

where:

T = MPC bulk average temperature (°F)

T_o = initial MPC bulk average temperature in the HI-STAR system (equal to 439°F)

t = time after start of forced circulation (hrs)

Q_D = decay heat load (Btu/hr) (equal to Design Basis maximum 19.0 kW (i.e., 64,847 Btu/hr))

m = helium circulation rate (lb/hr)

C_p = helium heat capacity (Btu/lb-°F) (equal to 1.24 Btu/lb-°F)

Q_c = heat rejection from cask exposed surfaces to ambient (Btu/hr) (conservatively

neglected)

C_h = thermal capacity of the loaded MPC (Btu/°F)

(For a bounding upper bound 100,000 lb loaded MPC weight, and heat capacity of Alloy X equal to 0.12 Btu/lb-°F, the heat capacity is equal to 12,000 Btu/°F.)

T_i = MPC helium inlet temperature (°F)

The differential equation is analytically solved, yielding the following expression for time-dependent MPC bulk temperature.

$$T(t) = (T_i + \frac{Q_D}{m\ C_p})\ (1 - e^{-\frac{m\ C_p}{C_h}t}) + T_o\ e^{-\frac{m\ C_p}{C_h}t}$$

This equation is used to determine the minimum helium mass flow rate which would cool the MPC cavity down from initially hot conditions to less than 200°F in 72 hours. The required helium mass flow rate is 546 lb/hr (i.e., 817 SCFM).

Once the helium gas circulation has cooled the MPC internals to less than 200°F, water can be injected to the MPC without risk of boiling and the associated thermal stress concerns. Because of the relatively long cooldown period, the thermal stress contribution to the total cladding stress would be negligible, and the total stress would therefore be bounded by the normal (dry) condition. The elimination of boiling eliminates any concern of over-pressurization due to steam production.

4.4.1.1.16 HI-STAR Temperature Field With Low Emitting Fuel

The HI-STAR 100 thermal evaluations for BWR fuel are divided in two groups of fuel assemblies proposed for storage in MPC-68. These groups are classified as Low Heat Emitting (LHE) fuel assemblies and Design Basis (DB) fuel assemblies. The LHE group of fuel assemblies are characterized by low burnup, long cooling time, and short active fuel lengths. Consequently, their heat loads are dwarfed by the DB group of fuel assemblies. The Dresden-1 (6x6 and 8x8), Quad+, and Humboldt Bay (7x7 and 6x6) fuel characteristics warrant their classification as LHE fuel. These characteristics, including burnup and cooling time limits imposed on this class of fuel, are presented in Table 2.1.6. This fuel (except Quad$^+$) is permitted to be loaded when encased in Damaged Fuel Containers (DFCs). As a result of interruption of radiation heat exchange between the fuel assembly and the fuel basket by the DFC boundary, this loading configuration is bounding for thermal evaluation. In Subsection 4.4.1.1.2, two canister designs for encasing LHE fuel are evaluated – a previously approved Holtec Design (Holtec Drawing-1783) and an existing canister in which some of the Dresden-1 fuel is currently stored (Transnuclear D-1 canister). The most resistive fuel assembly determined by analytical evaluation is considered for thermal evaluation (see Table 4.4.6). The MPC-68 basket effective conductivity, loaded with the most resistive fuel assembly from the LHE group of fuel (encased in a canister) is provided in Table 4.4.7. To this basket, LHE decay heat load is applied and a HI-STAR 100 System temperature field obtained. The low heat load burden limits the initial peak

cladding temperature to 595°F which is substantially below the temperature limit for long-cooled fuel (~643°F).

A thoria rod canister designed to hold a maximum of 20 fuel rods arrayed in a 5x4 configuration is currently stored at the Dresden-1 spent fuel pool. The fuel rods contain a mixture of enriched UO_2 and Thorium Oxide in the fuel pellets. The fuel rods were originally constituted as part of an 8x8 fuel assembly and used in the second and third cycle of Dresden-1 operation. The maximum fuel burnup of these rods is quite low (~14,400 MWD/MTU). The thoria rod canister internal design is a honeycomb structure formed from 12 gage stainless steel plates. The rods are loaded in individual square cells and are isolated from each other by the cell walls. The few number of rods (18 per assembly) and very low burnup of fuel stored in these Dresden-1 canisters render them as miniscule sources of decay heat. The canister all-metal internal honeycomb construction serves as an additional means of heat dissipation in the fuel cell space. In accordance with preferential fuel loading requirements imposed in the Technical Specifications, low burnup fuel shall be loaded toward the basket periphery (i.e., away from the hot central core of the fuel basket). All these considerations provide ample assurance that these fuel rods will be stored in a benign thermal environment and therefore remain protected during long-term storage.

4.4.1.2 Test Model

A detailed analytical model for thermal design of the HI-STAR 100 System was developed using the FLUENT CFD code and the industry standard ANSYS modeling package, as discussed in Subsection 4.4.1.1. As discussed throughout this chapter and specifically in Section 4.4.6, the analysis incorporates significant conservatisms so as to predict the fuel cladding temperature with considerable margins. Furthermore, compliance with specified limits of operation is demonstrated with adequate margins. In view of these considerations, the HI-STAR 100 System thermal design complies with the thermal criteria set forth in the design basis (Sections 2.1 and 2.2) for long-term storage under normal conditions. Additional experimental verification of the thermal design is therefore not required.

4.4.2 Maximum Temperatures

4.4.2.1 Maximum Temperatures Under Normal Storage Conditions

The two MPC basket designs developed for the HI-STAR 100 System have been analyzed to determine the temperature distribution under long-term normal storage conditions. The MPC baskets are considered to be loaded at design basis maximum heat loads with PWR or BWR fuel assemblies, as appropriate. The systems are considered to be arranged in an ISFSI array and subjected to design basis normal ambient conditions with insolation.

Applying the radiative blocking factor applicable for the worst case cask location, converged temperature contours are shown in Figures 4.4.17 and 4.4.18 for the MPC-24, and MPC-68 basket designs. The temperatures in these two figures are in degrees Kelvin. The calculated

temperatures presented in this chapter are based on an array of analyses that incorporate many

conservatisms. As such, the calculated temperatures are upper bound values which would exceed actual temperatures.

The maximum fuel clad temperatures for zircaloy clad fuel assemblies are listed in Tables 4.4.10 and 4.4.11, which also summarize maximum calculated temperatures in different parts of the HI-STAR 100 System. Figures 4.4.21 and 4.4.22 show the axial temperature variation of the hottest fuel rod in the MPC-24 and MPC-68 basket designs, respectively. Figures 4.4.24 and 4.4.25 show the radial temperature profile in the MPC-24 and MPC-68 basket designs, respectively, in the horizontal plane where maximum fuel cladding temperature is indicated.

As discussed in Subsection 4.4.1.1.1, the thermal analysis is performed using a submodeling process where the results of an analysis on an individual component are incorporated into the analysis of a larger set of components. Specifically, the submodeling process yields directly computed fuel temperatures from which fuel basket temperatures are indirectly calculated. This modeling process differs from previous analytical approaches wherein the basket temperatures were evaluated first and then a basket-to-cladding temperature difference calculation by Wooten-Epstein or other means provided a basis for cladding temperatures. Subsection 4.4.1.1.2 describes the calculation of an effective fuel assembly thermal conductivity for an equivalent homogenous region. It is important to note that the result of this analysis is a function for thermal conductivity versus temperature. This function for fuel thermal conductivity is then input to the fuel basket effective thermal conductivity calculation described in Subsection 4.4.1.1.4. This calculation uses a finite-element methodology, wherein each fuel cell region containing multiple finite-elements has temperature varying thermal conductivity properties. The resultant temperature varying fuel basket thermal conductivity computed by this basket-fuel composite model is then input to the fuel basket region of the FLUENT cask model.

Because the FLUENT cask model incorporates the results of the fuel basket submodel, which in turn incorporates the fuel assembly submodel, the peak temperature reported from the FLUENT model is the peak temperature in any component. In a dry storage cask, the hottest components are the fuel assemblies. It should be noted that, because the fuel assembly models described in Subsection 4.4.1.1.2 include the fuel pellets, the FLUENT calculated peak temperatures reported in Tables 4.4.10 and 4.4.11 are actually peak pellet centerline temperatures which bound the peak cladding temperatures. We conservatively assume that the peak clad temperature is equal to the peak pellet centerline temperature.

The following additional observations can be derived by inspecting the temperature field obtained from the finite volume analysis:

- The maximum fuel cladding temperature is well within the PNL [4.3.1] and the LLNL [4.3.6] recommended temperature limits.

- The maximum temperature of the basket structural material is within the stipulated Design Temperature.

- The maximum temperature of the Boral neutron absorber is below the material supplier's recommended limit.

- The maximum temperatures of the MPC pressure boundary materials are well below their respective ASME Code limits.

- The maximum temperatures of the overpack pressure boundary material are well below their respective ASME Code limits.

- The neutron shielding material (Holtite-A) will not experience temperatures in excess of its qualified limit.

- The local temperatures of the mechanical seals are well below their respective long-term limits (Table 4.3.1).

Noting that the allowable maximum initial peak cladding temperature is significantly lower for older fuel, parametric peak fuel cladding temperature versus total decay heat load tables for each of the two basket designs were developed. This lower than design basis heat load performance data is presented in Tables 4.4.18 and 4.4.19. The decay heat limit curve in Figure 2.1.8 is developed based on these tables and the allowable fuel cladding temperature limits listed in Table 2.2.3.

The above observations lead us to conclude that the temperature field in the HI-STAR 100 System with a fully loaded MPC containing design-basis heat emitting SNF complies with all regulatory and industry temperature limits. In other words, the thermal environment in the HI-STAR 100 System will be conducive to long-term safe storage of spent nuclear fuel.

4.4.2.2 Maximum MPC Basket Temperature Under Vacuum Conditions

A plot of typical steady-state temperature contours under vacuum conditions is shown in Figure 4.4.19. The peak fuel clad temperature during short-term vacuum drying operations is limited to less than 950°F for both baskets at design basis maximum heat loads by a significant margin. This limit is lower than the recommended fuel cladding temperature (see Table 4.3.1) limits for short-term conditions by a large margin.

4.4.3 Minimum Temperatures

In Table 2.2.2 of this report, the minimum ambient temperature condition required to be considered for HI-STAR 100 System design is specified to be -40°F. If, conservatively, a zero decay heat load (with no solar input) is applied to the stored fuel assemblies then every component of the system at steady state would be at this minimum ambient temperature. All HI-STAR 100 System materials of construction would satisfactorily perform their intended function in the storage mode at this minimum postulated temperature condition. Structural evaluations in Chapter 3 show the acceptable performance of the overpack and MPC steel material at low

temperature. Criticality and shielding functions of the

HI-STAR 100 System materials (Chapters 5 and 6) are unaffected by exposure to this minimum temperature.

4.4.4 Maximum Internal Pressure

The MPC is initially filled with helium after fuel loading and drying prior to installing the MPC closure ring. During normal storage, the gas temperature within the MPC rises to its maximum operating basis temperature as determined based on the thermal analysis methodology described earlier. The gas pressure inside the MPC will also increase with rising temperature. The pressure rise is determined using the ideal gas law which states that the absolute pressure of a fixed volume of confined gas is proportional to its absolute temperature. In Tables 4.4.13 and 4.4.14, a summary of calculations for determining the net free volume in the MPC-24 and MPC-68 are presented.

The maximum gas pressure in the MPC is considered for a postulated accidental release of fission product gases caused by fuel rods rupture. For these fuel rod rupture conditions, the amounts of each of the release gas constituents in the MPC cavity are summed and the resulting total pressures determined from the Ideal Gas Law. Based on fission gases release fractions (per NUREG-1536 criteria [4.1.3]), minimum net free volume and maximum initial fill gas pressure, bounding maximum gas pressures with 1% (normal), 10% (off-normal), and 100% (accident condition) rod rupture are given in Table 4.4.15. The MPC maximum gas pressures listed in Table 4.4.15 are all below the MPC design internal pressure listed in Table 2.2.1.

The inclusion of PWR non-fuel hardware (BPRA control elements and thimble plugs) to the MPC-24 influences the internal pressure in two ways. The presence of non-fuel hardware enhances heat dissipation, thus lowering fuel temperatures and the gas filling the space between fuel rods. The gas volume displaced by the mass of non-fuel hardware lowers the cavity free volume. These two effects, namely, temperature lowering and free volume reduction, have opposing influence in the MPC cavity pressure. The first effect lowers gas pressure while the second effect raises it. In the HI-STAR thermal analysis, the computed temperature field (with non-fuel hardware excluded) provides a conservatively bounding MPC-24 temperature field. The MPC cavity free space is computed based on volume displacement by the heaviest fuel (bounding weight) with non-fuel hardware included).

During in-core irradiation of BPRAs, the B-10 isotope in the neutron absorbing material is transformed to helium atoms. Two different forms of the neutron absorbing material are used in BPRAs: Borasilicate glass and B_4C in a refractory solid matrix (Al_2O_3). Borosilicate glass (primarily a constituent of Westinghouse BPRAs) is used in the shape of hollow pyrex glass tubes sealed within steel rods and supported on the inside by a thin walled steel liner. To accommodate helium diffusion from the glass rod into the rod internal space, a relatively high void volume (~40%) is engineered in this type of rod design. The rod internal pressure is thus designed to remain below reactor operating conditions (2,300 psia and approximately 600°F coolant temperature). The B_4C- Al_2O_3 neutron absorber material is principally used in B&W and

CE fuel BPRA designs. The relatively low temperature of the poison material in BPRA rods (relative to fuel pellets) favor the entrapment of helium atoms in the solid matrix.

Several BPRA designs are used in PWR fuel which differ in the number, diameter, and length of poison rods. The older Westinghouse fuel (W-14x14 and AW-15x15) has used 6,12, 16, and 20 rods per assembly BPRAs and the later (W-17x17) fuel uses up to 24 rods per BPRA. The BPRA rods in the older fuel are much larger than the later fuel and, therefore, the B-10 isotope inventory in the 20-rod BPRAs bound the newer W-17x17 fuel. Based on bounding BPRA rods internal pressure, a large hypothetical quantity of helium (7.2 g-moles/BPRA) is assumed to be available for release into the MPC cavity from each fuel assembly in the MPC-24. To accommodate this quantity of helium gas[†] at the NUREG-1536 stipulated rods rupture assumptions, the initial helium backfill in the MPC-24 is reduced such that the final confinement boundary pressures are approximately unchanged from inclusion of non-fuel hardware. The MPC cavity pressures are summarized in Table 4.4.15

4.4.5 Maximum Thermal Stresses

Thermal expansion induced mechanical stresses due to the non-uniform temperature distribution are reported in Chapter 3. Table 4.4.16 provides a summary of HI-STAR 100 System component temperature inputs for structural evaluation.

Table 4.4.22 provides a summary of confinement boundary temperatures during normal storage conditions. Structural evaluation in Section 3.4.4 references these temperature results to demonstrate confinement boundary integrity.

4.4.6 Evaluation of System Performance for Normal Conditions of Storage

The HI-STAR 100 System thermal analysis is based on a detailed and complete heat transfer model which properly accounts for radiation, conduction and natural convection modes of heat transfer in various portions of the MPC and overpack. The thermal model incorporates many conservative features that are listed below:

1. The most severe levels of environmental factors - bounding long-term annual ambient temperature with insolation - were coincidentally imposed on the HI-STAR 100 cask. A bounding solar absorbtivity of 1.0 was applied to all surfaces exposed to insolation.

2. No credit was considered for the thermosiphon heat transfer which is intrinsic to the HI-STAR fuel baskets.

3. The most adversely located HI-STAR 100 System in an ISFSI array was considered for analysis.

4. No credit was considered for conduction through the radial neutron shielding material.

[†] 3,875 liters of helium gas at STP from 100% BPRA rods rupture.

5. A uniform nominal radial gap between overpack-to-MPC was applied to the cask thermal model. No credit for gap reduction due to differential thermal expansion under the hot condition was considered. The MPC is considered to be in concentric alignment inside the overpack cavity. This is a worst case scenario since any eccentricity will improve conductive heat transport in this region.

6. Not Used.

7. Interfacial contact conductance of multilayered intermediate shell contacting layers was conservatively determined to bound surface finish, contact pressure, and base metal conductivity conditions.

8. No credit was considered for contact between fuel assemblies and the MPC basket wall or between the MPC basket and the basket supports. The fuel assemblies and MPC basket were conservatively considered to be in concentric alignment.

9. The MPC is assumed to be loaded with the SNF type which has the maximum equivalent thermal resistance of all fuel types in its category (BWR or PWR), as applicable.

10. The decay heat load, which is a function of burnup and decay time, varies in a narrow range within the group of PWR assemblies considered (Table 4.4.5) and also within the group of BWR assemblies considered (Table 4.4.6). The assembly type which gives the maximum decay heat load for a given burnup is used for defining the decay heat load vs. decay time. The B&W 15×15 is the limiting PWR SNF type (see Table 2.1.5). The governing BWR fuel is GE 7×7 (see Table 2.1.5). For other than the governing fuel types, there is a small conservatism in the decay heat load term.

11. The MPC basket axial conductivity is conservatively assumed to be equal to the lower basket cross sectional effective conductivity.

12. As discussed in Section 4.3, the NUREG-1536 endorsed DCCG [4.3.6] model yields temperature limits slightly higher (approximately 10°F) than the PNL [4.3.1] limits for allowable peak cladding temperature during storage. For conservatism, the lower PNL value (Table 2.2.3) is used as the permissible limit.

Temperature distribution results obtained from this conservative thermal model show that the established maximum fuel cladding temperature limits are met with adequate margins. Expected margins during normal storage will be larger due to the many conservative assumptions incorporated in the analysis. The long-term impact of decay heat induced temperature levels on the HI-STAR 100 System structural and neutron shielding materials is considered to be negligible. The maximum local MPC basket temperature level is below the recommended limits for structural materials in terms of susceptibility to stress, corrosion and creep induced degradation. Furthermore, structural evaluation (Chapter 3) has demonstrated that stresses (including those induced due to imposed temperature gradients) are within ASME B&PV Code limits. The maximum local neutron shield temperature is lower than design limits. Section 4.5

provides a discussion of compliance with regulatory criteria 1 through 8 listed in Section 4.0. The above-mentioned considerations lead to the conclusion that the HI-STAR 100 System thermal design is in compliance with 10CFR72 requirements.

Table 4.4.1

CLOSED CAVITY NUSSELT NUMBER RESULTS
FOR HELIUM-FILLED MPC PERIPHERAL VOIDS

Temperature [°F]	Nusselt Number (PWR Baskets)	Nusselt Number (BWR Basket)
200	3.17	2.41
450	2.56	1.95
700	2.21	1.68

Table 4.4.2

RELATIONSHIP BETWEEN HI-STAR 100 SYSTEM REGIONS
AND MATHEMATICAL MODEL DESCRIPTIONS

HI-STAR System Region	Mathematical Model	Subsections
Fuel Assembly	Fuel Region Effective Thermal Conductivity	4.4.1.1.2
MPC	Effective Thermal Conductivity of Boral/Sheathing/Box Wall Sandwich	4.4.1.1.3
	Basket In-Plane Conductive Heat Transport	4.4.1.1.4
	Heat Transfer in MPC Basket Peripheral Region	4.4.1.1.5
	Effective Thermal Conductivity of Flexible MPC Basket-to-Shell Aluminum Heat Conduction Elements	4.4.1.1.10
Overpack	Effective Conductivity of Multilayered Intermediate Shell Region	4.4.1.1.6
	Effective Thermal Conductivity of Holtite Neutron Shielding Region	4.4.1.1.9
Ambient Environment	Heat Rejection from Overpack Exterior Surfaces	4.4.1.1.7
	Solar Heat Input	4.4.1.1.8
Assembled Cask Model	Overview of the Thermal Model	4.4.1.1.1
	FLUENT Model for HI-STAR 100	4.4.1.1.11

Table 4.4.3

THIS TABLE IS INTENTIONALLY DELETED.

Table 4.4.4

THIS TABLE IS INTENTIONALLY DELETED.

Table 4.4.5

SUMMARY OF PWR FUEL ASSEMBLY EFFECTIVE THERMAL CONDUCTIVITIES

	Fuel	@ 200°F (Btu/ft-hr-°F)	@ 450°F (Btu/ft-hr-°F)	@ 700°F (Btu/ft-hr-°F)
1	W - 17×17 OFA	0.182	0.277	**0.402**
2	W - 17×17 Std	0.189	0.286	0.413
3	W - 17×17 Vantage	0.182	0.277	0.402
4	W - 15×15 Std	0.191	0.294	0.430
5	W - 14×14 Std	0.182	0.284	0.424
6	W - 14×14 OFA	**0.175**	**0.275**	0.413
7	B&W - 17×17	0.191	0.289	0.416
8	B&W - 15×15	0.195	0.298	0.436
9	CE - 16×16	0.183	0.281	0.411
10	CE - 14×14	0.189	0.293	0.435
11	HN† -15×15 SS	0.180	0.265	0.370
12	W-14×14 SS	0.170	0.254	0.361
13	B&W – 15x15	0.187	0.289	0.424
14	CE-14x14 (MP2)	0.188	0.293	0.434

Note: Boldface values denote the lowest thermal conductivity in each column.

† Haddam Neck B&W or Westinghouse stainless steel clad fuel assemblies.

Table 4.4.6
SUMMARY OF BWR FUEL ASSEMBLY EFFECTIVE
THERMAL CONDUCTIVITIES

	Fuel	@ 200°F (Btu/ft-hr-°F)	@ 450°F (Btu/ft-hr-°F)	@ 700°F (Btu/ft-hr-°F)
1	Dresden 1 - 8×8†	0.119	0.201	0.319
2	Dresden 1 - 6×6†	0.126	0.215	0.345
3	GE - 7×7	0.171	0.286	0.449
4	GE - 7×7R	0.171	0.286	0.449
5	GE - 8×8	0.168	0.278	0.433
6	GE - 8×8R	**0.166**	0.275	0.430
7	GE10 - 8×8	0.168	0.280	0.437
8	GE11 - 9×9	0.167	**0.273**	**0.422**
9	AC†† -10×10 SS	0.152	0.222	0.309
10	Exxon-10×10 SS	0.151	0.221	0.308
11	Humboldt Bay-7x7†	0.127	0.215	0.343
12	Dresden-1 Thin †Clad-6x6	0.124	0.212	0.343
13	Damaged Dresden-1 8×8† (in a damaged fuel container)	0.107	0.169	0.254
14	Damaged† Dresden-1 8x8 (in TN D-1 canister)	0.107	0.168	0.252
15	8x8 QUAD+ Westinghouse†	0.164	0.276	0.435

Note: Boldface values denote the lowest thermal conductivity in each column.

† Fuel cladding temperatures for low heat emitting (intact and damaged) fuel types in the HI-STAR 100 System will be bounded by design basis fuel cladding temperatures. Therefore, these fuel assembly types are excluded from the list of design basis fuel assemblies (Zircaloy clad) evaluated to determine the most resistive SNF type.

†† Allis-Chalmers stainless steel clad fuel assemblies.

Table 4.4.7

MPC BASKET EFFECTIVE THERMAL CONDUCTIVITY VALUES†

Basket	@200°F [Btu/ft-hr-°F]	@450°F [Btu/ft-hr-°F]	@700°F [Btu/ft-hr-°F]
MPC-24 (Zircaloy Clad Fuel)	1.108	1.495	1.954
MPC-68 (Zircaloy Clad Fuel)	0.959	1.188	1.432
MPC-24 (Stainless Steel Clad Fuel)	0.995	1.321	1.700 (a)
MPC-68 (Stainless Steel Clad Fuel)	0.931	1.125	1.311 (b)
MPC-68 (Dresden-1 8x8 in canister)	0.861	1.055	1.242

(a) Conductivity is 13% less than corresponding Zircaloy fueled basket.
(b) Conductivity is 9% less than corresponding Zircaloy fueled basket.

† The values reported in this table are conservatively understated.

Table 4.4.8

EFFECTIVE THERMAL CONDUCTIVITY OF THE NEUTRON SHIELD/RADIAL CHANNEL LEG REGION

Condition/Temperature (°F)	Thermal Conductivity (Btu/ft-hr-°F)
Normal condition:	
200	1.953
450	1.812
700	1.645
Fire condition:	
200	3.012
450	2.865
700	2.689

Table 4.4.9

THIS TABLE IS INTENTIONALLY DELETED.

Table 4.4.10

HI-STAR 100 SYSTEM LONG-TERM NORMAL STORAGE[†]
MAXIMUM TEMPERATURES [°F]
(24-PWR ASSEMBLIES, MPC)

	Maximum Temperature (°F)	Normal Condition Design Temperature (°F)
Fuel Cladding	709	720
MPC Basket Centerline	675	725
MPC Basket Periphery	451	725
MPC Outer Shell Surface	332	450
MPC/Overpack Helium Gap Outer Surface	292	400
Neutron Shield Inner Surface	274	300
Overpack Outer Enclosure Surface	229	350
Overpack Bolted Closure Plate[††]	155	400
Overpack Bottom Plate[††]	241	350

[†] Ambient Temperature = 80°F
Cask Array Pitch = 3 x Cask Radius = 12 ft.

[††] Overpack closure plate and vent/drain port plug seals normal condition design temperature is 400°F. The maximum seals temperatures are bounded by the reported closure plate and bottom plate maximum temperatures. Consequently, a large margin of safety exists to permit safe operation of seals in the overpack helium retention boundary.

Table 4.4.11

HI-STAR 100 SYSTEM LONG-TERM NORMAL STORAGE[†]
MAXIMUM TEMPERATURES [°F]
(68-BWR ASSEMBLIES, MPC)

	Maximum Temperature (°F)	Normal Condition Design Temperature (°F)
Fuel Cladding	741	749
MPC Basket Centerline	725	725
MPC Basket Periphery	393	725
MPC Outer Shell Surface	331	450
MPC/Overpack Helium Gap Outer Surface	292	400
Neutron Shield Inner Surface	273	300
Overpack Outer Enclosure Surface	228	350
Overpack Bolted Closure Plate[††]	155	400
Overpack Bottom Plate[††]	213	350

[†] Ambient Temperature = 80°F
Cask Array Pitch = 3 x Cask Radius = 12 ft.

[††] Overpack closure plate and vent/drain port plug seals normal condition design temperature is 400°F. The maximum seals temperatures are bounded by the reported closure plate and bottom plate maximum temperatures. Consequently, a large margin of safety exists to permit safe operation of seals in the overpack helium retention boundary.

Table 4.4.12

THIS TABLE IS INTENTIONALLY DELETED.

Table 4.4.13

SUMMARY OF MPC-24 FREE VOLUME CALCULATIONS

Item	Volume (ft^3)
Cavity Volume	367.9
Basket Metal Volume	37.9
Bounding Fuel Assemblies Volume	78.8
Basket Supports and Fuel Spacers Volume	6.1
Aluminum Conduction Elements	5.9†
Net Free Volume	237.5 (6,724 liters)

† Bounding 1,000 lbs weight.

Table 4.4.14

SUMMARY OF MPC-68 FREE VOLUME CALCULATIONS

Item	Volume (ft^3)
Cavity Volume	367.3
Basket Metal Volume	34.8
Bounding Fuel Assemblies Volume	93.0
Basket Supports and Fuel Spacers Volume	11.3
Aluminum Conduction Elements	5.9[†]
Net Free Volume	222.3 (6,294 liters)

[†] Bounding 1,000 lbs weight.

Table 4.4.15

SUMMARY OF MPC CONFINEMENT BOUNDARY PRESSURES[†] FOR NORMAL LONG-TERM STORAGE

Condition	Pressure (psig)
MPC-24[††]:	
Initial backfill (at 70°F)	22.2
Normal condition	43.8
With 1% rods rupture	44.3
With 10% rods rupture	49.1
With 100% rods rupture	97.3
MPC-68:	
Initial backfill (at 70°F)	28.5
Normal condition	57.5
With 1% rods rupture	57.8
With 10% rods rupture	60.2
With 100% rods rupture	84.6

[†] Pressure analysis is based on NUREG-1536 criteria (i.e., 100% of rods fill gas and 30% of radioactive gases are available for release from a ruptured rod).

[††] PWR fuel storage includes hypothetical BPRA rods rupture in the pressure calculations.

Table 4.4.16

SUMMARY OF HI-STAR 100 SYSTEM COMPONENTS
NORMAL STORAGE TEMPERATURES [°F]

Location	MPC-24	MPC-68
MPC Basket Top:		
Basket center	180	179
Basket periphery	168	168
MPC shell	166	167
Overpack inner shell	162	163
Overpack enclosure shell	159	160
MPC Basket Bottom:		
Basket center	251	220
Basket periphery	226	204
MPC shell	222	203
Overpack inner shell	218	201
Overpack enclosure shell	177	167

Table 4.4.17

THIS TABLE IS INTENTIONALLY DELETED.

Table 4.4.18

MPC-24 BASKET PEAK FUEL CLADDING TEMPERATURE AS A FUNCTION OF TOTAL HEAT LOAD

Total Basket Decay Heat Load (kW)	Peak Cladding Temperature (°F)
19.0†	708.8
18.5	696.9
17.0	660.1
15.5	621.9

† Design Basis Maximum (equivalent to 792 watts per assembly).

Table 4.4.19

MPC-68 BASKET PEAK CLADDING TEMPERATURE AS A FUNCTION OF TOTAL DECAY HEAT LOAD

Total Basket Decay Heat Load (kW)	Peak Cladding Temperature (°F)
18.5†	741.5
17.5	713.6
15.5	656.2

† Design Basis Maximum (equivalent to 272 watts per assembly).

Table 4.4.20

SUMMARY OF LOADED HI-STAR SYSTEM
BOUNDING COMPONENT WEIGHTS AND THERMAL INERTIAS

Component	Weight (lbs)	Heat Capacity (Btu/lb-°F)	Thermal Inertia (Btu/°F)
Holtite-A	11,000	0.39	4,290
Carbon Steel	140,000	0.1	14,000
Alloy-X MPC (empty)	35,000	0.12	4,200
Fuel	40,000	0.056	2,240
MPC Cavity Water†	6,500	1.0	6,500
			31,230 (Total)

† Based on smallest MPC-68 cavity net free volume with 50% credit for flooded water mass.

Table 4.4.21

MAXIMUM ALLOWABLE TIME DURATION FOR WET TRANSFER OPERATIONS

Initial Temperature (°F)	Time Duration (hr)
115	46.7
120	44.3
125	41.9
130	39.5
135	37.1
140	34.6
145	32.3
150	29.8

Table 4.4.22

SUMMARY OF MPC CONFINEMENT BOUNDARY TEMPERATURE DISTRIBUTION DURING NORMAL STORAGE CONDITIONS

Location	Figure 3.4.44 Designation	MPC-24 [°F]	MPC-68 [°F]
MPC Lid Inside Surface at Centerline	A	179	178
MPC Lid Outside Surface at Centerline	B	173	172
MPC Lid Inside Surface at Periphery	C	166	167
MPC Lid Outside Surface at Periphery	D	164	164
MPC Baseplate Inside Surface at Centerline	E	249	218
MPC Baseplate Outside Surface at Centerline	F	241	213
MPC Baseplate Inside Surface at Periphery	G	222	203
MPC Baseplate Outside Surface at Periphery	H	219	200
MPC Shell Maximum	I	332	331

Table 4.4.23

SUMMARY OF 10×10 ARRAY TYPE BWR FUEL ASSEMBLY EFFECTIVE THERMAL CONDUCTIVITIES†

FUEL	@200°F [Btu/ft-hr-°F]	@450°F [Btu/ft-hr-°F]	@700°F [Btu/ft-hr-°F]
GE-12/14	0.166	0.269	0.412
Atrium-10	0.164	0.266	0.409
SVEA-96	0.164	0.269	0.416

† The conductivities reported in this table are obtained by the simplified method described in the beginning of the Subsection 4.4.1.1.2.

Table 4.4.24

COMPARISON OF ATRIUM-10 BWR FUEL ASSEMBLY CONDUCTIVITY[†] WITH THE BOUNDING[††] BWR FUEL ASSEMBLY CONDUCTIVITY

Temperature [°F]	Atrium-10 BWR Assembly [Btu/ft-hr-°F]	Bounding BWR Assembly [Btu/ft-hr-°F]
200	0.225	0.171
450	0.345	0.271
700	0.504	0.410

[†] The reported effective conductivity has been obtained from a rigorous finite element model.

[††] The bounding BWR fuel assembly conductivity applied in the MPC-68 basket thermal analysis.

Table 4.4.25

PLANT SPECIFIC BWR FUEL TYPES EFFECTIVE THERMAL CONDUCTIVITY*

Fuel	@200° F [Btu/ft-hr-°F]	@ 450° F [Btu/ft-hr-°F]	@ 700° F [Btu/ft-hr-°F]
Oyster Creek (7x7)	0.165	0.273	0.427
Oyster Creek (8x8)	0.162	0.266	0.413
TVA Browns Ferry (8x8)	0.160	0.264	0.411
SPC-5 (9x9)	0.149	0.245	0.380

* The conductivities reported in this table are obtained by a simplified analytical method described in Subsection 4.4.1.2.

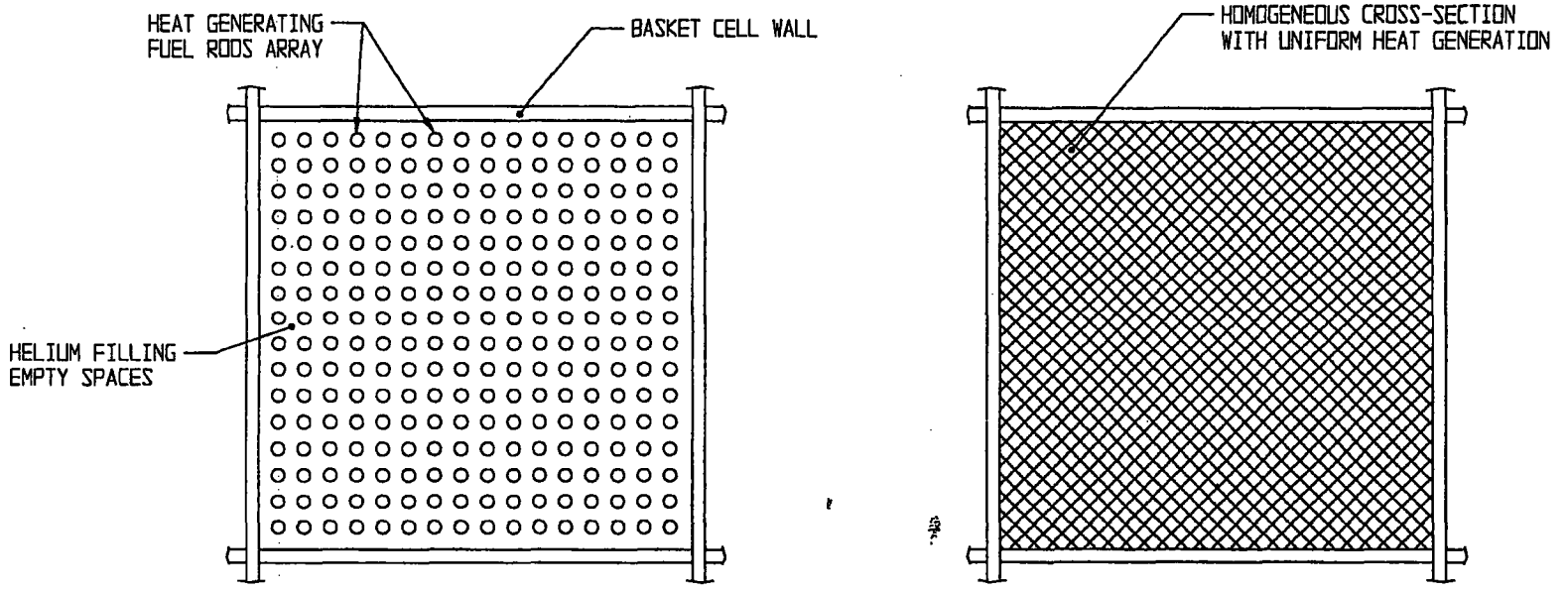

(a) TYPICAL FUEL CELL

(b) SOLID REGION OF
EFFECTIVE CONDUCTIVITY

FIGURE 4.4.1; HOMOGENIZATION OF THE STORAGE CELL CROSS-SECTION

\5014\HI941184\CH_4\4_4_1

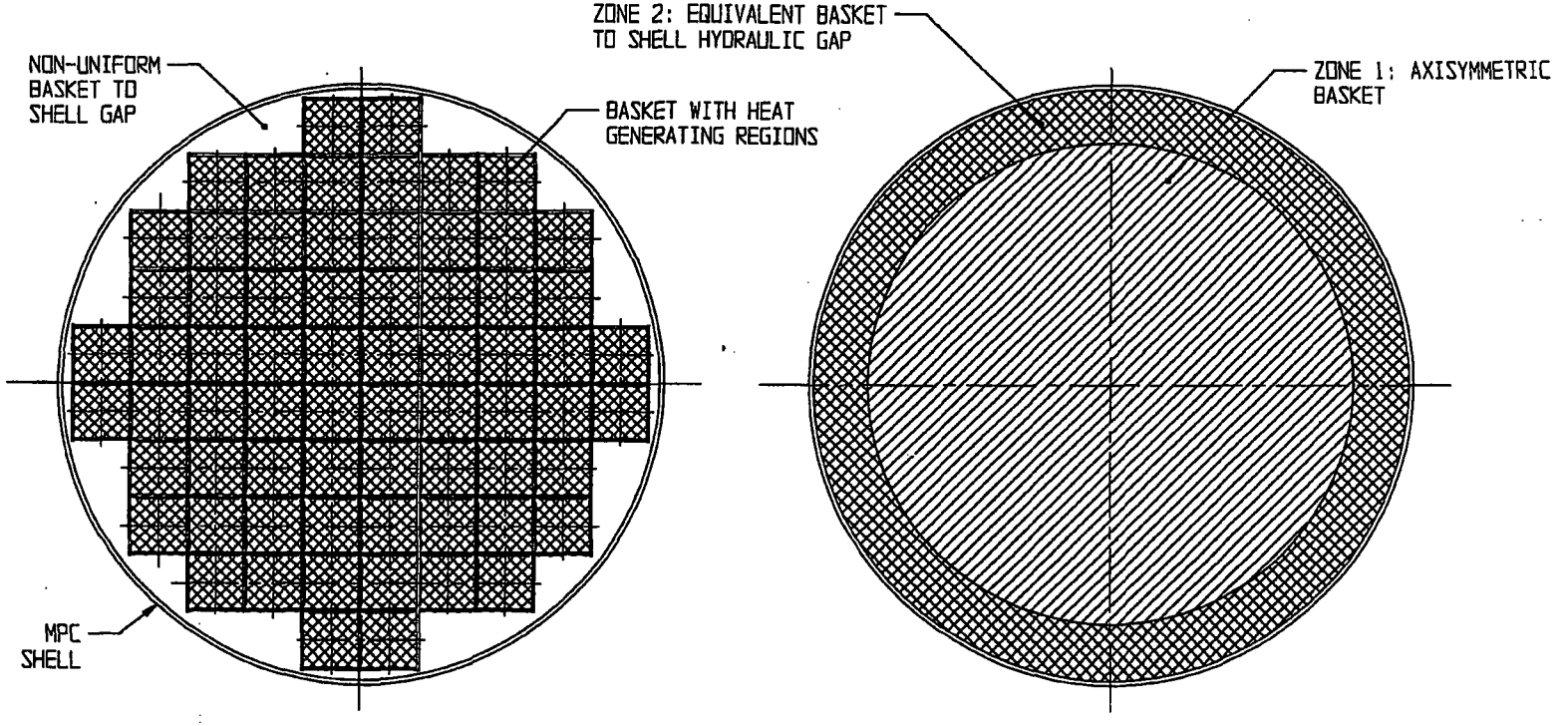

(a) TYPICAL MPC CROSS-SECTION

(b) EQUIVALENT TWO ZONE BODY

FIGURE 4.4.2; MPC CROSS-SECTION REPLACED WITH AN EQUIVALENT TWO ZONE AXISYMMETRIC BODY

\5014\HI941184\CH_4\4_4_2

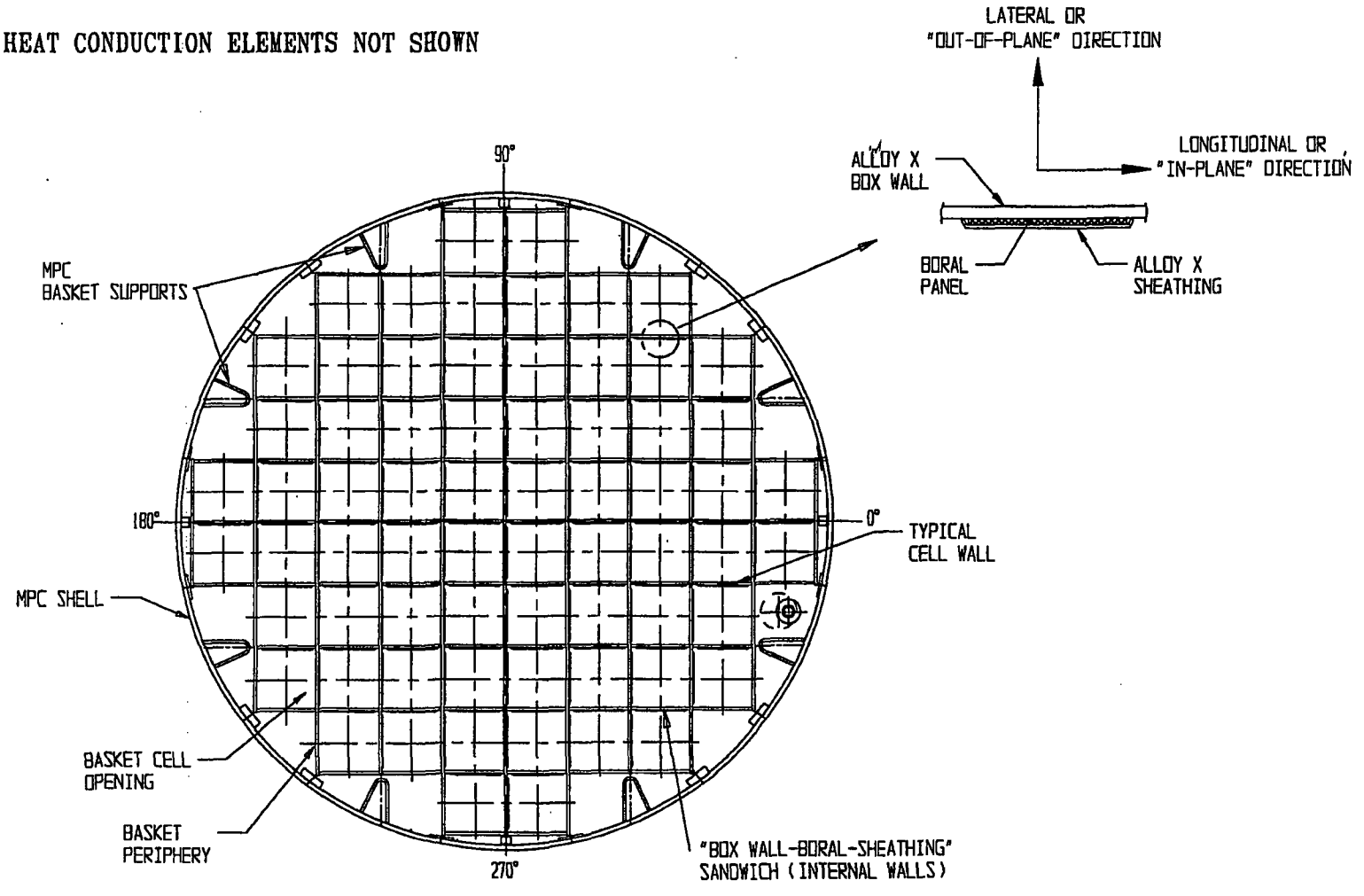

FIGURE 4.4.3; TYPICAL MPC BASKET PARTS IN A CROSS-SECTIONAL VIEW

\5014\HI941184\CH_4\4_4_3

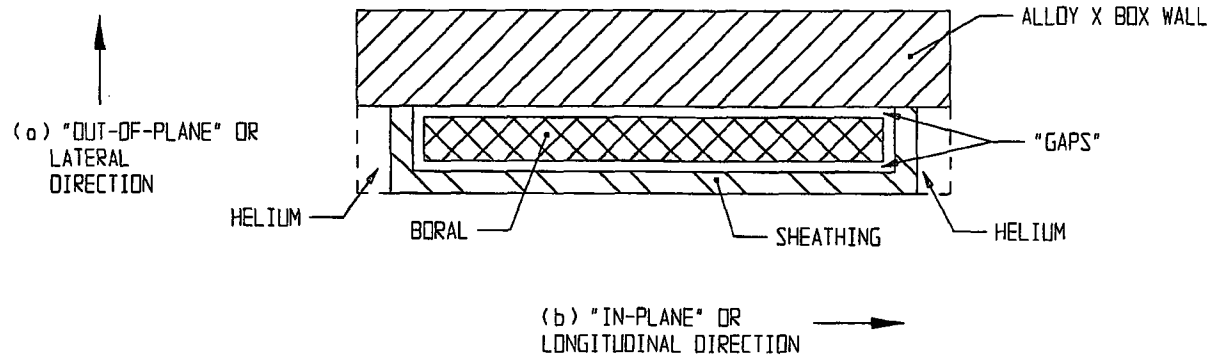

FIGURE 4.4.4; "BOX WALL-BORAL-SHEATHING" SANDWICH

FIGURE 4.4.5; ANSYS FINITE ELEMENT MODEL FOR EVALUATION OF RADIATIVE BLOCKING FACTOR FOR A CASK ARRAY AT AN ISFSI SITE

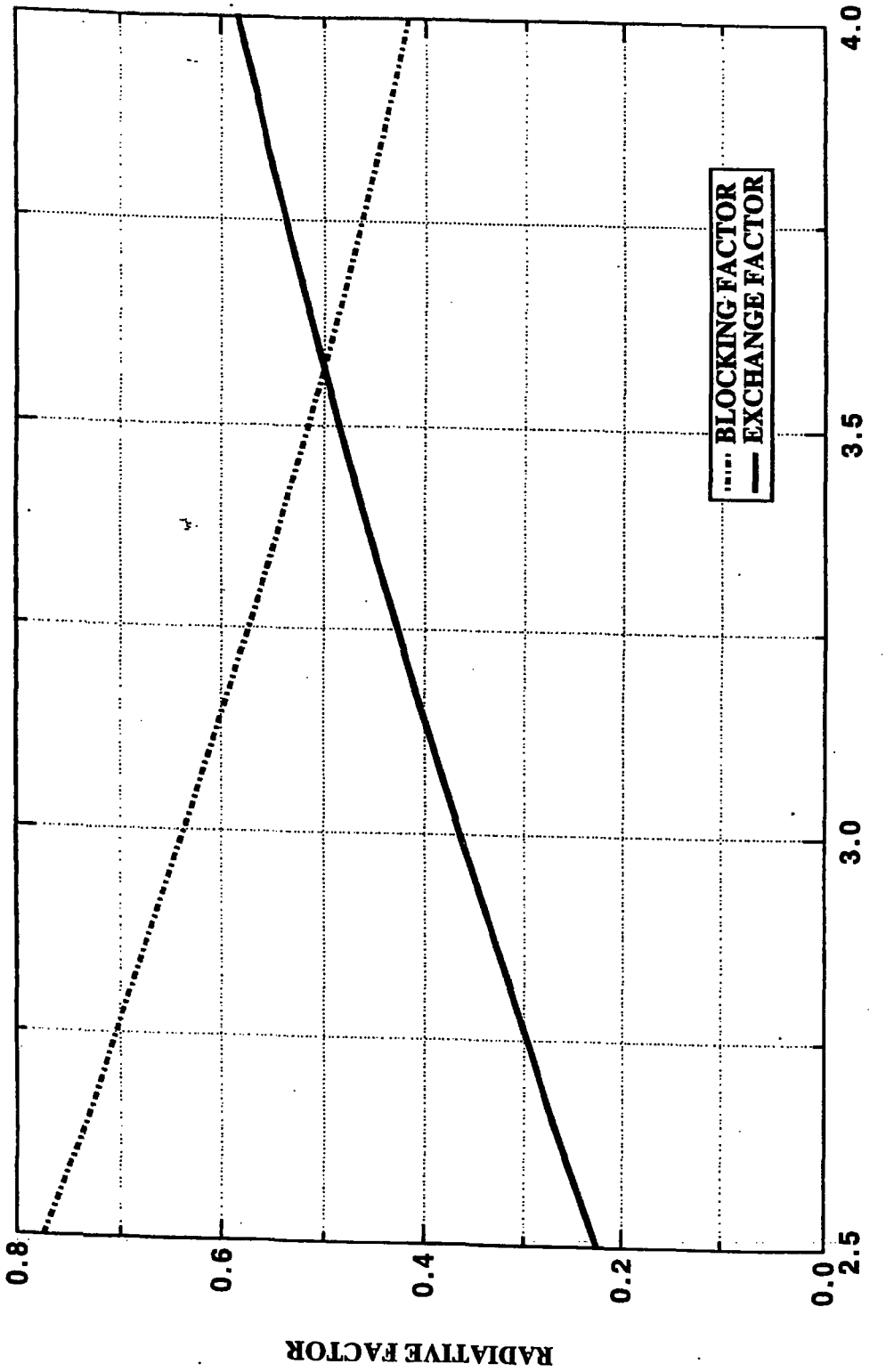

FIGURE 4.4.6; EFFECT OF ISFSI CASK ARRAY PITCH ON RADIATIVE BLOCKING AND EXCHANGE FACTORS

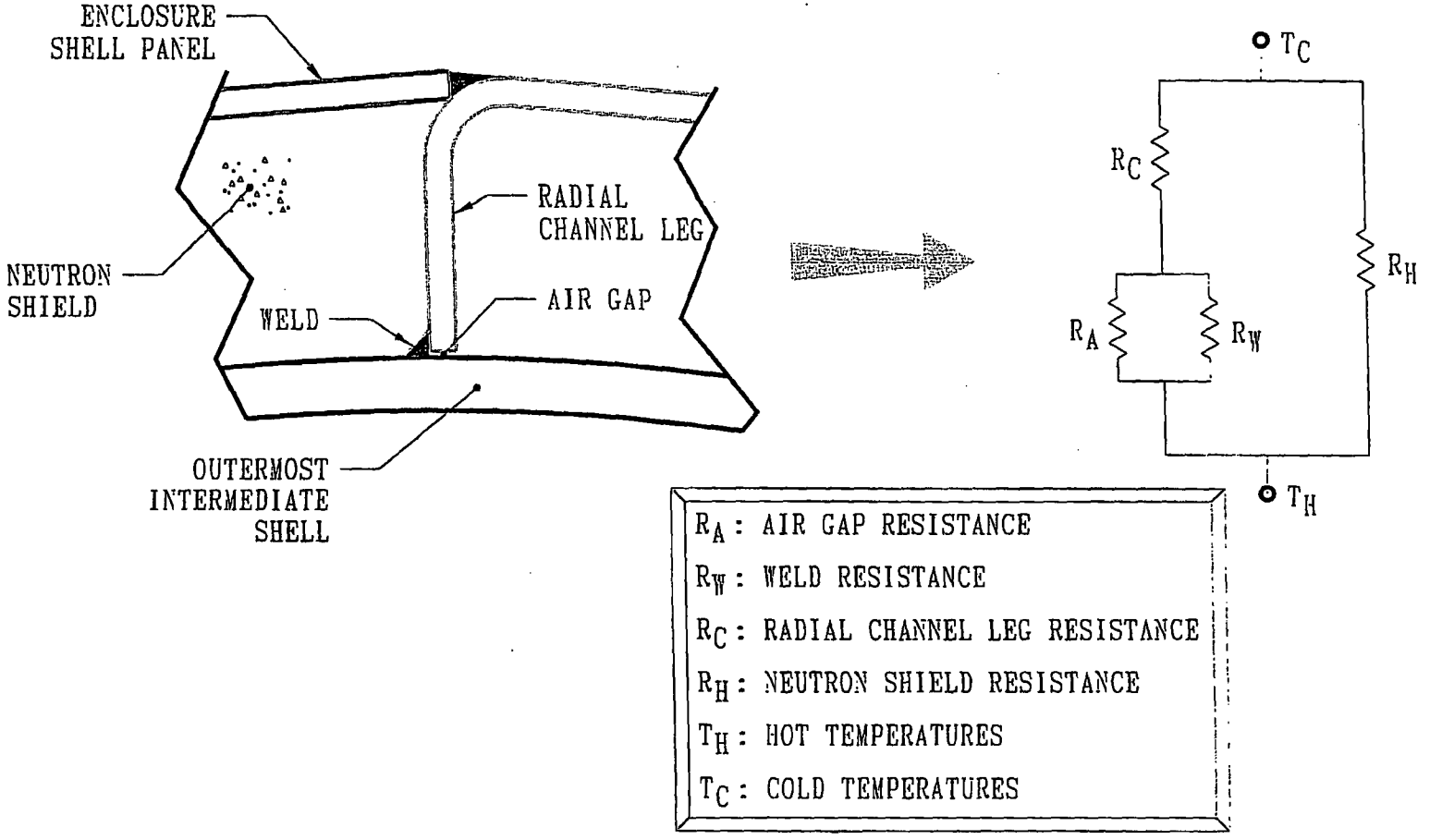

FIGURE 4.4.7; NEUTRON SHIELD REGION RESISTANCE NETWORK ANALOGY FOR EFFECTIVE CONDUCTIVITY CALCULATION

FIGURE 4.4.8: WESTINGHOUSE 17x17 OFA PWR FUEL ASSEMBLY MODEL

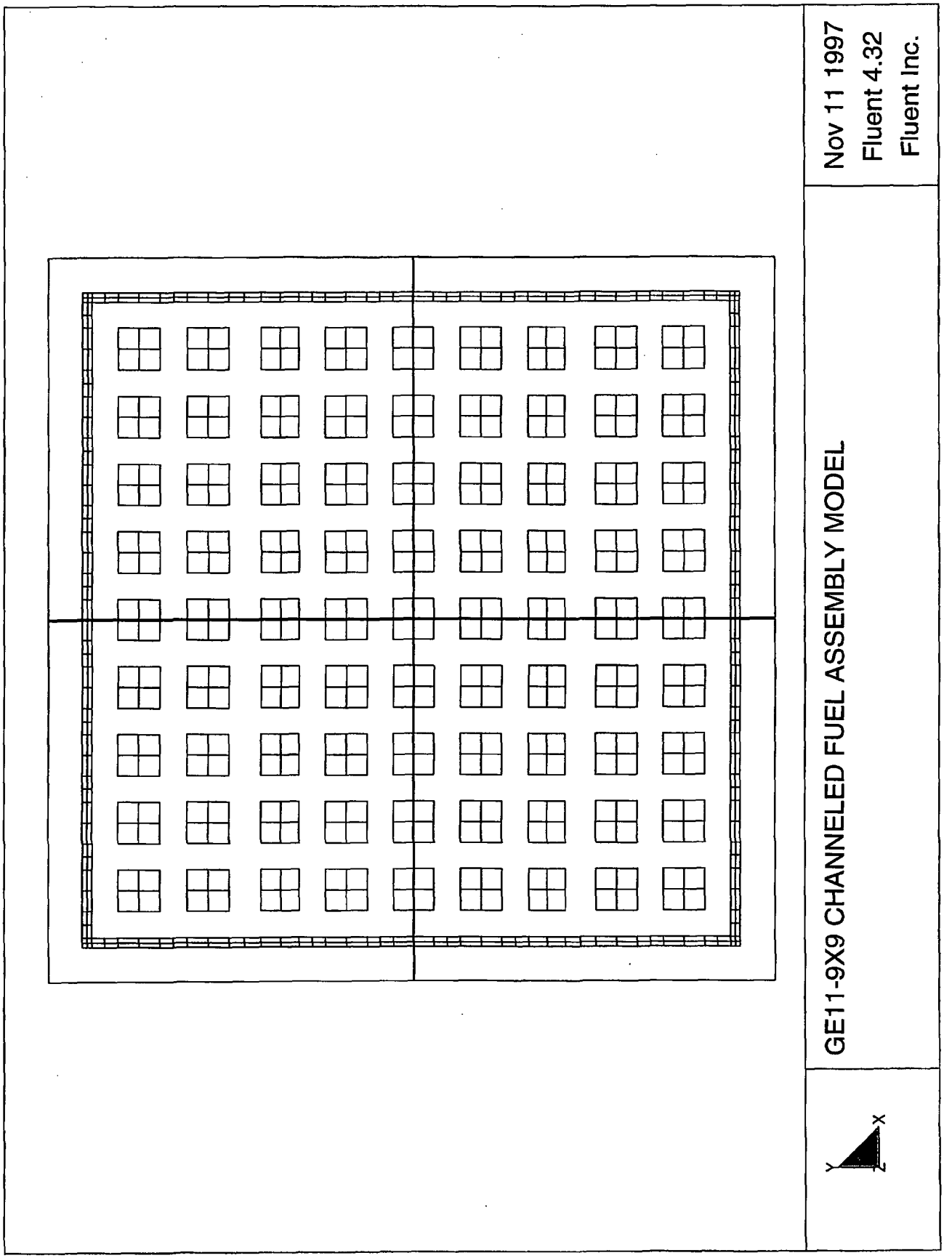

FIGURE 4.4.9: GENERAL ELECTRIC 9x9 BWR FUEL ASSEMBLY MODEL

FIGURE 4.4.10

THIS FIGURE IS INTENTIONALLY DELETED

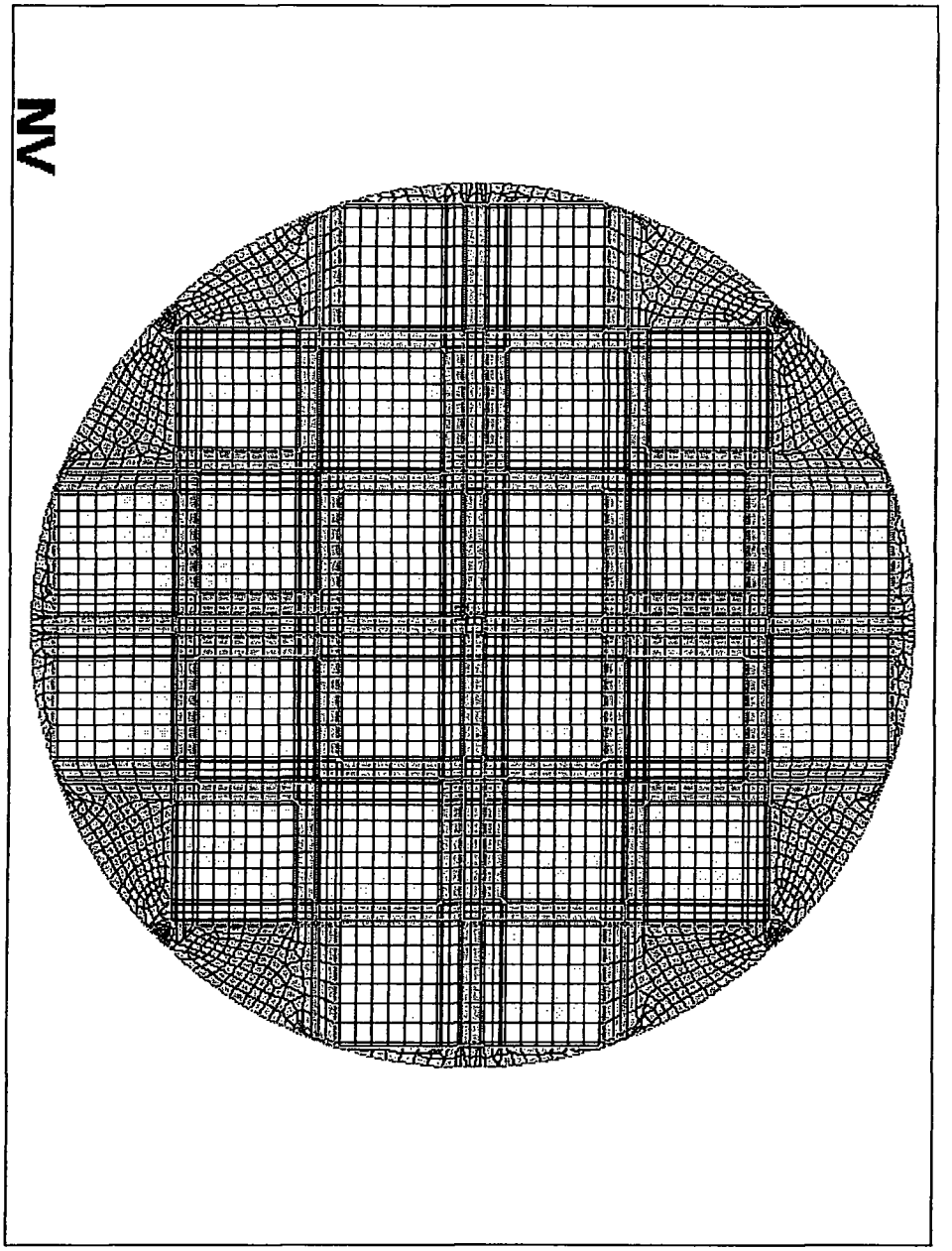

FIGURE 4.4.11; MPC-24 BASKET CROSS-SECTION ANSYS FINITE-ELEMENT MODEL

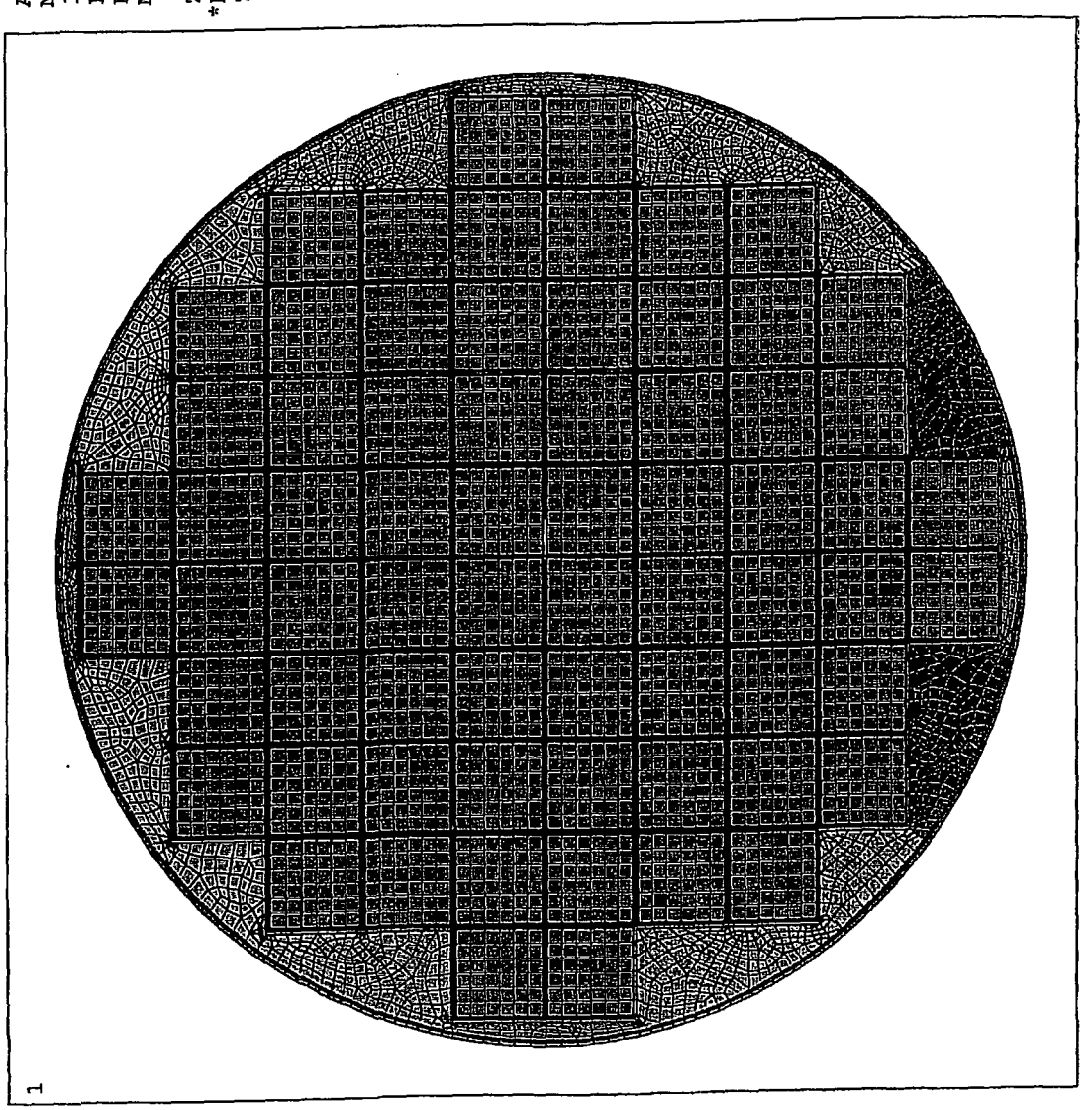

FIGURE 4.4.12; MPC-68 BASKET CROSS-SECTION ANSYS FINITE ELEMENT MODEL

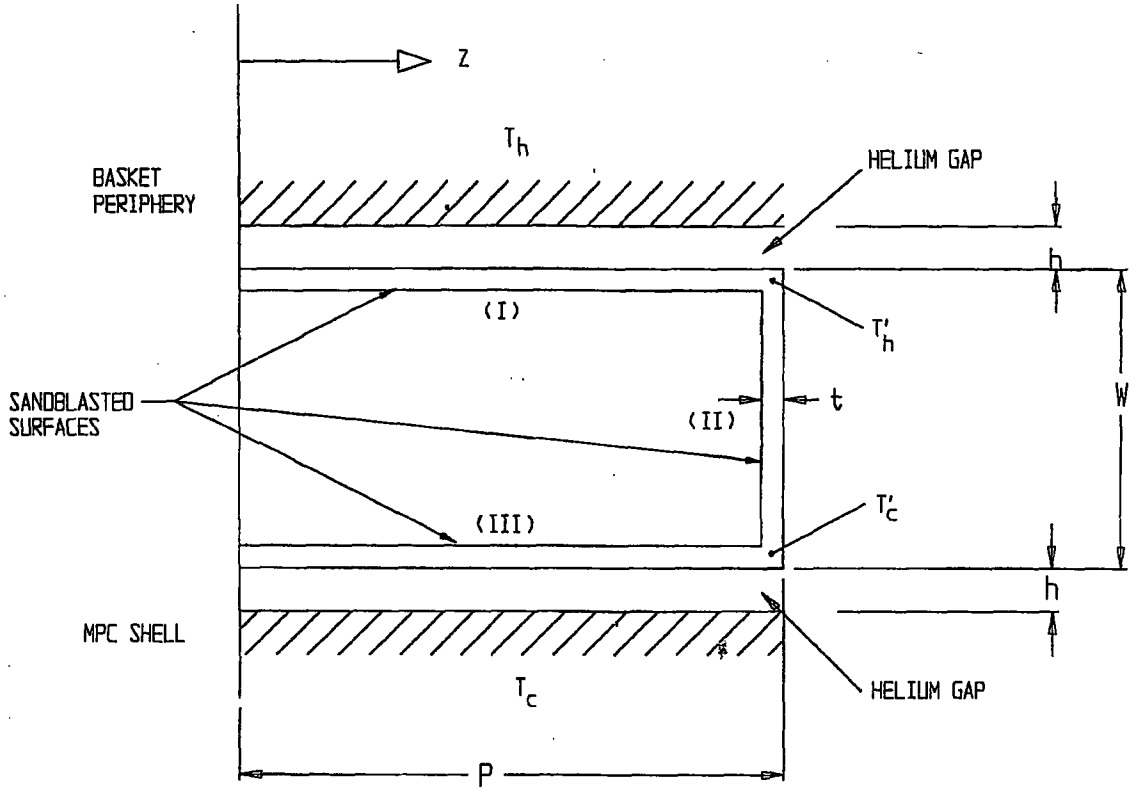

FIGURE 4.4.13; ILLUSTRATION OF AN MPC BASKET TO SHELL ALUMINUM HEAT CONDUCTION ELEMENT

\5014\HI941184\CH_4\4_4_13

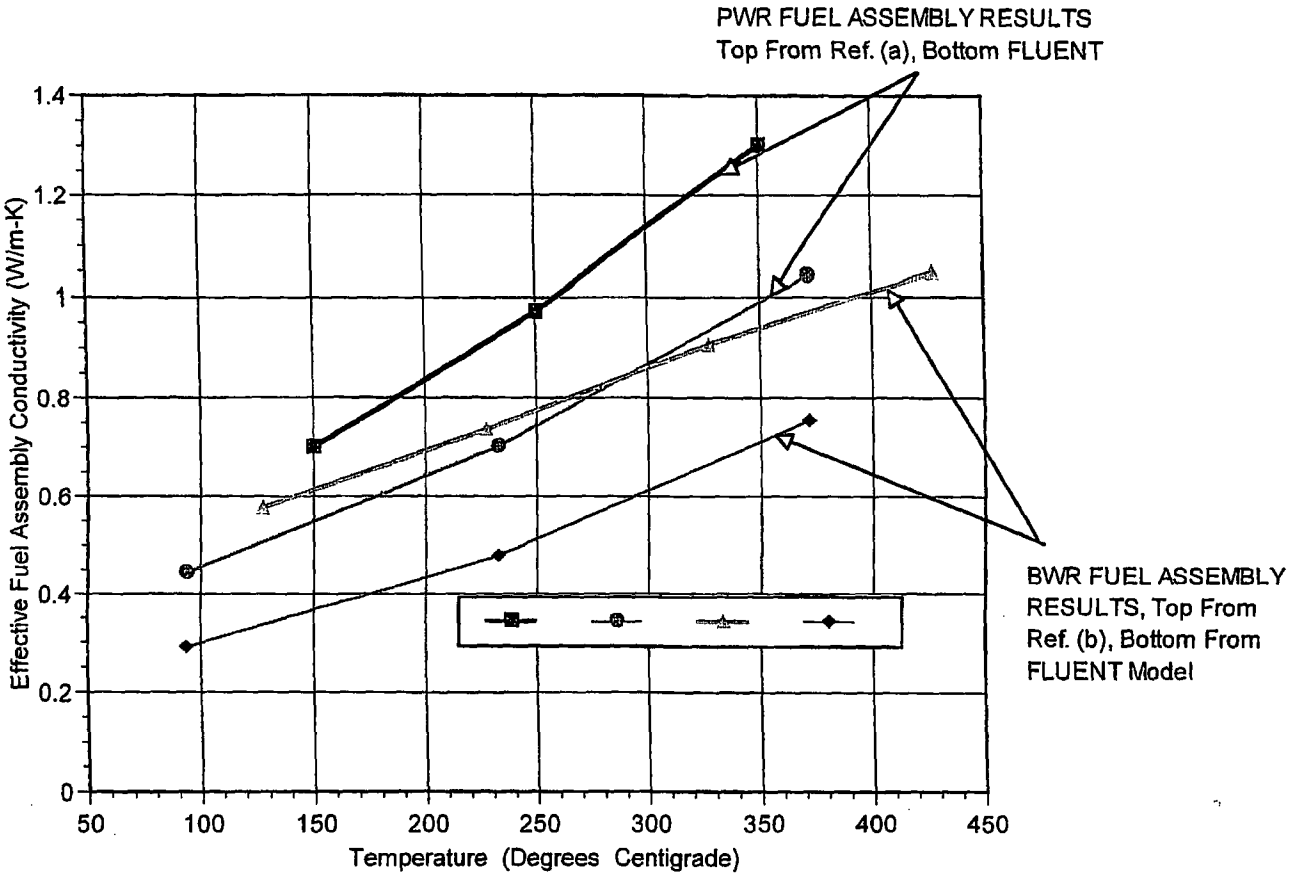

(a) "Determination of SNF Peak Temperatures in the Waste Package", Bahney & Doering, *HLRWM Sixth Annual Conf.*, Pages 671-673, (April 30 - May 5, 1995)
(b) "A Method for Determining the Spent-Fuel Contribution to Transport Cask Containment Requirements", *Sandia Report SAND90-2406*, page II-132, (1992)

FIGURE 4.4.14: COMPARISON OF FLUENT BASED FUEL ASSEMBLY EFFECTIVE CONDUCTIVITY RESULTS WITH PUBLISHED TECHNICAL DATA

FIGURE 4.4.15: TYPICAL HI-STAR 100 SYSTEM FINITE ELEMENT MESH FOR THERMAL ANALYSIS

FIGURE 4.4.16

THIS FIGURE IS INTENTIONALLY DELETED

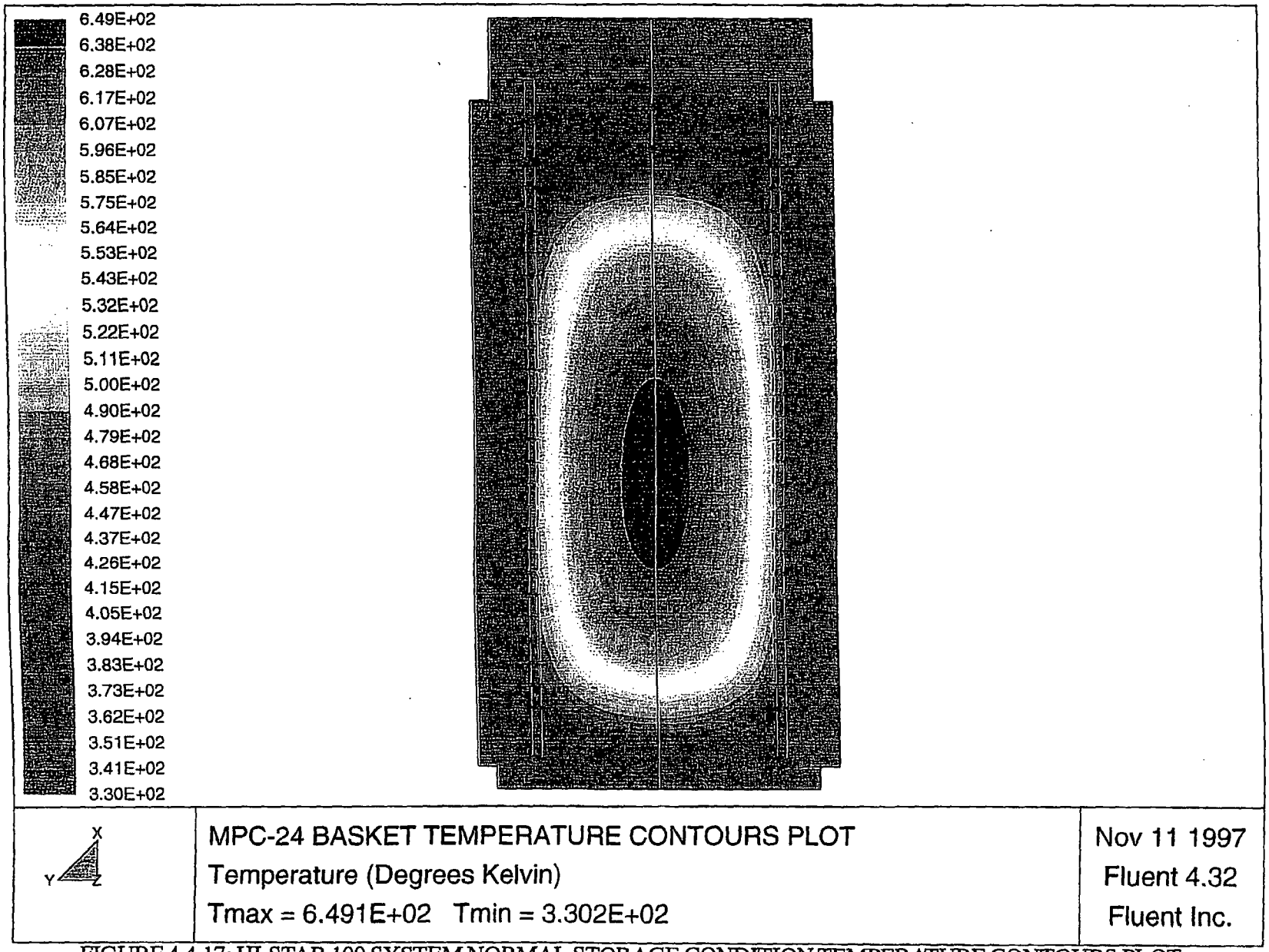

FIGURE 4.4.17: HI-STAR 100 SYSTEM NORMAL STORAGE CONDITION TEMPERATURE CONTOURS PLOT (MPC-24 BASKET)

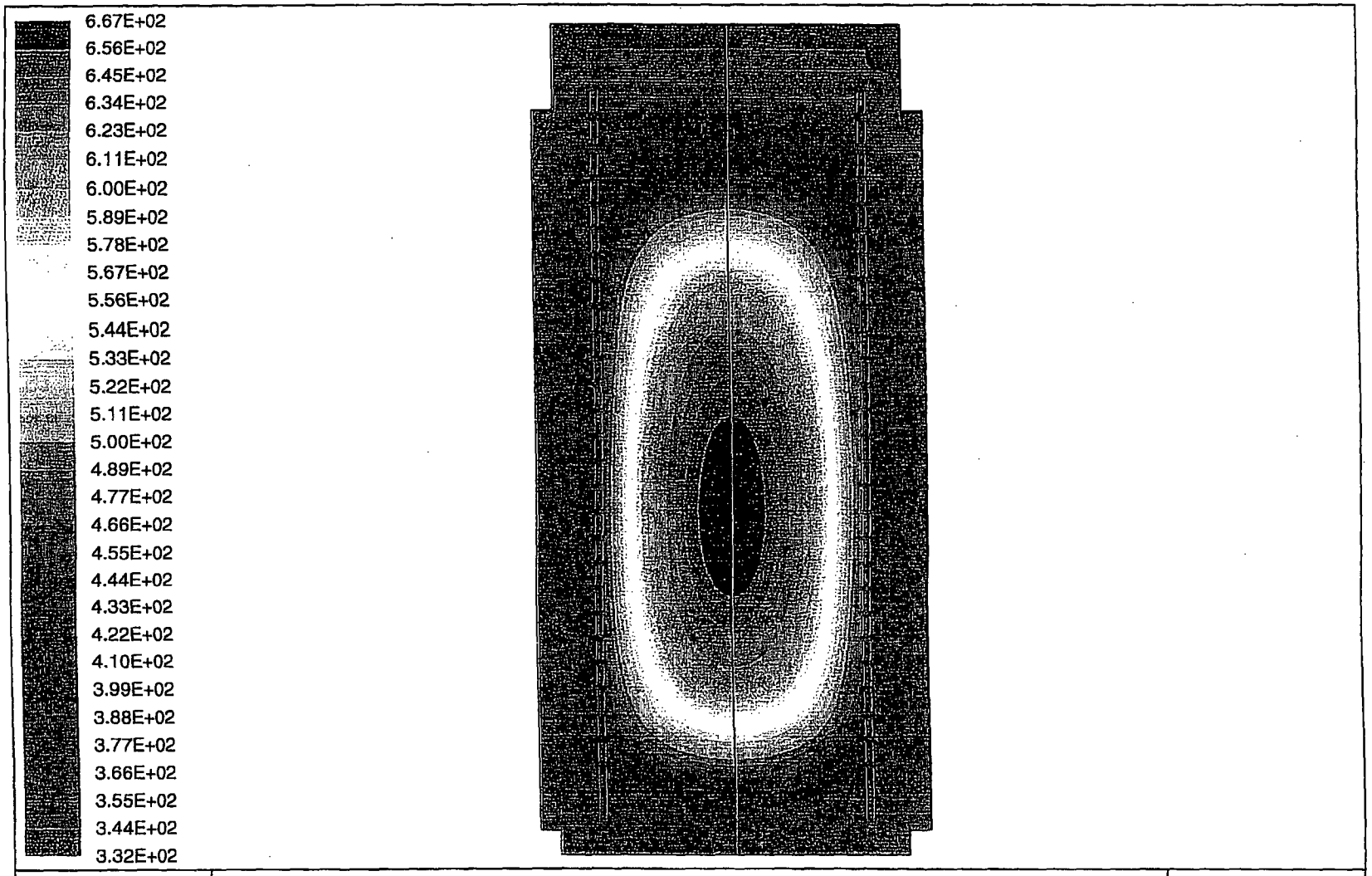

FIGURE 4.4.18: HI-STAR 100 SYSTEM NORMAL STORAGE CONDITION TEMPERATURE CONTOURS PLOT (MPC-68 BASKET)

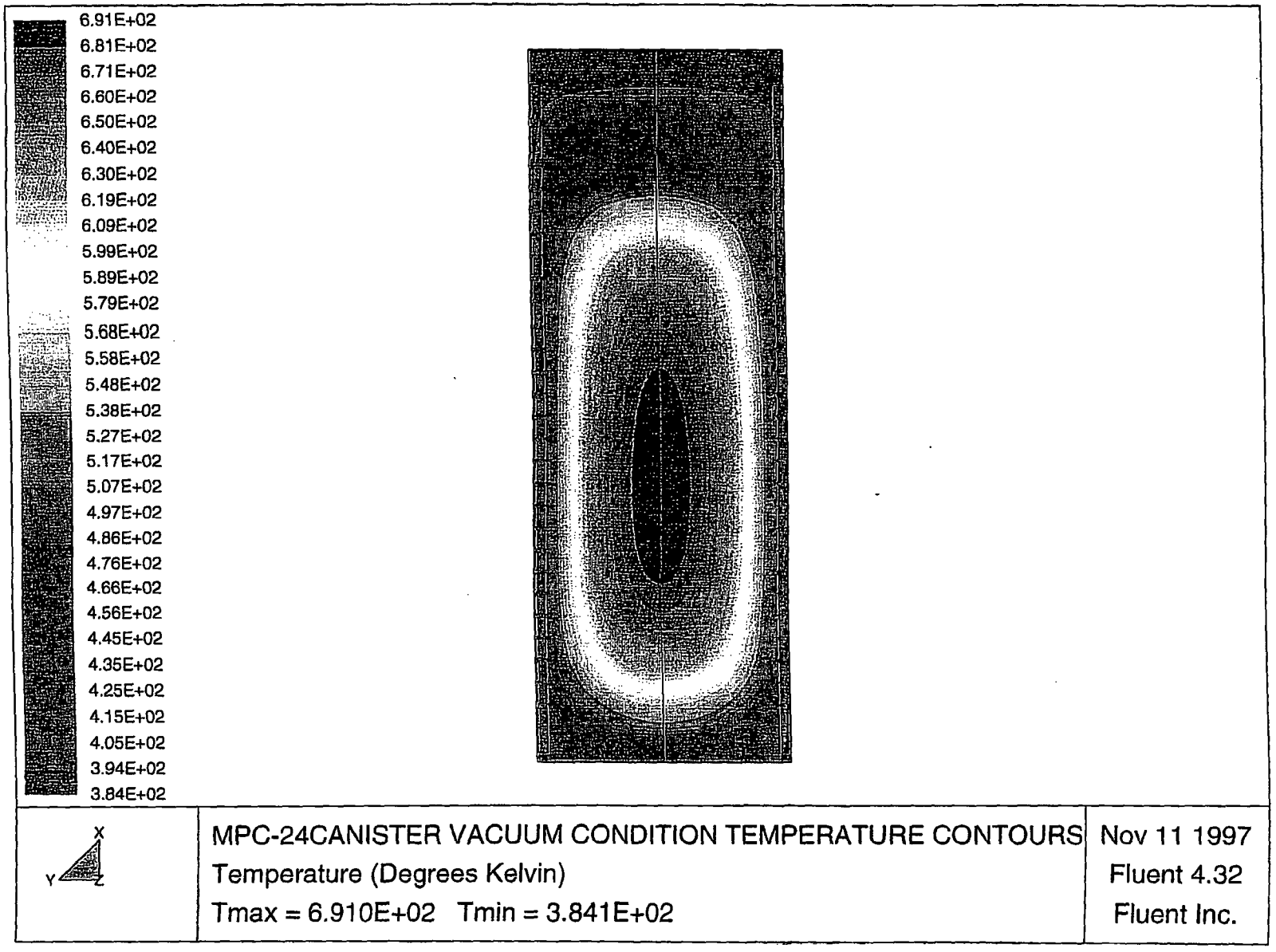

FIGURE 4.4.19: VACUUM CONDITION TEMPERATURE CONTOURS PLOT FOR BOUNDING MPC-24 BASKET

FIGURE 4.4.20

THIS FIGURE IS INTENTIONALLY DELETED

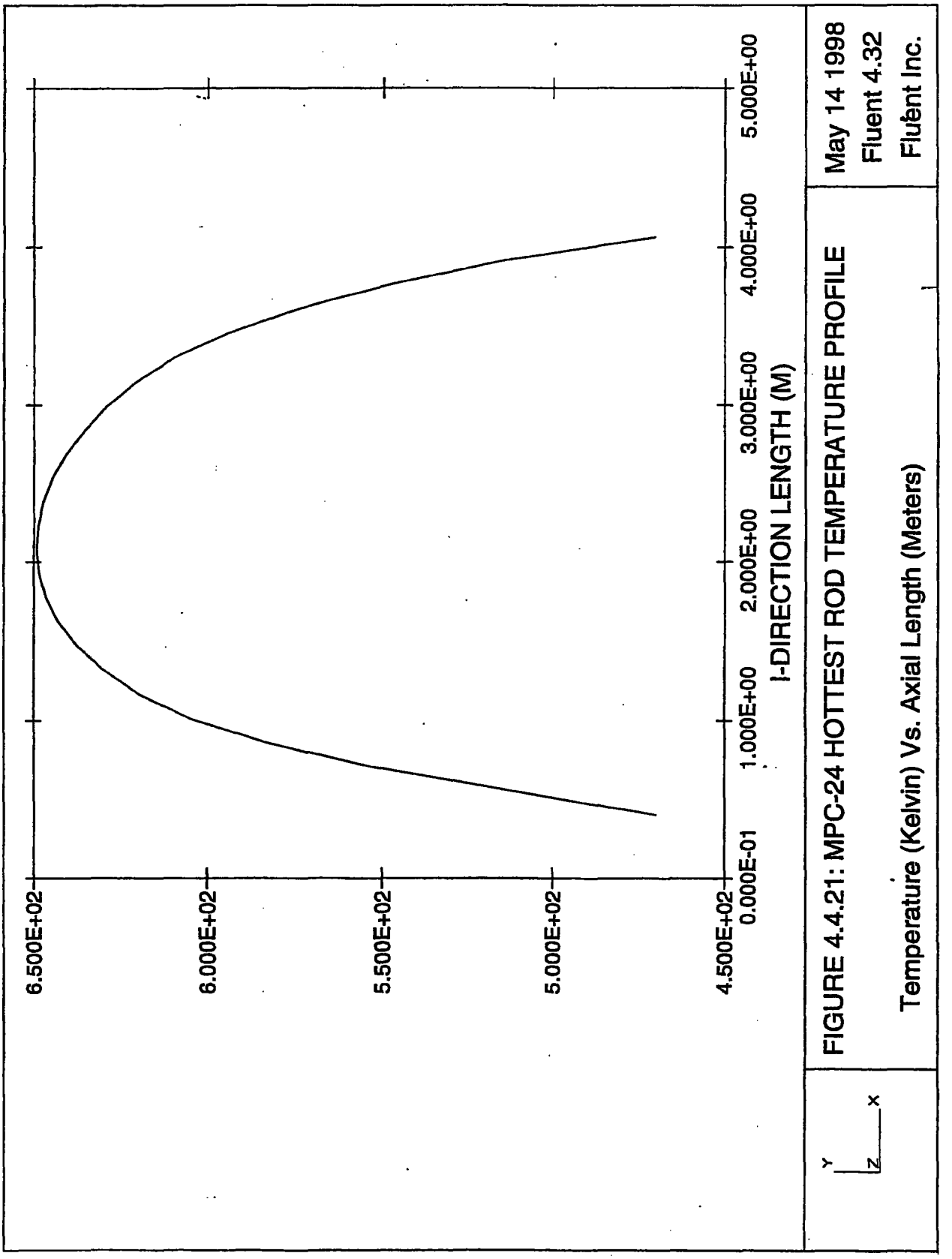
6.500E+02
6.000E+02
5.500E+02
5.000E+02
4.500E+02
0.000E-01
1.000E+00
2.000E+00
3.000E+00
4.000E+00
5.000E+00
I-DIRECTION LENGTH (M)
FIGURE 4.4.21: MPC-24 HOTTEST ROD TEMPERATURE PROFILE
Temperature (Kelvin) Vs. Axial Length (Meters)
May 14 1998
Fluent 4.32
Fluent Inc.
Y
Z
X

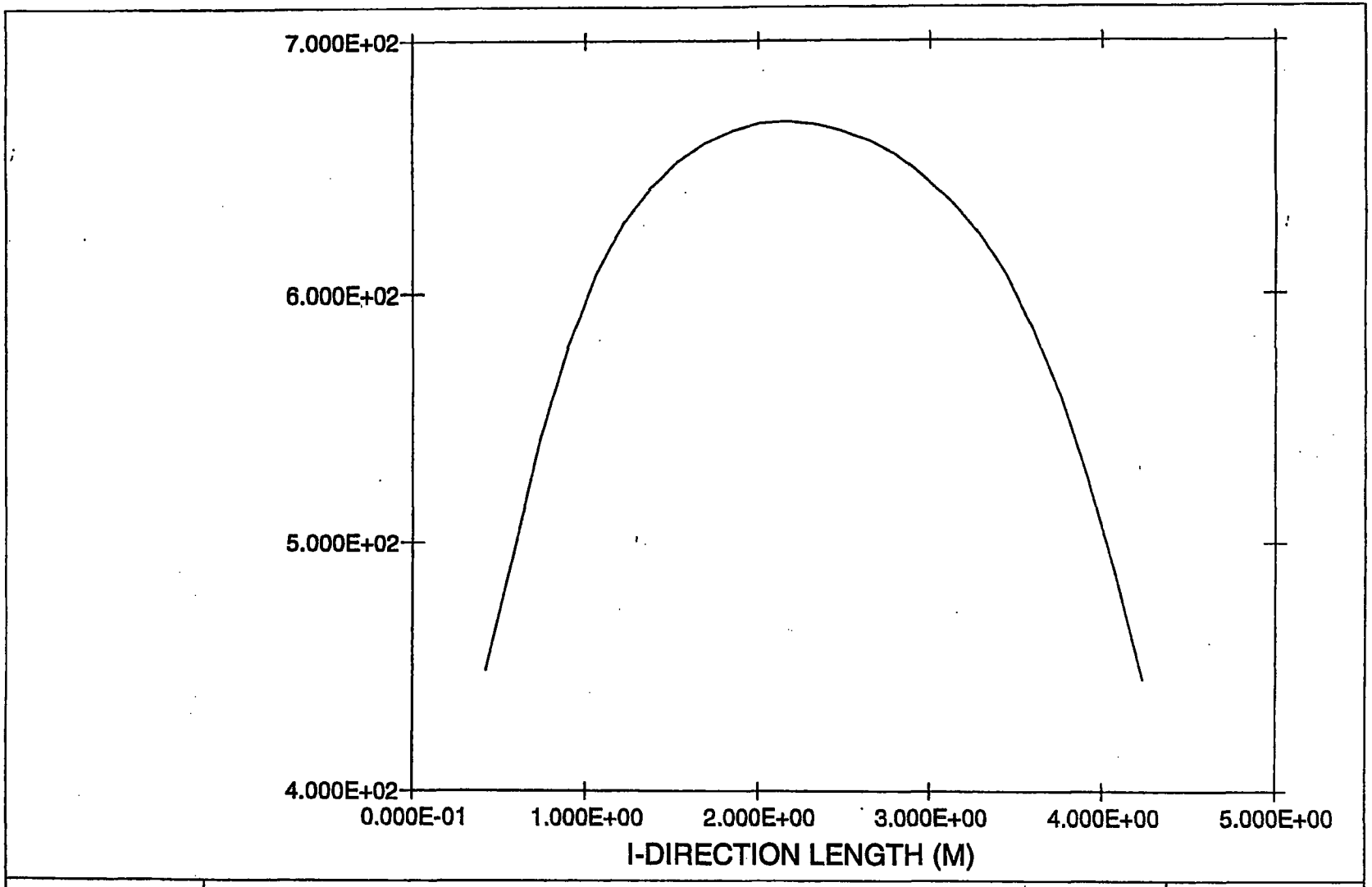

FIGURE 4.4.22: MPC-68 HOTTEST ROD TEMPERATURE PROFILE

Temperature (Kelvin) Vs. Axial Length (Meters)

May 14 1998
Fluent 4.32
Fluent Inc.

FIGURE 4.4.23

THIS FIGURE IS INTENTIONALLY DELETED

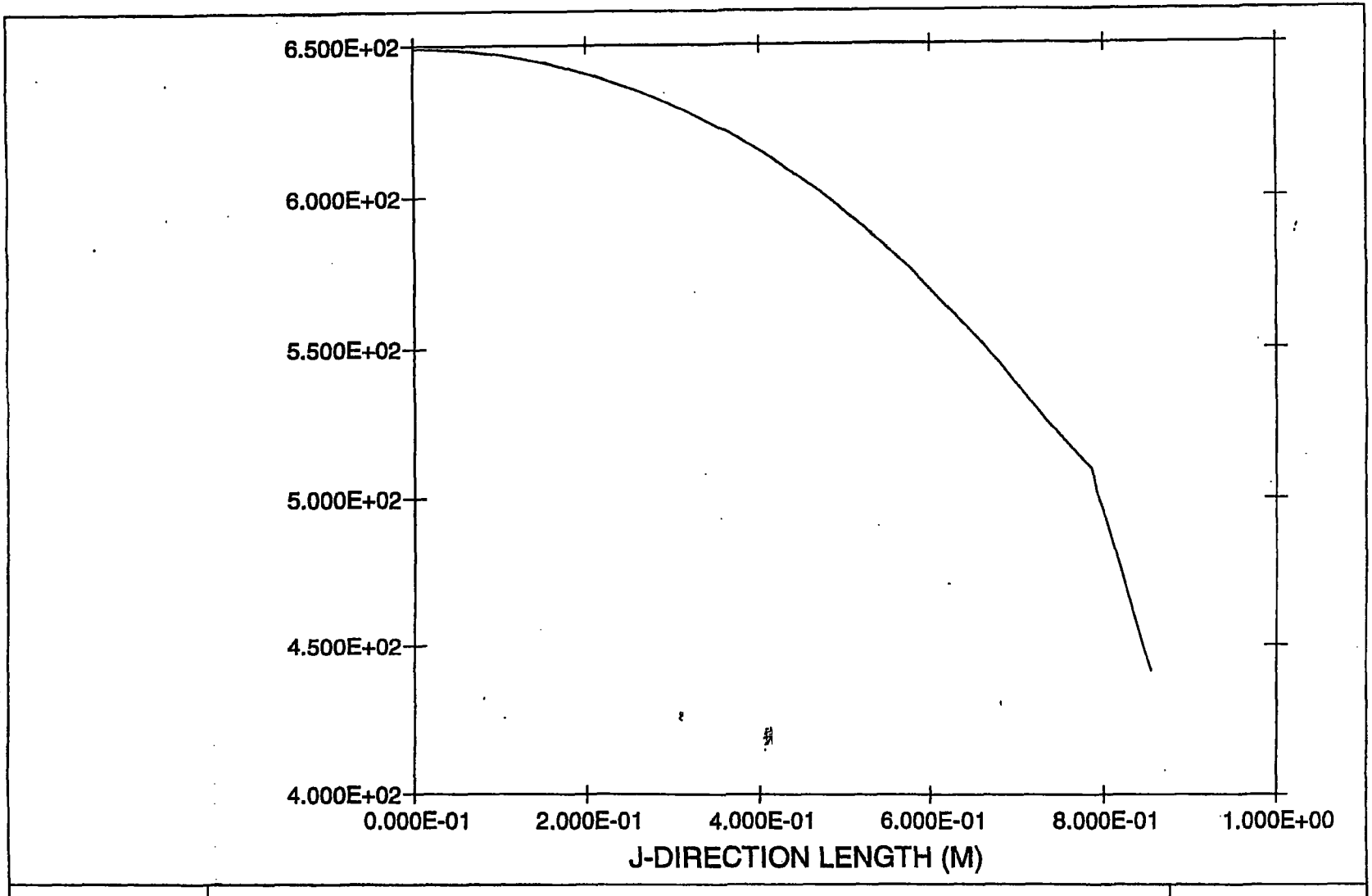

FIGURE 4.4.24: MPC-24 BASKET RADIAL TEMPERATURE PROFILE
(Hottest Basket Cross-Section)
Temperature (Kelvin) Vs. Radial Distance (Meters)

May 14 1998
Fluent 4.32
Fluent Inc.

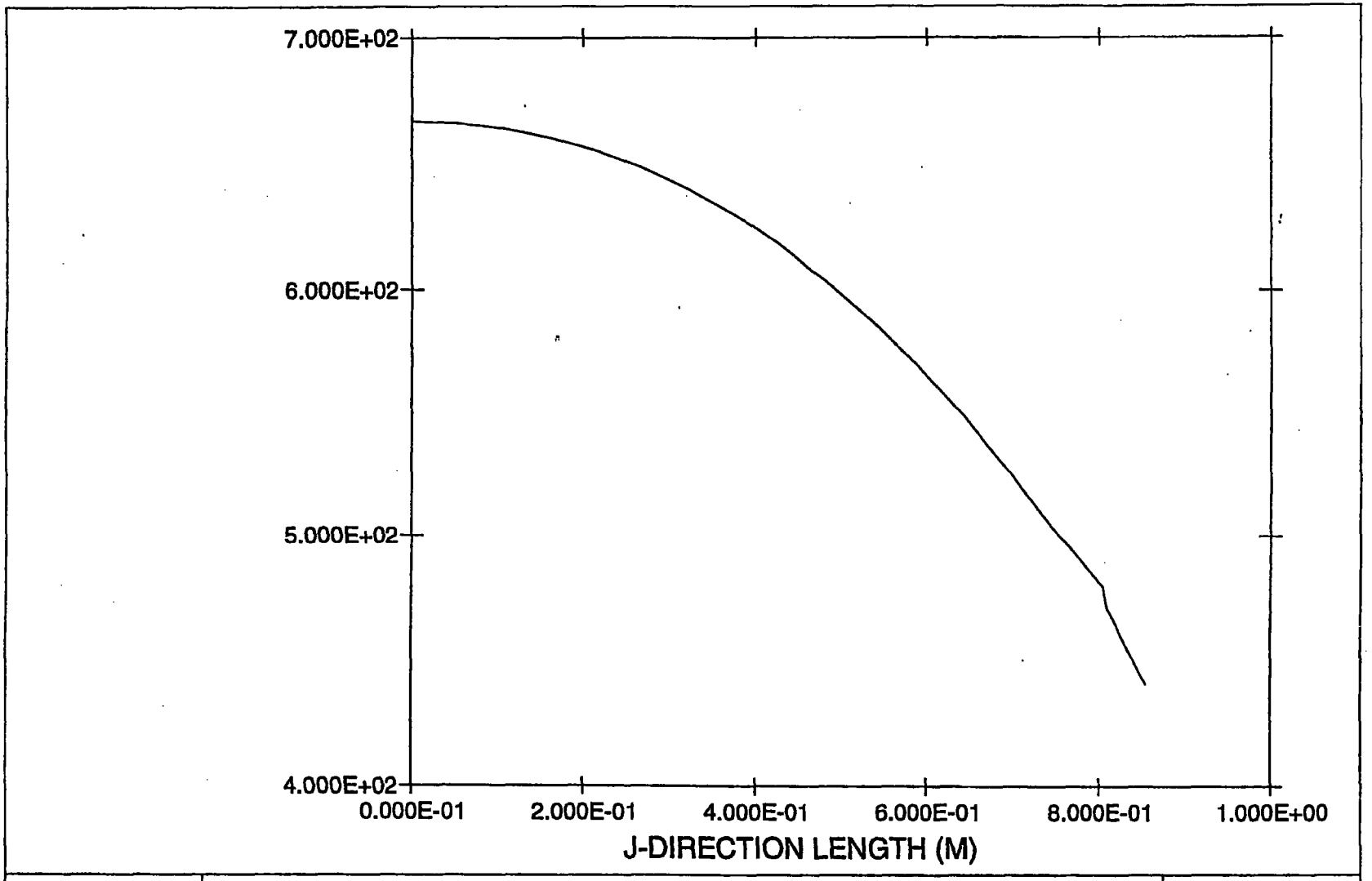

FIGURE 4.4.25: MPC-68 BASKET RADIAL TEMPERATURE PROFILE

Temperature (Kelvin) Vs. Radial Position (Meters)

May 14 1998
Fluent 4.32
Fluent Inc.

4.5 REGULATORY COMPLIANCE

NUREG-1536 ([4.1.3], IV) defines eight specific thermal acceptance criteria which are addressed in Sections 4.1 through 4.4. Each of the pertinent criteria and the conclusion of the evaluations are summarized here.

1. As required by NUREG-1536 ([4.1.3], 4.IV.1), the fuel cladding temperature at the beginning of dry cask storage is maintained below the anticipated damage-threshold temperatures for normal conditions and a minimum of 20 years of cask storage. Maximum clad temperatures for normal storage conditions are reported in Section 4.4.2.1. Anticipated damage-threshold temperatures, calculated as described in Section 4.3, are summarized in Table 2.2.3.

2. As required by NUREG-1536 ([4.1.3], 4.IV.2), the fuel cladding temperature is maintained below 570°C (1058°F) for short-term accident conditions, short-term off-normal conditions, and fuel transfer operations. Results of off-normal and accident condition evaluations presented in Chapter 11 comply with this limit. Maximum clad temperatures for vacuum drying conditions are reported in Section 4.4.2.2 which comply within this limit by large conservative margins.

3. As required by NUREG-1536 ([4.1.3], 4.IV.3), the maximum internal pressure of the cask remains within its design pressure for normal, off-normal, and accident conditions, assuming rupture of 1 percent, 10 percent, and 100 percent of the fuel rods, respectively. Assumptions for pressure calculations include release of 100 percent of the fill gas and 30 percent of the significant radioactive gases in the fuel rods. Maximum internal pressures are reported in Section 4.4.4. Design pressures are summarized in Table 2.2.1.

4. As required by NUREG-1536 ([4.1.3], 4.IV.4), all cask and fuel materials are maintained within their minimum and maximum temperatures for normal and off-normal conditions in order to enable components to perform their intended safety functions. During normal fuel handling operations (i.e., vacuum drying) the cask component temperatures are compared with short-term temperature limits (Section 4.4.2.2). Maximum and minimum temperatures for normal conditions are reported in Sections 4.4.2 and 4.4.3, respectively. Design temperature limits are summarized in Table 2.2.3. HI-STAR 100 System components defined as important to safety are listed in Table 2.2.6. Off-normal and accident condition thermal evaluations are discussed in Sections 11.1 and 11.2, respectively.

5. & 6. As required by NUREG-1536 ([4.1.3], 4.IV.5), the cask system ensures a very low probability of cladding breach during long-term storage. Further, NUREG-1536 ([4.1.3], 4.IV.6) requires that the fuel cladding damage resulting from creep cavitation should be limited to 15 percent of the original cladding cross section area during dry storage. The calculation methodology, described in Section 4.3, for determining initial dry storage fuel clad temperature limits, ensures that both of these requirements are satisfied. Maximum

fuel clad temperature limits are summarized in Table 2.2.3.

7. As required by NUREG-1536 ([4.1.3], 4.IV.7), the cask system is passively cooled. All heat rejection mechanisms described in this chapter, including conduction, natural convection, and thermal radiation, are completely passive.

8. As required by NUREG-1536 ([4.1.3], 4.IV.8), the thermal performance of the cask is within the allowable design criteria specified in FSAR Chapter 2 for normal storage and fuel handling conditions. During normal fuel handling operations (i.e., vacuum drying) the cask component temperatures are compared with short-term temperature limits. All thermal results reported in this chapter are within the design criteria allowable ranges for all normal storage and fuel handling conditions. Off-normal and fire accident condition responses are reported in Section 11.1 and 11.2, respectively.

Finally, the acceptance criteria set forth in NUREG-1536 ([4.1.3], 4.VI) can be demonstrated to have been satisfied on the strength of information provided in this FSAR. Specifically, it is noted that:

- Structures, systems, and components (SSCs) important to safety are described in sufficient detail in Chapters 1, 2 and 4 of this FSAR to enable an evaluations of their thermal effectiveness. Cask SSCs important to safety remain within their operating temperature ranges.

- The HI-STAR 100 System is designed with a heat-removal capability having verifiability and reliability consistent with its importance to safety. The cask is designed to provide adequate heat removal capacity without active cooling systems.

- The spent fuel cladding is protected against degradation leading to gross ruptures by maintaining the cladding temperature for five-year cooled fuel in an inert helium environment below 720°F for PWR fuel assemblies and below 749°F for BWR fuel assemblies. Protection of the cladding against degradation is expected to allow ready retrieval of spent fuel for further processing or disposal.

It is therefore concluded that the thermal design of the HI-STAR 100 System is in compliance with 10 CFR Part 72, and that the applicable design and acceptance criteria have been satisfied. The evaluation of the thermal design provides reasonable assurance that the HI-STAR 100 System will allow safe storage of spent fuel for its design life. This finding is reached on the basis of the technical data presented in this FSAR in conjunction with provisions of 10 CFR Part 72, appropriate regulatory guides, applicable codes and standards, and accepted engineering practices.

4.6 REFERENCES

[4.1.1] ANSYS Finite Element Modeling Package, Swanson Analysis Systems, Inc., Houston, PA, 1993.

[4.1.2] FLUENT Computational Fluid Dynamics Software, (Fluent, Inc., Centerra Resource Park, 10 Cavendish Court, Lebanon, NH 03766).

[4.1.3] NUREG-1536, "Standard Review Plan for Dry Cask Storage Systems", USNRC, January 1997

[4.1.4] "The TN-24P PWR Spent-Fuel Storage Cask: Testing and Analyses", EPRI NP-5128, (April 1987).

[4.1.5] Deleted.

[4.2.1] Baumeister, T., Avallone, E.A. and Baumeister III, T., "Marks' Standard Handbook for Mechanical Engineers", 8th Edition, McGraw Hill Book Co., 1978.

[4.2.2] Rohsenow, W.M. and Hartnett, J.P., "Handbook of Heat Transfer", McGraw Hill Book Co., New York, 1973.

[4.2.3] Creer et al., "The TN-24P Spent Fuel Storage Cask: Testing and Analyses", EPRI NP-5128, PNL-6054, UC-85, (April 1987).

[4.2.4] Rust, J.H., "Nuclear Power Plant Engineering", Haralson Publishing Co., (1979).

[4.2.5] Kern, D.Q., "Process Heat Transfer", McGraw Hill Kogakusha, (1950).

[4.2.6] "A Handbook of Materials Properties for Use in the Analysis of Light Water Reactor Fuel Rod Behavior", NUREG/CR-0497, (August 1981).

[4.2.7] "Safety Analysis Report for the NAC Storable Transport Cask", Docket No. 71-9235.

[4.2.8] ASME Boiler and Pressure Vessel Code, Section II, Part D, (1995).

[4.2.9] Jakob, M. and Hawkins, G.A., "Elements of Heat Transfer", John Wiley & Sons, New York, 1957.

[4.3.1] Levy, I.S., et al., "Recommended Temperature Limits for Dry Storage of Spent Light Water Reactor Zircaloy-Clad Fuel Rods in Inert Gas", PNL-6189, (May 1987).

[4.3.2] Deleted.

[4.3.3] "Characteristics of Spent Fuel High-Level Waste, and Other Radioactive Wastes Which May Require Long-Term Isolation", DOE/RW-0184, (December 1987).

[4.3.4] Johnson, Jr., A.B. and Gilbert, E.R., "Technical Basis for Storage of Zircaloy-Clad Spent Fuel in Inert Gases", PNL-4835, (September 1983).

[4.3.5] Cunningham et. al., "Evaluation of Expected Behavior of LWR Stainless Steel-Clad Fuel in Long-Term Dry Storage", EPRI TR-106440, (April 1996).

[4.3.6] Schwartz, M.W., Witte, M.C., "Spent Fuel Cladding Integrity During Dry Storage", LLNL, UCID-22181 (September 1987).

[4.3.7] "Temperature Limit Determination for the Inert Dry Storage of Spent Nuclear Fuel", EPRI TR-103949, (May 1994).

[4.4.1] Wooton, R.O. and Epstein, H.M., "Heat Transfer from a Parallel Rod Fuel Element in a Shipping Container", Battelle Memorial Institute, 1963.

[4.4.2] Rapp, D., "Solar Energy", Prentice-Hall, Inc., Englewood Cliffs, NJ, (1981).

[4.4.3] Deleted.

[4.4.4] Holman, J.P., "Heat Transfer," 6th ed., McGraw Hill Book Co., (1986).

[4.4.5] Sanders et al., "A Method for Determining the Spent-Fuel Contribution to Transport Cask Containment Requirements," Sandia Report SAND90-2406-TTC-1019UC-820, page II-127, (November 1992).

[4.4.6] Hewitt, G.F., Shires, G.L. and Bott, T.R., "Process Heat Transfer", CRC Press, (1994).

CHAPTER 5: SHIELDING EVALUATION

5.0 INTRODUCTION

The shielding analysis of the HI-STAR 100 System is presented in this chapter. The HI-STAR 100 System is designed to accommodate different MPCs within one standard HI-STAR overpack. The MPCs are designated as MPC-24 (24 PWR fuel assemblies) and MPC-68 (68 BWR fuel assemblies).

In addition to storing intact PWR and BWR fuel assemblies, the HI-STAR 100 System is designed to store damaged BWR fuel assemblies and BWR fuel debris. Damaged fuel assemblies and fuel debris are defined in Section 2.1.3 and Appendix B to the Certificate of Compliance. Both damaged BWR fuel assemblies and BWR fuel debris are required to be loaded into Damaged Fuel Containers (DFCs) prior to being loaded into the MPC. DFCs containing fuel debris must be stored in the MPC-68F. DFCs containing damaged fuel assemblies may be stored in either the MPC-68 or the MPC-68F. Only the fuel assemblies in the Dresden 1 and Humboldt Bay fuel assembly classes identified in Table 2.1.2 are authorized as contents for storage in the HI-STAR 100 system as either damaged fuel or fuel debris.

The MPC-68 and MPC-68F are also capable of storing Dresden Unit 1 antimony-beryllium neutron sources and the single Thoria rod canister which contains 18 thoria rods that were irradiated in two separate fuel assemblies.

PWR fuel assemblies may contain burnable poison rod assemblies (BPRAs) or thimble plug devices (TPDs) or similarly named devices. These devices are an integral yet removable part of PWR fuel assemblies and therefore the HI-STAR 100 System has been designed to store PWR fuel assemblies with or without BPRAs or TPDs. Since BPRAs and TPDs occupy the same space within a fuel assembly, a single PWR fuel assembly will not contain both devices.

The sections that follow will demonstrate that the design of the HI-STAR 100 dry cask storage system fulfills the following acceptance criteria outlined in the Standard Review Plan, NUREG-1536[5.2.1]:

Acceptance Criteria

1. The minimum distance from each spent fuel handling and storage facility to the controlled area boundary must be at least 100 meters. The "controlled area" is defined in 10CFR72.3 as the area immediately surrounding an ISFSI or monitored retrievable storage (MRS) facility, for which the licensee exercises authority regarding its use and within which ISFSI operations are performed.

2. The cask vendor must show that, during both normal operations and anticipated occurrences, the radiation shielding features of the proposed dry cask storage system are sufficient to meet the radiation dose requirements in Sections 72.104(a). Specifically, the vendor must demonstrate this capability for a typical array of casks in the most bounding site configuration. For example, the most bounding configuration might be located at the minimum distance (100 meters) to the controlled area boundary, without any shielding from other structures or topography.

3. Dose rates from the cask must be consistent with a well-established "as low as reasonably achievable" (ALARA) program for activities in and around the storage site.

4. After a design-basis accident, an individual at the boundary or outside the controlled area shall not receive a dose greater than the limits specified in 10 CFR 72.106.

5. The proposed shielding features must ensure that the dry cask storage system meets the regulatory requirements for occupational and radiation dose limits for individual members of the public, as prescribed in 10 CFR Part 20, Subparts C and D.

This chapter contains the following information which demonstrates full compliance with the Standard Review Plan, NUREG-1536:

- A description of the shielding features of the HI-STAR 100 System.
- A description of the bounding source terms.
- A general description of the shielding analysis methodology.
- A description of the analysis assumptions and results for the HI-STAR 100 System.
- Analyses are presented for each MPC showing that the radiation dose rates follow As-Low-As-Reasonably-Achievable (ALARA) practices.
- The HI-STAR 100 System has been analyzed to show that the 10CFR72.104 and 10CFR72.106 controlled area boundary radiation dose limits are met during normal, off-normal, and accident conditions of storage for non-effluent radiation from illustrative ISFSI configurations at a minimum distance of 100 meters.
- Analyses are also presented which demonstrate that the storage of damaged fuel and fuel debris in the HI-STAR 100 System is bounded by the BWR intact fuel analysis during normal, off-normal, and accident conditions.

Chapter 10, Radiation Protection, contains the following information:

- A discussion of the estimated occupational exposures for the HI-STAR 100 System.
- A summary of the estimated radiation exposure to the public.

Chapter 2 contains a detailed description of structures, systems, and components important to safety.

Chapter 7 contains an analysis of the estimated dose at the controlled area boundary during normal, off-normal, and accident conditions from the release of radioactive materials. Therefore, this chapter only calculates the dose from direct neutron and gamma radiation emanating from the HI-STAR 100 System.

5.1 DISCUSSION AND RESULTS

The principal sources of radiation in the HI-STAR 100 System are:

- Gamma radiation originating from the following sources

    1. Decay of radioactive fission products
    2. Secondary photons from neutron capture in fissile and non-fissile nuclides
    3. Hardware activation products generated during core operations

- Neutron radiation originating from the following sources

    1. Spontaneous fission
    2. α,n reactions in fuel materials
    3. Secondary neutrons produced by fission from subcritical multiplication
    4. γ,n reactions (this source is negligible)
    5. Dresden Unit 1 antimony-beryllium neutron sources

Shielding from gamma radiation is provided by the steel structure of the MPC and overpack. In order for the neutron shielding to be effective, the neutrons must be thermalized and then absorbed in a material of high neutron cross section. In the HI-STAR 100 design, a neutron shielding material, Holtite-A, is used to thermalize the neutrons. Boron carbide, dispersed in the neutron shield, utilizes the high neutron absorption cross section of ^{10}B to absorb the thermalized neutrons.

The shielding analyses were performed with MCNP-4A [5.1.1] from Los Alamos National Laboratory. The source terms for the design basis fuels were calculated with the SAS2H and ORIGEN-S modules from the SCALE 4.3 system [5.1.2, 5.1.3]. A detailed description of the MCNP models and the source term calculations is presented in Sections 5.3 and 5.2, respectively.

The design basis intact zircaloy clad fuel assemblies used for calculating the dose rates presented in this chapter are B&W 15x15 and the GE 7x7, for PWR and BWR fuel types, respectively. The design basis intact 6x6, damaged, and mixed oxide (MOX) fuel assemblies are the GE 6x6. Table 2.1.6 specifies the acceptable intact zircaloy clad fuel characteristics for storage. Table 2.1.7 specifies the acceptable damaged and MOX zircaloy clad fuel characteristics for storage.

The design basis intact stainless steel clad fuels are the WE 15x15 and the A/C 10x10, for PWR and BWR fuel types, respectively. Table 2.1.11 specifies the acceptable fuel characteristics of stainless steel clad fuel for storage.

The MPC-24 and MPC-68 are qualified for storage of SNF with different combinations of maximum burnup levels and minimum cooling times. Figure 2.1.6 specifies the acceptable maximum burnup levels and minimum cooling times for storage of zircaloy clad fuel in the MPC-24 and the MPC-68 (Appendix B to the Certificate of Compliance presents this data in tabular form). Table 2.1.11 specifies the acceptable maximum burnup levels and minimum cooling times for storage of stainless steel clad fuel. The values in Figure 2.1.6 and Table 2.1.11 were chosen based on an analysis of the maximum decay heat load that could be accommodated within each MPC. The shielding analyses presented in this chapter used the burnup and cooling time combinations listed below which are either equal to or conservatively bound the acceptable burnup levels and cooling times shown in Figure 2.1.6 and Table 2.1.11.

Maximum Burnup and Minimum Cooling Times Analyzed	
Zircaloy Clad Fuel	
MPC-24	**MPC-68**
40,000 MWD/MTU 5 year cooling	35,000 MWD/MTU 5 year cooling
47,500 MWD/MTU 8 year cooling	45,000 MWD/MTU 9 year cooling
N/A	30,000 MWD/MTU 18 year cooling (6x6 intact, damaged and MOX fuel)
Stainless Steel Clad Fuel	
MPC-24	**MPC-68**
30,000 MWD/MTU 9 year cooling	22,500 MWD/MTU 10 year cooling
40,000 MWD/MTU 15 year cooling	N/A

Appendix B to the Certificate of Compliance requires that, in the MPC-24, for a minimum cooling time of 5-years, the maximum burnup is 28,700 MWD/MTU, and for 15-year cooling the maximum burnup is 42,100 MWD/MTU for PWR fuel assemblies without Burnable Poison Rod Assemblies (BPRAs). PWR fuel assemblies containing BPRAs are limited to 28,300 MWD/MTU for 5 year cooling and 41,400 MWD/MTU for 15 year cooling. Since the burnup and cooling times analyzed in this chapter for the MPC-24 were 40,000 MWD/MTU and 5-year cooling and 47,500 MWD/MTU and 8-year cooling, the shielding analysis presented is conservatively bounding for the MPC-24.

Appendix B to the Certificate of Compliance requires that, in the MPC-68, for a minimum cooling time of 5-years, the maximum burnup is 26,000 MWD/MTU, and for 15-year cooling

the maximum burnup is 37,600 MWD/MTU. Since the burnup and cooling times analyzed in this chapter for the MPC-68 were 35,000 MWD/MTU and 5-year cooling and 45,000 MWD/MTU and 9-year cooling, the shielding analysis presented is conservatively bounding for the MPC-68.

The dose rates corresponding to the burnup and cooling time combination which resulted in the highest dose rates at the midplane of the cask during normal conditions are reported in this section. Dose rates for each of the combinations are listed in Section 5.4.

5.1.1 Normal and Off-Normal Operations

Chapter 11 discusses the potential off-normal conditions and their effect on the HI-STAR 100 System. None of the off-normal conditions have any impact on the shielding analysis. Therefore, off-normal and normal conditions are identical for the purpose of the shielding evaluation.

The 10CFR72.104 criteria for radioactive materials in effluents and direct radiation during normal operations are:

1. During normal operations and anticipated occurrences, the annual dose equivalent to any real individual who is located beyond the controlled area, must not exceed 25 mrem to the whole body, 75 mrem to the thyroid and 25 mrem to any other critical organ.

2. Operational restrictions must be established to meet as low as reasonably achievable objectives for radioactive materials in effluents and direct radiation.

10CFR20 Subparts C and D specify additional requirements for occupational dose limits and radiation dose limits for individual members of the public. Chapter 10 specifically addresses these regulations.

In accordance with ALARA practices, design objective dose rates are established for the HI-STAR 100 in Section 2.3.5.2 as: 125 mrem/hour on the radial surface of the overpack, and 375 mrem/hour in areas above and below the neutron shield in the radial direction.

The dose rates presented in this section are calculated at 40,000 MWD/MTU and 5-year cooling for the MPC-24, and 35,000 MWD/MTU and 5-year cooling for the MPC-68. Based on a comparison of the normal condition dose rates at the fuel mid-plane for the various burnup and cooling time combinations analyzed, these were chosen as the worst case for the MPC-24 and the MPC-68. Section 5.4 provides a detailed list of dose rates at several cask locations for all burnup and cooling times analyzed.

Figure 5.1.1 identifies the locations of the dose points referenced in the summary tables. The bottom shield shown in this figure is temporary shielding which may be used during on-site horizontal handling operations. Dose Point #7 is located directly below the overpack bottom plate or directly below the bottom shield when it is attached. Dose Points #1, #3, and #4 are not

contact doses, but rather, in-air doses at the locations shown. The dose values reported at the locations shown on Figure 5.1.1 are averaged over a region that is approximately 1 foot in width.

Tables 5.1.2 and 5.1.3 provide the maximum dose rates adjacent to the overpack during normal conditions for each of the MPCs. Tables 5.1.5 and 5.1.6 provide the maximum dose rates at one meter from the overpack.

The dose to any real individual at or beyond the controlled area boundary is required to be below 25 mrem per year. The minimum distance to the controlled area boundary is 100 meters from the ISFSI. Only the MPC-24 was used in the calculation of the dose rates at the controlled area boundary. The MPC-24 was chosen because its dose rates are equivalent or greater than the dose rates from the MPC-68 as shown in Tables 5.1.2, 5.1.3, 5.1.5, and 5.1.6. Table 5.1.7 presents the annual dose to an individual from a single cask and various arrays of casks, assuming 100% occupancy (8760 hours). The minimum distance required for the corresponding dose is also listed. These values were calculated for the MPC-24 with a burnup of 40,000 MWD/MTU and a 5-year cooling time. It will be shown in Section 5.4.3 that this burnup and cooling time results in the highest offsite dose for the combinations of maximum burnup and minimum cooling time analyzed. It is noted that these data are provided for illustrative purposes only. A detailed site specific evaluation of dose at the controlled area boundary will be performed for each ISFSI in accordance with 10CFR72.212, as stated in Chapter 12, Operating Controls and Limits. The site specific evaluation will consider dose from other portions of the facility and will consider the specifics of the fuel being stored (burnup and cooling time).

Figure 5.1.2 is an annual dose versus distance graph for the cask configurations provided in Table 5.1.7. This curve, which is based on 100% occupancy, is provided for illustrative purposes only and will be re-evaluated on a site-specific basis.

Section 5.2 lists the gamma and neutron sources for the design basis intact and damaged fuels. Since the source strengths of the damaged fuel and the MOX fuel are significantly smaller in all energy groups than those corresponding to the intact design basis fuel source strengths, the damaged and MOX fuel dose rates for normal conditions are bounded by the MPC-68 analysis with design basis intact fuel. Therefore, no explicit analysis is required to demonstrate that the MPC-68 with damaged or MOX fuel will meet the normal condition regulatory requirements.

Section 5.2.6 lists the gamma and neutron sources from the Dresden Unit 1 Thoria rod canister and demonstrates that the Thoria rod canister is bounded by the design basis Dresden Unit 1 6x6 intact fuel.

Section 5.2.4 presents the Co-60 sources from the BPRAs and TPDs that are permitted for storage in the HI-STAR 100. Section 5.4.6 demonstrates that the maximum dose rates presented in this section bound the dose rates from fuel assemblies containing either BPRAs or TPDs.

Section 5.4.7 demonstrates that the Dresden Unit 1 fuel assemblies containing antimony-beryllium neutron sources are bounded by the shielding analysis presented in this section.

Section 5.2.3 presents the gamma and neutron source for the design basis intact stainless steel clad fuel. The dose rates from this fuel are provided in Section 5.4.5.

The analyses summarized in this section demonstrate that the HI-STAR 100 System is in compliance with the 10CFR72.104 limits and ALARA practices.

5.1.2 Accident Conditions

The 10CFR72.106 radiation dose limits at the controlled area boundary for design basis accidents are:

> Any individual located on or beyond the nearest boundary of the controlled area may not receive from any design basis accident the more limiting of a total effective dose equivalent of 5 Rem, or the sum of the deep-dose equivalent and the committed dose equivalent to any individual organ or tissue (other than the lens of the eye) of 50 Rem. The lens dose equivalent shall not exceed 15 Rem and the shallow dose equivalent to skin or to any extremity shall not exceed 50 rem. The minimum distance from the spent fuel or high level radioactive waste handling and storage facilities to the nearest boundary of the controlled area shall be at least 100 meters.

The design basis accidents analyzed in Chapter 11 have one bounding consequence which affects the shielding materials. It is the damage to the neutron shield as a result of the design basis fire. Other design basis accidents result in damage to the outer enclosure shell and neutron shield; however, these accidents are localized. In a conservative fashion, the dose analysis assumes that as a result of the fire, the neutron shield is completely destroyed and replaced by a void. This is highly conservative as there will be limited sources of combustible materials stored in or around the ISFSI. Additionally, the neutron shield is assumed to be completely lost, whereas some portion of the neutron shield would be expected to remain, as the neutron shield material is fire retardant.

Throughout all design basis accident conditions the axial location of the fuel will remain fixed within the MPC because of the fuel spacers. Chapter 3 provides an analysis to show that the fuel spacers do not fail under all normal, off-normal, and accident conditions of storage. Chapter 3 also shows that the inner shell, intermediate shells, radial channels, and outer enclosure shell of the overpack remain unaltered throughout all design basis accident conditions. Localized damage of the overpack outer enclosure shell could be experienced. However, the localized deformations will have a negligible impact on the dose rate at the boundary of the controlled area.

The complete loss of the neutron shield significantly affects the dose at Dose Point #2 at the mid-height adjacent to the overpack neutron shield. Loss of the neutron shield has a small effect on the other dose points. To illustrate the impact of the design basis accident, the dose rates at Dose

Point #2 (see Figure 5.1.1) are provided in Tables 5.1.8 and 5.1.9. The normal condition dose rates are provided for reference.

Table 5.1.9 provides a comparison of the normal and accident condition dose rates at one meter from the overpack. By comparing the increase in dose rates from normal and accident conditions and the maximum normal condition controlled area dose rate, it is evident that the dose as a result of the design basis accident cannot exceed 5 Rem at the controlled area boundary for the short duration of the accident. Conservatively assuming a 1/R reduction in the dose rate, the dose rate at the 100 meter controlled area boundary would be less than 5 mrem/hr for a single HI-STAR 100 during the accident condition. At this dose rate, it would take more than 1000 hours (41 days) for the dose at the controlled area boundary to reach 5 Rem. This length of time greatly exceeds the time necessary to implement and complete the corrective actions outlined in Chapter 11 for the fire accident. Therefore, the dose requirement of 10CFR72.106 is satisfied.

The consequences of the design basis accident conditions for the MPC-68 storing damaged fuel and the MPC-68F storing damaged fuel and/or fuel debris differ slightly from those with intact fuel. It is conservatively assumed that during a drop accident (vertical, horizontal, or tip-over) the fuel collapses and the pellets rest in the bottom of the damaged fuel container. Since the damaged and MOX fuels are both Dresden 1 fuel, the MOX fuel can also be considered damaged fuel. Analysis in Section 5.4.2 demonstrates that the damaged fuel in the post-accident condition has lower source terms (both gamma and neutron) per inch than the intact BWR design basis fuel. Therefore, the damaged fuel post-accident dose rates are bounded by the BWR intact fuel post-accident dose rates.

Analyses summarized in this section demonstrate the HI-STAR 100 System's compliance with the 10CFR72.106 limits.

Table 5.1.1

DELETED

Table 5.1.2

DOSE RATES ADJACENT TO OVERPACK FOR NORMAL CONDITIONS
MPC-24 WITH DESIGN BASIS ZIRCALOY CLAD FUEL AT WORST CASE
BURNUP AND COOLING TIME
40,000 MWD/MTU AND 5-YEAR COOLING

Dose Point† Location	Fuel Gammas†† (mrem/hr)	^{60}Co Gammas (mrem/hr)	Neutrons (mrem/hr)	Totals (mrem/hr)
1	12.45	231.52	82.27	326.24
2	96.88	0.03	22.12	119.03
3	3.51	81.12	70.28	154.90
4	1.81	35.86	39.47	77.14
5	0.34	0.69	56.70	57.73
6 (dry MPC)†††	27.07	286.19	126.02	439.28
7 (no temp. shield)	100.36	1432.28	397.30	1929.94
7 (with temp. shield)	28.27	329.84	19.84	377.94

† Refer to Figure 5.1.1.

†† Gammas generated by neutron capture are included with fuel gammas.

††† Overpack closure plate not present.

Table 5.1.3

DOSE RATES ADJACENT TO OVERPACK FOR NORMAL CONDITIONS
MPC-68 WITH DESIGN BASIS ZIRCALOY CLAD FUEL AT WORST CASE
BURNUP AND COOLING TIME
35,000 MWD/MTU AND 5-YEAR COOLING

Dose Point† Location	Fuel Gammas†† (mrem/hr)	^{60}Co Gammas (mrem/hr)	Neutrons (mrem/hr)	Totals (mrem/hr)
1	10.26	297.76	65.63	373.64
2	100.42	0.02	19.40	119.85
3	0.97	127.41	29.88	158.26
4	0.44	51.49	17.76	69.69
5	0.13	0.72	26.45	27.30
6 (dry MPC)†††	9.32	329.17	65.38	403.87
7 (no temp. shield)	64.46	1794.41	325.90	2184.76
7 (with temp. shield)	20.36	381.90	14.52	416.78

† Refer to Figure 5.1.1.

†† Gammas generated by neutron capture are included with fuel gammas.

††† Overpack closure plate not present.

Table 5.1.4

DELETED

Table 5.1.5

DOSE RATES AT ONE METER FOR NORMAL CONDITIONS
MPC-24 WITH DESIGN BASIS ZIRCALOY CLAD FUEL AT WORST CASE
BURNUP AND COOLING TIME
40,000 MWD/MTU AND 5-YEAR COOLING

Dose Point† Location	Fuel Gammas†† (mrem/hr)	^{60}Co Gammas (mrem/hr)	Neutrons (mrem/hr)	TOTALS (mrem/hr)
1	10.11	25.00	8.69	43.79
2	42.67	1.06	7.74	51.47
3	7.10	14.06	9.04	30.21
4	4.59	14.69	9.33	28.61
5	0.11	0.32	16.67	17.11
7 (no temp. shield)	52.66	720.72	116.30	889.68
7 (with temp. shield)	11.46	139.22	15.19	165.87

† Refer to Figure 5.1.1.

†† Gammas generated by neutron capture are included with fuel gammas.

Table 5.1.6

DOSE RATES AT ONE METER FOR NORMAL CONDITIONS
MPC-68 WITH DESIGN BASIS ZIRCALOY CLAD FUEL AT WORST CASE
BURNUP AND COOLING TIME
35,000 MWD/MTU AND 5-YEAR COOLING

Dose Point† Location	Fuel Gammas†† (mrem/hr)	^{60}Co Gammas (mrem/hr)	Neutrons (mrem/hr)	Totals (mrem/hr)
1	10.47	34.29	7.52	52.28
2	43.01	0.60	7.50	51.11
3	4.37	21.32	4.23	29.91
4	2.60	22.51	4.19	29.30
5	0.06	0.37	7.44	7.86
7 (no temp. shield)	29.91	888.15	87.01	1005.07
7 (with temp. shield)	8.10	162.56	10.52	181.19

† Refer to Figure 5.1.1.

†† Gammas generated by neutron capture are included with fuel gammas.

Table 5.1.7

DOSE RATES FOR ARRAYS OF MPC-24
WITH DESIGN BASIS ZIRCALOY CLAD FUEL
40,000 MWD/MTU AND 5-YEAR COOLING

Array Configuration	1 cask	2x2	2x3	2x4	2x5
Annual Dose (mrem/year)[†]	13.55	18.60	13.84	18.45	23.06
Distance to Controlled Area Boundary (meters)[††], [†††]	300	350	400	400	400

[†] 100% occupancy is assumed.

[††] Dose location is at the center of the long side of the array.

[†††] Actual controlled area boundary dose rates will be lower because the maximum permissible burnup for 5-year cooling as specified in the Technical Specifications is lower than the burnup analyzed for the design basis fuel used in this chapter .

Table 5.1.8

DOSE RATES ADJACENT TO OVERPACK FOR ACCIDENT CONDITIONS
DESIGN BASIS ZIRCALOY CLAD FUEL
AT WORST CASE BURNUP AND COOLING TIME

Dose Point† Location	Fuel Gammas†† (mrem/hr)	^{60}Co Gammas (mrem/hr)	Neutrons (mrem/hr)	Totals (mrem/hr)
MPC-24 (40,000 MWD/MTU AND 5-YEAR COOLING)				
2 (Accident Condition)	221.84	0.04	1149.46	1371.34
2 (Normal Condition)	96.88	0.03	22.12	119.03
MPC-68 (35,000 MWD/MTU AND 5-YEAR COOLING)				
2 (Accident Condition)	223.20	0.04	1140.57	1363.82
2 (Normal Condition)	100.42	0.02	19.40	119.85

† Refer to Figure 5.1.1.

†† Gammas generated by neutron capture are included with fuel gammas.

Table 5.1.9

DOSE RATES AT ONE METER FOR ACCIDENT CONDITIONS
DESIGN BASIS ZIRCALOY CLAD FUEL
AT WORST CASE BURNUP AND COOLING TIME

Dose Point† Location	Fuel Gammas†† (mrem/hr)	^{60}Co Gammas (mrem/hr)	Neutrons (mrem/hr)	Totals (mrem/hr)
MPC-24 (40,000 MWD/MTU AND 5-YEAR COOLING)				
2 (Accident Condition)	100.98	1.80	388.94	491.73
2 (Normal Condition)	42.67	1.06	7.74	51.47
MPC-68 (35,000 MWD/MTU AND 5-YEAR COOLING)				
2 (Accident Condition)	98.28	1.48	360.93	460.69
2 (Normal Condition)	43.01	0.60	7.50	51.11

† Refer to Figure 5.1.1.

†† Gammas generated by neutron capture are included with fuel gammas.

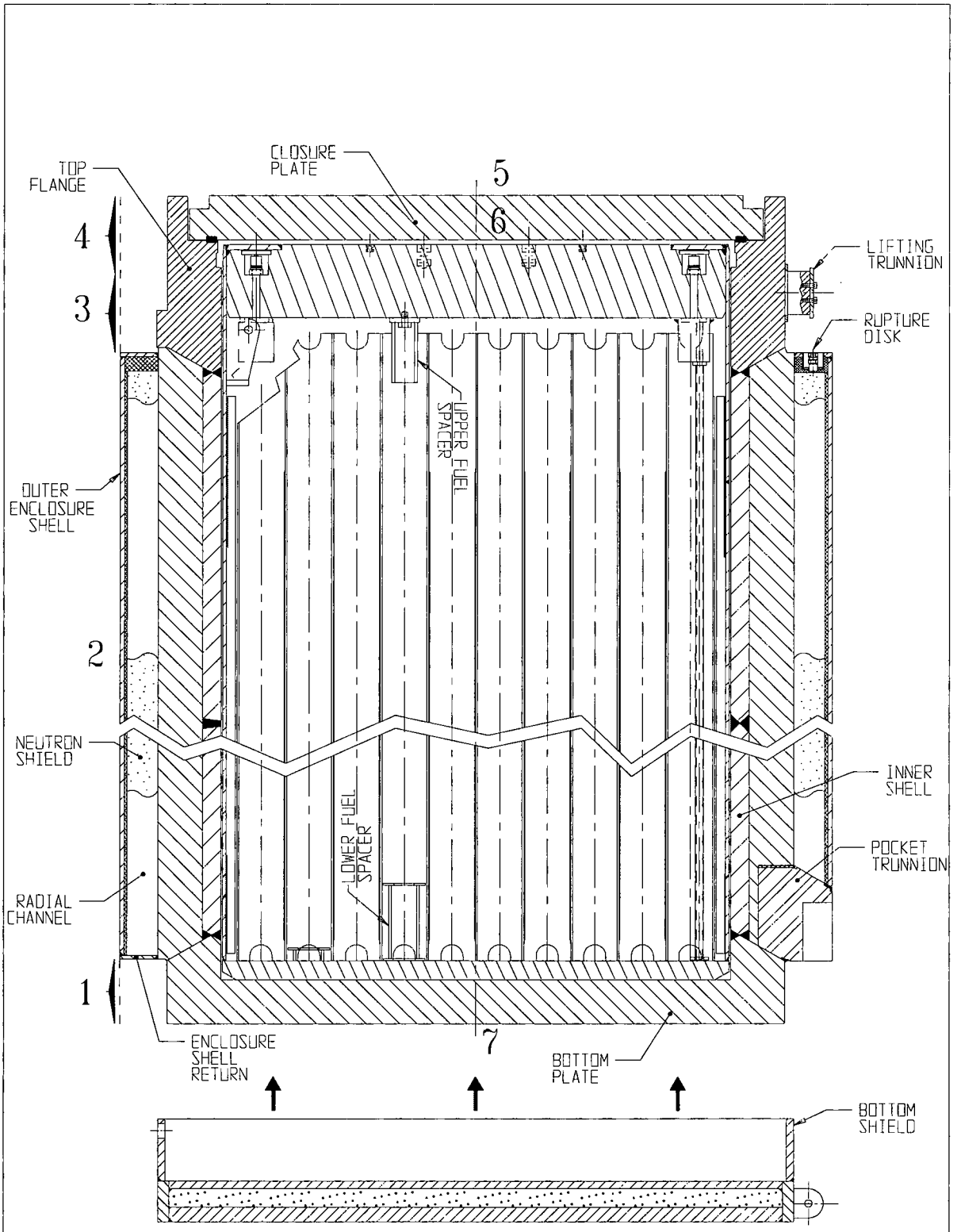

FIGURE 5.1.1; CROSS SECTION ELEVATION VIEW OF OVERPACK WITH DOSE POINT LOCATIONS

REPORT HI-2012610 REVISION 0

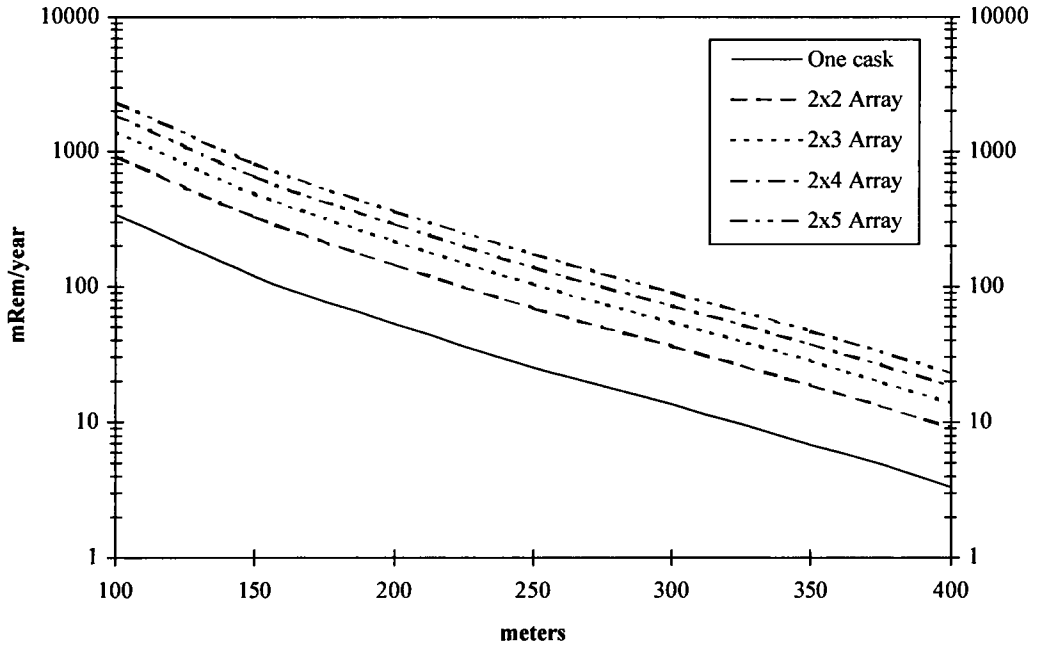

FIGURE 5.1.2; ANNUAL DOSE VERSUS DISTANCE FOR VARIOUS CONFIGURATIONS OF THE MPC-24
40,000 MWD/MTU AND 5-YEAR COOLING
100% OCCUPANCY ASSUMED

5.2 SOURCE SPECIFICATION

The neutron and gamma source terms, decay heat values, and quantities of radionuclides available for release, were calculated with the SAS2H and ORIGEN-S modules of the SCALE 4.3 system [5.1.2, 5.1.3]. Sample input files for SAS2H and ORIGEN-S are provided in Appendices 5.A and 5.B, respectively. The gamma source term is actually comprised of three distinct sources. The first is a gamma source term from the active fuel region due to decay of fission products. The second source term is from ^{60}Co activity of the steel structural material in the fuel element above and below the active fuel region. The third source is from (n,γ) reactions described below.

A description of the design basis intact zircaloy clad fuel for the source term calculations is provided in Table 5.2.1. The PWR fuel assembly described is the assembly that produces the highest neutron and gamma sources and the highest decay heat load from the following fuel assembly classes listed in Tables 2.1.1: B&W 15x15, B&W 17x17, CE 14x14, CE 16x16, WE 14x14, WE 15x15, WE 17x17, St. Lucie, and Ft. Calhoun. The BWR fuel assembly described is the assembly that produces the highest neutron and gamma sources and the highest decay heat load from the following fuel assembly classes listed in Table 2.1.2: GE BWR/2-3, GE BWR/4-6, Humboldt Bay 7x7, and Dresden 1 8x8. Multiple SAS2H and ORIGEN-S calculations were performed to confirm that the B&W 15x15 and the GE 7x7, which have the highest UO_2 mass, bound all other PWR and BWR fuel assemblies, respectively. Section 5.2.5 discusses, in detail, the determination of the design basis fuel assemblies.

The design basis Humboldt Bay and Dresden 1 6x6 fuel assembly, which is also the design basis damaged fuel assembly for the Humboldt Bay and Dresden 1 damaged fuel or fuel debris, is described in Table 5.2.2. The design basis damaged fuel assembly is also the design basis fuel assembly for fuel debris. The fuel assembly type listed produces the highest total neutron and gamma sources from the fuel assemblies at Dresden 1 and Humboldt Bay. Table 5.2.15 provides a description of the design basis Dresden 1 MOX fuel assembly used in this analysis. The design basis 6x6, damaged, and MOX fuel assemblies which are smaller than the GE 7x7, are assumed to have the same hardware characteristics as the GE 7x7. This is conservative because the larger hardware mass of the GE 7x7 results in a larger ^{60}Co activity.

The design basis stainless steel clad fuel assembly for the Haddam Neck and San Onofre 1 assembly classes is described in Table 5.2.18. This table also describes the design basis stainless steel clad LaCrosse fuel assembly.

In performing the SAS2H and ORIGEN-S calculations, a single full power cycle was used to achieve the desired burnup. This assumption, in conjunction with the above-average specific powers listed in Tables 5.2.1, 5.2.2, 5.2.15, and 5.2.18 resulted in conservative source term calculations.

Sections 5.2.1 and 5.2.2 describe the calculation of gamma and neutron source terms for zircaloy clad fuel while Section 5.2.3 discusses the calculation of the gamma and neutron source terms for the stainless steel clad fuel.

5.2.1 Gamma Source

Tables 5.2.4 through 5.2.6 provide the gamma source in MeV/s and photons/s as calculated with SAS2H and ORIGEN-S for the design bases intact fuels for the MPC-24 and MPC-68, and the design basis damaged fuel. Table 5.2.16 provides the gamma source in MeV/s and photons/s for the design basis MOX fuel. NUREG-1536 [5.2.1] states that "only gammas with energies from approximately 0.8 to 2.5 MeV will contribute significantly to the dose rate." Conservatively, only energies in the range of 0.7 MeV-3.0 MeV are used in the shielding calculations. Photons with energies below 0.7 MeV are too weak to penetrate the steel of the overpack, and photons with energies above 3.0 MeV are too few to contribute significantly to the external dose. This section provides the radiation source for each of the burnup levels and cooling times evaluated.

The primary source of activity in the non-fuel regions of an assembly arise from the activation of ^{59}Co to ^{60}Co. The primary source of ^{59}Co in a fuel assembly is the steel structural material above and below the fuel. The zircaloy in these regions is neglected since it does not have a significant ^{59}Co impurity level. Reference [5.2.2] indicates that the impurity level in steel is 800 ppm or 0.8 gm/kg. As a conservative measure, the impurity level of ^{59}Co was assumed to be 1000 ppm or 1.0 gm/kg. Therefore, Inconel and stainless steel in the non-fuel regions are both conservatively assumed to have the 1.0 gm/kg impurity level.

The gamma source from the activation of the grid spacers is negligible in comparison to the source from the active fuel. In addition, in most fuel elements that obtain high burnups, the grid spacers are manufactured from zircaloy which does not activate to produce a gamma source. Therefore, for the PWR fuel assembly, no contribution to the fuel region gamma source from activation of grid spacers is provided in the source term calculations. The BWR assembly grid spacers are zircaloy, however, some assembly designs have steel springs in conjunction with the grid spacers. The gamma source for the BWR fuel assembly includes the activation of these springs associated with the grid spacers.

The non-fuel data listed in Table 5.2.1 was taken from References [5.2.2], [5.2.4], and [5.2.5]. The BWR masses are for an 8x8 fuel assembly. These masses are also appropriate for the 7x7 assembly since the masses of the non-fuel hardware from a 7x7 and an 8x8 are approximately the same. The masses listed are those of the steel components. The zircaloy in these regions was not included because zircaloy does not produce significant activation. These masses are larger than most other fuel assemblies from other manufactures. This, in combination with the conservative ^{59}Co impurity level, results in a conservative estimate of the ^{60}Co activity.

The masses in Table 5.2.1 were used to calculate a ^{59}Co impurity level in the fuel material. The grams of impurity were then used in ORIGEN-S to calculate a ^{60}Co activity level for the desired

burnup and decay time. The methodology used to determine the activation level was developed from Reference [5.2.3] and is described here.

1. The activity of the ^{60}Co is calculated using ORIGEN-S. The flux used in the calculation was the in-core fuel region flux at full power.

2. The activity calculated in Step 1 for the region of interest was modified by the appropriate scaling factors listed in Table 5.2.7. These scaling factors were taken from Reference [5.2.3].

Tables 5.2.9 and 5.2.10 provide the ^{60}Co activity utilized in the shielding calculations in the non-fuel regions of the assemblies for the MPC-24 and the MPC-68. The design basis damaged and MOX fuel assemblies are conservatively assumed to have the same ^{60}Co source strength as the BWR intact design basis fuel. This is a conservative assumption as the design basis damaged fuel and MOX fuel are limited to a significantly lower burnup and longer cooling time than the intact design basis fuel.

In addition to the two sources already mentioned, a third source arises from (n,γ) reactions in the material of the MPC and the overpack. This source of photons is properly accounted for in MCNP when a neutron calculation is performed in a coupled neutron-gamma mode.

5.2.2 Neutron Source

It is well known that the neutron source strength increases as enrichment decreases, for a constant burnup and decay time. This is due to the increase in Pu content in the fuel which increases the inventory of other transuranium nuclides such as Cm. The gamma source also varies with enrichment, although only slightly. Because of this effect and in order to obtain conservative source terms, low initial fuel enrichments were chosen for the BWR and PWR design basis fuel assemblies. The enrichments are appropriately varied as a function of burnup. Table 5.2.23 presents the ^{235}U initial enrichments for various burnup ranges from 20,000 - 50,000 MWD/MTU for PWR and BWR zircaloy clad fuel. These enrichments are based on Reference [5.2.6]. Table 8 of this reference presents average enrichments for burnup ranges. The initial enrichments chosen in Table 5.2.23 are approximately the average enrichments for the burnup range that are 5,000 MWD/MTU less than the ranges listed in Table 5.2.23. These enrichments are below the enrichments typically required to achieve the burnups that were analyzed. Therefore, the source term calculations are conservative.

The neutron source calculated for the design basis intact fuel assemblies for the MPC-24 and MPC-68 and the design basis damaged fuel are listed in Tables 5.2.12 through 5.2.14 in neutrons/s. Table 5.2.17 provides the neutron source in neutrons/sec for the design basis MOX fuel assembly. ^{244}Cm accounts for approximately 96% of the total number of neutrons produced, with slightly over 2% originating from (α,n) reactions within the UO_2 fuel. The remaining 2% derive from spontaneous fission in various Pu and Cm radionuclides. In addition, any neutrons

generated from subcritical multiplication, (n,2n) or similar reactions are properly accounted for in the MCNP calculation.

5.2.3 Stainless Steel Clad Fuel Source

Table 5.2.18 lists the characteristics of the design basis stainless steel clad fuel. The fuel characteristics listed in this table are the input parameters that were used in the shielding calculations described in this chapter. The active fuel length listed in Table 5.2.18 is actually longer than the true active fuel length of 122 inches for the WE 15x15 and 83 inches for the A/C 10x10. Since the true active fuel length is shorter than the design basis zircaloy clad active fuel length, it would be incorrect to calculate source terms for the stainless steel fuel using the correct fuel length and compare them directly to the zircaloy clad fuel source terms because this type of approach would not reflect the potential change in dose rates at the center of the cask (center of the active fuel). As an example, if it is assumed that the source strength for both the stainless steel and zircaloy fuel is 144 photons/s and that the active fuel lengths of the stainless steel fuel and zircaloy fuel are 83 inches and 144 inches, respectively; the source strengths per inch of active fuel would be different for the two fuel types, 1.73 photons/s/inch and 1 photons/s/inch for the stainless steel and zircaloy fuel, respectively. The result would be a higher photon dose rate at the center of the cask with the stainless steel fuel than with the zircaloy clad fuel; a conclusion that would be overlooked by just comparing the source terms. This is an important consideration because the stainless steel clad fuel differs from the zircaloy clad in one important aspect: the stainless steel cladding will contain a significant photon source from Cobalt-60 which will be absent from the zircaloy clad fuel.

In order to eliminate the potential confusion when comparing source terms, the stainless steel clad fuel source terms were calculated with the same active fuel length as the design basis zircaloy clad fuel. Reference [5.2.2] indicates that the Cobalt-59 impurity level in steel is 800 ppm or 0.8 gm/kg. This impurity level was used for the stainless steel cladding in the source term calculations. It is assumed that the end fitting masses of the stainless steel clad fuel are the same as the end fitting masses of the zircaloy clad fuel. Therefore, separate source terms are not provided for the end fittings of the stainless steel fuel.

Tables 5.2.19 through 5.2.22 list the neutron and gamma source strengths for the design basis stainless steel clad fuel. It is obvious from these source terms that the neutron source strength for the stainless steel fuel is lower than for the zircaloy fuel. However, this is not true for all photon energy groups. The peak energy group is from 1.0 to 1.5 MeV which results from the large Cobalt activation in the cladding. Since some of the source strengths are higher for the stainless steel fuel, Section 5.4.5 presents the dose rates at the center of the overpack for the stainless steel fuel. The center dose location is the only location of concern since the end fittings are assumed to be the same mass as the end fittings for the zircaloy clad fuel. In addition, the burnup is lower and the cooling time is longer for the stainless steel fuel compared to the zircaloy clad fuel.

5.2.4 Non-Fuel Hardware

Rod cluster control assemblies and axial power shaping rods are not permitted for storage in the HI-STAR 100 system. However, burnable poison rod assemblies (BPRAs) and thimble plug devices (TPDs) are permitted for storage in the HI-STAR 100 System as an integral part of a PWR fuel assembly.

5.2.4.1 BPRAs and TPDs

Burnable poison rod assemblies (BPRA) (including wet annular burnable absorbers and similarly designed devices with different names) and thimble plug devices (TPD) (including orifice rod assemblies, guide tube plugs, and similarly designed devices with different names) are an integral, yet removable, part of a large portion of PWR fuel. The TPDs are not used in all assemblies in a reactor core but are reused from cycle to cycle. Therefore, these devices can achieve very high burnups. In contrast, BPRAs are burned with a fuel assembly in core and are not reused. In fact, many BPRAs are removed after one or two cycles before the fuel assembly is discharged. Therefore, the achieved burnup for BPRAs is not significantly different than fuel assemblies.

TPDs are made of stainless steel and contain a small amount of inconel. These devices extend down into the plenum region of the fuel assembly but do not extend into the active fuel region with the exception of the W 14x14 water displacement guide tube plugs. Since these devices are made of stainless steel, there is a significant amount of cobalt-60 produced during irradiation. This is the only significant radiation source from the activation of steel and inconel.

BPRAs are made of stainless steel in the region above the active fuel zone and may contain a small amount of inconel in this region. Within the active fuel zone the BPRAs may contain 2-24 rodlets which are burnable absorbers clad in either zircaloy or stainless steel. The stainless steel clad BPRAs create a significant radiation source (Co-60) while the zircaloy clad BPRAs create a negligible radiation source. Therefore the stainless steel clad BPRAs are bounding.

SAS2H and ORIGEN-S were used to calculate a radiation source term and decay heat level for the TPDs and BPRAs. In the ORIGEN-S calculations the cobalt-59 impurity level was conservatively assumed to be 0.8 gm/kg for stainless steel and 4.7 gm/kg for inconel. These calculations were performed by irradiating the appropriate mass of steel and inconel using the flux calculated for the design basis B&W 15x15 fuel assembly. The mass of material in the regions above the active fuel zone was scaled by the appropriate scaling factors listed in Table 5.2.10 in order to account for the reduced flux levels above the fuel assembly. The total curies of cobalt and the decay heat load were calculated for the TPDs and BPRAs as a function of burnup and cooling time. For burnups beyond 45,000 MWD/MTU, it was assumed, for the purpose of the calculation, that the burned fuel assembly was replaced with a fresh fuel assembly every 45,000 MWD/MTU. This was achieved in ORIGEN-S by resetting the flux levels and cross sections to the 0 MWD/MTU condition after every 45,000 MWD/MTU.

Since the HI-STAR 100 cask system is designed to store many varieties of PWR fuel, a bounding TPD and BPRA had to be determined for the purposes of the analysis. This was accomplished by analyzing all of the BPRAs and TPDs (Westinghouse and B&W 14x14 through 17x17) found in references [5.2.5] and [5.2.7] to determine the TPD and BPRA which produced the highest Cobalt-60 source term and decay heat for a specific burnup and cooling time. The bounding TPD was determined to be the Westinghouse 17x17 guide tube plug and the bounding BPRA was actually determined by combining the higher masses of the Westinghouse 17x17 and 15x15 BPRAs into a singly hypothetical BPRA. The masses of this TPD and BPRA are listed in Table 5.2.29. As mentioned above, reference [5.2.5] describes the Westinghouse 14x14 water displacement guide tube plug as having a steel portion which extends into the active fuel zone. This particular water displacement guide tube plug was analyzed and determined to be bounded by the design basis TPD and BPRA.

Once the bounding BPRA and TPD were determined, the allowable decay heat load and Co-60 source from the BPRA and TPD were specified: 0.77 watts and 50 curies Co-60 for each TPD, and 13.0 watts and 831 curies Co-60 for each BPRA. Table 5.2.30 shows the curies of Co-60 that were calculated for BPRAs and TPDs in each region of the fuel assembly (e.g. incore, plenum, top). The allowable decay heat load for the TPDs and BPRAs was subtracted from the allowable decay heat load per assembly to determine the allowable PWR fuel assembly burnup and cooling times listed in Table 1.1-6 of Appendix B of the Certificate of Compliance. Since the decay heat load of the TPDs is negligible the same burnup and cooling time is used for assemblies with or without TPDs. However, a different burnup and cooling time is used for assemblies that contain BPRAs to account for the allowable BPRA decay heat load of 13.0 watts. A separate allowable burnup and cooling time is used for BPRAs and TPDs. These burnup and cooling times assure that the decay heat load and Cobalt-60 activity remain below the allowable levels specified above. It should be noted that at very high burnups, greater than 200,000 MWD/MTU the TPD decay heat load for a given cooling time actually decreases as the burnup continues to increase. This is due to a decrease in the Cobalt-60 production rate as the initial Cobalt-59 impurity is being depleted. Conservatively, a constant cooling time has been specified for burnups from 180,000 to 630,000 MWD/MTU for the TPDs.

Section 5.4.6 demonstrates that the dose rates from fuel assemblies containing BPRAs or TPDs is bounded by the dose rates presented in Section 5.1.1.

5.2.5 Choice of Design Basis Assembly

The analysis presented in this chapter was performed to bound the fuel assembly classes listed in Tables 2.1.1 and 2.1.2. In order to perform a bounding analysis, a design basis fuel assembly must be chosen. Therefore, a fuel assembly from each fuel class was analyzed and a comparison of the neutrons/sec, photons/sec, and thermal power (watts) was performed. The fuel assembly which produced the highest source for a specified burnup, cooling time, and enrichment was

chosen as the design basis fuel assembly. A separate design basis assembly was chosen for the MPC-24 and the MPC-68.

5.2.5.1 PWR Design Basis Assembly

Table 2.1.1 lists the PWR fuel assembly classes that were evaluated to determine the design basis PWR fuel assembly. Within each class, the fuel assembly with the highest UO_2 mass was analyzed. Since the variations of fuel assemblies within a class are very minor (pellet diameter, clad thickness, etc.), it is conservative to choose the assembly with the highest UO_2 mass. For a given class of assemblies, the one with the highest UO_2 mass will produce the highest radiation source because, for a given burnup (MWD/MTU) and enrichment, the highest UO_2 mass will have produced the most energy and therefore the most fission products.

Table 5.2.24 presents the characteristics of the fuel assemblies analyzed to determine the design basis zircaloy clad PWR fuel assembly. The fuel assembly listed for each class is the assembly with the highest UO_2 mass. The St. Lucie and Ft. Calhoun classes are not present in Table 5.2.24. These assemblies are shorter versions of the CE 16x16 and CE 14x14 assembly classes, respectively. Therefore, these assemblies are bounded by the CE 16x16 and CE 14x14 classes and were not explicitly analyzed. Since the Haddam Neck and San Onofre 1 classes are stainless steel clad fuel, these classes were analyzed separately and are discussed below. All fuel assemblies in Table 5.2.24 were analyzed at the same burnup and cooling time. The initial enrichment used in the analysis is consistent with Table 5.2.23. The results of the comparison are provided in Table 5.2.26. These results indicate that the B&W 15x15 fuel assembly has the highest radiation source term of the zircaloy clad fuel assembly classes considered in Table 2.1.1. This fuel assembly also has the highest UO_2 mass (see Table 5.2.24) which confirms that, for a given initial enrichment, burnup, and cooling time, the assembly with the highest UO_2 mass produces the highest radiation source term.

The Haddam Neck and San Onofre 1 classes are shorter stainless steel clad versions of the WE 15x15 and WE 14x14 classes, respectively. Since these assemblies have stainless steel clad, they were analyzed separately as discussed in Section 5.2.3. Based on the results in Table 5.2.26, which show that the WE 15x15 assembly class has a higher source term than the WE 14x14 assembly class, the Haddam Neck, WE 15x15, fuel assembly was analyzed as the bounding PWR stainless steel clad fuel assembly.

5.2.5.2 BWR Design Basis Assembly

Table 2.1.2 lists the BWR fuel assembly classes that were evaluated to determine the design basis BWR fuel assembly. Since there are minor differences between the array types in the GE BWR/2-3 and GE BWR/4-6 assembly classes, these assembly classes were not considered individually but rather as a single class. Within that class, the array types, 7x7, 8x8, 9x9, and 10x10 were analyzed to determine the bounding BWR fuel assembly. Since the Humboldt Bay 7x7 and Dresden 1 8x8 are smaller versions of the 7x7 and 8x8 assemblies they are bounded by

the 7x7 and 8x8 assemblies in the GE BWR/2-3 and GE BWR/4-6 classes. Within each array type, the fuel assembly with the highest UO_2 mass was analyzed. Since the variations of fuel assemblies within an array type are very minor, it is conservative to choose the assembly with the highest UO_2 mass. For a given array type of assemblies, the one with the highest UO_2 mass will produce the highest radiation source because, for a given burnup (MWD/MTU) and enrichment, it will have produced the most energy and therefore the most fission products. The Humboldt Bay 6x6, Dresden 1 6x6, and LaCrosse assembly classes were not considered in the determination of the bounding fuel assembly. However, these assemblies were analyzed explicitly as discussed below.

Table 5.2.25 presents the characteristics of the fuel assemblies analyzed to determine the design basis zircaloy clad BWR fuel assembly. The fuel assembly listed for each array type is the assembly that has the highest UO_2 mass. All fuel assemblies in Table 5.2.25 were analyzed at the same burnup and cooling time. The initial enrichment used in these analyses is consistent with Table 5.2.23. The results of the comparison are provided in Table 5.2.27. These results indicate that the 7x7 fuel assembly has the highest radiation source term of the zircaloy clad fuel assembly classes considered in Table 2.1.2. This fuel assembly also has the highest UO_2 mass which confirms that, for a given initial enrichment, burnup, and cooling time, the assembly with the highest UO_2 mass produces the highest radiation source term. According to Reference [5.2.6], the last discharge of a 7x7 assembly was in 1985 and the maximum average burnup for a 7x7 during their operation was 29,000 MWD/MTU. This clearly indicates that the existing 7x7 assemblies have an average burnup and minimum cooling time that is well within the burnup and cooling time limits in Appendix B to the Certificate of Compliance. Therefore, the 7x7 assembly has never reached the burnup level analyzed in this chapter. However, in the interest of conservatism the 7x7 was chosen as the bounding fuel assembly array type.

Since the LaCrosse fuel assembly type is a stainless steel clad 10x10 assembly it was analyzed separately. The maximum burnup and minimum cooling times for this assembly are limited to 22,500 MWD/MTU and 10-year cooling as specified in Appendix B to the Certificate of Compliance. This assembly type is discussed further in Section 5.2.3.

The Humboldt Bay 6x6 and Dresden 1 6x6 fuel are older and shorter fuel than the other array types analyzed and therefore are considered separately. The Dresden 1 6x6 was chosen as the design basis fuel assembly for the Humboldt Bay 6x6 and Dresden 1 6x6 fuel assembly classes because it has the higher UO_2 mass. Dresden 1 also contains a few 6x6 MOX fuel assemblies which were explicitly analyzed as well.

Reference [5.2.6] indicates that the Dresden 1 6x6 fuel assembly has a higher UO_2 mass than the Dresden 1 8x8 or the Humboldt Bay fuel (6x6 and 7x7). Therefore, the Dresden 1 6x6 fuel assembly was also chosen as the bounding assembly for damaged fuel and fuel debris for the Humboldt Bay and Dresden 1 fuel assembly classes.

Since the design basis damaged fuel assembly and the design basis intact 6x6 fuel assembly are identical, the analysis presented in Section 5.4.2 for the damaged fuel assembly also demonstrates the acceptability of storing intact 6x6 fuel assemblies from the Dresden 1 and Humboldt Bay fuel assembly classes.

5.2.5.3 Decay Heat Loads

Section 2.1.5 describes the calculation of the burnup versus cooling time Technical Specification which is based on a maximum permissible decay heat per assembly. The decay heat values per assembly were calculated using the methodology described in Section 5.2. The design basis fuel assemblies, as described in Table 5.2.1, were used in the calculation of the burnup versus cooling time Technical Specification. The enrichments used in the calculation of the decay heats were consistent with Table 5.2.23. As demonstrated in Tables 5.2.26 and 5.2.27, the design basis fuel assembly produces a higher decay heat value than the other assembly types considered. This is due to the higher heavy metal mass in the design basis fuel assemblies. Conservatively, Appendix B of the Certificate of Compliance limits the heavy metal mass of the design basis fuel assembly classes to a value less than the design basis value utilized in this chapter. This provides additional assurance that the decay heat values are bounding values.

As further demonstration that the decay heat values (calculated using the design basis fuel assemblies) are conservative, a comparison between these calculated decay heats and the decay heats reported in Reference [5.2.7] are presented in Table 5.2.28. This comparison is made for a burnup of 30,000 MWD/MTU and a cooling time of 5 years. The burnup was chosen based on the limited burnup data available in Reference [5.2.7].

The heavy metal mass of the non-design basis fuel assembly classes in Appendix B of the Certificate of Compliance are limited to the masses used in Tables 5.2.24 and 5.2.25. No margin is applied between the allowable mass and the analyzed mass of heavy metal for the non-design basis fuel assemblies. This is acceptable because additional assurance that the decay heat values for the non-design basis fuel assemblies are bounding values is obtained by using the decay heat values for the design basis fuel assemblies to determine the acceptable storage criteria for all fuel assemblies. As mentioned above, Table 5.2.28 demonstrates the level of conservatism in applying the decay heat from the design basis fuel assembly to all fuel assemblies.

5.2.6 Thoria Rod Canister

Dresden Unit 1 has a single DFC containing 18 thoria rods which have obtained a relatively low burnup, 16,000 MWD/MTU. These rods were removed from two 8x8 fuel assemblies which contained 9 rods each. The irradiation of thorium produces an isotope which is not commonly found in depleted uranium fuel. Th-232 when irradiated produces U-233. The U-233 can undergo an (n,2n) reaction which produces U-232. The U-232 decays to produce Tl-208 which produces a 2.6 MeV gamma during Beta decay. This results in a significant source in the 2.5-3.0

MeV range which is not commonly present in depleted uranium fuel. Therefore, this single DFC container was analyzed to determine if it was bounded by the current shielding analysis.

A radiation source term was calculated for the 18 thoria rods using SAS2H and ORIGEN-S for a burnup of 16,000 MWD/MTU and a cooling time of 18 years. Table 5.2.31 describes the 8x8 fuel assembly that contains the thoria rods. Table 5.2.32 and 5.2.33 show the gamma and neutron source terms, respectively, that were calculated for the 18 thoria rods in the thoria rod canister. Comparing these source terms to the design basis 6x6 source terms for Dresden Unit 1 fuel in Tables 5.2.6 and 5.2.14 clearly indicates that the design basis source terms bound the thoria rods source terms in all neutron groups and in all gamma groups except the 2.5-3.0 MeV group. As mentioned above, the thoria rods have a significant source in this energy range due to the decay of Tl-208.

Section 5.4.8 provides a further discussion of the thoria rod cansiter and its acceptablity for storage in the HI-STAR 100 System.

5.2.7 Fuel Assembly Neutron Sources

Neutron sources are used in reactors during initial startup of reactor cores. There a different types of neutron sources (e.g. californium, americium-beryllium, plutonium-beryllium, antimony-beryllium). These neutron sources are typically inserted into the water rod of a fuel assembly and are usually removable.

Dresden Unit 1 has a few antimony-beryllium neutron sources. These sources have been analyzed in Section 5.4.7 to demonstrate that they are acceptable for storage in the HI-STAR 100 System. Currently these are the only neutron source permitted for storage in the HI-STAR 100 System.

Table 5.2.1

DESCRIPTION OF DESIGN BASIS INTACT ZIRCALOY CLAD FUEL

	PWR	BWR
Assembly type/class	B&W 15×15	GE 7×7
Active fuel length (in.)	144	144
No. of fuel rods	208	49
Rod pitch (in.)	0.568	0.738
Cladding material	zircaloy-4	zircaloy-2
Rod diameter (in.)	0.428	0.570
Cladding thickness (in.)	0.0230	0.0355
Pellet diameter (in.)	0.3742	0.488
Pellet material	UO_2	UO_2
Pellet density (gm/cc)	10.412 (95% of theoretical)	10.412 (95% of theoretical)
Enrichment (w/o ^{235}U)	3.4 and 3.6	2.9 and 3.2
Burnup (MWD/MTU)†	40,000 and 47,500 (MPC-24)	35,000 and 45,000 (MPC-68)
Cooling Time (years)†	5 and 8 (MPC-24)	5 and 9 (MPC-68)
Specific power (MW/MTU)	40	30
Weight of UO_2 (kg)††	562.029	225.177
Weight of U (kg)††	495.485	198.516

Notes:
1. The B&W 15x15 is the design basis assembly for the following fuel assembly classes listed in Table 2.1.1: B&W 15x15, B&W 17x17, CE 14x14, CE 16x16, WE 14x14, WE 15x15, WE 17x17, St. Lucie, and Ft. Calhoun.
2. The GE 7x7 is the design basis assembly for the following fuel assembly classes listed in Table 2.1.2: GE BWR/2-3, GE BWR/4-6, Humboldt Bay 7x7, and Dresden 1 8x8.

† Burnup and cooling time combinations conservatively bound the acceptable burnup and cooling times listed in Appendix B to the Certificate of Compliance.

†† Derived from parameters in this table.

Table 5.2.1 (continued)

DESCRIPTION OF DESIGN BASIS INTACT ZIRCALOY CLAD FUEL

	PWR	BWR
No. of Water Rods/Guide Tubes	17	0
Water Rod O.D. (in.)	0.53	N/A
Water Rod Thickness (in.)	0.0160	N/A
Lower End Fitting (kg)	9.46	4.8
Gas Plenum Springs (kg)	0.72176	1.1
Gas Plenum Spacer (kg)	0.82824	N/A
Expansion Springs (kg)	N/A	0.4
Upper End Fitting (kg)	9.28	2.0
Handle (kg)	N/A	0.5
Fuel Grid Spacer Springs (kg of steel)	N/A	0.33

Table 5.2.2

DESCRIPTION OF DESIGN BASIS DAMAGED ZIRCALOY CLAD FUEL

	BWR
Fuel type	GE 6x6
Active fuel length (in.)	110
No. of fuel rods	36
Rod pitch (in.)	0.694
Cladding material	zircaloy-2
Rod diameter (in.)	0.5645
Cladding thickness (in.)	0.035
Pellet diameter (in.)	0.494
Pellet material	UO_2
Pellet density (gm/cc)	10.412 (95% of theoretical)
Enrichment (w/o ^{235}U)	2.24
Burnup (MWD/MTU)	30,000
Cooling Time (years)	18
Specific power (MW/MTU)	16.5
Weight of UO_2 (kg)†	129.5
Weight of U (kg)†	114.2

Notes:
1. The 6x6 is the design basis damaged fuel assembly for the Humboldt Bay (all array types) and the Dresden 1 (all array types) damaged fuel assembly classes. It is also the design basis fuel assembly for the intact Humboldt Bay 6x6 and Dresden 1 6x6 fuel assembly classes.
2. This design basis damaged fuel assembly is also the design basis fuel assembly for fuel debris.

† Derived from parameters in this table.

Table 5.2.3

DELETED

Table 5.2.4

CALCULATED MPC-24 PWR FUEL GAMMA SOURCE PER ASSEMBLY
FOR DESIGN BASIS ZIRCALOY CLAD FUEL
FOR VARYING BURNUPS AND COOLING TIMES

Lower Energy	**Upper Energy**	**40,000 MWD/MTU 5-Year Cooling**		**47,500 MWD/MTU 8-Year Cooling**	
(MeV)	(MeV)	(MeV/s)	(Photons/s)	(MeV/s)	(Photons/s)
7.0e-01	1.0	5.96e+14	7.01e+14	3.06e+14	3.60e+14
1.0	1.5	1.38e+14	1.11e+14	9.68e+13	7.74e+13
1.5	2.0	8.94e+12	5.11e+12	4.61e+12	2.64e+12
2.0	2.5	6.85e+12	3.05e+12	6.28e+11	2.79e+11
2.5	3.0	2.67e+11	9.71e+10	3.96e+10	1.44e+10
Totals		7.50e+14	8.20e+14	4.08e+14	4.40e+14

Table 5.2.5

CALCULATED MPC-68 BWR FUEL GAMMA SOURCE PER ASSEMBLY
FOR DESIGN BASIS ZIRCALOY CLAD FUEL
FOR VARYING BURNUPS AND COOLING TIMES

Lower Energy	**Upper Energy**	**35,000 MWD/MTU 5-Year Cooling**		**45,000 MWD/MTU 9-Year Cooling**	
(MeV)	(MeV)	(MeV/s)	(Photons/s)	(MeV/s)	(Photons/s)
7.0e-01	1.0	1.84e+14	2.17e+14	7.92e+13	9.32e+13
1.0	1.5	4.28e+13	3.43e+13	2.85e+13	2.28e+13
1.5	2.0	2.81e+12	1.60e+12	1.37e+12	7.83e+11
2.0	2.5	2.13e+12	9.48e+11	9.25e+10	4.11e+10
2.5	3.0	8.50e+10	3.09e+10	6.78e+9	2.47e+9
Totals		2.32e+14	2.54e+14	1.09e+14	1.17e+14

Table 5.2.6

CALCULATED MPC-68 and MPC-68F BWR FUEL GAMMA SOURCE PER ASSEMBLY FOR DESIGN BASIS ZIRCALOY CLAD DAMAGED FUEL

Lower Energy	**Upper Energy**	**30,000 MWD/MTU 18-Year Cooling**	
(MeV)	(MeV)	(MeV/s)	(Photons/s)
7.0e-01	1.0	3.97e+12	4.67e+12
1.0	1.5	3.67e+12	2.94e+12
1.5	2.0	2.20e+11	1.26e+11
2.0	2.5	1.35e+9	5.99e+8
2.5	3.0	7.30e+7	2.66e+7
Totals		7.86e+12	7.74e+12

Table 5.2.7

SCALING FACTORS USED IN CALCULATING THE ^{60}Co SOURCE

Region	**PWR**	**BWR**
Handle	N/A	0.05
Upper end fitting	0.1	0.1
Gas plenum spacer	0.1	N/A
Expansion springs	N/A	0.1
Gas plenum springs	0.2	0.2
Grid spacer springs	N/A	1.0
Lower end fitting	0.2	0.15

Table 5.2.8

DELETED

Table 5.2.9

CALCULATED MPC-24 ^{60}Co SOURCE PER ASSEMBLY
FOR DESIGN BASIS ZIRCALOY CLAD FUEL
AT VARYING BURNUP AND COOLING TIMES

Location	**40,000 MWD/MTU 5-Year Cooling (curies)**	**47,500 MWD/MTU 8-Year Cooling (curies)**
Lower end fitting	154.95	118.06
Gas plenum springs	11.82	9.01
Gas plenum spacer	6.78	5.17
Expansion springs	N/A	N/A
Grid spacer springs	N/A	N/A
Upper end fitting	76.00	57.91
Handle	N/A	N/A

Table 5.2.10

CALCULATED MPC-68 ^{60}Co SOURCE PER ASSEMBLY
FOR DESIGN BASIS ZIRCALOY CLAD FUEL
AT VARYING BURNUP AND COOLING TIMES

Location	35,000 MWD/MTU 5-Year Cooling (curies)	45,000 MWD/MTU 9-Year Cooling (curies)
Lower end fitting	57.38	40.15
Gas plenum springs	17.53	12.27
Gas plenum spacer	N/A	N/A
Expansion springs	3.19	2.23
Grid spacer springs	26.30	18.40
Upper end fitting	15.94	11.15
Handle	1.99	1.39

Table 5.2.11

DELETED

Table 5.2.12

CALCULATED MPC-24 PWR NEUTRON SOURCE PER ASSEMBLY
FOR DESIGN BASIS ZIRCALOY CLAD FUEL
FOR VARYING BURNUP AND COOLING TIMES

Lower Energy (MeV)	**Upper Energy (MeV)**	**40,000 MWD/MTU 5-Year Cooling (Neutrons/s)**	**47,500 MWD/MTU 8-Year Cooling (Neutrons/s)**
1.0e-01	4.0e-01	1.11e+7	1.80e+7
4.0e-01	9.0e-01	5.69e+7	9.19e+7
9.0e-01	1.4	5.21e+7	8.41e+7
1.4	1.85	3.85e+7	6.20e+7
1.85	3.0	6.80e+7	1.10e+8
3.0	6.43	6.16e+7	9.94e+7
6.43	20.0	5.45e+6	8.81e+6
Totals		2.94e+8	4.74e+8

Table 5.2.13

CALCULATED MPC-68 BWR NEUTRON SOURCE PER ASSEMBLY
FOR DESIGN BASIS ZIRCALOY CLAD FUEL
FOR VARYING BURNUP AND COOLING TIMES

Lower Energy (MeV)	**Upper Energy (MeV)**	**35,000 MWD/MTU 5-Year Cooling (Neutrons/s)**	**45,000 MWD/MTU 9-Year Cooling (Neutrons/s)**
1.0e-01	4.0e-01	3.05e+6	6.23e+6
4.0e-01	9.0e-01	1.56e+7	3.18e+7
9.0e-01	1.4	1.43e+7	2.91e+7
1.4	1.85	1.06e+7	2.15e+7
1.85	3.0	1.87e+7	3.79e+7
3.0	6.43	1.69e+7	3.44e+7
6.43	20.0	1.49e+6	3.05e+6
Totals		8.06e+7	1.64e+8

Table 5.2.14

CALCULATED MPC-68 and MPC-68F BWR NEUTRON SOURCE PER ASSEMBLY FOR DESIGN BASIS DAMAGED ZIRCALOY CLAD FUEL

Lower Energy (MeV)	**Upper Energy (MeV)**	**30,000 MWD/MTU 18-Year Cooling (Neutrons/s)**
1.0e-01	4.0e-01	8.22e+5
4.0e-01	9.0e-01	4.20e+6
9.0e-01	1.4	3.87e+6
1.4	1.85	2.88e+6
1.85	3.0	5.18e+6
3.0	6.43	4.61e+6
6.43	20.0	4.02e+5
Totals		2.20e+7

Table 5.2.15

DESCRIPTION OF DESIGN BASIS ZIRCALOY CLAD MIXED OXIDE FUEL

	BWR
Fuel type	GE 6x6
Active fuel length (in.)	110
No. of fuel rods	36
Rod pitch (in.)	0.696
Cladding material	zircaloy-2
Rod diameter (in.)	0.5645
Cladding thickness (in.)	0.036
Pellet diameter (in.)	0.482
Pellet material	UO_2 and $PuUO_2$
No. of UO_2 Rods	27
No. of $PuUO_2$ rods	9
Pellet density (gm/cc)	10.412 (95% of theoretical)
Enrichment (w/o ^{235}U)†	2.24 (UO_2 rods) 0.711 ($PuUO_2$ rods)
Burnup (MWD/MTU)	30,000
Cooling Time (years)	18
Specific power (MW/MTU)	16.5
Weight of UO_2,$PuUO_2$ (kg)††	123.3
Weight of U,Pu (kg)††	108.7

† See Table 5.3.3 for detailed composition of $PuUO_2$ rods.

†† Derived from parameters in this table.

Table 5.2.16

CALCULATED MPC-68 BWR FUEL GAMMA SOURCE PER ASSEMBLY
FOR DESIGN BASIS ZIRCALOY CLAD MIXED OXIDE FUEL

Lower Energy	**Upper Energy**	**30,000 MWD/MTU 18-Year Cooling**	
(MeV)	(MeV)	(MeV/s)	(Photons/s)
7.0e-01	1.0	3.87e+12	4.56e+12
1.0	1.5	3.72e+12	2.98e+12
1.5	2.0	2.18e+11	1.25e+11
2.0	2.5	1.17e+9	5.22e+8
2.5	3.0	9.25e+7	3.36e+7
Totals		7.81e+12	7.67e+12

Table 5.2.17

CALCULATED MPC-68 BWR NEUTRON SOURCE PER ASSEMBLY
FOR DESIGN BASIS ZIRCALOY CLAD MIXED OXIDE FUEL

Lower Energy (MeV)	**Upper Energy (MeV)**	**30,000 MWD/MTU 18-Year Cooling (Neutrons/s)**
1.0e-01	4.0e-01	1.24e+6
4.0e-01	9.0e-01	6.36e+6
9.0e-01	1.4	5.88e+6
1.4	1.85	4.43e+6
1.85	3.0	8.12e+6
3.0	6.43	7.06e+6
6.43	20.0	6.07e+5
Totals		3.37e+7

Table 5.2.18

DESCRIPTION OF DESIGN BASIS INTACT STAINLESS STEEL CLAD FUEL

	PWR	**BWR**
Fuel type	WE 15x15	A/C 10x10
Active fuel length (in.)	144	144
No. of fuel rods	204	100
Rod pitch (in.)	0.563	0.565
Cladding material	304 SS	348H SS
Rod diameter (in.)	0.422	0.396
Cladding thickness (in.)	0.0165	0.02
Pellet diameter (in.)	0.3825	0.35
Pellet material	UO_2	UO_2
Pellet density (gm/cc)	10.412 (95% of theoretical)	10.412 (95% of theoretical)
Enrichment (w/o ^{235}U)	3.5	3.5
Burnup (MWD/MTU)	30,000 @ 9 yr (MPC-24) 40,000 @ 15 yr (MPC-24)	22,500 (MPC-68)
Cooling Time (years)	9 (MPC-24) 15 (MPC-24)	10 (MPC-68)
Specific power (MW/MTU)	37.96	29.17
No. of Water Rods	21	0
Water Rod O.D. (in.)	0.546	N/A
Water Rod Thickness (in.)	0.017	N/A

Notes:
1. The WE 15x15 is the design basis assembly for the following fuel assembly classes listed in Table 2.1.1: Haddam Neck and San Onofre 1.
2. The A/C 10x10 is the design basis assembly for the following fuel assembly class listed in Table 2.1.2: LaCrosse.

Table 5.2.19

CALCULATED BWR FUEL GAMMA SOURCE PER ASSEMBLY
FOR STAINLESS STEEL CLAD FUEL

Lower Energy	**Upper Energy**	**22,500 MWD/MTU 10-Year Cooling**	
(MeV)	(MeV)	(MeV/s)	(Photons/s)
7.0e-01	1.0	1.97e+13	2.31e+13
1.0	1.5	7.93e+13	6.34e+13
1.5	2.0	4.52e+11	2.58e+11
2.0	2.5	3.28e+10	1.46e+10
2.5	3.0	1.69e+9	6.14e+8
Totals		9.95e+13	8.68e+13

Note:
These source terms were calculated for a 144 inch active fuel length. The actual active fuel length is 83 inches.

Table 5.2.20

CALCULATED PWR FUEL GAMMA SOURCE PER ASSEMBLY
FOR STAINLESS STEEL CLAD FUEL

Lower Energy	**Upper Energy**	**30,000 MWD/MTU 9-Year Cooling**		**40,000 MWD/MTU 15-Year Cooling**	
(MeV)	(MeV)	(MeV/s)	(Photons/s)	(MeV/s)	(Photons/s)
7.0e-01	1.0	1.18e+14	1.39e+14	4.79e+13	5.63e+13
1.0	1.5	3.00e+14	2.40e+14	1.88e+14	1.50e+14
1.5	2.0	2.28e+12	1.30e+12	2.07e+12	1.18e+12
2.0	2.5	2.34e+11	1.04e+11	1.28e+10	5.71e+9
2.5	3.0	1.33e+10	4.83e+9	9.59e+8	3.49e+8
Totals		4.21e+14	3.80e+14	2.38e+14	2.07e+14

Note:
These source terms were calculated for a 144 inch active fuel length. The actual active fuel length is 122 inches.

Table 5.2.21

CALCULATED BWR NEUTRON SOURCE PER ASSEMBLY
FOR STAINLESS STEEL CLAD FUEL

Lower Energy (MeV)	**Upper Energy (MeV)**	**22,500 MWD/MTU 10-Year Cooling (Neutrons/s)**
1.0e-01	4.0e-01	2.23e+5
4.0e-01	9.0e-01	1.14e+6
9.0e-01	1.4	1.07e+6
1.4	1.85	8.20e+5
1.85	3.0	1.56e+6
3.0	6.43	1.30e+6
6.43	20.0	1.08e+5
Total		6.22e+6

Note:
These source terms were calculated for a 144 inch active fuel length. The actual active fuel length is 83 inches.

Table 5.2.22

CALCULATED PWR NEUTRON SOURCE PER ASSEMBLY
FOR STAINLESS STEEL CLAD FUEL

Lower Energy (MeV)	**Upper Energy (MeV)**	**30,000 MWD/MTU 9-Year Cooling (Neutrons/s)**	**40,000 MWD/MTU 15-Year Cooling (Neutrons/s)**
1.0e-01	4.0e-01	3.05e+6	8.02e+6
4.0e-01	9.0e-01	1.56e+7	4.10e+7
9.0e-01	1.4	1.44e+7	3.77e+7
1.4	1.85	1.07e+7	2.79e+7
1.85	3.0	1.93e+7	4.98e+7
3.0	6.43	1.71e+7	4.47e+7
6.43	20.0	1.49e+6	3.93e+6
Totals		8.16e+7	2.13e+8

Note:
These source terms were calculated for a 144 inch active fuel length. The actual active fuel length is 122 inches.

Table 5.2.23

INITIAL ENRICHMENTS USED IN THE SOURCE TERM CALCULATIONS

Burnup Range (MWD/MTU)	Initial Enrichment (wt.% ^{235}U)
BWR Fuel	
20,000-25,000	2.1
25,000-30,000	2.4
30,000-35,000	2.6
35,000-40,000	2.9
40,000-45,000	3.0
45,000-50,000	3.2
PWR Fuel	
20,000-25,000	2.3
25,000-30,000	2.6
30,000-35,000	2.9
35,000-40,000	3.2
40,000-45,000	3.4
45,000-50,000	3.6

Note: The burnup ranges do not overlap. Therefore, 20,000-25,000 MWD/MTU means 20,000-24,999.9 MWD/MTU, etc.

Table 5.2.24

DESCRIPTION OF EVALUATED INTACT ZIRCALOY CLAD PWR FUEL

Assembly class	WE 14×14	WE 15×15	WE 17×17	CE 14×14	CE 16×16	B&W 15×15	B&W 17×17
Active fuel length (in.)	144	144	144	144	150	144	144
No. of fuel rods	179	204	264	176	236	208	264
Rod pitch (in.)	0.556	0.563	0.496	0.580	0.5063	0.568	0.502
Cladding material	Zr-4	Zr-4	Zr-4	Zr-4	Zr-4	Zr-4	Zr-4
Rod diameter (in.)	0.422	0.422	0.374	0.440	0.382	0.428	0.377
Cladding thickness (in.)	0.0243	0.0245	0.0225	0.0280	0.0250	0.0230	0.0220
Pellet diameter (in.)	0.3659	0.366	0.3225	0.377	0.3255	0.3742	0.3252
Pellet material	UO_2	UO_2	UO_2	UO_2	UO_2	UO_2	UO_2
Pellet density (gm/cc) (95% of theoretical)	10.412	10.412	10.412	10.412	10.412	10.412	10.412
Enrichment (wt.% ^{235}U)	3.4	3.4	3.4	3.4	3.4	3.4	3.4
Burnup (MWD/MTU)	40,000	40,000	40,000	40,000	40,000	40,000	40,000
Cooling time (years)	5	5	5	5	5	5	5
Specific power (MW/MTU)	40	40	40	40	40	40	40
Weight of UO_2 (kg)†	462.451	527.327	529.848	482.706	502.609	562.029	538.757
Weight of U (kg)†	407.697	464.891	467.114	425.554	443.100	495.485	474.968
No. of Guide Tubes	17	21	25	5	5	17	25
Guide Tube O.D. (in.)	0.539	0.546	0.474	1.115	0.98	0.53	0.564
Guide Tube Thickness (in.)	0.0170	0.0170	0.0160	0.0400	0.0400	0.0160	0.0175

† Derived from parameters in this table.

Table 5.2.25

DESCRIPTION OF EVALUATED INTACT ZIRCALOY CLAD BWR FUEL

Array Type	7×7	8×8	9×9	10×10
Active fuel length (in.)	144	144	144	144
No. of fuel rods	49	63	74	92
Rod pitch (in.)	0.738	0.640	0.566	0.510
Cladding material	Zr-2	Zr-2	Zr-2	Zr-2
Rod diameter (in.)	0.570	0.493	0.440	0.404
Cladding thickness (in.)	0.0355	0.0340	0.0280	0.0260
Pellet diameter (in.)	0.488	0.416	0.376	0.345
Pellet material	UO_2	UO_2	UO_2	UO_2
Pellet density (gm/cc) (95% of theoretical)	10.412	10.412	10.412	10.412
Enrichment (wt.% ^{235}U)	3.0	3.0	3.0	3.0
Burnup (MWD/MTU)	40,000	40,000	40,000	40,000
Cooling time (years)	5	5	5	5
Specific power (MW/MTU)	30	30	30	30
Weight of UO_2 (kg)†	225.177	210.385	201.881	211.307
Weight of U (kg)†	198.516	185.475	177.978	186.288
No. of Water Rods	0	1	2	2
Water Rod O.D. (in.)	n/a	0.493	0.980	0.980
Water Rod Thickness (in.)	n/a	0.0340	0.0300	0.0300

† Derived from parameters in this table.

Table 5.2.26

COMPARISON OF SOURCE TERMS FOR INTACT ZIRCALOY CLAD PWR FUEL
3.4 wt.% ^{235}U - 40,000 MWD/MTU - 5 years cooling

Assembly class	WE 14x14	WE 15x15	WE 17x17	CE 14x14	CE 16x16	B&W 15x15	B&W 17x17
Neutrons/sec	2.29e+8 / 2.31e+8	2.63e+8 / 2.65e+8	2.62e+8	2.31e+8	2.34e+8	2.94e+8	2.64e+8
Photons/sec (0.7-3.0 MeV)	6.64e+14/ 7.11e+14	7.54e+14/ 8.12e+14	7.60e+14	6.77e+14	7.06e+14	8.20e+14	7.71e+14
Thermal power (watts)	926.6 / 936.8	1056 / 1068	1062	956.6	995.7	1137	1077

Note:
The WE 14x14 and WE 15x15 have both zircaloy and stainless steel guide tubes. The first value presented is for the assembly with zircaloy guide tubes and the second value is for the assembly with stainless steel guide tubes.

Table 5.2.27

COMPARISON OF SOURCE TERMS FOR INTACT ZIRCALOY CLAD BWR FUEL
3.0 wt.% ^{235}U - 40,000 MWD/MTU - 5 years cooling

Assembly class	7×7	8×8	9×9	10×10
Neutrons/sec	1.33e+8	1.17e+8	1.11e+8	1.22e+8
Photons/sec (0.7-3.0 MeV)	3.10e+14	2.83e+14	2.71e+14	2.89e+14
Thermal power (watts)	435.5	402.3	385.3	407.4

Table 5.2.28

COMPARISON OF CALCULATED DECAY HEATS FOR DESIGN BASIS FUEL AND VALUES REPORTED IN THE DOE CHARACTERISTICS DATABASE † FOR 30,000 MWD/MTU AND 5-YEAR COOLING

Fuel Assembly Class	Decay Heat from the DOE Database (watts/assembly)	Decay Heat from Design Basis Fuel (watts/assembly)
PWR Fuel		
B&W 15x15	752.0	827.5
B&W 17x17	732.9	827.5
CE 16x16	653.7	827.5
CE 14x14	601.3	827.5
WE 17x17	742.5	827.5
WE 15x15	762.2	827.5
WE 14x14	649.6	827.5
BWR Fuel		
7x7	310.9	315.7
8x8	296.6	315.7
9x9	275.0	315.7

Notes:
1. The PWR and BWR design basis fuels are the B&W 15x15 and the GE 7x7, respectively.
2. The decay heat values from the database include contributions from in-core material (e.g. spacer grids).
3. Information on the 10x10 was not available in the DOE database. However, based on the results in Table 5.2.27, the actual decay heat values from the 10x10 would be very similar to the values shown above for the 8x8.

† Reference [5.2.7].

Table 5.2.29

DESCRIPTION OF DESIGN BASIS BURNABLE POISON ROD ASSEMBLY AND THIMBLE PLUG DEVICE

Region	**BPRA**	**TPD**
Upper End Fitting (kg of steel)	2.62	2.3
Upper End Fitting (kg of inconel)	0.42	0.42
Gas Plenum Spacer (kg of steel)	0.77488	1.71008
Gas Plenum Springs (kg of steel)	0.67512	1.48992
In-core (kg of steel)	13.2	N/A

Table 5.2.30

DESIGN BASIS COBALT-60 ACTIVITIES FOR BURNABLE POISON ROD ASSEMBLIES AND THIMBLE PLUG DEVICES

Region	**BPRA**	**TPD**
Upper End Fitting (curies Co-60)	30.4	25.21
Gas Plenum Spacer (curies Co-60)	4.6	9.04
Gas Plenum Springs (curies Co-60)	8.2	15.75
In-core (curies Co-60)	787.8	N/A

Table 5.2.31

DESCRIPTION OF FUEL ASSEMBLY USED TO ANNALYZE THORIA RODS IN THE THORIA ROD CANISTER

	BWR
Fuel type	8x8
Active fuel length (in.)	110.5
No. of UO_2 fuel rods	55
No. of UO_2/ThO_2 fuel rods	9
Rod pitch (in.)	0.523
Cladding material	zircaloy
Rod diameter (in.)	0.412
Cladding thickness (in.)	0.025
Pellet diameter (in.)	0.358
Pellet material	98.2% ThO_2 and 1.8% UO_2 for UO_2/ThO_2 rods
Pellet density (gm/cc)	10.412
Enrichment (w/o ^{235}U)	93.5 in UO_2 for UO_2/ThO_2 rods and 1.8 for UO_2 rods
Burnup (MWD/MTIHM)	16,000
Cooling Time (years)	18
Specific power (MW/MTIHM)	16.5
Weight of THO_2 and UO_2 (kg)†	121.46
Weight of U (kg)†	92.29
Weight of Th (kg)†	14.74

† Derived from parameters in this table.

Table 5.2.32

CALCULATED FUEL GAMMA SOURCE FOR THORIA ROD CANISTER CONTAINING EIGHTEEN THORIA RODS

Lower Energy	**Upper Energy**	**16,000 MWD/MTIHM 18-Year Cooling**	
(MeV)	(MeV)	(MeV/s)	(Photons/s)
7.0e-01	1.0	5.79e+11	6.81e+11
1.0	1.5	3.79e+11	3.03e+11
1.5	2.0	4.25e+10	2.43e+10
2.0	2.5	4.16e+8	1.85e+8
2.5	3.0	2.31e+11	8.39e+10
Totals		1.23e+12	1.09e+12

Table 5.2.33

CALCULATED FUEL NEUTRON SOURCE FOR THORIA ROD CANISTER CONTAINING EIGHTEEN THORIA RODS

Lower Energy (MeV)	**Upper Energy (MeV)**	**16,000 MWD/MTIHM 18-Year Cooling (Neutrons/s)**
1.0e-01	4.0e-01	5.65e+2
4.0e-01	9.0e-01	3.19e+3
9.0e-01	1.4	6.79e+3
1.4	1.85	1.05e+4
1.85	3.0	3.68e+4
3.0	6.43	1.41e+4
6.43	20.0	1.60e+2
Totals		7.21e+4

5.3 MODEL SPECIFICATIONS

The shielding analysis of the HI-STAR 100 System was performed with MCNP-4A [5.1.1]. MCNP is a Monte Carlo transport code that offers a full three-dimensional combinatorial geometry modeling capability including such complex surfaces as cones and tori. This means that no gross approximations were required to represent the HI-STAR 100 System in the shielding analysis. A sample input file for MCNP is provided in Appendix 5.C.

As discussed in Section 5.1.1, off-normal conditions do not have any implications for the shielding analysis. Therefore, the MCNP models and results developed for the normal conditions also represent the off-normal condition. Section 5.1.2 discussed the accident conditions and stated that the only accident that would impact the shielding analysis would be a loss of the neutron shield. Therefore, the MCNP models of the HI-STAR 100 System normal condition have the neutron shield in place while the accident condition replaces the neutron shield with void.

5.3.1 Description of the Radial and Axial Shielding Configuration

Section 1.5 provides the drawings that describe the HI-STAR 100 System. These drawings were used to create the MCNP models used in the radiation transport calculations. Figures 5.3.2 and 5.3.3 show cross sectional views of the HI-STAR 100 overpack and MPC as it was modeled in MCNP for each of the MPCs. These figures were created with the MCNP two-dimensional plotter and are drawn to scale. The figures clearly illustrate the radial steel fins and pocket trunnions in the neutron shield region. Since the fins and pocket trunnions were modeled explicitly, neutron streaming through these components is accounted for in the calculations of the dose adjacent to the overpack and 1 meter dose. In Section 5.4.1, the dose effect of localized streaming through these compartments is analyzed. Figures 5.3.5 and 5.3.6 show the MCNP models of the MPC-24 and MPC-68 fuel baskets including the as-modeled dimensions. Figure 5.3.9 shows a cross sectional view of the HI-STAR 100 overpack with the as-modeled thickness of the various materials. Figure 5.3.10 is an axial representation of the HI-STAR 100 overpack with the various as-modeled dimensions indicated. As Figure 5.3.10 indicates, the thickness of the MPC-68 lid and the thickness of the MPC-24 lid are 10.0 and 9.5 inches, respectively. Correspondingly, the MPC-internal cavity heights differ by 0.5 inch. In the MCNP models of the MPC-24 and MPC-68, the actual lid thickness and internal cavity height for that particular MPC was used.

Calculations were performed to determine the acceptability of homogenizing the fuel assembly versus explicit modeling. Based on these calculations it was concluded that it was acceptable to homogenize the fuel assembly without loss of accuracy. The PWR fuel assembly modeled was the design basis fuel assembly, the B&W 15x15. The width of this homogenized fuel assembly in MCNP is equal to 15 times the pitch. The BWR fuel assembly modeled was an 8x8 fuel assembly. This is different from the 7x7 design basis fuel assembly used for the source term calculations. However, it is conservative to use an 8x8 fuel assembly in the MCNP model since it contains less fuel and therefore less shielding than the 7x7 fuel assembly. The width of the BWR

homogenized fuel assembly is equal to 8 times the pitch. Homogenization of the fuel assemblies resulted in a noticeable decrease in run time.

Several conservative approximations were made in modeling the MPC. The conservative approximations are listed below.

1. The basket material in the top and bottom 0.9 inches where the MPC basket flow holes are located is not modeled. The length of the basket not modeled (0.9 inches) was determined by calculating the equivalent area removed by the flow holes. This method of approximation is conservative because no material for the basket shielding is provided in the 0.9 inch area at the top and bottom of the MPC basket.

2. The upper and lower fuel spacers are not modeled. The fuel spacers are not needed on all fuel assembly types. However, most PWR fuel assemblies will have upper and lower fuel spacers. The positioning of the fuel assembly for the shielding analysis is determined by the fuel spacer length for the design basis fuel assembly type, but the fuel spacer materials are not modeled. This is conservative since it removes steel which would provide a small amount of additional shielding.

3. For the MPC-24 and the MPC-68, the MPC basket supports are not modeled. This is conservative since it removes steel which would provide a small increase in shielding. The aluminum heat conduction elements are also conservatively not modeled.

4. The MPC-24 basket is fabricated from 5/16 inch thick cell plates. It is conservatively assumed for modeling purposes that the structural portion of the MPC-24 basket is uniformly fabricated from 9/32 inch thick steel. The Boral and sheathing are modeled explicitly. This is conservative since it removes steel which would provide a small amount of additional shielding.

5. In the modeling of the BWR fuel assemblies, the zircaloy flow channel was not represented. This was done because it cannot be guaranteed that all BWR fuel assemblies will have an associated flow channel when placed in the MPC. The flow channel does not contribute to the source, but does provide some small amount of shielding. However, no credit is taken for this additional shielding.

6. In the MPC-24, conservatively, all Boral panels on the periphery were modeled with a reduced width of 5 inches compared to 6.25 inches or 7.5 inches.

7. The MPC-68 is designed for two lid thicknesses: 9.5 inches and 10 inches. Conservatively, all calculations reported in this chapter were performed with the 9.5 inch thick lid.

During this project several design changes occurred that affected the drawings, but did not significantly affect the MCNP models. Therefore, the models may not exactly represent the drawings. The discrepancies between models and drawings are listed and discussed here.

MPC Modeling Discprepancies

1. In the MPCs, there is a sump in the baseplate to enhance draining of the MPC. This localized reduction in the thickness of the baseplate was not modeled. Since there is significant shielding and distance in the HI-STAR outside the MPC baseplate, this localized reduction in shielding will not affect the calculated dose rates outside the HI-STAR.

2. The design configuration of the MPC-24 has been enhanced for criticality purposes. The general location of the 24 assemblies remains basically the same, therefore the shielding analysis continues to use the superseded configuration. Figure 5.3.11 shows the superseded and current configuration for the MPC-24 for comparison.

3. The sheathing thickness on the new MPC-24 configuration was reduced from 0.06 inches to 0.0235 inches. However, the model still uses 0.06 inches. This discrepancy is compensated for by the use of 9/32 inch cell walls and 5 inch boral on the periphery as described above. MCNP calculations were performed with the new MPC-24 configuration under Docket No. 72-1014 in the 100-ton HI-TRAC for comparison to the superceded configuration. These results indicate that on the side of the overpack, the dose rates decrease by approximately 12% on the surface. These results demonstrate that using the superceded MPC-24 design is conservative.

5.3.1.1 Fuel Configuration

As described above, the active fuel region is modeled as a homogenous zone. The end fittings and the plenum regions are also modeled as homogenous regions of steel. The masses of steel used in these regions are shown in Table 5.2.1. The axial description of the design basis fuel assemblies is provided in Table 5.3.1. Figures 5.3.7 and 5.3.8 graphically depict the location of the PWR and BWR fuel assemblies within the HI-STAR 100 System. The axial locations of the Boral, basket, pocket trunnion, and transition areas are shown in these figures.

5.3.1.2 Streaming Considerations

The streaming from the radial steel fins and pocket trunnions in the neutron shield is evaluated in Section 5.4.1. The MCNP model of the HI-STAR 100 completely describes the radial steel fins and pocket trunnions, thereby properly accounting for the streaming effect. This is discussed further in Section 5.4.1.

The design of the HI-STAR 100 System, as described in the drawings in Section 1.5, has eliminated all other possible streaming paths. Therefore, the MCNP model does not represent any additional streaming paths. A brief justification of this assumption is provided for each penetration.

- The lifting trunnions will remain installed in the overpack top flange. No credit is taken for any part of the trunnion that extends outside of the overpack.

- The pocket trunnions are modeled as solid blocks of steel. The pocket trunnion will be filled with a solid steel rotation trunnion attached to the transport frame during handling and a shield plug when located at the ISFSI pad.

- The threaded holes in the MPC lid are plugged with solid plugs during storage and, therefore, do not create a void in the MPC lid.

- The drain and vent ports in the MPC lid are designed to eliminate streaming paths. The steel lost in the MPC lid at the port location is replaced with a block of steel approximately 6 inches thick below the port opening and attached to the underside of the lid. This design feature is shown on the drawings in Section 1.5. The MCNP model did not explicitly represent this arrangement but, rather, modeled the MPC lid as a solid piece.

- The penetrations in the overpack are filled with bolts that extend into the penetration when in storage operations, thereby eliminating any potential direct streaming paths. Cover plates are also designed in such a way as to maintain the thickness of the overpack to the maximum extent practical. Therefore, the MCNP model does not represent any streaming paths due to penetrations in the overpack.

5.3.2 Regional Densities

Composition and densities of the various materials used in the HI-STAR 100 System shielding analyses are given in Tables 5.3.2 and 5.3.3. All of the materials and their actual geometries are represented in the MCNP model.

Sections 4.4 and 4.5 demonstrate that all materials used in the HI-STAR 100 System remain below their design temperatures as specified in Table 2.2.3 during all normal conditions. Therefore, the shielding analysis does not address changes in the material density or composition as a result of temperature changes.

Chapter 11 discusses the effect of the various accident conditions on the temperatures of the shielding materials and the resultant impact on their shielding effectiveness. As stated in Section

5.1.2, there is only one accident that has any significant impact on the shielding configuration. This accident is the loss of the neutron shield in the HI-STAR 100 System as a result of fire or other damage. The change in the neutron shield was conservatively analyzed by assuming that the entire volume of the neutron shield was replaced by void.

Table 5.3.1

DESCRIPTION OF THE AXIAL MCNP MODEL OF THE FUEL ASSEMBLIES[†]

Region	Start (in.)	Finish (in.)	Length (in.)	Actual Material	Modeled Material
PWR					
Lower End Fitting	0.0	7.375	7.375	SS304	SS304
Space	7.375	8.375	1.0	zircaloy	void
Fuel	8.375	152.375	144	fuel & zircaloy	fuel
Gas Plenum Springs	152.375	156.1875	3.8125	SS304 & zircaloy	SS304
Gas Plenum Spacer	156.1875	160.5625	4.375	SS304 & zircaloy	SS304
Upper End Fitting	160.5625	165.625	5.0625	SS304	SS304
BWR					
Lower End Fitting	0.0	7.385	7.385	SS304	SS304
Fuel	7.385	151.385	144	fuel & zircaloy	fuel
Space	151.385	157.385	6	zircaloy	void
Gas Plenum Springs	157.385	166.865	9.48	SS304 & zircaloy	SS304
Expansion Springs	166.865	168.215	1.35	SS304	SS304
Upper End Fitting	168.215	171.555	3.34	SS304	SS304
Handle	171.555	176	4.445	SS304	SS304

[†] All dimensions start at the bottom of the fuel assembly. The length of the lower fuel spacer must be added to the distances to determine the distance from the top of the MPC baseplate.

Table 5.3.2

COMPOSITION OF THE MATERIALS IN THE HI-STAR 100 SYSTEM

Component	Density (g/cm^3)	Elements	Mass Fraction (%)
Uranium Oxide	10.412	^{235}U	2.9971(BWR) 3.2615(PWR)
		^{238}U	85.1529(BWR) 84.8885(PWR)
		O	11.85
Boral	2.644	^{10}B	4.4226 (MPC-68) 4.367 (MPC-24)
		^{11}B	20.1474 (MPC-68) 19.893 (MPC-24)
		Al	68.61 (MPC-68) 69.01 (MPC-24)
		C	6.82 (MPC-68) 6.73 (MPC-24)
SS304	7.92	Cr	19
		Mn	2
		Fe	69.5
		Ni	9.5
Carbon Steel	7.82	C	0.5
		Fe	99.5
Zircaloy	6.55	Zr	100

Table 5.3.2 (continued)

COMPOSITION OF THE MATERIALS IN THE HI-STAR 100 SYSTEM

Component	Density (g/cm^3)	Elements	Mass Fraction (%)
Neutron Shield Holtite-A	1.61	C	27.66039
		H	5.92
		Al	21.285
		N	1.98
		O	42.372
		^{10}B	0.14087
		^{11}B	0.64174
BWR Fuel Region Mixture	3.979996	^{235}U	2.4483
		^{238}U	69.5601
		O	9.6801
		Zr	18.3115
PWR Fuel Region Mixture	3.853705	^{235}U	2.6944
		^{238}U	70.1276
		O	9.7895
		Zr	17.3885
Lower End Fitting (PWR)	1.0783	SS304	100
Gas Plenum Springs (PWR)	0.1591	SS304	100
Gas Plenum Spacer (PWR)	0.1591	SS304	100

Table 5.3.2 (continued)

COMPOSITION OF THE MATERIALS IN THE HI-STAR 100 SYSTEM

Component	Density (g/cm^3)	Elements	Mass Fraction (%)
Upper End Fitting (PWR)	1.5410	SS304	100
Lower End Fitting (BWR)	1.5130	SS304	100
Gas Plenum Springs (BWR)	0.2701	SS304	100
Expansion Springs (BWR)	0.6897	SS304	100
Upper End Fitting (BWR)	1.3939	SS304	100
Handle (BWR)	0.2619	SS304	100

Table 5.3.3

COMPOSITION OF THE FUEL IN THE MIXED OXIDE FUEL ASSEMBLIES IN THE MPC-68 OF THE HI-STAR 100 SYSTEM

Component	Density (g/cm^3)	Elements	Mass Fraction (%)
Mixed Oxide Pellets	10.412	^{238}U	84.498
		^{235}U	0.612
		^{238}Pu	0.421
		^{239}Pu	1.455
		^{240}Pu	0.034
		^{241}Pu	0.123
		^{242}Pu	0.007
		O	11.85
Uranium Oxide Pellets	10.412	^{238}U	86.175
		^{235}U	1.975
		O	11.85

FIGURE 5.3.1

DELETED

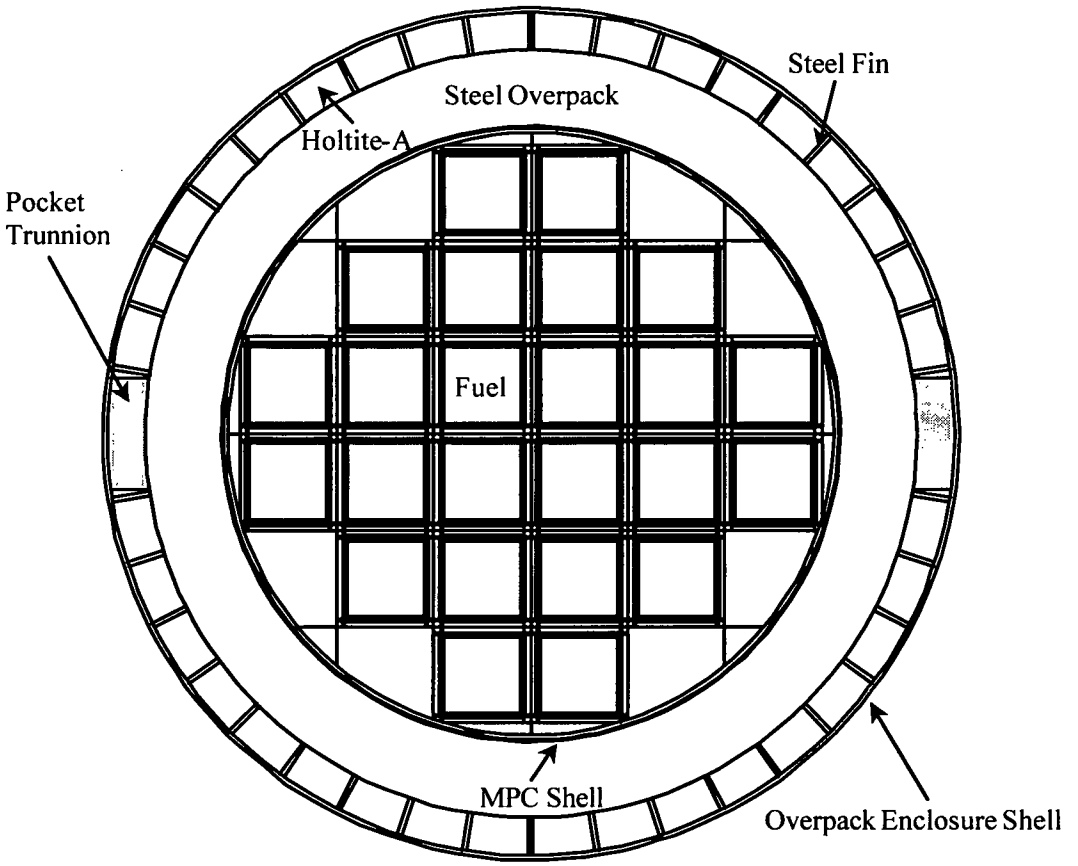

FIGURE 5.3.2; HI-STAR 100 OVERPACK WITH MPC-24 CROSS SECTIONAL VIEW AS MODELLED IN MCNP[†]

[†] This figure is drawn to scale using the MCNP plotter.

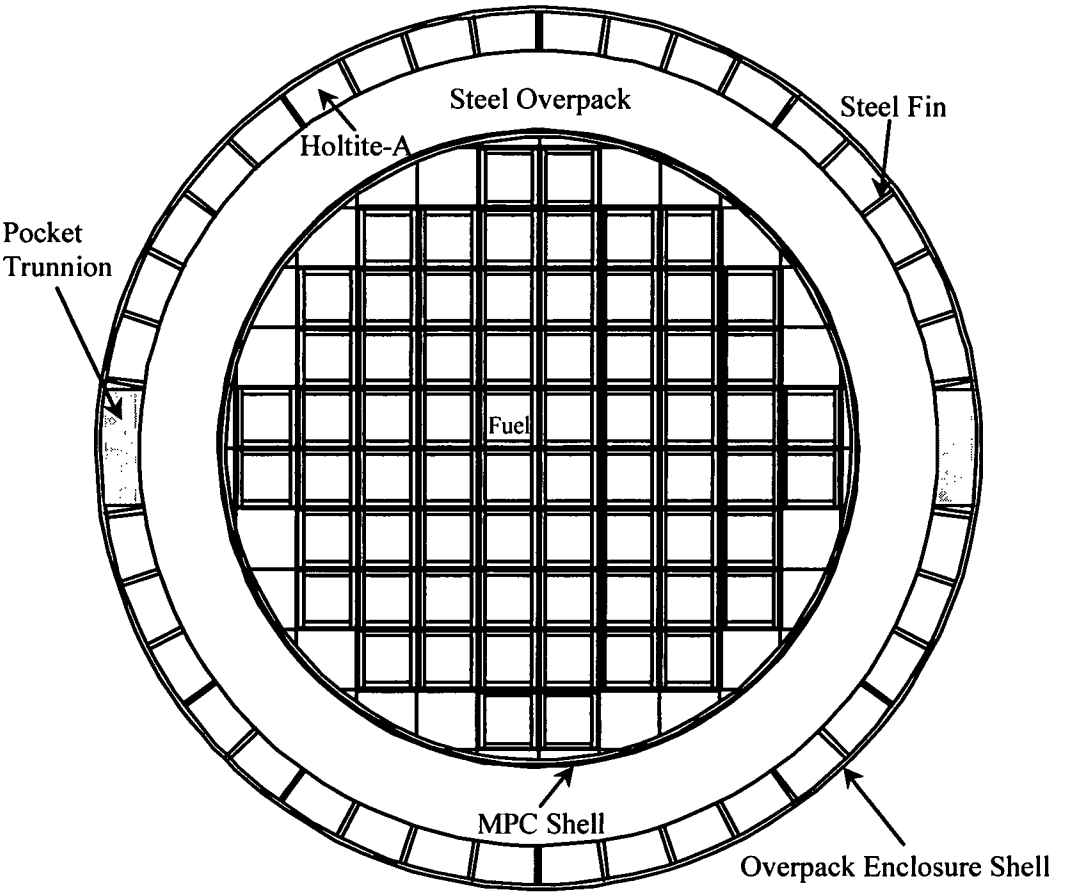

FIGURE 5.3.3; HI-STAR 100 OVERPACK WITH MPC-68 CROSS SECTIONAL VIEW AS MODELLED IN MCNP[†]

[†] This figure is drawn to scale using the MCNP plotter.

FIGURE 5.3.4

DELETED

Security-Related Information
Figure Withheld Under 10 CFR 2.390

FIGURE 5.3.5; CROSS SECTIONAL VIEW OF AN MPC-24 BASKET CELL AS MODELED IN MCNP

Security-Related Information
Figure Withheld Under 10 CFR 2.390

FIGURE 5.3.6; CROSS SECTIONAL VIEW OF AN MPC-68 BASKET CELL AS MODELED IN MCNP

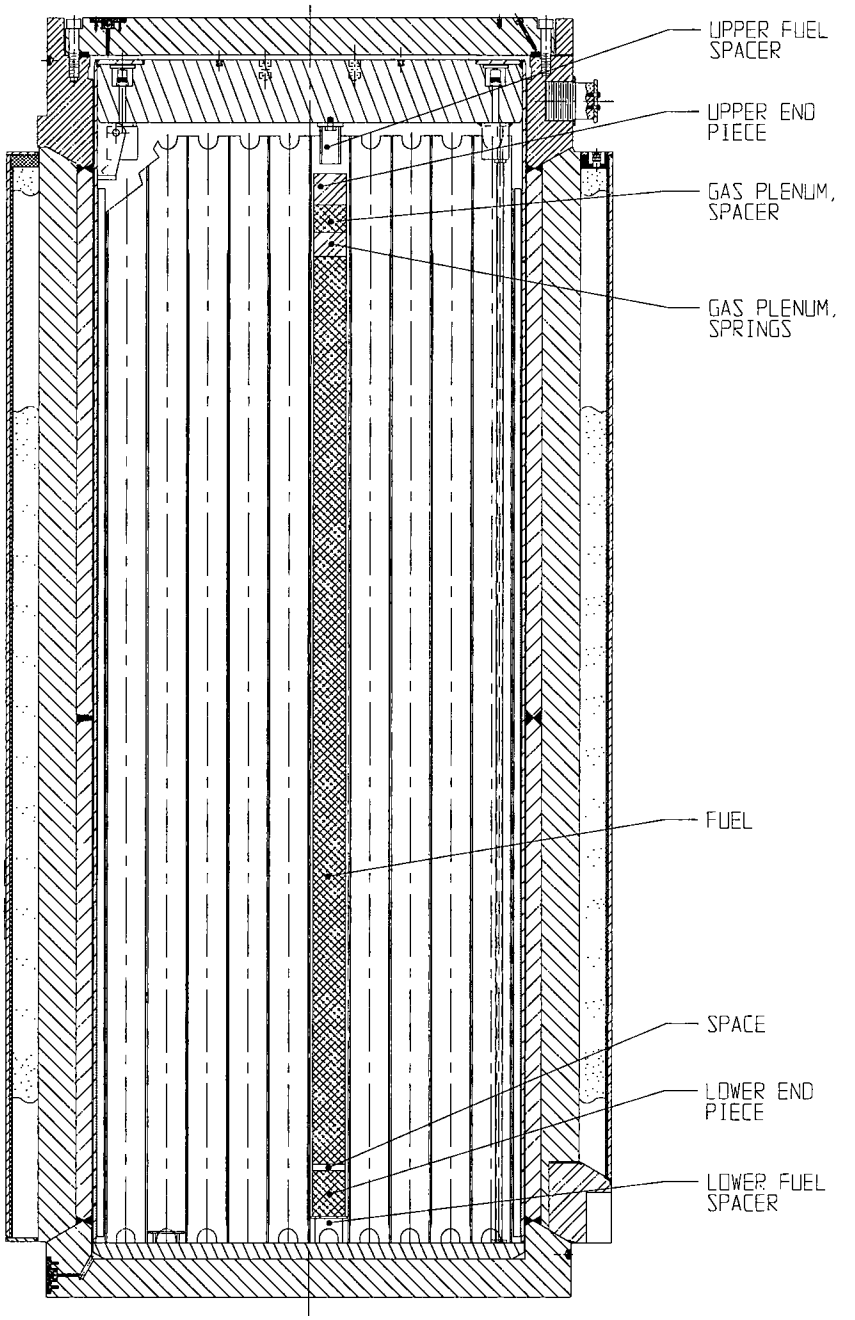

FIGURE 5.3.7; AXIAL LOCATION OF PWR DESIGN BASIS FUEL IN THE HI-STAR 100 SYSTEM

REPORT HI-2012610 | REVISION 0

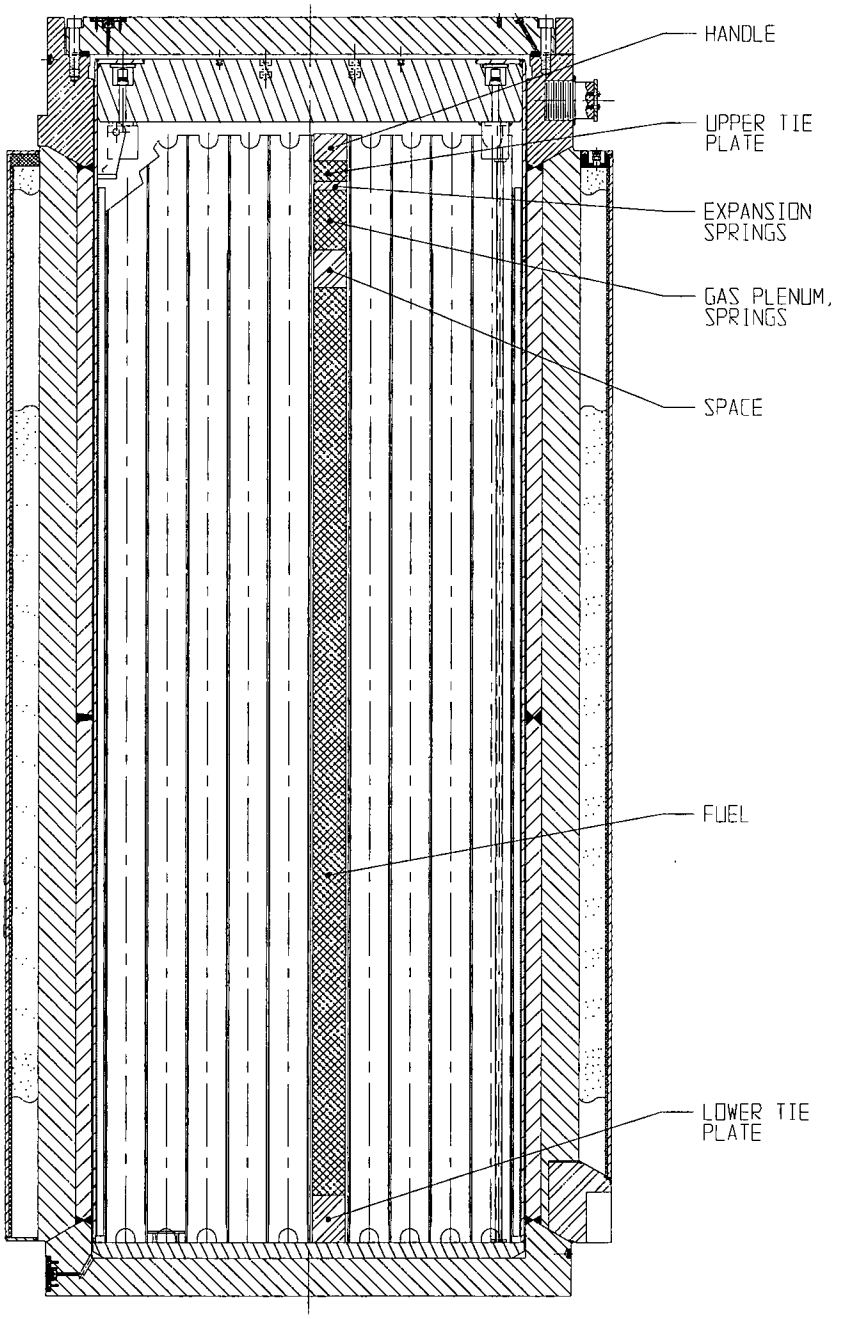

FIGURE 5.3.8; AXIAL LOCATION OF BWR DESIGN BASIS FUEL IN THE HI-STAR 100 SYSTEM

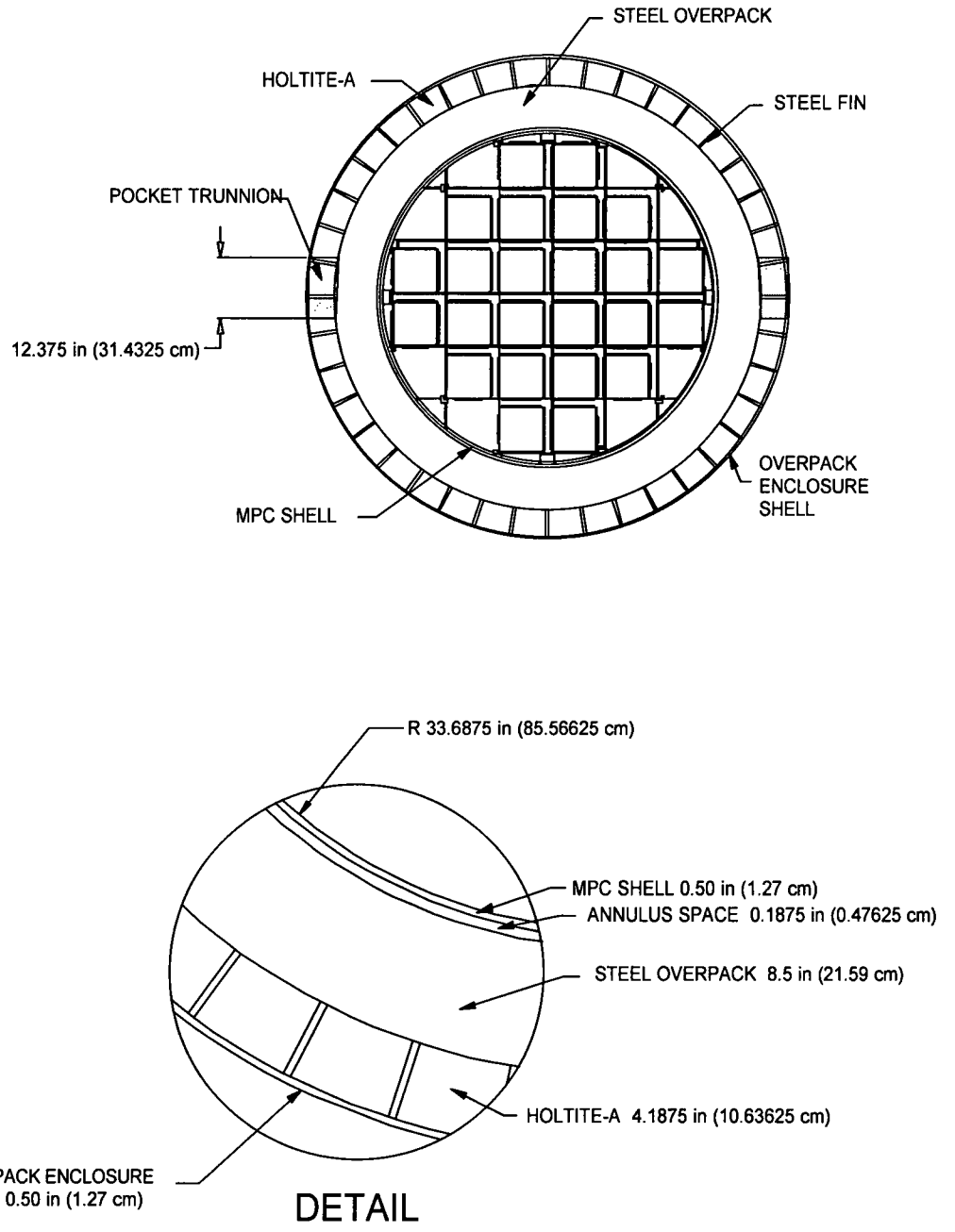

FIGURE 5.3.9; HI-STAR 100 OVERPACK WITH MPC-24 CROSS SECTIONAL VIEW SHOWING THE THICKNESS OF THE MPC SHELL AND OVERPACK AS MODELED IN MCNP

Security-Related Information
Figure Withheld Under 10 CFR 2.390

FIGURE 5.3.10; AXIAL VIEW OF HI-STAR 100 OVERPACK AND MPC WITH AXIAL DIMENSIONS SHOWN AS MODELED IN MCNP

REPORT HI-2012610 REV. 1

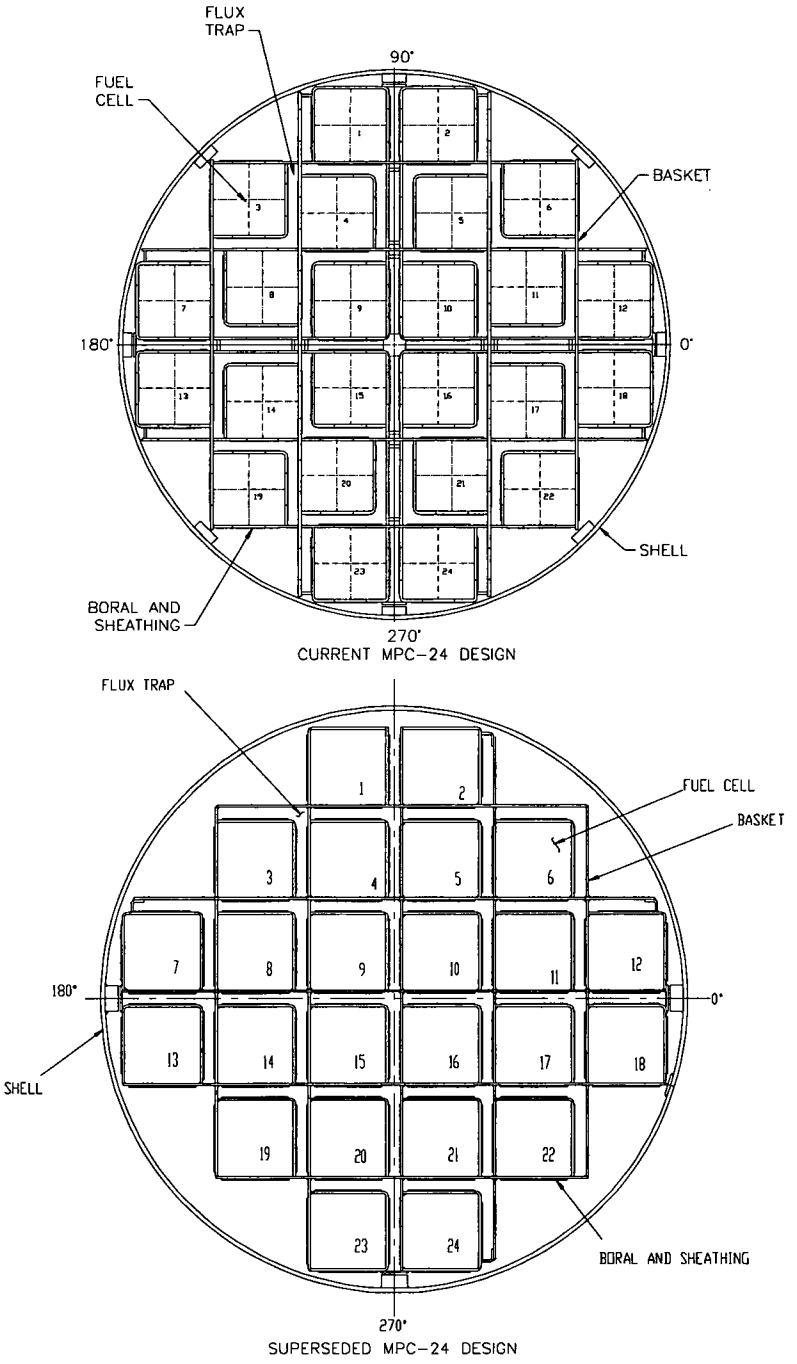

FIGURE 5.3.11; CROSS SECTIONAL VIEWS OF THE CURRENT MPC-24 DESIGN AND THE SUPERSEDED MPC-24 WHICH IS USED IN THE MCNP MODELS.

5.4 SHIELDING EVALUATION

The MCNP-4A code[5.1.1] was used for all of the shielding analyses. MCNP is a continuous energy, three-dimensional, coupled neutron-photon-electron Monte Carlo transport code. Continuous energy cross-section data is represented with sufficient energy points to permit linear-linear interpolation between these points. The individual cross-section libraries used for each nuclide are those recommended by the MCNP manual. All of these data are based on ENDF/B-V data. MCNP has been extensively benchmarked against experimental data by the large user community. References [5.4.2], [5.4.3], and [5.4.4] are three examples of the benchmarking that has been performed.

The energy distribution of the source term, as described earlier, is used explicitly in the MCNP model. A different MCNP calculation is performed for each of the three source terms (neutron, decay gamma, and ^{60}Co). The axial distribution of the fuel source term is described in Table 2.1.8 and Figures 2.1.3 and 2.1.4. The PWR and BWR axial burnup distributions were obtained from References [5.4.5] and [5.4.6] respectively. These axial distributions were obtained from operating plants and are representative of PWR and BWR fuel with burnups greater than 30,000 MWD/MTU. The ^{60}Co source in the activated hardware was assumed to be uniformly distributed over the appropriate regions.

It has been shown that the neutron source strength varies as the burnup level raised by the power of 4.2. Since this relationship is non-linear and since the burnup in the axial center of a fuel assembly is greater than the average burnup, the neutron source strength in the axial center of the assembly is greater than the relative burnup times the average neutron source strength. In order to account for this effect, the neutron source strength in each of the 10 axial nodes listed in Table 2.1.8 was determined by multiplying the average source strength by the relative burnup level raised to the power of 4.2. The peak relative burnups listed in Table 2.1.8 for the PWR and BWR fuels are 1.105 and 1.195 respectively. Using the power of 4.2 relationship results in a 37.6% ($1.105^{4.2}/1.105$) and 76.8% ($1.195^{4.2}/1.195$) increase in the neutron source strength in the peak nodes for the PWR and BWR fuel respectively. The total neutron source strength increases by 15.6% for the PWR fuel assemblies and 36.9% for the BWR fuel assemblies.

MCNP was used to calculate dose at the various desired locations. MCNP calculates neutron or photon flux which can be converted into dose by the use of dose response functions. This is done internally in MCNP and the dose response functions are listed in the input file. The response functions used in these calculations are listed in Table 5.4.1 and were taken from ANSI/ANS 6.1.1, 1977 [5.4.1].

Tables 5.4.2 through 5.4.7 list the normal condition dose rates (from each of the three radiation sources) adjacent to the overpack for each of the burnup levels and cooling times evaluated for the MPC-24 and MPC-68. Tables 5.4.8 and 5.4.9 provide the total dose rate for each burnup level and cooling time for the MPC-24 and MPC-68, respectively. This information was used to determine the worst case burnup level and cooling time and corresponding maximum dose rates

reported in Section 5.1. A detailed discussion of the normal, off-normal, and accident condition dose rates was provided in Sections 5.1.1 and 5.1.2.

Since MCNP is a statistical code, there is an uncertainty associated with the calculated values. In MCNP the uncertainty is expressed as the relative error which is defined as the standard deviation of the mean divided by the mean. Therefore, the standard deviation is represented as a percentage of the mean. The relative error for the total dose rates presented in this chapter were typically less than 3% and the relative error for the individual dose components was typically less than 5%.

5.4.1 Streaming Through Radial Steel Fins and Pocket Trunnions

The HI-STAR 100 overpack utilizes 0.5 inch thick radial steel fins for structural support and cooling. The attenuation of neutrons through steel is substantially less than the attenuation of neutrons through the Holtite-A. Therefore, it is possible to have neutron streaming through the fins which could result in a localized dose peak. The reverse is true for photons which would result in a localized reduction in the photon dose. Analyses were performed to determine the magnitude of the dose peaks and depressions and the impact on localized dose as compared to average total dose. This effect was evaluated at the radial surface of the cask and a distance of one meter from the cask.

In addition to the fins, the pocket trunnions are essentially blocks of steel that are approximately 12 inches wide and 12 inches high. The effect of the pocket trunnion on neutron streaming and photon transmission will be more substantial than the effect of a single fin. Therefore, analyses were performed to quantity this effect. Figure 5.1.1 illustrates the location of the pocket trunnion and its axial position relative to the active fuel. This position will be important in the discussion that follows.

The effect of streaming through the pocket trunnion and the fins was analyzed using MCNP. The model used was an infinite height radial model which consisted of the MPC and the surrounding overpack. The active fuel region of the fuel assemblies was represented in the MPC basket when the neutron source was used and the lower steel regions of the fuel elements were presented in the MPC basket when the cobalt source was used. The pocket trunnion was represented in this infinite model as being axially adjacent to the active fuel. A calculation was not performed with the photon source. Any depression of the gamma dose due to the steel will be evident when using the cobalt source and this will conservatively bound the effects due to the photon source. This is because the average energy of the photons from ^{60}Co is higher than the average energy of decay gammas.

The MPC-24 and the MPC-68 were analyzed. Figure 5.4.1 shows a quarter of the HI-STAR 100 overpack with 91 azimuthal bins drawn. There is one bin per steel fin and 8 bins in each Holtite-A region. This azimuthal binning structure was used in an infinite height two-dimensional model of the MPC and overpack. The dose was calculated in each of these bins and then compared to

the average dose calculated over the surface to determine a peak-to-average ratio for the dose in that bin. The location of the pocket trunnion is shown in Figure 5.4.1. The pocket trunnion was modeled as solid steel. During storage, a shield plug shall be placed in the pocket trunnion recess, and during handling operations a steel rotation trunnion shall be placed in the pocket trunnion recess. To conservatively evaluate the peak-to-average ratio, the pocket trunnion is assumed to be solid steel. The peak-to-average ratio was calculated for the entire pocket trunnion which would correspond to the first seven azimuthal bins.

Table 5.4.10 provides the peak-to-average ratios that were calculated for the various dose components and locations. The peak-to-average ratios were essentially the same for all MPCs, therefore, only one set of values is shown. The values presented for the pocket trunnions are very conservative since the two-dimensional model represented the trunnion as infinite in height whereas the actual height is approximately 12 inches. In addition, the pocket trunnion was represented as being axially adjacent to the active fuel which is not completely accurate for the design basis fuel. The infinite two-dimensional model therefore does not represent any leakage out of the pocket trunnion in the axial direction which would reduce the peaking effect.

Table 5.4.11 presents the dose rates at Dose Point #2 (see Figure 5.1.1) and the adjusted dose rates at this point to account for the streaming effects. An additional dose point labeled 2a is listed in this table. This location is axially adjacent to the pocket trunnion and approximately 6 feet below Dose Point #2. Based on these results it can be concluded that the streaming effect is noticeable but is not of significant concern.

5.4.2 Damaged Fuel Post-Accident Shielding Evaluation

As discussed in Section 5.2.5.2, the analysis presented below, even though it is for damaged fuel, demonstrates the acceptability of storing intact Humboldt Bay 6x6 and intact Dresden 1 6x6 fuel assemblies.

For the damaged fuel and fuel debris accident condition, it is conservatively assumed that the damaged fuel cladding ruptures and all the fuel pellets fall and collect at the bottom of the damaged fuel container. The inner dimension of the damaged fuel container, specified in the design drawings, and the design basis damaged fuel and fuel debris assembly dimensions in Table 5.2.2 are used to calculate the axial height of the rubble in the damaged fuel container assuming 50% compaction. Neglecting the fuel pellet to cladding inner diameter gap, the volume of cladding and fuel pellets available for deposit is calculated assuming the fuel rods are solid. Using the volume in conjunction with the damaged fuel container, the axial height of rubble is calculated to be 80 inches.

Dividing the total fuel gamma source for damaged fuel in Table 5.2.6 by the 80 inch rubble height provides a gamma source per inch of 9.68e+10 photon/s. Dividing the total neutron source for damaged fuel in Table 5.2.14 by 80 inches provides a neutron source per inch of 2.75e+5 neutron/s. These values are both bounded by the BWR design basis fuel gamma source

per inch and neutron source per inch values of 1.76e+12 photon/s and 5.60e+5 neutron/s. These BWR design basis values were calculated by dividing the total source strengths in Tables 5.2.5 and 5.2.13 by the active fuel length of 144 inches. Therefore, the design basis damaged fuel assembly is bounded by the design basis intact BWR fuel assembly for accident conditions. No explicit analysis of the damaged fuel dose rates are provided as they are bounded by the intact fuel analysis.

5.4.3 Site Boundary Evaluation

Since NUREG-1536 [5.2.1] states that detailed calculations need not be presented, Chapter 12 assigns ultimate compliance responsibilities to the site licensee. Therefore, this subsection describes, by example, the general methodology for performing site boundary dose calculations. The site-specific fuel characteristics, burnup, cooling time, and the site layout and boundary characteristics would be factored into the evaluation performed by the licensee.

As an example of the methodology, the dose from a single MPC-24 cask and various arrays of MPC-24 casks at a distance greater than 100 meters was evaluated with MCNP. In the model the casks were placed on an infinite slab of concrete to account for earth-shine effects. The atmosphere was represented as dry air at a uniform density corresponding to 20 degrees C. The height of air modeled was 800 meters. This is more than sufficient to properly account for skyshine effects.

The annual dose, assuming 100% occupancy (8760 hours), at 300 meters from one cask is presented in Table 5.4.12 at the varying maximum burnup and minimum cooling times analyzed. This table indicates that the 40,000 MWD/MTU and 5-year cooling is the bounding case for these combinations.

This table also indicates that the dose due to neutrons is 21% of the total dose. This is an important observation because it implies that simplistic analytical methods such as point kernel techniques may not properly account for the neutron transmission and could lead to low estimates of the site boundary dose.

One of the features of MCNP is the ability to calculate the dose from particles that have passed through certain geometrical regions (referred to as surface or cell flagging). This technique was used to estimate the fraction of the dose at distance from particles, both neutron and gamma, passing through the upper flange region of the overpack. This region is referred to as 3 and 4 on Figure 5.1.1. It was found that, for one cask, approximately 9% of the dose comes from this upper flange region. This is a significant fraction of the total dose and one that is only accounted for using three-dimensional analysis, such as MCNP, which properly includes the effects of neutron and gamma skyshine.

Since the upper flange region is located at the top of the cask, it is reasonable to conclude that this contribution to total dose would be unaffected by placing the cask in an array configuration.

The annual dose, assuming 100% occupancy, at distance from an array of casks was calculated in three steps.

1. The annual dose from the radiation leaving the side of a single HI-STAR 100 overpack was calculated at the distance desired. The side of the HI-STAR 100 overpack is defined as any surface between the bottom of the bottom plate and the top of the closure plate including the upper flange area. Dose value = A.

2. The annual dose from the radiation leaving the top of a single HI-STAR 100 overpack was calculated at the distance desired. The top of the HI-STAR 100 overpack is defined as the top of the closure plate. Dose value = B.

3. The annual dose from the radiation leaving the side of a HI-STAR 100 overpack, when it is in the center of a 3x3 array of casks, was calculated at the distance desired. The casks in the array have a 12 foot pitch. Dose value = C.

The annual dose calculated in each of these three steps was averaged over a cylindrical surface at various distances from the source cask for ease of calculation. In step 3, the dose at the cylindrical surface included contributions from radiation that traveled between the surrounding casks and from radiation that traveled above the surrounding casks and scattered in air to reach the dose location. Therefore, the average dose values from step 3 include all possible paths for radiation to reach the dose location. The values from step 3 represent the dose from a cask in the second row of an array which is shielded by casks in the front row.

The doses calculated in the steps above are listed in Table 5.4.13 for 40,000 MWD/MTU and 5-year cooling. Using these values, the annual dose (at the center of the long side) from an arbitrary 2 by Z array of HI-STAR 100 overpacks can easily be calculated. The following formula describes the method.

Z = number of casks along long side

Dose = ZA + 2ZB + ZC

As an example, the dose from a 2x3 array at 250 meters is presented.

1. The annual dose from the side of a single cask: Dose A = 24.53
2. The annual dose from the top of a single cask: Dose B = 0.63
3. The annual dose from the side of a cask in the center of a 3x3 array: Dose C = 8.81

Using the formula shown above (Z=3) the total dose at 250 meters from a 2x3 array of filled HI-STAR 100 overpacks is 103.80 mrem/year, assuming 100% occupancy.

An important point to notice here is that the dose from the side of the back row of casks is approximately 25% of the total dose. This is a significant contribution and one that would probably not be accounted for properly by simpler methods of analysis.

The results for various arrays of filled HI-STAR 100 overpacks can be found in Section 5.1.1.

5.4.4 Mixed Oxide Fuel Evaluation

The source terms calculated for the Dresden 1 GE 6x6 MOX fuel assemblies can be compared to the design basis source terms for the GE 7x7 assemblies which demonstrates that the MOX fuel source terms are bounded by the design basis source terms and no additional shielding analysis is needed.

Since the active fuel length of the MOX fuel assemblies is shorter than the active fuel length of the design basis fuel, the source terms must be compared on a per inch basis. Dividing the total fuel gamma source for the MOX fuel in Table 5.2.16 by the 110 inch active fuel height provides a gamma source per inch of 6.97e+10 photons/s. Dividing the total neutron source for the MOX fuel assemblies in Table 5.2.17 by 110 inches provides a neutron source strength per inch of 3.06e+5 neutrons/s. These values are both bounded by the BWR design basis fuel gamma source per inch and neutron source per inch values of 1.76e+12 photons/s and 5.60e+5 neutrons/s. These BWR design basis values were calculated by dividing the total source strength in Tables 5.2.5 and 5.2.13 by the active fuel length of 144 inches. This comparison shows that the MOX fuel source terms are bound by the design basis source terms. Therefore, no explicit analysis of dose rates is provided for MOX fuel.

Since the MOX fuel assemblies are Dresden 1 6x6 assemblies, they can also be considered as damaged fuel or fuel debris. Using the same methodology as described in Section 5.4.2, the source term for the MOX fuel is calculated on a per inch basis assuming a post accident rubble height of 80 inches. The resulting gamma and neutron source strengths are 9.59e+10 photons/s and 4.21e+5 neutrons/s. These values are also bounded by the design basis fuel gamma source per inch and neutron source per inch. Therefore, no explicit analysis of dose rates is provided for MOX fuel in a post accident configuration.

5.4.5 Stainless Steel Clad Fuel Evaluation

Table 5.4.14 presents the dose rates at the center of the HI-STAR 100 overpack, adjacent and at one meter distance, for the stainless steel clad fuel. These dose rates, when compared to Tables 5.1.2, 5.1.3, 5.1.5, and 5.1.6, are very close to the dose rates from the design basis zircaloy clad fuel indicating that these fuel assemblies are acceptable for storage.

As described in Section 5.2.3, it would be incorrect to compare the total source strength from the stainless steel clad fuel assemblies to the source strength from the design basis zircaloy clad fuel assemblies since these assemblies do not have the same active fuel length and since there is a

significant gamma source from Cobalt-60 activation in the stainless steel. Therefore it is necessary to calculate the dose rates from the stainless steel clad fuel and compare them to the dose rates from the zircaloy clad fuel. In calculating the dose rates, the source term for the stainless steel fuel was calculated with an artificial active fuel length of 144 inches to permit a simple comparison of dose rates from stainless steel clad fuel and zircaloy clad fuel at the center of the HI-STAR 100 overpack. Since the true active fuel length is shorter than 144 inches and since the end fitting masses of the stainless steel clad fuel are assumed to be identical to the end fitting masses of the zircaloy clad fuel, the dose rates at the other locations on the overpack are bounded by the dose rates from the design basis zircaloy clad fuel, and therefore, no additional dose rates are presented.

5.4.6 BPRAs and TPDs

In order to verify that the BPRAs and TPDs do not affect the shielding analysis, the total dose rates were calculated for the HI-STAR 100 assuming all fuel assemblies in the MPC contained either BPRAs or TPDs. For this calculation, three separate burnups, slightly higher than the allowable burnups listed in Appendix B of the Certificate of Compliance were used with the corresponding cooling time. Tables 5.4.16 and 5.4.17 present the comparison of the total dose rates around the HI-STAR 100 overpack for PWR fuel with and without BPRAs or TPDs. The design basis dose rates are provided in these tables for easy comparison. A comparison of accident condition dose rates is only performed for assemblies with BPRAs since the TPDs, which are in the upper portion of the fuel assembly, will not have a noticeable impact on the accident dose rates at the centerline of the overpack. These tables illustrate that the dose rates for fuel assemblies containing BPRAs and TPDs are bounded by the design basis 40,000 MWD/MTU and 5 year cooling dose rates listed in Section 5.1.1 and Section 5.1.2. Therefore, the addition of BPRAs and TPDs to the MPC-24 is bounded by the shielding analysis presented in this chapter.

5.4.7 Dresden Unit 1 Antimony-Beryllium Neutron Sources

Dresden Unit 1 has antimony-beryllium neutron sources which are placed in the water rod location of their fuel assemblies. These sources are steel rods which contain a cylindrical antimony-beryllium source which is 77.25 inches in length. The steel rod is approximately 95 inches in length. Information obtained from Dresden Unit 1 characterizes these sources in the following manner: "About one-quarter pound of beryllium will be employed as a special neutron source material. The beryllium produces neutrons upon gamma irradiation. The gamma rays for the source at initial start-up will be provided by neutron-activated antimony (about 865 curies). The source strength is approximately 1E+8 neutrons/second."

As stated above, beryllium produces neutrons through gamma irradiation and in this particular case antimony is used as the gamma source. The threshold gamma energy for producing neutrons from beryllium is 1.666 MeV. The outgoing neutron energy increases as the incident gamma energy increases. Sb-124, which decays by Beta decay with a half life of 60.2 days, produces a

gamma of energy 1.69 MeV which is just energetic enough to produce a neutron from beryllium. Approximately 54% of the Beta decays for Sb-124 produce gammas with energies greater than or equal to 1.69 MeV. Therefore, the neutron production rate in the neutron source can be specified as 5.8E-6 neutrons per gamma (1E+8/865/3.7e+10/0.54) with energy greater than 1.666 MeV or 1.16E+5 neutrons/curie (1E+8/865) of Sb-124.

With the short half life of 60.2 days all of the initial Sb-124 is decayed and any Sb-124 that was produced while the neutron source was in the reactor is also decayed since these neutron sources are assumed to have the same minimum cooling time as the Dresden 1 fuel assemblies (array classes 6x6A, 6x6B, 6x6C, and 8x8A) of 18 years. Therefore, there are only two possible gamma sources which can produce neutrons from this antimony-beryllium source. The first is the gammas from the decay of fission products in the fuel assemblies in the MPC. The second gamma source is from Sb-124 which is being produced in the MPC from neutron activation from neutrons from the decay of fission products.

MCNP calculations were performed to determine the gamma source as a result of decay gammas from fuel assemblies and Sb-124 activation. The calculations explicitly modeled the 6x6 fuel assembly described in Table 5.2.2. A single fuel rod was removed and replaced by a guide tube. In order to determine the amount of Sb-124 that is being activated from neutrons in the MPC it was necessary to estimate the amount of antimony in the neutron source. The O.D. of the source was assumed to be the I.D. of the steel rod encasing the source (0.345 in.). The length of the source is 77.25 inches. The beryllium is assumed to be annular in shape encompassing the antimony. Using the assumed O.D. of the beryllium and the mass and length, the I.D. of the beryllium was calculated to be 0.24 inches. The antimony is assumed to be a solid cylinder with an O.D. equal to the I.D. of the beryllium. These assumptions are conservative since the antimony and beryllium are probably encased in another material which would reduce the mass of antimony. A larger mass of antimony is conservative since the calculated activity of Sb-124 is directly proportional to the initial mass of antimony.

The number of gammas from fuel assemblies with energies greater than 1.666 MeV entering the 77.25 inch long neutron source was calculated to be 1.04E+8 gammas/sec which would produce a neutron source of 603.2 neutrons/sec (1.04E+8 * 5.8E-6). The steady state amount of Sb-124 activated in the antimony was calculated to be 39.9 curies. This activity level would produce a neutron source of 4.63E+6 neutrons/sec (39.9 * 1.16E+5) or 6.0E+4 neutrons/sec/inch (4.63E+6/77.25). These calculations conservatively neglect the reduction in antimony and beryllium which would have occurred while the neutron sources were in the core and being irradiated at full reactor power.

Since this is a localized source (77.25 inches in length) it is appropriate to compare the neutron source per inch from the design basis Dresden Unit 1 fuel assembly, 6x6, containing an Sb-Be neutron source to the design basis fuel neutron source per inch. This comparison, presented in Table 5.4.15, demonstrates that a Dresden Unit 1 fuel assembly containing an Sb-Be neutron source is bounded by the design basis fuel.

As stated above, the Sb-Be source is encased in a steel rod. Therefore, the gamma source from the activation of the steel was considered assuming a burnup of 120,000 MWD/MTU which is the maximum burnup assuming the Sb-Be source was in the reactor for the entire 18 year life of Dresden Unit 1. The cooling time assumed was 18 years which is the minimum cooling time for Dresden Unit 1 fuel. The source from the steel was bounded by the design basis fuel assembly. In conclusion, storage of a Dresden Unit 1 Sb-Be neutron source in a Dresden Unit 1 fuel assembly is acceptable and bounded by the current analysis.

5.4.8 Thoria Rod Canister

Based on a comparison of the gamma spectra from Tables 5.2.32 and 5.2.6 for the thoria rod canister and design basis 6x6 fuel assembly, respectively, it is difficult to determine if the thoria rods will be bounded by the 6x6 fuel assemblies. However, it is obvious that the neutron spectra from the 6x6, Table 5.2.14, bounds the thoria rod neutron spectra, Table 5.2.33, with a significant margin. In order to demonstrate that the gamma spectrum from the single thoria rod canister is bounded by the gamma spectrum from the design basis 6x6 fuel assembly, the gamma dose rate on the outer radial surface of the overpack was estimated conservatively assuming an MPC full of thoria rod canisters. This gamma dose rate was compared to an estimate of the dose rate from an MPC full of design basis 6x6 fuel assemblies. The gamma dose rate from the 6x6 fuel was higher than the dose rate from an MPC full of thoria rod canisters. This in conjunction with the significant margin in neutron spectrum and the fact that there is only one thoria rod canister clearly demonstrates that the thoria rod canister is acceptable for storage in the MPC-68 or the MPC-68F.

Table 5.4.1

FLUX-TO-DOSE CONVERSION FACTORS
(FROM [5.4.1])

Gamma Energy (MeV)	**(rem/hr)/ (photon/cm^2-s)**
0.01	3.96E-06
0.03	5.82E-07
0.05	2.90E-07
0.07	2.58E-07
0.1	2.83E-07
0.15	3.79E-07
0.2	5.01E-07
0.25	6.31E-07
0.3	7.59E-07
0.35	8.78E-07
0.4	9.85E-07
0.45	1.08E-06
0.5	1.17E-06
0.55	1.27E-06
0.6	1.36E-06
0.65	1.44E-06
0.7	1.52E-06
0.8	1.68E-06
1.0	1.98E-06
1.4	2.51E-06
1.8	2.99E-06
2.2	3.42E-06

Table 5.4.1 (continued)

FLUX-TO-DOSE CONVERSION FACTORS
(FROM [5.4.1])

Gamma Energy (MeV)	**(rem/hr)/ (photon/cm^2-s)**
2.6	3.82E-06
2.8	4.01E-06
3.25	4.41E-06
3.75	4.83E-06
4.25	5.23E-06
4.75	5.60E-06
5.0	5.80E-06
5.25	6.01E-06
5.75	6.37E-06
6.25	6.74E-06
6.75	7.11E-06
7.5	7.66E-06
9.0	8.77E-06
11.0	1.03E-05
13.0	1.18E-05
15.0	1.33E-05

Table 5.4.1 (continued)

FLUX-TO-DOSE CONVERSION FACTORS
(FROM [5.4.1])

Neutron Energy (MeV)	Quality Factor	(rem/hr)†/(n/cm^2-s)
2.5E-8	2.0	3.67E-6
1.0E-7	2.0	3.67E-6
1.0E-6	2.0	4.46E-6
1.0E-5	2.0	4.54E-6
1.0E-4	2.0	4.18E-6
1.0E-3	2.0	3.76E-6
1.0E-2	2.5	3.56E-6
0.1	7.5	2.17E-5
0.5	11.0	9.26E-5
1.0	11.0	1.32E-4
2.5	9.0	1.25E-4
5.0	8.0	1.56E-4
7.0	7.0	1.47E-4
10.0	6.5	1.47E-4
14.0	7.5	2.08E-4
20.0	8.0	2.27E-4

† Includes the Quality Factor.

Table 5.4.2

DOSE RATES FROM FUEL GAMMAS
DOSE LOCATION ADJACENT TO OVERPACK
NORMAL CONDITIONS
MPC-24 DESIGN BASIS ZIRCALOY CLAD FUEL AT VARYING BURNUP
AND COOLING TIMES[†]

Dose Point[††] Location	**40,000 MWD/MTU 5-Year Cooling (mrem/hr)**	**47,500 MWD/MTU 8-Year Cooling (mrem/hr)**
1	12.45	6.93
2	96.88	54.98
3	3.51	2.20
4	1.81	1.11
5	0.34	0.42
6 (dry MPC)[†††]	27.07	14.36
7 (no temp. shield)	100.36	50.68
7 (with temp. shield)	28.27	19.59

[†] Gammas generated by neutron capture are included with fuel gammas.

[††] Refer to Figure 5.1.1.

[†††] Overpack closure plate not present.

Table 5.4.3

DOSE RATES FROM ^{60}Co GAMMAS
DOSE LOCATION ADJACENT TO OVERPACK
NORMAL CONDITIONS
MPC-24 DESIGN BASIS ZIRCALOY CLAD FUEL AT VARYING BURNUP
AND COOLING TIMES

Dose Point† Location	**40,000 MWD/MTU 5-Year Cooling (mrem/hr)**	**47,500 MWD/MTU 8-Year Cooling (mrem/hr)**
1	231.52	176.39
2	0.03	0.02
3	81.12	61.80
4	35.86	27.32
5	0.69	0.53
6 (dry MPC)††	286.19	218.05
7 (no temp. shield)	1432.28	1091.26
7 (with temp. shield)	329.84	251.30

† Refer to Figure 5.1.1.

†† Overpack closure plate not present.

Table 5.4.4

DOSE RATES FROM NEUTRONS
DOSE LOCATION ADJACENT TO OVERPACK
NORMAL CONDITIONS
MPC-24 DESIGN BASIS ZIRCALOY CLAD FUEL AT VARYING BURNUP
AND COOLING TIMES

Dose Point† Location	**40,000 MWD/MTU 5-Year Cooling (mrem/hr)**	**47,500 MWD/MTU 8-Year Cooling (mrem/hr)**
1	82.27	132.74
2	22.12	35.69
3	70.28	113.40
4	39.47	63.68
5	56.70	91.48
6 (dry MPC)††	126.02	203.29
7 (no temp. shield)	397.30	641.02
7 (with temp. shield)	19.84	32.01

† Refer to Figure 5.1.1.

†† Overpack closure plate not included.

Table 5.4.5

DOSE RATES FROM FUEL GAMMAS
DOSE LOCATION ADJACENT TO OVERPACK
NORMAL CONDITIONS
MPC-68 DESIGN BASIS ZIRCALOY CLAD FUEL AT VARYING BURNUP
AND COOLING TIMES[†]

Dose Point[††] Location	**35,000 MWD/MTU 5-Year Cooling (mrem/hr)**	**45,000 MWD/MTU 9-Year Cooling (mrem/hr)**
1	10.26	5.47
2	100.42	52.26
3	0.97	0.81
4	0.44	0.37
5	0.13	0.20
6 (dry MPC)[†††]	9.32	4.52
7 (no temp. shield)	64.46	31.28
7 (with temp. shield)	20.36	16.04

[†] Gammas generated by neutron capture are included with fuel gammas.

[††] Refer to Figure 5.1.1.

[†††] Overpack closure plate not included.

Table 5.4.6

DOSE RATES FROM ^{60}Co GAMMAS
DOSE LOCATION ADJACENT TO OVERPACK
NORMAL CONDITIONS
MPC-68 DESIGN BASIS ZIRCALOY CLAD FUEL AT VARYING BURNUP
AND COOLING TIMES

Dose Point† Location	**35,000 MWD/MTU 5-Year Cooling (mrem/hr)**	**45,000 MWD/MTU 9-Year Cooling (mrem/hr)**
1	297.76	208.32
2	0.02	0.01
3	127.41	89.14
4	51.49	36.02
5	0.72	0.50
6 (dry MPC)††	329.17	230.30
7 (no temp. shield)	1794.41	1255.40
7 (with temp. shield)	381.90	267.18

† Refer to Figure 5.1.1.

†† Overpack closure plate not included.

Table 5.4.7

DOSE RATES FROM NEUTRONS
DOSE LOCATION ADJACENT TO OVERPACK
NORMAL CONDITIONS
MPC-68 DESIGN BASIS ZIRCALOY CLAD FUEL AT VARYING BURNUP
AND COOLING TIMES

Dose Point† Location	**35,000 MWD/MTU 5-Year Cooling (mrem/hr)**	**45,000 MWD/MTU 9-Year Cooling (mrem/hr)**
1	65.63	133.56
2	19.40	43.08
3	29.88	60.80
4	17.76	36.14
5	26.45	53.81
6 (dry MPC)††	65.38	133.03
7 (no temp. shield)	325.90	663.17
7 (with temp. shield)	14.52	29.55

† Refer to Figure 5.1.1.

†† Overpack closure plate not included.

Table 5.4.8

TOTAL DOSE RATES
DOSE LOCATION ADJACENT TO OVERPACK
NORMAL CONDITIONS
MPC-24 DESIGN BASIS ZIRCALOY CLAD FUEL AT VARYING BURNUP
AND COOLING TIMES

Dose Point† Location	**40,000 MWD/MTU 5-Year Cooling (mrem/hr)**	**47,500 MWD/MTU 8-Year Cooling (mrem/hr)**
1	326.24	316.06
2	119.03	90.69
3	154.90	177.40
4	77.14	92.12
5	57.73	92.43
6 (dry MPC)††	439.28	435.70
7 (no temp. shield)	1929.94	1782.95
7 (with temp. shield)	377.94	302.90

† Refer to Figure 5.1.1.

†† Overpack closure plate not included.

Table 5.4.9

TOTAL DOSE RATES
DOSE LOCATION ADJACENT TO OVERPACK
NORMAL CONDITIONS
MPC-68 DESIGN BASIS ZIRCALOY CLAD FUEL AT VARYING BURNUP
AND COOLING TIMES

Dose Point† Location	**35,000 MWD/MTU 5-Year Cooling (mrem/hr)**	**45,000 MWD/MTU 9-Year Cooling (mrem/hr)**
1	373.64	347.35
2	119.85	95.35
3	158.26	150.75
4	69.69	72.52
5	27.30	54.52
6 (dry MPC)††	403.87	367.85
7 (no temp. shield)	2184.76	1949.86
7 (with temp. shield)	416.78	312.77

† Refer to Figure 5.1.1.

†† Overpack closure plate not included.

Table 5.4.10

PEAK-TO-AVERAGE RATIOS FOR THE DOSE COMPONENTS
AT VARIOUS LOCATIONS

Location	Fuel Gammas	Gammas from Neutrons	^{60}Co Gammas	Neutron
Pocket Trunnion (surface)	0.06	0.33	0.06	7.94
Steel Fin (surface)	0.74	0.95	0.74	2.16
Holtite-A (surface)	1.17	1.05	1.17	0.71
Pocket Trunnion (1 meter)	0.6	0.86	0.6	2.82
Steel Fin (1 meter)	1.0	1.0	1.0	1.05
Holtite-A (1 meter)	1.0	1.0	1.0	0.92

Table 5.4.11

DOSE RATES FOR NORMAL CONDITIONS SHOWING THE
EFFECT OF PEAKING
MPC-24 DESIGN BASIS ZIRCALOY CLAD FUEL
40,000 MWD/MTU 5-YEAR COOLING

Dose Point† Location	Fuel Gammas (mrem/hr)	Gammas from Neutrons (mrem/hr)	^{60}Co Gammas (mrem/hr)	Neutrons (mrem/hr)	Total (mrem/hr)
SURFACE					
2	90.55	6.33	0.03	22.12	119.03
2 (fin)	67.01	6.01	0.02	47.78	120.82
2 (Holtite)	105.94	6.65	0.04	15.71	128.34
2a (Holtite)††	12.35	1.49	77.43	10.08	101.35
2a (pocket trunnion)††	0.63	0.47	3.97	112.75	117.82
ONE METER					
2	40.47	2.20	1.06	7.74	51.47
2 (fin)	40.47	2.20	1.06	8.13	51.86
2 (Holtite)	40.47	2.20	1.06	7.12	50.85
2a (Holtite)††	14.67	0.93	16.58	6.90	39.08
2a (pocket trunnion)††	8.80	0.80	9.95	21.14	40.69

† Refer to Figure 5.1.1.

†† Dose point #2a is axially located next to either the Holtite (neutron shield) or pocket trunnion and approximately 6 feet below Dose point #2.

Table 5.4.12

ANNUAL DOSE AT 300 METERS FROM A SINGLE CASK[†]

	40,000 MWD/MTU 5-Year Cooling (mrem/yr)	**47,500 MWD/MTU 8-Year Cooling (mrem/yr)**
Fuel gammas[††]	8.15	4.34
^{60}Co Gammas	2.46	1.88
Neutrons	2.94	4.74
Total	13.55	10.96

[†] 100% occupancy (8760 hours) is assumed.

[††] Gammas generated by neutron capture are included with fuel gammas.

Table 5.4.13

DOSE VALUES USED IN CALCULATING ANNUAL DOSE FROM
VARIOUS ISFSI CONFIGURATIONS
40,000 MWD/MTU AND 5-YEAR COOLING[†]

	A **Side of Overpack (mrem/yr)**	**B** **Top of Overpack (mrem/yr)**	**C** **Side of Shielded Overpack (mrem/yr)**
100 meters	337.58	7.40	110.31
150 meters	115.93	3.07	40.56
200 meters	51.52	1.35	17.54
250 meters	24.53	0.63	8.81
300 meters	13.28	0.27	4.15
350 meters	6.76	0.15	2.23
400 meters	3.28	0.09	1.16

[†] 100% occupancy (8760 hours) is assumed.

Table 5.4.14

DOSE RATES AT THE CENTERLINE OF THE OVERPACK FOR
DESIGN BASIS STAINLESS STEEL CLAD FUEL

Dose Point† Location	Fuel Gammas†† (mrem/hr)	^{60}Co Gammas (mrem/hr)	Neutrons (mrem/hr)	Totals (mrem/hr)
MPC-24 (30,000 MWD/MTU AND 9-YEAR COOLING)				
2 (Adjacent)	101.34	0.06	5.13	106.53
2 (One Meter)	43.64	0.40	2.16	46.20
MPC-24 (40,000 MWD/MTU AND 15-YEAR COOLING)				
2 (Adjacent)	64.26	0.01	16.06	80.33
2 (One Meter)	28.38	0.19	5.63	34.19
MPC-68 (22,500 MWD/MTU AND 10-YEAR COOLING)				
2 (Adjacent)	80.71	0.01	1.51	82.23
2 (One Meter)	34.70	0.30	0.58	35.59

† Refer to Figure 5.1.1.

†† Gammas generated by neutron capture are included with fuel gammas.

Table 5.4.15

COMPARISON OF NEUTRON SOURCE PER INCH PER SECOND FOR DESIGN BASIS 7X7 FUEL AND DESIGN BASIS DRESDEN UNIT 1 FUEL

Assembly	**Active fuel length (inch)**	**Neutrons per sec per inch**	**Neutrons per sec per inch with Sb-Be source**	**Reference for neutrons per sec per inch**
7x7 design basis	144	5.60E+5	N/A	Table 5.2.13 - 35 GWD/MTU and 5 year cooling
6x6 design basis	110	2.0e+5	2.6E+5	Table 5.2.14
6x6 design basis MOX	110	3.06E+5	3.66E+5	Table 5.2.17

Table 5.4.16

COMPARISON OF TOTAL DOSE RATES FOR DESIGN BASIS PWR FUEL
AND PWR FUEL WITH BPRAS
MPC-24 NORMAL AND ACCIDENT CONDITIONS

Dose Point† Location	**40 GWD/MTU 5 year cooling DESIGN BASIS (mrem/hr)**	**29 GWD/MTU 5 year cooling (mrem/hr)**	**39 GWD/MTU 10 year cooling (mrem/hr)**	**42.5 GWD/MTU 15 year cooling (mrem/hr)**
BPRAs ?	NO	YES	YES	YES
SURFACE - NORMAL CONDITION				
1	326.24	244.72	195.95	143.2
2	119.03	99.66	69.57	61.70
3	154.90	136.39	136.84	120.32
4	77.14	64.13	67.66	60.70
5	57.73	25.15	48.25	50.53
6 (dry MPC)††	439.28	445.46	389.94	324.45
7 (no temp. shield)	1929.94	1557.87	1165.15	810.77
ONE METER - NORMAL CONDITION				
1	43.79	34.47	25.62	19.12
2	51.47	44.42	29.32	25.50
3	30.21	28.68	24.86	21.27
4	28.61	27.06	24.19	20.68
5	17.11	7.55	14.3	14.95
7 (no temp. shield)	889.68	717.64	501.61	329.5
SURFACE - ACCIDENT CONDITION				
2	1371.34	699.45	1074.98	1101.53
ONE METER - ACCIDENT CONDITION				
2	491.73	263.82	378.91	384.75

† Refer to Figure 5.1.1.

†† Overpack closure plate not present.

Table 5.4.17

COMPARISON OF TOTAL DOSE RATES FOR DESIGN BASIS PWR FUEL
AND PWR FUEL WITH TPDS
MPC-24 NORMAL CONDITIONS

Dose Point† Location	**40 GWD/MTU 5 year cooling DESIGN BASIS (mrem/hr)**	**29 GWD/MTU 5 year cooling (mrem/hr)**	**39 GWD/MTU 10 year cooling (mrem/hr)**	**42.5 GWD/MTU 15 year cooling (mrem/hr)**
TPDs ?	NO	YES	YES	YES
SURFACE - NORMAL CONDITION				
1	326.24	241.88	193.11	140.36
2	119.03	78.00	47.91	40.04
3	154.90	134.01	134.47	117.95
4	77.14	63.09	66.62	59.66
5	57.73	25.12	48.22	50.51
6 (dry MPC)††	439.28	439.39	383.86	318.38
7 (no temp. shield)	1929.94	1531.39	1138.67	784.28
ONE METER - NORMAL CONDITION				
1	43.79	32.23	23.39	16.88
2	51.47	34.70	19.61	15.78
3	30.21	27.55	23.74	20.15
4	28.61	26.11	23.25	19.73
5	17.11	7.54	14.29	14.94
7 (no temp. shield)	889.68	703.89	487.86	315.76

† Refer to Figure 5.1.1.

†† Overpack closure plate not present.

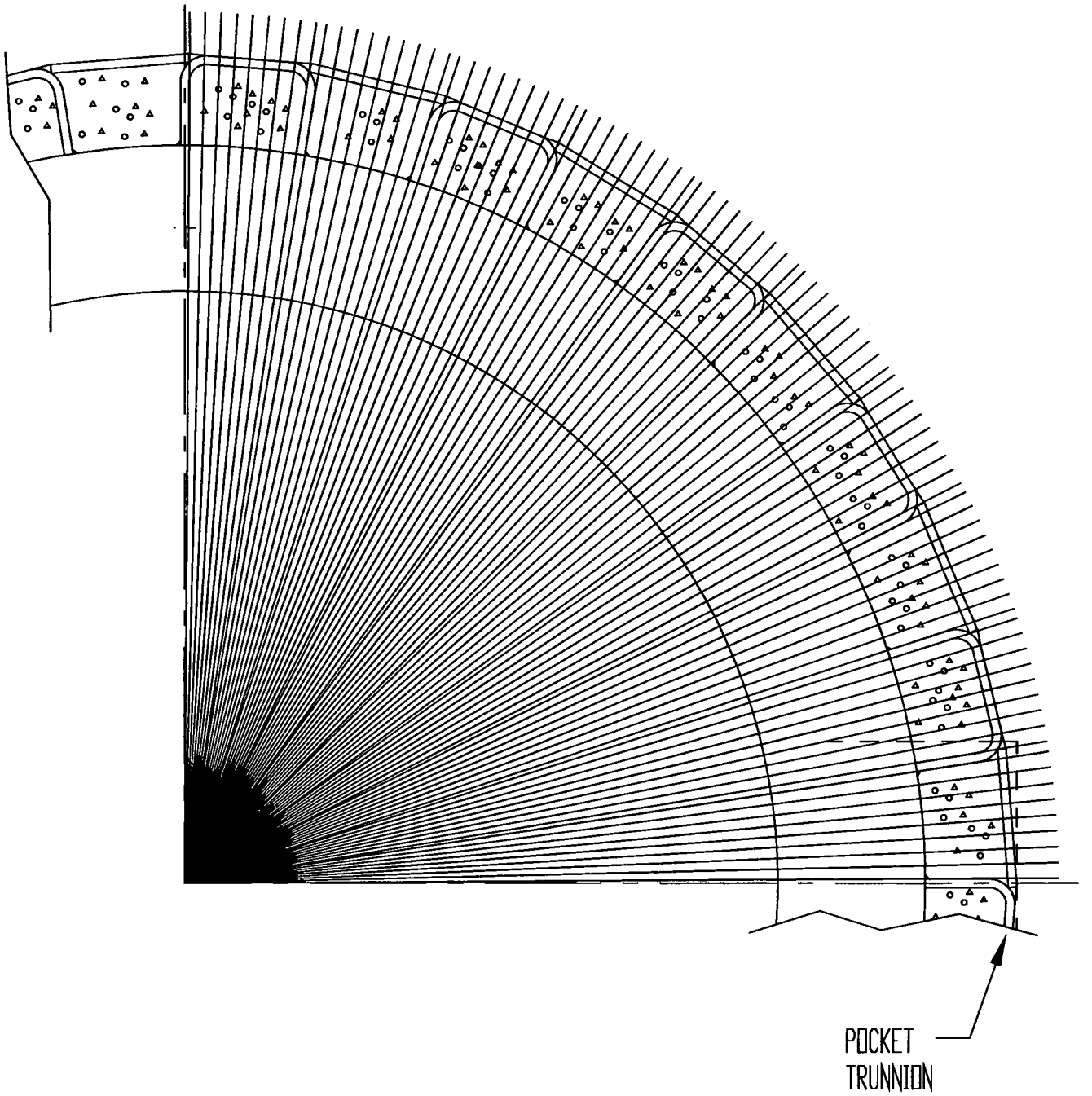

FIGURE 5.4.1; DEPICTION OF THE AZIMUTHAL SEGMENTATION OF THE OVERPACK USED IN ANALYZING NEUTRON AND PHOTON STREAMING

5.5 REGULATORY COMPLIANCE

Chapters 1 and 2 and this chapter of this FSAR describe in detail the shielding structures, systems, and components (SSCs) important to safety.

This chapter has evaluated these shielding SSCs important to safety and has assessed the impact on health and safety resulting from operation of an independent spent fuel storage installation (ISFSI) utilizing the HI-STAR 100 System.

It has been shown that the design of the shielding system of the HI-STAR 100 System is in compliance with 10CFR72 and that the applicable design and acceptance criteria including 10CFR20 have been satisfied. Thus, this shielding evaluation provides reasonable assurance that the HI-STAR 100 System will allow safe storage of spent fuel.

5.6 REFERENCES

[5.1.1] J.F. Briesmeister, Ed., "MCNP - A General Monte Carlo N-Particle Transport Code, Version 4A." Los Alamos National Laboratory, LA-12625-M (1993).

[5.1.2] O.W. Hermann, C.V. Parks, "SAS2H: A Coupled One-Dimensional Depletion and Shielding Analysis Module," NUREG/CR-0200, Revision 5, (ORNL/NUREG/CSD-2/V2/R5), Oak Ridge National Laboratory, September 1995.

[5.1.3] O.W. Hermann, R.M. Westfall, "ORIGEN-S: SCALE System Module to Calculate Fuel Depletion, Actinide Transmutation, Fission Product Buildup and Decay, and Associated Radiation Source Terms," NUREG/CR-0200, Revision 5, (ORNL/NUREG/CSD-2/V2/R5), Oak Ridge National Laboratory, September 1995.

[5.2.1] NUREG-1536, SRP for Dry Cask Storage Systems, USNRC, Washington, DC, January 1997.

[5.2.2] A.G. Croff, M.A. Bjerke, G.W. Morrison, L.M. Petrie, "Revised Uranium-Plutonium Cycle PWR and BWR Models for the ORIGEN Computer Code," ORNL/TM-6051, Oak Ridge National Laboratory, September 1978.

[5.2.3] A. Luksic, "Spent Fuel Assembly Hardware: Characterization and 10CFR 61 Classification for Waste Disposal," PNL-6906-vol. 1, Pacific Northwest Laboratory, June 1989.

[5.2.4] J.W. Roddy et al., "Physical and Decay Characteristics of Commercial LWR Spent Fuel," ORNL/TM-9591/V1&R1, Oak Ridge National Laboratory, January 1996.

[5.2.5] "Characteristics of Spent Fuel, High Level Waste, and Other Radioactive Wastes Which May Require Long-Term Isolation," DOE/RW-0184, U.S. Department of Energy, December 1987.

[5.2.6] "Spent Nuclear Fuel Discharges from U.S. Reactors 1994," SR/CNEAF/96-01, Energy Information Administration, U.S. Department of Energy, February 1996.

[5.2.7] "Characteristics Database System LWR Assemblies Database," DOE/RW-0184-R1, U.S. Department of Energy, July 1992.

[5.4.1] "American National Standard Neutron and Gamma-Ray Flux-to-Dose Rate Factors", ANSI/ANS-6.1.1-1977.

[5.4.2] D. J. Whalen, et al., 'MCNP: Photon Benchmark Problems," LA-12196, Los Alamos National Laboratory, September 1991.

[5.4.3] D. J. Whalen, et al., 'MCNP: Neutron Benchmark Problems,"LA-12212, Los Alamos National Laboratory, November 1991.

[5.4.4] J. C. Wagner, et al., 'MCNP: Criticality Safety Benchmark Problems," LA-12415, Los Alamos National Laboratory, October 1992.

[5.4.5] S. E. Turner, "Uncertainty Analysis - Axial Burnup Distribution Effects," presented in "Proceedings of a Workshop on the Use of Burnup Credit in Spent Fuel Transport Casks," SAND-89-0018, Sandia National Laboratory, Oct. 1989.

[5.4.6] Commonwealth Edison Company, Letter No. NFS-BND-95-083, Chicago, Illinois.

APPENDIX 5.A

SAMPLE INPUT FILE FOR SAS2H

(Total number of pages in this appendix : 3)

```
=SAS2H     PARM='halt08,skipshipdata'
bw 15x15 PWR assembly
' fuel temp 923
44groupndf5     LATTICECELL
UO2 1 0.95 923 92234 0.03026 92235 3.4 92236 0.01564
    92238 96.5541 END
'
' Zirc 4 composition
ARBM-ZIRC4 6.55 4 1 0 0 50000 1.7 26000 0.24 24000 0.13 40000 97.93
           2 1.0 595 END
'
' water with 652.5 ppm boron
H2O        3 DEN=0.7135 1  579 END
ARBM-BORMOD  0.7135 1 1 0 0 5000 100 3 652.5E-6  579  END
'
co-59  3 0 1-20 579 end
kr-83  1 0 1-20 923 end
kr-84  1 0 1-20 923 end
kr-85  1 0 1-20 923 end
kr-86  1 0 1-20 923 end
sr-90  1 0 1-20 923 end
y-89   1 0 1-20 923 end
zr-94  1 0 1-20 923 end
zr-95  1 0 1-20 923 end
mo-94  1 0 1-20 923 end
mo-95  1 0 1-20 923 end
nb-94  1 0 1-20 923 end
nb-95  1 0 1-20 923 end
tc-99  1 0 1-20 923 end
ru-106  1 0 1-20 923 end
rh-103  1 0 1-20 923 end
rh-105  1 0 1-20 923 end
sb-124  1 0 1-20 923 end
sn-126  1 0 1-20 923 end
xe-131  1 0 1-20 923 end
xe-132  1 0 1-20 923 end
xe-134  1 0 1-20 923 end
'
xe-135  1 0 1-09 923 end
'
xe-136  1 0 1-20 923 end
cs-133  1 0 1-20 923 end
cs-134  1 0 1-20 923 end
cs-135  1 0 1-20 923 end
cs-137  1 0 1-20 923 end
ba-136  1 0 1-20 923 end
la-139  1 0 1-20 923 end
ce-144  1 0 1-20 923 end
pr-143  1 0 1-20 923 end
nd-143  1 0 1-20 923 end
nd-144  1 0 1-20 923 end
nd-145  1 0 1-20 923 end
nd-146  1 0 1-20 923 end
nd-147  1 0 1-20 923 end
nd-148  1 0 1-20 923 end
nd-150  1 0 1-20 923 end
pm-147  1 0 1-20 923 end
pm-148  1 0 1-20 923 end
```

```
pm-149  1 0 1-20 923 end
sm-147  1 0 1-20 923 end
sm-148  1 0 1-20 923 end
sm-149  1 0 1-20 923 end
sm-150  1 0 1-20 923 end
sm-151  1 0 1-20 923 end
sm-152  1 0 1-20 923 end
eu-151  1 0 1-20 923 end
eu-153  1 0 1-20 923 end
eu-154  1 0 1-20 923 end
eu-155  1 0 1-20 923 end
gd-154  1 0 1-20 923 end
gd-155  1 0 1-20 923 end
gd-157  1 0 1-20 923 end
gd-158  1 0 1-20 923 end
gd-160  1 0 1-20 923 end
'
END COMP
'
' - - - - - - - - - - - - - - - - - - - - - - - - - - - - - - - - - - -
'
'  FUEL-PIN-CELL GEOMETRY:
'
SQUAREPITCH  1.44272 0.950468 1 3 1.08712 2 0.97028 0 END
'
' - - - - - - - - - - - - - - - - - - - - - - - - - - - - - - - - - - -
'
'  MTU in this model is 0.495485 based on fuel dimensions provided
'
'  1 power cycle will be used and a library will be generated every
'  2500 MWD/MTU  power level is 40 MW/MTU
'  therefore 62.5 days per 2500 MWD/MTU
'  Below
'  BURN=62.5*NLIB/CYC
'  POWER=MTU*40
'
'  Number of libraries is 17 which is 42,500 MWD/MTU burnup (17*2500)
'
'  ASSEMBLY AND CYCLE PARAMETERS:
'
NPIN/ASSM=208 FUELNGTH=365.76 NCYCLES=1 NLIB/CYC=17
PRINTLEVEL=1
LIGHTEL=5  INPLEVEL=1   NUMHOLES=17
NUMINStr= 0  ORTUBE= 0.6731  SRTUBE=0.63246   END
POWER=19.81938 BURN=1062.5 END
'
 O  66.54421
 FE  0.24240868
 ZR 98.78151  CR  0.1311304   SN  1.714782
'
END
=SAS2H    PARM='restarts,halt17,skipshipdata'
bw 15x15 PWR assembly
END
```

APPENDIX 5.B

SAMPLE INPUT FILE FOR ORIGEN-S

(Total number of pages in this appendix : 6)

```
#ORIGENS
0$$  A4 33 A8 26 A11 71  E
1$$  1 T
bw 15x15 FUEL -- FT33F001 -
'
' SUBCASE  1 LIBRARY POSITION  1
'
'   lib     pos      grms   photon group
3$$ 33  A3  1  0  A16 2   E T
35$$ 0 T
56$$  5  5  A6 3  A10  0  A13 9  A15 3 A19 1 E
57** 0.0 A3 1.E-5 0.0625 E T
 FUEL 3.4
BW 15x15 0.495485 MTU
58** 19.81938  19.81938 19.81938 19.81938  19.81938
60**  1.0000   3.0000  15.0000  30.0000  62.5
66$$ A1 2 A5 2 A9 2  E
73$$  922350  922340  922360  922380  80000  500000
      260000  240000  400000
74** 16846.48 149.9336 77.49379 478410.7 66544.21 1714.782
     242.0868 131.1304 98781.51
75$$  2  2  2  2  4  4  4  4  4  T
'
' SUBCASE  2 LIBRARY POSITION  2
'
3$$ 33  A3   2  0  A16 2  A33 0  E T
35$$ 0 T
56$$  3  3  A6 3  A10   5  A15 3 A19 1 E
57** 0.0 A3 1.E-5  0.0625 E T
 fuel
BW 15X15
58** 19.81938 19.81938 19.81938
60** 18.5 37.0 62.5
66$$ A1 2 A5 2 A9 2  E T
'
' SUBCASE  3 LIBRARY POSITION  3
'
3$$ 33  A3   3  0  A16 2  A33 0  E T
35$$ 0 T
56$$  3  3  A6 3  A10   3  A15 3 A19 1 E
57** 0.0 A3 1.E-5  0.0625 E T
 fuel
BW 15X15
58** 19.81938 19.81938 19.81938
60** 18.5 37.0 62.5
66$$ A1 2 A5 2 A9 2  E T
'
' SUBCASE  4 LIBRARY POSITION  4
'
3$$ 33  A3   4  0  A16 2  A33 0  E T
35$$ 0 T
56$$  3  3  A6 3  A10   3  A15 3 A19 1 E
57** 0.0 A3 1.E-5  0.0625 E T
 fuel
BW 15X15
58** 19.81938 19.81938 19.81938
60** 18.5 37.0 62.5
66$$ A1 2 A5 2 A9 2  E T
'
```

```
' SUBCASE  5 LIBRARY POSITION  5
'
3$$ 33  A3   5  0  A16 2  A33 0  E T
35$$ 0 T
56$$  3  3  A6 3  A10   3  A15 3 A19 1 E
57** 0.0 A3 1.E-5  0.0625 E T
 fuel
BW 15X15
58** 19.81938 19.81938 19.81938
60** 18.5 37.0 62.5
66$$ A1 2 A5 2 A9 2  E T
'
' SUBCASE  6 LIBRARY POSITION  6
'
3$$ 33  A3   6  0  A16 2  A33 0  E T
35$$ 0 T
56$$  3  3  A6 3  A10   3  A15 3 A19 1 E
57** 0.0 A3 1.E-5  0.0625 E T
 fuel
BW 15X15
58** 19.81938 19.81938 19.81938
60** 18.5 37.0 62.5
66$$ A1 2 A5 2 A9 2  E T
'
' SUBCASE  7 LIBRARY POSITION  7
'
3$$ 33  A3   7  0  A16 2  A33 0  E T
35$$ 0 T
56$$  3  3  A6 3  A10   3  A15 3 A19 1 E
57** 0.0 A3 1.E-5  0.0625 E T
 fuel
BW 15X15
58** 19.81938 19.81938 19.81938
60** 18.5 37.0 62.5
66$$ A1 2 A5 2 A9 2  E T
'
' SUBCASE  8 LIBRARY POSITION  8
'
3$$ 33  A3   8  0  A16 2  A33 0  E T
35$$ 0 T
56$$  3  3  A6 3  A10   3  A15 3 A19 1 E
57** 0.0 A3 1.E-5  0.0625 E T
 fuel
BW 15X15
58** 19.81938 19.81938 19.81938
60** 18.5 37.0 62.5
66$$ A1 2 A5 2 A9 2  E T
'
' SUBCASE  9 LIBRARY POSITION  9
'
3$$ 33  A3   9  0  A16 2  A33 0  E T
35$$ 0 T
56$$  3  3  A6 3  A10   3  A15 3 A19 1 E
57** 0.0 A3 1.E-5  0.0625 E T
 fuel
BW 15X15
58** 19.81938 19.81938 19.81938
60** 18.5 37.0 62.5
66$$ A1 2 A5 2 A9 2  E T
```

```
'
' SUBCASE 10 LIBRARY POSITION 10
'
3$$ 33  A3  10  0  A16 2  A33 0  E T
35$$ 0 T
56$$  3  3  A6 3  A10   3  A15 3 A19 1 E
57** 0.0 A3 1.E-5  0.0625 E T
 fuel
BW 15X15
58** 19.81938 19.81938 19.81938
60** 18.5 37.0 62.5
66$$ A1 2 A5 2 A9 2  E T
'
' SUBCASE 11 LIBRARY POSITION 11
'
3$$ 33  A3  11  0  A16 2  A33 0  E T
35$$ 0 T
56$$  3  3  A6 3  A10   3  A15 3 A19 1 E
57** 0.0 A3 1.E-5  0.0625 E T
 fuel
BW 15X15
58** 19.81938 19.81938 19.81938
60** 18.5 37.0 62.5
66$$ A1 2 A5 2 A9 2  E T
'
' SUBCASE 12 LIBRARY POSITION 12
'
3$$ 33  A3  12  0  A16 2  A33 0  E T
35$$ 0 T
56$$  3  3  A6 3  A10   3  A15 3 A19 1 E
57** 0.0 A3 1.E-5  0.0625 E T
 fuel
BW 15X15
58** 19.81938 19.81938 19.81938
60** 18.5 37.0 62.5
66$$ A1 2 A5 2 A9 2  E T
'
' SUBCASE 13 LIBRARY POSITION 13
'
3$$ 33  A3  13  0  A16 2  A33 0  E T
35$$ 0 T
56$$  3  3  A6 3  A10   3  A15 3 A19 1 E
57** 0.0 A3 1.E-5  0.0625 E T
 fuel
BW 15X15
58** 19.81938 19.81938 19.81938
60** 18.5 37.0 62.5
66$$ A1 2 A5 2 A9 2  E T
'
' SUBCASE 14 LIBRARY POSITION 14
'
3$$ 33  A3  14  0  A16 2  A33 0  E T
35$$ 0 T
56$$  3  3  A6 3  A10   3  A15 3 A19 1 E
57** 0.0 A3 1.E-5  0.0625 E T
 fuel
BW 15X15
58** 19.81938 19.81938 19.81938
60** 18.5 37.0 62.5
```

```
66$$ A1 2 A5 2 A9 2  E T
'
' SUBCASE 15 LIBRARY POSITION 15
'
3$$ 33  A3  15  0  A16 2  A33 0  E T
35$$ 0 T
56$$  3  3  A6 3  A10   3  A15 3 A19 1 E
57** 0.0 A3 1.E-5  0.0625 E T
 fuel
BW 15X15
58** 19.81938 19.81938 19.81938
60** 18.5 37.0 62.5
66$$ A1 2 A5 2 A9 2  E T
'
' SUBCASE 16 LIBRARY POSITION 16
'
3$$ 33  A3  16  A4 7 0  A16 2  A33 18  E T
35$$ 0 T
56$$  3  3  A6 1  A10  3  A15 3 A19 1 E
57** 0.0 A3 1.E-5  0.0625 E T
 fuel
BW 15X15
58** 19.81938 19.81938 19.81938
60** 18.5 37.0 62.5
66$$ A1 2 A5 2 A9 2  E T
'
' SUBCASE - decay
'
54$$ A8 1 E
56$$ 0 9 A6 1 A10 3 A14 3 A15 1 A19 1 E
57** 0.0 0 1.E-5  E T
 fuel enrichment above
60** 0.5 0.75 1.0 4.0 8.0 12.0 24.0 48.0 96.0
61** F0.1
65$$
'GRAM-ATOMS   GRAMS    CURIES     WATTS-ALL  WATTS-GAMMA
     3Z     0  1  0     0 0 0      1 0 0         3Z         6Z
     3Z     0  1  0     0 0 0      1 0 0         3Z         6Z
     3Z     0  1  0     0 0 0      1 0 0         3Z         6Z  T
'
' SUBCASE - decay
'
54$$ A8 1 E
56$$ 0 9 A6 1 A10 9 A14 4 A15 1 A19 1 E
57** 4.0 0 1.E-5  E T
 fuel enrichment above
60** 10.0 20.0 30.0 60.0 90.0 120.0 180.0 240.0 365.0
61** F0.1
65$$
'GRAM-ATOMS   GRAMS    CURIES     WATTS-ALL  WATTS-GAMMA
     3Z     0  1  0     0 0 0      1 0 0         3Z         6Z
     3Z     0  1  0     0 0 0      1 0 0         3Z         6Z
     3Z     0  1  0     0 0 0      1 0 0         3Z         6Z  T
'
' SUBCASE - decay
'
54$$ A8 0 E
56$$ 0 9 A6 1 A10 9 A14 5 A15 1 A19 1 E
57** 1.0 0 1.E-5  E T
```

```
 fuel enrichment above
60** 1.5 3.0 4.0 5.0 6.0 7.0 8.0 9.0 10.0
61** F1.0e-5
65$$
'GRAM-ATOMS   GRAMS    CURIES     WATTS-ALL  WATTS-GAMMA
     3Z     0  1  0     1 0 0      1 0 0         3Z         6Z
     3Z     0  1  0     1 0 0      1 0 0         3Z         6Z
     3Z     0  1  0     1 0 0      1 0 0         3Z         6Z
81$$ 2 0 26 1 E
82$$ 0 2 2 2 2 2 2 2 2
83**  1.1E+7  8.0E+6 6.0E+6 4.0E+6 3.0E+6 2.5E+6 2.0E+6 1.5E+6
      1.0E+6  7.0E+5 4.5E+5 3.0E+5 1.5E+5 1.0E+5 7.0E+4 4.5E+4
      3.0E+4  2.0E+4 1.0E+4
84**  20.0E+6 6.43E+6 3.0E+6 1.85E+6 1.40E+6 9.00E+5 4.00E+5 1.0E+5 T
'
'
'
'
'
'
'
'
' SUBCASE - decay
'
54$$ A8 0 E
56$$ 0 10 A6 1 A10 9 A14 5 A15 1 A19 1 E
57** 10.0 0 1.E-5  E T
 fuel enrichment above
60** 11.0 12.0 13.0 14.0 15.0 16.0 17.0 18.0 19.0 20.0
61** F1.0e-5
65$$
'GRAM-ATOMS   GRAMS    CURIES     WATTS-ALL  WATTS-GAMMA
     3Z     0  1  0     1 0 0      1 0 0         3Z         6Z
     3Z     0  1  0     1 0 0      1 0 0         3Z         6Z
     3Z     0  1  0     1 0 0      1 0 0         3Z         6Z
81$$ 2 0 26 1 E
82$$ 2 2 2 2 2 2 2 2 2 2
83**  1.1E+7  8.0E+6 6.0E+6 4.0E+6 3.0E+6 2.5E+6 2.0E+6 1.5E+6
      1.0E+6  7.0E+5 4.5E+5 3.0E+5 1.5E+5 1.0E+5 7.0E+4 4.5E+4
      3.0E+4  2.0E+4 1.0E+4
84**  20.0E+6 6.43E+6 3.0E+6 1.85E+6 1.40E+6 9.00E+5 4.00E+5 1.0E+5 T
'
'
'
'
'
'
'
'
'
'
' END
'
56$$ F0 T
END
```

APPENDIX 5.C

SAMPLE INPUT FILE FOR MCNP

(Total number of pages in this appendix : 35)

```
message:   outp=m68n65ao  srctp=m68n65as  runtpe=m68n65ar
           mctal=m68n65am  wssa=m68n65aw  rssa=pt001w

m68n65a
c       HI STAR 100 MPC68
c
c
c     two pocket trunions modeled
c     holtite present
c     impact limiters not present
c     axial model
c
c     origen is at the bottom of the overpack - as an example of the origen
c     item 1 on drawing 1397 is 6 inches thick and extends
c     from 0.0 to 6.0 inches in the axial direction
c
c     only cells that contain material are split axially
c     importance splitting is not done in cells with 0 material
c
c     universe 1
c
c      egg crate
301     0            -30            -400 u=1
302     0             31            -400 u=1
303     0        30 -31 -32         -400 u=1
304     0        30 -31  33         -400 u=1
305     5 -7.92          28     400 -420 u=1
306     5 -7.92             -23 400 -420 u=1
307     5 -7.92     -15 23 -28 400 -420 u=1
308     5 -7.92  20     23 -28 400 -420 u=1
309     5 -7.92          28     420 -430 u=1
310     5 -7.92             -23 420 -430 u=1
311     5 -7.92     -15 23 -28 420 -430 u=1
312     5 -7.92  20     23 -28 420 -430 u=1
313     5 -7.92          28     430 -440 u=1
314     5 -7.92             -23 430 -440 u=1
315     5 -7.92     -15 23 -28 430 -440 u=1
316     5 -7.92  20     23 -28 430 -440 u=1
317     5 -7.92          28     440 -670 u=1
318     5 -7.92             -23 440 -670 u=1
319     5 -7.92     -15 23 -28 440 -670 u=1
320     5 -7.92  20     23 -28 440 -670 u=1
321     5 -7.92          28     670 -460 u=1
322     5 -7.92             -23 670 -460 u=1
323     5 -7.92     -15 23 -28 670 -460 u=1
324     5 -7.92  20     23 -28 670 -460 u=1
c      boral and inside of egg crate and outside of fuel
326     0        15 -30 23 -28 400 -410 u=-1
327     0        31 -20 23 -28 400 -410 u=-1
328     0        30 -31 33 -28 400 -410 u=-1
329     0        30 -31 23 -32 400 -410 u=-1
330     0        15 -18 26 -28 410 -435 u=-1
331     0        19 -20 26 -28 410 -435 u=-1
332     0        15 -17 23 -24 410 -435 u=-1
333     0        15 -17 25 -26 410 -435 u=-1
334     6 -2.644 18 -19 27 -28 410 -420 u=-1
335     5 -7.92  18 -19 26 -27 410 -420 u=-1
336     6 -2.644 15 -16 24 -25 410 -420 u=-1
337     5 -7.92  16 -17 24 -25 410 -420 u=-1
338     6 -2.644 18 -19 27 -28 420 -430 u=-1
339     5 -7.92  18 -19 26 -27 420 -430 u=-1
340     6 -2.644 15 -16 24 -25 420 -430 u=-1
341     5 -7.92  16 -17 24 -25 420 -430 u=-1
342     6 -2.644 18 -19 27 -28 430 -435 u=-1
343     5 -7.92  18 -19 26 -27 430 -435 u=-1
344     6 -2.644 15 -16 24 -25 430 -435 u=-1
345     5 -7.92  16 -17 24 -25 430 -435 u=-1
346     0        17 -30 23 -26 410 -435 u=-1
347     0        31 -20 23 -26 410 -435 u=-1
```

```
348     0         30 -31 23 -32 410 -435 u=-1
349     0         30 -31 33 -26 410 -435 u=-1
350     0         15 -30 23 -28 435 -460 u=-1
351     0         31 -20 23 -28 435 -460 u=-1
352     0         30 -31 33 -28 435 -460 u=-1
353     0         30 -31 23 -32 435 -460 u=-1
c       fuel element
354     5 -1.51304  30 -31 32 -33      -420 u=1
355     2 -3.979996 30 -31 32 -33 420 -425 u=-1
356     0           30 -31 32 -33 425 -430 u=-1
357     5 -0.270112 30 -31 32 -33 430 -440 u=-1
358     5 -0.689740 30 -31 32 -33 440 -445 u=-1
359     5 -1.393935 30 -31 32 -33 445 -450 u=-1
360     5 -0.261853 30 -31 32 -33 450 -670 u=-1
361     5 -0.261853 30 -31 32 -33 670 -455 u=-1
362     0           30 -31 32 -33 455  u=1
363     0           -30            460 u=1
364     0            31            460 u=1
365     0         30 -31 -32       460 u=1
366     0         30 -31  33       460 u=1
c
c     universe 2
c
c       egg crate
401     0           -30            -400 u=2
402     0            31            -400 u=2
403     0         30 -31 -32       -400 u=2
404     0         30 -31  33       -400 u=2
405     5 -7.92          28     400 -420 u=2
406     5 -7.92             -23 400 -420 u=2
407     5 -7.92     -15 23 -28 400 -420 u=2
408     5 -7.92  20     23 -28 400 -420 u=2
409     5 -7.92          28     420 -430 u=2
410     5 -7.92             -23 420 -430 u=2
411     5 -7.92     -15 23 -28 420 -430 u=2
412     5 -7.92  20     23 -28 420 -430 u=2
413     5 -7.92          28     430 -440 u=2
414     5 -7.92             -23 430 -440 u=2
415     5 -7.92     -15 23 -28 430 -440 u=2
416     5 -7.92  20     23 -28 430 -440 u=2
417     5 -7.92          28     440 -670 u=2
418     5 -7.92             -23 440 -670 u=2
419     5 -7.92     -15 23 -28 440 -670 u=2
420     5 -7.92  20     23 -28 440 -670 u=2
421     5 -7.92          28     670 -460 u=2
422     5 -7.92             -23 670 -460 u=2
423     5 -7.92     -15 23 -28 670 -460 u=2
424     5 -7.92  20     23 -28 670 -460 u=2
c       boral and inside of egg crate and outside of fuel
426     0         15 -30 23 -28 400 -460 u=-2
427     0         31 -20 23 -28 400 -460 u=-2
428     0         30 -31 33 -28 400 -460 u=-2
429     0         30 -31 23 -32 400 -460 u=-2
c       fuel element
454     5 -1.51304  30 -31 32 -33      -420 u=2
455     2 -3.979996 30 -31 32 -33 420 -425 u=-2
456     0           30 -31 32 -33 425 -430 u=-2
457     5 -0.270112 30 -31 32 -33 430 -440 u=-2
458     5 -0.689740 30 -31 32 -33 440 -445 u=-2
459     5 -1.393935 30 -31 32 -33 445 -450 u=-2
460     5 -0.261853 30 -31 32 -33 450 -670 u=-2
461     5 -0.261853 30 -31 32 -33 670 -455 u=-2
462     0           30 -31 32 -33 455  u=2
463     0           -30            460 u=2
464     0            31            460 u=2
465     0         30 -31 -32       460 u=2
466     0         30 -31  33       460 u=2
c
c     universe 3
```

```
c
c       egg crate
501     0             -30             -400 u=3
502     0              31             -400 u=3
503     0         30 -31 -32          -400 u=3
504     0         30 -31  33          -400 u=3
505     5 -7.92           28      400 -420 u=3
506     5 -7.92              -23 400 -420 u=3
507     5 -7.92       -15 23 -28 400 -420 u=3
508     5 -7.92  20       23 -28 400 -420 u=3
509     5 -7.92           28      420 -430 u=3
510     5 -7.92              -23 420 -430 u=3
511     5 -7.92       -15 23 -28 420 -430 u=3
512     5 -7.92  20       23 -28 420 -430 u=3
513     5 -7.92           28      430 -440 u=3
514     5 -7.92              -23 430 -440 u=3
515     5 -7.92       -15 23 -28 430 -440 u=3
516     5 -7.92  20       23 -28 430 -440 u=3
517     5 -7.92           28      440 -670 u=3
518     5 -7.92              -23 440 -670 u=3
519     5 -7.92       -15 23 -28 440 -670 u=3
520     5 -7.92  20       23 -28 440 -670 u=3
521     5 -7.92           28      670 -460 u=3
522     5 -7.92              -23 670 -460 u=3
523     5 -7.92       -15 23 -28 670 -460 u=3
524     5 -7.92  20       23 -28 670 -460 u=3
c       boral and inside of egg crate and outside of fuel
526     0         15 -30 23 -28 400 -410 u=-3
527     0         31 -20 23 -28 400 -410 u=-3
528     0         30 -31 33 -28 400 -410 u=-3
529     0         30 -31 23 -32 400 -410 u=-3
530     0         15 -18 26 -28 410 -435 u=-3
531     0         19 -20 26 -28 410 -435 u=-3
534     6 -2.644 18 -19 27 -28 410 -420 u=-3
535     5 -7.92  18 -19 26 -27 410 -420 u=-3
538     6 -2.644 18 -19 27 -28 420 -430 u=-3
539     5 -7.92  18 -19 26 -27 420 -430 u=-3
542     6 -2.644 18 -19 27 -28 430 -435 u=-3
543     5 -7.92  18 -19 26 -27 430 -435 u=-3
546     0         15 -30 23 -26 410 -435 u=-3
547     0         31 -20 23 -26 410 -435 u=-3
548     0         30 -31 23 -32 410 -435 u=-3
549     0         30 -31 33 -26 410 -435 u=-3
550     0         15 -30 23 -28 435 -460 u=-3
551     0         31 -20 23 -28 435 -460 u=-3
552     0         30 -31 33 -28 435 -460 u=-3
553     0         30 -31 23 -32 435 -460 u=-3
c       fuel element
554     5 -1.51304  30 -31 32 -33      -420 u=3
555     2 -3.979996 30 -31 32 -33 420 -425 u=-3
556     0           30 -31 32 -33 425 -430 u=-3
557     5 -0.270112 30 -31 32 -33 430 -440 u=-3
558     5 -0.689740 30 -31 32 -33 440 -445 u=-3
559     5 -1.393935 30 -31 32 -33 445 -450 u=-3
560     5 -0.261853 30 -31 32 -33 450 -670 u=-3
561     5 -0.261853 30 -31 32 -33 670 -455 u=-3
562     0           30 -31 32 -33 455  u=3
563     0           -30             460 u=3
564     0            31             460 u=3
565     0         30 -31 -32         460 u=3
566     0         30 -31  33         460 u=3
c
c      universe 4
c
c       egg crate
601     0             -30             -400 u=4
602     0              31             -400 u=4
603     0         30 -31 -32          -400 u=4
604     0         30 -31  33          -400 u=4
```

```
605     5 -7.92          28      400 -420 u=4
606     5 -7.92             -23 400 -420 u=4
607     5 -7.92      -15 23 -28 400 -420 u=4
608     5 -7.92  20      23 -28 400 -420 u=4
609     5 -7.92          28      420 -430 u=4
610     5 -7.92             -23 420 -430 u=4
611     5 -7.92      -15 23 -28 420 -430 u=4
612     5 -7.92  20      23 -28 420 -430 u=4
613     5 -7.92          28      430 -440 u=4
614     5 -7.92             -23 430 -440 u=4
615     5 -7.92      -15 23 -28 430 -440 u=4
616     5 -7.92  20      23 -28 430 -440 u=4
617     5 -7.92          28      440 -670 u=4
618     5 -7.92             -23 440 -670 u=4
619     5 -7.92      -15 23 -28 440 -670 u=4
620     5 -7.92  20      23 -28 440 -670 u=4
621     5 -7.92          28      670 -460 u=4
622     5 -7.92             -23 670 -460 u=4
623     5 -7.92      -15 23 -28 670 -460 u=4
624     5 -7.92  20      23 -28 670 -460 u=4
c       boral and inside of egg crate and outside of fuel
626     0         15 -30 23 -28 400 -410 u=-4
627     0         31 -20 23 -28 400 -410 u=-4
628     0         30 -31 33 -28 400 -410 u=-4
629     0         30 -31 23 -32 400 -410 u=-4
632     0         15 -17 23 -24 410 -435 u=-4
633     0         15 -17 25 -28 410 -435 u=-4
636     6 -2.644 15 -16 24 -25 410 -420 u=-4
637     5 -7.92  16 -17 24 -25 410 -420 u=-4
640     6 -2.644 15 -16 24 -25 420 -430 u=-4
641     5 -7.92  16 -17 24 -25 420 -430 u=-4
644     6 -2.644 15 -16 24 -25 430 -435 u=-4
645     5 -7.92  16 -17 24 -25 430 -435 u=-4
646     0         17 -30 23 -28 410 -435 u=-4
647     0         31 -20 23 -28 410 -435 u=-4
648     0         30 -31 23 -32 410 -435 u=-4
649     0         30 -31 33 -28 410 -435 u=-4
650     0         15 -30 23 -28 435 -460 u=-4
651     0         31 -20 23 -28 435 -460 u=-4
652     0         30 -31 33 -28 435 -460 u=-4
653     0         30 -31 23 -32 435 -460 u=-4
c       fuel element
654     5 -1.51304  30 -31 32 -33      -420 u=4
655     2 -3.979996 30 -31 32 -33 420 -425 u=-4
656     0           30 -31 32 -33 425 -430 u=-4
657     5 -0.270112 30 -31 32 -33 430 -440 u=-4
658     5 -0.689740 30 -31 32 -33 440 -445 u=-4
659     5 -1.393935 30 -31 32 -33 445 -450 u=-4
660     5 -0.261853 30 -31 32 -33 450 -670 u=-4
661     5 -0.261853 30 -31 32 -33 670 -455 u=-4
662     0           30 -31 32 -33 455  u=4
663     0           -30             460 u=4
664     0            31             460 u=4
665     0         30 -31 -32        460 u=4
666     0         30 -31  33        460 u=4
c
c     universe 5
c
701     0              -400 u=5
702     5 -7.92 20 400 -420 u=5
703     5 -7.92 20 420 -430 u=5
704     5 -7.92 20 430 -440 u=5
705     5 -7.92 20 440 -670 u=5
706     5 -7.92 20 670 -460 u=5
707     0      -20 400 -460 u=5
708     0          460      u=5
c
c     universe 6
c
```

```
710    0                    -400 u=6
711    5 -7.92  -23 400 -420 u=6
712    5 -7.92  -23 420 -430 u=6
713    5 -7.92  -23 430 -440 u=6
714    5 -7.92  -23 440 -670 u=6
715    5 -7.92  -23 670 -460 u=6
716    0         23 400 -460 u=6
717    0            460      u=6
c
c     universe 7
c
720    0                        -400 u=7
721    5 -7.92 20       23 400 -420 u=7
722    5 -7.92    -23       400 -420 u=7
723    5 -7.92 20       23 420 -430 u=7
724    5 -7.92    -23       420 -430 u=7
725    5 -7.92 20       23 430 -440 u=7
726    5 -7.92    -23       430 -440 u=7
727    5 -7.92 20       23 440 -670 u=7
728    5 -7.92    -23       440 -670 u=7
729    5 -7.92 20       23 670 -460 u=7
730    5 -7.92    -23       670 -460 u=7
731    0          -20  23 400 -460 u=7
732    0               460      u=7
c
c     universe 8
c
735    0                           -400 u=8
736    0        15             400 -460 u=8
747    5 -7.92     -15         400 -420 u=8
748    5 -7.92     -15         420 -430 u=8
749    5 -7.92     -15         430 -440 u=8
750    5 -7.92     -15         440 -670 u=8
751    5 -7.92     -15         670 -460 u=8
752    0                       460      u=8
c
c     universe 9
c
755    0        15     23      400 -460 u=9
766    0                           -400 u=9
767    5 -7.92     -15 23      400 -420 u=9
768    5 -7.92     -23         400 -420 u=9
769    5 -7.92     -15 23      420 -430 u=9
770    5 -7.92     -23         420 -430 u=9
771    5 -7.92     -15 23      430 -440 u=9
772    5 -7.92     -23         430 -440 u=9
773    5 -7.92     -15 23      440 -670 u=9
774    5 -7.92     -23         440 -670 u=9
775    5 -7.92     -15 23      670 -460 u=9
776    5 -7.92     -23         670 -460 u=9
777    0                       460      u=9
c
c     universe 10
c
780    0        15         -28 400 -460 u=10
799    0                           -400 u=10
800    5 -7.92     -15     -28 400 -420 u=10
801    5 -7.92         28      400 -420 u=10
802    5 -7.92     -15     -28 420 -430 u=10
803    5 -7.92         28      420 -430 u=10
804    5 -7.92     -15     -28 430 -440 u=10
805    5 -7.92         28      430 -440 u=10
806    5 -7.92     -15     -28 440 -670 u=10
807    5 -7.92         28      440 -670 u=10
808    5 -7.92     -15     -28 670 -460 u=10
809    5 -7.92         28      670 -460 u=10
810    0                       460      u=10
c
c     universe 11
```

```
c
811   0                    -28 400 -460 u=11
822   0                        -400 u=11
823   5 -7.92          28      400 -420 u=11
824   5 -7.92          28      420 -430 u=11
825   5 -7.92          28      430 -440 u=11
826   5 -7.92          28      440 -670 u=11
827   5 -7.92          28      670 -460 u=11
828   0                        460      u=11
c
c     universe 12
c
830   0           -20    -28 400 -460 u=12
841   0                        -400 u=12
842   5 -7.92     -20 28      400 -420 u=12
843   5 -7.92  20             400 -420 u=12
844   5 -7.92     -20 28      420 -430 u=12
845   5 -7.92  20             420 -430 u=12
846   5 -7.92     -20 28      430 -440 u=12
847   5 -7.92  20             430 -440 u=12
848   5 -7.92     -20 28      440 -670 u=12
849   5 -7.92  20             440 -670 u=12
850   5 -7.92     -20 28      670 -460 u=12
851   5 -7.92  20             670 -460 u=12
852   0                       460      u=12
c
c     universe 13
c
c     810   0          -420  u=13
c     811   0    420   -430  u=13
c     812   0    430   -440  u=13
c     813   0    440   -670  u=13
c     814   0    670         u=13
c     storage locations
c
201   0  -301  -106 212 620 -675
202   0  -301  106 -107 212 620 -675
         fill=6 (-8.2423 90.6653 0.0)
203   0  -301  107 -108 212 620 -675
         fill=6 ( 8.2423 90.6653 0.0)
204   0  -301  108 212 620 -675
c
205   0  -301 -104 211 620 -675
206   0  -301 104 -105 211 620 -675
         fill=6 (-41.2115 74.1807 0.0)
207   0  -301 105 -106 211 -212 620 -675
         fill=7 (-24.7269 74.1807 0.0)
c
101   0  106 -107 211 -212  620 -675
         fill=2 (-8.2423 74.1807 0.0)
102   0  107 -108 211 -212  620 -675
         fill=4 ( 8.2423 74.1807 0.0)
c
208   0  -301 108 -109 211 -212 620 -675
         fill=9 (24.7269 74.1807 0.0)
209   0  -301 109 -110 211 620 -675
         fill=6 (41.2115 74.1807 0.0)
210   0  -301 110 211 620 -675
c
211   0  -301 -103 210 620 -675
212   0  -301 103 -104 210 -211 620 -675
         fill=7 (-57.6961 57.6961 0.0)
c
103   0  104 -105 210 -211  620 -675
         fill=2 (-41.2115 57.6961 0.0)
104   0  105 -106 210 -211  620 -675
         fill=4 (-24.7269 57.6961 0.0)
105   0  106 -107 210 -211  620 -675
         fill=1 (-8.2423 57.6961 0.0)
```

```
106    0   107 -108 210 -211  620 -675
           fill=1 ( 8.2423 57.6961 0.0)
107    0   108 -109 210 -211  620 -675
           fill=4 ( 24.7269 57.6961 0.0)
108    0   109 -110 210 -211  620 -675
           fill=4 ( 41.2115 57.6961 0.0)
c
213    0   -301 110 -111 210 -211 620 -675
           fill=9 ( 57.6961 57.6961 0.0)
214    0   -301 111 210 620 -675
c
215    0   -301 -103 209 -210 620 -675
           fill=5 (-74.1807 41.2115 0.0)
c
109    0   103 -104 209 -210  620 -675
           fill=2 (-57.6961 41.2115 0.0)
110    0   104 -105 209 -210  620 -675
           fill=1 (-41.2115 41.2115 0.0)
111    0   105 -106 209 -210  620 -675
           fill=1 (-24.7269 41.2115 0.0)
112    0   106 -107 209 -210  620 -675
           fill=1 (-8.2423 41.2115 0.0)
113    0   107 -108 209 -210  620 -675
           fill=1 ( 8.2423 41.2115 0.0)
114    0   108 -109 209 -210  620 -675
           fill=1 ( 24.7269 41.2115 0.0)
115    0   109 -110 209 -210  620 -675
           fill=1 ( 41.2115 41.2115 0.0)
116    0   110 -111 209 -210  620 -675
           fill=4 ( 57.6961 41.2115 0.0)
c
216    0   -301 111 209 -210 620 -675
           fill=8 (74.1807 41.2115 0.0)
c
217    0   -301 -102 208 620 -675
218    0   -301 102 -103 208 -209 620 -675
           fill=7 (-74.1807 24.7269 0.0)
c
117    0   103 -104 208 -209  620 -675
           fill=3 (-57.6961 24.7269 0.0)
118    0   104 -105 208 -209  620 -675
           fill=1 (-41.2115 24.7269 0.0)
119    0   105 -106 208 -209  620 -675
           fill=1 (-24.7269 24.7269 0.0)
120    0   106 -107 208 -209  620 -675
           fill=1 (-8.2423 24.7269 0.0)
121    0   107 -108 208 -209  620 -675
           fill=1 ( 8.2423 24.7269 0.0)
122    0   108 -109 208 -209  620 -675
           fill=1 ( 24.7269 24.7269 0.0)
123    0   109 -110 208 -209  620 -675
           fill=1 ( 41.2115 24.7269 0.0)
124    0   110 -111 208 -209  620 -675
           fill=1 ( 57.6961 24.7269 0.0)
c
219    0   -301 111 -112 208 -209 620 -675
           fill=9 (74.1807 24.7269 0.0)
220    0   -301 112 208 620 -675
c
221    0   -301 -102 207 -208 620 -675
           fill=5 (-90.6653 8.2423 0.0)
c
125    0   102 -103 207 -208  620 -675
           fill=2 (-74.1807 8.2423 0.0)
126    0   103 -104 207 -208  620 -675
           fill=1 (-57.6961 8.2423 0.0)
127    0   104 -105 207 -208  620 -675
           fill=1 (-41.2115 8.2423 0.0)
128    0   105 -106 207 -208  620 -675
```

```
          fill=1 (-24.7269 8.2423 0.0)
129   0   106 -107 207 -208  620 -675
          fill=1 (-8.2423 8.2423 0.0)
130   0   107 -108 207 -208  620 -675
          fill=1 ( 8.2423 8.2423 0.0)
131   0   108 -109 207 -208  620 -675
          fill=1 ( 24.7269 8.2423 0.0)
132   0   109 -110 207 -208  620 -675
          fill=1 ( 41.2115 8.2423 0.0)
133   0   110 -111 207 -208  620 -675
          fill=1 ( 57.6961 8.2423 0.0)
134   0   111 -112 207 -208  620 -675
          fill=4 ( 74.1807 8.2423 0.0)
c
222   0   -301 112 207 -208 620 -675
          fill=8 (90.6653 8.2423 0.0)
c
223   0   -301 -102 206 -207 620 -675
          fill=5 (-90.6653 -8.2423 0.0)
c
135   0   102 -103 206 -207  620 -675
          fill=3 (-74.1807 -8.2423 0.0)
136   0   103 -104 206 -207  620 -675
          fill=1 (-57.6961 -8.2423 0.0)
137   0   104 -105 206 -207  620 -675
          fill=1 (-41.2115 -8.2423 0.0)
138   0   105 -106 206 -207  620 -675
          fill=1 (-24.7269 -8.2423 0.0)
139   0   106 -107 206 -207  620 -675
          fill=1 (-8.2423 -8.2423 0.0)
140   0   107 -108 206 -207  620 -675
          fill=1 ( 8.2423 -8.2423 0.0)
141   0   108 -109 206 -207  620 -675
          fill=1 ( 24.7269 -8.2423 0.0)
142   0   109 -110 206 -207  620 -675
          fill=1 ( 41.2115 -8.2423 0.0)
143   0   110 -111 206 -207  620 -675
          fill=1 ( 57.6961 -8.2423 0.0)
144   0   111 -112 206 -207  620 -675
          fill=1 ( 74.1807 -8.2423 0.0)
c
224   0   -301 112 206 -207 620 -675
          fill=8 (90.6653 -8.2423 0.0)
c
225   0   -301 -102 -206 620 -675
226   0   -301 102 -103 205 -206 620 -675
          fill=12 (-74.1807 -24.7269 0.0)
c
145   0   103 -104 205 -206  620 -675
          fill=3 (-57.6961 -24.7269 0.0)
146   0   104 -105 205 -206  620 -675
          fill=1 (-41.2115 -24.7269 0.0)
147   0   105 -106 205 -206  620 -675
          fill=1 (-24.7269 -24.7269 0.0)
148   0   106 -107 205 -206  620 -675
          fill=1 (-8.2423  -24.7269 0.0)
149   0   107 -108 205 -206  620 -675
          fill=1 ( 8.2423  -24.7269 0.0)
150   0   108 -109 205 -206  620 -675
          fill=1 ( 24.7269 -24.7269 0.0)
151   0   109 -110 205 -206  620 -675
          fill=1 ( 41.2115 -24.7269 0.0)
152   0   110 -111 205 -206  620 -675
          fill=1 ( 57.6961 -24.7269 0.0)
c
227   0   -301 111 -112 205 -206 620 -675
          fill=10 (74.1807 -24.7269 0.0)
228   0   -301 112 -206 620 -675
c
```

```
229    0  -301 -103 204 -205 620 -675
          fill=5 (-74.1807 -41.2115 0.0)
c
153    0  103 -104 204 -205  620 -675
          fill=3 (-57.6961 -41.2115 0.0)
154    0  104 -105 204 -205  620 -675
          fill=1 (-41.2115 -41.2115 0.0)
155    0  105 -106 204 -205  620 -675
          fill=1 (-24.7269 -41.2115 0.0)
156    0  106 -107 204 -205  620 -675
          fill=1 (-8.2423  -41.2115 0.0)
157    0  107 -108 204 -205  620 -675
          fill=1 ( 8.2423  -41.2115 0.0)
158    0  108 -109 204 -205  620 -675
          fill=1 ( 24.7269 -41.2115 0.0)
159    0  109 -110 204 -205  620 -675
          fill=1 ( 41.2115 -41.2115 0.0)
160    0  110 -111 204 -205  620 -675
          fill=1 ( 57.6961 -41.2115 0.0)
c
230    0  -301 111 204 -205 620 -675
          fill=8 (74.1807 -41.2115 0.0)
c
231    0  -301 -103 -204 620 -675
232    0  -301 103 -104 203 -204 620 -675
          fill=12 (-57.6961 -57.6961 0.0)
c
161    0  104 -105 203 -204  620 -675
          fill=3 (-41.2115 -57.6961 0.0)
162    0  105 -106 203 -204  620 -675
          fill=1 (-24.7269 -57.6961 0.0)
163    0  106 -107 203 -204  620 -675
          fill=1 (-8.2423 -57.6961 0.0)
164    0  107 -108 203 -204  620 -675
          fill=1 ( 8.2423 -57.6961 0.0)
165    0  108 -109 203 -204  620 -675
          fill=1 ( 24.7269 -57.6961 0.0)
166    0  109 -110 203 -204  620 -675
          fill=1 ( 41.2115 -57.6961 0.0)
c
233    0  -301 110 -111 203 -204 620 -675
          fill=10 ( 57.6961 -57.6961 0.0)
234    0  -301 111 -204 620 -675
c
235    0  -301 -104 -203 620 -675
236    0  -301 104 -105 -203 620 -675
          fill=11 (-41.2115 -74.1807 0.0)
237    0  -301 105 -106 202 -203 620 -675
          fill=12 (-24.7269 -74.1807 0.0)
c
167    0  106 -107 202 -203  620 -675
          fill=3 (-8.2423 -74.1807 0.0)
168    0  107 -108 202 -203  620 -675
          fill=1 ( 8.2423 -74.1807 0.0)
c
238    0  -301 108 -109 202 -203 620 -675
          fill=10 (24.7269 -74.1807 0.0)
239    0  -301 109 -110 -203 620 -675
          fill=11 (41.2115 -74.1807 0.0)
240    0  -301 110 -203 620 -675
c
241    0  -301  -106 -202 620 -675
242    0  -301  106 -107 -202 620 -675
          fill=11 (-8.2423 -90.6653 0.0)
243    0  -301  107 -108 -202 620 -675
          fill=11 ( 8.2423 -90.6653 0.0)
244    0  -301  108 -202 620 -675
c
1821   5 -7.92 301 -302 610 -615  $ MPC shell
```

```
1822   0        302 -501 610 -615  $ Air gap
1823   5 -7.92  301 -302 615 -630  $ MPC shell
1824   0        302 -501 615 -630  $ Air gap
1825   5 -7.92  301 -302 630 -420  $ MPC shell
1826   0        302 -501 630 -420  $ Air gap
1827   5 -7.92  301 -302 420 -430  $ MPC shell
1828   0        302 -501 420 -430  $ Air gap
1829   5 -7.92  301 -302 430 -440  $ MPC shell
1830   0        302 -501 430 -440  $ Air gap
1831   5 -7.92  301 -302 440 -670  $ MPC shell
1832   0        302 -501 440 -670  $ Air gap
1833   5 -7.92  301 -302 670 -675  $ MPC shell
1834   0        302 -501 670 -675  $ Air gap
1835   5 -7.92  301 -302 675 -651  $ MPC shell
1836   0        302 -501 675 -651  $ Air gap
1837   5 -7.92  301 -302 651 -652  $ MPC shell
1838   0        302 -501 651 -652  $ Air gap
1839   5 -7.92  301 -302 652 -653  $ MPC shell
1840   0        302 -501 652 -653  $ Air gap
1841   5 -7.92  301 -302 653 -654  $ MPC shell
1842   0        302 -501 653 -654  $ Air gap
1843   5 -7.92  301 -302 654 -655  $ MPC shell
1844   0        302 -501 654 -655  $ Air gap
1845   5 -7.92  301 -302 655 -656  $ MPC shell
1846   0        302 -501 655 -656  $ Air gap
1847   5 -7.92  301 -302 656 -657  $ MPC shell
1848   0        302 -501 656 -657  $ Air gap
1849   5 -7.92  301 -302 657 -680  $ MPC shell
1850   0        301 -302 680 -685  $ Air gap
1851   0        302 -501 657 -685  $ Air gap
c
1854   5 -7.92      -301 610 -615  $ MPC baseplate
1855   5 -7.92      -301 615 -620  $ MPC baseplate
1860   5 -7.92      -301 675 -651  $ MPC lid (both)
1861   5 -7.92      -301 651 -652  $ MPC lid (both)
1862   5 -7.92      -301 652 -653  $ MPC lid (both)
1863   5 -7.92      -301 653 -654  $ MPC lid (both)
1864   5 -7.92      -301 654 -655  $ MPC lid (both)
1865   5 -7.92      -301 655 -656  $ MPC lid (both)
1866   5 -7.92      -301 656 -657  $ MPC lid (both)
1867   5 -7.92      -301 657 -680  $ MPC lid (both)
1868   0            -301 680 -685  $ Air gap
c     OVERPACK \/ \/ \/ \/ \/
c
1001  8 -7.82 501 -508 630 -420 $ steel shell
1002  8 -7.82 501 -508 420 -430 $ steel shell
1003  8 -7.82 501 -508 430 -440 $ steel shell
1004  8 -7.82 501 -508 440 -670 $ steel shell
1005  0       508 -512 630 -420  fill=20
1006  0       508 -512 420 -430  fill=20
1007  0       508 -512 430 -440  fill=20
1008  0       508 -512 440 -670  fill=20
1009  8 -7.82 512 -513 630 -420 $ outer steel shell
1010  8 -7.82 512 -513 420 -430 $ outer steel shell
1011  8 -7.82 512 -513 430 -440 $ outer steel shell
1012  8 -7.82 512 -513 440 -670 $ outer steel shell
c     1012  8 -7.82  512 -513 640 -670             $ outer steel shell
c     1013  0        512 -513 630 -640  1103 -1102 $ air in pocket trun.
c     1014  0        512 -513 630 -640  2103 -2102 $ air in pocket trun.
c     1015  8 -7.82  512 -513 630 -640  1102  2102 $ outer steel shell
c     1016  8 -7.82  512 -513 630 -640  1102 -2103 $ outer steel shell
c     1017  8 -7.82  512 -513 630 -640 -1103 -2103 $ outer steel shell
c     1018  8 -7.82  512 -513 630 -640 -1103  2102 $ outer steel shell
c
c      steel spines and holtite
10101   8 -7.82   2000 -2002  645 -660   1000  u=20 $ steel spine
10102   7 -1.61   2002 -2011  645 -660   2000  u=20 $ holtite
10103   8 -7.82   2011 -2012  645 -660   2000  u=20 $ steel spine
10104   7 -1.61   2012 -2021  645 -660   2000  u=20 $ holtite
```

```
10105   8 -7.82   2021 -2022  645 -660   2000  u=20 $ steel spine
10106   7 -1.61   2022 -2031  645 -660   2000  u=20 $ holtite
10107   8 -7.82   2031 -2032  645 -660   2000  u=20 $ steel spine
10108   7 -1.61   2032 -2041  645 -660   2000  u=20 $ holtite
10109   8 -7.82   2041 -2042  645 -660   2000  u=20 $ steel spine
10110   7 -1.61   2042 -2051  645 -660   2000  u=20 $ holtite
10111   8 -7.82   2051 -2052  645 -660   2000  u=20 $ steel spine
10112   7 -1.61   2052 -2061  645 -660   2000  u=20 $ holtite
10113   8 -7.82   2061 -2062  645 -660   2000  u=20 $ steel spine
10114   7 -1.61   2062 -2071  645 -660   2000  u=20 $ holtite
10115   8 -7.82   2071 -2072  645 -660   2000  u=20 $ steel spine
10116   7 -1.61   2072 -2081  645 -660   2000  u=20 $ holtite
10117   8 -7.82   2081 -2082  645 -660   2000  u=20 $ steel spine
10118   7 -1.61   2082 -2091  645 -660   2000  u=20 $ holtite
10119   8 -7.82   2091 -2092  645 -660   2000  u=20 $ steel spine
10120   7 -1.61   2092  1002  645 -660   2000  u=20 $ holtite
10121   8 -7.82   1000 -1002  645 -660   2000  u=20 $ steel spine
c
10122   8 -7.82   1001 -1000  645 -660   2000  u=20 $ steel spine
10123   7 -1.61   1012 -1001  645 -660   2000  u=20 $ holtite
10124   8 -7.82   1011 -1012  645 -660   2000  u=20 $ steel spine
10125   7 -1.61   1022 -1011  645 -660   2000  u=20 $ holtite
10126   8 -7.82   1021 -1022  645 -660   2000  u=20 $ steel spine
10127   7 -1.61   1032 -1021  645 -660   2000  u=20 $ holtite
10128   8 -7.82   1031 -1032  645 -660   2000  u=20 $ steel spine
10129   7 -1.61   1042 -1031  645 -660   2000  u=20 $ holtite
10130   8 -7.82   1041 -1042  645 -660   2000  u=20 $ steel spine
10131   7 -1.61   1052 -1041  645 -660   2000  u=20 $ holtite
10132   8 -7.82   1051 -1052  645 -660   2000  u=20 $ steel spine
10133   7 -1.61   1062 -1051  645 -660   2000  u=20 $ holtite
10134   8 -7.82   1061 -1062  645 -660   2000  u=20 $ steel spine
10135   7 -1.61   1072 -1061  645 -660   2000  u=20 $ holtite
10136   8 -7.82   1071 -1072  645 -660   2000  u=20 $ steel spine
10137   7 -1.61   1082 -1071  645 -660   2000  u=20 $ holtite
10138   8 -7.82   1081 -1082  645 -660   2000  u=20 $ steel spine
10139   7 -1.61   1092 -1081  645 -660   2000  u=20 $ holtite
10140   8 -7.82   1091 -1092  645 -660   2000  u=20 $ steel spine
10141   7 -1.61   2002 -1091  645 -660   2000  u=20 $ holtite
10142   8 -7.82   2000 -2002  645 -660  -1000  u=20 $ steel spine
c
10143   8 -7.82   2001 -2000  645 -660  -1000  u=20 $ steel spine
10144   7 -1.61   2012 -2001  645 -660  -2000  u=20 $ holtite
10145   8 -7.82   2011 -2012  645 -660  -2000  u=20 $ steel spine
10146   7 -1.61   2022 -2011  645 -660  -2000  u=20 $ holtite
10147   8 -7.82   2021 -2022  645 -660  -2000  u=20 $ steel spine
10148   7 -1.61   2032 -2021  645 -660  -2000  u=20 $ holtite
10149   8 -7.82   2031 -2032  645 -660  -2000  u=20 $ steel spine
10150   7 -1.61   2042 -2031  645 -660  -2000  u=20 $ holtite
10151   8 -7.82   2041 -2042  645 -660  -2000  u=20 $ steel spine
10152   7 -1.61   2052 -2041  645 -660  -2000  u=20 $ holtite
10153   8 -7.82   2051 -2052  645 -660  -2000  u=20 $ steel spine
10154   7 -1.61   2062 -2051  645 -660  -2000  u=20 $ holtite
10155   8 -7.82   2061 -2062  645 -660  -2000  u=20 $ steel spine
10156   7 -1.61   2072 -2061  645 -660  -2000  u=20 $ holtite
10157   8 -7.82   2071 -2072  645 -660  -2000  u=20 $ steel spine
10158   7 -1.61   2082 -2071  645 -660  -2000  u=20 $ holtite
10159   8 -7.82   2081 -2082  645 -660  -2000  u=20 $ steel spine
10160   7 -1.61   2092 -2081  645 -660  -2000  u=20 $ holtite
10161   8 -7.82   2091 -2092  645 -660  -2000  u=20 $ steel spine
10162   7 -1.61  -1001 -2091  645 -660  -2000  u=20 $ holtite
10163   8 -7.82   1001 -1000  645 -660  -2000  u=20 $ steel spine
c
10164   8 -7.82   1000 -1002  645 -660  -2000  u=20 $ steel spine
10165   7 -1.61   1002 -1011  645 -660  -2000  u=20 $ holtite
10166   8 -7.82   1011 -1012  645 -660  -2000  u=20 $ steel spine
10167   7 -1.61   1012 -1021  645 -660  -2000  u=20 $ holtite
10168   8 -7.82   1021 -1022  645 -660  -2000  u=20 $ steel spine
10169   7 -1.61   1022 -1031  645 -660  -2000  u=20 $ holtite
10170   8 -7.82   1031 -1032  645 -660  -2000  u=20 $ steel spine
```

```
10171    7 -1.61    1032 -1041   645 -660   -2000   u=20 $ holtite
10172    8 -7.82    1041 -1042   645 -660   -2000   u=20 $ steel spine
10173    7 -1.61    1042 -1051   645 -660   -2000   u=20 $ holtite
10174    8 -7.82    1051 -1052   645 -660   -2000   u=20 $ steel spine
10175    7 -1.61    1052 -1061   645 -660   -2000   u=20 $ holtite
10176    8 -7.82    1061 -1062   645 -660   -2000   u=20 $ steel spine
10177    7 -1.61    1062 -1071   645 -660   -2000   u=20 $ holtite
10178    8 -7.82    1071 -1072   645 -660   -2000   u=20 $ steel spine
10179    7 -1.61    1072 -1081   645 -660   -2000   u=20 $ holtite
10180    8 -7.82    1081 -1082   645 -660   -2000   u=20 $ steel spine
10181    7 -1.61    1082 -1091   645 -660   -2000   u=20 $ holtite
10182    8 -7.82    1091 -1092   645 -660   -2000   u=20 $ steel spine
10183    7 -1.61    1092 -2001   645 -660   -2000   u=20 $ holtite
10184    8 -7.82    2001 -2000   645 -660    1000   u=20 $ steel spine
c
c    10201    8 -7.82    2000 -2002   635 -645    1000   u=20 $ steel spine
c    10202    7 -1.61    2002 -2011   635 -645    2000   u=20 $ holtite
10202    7 -1.61    2101 -2011   635 -645    2000   u=20 $ holtite
10203    8 -7.82    2011 -2012   635 -645    2000   u=20 $ steel spine
10204    7 -1.61    2012 -2021   635 -645    2000   u=20 $ holtite
10205    8 -7.82    2021 -2022   635 -645    2000   u=20 $ steel spine
10206    7 -1.61    2022 -2031   635 -645    2000   u=20 $ holtite
10207    8 -7.82    2031 -2032   635 -645    2000   u=20 $ steel spine
10208    7 -1.61    2032 -2041   635 -645    2000   u=20 $ holtite
10209    8 -7.82    2041 -2042   635 -645    2000   u=20 $ steel spine
10210    7 -1.61    2042 -2051   635 -645    2000   u=20 $ holtite
10211    8 -7.82    2051 -2052   635 -645    2000   u=20 $ steel spine
10212    7 -1.61    2052 -2061   635 -645    2000   u=20 $ holtite
10213    8 -7.82    2061 -2062   635 -645    2000   u=20 $ steel spine
10214    7 -1.61    2062 -2071   635 -645    2000   u=20 $ holtite
10215    8 -7.82    2071 -2072   635 -645    2000   u=20 $ steel spine
10216    7 -1.61    2072 -2081   635 -645    2000   u=20 $ holtite
10217    8 -7.82    2081 -2082   635 -645    2000   u=20 $ steel spine
10218    7 -1.61    2082 -2091   635 -645    2000   u=20 $ holtite
10219    8 -7.82    2091 -2092   635 -645    2000   u=20 $ steel spine
c    10220    7 -1.61    2092  1101   635 -645    2000   u=20 $ holtite
10220    7 -1.61    2092  1002   635 -645    2000   u=20 $ holtite
10221    8 -7.82    1000 -1002   635 -645    2000   u=20 $ steel spine
c
10222    8 -7.82    1001 -1000   635 -645    2000   u=20 $ steel spine
10223    7 -1.61    1012 -1001   635 -645    2000   u=20 $ holtite
c    10223    7 -1.61    1012 -1104   635 -645    2000   u=20 $ holtite
10224    8 -7.82    1011 -1012   635 -645    2000   u=20 $ steel spine
10225    7 -1.61    1022 -1011   635 -645    2000   u=20 $ holtite
10226    8 -7.82    1021 -1022   635 -645    2000   u=20 $ steel spine
10227    7 -1.61    1032 -1021   635 -645    2000   u=20 $ holtite
10228    8 -7.82    1031 -1032   635 -645    2000   u=20 $ steel spine
10229    7 -1.61    1042 -1031   635 -645    2000   u=20 $ holtite
10230    8 -7.82    1041 -1042   635 -645    2000   u=20 $ steel spine
10231    7 -1.61    1052 -1041   635 -645    2000   u=20 $ holtite
10232    8 -7.82    1051 -1052   635 -645    2000   u=20 $ steel spine
10233    7 -1.61    1062 -1051   635 -645    2000   u=20 $ holtite
10234    8 -7.82    1061 -1062   635 -645    2000   u=20 $ steel spine
10235    7 -1.61    1072 -1061   635 -645    2000   u=20 $ holtite
10236    8 -7.82    1071 -1072   635 -645    2000   u=20 $ steel spine
10237    7 -1.61    1082 -1071   635 -645    2000   u=20 $ holtite
10238    8 -7.82    1081 -1082   635 -645    2000   u=20 $ steel spine
10239    7 -1.61    1092 -1081   635 -645    2000   u=20 $ holtite
10240    8 -7.82    1091 -1092   635 -645    2000   u=20 $ steel spine
10241    7 -1.61    2101 -1091   635 -645    2000   u=20 $ holtite
c    10241    7 -1.61    2002 -1091   635 -645    2000   u=20 $ holtite
c    10242    8 -7.82    2000 -2002   635 -645   -1000   u=20 $ steel spine
c
c    10243    8 -7.82    2001 -2000   635 -645   -1000   u=20 $ steel spine
c    10244    7 -1.61    2012 -2001   635 -645   -2000   u=20 $ holtite
10244    7 -1.61    2012 -2104   635 -645   -2000   u=20 $ holtite
10245    8 -7.82    2011 -2012   635 -645   -2000   u=20 $ steel spine
10246    7 -1.61    2022 -2011   635 -645   -2000   u=20 $ holtite
10247    8 -7.82    2021 -2022   635 -645   -2000   u=20 $ steel spine
```

```
10248   7 -1.61   2032 -2021  635 -645  -2000  u=20 $ holtite
10249   8 -7.82   2031 -2032  635 -645  -2000  u=20 $ steel spine
10250   7 -1.61   2042 -2031  635 -645  -2000  u=20 $ holtite
10251   8 -7.82   2041 -2042  635 -645  -2000  u=20 $ steel spine
10252   7 -1.61   2052 -2041  635 -645  -2000  u=20 $ holtite
10253   8 -7.82   2051 -2052  635 -645  -2000  u=20 $ steel spine
10254   7 -1.61   2062 -2051  635 -645  -2000  u=20 $ holtite
10255   8 -7.82   2061 -2062  635 -645  -2000  u=20 $ steel spine
10256   7 -1.61   2072 -2061  635 -645  -2000  u=20 $ holtite
10257   8 -7.82   2071 -2072  635 -645  -2000  u=20 $ steel spine
10258   7 -1.61   2082 -2071  635 -645  -2000  u=20 $ holtite
10259   8 -7.82   2081 -2082  635 -645  -2000  u=20 $ steel spine
10260   7 -1.61   2092 -2081  635 -645  -2000  u=20 $ holtite
10261   8 -7.82   2091 -2092  635 -645  -2000  u=20 $ steel spine
c    10262   7 -1.61  -1104 -2091  635 -645  -2000  u=20 $ holtite
10262   7 -1.61  -1001 -2091  635 -645  -2000  u=20 $ holtite
10263   8 -7.82   1001 -1000  635 -645  -2000  u=20 $ steel spine
c
10264   8 -7.82   1000 -1002  635 -645  -2000  u=20 $ steel spine
10265   7 -1.61   1002 -1011  635 -645  -2000  u=20 $ holtite
c    10265   7 -1.61   1101 -1011  635 -645  -2000  u=20 $ holtite
10266   8 -7.82   1011 -1012  635 -645  -2000  u=20 $ steel spine
10267   7 -1.61   1012 -1021  635 -645  -2000  u=20 $ holtite
10268   8 -7.82   1021 -1022  635 -645  -2000  u=20 $ steel spine
10269   7 -1.61   1022 -1031  635 -645  -2000  u=20 $ holtite
10270   8 -7.82   1031 -1032  635 -645  -2000  u=20 $ steel spine
10271   7 -1.61   1032 -1041  635 -645  -2000  u=20 $ holtite
10272   8 -7.82   1041 -1042  635 -645  -2000  u=20 $ steel spine
10273   7 -1.61   1042 -1051  635 -645  -2000  u=20 $ holtite
10274   8 -7.82   1051 -1052  635 -645  -2000  u=20 $ steel spine
10275   7 -1.61   1052 -1061  635 -645  -2000  u=20 $ holtite
10276   8 -7.82   1061 -1062  635 -645  -2000  u=20 $ steel spine
10277   7 -1.61   1062 -1071  635 -645  -2000  u=20 $ holtite
10278   8 -7.82   1071 -1072  635 -645  -2000  u=20 $ steel spine
10279   7 -1.61   1072 -1081  635 -645  -2000  u=20 $ holtite
10280   8 -7.82   1081 -1082  635 -645  -2000  u=20 $ steel spine
10281   7 -1.61   1082 -1091  635 -645  -2000  u=20 $ holtite
10282   8 -7.82   1091 -1092  635 -645  -2000  u=20 $ steel spine
10283   7 -1.61   1092 -2104  635 -645  -2000  u=20 $ holtite
c    10283   7 -1.61    1092 -2001  635 -645  -2000  u=20 $ holtite
c    10284   8 -7.82   2001 -2000  635 -645   1000  u=20 $ steel spine
c
11000   0         660 -665   u=20 $ foam
11001   8 -7.82   665        u=20 $ item 17 top
c    11002   8 -7.82   1101  2101  -635  u=20 $ item 17 bot
c    11003   8 -7.82  -2104  1101  -635  u=20 $ item 17 bot
c    11004   8 -7.82  -1104 -2104  -635  u=20 $ item 17 bot
c    11005   8 -7.82   2101 -1104  -635  u=20 $ item 17 bot
11002   8 -7.82         2101  -635  u=20 $ item 17 bot
11003   8 -7.82  -2104        -635  u=20 $ item 17 bot
c
c    pocket trunion
c
c    11101   8 -7.82  -514  1104 -1101 -640  u=20 $ pocket trunion before hole
c    11102   8 -7.82   514  1104 -1103 -640  u=20 $ steel on side of hole
c    11103   8 -7.82   514  1103 -1102 -640  u=20 $ hole
c    11104   8 -7.82   514  1102 -1101 -640  u=20 $ steel on side of hole
c    11105   8 -7.82        1104 -1101  640 -645  u=20 $ steel above hole
c
11111   8 -7.82  -514  2104 -2101 -640  u=20 $ pocket trunion before hole
11112   8 -7.82   514  2104 -2103 -640  u=20 $ steel on side of hole
11113   8 -7.82   514  2103 -2102 -640  u=20 $ hole
11114   8 -7.82   514  2102 -2101 -640  u=20 $ steel on side of hole
11115   8 -7.82        2104 -2101  640 -645  u=20 $ steel above hole
c
c     overpack base plate
c
2000  8 -7.82     -501 600 -601
2001  8 -7.82     -501 601 -602
```

```
2002  8 -7.82      -501 602 -603
2003  8 -7.82      -501 603 -604
2004  8 -7.82      -501 604 -610
c
2010  8 -7.82 501 -515 600 -601
2011  8 -7.82 501 -515 601 -602
2012  8 -7.82 501 -515 602 -603
2013  8 -7.82 501 -515 603 -604
2014  8 -7.82 501 -515 604 -610
2015  8 -7.82 501 -515 610 -615
2016  8 -7.82 501 -515 615 -630
2020  0    515 -513 600 -601
2021  0    515 -513 601 -602
2022  0    515 -513 602 -603
2023  0    515 -513 603 -604
2024  0    515 -513 604 -610
2025  0    515 -513 610 -615
2026  0    515 -513 615 -630
c
c     overpack lid
c
3000  8 -7.82      -506 685 -686
3001  8 -7.82      -506 686 -687
3002  8 -7.82      -506 687 -688
3003  8 -7.82      -506 688 -689
3004  8 -7.82      -506 689 -695
3010  0    506 -513 685 -686
3011  0    506 -513 686 -687
3012  0    506 -513 687 -688
3013  0    506 -513 688 -689
3014  0    506 -513 689 -695
c
3020  8 -7.82 501 -517 675 -676
3021  8 -7.82 501 -516 676 -651
3022  8 -7.82 501 -516 651 -652
3023  8 -7.82 501 -516 652 -653
3024  8 -7.82 501 -516 653 -654
3025  8 -7.82 501 -516 654 -655
3026  8 -7.82 501 -516 655 -656
3027  8 -7.82 501 -516 656 -677
3028  8 -7.82 501 -506 677 -657
3029  8 -7.82 501 -506 657 -685
3030  0    517 -513 675 -676
3031  0    516 -513 676 -651
3032  0    516 -513 651 -652
3033  0    516 -513 652 -653
3034  0    516 -513 653 -654
3035  0    516 -513 654 -655
3036  0    516 -513 655 -656
3037  0    516 -513 656 -677
3038  0    506 -513 677 -657
3039  0    506 -513 657 -685
c
3042  8 -7.82 501 -517 670 -675
3047  0    517 -513 670 -675
c
c     surrounding air regions
9000  9 -1.17e-3       -506 695 -830
9001  9 -1.17e-3       -506 830 -831
9002  9 -1.17e-3       -506 831 -832
9003  9 -1.17e-3       -506 832 -833
9004  9 -1.17e-3       -506 833 -837
9010  0    506 -527 695 -830
9011  0    506 -527 830 -831
9012  0    506 -527 831 -832
9013  0    506 -527 832 -833
9014  0    506 -527 833 -837
c
9100  9 -1.17e-3       -515 810 -600
```

```
9101   9 -1.17e-3        -515 811 -810
9102   9 -1.17e-3        -515 812 -811
9103   9 -1.17e-3        -515 813 -812
9104   9 -1.17e-3        -515 817 -813
9110   0    515 -527 810 -600
9111   0    515 -527 811 -810
9112   0    515 -527 812 -811
9113   0    515 -527 813 -812
9114   0    515 -527 817 -813
c
9200   0    513 -527 600 -601
9201   0    513 -527 601 -602
9202   0    513 -527 602 -603
9203   0    513 -527 603 -604
9204   0    513 -527 604 -610
9205   0    513 -527 610 -615
9206   0    513 -527 615 -630
9207   0    513 -527 630 -420
9208   0    513 -527 420 -430
9209   0    513 -527 430 -440
9210   0    513 -527 440 -670
9211   0    513 -527 670 -675
9212   0    513 -527 675 -651
9213   0    513 -527 651 -652
9214   0    513 -527 652 -653
9215   0    513 -527 653 -654
9216   0    513 -527 654 -655
9217   0    513 -527 655 -656
9218   0    513 -527 656 -657
9219   0    513 -527 657 -685
9220   0    513 -527 685 -686
9221   0    513 -527 686 -687
9222   0    513 -527 687 -688
9223   0    513 -527 688 -689
9224   0    513 -527 689 -695
c
c
c
9999   0   527:-817:837
c
c      BLANK LINE

c      BLANK LINE
c
c      MPC surfaces\/ \/ \/ \/ \/
c
1      cz          0.52832
2      cz          0.53213
3      cz          0.61341
4      cz          0.67437
5      cz          0.75057
6      px          0.8128
7      px         -0.8128
8      py          0.8128
9      py         -0.8128
10     px         -4.445
11     px          4.445
12     py         -4.445
13     py          4.445
c      14    px          -8.2423
14     px         -8.242301
15     px         -7.9248
16     px         -7.66826
17     px         -7.47776
18     px         -6.0325
19     px          6.0325
20     px          7.9248
c      21    px          8.2423
c      22    py         -8.2423
```

```
21    px         8.242301
22    py        -8.242301
23    py        -7.9248
24    py        -6.0325
25    py         6.0325
26    py         7.47776
27    py         7.66826
28    py         7.9248
c     29    py         8.2423
29    py         8.242301
c
30    px   -6.5024
31    px    6.5024
32    py   -6.5024
33    py    6.5024
c
101   px  -98.9076
102   px  -82.423
103   px  -65.9384
104   px  -49.4538
105   px  -32.9692
106   px  -16.4846
107   px   0.0
108   px   16.4846
109   px   32.9692
110   px   49.4538
111   px   65.9384
112   px   82.423
113   px   98.9076
c
201   py  -98.9076
202   py  -82.423
203   py  -65.9384
204   py  -49.4538
205   py  -32.9692
206   py  -16.4846
207   py   0.0
208   py   16.4846
209   py   32.9692
210   py   49.4538
211   py   65.9384
212   py   82.423
213   py   98.9076
c
301   cz   85.4075
302   cz   86.6775
c
c     620   pz    21.59     $ MPC baseplate        - 2.5 inches
c     400   pz   24.765  $ start of egg crate
400   pz   23.876  $ start of egg crate
410   pz   33.9725  $ start of boral
420   pz   40.3479 $ beginning of fuel
425   pz   406.1079 $ end of fuel
430   pz   421.3479 $ space
435   pz   430.2125  $ end  of boral
440   pz   445.4271 $ plenum
445   pz   448.8561 $ expansion springs
450   pz   457.3397 $ top end fitting
455   pz   468.63   $ top of element
460   pz   466.344  $ top of egg crate
c
c     MPC surfaces/\ /\ /\ /\ /\
c
c
c     OVERPACK survaces \/ \/ \/ \/ \/
c
501   cz    87.3125  $ IR for overpack
502   cz    90.4875  $ item 2  1.25 inch
503   cz    93.6625  $ item 2  1.25 inch
```

```
504   cz    96.8375    $ item 12  1.25 inch
505   cz    100.0125   $ item 13  1.25 inch
506   cz    103.1875   $ item 14  1.25 inch
507   cz    106.3625   $ item 15  1.25 inch
508   cz    108.9025   $ item 16  1 inch
509   cz    111.521875  $ holtite
510   cz    114.14125   $ holtite
511   cz    116.760625  $ holtite
512   cz    119.53875      $ holtite - total 4.1875 inches
513   cz    120.80875      $ outer steel shell - 0.5 inches
c     512   cz    119.38      $ holtite - total 4.125 inches
c     513   cz    120.65      $ outer steel shell - 0.5 inches
514   cz    111.54      $ hole in pocket trunion
515   cz    105.7275    $ flange bottom of overpack
516   cz    105.7275    $ flange top    of overpack
517   cz    109.5375    $ shear ring
518   cz    103.1875    $ item 14  1.25 inch
519   cz    108.2675    $ impact limiter - 2 inch steel
c
521   cz    162.56      $ surface of impact limiters
522   cz    203.1875    $ 1 meter from 506 - upper and lower part overpack
523   cz    220.80875   $ 1 meter from 513 - outer steel
524   cz    303.1875    $ 2 meter from 506 - upper and lower part overpack
525   cz    320.80875   $ 2 meter from 513 - outer steel
526   cz    362.56      $ 2 meter from 521 - edge of impact limiters
527   cz    400.00
c
600   pz    0.0       $ bottom of overpack
601   pz    3.048
602   pz    6.096
603   pz    9.144
604   pz    12.192
610   pz    15.24     $ overpack baseplate   - 6 inches
615   pz    18.415
620   pz    21.59     $ MPC baseplate        - 2.5 inches
630   pz    22.225    $ beginning of item 17 - 0.25 inches
635   pz    23.495    $ item 17              - 0.5 inches
640   pz    41.75125  $ hole in pocket trun  - 7.6875 inches from 630
645   pz    54.61     $ top of pocket trun   - 12.75 inches from 630
660   pz    455.6125  $ top of holtite       - 170.125 inches from 635
665   pz    460.6925  $ top of foam          - 2 inches
670   pz    461.9625  $ top of item 17 on top- 0.5 inches
675   pz    473.71    $ bottom of MPC in lid - 178 inches from 620
676   pz    476.5675  $ top of shear ring
677   pz    494.03    $ top of add steel
651   pz    476.885
652   pz    480.06
653   pz    483.235
654   pz    486.41
655   pz    489.585
656   pz    492.76
657   pz    495.935
680   pz    499.11    $ top of MPC outer lid
685   pz    500.6975  $ bot of overpack lid  - 5/8 inch
686   pz    503.7455
687   pz    506.7935
688   pz    509.8415
689   pz    512.8895
695   pz    515.9375  $ top of overpack lid  - 6 inches
c
c     tally segment surfaces
c
701   pz    -121.92
702   pz    -91.44
703   pz    -60.96
704   pz    -30.48
c     600   pz    0.0       $ bottom of overpack
c     630   pz    22.225    $ beginning of item 17 - 0.25 inches
705   pz    51.5408
```

```
706   pz    80.8567
707   pz    110.1725
708   pz    139.4883
709   pz    168.8042
710   pz    198.1200
711   pz    227.4358
712   pz    256.7517
713   pz    286.0675
714   pz    315.3833
715   pz    344.6992
716   pz    374.0150
717   pz    403.3308
718   pz    432.6467
c     670   pz    461.9625  $ top of item 17 on top- 0.5 inches
719   pz    488.3150
c     695   pz    514.6675  $ top of overpack lid  - 6 inches
720   pz    545.1475
721   pz    575.6275
722   pz    606.1075
723   pz    636.5875
c
740   cz    15.24
741   cz    45.72
742   cz    76.2
743   cz    106.68
744   cz    137.16
745   cz    167.64
746   cz    198.12
747   cz    228.6
748   cz    259.08
749   cz    289.56
750   cz    320.04
751   cz    350.52
752   cz    381.0
c
801   pz    -2.54    $ steel disk
802   pz    -5.715   $ holtite
803   pz    -8.89    $ holtite
804   pz    -9.2075  $ cover over holtite
805   pz    -53.34   $ item 2 on impact limiters
810   pz    -100.0   $ 1 meter from surface overpack
811   pz    -105.7275 $ edge of impact limiter
812   pz    -200.0    $ 2 meter from surface overpack
813   pz    -305.7275 $ 2 meter from surface impact limiter
814   pz    -427.6475 $ 2 meter + 4 feet
815   pz    -488.6075 $ 2 meter + 6 feet
816   pz    -671.4875 $ 2 meter + 12 feet
817   pz    -700.00
c
821   pz    518.4775    $ steel disk
822   pz    521.6525    $ holtite
823   pz    524.8275    $ holtite
824   pz    525.145     $ cover over holtite
825   pz    569.2775    $ item 2 on impact limiters
830   pz    615.9375    $ 1 meter from surface overpack
831   pz    621.6650    $ edge of impact limiter
832   pz    715.9375    $ 2 meter from surface overpack
833   pz    821.6650    $ 2 meter from surface impact limiter
834   pz    943.5850    $ 2 meter + 4 feet
835   pz    1004.545    $ 2 meter + 6 feet
836   pz    1187.425    $ 2 meter + 12 feet
837   pz    1200.00
c
c         steel spine and holtite cells
c
1000      px    0.0
1001      px  -0.635
1002      px   0.635
1011   1  px  -0.635
```

```
1012    1  px    0.635
1021    2  px   -0.635
1022    2  px    0.635
1031    3  px   -0.635
1032    3  px    0.635
1041    4  px   -0.635
1042    4  px    0.635
1051    5  px   -0.635
1052    5  px    0.635
1061    6  px   -0.635
1062    6  px    0.635
1071    7  px   -0.635
1072    7  px    0.635
1081    8  px   -0.635
1082    8  px    0.635
1091    9  px   -0.635
1092    9  px    0.635
c
1101    px   15.71625  $ pocket trunion
1102    px   8.09625   $ pocket trunion opening
1103    px  -8.09625   $ pocket trunion opening 6 3/8 inches thick
1104    px  -15.71625  $ pocket trunion - 9 3/8 inches thick
c
2000       py   0.0
2001       py  -0.635
2002       py   0.635
2011    1  py  -0.635
2012    1  py   0.635
2021    2  py  -0.635
2022    2  py   0.635
2031    3  py  -0.635
2032    3  py   0.635
2041    4  py  -0.635
2042    4  py   0.635
2051    5  py  -0.635
2052    5  py   0.635
2061    6  py  -0.635
2062    6  py   0.635
2071    7  py  -0.635
2072    7  py   0.635
2081    8  py  -0.635
2082    8  py   0.635
2091    9  py  -0.635
2092    9  py   0.635
c
2101    py   15.71625  $ pocket trunion
2102    py   8.09625   $ pocket trunion opening
2103    py  -8.09625   $ pocket trunion opening 6 3/8 inches thick
2104    py  -15.71625  $ pocket trunion - 9 3/8 inches thick
c
c     OVERPACK surfaces /\ /\ /\ /\ /\
c
c     BLANK LINE

c     BLANK LINE
c
*tr1    0 0 0  9 279 90  99  9 90 90 90 0
*tr2    0 0 0 18 288 90 108 18 90 90 90 0
*tr3    0 0 0 27 297 90 117 27 90 90 90 0
*tr4    0 0 0 36 306 90 126 36 90 90 90 0
*tr5    0 0 0 45 315 90 135 45 90 90 90 0
*tr6    0 0 0 54 324 90 144 54 90 90 90 0
*tr7    0 0 0 63 333 90 153 63 90 90 90 0
*tr8    0 0 0 72 342 90 162 72 90 90 90 0
*tr9    0 0 0 81 351 90 171 81 90 90 90 0
c
c        PHOTON MATERIALS
c
c     fuel 3.4 w/o U235  10.412 gm/cc
```

```
c     m1           92235.01p   -0.029971
c                  92238.01p   -0.851529
c                  8016.01p    -0.1185
c     c     homogenized fuel  density 3.979996 gm/cc
c     m2           92235.01p   -0.024483
c                  92238.01p   -0.695601
c                   8016.01p   -0.096801
c                  40000.01p   -0.183115
c     c     zirconium 6.55 gm/cc
c     m3           40000.01p   1.          $ Zr Clad
c     c     stainless steel 7.92 gm/cc
c     m5           24000.01p   -0.19
c                  25055.01p   -0.02
c                  26000.01p   -0.695
c                  28000.01p   -0.095
c     c     boral  2.644 gm/cc
c     m6           5010.01p    -0.044226
c                  5011.01p    -0.201474
c                  13027.01p   -0.6861
c                  6000.01p    -0.0682
c     c     holtite 1.61 gm/cc
c     m7           6000.01p  -0.2766039
c                 13027.01p  -0.21285
c                  1001.01p  -0.0592
c                  8016.01p  -0.42372
c                  7014.01p  -0.0198
c                  5010.01p  -0.0014087
c                  5011.01p  -0.0064174
c     c     carbon steel 7.82 gm/cc
c     m8      6000.01p -0.005 26000.01p -0.995
c     c     air density 1.17e-3 gm/cc
c     m9      7014.01p 0.78 8016.01p 0.22
c     c
c     c         NEUTRON MATERIALS
c
c     fuel 3.4 w/o U235  10.412 gm/cc
m1           92235.50c   -0.029971
             92238.50c   -0.851529
             8016.50c    -0.1185
c     homogenized fuel  density 3.979996 gm/cc
m2           92235.50c   -0.024483
             92238.50c   -0.695601
              8016.50c   -0.096801
             40000.35c   -0.183115
c     helium  1e-4 gm/cc
m3     2004.50c 1.0
c     stainless steel 7.92 gm/cc
m5           24000.50c   -0.19
             25055.50c   -0.02
             26000.55c   -0.695
             28000.50c   -0.095
c     boral  2.644 gm/cc
m6           5010.50c    -0.044226
             5011.56c    -0.201474
             13027.50c   -0.6861
             6000.50c    -0.0682
c     holtite 1.61 gm/cc
m7           6000.50c  -0.2766039
            13027.50c  -0.21285
             1001.50c  -0.0592
             8016.50c  -0.42372
             7014.50c  -0.0198
             5010.50c  -0.0014087
             5011.56c  -0.0064174
mt7    lwtr.01t
c     carbon steel 7.82 gm/cc
m8      6000.50c -0.005 26000.55c -0.995
c     air density 1.17e-3 gm/cc
m9      7014.50c 0.78 8016.50c 0.22
```

```
c
phys:n   20 0.0
phys:p   100 0
c     imp:n   1 228r 0
c     imp:p   1 228r 0
nps     500000
prdmp    j   -30   1   2
c     print   10 110 160 161 20 170
print
mode n p
c
sdef  par=1  erg=d1 axs=0 0 1 x=d4 y=fx d5 z=d3
c
c    energy dist for gammas in the fuel
c
c    si1  h  0.7 1.0 1.5 2.0 2.5 3.0
c    sp1     0  0.31 0.31 0.15 0.15 0.08
c
c    energy dist for neutrons in the fuel
c
si1  h  0.1 0.4 0.9 1.4 1.85 3.0 6.43 20.0
sp1     0   0.03787 0.1935 0.1773 0.1310 0.2320 0.2098 0.01853
c
c    energy dist for Co60 gammas
c
c    si1  d 1.3325 1.1732
c    sp1    0.5    0.5
c
c    axial dist for neut and phot in fuel
c
si3  h 40.3479 55.5879 70.8279 101.3079 162.2679 223.2279
       284.1879 345.1479 375.6279 390.8679 406.1079
sp3    0 0.00005 0.00961 0.07031 0.23323 0.25719 0.22907
         0.16330 0.03309 0.00409 0.00005
sb3    0 1 1 1 1 1 1 1 1 1 1
c
c    axial dist for Co60 - a zero prob is in the fuel
c
c    si3  h 21.59 40.3479 421.3479 445.4271 448.8561 457.3397 468.63
c    sp3    0     0.547   0.0      0.125    0.045    0.227    0.056
c
si4  s                15 16
                 13 14 15 16 17 18
              12 13 14 15 16 17 18 19
              12 13 14 15 16 17 18 19
           11 12 13 14 15 16 17 18 19 20
           11 12 13 14 15 16 17 18 19 20
              12 13 14 15 16 17 18 19
              12 13 14 15 16 17 18 19
                 13 14 15 16 17 18
                       15 16
sp4  1 67r
c
ds5  s                30 30
                 29 29 29 29 29 29
              28 28 28 28 28 28 28 28
              27 27 27 27 27 27 27 27
           26 26 26 26 26 26 26 26 26 26
           25 25 25 25 25 25 25 25 25 25
              24 24 24 24 24 24 24 24
              23 23 23 23 23 23 23 23
                 22 22 22 22 22 22
                       21 21
c
si11  -80.6831 -67.6783
si12  -64.1985 -51.1937
si13  -47.7139 -34.7091
si14  -31.2293 -18.2245
si15  -14.7447 -1.7399
```

```
si16   1.7399   14.7447
si17   18.2245  31.2293
si18   34.7091  47.7139
si19   51.1937  64.1985
si20   67.6783  80.6831
c
si21  -80.6831 -67.6783
si22  -64.1985 -51.1937
si23  -47.7139 -34.7091
si24  -31.2293 -18.2245
si25  -14.7447 -1.7399
si26   1.7399   14.7447
si27   18.2245  31.2293
si28   34.7091  47.7139
si29   51.1937  64.1985
si30   67.6783  80.6831
sp11   0 1
sp12   0 1
sp13   0 1
sp14   0 1
sp15   0 1
sp16   0 1
sp17   0 1
sp18   0 1
sp19   0 1
sp20   0 1
sp21   0 1
sp22   0 1
sp23   0 1
sp24   0 1
sp25   0 1
sp26   0 1
sp27   0 1
sp28   0 1
sp29   0 1
sp30   0 1
c
#         imp:n     imp:p
    301       1         1
    302       1         1
    303       1         1
    304       1         1
    305       2         1
    306       2         1
    307       2         1
    308       2         1
    309       1         1
    310       1         1
    311       1         1
    312       1         1
    313       2         1
    314       2         1
    315       2         1
    316       2         1
    317       4         1
    318       4         1
    319       4         1
    320       4         1
    321       4         1
    322       4         1
    323       4         1
    324       4         1
    326       1         1
    327       1         1
    328       1         1
    329       1         1
    330       1         1
    331       1         1
    332       1         1
```

333	1	1
334	2	1
335	2	1
336	2	1
337	2	1
338	1	1
339	1	1
340	1	1
341	1	1
342	2	1
343	2	1
344	2	1
345	2	1
346	1	1
347	1	1
348	1	1
349	1	1
350	1	1
351	1	1
352	1	1
353	1	1
354	2	1
355	1	1
356	1	1
357	2	1
358	4	1
359	4	1
360	4	1
361	4	1
362	1	1
363	1	1
364	1	1
365	1	1
366	1	1
401	1	1
402	1	1
403	1	1
404	1	1
405	2	1
406	2	1
407	2	1
408	2	1
409	1	1
410	1	1
411	1	1
412	1	1
413	2	1
414	2	1
415	2	1
416	2	1
417	4	1
418	4	1
419	4	1
420	4	1
421	4	1
422	4	1
423	4	1
424	4	1
426	1	1
427	1	1
428	1	1
429	1	1
454	2	1
455	1	1
456	1	1
457	2	1
458	4	1
459	4	1
460	4	1

461	4	1
462	1	1
463	1	1
464	1	1
465	1	1
466	1	1
501	1	1
502	1	1
503	1	1
504	1	1
505	2	1
506	2	1
507	2	1
508	2	1
509	1	1
510	1	1
511	1	1
512	1	1
513	2	1
514	2	1
515	2	1
516	2	1
517	4	1
518	4	1
519	4	1
520	4	1
521	4	1
522	4	1
523	4	1
524	4	1
526	1	1
527	1	1
528	1	1
529	1	1
530	1	1
531	1	1
534	2	1
535	2	1
538	1	1
539	1	1
542	2	1
543	2	1
546	1	1
547	1	1
548	1	1
549	1	1
550	1	1
551	1	1
552	1	1
553	1	1
554	2	1
555	1	1
556	1	1
557	2	1
558	4	1
559	4	1
560	4	1
561	4	1
562	1	1
563	1	1
564	1	1
565	1	1
566	1	1
601	1	1
602	1	1
603	1	1
604	1	1
605	2	1
606	2	1

607	2	1
608	2	1
609	1	1
610	1	1
611	1	1
612	1	1
613	2	1
614	2	1
615	2	1
616	2	1
617	4	1
618	4	1
619	4	1
620	4	1
621	4	1
622	4	1
623	4	1
624	4	1
626	1	1
627	1	1
628	1	1
629	1	1
632	1	1
633	1	1
636	2	1
637	2	1
640	1	1
641	1	1
644	2	1
645	2	1
646	1	1
647	1	1
648	1	1
649	1	1
650	1	1
651	1	1
652	1	1
653	1	1
654	2	1
655	1	1
656	1	1
657	2	1
658	4	1
659	4	1
660	4	1
661	4	1
662	1	1
663	1	1
664	1	1
665	1	1
666	1	1
701	1	1
702	2	1
703	1	1
704	2	1
705	4	1
706	4	1
707	1	1
708	1	1
710	1	1
711	2	1
712	1	1
713	2	1
714	4	1
715	4	1
716	1	1
717	1	1
720	1	1
721	2	1

722	2	1
723	1	1
724	1	1
725	2	1
726	2	1
727	4	1
728	4	1
729	4	1
730	4	1
731	1	1
732	1	1
735	1	1
736	1	1
747	2	1
748	1	1
749	2	1
750	4	1
751	4	1
752	1	1
755	1	1
766	1	1
767	2	1
768	2	1
769	1	1
770	1	1
771	2	1
772	2	1
773	4	1
774	4	1
775	4	1
776	4	1
777	1	1
780	1	1
799	1	1
800	2	1
801	2	1
802	1	1
803	1	1
804	2	1
805	2	1
806	4	1
807	4	1
808	4	1
809	4	1
810	1	1
811	1	1
822	1	1
823	2	1
824	1	1
825	2	1
826	4	1
827	4	1
828	1	1
830	1	1
841	1	1
842	2	1
843	2	1
844	1	1
845	1	1
846	2	1
847	2	1
848	4	1
849	4	1
850	4	1
851	4	1
852	1	1
201	1	1
202	1	1
203	1	1

204	1	1
205	1	1
206	1	1
207	1	1
101	1	1
102	1	1
208	1	1
209	1	1
210	1	1
211	1	1
212	1	1
103	1	1
104	1	1
105	1	1
106	1	1
107	1	1
108	1	1
213	1	1
214	1	1
215	1	1
109	1	1
110	1	1
111	1	1
112	1	1
113	1	1
114	1	1
115	1	1
116	1	1
216	1	1
217	1	1
218	1	1
117	1	1
118	1	1
119	1	1
120	1	1
121	1	1
122	1	1
123	1	1
124	1	1
219	1	1
220	1	1
221	1	1
125	1	1
126	1	1
127	1	1
128	1	1
129	1	1
130	1	1
131	1	1
132	1	1
133	1	1
134	1	1
222	1	1
223	1	1
135	1	1
136	1	1
137	1	1
138	1	1
139	1	1
140	1	1
141	1	1
142	1	1
143	1	1
144	1	1
224	1	1
225	1	1
226	1	1
145	1	1
146	1	1

147	1	1
148	1	1
149	1	1
150	1	1
151	1	1
152	1	1
227	1	1
228	1	1
229	1	1
153	1	1
154	1	1
155	1	1
156	1	1
157	1	1
158	1	1
159	1	1
160	1	1
230	1	1
231	1	1
232	1	1
161	1	1
162	1	1
163	1	1
164	1	1
165	1	1
166	1	1
233	1	1
234	1	1
235	1	1
236	1	1
237	1	1
167	1	1
168	1	1
238	1	1
239	1	1
240	1	1
241	1	1
242	1	1
243	1	1
244	1	1
1821	4	1
1822	4	1
1823	4	1
1824	4	1
1825	2	1
1826	2	1
1827	1	1
1828	1	1
1829	2	1
1830	2	1
1831	4	1
1832	4	1
1833	4	1
1834	4	1
1835	8	1
1836	8	1
1837	8	1
1838	8	1
1839	16	1
1840	16	1
1841	16	1
1842	16	1
1843	32	1
1844	32	1
1845	32	1
1846	32	1
1847	64	1
1848	64	1
1849	64	1

1850	64	1
1851	64	1
1854	4	1
1855	4	1
1860	8	1
1861	8	1
1862	16	1
1863	16	1
1864	32	1
1865	32	1
1866	64	1
1867	64	1
1868	64	1
1001	2	1
1002	1	1
1003	2	1
1004	4	1
1005	2	1
1006	1	1
1007	2	1
1008	4	1
1009	2	1
1010	1	1
1011	2	1
1012	4	1
10101	1	1
10102	1	1
10103	1	1
10104	1	1
10105	1	1
10106	1	1
10107	1	1
10108	1	1
10109	1	1
10110	1	1
10111	1	1
10112	1	1
10113	1	1
10114	1	1
10115	1	1
10116	1	1
10117	1	1
10118	1	1
10119	1	1
10120	1	1
10121	1	1
10122	1	1
10123	1	1
10124	1	1
10125	1	1
10126	1	1
10127	1	1
10128	1	1
10129	1	1
10130	1	1
10131	1	1
10132	1	1
10133	1	1
10134	1	1
10135	1	1
10136	1	1
10137	1	1
10138	1	1
10139	1	1
10140	1	1
10141	1	1
10142	1	1
10143	1	1
10144	1	1

10145	1	1
10146	1	1
10147	1	1
10148	1	1
10149	1	1
10150	1	1
10151	1	1
10152	1	1
10153	1	1
10154	1	1
10155	1	1
10156	1	1
10157	1	1
10158	1	1
10159	1	1
10160	1	1
10161	1	1
10162	1	1
10163	1	1
10164	1	1
10165	1	1
10166	1	1
10167	1	1
10168	1	1
10169	1	1
10170	1	1
10171	1	1
10172	1	1
10173	1	1
10174	1	1
10175	1	1
10176	1	1
10177	1	1
10178	1	1
10179	1	1
10180	1	1
10181	1	1
10182	1	1
10183	1	1
10184	1	1
10202	1	1
10203	1	1
10204	1	1
10205	1	1
10206	1	1
10207	1	1
10208	1	1
10209	1	1
10210	1	1
10211	1	1
10212	1	1
10213	1	1
10214	1	1
10215	1	1
10216	1	1
10217	1	1
10218	1	1
10219	1	1
10220	1	1
10221	1	1
10222	1	1
10223	1	1
10224	1	1
10225	1	1
10226	1	1
10227	1	1
10228	1	1
10229	1	1
10230	1	1

10231	1	1
10232	1	1
10233	1	1
10234	1	1
10235	1	1
10236	1	1
10237	1	1
10238	1	1
10239	1	1
10240	1	1
10241	1	1
10244	1	1
10245	1	1
10246	1	1
10247	1	1
10248	1	1
10249	1	1
10250	1	1
10251	1	1
10252	1	1
10253	1	1
10254	1	1
10255	1	1
10256	1	1
10257	1	1
10258	1	1
10259	1	1
10260	1	1
10261	1	1
10262	1	1
10263	1	1
10264	1	1
10265	1	1
10266	1	1
10267	1	1
10268	1	1
10269	1	1
10270	1	1
10271	1	1
10272	1	1
10273	1	1
10274	1	1
10275	1	1
10276	1	1
10277	1	1
10278	1	1
10279	1	1
10280	1	1
10281	1	1
10282	1	1
10283	1	1
11000	1	1
11001	1	1
11002	1	1
11003	1	1
11111	1	1
11112	1	1
11113	1	1
11114	1	1
11115	1	1
2000	32	1
2001	16	1
2002	16	1
2003	8	1
2004	8	1
2010	32	1
2011	16	1
2012	16	1
2013	8	1

2014	8	1
2015	4	1
2016	4	1
2020	1	1
2021	1	1
2022	1	1
2023	1	1
2024	1	1
2025	1	1
2026	1	1
3000	128	1
3001	128	1
3002	256	1
3003	256	1
3004	512	1
3010	1	1
3011	1	1
3012	1	1
3013	1	1
3014	1	1
3020	8	1
3021	8	1
3022	8	1
3023	16	1
3024	16	1
3025	32	1
3026	32	1
3027	64	1
3028	64	1
3029	64	1
3030	1	1
3031	1	1
3032	1	1
3033	1	1
3034	1	1
3035	1	1
3036	1	1
3037	1	1
3038	1	1
3039	1	1
3042	4	1
3047	1	1
9000	512	1
9001	512	1
9002	512	1
9003	512	1
9004	512	1
9010	1	1
9011	1	1
9012	1	1
9013	1	1
9014	1	1
9100	32	1
9101	32	1
9102	32	1
9103	32	1
9104	32	1
9110	1	1
9111	1	1
9112	1	1
9113	1	1
9114	1	1
9200	1	1
9201	1	1
9202	1	1
9203	1	1
9204	1	1
9205	1	1
9206	1	1

```
  9207      1         1
  9208      1         1
  9209      1         1
  9210      1         1
  9211      1         1
  9212      1         1
  9213      1         1
  9214      1         1
  9215      1         1
  9216      1         1
  9217      1         1
  9218      1         1
  9219      1         1
  9220      1         1
  9221      1         1
  9222      1         1
  9223      1         1
  9224      1         1
  9999      0         0
c
c       neutron dose factors
c
c    2.5e-8   1.0e-7   1.0e-6   1.0e-5   1.0e-4   1.0e-3   1.0e-2     0.1
c        0.5      1.0      2.5      5.0      7.0      10.0     14.0     20.0
c    3.67e-6  3.67e-6  4.46e-6  4.54e-6  4.18e-6  3.76e-6  3.56e-6 2.17e-5
c        9.26e-5  1.32e-4  1.25e-4  1.56e-4  1.47e-4  1.47e-4  2.08e-4 2.27e-4
c
c       photon dose factors
c
c    0.01  0.03  0.05  0.07  0.1  0.15  0.2  0.25  0.3  0.35  0.4  0.45
c         0.5  0.55  0.6  0.65  0.7  0.8  1.0  1.4  1.8  2.2  2.6  2.8  3.25
c         3.75  4.25  4.75  5.0  5.25  5.75  6.25  6.75  7.5  9.0  11.0
c         13.0  15.0
c   3.96e-06  5.82e-07  2.90e-07  2.58e-07  2.83e-07  3.79e-07  5.01e-07
c        6.31e-07  7.59e-07  8.78e-07  9.85e-07  1.08e-06  1.17e-06  1.27e-06
c        1.36e-06  1.44e-06  1.52e-06  1.68e-06  1.98e-06  2.51e-06  2.99e-06
c        3.42e-06  3.82e-06  4.01e-06  4.41e-06  4.83e-06  5.23e-06  5.60e-06
c        5.80e-06  6.01e-06  6.37e-06  6.74e-06  7.11e-06  7.66e-06  8.77e-06
c        1.03e-05  1.18e-05  1.33e-05
c
f2:n   600 810 811 812 813
fs2    -740 -741 -742 -743 -744 -745 -746 -747 -748 -749 -750 -751 -752 t
fc2    1ft all
ft2    scx 1
de2   2.5e-8   1.0e-7   1.0e-6   1.0e-5   1.0e-4   1.0e-3   1.0e-2     0.1
      0.5      1.0      2.5      5.0      7.0      10.0      14.0     20.0
df2   3.67e-6  3.67e-6  4.46e-6  4.54e-6  4.18e-6  3.76e-6  3.56e-6 2.17e-5
      9.26e-5  1.32e-4  1.25e-4  1.56e-4  1.47e-4  1.47e-4  2.08e-4 2.27e-4
fq2   u s
tf2   3j 2
c
f12:n  695 830 831 832 833
fs12   -740 -741 -742 -743 -744 -745 -746 -747 -748 -749 -750 -751 -752 t
fc12    1ft all
ft12    scx 1
de12   2.5e-8   1.0e-7   1.0e-6   1.0e-5   1.0e-4   1.0e-3   1.0e-2     0.1
      0.5      1.0      2.5      5.0      7.0      10.0      14.0     20.0
df12   3.67e-6  3.67e-6  4.46e-6  4.54e-6  4.18e-6  3.76e-6  3.56e-6 2.17e-5
      9.26e-5  1.32e-4  1.25e-4  1.56e-4  1.47e-4  1.47e-4  2.08e-4 2.27e-4
fq12   u s
tf12   3j 2
c
c      PHOTON TALLIES
c
f102:p   600 810 811 812 813
fs102    -740 -741 -742 -743 -744 -745 -746 -747 -748 -749 -750 -751 -752 t
fc102    1ft all
ft102    scx 1
de102    0.01  0.03  0.05  0.07  0.1  0.15  0.2  0.25  0.3  0.35  0.4  0.45
```

```
          0.5  0.55  0.6  0.65  0.7  0.8  1.0  1.4  1.8  2.2  2.6  2.8  3.25
          3.75  4.25  4.75  5.0  5.25  5.75  6.25  6.75  7.5  9.0  11.0
          13.0  15.0
df102     3.96e-06  5.82e-07  2.90e-07  2.58e-07  2.83e-07  3.79e-07  5.01e-07
          6.31e-07  7.59e-07  8.78e-07  9.85e-07  1.08e-06  1.17e-06  1.27e-06
          1.36e-06  1.44e-06  1.52e-06  1.68e-06  1.98e-06  2.51e-06  2.99e-06
          3.42e-06  3.82e-06  4.01e-06  4.41e-06  4.83e-06  5.23e-06  5.60e-06
          5.80e-06  6.01e-06  6.37e-06  6.74e-06  7.11e-06  7.66e-06  8.77e-06
          1.03e-05  1.18e-05  1.33e-05
fq102     u s
tf102     3j 2
c
f112:p     695 830 831 832 833
fs112      -740 -741 -742 -743 -744 -745 -746 -747 -748 -749 -750 -751 -752 t
fc112      1ft all
ft112      scx 1
de112      0.01  0.03  0.05  0.07  0.1  0.15  0.2  0.25  0.3  0.35  0.4  0.45
           0.5  0.55  0.6  0.65  0.7  0.8  1.0  1.4  1.8  2.2  2.6  2.8  3.25
           3.75  4.25  4.75  5.0  5.25  5.75  6.25  6.75  7.5  9.0  11.0
           13.0  15.0
df112      3.96e-06  5.82e-07  2.90e-07  2.58e-07  2.83e-07  3.79e-07  5.01e-07
           6.31e-07  7.59e-07  8.78e-07  9.85e-07  1.08e-06  1.17e-06  1.27e-06
           1.36e-06  1.44e-06  1.52e-06  1.68e-06  1.98e-06  2.51e-06  2.99e-06
           3.42e-06  3.82e-06  4.01e-06  4.41e-06  4.83e-06  5.23e-06  5.60e-06
           5.80e-06  6.01e-06  6.37e-06  6.74e-06  7.11e-06  7.66e-06  8.77e-06
           1.03e-05  1.18e-05  1.33e-05
fq112      u s
tf112      3j 2
```

CHAPTER 6: CRITICALITY EVALUATION

This chapter documents the criticality evaluation of the HI-STAR 100 System for the storage of spent nuclear fuel in accordance with 10CFR72.124. The results of this evaluation demonstrate that the HI-STAR 100 System is consistent with the Standard Review Plan for Dry Cask Storage Systems, NUREG-1536, and thus, fulfills the following acceptance criteria:

1. The multiplication factor (k_{eff}), including all biases and uncertainties at a 95-percent confidence level, should not exceed 0.95 under all credible normal, off-normal, and accident conditions.

2. At least two unlikely, independent, and concurrent or sequential changes to the conditions essential to criticality safety, under normal, off-normal, and accident conditions, should occur before an accidental criticality is deemed to be possible.

3. When practicable, criticality safety of the design should be established on the basis of favorable geometry, permanent fixed neutron-absorbing materials (poisons), or both. Where solid neutron absorbing materials are used, the design should provide for a positive means to verify their continued efficacy during the storage period.

4. Criticality safety of the cask system should not rely on use of the following credits:

    a. burnup of the fuel
    b. fuel-related burnable neutron absorbers
    c. more than 75 percent for fixed neutron absorbers when subject to standard acceptance test.

In addition to demonstrating that the criticality safety acceptance criteria are satisfied, this chapter describes the HI-STAR 100 System design structures and components important to criticality safety and defines the limiting fuel characteristics.

6.1 DISCUSSION AND RESULTS

In conformance with the principles established in NUREG-1536 [6.1.1], 10CFR72.124 [6.1.2], and NUREG-0800 Section 9.1.2 [6.1.3], the results in this chapter demonstrate that the effective multiplication factor (k_{eff}) of the HI-STAR 100 System, including all biases and uncertainties evaluated with a 95% probability at the 95% confidence level, does not exceed 0.95 under all credible normal, off-normal, and accident conditions. Moreover, these results demonstrate that the HI-STAR 100 System is designed and maintained such that at least two unlikely, independent, and concurrent or sequential changes must occur to the conditions essential to criticality safety before a nuclear criticality accident is possible. These criteria provide a large subcritical margin, sufficient to assure the criticality safety of the HI-STAR 100 System when fully loaded with fuel of the highest permissible reactivity.

Criticality safety of the HI-STAR 100 System depends on the following three principal design parameters:

1. The inherent geometry of the fuel basket designs within the MPC (and the flux-trap water gaps in the MPC-24);

2. The incorporation of permanent fixed neutron-absorbing panels (Boral) in the fuel basket structure; and

3. An administrative limit on the maximum enrichment for PWR fuel and maximum planar-average enrichment for BWR fuel.

The normal conditions for loading/unloading, handling, packaging, transfer, and storage of the HI-STAR 100 System conservatively include: full flooding with ordinary water corresponding to the highest reactivity, and the worst case (most conservative) combination of manufacturing and fabrication tolerances. The off-normal and accident conditions defined in Chapter 2 and considered in Chapter 11 have no adverse effect on the design parameters important to criticality safety, and thus, the off-normal and accident conditions are identical to those for normal conditions.

The HI-STAR 100 System is designed such that the fixed neutron absorber (Boral) will remain effective for a storage period greater than 20 years, and there are no credible means to lose it. Therefore, in accordance with 10CFR72.124(b), there is no need to provide a surveillance or monitoring program to verify the continued efficacy of the neutron absorber.

Criticality safety of the HI-STAR 100 System does not rely on the use of any of the following credits:

- burnup of fuel
- fuel-related burnable neutron absorbers
- more than 75 percent of the B-10 content for the fixed neutron absorber (Boral).

The following two interchangeable basket designs are available for use in the HI-STAR 100 System:

- a 24-cell basket (MPC-24), designed for intact PWR fuel assemblies with a specified maximum enrichment
- a 68-cell basket (MPC-68), designed for both intact and damaged BWR fuel assemblies with a specified maximum planar-average enrichment. Additionally, a variation in the MPC-68, designated MPC-68F, is designed for damaged BWR fuel assemblies and BWR fuel debris with a specified maximum planar-average enrichment.

The HI-STAR 100 System for storage is dry (no moderator), and thus, the reactivity is very low ($k_{eff} < 0.40$). However, the HI-STAR 100 System for loading and unloading operations is flooded, and thus, represents the limiting case in terms of reactivity.

Confirmation of the criticality safety of the HI-STAR 100 System under flooded conditions, when filled with fuel of the maximum permissible reactivity for which they are designed, was accomplished with the three-dimensional Monte Carlo code MCNP4a [6.1.4]. Independent confirmatory calculations were made with NITAWL-KENO5a from the SCALE-4.3 package. KENO5a [6.1.5] calculations used the 238-group SCALE cross-section library compiled with the NITAWL-II program [6.1.6], which adjusts the uranium-238 cross sections to compensate for resonance self-shielding effects. The Dancoff factors required by NITAWL-II were calculated with the CELLDAN code [6.1.13], which includes the SUPERDAN code [6.1.7] as a subroutine. K-factors for one-sided statistical tolerance limits with 95% probability at the 95% confidence level were obtained from the National Bureau of Standards (now NIST) Handbook 91 [6.1.8].

CASMO-3, a two-dimensional transport theory code [6.1.9-6.1.12] for fuel assemblies, was used to assess the incremental reactivity effects due to manufacturing tolerances. The CASMO-3 calculations identify those tolerances that cause a positive reactivity effect, enabling the Monte Carlo code input to define the worst case (most conservative) conditions. CASMO-3 was not used for quantitative information, but only to qualitatively indicate the direction and approximate magnitude of the reactivity effects of the manufacturing tolerances.

Benchmark calculations were made to compare the primary code packages (MCNP4a and KENO5a) with experimental data, using critical experiments selected to encompass, insofar as practical, the design parameters of the HI-STAR 100 System. The most important parameters are (1) the enrichment, (2) the water-gap size (MPC-24) or cell spacing (MPC-68), and (3) the ^{10}B loading of the neutron absorber panels. Benchmark calculations are presented in Appendix 6.A.

Applicable codes, standards, and regulations, or pertinent sections thereof, include the following:

- NUREG-1536, Standard Review Plan for Dry Cask Storage Systems, USNRC, Washington D.C., January 1997.
- 10CFR72.124, Criteria For Nuclear Criticality Safety.
- Code of Federal Regulations, Title 10, Part 50, Appendix A, General Design Criterion 62, Prevention of Criticality in Fuel Storage and Handling.
- USNRC Standard Review Plan, NUREG-0800, Section 9.1.2, Spent Fuel Storage, Rev. 3, July 1981.

To assure the true reactivity will always be less than the calculated reactivity, the following conservative assumptions were made:

- The MPCs are assumed to contain the most reactive fresh fuel authorized to be loaded into a specific basket design.
- Consistent with NUREG-1536, no credit for fuel burnup is assumed, either in depleting the quantity of fissile nuclides or in producing fission product poisons.
- Consistent with NUREG-1536, the criticality analyses assume 75% of the manufacturer's minimum Boron-10 content for the Boral neutron absorber.
- The fuel stack density is conservatively assumed to be 96% of theoretical (10.522 g/cm^3) for all criticality analyses. No credit is taken for fuel pellet dishing or chamfering.
- No credit is taken for the ^{234}U and ^{236}U in the fuel.
- When flooded, the moderator is assumed to be pure, unborated water at a temperature corresponding to the highest reactivity within the expected operating range (i.e., water density of 1.000 g/cc).

- Neutron absorption in minor structural members and heat conduction elements is neglected, i.e., spacer grids, basket supports, and aluminum heat conduction elements are replaced by water.

- Consistent with NUREG-1536, the worst hypothetical combination of tolerances (most conservative values within the range of acceptable values), as identified in Section 6.3, is assumed.

- When flooded, the fuel rod pellet-to-clad gap regions are assumed to be flooded.

- Planar-averaged enrichments are assumed for BWR fuel. (In accordance with NUREG-1536, analysis is presented in Appendix 6.B to demonstrate that the use of planar-average enrichments produces conservative results.)

- Consistent with NUREG-1536, fuel-related burnable neutron absorbers, such as the Gadolinia normally used in BWR fuel and IFBA normally used in PWR fuel, are neglected.

- Higher temperatures of the fuel and moderator resulting from decay heat are neglected.

- For evaluation of the bias, all benchmark calculations that result in a k_{eff} greater than 1.0 are conservatively truncated to 1.0000, consistent with NUREG-1536.

- The water reflector above and below the fuel is assumed to be unborated water.

- For fuel assemblies that contain low-enriched axial blankets, the governing enrichment is that of the highest planar average, and the blankets are not included in determining the average enrichment.

- For intact fuel assemblies, as defined in Appendix B to the Certificate of Compliance, missing fuel rods are assumed to be replaced with dummy rods that displace an amount of water greater than or equal to the original rods.

Results of the design basis criticality safety calculations for single unreflected, internally flooded casks (limiting cases) are listed in Tables 6.1.1 through 6.1.3, conservatively evaluated for the worst combination of manufacturing tolerances (as identified in Section 6.3), and including the calculational bias, uncertainties, and calculational statistics. For each of the MPC designs and

fuel assembly classes[†], Tables 6.1.1 through 6.1.3 list the bounding maximum k_{eff} value and the associated maximum allowable enrichment. The maximum allowed enrichments are defined in Appendix B to the Certificate of Compliance. Maximum k_{eff} values for each of the candidate fuel assemblies and basket configurations, that are bounded by those listed in Tables 6.1.1 through 6.1.3, are given in Section 6.2.

A table listing the maximum k_{eff} (including bias, uncertainties, and calculational statistics), calculated k_{eff}, standard deviation, and energy of the average lethargy causing fission (EALF) for each of the candidate fuel assemblies and basket configurations is provided in Appendix 6.C. These results confirm that the maximum k_{eff} values for the HI-STAR 100 System are below the limiting design criteria ($k_{eff} < 0.95$) when fully flooded and loaded with any of the candidate fuel assemblies and basket configurations. Analyses for the various conditions of flooding that support the conclusion that the fully flooded condition corresponds to the highest reactivity, and thus is most limiting, are presented in Section 6.4. The capability of the HI-STAR 100 System to safely accommodate damaged fuel and fuel debris is demonstrated in Subsection 6.4.4.

Accident conditions have also been considered and no credible accident has been identified that would result in exceeding the design criteria limit on reactivity. After the MPC is loaded with spent fuel, it is seal-welded and cannot be internally flooded. The HI-STAR 100 System for storage is dry (no moderator) and the reactivity is very low. For arrays of HI-STAR 100 casks, the radiation shielding and the physical separation between overpacks due to the large diameter and cask pitch preclude any significant neutronic coupling between the casks.

[†] For each array size (e.g., 6x6, 7x7, 14x14, etc.), the fuel assemblies have been subdivided into a number of assembly classes, where an assembly class is defined in terms of the (1) number of fuel rods; (2) pitch; (3) number and location of guide tubes (PWR) or water rods (BWR); and (4) cladding material. The assembly classes for BWR and PWR fuel are defined in Section 6.2.

Table 6.1.1

BOUNDING MAXIMUM k_{eff} VALUES FOR EACH ASSEMBLY CLASS IN THE MPC-24

Fuel Assembly Class	Maximum Allowable Enrichment (wt% ^{235}U)	Maximum† k_{eff}
14x14A	4.6	0.9296
14x14B	4.6	0.9228
14x14C	4.6	0.9287
14x14D	4.0	0.8507
15x15A	4.1	0.9204
15x15B	4.1	0.9388
15x15C	4.1	0.9361
15x15D	4.1	0.9367
15x15E	4.1	0.9368
15x15F	4.1	0.9395††
15x15G	4.0	0.8876
15x15H	3.8	0.9337
16x16A	4.6	0.9287
17x17A	4.0	0.9368
17x17B	4.0	0.9324
17x17C	4.0	0.9336

Note: These calculations are for single unreflected, fully flooded casks. However, comparable reactivities were obtained for fully reflected casks and for arrays of casks.

† The term "maximum k_{eff} " as used here, and elsewhere in this document, means the highest possible k-effective, including bias, uncertainties, and calculational statistics, evaluated for the worst case combination of manufacturing tolerances.

†† KENO5a verification calculation resulted in a maximum k_{eff} of 0.9378.

Table 6.1.2

BOUNDING MAXIMUM k_{eff} VALUES FOR EACH ASSEMBLY CLASS IN THE MPC-68

Fuel Assembly Class	Maximum Allowable Planar-Average Enrichment (wt% ^{235}U)	Maximum† k_{eff}
6x6A	2.7††	0.7888†††
6x6B‡	2.7††	0.7824†††
6x6C	2.7††	0.8021†††
7x7A	2.7††	0.7974†††
7x7B	4.2	0.9386
8x8A	2.7††	0.7697†††
8x8B	4.2	0.9416
8x8C	4.2	0.9425
8x8D	4.2	0.9403
8x8E	4.2	0.9312
8x8F	3.6	0.9153

Note: These calculations are for single unreflected, fully flooded casks. However, comparable reactivities were obtained for fully reflected casks and for arrays of casks.

---

† The term "maximum k_{eff}" as used here, and elsewhere in this document, means the highest possible k-effective, including bias, uncertainties, and calculational statistics, evaluated for the worst case combination of manufacturing tolerances.

†† This calculation was performed for 3.0% planar-average enrichment, however, the actual fuel is limited, as specified in Appendix B to the CoC, to a maximum planar-average enrichment of 2.7%. Therefore, the listed maximum k_{eff} value is conservative.

††† This calculation was performed for a ^{10}B loading of 0.0067 g/cm^2, which is 75% of a minimum ^{10}B loading of 0.0089 g/cm^2. The minimum ^{10}B loading in the MPC-68 is 0.0372 g/cm^2. Therefore, the listed maximum k_{eff} value is conservative.

‡ Assemblies in this class contain both MOX and UO_2 pins. The composition of the MOX fuel pins is given in Table 6.3.4. The maximum allowable planar-average enrichment for the MOX pins is given in the Appendix B to the Certificate of Compliance.

Table 6.1.2 (continued)

BOUNDING MAXIMUM k_{eff} VALUES FOR EACH ASSEMBLY CLASS IN THE MPC-68

Fuel Assembly Class	Maximum Allowable Planar-Average Enrichment (wt% ^{235}U)	Maximum† k_{eff}
9x9A	4.2	0.9417
9x9B	4.2	0.9436
9x9C	4.2	0.9395
9x9D	4.2	0.9394
9x9E	4.1	0.9424
9x9F	4.1	0.9424
10x10A	4.2	0.9457††
10x10B	4.2	0.9436
10x10C	4.2	0.9433
10x10D	4.0	0.9376
10x10E	4.0	0.9185

Note: These calculations are for single unreflected, fully flooded casks. However, comparable reactivities were obtained for fully reflected casks and for arrays of casks.

† The term "maximum k_{eff} " as used here, and elsewhere in this document, means the highest possible k-effective, including bias, uncertainties, and calculational statistics, evaluated for the worst case combination of manufacturing tolerances.

†† KENO5a verification calculation resulted in a maximum k_{eff} of 0.9453.

Table 6.1.3

BOUNDING MAXIMUM k_{eff} VALUES FOR EACH ASSEMBLY CLASS IN THE MPC-68F

Fuel Assembly Class	**Maximum Allowable Planar-Average Enrichment (wt% ^{235}U)**	**Maximum† k_{eff}**
6x6A	2.7††	0.7888
6x6B†††	2.7	0.7824
6x6C	2.7	0.8021
7x7A	2.7	0.7974
8x8A	2.7	0.7697

Note:

1. These calculations are for single unreflected, fully flooded casks. However, comparable reactivities were obtained for fully reflected casks and for arrays of casks.

2. These calculations were performed for a ^{10}B loading of 0.0067 g/cm^2, which is 75% of a minimum ^{10}B loading of 0.0089 g/cm^2. The minimum ^{10}B loading in the MPC-68F is 0.010 g/cm^2. Therefore, the listed maximum k_{eff} values are conservative.

† The term "maximum k_{eff} " as used here, and elsewhere in this document, means the highest possible k-effective, including bias, uncertainties, and calculational statistics, evaluated for the worst case combination of manufacturing tolerances.

†† These calculations were performed for 3.0% planar-average enrichment, however, the actual fuel is limited, as specified in Appendix B to the CoC, to a maximum planar-average enrichment of 2.7%. Therefore, the listed maximum k_{eff} values are conservative.

††† Assemblies in this class contain both MOX and UO_2 pins. The composition of the MOX fuel pins is given in Table 6.3.4. The maximum allowable planar-average enrichment for the MOX pins is specified in Appendix B to the Certificate of Compliance.

6.2 SPENT FUEL LOADING

Specifications for the BWR and PWR fuel assemblies that were analyzed in this criticality evaluation are given in Tables 6.2.1 and 6.2.2, respectively. For the BWR fuel characteristics, the number and dimensions for the water rods are the actual number and dimensions. For the PWR fuel characteristics, the actual number and dimensions of the control rod guide tubes and thimbles are used. Table 6.2.1 lists 56 unique BWR assemblies while Table 6.2.2 lists 41 unique PWR assemblies, all of which were explicitly analyzed for this evaluation. Examination of Tables 6.2.1 and 6.2.2 reveals that there are a large number of minor variations in fuel assembly dimensions.

Due to the large number of minor variations in the fuel assembly dimensions, the use of explicit dimensions in the Certificate of Compliance could limit the applicability of the HI-STAR 100 System. To resolve this limitation, bounding criticality analyses are presented in this section for a number of defined fuel assembly classes for both fuel types (PWR and BWR). The results of the bounding criticality analyses justify using bounding specifications for fuel dimensions in the Certificate of Compliance.

6.2.1 Definition of Assembly Classes

For each array size (e.g., 6x6, 7x7, 15x15, etc.), the fuel assemblies have been subdivided into a number of defined classes, where a class is defined in terms of (1) the number of fuel rods; (2) pitch; (3) number and locations of guide tubes (PWR) or water rods (BWR); and (4) cladding material. The assembly classes for BWR and PWR fuel are defined in Tables 6.2.1 and 6.2.2, respectively. It should be noted that these assembly classes are unique to this evaluation and are not known to be consistent with any class designations in the open literature.

For each assembly class, calculations have been performed for all of the dimensional variations for which data is available (i.e., all data in Tables 6.2.1 and 6.2.2). These calculations demonstrate that the maximum reactivity corresponds to:

- maximum active fuel length,
- maximum fuel pellet diameter,
- minimum cladding outside diameter (OD),
- maximum cladding inside diameter (ID),
- minimum guide tube/water rod thickness, and
- maximum channel thickness (for BWR assemblies only).

Therefore, for each assembly class, a bounding assembly was defined based on the above characteristics and a calculation for the bounding assembly was performed to demonstrate compliance with the regulatory requirement of $k_{eff} < 0.95$. In some assembly classes this bounding assembly corresponds directly to one of the actual (real) assemblies; while in most

assembly classes, the bounding assembly is artificial (i.e., based on bounding dimensions from more than one of the actual assemblies). In classes where the bounding assembly is artificial, the reactivity of the actual (real) assemblies is typically much less than that of the bounding assembly; thereby providing additional conservatism. As a result of these analyses, the Certificate of Compliance will define acceptability in terms of the bounding assembly parameters for each class.

To demonstrate that the aforementioned characteristics are bounding, a parametric study was performed for a reference BWR assembly, designated herein as 8x8C04 (identified generally as a GE8x8R). The results of this study are shown in Table 6.2.3, and verify the positive reactivity effect associated with (1) increasing the pellet diameter, (2) maximizing the cladding ID (while maintaining a constant cladding OD), (3) minimizing the cladding OD (while maintaining a constant cladding ID), (4) decreasing the water rod thickness, (5) artificially replacing the Zircaloy water rod tubes with water, and (6) maximizing the channel thickness. These results, and the many that follow, justify the approach for using bounding dimensions in the Certificate of Compliance. Where margins permit, the Zircaloy water rod tubes (BWR assemblies) are artificially replaced by water in the bounding cases to remove the requirement for water rod thickness from the Certificate of Compliance.

As mentioned, the bounding approach used in these analyses often results in a maximum k_{eff} value for a given class of assemblies that is much greater than the reactivity of any of the actual (real) assemblies within the class, and yet, is still below the 0.95 regulatory limit.

6.2.2 PWR Fuel Assemblies in the MPC-24

For PWR fuel assemblies (specifications listed in Table 6.2.2) the 15x15F01 fuel assembly at 4.1% enrichment has the highest reactivity (maximum k_{eff} of 0.9395). The 17x17A01 assembly (otherwise known as a Westinghouse 17x17 OFA) has a similar reactivity (see Table 6.2.17) and was used throughout this criticality evaluation as a reference PWR assembly. The 17x17A01 assembly is a representative PWR fuel assembly in terms of design and reactivity and is useful for the reactivity studies presented in Sections 6.3 and 6.4. Calculations for the various PWR fuel assemblies in the MPC-24 are summarized in Tables 6.2.4 through 6.2.19 for the fully flooded condition.

Tables 6.2.4 through 6.2.19 show the maximum k_{eff} values for the assembly classes that are acceptable for storage in the MPC-24. All maximum k_{eff} values include the bias, uncertainties, and calculational statistics, evaluated for the worst combination of manufacturing tolerances. All calculations for the MPC-24 were performed for a ^{10}B loading of 0.020 g/cm^2, which is 75% of the minimum loading, 0.0267 g/cm^2, specified on the MPC-24 drawing in Section 1.5. The maximum allowable enrichment in the MPC-24 varies from 4.0 to 4.6 wt% ^{235}U, depending on the assembly class, and is defined in Tables 6.2.4 through 6.2.19. It should be noted that the maximum allowable enrichment does not vary within an assembly class. Table 6.1.1 summarizes

the maximum allowable enrichments for each of the assembly classes that are acceptable for storage in the MPC-24.

Tables 6.2.4 through 6.2.19 are formatted with the assembly class information in the top row, the unique assembly designations, dimensions, and k_{eff} values in the following rows above the bold double lines, and the bounding dimensions selected for the Certificate of Compliance and corresponding bounding k_{eff} values in the final rows. Where the bounding assembly corresponds directly to one of the actual assemblies, the fuel assembly designation is listed in the bottom row in parentheses (e.g., Table 6.2.4). Otherwise, the bounding assembly is given a unique designation. For an assembly class that contains only a single assembly (e.g., 14x14D, see Table 6.2.7), the Certificate of Compliance dimensions are based on the assembly dimensions from that single assembly. All of the maximum k_{eff} values corresponding to the selected bounding dimensions are greater than or equal to those for the actual assembly dimensions and are below the 0.95 regulatory limit.

6.2.3 BWR Fuel Assemblies in the MPC-68

For BWR fuel assemblies (specifications listed in Table 6.2.1) the artificial bounding assembly for the 10x10A assembly class at 4.2% enrichment has the highest reactivity (maximum k_{eff} of 0.9457). Calculations for the various BWR fuel assemblies in the MPC-68 are summarized in Tables 6.2.20 through 6.2.36 for the fully flooded condition. In all cases, the gadolinia (Gd_2O_3) normally incorporated in BWR fuel was conservatively neglected.

For calculations involving BWR assemblies, the use of a uniform (planar-average) enrichment, as opposed to the distributed enrichments normally used in BWR fuel, produces conservative results. Calculations confirming this statement are presented in Appendix 6.B for several representative BWR fuel assembly designs. These calculations justify the specification of planar-average enrichments to define acceptability of BWR fuel for loading into the MPC-68.

Tables 6.2.20 through 6.2.36 show the maximum k_{eff} values for assembly classes that are acceptable for storage in the MPC-68. All maximum k_{eff} values include the bias, uncertainties, and calculational statistics, evaluated for the worst combination of manufacturing tolerances. With the exception of assembly classes 6x6A, 6x6B, 6x6C, 7x7A, and 8x8A, which will be discussed in Section 6.2.4, all calculations for the MPC-68 were performed with a ^{10}B loading of 0.0279 g/cm^2, which is 75% of the minimum loading, 0.0372 g/cm^2, specified on the MPC-68 drawing in Section 1.5. Calculations for assembly classes 6x6A, 6x6B, 6x6C, 7x7A, and 8x8A were conservatively performed with a ^{10}B loading of 0.0067 g/cm^2. The maximum allowable enrichment in the MPC-68 varies from 2.7 to 4.2 wt% ^{235}U, depending on the assembly class. It should be noted that the maximum allowable enrichment does not vary within an assembly class. Table 6.1.2 summarizes the maximum allowable enrichments for all assembly classes that are acceptable for storage in the MPC-68.

Tables 6.2.20 through 6.2.36 are formatted with the assembly class information in the top row, the unique assembly designations, dimensions, and k_{eff} values in the following rows above the bold double lines, and the bounding dimensions selected for the Certificate of Compliance and corresponding bounding k_{eff} values in the final rows. Where an assembly class contains only a single assembly (e.g., 8x8E, see Table 6.2.24), the Certificate of Compliance dimensions are based on the assembly dimensions from that single assembly. For assembly classes that are suspected to contain assemblies with thicker channels (e.g., 120 mils), bounding calculations are also performed to qualify the thicker channels (e.g. 7x7B, see Table 6.2.20). All of the maximum k_{eff} values corresponding to the selected bounding dimensions are shown to be greater than or equal to those for the actual assembly dimensions and are below the 0.95 regulatory limit.

For assembly classes that contain partial length rods (i.e., 9x9A, 10x10A, and 10x10B), calculations were performed for the actual (real) assembly configuration and for the axial segments (assumed to be full length) with and without the partial length rods. In all cases, the axial segment with only the full length rods present (where the partial length rods are absent) is bounding. Therefore, the bounding maximum k_{eff} values reported for assembly classes that contain partial length rods bound the reactivity regardless of the active fuel length of the partial length rods. As a result, the Certificate of Compliance have no minimum requirement for the active fuel length of the partial length rods.

For BWR fuel assembly classes where margins permit, the Zircaloy water rod tubes are artificially replaced by water in the bounding cases to remove the requirement for water rod thickness from the Certificate of Compliance. For these cases, the bounding water rod thickness is listed as zero.

As mentioned, the highest observed maximum k_{eff} value is 0.9457, corresponding to the artificial bounding assembly in the 10x10A assembly class. This assembly has the following bounding characteristics: (1) the partial length rods are assumed to be zero length (most reactive configuration); (2) the channel is assumed to be 120 mils thick; and (3) the active fuel length of the full length rods is 155 inches. Therefore, the maximum reactivity value is bounding compared to any of the real BWR assemblies listed.

6.2.4 Damaged BWR Fuel Assemblies and BWR Fuel Debris

In addition to storing intact PWR and BWR fuel assemblies, the HI-STAR 100 System is designed to store damaged BWR fuel assemblies and BWR fuel debris. Damaged fuel assemblies and fuel debris are defined in Section 2.1.3 and Appendix B to the Certificate of Compliance. Both damaged BWR fuel assemblies and BWR fuel debris are required to be loaded into Damaged Fuel Containers (DFCs) prior to being loaded into the MPC. Two different DFC types with slightly different cross sections are considered. DFCs containing fuel debris must be stored in the MPC-68F. DFCs containing damaged fuel assemblies may be stored in either the MPC-68

or MPC-68F. The criticality evaluation of various possible damaged conditions of the fuel is presented in Subsection 6.4.4 for both DFC types.

Tables 6.2.37 through 6.2.41 show the maximum k_{eff} values for the six assembly classes that may be stored as damaged fuel or fuel debris. All maximum k_{eff} values include the bias, uncertainties, and calculational statistics, evaluated for the worst combination of manufacturing tolerances. All calculations were performed for a ^{10}B loading of 0.0067 g/cm^2, which is 75% of a minimum loading, 0.0089 g/cm^2. However, because the practical manufacturing lower limit for minimum ^{10}B loading is 0.01 g/cm^2, the minimum ^{10}B loading of 0.01 g/cm^2 is specified on the MPC-68 drawing in Section 1.5, for the MPC-68F. As an additional level of conservatism in the analyses, the calculations were performed for an enrichment of 3.0 wt% ^{235}U, while the maximum allowable enrichment for these assembly classes is limited to 2.7 wt% ^{235}U in the Certificate of Compliance. Therefore, the maximum k_{eff} values for damaged BWR fuel assemblies and fuel debris are conservative. Calculations for the various BWR fuel assemblies in the MPC-68F are summarized in Tables 6.2.37 through 6.2.41 for the fully flooded condition.

For the assemblies that may be stored as damaged fuel or fuel debris, the 6x6C01 assembly at 3.0 wt% ^{235}U enrichment has the highest reactivity (maximum k_{eff} of 0.8021). Considering all of the conservatism built into this analysis (e.g., higher than allowed enrichment and lower than actual ^{10}B loading), the actual reactivity will be lower.

Because the analysis for the damaged BWR fuel assemblies and fuel debris was performed for a ^{10}B loading of 0.0089 g/cm^2, which conservatively bounds damaged BWR fuel assemblies in a standard MPC-68 with a minimum ^{10}B loading of 0.0372 g/cm^2, damaged BWR fuel assemblies may also be stored in the standard MPC-68. However, fuel debris is limited to the MPC-68F by Appendix B to the Certificate of Compliance.

Tables 6.2.37 through 6.2.41 are formatted with the assembly class information in the top row, the unique assembly designations, dimensions, and k_{eff} values in the following rows above the bold double lines, and the bounding dimensions selected for the Certificate of Compliance and corresponding bounding k_{eff} values in the final rows. Where an assembly class contains only a single assembly (e.g., 6x6C, see Table 6.2.39), the Certificate of Compliance dimensions are based on the assembly dimensions from that single assembly. All of the maximum k_{eff} values corresponding to the selected bounding dimensions are greater than or equal to those for the actual assembly dimensions and are well below the 0.95 regulatory limit.

6.2.5 Thoria Rod Canister

Additionally, th HI-STAR 100 System is designed to store a Thoria Rod Canister in the MPC68 or MPC68F. The canister is similar to a DFC and contains 18 intact Thoria Rods placed in a separator assembly. The reactivity of the canister in the MPC68 or MPC68F is very low compared to the reactivity of the approved fuel assemblies (The ^{235}U content of these rods corresponds to UO_2 rods with an initial enrichment of approximately 1.7 wt% ^{235}U). It is

therefore permissible to store the Thoria Rod Canister together with any other approved content in a MPC68 or MPC68F. Specifications of the canister and the Thoria Rods that are used in the criticality evaluation are given in Table 6.2.42. The criticality evaluation is presented in Subsection 6.4.6.

Table 6.2.1 (page 1 of 6)
BWR FUEL CHARACTERISTICS AND ASSEMBLY CLASS DEFINITIONS
(all dimensions are in inches)

Fuel Assembly Designation	Clad Material	Pitch	Number of Fuel Rods	Cladding OD	Cladding Thickness	Pellet Diameter	Active Fuel Length	Number of Water Rods	Water Rod OD	Water Rod ID	Channel Thickness	Channel ID
6x6A Assembly Class												
6x6A01	Zr	0.694	36	0.5645	0.0350	0.4940	110.0	0	n/a	n/a	0.060	4.290
6x6A02	Zr	0.694	36	0.5645	0.0360	0.4820	110.0	0	n/a	n/a	0.060	4.290
6x6A03	Zr	0.694	36	0.5645	0.0350	0.4820	110.0	0	n/a	n/a	0.060	4.290
6x6A04	Zr	0.694	36	0.5550	0.0350	0.4820	110.0	0	n/a	n/a	0.060	4.290
6x6A05	Zr	0.696	36	0.5625	0.0350	0.4820	110.0	0	n/a	n/a	0.060	4.290
6x6A06	Zr	0.696	35	0.5625	0.0350	0.4820	110.0	1	0.0	0.0	0.060	4.290
6x6A07	Zr	0.700	36	0.5555	0.03525	0.4780	110.0	0	n/a	n/a	0.060	4.290
6x6A08	Zr	0.710	36	0.5625	0.0260	0.4980	110.0	0	n/a	n/a	0.060	4.290
6x6B (MOX) Assembly Class												
6x6B01	Zr	0.694	36	0.5645	0.0350	0.4820	110.0	0	n/a	n/a	0.060	4.290
6x6B02	Zr	0.694	36	0.5625	0.0350	0.4820	110.0	0	n/a	n/a	0.060	4.290
6x6B03	Zr	0.696	36	0.5625	0.0350	0.4820	110.0	0	n/a	n/a	0.060	4.290
6x6B04	Zr	0.696	35	0.5625	0.0350	0.4820	110.0	1	0.0	0.0	0.060	4.290
6x6B05	Zr	0.710	35	0.5625	0.0350	0.4820	110.0	1	0.0	0.0	0.060	4.290
6x6C Assembly Class												
6x6C01	Zr	0.740	36	0.5630	0.0320	0.4880	77.5	0	n/a	n/a	0.060	4.542
7x7A Assembly Class												
7x7A01	Zr	0.631	49	0.4860	0.0328	0.4110	80	0	n/a	n/a	0.060	4.542

Table 6.2.1 (page 2 of 6)
BWR FUEL CHARACTERISTICS AND ASSEMBLY CLASS DEFINITIONS
(all dimensions are in inches)

Fuel Assembly Designation	Clad Material	Pitch	Number of Fuel Rods	Cladding OD	Cladding Thickness	Pellet Diameter	Active Fuel Length	Number of Water Rods	Water Rod OD	Water Rod ID	Channel Thickness	Channel ID
7x7B Assembly Class												
7x7B01	Zr	0.738	49	0.5630	0.0320	0.4870	150	0	n/a	n/a	0.080	5.278
7x7B02	Zr	0.738	49	0.5630	0.0370	0.4770	150	0	n/a	n/a	0.102	5.291
7x7B03	Zr	0.738	49	0.5630	0.0370	0.4770	150	0	n/a	n/a	0.080	5.278
7x7B04	Zr	0.738	49	0.5700	0.0355	0.4880	150	0	n/a	n/a	0.080	5.278
7x7B05	Zr	0.738	49	0.5630	0.0340	0.4775	150	0	n/a	n/a	0.080	5.278
7x7B06	Zr	0.738	49	0.5700	0.0355	0.4910	150	0	n/a	n/a	0.080	5.278
8x8A Assembly Class												
8x8A01	Zr	0.523	64	0.4120	0.0250	0.3580	110	0	n/a	n/a	0.100	4.290
8x8A02	Zr	0.523	63	0.4120	0.0250	0.3580	120	0	n/a	n/a	0.100	4.290

Table 6.2.1 (page 3 of 6)
BWR FUEL CHARACTERISTICS AND ASSEMBLY CLASS DEFINITIONS
(all dimensions are in inches)

Fuel Assembly Designation	Clad Material	Pitch	Number of Fuel Rods	Cladding OD	Cladding Thickness	Pellet Diameter	Active Fuel Length	Number of Water Rods	Water Rod OD	Water Rod ID	Channel Thickness	Channel ID
8x8B Assembly Class												
8x8B01	Zr	0.641	63	0.4840	0.0350	0.4050	150	1	0.484	0.414	0.100	5.278
8x8B02	Zr	0.636	63	0.4840	0.0350	0.4050	150	1	0.484	0.414	0.100	5.278
8x8B03	Zr	0.640	63	0.4930	0.0340	0.4160	150	1	0.493	0.425	0.100	5.278
8x8B04	Zr	0.642	64	0.5015	0.0360	0.4195	150	0	n/a	n/a	0.100	5.278
8x8C Assembly Class												
8x8C01	Zr	0.641	62	0.4840	0.0350	0.4050	150	2	0.484	0.414	0.100	5.278
8x8C02	Zr	0.640	62	0.4830	0.0320	0.4100	150	2	0.591	0.531	0.000	no channel
8x8C03	Zr	0.640	62	0.4830	0.0320	0.4100	150	2	0.591	0.531	0.080	5.278
8x8C04	Zr	0.640	62	0.4830	0.0320	0.4100	150	2	0.591	0.531	0.100	5.278
8x8C05	Zr	0.640	62	0.4830	0.0320	0.4100	150	2	0.591	0.531	0.120	5.278
8x8C06	Zr	0.640	62	0.4830	0.0320	0.4110	150	2	0.591	0.531	0.100	5.278
8x8C07	Zr	0.640	62	0.4830	0.0340	0.4100	150	2	0.591	0.531	0.100	5.278
8x8C08	Zr	0.640	62	0.4830	0.0320	0.4100	150	2	0.493	0.425	0.100	5.278
8x8C09	Zr	0.640	62	0.4930	0.0340	0.4160	150	2	0.493	0.425	0.100	5.278
8x8C10	Zr	0.640	62	0.4830	0.0340	0.4100	150	2	0.591	0.531	0.120	5.278
8x8C11	Zr	0.640	62	0.4830	0.0340	0.4100	150	2	0.591	0.531	0.120	5.215
8x8C12	Zr	0.636	62	0.4830	0.0320	0.4110	150	2	0.591	0.531	0.120	5.215

Table 6.2.1 (page 4 of 6)
BWR FUEL CHARACTERISTICS AND ASSEMBLY CLASS DEFINITIONS
(all dimensions are in inches)

Fuel Assembly Designation	Clad Material	Pitch	Number of Fuel Rods	Cladding OD	Cladding Thickness	Pellet Diameter	Active Fuel Length	Number of Water Rods	Water Rod OD	Water Rod ID	Channel Thickness	Channel ID
8x8D Assembly Class												
8x8D01	Zr	0.640	60	0.4830	0.0320	0.4110	150	2 large/ 2 small	0.591/ 0.483	0.531/ 0.433	0.100	5.278
8x8D02	Zr	0.640	60	0.4830	0.0320	0.4110	150	4	0.591	0.531	0.100	5.278
8x8D03	Zr	0.640	60	0.4830	0.0320	0.4110	150	4	0.483	0.433	0.100	5.278
8x8D04	Zr	0.640	60	0.4830	0.0320	0.4110	150	1	1.34	1.26	0.100	5.278
8x8D05	Zr	0.640	60	0.4830	0.0320	0.4100	150	1	1.34	1.26	0.100	5.278
8x8D06	Zr	0.640	60	0.4830	0.0320	0.4110	150	1	1.34	1.26	0.120	5.278
8x8D07	Zr	0.640	60	0.4830	0.0320	0.4110	150	1	1.34	1.26	0.080	5.278
8x8D08	Zr	0.640	61	0.4830	0.0300	0.4140	150	3	0.591	0.531	0.080	5.278
8x8E Assembly Class												
8x8E01	Zr	0.640	59	0.4930	0.0340	0.4160	150	5	0.493	0.425	0.100	5.278
8x8F Assembly Class												
8x8F01	Zr	0.609	64	0.4576	0.0290	0.3913	150	4†	0.291†	0.228†	0.055	5.390
9x9A Assembly Class												
9x9A01	Zr	0.566	74	0.4400	0.0280	0.3760	150	2	0.98	0.92	0.100	5.278
9x9A02	Zr	0.566	66	0.4400	0.0280	0.3760	150	2	0.98	0.92	0.100	5.278
9x9A03	Zr	0.566	74/66	0.4400	0.0280	0.3760	150/90	2	0.98	0.92	0.100	5.278
9x9A04	Zr	0.566	74/66	0.4400	0.0280	0.3760	150/90	2	0.98	0.92	0.120	5.278

† Four rectangular water cross segments dividing the assembly into four quadrants

Table 6.2.1 (page 5 of 6)
BWR FUEL CHARACTERISTICS AND ASSEMBLY CLASS DEFINITIONS
(all dimensions are in inches)

Fuel Assembly Designation	Clad Material	Pitch	Number of Fuel Rods	Cladding OD	Cladding Thickness	Pellet Diameter	Active Fuel Length	Number of Water Rods	Water Rod OD	Water Rod ID	Channel Thickness	Channel ID
9x9B Assembly Class												
9x9B01	Zr	0.569	72	0.4330	0.0262	0.3737	150	1	1.516	1.459	0.100	5.278
9x9B02	Zr	0.569	72	0.4330	0.0260	0.3737	150	1	1.516	1.459	0.100	5.278
9x9B03	Zr	0.572	72	0.4330	0.0260	0.3737	150	1	1.516	1.459	0.100	5.278
9x9C Assembly Class												
9x9C01	Zr	0.572	80	0.4230	0.0295	0.3565	150	1	0.512	0.472	0.100	5.278
9x9D Assembly Class												
9x9D01	Zr	0.572	79	0.4240	0.0300	0.3565	150	2	0.424	0.364	0.100	5.278
9x9E Assembly Class†												
9x9E01	Zr	0.572	76	0.4170	0.0265	0.3530	150	5	0.546	0.522	0.120	5.215
9x9E02	Zr	0.572	48 28	0.4170 0.4430	0.0265 0.0285	0.3530 0.3745	150	5	0.546	0.522	0.120	5.215
9x9F Assembly Class†												
9x9F01	Zr	0.572	76	0.4430	0.0285	0.3745	150	5	0.546	0.522	0.120	5.215
9x9F02	Zr	0.572	48 28	0.4170 0.4430	0.0265 0.0285	0.3530 0.3745	150	5	0.546	0.522	0.120	5.215

† The 9x9E and 9x9F fuel assembly classes represent a single fuel type containing fuel rods with different dimensions (SPC 9x9-5). In addition to the actual configuration (9x9E02 and 9x9F02), the 9x9E class contains a hypothetical assembly with only small fuel rods (9x9E01), and the 9x9F class contains a hypothetical assembly with only large rods (9x9F01). This was done in order to simplify the specification of this assembly in the CoC.

Table 6.2.1 (page 6 of 6)
BWR FUEL CHARACTERISTICS AND ASSEMBLY CLASS DEFINITIONS
(all dimensions are in inches)

Fuel Assembly Designation	Clad Material	Pitch	Number of Fuel Rods	Cladding OD	Cladding Thickness	Pellet Diameter	Active Fuel Length	Number of Water Rods	Water Rod OD	Water Rod ID	Channel Thickness	Channel ID
10x10A Assembly Class												
10x10A01	Zr	0.510	92	0.4040	0.0260	0.3450	155	2	0.980	0.920	0.100	5.278
10x10A02	Zr	0.510	78	0.4040	0.0260	0.3450	155	2	0.980	0.920	0.100	5.278
10x10A03	Zr	0.510	92/78	0.4040	0.0260	0.3450	155/90	2	0.980	0.920	0.100	5.278
10x10B Assembly Class												
10x10B01	Zr	0.510	91	0.3957	0.0239	0.3413	155	1	1.378	1.321	0.100	5.278
10x10B02	Zr	0.510	83	0.3957	0.0239	0.3413	155	1	1.378	1.321	0.100	5.278
10x10B03	Zr	0.510	91/83	0.3957	0.0239	0.3413	155/90	1	1.378	1.321	0.100	5.278
10x10C Assembly Class												
10x10C01	Zr	0.488	96	0.3780	0.0243	0.3224	150	5	1.227	1.165	0.055	5.457
10x10D Assembly Class												
10x10D01	SS	0.565	100	0.3960	0.0200	0.3500	83	0	n/a	n/a	0.08	5.663
10x10E Assembly Class												
10x10E01	SS	0.557	96	0.3940	0.0220	0.3430	83	4	0.3940	0.3500	0.08	5.663

Table 6.2.2 (page 1 of 3)
PWR FUEL CHARACTERISTICS AND ASSEMBLY CLASS DEFINITIONS
(all dimensions are in inches)

Fuel Assembly Designation	Clad Material	Pitch	Number of Fuel Rods	Cladding OD	Cladding Thickness	Pellet Diameter	Active Fuel Length	Number of Guide Tubes	Guide Tube OD	Guide Tube ID	Guide Tube Thickness
14x14A Assembly Class											
14x14A01	Zr	0.556	179	0.400	0.0243	0.3444	150	17	0.527	0.493	0.0170
14x14A02	Zr	0.556	179	0.400	0.0243	0.3444	150	17	0.528	0.490	0.0190
14x14A03	Zr	0.556	179	0.400	0.0243	0.3444	150	17	0.526	0.492	0.0170
14x14B Assembly Class											
14x14B01	Zr	0.556	179	0.422	0.0243	0.3659	150	17	0.539	0.505	0.0170
14x14B02	Zr	0.556	179	0.417	0.0295	0.3505	150	17	0.541	0.507	0.0170
14x14B03	Zr	0.556	179	0.424	0.0300	0.3565	150	17	0.541	0.507	0.0170
14x14B04	Zr	0.556	179	0.426	0.0310	0.3565	150	17	0.541	0.507	0.0170
14x14C Assembly Class											
14x14C01	Zr	0.580	176	0.440	0.0280	0.3765	150	5	1.115	1.035	0.0400
14x14C02	Zr	0.580	176	0.440	0.0280	0.3770	150	5	1.115	1.035	0.0400
14x14C03	Zr	0.580	176	0.440	0.0260	0.3805	150	5	1.111	1.035	0.0380
14x14D Assembly Class											
14x14D01	SS	0.556	180	0.422	0.0165	0.3835	144	16	0.543	0.514	0.0145
15x15A Assembly Class											
15x15A01	Zr	0.550	204	0.418	0.0260	0.3580	150	21	0.533	0.500	0.0165

Table 6.2.2 (page 2 of 3)
PWR FUEL CHARACTERISTICS AND ASSEMBLY CLASS DEFINITIONS
(all dimensions are in inches)

Fuel Assembly Designation	Clad Material	Pitch	Number of Fuel Rods	Cladding OD	Cladding Thickness	Pellet Diameter	Active Fuel Length	Number of Guide Tubes	Guide Tube OD	Guide Tube ID	Guide Tube Thickness
15x15B Assembly Class											
15x15B01	Zr	0.563	204	0.422	0.0245	0.3660	150	21	0.533	0.499	0.0170
15x15B02	Zr	0.563	204	0.422	0.0245	0.3660	150	21	0.546	0.512	0.0170
15x15B03	Zr	0.563	204	0.422	0.0243	0.3660	150	21	0.533	0.499	0.0170
15x15B04	Zr	0.563	204	0.422	0.0243	0.3659	150	21	0.545	0.515	0.0150
15x15B05	Zr	0.563	204	0.422	0.0242	0.3659	150	21	0.545	0.515	0.0150
15x15B06	Zr	0.563	204	0.420	0.0240	0.3671	150	21	0.544	0.514	0.0150
15x15C Assembly Class											
15x15C01	Zr	0.563	204	0.424	0.0300	0.3570	150	21	0.544	0.493	0.0255
15x15C02	Zr	0.563	204	0.424	0.0300	0.3570	150	21	0.544	0.511	0.0165
15x15C03	Zr	0.563	204	0.424	0.0300	0.3565	150	21	0.544	0.511	0.0165
15x15C04	Zr	0.563	204	0.417	0.0300	0.3565	150	21	0.544	0.511	0.0165
15x15D Assembly Class											
15x15D01	Zr	0.568	208	0.430	0.0265	0.3690	150	17	0.530	0.498	0.0160
15x15D02	Zr	0.568	208	0.430	0.0265	0.3686	150	17	0.530	0.498	0.0160
15x15D03	Zr	0.568	208	0.430	0.0265	0.3700	150	17	0.530	0.499	0.0155
15x15D04	Zr	0.568	208	0.430	0.0250	0.3735	150	17	0.530	0.500	0.0150
15x15E Assembly Class											
15x15E01	Zr	0.568	208	0.428	0.0245	0.3707	150	17	0.528	0.500	0.0140
15x15F Assembly Class											
15x15F01	Zr	0.568	208	0.428	0.0230	0.3742	150	17	0.528	0.500	0.0140

Table 6.2.2 (page 3 of 3)
PWR FUEL CHARACTERISTICS AND ASSEMBLY CLASS DEFINITIONS
(all dimensions are in inches)

Fuel Assembly Designation	Clad Material	Pitch	Number of Fuel Rods	Cladding OD	Cladding Thickness	Pellet Diameter	Active Fuel Length	Number of Guide Tubes	Guide Tube OD	Guide Tube ID	Guide Tube Thickness
15x15G Assembly Class											
15x15G01	SS	0.563	204	0.422	0.0165	0.3825	144	21	0.543	0.514	0.0145
15x15H Assembly Class											
15x15H01	Zr	0.568	208	0.414	0.0220	0.3622	150	17	0.528	0.500	0.0140
16x16A Assembly Class											
16x16A01	Zr	0.506	236	0.382	0.0250	0.3255	150	5	0.980	0.900	0.0400
16x16A02	Zr	0.506	236	0.382	0.0250	0.3250	150	5	0.980	0.900	0.0400
17x17A Assembly Class											
17x17A01	Zr	0.496	264	0.360	0.0225	0.3088	144	25	0.474	0.442	0.0160
17x17A02	Zr	0.496	264	0.360	0.0225	0.3088	150	25	0.474	0.442	0.0160
17x17A03	Zr	0.496	264	0.360	0.0250	0.3030	150	25	0.480	0.448	0.0160
17x17B Assembly Class											
17x17B01	Zr	0.496	264	0.374	0.0225	0.3225	150	25	0.482	0.450	0.0160
17x17B02	Zr	0.496	264	0.374	0.0225	0.3225	150	25	0.474	0.442	0.0160
17x17B03	Zr	0.496	264	0.376	0.0240	0.3215	150	25	0.480	0.448	0.0160
17x17B04	Zr	0.496	264	0.372	0.0205	0.3232	150	25	0.427	0.399	0.0140
17x17B05	Zr	0.496	264	0.374	0.0240	0.3195	150	25	0.482	0.450	0.0160
17x17B06	Zr	0.496	264	0.372	0.0205	0.3232	150	25	0.480	0.452	0.0140
17x17C Assembly Class											
17x17C01	Zr	0.502	264	0.379	0.0240	0.3232	150	25	0.472	0.432	0.0200
17x17C02	Zr	0.502	264	0.377	0.0220	0.3252	150	25	0.472	0.432	0.0200

Table 6.2.3
REACTIVITY EFFECT OF ASSEMBLY PARAMETER VARIATIONS
(all dimensions are in inches)

Fuel Assembly/ Parameter Variation	reactivity effect	calculated k_{eff}	standard deviation	cladding OD	cladding ID	cladding thickness	pellet OD	water rod thickness	channel thickness
8x8C04 (GE8x8R)	reference	0.9307	0.0007	0.483	0.419	0.032	0.410	0.030	0.100
increase pellet OD (+0.001)	+0.0005	0.9312	0.0007	0.483	0.419	0.032	0.411	0.030	0.100
decrease pellet OD (-0.001)	-0.0008	0.9299	0.0009	0.483	0.419	0.032	0.409	0.030	0.100
increase clad ID (+0.004)	+0.0027	0.9334	0.0007	0.483	0.423	0.030	0.410	0.030	0.100
decrease clad ID (-0.004)	-0.0034	0.9273	0.0007	0.483	0.415	0.034	0.410	0.030	0.100
increase clad OD (+0.004)	-0.0041	0.9266	0.0008	0.487	0.419	0.034	0.410	0.030	0.100
decrease clad OD (-0.004)	+0.0023	0.9330	0.0007	0.479	0.419	0.030	0.410	0.030	0.100
increase water rod thickness (+0.015)	-0.0019	0.9288	0.0008	0.483	0.419	0.032	0.410	0.045	0.100
decrease water rod thickness (-0.015)	+0.0001	0.9308	0.0008	0.483	0.419	0.032	0.410	0.015	0.100
remove water rods (i.e., replace the water rod tubes with water)	+0.0021	0.9328	0.0008	0.483	0.419	0.032	0.410	0.000	0.100
remove channel	-0.0039	0.9268	0.0009	0.483	0.419	0.032	0.410	0.030	0.000
increase channel thickness (+0.020)	+0.0005	0.9312	0.0007	0.483	0.419	0.032	0.410	0.030	0.120

Table 6.2.4
MAXIMUM K_{EFF} VALUES FOR THE 14X14A ASSEMBLY CLASS IN THE MPC-24
(all dimensions are in inches)

14x14A (4.6% Enrichment, Boral ^{10}B minimum loading of 0.02 g/cm^2) 179 fuel rods, 17 guide tubes, pitch=0.556, Zr clad									
Fuel Assembly Designation	maximum k_{eff}	calculated k_{eff}	standard deviation	cladding OD	cladding ID	cladding thickness	pellet OD	fuel length	guide tube thickness
14x14A01	0.9295	0.9252	0.0008	0.400	0.3514	0.0243	0.3444	150	0.017
14x14A02	0.9286	0.9242	0.0009	0.400	0.3514	0.0243	0.3444	150	0.019
14x14A03	0.9296	0.9253	0.0008	0.400	0.3514	0.0243	0.3444	150	0.017
Dimensions Listed in Certificate of Compliance				0.400 (min.)	0.3514 (max.)		0.3444 (max.)	150 (max.)	0.017 (min.)
bounding dimensions (14x14A03)	0.9296	0.9253	0.0008	0.400	0.3514	0.0243	0.3444	150	0.017

Table 6.2.5
MAXIMUM K_{EFF} VALUES FOR THE 14X14B ASSEMBLY CLASS IN THE MPC-24
(all dimensions are in inches)

14x14B (4.6% Enrichment, Boral ^{10}B minimum loading of 0.02 g/cm^2) 179 fuel rods, 17 guide tubes, pitch=0.556, Zr clad									
Fuel Assembly Designation	maximum k_{eff}	calculated k_{eff}	standard deviation	cladding OD	cladding ID	cladding thickness	pellet OD	fuel length	guide tube thickness
14x14B01	0.9159	0.9117	0.0007	0.422	0.3734	0.0243	0.3659	150	0.017
14x14B02	0.9169	0.9126	0.0008	0.417	0.3580	0.0295	0.3505	150	0.017
14x14B03	0.9110	0.9065	0.0009	0.424	0.3640	0.0300	0.3565	150	0.017
14x14B04	0.9084	0.9039	0.0009	0.426	0.3640	0.0310	0.3565	150	0.017
Dimensions Listed in Certificate of Compliance				0.417 (min.)	0.3734 (max.)		0.3659 (max.)	150 (max.)	0.017 (min.)
bounding dimensions (B14x14B01)	0.9228	0.9185	0.0008	0.417	0.3734	0.0218	0.3659	150	0.017

Table 6.2.6
MAXIMUM K_{EFF} VALUES FOR THE 14X14C ASSEMBLY CLASS IN THE MPC-24
(all dimensions are in inches)

14x14C (4.6% Enrichment, Boral ^{10}B minimum loading of 0.02 g/cm^2) 176 fuel rods, 5 guide tubes, pitch=0.580, Zr clad									
Fuel Assembly Designation	maximum k_{eff}	calculated k_{eff}	standard deviation	cladding OD	cladding ID	cladding thickness	pellet OD	fuel length	guide tube thickness
14x14C01	0.9258	0.9215	0.0008	0.440	0.3840	0.0280	0.3765	150	0.040
14x14C02	0.9265	0.9222	0.0008	0.440	0.3840	0.0280	0.3770	150	0.040
14x14C03	0.9287	0.9242	0.0009	0.440	0.3880	0.0260	0.3805	150	0.038
Dimensions Listed in Certificate of Compliance				0.440 (min.)	0.3880 (max.)		0.3805 (max.)	150 (max.)	0.038 (min.)
bounding dimensions (14x14C01)	0.9287	0.9242	0.0009	0.440	0.3880	0.0260	0.3805	150	0.038

Table 6.2.7
MAXIMUM K_{EFF} VALUES FOR THE 14X14D ASSEMBLY CLASS IN THE MPC-24
(all dimensions are in inches)

14x14D (4.0% Enrichment, Boral ^{10}B minimum loading of 0.02 g/cm^2) 180 fuel rods, 16 guide tubes, pitch=0.556, SS clad									
Fuel Assembly Designation	maximum k_{eff}	calculated k_{eff}	standard deviation	cladding OD	cladding ID	cladding thickness	pellet OD	fuel length	guide tube thickness
14x14D01	0.8507	0.8464	0.0008	0.422	0.3890	0.0165	0.3835	144	0.0145
Dimensions Listed in Certificate of Compliance				0.422 (min.)	0.3890 (max.)		0.3835 (max.)	144 (max.)	0.0145 (min.)

Table 6.2.8
MAXIMUM K_{EFF} VALUES FOR THE 15X15A ASSEMBLY CLASS IN THE MPC-24
(all dimensions are in inches)

15x15A (4.1% Enrichment, Boral ^{10}B minimum loading of 0.02 g/cm^2) 204 fuel rods, 21 guide tubes, pitch=0.550, Zr clad									
Fuel Assembly Designation	maximum k_{eff}	calculated k_{eff}	standard deviation	cladding OD	cladding ID	cladding thickness	pellet OD	fuel length	guide tube thickness
15x15A01	0.9204	0.9159	0.0009	0.418	0.3660	0.0260	0.3580	150	0.0165
Dimensions Listed in Certificate of Compliance				0.418 (min.)	0.3660 (max.)		0.3580 (max.)	150 (max.)	0.0165 (min.)

Table 6.2.9
MAXIMUM K_{EFF} VALUES FOR THE 15X15B ASSEMBLY CLASS IN THE MPC-24
(all dimensions are in inches)

15x15B (4.1% Enrichment, Boral ^{10}B minimum loading of 0.02 g/cm^2) 204 fuel rods, 21 guide tubes, pitch=0.563, Zr clad									
Fuel Assembly Designation	maximum k_{eff}	calculated k_{eff}	standard deviation	cladding OD	cladding ID	cladding thickness	pellet OD	fuel length	guide tube thickness
15x15B01	0.9369	0.9326	0.0008	0.422	0.3730	0.0245	0.3660	150	0.017
15x15B02	0.9338	0.9295	0.0008	0.422	0.3730	0.0245	0.3660	150	0.017
15x15B03	0.9362	0.9318	0.0008	0.422	0.3734	0.0243	0.3660	150	0.017
15x15B04	0.9370	0.9327	0.0008	0.422	0.3734	0.0243	0.3659	150	0.015
15x15B05	0.9356	0.9313	0.0008	0.422	0.3736	0.0242	0.3659	150	0.015
15x15B06	0.9366	0.9324	0.0007	0.420	0.3720	0.0240	0.3671	150	0.015
Dimensions Listed in Certificate of Compliance				0.420 (min.)	0.3736 (max.)		0.3671 (max.)	150 (max.)	0.015 (min.)
bounding dimensions (B15x15B01)	0.9388	0.9343	0.0009	0.420	0.3736	0.0232	0.3671	150	0.015

Table 6.2.10
MAXIMUM K_{EFF} VALUES FOR THE 15X15C ASSEMBLY CLASS IN THE MPC-24
(all dimensions are in inches)

15x15C (4.1% Enrichment, Boral ^{10}B minimum loading of 0.02 g/cm^2) 204 fuel rods, 21 guide tubes, pitch=0.563, Zr clad									
Fuel Assembly Designation	maximum k_{eff}	calculated k_{eff}	standard deviation	cladding OD	cladding ID	cladding thickness	pellet OD	fuel length	guide tube thickness
15x15C01	0.9255	0.9213	0.0007	0.424	0.3640	0.0300	0.3570	150	0.0255
15x15C02	0.9297	0.9255	0.0007	0.424	0.3640	0.0300	0.3570	150	0.0165
15x15C03	0.9297	0.9255	0.0007	0.424	0.3640	0.0300	0.3565	150	0.0165
15x15C04	0.9311	0.9268	0.0008	0.417	0.3570	0.0300	0.3565	150	0.0165
Dimensions Listed in Certificate of Compliance				0.417 (min.)	0.3640 (max.)		0.3570 (max.)	150 (max.)	0.0165 (min.)
bounding dimensions (B15x15C01)	0.9361	0.9316	0.0009	0.417	0.3640	0.0265	0.3570	150	0.0165

Table 6.2.11
MAXIMUM K_{EFF} VALUES FOR THE 15X15D ASSEMBLY CLASS IN THE MPC-24
(all dimensions are in inches)

15x15D (4.1% Enrichment, Boral ^{10}B minimum loading of 0.02 g/cm^2) 208 fuel rods, 17 guide tubes, pitch=0.568, Zr clad									
Fuel Assembly Designation	maximum k_{eff}	calculated k_{eff}	standard deviation	cladding OD	cladding ID	cladding thickness	pellet OD	fuel length	guide tube thickness
15x15D01	0.9341	0.9298	0.0008	0.430	0.3770	0.0265	0.3690	150	0.0160
15x15D02	0.9367	0.9324	0.0008	0.430	0.3770	0.0265	0.3686	150	0.0160
15x15D03	0.9354	0.9311	0.0008	0.430	0.3770	0.0265	0.3700	150	0.0155
15x15D04	0.9339	0.9292	0.0010	0.430	0.3800	0.0250	0.3735	150	0.0150
Dimensions Listed in Certificate of Compliance				0.430 (min.)	0.3800 (max.)		0.3735 (max.)	150 (max.)	0.0150 (min.)
bounding dimensions (15x15D04)	0.9339†	0.9292	0.0010	0.430	0.3800	0.0250	0.3735	150	0.0150

† The k_{eff} value listed for the 15x15D02 case is higher than that for the case with the bounding dimensions. Therefore, the 0.9367 value from case 15x15D02 is listed in Table 6.1.1 as the maximum.

Table 6.2.12
MAXIMUM K_{EFF} VALUES FOR THE 15X15E ASSEMBLY CLASS IN THE MPC-24
(all dimensions are in inches)

15x15E (4.1% Enrichment, Boral ^{10}B minimum loading of 0.02 g/cm^2) 208 fuel rods, 17 guide tubes, pitch=0.568, Zr clad									
Fuel Assembly Designation	maximum k_{eff}	calculated k_{eff}	standard deviation	cladding OD	cladding ID	cladding thickness	pellet OD	fuel length	guide tube thickness
15x15E01	0.9368	0.9325	0.0008	0.428	0.3790	0.0245	0.3707	150	0.0140
Dimensions Listed in Certificate of Compliance				0.428 (min.)	0.3790 (max.)		0.3707 (max.)	150 (max.)	0.0140 (min.)

Table 6.2.13
MAXIMUM K_{EFF} VALUES FOR THE 15X15F ASSEMBLY CLASS IN THE MPC-24
(all dimensions are in inches)

15x15F (4.1% Enrichment, Boral ^{10}B minimum loading of 0.02 g/cm^2) 208 fuel rods, 17 guide tubes, pitch=0.568, Zr clad									
Fuel Assembly Designation	maximum k_{eff}	calculated k_{eff}	standard deviation	cladding OD	cladding ID	cladding thickness	pellet OD	fuel length	guide tube thickness
15x15F01	0.9395[†]	0.9350	0.0009	0.428	0.3820	0.0230	0.3742	150	0.0140
Dimensions Listed in Certificate of Compliance				0.428 (min.)	0.3820 (max.)		0.3742 (max.)	150 (max.)	0.0140 (min.)

[†] KENO5a verification calculation resulted in a maximum k_{eff} of 0.9383.

Table 6.2.14
MAXIMUM K_{EFF} VALUES FOR THE 15X15G ASSEMBLY CLASS IN THE MPC-24
(all dimensions are in inches)

15x15G (4.0% Enrichment, Boral ^{10}B minimum loading of 0.02 g/cm^2) 204 fuel rods, 21 guide tubes, pitch=0.563, SS clad									
Fuel Assembly Designation	maximum k_{eff}	calculated k_{eff}	standard deviation	cladding OD	cladding ID	cladding thickness	pellet OD	fuel length	guide tube thickness
15x15G01	0.8876	0.8833	0.0008	0.422	0.3890	0.0165	0.3825	144	0.0145
Dimensions Listed in Certificate of Compliance				0.422 (min.)	0.3890 (max.)		0.3825 (max.)	144 (max.)	0.0145 (min.)

Table 6.2.15
MAXIMUM K_{EFF} VALUES FOR THE 15X15H ASSEMBLY CLASS IN THE MPC-24
(all dimensions are in inches)

15x15H (3.8% Enrichment, Boral ^{10}B minimum loading of 0.02 g/cm^2) 208 fuel rods, 17 guide tubes, pitch=0.568, Zr clad									
Fuel Assembly Designation	maximum k_{eff}	calculated k_{eff}	standard deviation	cladding OD	cladding ID	cladding thickness	pellet OD	fuel length	guide tube thickness
15x15H01	0.9337	0.9292	0.0009	0.414	0.3700	0.0220	0.3622	150	0.0140
Dimensions Listed in Certificate of Compliance				0.414 (min.)	0.3700 (max.)		0.3622 (max.)	150 (max.)	0.0140 (min.)

Table 6.2.16
MAXIMUM K_{EFF} VALUES FOR THE 16X16A ASSEMBLY CLASS IN THE MPC-24
(all dimensions are in inches)

16x16A (4.6% Enrichment, Boral ^{10}B minimum loading of 0.02 g/cm^2) 236 fuel rods, 5 guide tubes, pitch=0.506, Zr clad									
Fuel Assembly Designation	maximum k_{eff}	calculated k_{eff}	standard deviation	cladding OD	cladding ID	cladding thickness	pellet OD	fuel length	guide tube thickness
16x16A01	0.9287	0.9244	0.0008	0.382	0.3320	0.0250	0.3255	150	0.0400
16x16A02	0.9263	0.9221	0.0007	0.382	0.3320	0.0250	0.3250	150	0.0400
Dimensions Listed in Certificate of Compliance				0.382 (min.)	0.3320 (max.)		0.3255 (max.)	150 (max.)	0.0400 (min.)
bounding dimensions (16x16A01)	0.9287	0.9244	0.0008	0.382	0.3320	0.0250	0.3255	150	0.0400

Table 6.2.17
MAXIMUM K_{EFF} VALUES FOR THE 17X17A ASSEMBLY CLASS IN THE MPC-24
(all dimensions are in inches)

17x17A (4.0% Enrichment, Boral ^{10}B minimum loading of 0.02 g/cm^2) 264 fuel rods, 25 guide tubes, pitch=0.496, Zr clad									
Fuel Assembly Designation	maximum k_{eff}	calculated k_{eff}	standard deviation	cladding OD	cladding ID	cladding thickness	pellet OD	fuel length	guide tube thickness
17x17A01	0.9368	0.9325	0.0008	0.360	0.3150	0.0225	0.3088	144	0.016
17x17A02	0.9368	0.9325	0.0008	0.360	0.3150	0.0225	0.3088	150	0.016
17x17A03	0.9329	0.9286	0.0008	0.360	0.3100	0.0250	0.3030	150	0.016
Dimensions Listed in Certificate of Compliance				0.360 (min.)	0.3150 (max.)		0.3088 (max.)	150 (max.)	0.016 (min.)
bounding dimensions (17x17A02)	0.9368	0.9325	0.0008	0.360	0.3150	0.0225	0.3088	150	0.016

Table 6.2.18
MAXIMUM K_{EFF} VALUES FOR THE 17X17B ASSEMBLY CLASS IN THE MPC-24
(all dimensions are in inches)

17x17B (4.0% Enrichment, Boral ^{10}B minimum loading of 0.02 g/cm^2) 264 fuel rods, 25 guide tubes, pitch=0.496, Zr clad									
Fuel Assembly Designation	maximum k_{eff}	calculated k_{eff}	standard deviation	cladding OD	cladding ID	cladding thickness	pellet OD	fuel length	guide tube thickness
17x17B01	0.9288	0.9243	0.0009	0.374	0.3290	0.0225	0.3225	150	0.016
17x17B02	0.9290	0.9247	0.0008	0.374	0.3290	0.0225	0.3225	150	0.016
17x17B03	0.9243	0.9199	0.0008	0.376	0.3280	0.0240	0.3215	150	0.016
17x17B04	0.9324	0.9279	0.0009	0.372	0.3310	0.0205	0.3232	150	0.014
17x17B05	0.9266	0.9222	0.0008	0.374	0.3260	0.0240	0.3195	150	0.016
17x17B06	0.9311	0.9268	0.0008	0.372	0.3310	0.0205	0.3232	150	0.014
Dimensions Listed in Certificate of Compliance				0.372 (min.)	0.3310 (max.)		0.3232 (max.)	150 (max.)	0.014 (min.)
bounding dimensions (17x17B06)	0.9311†	0.9268	0.0008	0.372	0.3310	0.0205	0.3232	150	0.014

† The k_{eff} value listed for the 17x17B04 case is higher than that for the case with the bounding dimensions. Therefore, the 0.9324 value from case 17x17B04 is listed in Table 6.1.1 as the maximum.

Table 6.2.19
MAXIMUM K_{EFF} VALUES FOR THE 17X17C ASSEMBLY CLASS IN THE MPC-24
(all dimensions are in inches)

17x17C (4.0% Enrichment, Boral ^{10}B minimum loading of 0.02 g/cm^2) 264 fuel rods, 25 guide tubes, pitch=0.502, Zr clad									
Fuel Assembly Designation	maximum k_{eff}	calculated k_{eff}	standard deviation	cladding OD	cladding ID	cladding thickness	pellet OD	fuel length	guide tube thickness
17x17C01	0.9293	0.9250	0.0008	0.379	0.3310	0.0240	0.3232	150	0.020
17x17C02	0.9336	0.9293	0.0008	0.377	0.3330	0.0220	0.3252	150	0.020
Dimensions Listed in Certificate of Compliance				0.377 (min.)	0.3330 (max.)		0.3252 (max.)	150 (max.)	0.020 (min.)
bounding dimensions (17x17C02)	0.9336	0.9293	0.0008	0.377	0.3330	0.0220	0.3252	150	0.020

Table 6.2.20
MAXIMUM K_{EFF} VALUES FOR THE 7X7B ASSEMBLY CLASS IN THE MPC-68
(all dimensions are in inches)

7x7B (4.2% Enrichment, Boral ^{10}B minimum loading of 0.0279 g/cm^2) 49 fuel rods, 0 water rods, pitch=0.738, Zr clad										
Fuel Assembly Designation	maximum k_{eff}	calculated k_{eff}	standard deviation	cladding OD	cladding ID	cladding thickness	pellet OD	fuel length	water rod thickness	channel thickness
7x7B01	0.9372	0.9330	0.0007	0.5630	0.4990	0.0320	0.4870	150	n/a	0.080
7x7B02	0.9301	0.9260	0.0007	0.5630	0.4890	0.0370	0.4770	150	n/a	0.102
7x7B03	0.9313	0.9271	0.0008	0.5630	0.4890	0.0370	0.4770	150	n/a	0.080
7x7B04	0.9311	0.9270	0.0007	0.5700	0.4990	0.0355	0.4880	150	n/a	0.080
7x7B05	0.9350	0.9306	0.0008	0.5630	0.4950	0.0340	0.4775	150	n/a	0.080
7x7B06	0.9298	0.9260	0.0006	0.5700	0.4990	0.0355	0.4910	150	n/a	0.080
Dimensions Listed in Certificate of Compliance				0.5630 (min.)	0.4990 (max.)		0.4910 (max.)	150 (max.)	n/a	0.120 (max.)
bounding dimensions (B7x7B01)	0.9375	0.9332	0.0008	0.5630	0.4990	0.0320	0.4910	150	n/a	0.102
bounding dimensions with 120 mil channel (B7x7B02)	0.9386	0.9344	0.0007	0.5630	0.4990	0.0320	0.4910	150	n/a	0.120

Table 6.2.21
MAXIMUM K_{EFF} VALUES FOR THE 8X8B ASSEMBLY CLASS IN THE MPC-68
(all dimensions are in inches)

8x8B (4.2% Enrichment, Boral ^{10}B minimum loading of 0.0279 g/cm^2) 63 or 64 fuel rods†, 1 or 0 water rods†, pitch† = 0.636-0.642, Zr clad												
Fuel Assembly Designation	maximum k_{eff}	calculated k_{eff}	standard deviation	Fuel rods	pitch	cladding OD	cladding ID	cladding thickness	pellet OD	fuel length	water rod thickness	channel thickness
8x8B01	0.9310	0.9265	0.0009	63	0.641	0.4840	0.4140	0.0350	0.4050	150	0.035	0.100
8x8B02	0.9227	0.9185	0.0007	63	0.636	0.4840	0.4140	0.0350	0.4050	150	0.035	0.100
8x8B03	0.9299	0.9257	0.0008	63	0.640	0.4930	0.4250	0.0340	0.4160	150	0.034	0.100
8x8B04	0.9236	0.9194	0.0008	64	0.642	0.5015	0.4295	0.0360	0.4195	150	n/a	0.100
Dimensions Listed in Certificate of Compliance				63 or 64	0.636-0.642	0.4840 (min.)	0.4295 (max.)		0.4195 (max.)	150 (max.)	0.034	0.120 (max.)
bounding (pitch=0.636) (B8x8B01)	0.9346	0.9301	0.0009	63	0.636	0.4840	0.4295	0.02725	0.4195	150	0.034	0.120
bounding (pitch=0.640) (B8x8B02)	0.9385	0.9343	0.0008	63	0.640	0.4840	0.4295	0.02725	0.4195	150	0.034	0.120
bounding (pitch=0.642) (B8x8B03)	0.9416	0.9375	0.0007	63	0.642	0.4840	0.4295	0.02725	0.4195	150	0.034	0.120

† This assembly class was analyzed and qualified for a small variation in the pitch and a variation in the number of fuel and water rods.

Table 6.2.22
MAXIMUM K_{EFF} VALUES FOR THE 8X8C ASSEMBLY CLASS IN THE MPC-68
(all dimensions are in inches)

8x8C (4.2% Enrichment, Boral ^{10}B minimum loading of 0.0279 g/cm^2) 62 fuel rods, 2 water rods, pitch† = 0.636-0.641, Zr clad											
Fuel Assembly Designation	maximum k_{eff}	calculated k_{eff}	standard deviation	pitch	cladding OD	cladding ID	cladding thickness	pellet OD	fuel length	water rod thickness	channel thickness
8x8C01	0.9315	0.9273	0.0007	0.641	0.4840	0.4140	0.0350	0.4050	150	0.035	0.100
8x8C02	0.9313	0.9268	0.0009	0.640	0.4830	0.4190	0.0320	0.4100	150	0.030	0.000
8x8C03	0.9329	0.9286	0.0008	0.640	0.4830	0.4190	0.0320	0.4100	150	0.030	0.800
8x8C04	0.9348††	0.9307	0.0007	0.640	0.4830	0.4190	0.0320	0.4100	150	0.030	0.100
8x8C05	0.9353	0.9312	0.0007	0.640	0.4830	0.4190	0.0320	0.4100	150	0.030	0.120
8x8C06	0.9353	0.9312	0.0007	0.640	0.4830	0.4190	0.0320	0.4110	150	0.030	0.100
8x8C07	0.9314	0.9273	0.0007	0.640	0.4830	0.4150	0.0340	0.4100	150	0.030	0.100
8x8C08	0.9339	0.9298	0.0007	0.640	0.4830	0.4190	0.0320	0.4100	150	0.034	0.100
8x8C09	0.9301	0.9260	0.0007	0.640	0.4930	0.4250	0.0340	0.4160	150	0.034	0.100
8x8C10	0.9317	0.9275	0.0008	0.640	0.4830	0.4150	0.0340	0.4100	150	0.030	0.120
8x8C11	0.9328	0.9287	0.0007	0.640	0.4830	0.4150	0.0340	0.4100	150	0.030	0.120
8x8C12	0.9285	0.9242	0.0008	0.636	0.4830	0.4190	0.0320	0.4110	150	0.030	0.120
Dimensions Listed in Certificate of Compliance				0.636-0.641	0.4830 (min.)	0.4250 (max.)		0.4160 (max.)	150 (max.)	0.000 (min.)	0.120 (max.)
bounding (pitch=0.636) (B8x8C01)	0.9357	0.9313	0.0009	0.636	0.4830	0.4250	0.0290	0.4160	150	0.000	0.120
bounding (pitch=0.640) (B8x8C02)	0.9425	0.9384	0.0007	0.640	0.4830	0.4250	0.0290	0.4160	150	0.000	0.120
Bounding (pitch=0.641) (B8x8C03)	0.9418	0.9375	0.0008	0.641	0.4830	0.4250	0.0290	0.4160	150	0.000	0.120

† This assembly class was analyzed and qualified for a small variation in the pitch.
†† KENO5a verification calculation resulted in a maximum k_{eff} of 0.9343.

Table 6.2.23
MAXIMUM K_{EFF} VALUES FOR THE 8X8D ASSEMBLY CLASS IN THE MPC-68
(all dimensions are in inches)

8x8D (4.2% Enrichment, Boral ^{10}B minimum loading of 0.0279 g/cm^2) 60-61 fuel rods, 1-4 water rods†, pitch=0.640, Zr clad										
Fuel Assembly Designation	maximum k_{eff}	calculated k_{eff}	standard deviation	cladding OD	cladding ID	cladding thickness	pellet OD	fuel length	water rod thickness	channel thickness
8x8D01	0.9342	0.9302	0.0006	0.4830	0.4190	0.0320	0.4110	150	0.03/0.025	0.100
8x8D02	0.9325	0.9284	0.0007	0.4830	0.4190	0.0320	0.4110	150	0.030	0.100
8x8D03	0.9351	0.9309	0.0008	0.4830	0.4190	0.0320	0.4110	150	0.025	0.100
8x8D04	0.9338	0.9296	0.0007	0.4830	0.4190	0.0320	0.4110	150	0.040	0.100
8x8D05	0.9339	0.9294	0.0009	0.4830	0.4190	0.0320	0.4100	150	0.040	0.100
8x8D06	0.9365	0.9324	0.0007	0.4830	0.4190	0.0320	0.4110	150	0.040	0.120
8x8D07	0.9341	0.9297	0.0009	0.4830	0.4190	0.0320	0.4110	150	0.040	0.080
8x8D08	0.9376	0.9332	0.0009	0.4830	0.4230	0.0300	0.4140	150	0.030	0.080
Dimensions Listed in Certificate of Compliance				0.4830 (min.)	0.4230 (max.)		0.4140 (max.)	150 (max.)	0.000 (min.)	0.120 (max.)
bounding dimensions (B8x8D01)	0.9403	0.9363	0.0007	0.4830	0.4230	0.0300	0.4140	150	0.000	0.120

† Fuel assemblies 8x8D01 through 8x8D03 have 4 water rods that are similar in size to the fuel rods, while assemblies 8x8D04 through 8x8D07 have 1 large water rod that takes the place of the 4 water rods. Fuel assembly 8x8D08 contains 3 water rods that are similar in size to the fuel rods.

Table 6.2.24
MAXIMUM K_{EFF} VALUES FOR THE 8X8E ASSEMBLY CLASS IN THE MPC-68
(all dimensions are in inches)

8x8E (4.2% Enrichment, Boral ^{10}B minimum loading of 0.0279 g/cm^2) 59 fuel rods, 5 water rods, pitch=0.640, Zr clad										
Fuel Assembly Designation	maximum k_{eff}	calculated k_{eff}	standard deviation	cladding OD	cladding ID	cladding thickness	pellet OD	fuel length	water rod thickness	channel thickness
8x8E01	0.9312	0.9270	0.0008	0.4930	0.4250	0.0340	0.4160	150	0.034	0.100
Dimensions Listed in Certificate of Compliance				0.4930 (min.)	0.4250 (max.)		0.4160 (max.)	150 (max.)	0.034 (min.)	0.100 (max.)

Table 6.2.25
MAXIMUM K_{EFF} VALUES FOR THE 8X8F ASSEMBLY CLASS IN THE MPC-68
(all dimensions are in inches)

8x8F (3.6% Enrichment, Boral ^{10}B minimum loading of 0.0279 g/cm^2) 64 fuel rods, 4 rectangular water cross segments dividing the assembly into four quadrants, pitch=0.609, Zr clad										
Fuel Assembly Designation	maximum k_{eff}	calculated k_{eff}	standard deviation	cladding OD	cladding ID	cladding thickness	pellet OD	fuel length	water rod thickness	channel thickness
8x8F01	0.9153	0.9111	0.0007	0.4576	0.3996	0.0290	0.3913	150	0.0315	0.055
Dimensions Listed in Certificate of Compliance				0.4576 (min.)	0.3996 (max.)		0.3913 (max.)	150 (max.)	0.0315 (min.)	0.055 (max.)

Table 6.2.26
MAXIMUM K_{EFF} VALUES FOR THE 9X9A ASSEMBLY CLASS IN THE MPC-68
(all dimensions are in inches)

9x9A (4.2% Enrichment, Boral ^{10}B minimum loading of 0.0279 g/cm^2) 74/66 fuel rods†, 2 water rods, pitch=0.566, Zr clad										
Fuel Assembly Designation	maximum k_{eff}	calculated k_{eff}	standard deviation	cladding OD	cladding ID	cladding thickness	pellet OD	fuel length	water rod thickness	channel thickness
9x9A01 (axial segment with all rods)	0.9353	0.9310	0.0008	0.4400	0.3840	0.0280	0.3760	150	0.030	0.100
9x9A02 (axial segment with only the full length rods)	0.9388	0.9345	0.0008	0.4400	0.3840	0.0280	0.3760	150	0.030	0.100
9x9A03 (actual three-dimensional representation of all rods)	0.9351	0.9310	0.0007	0.4400	0.3840	0.0280	0.3760	150/90	0.030	0.100
9x9A04 (axial segment with only the full length rods)	0.9396	0.9355	0.0007	0.4400	0.3840	0.0280	0.3760	150	0.030	0.120
Dimensions Listed in Certificate of Compliance				0.4400 (min.)	0.3840 (max.)		0.3760 (max.)	150 (max.)	0.000 (min.)	0.120 (max.)
bounding dimensions (axial segment with only the full length rods) (B9x9A01)	0.9417	0.9374	0.0008	0.4400	0.3840	0.0280	0.3760	150	0.000	0.120

† This assembly class contains 66 full length rods and 8 partial length rods. In order to eliminate a requirement on the length of the partial length rods, separate calculations were performed for the axial segments with and without the partial length rods.

Table 6.2.27
MAXIMUM K_{EFF} VALUES FOR THE 9X9B ASSEMBLY CLASS IN THE MPC-68
(all dimensions are in inches)

9x9B (4.2% Enrichment, Boral ^{10}B minimum loading of 0.0279 g/cm^2) 72 fuel rods, 1 water rod (square, replacing 9 fuel rods), pitch=0.569 to 0.572†, Zr clad											
Fuel Assembly Designation	maximum k_{eff}	calculated k_{eff}	standard deviation	pitch	cladding OD	cladding ID	cladding thickness	pellet OD	fuel length	water rod thickness	channel thickness
9x9B01	0.9380	0.9336	0.0008	0.569	0.4330	0.3807	0.0262	0.3737	150	0.0285	0.100
9x9B02	0.9373	0.9329	0.0009	0.569	0.4330	0.3810	0.0260	0.3737	150	0.0285	0.100
9x9B03	0.9417	0.9374	0.0008	0.572	0.4330	0.3810	0.0260	0.3737	150	0.0285	0.100
Dimensions Listed in Certificate of Compliance				0.572	0.4330 (min.)	0.3810 (max.)		0.3740 (max.)	150 (max.)	0.000 (min.)	0.120 (max.)
bounding dimensions (B9x9B01)	0.9436	0.9394	0.0008	0.572	0.4330	0.3810	0.0260	0.3740††	150	0.000	0.120

† This assembly class was analyzed and qualified for a small variation in the pitch.
†† This value was conservatively defined to be larger than any of the actual pellet diameters.

Table 6.2.28
MAXIMUM K_{EFF} VALUES FOR THE 9X9C ASSEMBLY CLASS IN THE MPC-68
(all dimensions are in inches)

9x9C (4.2% Enrichment, Boral ^{10}B minimum loading of 0.0279 g/cm^2) 80 fuel rods, 1 water rods, pitch=0.572, Zr clad										
Fuel Assembly Designation	maximum k_{eff}	calculated k_{eff}	standard deviation	cladding OD	cladding ID	cladding thickness	pellet OD	fuel length	water rod thickness	channel thickness
9x9C01	0.9395	0.9352	0.0008	0.4230	0.3640	0.0295	0.3565	150	0.020	0.100
Dimensions Listed in Certificate of Compliance				0.4230 (min.)	0.3640 (max.)		0.3565 (max.)	150 (max.)	0.020 (min.)	0.100 (max.)

Table 6.2.29
MAXIMUM K_{EFF} VALUES FOR THE 9X9D ASSEMBLY CLASS IN THE MPC-68
(all dimensions are in inches)

9x9D (4.2% Enrichment, Boral ^{10}B minimum loading of 0.0279 g/cm^2) 79 fuel rods, 2 water rods, pitch=0.572, Zr clad										
Fuel Assembly Designation	maximum k_{eff}	calculated k_{eff}	standard deviation	cladding OD	cladding ID	cladding thickness	pellet OD	fuel length	water rod thickness	channel thickness
9x9D01	0.9394	0.9350	0.0009	0.4240	0.3640	0.0300	0.3565	150	0.0300	0.100
Dimensions Listed in Certificate of Compliance				0.4240 (min.)	0.3640 (max.)		0.3565 (max.)	150 (max.)	0.0300 (min.)	0.100 (max.)

Table 6.2.30
MAXIMUM K_{EFF} VALUES FOR THE 9X9E ASSEMBLY CLASS IN THE MPC-68
(all dimensions are in inches)

9x9E (4.1% Enrichment, Boral ^{10}B minimum loading of 0.0279 g/cm^2) 76 fuel rods, 5 water rods, pitch=0.572, Zr clad										
Fuel Assembly Designation	maximum k_{eff}	calculated k_{eff}	standard deviation	cladding OD	cladding ID	cladding thickness	pellet OD	fuel length	water rod thickness	channel thickness
9x9E01	0.9402	0.9359	0.0008	0.4170	0.3640	0.0265	0.3530	150	0.0120	0.120
9x9E02	0.9424	0.9380	0.0008	0.4170 0.4430	0.3640 0.3860	0.0265 0.0285	0.3530 0.3745	150	0.0120	0.120
Dimensions Listed in Certificate of Compliance†				0.4170 (min.)	0.3640 (max.)		0.3530 (max.)	150 (max.)	0.0120 (min.)	0.120 (max.)
bounding dimensions (9x9E02)	0.9424	0.9380	0.0008	0.4170 0.4430	0.3640 0.3860	0.0265 0.0285	0.3530 0.3745	150	0.0120	0.120

† This fuel assembly, also known as SPC 9x9-5, contains fuel rods with different cladding and pellet diameters which do not bound each other. To be consistent in the way fuel assemblies are listed in the Certificate of Compliance, two assembly classes (9x9E and 9x9F) are required to specify this assembly. Each class contains the actual geometry (9x9E02 and 9x9F02), as well as a hypothetical geometry with either all small rods (9x9E01) or all large rods (9x9F01). The Certificate of Compliance lists the small rod dimensions for class 9x9E and the large rod dimensions for class 9x9F, and a note that both classes are used to qualify the assembly. The analyses demonstrate that all configurations, including the actual geometry, are acceptable.

Table 6.2.31
MAXIMUM K_{EFF} VALUES FOR THE 9X9F ASSEMBLY CLASS IN THE MPC-68
(all dimensions are in inches)

9x9F (4.1% Enrichment, Boral ^{10}B minimum loading of 0.0279 g/cm^2) 76 fuel rods, 5 water rods, pitch=0.572, Zr clad										
Fuel Assembly Designation	maximum k_{eff}	calculated k_{eff}	standard deviation	cladding OD	cladding ID	cladding thickness	pellet OD	fuel length	water rod thickness	channel thickness
9x9F01	0.9369	0.9326	0.0007	0.4430	0.3860	0.0285	0.3745	150	0.0120	0.120
9x9F02	0.9424	0.9380	0.0008	0.4170 0.4430	0.3640 0.3860	0.0265 0.0285	0.3530 0.3745	150	0.0120	0.120
Dimensions Listed in Certificate of Compliance†				0.4430 (min.)	0.3860 (max.)		0.3745 (max.)	150 (max.)	0.0120 (min.)	0.120 (max.)
bounding dimensions (9x9F02)	0.9424	0.9380	0.0008	0.4170 0.4430	0.3640 0.3860	0.0265 0.0285	0.3530 0.3745	150	0.0120	0.120

† This fuel assembly, also known as SPC 9x9-5, contains fuel rods with different cladding and pellet diameters which do not bound each other. To be consistent in the way fuel assemblies are listed in the Certificate of Compliance, two assembly classes (9x9E and 9x9F) are required to specify this assembly. Each class contains the actual geometry (9x9E02 and 9x9F02), as well as a hypothetical geometry with either all small rods (9x9E01) or all large rods (9x9F01). The Certificate of Compliance lists the small rod dimensions for class 9x9E and the large rod dimensions for class 9x9F, and a note that both classes are used to qualify the assembly. The analyses demonstrate that all configurations, including the actual geometry, are acceptable.

Table 6.2.32
MAXIMUM K_{EFF} VALUES FOR THE 10X10A ASSEMBLY CLASS IN THE MPC-68
(all dimensions are in inches)

10x10A (4.2% Enrichment, Boral ^{10}B minimum loading of 0.0279 g/cm^2) 92/78 fuel rods†, 2 water rods, pitch=0.510, Zr clad										
Fuel Assembly Designation	maximum k_{eff}	calculated k_{eff}	standard deviation	cladding OD	cladding ID	cladding thickness	pellet OD	fuel length	water rod thickness	channel thickness
10x10A01 (axial segment with all rods)	0.9377	0.9335	0.0008	0.4040	0.3520	0.0260	0.3450	155	0.030	0.100
10x10A02 (axial segment with only the full length rods)	0.9426	0.9386	0.0007	0.4040	0.3520	0.0260	0.3450	155	0.030	0.100
10x10A03 (actual three-dimensional representation of all rods)	0.9396	0.9356	0.0007	0.4040	0.3520	0.0260	0.3450	155/90	0.030	0.100
Dimensions Listed in Certificate of Compliance				0.4040 (min.)	0.3520 (max.)		0.3455 (max.)	150†† (max.)	0.030 (min.)	0.120 (max.)
bounding dimensions (axial segment with only the full length rods) (B10x10A01)	0.9457†††	0.9414	0.0008	0.4040	0.3520	0.0260	0.3455‡	155	0.030	0.120

† This assembly class contains 78 full-length rods and 14 partial-length rods. In order to eliminate the requirement on the length of the partial length rods, separate calculations were performed for axial segments with and without the partial length rods.

†† Although the analysis qualifies this assembly for a maximum active fuel length of 155 inches, the Certificate of Compliance limits the active fuel length to 150 inches. This is due to the fact that the Boral panels are 156 inches in length.

††† KENO5a verification calculation resulted in a maximum k_{eff} of 0.9453.

‡ This value was conservatively defined to be larger than any of the actual pellet diameters.

Table 6.2.33
MAXIMUM K_{EFF} VALUES FOR THE 10X10B ASSEMBLY CLASS IN THE MPC-68
(all dimensions are in inches)

10x10B (4.2% Enrichment, Boral ^{10}B minimum loading of 0.0279 g/cm^2) 91/83 fuel rods†, 1 water rods (square, replacing 9 fuel rods), pitch=0.510, Zr clad										
Fuel Assembly Designation	maximum k_{eff}	calculated k_{eff}	standard deviation	cladding OD	cladding ID	cladding thickness	pellet OD	fuel length	water rod thickness	channel thickness
10x10B01 (axial segment with all rods)	0.9384	0.9341	0.0008	0.3957	0.3480	0.0239	0.3413	155	0.0285	0.100
10x10B02 (axial segment with only the full length rods)	0.9416	0.9373	0.0008	0.3957	0.3480	0.0239	0.3413	155	0.0285	0.100
10x10B03 (actual three-dimensional representation of all rods)	0.9375	0.9334	0.0007	0.3957	0.3480	0.0239	0.3413	155/90	0.0285	0.100
Dimensions Listed in Certificate of Compliance				0.3957 (min.)	0.3480 (max.)		0.3420 (max.)	150†† (max.)	0.000 (min.)	0.120 (max.)
bounding dimensions (axial segment with only the full length rods) (B10x10B01)	0.9436	0.9395	0.0007	0.3957	0.3480	0.0239	0.3420†††	155	0.000	0.120

† This assembly class contains 83 full length rods and 8 partial length rods. In order to eliminate a requirement on the length of the partial length rods, separate calculations were performed for the axial segments with and without the partial length rods.

†† Although the analysis qualifies this assembly for a maximum active fuel length of 155 inches, the Certificate of Compliance limits the active fuel length to 150 inches. This is due to the fact that the Boral panels are 156 inches in length.

††† This value was conservatively defined to be larger than any of the actual pellet diameters.

Table 6.2.34
MAXIMUM K_{EFF} VALUES FOR THE 10X10C ASSEMBLY CLASS IN THE MPC-68
(all dimensions are in inches)

10x10C (4.2% Enrichment, Boral ^{10}B minimum loading of 0.0279 g/cm^2) 96 fuel rods, 5 water rods (1 center diamond and 4 rectangular), pitch=0.488, Zr clad										
Fuel Assembly Designation	maximum k_{eff}	calculated k_{eff}	standard deviation	cladding OD	cladding ID	cladding thickness	pellet OD	fuel length	water rod thickness	channel thickness
10x10C01	0.9433	0.9392	0.0007	0.3780	0.3294	0.0243	0.3224	150	0.031	0.055
Dimensions Listed in Certificate of Compliance				0.3780 (min.)	0.3294 (max.)		0.3224 (max.)	150 (max.)	0.031 (min.)	0.055 (max.)

Table 6.2.35
MAXIMUM K_{EFF} VALUES FOR THE 10X10D ASSEMBLY CLASS IN THE MPC-68
(all dimensions are in inches)

10x10D (4.0% Enrichment, Boral ^{10}B minimum loading of 0.0279 g/cm^2) 100 fuel rods, 0 water rods, pitch=0.565, SS clad										
Fuel Assembly Designation	maximum k_{eff}	calculated k_{eff}	standard deviation	cladding OD	cladding ID	cladding thickness	pellet OD	fuel length	water rod thickness	channel thickness
10x10D01	0.9376	0.9333	0.0008	0.3960	0.3560	0.0200	0.350	83	n/a	0.080
Dimensions Listed in Certificate of Compliance				0.3960 (min.)	0.3560 (max.)		0.350 (max.)	83 (max.)	n/a	0.080 (max.)

Table 6.2.36
MAXIMUM K_{EFF} VALUES FOR THE 10X10E ASSEMBLY CLASS IN THE MPC-68
(all dimensions are in inches)

10x10E (4.0% Enrichment, Boral ^{10}B minimum loading of 0.0279 g/cm^2) 96 fuel rods, 4 water rods, pitch=0.557, SS clad										
Fuel Assembly Designation	maximum k_{eff}	calculated k_{eff}	standard deviation	cladding OD	cladding ID	cladding thickness	pellet OD	fuel length	water rod thickness	channel thickness
10x10E01	0.9185	0.9144	0.0007	0.3940	0.3500	0.0220	0.3430	83	0.022	0.080
Dimensions Listed in Certificate of Compliance				0.3940 (min.)	0.3500 (max.)		0.3430 (max.)	83 (max.)	0.022 (min.)	0.080 (max.)

Table 6.2.37
MAXIMUM K_{EFF} VALUES FOR THE 6X6A ASSEMBLY CLASS IN THE MPC-68F
(all dimensions are in inches)

6x6A (3.0% Enrichment†, Boral ^{10}B minimum loading of 0.0067 g/cm^2) 35 or 36 fuel rods††, 1 or 0 water rods††, pitch††=0.694 to 0.710, Zr clad												
Fuel Assembly Designation	maximum k_{eff}	calculated k_{eff}	standard deviation	pitch	fuel rods	cladding OD	cladding ID	cladding thickness	pellet OD	fuel length	water rod thickness	channel thickness
6x6A01	0.7539	0.7498	0.0007	0.694	36	0.5645	0.4945	0.0350	0.4940	110	n/a	0.060
6x6A02	0.7517	0.7476	0.0007	0.694	36	0.5645	0.4925	0.0360	0.4820	110	n/a	0.060
6x6A03	0.7545	0.7501	0.0008	0.694	36	0.5645	0.4945	0.0350	0.4820	110	n/a	0.060
6x6A04	0.7537	0.7494	0.0008	0.694	36	0.5550	0.4850	0.0350	0.4820	110	n/a	0.060
6x6A05	0.7555	0.7512	0.0008	0.696	36	0.5625	0.4925	0.0350	0.4820	110	n/a	0.060
6x6A06	0.7618	0.7576	0.0008	0.696	35	0.5625	0.4925	0.0350	0.4820	110	0.0	0.060
6x6A07	0.7588	0.7550	0.0007	0.700	36	0.5555	0.4850	0.03525	0.4780	110	n/a	0.060
6x6A08	0.7808	0.7766	0.0007	0.710	36	0.5625	0.5105	0.0260	0.4980	110	n/a	0.060
Dimensions Listed in Certificate of Compliance				0.710 (max.)	35 or 36	0.5550 (min.)	0.5105 (max.)	0.02225	0.4980 (max.)	120 (max.)	0.0	0.060 (max.)
bounding dimensions (B6x6A01)	0.7727	0.7685	0.0007	0.694	35	0.5550	0.5105	0.02225	0.4980	120	0.0	0.060
bounding dimensions (B6x6A02)	0.7782	0.7738	0.0008	0.700	35	0.5550	0.5105	0.02225	0.4980	120	0.0	0.060
bounding dimensions (B6x6A03)	0.7888	0.7846	0.0007	0.710	35	0.5550	0.5105	0.02225	0.4980	120	0.0	0.060

† Although the calculations were performed for 3.0%, the enrichment is limited in the Certificate of Compliance to 2.7%.
†† This assembly class was analyzed and qualified for a small variation in the pitch and a variation in the number of fuel and water rods.

Table 6.2.38
MAXIMUM K_{EFF} VALUES FOR THE 6X6B ASSEMBLY CLASS IN THE MPC-68F
(all dimensions are in inches)

6x6B (3.0% Enrichment†, Boral ^{10}B minimum loading of 0.0067 g/cm^2) 35 or 36 fuel rods†† (up to 9 MOX rods), 1 or 0 water rods††, pitch††=0.694 to 0.710, Zr clad												
Fuel Assembly Designation	maximum k_{eff}	calculated k_{eff}	standard deviation	pitch	fuel rods	cladding OD	cladding ID	cladding thickness	pellet OD	fuel length	water rod thickness	channel thickness
6x6B01	0.7604	0.7563	0.0007	0.694	36	0.5645	0.4945	0.0350	0.4820	110	n/a	0.060
6x6B02	0.7618	0.7577	0.0007	0.694	36	0.5625	0.4925	0.0350	0.4820	110	n/a	0.060
6x6B03	0.7619	0.7578	0.0007	0.696	36	0.5625	0.4925	0.0350	0.4820	110	n/a	0.060
6x6B04	0.7686	0.7644	0.0008	0.696	35	0.5625	0.4925	0.0350	0.4820	110	0.0	0.060
6x6B05	0.7824	0.7785	0.0006	0.710	35	0.5625	0.4925	0.0350	0.4820	110	0.0	0.060
Dimensions Listed in Certificate of Compliance				0.710 (max.)	35 or 36	0.5625 (min.)	0.4945 (max.)		0.4820 (max.)	120 (max.)	0.0	0.060 (max.)
bounding dimensions (B6x6B01)	0.7822†††	0.7783	0.0006	0.710	35	0.5625	0.4945	0.0340	0.4820	120	0.0	0.060

Note:

1. These assemblies contain up to 9 MOX pins. The composition of the MOX fuel pins is given in Table 6.3.4.

† The ^{235}U enrichment of the MOX and UO_2 pins is assumed to be 0.711% and 3.0%, respectively.

†† This assembly class was analyzed and qualified for a small variation in the pitch and a variation in the number of fuel and water rods.

††† The k_{eff} value listed for the 6x6B05 case is slightly higher than that for the case with the bounding dimensions. However, the difference (0.0002) is well within the statistical uncertainties, and thus, the two values are statistically equivalent (within 1σ). Therefore, the 0.7824 value is listed in Tables 6.1.2 and 6.1.3 as the maximum.

Table 6.2.39
MAXIMUM K_{EFF} VALUES FOR THE 6X6C ASSEMBLY CLASS IN THE MPC-68F
(all dimensions are in inches)

6x6C (3.0% Enrichment†, Boral ^{10}B minimum loading of 0.0067 g/cm^2) 36 fuel rods, 0 water rods, pitch=0.740, Zr clad										
Fuel Assembly Designation	maximum k_{eff}	calculated k_{eff}	standard deviation	cladding OD	cladding ID	cladding thickness	pellet OD	fuel length	water rod thickness	channel thickness
6x6C01	0.8021	0.7980	0.0007	0.5630	0.4990	0.0320	0.4880	77.5	n/a	0.060
Dimensions Listed in Certificate of Compliance				0.5630 (min.)	0.4990 (max.)		0.4880 (max.)	77.5 (max.)	n/a	0.060 (max.)

† Although the calculations were performed for 3.0%, the enrichment is limited in the Certificate of Compliance to 2.7%.

Table 6.2.40
MAXIMUM K_{EFF} VALUES FOR THE 7X7A ASSEMBLY CLASS IN THE MPC-68F
(all dimensions are in inches)

7x7A (3.0% Enrichment†, Boral ^{10}B minimum loading of 0.0067 g/cm^2) 49 fuel rods, 0 water rods, pitch=0.631, Zr clad										
Fuel Assembly Designation	maximum k_{eff}	calculated k_{eff}	standard deviation	cladding OD	cladding ID	cladding thickness	pellet OD	fuel length	water rod thickness	channel thickness
7x7A01	0.7974	0.7932	0.0008	0.4860	0.4204	0.0328	0.4110	80	n/a	0.060
Dimensions Listed in Certificate of Compliance				0.4860 (min.)	0.4204 (max.)		0.4110 (max.)	80 (max.)	n/a	0.060 (max.)

† Although the calculations were performed for 3.0%, the enrichment is limited in the Certificate of Compliance to 2.7%.

Table 6.2.41
MAXIMUM K_{EFF} VALUES FOR THE 8X8A ASSEMBLY CLASS IN THE MPC-68F
(all dimensions are in inches)

8x8A (3.0% Enrichment†, Boral ^{10}B minimum loading of 0.0067 g/cm^2) 63 or 64 fuel rods††, 0 water rods, pitch=0.523, Zr clad											
Fuel Assembly Designation	maximum k_{eff}	calculated k_{eff}	standard deviation	fuel rods	cladding OD	cladding ID	cladding thickness	pellet OD	fuel length	water rod thickness	channel thickness
8x8A01	0.7685	0.7644	0.0007	64	0.4120	0.3620	0.0250	0.3580	110	n/a	0.100
8x8A02	0.7697	0.7656	0.0007	63	0.4120	0.3620	0.0250	0.3580	120	n/a	0.100
Dimensions Listed in Certificate of Compliance				63	0.4120 (min.)	0.3620 (max.)		0.3580 (max.)	120 (max.)	n/a	0.100 (max.)
bounding dimensions (8x8A02)	0.7697	0.7656	0.0007	63	0.4120	0.3620	0.0250	0.3580	120	n/a	0.100

† Although the calculations were performed for 3.0%, the enrichment is limited in the Certificate of Compliance to 2.7%.
†† This assembly class was analyzed and qualified for a variation in the number of fuel rods.

Table 6.2.42

SPECIFICATION OF THE THORIA ROD CANISTER AND THE THORIA RODS

Canister ID	4.81"
Canister Wall Thickness	0.11"
Separator Assembly Plates Thickness	0.11"
Cladding OD	0.412"
Cladding ID	0.362"
Pellet OD	0.358"
Active Length	110.5"
Fuel Composition	1.8% UO_2 and 98.2% ThO_2
Initial Enrichment	93.5 wt% ^{235}U for 1.8% of the fuel
Maximum k_{eff}	0.1813
Calculated k_{eff}	0.1779
Standard Deviation	0.0004

6.3 MODEL SPECIFICATION

6.3.1 Description of Calculational Model

Figures 6.3.1 and 6.3.3 show representative horizontal cross sections of the two types of cells used in the calculations, and Figures 6.3.4 and 6.3.6 illustrate the basket configurations used. Two different MPC fuel basket designs were evaluated as follows:

- a 24 PWR assembly basket
- a 68 BWR assembly basket.

Full three-dimensional calculations were used, assuming the axial configuration shown in Figure 6.3.7, and conservatively neglecting the absorption in the overpack neutron shielding material (Holtite-A). Although the Boral neutron absorber panels are 156 inches in length, which is much longer than the active fuel length (maximum of 150 inches), they are assumed equal to the active fuel length in the calculations. As shown on the drawings in Section 1.5, 16 of the 24 periphery Boral panels on the MPC-24 have reduced width (i.e., 6.25 inches wide as opposed to 7.5 inches). However, the calculational models for the MPC-24 conservatively assume all of the periphery Boral panels are 6.25 inches in width.

The off-normal and accident conditions defined in Chapter 2 and considered in Chapter 11 have no adverse effect on the design conditions important to criticality safety, and thus from a criticality standpoint, the normal, off-normal, and accident conditions are identical and do not require individual models.

The calculational model explicitly defines the fuel rods and cladding, the guide tubes (or water rods for BWR assemblies), the water-gaps and Boral absorber panels on the stainless steel walls of the storage cells. Under the conditions of storage, when the MPC is dry, the resultant reactivity with the design basis fuel is very low ($k_{eff} < 0.4$). For the flooded condition (loading and unloading), water was assumed to be present in the fuel rod pellet-to-clad gaps. Appendix 6.D provides sample input files for each of the two MPC basket designs in the HI-STAR 100 System.

The water thickness above and below the fuel is intentionally maintained less than or equal to the actual water thickness. This assures that any positive reactivity effect of the steel in the MPC is conservatively included.

As indicated in Figures 6.3.1 and 6.3.3 and in Tables 6.3.1 and 6.3.2, calculations were made with dimensions assumed to be at their most conservative value with respect to criticality. CASMO-3 was used to determine the direction of the manufacturing tolerances which produced

the most adverse effect on criticality. After the directional effect (positive effect with an increase in reactivity; or negative effect with a decrease in reactivity) of the manufacturing tolerances was determined, the criticality analyses were performed using the worst case tolerances in the direction which would increase reactivity. These effects are shown in Table 6.3.1 which also identifies the approximate magnitude of the tolerances on reactivity.

The various basket dimensions are inter-dependent, and therefore cannot be individually varied (i.e., reduction in one parameter requires a corresponding reduction or increase in another parameter). Thus, it is not possible to determine the reactivity effect of each individual dimensional tolerance separately. However, it is possible to determine the reactivity effect of the dimensional tolerances by evaluating the various possible dimensional combinations. To this end, an evaluation of the various possible dimensional combinations was performed using MCNP4a. Calculated k_{eff} results (which do not include the bias, uncertainties, or calculational statistics), along with the actual dimensions, for a number of dimensional combinations are shown in Table 6.3.2 for the reference PWR and BWR assemblies. In Table 6.3.2, the box I.D. is the inner box dimension and the minimum, nominal, and maximum values correspond to those values permitted by the tolerances in the drawings in Section 1.5. For each of the MPC designs, the reactivity effects of the tolerances are very small, generally within one standard deviation. The effect of the box wall thickness tolerance is negligible, being either slightly negative or within one standard deviation of the reference.

Based on the MCNP4a and CASMO-3 calculations, the conservative dimensional assumptions listed in Table 6.3.3 were determined. Because the reactivity effect (positive or negative) of the manufacturing tolerances are not assembly dependent, these dimensional assumptions were employed for the criticality analyses.

As demonstrated in this section, design parameters important to criticality safety are: fuel enrichment, the inherent geometry of the fuel basket structure, and the fixed neutron absorbing panels (Boral). As shown in Chapter 11, none of these parameters are affected during any of the design basis off-normal or accident conditions involving handling, packaging, transfer or storage.

6.3.2 Cask Regional Densities

Composition of the various components of the principal designs of the HI-STAR 100 Systems are listed in Table 6.3.4.

The HI-STAR 100 System is designed such that the fixed neutron absorber (Boral) will remain effective for a storage period greater than 20 years, and there are no credible means to lose it. A detailed physical description, historical applications, unique characteristics, service experience, and manufacturing quality assurance of Boral are provided in Section 1.2.1.3.1.

The continued efficacy of the Boral is assured by acceptance testing, documented in Section 9.1.5.3, to validate the ^{10}B (poison) concentration in the Boral. To demonstrate that the neutron flux from the irradiated fuel results in a negligible depletion of the poison material over the storage period, an MCNP4a calculation of the number of neutrons absorbed in the ^{10}B was performed. The calculation conservatively assumed a constant neutron source for 50 years equal to the initial source for the design basis fuel, as determined in Section 5.2, and shows that the fraction of ^{10}B atoms destroyed is only 2.6E-09 in 50 years. Thus, the reduction in ^{10}B concentration in the Boral by neutron absorption is negligible. In addition, analysis in Appendix 3.M.1 demonstrates that the sheathing, which affixes the Boral panel, remains in place during all credible accident conditions, and thus, the Boral panel remains permanently fixed. Therefore, in accordance with NUREG-1536, there is no need to provide a surveillance or monitoring program to verify the continued efficacy of the neutron absorber, as required by 10CFR72.124(b).

Table 6.3.1

CASMO-3 CALCULATIONS FOR EFFECT OF TOLERANCES AND TEMPERATURE

Change in Nominal Parameter†	Δk for Maximum Tolerance		Action/Modeling Assumption
	MPC-24‡	MPC-68	
Reduce Boral Width to Minimum	N/A††† min.= nom.= 7.5" and 6.25"	N/A††† min. = nom. = 4.75"	Assume minimum Boral width
Increase UO_2 Density to Maximum	+0.0017 max. = 10.522 g/cc nom. = 10.412 g/cc	+0.0014 max. = 10.522 g/cc nom. = 10.412 g/cc	Assume maximum UO_2 density
Reduce Box Inside Dimension (I.D.) to Minimum	-0.0005 min.= 8.86" nom. = 8.92"	See Table 6.3.2	Assume maximum box I.D. for the MPC-24
Increase Box Inside Dimension (I.D.) to Maximum	+0.0007 max. = 8.98" nom. = 8.92"	-0.0030 max. = 6.113" nom. = 6.053"	Assume minimum box I.D. for the MPC-68
Decrease Water Gap to Minimum	+0.0069 min. = 1.09" nom. = 1.15"	N/A	Assume minimum water gap in the MPC-24

† Reduction (or increase) in a parameter indicates that the parameter is changed to its minimum (or maximum) value.

‡ Calculations for the MPC-24 were performed with CASMO-4 [6.3.1–6.3.3]

††† The Boral width for the MPC-68 is 4.75" +0.125", -0", The Boral widths for the MPC-24 are 7.5" +0.125", -0" and 6.25" +0.125", -0" (i.e., the nominal and minimum values are the same).

Table 6.3.1 (continued)

CASMO-3 CALCULATIONS FOR EFFECT OF TOLERANCES AND TEMPERATURE

Change in Nominal Parameter	Δk Maximum Tolerance		Action/Modeling Assumption
	MPC-24	MPC-68	
Increase in Temperature			Assume 20°C
20°C	Ref.	Ref.	
40°C	-0.0030	-0.0039	
70°C	-0.0089	-0.0136	
100°C	-0.0162	-0.0193	
10% Void in Moderator			Assume no void
20°C with no void	Ref.	Ref.	
20°C	-0.0251	-0.0241	
100°C	-0.0412	-0.0432	
Removal of Flow Channel (BWR)	N/A	-0.0073	Assume flow channel present for MPC-68

Table 6.3.2

MCNP4a EVALUATION OF BASKET MANUFACTURING TOLERANCES[†]

Pitch	Box I.D.	Box Wall Thickness	MCNP4a Calculated k_{eff}
MPC-24[††] (17x17A01 @ 4.0% Enrichment)			
nominal (10.906")	maximum (8.98")	nominal (5/16")	0.9325±0.0008[†††]
minimum (10.846")	nominal (8.92")	nominal (5/16")	0.9300±0.0008
nominal (10.906")	nom. - 0.04" (8.88")	nom. + 0.05" (0.3625")	0.9305±0.0007
MPC-68 (8x8C04 @ 4.2% Enrichment)			
minimum (6.43")	minimum (5.993")	nominal (1/4")	0.9307±0.0007
nominal (6.49")	nominal (6.053")	nominal (1/4")	0.9274±0.0007
maximum (6.55")	maximum (6.113")	nominal (1/4")	0.9272±0.0008
nom. + 0.05" (6.54")	nominal (6.053")	nom. + 0.05" (0.30")	0.9267±0.0007

Note: Values in parentheses are the actual value used.

† Tolerance for pitch and box I.D. are ± 0.06".
Tolerance for box wall thickness is +0.05", -0.00".

†† All calculations for the MPC-24 assume minimum water gap thickness (1.09").

††† Numbers are 1σ statistical uncertainties.

Table 6.3.3

BASKET DIMENSIONAL ASSUMPTIONS

Basket Type	Pitch	Box I.D.	Box Wall Thickness	Water-Gap Flux Trap
MPC-24	nominal (10.906")	maximum (8.98")	nominal (5/16")	minimum (1.09")
MPC-68	minimum (6.43")	minimum (5.993")	nominal (1/4")	N/A

Table 6.3.4

COMPOSITION OF THE MAJOR COMPONENTS OF THE HI-STAR 100 SYSTEM

MPC-24		
UO_2 4.0% ENRICHMENT, DENSITY (g/cc) = 10.522		
Nuclide	**Atom-Density**	**Wgt. Fraction**
8016	4.693E-02	1.185E-01
92235	9.505E-04	3.526E-02
92238	2.252E-02	8.462E-01
BORAL (0.02 g ^{10}B/cm sq), DENSITY (g/cc) = 2.660		
Nuclide	**Atom-Density**	**Wgt. Fraction**
5010	8.707E-03	5.443E-02
5011	3.512E-02	2.414E-01
6012	1.095E-02	8.210E-02
13027	3.694E-02	6.222E-01

Table 6.3.4 (continued)

COMPOSITION OF THE MAJOR COMPONENTS OF THE HI-STAR 100 SYSTEM

MPC-68		
UO_2 4.2% ENRICHMENT, DENSITY (g/cc) = 10.522		
Nuclide	**Atom-Density**	**Wgt. Fraction**
8016	4.697E-02	1.185E-01
92235	9.983E-04	3.702E-02
92238	2.248E-02	8.445E-01
UO_2 3.0% ENRICHMENT, DENSITY (g/cc) = 10.522		
Nuclide	**Atom-Density**	**Wgt. Fraction**
8016	4.695E-02	1.185E-01
92235	7.127E-04	2.644E-02
92238	2.276E-02	8.550E-01
MOX FUEL†, DENSITY (g/cc) = 10.522		
Nuclide	**Atom-Density**	**Wgt. Fraction**
8016	4.714E-02	1.190E-01
92235	1.719E-04	6.380E-03
92238	2.285E-02	8.584E-01
94239	3.876E-04	1.461E-02
94240	9.177E-06	3.400E-04
94241	3.247E-05	1.240E-03
94242	2.118E-06	7.000E-05

† The Pu-238, which is an absorber, was conservatively neglected in the MOX description for analysis purposes.

Table 6.3.4 (continued)

COMPOSITION OF THE MAJOR COMPONENTS OF THE HI-STAR 100 SYSTEM

BORAL (0.0279 g ^{10}B/cm sq), DENSITY (g/cc) = 2.660		
Nuclide	**Atom-Density**	**Wgt. Fraction**
5010	8.071E-03	5.089E-02
5011	3.255E-02	2.257E-01
6012	1.015E-02	7.675E-02
13027	3.805E-02	6.467E-01
FUEL IN THORIA RODS, DENSITY (g/cc) = 10.522		
Nuclide	**Atom-Density**	**Wgt. Fraction**
8016	4.798E-02	1.212E-01
92235	4.001E-04	1.484E-02
92238	2.742E-05	1.030E-03
90232	2.357E-02	8.630E-01

Table 6.3.4 (continued)

COMPOSITION OF THE MAJOR COMPONENTS OF THE HI-STAR 100 SYSTEM

COMMON MATERIALS		
ZR CLAD, DENSITY (g/cc) = 6.550		
Nuclide	**Atom-Density**	**Wgt. Fraction**
40000	4.323E-02	1.000E+00
MODERATOR (H_2O), DENSITY (g/cc) = 1.000		
Nuclide	**Atom-Density**	**Wgt. Fraction**
1001	6.688E-02	1.119E-01
8016	3.344E-02	8.881E-01
STAINLESS STEEL, DENSITY (g/cc) = 7.840		
Nuclide	**Atom-Density**	**Wgt. Fraction**
24000	1.761E-02	1.894E-01
25055	1.761E-03	2.001E-02
26000	5.977E-02	6.905E-01
28000	8.239E-03	1.000E-01
ALUMINUM, DENSITY (g/cc) = 2.700		
Nuclide	**Atom-Density**	**Wgt. Fraction**
13027	6.026E-02	1.000E+00

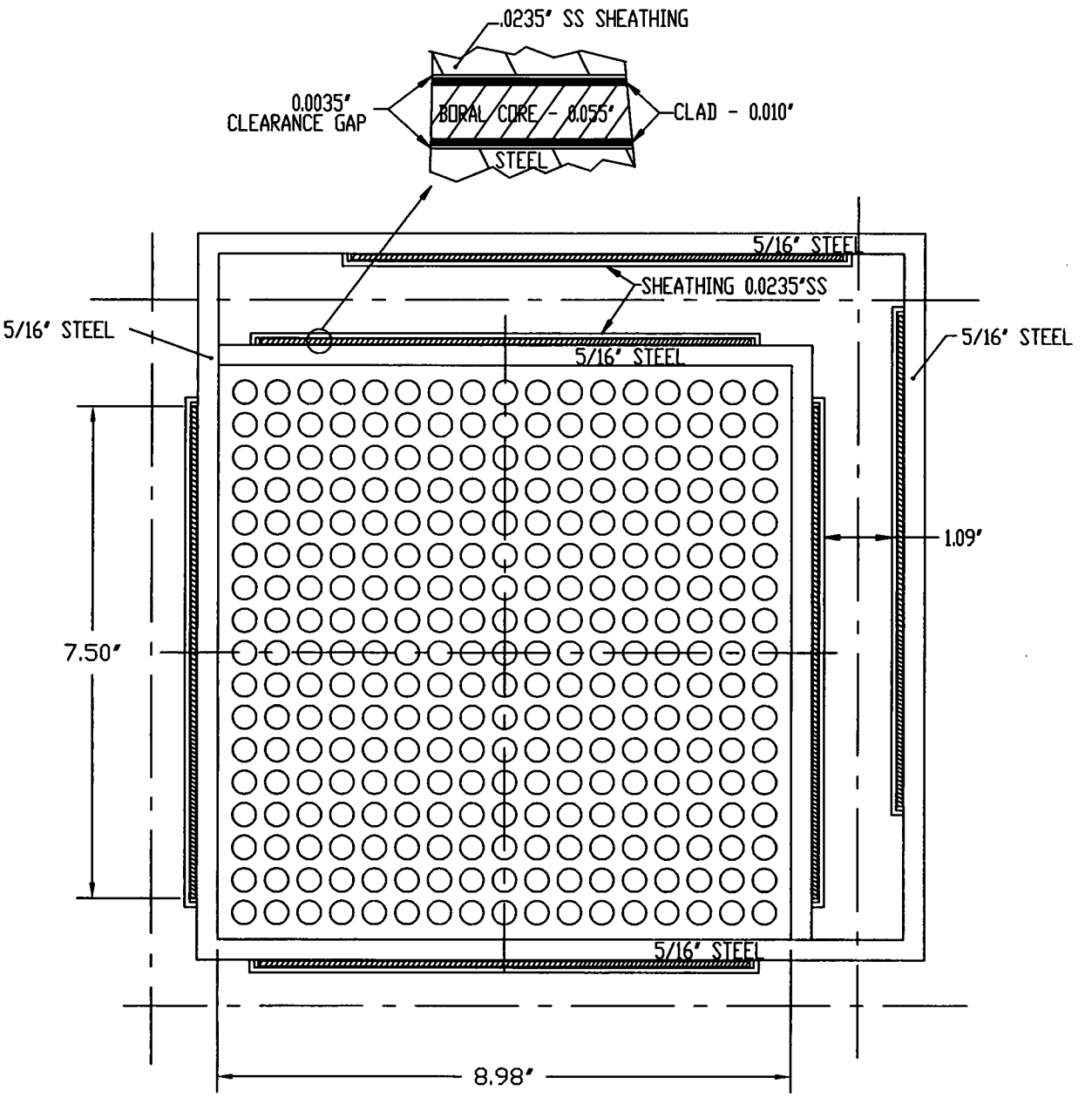

FIGURE 6.3.1; TYPICAL CELL IN THE CALCULATION MODEL (PLANAR CROSS-SECTION) WITH REPRESENTATIVE FUEL IN THE MPC-24 BASKET

(SEE CHAPTER 1 FOR TRUE BASKET DIMENSIONS)

NOTE: THESE DIMENSIONS WERE CONSERVATIVELY USED FOR CRITICALITY ANALYSES.

DELETED

FIGURE 6.3.2

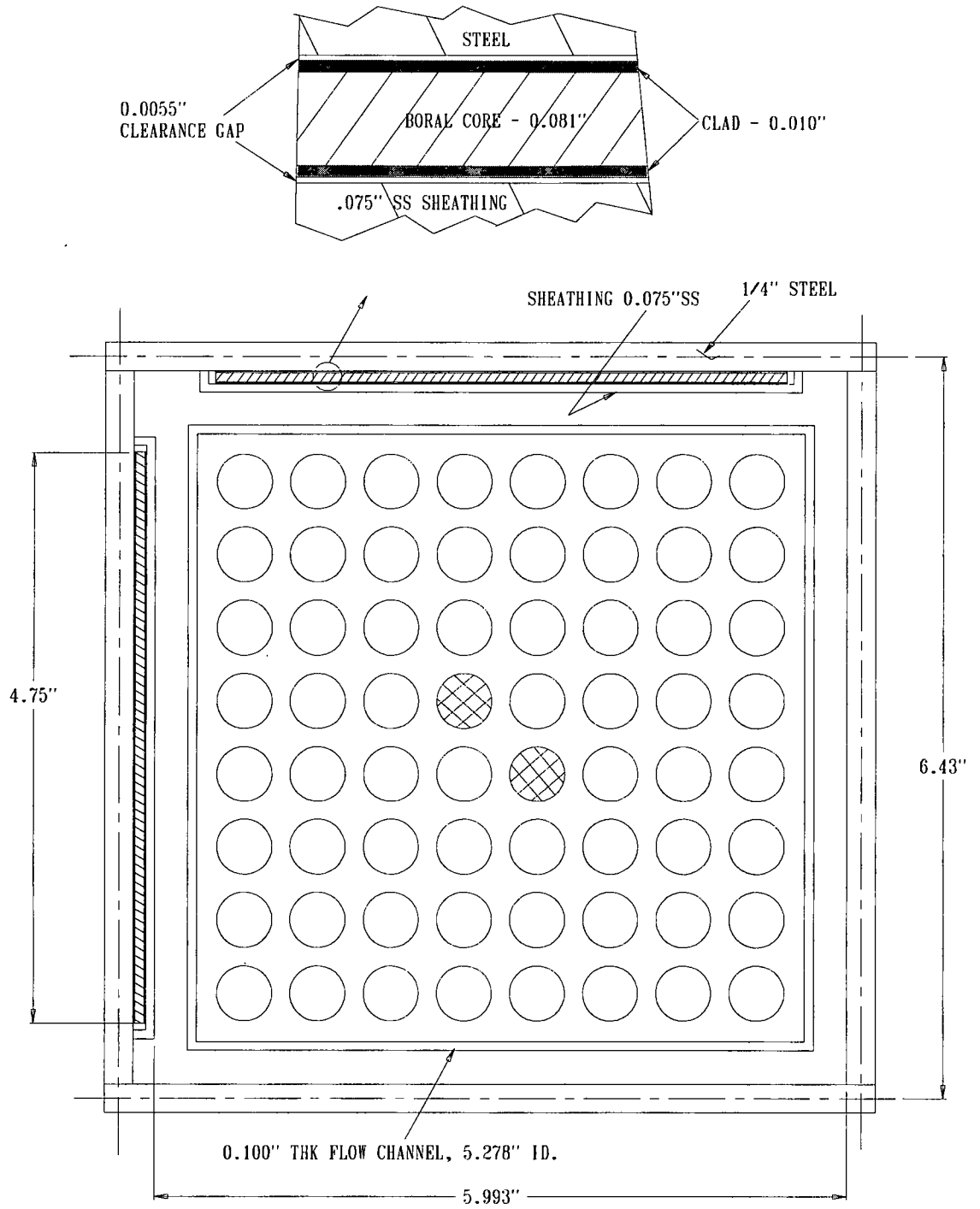

FIGURE 6.3.3; TYPICAL CELL IN THE CALCULATION MODEL (PLANAR CROSS-SECTION) WITH REPRESENTATIVE FUEL IN THE MPC-68 BASKET

(SEE CHAPTER 1 FOR TRUE BASKET DIMENSIONS)

NOTE: THESE DIMENSIONS WERE CONSERVATIVELY USED FOR CRITICALITY ANALYSES.

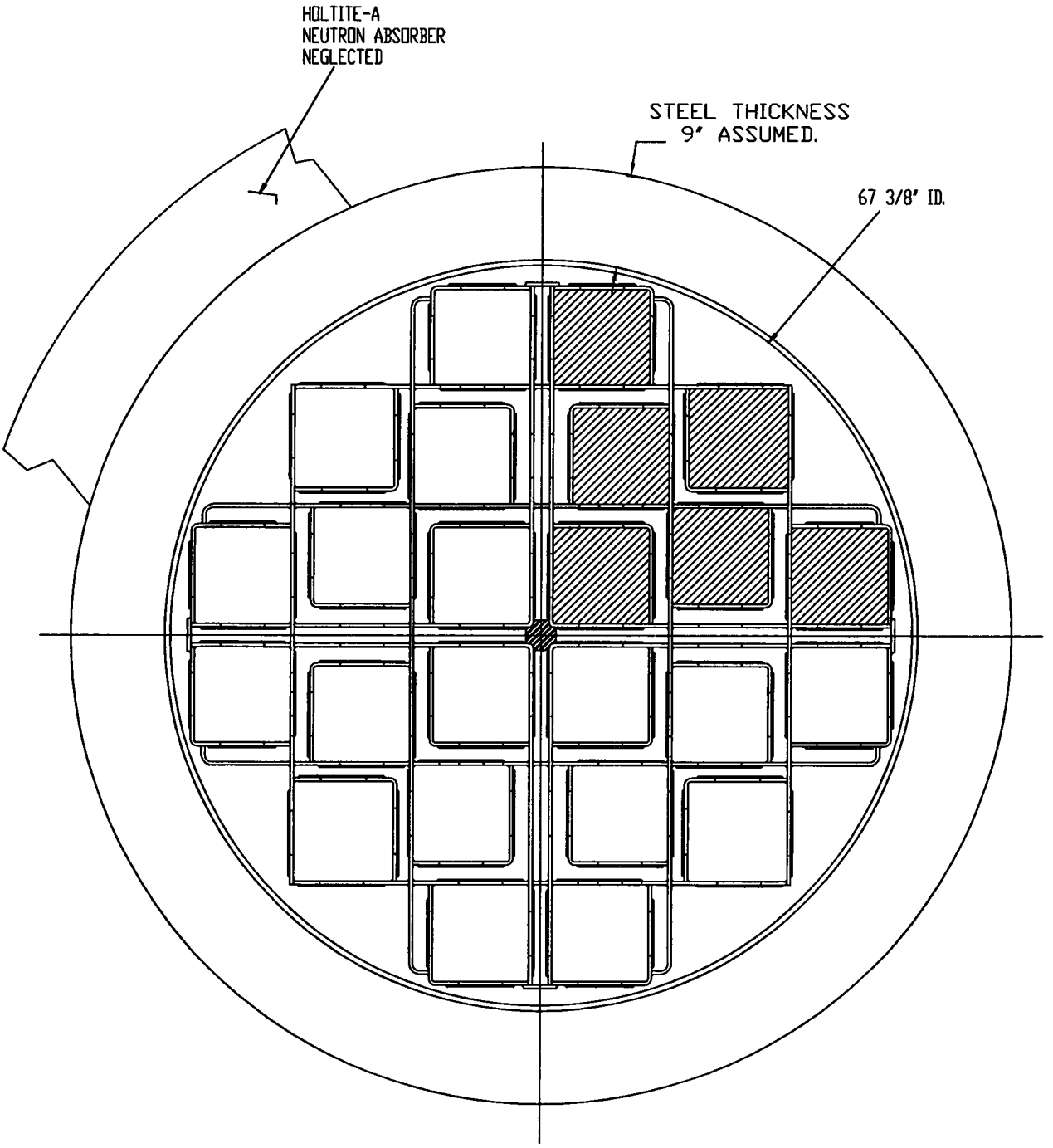

FIGURE 6.3.4; CALCULATION MODEL (PLANAR CROSS-SECTION)
WITH FUEL ILLUSTRATED IN ONE QUADRANT OF
THE MPC -24

(SEE CHAPTER 1 FOR TRUE BASKET DIMENSIONS)

DELETED

FIGURE 6.3.5

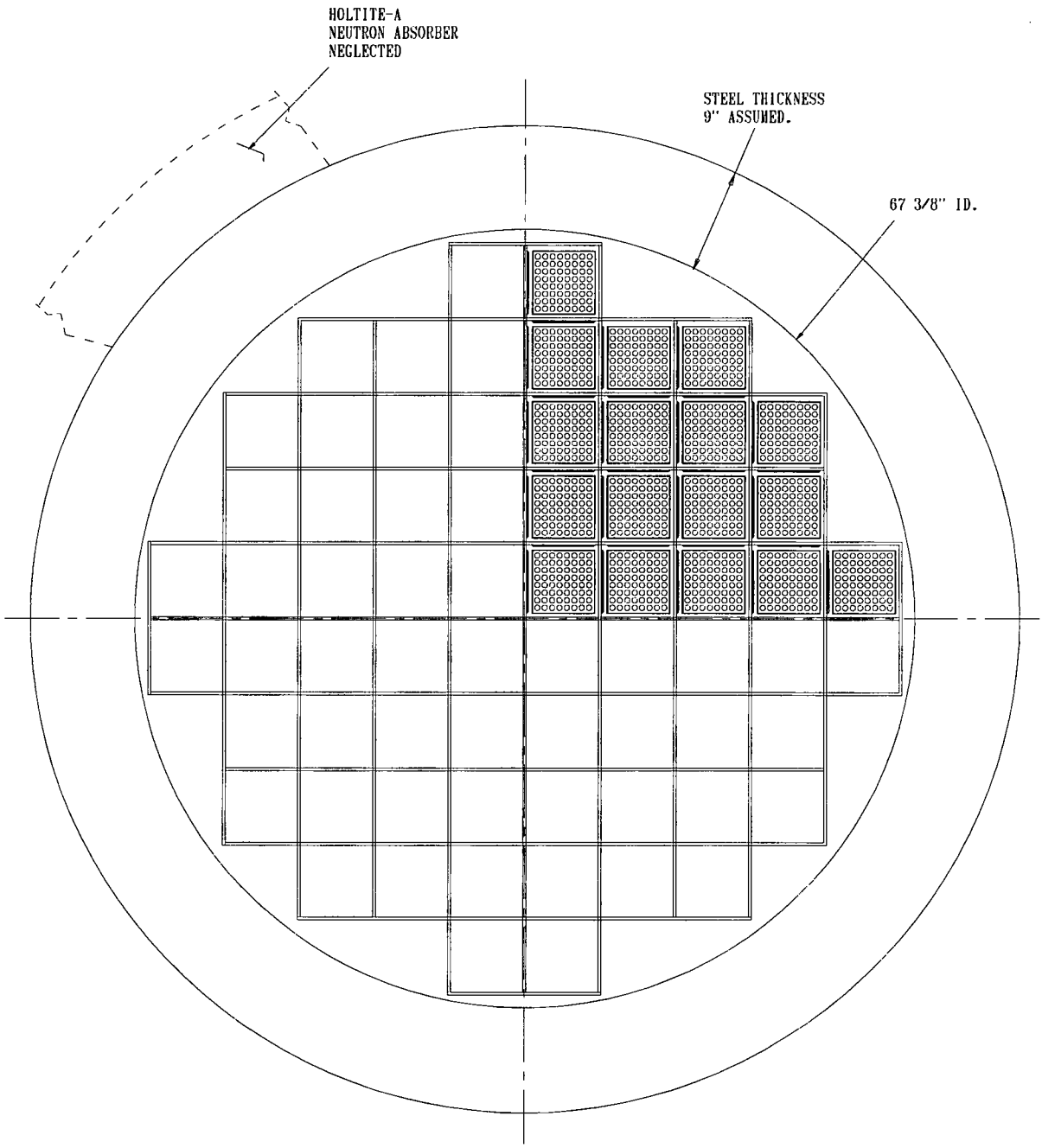

FIGURE 6.3.6; CALCULATION MODEL (PLANAR CROSS-SECTION) WITH FUEL ILLUSTRATED IN ONE QUADRANT OF THE MPC-68

(SEE CHAPTER 1 FOR TRUE BASKET DIMENSIONS)

	ACTIVE FUEL LENGTH	LOWER WATER THICKNESS	UPPER WATER THICKNESS
MPC-68	SEE TABLE 6.2.1	7.30 IN.	8.46 IN.
MPC-24	SEE TABLE 6.2.2	4.0 IN.	6.0 IN.

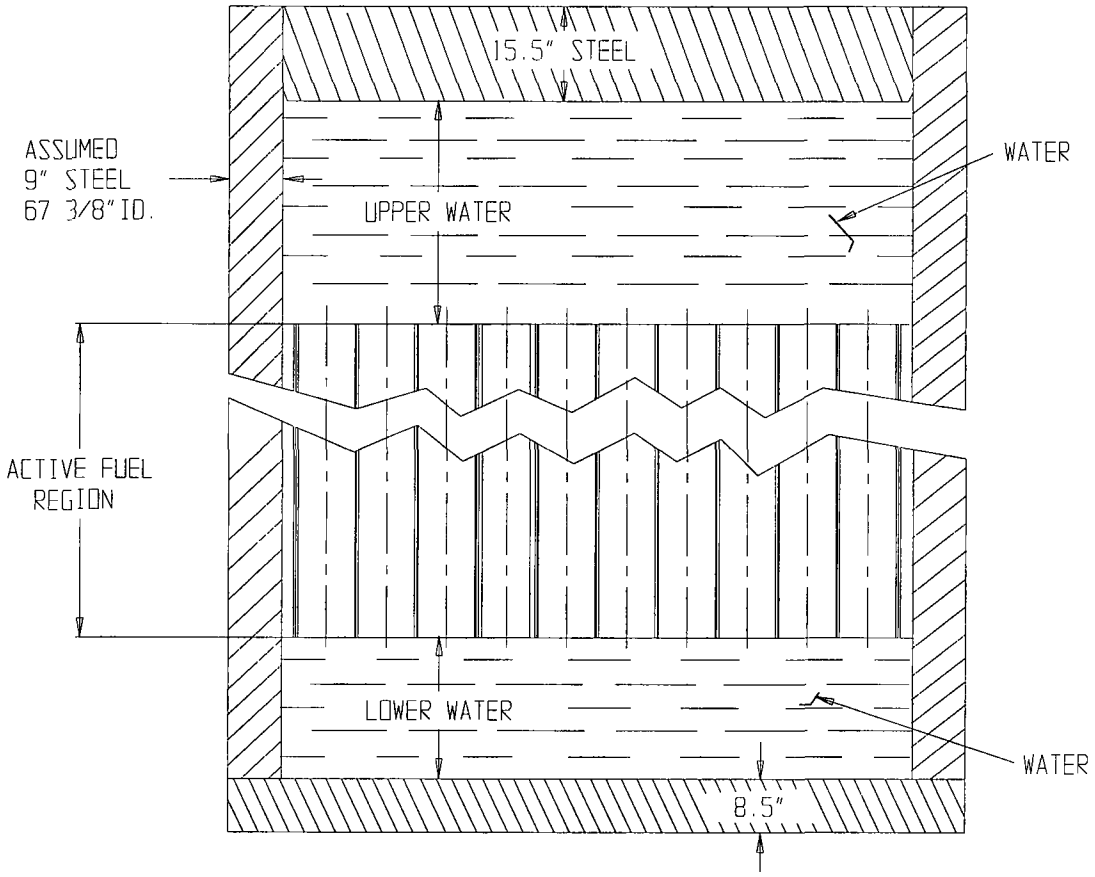

FIGURE 6.3.7; SKETCH OF THE CALCULATIONAL MODEL IN THE AXIAL DIRECTION

6.4 CRITICALITY CALCULATIONS

6.4.1 Calculational or Experimental Method

6.4.1.1 Basic Criticality Safety Calculations

The principal method for the criticality analysis is the general three-dimensional continuous energy Monte Carlo N-Particle code MCNP4a [6.1.4] developed at the Los Alamos National Laboratory. MCNP4a was selected because it has been extensively used and verified and has all of the necessary features for this analysis. MCNP4a calculations used continuous energy cross-section data based on ENDF/B-V, as distributed with the code [6.1.4]. Independent verification calculations were performed with NITAWL-KENO5a [6.1.5], which is a three-dimensional multigroup Monte Carlo code developed at the Oak Ridge National Laboratory. The KENO5a calculations used the 238-group cross-section library, which is based on ENDF/B-V data and is distributed as part of the SCALE-4.3 package [6.4.1], compiled with the NITAWL-II program [6.1.6], which adjusts the uranium-238 cross sections to compensate for resonance self-shielding effects. The Dancoff factors required by NITAWL-II were calculated with the CELLDAN code [6.1.13], which includes the SUPERDAN code [6.1.7] as a subroutine.

The convergence of a Monte Carlo criticality problem is sensitive to the following parameters: (1) number of histories per cycle, (2) the number of cycles skipped before averaging, (3) the total number of cycles and (4) the initial source distribution. The MCNP4a criticality output contains a great deal of useful information that may be used to determine the acceptability of the problem convergence. This information was used in parametric studies to develop appropriate values for the aforementioned criticality parameters to be used in the criticality calculations for this submittal. Based on these studies, a minimum of 5,000 histories were simulated per cycle, a minimum of 20 cycles were skipped before averaging, a minimum of 100 cycles were accumulated, and the initial source was specified as uniform over the fueled regions (assemblies). Further, the output was examined to ensure that each calculation achieved acceptable convergence. These parameters represent an acceptable compromise between calculational precision and computational time. Appendix 6.D provides sample input files for each of the MPC baskets in the HI-STAR 100 System.

CASMO-3 [6.1.9] was used for determining the small incremental reactivity effects of manufacturing tolerances. Although CASMO-3 has been extensively benchmarked, these calculations are used only to establish direction of reactivity uncertainties due to manufacturing tolerances (and their magnitude). This allows the MCNP4a calculational model to use the worst combination of manufacturing tolerances. Table 6.3.1 shows results of the CASMO-3 calculations.

6.4.2 Fuel Loading or Other Contents Loading Optimization

The basket designs are intended to safely accommodate fuel with enrichments indicated in Tables 6.1.1 and 6.1.2. These calculations were based on the assumption that the HI-STAR 100 System was fully flooded with clean unborated water. In all cases, the calculations include bias and calculational uncertainties, as well as the reactivity effects of manufacturing tolerances, determined by assuming the worst case geometry.

Nominally, the fuel assemblies would be centrally positioned in each MPC basket cell. However, in accordance with NUREG-1536, the consequence of eccentric positioning was also evaluated and found to be negligible. To simulate eccentric positioning (and possible closer approach to the thick steel shield), calculations were made analytically decreasing the inner radius of the steel until it was 1 cm away† from the nearest fuel. Results showed a minor increase in reactivity of 0.0026 Δk maximum (MPC-68) which implies that the effect of eccentric location of fuel is negligible at the actual reflector spacing.

6.4.2.1 Internal and External Moderation

As required by NUREG-1536, calculations in this section demonstrate that the HI-STAR 100 System remains subcritical for all credible conditions of moderation.

With a neutron absorber present (i.e., the Boral sheets or the steel walls of the storage compartments), the phenomenon of a peak in reactivity at a hypothetical low moderator density (sometimes called "optimum" moderation) does not occur to any significant extent. In a definitive study, Cano, et al. [6.4.2] has demonstrated that the phenomenon of a peak in reactivity at low moderator densities does not occur when strong neutron absorbing material is present or in the absence of large water spaces between fuel assemblies in storage. Nevertheless, calculations for a single reflected cask were made to confirm that the phenomenon does not occur with low density water inside or outside the casks.

Calculations for the MPC designs with internal and external moderators of various densities are shown in Table 6.4.1. For comparison purposes, a calculation for a single unreflected cask (Case 1) is also included in Table 6.4.1. At 100% external moderator density, Case 2 corresponds to a single fully-flooded cask, fully reflected by water. Results listed in Table 6.4.1 support the following conclusions:

† PNL critical experiments have shown a small positive reactivity effect of thick steel reflectors, with the maximum effect at 1 cm distance from the fuel. In the cask designs, the fuel is mechanically prohibited from being positioned at a 1 cm spacing from the overpack steel.

- For each type of MPC, the calculated k_{eff} for a fully-flooded cask is independent of the external moderator (the small variations in the listed values are due to statistical uncertainties which are inherent to the calculational method (Monte Carlo)), and

- For each type of MPC, reducing the internal moderation results in a monotonic reduction in reactivity, with no evidence of any optimum moderation. Thus, the fully flooded condition corresponds to the highest reactivity, and the phenomenon of optimum low-density moderation does not occur and is not applicable to the HI-STAR 100 System.

For each of the MPC designs, the maximum k_{eff} values are shown to be less than or statistically equal to that of a single internally flooded unreflected cask and are below the regulatory limit of 0.95.

6.4.2.2 Partial Flooding

As required by NUREG-1536, calculations in this section address partial flooding in the HI-STAR 100 System and demonstrate that the fully flooded condition is the most reactive.

The reactivity changes during the flooding process were evaluated in both the vertical and horizontal positions for all MPC designs. For these calculations, the cask is partially filled (at various levels) with full density (1.0 g/cc) water and the reminder of the cask is filled with steam consisting of ordinary water at partial density (0.002 g/cc), as suggested in NUREG-1536. Results of these calculations are shown in Table 6.4.2. In all cases, the reactivity increases monotonically as the water level rises, confirming that the most reactive condition is fully flooded.

6.4.2.3 Clad Gap Flooding

As required by NUREG-1536, the reactivity effect of flooding the fuel rod pellet-to-clad gap regions, in the fully flooded condition, has been investigated. Table 6.4.3 presents maximum k_{eff} values that demonstrate the positive reactivity effect associated with flooding the pellet-to-clad gap regions. These results confirm that it is conservative to assume that the pellet-to-clad gap regions are flooded. For all cases that involve flooding, the pellet-to-clad gap regions are assumed to be flooded.

6.4.2.4 Preferential Flooding

Preferential or uneven flooding within the HI-STAR 100 System was not evaluated because such a condition is not credible for any of the MPC basket designs loaded in the HI-STAR cask. Preferential flooding of any of the MPC fuel basket designs is not possible because flow holes are present on all four walls of each basket cell and on the two flux trap walls at both the top and bottom of the MPC basket. The flow holes are sized to ensure that they cannot be blocked by crud deposits (see Chapter 11). Because the fuel cladding temperatures remain below their design limits (as demonstrated in Chapter 4) and the inertial loading remains below 63g's (the inertial loadings associated with the design basis drop accidents discussed in Chapter 11 are limited to 60g's), the cladding remains intact (see Section 3.5). For damaged BWR fuel assemblies and BWR fuel debris, the assemblies or debris are pre-loaded into stainless steel Damaged Fuel Containers fitted with 250 micron fine mesh screens which prevent damaged fuel assemblies or fuel debris from blocking the basket flow holes. Therefore, the flow holes cannot be blocked.

Once established, the integrity of the MPC confinement boundary is maintained during all credible off-normal and accident conditions, and thus, the MPC cannot be flooded. Therefore, it is concluded that the MPC fuel baskets cannot be preferentially flooded.

6.4.2.5 Design Basis Accidents

The analyses presented in Chapters 3 and 11 demonstrate that the damage resulting from the design basis accidents is limited to a loss of the neutron shield material as a result of the fire accident. Because the criticality analyses do not take credit for the neutron shield material (Holtite-A), this condition has no effect on the criticality analyses.

As reported in Chapter 3, the minimum factor of safety for the MPC-24 as a result of the hypothetical cask drop or tip-over accident is 1.17 against the Level D allowables for Subsection NG, Section III of the ASME Code. Therefore, because the maximum box wall stresses are well within the ASME Level D allowables, the flux-trap gap change will be insignificant compared to the characteristic dimension of the flux trap.

In summary, the design basis accidents have no adverse effect on the design parameters important to criticality safety, and therefore, there is no increase in reactivity as a result of any of the credible off-normal or accident conditions involving handling, packaging, transfer or storage. Consequently, the HI-STAR 100 System is in full compliance with the requirement of 10CRF72.124, which states that "before a nuclear criticality accident is possible, at least two unlikely, independent, and concurrent or sequential changes have occurred in the conditions essential to nuclear criticality safety."

6.4.3 Criticality Results

Results of the criticality safety calculations for the condition of flooding with clean unborated water are presented in Section 6.2 and summarized in Section 6.1. These data confirm that for each of the candidate fuel types and basket configurations the effective multiplication factor (k_{eff}), including all biases and uncertainties at a 95-percent confidence level, do not exceed 0.95 under all credible normal, off-normal, and accident conditions.

Additional calculations (CASMO-3) at elevated temperatures confirm that the temperature coefficients of reactivity are negative as shown in Table 6.3.1. This confirms that the calculations for the storage baskets are conservative.

In calculating the maximum reactivity, the analysis used the following equation:

$$k_{eff}^{max} = k_c + K_c \sigma_c + Bias + \sigma_B$$

where:

- $\Rightarrow$ k_c is the calculated k_{eff} under the worst combination of tolerances;
- $\Rightarrow$ K_c is the K multiplier for a one-sided statistical tolerance limit with 95% probability at the 95% confidence level [6.1.8]. Each final k_{eff} value calculated by MCNP4a (or KENO5a) is the result of averaging 100 (or more) cycle k_{eff} values, and thus, is based on a sample size of 100. The K multiplier corresponding to a sample size of 100 is 1.93. However, for this analysis a value of 2.00 was assumed for the K multiplier, which is larger (more conservative) than the value corresponding to a sample size of 100;
- $\Rightarrow$ σ_c is the standard deviation of the calculated k_{eff}, as determined by the computer code (MCNP4a or KENO5a);
- $\Rightarrow$ ***Bias*** is the systematic error in the calculations (code dependent) determined by comparison with critical experiments in Appendix 6.A; and
- $\Rightarrow$ σ_B is the standard error of the bias (which includes the K multiplier for 95% probability at the 95% confidence level; see Appendix 6.A).

Appendix 6.A presents the critical experiment benchmarking and the derivation of the bias and standard error of the bias (95% probability at the 95% confidence level).

6.4.4 Damaged Fuel Container

Both damaged BWR fuel assemblies and BWR fuel debris are required to be loaded into Damaged Fuel Containers (DFCs) prior to being loaded into the MPC. Two different DFC types

with slightly different cross sections are analyzed. DFCs containing fuel debris must be stored in the MPC-68F. DFCs containing damaged fuel assemblies may be stored in either the MPC-68 or MPC-68F. Evaluation of the capability of storing damaged fuel and fuel debris (loaded in DFCs) is limited to very low reactivity fuel in the MPC-68F. Because the MPC-68 has a higher specified ^{10}B loading, the evaluation of the MPC-68F conservatively bounds the storage of damaged BWR fuel assemblies in a standard MPC-68 Although the maximum planar-average enrichment of the damaged fuel is limited to 2.7% ^{235}U as specified in Appendix B to the Certificate of Compliance, analyses have been made for three possible scenarios, conservatively assuming fuel[††] of 3.0% enrichment. The scenarios considered included the following:

1. Lost or missing fuel rods, calculated for various numbers of missing rods in order to determine the maximum reactivity. The configurations assumed for analysis are illustrated in Figures 6.4.2 through 6.4.8.
2. Broken fuel assembly with the upper segments falling into the lower segment creating a close-packed array (described as a 8x8 array). For conservatism, the array analytically retained the same length as the original fuel assemblies in this analysis. This configuration is illustrated in Figure 6.4.9.
3. Fuel pellets lost from the assembly and forming powdered fuel dispersed through a volume equivalent to the height of the original fuel. (Flow channel and clad material assumed to disappear).

Results of the analyses, shown in Table 6.4.5, confirm that, in all cases, the maximum reactivity is well below the regulatory limit. There is no significant difference in reactivity between the two DFC types. Collapsed fuel reactivity (simulating fuel debris) is low because of the reduced moderation. Dispersed powdered fuel results in low reactivity because of the increase in ^{238}U neutron capture (higher effective resonance integral for ^{238}U absorption).

The loss of fuel rods results in a small increase in reactivity (i.e., rods assumed to collapse, leaving a smaller number of rods still intact). The peak reactivity occurs for 8 missing rods, and a smaller (or larger) number of intact rods will have a lower reactivity, as indicated in Table 6.4.5.

The analyses performed and summarized in Table 6.4.5 provides the relative magnitude of the effects on the reactivity. This information coupled with the maximum k_{eff} values listed in Table 6.1.3 and the conservatism in the analyses, demonstrate that the maximum k_{eff} of the damaged fuel in the most adverse post-accident condition will remain well below the regulatory requirement of $k_{eff} < 0.95$.

Appendix 6.D provides sample input files for the damaged fuel analysis.

---

†† 6x6A01 and 7x7A01 fuel assemblies were used as representative assemblies.

6.4.5 Fuel Assemblies with Missing Rods

For fuel assemblies that are qualified for damaged fuel storage, missing and/or damaged fuel rods are acceptable. However, for fuel assemblies to meet the limitations of intact fuel assembly storage, missing fuel rods must be replaced with dummy rods that displace a volume of water that is equal to, or larger than, that displaced by the original rods.

6.4.6 Thoria Rod Canister

The Thoria Rod Canister is similar to a DFC with an internal separator assembly containing 18 intact fuel rods. The configuration is illustrated in Figure 6.4.10. The k_{eff} value for an MPC-68F filled with Thoria Rod Canisters is calculated to be 0.1813. This low reactivity is attributed to the relatively low content in ^{235}U (equivalent to UO_2 fuel with an enrichment of approximately 1.7 wt% ^{235}U), the large spacing between the rods (the pitch is approximately 1", the cladding OD is 0.412") and the absorption in the separator assembly. Together with the maximum k_{eff} values listed in Tables 6.1.2 and 6.1.3 this result demonstrates, that the k_{eff} for a Thoria Rod Canister loaded into the MPC68 or the MPC68F together with other approved fuel assemblies or DFCs will remain well below the regulatory requirement of $k_{eff} < 0.95$.

6.4.7 Sealed Rods replacing BWR Water Rods

Some BWR fuel assemblies contain sealed rods filled with a non-fissile instead of water rods. Compared to the configuration with water rods, the configuration with sealed rods has a reduced amount of moderator, while the amount of fissile material is maintained. Thus, the reactivity of the configuration with sealed rods will be lower compared to the configuration with water rods. Any configuration containing sealed rods instead of water rods is therefore bounded by the analysis for the configuration with water rods and no further analysis is required to demonstrate the acceptability. Therefore, for all BWR fuel assemblies analyzed, it is permissible that water rods are replaced by sealed rods filled with a non-fissile material.

6.4.8 Inserts in PWR Fuel Assemblies

Inserts into PWR fuel assemblies such as Thimble Plugs (TPs) and Burnable Poison Rod Assemblies (BPRAs) and similar devices are permitted for storage with all PWR fuel types. The reactivity of any PWR assembly with inserts is bounded by (i.e. lower than) the reactivity of the same assembly without the insert. This is due to the fact that the insert reduces the amount of moderator in the assembly, while the amount of fissile material remains unchanged. Therefore,

from a criticality safety perspective, inserts into PWR assemblies are acceptable for all allowable PWR types, and increase the safety margin.

6.4.9 Neutron Sources in Fuel Assemblies

Fuel assemblies containing start-up neutron sources are permitted for storage in the HI-STAR 100 System. The reactivity of a fuel assembly is not affected by the presence of a neutron source (other than by the presence of the material of the source, which is discussed later). This true because in a system with a keff less than 1.0, any given neutron population at any time, regardless of its origin or size, will decrease over time. Therefore, a neutron source of any strength will not increase reactivity, but only the neutron flux in a system, and no additional criticality analyses are required. Sources are inserted as rods into fuel assemblies, i.e. they replace either a fuel rod or water rod (moderator). Therefore, the insertion of the material of the source into a fuel assembly will not lead to an increase of reactivity either.

Table 6.4.1

MAXIMUM REACTIVITIES WITH REDUCED WATER DENSITIES FOR CASK ARRAYS[†]

	Water Density		MCNP4a Maximum k_{eff}[††]	
Case Number	Internal	External	MPC-24 (17x17A01 @ 4.0%)	MPC-68 (8x8C04 @ 4.2%)
1	100%	single cask	0.9368	0.9348
2	100%	100%	0.9354	0.9339
3	100%	70%	0.9362	0.9339
4	100%	50%	0.9352	0.9347
5	100%	20%	0.9372	0.9338
6	100%	10%	0.9380	0.9336
7	100%	5%	0.9351	0.9333
8	100%	0%	0.9342	0.9338
9	70%	0%	0.8337	0.8488
10	50%	0%	0.7426	0.7631
11	20%	0%	0.5606	0.5797
12	10%	0%	0.4834	0.5139
13	5%	0%	0.4432	0.4763
14	10%	100%	0.4793	0.4946

† For an infinite square array of casks with 60cm spacing between cask surfaces

†† Maximum k_{eff} includes the bias, uncertainties, and calculational statistics, evaluated for the worst case combination of manufacturing tolerances.

Table 6.4.2

REACTIVITY EFFECTS OF PARTIAL CASK FLOODING

MPC-24 (17x17A01 @ 4.0% ENRICHMENT)			
Flooded Condition (% Full)	Vertical Orientation	Flooded Condition (% Full)	Horizontal Orientation
25	0.9157	25	0.8766
50	0.9305	50	0.9240
75	0.9330	75	0.9329
100	0.9368	100	0.9368
MPC-68 (8x8C04 @ 4.2% ENRICHMENT)			
Flooded Condition (% Full)	Vertical Orientation	Flooded Condition (% Full)	Horizontal Orientation
25	0.9132	23.5	0.8586
50	0.9307	50	0.9088
75	0.9312	76.5	0.9275
100	0.9348	100	0.9348

Notes:

1. All values are maximum k_{eff} which include bias, uncertainties, and calculational statistics, evaluated for the worst case combination of manufacturing tolerances.

Table 6.4.3

REACTIVITY EFFECT OF FLOODING THE PELLET-TO-CLAD GAP

Pellet-to-Clad Condition	MPC-24 17x17A01 4.0% Enrichment	MPC-68 8x8C04 4.2% Enrichment
dry	0.9295	0.9279
flooded	0.9368	0.9348

Notes:

1. All values are maximum k_{eff} which includes bias, uncertainties, and calculational statistics, evaluated for the worst case combination of manufacturing tolerances.

Table 6.4.4

DELETED

Table 6.4.5

MAXIMUM k_{eff} VALUES† IN THE DAMAGED FUEL CONTAINER

Condition	MCNP4a Maximum†† k_{eff}	
	DFC Dimensions: ID 4.93" THK. 0.12"	**DFC Dimensions: ID 4.81" THK. 0.11"**
6x6 Fuel Assembly		
6x6 Intact Fuel	0.7086	0.7016
w/32 Rods Standing	0.7183	0.7117
w/28 Rods Standing	0.7315	0.7241
w/24 Rods Standing	0.7086	0.7010
w/18 Rods Standing	0.6524	0.6453
Collapsed to 8x8 array	0.7845	0.7857
Dispersed Powder	0.7628	0.7440
7x7 Fuel Assembly		
7x7 Intact Fuel	0.7463	0.7393
w/41 Rods Standing	0.7529	0.7481
w/36 Rods Standing	0.7487	0.7444
w/25 Rods Standing	0.6718	0.6644

† These calculations were performed with a planar-average enrichment of 3.0% and a ^{10}B loading of 0.0067 g/cm^2, which is 75% of a minimum ^{10}B loading of 0.0089 g/cm^2. The minimum ^{10}B loading in the MPC-68F is 0.010 g/cm^2. Therefore, the listed maximum k_{eff} values are conservative.

†† Maximum k_{eff} includes bias, uncertainties, and calculational statistics, evaluated for the worst case combination of manufacturing tolerances.

DELETED

FIGURE 6.4.1

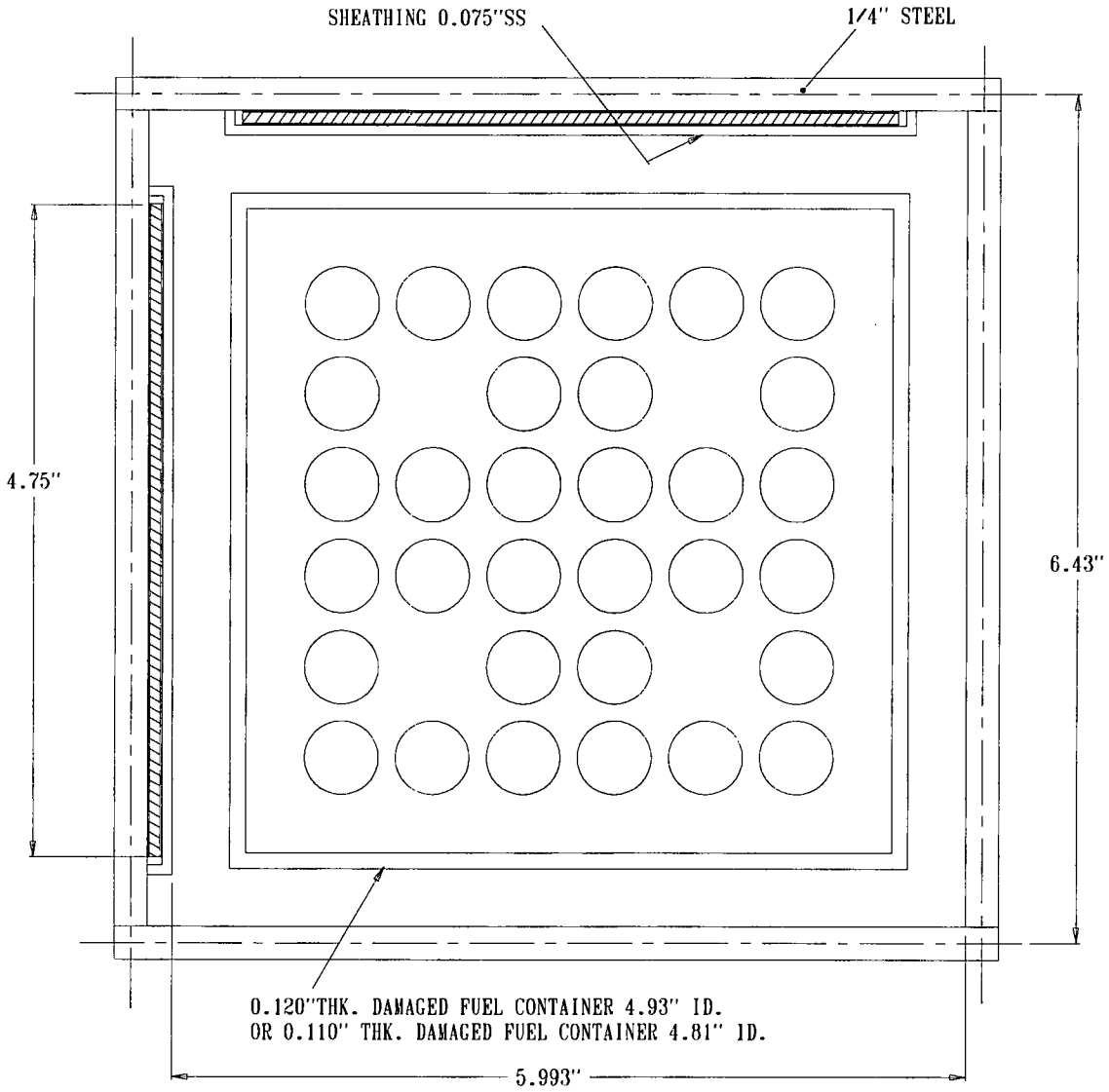

FIGURE 6.4.2; FAILED FUEL CALCULATION MODEL (PLANAR CROSS-SECTION) WITH 6X6 ARRAY WITH 4 MISSING RODS IN THE MPC-68 BASKET (SEE CHAPTER 1 FOR TRUE BASKET DIMENSIONS)

NOTE: THESE DIMENSIONS WERE CONSERVATIVELY USED FOR CRITICALITY ANALYSES.

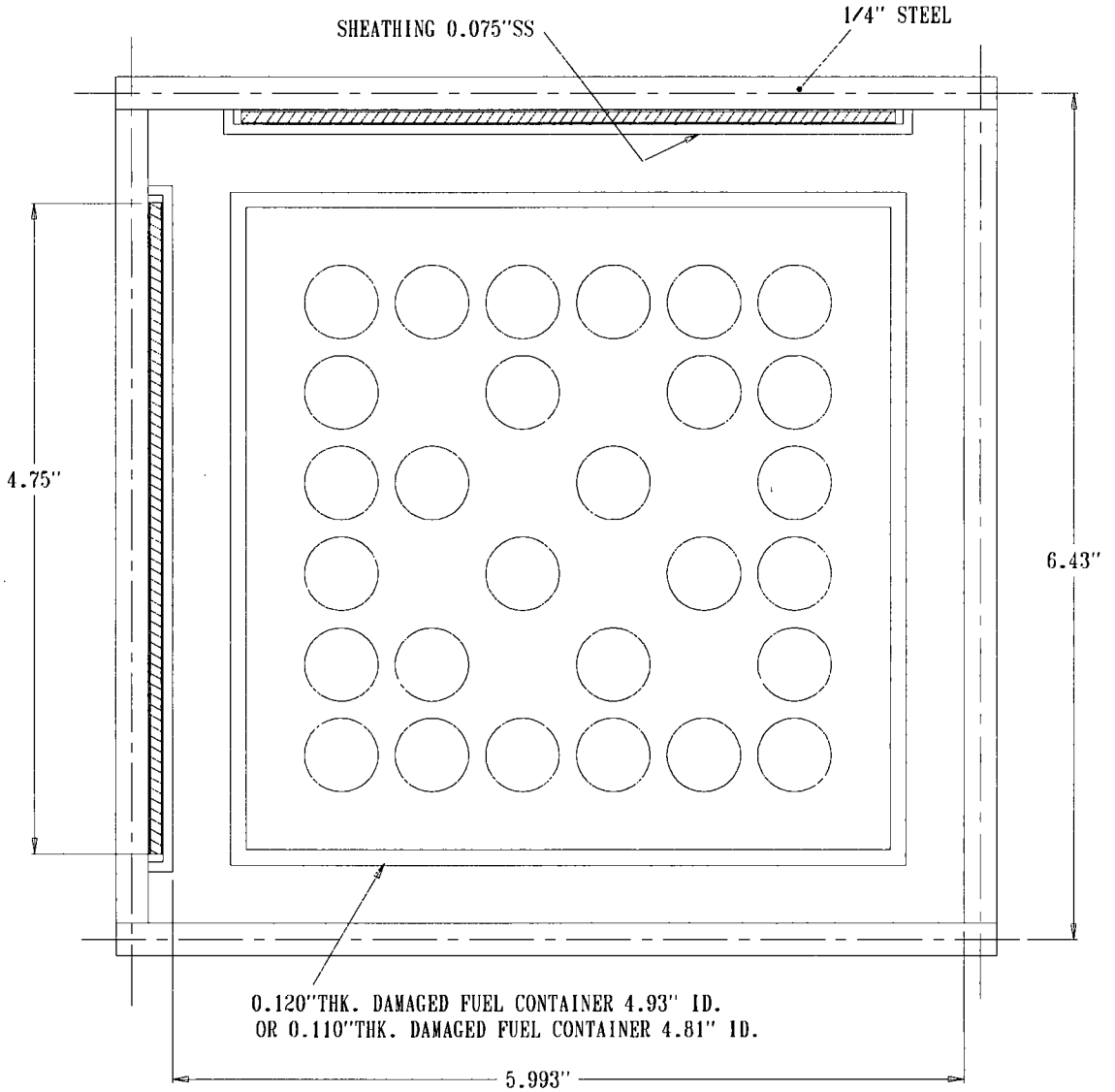

FIGURE 6.4.3; FAILED FUEL CALCULATION MODEL (PLANAR CROSS-SECTION) WITH 6X6 ARRAY WITH 8 MISSING RODS IN THE MPC-68 BASKET (SEE CHAPTER 1 FOR TRUE BASKET DIMENSIONS)

NOTE: THESE DIMENSIONS WERE CONSERVATIVELY USED FOR CRITICALITY ANALYSES.

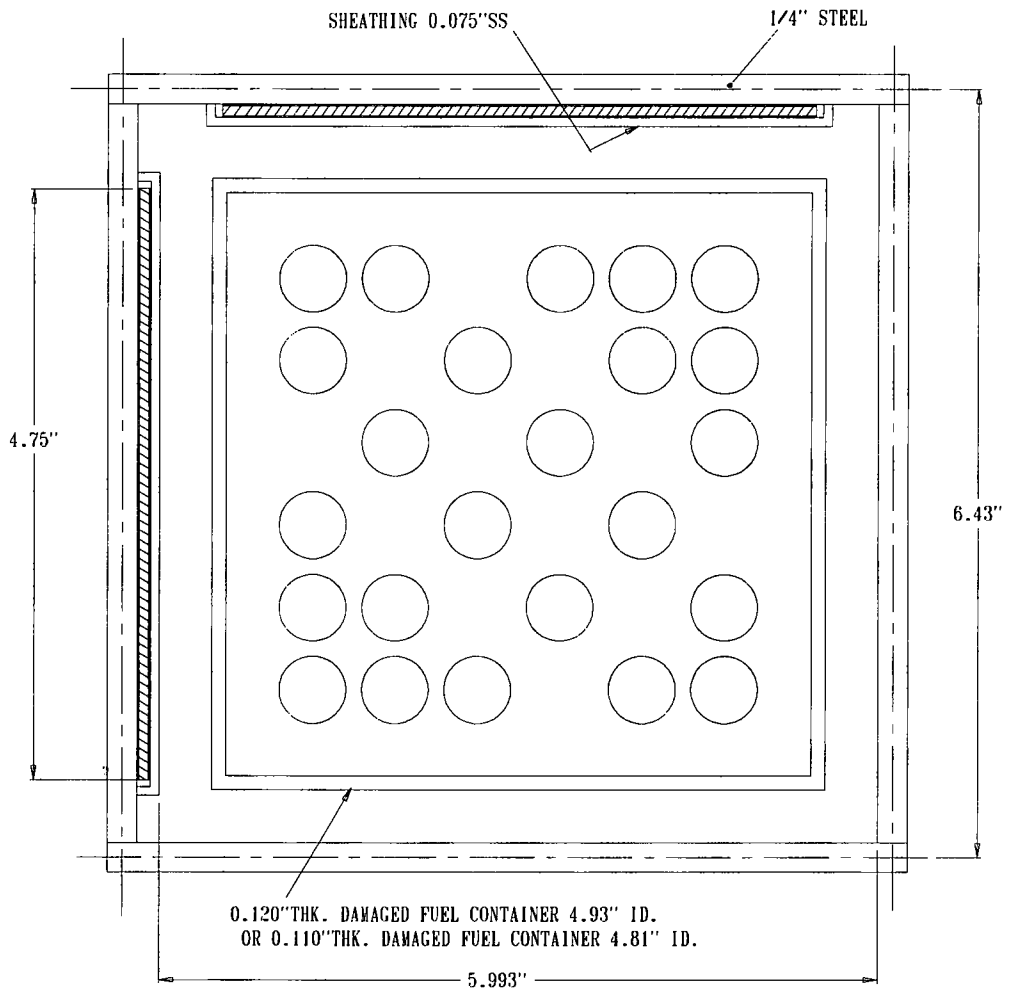

FIGURE 6.4.4; FAILED FUEL CALCULATION MODEL (PLANAR CROSS-SECTION) WITH 6X6 ARRAY WITH 12 MISSING RODS IN THE MPC-68 BASKET (SEE CHAPTER 1 FOR TRUE BASKET DIMENSIONS)

NOTE: THESE DIMENSIONS WERE CONSERVATIVELY USED FOR CRITICALITY ANALYSES.

REPORT HI-2012610 REVISION 0

e\PROJECTS\5014\HI941184\CH 6\6 4 4

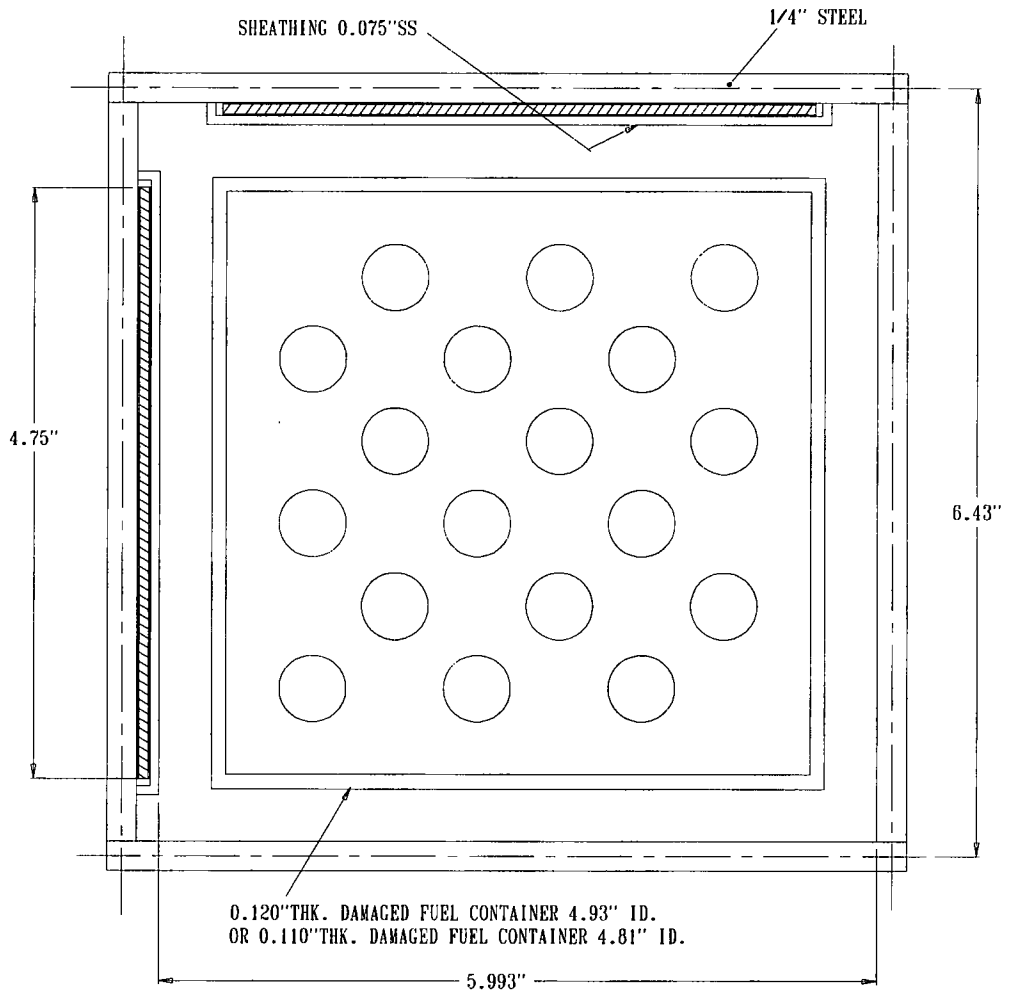

FIGURE 6.4.5; FAILED FUEL CALCULATION MODEL (PLANAR CROSS-SECTION)
WITH 6X6 ARRAY WITH 18 MISSING RODS IN THE MPC-68 BASKET
(SEE CHAPTER 1 FOR TRUE BASKET DIMENSIONS)

NOTE: THESE DIMENSIONS WERE CONSERVATIVELY USED FOR CRITICALITY ANALYSES.

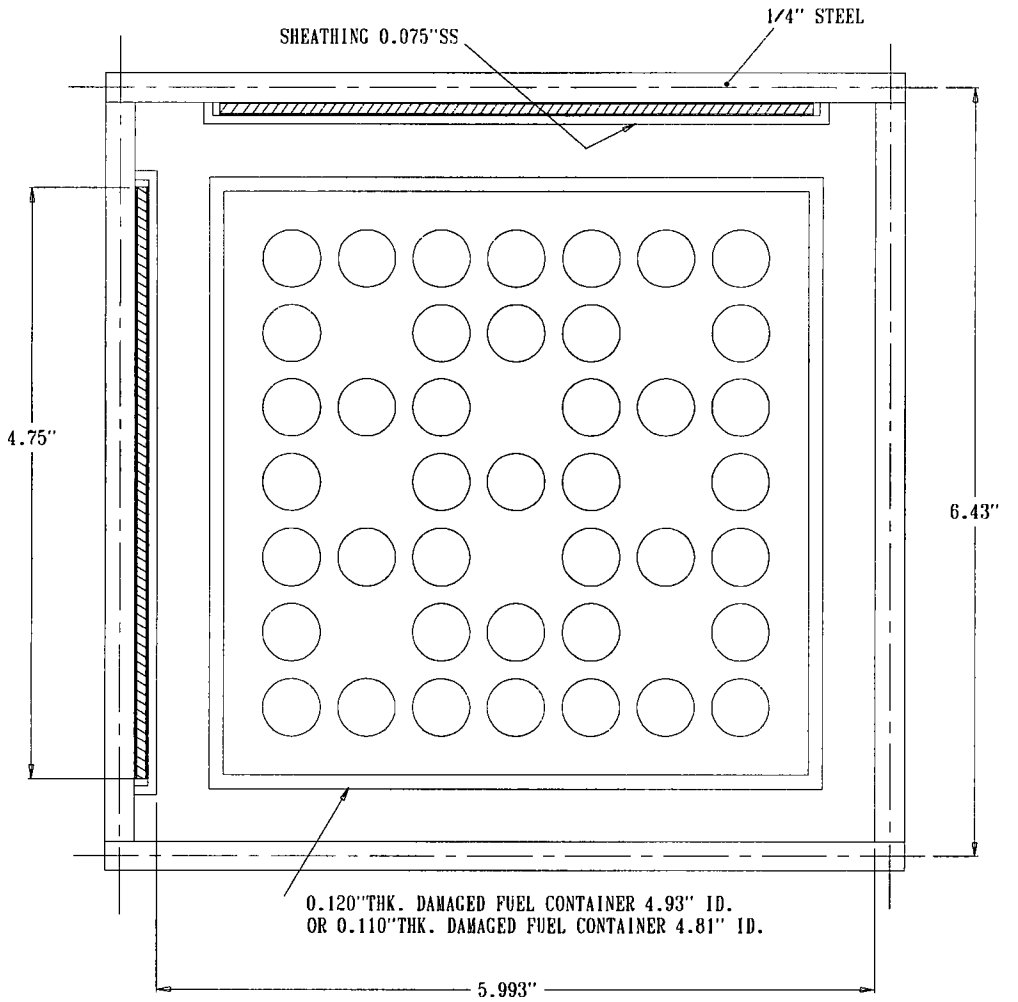

FIGURE 6.4.6; FAILED FUEL CALCULATION MODEL (PLANAR CROSS-SECTION) WITH 7X7 ARRAY WITH 8 MISSING RODS IN THE MPC-68 BASKET (SEE CHAPTER 1 FOR TRUE BASKET DIMENSIONS)

NOTE: THESE DIMENSIONS WERE CONSERVATIVELY USED FOR CRITICALITY ANALYSES.

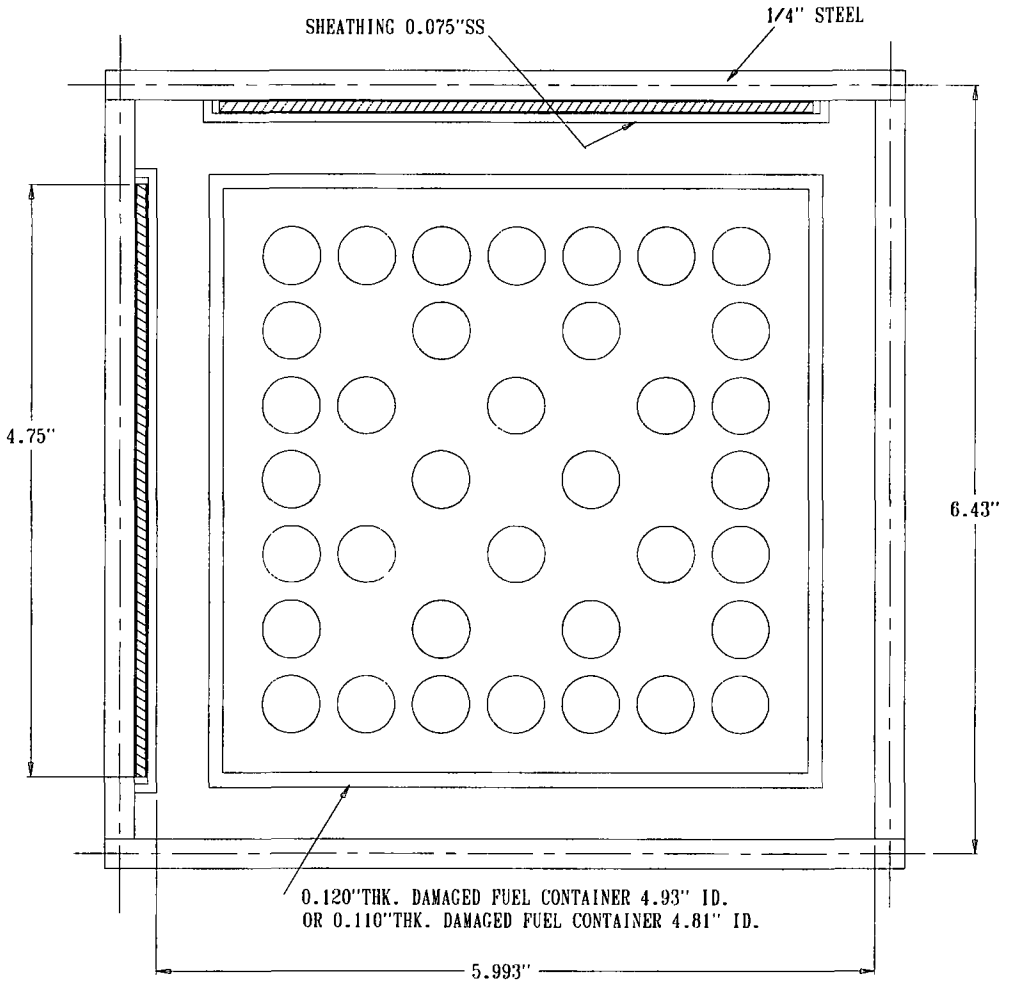

FIGURE 6.4.7; FAILED FUEL CALCULATION MODEL (PLANAR CROSS-SECTION)
WITH 7X7 ARRAY WITH 13 MISSING RODS IN THE MPC-68 BASKET
(SEE CHAPTER 1 FOR TRUE BASKET DIMENSIONS)

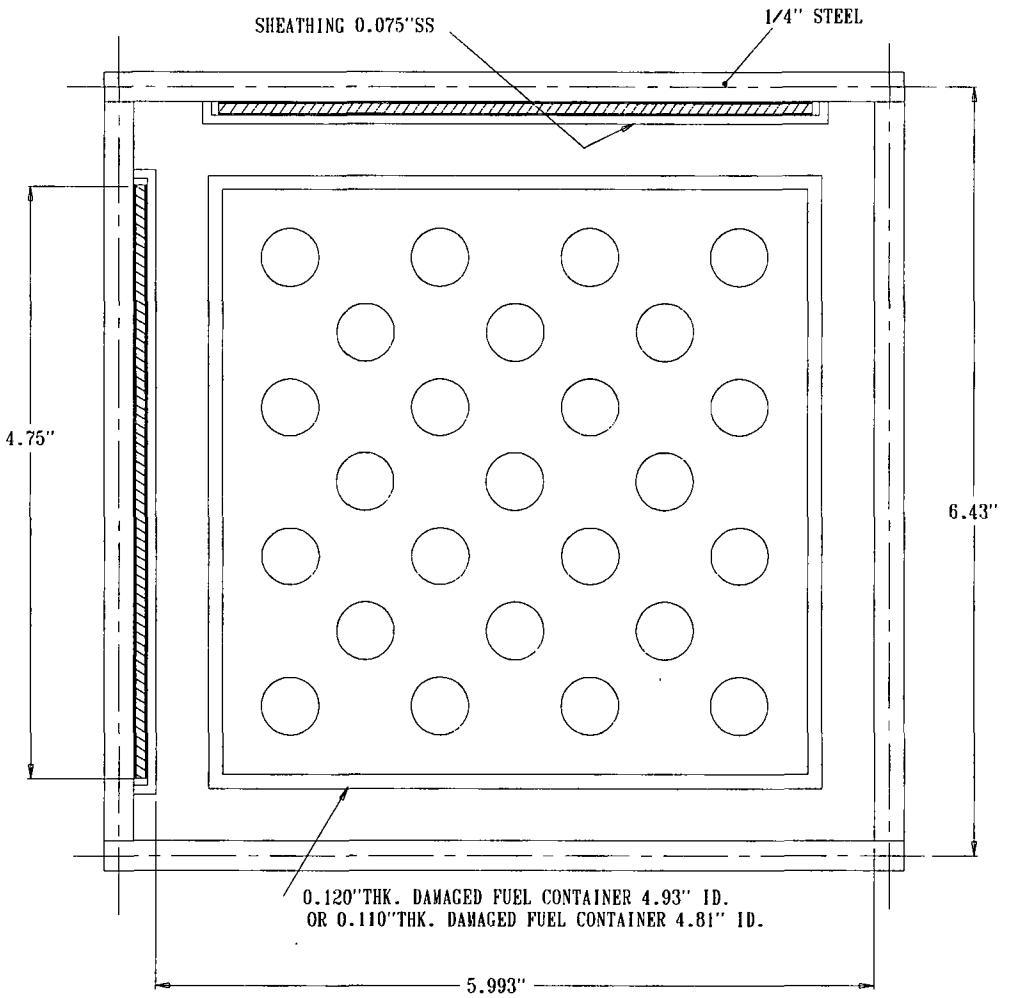

FIGURE 6.4.8; FAILED FUEL CALCULATION MODEL (PLANAR CROSS-SECTION) WITH 7X7 ARRAY WITH 24 MISSING RODS IN THE MPC-68 BASKET (SEE CHAPTER 1 FOR TRUE BASKET DIMENSIONS)

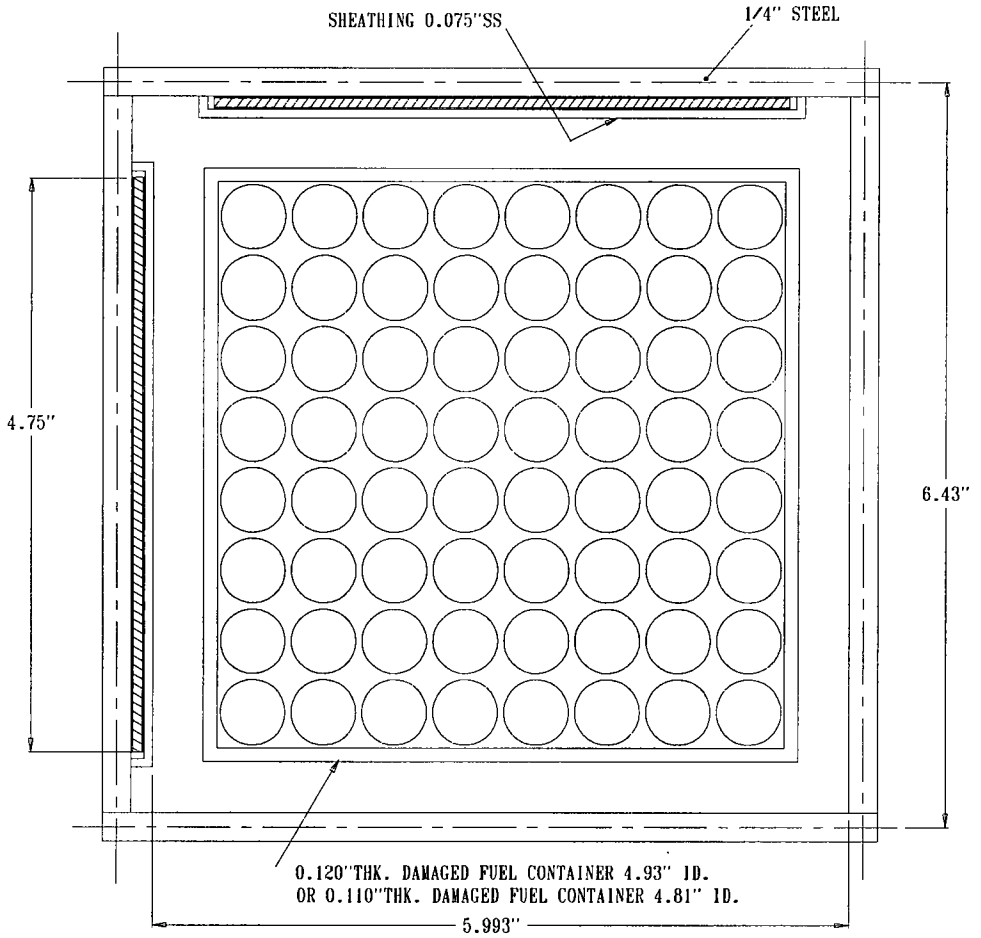

FIGURE 6.4.9; FAILED FUEL CALCULATION MODEL (PLANAR CROSS-SECTION) WITH DAMAGED FUEL COLLAPSED INTO 8X8 ARRAY IN THE MPC-68 BASKET (SEE CHAPTER 1 FOR TRUE BASKET DIMENSIONS)

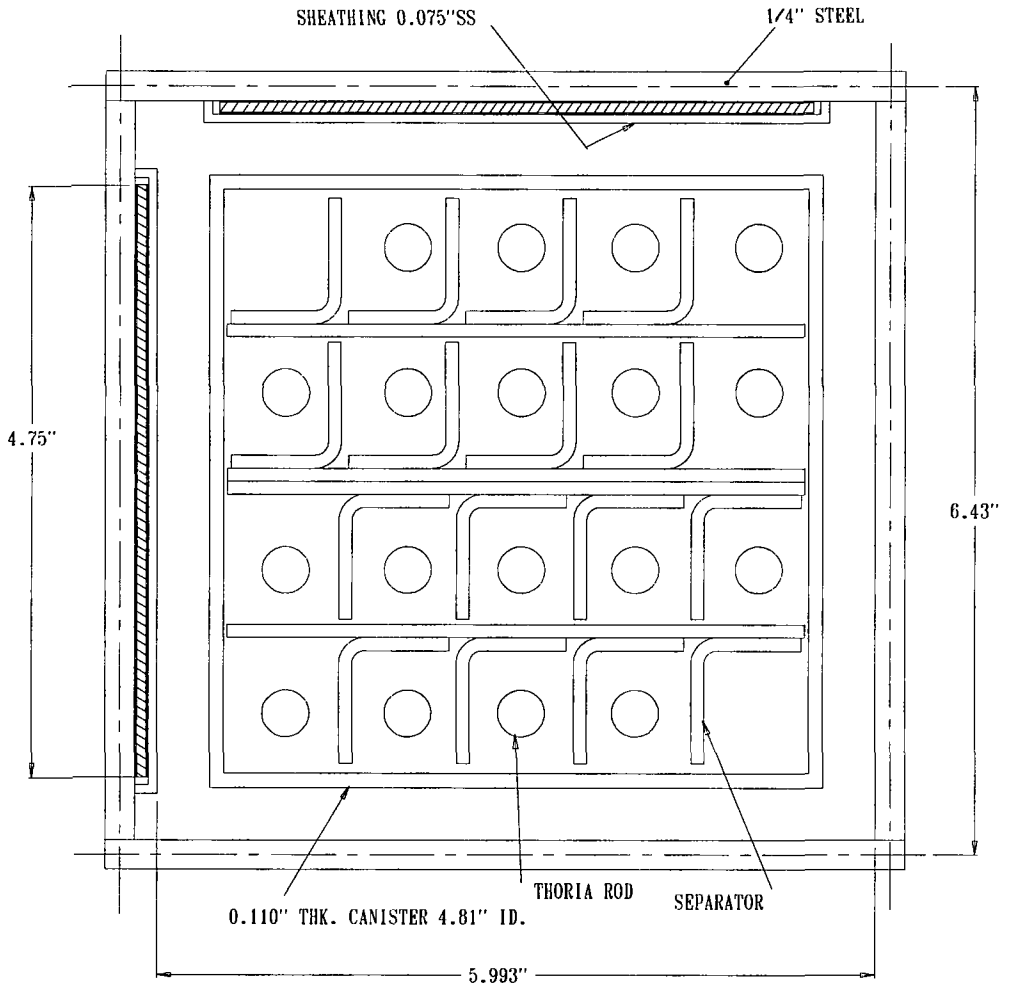

FIGURE 6.4.10; THORIA ROD CANISTER (PLANAR CROSS-SECTION)
WITH 18 THORIA RODS IN THE MPC-68 BASKET
(SEE CHAPTER 1 FOR TRUE BASKET DIMENSIONS)

6.5 CRITICALITY BENCHMARK EXPERIMENTS

Benchmark calculations have been made on selected critical experiments, chosen, insofar as possible, to bound the range of variables in the cask designs. The most important parameters are (1) the enrichment, (2) the water-gap size (MPC-24) or cell spacing (MPC-68), and (3) the ^{10}B loading of the neutron absorber panels. Other parameters, within the normal range of cask and fuel designs, have a smaller effect, but are also included. No significant trends were evident in the benchmark calculations or the derived bias. Detailed benchmark calculations are presented in Appendix 6.A.

The benchmark calculations were performed with the same computer codes and cross-section data, described in Section 6.4, that were used to calculate the k_{eff} values for the cask. Further, all calculations were performed on the same computer hardware, specifically, personal computers using the pentium processor.

6.6 REGULATORY COMPLIANCE

This chapter documents the criticality evaluation of the HI-STAR 100 System for the storage of spent nuclear fuel. This evaluation demonstrates that the HI-STAR 100 System is in full compliance with the criticality requirements of 10CFR72 and NUREG-1536.

Structures, systems, and components important to criticality safety are described in sufficient detail in this chapter to enable an evaluation of their effectiveness.

The HI-STAR 100 System is designed to be subcritical under all credible conditions. The criticality design is based on favorable geometry and fixed neutron poisons (Boral). An appraisal of the fixed neutron poisons has shown that they will remain effective for a storage period greater than 20 years, and there is no credible way to lose it, therefore there is no need to provide a positive means to verify their continued efficacy as required by 10CFR72.124(b).

The criticality evaluation has demonstrated that the cask will enable the storage of spent fuel for a minimum of 20 years with an adequate margin of safety. Further, the evaluation has demonstrated that the design basis accidents have no adverse effect on the design parameters important to criticality safety, and therefore, the HI-STAR 100 System is in full compliance with the double contingency requirements of 10CRF72.124. Therefore, it is concluded that the criticality design features for the HI-STAR 100 System are in compliance with 10 CFR Part 72 and that the applicable design and acceptance criteria have been satisfied. The criticality evaluation provides reasonable assurance that the HI-STAR 100 System will allow safe storage of spent fuel.

6.7 REFERENCES

[6.1.1] NUREG-1536, Standard Review Plan for Dry Cask Storage Systems, USNRC, Washington, D.C., January 1997.

[6.1.2] 10CFR72.124, "Criteria For Nuclear Criticality Safety."

[6.1.3] USNRC Standard Review Plan, NUREG-0800, Section 9.1.2, Spent Fuel Storage, Rev. 2 - July 1981.

[6.1.4] J.F. Briesmeister, Ed., "MCNP - A General Monte Carlo N-Particle Transport Code, Version 4A," Los Alamos National Laboratory, LA-12625-M (1993).

[6.1.5] L.M. Petrie and N.F. Landers, "KENOVa - An Improved Monte Carlo Criticality Program with Supergrouping," Volume 2, Section F11 from "SCALE: A Modular System for Performing Standardized Computer Analysis for Licensing Evaluation," NUREG/CR-0200, Rev. 4, January 1990.

[6.1.6] N.M. Greene, L.M. Petrie and R.M. Westfall, "NITAWL-II: Scale System Module For Performing Resonance Shielding and Working Library Production," Volume 1, Section F1 from "SCALE: A Modular System for Performing Standardized Computer Analysis for Licensing Evaluation," NUREG/CR-0200, Rev. 4, January 1990.

[6.1.7] J.R. Knight, "SUPERDAN: Computer Programs for Calculating the Dancoff Factor of Spheres, Cylinders, and Slabs," Oak Ridge National Laboratory, ORNL/NUREG/CSD/TM-2, March 1978, with correction published in "Proceedings of Seminar on SCALE-4," Saclay, France, 1991.

[6.1.8] M.G. Natrella, Experimental Statistics, National Bureau of Standards, Handbook 91, August 1963.

[6.1.9] A. Ahlin, M. Edenius, and H. Haggblom, "CASMO - A Fuel Assembly Burnup Program," AE-RF-76-4158, Studsvik report.

[6.1.10] A. Ahlin and M. Edenius, "CASMO - A Fast Transport Theory Depletion Code for LWR Analysis," *Trans. Am. Nucl. Soc.*, **26**, 604 (1977).

[6.1.11] "CASMO-3 A Fuel Assembly Burnup Program, Users Manual," Studsvik/NFA-87/7, Studsvik Energitechnik AB, November 1986.

[6.1.12] M. Edenius and A. Ahlin, "CASMO-3: New Features, Benchmarking, and Advanced Applications," *Nucl. Sci. Eng.*, **100**, 342-351, (1988).

[6.1.13] "QA Validation Manual for Computer Code CELLDAN," Holtec International Report HI-90577.

[6.3.1] "CASMO-4 Methodology", Studsvik/SOA-95/2, Rev. 0, 1995.

[6.3.2] "CASMO-4 A Fuel Assembly Burnup Program, Users Manual," SSP-01/400, Rev. 1, Studsvik Scandpower, Inc., 2001.

[6.3.3] "CASMO-4 Benchmark Against Critical Experiments", Studsvik/SOA-94/13, Studsvik of America, 1995.

[6.4.1] "SCALE 4.3: A Modular System for Performing Standardized Computer Analysis for Licensing Evaluations," NUREG-CR-0200, Rev. 5, Oak Ridge National Laboratory (1995).

[6.4.2] J.M. Cano, R. Caro, and J.M Martinez-Val, "Supercriticality Through Optimum Moderation in Nuclear Fuel Storage," *Nucl. Technol.*, **48**, 251-260, (1980).

APPENDIX 6.A: BENCHMARK CALCULATIONS

6.A.1 INTRODUCTION AND SUMMARY

Benchmark calculations have been made on selected critical experiments, chosen, in so far as possible, to bound the range of variables in the cask designs. Two independent methods of analysis were used, differing in cross section libraries and in the treatment of the cross sections. MCNP4a [6.A.1] is a continuous energy Monte Carlo code and KENO5a [6.A.2] uses group-dependent cross sections. For the KENO5a analyses reported here, the 238-group library was chosen, processed through the NITAWL-II [6.A.2] program to create a working library and to account for resonance self-shielding in uranium-238 (Nordheim integral treatment). The 238 group library was chosen to avoid or minimize the errors[†] (trends) that have been reported (e.g., [6.A.3 through 6.A.5]) for calculations with collapsed cross section sets.

In cask designs, the three most significant parameters affecting criticality are (1) the fuel enrichment, (2) the ^{10}B loading in the neutron absorber, and (3) the lattice spacing (or water-gap thickness if a flux-trap design is used). Other parameters, within the normal range of cask and fuel designs, have a smaller effect, but are also included in the analyses.

Table 6.A.1 summarizes results of the benchmark calculations for all cases selected and analyzed, as referenced in the table. The effect of the major variables are discussed in subsequent sections below. It is important to note that there is obviously considerable overlap in parameters since it is not possible to vary a single parameter and maintain criticality; some other parameter or parameters must be concurrently varied to maintain criticality.

One possible way of representing the data is through a spectrum index that incorporates all of the variations in parameters. KENO5a computes and prints the "energy of the average lethargy causing fission". In MCNP4a, by utilizing the tally option with the identical 238-group energy structure as in KENO5a, the number of fissions in each group may be collected and the energy of the average lethargy causing fission determined (post-processing).

Figures 6.A.1 and 6.A.2 show the calculated k_{eff} for the benchmark critical experiments as a function of the "energy of the average lethargy causing fission" for MCNP4a and KENO5a, respectively (UO_2 fuel only). The scatter in the data (even for comparatively minor variation in

---

† Small but observable trends (errors) have been reported for calculations with the 27-group and 44-group collapsed libraries. These errors are probably due to the use of a single collapsing spectrum when the spectrum should be different for the various cases analyzed, as evidenced by the spectrum indices.

critical parameters) represents experimental error[†] in performing the critical experiments within each laboratory, as well as between the various testing laboratories. The B&W critical experiments show a larger experimental error than the PNL criticals. This would be expected since the B&W criticals encompass a greater range of critical parameters than the PNL criticals.

Linear regression analysis of the data in Figures 6.A.1 and 6.A.2 show that there are no trends, as evidenced by very low values of the correlation coefficient (0.13 for MCNP4a and 0.21 for KENO5a). The total bias (systematic error, or mean of the deviation from a k_{eff} of exactly 1.000) for the two methods of analysis are shown in the table below.

Calculational Bias of MCNP4a and KENO5a		
	Total	Truncated
MCNP4a	0.0009 ± 0.0011	0.0021 ± 0.0006
KENO5a	0.0030 ± 0.0012	0.0036 ± 0.0009

The values of bias shown in this table include both the bias derived directly from the calculated k_{eff} values in Table 6.A.1, and a more conservative value derived by arbitrarily truncating to 1.000 any calculated value that exceeds 1.000. The bias and standard error of the bias were calculated by the following equations[††], with the standard error multiplied by the one-sided K-factor for 95% probability at the 95% confidence level from NBS Handbook 91 [6.A.18] (for the number of cases analyzed, the K-factor is ~2.05 or slightly more than 2).

$$\bar{k} = \frac{1}{n}\sum_{i=1}^{n} k_i \qquad (6.A.1)$$

[†] A classical example of experimental error is the corrected enrichment in the PNL experiments, first as an addendum to the initial report and, secondly, by revised values in subsequent reports for the same fuel rods.

[††] These equations may be found in any standard text on statistics, for example, reference [6.A.6] (or the MCNP4a manual) and is the same methodology used in MCNP4a and in KENO5a.

$$\sigma_{\bar{k}}^2 = \frac{\sum_{i=1}^{n} k_i^2 - (\sum_{i=1}^{n} k_i)^2 / n}{n(n-1)} \qquad (6.A.2)$$

$$\text{Bias} = (1 - \bar{k}) \pm K\sigma_{\bar{k}} \qquad (6.A.3)$$

where k_i are the calculated reactivities for n critical experiments; $\sigma_{\bar{k}}$ is the unbiased estimator of the standard deviation of the mean (also called the standard error of the bias (mean)); and K is the one-sided multiplier for 95% probability at the 95% confidence level (NBS Handbook 91 [6.A.18]).

Formula 6.A.3 is based on the methodology of the National Bureau of Standards (now NIST) and is used to calculate the values presented on page 6.A-2. The first portion of the equation, $(1-\bar{k})$, is the actual bias which is added to the MCNP4a and KENO5a results. The second term, $K\sigma_{\bar{k}}$, which corresponds to σ_B in Section 6.4.3, is the uncertainty or standard error associated with the bias. The K values used were obtained from the National Bureau of Standards Handbook 91 and are for one-sided statistical tolerance limits for 95% probability at the 95% confidence level. The actual K values for the 56 critical experiments evaluated with MCNP4a and the 53 critical experiments evaluated with KENO5a are 2.04 and 2.05, respectively.

The larger of the calculational biases (truncated bias) was used to evaluate the maximum k_{eff} values for the cask designs.

6.A.2 Effect of Enrichment

The benchmark critical experiments include those with enrichments ranging from 2.46% to 5.74% and therefore span the enrichment range for the MPC designs. Figures 6.A.3 and 6.A.4 show the calculated k_{eff} values (Table 6.A.1) as a function of the fuel enrichment reported for the critical experiments. Linear regression analyses for these data confirms that there are no trends, as indicated by low values of the correlation coefficients (0.03 for MCNP4a and 0.38 for KENO5a). Thus, there are no corrections to the bias for the various enrichments.

As further confirmation of the absence of any trends with enrichment, the MPC-68 configuration was calculated with both MCNP4a and KENO5a for various enrichments. The cross-comparison of calculations with codes of comparable sophistication is suggested in Reg. Guide 3.41. Results of this comparison, shown in Table 6.A.2 and Figure 6.A.5, confirm no significant difference in the calculated values of k_{eff} for the two independent codes as evidenced by the 45° slope of the curve. Since it is very unlikely that two independent methods of analysis would be subject to the

same error, this comparison is considered confirmation of the absence of an enrichment effect (trend) in the bias.

6.A.3 Effect of ^{10}B Loading

Several laboratories have performed critical experiments with a variety of thin absorber panels similar to the Boral panels in the cask designs. Of these critical experiments, those performed by B&W are the most representative of the cask designs. PNL has also made some measurements with absorber plates, but, with one exception (a flux-trap experiment), the reactivity worth of the absorbers in the PNL tests is very low and any significant errors that might exist in the treatment of strong thin absorbers could not be revealed.

Table 6.A.3 lists the subset of experiments using thin neutron absorbers (from Table 6.A.1) and shows the reactivity worth (Δk) of the absorber.[†]

No trends with reactivity worth of the absorber are evident, although based on the calculations shown in Table 6.A.3, some of the B&W critical experiments seem to have unusually large experimental errors. B&W made an effort to report some of their experimental errors. Other laboratories did not evaluate their experimental errors.

To further confirm the absence of a significant trend with ^{10}B concentration in the absorber, a cross-comparison was made with MCNP4a and KENO5a (as suggested in Reg. Guide 3.41). Results are shown in Figure 6.A.6 and Table 6.A.4 for the MPC-68 cask[††] geometry. These data substantiate the absence of any error (trend) in either of the two codes for the conditions analyzed (data points fall on a 45° line, within an expected 95% probability limit).

---

† The reactivity worth of the absorber panels was determined by repeating the calculation with the absorber analytically removed and calculating the incremental (Δk) change in reactivity due to the absorber.

†† The MPC-68 geometry was chosen for this comparison since it contains the greater number of Boral panels and would therefore be expected to be the most sensitive to trends (errors) in calculations.

6.A.4 Miscellaneous and Minor Parameters

6.A.4.1 Reflector Material and Spacings

PNL has performed a number of critical experiments with thick steel and lead reflectors.[†] Analysis of these critical experiments are listed in Table 6.A.5 (subset of data in Table 6.A.1). There appears to be a small tendency toward overprediction of k_{eff} at the lower spacing, although there are an insufficient number of data points in each series to allow a quantitative determination of any trends. The tendency toward overprediction at close spacing means that the cask calculations may be slightly more conservative than otherwise.

6.A.4.2 Fuel Pellet Diameter and Lattice Pitch

The critical experiments selected for analysis cover a range of fuel pellet diameters from 0.311 to 0.444 inches, and lattice spacings from 0.476 to 1.00 inches. In the cask designs, the fuel pellet diameters range from 0.303 to 0.3835 inches O.D. (0.496 to 0.580 inch lattice spacing) for PWR fuel and from 0.3224 to 0.498 inches O.D. (0.488 to 0.740 inch lattice spacing) for BWR fuel. Thus, the critical experiments analyzed provide a reasonable representation of the fuel in the MPC designs. Based on the data in Table 6.A.1, there does not appear to be any observable trend with either fuel pellet diameter or lattice pitch, at least over the range of the critical experiments or the cask designs.

6.A.4.3 Soluble Boron Concentration Effects

Various soluble boron concentrations were used in the B&W series of critical experiments and in one PNL experiment, with boron concentrations ranging up to 2550 ppm. Results of MCNP4a (and one KENO5a) calculations are shown in Table 6.A.6. Analyses of the very high boron concentration experiments (>1300 ppm) show a tendency to slightly overpredict reactivity for the three experiments exceeding 1300 ppm. In turn, this would suggest that the evaluation of the MPC-32 with various soluble boron concentration could be slightly conservative for the high soluble boron concentration.

6.A.5 MOX Fuel

The number of critical experiments with PuO_2 bearing fuel (MOX) is more limited than for UO_2 fuel. However, a number of MOX critical experiments have been analyzed and the results are

[†]Parallel experiments with a depleted uranium reflector were also performed but not included in the present analysis since they are not pertinent to the Holtec cask design. A lead reflector is also not directly pertinent, but might be used in future designs.

shown in Table 6.A.7. Results of these analyses are generally above a k_{eff} of 1.00, indicating that when Pu is present, MCNP4a and KENO5a overpredict the reactivity.

This may indicate that calculation for MOX fuel will be expected to be conservative, especially with MCNP4a. It may be noted that for the larger lattice spacings, the KENO5a calculated reactivities are below 1.00, suggested that a small trend may exist with KENO5a. It is also possible that the overprediction in k_{eff} in both codes may be due to a small inadequacy in the determination of the Pu-241 decay and Am-241 growth. This possibility is supported by the consistency in calculated k_{eff} over a wide range of the spectral index (energy of the average lethargy causing fission).

6.A.6 References

[6.A.1] J.F. Briesmeister, Ed., "MCNP - A General Monte Carlo N-Particle Transport Code, Version 4A; Los Alamos National Laboratory, LA-12625-M (1993).

[6.A.2] SCALE 4.3, "A Modular Code System for Performing Standardized Computer Analyses for Licensing Evaluation", NUREG-0200 (ORNL-NUREG-CSD-2/U2/R5, Revision 5, Oak Ridge National Laboratory, September 1995.

[6.A.3] M.D. DeHart and S.M. Bowman, "Validation of the SCALE Broad Structure 44-Group ENDF/B-V Cross-Section Library for Use in Criticality Safety Analyses", NUREG/CR-6102 (ORNL/TM-12460) Oak Ridge National Laboratory, September 1994.

[6.A.4] W.C. Jordan et al., "Validation of KENOV.a", CSD/TM-238, Martin Marietta Energy Systems, Inc., Oak Ridge National Laboratory, December 1986.

[6.A.5] O.W. Hermann et al., "Validation of the Scale System for PWR Spent Fuel Isotopic Composition Analysis", ORNL-TM-12667, Oak Ridge National Laboratory, undated.

[6.A.6] R.J. Larsen and M.L. Marx, An Introduction to Mathematical Statistics and its Applications, Prentice-Hall, 1986.

[6.A.7] M.N. Baldwin et al., Critical Experiments Supporting Close Proximity Water Storage of Power Reactor Fuel, BAW-1484-7, Babcock and Wilcox Company, July 1979.

[6.A.8] G.S. Hoovier et al., Critical Experiments Supporting Underwater Storage of Tightly Packed Configurations of Spent Fuel Pins, BAW-1645-4, Babcock & Wilcox Company, November 1991.

[6.A.9] L.W. Newman et al., Urania Gadolinia: Nuclear Model Development and Critical Experiment Benchmark, BAW-1810, Babcock and Wilcox Company, April 1984.

[6.A.10] J.C. Manaranche et al., "Dissolution and Storage Experimental Program with 4.75% Enriched Uranium-Oxide Rods," Trans. Am. Nucl. Soc. 33: 362-364 (1979).

[6.A.11] S.R. Bierman and E.D. Clayton, Criticality Experiments with Subcritical Clusters of 2.35 wt % and 4.31 wt % ^{235}U Enriched UO_2 Rods in Water with Steel Reflecting Walls, PNL-3602, Battelle Pacific Northwest Laboratory, April 1981.

[6.A.12] S.R. Bierman et al., Criticality Experiments with Subcritical Clusters of 2.35 Wt% and 4.31 Wt% ^{235}U Enriched UO_2 Rods in Water with Uranium or Lead Reflecting Walls, PNL-3926, Battelle Pacific Northwest Laboratory, December, 1981.

[6.A.13] S.R. Bierman et al., Critical Separation Between Subcritical Clusters of 4.31 Wt % ^{235}U Enriched UO_2 Rods in Water with Fixed Neutron Poisons, PNL-2615, Battelle Pacific Northwest Laboratory, October 1977.

[6.A.14] S.R. Bierman, Criticality Experiments with Neutron Flux Traps Containing Voids, PNL-7167, Battelle Pacific Northwest Laboratory, April 1990.

[6.A.15] B.M. Durst et al., Critical Experiments with 4.31 wt % ^{235}U Enriched UO_2 Rods in Highly Borated Water Lattices, PNL-4267, Battelle Pacific Northwest Laboratory, August 1982.

[6.A.16] S.R. Bierman, Criticality Experiments with Fast Test Reactor Fuel Pins in Organic Moderator, PNL-5803, Battelle Pacific Northwest Laboratory, December 1986.

[6.A.17] E.G. Taylor et al., Saxton Plutonium Program Critical Experiments for the Saxton Partial Plutonium core, WCAP-3385-54, Westinghouse Electric Corp., Atomic Power Division, December 1965.

[6.A.18] M.G. Natrella, Experimental Statistics, National Bureau of Standards, Handbook 91, August 1963.

Table 6.A.1
Summary of Criticality Benchmark Calculations

	Reference	Identification	Enrich.	Calculated k_{eff}		EALF (eV)	
				MCNP4a	KENO5a	MCNP4a	KENO5a
1	B&W-1484 (6.A.7)	Core I	2.46	0.9964 ± 0.0010	0.9898 ± 0.0006	0.1759	0.1753
2	B&W-1484 (6.A.7)	Core II	2.46	1.0008 ± 0.0011	1.0015 ± 0.0005	0.2553	0.2446
3	B&W-1484 (6.A.7)	Core III	2.46	1.0010 ± 0.0012	1.0005 ± 0.0005	0.1999	0.1939
4	B&W-1484 (6.A.7)	Core IX	2.46	0.9956 ± 0.0012	0.9901 ± 0.0006	0.1422	0.1426
5	B&W-1484 (6.A.7)	Core X	2.46	0.9980 ± 0.0014	0.9922 ± 0.0006	0.1513	0.1499
6	B&W-1484 (6.A.7)	Core XI	2.46	0.9978 ± 0.0012	1.0005 ± 0.0005	0.2031	0.1947
7	B&W-1484 (6.A.7)	Core XII	2.46	0.9988 ± 0.0011	0.9978 ± 0.0006	0.1718	0.1662
8	B&W-1484 (6.A.7)	Core XIII	2.46	1.0020 ± 0.0010	0.9952 ± 0.0006	0.1988	0.1965
9	B&W-1484 (6.A.7)	Core XIV	2.46	0.9953 ± 0.0011	0.9928 ± 0.0006	0.2022	0.1986
10	B&W-1484 (6.A.7)	Core XV[††]	2.46	0.9910 ± 0.0011	0.9909 ± 0.0006	0.2092	0.2014
11	B&W-1484 (6.A.7)	Core XVI[††]	2.46	0.9935 ± 0.0010	0.9889 ± 0.0006	0.1757	0.1713
12	B&W-1484 (6.A.7)	Core XVII	2.46	0.9962 ± 0.0012	0.9942 ± 0.0005	0.2083	0.2021

Table 6.A.1
Summary of Criticality Benchmark Calculations

	Reference	Identification	Enrich.	Calculated k_{eff}		EALF (eV)	
				MCNP4a	KENO5a	MCNP4a	KENO5a
13	B&W-1484 (6.A.7)	Core XVIII	2.46	1.0036 ± 0.0012	0.9931 ± 0.0006	0.1705	0.1708
14	B&W-1484 (6.A.7)	Core XIX	2.46	0.9961 ± 0.0012	0.9971 ± 0.0005	0.2103	0.2011
15	B&W-1484 (6.A.7)	Core XX	2.46	1.0008 ± 0.0011	0.9932 ± 0.0006	0.1724	0.1701
16	B&W-1484 (6.A.7)	Core XXI	2.46	0.9994 ± 0.0010	0.9918 ± 0.0006	0.1544	0.1536
17	B&W-1645 (6.A.8)	S-type Fuel, w/886 ppm B	2.46	0.9970 ± 0.0010	0.9924 ± 0.0006	1.4475	1.4680
18	B&W-1645 (6.A.8)	S-type Fuel, w/746 ppm B	2.46	0.9990 ± 0.0010	0.9913 ± 0.0006	1.5463	1.5660
19	B&W-1645 (6.A.8)	SO-type Fuel, w/1156 ppm B	2.46	0.9972 ± 0.0009	0.9949 ± 0.0005	0.4241	0.4331
20	B&W-1810 (6.A.9)	Case 1 1337 ppm B	2.46	1.0023 ± 0.0010	NC	0.1531	NC
21	B&W-1810 (6.A.9)	Case 12 1899 ppm B	2.46/4.02	1.0060 ± 0.0009	NC	0.4493	NC
22	French (6.A.10)	Water Moderator 0 gap	4.75	0.9966 ± 0.0013	NC	0.2172	NC
23	French (6.A.10)	Water Moderator 2.5 cm gap	4.75	0.9952 ± 0.0012	NC	0.1778	NC
24	French (6.A.10)	Water Moderator 5 cm gap	4.75	0.9943 ± 0.0010	NC	0.1677	NC

Table 6.A.1
Summary of Criticality Benchmark Calculations

	Reference	Identification	Enrich.	Calculated k_{eff}		EALF (eV)	
				MCNP4a	KENO5a	MCNP4a	KENO5a
25	French (6.A.10)	Water Moderator 10 cm gap	4.75	0.9979 ± 0.0010	NC	0.1736	NC
26	PNL-3602 (6.A.11)	Steel Reflector, 0 cm separation	2.35	NC	1.0004 ± 0.0006	NC	0.1018
27	PNL-3602 (6.A.11)	Steel Reflector, 1.321 cm separation	2.35	0.9980 ± 0.0009	0.9992 ± 0.0006	0.1000	0.0909
28	PNL-3602 (6.A.11)	Steel Reflector, 2.616 cm separation	2.35	0.9968 ± 0.0009	0.9964 ± 0.0006	0.0981	0.0975
29	PNL-3602 (6.A.11)	Steel Reflector, 3.912 cm separation	2.35	0.9974 ± 0.0010	0.9980 ± 0.0006	0.0976	0.0970
30	PNL-3602 (6.A.11)	Steel Reflector, Infinite separation	2.35	0.9962 ± 0.0008	0.9939 ± 0.0006	0.0973	0.0968
31	PNL-3602 (6.A.11)	Steel Reflector, 0 cm separation	4.306	NC	1.0003 ± 0.0007	NC	0.3282
32	PNL-3602 (6.A.11)	Steel Reflector, 1.321 cm separation	4.306	0.9997 ± 0.0010	1.0012 ± 0.0007	0.3016	0.3039
33	PNL-3602 (6.A.11)	Steel Reflector, 2.616 cm separation	4.306	0.9994 ± 0.0012	0.9974 ± 0.0007	0.2911	0.2927
34	PNL-3602 (6.A.11)	Steel Reflector, 5.405 cm separation	4.306	0.9969 ± 0.0011	0.9951 ± 0.0007	0.2828	0.2860
35	PNL-3602 (6.A.11)	Steel Reflector, Infinite separation	4.306	0.9910 ± 0.0020	0.9947 ± 0.0007	0.2851	0.2864
36	PNL-3602 (6.A.11)	Steel Reflector, with Boral Sheets	4.306	0.9941 ± 0.0011	0.9970 ± 0.0007	0.3135	0.3150

Table 6.A.1
Summary of Criticality Benchmark Calculations

				Calculated k_{eff}		EALF (eV)	
	Reference	Identification	Enrich.	MCNP4a	KENO5a	MCNP4a	KENO5a
37	PNL-3626 (6.A.12)	Lead Reflector, 0 cm sepn.	4.306	NC	1.0003 ± 0.0007	NC	0.3159
38	PNL-3626 (6.A.12)	Lead Reflector, 0.55 cm sepn.	4.306	1.0025 ± 0.0011	0.9997 ± 0.0007	0.3030	0.3044
39	PNL-3626 (6.A.12)	Lead Reflector, 1.956 cm sepn.	4.306	1.0000 ± 0.0012	0.9985 ± 0.0007	0.2883	0.2930
40	PNL-3626 (6.A.12)	Lead Reflector, 5.405 cm sepn.	4.306	0.9971 ± 0.0012	0.9946 ± 0.0007	0.2831	0.2854
41	PNL-2615 (6.A.13)	Experiment 004/032 – no absorber	4.306	0.9925 ± 0.0012	0.9950 ± 0.0007	0.1155	0.1159
42	PNL-2615 (6.A.13)	Experiment 030 – Zr plates	4.306	NC	0.9971 ± 0.0007	NC	0.1154
43	PNL-2615 (6.A.13)	Experiment 013 – Steel plates	4.306	NC	0.9965 ± 0.0007	NC	0.1164
44	PNL-2615 (6.A.13)	Experiment 014 – Steel plates	4.306	NC	0.9972 ± 0.0007	NC	0.1164
45	PNL-2615 (6.A.13)	Exp. 009 1.05% Boron Steel plates	4.306	0.9982 ± 0.0010	0.9981 ± 0.0007	0.1172	0.1162
46	PNL-2615 (6.A.13)	Exp. 009 1.62% Boron Steel plates	4.306	0.9996 ± 0.0012	0.9982 ± 0.0007	0.1161	0.1173
47	PNL-2615 (6.A.13)	Exp. 031 – Boral plates	4.306	0.9994 ± 0.0012	0.9969 ± 0.0007	0.1165	0.1171
48	PNL-7167 (6.A.14)	Experiment 214R – with flux traps	4.306	0.9991 ± 0.0011	0.9956 ± 0.0007	0.3722	0.3812

Table 6.A.1
Summary of Criticality Benchmark Calculations

				Calculated k_{eff}		EALF (eV)	
	Reference	Identification	Enrich.	MCNP4a	KENO5a	MCNP4a	KENO5a
49	PNL-7167 (6.A.14)	Experiment 214V3 –with flux trap	4.306	0.9969 ± 0.0011	0.9963 ± 0.0007	0.3742	0.3826
50	PNL-4267 (6.A.15)	Case 173 – 0 ppm B	4.306	0.9974 ± 0.0012	NC	0.2893	NC
51	PNL-4267 (6.A.15)	Case 177 – 2550 ppm B	4.306	1.0057 ± 0.0010	NC	0.5509	NC
52	PNL-5803 (6.A.16)	MOX Fuel – Type 3.2 Exp. 21	20% Pu	1.0041 ± 0.0011	1.0046 ± 0.0006	0.9171	0.8868
53	PNL-5803 (6.A.16)	MOX Fuel – Type 3.2 Exp. 43	20% Pu	1.0058 ± 0.0012	1.0036 ± 0.0006	0.2968	0.2944
54	PNL-5803 (6.A.16)	MOX Fuel – Type 3.2 Exp. 13	20% Pu	1.0083 ± 0.0011	0.9989 ± 0.0006	0.1665	0.1706
55	PNL-5803 (6.A.16)	MOX Fuel – Type 3.2 Exp. 32	20% Pu	1.0079 ± 0.0011	0.9966 ± 0.0006	0.1339	0.1165
56	WCAP-3385 (6.A.17)	Saxton Case 52 PuO_2 0.52" pitch	6.6% Pu	0.9996 ± 0.0011	1.0005 ± 0.0006	0.8665	0.8417
57	WCAP-3385 (6.A.17)	Saxton Case 52 U 0.52" pitch	5.74	1.0000 ± 0.0010	0.9956 ± 0.0007	0.4476	0.4580
58	WCAP-3385 (6.A.17)	Saxton Case 56 PuO_2 0.56" pitch	6.6% Pu	1.0036 ± 0.0011	1.0047 ± 0.0006	0.5289	0.5197
59	WCAP-3385 (6.A.17)	Saxton Case 56 borated PuO_2	6.6% Pu	1.0008 ± 0.0010	NC	0.6389	NC
60	WCAP-3385 (6.A.17)	Saxton Case 56 U 0.56" pitch	5.74	0.9994 ± 0.0011	0.9967 ± 0.0007	0.2923	0.2954

Table 6.A.2

COMPARISON OF MCNP4a AND KENO5a CALCULATED REACTIVITIES[†] FOR VARIOUS ENRICHMENTS (UO_2)

Enrichment	Calculated $k_{eff} \pm 1\sigma$	
	MCNP4a	**KENO5a**
3.0	0.8465 ± 0.0011	0.8478 ± 0.0004
3.5	0.8820 ± 0.0011	0.8841 ±0.0004
3.75	0.9019 ± 0.0011	0.8987 ± 0.0004
4.0	0.9132 ± 0.0010	0.9140 ± 0.0004
4.2	0.9276 ± 0.0011	0.9237 ± 0.0004
4.5	0.9400 ± 0.0011	0.9388 ± 0.0004

† Based on the MPC-68 with the GE 8x8R

Table 6.A.3

MCNP4a CALCULATED REACTIVITIES FOR
CRITICAL EXPERIMENTS WITH NEUTRON ABSORBERS (UO_2)

Ref.	Experiment		Δk Worth of Absorber	MCNP4a Calculated k_{eff}	EALF† (eV)
6.A.13	PNL-2615	Boral Sheet	0.0139	0.9994 ± 0.0012	0.1165
6.A.7	BAW-1484	Core XX	0.0165	1.0008 ± 0.0011	0.1724
6.A.13	PNL-2615	1.62% Boron-steel	0.0165	0.9996 ± 0.0012	0.1161
6.A.7	BAW-1484	Core XIX	0.0202	0.9961 ± 0.0012	0.2103
6.A.7	BAW-1484	Core XXI	0.0243	0.9994 ± 0.0010	0.1544
6.A.7	BAW-1484	Core XVII	0.0519	0.9962 ± 0.0012	0.2083
6.A.11	PNL-3602	Boral Sheet	0.0708	0.9941 ± 0.0011	0.3135
6.A.7	BAW-1484	Core XV	0.0786	0.9910 ± 0.0011	0.2092
6.A.7	BAW-1484	Core XVI	0.0845	0.9935 ± 0.0010	0.1757
6.A.7	BAW-1484	Core XIV	0.1575	0.9953 ± 0.0011	0.2022
6.A.7	BAW-1484	Core XIII	0.1738	1.0020 ± 0.0011	0.1988
6.A.14	PNL-7167	Expt 214R flux trap	0.1931	0.9991 ± 0.0011	0.3722

† EALF is the energy of the average lethargy causing fission

Table 6.A.4
COMPARISON OF MCNP4a AND KENO5a
CALCULATED REACTIVITIES† FOR VARIOUS BORON LOADINGS (UO_2)

^{10}B, g/cm^2	**Calcualted $k_{eff} \pm 1\sigma$**	
	MCNP4a	**KENO5a**
0.005	1.0381 ± 0.0012	1.0340 ± 0.0004
0.010	0.9960 ±0.0010	0.9941 ± 0.0004
0.015	0.9727 ± 0.0009	0.9713 ± 0.0004
0.020	0.9541 ± 0.0012	0.9560 ± 0.0004
0.025	0.9433 ± 0.0011	0.9428 ± 0.0004
0.03	0.9325 ± 0.0011	0.9338 ± 0.0004
0.035	0.9234 ± 0.0011	0.9251 ± 0.0004
0.04	0.9173 ± 0.0011	0.9179 ± 0.0004

† based on 4.5% enrichment GE 8x8R in the MPC-68 cask.

Table 6.A.5

CALCULATIONS FOR CRITICAL EXPERIMENTS WITH
THICK LEAD AND STEEL REFLECTORS† (UO_2)

Ref.	Case	Enrichment, wt%	Separation, cm	MCNP4a k_{eff}	KENO5a k_{eff}
6.A.11	Steel Reflector	2.35	1.321	0.9980 ± 0.0009	0.9992 ± 0.0006
		2.35	2.616	0.9968 ± 0.0009	0.9964 ± 0.0006
		2.35	3.912	0.9974 ± 0.0010	0.9980 ± 0.0006
		2.35	∞	0.9962 ± 0.0008	0.9939 ± 0.0006
6.A.11	Steel Reflector	4.306	1.321	0.9997 ± 0.0010	1.0012 ± 0.0007
		4.306	2.616	0.9994 ± 0.0012	0.9974 ± 0.0007
		4.306	3.405	0.9969 ± 0.0011	0.9951 ± 0.0007
		4.306	∞	0.9910 ± 0.0020	0.9947 ± 0.0007
6.A.11	Lead Reflector	4.306	0.55	1.0025 ± 0.0011	0.9997 ± 0.0007
		4.306	1.956	1.0000 ± 0.0012	0.9985 ± 0.0007
		4.306	5.405	0.9971 ± 0.0012	0.9946 ± 0.0007

† Arranged in order of increasing reflector fuel spacing.

Table 6.A.1
Summary of Criticality Benchmark Calculations

				Calculated k_{eff}		EALF (eV)	
	Reference	Identification	Enrich.	MCNP4a	KENO5a	MCNP4a	KENO5a
61	WCAP-3385 (6.A.17)	Saxton Case 79 PuO_2 0.79" pitch	6.6% Pu	1.0063 ± 0.0011	1.0133 ± 0.0006	0.1520	0.1555
62	WCAP-3385 (6.A.17)	Saxton Case 79 U 0.79" pitch	5.74	1.0039 ± 0.0011	1.0008 ± 0.0006	0.1036	0.1047

Notes: NC stands for not calculated.

† EALF is the energy of the average lethargy causing fission

†† The experimental results appear to be statistical outliers (>3σ) suggesting the possibility of unusually large experimental error. Although they could be justifiably excluded, for conservatism, they were retained in determining the calculational basis.

Table 6.A.6

CALCULATIONS FOR CRITICAL EXPERIMENTS WITH VARIOUS SOLUBLE BORON CONCENTRATIONS (UO_2)

Reference	Experiment	Boron Concentration ppm	Calculated k_{eff}	
			MCNP4a	KENO5a
6.A.15	PNL-4267	0	0.9974 ± 0.0012	-
6.A.8	BAW-1645-4	886	0.9970 ± 0.0010	0.9924 ± 0.0006
6.A.9	BAW-1810	1337	1.0023 ± 0.0010	-
6.A.9	BAW-1810	1899	1.0060 ± 0.0009	-
6.A.15	PNL-4267	2550	1.0057 ± 0.0010	-

Table 6.A.7

CALCULATIONS FOR CRITICAL EXPERIMENTS WITH MOX FUEL

Reference	Case†	MCNP4a		KENO 5a	
		k_{eff}	EALF†† (eV)	k_{eff}	EALF†† (eV)
PNL-5803 [6.A.16]	MOX Fuel – Exp No 21	1.0041±0.0011	0.9171	1.0046±0.0006	0.8868
	MOX Fuel – Exp No 43	1.0058±0.0012	0.2968	1.0036±0.0006	0.2944
	MOX Fuel – Exp No 13	1.0083±0.0011	0.1665	0.9989±0.0006	0.1706
	MOX Fuel – Exp No 32	1.0079±0.0011	0.1139	0.9966±0.0006	0.1165
WCAP- 3385-54 [6.A.17]	Saxton @ 0.52" pitch	0.9996±0.0011	0.8665	1.0005±0.0006	0.8417
	Saxton @ 0.56" pitch	1.0036±0.0011	0.5289	1.0047±0.0006	0.5197
	Saxton @ 0.56" pitch borated	1.0008±0.0010	0.6389	NC	NC
	Saxton @ 0.79" pitch	1.0063±0.0011	0.1520	1.0133±0.0006	0.1555

† Arranged in order of increasing lattice spacing.

†† EALF is the energy of the average lethargy causing fission.

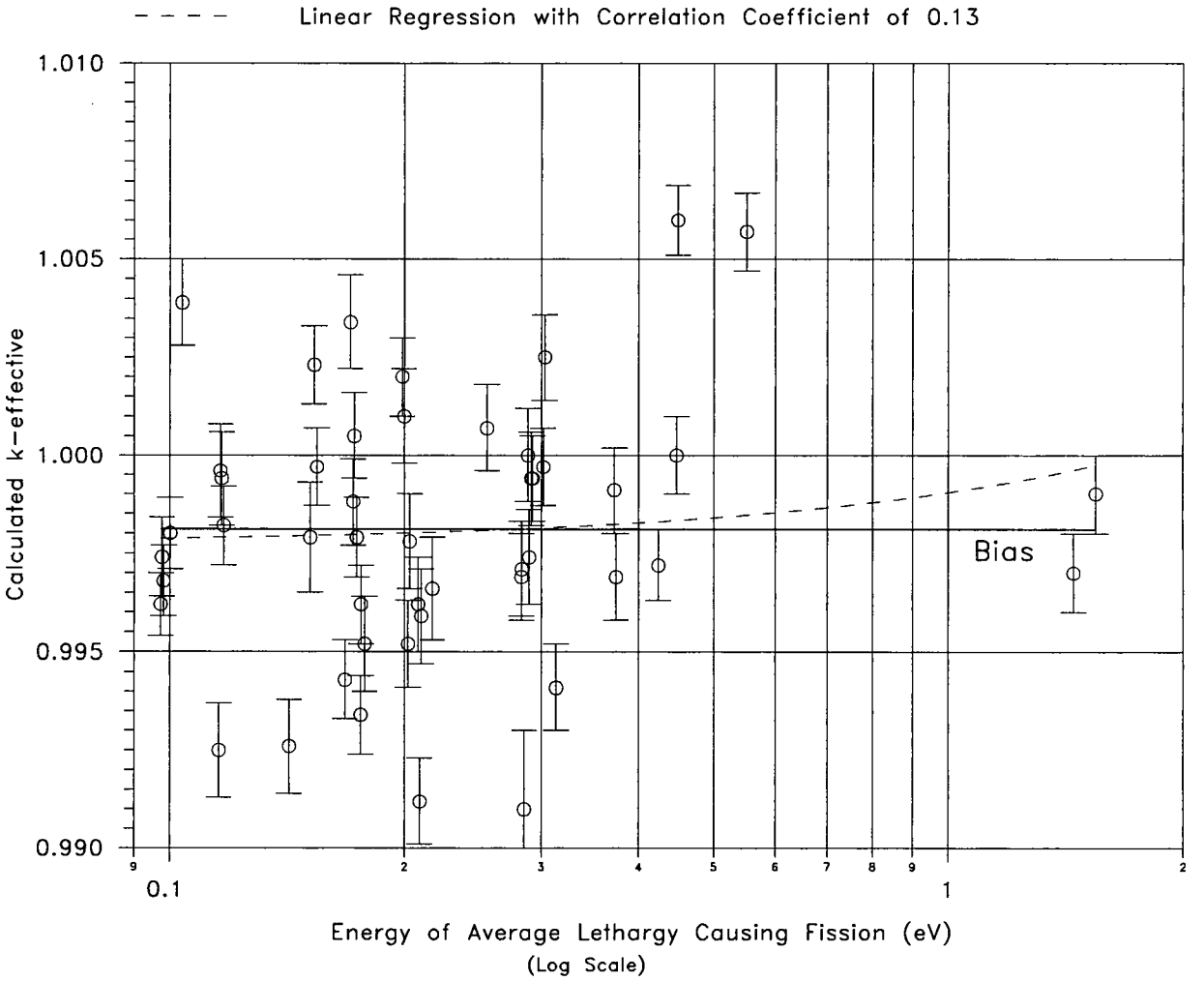

FIGURE 6.A.1 MCNP4a CALCULATED k-eff VALUES FOR VARIOUS VALUES OF THE SPECTRAL INDEX

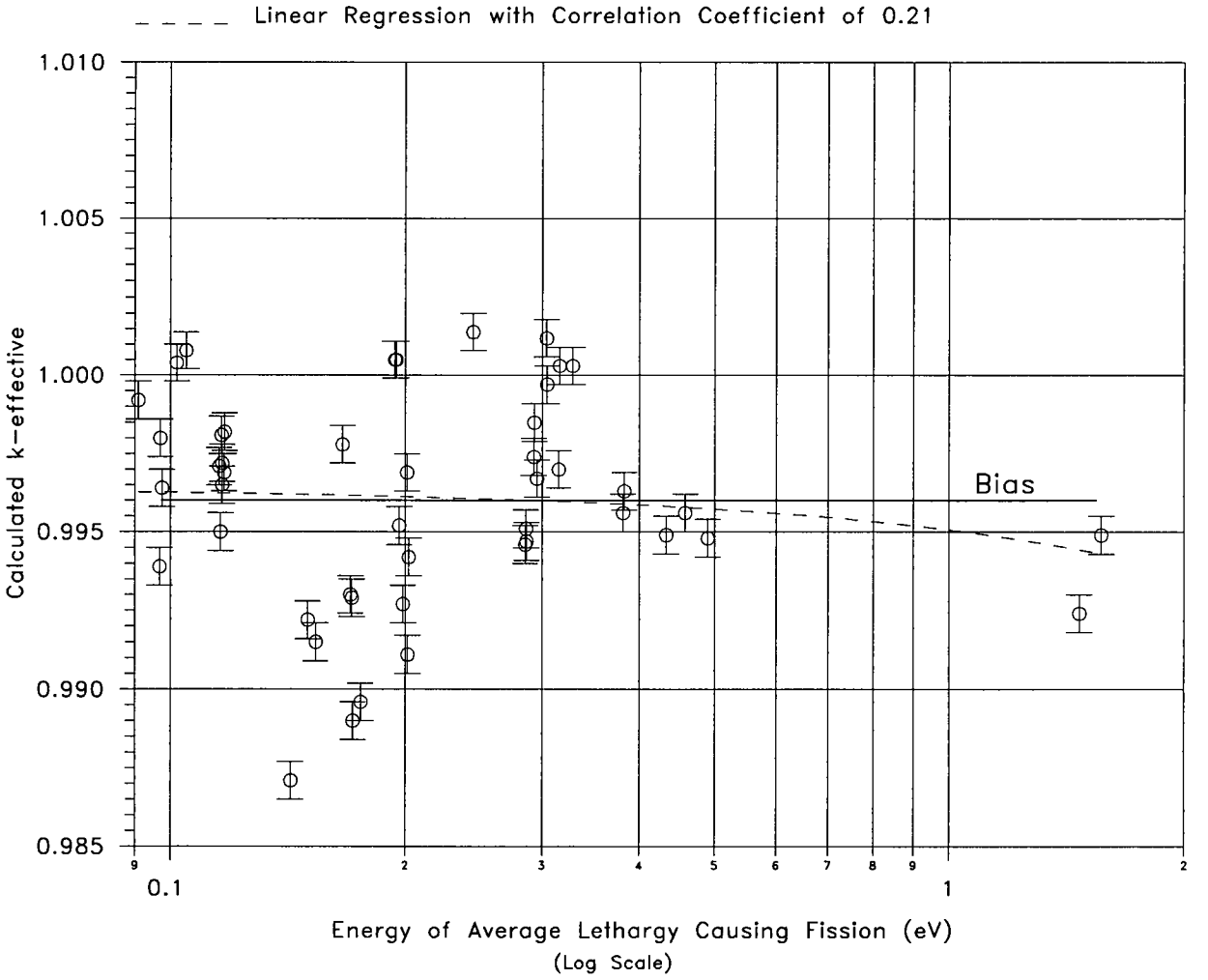

FIGURE 6.A.2 KENO5a CALCULATED k-eff VALUES FOR VARIOUS VALUES OF THE SPECTRAL INDEX

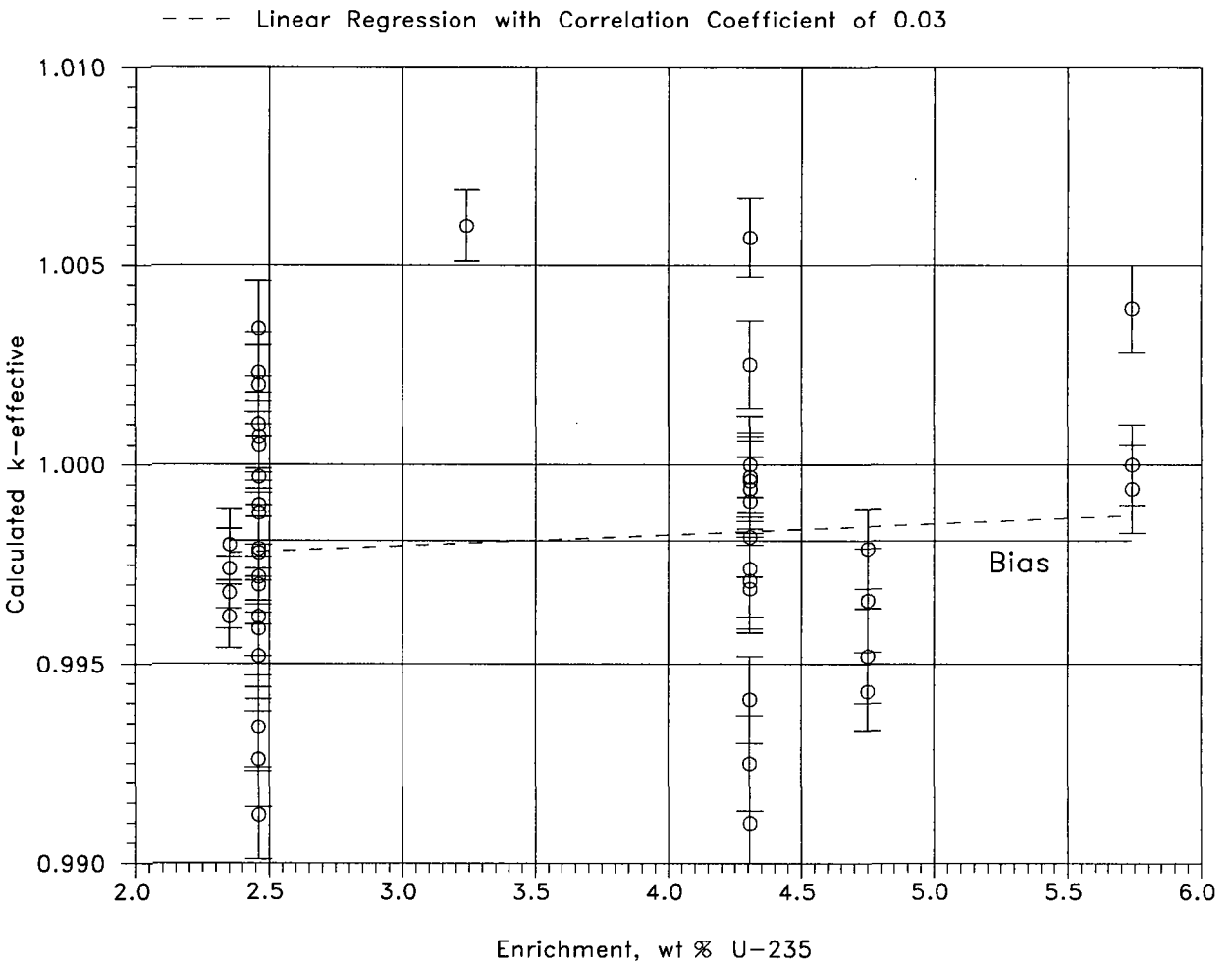

FIGURE 6.A.3 MCNP4a CALCULATED k-eff VALUES AT VARIOUS U-235 ENRICHMENTS

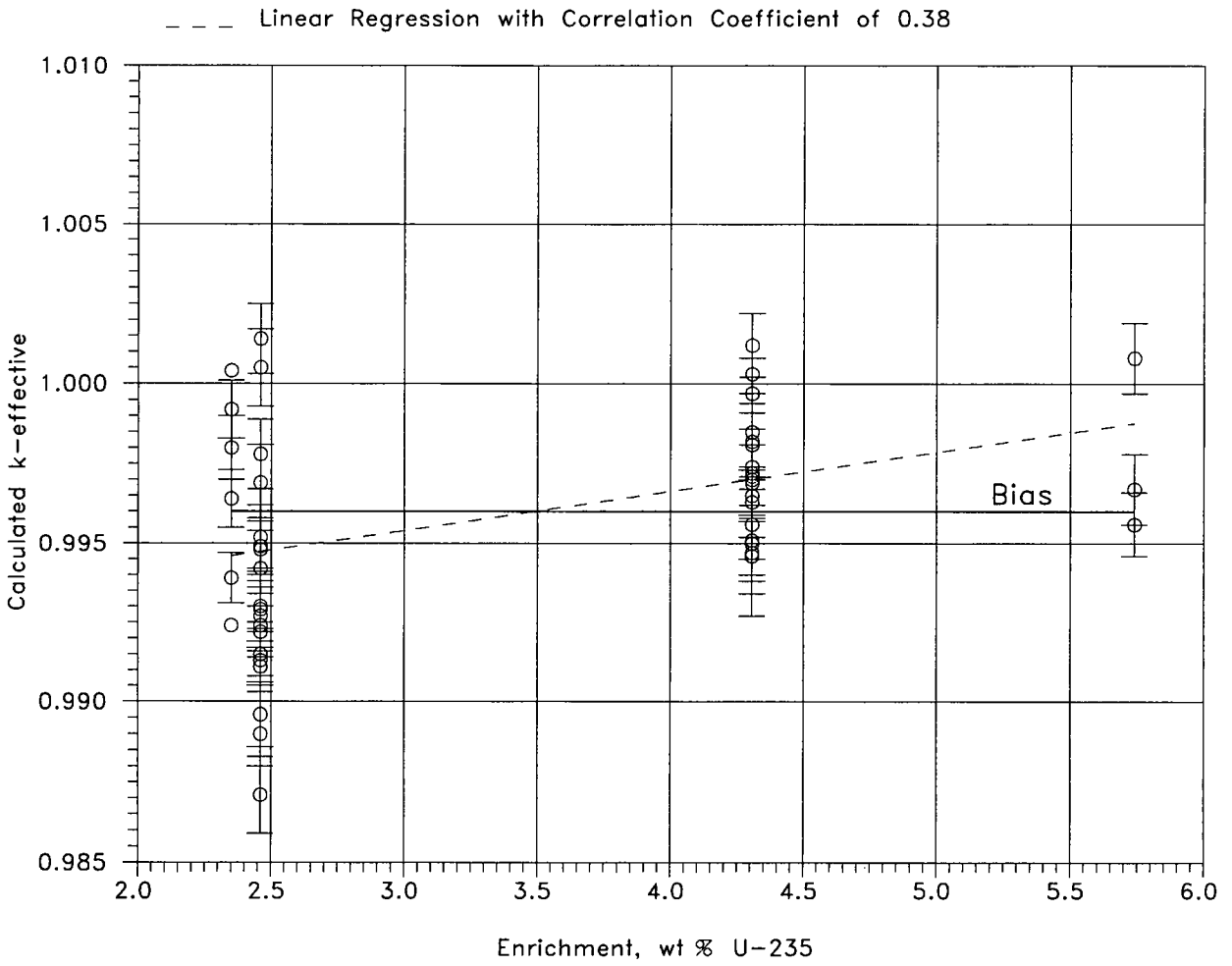

FIGURE 6.A.4 KENO5a CALCULATED k-eff VALUES AT VARIOUS U-235 ENRICHMENTS

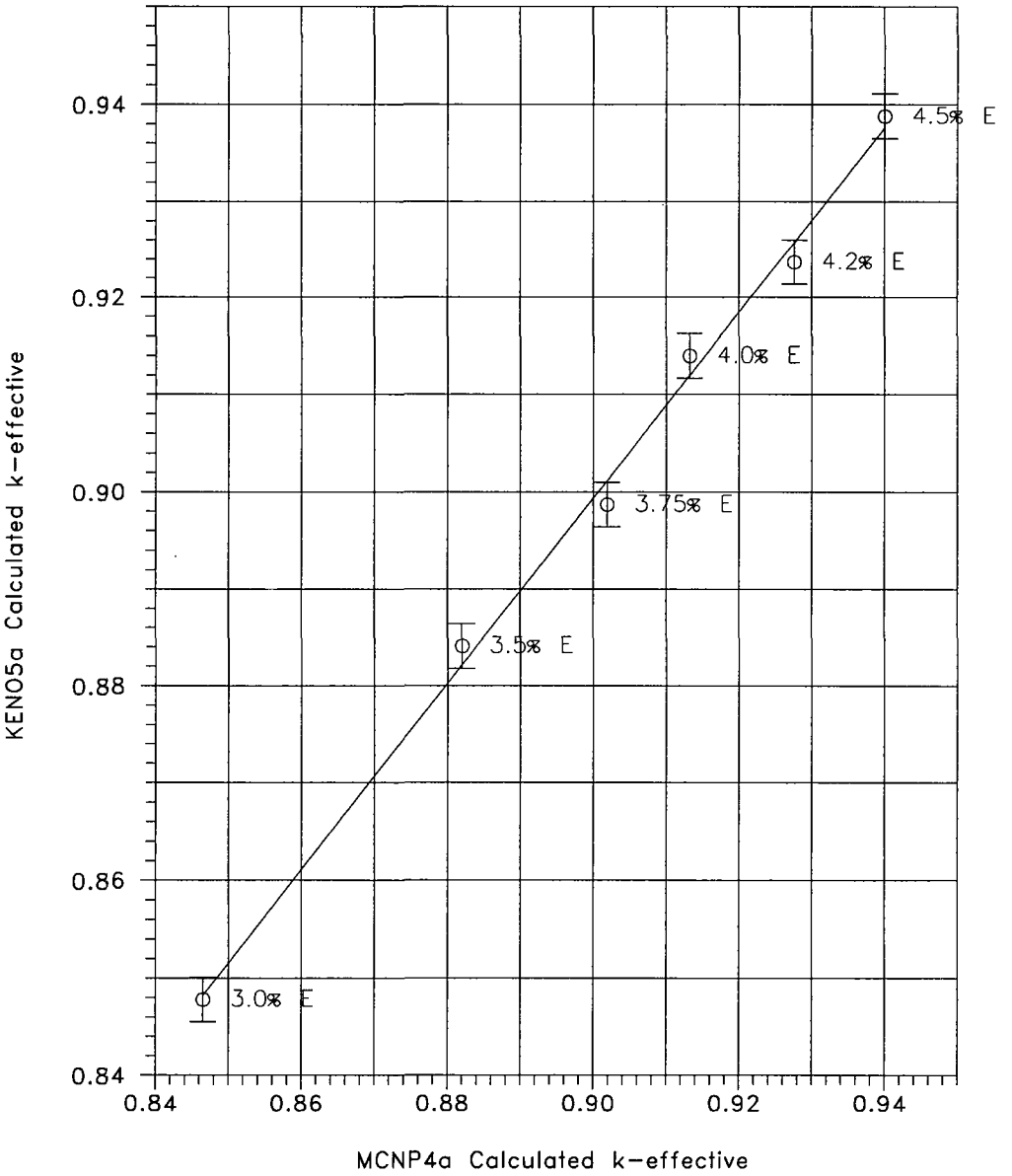

FIGURE 6.A.5 COMPARISON OF MCNP4a AND KENO5a CALCULATIONS FOR VARIOUS FUEL ENRICHMENTS

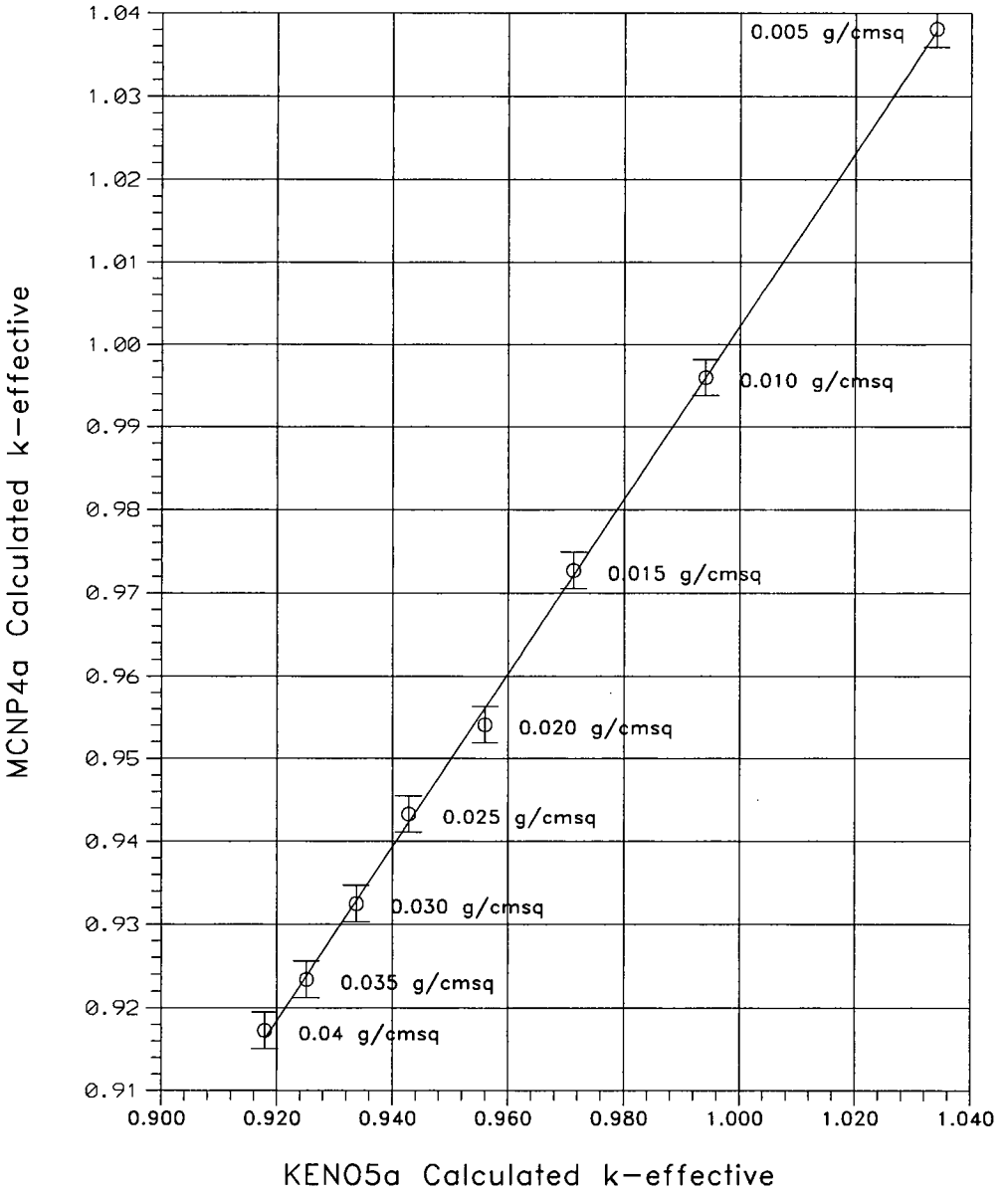

FIGURE 6.A.6 COMPARISON OF MCNP4a AND KENO5a CALCULATIONS FOR VARIOUS BORON-10 AREAL DENSITIES

APPENDIX 6.B: DISTRIBUTED ENRICHMENTS IN BWR FUEL

Fuel assemblies used in BWRs utilize fuel rods of varying enrichments as a means of controlling power peaking during in-core operation. For calculations involving BWR assemblies, the use of a uniform (planar-average) enrichment, as opposed to the distributed enrichments normally used in BWR fuel, produces conservative results. Calculations have been performed to confirm that this statement remains valid in the geometry of the MPC-68. These calculations are based on fuel assembly designs currently in use and two hypothetical distributions, all intended to illustrate that calculations with uniform average enrichments are conservative.

The average enrichment is calculated as the linear average of the various fuel rod enrichments, i.e.,

$$\overline{E} = \frac{1}{n} \sum_{i=1}^{n} E_i,$$

where E_i is the enrichment in each of the n rods, and $\overline{E}$ is the assembly average enrichment. This parameter conservatively characterizes the fuel assembly and is readily available for specific fuel assemblies in determining the acceptability of the assembly for placement in the MPC-68 cask.

The criticality calculations for average and distributed enrichment cases are compared in Table 6.B.1 to illustrate and confirm the conservatism inherent in using average enrichments. With two exceptions, the cases analyzed represent realistic designs currently in use and encompass fuel with different ratios of maximum pin enrichment to average assembly enrichment. The two exceptions are hypothetical cases intended to extend the models to higher enrichments and to demonstrate that using the average enrichment remains conservative.

Table 6.B.1 shows that, in all cases, the averaged enrichment yields conservative values of reactivity relative to distributed enrichments for both the actual fuel designs and the hypothetical higher enrichment cases. Thus, it is concluded that uniform average enrichments will always yield higher (more conservative) values for reactivity than the corresponding distributed enrichments†.

† This conclusion implicitly assumes the higher enrichment fuel rods are located internal to the assembly (as in BWR fuel), and the lower enriched rods are on the outside.

Table 6.B.1

COMPARISON CALCULATIONS FOR BWR FUEL WITH AVERAGE AND DISTRIBUTED ENRICHMENTS

Case	Average %E	Peak Rod E%	Calculated k_{eff}	
			Average E	Distributed E
8x8C04	3.01	3.80	0.8549	0.8429
8x8C04	3.934	4.9	0.9128	0.9029
8x8D05	3.42	3.95	0.8790	0.8708
8x8D05	3.78	4.40	0.9030	0.8974
8x8D05	3.90	4.90	0.9062	0.9042
9x9B01	4.34	4.71	0.9347	0.9285
9x9D01	3.35	4.34	0.8793	0.8583
Hypothetical #1 (48 outer rods of 3.967%E,14 inner rods of 5.0%)	4.20	5.00	0.9289	0.9151
Hypothetical #2 (48 outer rods of 4.354%E,14 inner rods of 5.0%)	4.50	5.00	0.9422	0.9384

APPENDIX 6.C: CALCULATIONAL SUMMARY

The following table lists the maximum k_{eff} (including bias, uncertainties, and calculational statistics), MCNP calculated k_{eff}, standard deviation, and energy of average lethargy causing fission (EALF) for each of the candidate fuel types and basket configurations.

Table 6.C.1
CALCULATIONAL SUMMARY FOR ALL CANDIDATE FUEL TYPES
AND BASKET CONFIGURATIONS

MPC-24				
Fuel Assembly Designation	**Maximum k_{eff}**	**Calculated k_{eff}**	**Std. Dev. (1-sigma)**	**EALF (eV)**
14x14A01	0.9295	0.9252	0.0008	0.2084
14x14A02	0.9286	0.9242	0.0008	0.2096
14x14A03	0.9296	0.9253	0.0008	0.2093
14x14B01	0.9159	0.9117	0.0007	0.2727
14x14B02	0.9169	0.9126	0.0008	0.2345
14x14B03	0.9110	0.9065	0.0009	0.2545
14x14B04	0.9084	0.9039	0.0009	0.2563
B14x14B01	0.9228	0.9185	0.0008	0.2675
14x14C01	0.9258	0.9215	0.0008	0.2729
14x14C02	0.9265	0.9222	0.0008	0.2765
14x14C03	0.9287	0.9242	0.0009	0.2825
14x14D01	0.8507	0.8464	0.0008	0.3308
15x15A01	0.9204	0.9159	0.0009	0.2608
15x15B01	0.9369	0.9326	0.0008	0.2632
15C15B02	0.9338	0.9295	0.0008	0.2640
15x15B03	0.9362	0.9318	0.0008	0.2632
15x15B04	0.9370	0.9327	0.0008	0.2612
15x15B05	0.9356	0.9313	0.0008	0.2606
15x15B06	0.9366	0.9324	0.0007	0.2638
B15x15B01	0.9388	0.9343	0.0009	0.2626
15x15C01	0.9255	0.9213	0.0007	0.2493

Table 6.C.1 (continued)
CALCULATIONAL SUMMARY FOR ALL CANDIDATE FUEL TYPES
AND BASKET CONFIGURATIONS

MPC-24				
Fuel Assembly Designation	**Maximum k_{eff}**	**Calculated k_{eff}**	**Std. Dev. (1-sigma)**	**EALF (eV)**
15x15C02	0.9297	0.9255	0.0007	0.2457
15x15C03	0.9297	0.9255	0.0007	0.2440
15x15C04	0.9311	0.9268	0.0008	0.2435
B15x15C01	0.9361	0.9316	0.0009	0.2385
15x15D01	0.9341	0.9298	0.0008	0.2822
15x15D02	0.9367	0.9324	0.0008	0.2802
15x15D03	0.9354	0.9311	0.0008	0.2844
15x15D04	0.9339	0.9292	0.0010	0.2958
15x15E01	0.9368	0.9325	0.0008	0.2826
15x15F01	0.9395	0.9350	0.0009	0.2903
15x15G01	0.8876	0.8833	0.0008	0.3357
15x15H01	0.9337	0.9292	0.0009	0.2349
16x16A01	0.9287	0.9244	0.0008	0.2704
16x16A02	0.9263	0.9221	0.0007	0.2702
17x17A01	0.9368	0.9325	0.0008	0.2131
17x17A02	0.9368	0.9325	0.0008	0.2131
17x17A03	0.9329	0.9286	0.0008	0.2018
17x17B01	0.9288	0.9243	0.0009	0.2607
17x17B02	0.9290	0.9247	0.0008	0.2596
17x17B03	0.9243	0.9199	0.0008	0.2625
17x17B04	0.9324	0.9279	0.0009	0.2576
17x17B05	0.9266	0.9222	0.0008	0.2539

Table 6.C.1 (continued)
CALCULATIONAL SUMMARY FOR ALL CANDIDATE FUEL TYPES
AND BASKET CONFIGURATIONS

MPC-24				
Fuel Assembly Designation	**Maximum k_{eff}**	**Calculated k_{eff}**	**Std. Dev. (1-sigma)**	**EALF (eV)**
17x17B06	0.9311	0.9268	0.0008	0.2593
17x17C01	0.9293	0.9250	0.0008	0.2595
17x17C02	0.9336	0.9293	0.0008	0.2624

MPC-68				
Fuel Assembly Designation	**Maximum k_{eff}**	**Calculated k_{eff}**	**Std. Dev. (1-sigma)**	**EALF (eV)**
6x6A01	0.7539	0.7498	0.0007	0.2754
6x6A02	0.7517	0.7476	0.0007	0.2510
6x6A03	0.7545	0.7501	0.0008	0.2494
6x6A04	0.7537	0.7494	0.0008	0.2494
6x6A05	0.7555	0.7512	0.0008	0.2470
6x6A06	0.7618	0.7576	0.0008	0.2298
6x6A07	0.7588	0.7550	0.0005	0.2360
6x6A08	0.7808	0.7766	0.0007	0.2527
B6x6A01	0.7888	0.7846	0.0007	0.2310
6x6B01	0.7604	0.7563	0.0007	0.2461
6x6B02	0.7618	0.7577	0.0006	0.2450
6x6B03	0.7619	0.7578	0.0007	0.2439
6x6B04	0.7686	0.7644	0.0008	0.2286
6x6B05	0.7824	0.7785	0.0006	0.2184
B6x6B01	0.7822	0.7783	0.0006	0.2190

Table 6.C.1 (continued)
CALCULATIONAL SUMMARY FOR ALL CANDIDATE FUEL TYPES
AND BASKET CONFIGURATIONS

MPC-68				
Fuel Assembly Designation	**Maximum k_{eff}**	**Calculated k_{eff}**	**Std. Dev. (1-sigma)**	**EALF (eV)**
6x6C01	0.8021	0.7980	0.0007	0.2139
7x7A01	0.7973	0.7930	0.0008	0.2015
7x7B01	0.9372	0.9330	0.0007	0.3658
7x7B02	0.9301	0.9260	0.0007	0.3524
7x7B03	0.9313	0.9271	0.0008	0.3438
7x7B04	0.9311	0.9270	0.0007	0.3816
7x7B05	0.9350	0.9306	0.0008	0.3382
7x7B06	0.9298	0.9260	0.0006	0.3957
B7x7B01	0.9375	0.9332	0.0008	0.3887
B7x7B02	0.9386	0.9344	0.0007	0.3983
8x8A01	0.7685	0.7644	0.0007	0.2227
8x8A02	0.7697	0.7656	0.0007	0.2158
8x8B01	0.9310	0.9265	0.0009	0.2935
8x8B02	0.9227	0.9185	0.0007	0.2993
8x8B03	0.9299	0.9257	0.0008	0.3319
8x8B04	0.9236	0.9194	0.0008	0.3700
B8x8B01	0.9346	0.9301	0.0009	0.3389
B8x8B02	0.9385	0.9343	0.0008	0.3329
B8x8B03	0.9416	0.9375	0.0007	0.3293
8x8C01	0.9315	0.9273	0.0007	0.2822
8x8C02	0.9313	0.9268	0.0009	0.2716
8x8C03	0.9329	0.9286	0.0008	0.2877

Table 6.C.1 (continued)
CALCULATIONAL SUMMARY FOR ALL CANDIDATE FUEL TYPES
AND BASKET CONFIGURATIONS

MPC-68				
Fuel Assembly Designation	**Maximum k_{eff}**	**Calculated k_{eff}**	**Std. Dev. (1-sigma)**	**EALF (eV)**
8x8C04	0.9348	0.9307	0.0007	0.2915
8x8C05	0.9353	0.9312	0.0007	0.2971
8x8C06	0.9353	0.9312	0.0007	0.2944
8x8C07	0.9314	0.9273	0.0007	0.2972
8x8C08	0.9339	0.9298	0.0007	0.2915
8x8C09	0.9301	0.9260	0.0007	0.3183
8x8C10	0.9317	0.9275	0.0008	0.3018
8x8C11	0.9328	0.9287	0.0007	0.3001
8x8C12	0.9285	0.9242	0.0008	0.3062
B8x8C01	0.9357	0.9313	0.0009	0.3141
B8x8C02	0.9425	0.9384	0.0007	0.3081
B8x8C03	0.9418	0.9375	0.0008	0.3056
8x8D01	0.9342	0.9302	0.0006	0.2733
8x8D02	0.9325	0.9284	0.0007	0.2750
8x8D03	0.9351	0.9309	0.0008	0.2731
8x8D04	0.9338	0.9296	0.0007	0.2727
8x8D05	0.9339	0.9294	0.0009	0.2700
8x8D06	0.9365	0.9324	0.0007	0.2777
8x8D07	0.9341	0.9297	0.0009	0.2694
8x8D08	0.9376	0.9332	0.0009	0.2841
B8x8D01	0.9403	0.9363	0.0007	0.2778
8x8E01	0.9312	0.9270	0.0008	0.2831

Table 6.C.1 (continued)
CALCULATIONAL SUMMARY FOR ALL CANDIDATE FUEL TYPES
AND BASKET CONFIGURATIONS

MPC-68				
Fuel Assembly Designation	**Maximum k_{eff}**	**Calculated k_{eff}**	**Std. Dev. (1-sigma)**	**EALF (eV)**
8x8F01	0.9153	0.9111	0.0007	0.2143
9x9A01	0.9353	0.9310	0.0008	0.2875
9x9A02	0.9388	0.9345	0.0008	0.2228
9x9A03	0.9351	0.9310	0.0007	0.2837
9x9A04	0.9396	0.9355	0.0007	0.2262
B9x9A01	0.9417	0.9374	0.0008	0.2236
9x9B01	0.9380	0.9336	0.0008	0.2576
9x9B02	0.9373	0.9329	0.0009	0.2578
9x9B03	0.9417	0.9374	0.0008	0.2545
B9x9B01	0.9436	0.9394	0.0008	0.2506
9x9C01	0.9395	0.9352	0.0008	0.2698
9x9D01	0.9394	0.9350	0.0009	0.2625
9x9E01	0.9402	0.9359	0.0008	0.2249
9x9E02	0.9424	0.9380	0.0008	0.2088
9x9F01	0.9369	0.9326	0.0008	0.2954
9x9F02	0.9424	0.9380	0.0008	0.2088
10x10A01	0.9377	0.9335	0.0008	0.3170
10x10A02	0.9426	0.9386	0.0007	0.2159
10x10A03	0.9396	0.9356	0.0007	0.3169
B10x10A01	0.9457	0.9414	0.0008	0.2212
10x10B01	0.9384	0.9341	0.0008	0.2881
10x10B02	0.9416	0.9373	0.0008	0.2333

Table 6.C.1 (continued)
CALCULATIONAL SUMMARY FOR ALL CANDIDATE FUEL TYPES
AND BASKET CONFIGURATIONS

MPC-68				
Fuel Assembly Designation	**Maximum k_{eff}**	**Calculated k_{eff}**	**Std. Dev. (1-sigma)**	**EALF (eV)**
10x10B03	0.9375	0.9334	0.0007	0.2856
B10x10B01	0.9436	0.9395	0.0007	0.2366
10x10C01	0.9433	0.9392	0.0007	0.2416
10x10D01	0.9376	0.9333	0.0008	0.3355
10x10E01	0.9185	0.9144	0.0007	0.2936

Note: Maximum k_{eff} = Calculated k_{eff} + $K_c \times \sigma_c$ + Bias + σ_B
where:

K_c = 2.0
σ_c = Std. Dev. (1-sigma)
Bias = 0.0021
σ_B = 0.0006

See Subsection 6.4.3 for further explanation.

APPENDIX 6.D: SAMPLE INPUT FILES

(Total number of pages in this appendix : 46)

```
c
c Bounding Assembly in Class 15x15F
c
c MPC-24/24E cell configuration
c
c HI-STAR with active length 150 inch
c
c Cask Input Preprocessor
c cskinp 15f 15f mpc24n mpc24n histar star150 4.1 4rf5f45 pure
c ------     cpp\15f.bat
c   added 15f.co
c   added 15f.ce
c   added 15f.su
c   added 15f.sp
c ------     cpp\mpc24n.bat
c   added mpc24n.co
c   added mpc24n.ce
c   added mpc24n.su
c   added mpc24n.sp
c ------      cpp\histar.bat
c   added histar.co
c   added histar.ce
c   added histar.su
c   added histar.sp
c end of comments
c
c start of cells
c
c 15x15f
c
c number of cells: 6
c cell numbers:      1 to 7 and 201 to 299
c univers numbers:   1 to 3 and 201 to 299
c surface numbers:   1 to 9 and 201 to 299
c
c number of cells: 1
1     1 -10.522     -1  u=2       $ fuel
2     4 -1.0     1  -2  u=2       $ gap
3     3 -6.55    2  -3  u=2       $ Zr Clad
4     4 -1.0        3  u=2       $ water in fuel region
5     4 -1.0  -4:5     u=3       $ water in guide tubes
6     3 -6.55   4 -5    u=3        $ guide tubes
7     4 -1.0  -6   +7   -8   +9   u=1  lat=1
      fill= -8:8    -8:8   0:0
      1 1 1 1 1 1 1 1 1 1 1 1 1 1 1 1 1
      1 2 2 2 2 2 2 2 2 2 2 2 2 2 2 2 1
      1 2 2 2 2 2 2 2 2 2 2 2 2 2 2 2 1
      1 2 2 2 2 2 3 2 2 2 3 2 2 2 2 2 1
      1 2 2 2 3 2 2 2 2 2 2 2 3 2 2 2 1
      1 2 2 2 2 2 2 2 2 2 2 2 2 2 2 2 1
      1 2 2 3 2 2 3 2 2 2 3 2 2 3 2 2 1
      1 2 2 2 2 2 2 2 2 2 2 2 2 2 2 2 1
      1 2 2 2 2 2 2 2 3 2 2 2 2 2 2 2 1
      1 2 2 2 2 2 2 2 2 2 2 2 2 2 2 2 1
      1 2 2 3 2 2 3 2 2 2 3 2 2 3 2 2 1
      1 2 2 2 2 2 2 2 2 2 2 2 2 2 2 2 1
      1 2 2 2 3 2 2 2 2 2 2 2 3 2 2 2 1
      1 2 2 2 2 2 2 3 2 2 2 3 2 2 2 2 1
      1 2 2 2 2 2 2 2 2 2 2 2 2 2 2 2 1
      1 2 2 2 2 2 2 2 2 2 2 2 2 2 2 2 1
```

```
      1 1 1 1 1 1 1 1 1 1 1 1 1 1 1 1 1
c
c     MPC-24
c
c number of cells: 102
c cell numbers :      400   to  699
c universe numbers :    4   to    9
c surface numbers :   400   to  699
c
c     Right Side
c
408     0          -410   411  -412   413    u=4 fill=1 (1)
409     5  -7.84    410  -424   413  -426    u=4
410    4 -1.0     424  -428   448  -445    u=4
411    7  -2.7     428  -528  448  -445    u=4
412    6  -2.66   528  -532  448  -445    u=4
413    7  -2.7    532  -432   448  -445    u=4
414    4 -1.0     432  -436   448  -445    u=4
415    5  -7.84    436  -440   448  -445    u=4
416    4 -1.0     440        413         u=4
417    4 -1.0     424  -440   413  -447    u=4
418    4 -1.0     424  -440   446         u=4
419    5  -7.84    424  -440   447  -448    u=4
420    5  -7.84    424  -440   445  -446    u=4
c
c    Left Side
c
421    5  -7.84    425  -411   413         u=4
422    4 -1.0     429  -425   448  -445    u=4
423    7  -2.7    529  -429   448  -445    u=4
424    6  -2.66   533 -529   448  -445    u=4
425    7  -2.7     433 -533   448  -445    u=4
426    4 -1.0     437  -433   448  -445    u=4
427    5  -7.84    441  -437   448  -445    u=4
428    4 -1.0        -441   413         u=4
429    4 -1.0     441  -425   413  -447    u=4
430    4 -1.0     441  -425   446         u=4
431    5  -7.84    441  -425   447  -448    u=4
432    5  -7.84    441  -425   445  -446    u=4
c
c     Top
c
433    5  -7.84    411  -410   412  -426    u=4
434    4 -1.0     451  -452   426  -430    u=4
435    7  -2.7     451  -452   430 -530    u=4
436    6  -2.66    451  -452  530 -534    u=4
437    7  -2.7     451  -452  534  -434    u=4
438    4 -1.0     451  -452   434  -438    u=4
439    5  -7.84    451  -452   438  -442    u=4
440    4 -1.0     411  -424   442         u=4
441    4 -1.0     411  -450   426  -442    u=4
442    4 -1.0     453  -424   426  -442    u=4
443    5  -7.84    450  -451   426  -442    u=4
444    5  -7.84    452  -453   426  -442    u=4
c
c     Bottom
c
445    5  -7.84    427            -413    u=4
446    4 -1.0     451  -452   431  -427    u=4
447    7  -2.7     451  -452  531  -431    u=4
448    6  -2.66    451  -452  535 -531    u=4
```

```
449    7  -2.7     451  -452   435 -535    u=4
450    4 -1.0     451  -452   439  -435    u=4
451    5  -7.84    451  -452   443  -439    u=4
452    4 -1.0     411           -443    u=4
453    4 -1.0     411  -450   443  -427    u=4
454    4 -1.0     453        443  -427    u=4
455    5  -7.84    450  -451   443  -427    u=4
456    5  -7.84    452  -453   443  -427    u=4
457    5  -7.84    425  -411       -427    u=4
458    4 -1.0        -425       -427    u=4
c
c     TYPE B CELL  -  Short Boral on top and right
c
c     Right Side
c
459    0          -410   411  -412   413    u=5 fill=1 (1)
460    5  -7.84    410  -424   413  -426    u=5
470    4 -1.0     424  -428  548 -545    u=5
471    7  -2.7     428  -528 548 -545    u=5
472    6  -2.66   528  -532 548 -545    u=5
473    7  -2.7    532  -432  548 -545    u=5
474    4 -1.0     432  -436  548 -545    u=5
475    5  -7.84    436  -440  548 -545    u=5
476    4 -1.0     440        413         u=5
477    4 -1.0     424  -440   413 -547    u=5
478    4 -1.0     424  -440  546         u=5
479    5  -7.84    424  -440  547 -548    u=5
480    5  -7.84    424  -440  545 -546    u=5
c
c    Left Side
c
481    5  -7.84    425  -411   413         u=5
482    4 -1.0     429  -425   448  -445    u=5
483    7  -2.7    529  -429   448  -445    u=5
484    6  -2.66   533 -529   448  -445    u=5
485    7  -2.7     433 -533   448  -445    u=5
486    4 -1.0     437  -433   448  -445    u=5
487    5  -7.84    441  -437   448  -445    u=5
488    4 -1.0        -441   413         u=5
489    4 -1.0     441  -425   413  -447    u=5
490    4 -1.0     441  -425   446         u=5
491    5  -7.84    441  -425   447  -448    u=5
492    5  -7.84    441  -425   445  -446    u=5
c
c     Top
c
493    5  -7.84    411  -410   412  -426    u=5
494    4 -1.0    551 -552   426  -430    u=5
495    7  -2.7    551 -552   430 -530    u=5
496    6  -2.66   551 -552  530 -534    u=5
497    7  -2.7    551 -552  534  -434    u=5
498    4 -1.0    551 -552   434  -438    u=5
499    5  -7.84   551 -552   438  -442    u=5
500   4 -1.0     411  -424   442         u=5
501   4 -1.0     411 -550   426  -442    u=5
502   4 -1.0    553  -424   426  -442    u=5
503   5  -7.84   550 -551   426  -442    u=5
504   5  -7.84   552 -553   426  -442    u=5
c
c     Bottom
c
```

```
505   5  -7.84    427            -413    u=5
506   4 -1.0     451  -452   431  -427    u=5
507   7  -2.7     451  -452  531  -431    u=5
508   6  -2.66    451  -452  535 -531    u=5
509   7  -2.7     451  -452   435 -535    u=5
510   4 -1.0     451  -452   439  -435    u=5
511   5  -7.84    451  -452   443  -439    u=5
512   4 -1.0     411            -443    u=5
513   4 -1.0     411  -450   443  -427    u=5
514   4 -1.0     453         443  -427    u=5
515   5  -7.84    450  -451   443  -427    u=5
516   5  -7.84    452  -453   443  -427    u=5
517   5  -7.84    425  -411        -427    u=5
518   4 -1.0        -425        -427    u=5
c
c
c
c     TYPE D CELL  -  Short Boral on left and bottom, different cell ID
c
c number of cells: 51
c
c     Right Side
c
1570   0          -1410   1411  -1412   1413    u=17 fill=1 (1)
1571   5  -7.84    1410  -1424   1413  -1426    u=17
1572   4 -1.0     1424  -1428   1448  -1445    u=17
1573   7  -2.7     1428  -1528  1448  -1445    u=17
1574   6  -2.66   1528  -1532  1448  -1445    u=17
1575   7  -2.7    1532  -1432   1448  -1445    u=17
1576   4 -1.0     1432  -1436   1448  -1445    u=17
1577   5  -7.84    1436  -1440   1448  -1445    u=17
1578   4 -1.0     1440        1413         u=17
1579   4 -1.0     1424  -1440   1413  -1447    u=17
1580   4 -1.0     1424  -1440   1446         u=17
1581   5  -7.84    1424  -1440   1447  -1448    u=17
1582   5  -7.84    1424  -1440   1445  -1446    u=17
c
c    Left Side
c
1583   5  -7.84    1425  -1411   1413         u=17
1584   4 -1.0     1429  -1425  1548 -1545    u=17
1585   7  -2.7    1529  -1429  1548 -1545    u=17
1586   6  -2.66   1533 -1529  1548 -1545    u=17
1587   7  -2.7     1433 -1533  1548 -1545    u=17
1588   4 -1.0     1437  -1433  1548 -1545    u=17
1589   5  -7.84    1441  -1437  1548 -1545    u=17
1590   4 -1.0        -1441   1413         u=17
1591   4 -1.0     1441  -1425   1413 -1547    u=17
1592   4 -1.0     1441  -1425  1546         u=17
1593   5  -7.84    1441  -1425  1547 -1548    u=17
1594   5  -7.84    1441  -1425  1545 -1546    u=17
c
c     Top
c
1595   5  -7.84    1411  -1410   1412  -1426    u=17
1596   4 -1.0     1451  -1452   1426  -1430    u=17
1597   7  -2.7     1451  -1452   1430 -1530    u=17
1598   6  -2.66    1451  -1452  1530 -1534    u=17
1599   7  -2.7     1451  -1452  1534  -1434    u=17
1600   4 -1.0     1451  -1452   1434  -1438    u=17
1601   5  -7.84    1451  -1452   1438  -1442    u=17
```

```
1602   4 -1.0     1411  -1424   1442          u=17
1603   4 -1.0     1411  -1450   1426  -1442    u=17
1604   4 -1.0     1453  -1424   1426  -1442    u=17
1605   5  -7.84    1450  -1451   1426  -1442    u=17
1606   5  -7.84    1452  -1453   1426  -1442    u=17
c
c     Bottom
c
1607   5  -7.84    1427            -1413    u=17
1608   4 -1.0    1551 -1552   1431  -1427    u=17
1609   7  -2.7    1551 -1552  1531  -1431    u=17
1610   6  -2.66   1551 -1552  1535 -1531    u=17
1611   7  -2.7    1551 -1552   1435 -1535    u=17
1612   4 -1.0    1551 -1552   1439  -1435    u=17
1613   5  -7.84   1551 -1552   1443  -1439    u=17
1614   4 -1.0     1411            -1443    u=17
1615   4 -1.0     1411 -1550   1443  -1427    u=17
1616   4 -1.0    1553        1443  -1427    u=17
1617   5  -7.84   1550 -1551   1443  -1427    u=17
1618   5  -7.84   1552 -1553   1443  -1427    u=17
1619   5  -7.84    1425  -1411       -1427    u=17
1620   4 -1.0        -1425       -1427    u=17
c
c number of cells: 29
c
c empty cell no boral, no top
c
c
751     4 -1.0   -410   411  -412   413    u=14
752     5  -7.84    410  -424   413  -426    u=14
753    5  -7.84    425  -411   413         u=14
754    4 -1.0     411  -410   412  -426    u=14
755    5  -7.84    427            -413    u=14
756    5  -7.84    425  -411      -427    u=14
757    4 -1.0     411   426              u=14
758    4 -1.0     411  -427              u=14
759    4 -1.0    -425   413              u=14
760    4 -1.0     424   413   -426       u=14
761    4 -1.0    -425  -427              u=14
c
c
701   5   -7.84   701 -702 711 -713     u=9   $ steel post
702   5   -7.84   702 -703 711 -712     u=9   $ steel post
c
711   0           701 -705 711 -715 (702:713) (703:712)
                  fill=4 (13.8506 13.8506 0) u=9
712   0           704 (-706:-716) (705:715) -717 -710
                  fill=4 (17.9489 41.5518 0  0 1 0  -1 0 0   0 0 1) u=9
713   0           (705:715) -707 714 (-706:-716)  710
                  fill=4 (41.5518 17.9489 0  0 -1 0  1 0 0   0 0 1) u=9
714   0           701 -705 717 -719
                  fill=5 (13.8506 69.253 0) u=9
715   0           707 -709 711 -715
                  fill=5 (69.253 13.8506 0) u=9
716   0           706 -708 716 -718
                  fill=17 (45.6501 45.6501 0  -1 0 0  0 -1 0  0 0 1) u=9
717   0           705 -706 717 -719
                  fill=14 (41.5518 69.253 0) u=9
718   0           707 -709 715 -716
                  fill=14 (69.253 41.5518 0 0 1 0   1 0 0   0 0 1) u=9
719   0           701 -704 715 -717
```

```
                fill=14 (-9.75233 41.5518 0  -1 0 0  0 1 0   0 0 1) u=9
720   0         705 -707 711 -714
                fill=14 (41.5518 -9.75233 0   0 -1 0  1 0 0   0 0 1) u=9
721   4 -1.0    (706:719) (708:718) (709:716) u=9
c
c
c q-offset  0 inch
c
731   4 -1.0     720  721   fill=9 (0 0 0) u=19
732   4 -1.0    -720  721   fill=9 (0 0 0
                            -1 0 0  0  1 0  0 0 1) u=19
733   4 -1.0     720 -721   fill=9 (0 0 0
                              1 0 0  0 -1 0  0 0 1) u=19
734   4 -1.0    -720 -721   fill=9 (0 0 0
                            -1 0 0  0 -1 0  0 0 1) u=19
c
673   0          -41              39  -40  fill=19
c
c number of cells: 6
102   4  -1.0    -41       40  -44            $ 6.0" Water above Fuel
103   5  -7.84   -41       44  -45            $ 15.5" Steel above Fuel
104   4  -1.0    -41      -39   43            $ 7.3" Water below Fuel
105   5  -7.84   -41      -43   46            $ 8.5" Steel below Fuel
106   5  -7.84   46  -45 41 -42               $ 6.0" Radial Steel Shield
107   0           -46:45:42                   $ Outside world
c end of cells
c --- empty line

c --- empty line
c start of surfaces
1     cz         0.4752    $ fuel
2     cz         0.4851    $ clad ID
3     cz         0.5436    $ clad OD
4     cz         0.6350    $ guide ID
5     cz         0.6706    $ guide OD
6     px         0.7214    $ pin pitch
7     px        -0.7214
8     py         0.7214
9     py        -0.7214
c
c
c cell-id      8.98
c cell-pitch   10.906
c wall-thkns   5/16
c angle-thkns  5/16
c boral-gap    0.0035
c boral-gap-o  0.0035
c boral-thkns  0.075
c boral-clad   0.01
c sheathing    0.0235
c boral-wide   7.5
c boral-narrow 6.25
c
c gap size     1.09
c basket-od    67.335
c
410    px         11.40460 $x 8.98/2
411    px        -11.40460 $x {410} *-1
412    py         11.40460 $x {410}
413    py        -11.40460 $x {411}
424    px         12.19835 $x {410} + 5/16     $ angle
```

```
425    px        -12.19835 $x {411} - 5/16     $ box wall
426    py         12.19835 $x {412} + 5/16
427    py        -12.19835 $x {413} - 5/16
428    px         12.20724 $x {424} + 0.0035   $ wall to boral gap
429    px        -12.20724 $x {425} - 0.0035
430    py         12.20724 $x {426} + 0.0035
431    py        -12.20724 $x {427} - 0.0035
432    px         12.39774 $x {428} + 0.075    $ boral
433    px        -12.39774 $x {429} - 0.075
434    py         12.39774 $x {430} + 0.075
435    py        -12.39774 $x {431} - 0.075
436    px         12.40663 $x {432} + 0.0035   $ boral to sheathing gap
437    px        -12.40663 $x {433} - 0.0035
438    py         12.40663 $x {434} + 0.0035
439    py        -12.40663 $x {435} - 0.0035
440    px         12.46632 $x {436} + 0.0235   $ sheathing
441    px        -12.46632 $x {437} - 0.0235
442    py         12.46632 $x {438} + 0.0235
443    py        -12.46632 $x {439} - 0.0235
445    py          9.52500 $x 7.5/2
446    py          9.58469 $x {445} + 0.0235   $ sheathing
447    py         -9.58469 $x {446} *-1
448    py         -9.52500 $x {445} *-1
450    px         -9.58469 $x {447}
451    px         -9.52500 $x {448}
452    px          9.52500 $x {445}
453    px          9.58469 $x {446}
528   px         12.23264 $x {428} + 0.01  $ Aluminum on the outside of boral
529   px        -12.23264 $x {429} - 0.01
530   py         12.23264 $x {430} + 0.01
531   py        -12.23264 $x {431} - 0.01
532   px         12.37234 $x {432} - 0.01
533   px        -12.37234 $x {433} + 0.01
534   py         12.37234 $x {434} - 0.01
535   py        -12.37234 $x {435} + 0.01
545   py         7.93750 $x 6.25/2
546   py         7.99719 $x {545} + 0.0235   $ sheathing
547   py        -7.99719 $x {546} *-1
548   py        -7.93750 $x {545} *-1
550   px        -7.99719 $x {547}
551   px        -7.93750 $x {548}
552   px         7.93750 $x {545}
553   px         7.99719 $x {546}
c
c cell-id-2 8.98
c gap-o     1.09
c
701   px        -5.0
702   px        1.90627 $x (10.906 - 8.98)/2 - 5/16 + 0.1
703   px        3.45694 $x 2.722/2
704   px        4.09829 $x 10.906 - 8.98 - 5/16
705   px        27.70124 $x 10.906
706   px        31.79953 $x 2 * 10.906 - (8.98+8.98)/2 - 5/16
707   px        55.40248 $x 2 * 10.906
708   px        59.50077 $x {707} + {704}
709   px        83.10372 $x 3 * 10.906
710   p     1  -1  0  0.1 $ diagonal x=y, offset by 0.1 to avoid intersecting corners
711   py        -4.99999 $x {701}
712   py        1.90627 $x {702}
713   py        3.45694 $x {703}
714   py        4.09829 $x {704}
```

```
715   py        27.70124 $x {705}
716   py        31.79953 $x {706}
717   py        55.40248 $x {707}
718   py        59.50077 $x {708}
719   py        83.10372 $x {709}
720   px        0.0
721   py        0.0
1410    px         11.40460 $x 8.98/2
1411    px        -11.40460 $x {1410} *-1
1412    py         11.40460 $x {1410}
1413    py        -11.40460 $x {1411}
1424    px         12.19835 $x {1410} + 5/16     $ angle
1425    px        -12.19835 $x {1411} - 5/16     $ box wall
1426    py         12.19835 $x {1412} + 5/16
1427    py        -12.19835 $x {1413} - 5/16
1428    px         12.20724 $x {1424} + 0.0035   $ wall to boral gap
1429    px        -12.20724 $x {1425} - 0.0035
1430    py         12.20724 $x {1426} + 0.0035
1431    py        -12.20724 $x {1427} - 0.0035
1432    px         12.39774 $x {1428} + 0.075    $ boral
1433    px        -12.39774 $x {1429} - 0.075
1434    py         12.39774 $x {1430} + 0.075
1435    py        -12.39774 $x {1431} - 0.075
1436    px         12.40663 $x {1432} + 0.0035   $ boral to sheathing gap
1437    px        -12.40663 $x {1433} - 0.0035
1438    py         12.40663 $x {1434} + 0.0035
1439    py        -12.40663 $x {1435} - 0.0035
1440    px         12.46632 $x {1436} + 0.0235   $ sheathing
1441    px        -12.46632 $x {1437} - 0.0235
1442    py         12.46632 $x {1438} + 0.0235
1443    py        -12.46632 $x {1439} - 0.0235
1445    py          9.52500 $x 7.5/2
1446    py          9.58469 $x {1445} + 0.0235   $ sheathing
1447    py         -9.58469 $x {1446} *-1
1448    py         -9.52500 $x {1445} *-1
1450    px         -9.58469 $x {1447}
1451    px         -9.52500 $x {1448}
1452    px          9.52500 $x {1445}
1453    px          9.58469 $x {1446}
1528   px         12.23264 $x {1428} + 0.01  $ Aluminum on the outside of boral
1529   px        -12.23264 $x {1429} - 0.01
1530   py         12.23264 $x {1430} + 0.01
1531   py        -12.23264 $x {1431} - 0.01
1532   px         12.37234 $x {1432} - 0.01
1533   px        -12.37234 $x {1433} + 0.01
1534   py         12.37234 $x {1434} - 0.01
1535   py        -12.37234 $x {1435} + 0.01
1545   py         7.93750 $x 6.25/2
1546   py         7.99719 $x {1545} + 0.0235   $ sheathing
1547   py        -7.99719 $x {1546} *-1
1548   py        -7.93750 $x {1545} *-1
1550   px        -7.99719 $x {1547}
1551   px        -7.93750 $x {1548}
1552   px         7.93750 $x {1545}
1553   px         7.99719 $x {1546}
46    pz        -31.75       $ 8.5"  lower steel thickness
43    pz        -10.16       $ lower water thickness
39    pz          0.0        $ bottom of active fuel assembly
40    pz        381.0        $ top of active fuel assembly
44    pz        396.24       $ upper water thickness
45    pz        435.61       $ 15.5" upper steel thickness
```

```
41    cz          85.57       $ mpc steel ID
42    cz         108.43       $ mpc water
c end of surfaces
c --- empty line

c --- empty line
trl 0 0 0
kcode    10000  .94  20  120
sdef  par=1  erg=d1 axs=0 0 1 x=d4 y=fx d5 z=d3
c
sp1  -2 1.2895
c
sp3  0 1
c
si4  s         13 14
           12 13 14 15
        11 12 13 14 15 16
        11 12 13 14 15 16
           12 13 14 15
              13 14
sp4  1 23r
c
ds5  s               26 26
                  25 25 25 25
               24 24 24 24 24 24
               23 23 23 23 23 23
                  22 22 22 22
                     21 21
c
si11  -79.25435 -57.61355
si12  -51.88077 -30.23997
si13  -24.50719 -2.86639
si14   2.86639   24.50719
si15   30.23997  51.88077
si16   57.61355  79.25435
c
si21  -79.25435 -57.61355
si22  -51.88077 -30.23997
si23  -24.50719 -2.86639
si24   2.86639   24.50719
si25   30.23997  51.88077
si26   57.61355  79.25435
c
sp11  0 1
sp12  0 1
sp13  0 1
sp14  0 1
sp15  0 1
sp16  0 1
sp21  0 1
sp22  0 1
sp23  0 1
sp24  0 1
sp25  0 1
sp26  0 1
c
m3           40000.56c   1.          $ Zr Clad
m4           1001.50c    0.6667      $ Water
             8016.50c    0.3333
m5           24000.50c   0.01761     $ Steel
             25055.50c   0.001761
```

```
             26000.55c   0.05977
             28000.50c   0.008239
m6           5010.50c   -0.054427     $ Boral Central Section @ 0.02 g/cmsq
             5011.50c   -0.241373
             13027.50c  -0.6222
             6000.50c   -0.0821
m7           13027.50c   1.0
mt4         lwtr.01t
prdmp    j   -120   j   2
fm4      1000   1   -6
f4:n   1
sd4      1000
e4    1.000E-11   1.000E-10   5.000E-10   7.500E-10   1.000E-09   1.200E-09
      1.500E-09   2.000E-09   2.500E-09   3.000E-09
      4.700E-09   5.000E-09   7.500E-09   1.000E-08   2.530E-08
      3.000E-08   4.000E-08   5.000E-08   6.000E-08   7.000E-08
      8.000E-08   9.000E-08   1.000E-07   1.250E-07   1.500E-07
      1.750E-07   2.000E-07   2.250E-07   2.500E-07   2.750E-07
      3.000E-07   3.250E-07   3.500E-07   3.750E-07   4.000E-07
      4.500E-07   5.000E-07   5.500E-07   6.000E-07   6.250E-07
      6.500E-07   7.000E-07   7.500E-07   8.000E-07   8.500E-07
      9.000E-07   9.250E-07   9.500E-07   9.750E-07   1.000E-06
      1.010E-06   1.020E-06   1.030E-06   1.040E-06   1.050E-06
      1.060E-06   1.070E-06   1.080E-06   1.090E-06   1.100E-06
      1.110E-06   1.120E-06   1.130E-06   1.140E-06   1.150E-06
      1.175E-06   1.200E-06   1.225E-06   1.250E-06   1.300E-06
      1.350E-06   1.400E-06   1.450E-06   1.500E-06   1.590E-06
      1.680E-06   1.770E-06   1.860E-06   1.940E-06   2.000E-06
      2.120E-06   2.210E-06   2.300E-06   2.380E-06   2.470E-06
      2.570E-06   2.670E-06   2.770E-06   2.870E-06   2.970E-06
      3.000E-06   3.050E-06   3.150E-06   3.500E-06   3.730E-06
      4.000E-06   4.750E-06   5.000E-06   5.400E-06   6.000E-06
      6.250E-06   6.500E-06   6.750E-06   7.000E-06   7.150E-06
      8.100E-06   9.100E-06   1.000E-05   1.150E-05   1.190E-05
      1.290E-05   1.375E-05   1.440E-05   1.510E-05   1.600E-05
      1.700E-05   1.850E-05   1.900E-05   2.000E-05   2.100E-05
      2.250E-05   2.500E-05   2.750E-05   3.000E-05   3.125E-05
      3.175E-05   3.325E-05   3.375E-05   3.460E-05   3.550E-05
      3.700E-05   3.800E-05   3.910E-05   3.960E-05   4.100E-05
      4.240E-05   4.400E-05   4.520E-05   4.700E-05   4.830E-05
      4.920E-05   5.060E-05   5.200E-05   5.340E-05   5.900E-05
      6.100E-05   6.500E-05   6.750E-05   7.200E-05   7.600E-05
      8.000E-05   8.200E-05   9.000E-05   1.000E-04   1.080E-04
      1.150E-04   1.190E-04   1.220E-04   1.860E-04   1.925E-04
      2.075E-04   2.100E-04   2.400E-04   2.850E-04   3.050E-04
      5.500E-04   6.700E-04   6.830E-04   9.500E-04   1.150E-03
      1.500E-03   1.550E-03   1.800E-03   2.200E-03   2.290E-03
      2.580E-03   3.000E-03   3.740E-03   3.900E-03   6.000E-03
      8.030E-03   9.500E-03   1.300E-02   1.700E-02   2.500E-02
      3.000E-02   4.500E-02   5.000E-02   5.200E-02   6.000E-02
      7.300E-02   7.500E-02   8.200E-02   8.500E-02   1.000E-01
      1.283E-01   1.500E-01   2.000E-01   2.700E-01   3.300E-01
      4.000E-01   4.200E-01   4.400E-01   4.700E-01   4.995E-01
      5.500E-01   5.730E-01   6.000E-01   6.700E-01   6.790E-01
      7.500E-01   8.200E-01   8.611E-01   8.750E-01   9.000E-01
      9.200E-01   1.010E+00   1.100E+00   1.200E+00   1.250E+00
      1.317E+00   1.356E+00   1.400E+00   1.500E+00   1.850E+00
      2.354E+00   2.479E+00   3.000E+00   4.304E+00   4.800E+00
      6.434E+00   8.187E+00   1.000E+01   1.284E+01   1.384E+01
      1.455E+01   1.568E+01   1.733E+01   2.000E+01
si3  h 0 381.00
```

```
imp:n 1 193r 0
c fuel enrichment 4.1 %
m1      92235.50c     -0.03614
        92238.50c     -0.84536
         8016.50c     -0.11850
c end of file
c
```

```
HI-STAR containing MPC68, 08x08 @ 4.2 wt% Enrich.
c     4.20 % uniform enrichment,  unreflected cask, 0.0279 g/cmsq B-10 in Boral
c
c
1     1 -10.522      -1  u=2       $ fuel
2     4 -1.0      1  -2  u=2       $ gap
3     3 -6.55     2  -3  u=2       $ Zr Clad
4     4 -1.0          3  u=2       $ water in fuel region
5     4 -1.0   -4:5      u=3       $ water in guide tubes
6     3 -6.55   4 -5     u=3       $ guide tubes
7     4 -1.0   -6   +7   -8   +9   u=1  lat=1
      fill= -5:4    -5:4   0:0
      1  1 1 1 1 1 1 1 1  1
      1  2 2 2 2 2 2 2 2  1
      1  2 2 2 2 2 2 2 2  1
      1  2 2 2 2 2 2 2 2  1
      1  2 2 2 3 2 2 2 2  1
      1  2 2 2 2 3 2 2 2  1
      1  2 2 2 2 2 2 2 2  1
      1  2 2 2 2 2 2 2 2  1
      1  2 2 2 2 2 2 2 2  1
      1  1 1 1 1 1 1 1 1  1
c
C  BOX TYPE R
c
8     0  -10   11  -12   13          u=4 fill=1 (0.8128  0.8128  0)
9     3  -6.55    60   -61    62   -63  #8       u=4     $ Zr flow channel
10    4  -1.      64   -65    66   -67  #8 #9    u=4     $ water
11    5  -7.84    20   -23    67   -14           u=4     $ 0.075" STEEL
12    4  -1.      20   -23    14   -15           u=4     $ WATER POCKET
13    7  -2.7     20   -23    15   -16           u=4     $ Al CLAD
14    6  -2.66    20   -23    16   -17           u=4     $ BORAL Absorber
15    7  -2.7     20   -23    17   -18           u=4     $ Al Clad
16    4  -1.      20   -23    18  -118           u=4     $ Water
17    5  -7.84    118:-129:65:-66                u=4     $ Steel
18    4  -1.      64   -21    67   -118          u=4     $ Water
19    4  -1.      24   -65    67   -118          u=4     $ water
20    5  -7.84    21   -20    67   -118          u=4     $ Steel
21    5  -7.84    23   -24    67   -118          u=4     $ Steel
22    4  -1.     129   -64    33   -118          u=4     $ Water
c
23    5  -7.84    25   -64    30   -31           u=4     $ Steel
24    4  -1.      26   -25    30   -31           u=4     $ Water
25    7  -2.7     27   -26    30   -31           u=4     $ Al clad
26    6  -2.66    28   -27    30   -31           u=4     $ Boral
27    7  -2.7     29   -28    30   -31           u=4     $ Al clad
28    4  -1.     129   -29    30   -31           u=4     $ water
29    5  -7.84   129   -64    32   -30           u=4     $ Steel ends
30    5  -7.84   129   -64    31   -33           u=4     $ Steel ends
31    4  -1.     129   -64    66   -32           u=4     $ Water
c
c    Type A box - Boral only on left side
c
32    0  -10   11  -12   13          u=6 fill=1 (0.8128  0.8128  0)
33    3  -6.55    60   -61    62   -63  #8       u=6     $ Zr flow channel
34    4  -1.      64   -65    66  -118  #8 #9    u=6     $ water
35    5  -7.84    118:-129:65:-66                u=6     $ Steel
36    4  -1.     129   -64    67   -118          u=6     $ Water
c
37    5  -7.84    25   -64    30   -31           u=6     $ Steel
38    4  -1.      26   -25    30   -31           u=6     $ Water
```

```
39    7  -2.7     27   -26    30   -31          u=6     $ Al clad
40    6  -2.66    28   -27    30   -31          u=6     $ Boral
41    7  -2.7     29   -28    30   -31          u=6     $ Al clad
42    4  -1.     129   -29    30   -31          u=6     $ water
43    4  -1.     129   -64    33   -67          u=6     $ Water
44    5  -7.84   129   -64    32   -30          u=6     $ Steel ends
45    5  -7.84   129   -64    31   -33          u=6     $ Steel ends
46    4  -1.     129   -64    66   -32          u=6     $ Water
c
c    Type B box -  Boral on Top only
c
47    0  -10   11  -12   13         u=7 fill=1 (0.8128  0.8128  0)
48    3  -6.55    60   -61    62   -63  #8      u=7     $ Zr flow channel
49    4  -1.      64   -65    66   -67  #8 #9   u=7     $ water
50    5  -7.84    20   -23    67   -14          u=7     $ 0.075" STEEL
51    4  -1.      20   -23    14   -15          u=7     $ WATER POCKET
52    7  -2.7     20   -23    15   -16          u=7     $ Al CLAD
53    6  -2.66    20   -23    16   -17          u=7     $ BORAL Absorber
54    7  -2.7     20   -23    17   -18          u=7     $ water
55    4  -1.      20   -23    18  -118          u=7     $ Water
56    5  -7.84    118:-129:65:-66               u=7     $ Steel
57    4  -1.      64   -21    67   -118         u=7     $ Water
58    4  -1.      24   -65    67   -118         u=7     $ water
59    5  -7.84    21   -20    67   -118         u=7     $ Steel
60    5  -7.84    23   -24    67   -118         u=7     $ Steel
61    4  -1.     129   -64    66   -118         u=7     $ Water
c
c    Type E box  - No Boral Panels
c
62    0  -10   11  -12   13         u=8 fill=1 (0.8128  0.8128  0)
63    3  -6.55    60   -61    62   -63  #8      u=8     $ Zr flow channel
64    4  -1.     129   -65    66  -118  #8 #9   u=8     $ water
65    5  -7.84    118:-129:65:-66               u=8     $ Steel
c
c    Type F box  - No Boral Panels or fuel
c
66    4  -1.     129   -65    66  -118          u=9     $ water
67    5  -7.84    118:-129:65:-66               u=9     $ Steel
c
68    4  -1.0    -34  35  -36  37  u=5  lat=1  fill=-7:6  -7:6  0:0
                5 5 5 5 5 5 5 5 5 5 5 5 5 5
                5 9 9 9 9 9 9 9 9 9 9 9 9 5
                5 9 9 9 9 9 7 4 9 9 9 9 9 5
                5 9 9 9 7 4 4 4 4 4 9 9 9 5
                5 9 9 7 4 4 4 4 4 4 4 9 9 5
                5 9 9 7 4 4 4 4 4 4 4 9 9 5
                5 9 7 4 4 4 4 4 4 4 4 4 9 5
                5 9 8 4 4 4 4 4 4 4 4 6 9 5
                5 9 9 7 4 4 4 4 4 4 4 9 9 5
                5 9 9 8 4 4 4 4 4 4 6 9 9 5
                5 9 9 9 8 4 4 4 4 6 6 9 9 5
                5 9 9 9 9 9 9 8 6 9 9 9 9 9 5
                5 9 9 9 9 9 9 9 9 9 9 9 9 9 5
                5 5 5 5 5 5 5 5 5 5 5 5 5 5 5
69    0          -41              50  -49  fill=5 (8.1661  8.1661  0)
70    4  -1.0    -41       43  -50            $ Water below Fuel
71    4  -1.0    -41       49  -44            $ Water above Fuel
72    5  -7.84   -42       68  -43            $ Steel below Fuel
73    5  -7.84   -42       44  -69            $ Steel above Fuel
74    5  -7.84    41  -42  43  -44            $ Radial Steel
75    0           42 :-68:  69                $ outside world
```

```
1      cz          0.5207      $ Fuel OD
2      cz          0.5321      $ Clad ID
3      cz          0.6134      $ Clad OD
4      cz          0.6744      $ Thimble ID
5      cz          0.7506      $ Thimble OD
6      px          0.8128      $ Pin Pitch
7      px         -0.8128
8      py          0.8128
9      py         -0.8128
10     px          6.7031      $ Channel ID
11     px         -6.7031
12     py          6.7031
13     py         -6.7031
14     py          7.8016
15     py          7.8155
16     py          7.8410
17     py          8.0467
18     py          8.0721
118    py          8.0861
20     px         -6.0325
21     px         -6.2230
23     px          6.0325
24     px          6.2230
25     px         -7.8016
26     px         -7.8155
27     px         -7.8410
28     px         -8.0467
29     px         -8.0721
129    px         -8.0861
30     py         -6.0325
31     py          6.0325
32     py         -6.2230
33     py          6.2230
34     px          7.6111
35     px         -8.7211
36     py          8.7211
37     py         -7.6111
41     cz          85.57
42     cz          108.43
43     pz         -18.54
44     pz          402.5
49     pz          381.        $ Top of Active Fuel
50     pz            0         $ Start of Active Fuel
60     px         -6.9571      $ Channel OD
61     px          6.9571
62     py         -6.9571
63     py          6.9571
64     px         -7.6111      $ Cell Box ID
65     px          7.6111
66     py         -7.6111
67     py          7.6111
68     pz         -40.13
69     pz          441.9

imp:n     1 73r 0
kcode   10000  0.94   20  120
c
sdef  par=1  erg=d1 axs=0 0 1 x=d4 y=fx d5 z=d3
c
sp1 -2 1.2895
```

```
c
c
si3  h 0 365.76
sp3  0 1
c
c
si4  s                15 16
                   13 14 15 16 17 18
               12 13 14 15 16 17 18 19
               12 13 14 15 16 17 18 19
            11 12 13 14 15 16 17 18 19 20
            11 12 13 14 15 16 17 18 19 20
               12 13 14 15 16 17 18 19
               12 13 14 15 16 17 18 19
                  13 14 15 16 17 18
                        15 16
sp4  1 67r
c
ds5  s                30 30
                   29 29 29 29 29 29
               28 28 28 28 28 28 28 28
               27 27 27 27 27 27 27 27
            26 26 26 26 26 26 26 26 26 26
            25 25 25 25 25 25 25 25 25 25
               24 24 24 24 24 24 24 24
               23 23 23 23 23 23 23 23
                  22 22 22 22 22 22
                        21 21
c
si11  -80.6831 -67.6783
si12  -64.1985 -51.1937
si13  -47.7139 -34.7091
si14  -31.2293 -18.2245
si15  -14.7447 -1.7399
si16   1.7399   14.7447
si17   18.2245  31.2293
si18   34.7091  47.7139
si19   51.1937  64.1985
si20   67.6783  80.6831
c
si21  -80.6831 -67.6783
si22  -64.1985 -51.1937
si23  -47.7139 -34.7091
si24  -31.2293 -18.2245
si25  -14.7447 -1.7399
si26   1.7399   14.7447
si27   18.2245  31.2293
si28   34.7091  47.7139
si29   51.1937  64.1985
si30   67.6783  80.6831
sp11  0 1
sp12  0 1
sp13  0 1
sp14  0 1
sp15  0 1
sp16  0 1
sp17  0 1
sp18  0 1
sp19  0 1
sp20  0 1
sp21  0 1
```

```
sp22  0 1
sp23  0 1
sp24  0 1
sp25  0 1
sp26  0 1
sp27  0 1
sp28  0 1
sp29  0 1
sp30  0 1
c
m1          92235.50c   9.98343E-04  $ 4.20% E Fuel
            92238.50c   0.022484
            8016.50c    0.046965
m2          8016.50c    1.           $ Void
m3          40000.56c   1.           $ Zr Clad
m4          1001.50c    0.6667       $ Water
            8016.50c    0.3333
m5          24000.50c   0.01761      $ Steel
            25055.50c   0.001761
            26000.55c   0.05977
            28000.50c   0.008239
m6          5010.50c    8.0707E-03   $ Boral
            5011.50c    3.2553E-02
            6000.50c    1.0146E-02
            13027.50c   3.8054E-02
m7          13027.50c    1.           $ Al Clad
mt4        lwtr.01t
prdmp    j   -30   1   2
fm4      1000   1   -6
f4:n   1
sd4      1000
e4    1.000E-11   1.000E-10   5.000E-10   7.500E-10   1.000E-09   1.200E-09
      1.500E-09   2.000E-09   2.500E-09   3.000E-09
      4.700E-09   5.000E-09   7.500E-09   1.000E-08   2.530E-08
      3.000E-08   4.000E-08   5.000E-08   6.000E-08   7.000E-08
      8.000E-08   9.000E-08   1.000E-07   1.250E-07   1.500E-07
      1.750E-07   2.000E-07   2.250E-07   2.500E-07   2.750E-07
      3.000E-07   3.250E-07   3.500E-07   3.750E-07   4.000E-07
      4.500E-07   5.000E-07   5.500E-07   6.000E-07   6.250E-07
      6.500E-07   7.000E-07   7.500E-07   8.000E-07   8.500E-07
      9.000E-07   9.250E-07   9.500E-07   9.750E-07   1.000E-06
      1.010E-06   1.020E-06   1.030E-06   1.040E-06   1.050E-06
      1.060E-06   1.070E-06   1.080E-06   1.090E-06   1.100E-06
      1.110E-06   1.120E-06   1.130E-06   1.140E-06   1.150E-06
      1.175E-06   1.200E-06   1.225E-06   1.250E-06   1.300E-06
      1.350E-06   1.400E-06   1.450E-06   1.500E-06   1.590E-06
      1.680E-06   1.770E-06   1.860E-06   1.940E-06   2.000E-06
      2.120E-06   2.210E-06   2.300E-06   2.380E-06   2.470E-06
      2.570E-06   2.670E-06   2.770E-06   2.870E-06   2.970E-06
      3.000E-06   3.050E-06   3.150E-06   3.500E-06   3.730E-06
      4.000E-06   4.750E-06   5.000E-06   5.400E-06   6.000E-06
      6.250E-06   6.500E-06   6.750E-06   7.000E-06   7.150E-06
      8.100E-06   9.100E-06   1.000E-05   1.150E-05   1.190E-05
      1.290E-05   1.375E-05   1.440E-05   1.510E-05   1.600E-05
      1.700E-05   1.850E-05   1.900E-05   2.000E-05   2.100E-05
      2.250E-05   2.500E-05   2.750E-05   3.000E-05   3.125E-05
      3.175E-05   3.325E-05   3.375E-05   3.460E-05   3.550E-05
      3.700E-05   3.800E-05   3.910E-05   3.960E-05   4.100E-05
      4.240E-05   4.400E-05   4.520E-05   4.700E-05   4.830E-05
      4.920E-05   5.060E-05   5.200E-05   5.340E-05   5.900E-05
      6.100E-05   6.500E-05   6.750E-05   7.200E-05   7.600E-05
```

8.000E-05	8.200E-05	9.000E-05	1.000E-04	1.080E-04
1.150E-04	1.190E-04	1.220E-04	1.860E-04	1.925E-04
2.075E-04	2.100E-04	2.400E-04	2.850E-04	3.050E-04
5.500E-04	6.700E-04	6.830E-04	9.500E-04	1.150E-03
1.500E-03	1.550E-03	1.800E-03	2.200E-03	2.290E-03
2.580E-03	3.000E-03	3.740E-03	3.900E-03	6.000E-03
8.030E-03	9.500E-03	1.300E-02	1.700E-02	2.500E-02
3.000E-02	4.500E-02	5.000E-02	5.200E-02	6.000E-02
7.300E-02	7.500E-02	8.200E-02	8.500E-02	1.000E-01
1.283E-01	1.500E-01	2.000E-01	2.700E-01	3.300E-01
4.000E-01	4.200E-01	4.400E-01	4.700E-01	4.995E-01
5.500E-01	5.730E-01	6.000E-01	6.700E-01	6.790E-01
7.500E-01	8.200E-01	8.611E-01	8.750E-01	9.000E-01
9.200E-01	1.010E+00	1.100E+00	1.200E+00	1.250E+00
1.317E+00	1.356E+00	1.400E+00	1.500E+00	1.850E+00
2.354E+00	2.479E+00	3.000E+00	4.304E+00	4.800E+00
6.434E+00	8.187E+00	1.000E+01	1.284E+01	1.384E+01
1.455E+01	1.568E+01	1.733E+01	2.000E+01	

```
HI-STAR containing MPC68F, 06x06 @ 3.0 wt% Enrich.
c     3.00 % uniform enrichment, unreflected cask, 0.0067 g/cmsq B-10 in Boral
c     Dresden-1 6x6
c
c
1     1 -10.522      -1  u=2       $ fuel
2     4 -1.0      1  -2  u=2       $ gap
3     3 -6.55     2  -3  u=2       $ Zr Clad
4     4 -1.0          3  u=2       $ water in fuel region
5     4 -1.0   -4:5      u=3       $ water in guide tubes
6     3 -6.55   4 -5     u=3       $ guide tubes
7     4 -1.0   -6   +7   -8   +9   u=1  lat=1
      fill= -4:3    -4:3   0:0
      1  1 1 1 1 1 1  1
      1  2 2 2 2 2 2  1
      1  2 2 2 2 2 2  1
      1  2 2 2 2 2 2  1
      1  2 2 2 2 2 2  1
      1  2 2 2 2 2 2  1
      1  2 2 2 2 2 2  1
      1  1 1 1 1 1 1  1
c
C  BOX TYPE R
c
8     0  -10   11  -12   13          u=4 fill=1 (0.8814  0.8814  0)
9     3  -6.55    60   -61    62   -63  #8       u=4     $ Zr flow channel
10    4  -1.      64   -65    66   -67  #8 #9    u=4     $ water
11    5  -7.84    20   -23    67   -14           u=4     $ 0.075" STEEL
12    4  -1.      20   -23    14   -15           u=4     $ WATER POCKET
13    7  -2.7     20   -23    15   -16           u=4     $ Al CLAD
14    6  -2.66    20   -23    16   -17           u=4     $ BORAL Absorber
15    7  -2.7     20   -23    17   -18           u=4     $ Al Clad
16    4  -1.      20   -23    18  -118           u=4     $ Water
17    5  -7.84    118:-129:65:-66                u=4     $ Steel
18    4  -1.      64   -21    67   -118          u=4     $ Water
19    4  -1.      24   -65    67   -118          u=4     $ water
20    5  -7.84    21   -20    67   -118          u=4     $ Steel
21    5  -7.84    23   -24    67   -118          u=4     $ Steel
22    4  -1.     129   -64    33   -118          u=4     $ Water
c
23    5  -7.84    25   -64    30   -31           u=4     $ Steel
24    4  -1.      26   -25    30   -31           u=4     $ Water
25    7  -2.7     27   -26    30   -31           u=4     $ Al clad
26    6  -2.66    28   -27    30   -31           u=4     $ Boral
27    7  -2.7     29   -28    30   -31           u=4     $ Al clad
28    4  -1.     129   -29    30   -31           u=4     $ water
29    5  -7.84   129   -64    32   -30           u=4     $ Steel ends
30    5  -7.84   129   -64    31   -33           u=4     $ Steel ends
31    4  -1.     129   -64    66   -32           u=4     $ Water
c
c    Type A box - Boral only on left side
c
32    0  -10   11  -12   13          u=6 fill=1 (0.8814  0.8814  0)
33    3  -6.55    60   -61    62   -63  #8       u=6     $ Zr flow channel
34    4  -1.      64   -65    66  -118  #8 #9    u=6     $ water
35    5  -7.84    118:-129:65:-66                u=6     $ Steel
36    4  -1.     129   -64    67   -118          u=6     $ Water
c
37    5  -7.84    25   -64    30   -31           u=6     $ Steel
38    4  -1.      26   -25    30   -31           u=6     $ Water
39    7  -2.7     27   -26    30   -31           u=6     $ Al clad
```

```
40    6  -2.66    28   -27    30   -31          u=6     $ Boral
41    7  -2.7     29   -28    30   -31          u=6     $ Al clad
42    4  -1.     129   -29    30   -31          u=6     $ water
43    4  -1.     129   -64    33   -67          u=6     $ Water
44    5  -7.84   129   -64    32   -30          u=6     $ Steel ends
45    5  -7.84   129   -64    31   -33          u=6     $ Steel ends
46    4  -1.     129   -64    66   -32          u=6     $ Water
c
c    Type B box -  Boral on Top only
c
47    0  -10   11  -12   13         u=7 fill=1 (0.8814  0.8814  0)
48    3  -6.55    60   -61    62   -63  #8      u=7     $ Zr flow channel
49    4  -1.      64   -65    66   -67  #8 #9   u=7     $ water
50    5  -7.84    20   -23    67   -14          u=7     $ 0.075" STEEL
51    4  -1.      20   -23    14   -15          u=7     $ WATER POCKET
52    7  -2.7     20   -23    15   -16          u=7     $ Al CLAD
53    6  -2.66    20   -23    16   -17          u=7     $ BORAL Absorber
54    7  -2.7     20   -23    17   -18          u=7     $ water
55    4  -1.      20   -23    18  -118          u=7     $ Water
56    5  -7.84    118:-129:65:-66               u=7     $ Steel
57    4  -1.      64   -21    67   -118         u=7     $ Water
58    4  -1.      24   -65    67   -118         u=7     $ water
59    5  -7.84    21   -20    67   -118         u=7     $ Steel
60    5  -7.84    23   -24    67   -118         u=7     $ Steel
61    4  -1.     129   -64    66   -118         u=7     $ Water
c
c    Type E box  - No Boral Panels
c
62    0  -10   11  -12   13         u=8 fill=1 (0.8814  0.8814  0)
63    3  -6.55    60   -61    62   -63  #8      u=8     $ Zr flow channel
64    4  -1.     129   -65    66  -118  #8 #9   u=8     $ water
65    5  -7.84    118:-129:65:-66               u=8     $ Steel
c
c    Type F box  - No Boral Panels or fuel
c
66    4  -1.     129   -65    66  -118          u=9     $ water
67    5  -7.84    118:-129:65:-66               u=9     $ Steel
c
68    4  -1.0    -34  35  -36  37  u=5  lat=1  fill=-7:6  -7:6  0:0
                5 5 5 5 5 5 5 5 5 5 5 5 5 5
                5 9 9 9 9 9 9 9 9 9 9 9 9 5
                5 9 9 9 9 9 7 4 9 9 9 9 9 5
                5 9 9 9 7 4 4 4 4 4 9 9 9 5
                5 9 9 7 4 4 4 4 4 4 4 9 9 5
                5 9 9 7 4 4 4 4 4 4 4 9 9 5
                5 9 7 4 4 4 4 4 4 4 4 4 9 5
                5 9 8 4 4 4 4 4 4 4 4 6 9 5
                5 9 9 7 4 4 4 4 4 4 4 9 9 5
                5 9 9 8 4 4 4 4 4 4 6 9 9 5
                5 9 9 9 8 4 4 4 6 6 9 9 9 5
                5 9 9 9 9 9 8 6 9 9 9 9 9 5
                5 9 9 9 9 9 9 9 9 9 9 9 9 5
                5 5 5 5 5 5 5 5 5 5 5 5 5 5
69    0          -41               50  -49  fill=5 (8.1661  8.1661  0)
70    4  -1.0    -41       43  -50            $ Water below Fuel
71    4  -1.0    -41       49  -44            $ Water above Fuel
72    5  -7.84   -42       68  -43            $ Steel below Fuel
73    5  -7.84   -42       44  -69            $ Steel above Fuel
74    5  -7.84    41  -42  43  -44            $ Radial Steel
75    0           42 :-68:  69                $ outside world
```

```
1      cz          0.6274        $ Fuel OD
2      cz          0.6280        $ Clad ID
3      cz          0.7169        $ Clad OD
4      cz          0.6280        $ Thimble ID
5      cz          0.7169        $ Thimble OD
6      px          0.8814        $ Pin Pitch
7      px         -0.8814
8      py          0.8814
9      py         -0.8814
10     px          5.4483        $ Channel ID
11     px         -5.4483
12     py          5.4483
13     py         -5.4483
14     py          7.8016
15     py          7.8155
16     py          7.8410
17     py          8.0467
18     py          8.0721
118    py          8.0861
20     px         -6.0325
21     px         -6.2230
23     px          6.0325
24     px          6.2230
25     px         -7.8016
26     px         -7.8155
27     px         -7.8410
28     px         -8.0467
29     px         -8.0721
129    px         -8.0861
30     py         -6.0325
31     py          6.0325
32     py         -6.2230
33     py          6.2230
34     px          7.6111
35     px         -8.7211
36     py          8.7211
37     py         -7.6111
41     cz          85.57
42     cz          108.43
43     pz          11.46
44     pz          331.0
49     pz          309.4          $ Top of Active F
50     pz           30.           $ Start of Active
60     px         -5.6007         $ Channel OD
61     px          5.6007
62     py         -5.6007
63     py          5.6007
64     px         -7.6111         $ Cell Box ID
65     px          7.6111
66     py         -7.6111
67     py          7.6111
68     pz         -10.13
69     pz          370.36

imp:n     1 73r 0
kcode    10000  0.94   20  120
c
sdef  par=1  erg=d1 axs=0 0 1 x=d4 y=fx d5 z=d3
c
sp1 -2 1.2895
c
```

```
si3  h 30. 309.
sp3  0 1
c
c
si4  s                15 16
                   13 14 15 16 17 18
               12 13 14 15 16 17 18 19
               12 13 14 15 16 17 18 19
            11 12 13 14 15 16 17 18 19 20
            11 12 13 14 15 16 17 18 19 20
               12 13 14 15 16 17 18 19
               12 13 14 15 16 17 18 19
                  13 14 15 16 17 18
                        15 16
sp4  1 67r
c
ds5  s                30 30
                   29 29 29 29 29 29
               28 28 28 28 28 28 28 28
               27 27 27 27 27 27 27 27
            26 26 26 26 26 26 26 26 26 26
            25 25 25 25 25 25 25 25 25 25
               24 24 24 24 24 24 24 24
               23 23 23 23 23 23 23 23
                  22 22 22 22 22 22
                        21 21
c
si11  -80.6831 -67.6783
si12  -64.1985 -51.1937
si13  -47.7139 -34.7091
si14  -31.2293 -18.2245
si15  -14.7447 -1.7399
si16   1.7399   14.7447
si17   18.2245  31.2293
si18   34.7091  47.7139
si19   51.1937  64.1985
si20   67.6783  80.6831
c
si21  -80.6831 -67.6783
si22  -64.1985 -51.1937
si23  -47.7139 -34.7091
si24  -31.2293 -18.2245
si25  -14.7447 -1.7399
si26   1.7399   14.7447
si27   18.2245  31.2293
si28   34.7091  47.7139
si29   51.1937  64.1985
si30   67.6783  80.6831
sp11  0 1
sp12  0 1
sp13  0 1
sp14  0 1
sp15  0 1
sp16  0 1
sp17  0 1
sp18  0 1
sp19  0 1
sp20  0 1
sp21  0 1
sp22  0 1
sp23  0 1
```

```
sp24  0 1
sp25  0 1
sp26  0 1
sp27  0 1
sp28  0 1
sp29  0 1
sp30  0 1
c
m1          92235.50c   -0.02644      $ 3.00% E Fuel
            92238.50c   -0.85504
            8016.50c    -0.11852
m3          40000.56c   1.           $ Zr Clad
m4          1001.50c    0.6667       $ Water
            8016.50c    0.3333
m5          24000.50c   0.01761      $ Steel
            25055.50c   0.001761
            26000.55c   0.05977
            28000.50c   0.008239
m6          5010.50c  1.9592E-03      $ Boral 0.0067 gm/cm2
            5011.50c  8.1175E-03
            6000.50c  2.5176E-03
            13027.50c 5.4933E-02
m7          13027.50c    1.           $ Al Clad
mt4        lwtr.01t
prdmp    j   -120   j   2
fm4      1000   1   -6
f4:n   1
sd4      1000
e4    1.000E-11   1.000E-10   5.000E-10   7.500E-10   1.000E-09   1.200E-09
      1.500E-09   2.000E-09   2.500E-09   3.000E-09
      4.700E-09   5.000E-09   7.500E-09   1.000E-08   2.530E-08
      3.000E-08   4.000E-08   5.000E-08   6.000E-08   7.000E-08
      8.000E-08   9.000E-08   1.000E-07   1.250E-07   1.500E-07
      1.750E-07   2.000E-07   2.250E-07   2.500E-07   2.750E-07
      3.000E-07   3.250E-07   3.500E-07   3.750E-07   4.000E-07
      4.500E-07   5.000E-07   5.500E-07   6.000E-07   6.250E-07
      6.500E-07   7.000E-07   7.500E-07   8.000E-07   8.500E-07
      9.000E-07   9.250E-07   9.500E-07   9.750E-07   1.000E-06
      1.010E-06   1.020E-06   1.030E-06   1.040E-06   1.050E-06
      1.060E-06   1.070E-06   1.080E-06   1.090E-06   1.100E-06
      1.110E-06   1.120E-06   1.130E-06   1.140E-06   1.150E-06
      1.175E-06   1.200E-06   1.225E-06   1.250E-06   1.300E-06
      1.350E-06   1.400E-06   1.450E-06   1.500E-06   1.590E-06
      1.680E-06   1.770E-06   1.860E-06   1.940E-06   2.000E-06
      2.120E-06   2.210E-06   2.300E-06   2.380E-06   2.470E-06
      2.570E-06   2.670E-06   2.770E-06   2.870E-06   2.970E-06
      3.000E-06   3.050E-06   3.150E-06   3.500E-06   3.730E-06
      4.000E-06   4.750E-06   5.000E-06   5.400E-06   6.000E-06
      6.250E-06   6.500E-06   6.750E-06   7.000E-06   7.150E-06
      8.100E-06   9.100E-06   1.000E-05   1.150E-05   1.190E-05
      1.290E-05   1.375E-05   1.440E-05   1.510E-05   1.600E-05
      1.700E-05   1.850E-05   1.900E-05   2.000E-05   2.100E-05
      2.250E-05   2.500E-05   2.750E-05   3.000E-05   3.125E-05
      3.175E-05   3.325E-05   3.375E-05   3.460E-05   3.550E-05
      3.700E-05   3.800E-05   3.910E-05   3.960E-05   4.100E-05
      4.240E-05   4.400E-05   4.520E-05   4.700E-05   4.830E-05
      4.920E-05   5.060E-05   5.200E-05   5.340E-05   5.900E-05
      6.100E-05   6.500E-05   6.750E-05   7.200E-05   7.600E-05
      8.000E-05   8.200E-05   9.000E-05   1.000E-04   1.080E-04
      1.150E-04   1.190E-04   1.220E-04   1.860E-04   1.925E-04
      2.075E-04   2.100E-04   2.400E-04   2.850E-04   3.050E-04
```

5.500E-04	6.700E-04	6.830E-04	9.500E-04	1.150E-03
1.500E-03	1.550E-03	1.800E-03	2.200E-03	2.290E-03
2.580E-03	3.000E-03	3.740E-03	3.900E-03	6.000E-03
8.030E-03	9.500E-03	1.300E-02	1.700E-02	2.500E-02
3.000E-02	4.500E-02	5.000E-02	5.200E-02	6.000E-02
7.300E-02	7.500E-02	8.200E-02	8.500E-02	1.000E-01
1.283E-01	1.500E-01	2.000E-01	2.700E-01	3.300E-01
4.000E-01	4.200E-01	4.400E-01	4.700E-01	4.995E-01
5.500E-01	5.730E-01	6.000E-01	6.700E-01	6.790E-01
7.500E-01	8.200E-01	8.611E-01	8.750E-01	9.000E-01
9.200E-01	1.010E+00	1.100E+00	1.200E+00	1.250E+00
1.317E+00	1.356E+00	1.400E+00	1.500E+00	1.850E+00
2.354E+00	2.479E+00	3.000E+00	4.304E+00	4.800E+00
6.434E+00	8.187E+00	1.000E+01	1.284E+01	1.384E+01
1.455E+01	1.568E+01	1.733E+01	2.000E+01	

```
HI-STAR containing MPC68F, 06x06 in DFC with 08 missing rods
c     3.00 % uniform enrichment, unreflected cask, 0.0067 g/cmsq B-10 in Boral
c
c
1     1 -10.522      -1  u=2       $ fuel
2     4 -1.0      1  -2  u=2       $ gap
3     3 -6.55     2  -3  u=2       $ Zr Clad
4     4 -1.0          3  u=2       $ water in fuel region
5     4 -1.0   -4:5      u=3       $ water in guide tubes
6     3 -6.55   4 -5     u=3       $ guide tubes
7     4 -1.0   -6   +7   -8   +9   u=1  lat=1
      fill= -4:3    -4:3   0:0
      1  1 1 1 1 1 1  1
      1  2 2 2 2 2 2  1
      1  2 1 2 1 2 2  1
      1  2 2 1 2 1 2  1
      1  2 1 2 1 2 2  1
      1  2 2 1 2 1 2  1
      1  2 2 2 2 2 2  1
      1  1 1 1 1 1 1  1
c
C  BOX TYPE R
c
8     0  -10   11  -12   13          u=4 fill=1 (0.8814  0.8814  0)
9     3  -6.55    60   -61    62   -63  #8       u=4      $ Zr flow channel
100   5  -7.84   74 -75 76 -77 (-70:71:-72:73)  u=4      $ DFC
10    4  -1.       64   -65    66   -67  #8 #9 #100  u=4 $ water
11    5  -7.84    20   -23    67   -14           u=4      $ 0.075" STEEL
12    4  -1.      20   -23    14   -15           u=4      $ WATER POCKET
13    7  -2.7     20   -23    15   -16           u=4      $ Al CLAD
14    6  -2.66    20   -23    16   -17           u=4      $ BORAL Absorber
15    7  -2.7     20   -23    17   -18           u=4      $ Al Clad
16    4  -1.      20   -23    18  -118           u=4      $ Water
17    5  -7.84    118:-129:65:-66                u=4      $ Steel
18    4  -1.      64   -21    67   -118          u=4      $ Water
19    4  -1.      24   -65    67   -118          u=4      $ water
20    5  -7.84    21   -20    67   -118          u=4      $ Steel
21    5  -7.84    23   -24    67   -118          u=4      $ Steel
22    4  -1.     129   -64    33   -118          u=4      $ Water
c
23    5  -7.84    25   -64    30   -31           u=4      $ Steel
24    4  -1.      26   -25    30   -31           u=4      $ Water
25    7  -2.7     27   -26    30   -31           u=4      $ Al clad
26    6  -2.66    28   -27    30   -31           u=4      $ Boral
27    7  -2.7     29   -28    30   -31           u=4      $ Al clad
28    4  -1.     129   -29    30   -31           u=4      $ water
29    5  -7.84   129   -64    32   -30           u=4      $ Steel ends
30    5  -7.84   129   -64    31   -33           u=4      $ Steel ends
31    4  -1.     129   -64    66   -32           u=4      $ Water
c
c    Type A box - Boral only on left side
c
32    0  -10   11  -12   13          u=6 fill=1 (0.8814  0.8814  0)
33    3  -6.55    60   -61    62   -63  #8       u=6      $ Zr flow channel
101   5  -7.84   74 -75 76 -77 (-70:71:-72:73)  u=6      $ DFC
34    4  -1.      64   -65    66  -118  #8 #9 #101 u=6  $ water
35    5  -7.84    118:-129:65:-66                u=6      $ Steel
36    4  -1.     129   -64    67   -118          u=6      $ Water
c
37    5  -7.84    25   -64    30   -31           u=6      $ Steel
38    4  -1.      26   -25    30   -31           u=6      $ Water
```

```
39    7  -2.7     27   -26    30   -31          u=6     $ Al clad
40    6  -2.66    28   -27    30   -31          u=6     $ Boral
41    7  -2.7     29   -28    30   -31          u=6     $ Al clad
42    4  -1.     129   -29    30   -31          u=6     $ water
43    4  -1.     129   -64    33   -67          u=6     $ Water
44    5  -7.84   129   -64    32   -30          u=6     $ Steel ends
45    5  -7.84   129   -64    31   -33          u=6     $ Steel ends
46    4  -1.     129   -64    66   -32          u=6     $ Water
c
c    Type B box -  Boral on Top only
c
47    0  -10   11  -12   13         u=7 fill=1 (0.8814  0.8814  0)
48    3  -6.55    60   -61    62   -63  #8      u=7     $ Zr flow channel
102   5  -7.84   74 -75 76 -77 (-70:71:-72:73)  u=7     $ DFC
49    4  -1.      64   -65    66   -67  #8 #9 #102 u=7  $ water
50    5  -7.84    20   -23    67   -14          u=7     $ 0.075" STEEL
51    4  -1.      20   -23    14   -15          u=7     $ WATER POCKET
52    7  -2.7     20   -23    15   -16          u=7     $ Al CLAD
53    6  -2.66    20   -23    16   -17          u=7     $ BORAL Absorber
54    7  -2.7     20   -23    17   -18          u=7     $ water
55    4  -1.      20   -23    18  -118          u=7     $ Water
56    5  -7.84    118:-129:65:-66               u=7     $ Steel
57    4  -1.      64   -21    67   -118         u=7     $ Water
58    4  -1.      24   -65    67   -118         u=7     $ water
59    5  -7.84    21   -20    67   -118         u=7     $ Steel
60    5  -7.84    23   -24    67   -118         u=7     $ Steel
61    4  -1.     129   -64    66   -118         u=7     $ Water
c
c    Type E box  - No Boral Panels
c
62    0  -10   11  -12   13         u=8 fill=1 (0.8814  0.8814  0)
63    3  -6.55    60   -61    62   -63  #8      u=8     $ Zr flow channel
103   5  -7.84   74 -75 76 -77 (-70:71:-72:73)  u=8     $ DFC
64    4  -1.     129   -65    66  -118  #8 #9 #103 u=8  $ water
65    5  -7.84    118:-129:65:-66               u=8     $ Steel
c
c    Type F box  - No Boral Panels or fuel
c
66    4  -1.     129   -65    66  -118          u=9     $ water
67    5  -7.84    118:-129:65:-66               u=9     $ Steel
c
68    4  -1.0    -34  35  -36  37  u=5  lat=1  fill=-7:6  -7:6  0:0
                5 5 5 5 5 5 5 5 5 5 5 5 5 5
                5 9 9 9 9 9 9 9 9 9 9 9 9 5
                5 9 9 9 9 9 7 4 9 9 9 9 9 5
                5 9 9 9 7 4 4 4 4 4 9 9 9 5
                5 9 9 7 4 4 4 4 4 4 4 9 9 5
                5 9 9 7 4 4 4 4 4 4 4 9 9 5
                5 9 7 4 4 4 4 4 4 4 4 4 9 5
                5 9 8 4 4 4 4 4 4 4 4 6 9 5
                5 9 9 7 4 4 4 4 4 4 4 9 9 5
                5 9 9 8 4 4 4 4 4 4 6 9 9 5
                5 9 9 9 8 4 4 4 6 6 9 9 9 5
                5 9 9 9 9 9 8 6 9 9 9 9 9 5
                5 9 9 9 9 9 9 9 9 9 9 9 9 5
                5 5 5 5 5 5 5 5 5 5 5 5 5 5
69    0          -41              50  -49  fill=5 (8.1661  8.1661  0)
70    4  -1.0    -41       43  -50            $ Water below Fuel
71    4  -1.0    -41       49  -44            $ Water above Fuel
72    5  -7.84   -42       68  -43            $ Steel below Fuel
73    5  -7.84   -42       44  -69            $ Steel above Fuel
```

```
74    5  -7.84    41  -42  43  -44            $ Radial Steel
75    0            42 :-68:  69               $ outside world

1     cz          0.6274       $ Fuel OD
2     cz          0.6280       $ Clad ID
3     cz          0.7169       $ Clad OD
4     cz          0.6280       $ Thimble ID
5     cz          0.7169       $ Thimble OD
6     px          0.8814       $ Pin Pitch
7     px         -0.8814
8     py          0.8814
9     py         -0.8814
10    px          5.4483       $ Channel ID
11    px         -5.4483
12    py          5.4483
13    py         -5.4483
14    py          7.8016
15    py          7.8155
16    py          7.8410
17    py          8.0467
18    py          8.0721
118   py          8.0861
20    px         -6.0325
21    px         -6.2230
23    px          6.0325
24    px          6.2230
25    px         -7.8016
26    px         -7.8155
27    px         -7.8410
28    px         -8.0467
29    px         -8.0721
129   px         -8.0861
30    py         -6.0325
31    py          6.0325
32    py         -6.2230
33    py          6.2230
34    px          7.6111
35    px         -8.7211
36    py          8.7211
37    py         -7.6111
41    cz          85.57
42    cz          108.43
43    pz          11.46
44    pz          331.0
49    pz          309.4         $ Top of Active F
50    pz           30.          $ Start of Active
60    px         -5.6007       $ Channel OD
61    px          5.6007
62    py         -5.6007
63    py          5.6007
64    px         -7.6111       $ Cell Box ID
65    px          7.6111
66    py         -7.6111
67    py          7.6111
68    pz         -10.13
69    pz          370.36
70    px         -6.2611       $ DFC ID
71    px          6.2611
72    py         -6.2611
73    py          6.2611
74    px         -6.5659       $ DFC OD
```

```
75    px          6.5659
76    py         -6.5659
77    py          6.5659

imp:n     1 77r 0
kcode    10000  0.94   20  120
c
sdef  par=1  erg=d1 axs=0 0 1 x=d4 y=fx d5 z=d3
c
sp1 -2 1.2895
c
si3  h 30. 309.
sp3  0 1
c
c
si4  s               15 16
                  13 14 15 16 17 18
               12 13 14 15 16 17 18 19
               12 13 14 15 16 17 18 19
            11 12 13 14 15 16 17 18 19 20
            11 12 13 14 15 16 17 18 19 20
               12 13 14 15 16 17 18 19
               12 13 14 15 16 17 18 19
                  13 14 15 16 17 18
                        15 16
sp4  1 67r
c
ds5  s               30 30
                  29 29 29 29 29 29
               28 28 28 28 28 28 28 28
               27 27 27 27 27 27 27 27
            26 26 26 26 26 26 26 26 26 26
            25 25 25 25 25 25 25 25 25 25
               24 24 24 24 24 24 24 24
               23 23 23 23 23 23 23 23
                  22 22 22 22 22 22
                        21 21
c
si11  -80.6831 -67.6783
si12  -64.1985 -51.1937
si13  -47.7139 -34.7091
si14  -31.2293 -18.2245
si15  -14.7447 -1.7399
si16   1.7399   14.7447
si17   18.2245  31.2293
si18   34.7091  47.7139
si19   51.1937  64.1985
si20   67.6783  80.6831
c
si21  -80.6831 -67.6783
si22  -64.1985 -51.1937
si23  -47.7139 -34.7091
si24  -31.2293 -18.2245
si25  -14.7447 -1.7399
si26   1.7399   14.7447
si27   18.2245  31.2293
si28   34.7091  47.7139
si29   51.1937  64.1985
si30   67.6783  80.6831
sp11  0 1
sp12  0 1
```

```
sp13  0 1
sp14  0 1
sp15  0 1
sp16  0 1
sp17  0 1
sp18  0 1
sp19  0 1
sp20  0 1
sp21  0 1
sp22  0 1
sp23  0 1
sp24  0 1
sp25  0 1
sp26  0 1
sp27  0 1
sp28  0 1
sp29  0 1
sp30  0 1
c
m1           92235.50c   -0.02644      $ 3.00% E Fuel
             92238.50c   -0.85504
             8016.50c    -0.11852
m3           40000.56c   1.           $ Zr Clad
m4           1001.50c    0.6667       $ Water
             8016.50c    0.3333
m5           24000.50c   0.01761      $ Steel
             25055.50c   0.001761
             26000.55c   0.05977
             28000.50c   0.008239
m6           5010.50c  1.9592E-03      $ Boral 0.0067 gm/cm2
             5011.50c  8.1175E-03
             6000.50c  2.5176E-03
             13027.50c 5.4933E-02
m7           13027.50c    1.           $ Al Clad
mt4         lwtr.01t
prdmp    j   -120   j   2
fm4      1000   1   -6
f4:n   1
sd4      1000
e4    1.000E-11   1.000E-10   5.000E-10   7.500E-10   1.000E-09   1.200E-09
      1.500E-09   2.000E-09   2.500E-09   3.000E-09
      4.700E-09   5.000E-09   7.500E-09   1.000E-08   2.530E-08
      3.000E-08   4.000E-08   5.000E-08   6.000E-08   7.000E-08
      8.000E-08   9.000E-08   1.000E-07   1.250E-07   1.500E-07
      1.750E-07   2.000E-07   2.250E-07   2.500E-07   2.750E-07
      3.000E-07   3.250E-07   3.500E-07   3.750E-07   4.000E-07
      4.500E-07   5.000E-07   5.500E-07   6.000E-07   6.250E-07
      6.500E-07   7.000E-07   7.500E-07   8.000E-07   8.500E-07
      9.000E-07   9.250E-07   9.500E-07   9.750E-07   1.000E-06
      1.010E-06   1.020E-06   1.030E-06   1.040E-06   1.050E-06
      1.060E-06   1.070E-06   1.080E-06   1.090E-06   1.100E-06
      1.110E-06   1.120E-06   1.130E-06   1.140E-06   1.150E-06
      1.175E-06   1.200E-06   1.225E-06   1.250E-06   1.300E-06
      1.350E-06   1.400E-06   1.450E-06   1.500E-06   1.590E-06
      1.680E-06   1.770E-06   1.860E-06   1.940E-06   2.000E-06
      2.120E-06   2.210E-06   2.300E-06   2.380E-06   2.470E-06
      2.570E-06   2.670E-06   2.770E-06   2.870E-06   2.970E-06
      3.000E-06   3.050E-06   3.150E-06   3.500E-06   3.730E-06
      4.000E-06   4.750E-06   5.000E-06   5.400E-06   6.000E-06
      6.250E-06   6.500E-06   6.750E-06   7.000E-06   7.150E-06
      8.100E-06   9.100E-06   1.000E-05   1.150E-05   1.190E-05
```

1.290E-05	1.375E-05	1.440E-05	1.510E-05	1.600E-05
1.700E-05	1.850E-05	1.900E-05	2.000E-05	2.100E-05
2.250E-05	2.500E-05	2.750E-05	3.000E-05	3.125E-05
3.175E-05	3.325E-05	3.375E-05	3.460E-05	3.550E-05
3.700E-05	3.800E-05	3.910E-05	3.960E-05	4.100E-05
4.240E-05	4.400E-05	4.520E-05	4.700E-05	4.830E-05
4.920E-05	5.060E-05	5.200E-05	5.340E-05	5.900E-05
6.100E-05	6.500E-05	6.750E-05	7.200E-05	7.600E-05
8.000E-05	8.200E-05	9.000E-05	1.000E-04	1.080E-04
1.150E-04	1.190E-04	1.220E-04	1.860E-04	1.925E-04
2.075E-04	2.100E-04	2.400E-04	2.850E-04	3.050E-04
5.500E-04	6.700E-04	6.830E-04	9.500E-04	1.150E-03
1.500E-03	1.550E-03	1.800E-03	2.200E-03	2.290E-03
2.580E-03	3.000E-03	3.740E-03	3.900E-03	6.000E-03
8.030E-03	9.500E-03	1.300E-02	1.700E-02	2.500E-02
3.000E-02	4.500E-02	5.000E-02	5.200E-02	6.000E-02
7.300E-02	7.500E-02	8.200E-02	8.500E-02	1.000E-01
1.283E-01	1.500E-01	2.000E-01	2.700E-01	3.300E-01
4.000E-01	4.200E-01	4.400E-01	4.700E-01	4.995E-01
5.500E-01	5.730E-01	6.000E-01	6.700E-01	6.790E-01
7.500E-01	8.200E-01	8.611E-01	8.750E-01	9.000E-01
9.200E-01	1.010E+00	1.100E+00	1.200E+00	1.250E+00
1.317E+00	1.356E+00	1.400E+00	1.500E+00	1.850E+00
2.354E+00	2.479E+00	3.000E+00	4.304E+00	4.800E+00
6.434E+00	8.187E+00	1.000E+01	1.284E+01	1.384E+01
1.455E+01	1.568E+01	1.733E+01	2.000E+01	

```
HI-STAR containing MPC68F, 07x07 in DFC with 13 missing rods
c     3.00 % uniform enrichment, unreflected cask, 0.0067 g/cmsq B-10 in Boral
c
c
1     1 -10.522      -1  u=2       $ fuel
2     4 -1.0      1  -2  u=2       $ gap
3     3 -6.55     2  -3  u=2       $ Zr Clad
4     4 -1.0          3  u=2       $ water in fuel region
5     4 -1.0   -4:5      u=3       $ water in guide tubes
6     3 -6.55   4 -5     u=3       $ guide tubes
7     4 -1.0   -6   +7   -8   +9   u=1  lat=1
      fill= -4:4    -4:4   0:0
      1  1 1 1 1 1 1 1  1
      1  2 2 2 2 2 2 2  1
      1  2 1 2 1 2 1 2  1
      1  2 2 1 2 1 2 2  1
      1  2 1 2 1 2 1 2  1
      1  2 2 1 2 1 2 2  1
      1  2 1 2 1 2 1 2  1
      1  2 2 2 2 2 2 2  1
      1  1 1 1 1 1 1 1  1
c
C  BOX TYPE R
c
8     0  -10   11  -12   13          u=4 fill=1
9     3  -6.55    60   -61    62   -63  #8      u=4     $ Zr flow channel
100   5  -7.84   74 -75 76 -77 (-70:71:-72:73)  u=4     $ DFC
10    4  -1.      64   -65    66   -67  #8 #9 #100 u=4  $ water
11    5  -7.84    20   -23    67   -14          u=4     $ 0.075" STEEL
12    4  -1.      20   -23    14   -15          u=4     $ WATER POCKET
13    7  -2.7     20   -23    15   -16          u=4     $ Al CLAD
14    6  -2.66    20   -23    16   -17          u=4     $ BORAL Absorber
15    7  -2.7     20   -23    17   -18          u=4     $ Al Clad
16    4  -1.      20   -23    18  -118          u=4     $ Water
17    5  -7.84    118:-129:65:-66               u=4     $ Steel
18    4  -1.      64   -21    67   -118         u=4     $ Water
19    4  -1.      24   -65    67   -118         u=4     $ water
20    5  -7.84    21   -20    67   -118         u=4     $ Steel
21    5  -7.84    23   -24    67   -118         u=4     $ Steel
22    4  -1.     129   -64    33   -118         u=4     $ Water
c
23    5  -7.84    25   -64    30   -31          u=4     $ Steel
24    4  -1.      26   -25    30   -31          u=4     $ Water
25    7  -2.7     27   -26    30   -31          u=4     $ Al clad
26    6  -2.66    28   -27    30   -31          u=4     $ Boral
27    7  -2.7     29   -28    30   -31          u=4     $ Al clad
28    4  -1.     129   -29    30   -31          u=4     $ water
29    5  -7.84   129   -64    32   -30          u=4     $ Steel ends
30    5  -7.84   129   -64    31   -33          u=4     $ Steel ends
31    4  -1.     129   -64    66   -32          u=4     $ Water
c
c    Type A box - Boral only on left side
c
32    0  -10   11  -12   13          u=6 fill=1
33    3  -6.55    60   -61    62   -63  #8      u=6     $ Zr flow channel
101   5  -7.84   74 -75 76 -77 (-70:71:-72:73)  u=6     $ DFC
34    4  -1.      64   -65    66   -118 #8 #9 #101 u=6  $ water
35    5  -7.84    118:-129:65:-66               u=6     $ Steel
36    4  -1.     129   -64    67   -118         u=6     $ Water
c
37    5  -7.84    25   -64    30   -31          u=6     $ Steel
```

```
38    4  -1.      26   -25    30   -31          u=6     $ Water
39    7  -2.7     27   -26    30   -31          u=6     $ Al clad
40    6  -2.66    28   -27    30   -31          u=6     $ Boral
41    7  -2.7     29   -28    30   -31          u=6     $ Al clad
42    4  -1.     129   -29    30   -31          u=6     $ water
43    4  -1.     129   -64    33   -67          u=6     $ Water
44    5  -7.84   129   -64    32   -30          u=6     $ Steel ends
45    5  -7.84   129   -64    31   -33          u=6     $ Steel ends
46    4  -1.     129   -64    66   -32          u=6     $ Water
c
c    Type B box -  Boral on Top only
c
47    0  -10   11  -12   13         u=7 fill=1
48    3  -6.55    60   -61    62   -63  #8      u=7     $ Zr flow channel
102   5  -7.84   74 -75 76 -77 (-70:71:-72:73)  u=7     $ DFC
49    4  -1.      64   -65    66   -67  #8 #9 #102 u=7  $ water
50    5  -7.84    20   -23    67   -14          u=7     $ 0.075" STEEL
51    4  -1.      20   -23    14   -15          u=7     $ WATER POCKET
52    7  -2.7     20   -23    15   -16          u=7     $ Al CLAD
53    6  -2.66    20   -23    16   -17          u=7     $ BORAL Absorber
54    7  -2.7     20   -23    17   -18          u=7     $ water
55    4  -1.      20   -23    18  -118          u=7     $ Water
56    5  -7.84    118:-129:65:-66               u=7     $ Steel
57    4  -1.      64   -21    67   -118         u=7     $ Water
58    4  -1.      24   -65    67   -118         u=7     $ water
59    5  -7.84    21   -20    67   -118         u=7     $ Steel
60    5  -7.84    23   -24    67   -118         u=7     $ Steel
61    4  -1.     129   -64    66   -118         u=7     $ Water
c
c    Type E box  - No Boral Panels
c
62    0  -10   11  -12   13         u=8 fill=1
63    3  -6.55    60   -61    62   -63  #8      u=8     $ Zr flow channel
103   5  -7.84   74 -75 76 -77 (-70:71:-72:73)  u=8     $ DFC
64    4  -1.     129   -65    66  -118  #8 #9 #103 u=8  $ water
65    5  -7.84    118:-129:65:-66               u=8     $ Steel
c
c    Type F box  - No Boral Panels or fuel
c
66    4  -1.     129   -65    66  -118          u=9     $ water
67    5  -7.84    118:-129:65:-66               u=9     $ Steel
c
68    4  -1.0    -34  35  -36  37  u=5  lat=1  fill=-7:6  -7:6  0:0
                5 5 5 5 5 5 5 5 5 5 5 5 5
                5 9 9 9 9 9 9 9 9 9 9 9 5
                5 9 9 9 9 9 7 4 9 9 9 9 5
                5 9 9 9 7 4 4 4 4 4 9 9 5
                5 9 9 7 4 4 4 4 4 4 4 9 5
                5 9 9 7 4 4 4 4 4 4 4 9 5
                5 9 7 4 4 4 4 4 4 4 4 9 5
                5 9 8 4 4 4 4 4 4 4 6 9 5
                5 9 9 7 4 4 4 4 4 4 9 9 5
                5 9 9 8 4 4 4 4 4 4 6 9 5
                5 9 9 9 8 4 4 4 6 6 9 9 5
                5 9 9 9 9 9 8 6 9 9 9 9 5
                5 9 9 9 9 9 9 9 9 9 9 9 5
                5 5 5 5 5 5 5 5 5 5 5 5 5
69    0          -41              50  -49  fill=5 (8.1661  8.1661  0)
70    4  -1.0    -41       43  -50           $ Water below Fuel
71    4  -1.0    -41       49  -44           $ Water above Fuel
72    5  -7.84   -42       68  -43           $ Steel below Fuel
```

```
73    5  -7.84   -42       44  -69             $ Steel above Fuel
74    5  -7.84    41  -42  43  -44             $ Radial Steel
75    0            42 :-68:  69                $ outside world

1     cz          0.5220     $ Fuel OD
2     cz          0.5334     $ Clad ID
3     cz          0.6172     $ Clad OD
4     cz          0.5398     $ Thimble ID
5     cz          0.6261     $ Thimble OD
6     px          0.8014     $ Pin Pitch
7     px         -0.8014
8     py          0.8014
9     py         -0.8014
10    px          5.7684     $ Channel ID
11    px         -5.7684
12    py          5.7684
13    py         -5.7684
14    py          7.8016
15    py          7.8155
16    py          7.8410
17    py          8.0467
18    py          8.0721
118   py          8.0861
20    px         -6.0325
21    px         -6.2230
23    px          6.0325
24    px          6.2230
25    px         -7.8016
26    px         -7.8155
27    px         -7.8410
28    px         -8.0467
29    px         -8.0721
129   px         -8.0861
30    py         -6.0325
31    py          6.0325
32    py         -6.2230
33    py          6.2230
34    px          7.6111
35    px         -8.7211
36    py          8.7211
37    py         -7.6111
41    cz          85.57
42    cz          108.43
43    pz          11.46
44    pz          252.15
49    pz          230.66     $ Top of Active Fuel
50    pz          30.        $ Start of Active Fuel
60    px         -5.9207     $ Channel OD
61    px          5.9207
62    py         -5.9207
63    py          5.9207
64    px         -7.6111     $ Cell Box ID
65    px          7.6111
66    py         -7.6111
67    py          7.6111
68    pz         -10.13
69    pz          291.52
70    px         -6.2611       $ DFC ID
71    px          6.2611
72    py         -6.2611
73    py          6.2611
```

```
74    px          -6.5659       $ DFC OD
75    px           6.5659
76    py          -6.5659
77    py           6.5659

imp:n     1 77r 0
kcode   10000  0.94   20  120
c
sdef  par=1  erg=d1 axs=0 0 1 x=d4 y=fx d5 z=d3
c
sp1 -2 1.2895
c
si3  h 30. 230.66
sp3  0 1
c
c
si4  s                15 16
                   13 14 15 16 17 18
               12 13 14 15 16 17 18 19
               12 13 14 15 16 17 18 19
            11 12 13 14 15 16 17 18 19 20
            11 12 13 14 15 16 17 18 19 20
               12 13 14 15 16 17 18 19
               12 13 14 15 16 17 18 19
                  13 14 15 16 17 18
                        15 16
sp4  1 67r
c
ds5  s                30 30
                   29 29 29 29 29 29
               28 28 28 28 28 28 28 28
               27 27 27 27 27 27 27 27
            26 26 26 26 26 26 26 26 26 26
            25 25 25 25 25 25 25 25 25 25
               24 24 24 24 24 24 24 24
               23 23 23 23 23 23 23 23
                  22 22 22 22 22 22
                        21 21
c
si11  -80.6831 -67.6783
si12  -64.1985 -51.1937
si13  -47.7139 -34.7091
si14  -31.2293 -18.2245
si15  -14.7447 -1.7399
si16   1.7399   14.7447
si17   18.2245  31.2293
si18   34.7091  47.7139
si19   51.1937  64.1985
si20   67.6783  80.6831
c
si21  -80.6831 -67.6783
si22  -64.1985 -51.1937
si23  -47.7139 -34.7091
si24  -31.2293 -18.2245
si25  -14.7447 -1.7399
si26   1.7399   14.7447
si27   18.2245  31.2293
si28   34.7091  47.7139
si29   51.1937  64.1985
si30   67.6783  80.6831
sp11  0 1
```

```
sp12  0 1
sp13  0 1
sp14  0 1
sp15  0 1
sp16  0 1
sp17  0 1
sp18  0 1
sp19  0 1
sp20  0 1
sp21  0 1
sp22  0 1
sp23  0 1
sp24  0 1
sp25  0 1
sp26  0 1
sp27  0 1
sp28  0 1
sp29  0 1
sp30  0 1
c
m1          92235.50c   -0.02644      $ 3.00% E Fuel
            92238.50c   -0.85504
            8016.50c    -0.11852
m3          40000.56c   1.           $ Zr Clad
m4          1001.50c    0.6667       $ Water
            8016.50c    0.3333
m5          24000.50c   0.01761      $ Steel
            25055.50c   0.001761
            26000.55c   0.05977
            28000.50c   0.008239
m6          5010.50c  1.9592E-03      $ Boral 0.0067 gm/cm2
            5011.50c  8.1175E-03
            6000.50c  2.5176E-03
            13027.50c 5.4933E-02
m7          13027.50c    1.          $ Al Clad
mt4        lwtr.01t
prdmp    j   -120   j   2
fm4      1000   1   -6
f4:n   1
sd4      1000
e4    1.000E-11   1.000E-10   5.000E-10   7.500E-10   1.000E-09   1.200E-09
      1.500E-09   2.000E-09   2.500E-09   3.000E-09
      4.700E-09   5.000E-09   7.500E-09   1.000E-08   2.530E-08
      3.000E-08   4.000E-08   5.000E-08   6.000E-08   7.000E-08
      8.000E-08   9.000E-08   1.000E-07   1.250E-07   1.500E-07
      1.750E-07   2.000E-07   2.250E-07   2.500E-07   2.750E-07
      3.000E-07   3.250E-07   3.500E-07   3.750E-07   4.000E-07
      4.500E-07   5.000E-07   5.500E-07   6.000E-07   6.250E-07
      6.500E-07   7.000E-07   7.500E-07   8.000E-07   8.500E-07
      9.000E-07   9.250E-07   9.500E-07   9.750E-07   1.000E-06
      1.010E-06   1.020E-06   1.030E-06   1.040E-06   1.050E-06
      1.060E-06   1.070E-06   1.080E-06   1.090E-06   1.100E-06
      1.110E-06   1.120E-06   1.130E-06   1.140E-06   1.150E-06
      1.175E-06   1.200E-06   1.225E-06   1.250E-06   1.300E-06
      1.350E-06   1.400E-06   1.450E-06   1.500E-06   1.590E-06
      1.680E-06   1.770E-06   1.860E-06   1.940E-06   2.000E-06
      2.120E-06   2.210E-06   2.300E-06   2.380E-06   2.470E-06
      2.570E-06   2.670E-06   2.770E-06   2.870E-06   2.970E-06
      3.000E-06   3.050E-06   3.150E-06   3.500E-06   3.730E-06
      4.000E-06   4.750E-06   5.000E-06   5.400E-06   6.000E-06
      6.250E-06   6.500E-06   6.750E-06   7.000E-06   7.150E-06
```

8.100E-06	9.100E-06	1.000E-05	1.150E-05	1.190E-05
1.290E-05	1.375E-05	1.440E-05	1.510E-05	1.600E-05
1.700E-05	1.850E-05	1.900E-05	2.000E-05	2.100E-05
2.250E-05	2.500E-05	2.750E-05	3.000E-05	3.125E-05
3.175E-05	3.325E-05	3.375E-05	3.460E-05	3.550E-05
3.700E-05	3.800E-05	3.910E-05	3.960E-05	4.100E-05
4.240E-05	4.400E-05	4.520E-05	4.700E-05	4.830E-05
4.920E-05	5.060E-05	5.200E-05	5.340E-05	5.900E-05
6.100E-05	6.500E-05	6.750E-05	7.200E-05	7.600E-05
8.000E-05	8.200E-05	9.000E-05	1.000E-04	1.080E-04
1.150E-04	1.190E-04	1.220E-04	1.860E-04	1.925E-04
2.075E-04	2.100E-04	2.400E-04	2.850E-04	3.050E-04
5.500E-04	6.700E-04	6.830E-04	9.500E-04	1.150E-03
1.500E-03	1.550E-03	1.800E-03	2.200E-03	2.290E-03
2.580E-03	3.000E-03	3.740E-03	3.900E-03	6.000E-03
8.030E-03	9.500E-03	1.300E-02	1.700E-02	2.500E-02
3.000E-02	4.500E-02	5.000E-02	5.200E-02	6.000E-02
7.300E-02	7.500E-02	8.200E-02	8.500E-02	1.000E-01
1.283E-01	1.500E-01	2.000E-01	2.700E-01	3.300E-01
4.000E-01	4.200E-01	4.400E-01	4.700E-01	4.995E-01
5.500E-01	5.730E-01	6.000E-01	6.700E-01	6.790E-01
7.500E-01	8.200E-01	8.611E-01	8.750E-01	9.000E-01
9.200E-01	1.010E+00	1.100E+00	1.200E+00	1.250E+00
1.317E+00	1.356E+00	1.400E+00	1.500E+00	1.850E+00
2.354E+00	2.479E+00	3.000E+00	4.304E+00	4.800E+00
6.434E+00	8.187E+00	1.000E+01	1.284E+01	1.384E+01
1.455E+01	1.568E+01	1.733E+01	2.000E+01	

```
=NITAWL
' k4rf5f45, HI-STAR containing MPC24, 15x15 assembly a17 @ 4.1% E
0$$ 84 E
1$$ 0 13  0  4R0  1  E T
2$$ 92235    92238
    40000    1001     8016     5010      5011      6012
    13027    24000    25055     26000     28000
3** 92238 294.6    2   .4752    .1928     0.      0.02251     1
   16.0   7.8209   1   235.04  0.5154    1      1.0           T
END
=KENO5A
k4rf5f45, HI-STAR containing MPC24, 15x15 assembly a17 @ 4.1% E
READ PARAM TME=10000 GEN=300 NPG=10000 NSK=50 LIB=4 TBA=5
END PARAM
READ MIXT SCT=2  EPS=1.0
MIX=1    92235  9.7463E-04
         92238  0.02251
         8016   0.04694
MIX=2    40000  0.04323
MIX=3    1001   0.06688
         8016   0.03344
MIX=4    24000  0.01761
         25055  0.001761
         26000  0.05977
         28000  0.008239
MIX=5    5010   8.7066E-03
         5011   3.5116E-02
         6012   1.0948E-02
         13027  3.6936E-02
MIX=6    1001   0.06688
         8016   0.03344
MIX=7    13027  0.06026
END MIXT
'
' cell-id      8.98
' cell-pitch   10.906
' wall-thkns   5/16
' angle-thkns  5/16
' boral-gap    0.0035
' boral-pocket 0.082
' boral-thkns  0.075
' boral-clad   0.01
' boral-core   0.055
' sheathing    0.0235
' boral-wide   7.500
' boral-narrow 6.250
'
' gap size     1.09
'
READ GEOM
UNIT           1
COM="FUEL ROD"
CYLINDER        1  1  0.4752                                  381.0   0.
CYLINDER        3  1  0.4851                                  381.0   0.
CYLINDER        2  1  0.5436                                  381.0   0.
CUBOID          3  1  0.7214   -0.7214    0.7214    -0.7214    381.0   0.
UNIT           2
COM="GUIDE  TUBE CELL"
CYLINDER        3  1  0.6350                                  381.0   0.
CYLINDER        2  1  0.6706                                  381.0   0.
CUBOID          3  1  0.7214   -0.7214    0.7214    -0.7214    381.0   0.
```

```
UNIT          4
COM="LONG HORIZONTAL BORAL PANEL - NORTH"
CUBOID        5  1  9.525  -9.525   0.06985    -0.06985     381.0   0.
CUBOID        7  1  9.525  -9.525   0.09525    -0.09525     381.0   0.
CUBOID        3  1  9.525  -9.525   0.10414    -0.10414     381.0   0.
CUBOID        4  1  9.58469  -9.58469   0.16383      -0.10414     381.0   0.
UNIT          5
COM="LONG VERTICAL BORAL PANEL - EAST"
CUBOID        5  1  0.06985    -0.06985    9.525  -9.525    381.0   0.
CUBOID        7  1  0.09525    -0.09525    9.525  -9.525    381.0   0.
CUBOID        3  1  0.10414    -0.10414    9.525  -9.525    381.0   0.
CUBOID        4  1  0.16383      -0.10414    9.58469  -9.58469    381.0   0.
UNIT          6
COM="LONG HORIZONTAL BORAL PANEL - SOUTH"
CUBOID        5  1  9.525  -9.525    0.06985   -0.06985     381.0   0.
CUBOID        7  1  9.525  -9.525    0.09525   -0.09525     381.0   0.
CUBOID        3  1  9.525  -9.525    0.10414   -0.10414     381.0   0.
CUBOID        4  1  9.58469  -9.58469    0.10414   -0.16383       381.0   0.
UNIT          7
COM="LONG VERTICAL BORAL PANEL - WEST"
CUBOID        5  1  0.06985    -0.06985    9.525  -9.525    381.0   0.
CUBOID        7  1  0.09525    -0.09525    9.525  -9.525    381.0   0.
CUBOID        3  1  0.10414    -0.10414    9.525  -9.525    381.0   0.
CUBOID        4  1  0.10414    -0.16383      9.58469  -9.58469    381.0   0.
UNIT          8  ARRAY 1  -10.8204    -10.8204       0.
COM="CENTRAL FUEL ASSEMBLIES - 4 BORAL PANELS"
CUBOID        3  1  11.4046  -11.4046   11.4046  -11.4046     381.0   0.
CUBOID        4  1  12.1984  -12.1984   12.1984  -12.1984     381.0   0.
CUBOID        3  1  12.4673  -12.4673   12.4673  -12.4673     381.0   0.
HOLE          4    0.         12.3026     0.
HOLE          5   12.3026       0.        0.
HOLE          6  0.          -12.3026    0.
HOLE          7  -12.3026      0.        0.
UNIT         21  ARRAY 1  -10.8204    -10.8204       0.
COM="CENTRAL FUEL ASSEMBLIES - 4 BORAL PANELS, W/O EAST WALL"
CUBOID        3  1  11.4046  -11.4046   11.4046  -11.4046     381.0   0.
CUBOID        4  1  11.4046  -12.1984   12.1984  -12.1984     381.0   0.
CUBOID        3  1  11.4046  -12.4673   12.4673  -12.4673     381.0   0.
HOLE          4    0.         12.3026     0.
HOLE          6  0.          -12.3026    0.
HOLE          7  -12.3026      0.        0.
UNIT         22  ARRAY 1  -10.8204    -10.8204       0.
COM="CENTRAL FUEL ASSEMBLIES - 4 BORAL PANELS, W/O WEST WALL"
CUBOID        3  1  11.4046  -11.4046   11.4046  -11.4046     381.0   0.
CUBOID        4  1  12.1984  -11.4046   12.1984  -12.1984     381.0   0.
CUBOID        3  1  12.4673  -11.4046   12.4673  -12.4673     381.0   0.
HOLE          4    0.         12.3026     0.
HOLE          5   12.3026       0.        0.
HOLE          6  0.          -12.3026    0.
UNIT         23
COM="CELL WALL BETWEEN UNITS 21 AND 22"
CUBOID        4  1  0.396775  -0.396775   23.9998  -23.9998     381.0   0.
UNIT          9
COM="SHORT HORIZONTAL BORAL PANEL - NORTH"
CUBOID        5  1  7.9375  -7.9375   0.06985    -0.06985     381.0   0.
CUBOID        7  1  7.9375  -7.9375   0.09525    -0.09525     381.0   0.
CUBOID        3  1  7.9375  -7.9375   0.10414    -0.10414     381.0   0.
CUBOID        4  1  7.99719  -7.99719   0.16383      -0.10414     381.0   0.
UNIT         10
COM="SHORT VERTICAL BORAL PANEL - EAST"
CUBOID        5  1  0.06985    -0.06985    7.9375  -7.9375    381.0   0.
```

```
CUBOID          7  1  0.09525    -0.09525    7.9375  -7.9375    381.0   0.
CUBOID          3  1  0.10414    -0.10414    7.9375  -7.9375    381.0   0.
CUBOID          4  1  0.16383      -0.10414    7.99719  -7.99719    381.0   0.
UNIT           11
COM="SHORT HORIZONTAL BORAL PANEL - SOUTH"
CUBOID          5  1  7.9375  -7.9375    0.06985   -0.06985     381.0   0.
CUBOID          7  1  7.9375  -7.9375    0.09525   -0.09525     381.0   0.
CUBOID          3  1  7.9375  -7.9375    0.10414   -0.10414     381.0   0.
CUBOID          4  1  7.99719  -7.99719    0.10414   -0.16383       381.0   0.
UNIT           12
COM="SHORT VERTICAL BORAL PANEL - WEST"
CUBOID          5  1  0.06985    -0.06985    7.9375  -7.9375    381.0   0.
CUBOID          7  1  0.09525    -0.09525    7.9375  -7.9375    381.0   0.
CUBOID          3  1  0.10414    -0.10414    7.9375  -7.9375    381.0   0.
CUBOID          4  1  0.10414    -0.16383      7.99719  -7.99719    381.0   0.
UNIT           13  ARRAY 1  -10.8204    -10.8204       0.
COM="Array B short Boral N & E "
CUBOID          3  1  11.4046  -11.4046   11.4046  -11.4046     381.0   0.
CUBOID          4  1  12.1984  -12.1984   12.1984  -12.1984     381.0   0.
CUBOID          3  1  12.4673  -12.4673   12.4673  -12.4673     381.0   0.
HOLE            9    0.         12.3026     0.
HOLE           10   12.3026       0.        0.
HOLE            6  0.          -12.3026    0.
HOLE            7  -12.3026      0.        0.
UNIT           14  ARRAY 1  -10.8204    -10.8204       0.
COM="Array C short Boral E & S "
CUBOID          3  1  11.4046  -11.4046   11.4046  -11.4046     381.0   0.
CUBOID          4  1  12.1984  -12.1984   12.1984  -12.1984     381.0   0.
CUBOID          3  1  12.4673  -12.4673   12.4673  -12.4673     381.0   0.
HOLE            4    0.         12.3026     0.
HOLE           10   12.3026       0.        0.
HOLE           11  0.          -12.3026    0.
HOLE            7  -12.3026      0.        0.
UNIT           15  ARRAY 1  -10.8204    -10.8204       0.
COM="Array D short Boral S & W "
CUBOID          3  1  11.4046  -11.4046   11.4046  -11.4046     381.0   0.
CUBOID          4  1  12.1984  -12.1984   12.1984  -12.1984     381.0   0.
CUBOID          3  1  12.4673  -12.4673   12.4673  -12.4673     381.0   0.
HOLE            4    0.         12.3026     0.
HOLE            5   12.3026       0.        0.
HOLE           11  0.          -12.3026    0.
HOLE           12  -12.3026      0.        0.
UNIT           16  ARRAY 1  -10.8204    -10.8204       0.
COM="Array E short Boral N & W "
CUBOID          3  1  11.4046  -11.4046   11.4046  -11.4046     381.0   0.
CUBOID          4  1  12.1984  -12.1984   12.1984  -12.1984     381.0   0.
CUBOID          3  1  12.4673  -12.4673   12.4673  -12.4673     381.0   0.
HOLE            9    0.         12.3026     0.
HOLE            5   12.3026       0.        0.
HOLE            6  0.          -12.3026    0.
HOLE           12  -12.3026      0.        0.
UNIT           17
CUBOID          4  1  0.7938   -0.        1.60      -0.         381.0   0.
UNIT           18
CUBOID          4  1  1.60     -0.        0.7938    -0.         381.0   0.
UNIT           30
CUBOID          4  1  1.37332  -1.37332   3.4925  -3.4925     381.0   0.
UNIT           31
CUBOID          4  1  1.05959  -1.05959   1.37332  -1.37332     381.0   0.
UNIT           41
CUBOID          3  1  14.6768  -14.6768   1.65227  -1.65227     381.0   0.
```

```
CUBOID          4  1  14.6768  -14.6768   2.44602  -2.44602     381.0   0.
UNIT           42
CUBOID          3  1  1.65227  -1.65227   14.6768  -14.6768     381.0   0.
CUBOID          4  1  2.44602  -2.44602   14.6768  -14.6768     381.0   0.
GLOBAL
UNIT           19
COM="ASSEMBLY ARRAY + X DIRECTION"
CYLINDER        3  1  86.57                                  396.24  -10.16
HOLE            8   13.8506    13.8506    0.
HOLE            8   13.8506   -13.8506    0.
HOLE           21   17.949    41.5519    0.
HOLE           21   17.949   -41.5519    0.
HOLE           13   13.8506    69.2531    0.
HOLE           14   13.8506   -69.2531    0.
HOLE           22   41.5519    17.949    0.
HOLE           22   41.5519   -17.949    0.
HOLE           13   45.6502    45.6502    0.
HOLE           14   45.6502   -45.6502    0.
HOLE           13   69.2531    13.8506    0.
HOLE           14   69.2531   -13.8506    0.
HOLE            8  -13.8506    13.8506    0.
HOLE            8  -13.8506   -13.8506    0.
HOLE           22  -17.949    41.5519    0.
HOLE           22  -17.949   -41.5519    0.
HOLE           16  -13.8506    69.2531    0.
HOLE           15  -13.8506   -69.2531    0.
HOLE           21  -41.5519    17.949    0.
HOLE           21  -41.5519   -17.949    0.
HOLE           16  -45.6502    45.6502    0.
HOLE           15  -45.6502   -45.6502    0.
HOLE           16  -69.2531    13.8506    0.
HOLE           15  -69.2531   -13.8506    0.
HOLE           23   29.7505    29.7505    0.
HOLE           23  -29.7505    29.7505    0.
HOLE           23   29.7505   -29.7505    0.
HOLE           23  -29.7505   -29.7505    0.
HOLE            5   30.2516    41.5519    0.
HOLE            5   30.2516   -41.5519    0.
HOLE            7  -30.2516    41.5519    0.
HOLE            7  -30.2516   -41.5519    0.
HOLE            7   29.2494    17.949    0.
HOLE            7   29.2494   -17.949    0.
HOLE            5  -29.2494    17.949    0.
HOLE            5  -29.2494   -17.949    0.
HOLE           30      0.       0.    0.
HOLE           31   2.43291       0.    0.
HOLE           31  -2.43291       0.    0.
HOLE           41   41.5519       0.    0.
HOLE           41  -41.5519       0.    0.
HOLE           42      0.    41.5519    0.
HOLE           42      0.   -41.5519    0.
CYLINDER        4  1  108.43                                 435.61  -31.75
CUBOID          3  1  139   -139    139   -139    435.61   -31.75
END GEOM
READ ARRAY
ARA=1  NUX=15  NUY=15  NUZ=1
COM="15 X 15 FUEL ASSEMBLY"
FILL
      1 1 1 1 1 1 1 1 1 1 1 1 1 1 1
      1 1 1 1 1 1 1 1 1 1 1 1 1 1 1
      1 1 1 1 1 2 1 1 1 2 1 1 1 1 1
```

```
      1 1 1 2 1 1 1 1 1 1 1 2 1 1 1
      1 1 1 1 1 1 1 1 1 1 1 1 1 1 1
      1 1 2 1 1 2 1 1 1 2 1 1 2 1 1
      1 1 1 1 1 1 1 1 1 1 1 1 1 1 1
      1 1 1 1 1 1 1 2 1 1 1 1 1 1 1
      1 1 1 1 1 1 1 1 1 1 1 1 1 1 1
      1 1 2 1 1 2 1 1 1 2 1 1 2 1 1
      1 1 1 1 1 1 1 1 1 1 1 1 1 1 1
      1 1 1 2 1 1 1 1 1 1 1 2 1 1 1
      1 1 1 1 1 2 1 1 1 2 1 1 1 1 1
      1 1 1 1 1 1 1 1 1 1 1 1 1 1 1
      1 1 1 1 1 1 1 1 1 1 1 1 1 1 1
END FILL
END ARRAY
END DATA
END
```

```
=NITAWL
' HI-STAR containing MPC68, 08x08 @ 4.2% E
0$$ 84 E
1$$ 0 13  0  4R0  1  E T
2$$ 92235    92238
    40000    1001     8016     5010      5011      6012
    13027    24000    25055     26000     28000
3** 92238 294.6    2   .5207    .1623     0.      0.02248     1
   16.0   7.8330   1   235.04  0.5662    1      1.0           T
END
=KENO5A
HI-STAR containing MPC68, 08x08 @ 4.2% E
'  GE 8X8R FUEL 2 WATER HOLES
READ PARAM TME=10000 GEN=1100 NPG=5000 NSK=100
     LIB=4 TBA=5  LNG=400000   NB8=900
END PARAM
READ MIXT SCT=2  EPS=1.
MIX=1    92235  9.983E-04
         92238  0.02248
         8016   0.04697
MIX=2    40000  0.04323
MIX=3    1001   0.06688
         8016   0.03344
MIX=4    24000  0.01761
         25055  0.001761
         26000  0.05977
         28000  0.008239
MIX=5    5010   8.071E-03
         5011   3.255E-02
         6012   1.015E-02
         13027  3.805E-02
MIX=6    13027  0.06026
END MIXT
READ GEOM
UNIT           1
COM=           "FUEL ROD"
CYLINDER        1  1  0.5207                                  381.0   0.
CYLINDER        3  1  0.5321                                  381.0   0.
CYLINDER        2  1  0.6134                                  381.0   0.
CUBOID          3  1  0.8128   -0.8128    0.8128    -0.8128    381.0   0.
UNIT           2
COM=           "GUIDE  TUBE CELL"
CYLINDER        3  1  0.6744                                  381.0   0.
CYLINDER        2  1  0.7506                                  381.0   0.
CUBOID          3  1  0.8128   -0.8128    0.8128    -0.8128    381.0   0.
UNIT           4
COM=           "HORIZONTAL BORAL PANEL"
CUBOID          5  1  6.0325   -6.0325    0.1027    -0.1027    381.0   0.
CUBOID          6  1  6.0325   -6.0325    0.1283    -0.1283    381.0   0.
CUBOID          3  1  6.0325   -6.0325    0.1422    -0.1422    381.0   0.
CUBOID          4  1  6.4611   -6.4611    0.1422    -0.3327    381.0   0.
UNIT           5
COM=           "VERTICAL BORAL PANEL"
CUBOID          5  1  0.1027   -0.1027     6.0325   -6.0325   381.0   0.
CUBOID          6  1  0.1283   -0.1283     6.0325   -6.0325   381.0   0.
CUBOID          3  1  0.1422   -0.1422     6.0325   -6.0325   381.0   0.
CUBOID          4  1  0.3327   -0.1422     6.4611   -6.4611   381.0   0.
UNIT           8  ARRAY 1  -6.5024     -6.5024       0.
COM=           "FUEL ASSEMBLIES - 2 BORAL PANELS"
CUBOID          3  1  6.7031   -6.7031    6.7031   -6.7031          381.0   0.
CUBOID          2  1  6.9571   -6.9571    6.9571   -6.9571          381.0   0.
```

```
CUBOID      3  1  7.6111   -8.0861    8.0861   -7.6111          381.0   0.
HOLE        4    0.          7.9438     0.
HOLE        5  -7.9438        0.        0.
CUBOID      4  1  7.6111   -8.7211    8.7211   -7.6111          381.0   0.
UNIT        9  ARRAY 1  -6.5024     -6.5024        0.
COM=        "FUEL ASSEMBLIES - Type A"
CUBOID      3  1  6.7031   -6.7031    6.7031   -6.7031          381.0   0.
CUBOID      2  1  6.9571   -6.9571    6.9571   -6.9571          381.0   0.
CUBOID      3  1  7.6111   -8.0861    8.0861   -7.6111          381.0   0.
HOLE        5  -7.9438        0.        0.
CUBOID      4  1  8.2461   -8.7211    8.7211   -7.6111          381.0   0.
UNIT       10  ARRAY 1  -6.5024     -6.5024        0.
COM=        "FUEL ASSEMBLIES - Type B"
CUBOID      3  1  6.7031   -6.7031    6.7031   -6.7031          381.0   0.
CUBOID      2  1  6.9571   -6.9571    6.9571   -6.9571          381.0   0.
CUBOID      3  1  7.6111   -8.0861    8.0861   -7.6111          381.0   0.
HOLE        5  -7.9438        0.        0.
CUBOID      4  1  7.6111   -8.7211    8.7211   -7.6111          381.0   0.
UNIT       11  ARRAY 1  -6.5024     -6.5024        0.
COM=        "FUEL ASSEMBLIES - Type C"
CUBOID      3  1  6.7031   -6.7031    6.7031   -6.7031          381.0   0.
CUBOID      2  1  6.9571   -6.9571    6.9571   -6.9571          381.0   0.
CUBOID      3  1  7.6111   -8.0861    8.0861   -7.6111          381.0   0.
HOLE        4    0.          7.9438     0.
HOLE        5  -7.9438        0.        0.
CUBOID      4  1  8.2461   -8.7211    8.7211   -7.6111          381.0   0.
UNIT       12  ARRAY 1  -6.5024     -6.5024        0.
COM=        "FUEL ASSEMBLIES - Type D"
CUBOID      3  1  6.7031   -6.7031    6.7031   -6.7031          381.0   0.
CUBOID      2  1  6.9571   -6.9571    6.9571   -6.9571          381.0   0.
CUBOID      3  1  7.6111   -8.0861    8.0861   -7.6111          381.0   0.
HOLE        4    0.          7.9438     0.
HOLE        5  -7.9438        0.        0.
CUBOID      4  1  8.2461   -8.7211    8.7211   -8.2461          381.0   0.
UNIT       13  ARRAY 1  -6.5024     -6.5024        0.
COM=        "FUEL ASSEMBLIES - Type E"
CUBOID      3  1  6.7031   -6.7031    6.7031   -6.7031          381.0   0.
CUBOID      2  1  6.9571   -6.9571    6.9571   -6.9571          381.0   0.
CUBOID      3  1  7.6111   -8.0861    8.0861   -7.6111          381.0   0.
HOLE        4    0.          7.9438     0.
HOLE        5  -7.9438        0.        0.
CUBOID      4  1  7.6111   -8.7211    8.7211   -8.2461          381.0   0.
UNIT       14  ARRAY 1  -6.5024     -6.5024        0.
COM=        "FUEL ASSEMBLIES - Type F"
CUBOID      3  1  6.7031   -6.7031    6.7031   -6.7031          381.0   0.
CUBOID      2  1  6.9571   -6.9571    6.9571   -6.9571          381.0   0.
CUBOID      3  1  7.6111   -8.0861    8.0861   -7.6111          381.0   0.
HOLE        4    0.          7.9438     0.
CUBOID      4  1  7.6111   -8.7211    8.7211   -8.2461          381.0   0.
UNIT       15  ARRAY 1  -6.5024     -6.5024        0.
COM=        "FUEL ASSEMBLIES - TYPE G"
CUBOID      3  1  6.7031   -6.7031    6.7031   -6.7031          381.0   0.
CUBOID      2  1  6.9571   -6.9571    6.9571   -6.9571          381.0   0.
CUBOID      3  1  7.6111   -8.0861    8.0861   -7.6111          381.0   0.
HOLE        4    0.          7.9438     0.
CUBOID      4  1  7.6111   -8.7211    8.7211   -7.6111          381.0   0.
UNIT       16  ARRAY 1  -6.5024     -6.5024        0.
COM=        "FUEL ASSEMBLIES - TYPE H"
CUBOID      3  1  6.7031   -6.7031    6.7031   -6.7031          381.0   0.
CUBOID      2  1  6.9571   -6.9571    6.9571   -6.9571          381.0   0.
CUBOID      3  1  7.6111   -8.0861    8.0861   -7.6111          381.0   0.
```

```
CUBOID          4  1  7.6111    -8.7211     8.7211    -7.6111          381.0    0.
UNIT           17  ARRAY 2      -48.9966   -48.9966          0
UNIT           18  ARRAY 3      -16.3322   -7.6111           0.
UNIT           19  ARRAY 4      -48.9966   -7.6111           0.
UNIT           20  ARRAY 5      -8.7211    -16.3322          0.
UNIT           21  ARRAY 6      -8.7211    -50.1068          0.
UNIT           22  ARRAY 7      -8.7211    -16.3322          0.
UNIT           23  ARRAY 8      -8.7211    -16.3322          0.
UNIT           24  ARRAY 9      -8.7211    -16.3322          0.
UNIT           25  ARRAY 10     -8.7211    -16.3322          0.
UNIT           26  ARRAY 11     -16.3322   -8.7213           0.
UNIT           27  ARRAY 12     -16.3322   -7.6111           0.
UNIT           28  ARRAY 13     -16.3322   -8.7213           0.
UNIT           29  ARRAY 14     -16.3322   -8.7213           0.
GLOBAL
UNIT           30
CYLINDER        3  1   85.57                                  402.5   -18.54.
HOLE           17      0.0         0.0         0.
HOLE           18      0.0        73.4949      0.
HOLE           19      0.0        57.1627      0.
HOLE           20    -73.4949      0.0         0.
HOLE           21    -56.6077      0.0         0.
HOLE           22     57.7177     32.6644      0.
HOLE           23     57.7177      0.0         0.
HOLE           24     74.052       0.0         0.
HOLE           25     57.7177    -32.6644      0.
HOLE           26     32.6644    -57.7177      0.
HOLE           27      0.0       -57.7177      0.
HOLE           28    -32.6644    -57.7177      0.
HOLE           29      0.0       -74.052       0.
CYLINDER        4   1   108.43                          441.85  -40.13
CUBOID          3   1   109.     -109.      109.     -109.    442     -40.2
END GEOM
READ ARRAY
ARA=1  NUX=8   NUY=8   NUZ=1
COM=   "8 X 8 FUEL ASSEMBLY"
FILL
 1 1 1 1 1 1 1 1
 1 1 1 1 1 1 1 1
 1 1 1 1 1 1 1 1
 1 1 1 2 1 1 1 1
 1 1 1 1 2 1 1 1
 1 1 1 1 1 1 1 1
 1 1 1 1 1 1 1 1
 1 1 1 1 1 1 1 1
END FILL
ARA=2  NUX=6   NUY=6   NUZ=1
COM=   "6 X 6 CENTRAL ARRAY OF FUEL ASSEMBLIES"
FILL
  8 8 8 8 8 8
  8 8 8 8 8 8
  8 8 8 8 8 8
  8 8 8 8 8 8
  8 8 8 8 8 8
  8 8 8 8 8 8
END FILL
ARA=3  NUX=2   NUY=1   NUZ=1
COM=   "2 X 1  ARRAY OF FUEL ASSEMBLIES - TOP ROW"
FILL
 16  9
END FILL
```

```
ARA=4  NUX=6   NUY=1   NUZ=1
COM=   "6 X 1  ARRAY OF FUEL ASSEMBLIES - 2ND ROW"
FILL
  16  10  8  8  10  9
END FILL
ARA=5  NUX=1   NUY=2   NUZ=1
COM=   "2 X 1  ARRAY OF FUEL ASSEMBLIES - OUTER LEFT"
FILL
  14
  16
END FILL
ARA=6  NUX=1   NUY=6   NUZ=1
COM=   "1 X 6  ARRAY OF FUEL ASSEMBLIES - 2ND ROW LEFT"
FILL
  14  15  8  8  15  16
END FILL
ARA=7  NUX=1   NUY=2   NUZ=1
COM=   "1 X 2  ARRAY OF FUEL ASSEMBLIES - UPPER RIGHT"
FILL
  11
   9
END FILL
ARA=8  NUX=1   NUY=2   NUZ=1
COM=   "1 X 2  ARRAY OF FUEL ASSEMBLIES - MIDDLE RIGHT"
FILL
   8
   8
END FILL
ARA=9  NUX=1   NUY=2   NUZ=1
COM=   "1 X 2  ARRAY OF FUEL ASSEMBLIES - MIDDLE RIGHT"
FILL
   11
    9
END FILL
ARA=10  NUX=1   NUY=2   NUZ=1
COM=   "1 X 2  ARRAY OF FUEL ASSEMBLIES - LOWER RIGHT"
FILL
  11
  11
END FILL
ARA=11  NUX=2   NUY=1   NUZ=1
COM=   "2 X 1  ARRAY OF FUEL ASSEMBLIES - 2ND BOTTOM ROW"
FILL
  13  13
END FILL
ARA=12  NUX=2   NUY=1   NUZ=1
COM=   "2 X 1  ARRAY OF FUEL ASSEMBLIES - BOTTOM ROW"
FILL
  8  8
END FILL
ARA=13  NUX=2   NUY=1   NUZ=1
COM=   "2 X 1  ARRAY OF FUEL ASSEMBLIES - BOTTOM ROW"
FILL
  14  13
END FILL
ARA=14  NUX=2   NUY=1   NUZ=1
COM=   "2 X 1  ARRAY OF FUEL ASSEMBLIES - BOTTOM ROW"
FILL
  14 13
END FILL
END ARRAY
```

```
END DATA
END
```

CHAPTER 7: CONFINEMENT

7.0 INTRODUCTION

Confinement of all radioactive materials in the HI-STAR 100 System is provided by the MPC. The design of the HI-STAR 100 confinement boundary assures that there are no credible design basis events that would result in a radiological release to the environment. The HI-STAR 100 Overpack is designed to provide physical protection for an MPC during normal, off-normal, and postulated accident conditions to assure that the integrity of the MPC confinement boundary is maintained. The inert atmosphere in the MPC and the passive heat removal capabilities of the HI-STAR 100 also assure that the SNF assemblies remain protected from degradation, which might otherwise lead to gross cladding ruptures during dry storage.

The HI-STAR 100 System is classified as important to safety. Therefore, the individual structures, systems, and components (SSC's) that make up the HI-STAR 100 System shall be designed, fabricated, assembled, inspected, tested, accepted, and maintained in accordance with a quality program commensurate with the particular SSC's graded quality category. Tables 2.2.6 and 8.1.4 provide the quality category for each major item or component of the HI-STAR 100 System and required ancillary equipment and systems.

A detailed description of the confinement structures, systems, and components important to safety is provided in Chapter 2. The structural adequacy of the MPC is demonstrated by the analyses documented in Chapter 3. The physical protection of the MPC provided by the overpack for normal conditions of storage is demonstrated by the structural analyses documented in Chapter 3 and for off-normal and postulated accident conditions in Chapter 11. The heat removal capabilities of the HI-STAR 100 System are demonstrated by the thermal analyses documented in Chapter 4.

This chapter describes the HI-STAR 100 confinement boundary design and describes how the design satisfies the confinement requirements of 10CFR72 [7.0.1]. It also provides an evaluation of postulated radiological releases to the environment under normal, off-normal, and accident conditions of storage to ensure compliance with the limits established by the regulations.

This chapter is in compliance with NUREG-1536 except as noted in Table 1.0.3.

7.1 CONFINEMENT BOUNDARY

The primary confinement boundary against the release of radionuclides is the cladding of the individual fuel rods. The spent fuel rods are protected from degradation by maintaining an inert gas atmosphere (helium) inside the MPC and keeping the fuel cladding temperatures below the design basis values specified in Chapter 2.

The HI-STAR 100 confinement boundary consists of any one of the two fully-welded MPC designs described in Chapter 1. Each MPC is identical from a confinement perspective so the following discussion applies to all MPCs. The confinement boundary of the MPC consists of:

- MPC shell
- Bottom baseplate
- MPC lid (including the vent and drain port cover plates)
- MPC closure ring
- Associated welds

The above items form a totally seal-welded vessel for the storage of design basis spent fuel assemblies.

The MPC requires no valves, gaskets or mechanical seals for confinement. Figure 7.1.1 shows an elevation cross-section of the MPC confinement boundary. All components of the confinement boundary are Important to Safety, Category A, as specified in Table 2.2.6. The MPC confinement boundary is designed and fabricated in accordance with the ASME Code, Section III, Subsection NB [7.1.1] to the maximum extent practicable. Chapter 2 provides design criteria for the confinement design. Section 2.2.4 and Table 2.2.7 provide applicable Code requirements. Exceptions to specific Code requirements with complete justifications are presented in Table 2.2.15.

No additional credit is required or taken for confinement of the radionuclides by the overpack. The overpack helium retention boundary (containment boundary), which surrounds the MPC confinement boundary consists of the following (see Figure 7.1.2):

- inner shell, top flange, and bottom plate welded together with full penetration radiographed welds.
- a bolted closure plate with two concentric metallic seals to form a closure between the top flange surface and the closure plate, and redundant sealing of the inner metallic seal with a threaded test port plug containing a metallic seal which is compressed between the underside of the threaded plug head and the recessed seating surface on the closure plate.

- vent and drain ports with threaded plugs containing a metallic seal which is compressed between the underside of the threaded plug head and the overpack body.

- redundant sealing of the vent and drain ports by a bolted cover plate with a metallic seal which is compressed between the cover plate and the the overpack body

Table 7.1.1 provides design operating limits for the seals described above.

The HI-STAR helium retention boundary described above is identical to the HI-STAR 100 containment boundary defined and analyzed in the HI-STAR Safety Analysis Report submitted for transport certification [7.1.2].

7.1.1 Confinement Vessel

The HI-STAR 100 confinement vessel is the MPC. The MPC is designed to provide confinement of all radionuclides under normal, off-normal and accident conditions. The MPC is designed, fabricated, and tested in accordance with the applicable requirements of ASME, Section III, Subsection NB [7.1.1] to the maximum extent practicable. The MPC shell and baseplate assembly and basket structure are delivered to the loading facility as one complete component. The MPC lid, vent and drain port cover plates, and closure ring are supplied separately and are installed following fuel loading. The MPC lid (with the vent and drain port cover plates welded to the MPC lid) and closure ring are welded to the upper part of the MPC shell at the loading site to provide redundant sealing of the confinement boundary. The vent and drain port cover plates are welded to the MPC lid after the lid is welded to the MPC. Confinement boundary welds are described in detail in the drawing(s) in Section 1.5.

The MPC lid is made intentionally thick to minimize radiation exposure to workers during MPC closure operations, and is welded to the MPC shell. The vent and drain port cover plates are welded to the MPC lid following completion of MPC draining, vacuum drying, and helium backfill activities to close the MPC vent and drain openings. The MPC lid has a stepped recess around the perimeter for accommodating the closure ring. The MPC closure ring is welded to the MPC lid on the inner diameter of the ring and to the MPC shell on the outer diameter. The combination of the welded MPC lid and closure ring form the redundant closure of the MPC.

Table 7.1.1 provides a summary of the design ratings for normal, off-normal and accident conditions for the MPC confinement vessel. Tables 1.2.2, 2.2.1, and 2.2.3 provide additional design basis information.

The MPC shell and baseplate are helium leakage tested during fabrication in accordance with the requirements defined in Chapter 9. Following fuel loading and MPC lid welding, the MPC lid-to-shell weld is examined by liquid penetrant method (root and final), volumetrically examined (if volumetric examination is not performed, multi-layer liquid penetrant examination must be performed), helium leakage tested, and hydrostatically tested. If the MPC lid weld is acceptable, the vent and drain port cover plates are welded in place, examined by the liquid penetrant method (root and final), and a leakage rate test is performed. Finally, the MPC closure ring is

installed, welded and inspected by the liquid penetrant method (root and final), volumetrically examined (if volumentric examination is not performed, multi-layer liquid penetrant examination must be performed), helium leakage tested, and hydrostatically tested. If the MPC lid weld is acceptable, the vent and drain port cover plates are welded in place, examined by liquid penetrant method (root and final), and a leakage rate test is performed. Finally, the MPC closure ring is installed, welded and inspected by the liquid penetrant method (root, if multiple pass, and final). Chapters 8, 9, and the Certificate of Compliance provide procedural guidance, acceptance criteria, and Technical Specifications, respectively, for performance and acceptance of liquid penetrant examinations, volumetric examination, hydrostatic testing, and leakage rate testing of the field welds on the MPC.

After final vacuum drying, the MPC cavity is backfilled with helium. The helium backfill provides an inert atmosphere within the MPC cavity that precludes oxidation and hydride attack of the SNF cladding. Use of a helium atmosphere within the MPC contributes to the long-term integrity of the fuel cladding, reducing the potential for release of fission gas or other radioactive products to the MPC cavity. Helium also aids in heat transfer within the MPC and reduces the maximum fuel cladding temperatures. MPC inerting, in conjunction with the thermal design features of the MPC and storage cask, assures that the fuel assemblies are sufficiently protected against degradation, which might otherwise lead to gross cladding ruptures during long-term storage.

7.1.2 Confinement Penetrations

The MPC penetrations are designed to prevent the release of radionuclides under all normal, off-normal and accident conditions of storage. Two penetrations (the MPC vent and drain ports) are provided in the MPC lid for MPC draining, vacuum drying and backfilling during MPC loading operations, and for fuel cool-down and MPC flooding during unloading operations. No other confinement penetrations exist in the MPC. The MPC vent and drain ports are equipped with metal-to-metal seals to minimize leakage and withstand the long-term effects of temperature and radiation. The vent and drain connectors allow the vent and drain ports to be operated like valves and prevent the need to hot tap into the penetrations during unloading operations. The MPC vent and drain ports are sealed by cover plates which are seal welded to the MPC lid. No credit is taken for the seal provided by the vent and drain ports. The MPC closure ring covers the vent and drain port cover plate welds and the MPC lid-to-shell weld providing the redundant closure of the MPC vessel. The redundant closures of the MPC satisfy the requirements of 10CFR72.236(e) [7.0.1].

The MPC has no bolted closures or mechanical seals. The confinement boundary contains no external penetrations for pressure monitoring or overpressure protection.

7.1.3 Seals and Welds

The MPC is designed, fabricated, and tested in accordance with the applicable requirements of ASME, Section III, Subsection NB [7.1.1] to the maximum extent practicable. The MPC has no bolted closures or mechanical seals. Section 7.1.1 describes the design of the confinement vessel welds. The welds forming the confinement boundary are summarized in Table 7.1.2.

Confinement boundary welds are performed, inspected, and tested in accordance with the applicable requirements of ASME Section III, Subsection NB [7.1.1] to the maximum extent practicable. The use of multi-pass welds, root pass for multiple pass welds and final surface liquid penetrant inspection, and volumetric examination (if volumetric examination is not performed, multi-layer liquid penetrant examination must be performed) essentially eliminates the chance of a pinhole leak through the weld. Welds are also helium leak tested, providing added assurance of weld integrity. Additionally, a hydrostatic test is performed on the MPC lid-to-shell weld to confirm the weld's structural integrity. Fit-up of all field-welded components performed at the licensee's facility will result in a uniform root opening of the minimum size and will eliminate the need for backing that could restrain the weld joint and induce residual weld stresses. The ductile stainless steel material used for the MPC confinement boundary is not susceptible to delamination or hydrogen-induced weld degradation. The closure weld redundancy assures that failure of any single MPC confinement boundary closure weld does not result in release of radioactive material to the environment. Table 7.1.3 provides a summary of the closure weld examinations and tests.

7.1.4 Closure

The MPC is a totally seal-welded pressure vessel. The MPC has no bolted closure or mechanical seals. The MPC's redundant closures are designed to maintain confinement integrity during normal conditions of storage, and off-normal and postulated accident conditions. There are no unique or special closure devices. Primary closure welds are examined and leakage tested to ensure their integrity. A description of the MPC weld examinations is provided in Chapter 9.

Since the MPC uses an entirely welded redundant closure system, no direct monitoring of the closure is required. Section 11.2.1.4 describes requirements for verifying the continued confinement capabilities of the MPC in the event of off-normal or accident conditions. As discussed in Section 2.3.3.2, no instrumentation is required or provided for HI-STAR 100 storage operations, other than normal security service instruments and TLDs.

7.1.5 Damaged Fuel Container

The MPC is designed to allow for the storage of specified damaged fuel assemblies and fuel debris in a specially designed damaged fuel container (DFC). Fuel assemblies classified as damaged fuel or fuel debris (assembly array/class 6x6A, 6x6B, 6x6C, 7x7A, and 8x8A) as specified in the Technical Specifications have been evaluated.

To aid in loading and unloading, damaged fuel assemblies and fuel debris will be loaded into stainless steel DFCs prior to placement in the HI-STAR 100 System. Up to 68 damaged fuel assemblies in DFC's may be stored in an MPC-68 or MPC-68F. The DFC is shown in Figure 2.1.1 and detailed in the drawings in Section 1.5. The DFC is designed to provide SNF loose component retention and handling capabilities. The DFC consists of a smooth-walled, welded stainless steel container with a removable lid. The canister lid provides the means of DFC closure and handling. The DFC is provided with stainless steel wire mesh screens in the top and bottom for draining, vacuum drying and helium backfill operations. The screens are specified as a 250-by-250-mesh with an effective opening of 0.0024 inches. There are no other openings in the DFC. The Technical Specifications specify the fuel assembly characteristics for damaged

fuel acceptable for loading in the MPC-68 or MPC-68F and for fuel debris acceptable for loading in the MPC-68F.

Since the DFC has screens on the top and bottom, the DFC provides no pressure retention function. The confinement function of the DFC is limited to minimizing the release of loose particulates within the sealed MPC. The storage design basis leakage rates are not altered by the presence of the DFCs. The radioactive material available for release from the specified fuel assemblies are bounded by the design basis fuel assemblies analyzed herein.

Table 7.1.1

SUMMARY OF CONFINEMENT AND HELIUM RETENTION BOUNDARY DESIGN SPECIFICATIONS

Design Attribute	Design Rating
Internal Design Pressure (normal)	100 psig
Design Temperature (normal)	550°F (MPC lid)
Internal Design Pressure (off-normal)	100 psig
Design Temperature (off-normal)	775°F (MPC lid)
Internal Design Pressure (accident)	125 psig
Design Temperature (accident)	950°F (MPC basket)
Design Basis Leakage Rate	$5x10^{-6}$ atm cm^3/sec (helium)
Closure Plate Mechanical Seal[†,††] Design Temperature Pressure Limits Design Leakage Rate	 1200°F 1000 psig $1x10^{-6}$ cm^3/sec, Helium
Overpack Vent and Drain Port Cover Plate Mechanical Seals[†,††] Design Temperature Pressure Limits Design Leakage Rate	 1200 °F 1000 psig $1x10^{-6}$ cm^3/sec, Helium
Overpack Vent and Drain Port Plug Mechanical Seals[†,††] Design Temperature Pressure Limits Design Leakage Rate	 1200 °F 1000 psig $1x10^{-6}$ cm^3/sec, Helium

† For overpack helium retention only. No confinement credit is taken for the overpack mechanical seals.

†† Per Manufacturer's recommended operating limits.

Table 7.1.2

MPC CONFINEMENT BOUNDARY WELDS

Confinement Boundary Welds		
MPC Weld Location	**Weld Type†**	**ASME Code Category (Section III, Subsection NB)**
Shell longitudinal seam	Full Penetration Groove (shop weld)	A
Shell circumferential seam	Full Penetration Groove (shop weld)	B
Baseplate to shell	Full Penetration Groove (shop weld)	C
MPC lid to shell	Partial Penetration Groove (field weld)	C
MPC closure ring to shell	Fillet (field weld)	††
Vent and drain port cover plates to MPC lid	Partial Penetration Groove (field weld)	D
MPC closure ring to closure ring radial	Partial Penetration Groove (field weld)	††
MPC closure ring to MPC lid	Partial Penetration Groove (field weld)	C

† The tests and inspections for the confinement boundary welds are listed in Section 9.1.1.

†† This joint is covered by NB-5271 (liquid penetrant examination).

Table 7.1.3

CLOSURE WELD EXAMINATIONS AND TESTS

Closure Weld Description	Inspections/Tests	ASME Acceptance Criteria
MPC Lid-to-Shell	VT on Tack Welds PT Root Pass PT Final Pass VT Final Pass Volumetric Examination of Weld (UT) or multi-layer PT Hydrostatic Test Post Hydrostatic Test - PT Helium Leakage Test	NF-5360 NB-5350 NB-5350 NF-5360 NB-5332 NB-6000 NB-5350 Sect. V and ANSI N14.5
Vent/Drain Cover Plate to MPC Lid	VT on Tack Welds PT Root Pass PT Final Pass VT Final Pass Helium Leakage Test	NF-5360 NB-5350 NB-5350 NF-5360 Sect. V and ANSI N14.5
Closure Ring Radial Welds	VT on Tack Welds PT Root Pass (if multiple pass) PT Final Pass VT Final Pass	NF-5360 NB-5350 NB-5350 NF-5360
Closure Ring-to-MPC Shell	VT on Tack Welds PT Root Pass (if multiple pass) PT Final Pass VT Final Pass	NF-5360 NB-5350 NB-5350 NF-5360
Closure Ring-to-MPC Lid	VT on Tack Welds PT Root Pass PT Final Pass VT Final Pass	NF-5360 NB-5350 NB-5350 NF-5360

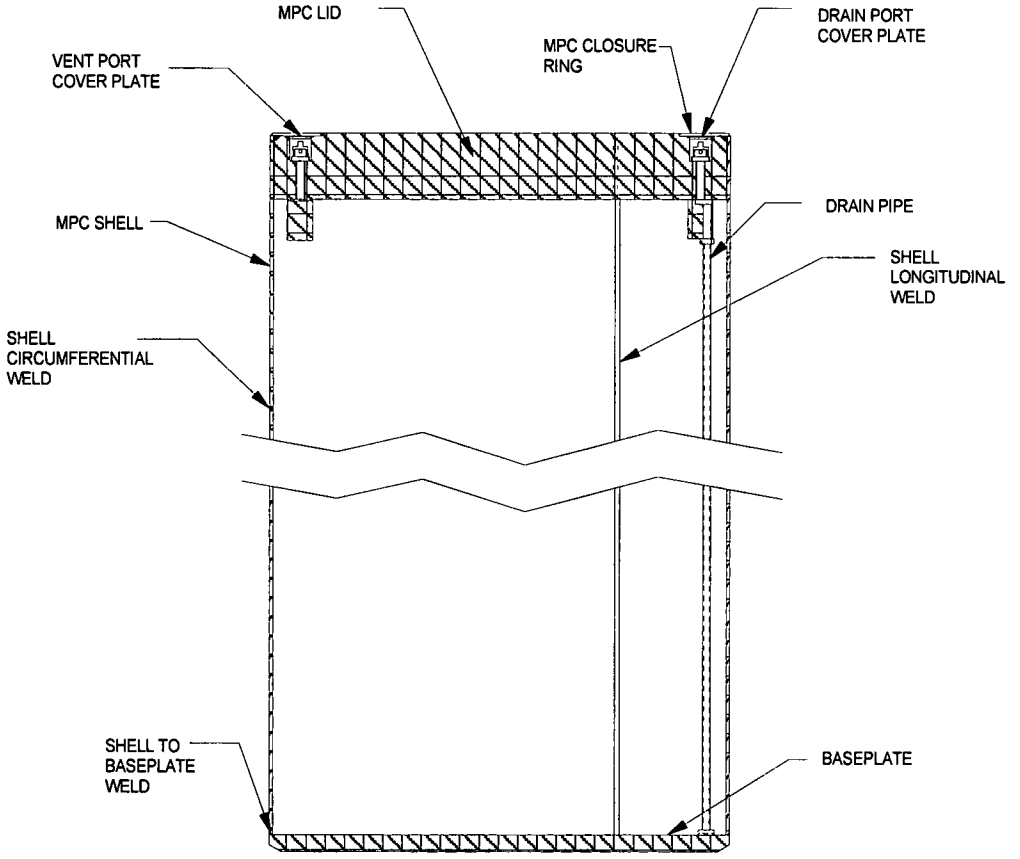

Figure 7.1.1; HI-STAR 100 System Confinement Boundary

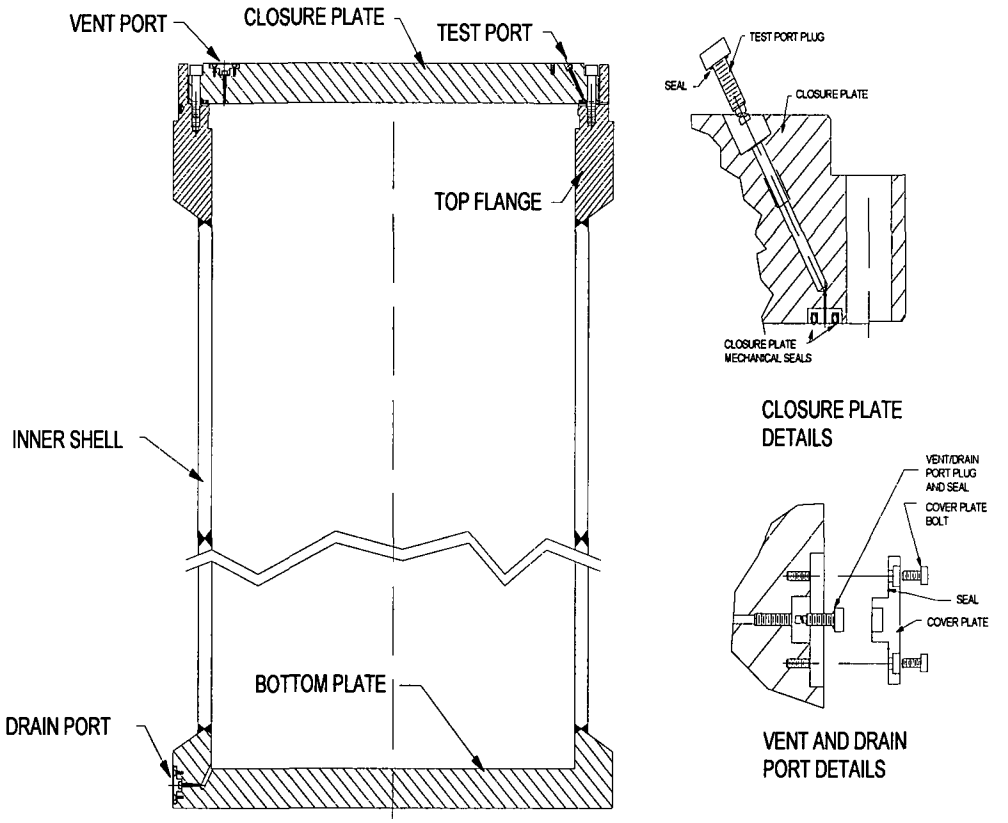

Figure 7.1.2; HI-STAR 100 System Containment Boundary

FIGURE 7.1.3

DELETED

7.2 REQUIREMENTS FOR NORMAL AND OFF-NORMAL CONDITIONS OF STORAGE

The MPC uses multiple confinement barriers provided by the fuel cladding and the MPC enclosure vessel to assure that there is no release of radioactive material to the environment. Chapter 3 shows that all confinement boundary components are maintained within their Code-allowable stress limits during normal storage conditions. Chapter 4 shows that the peak confinement boundary component temperatures and pressures are within the design basis limits for all normal conditions of storage. Since the MPC confinement vessel remains intact, and the design bases temperatures and pressure are not exceeded, the design basis leakage rate is not exceeded during normal conditions of storage.

7.2.1 Release of Radioactive Material

The MPC is closed by the MPC lid, the vent and drain port cover plates, and the MPC closure ring. Weld examinations, including multiple surface examinations, volumetric examination, hydrostatic testing, and leakage rate testing on the MPC lid weld, and multiple surface examinations and leakage rate testing of the vent and drain port cover plate welds, assure the integrity of the MPC closure. The MPC is a seal-welded pressure vessel designed to meet the stress criteria of the ASME Code, Section III, Subsection NB [7.1.1]. The all-welded construction of the MPC with redundant closure provided by the fully welded MPC closure ring, and extensive inspections and testing ensures that no release of fission gas or crud for normal storage and transfer conditions will occur. The above discussion notwithstanding, an analysis is performed in Section 7.2.7 to calculate the annual dose at 100 meters based on an assumed leakage rate of 5×10^{-6} atm-cm^3/sec plus the minimum test sensitivity of 2.5×10^{-6} atm-cm^3/sec under normal and off-normal conditions of storage.

7.2.2 Pressurization of the Confinement Vessel

The loaded and sealed MPC is drained, vacuum dried, and backfilled with helium gas. This process provides a chemically non-reactive environment for storage of spent fuel assemblies. First, air in the MPC is displaced with water and then the water is displaced by helium or nitrogen gas during MPC blowdown. The MPC is then vacuum dried, and backfilled with a predetermined mass of helium as specified in the Technical Specifications. Chapter 8 describes the steps of these processes and the Technical Specifications provide the acceptance criteria. This drying and backfilling process ensures that the resulting inventory of oxidizing gases in the MPC remains below 0.25% by volume, and that the MPC pressure is maintained within the design limitations. In addition, the MPC basket fluid contact areas are stainless steel alloy material or aluminum of extremely high corrosion and erosion resistance. The aluminum oxide layer on the aluminum components (e.g., heat conduction elements and Boral neutron absorption plates) ensures that there is a minimal amount of reaction during the short duration of exposure to the fuel pool water (see Section 3.4.1 for discussion of combustible gas control during lid welding). Carbon steels are not employed in the construction of the MPCs. Therefore, no protective coatings which could interact with borated spent fuel pool water are used.

The only means of pressure increase in the MPC is from the temperature rise to normal heat-up

to normal operating temperatures and the release of backfill and fission gas contents from fuel rods into the MPC cavity. Under the most adverse conditions of normal ambient temperature, full insolation, and design basis decay heat, the calculated pressure increase assuming 1% fuel rod failure is well below the system design pressure as shown in Chapter 4. The heavy HI-STAR 100 overpack provides protection from ambient day-night temperature swings thereby providing a relatively stable thermal environment for fuel storage. For off-normal conditions of storage, failure of up to 10% of the fuel rods has been analyzed and would result in an MPC internal pressure below the value specified as the normal design pressure.

7.2.3 Confinement Integrity During Dry Storage

There is no credible mechanism or event that results in a release of radioactive material from the MPC under normal conditions. Since the MPC remains structurally intact and provides redundant welded closures as discussed above, the postulated leakage of radioactive material from the MPC will be limited to a leakage rate equivalent to the acceptance test criteria specified for the MPC helium leak tests. Leakage from the MPC during normal conditions of storage could result in the release of gaseous fission products, fines, volatiles and airborne crud particulates as discussed in Section 7.3.1. The conservative assumption is made that 1% of the fuel inventory is available for release under normal conditions of storage and 10% of the fuel inventory is available for release under off-normal conditions of storage. The maximum cavity internal operating pressure with 10% fuel rod failure reported in Chapter 4 is bounded by the use of an internal cavity pressure of 58.7 psia (4.99 ATM), which is assumed as an initial condition for this evaluation.

The following doses to an individual at the site boundary (100 meters) as a result of an assumed effluent release under normal and off-normal conditions of storage were determined; the inhaled committed dose equivalent for critical organs and tissues (gonad, breast, lung, red marrow, bone surface, thyroid, skin, lens of the eye), the effective dose from external submersion in the plume, and the resulting Total Effective Dose Equivalent (TEDE). These doses were determined for each type of MPC. The ISFSI controlled area boundary must be at least 100 meters from the nearest loaded HI-STAR 100 System in accordance with 10CFR72.106(b) [7.0.1]. The doses are compared to the regulatory limits specified in 10CFR72.104 [7.0.1].

Confinement boundary welds performed at the fabricator's facility are inspected by volumetric and liquid penetrant examination methods as detailed in Section 9.1. Field welds are performed on the MPC lid, the MPC vent and drain port covers, and MPC closure ring. The weld of the MPC lid-to-shell is liquid penetrant examined on the root and final pass, volumetrically (or multilayer liquid penetrant) examined, hydrostatically tested, and leak rate tested. The vent and drain port cover plates are liquid penetrant examined on the root and final pass and leak rate tested. The MPC closure ring welds are inspected by the liquid penetrant examination method on the root pass, if multiple pass, and final pass. In Chapter 11, the MPC lid-to-shell weld is postulated to fail to confirm the safety of the HI-STAR 100 confinement boundary. The failure of the MPC lid weld is equivalent to the MPC drain or vent port cover weld failing. The MPC lid weld failure affects the MPC confinement boundary; however, no leakage will occur due to redundant sealing provided by the MPC closure ring.

7.2.4 Control of Radioactive Material During Fuel Loading Operations

The procedures for closure of the MPC, described in Section 8.1, are intended to assure that there is no unintended release of gas, liquid, or solid materials from the MPC during dry storage. During MPC closure operations, the lines used for venting or draining are routed to the plant's spent fuel pool or radioactive waste processing systems. MPC closure operations are performed inside the plant's fuel building in a controlled and monitored environment.

Radioactive effluent handling during fuel loading and MPC draining, vacuum drying, helium backfilling, and sealing operations is in accordance with the plant's 10CFR50 license and radioactive waste management system.

7.2.5 External Contamination Control

The external surface of the MPC is protected from contamination by preventing it from coming in contact with the spent fuel pool water. Prior to submergence in the spent fuel pool, an inflatable seal is installed at the top of the annulus formed between the MPC shell and the HI-TRAC transfer cask cavity. This annulus is filled with clean demineralized water and the seal is inflated. The inflated seal, backed by the demineralized water maintained at a slight positive pressure, is sufficient to preclude the entry of contaminated water into the annulus. These steps assure that the MPC surface is free of contamination that could become airborne during storage.

Additionally, following fuel loading operations and removal from the spent fuel pool, the upper end of the MPC shell is surveyed for loose surface contamination in accordance with the Technical Specifications.

7.2.6 Confinement Vessel Releasable Source Term

As discussed in Section 7.3.1, the source term used to evaluate the annual dose at the minimum controlled area boundary of 100 meters due to leakage from the MPC confinement boundary consists of gaseous fission products, fines, volatiles and airborne crud particulates. For this evaluation, it is conservatively assumed that 1% of the fuel inventory is available for release under normal conditions of storage and 10% of the fuel inventory is available for release under off-normal conditions of storage. A summary of the isotopes available for release is provided in Table 7.3.1.

7.2.7 Release of Contents Under Normal and Off-Normal Storage Conditions

7.2.7.1 Seal Leakage Rate

The methodology presented in Section 7.3.3.1 was used to determine the leakage rate at the upstream conditions. Using the capillary diameter determined in Section 7.3.3.1, and the parameters for normal and off-normal conditions provided in Table 7.3.6, Equation 7-3 was solved for the leakage rate at the upstream conditions. The resultant normal and off-normal condition leakage rate, 8.8×10^{-6} cm^3/s (at 499.2 K, 4.99 ATM) was calculated.

7.2.7.2 Fraction of Volume Released

The minimum free volume of each MPC design is presented in Tables 4.4.13 and 4.4.14 Using conservatively reduced values of these volumes and the upstream normal and off-normal condition leakage rate of 8.8×10^{-6} cm^3/s, the fraction of the volume released per second is calculated.

7.2.7.3 Release Fraction

The release fraction is that portion of the total radionuclide inventory that is released from the confinement boundary to the atmosphere (i.e., outside the MPC). The release fractions provided in NUREG/CR-6487 [7.3.2] are used. A summary of the release fractions is provided in Table 7.3.1.

7.2.7.4 Radionuclide Release Rate

The radionuclide release rate is the product of the quantity of isotopes available for release, the number of assemblies, the fraction of volume released, and the release fraction.

7.2.7.5 Atmospheric Dispersion Factor

For the evaluation of the dose at the controlled area boundary, the instantaneous χ/Q calculated for accident conditions (8.0×10^{-3} sec/m^3) was reduced to 1.6×10^{-4} sec/m^3 based on the long term nature of the release (1 year); the height of the release being essentially a ground level release ($h_e = 0$); all 16 compass directions (22.5 degree sectors) will be similarly affected due to the long term nature of the continuous release (over one year); the increase in average wind speeds (>1 m/s); and the additional effects of a reduction in atmospheric stability. Therefore, the χ/Q reduction factor of 50 used to correct the short term accident release χ/Q is conservative.

7.2.7.6 Dose Conversion Factors

Dose Conversion Factors (DCF) from EPA Federal Guidance Report No. 11, Table 2.1 [7.3.5] and EPA Federal Guidance Report No. 12, Table III.1 [7.3.6] were used for the analysis. The DCFs are provided on the spread sheets included as Appendix 7.A.

7.2.7.7 Occupancy Time

An occupancy time of 8,760 hours is used for the analysis [7.0.2]. This conservatively assumes that the individual is exposed 24 hours per day for 365 days at the minimum controlled area boundary of 100 meters.

7.2.7.8 Breathing Rate

A breathing rate of 3.3×10^{-4} m^3/sec for a worker is used for the analysis. This assumption is in accordance with the guidance provided in NUREG-1536 [7.0.2] for a worker.

7.2.8 Postulated Doses Under Normal and Off-Normal Conditions of Storage

The following doses to an individual at the site boundary (100 meters) as a result of an assumed effluent release under normal and off-normal conditions of storage were determined; the inhaled committed dose equivalent for critical organs and tissues (gonad, breast, lung, red marrow, bone surface, thyroid, skin, lens of the eye), the effective dose from external submersion in the plume, and the resulting Total Effective Dose Equivalent (TEDE). These doses are determined for each type of MPC and for each condition of storage (i.e., normal and off-normal). The postulated doses as a result of exposure to soil with ground surface contamination and soil contaminated to a depth of 15 cm were also determined. The resultant doses were negligible compared to the those resulting from submersion in the plume and are therefore not reported.

The doses were determined using spreadsheet software. The resultant doses are summarized for each MPC type in Tables 7.3.2, 7.3.3, and 7.3.4. Example spread sheets used for the dose estimates are presented in Appendix 7.A.

7.2.8.1 Whole Body Dose (Total Effective Dose Equivalent)

The whole body dose is the sum of the inhaled committed effective dose equivalent (CEDE) and the external exposure from submersion in the plume. The postulated doses were determined using spreadsheet software. Example spread sheets are provided in Appendix 7.A.

The CEDE is the product of radionuclide release rate, the atmospheric dispersion factor, the occupancy time, the breathing rate, and the effective dose conversion factor.

External exposure from submersion is the product of the nuclide release rate, the atmospheric dispersion factor, the occupancy time, and the effective dose conversion factor.

7.2.8.2 Critical Organ Dose

The dose to the critical organ (or tissue) is the sum of the committed dose equivalent to the critical organ or tissue from inhalation and the dose equivalent to the organ or tissue from submersion in the plume. The postulated doses as a result of exposure to soil with ground surface contamination and soil contaminated to a depth of 15 cm were also determined. The resultant doses were negligible compared to the those resulting from submersion in the plume and are therefore not reported.

The committed dose equivalent to the organ or tissue from inhalation is the product of radionuclide release rate, the atmospheric dispersion factor, the occupancy time, the breathing rate, and the organ/tissue dose conversion factor. The dose equivalent to the organ or tissue from submersion in the plume is the product of the nuclide release rate, the atmospheric dispersion factor, the occupancy time, and the organ/tissue dose conversion factor.

The doses for tissues and organs other than lens of the eye were determined using spreadsheet software. The dose to the lens of the eye as a result of submersion in the plume was estimated using guidance from Dr. James Turner in his book, Atoms, Radiation, and Radiation Protection

[7.3.10]]. Dr. Turner states that alpha particles and low-energy beta particles, such as those from tritium, cannot penetrate to the lens of the eye (at a depth of 3 mm). The discussion continues that many noble gases emit photons and energetic beta particles, which in turn must be considered in the dose estimate. Dr. Turner states that the dose-equivalent rate to tissues near the surface of the body (e.g., lens of the eye) is more than 130 times the dose-equivalent rate in the lung from gases contained in the lung. The estimated dose to the lens of the eye is greatest using the accident condition of storage for the MPC-68. Section 7.3.4.2 presents the detailed discussion of the dose to the lens of the eye.

7.2.9 Site Boundary

The estimated annual dose at the controlled area boundary is highest due to anticipated occurrences (off-normal) using the MPC-68. The estimated TEDE (0.87 mrem/yr) is a small fraction of the annual 25 mrem whole body limit imposed by 10 CFR 72.104(a). The estimated thyroid dose (0.10 mrem/yr) is a small fraction of the annual 75 mrem thyroid limit imposed by 10 CFR 72.104(a). Additionally, the dose estimates to other critical organs are small fractions of the annual 25 mrem critical organ limit imposed by 10 CFR 72.104(a). The highest of the "other critical organs" is 8.01 mrem to the bone surface.

7.2.10 Assumptions

The following presents a summary of assumptions for the normal and off-normal condition confinement analysis of the HI-STAR 100 System.

- The distance from the cask to the site boundary is 100 meters.
- Under normal conditions of storage, 1% of the fuel rods have ruptured. This assumption is in accordance with NUREG-1536 for normal storage conditions.
- Under off-normal conditions of storage, 10% of the fuel rods have ruptured. This assumption is in accordance with ISG-5 and NUREG-1536 for off-normal storage conditions.
- Unchoked flow correlations were used as the unchoked flow correlations better approximate the true measured flow rate for the leakage rates associated with transportation packages.
- The capillary length required for Equation 7-3 was chosen to be the smaller of the MPC lid closure weld sizes (MPC 24 and MPC-68, a=1.9cm and MPC-68F, a=3.2), which is 1.9 cm. The shorter leak path assumptions conservatively over estimates the leak rate in the thicker (MPC-68F) weld.
- For conservatism, the upstream pressure at test conditions (inside of the MPC) is assumed to be 2 ATM and the down stream pressure (outside of the MPC) is assumed to be 1 ATM.

- The temperature at test conditions is assumed to be equal to a temperature, 212° F based on the maximum temperature achievable by the water in the MPC during performance of the leak test. This is conservative because the leak hole diameter computed from test conditions is larger.

- The majority of the activity associated with crud is due to ^{60}Co. This assumption follows from the discussion provided in NUREG/CR-6487 [7.3.2].

- The normal and off-normal condition leakage rate persists for one year without a decrease in the rate or nuclide concentration.

- The individual at the site boundary is exposed for 8,760 hours [7.0.2]. This conservatively assumes that the individual is exposed 24 hours per day for 365 days.

- In accordance with the International Commission on Radiological Protection (ICRP) Publication 30 [7.3.7 "*for exposure in radioisotopes of the noble gases, external irradiation will be of such overriding importance that it alone need be considered.*" Therefore, the contribution to the committed effective dose equivalent from ^{85}Kr is neglected.

- A breathing rate of 3.3×10^{-4} m^3/sec for a worker is used for the analysis [7.0.2]. This assumption is in accordance with the guidance provided in NUREG-1536 for a worker.

- All fuel stored in the MPC is of the design basis type with a bounding burnup and cooling time.

- Exposure to dose conversion factors for inhalation reported in EPA Federal Guidance Report No. 11, Table 2.1 [7.3.5] were selected by lung clearance class which reports the most conservative values.

7.3 CONFINEMENT REQUIREMENTS FOR HYPOTHETICAL ACCIDENT CONDITIONS

The MPC uses redundant confinement closures to assure that there is no release of radioactive materials, including fission gases, volatiles, fuel fines or crud, for postulated storage accident conditions. The analyses presented in Chapters 3 and 11 demonstrate that the MPC remains intact during all normal, off-normal and postulated accident conditions, including the associated increased internal pressure due to decay heat generated by the stored fuel. The MPC is designed, fabricated, and tested in accordance with the applicable requirements of ASME, Section III, Subsection NB [7.1.1] to the maximum extent practicable. In summary, there is no mechanistic failure that results in a breach of the MPC confinement boundary.

The above discussion notwithstanding, this section evaluates the consequences of a non-mechanistic postulated ground level breach of the MPC confinement boundary. This breach could result in the release of gaseous fission products, fines, volatiles and airborne crud particulates. The internal accident pressure of 125 psig, as specified in Table 7.1.1, is assumed as an initial condition for this evaluation. The following doses to an individual at the site boundary (100 meters) as a result of an assumed effluent release under accident conditions of storage were determined; the inhaled committed dose equivalent for critical organs and tissues (gonad, breast, lung, red marrow, bone surface, thyroid, skin, lens of the eye), the effective dose from external submersion in the plume, and the resulting Total Effective Dose Equivalent (TEDE). These doses were determined for each type of MPC. The ISFSI controlled area boundary must be at least 100 meters from the nearest loaded HI-STAR 100 System in accordance with 10CFR72.106(b) [7.0.1]. The doses are compared to the regulatory limits specified in 10CFR72.106(b) [7.0.1].

7.3.1 Confinement Vessel Releasable Source Term

In accordance with NUREG/CR-6487 [7.3.2], the following contributions are considered in determining the releasable source term for packages designed to transport irradiated fuel rods: (1) the radionuclides comprising the fuel rods, (2) the radionuclides on the surface of the fuel rods, and (3) the residual contamination on the inside surfaces of the vessel. NUREG/CR-6487 goes on to state that a radioactive aerosol can be generated inside a vessel when radioactive material from the fuel rods or from the inside surfaces of the container become airborne. The sources for the airborne material are (1) residual activity on the cask interior, (2) fission and activation-product activity associated with corrosion-deposited material (crud) on the fuel assembly surface, and (3) the radionuclides within the individual fuel rods. In accordance with NUREG/CR-6487, contamination due to residual activity on the cask interior surfaces is negligible as compared to crud deposits on the fuel rods themselves and therefore may be neglected. The source term considered for this calculation results from the spallation of crud from the fuel rods and from the fines, gases and volatiles which result from cladding breaches. The methodology of NUREG/CR-6487 is conservatively applied to the storage confinement accident analysis as dry storage conditions are less severe than transport conditions.

The inventory for isotopes other than ^{60}Co is calculated with the SAS2H and ORIGEN-S modules of the SCALE 4.3 system as described in Section 5.2. The inventory for the MPC-24 was conservatively based on the B&W 15x15 fuel assembly with a burnup of 40,000 MWD/MTU, 5 years of cooling time, and an enrichment of 3.4%. The inventory for the MPC-68 was based the GE

7x7 fuel assembly with a burnup of 40,000 MWD/MTU, 5 years of cooling time, and 3.0% enrichment. The Technical Specifications limit the fuel assembly burnup well below 40,000 MWD/MTU for both BWR and PWR fuel at 5 years of cooling time. This ensures that the inventory used in this calculation exceeds that of the fuel authorized for storage in accordance with the Technical Specifications. The inventory for the MPC-68F was based on the GE 6x6 fuel assembly with a burnup of 30,000 MWD/MTU, 18 years of cooling time, and 2.24% enrichment. The Technical Specifications limit the burnup and cooling time of fuel debris in an MPC-68F to a maximum of 30,000 MWD/MTU at a minimum of 18 years cooling time. Additionally, an MPC-68F was analyzed containing 67 GE 6x6 assemblies and a DFC containing 18 thorium rods. Finally, an Sb-Be source stored in one fuel rod in one assembly with 67 GE 6x6 assemblies was analyzed. The isotopes which contribute greater than 0.1% to the total curie inventory for the fuel assembly are considered in the evaluation as fines. The analysis also includes actinides as the dose conversion factors for these isotopes are in general, orders of magnitude greater than other isotopes (e.g., isotopes of plutonium, americium, curium, and neptunium were included regardless of their contribution to the inventory). A summary of the isotopes available for release is provided in Table 7.3.1.

7.3.2 Crud Radionuclides

The majority of the activity associated with crud is due to ^{60}Co [7.3.2]. The inventory for ^{60}Co was determined by using the crud surface activity for PWR rods ($140x10^{-6}$ Ci/cm^2) and for BWR rods ($1254x10^{-6}$ Ci/cm^2) provided in NUREG/CR-6487 [7.3.2] multiplied by the surface area per assembly ($3x10^5$ cm^2 and $1x10^5$ cm^2 for PWR and BWR, respectively, also provided in NUREG/CR-6487). The source terms were then decay corrected (5 years for the MPC-24 and MPC-68; 18 years for the MPC-68F) using the basic radioactive decay equation:

Equation 7-1

$$A(t) = A_0 e^{-\lambda t}$$

where:

A(t)	is activity at time t [Ci]
A_0	is the initial activity [Ci]
λ	is the $\ln 2/t_{1/2}$ (where $t_{1/2}$ = 5.272 years for ^{60}Co)
t	is the time in years (5 years for the MPC-24 and MPC-68; 18 years for the MPC-68F)

Total ^{60}Co crud is 140 μCi/cm^2 for PWR and 1254 μCi/cm^2 for BWR [7.3.2].

PWR	**BWR**
Surface area per Assy = 3.0E+05 cm^2	Surface area per Assy = 1.0E+05 cm^2

140 $\mu Ci/cm^2$ x 3.0E+05 cm^2 = 42.0 Ci 1254 $\mu Ci/cm^2$ x 1.0E+05 cm^2 = 125.4 Ci

$^{60}Co(t) = {}^{60}Co_0\, e^{-(\lambda t)}$, where $\lambda = \ln 2/t_{1/2}$, t = 5 years (for the MPC-24 and MPC-68), t = 18 years (MPC-68F), $t_{1/2}$ = 5.272 years for ^{60}Co [7.3.3]

MPC-24

$^{60}Co(5) = 42.0\ Ci\ e^{-(\ln 2/5.272)(5)}$
$^{60}Co(5) = 21.77$ Ci

MPC-68

$^{60}Co(5) = 125.4\ Ci\ e^{-(\ln 2/5.272)(5)}$
$^{60}Co(5) = 64.98$ Ci

MPC-68F

$^{60}Co(18) = 125.4\ Ci\ e^{-(\ln 2/5.272)(18)}$
$^{60}Co(18) = 11.76$ Ci

A summary of the ^{60}Co inventory available for release is provided in Table 7.3.1.

7.3.3 Release of Contents Under Non-Mechanistic Accident Conditions of Storage

7.3.3.1 Seal Leakage Rate

The helium leak rate testing performed on the MPC confinement boundary verifies the helium leak rate to be less than or equal to $5x10^{-6}$ atm-cm^3/s[1] as required by the Technical Specifications with a minimum sensitivity of $2.5x10^{-6}$ atm-cm^3/s. As demonstrated by analysis, the MPC confinement boundary is not compromised as a result of normal, off-normal, and accident conditions. Based on the robust nature of the MPC confinement boundary, the NDE inspection of the welds, and the measurement of the helium leakage rate, there is essentially no leakage. However, it is conservatively assumed that the maximum possible leakage rate from the confinement vessel is the maximum leakage rate acceptance criteria plus the sensitivity. This yields an assumed helium leakage rate of $7.5x10^{-6}$ atm-cm^3/s.

Equation B-1 of ANSI N14.5 (1997) [7.3.8] is used to express this mass-like helium flow rate (Q_u) measured in atm-cm^3/s as a function of the upstream volumetric leakage rate (L_u) as follows:

Equation 7-2

[1] According to ANSI N14.5 (1997), the mass-like leakage rate specified herein is often used in leakage testing. This is defined as the rate of change of the pressure-volume product of the leaking fluid at test conditions.

$$Q_u = L_u * P_u \quad \text{atm-cm}^3/\text{sec (Equation B-1 from ANSI N14.5(1997))}$$

$$L_u = Q_u/P_u \quad \text{cm}^3/\text{sec}$$

where:

L_u is the upstream volumetric leakage rate [cm^3/s],
Q_u is the mass-like helium leak rate [atm cm^3/s], and
P_u is the upstream pressure [ATM]

The corresponding leakage rate at accident conditions is determined using the following methodology. For conservatism, unchoked flow correlations were used as the unchoked flow correlations better approximate the true measured flowrate for the leakage rates.

For conservatism, the upstream pressure at test conditions (inside of the MPC) is assumed to be 2 ATM (minimum) and the down stream pressure (outside of the MPC) is assumed to be 1 ATM (at 298 K), therefore, the average pressure is 1.5 ATM. The evaluation was performed using the helium gas temperature at test conditions of both 70°F and 212°F. These temperatures are representative of the possible temperature of the helium gas in the confinement vessel during the helium leak test. The 212°F helium temperature is the upper bound because the water inside the MPC is shown not to boil in Chapter 4 as long as the "time-to-boil" time limit is not exceeded. From the two calculations using the two temperatures, it was determined that the higher temperature (212°F) results in a greater capillary diameter.

Using the equations for molecular and continuum flow, Equation B-5 provided in ANSI N14.5-1997 [7.3.8], the corresponding capillary diameter, D, was calculated. The capillary length required for Equation 7-3 was conservatively chosen to be the minimum MPC lid closure weld which is 1.9 cm. Table 7.3.6 provides a summary of the parameters used in the calculation.

Equation 7-3

$$L_u = \left[\frac{2.49x10^6 D^4}{a\,u} + \frac{3.81x10^3 D^3 \sqrt{\frac{T}{M}}}{a\,P_a}\right][P_u - P_d]\left[\frac{P_a}{P_u}\right]$$

where:

L_u is the allowable leakage rate at the upstream pressure [cm^3/s],
a is the capillary length [cm],
T is the temperature [°K],
M is the gas molecular weight [g/mole] from ANSI N14.5, Table B1 [7.3.8],
u is the fluid viscosity for helium [cP] from Rosenhow and Hartnett [7.3.9]
P_u is the upstream pressure [ATM],
P_d is the downstream pressure [ATM], and
P_a is the average pressure; $P_a = (P_u + P_d)/2$ [ATM].

D is the capillary diameter [cm].

The capillary diameter (D) computed from the above equation is equal to 4.96×10^{-4} cm.

Using the capillary diameter determined above, and the parameters for accident conditions provided in Table 7.3.6, Equation 7-3 was solved for the leakage rate at the upstream conditions. The resultant hypothetical accident leakage rate, 1.25×10^{-5} cm^3/s (at 843 K, 9.5 ATM) was calculated.

7.3.3.2 Fraction of Volume Released

The minimum free volume of each MPC design is presented in Tables 4.4.13 and 4.4.14. Using conservatively reduced values of these volumes and the upstream hypothetical accident leakage rate of 1.25×10^{-5} cm^3/s, the fraction of the volume released per second is calculated.

7.3.3.3 Release Fraction

The release fraction is that portion of the total radionuclide inventory that is released from the confinement boundary to the atmosphere (i.e., outside the MPC). The release fractions provided in NUREG/CR-6487 [7.3.2] are used. A summary of the release fractions is provided in Table 7.3.1.

7.3.3.4 Radionuclide Release Rate

The radionuclide release rate is the product of the quantity of isotopes available for release, the number of assemblies, the fraction of volume released, and the release fraction.

7.3.3.5 Atmospheric Dispersion Factor

The short-term accident condition atmospheric dispersion factor at 100 meters was determined using Regulatory Guide 1.145 [7.3.4]. In accordance with NUREG-1536 [7.0.2], the dispersion factor was determined on the basis of F-stability diffusion, a wind speed of 1 m/s, and plume meandering.

Reg Guide 1.145 [7.3.4] specifies that χ/Q be calculated using the following three equations. The values determined using Equations 7-4 and 7-5 should be compared and the higher value selected. This value should be compared with the value determined using Equation 7-6, and the lower value of these two should be selected as the appropriate χ/Q value. This methodology was used to determine the value for χ/Q.

Equation 7-4

$$\frac{\chi}{Q} = \frac{1}{U(\pi \sigma_y \sigma_z + A/2)}$$

Equation 7-5
Equation 7-6

$$\frac{\chi}{Q} = \frac{1}{U(3\pi\sigma_y\sigma_z)}$$

$$\frac{\chi}{Q} = \frac{1}{U\pi\Sigma_y\sigma_z}$$

where:

χ/Q is relative concentration, in sec/m^3,
π is 3.14159,
U is windspeed at 10 meters above plant grade, in m/sec,
σ_y is lateral plume spread, in meters, a function of atmospheric stability and distance (Figure 1, Reg Guide 1.145 [7.3.4]),
σ_z is vertical plume spread, in meters, a function of atmospheric stability and distance (Figure 2, Reg Guide 1.145 [7.3.4]),
Σ_y is lateral plume spread with meander and building wake effects, in m, = M σ_y, where M is determined from Figure 3, Reg Guide 1.145 [7.3.4], and
A is the smallest vertical-plane cross-sectional area of the structure (cross section of the MPC), m^2.

Equations 7-4 through 7-6 were solved using the parameters presented in Table 7.3.5. The atmospheric dispersion factor, χ/Q, at 100 meters was selected in accordance with the methodology described above. The χ/Q value used to determine the dose is 8.0×10^{-3} sec/m^3. This short term accident condition χ/Q is deemed conservative for an accident evaluation period of 30 days.

7.3.3.6 Dose Conversion Factors

Dose Conversion Factors (DCF) from EPA Federal Guidance Report No. 11, Table 2.1 [7.3.5] and EPA Federal Guidance Report No. 12, Table III.1 [7.3.6] were used for the analysis. The DCFs are provided on the spread sheets included as Appendix 7.A.

7.3.3.7 Occupancy Time

An occupancy time of 720 hours (30 days) is used for the analysis [7.0.2]. This conservatively assumes that the individual is exposed 24 hours per day for 30 days at the minimum controlled area boundary of 100 meters. The accident event duration is considered conservative as any accident condition of storage resulting in the failure of 100% of the stored fuel rods would be detected by the routine security and surveillance inspections and corrective actions would be completed prior to the end of this 30-day period.

7.3.3.8 Breathing Rate

A breathing rate of 3.3×10^{-4} m^3/sec for a worker is used for the analysis. This assumption is in

accordance with the guidance provided in NUREG-1536 [7.0.2] for a worker.

7.3.4 Postulated Accident Doses

The following doses to an individual at the site boundary (100 meters) as a result of an assumed effluent release under accident conditions of storage were determined; the inhaled committed dose equivalent for critical organs and tissues (gonad, breast, lung, red marrow, bone surface, thyroid, skin, lens of the eye), the effective dose from external submersion in the plume, and the resulting Total Effective Dose Equivalent (TEDE). These doses are determined for each type of MPC. The postulated doses as a result of exposure to soil with ground surface contamination and soil contaminated to a depth of 15 cm were also determined. The resultant doses were negligible compared to the those resulting from submersion in the plume and are therefore not reported.

The doses were determined using spreadsheet software. The resultant doses are summarized for each MPC type in Tables 7.3.2, 7.3.3, and 7.3.4 of the HI-STAR FSAR. Example spread sheets used for the dose estimates are presented in Appendix 7.A.

7.3.4.1 Whole Body Dose (Total Effective Dose Equivalent)

The whole body dose is the sum of the inhaled committed effective dose equivalent (CEDE) and the external exposure from submersion in the plume. The postulated doses were determined using spreadsheet software. Example spread sheets are provided in Appendix 7.A.

The CEDE is the product of radionuclide release rate, the atmospheric dispersion factor, the occupancy time, the breathing rate, and the effective dose conversion factor.

External exposure from submersion is the product of the nuclide release rate, the atmospheric dispersion factor, the occupancy time, and the effective dose conversion factor.

7.3.4.2 Critical Organ Dose

The dose to the critical organ (or tissue) is the sum of the committed dose equivalent to the critical organ or tissue from inhalation and the dose equivalent to the organ or tissue from submersion in the plume. The postulated doses as a result of exposure to soil with ground surface contamination and soil contaminated to a depth of 15 cm were also determined. The resultant doses were negligible compared to the those resulting from submersion in the plume and are therefore not reported.

The committed dose equivalent to the organ or tissue from inhalation is the product of radionuclide release rate, the atmospheric dispersion factor, the occupancy time, the breathing rate, and the organ/tissue dose conversion factor. The dose equivalent to the organ or tissue from submersion in the plume is the product of the nuclide release rate, the atmospheric dispersion factor, the occupancy time, and the organ/tissue dose conversion factor.

The dose to the lens of the eye as a result of submersion in the plume was estimated using guidance from Dr. James Turner in his book, Atoms, Radiation, and Radiation Protection [7.3.10]. Dr. Turner states that alpha particles and low-energy beta particles, such as those from tritium, cannot penetrate to the lens of the eye (at a depth of 3 mm). The discussion continues that many noble gases emit

photons and energetic beta particles, which in turn must be considered in the dose estimate. Dr. Turner states that the dose-equivalent rate to tissues near the surface of the body (e.g., lens of the eye) is more than 130 times the dose-equivalent rate in the lung from gases contained in the lung. Using the accident condition of storage for the MPC-68 (which is the highest dose to the lung), the estimated dose to the lung from gases in the lung is 5.34×10^{-4} mrem. Conservatively multiplying this value by 150, the estimated dose to the lens of the eye is 8.01×10^{-2} mrem. This estimated dose to the lens of the eye, 8.01×10^{-2} mrem, is a small fraction of the 15 rem limit imposed by 10 CFR 72.106(b).

7.3.5 Site Boundary

The estimated accident doses at the controlled area boundary are highest for the accident condition of storage for the MPC-68. The estimated TEDE (44.1 mrem) is a small fraction of the 5 rem whole body limit imposed by 10 CFR 72.106(b). The estimated bone surface dose which is the highest critical organ dose (468 mrem) is a small fraction of the 50 rem critical organ limit imposed by 10 CFR 72.106(b). Additionally, the shallow dose estimate to skin (0.17 mrem) is a small fraction of the 50 rem shallow dose equivalent to skin or other extremity limit imposed by 10 CFR 72.106(b).

7.3.6 Assumptions

The following presents a summary of assumptions for the accident condition confinement analysis of the HI-STAR 100 System.

- The distance from the cask to the site boundary is 100 meters.
- 100% of the fuel rods have ruptured. This assumption is conservative because it results in the greatest potential release of radioactive material.
- Unchoked flow correlations were used as the unchoked flow correlations better approximate the true measured flowrate for the leakage rates associated with transportation packages.
- For conservatism, the upstream pressure at test conditions (inside of the MPC) is assumed to be 2 atm and the down stream pressure (outside of the MPC) is assumed to be 1 atm.
- The temperature at test conditions is assumed to be equal to an ambient reference temperature, 212° F based on the maximum temperature achievable by the water in the MPC during performance of the leak test. This is conservative because the leak hole diameter computed from test conditions is larger.
- Bounding accident conditions (i.e., MPC cavity at design pressure (125 psig) at peak cladding temperature limit (570° C)) are postulated for this analysis.
- The capillary length required for Equation 2-3 was conservatively chosen to be smaller ofthe MPC lid closure weld sizes (MPC-24 and MPC-68, a=1.9 cm and MPC-68, a=3.2 cm) which is 1.9 cm. The shorter leak path assumption conservatively over estimates the leak rate in the thicker (MPC-68F) weld.

- The majority of the activity associated with crud is due to ^{60}Co. This assumption follows from the discussion provided in NUREG/CR-6487 [7.3.2].

- The accident condition leakage rate persists for 30 days without a decrease in the rate or nuclide concentration.

- The individual at the site boundary is exposed for 720 hours (30 days). This conservatively assumes that the individual is exposed 24 hours per day for 30 days.

- A breathing rate of 3.3×10^{-4} m^3/sec for a worker is used for the analysis [7.0.2]. This assumption is in accordance with the guidance provided in NUREG-1536 for a worker.

- All fuel stored in the MPC is of the design basis type with a bounding burnup and cooling time.

- In accordance with the International Commission on Radiological Protection (ICRP) Publication 30 [7.3.7 *"for exposure in radioisotopes of the noble gases, external irraditaion will be of such overridding importance that it alone need be considered."* Therefore, the contribution to the committed effective dose equivalent from ^{85}Kr is neglected.

- Exposure to dose conversion factors for inhalation reported in EPA Federal Guidance Report No. 11, Table 2.1 [7.3.5] were selected by lung clearance class which reports the most conservative values.

Table 7.3.1

Isotope Inventory and Release Fraction

Nuclide	MPC-24 Ci/Assembly	MPC-68 Ci/Assembly	MPC-68F Ci/Assembly	Release Fraction [7.3.2]
Gases				
^{3}H	2.21E+02	8.72E+01	1.76E+01	0.30
^{129}I	1.93E-02	7.72E-03	--	0.30
^{85}Kr	3.75E+03	1.43E+03	2.54E+02	0.30
Crud				
^{60}Co	2.18E+01	6.50E+01	1.18E+01	0.15 normal/off-normal 1.0 accident
Volatiles				
^{90}Sr	3.91E+04	1.52E+04	4.64E+03	2.0E-04
^{106}Ru	1.18E+04	4.16E+03	--	2.0E-04
^{134}Cs	1.90E+04	7.20E+03	2.96E+01	2.0E-04
^{137}Cs	5.77E+04	2.29E+04	7.21E+03	2.0E-04
Fines				
^{241}Pu	6.33E+04	2.10E+04	4.99E+03	3.0 E-05
^{90}Y	3.91E+04	1.52E+04	4.64E+03	3.0 E-05
^{147}Pm	2.48E+04	8.88E+03	1.24E+02	3.0 E-05
^{144}Ce	7.97E+03	2.46E+03	--	3.0 E-05
^{144}Pr	7.97E+03	2.46E+03	--	3.0 E-05
^{154}Eu	2.89E+03	1.07E+03	1.37E+02	3.0 E-05
^{244}Cm	2.06E+03	9.30E+02	1.50E+02	3.0 E-05
^{238}Pu	1.98E+03	7.49E+02	2.41E+02	3.0 E-05
^{125}Sb	1.57E+03	6.40E+02	--	3.0 E-05
^{155}Eu	8.53E+02	3.51E+02	2.01E+01	3.0 E-05

Table 7.3.1
(continued)

Isotope Inventory and Release Fractions

Nuclide	MPC-24 Ci/Assembly	MPC-68 Ci/Assembly	MPC-68F Ci/Assembly	Release Fraction [7.3.2]
^{241}Am	6.46E+02	2.20E+02	2.45E+02	3.0 E-05
^{125m}Te	3.84E+02	1.56E+02	--	3.0 E-05
^{240}Pu	3.06E+02	1.26E+02	6.42E+01	3.0 E-05
^{151}Sm	2.37E+02	--	2.67E+01	3.0 E-05
^{239}Pu	1.86E+02	6.16E+01	3.05E+01	3.0 E-05
^{137m}Ba	5.44E+04	2.16E+04	6.81E+03	3.0 E-05
^{106}Rh	1.18E+04	4.16E+03	--	3.0 E-05
^{144m}Pr	1.12E+02	--	--	3.0 E-05
^{243}Am	1.73E+01	7.39E+00	2.55E+00	3.0 E-05
^{242}Cm	1.54E+01	6.10E+00	7.91E-01	3.0 E-05
^{243}Cm	1.14E+01	4.81E+00	1.30E+00	3.0 E-05
^{239}Np	1.73E+01	7.39E+00	--	3.0 E-05
^{237}Np	2.02E-01	7.05E-02	2.72E-02	3.0 E-05
^{242}Pu	1.38E+00	5.95E-01	2.51E-01	3.0 E-05
^{242}Am	4.69E+00	1.69E+00	9.55E-01	3.0 E-05
^{242m}Am	4.72E+00	1.70E+00	9.59E-01	3.0 E-05

Note: The isotopes which contribute greater than 0.1% to the total curie inventory for the fuel assembly are considered in the evaluation as fines. The analysis also includes actinides as the dose conversion factors for these isotopes are in general, orders of magnitude greater than other isotopes (e.g., isotopes of plutonium, americium, curium, and neptunium were included regardless of their contribution to the inventory).

Table 7.3.2

MPC-24
Postulated Doses
To An Individual at the Controlled Area Boundary (100 meters)
As a Result of an Assumed Effluent Release

	Normal Conditions of Storage			Off-Normal Conditions of Storage			Accident Conditions of Storage		
Organ or Tissue	Dose from Inhalation [mrem/yr]	Dose from Submersion [mrem/yr]	Total [mrem/yr]	Dose from Inhalation [mrem/yr]	Dose from Submersion [mrem/yr]	Total [mrem/yr]	Dose from Inhalation [mrem*]	Dose from Submersion [mrem*]	Total [mrem*]
Gonad	1.35E-02	2.45E-04	1.37E-02	1.07E-01	2.71E-04	1.07E-01	6.22E+00	1.11E-02	6.23E+00
Breast	1.22E-02	2.77E-04	1.25E-02	1.48E-02	3.06E-04	1.51E-02	6.32E-01	1.26E-02	6.45E-01
Lung	2.80E-01	2.47E-04	2.80E-01	7.82E-01	2.72E-04	7.82E-01	4.15E+01	1.12E-02	4.15E+01
Red Marrow	6.62E-02	2.45E-04	6.64E-02	5.62E-01	2.69E-04	5.62E-01	3.27E+01	1.11E-02	3.27E+01
Bone Surface	6.87E-01	3.55E-04	6.87E-01	6.79E+00	3.99E-04	6.79E+00	3.98E+02	1.65E-02	3.98E+02
Thyroid	1.08E-02	2.53E-04	1.11E-02	1.35E-02	2.79E-04	1.38E-02	5.88E-01	1.15E-02	6.00E-01
Skin	N/A	3.80E-04	3.80E-04	N/A	1.23E-03	1.23E-03	N/A	6.62E-02	6.62E-02
Effective	8.23E-02	2.51E-04	**8.26E-02**	4.77E-01	2.77E-04	**4.77E-01**	2.72E+01	1.14E-02	**2.72E+01**

*The accident duration is 30 days.

Table 7.3.3

MPC-68
Postulated Doses
To An Individual at the Controlled Area Boundary (100 meters)
As a Result of an Assumed Effluent Release

	Normal Conditions of Storage			Off-Normal Conditions of Storage			Accident Conditions of Storage		
Organ or Tissue	Dose from Inhalation [mrem/yr]	Dose from Submersion [mrem/yr]	Total [mrem/yr]	Dose from Inhalation [mrem/yr]	Dose from Submersion [mrem/yr]	Total [mrem/yr]	Dose from Inhalation [mrem*]	Dose from Submersion [mrem*]	Total [mrem*]
Gonad	4.06E-02	2.24E-03	4.28E-02	1.50E-01	2.27E-03	1.52E-01	8.21E+00	8.92E-02	8.29E+00
Breast	1.11E-01	2.53E-03	1.14E-01	1.14E-01	2.56E-03	1.17E-01	4.51E+00	1.01E-01	4.61E+00
Lung	2.13E+00	2.26E-03	2.13E+00	2.73E+00	2.29E-03	2.73E+00	1.20E+02	8.99E-02	1.20E+02
Red Marrow	1.67E-01	2.24E-03	1.70E-01	7.47E-01	2.27E-03	7.49E-01	4.18E+01	8.91E-02	4.18E+01
Bone Surface	8.75E-01	3.24E-03	8.77E-01	8.02E+00	3.29E-03	8.02E+00	4.68E+02	1.30E-01	4.68E+02
Thyroid	9.75E-02	2.31E-03	9.98E-02	1.01E-01	2.34E-03	1.03E-01	4.01E+00	9.21E-02	4.10E+00
Skin	N/A	2.74E-03	2.74E-03	N/A	3.74E-03	3.74E-03	N/A	1.68E-01	1.68E-01
Effective	4.06E-01	2.29E-03	**4.08E-01**	8.70E-01	2.32E-03	**8.72E-01**	4.41E+01	9.14E-02	**4.41E+01**

*The accident duration is 30 days.

Table 7.3.4

MPC-68F
Postulated Doses
To An Individual at the Controlled Area Boundary (100 meters)
As a Result of an Assumed Effluent Release

	Normal Conditions of Storage			Off-Normal Conditions of Storage			Accident Conditions of Storage		
Organ or Tissue	Dose from Inhalation [mrem/yr]	Dose from Submersion [mrem/yr]	Total [mrem/yr]	Dose from Inhalation [mrem/yr]	Dose from Submersion [mrem/yr]	Total [mrem/yr]	Dose from Inhalation [mrem*]	Dose from Submersion [mrem*]	Total [mrem*]
Gonad	9.62E-03	4.06E-04	1.00E-02	4.33E-02	4.08E-04	4.37E-02	2.80E+00	1.60E-02	2.82E+00
Breast	2.01E-02	4.59E-04	2.06E-02	2.07E-02	4.62E-04	2.12E-02	8.22E-01	1.80E-02	8.40E-01
Lung	3.94E-01	4.09E-04	3.94E-01	5.65E-01	4.12E-04	5.65E-01	2.57E+01	1.61E-02	2.57E+01
Red Marrow	4.24E-02	4.06E-04	4.28E-02	2.25E-01	4.08E-04	2.25E-01	1.46E+01	1.59E-02	1.46E+01
Bone Surface	3.07E-01	5.87E-04	3.08E-01	2.56E+00	5.92E-04	2.56E+00	1.72E+02	2.31E-02	1.72E+02
Thyroid	1.77E-02	4.19E-04	1.81E-02	1.84E-02	4.22E-04	1.88E-02	7.29E-01	1.65E-02	7.45E-01
Skin	N/A	4.98E-04	4.98E-04	N/A	6.73E-04	6.73E-04	N/A	3.00E-02	3.00E-02
Effective	8.26E-02	4.16E-04	**8.30E-02**	2.26E-01	4.18E-04	**2.26E-01**	1.32E+01	1.63E-02	**1.32E+01**

*The accident duration is 30 days.

Table 7.3.5
χ/Q Parameters

Parameter	Value	Reference
U	1 m/s	NUREG-1536 [7.0.2]
σ_y	4.0 m	Figure 1, Reg Guide 1.145 [7.3.4]
σ_z	2.5 m	Figure 2, Reg Guide 1.145 [7.3.4]
$\Sigma_y = M\,\sigma_y$	16	M is determined from Figure 3, Reg Guide 1.145 [7.3.4]
A	8.41 m^2	Chapter 1, Section 1.5

Table 7.3.6

Parameters for Test and Hypothetical Accident Conditions

Parameter	Test	Normal/Off-Normal	Hypothetical Accident
P_u	2 ATM (min)	4.99 ATM	9.5 ATM
P_d	1 ATM	1 ATM	1 ATM
T	373 K	499.2 K	843 K
M	4 g/mol	4 g/mol	4 g/mol
u (helium)	0.0231 cP	0.0283 cP	0.0397 cP
a	1.9 cm	1.9 cm	1.9 cm

7.4 REGULATORY COMPLIANCE

Chapter 7 of this FSAR has been prepared to summarize the confinement features and capabilities of the HI-STAR 100 System. The confinement boundary of the HI-STAR 100 System is designed to provide confinement of radionuclides under normal, off-normal, and accident conditions. The evaluations presented in Chapter 7 provides detailed analyses of the confinement system to show that the radiological releases to the environment during normal storage conditions and from a non-mechanistic accident will be within the limits established by the regulations. The inert atmosphere in the MPC and the passive heat removal capabilities of the HI-STAR 100 assure that the SNF assemblies remain protected from degradation, which might otherwise lead to gross cladding ruptures during storage.

The confinement features and capabilities of the HI-STAR 100 System can be summarized in the following evaluation statements:

1. Section 2 of this FSAR describes confinement structures, systems, and components (SSCs) important to safety in sufficient detail to permit evaluation of their effectiveness.

2. The design of the HI-STAR 100 System adequately protects the spent fuel cladding against degradation that might otherwise lead to gross cladding ruptures. The spent fuel rods are protected from degradation by maintaining an inert gas atmosphere (helium) inside the MPC and keeping the fuel cladding temperatures below the design basis values specified in Chapter 2. Chapter 4 of the FSAR discusses the relevant temperature analyses.

3. The design of the HI-STAR 100 System provides redundant sealing of the confinement system closure joints by the combination of the welded MPC lid, vent and drain port cover plates, and MPC closure ring. The MPC lid has a recess around the perimeter for installation of the closure ring. The MPC closure ring is welded to the MPC lid on the inner diameter of the ring and to the MPC shell on the outer diameter, thereby covering the vent and drain port cover plates, and the MPC lid-to-shell weld.

4. The confinement system is not required to be monitored.

5. The quantity of radionuclides postulated to be released to the environment is discussed in Section 7.2.6, 7.3.1 and 7.3.2 and is summarized in Table 7.3.1. Chapter 7 demonstrates that the incremental dose at the minimum controlled area boundary due to an atmospheric release resulting from leakage from the confinement boundary results in a minor contribution to the annual dose limit in effluents and direct radiation during normal operations or anticipated occurrences which meets the requirements in 10CFR72.104(a) [7.0.1]. The annual dose from normal and off-normal storage operations is provided in Table 7.3.2, 7.3.3 and 7.3.4 and reported in Chapter 10. The potential dose to an individual located at the minimum controlled area boundary (100 meters) from a non-mechanistic accident event is determined for each type of MPC and is summarized in Tables 7.3.2, 7.3.3 and 7.3.4. The licensee is required to perform a site-specific dose evaluation as part of the ISFSI design as dictated in 10CFR72.212 and Chapter 12 to demonstrate compliance with 10CFR72.104. The licensee's evaluation will account for the location of the controlled area boundary, ISFSI size and

configuration, fuel assembly specifics, and the effects of radiation from other on-site operations. Chapter 11 presents the results of the evaluations performed to demonstrate that the HI-STAR 100 System can withstand the effects of all credible accident conditions and natural phenomena with minimal contribution to the site boundary dose. Chapter 5 demonstrates that the direct radiation doses that result from the loss of the neutron shield are far below the requirements of 10CFR72.106. These doses combined with the doses presented in Chapter 7, satisfy the regulatory requirement of 10CFR72.106. The licensee is responsible for demonstrating site-specific compliance with 10CFR72.106.

6. The HI-STAR 100 System confinement boundary is designed and fabricated in accordance with the ASME Code, Section III, Subsection NB to the maximum extent practicable. Chapter 2 provides design criteria for the confinement design. Table 2.2.7 provides applicable Code requirements. Exceptions to specific Code requirements with complete justifications are presented in Table 2.2.15. The structural adequacy of the MPC is demonstrated by the analyses documented in Chapter 3. The HI-STAR 100 System confinement boundary is adequately designed to maintain confinement of all radionuclides under normal, off-normal and accident conditions.

7. The design of the confinement system of the HI-STAR 100 is in compliance with 10CFR72 and the applicable design and acceptance criteria are satisfied. The evaluation of the confinement system design provides reasonable assurance that the HI-STAR 100 System will allow the long term, safe storage of spent fuel.

7.5 REFERENCES

[7.0.1] 10CFR72, Licensing Requirements for the Independent Storage of Spent Nuclear Fuel and High-Level Radioactive Waste.

[7.0.2] NUREG-1536, "Standard Review Plan for Dry Cask Storage Systems", January, 1997.

[7.1.1] American Society of Mechanical Engineers (ASME), Boiler and Pressure Vessel Code, Section III, Division 1, Subsection NB, Class 1 Components, 1995 Edition.

[7.1.2] HI-STAR 100 Safety Analysis Report, Holtec International Report No. HI-951251, most current revision.

[7.3.1] Deleted.

[7.3.2] Anderson, B.L. et al. *Containment Analysis for Type B Packages Used to Transport Various Contents.* NUREG/CR-6487, UCRL-ID-124822. Lawrence Livermore National Laboratory, November 1996.

[7.3.3] Shleien, B, *The Health Physics and Radiological Health Handbook*, Scinta, Inc. Silver Spring, MD, 1992.

[7.3.4] U.S. Nuclear Regulatory Commission, "Atmospheric Dispersion Models for Potential Accident Consequence Assessments at Nuclear Power Plants," Regulatory Guide 1.145, November 1982.

[7.3.5] U.S. EPA, Federal Guidance Report No. 11, *Limiting Values of Radionuclide Intake and Air Concentration and Dose Conversion Factors for Inhalation, Submersion, and Ingestion*, DE89-011065, 1988.

[7.3.6] U.S. EPA, Federal Guidance Report No. 12, *External Exposure to Radionuclides in Air, Water, and Soil*, EPA 402-R-93-081, 1993.

[7.3.7] International Commission on Radiological Protection, Limits for Intakes of Radionuclides by Workers, ICRP Publication 30, Part 1; Pergamon Press; Oxford; 1978.

[7.3.8] ANSI N14.5-1997. "American National Standard for Radioactive Material Leakage Tests on Packages for Shipment."

[7.3.9] Rosenhow, W.M.. and Hartnett, J.P., *Handbook of Heat Transfer*, McGraw Hill Book Company, New York, 1973.

[7.3.10] Turner, James E. *Atoms, Radiation , and Radiation Protection*, McGraw Hill Book Company, New York, 1992.

APPENDIX 7.A

EXAMPLE DOSE CALCULATIONS FOR NORMAL, OFF-NORMAL, AND ACCIDENT CONDITIONS OF STORAGE

MPC-68, Normal Conditions of Storage, Dose from Inhalation: 7 pages
MPC-68, Off-Normal Conditions of Storage, Dose from Inhalation: 7 pages
MPC-68, Accident Conditions of Storage, Dose from Inhalation: 7 pages

MPC-68, Normal Conditions of Storage, Dose from Submersion: 8 pages
MPC-68, Off-Normal Conditions of Storage, Dose from Submersion: 8 pages
MPC-68, Accident Conditions of Storage, Dose from Submersion: 8 pages

MPC-68														
Normal Conditions														
Committed Effective Dose Equivalent From Inhalation														
Nuclide	Inventory (Ci/Assy)	1% for normal storage	No. Assy	MPC Vol (cm3)	L_{nor} Rate at Upstream (cm3/s)	Fraction Released per sec	Release Fraction	Release Rate (Ci/sec)	X/Q (sec/m3)	Breathing Rate (m3/sec)	DCF (Sv/Bq)	DCF (mRem/uCi)	Occ Time (sec)	CEDE (mRem)
								Gases						
H-3	8.72E+01	1.00E-02	68	5.99E+06	8.80E-06	1.47E-12	0.30	2.61E-11	1.60E-04	3.30E-04	1.73E-11	6.40E-02	3.15E+07	2.78E-06
I-129	7.72E-03	1.00E-02	68	5.99E+06	8.80E-06	1.47E-12	0.30	2.31E-15	1.60E-04	3.30E-04	8.69E-11	3.22E-01	3.15E+07	1.24E-09
Kr-85	1.43E+03	1.00E-02	68	5.99E+06	8.80E-06	1.47E-12	0.30	4.29E-10	1.60E-04	3.30E-04	0.00E+00	0.00E+00	3.15E+07	0.00E+00
								Crud						
Co-60	6.50E+01	1.00E+00	68	5.99E+06	8.80E-06	1.47E-12	0.15	9.74E-10	1.60E-04	3.30E-04	4.76E-09	1.76E+01	3.15E+07	2.85E-02
								Volatiles						
Sr-90	1.52E+04	1.00E-02	68	5.99E+06	8.80E-06	1.47E-12	2.00E-04	3.04E-12	1.60E-04	3.30E-04	2.69E-10	9.95E-01	3.15E+07	5.03E-06
Ru-106	4.16E+03	1.00E-02	68	5.99E+06	8.80E-06	1.47E-12	2.00E-04	8.31E-13	1.60E-04	3.30E-04	1.30E-09	4.81E+00	3.15E+07	6.65E-06
Cs-134	7.20E+03	1.00E-02	68	5.99E+06	8.80E-06	1.47E-12	2.00E-04	1.44E-12	1.60E-04	3.30E-04	1.30E-08	4.81E+01	3.15E+07	1.15E-04
Cs-137	2.29E+04	1.00E-02	68	5.99E+06	8.80E-06	1.47E-12	2.00E-04	4.58E-12	1.60E-04	3.30E-04	8.76E-09	3.24E+01	3.15E+07	2.47E-04
								Fines						
PU241	2.10E+04	1.00E-02	68	5.99E+06	8.80E-06	1.47E-12	3.00E-05	6.29E-13	1.60E-04	3.30E-04	6.82E-07	2.52E+03	3.15E+07	2.64E-03
Y 90	1.52E+04	1.00E-02	68	5.99E+06	8.80E-06	1.47E-12	3.00E-05	4.56E-13	1.60E-04	3.30E-04	9.52E-12	3.52E-02	3.15E+07	2.67E-08
PM147	8.88E+03	1.00E-02	68	5.99E+06	8.80E-06	1.47E-12	3.00E-05	2.66E-13	1.60E-04	3.30E-04	8.25E-15	3.05E-05	3.15E+07	1.35E-11
CE144	2.46E+03	1.00E-02	68	5.99E+06	8.80E-06	1.47E-12	3.00E-05	7.37E-14	1.60E-04	3.30E-04	1.93E-09	7.14E+00	3.15E+07	8.76E-07
PR144	2.46E+03	1.00E-02	68	5.99E+06	8.80E-06	1.47E-12	3.00E-05	7.37E-14	1.60E-04	3.30E-04	2.41E-15	8.92E-06	3.15E+07	1.09E-12
EU154	1.07E+03	1.00E-02	68	5.99E+06	8.80E-06	1.47E-12	3.00E-05	3.21E-14	1.60E-04	3.30E-04	1.17E-08	4.33E+01	3.15E+07	2.31E-06
CM244	9.30E+02	1.00E-02	68	5.99E+06	8.80E-06	1.47E-12	3.00E-05	2.79E-14	1.60E-04	3.30E-04	1.59E-05	5.88E+04	3.15E+07	2.73E-03
PU238	7.49E+02	1.00E-02	68	5.99E+06	8.80E-06	1.47E-12	3.00E-05	2.24E-14	1.60E-04	3.30E-04	2.80E-05	1.04E+05	3.15E+07	3.87E-03
SB125	6.40E+02	1.00E-02	68	5.99E+06	8.80E-06	1.47E-12	3.00E-05	1.92E-14	1.60E-04	3.30E-04	3.60E-10	1.33E+00	3.15E+07	4.25E-08
EU155	3.51E+02	1.00E-02	68	5.99E+06	8.80E-06	1.47E-12	3.00E-05	1.05E-14	1.60E-04	3.30E-04	3.56E-10	1.32E+00	3.15E+07	2.30E-08
AM241	2.20E+02	1.00E-02	68	5.99E+06	8.80E-06	1.47E-12	3.00E-05	6.59E-15	1.60E-04	3.30E-04	3.25E-05	1.20E+05	3.15E+07	1.32E-03
TE125M	1.56E+02	1.00E-02	68	5.99E+06	8.80E-06	1.47E-12	3.00E-05	4.68E-15	1.60E-04	3.30E-04	1.24E-10	4.59E-01	3.15E+07	3.57E-09
PU240	1.26E+02	1.00E-02	68	5.99E+06	8.80E-06	1.47E-12	3.00E-05	3.78E-15	1.60E-04	3.30E-04	3.18E-05	1.18E+05	3.15E+07	7.39E-04
151Sm	0.00E+00	1.00E-02	68	5.99E+06	8.80E-06	1.47E-12	3.00E-05	0.00E+00	1.60E-04	3.30E-04	4.03E-14	1.49E-04	3.15E+07	0.00E+00
239Pu	6.16E+01	1.00E-02	68	5.99E+06	8.80E-06	1.47E-12	3.00E-05	1.85E-15	1.60E-04	3.30E-04	3.18E-05	1.18E+05	3.15E+07	3.61E-04
137mBa	2.16E+04	1.00E-02	68	5.99E+06	8.80E-06	1.47E-12	3.00E-05	6.47E-13	1.60E-04	3.30E-04	0.00E+00	0.00E+00	3.15E+07	0.00E+00
106Rh	4.16E+03	1.00E-02	68	5.99E+06	8.80E-06	1.47E-12	3.00E-05	1.25E-13	1.60E-04	3.30E-04	0.00E+00	0.00E+00	3.15E+07	0.00E+00
144mPr	0.00E+00	1.00E-02	68	5.99E+06	8.80E-06	1.47E-12	3.00E-05	0.00E+00	1.60E-04	3.30E-04	0.00E+00	0.00E+00	3.15E+07	0.00E+00
243Am	7.39E+00	1.00E-02	68	5.99E+06	8.80E-06	1.47E-12	3.00E-05	2.21E-16	1.60E-04	3.30E-04	3.26E-05	1.21E+05	3.15E+07	4.44E-05
242Cm	6.10E+00	1.00E-02	68	5.99E+06	8.80E-06	1.47E-12	3.00E-05	1.83E-16	1.60E-04	3.30E-04	5.70E-07	2.11E+03	3.15E+07	6.41E-07
243Cm	4.81E+00	1.00E-02	68	5.99E+06	8.80E-06	1.47E-12	3.00E-05	1.44E-16	1.60E-04	3.30E-04	2.07E-05	7.66E+04	3.15E+07	1.84E-05
239Np	7.39E+00	1.00E-02	68	5.99E+06	8.80E-06	1.47E-12	3.00E-05	2.21E-16	1.60E-04	3.30E-04	7.45E-11	2.76E-01	3.15E+07	1.02E-10
237Np	7.05E-02	1.00E-02	68	5.99E+06	8.80E-06	1.47E-12	3.00E-05	2.11E-18	1.60E-04	3.30E-04	2.96E-05	1.10E+05	3.15E+07	3.85E-07
242Pu	5.95E-01	1.00E-02	68	5.99E+06	8.80E-06	1.47E-12	3.00E-05	1.78E-17	1.60E-04	3.30E-04	3.02E-05	1.12E+05	3.15E+07	3.31E-06
242Am	1.69E+00	1.00E-02	68	5.99E+06	8.80E-06	1.47E-12	3.00E-05	5.06E-17	1.60E-04	3.30E-04	1.94E-09	7.18E+00	3.15E+07	6.05E-10
242mAm	1.70E+00	1.00E-02	68	5.99E+06	8.80E-06	1.47E-12	3.00E-05	5.09E-17	1.60E-04	3.30E-04	3.21E-05	1.19E+05	3.15E+07	1.01E-05
													Total	4.06E-02

MPC-68														
Normal Conditions														
Committed Effective Dose Equivalent From Inhalation														
Nuclide	Inventory (Ci/Assy)	1% for normal storage	No. Assy	MPC Vol (cm3)	L_{nor} Rate at Upstream (cm3/s)	Fraction Released per sec	Release Fraction	Release Rate (Ci/sec)	X/Q (sec/m3)	Breathing Rate (m3/sec)	DCF (Sv/Bq)	DCF (mRem/uCi)	Occ Time (sec)	CEDE (mRem)
								Gases						
H-3	8.72E+01	1.00E-02	68	5.99E+06	8.80E-06	1.47E-12	0.30	2.61E-11	1.60E-04	3.30E-04	1.73E-11	6.40E-02	3.15E+07	2.78E-06
I-129	7.72E-03	1.00E-02	68	5.99E+06	8.80E-06	1.47E-12	0.30	2.31E-15	1.60E-04	3.30E-04	2.09E-10	7.73E-01	3.15E+07	2.98E-09
Kr-85	1.43E+03	1.00E-02	68	5.99E+06	8.80E-06	1.47E-12	0.30	4.29E-10	1.60E-04	3.30E-04	0.00E+00	0.00E+00	3.15E+07	0.00E+00
								Crud						
Co-60	6.50E+01	1.00E+00	68	5.99E+06	8.80E-06	1.47E-12	0.15	9.74E-10	1.60E-04	3.30E-04	1.84E-08	6.81E+01	3.15E+07	1.10E-01
								Volatiles						
Sr-90	1.52E+04	1.00E-02	68	5.99E+06	8.80E-06	1.47E-12	2.00E-04	3.04E-12	1.60E-04	3.30E-04	2.69E-10	9.95E-01	3.15E+07	5.03E-06
Ru-106	4.16E+03	1.00E-02	68	5.99E+06	8.80E-06	1.47E-12	2.00E-04	8.31E-13	1.60E-04	3.30E-04	1.78E-09	6.59E+00	3.15E+07	9.10E-06
Cs-134	7.20E+03	1.00E-02	68	5.99E+06	8.80E-06	1.47E-12	2.00E-04	1.44E-12	1.60E-04	3.30E-04	1.08E-08	4.00E+01	3.15E+07	9.56E-05
Cs-137	2.29E+04	1.00E-02	68	5.99E+06	8.80E-06	1.47E-12	2.00E-04	4.58E-12	1.60E-04	3.30E-04	7.84E-09	2.90E+01	3.15E+07	2.21E-04
								Fines						
PU241	2.10E+04	1.00E-02	68	5.99E+06	8.80E-06	1.47E-12	3.00E-05	6.29E-13	1.60E-04	3.30E-04	3.06E-11	1.13E-01	3.15E+07	1.19E-07
Y 90	1.52E+04	1.00E-02	68	5.99E+06	8.80E-06	1.47E-12	3.00E-05	4.56E-13	1.60E-04	3.30E-04	9.52E-12	3.52E-02	3.15E+07	2.67E-08
PM147	8.88E+03	1.00E-02	68	5.99E+06	8.80E-06	1.47E-12	3.00E-05	2.66E-13	1.60E-04	3.30E-04	3.60E-14	1.33E-04	3.15E+07	5.90E-11
CE144	2.46E+03	1.00E-02	68	5.99E+06	8.80E-06	1.47E-12	3.00E-05	7.37E-14	1.60E-04	3.30E-04	1.97E-09	7.29E+00	3.15E+07	8.94E-07
PR144	2.46E+03	1.00E-02	68	5.99E+06	8.80E-06	1.47E-12	3.00E-05	7.37E-14	1.60E-04	3.30E-04	1.05E-14	3.89E-05	3.15E+07	4.76E-12
EU154	1.07E+03	1.00E-02	68	5.99E+06	8.80E-06	1.47E-12	3.00E-05	3.21E-14	1.60E-04	3.30E-04	1.55E-08	5.74E+01	3.15E+07	3.06E-06
CM244	9.30E+02	1.00E-02	68	5.99E+06	8.80E-06	1.47E-12	3.00E-05	2.79E-14	1.60E-04	3.30E-04	1.04E-09	3.85E+00	3.15E+07	1.78E-07
PU238	7.49E+02	1.00E-02	68	5.99E+06	8.80E-06	1.47E-12	3.00E-05	2.24E-14	1.60E-04	3.30E-04	1.00E-09	3.70E+00	3.15E+07	1.38E-07
SB125	6.40E+02	1.00E-02	68	5.99E+06	8.80E-06	1.47E-12	3.00E-05	1.92E-14	1.60E-04	3.30E-04	4.16E-10	1.54E+00	3.15E+07	4.91E-08
EU155	3.51E+02	1.00E-02	68	5.99E+06	8.80E-06	1.47E-12	3.00E-05	1.05E-14	1.60E-04	3.30E-04	6.14E-10	2.27E+00	3.15E+07	3.97E-08
AM241	2.20E+02	1.00E-02	68	5.99E+06	8.80E-06	1.47E-12	3.00E-05	6.59E-15	1.60E-04	3.30E-04	2.67E-09	9.88E+00	3.15E+07	1.08E-07
TE125M	1.56E+02	1.00E-02	68	5.99E+06	8.80E-06	1.47E-12	3.00E-05	4.68E-15	1.60E-04	3.30E-04	1.07E-10	3.96E-01	3.15E+07	3.08E-09
PU240	1.26E+02	1.00E-02	68	5.99E+06	8.80E-06	1.47E-12	3.00E-05	3.78E-15	1.60E-04	3.30E-04	9.51E-10	3.52E+00	3.15E+07	2.21E-08
151Sm	0.00E+00	1.00E-02	68	5.99E+06	8.80E-06	1.47E-12	3.00E-05	0.00E+00	1.60E-04	3.30E-04	1.49E-13	5.51E-04	3.15E+07	0.00E+00
239Pu	6.16E+01	1.00E-02	68	5.99E+06	8.80E-06	1.47E-12	3.00E-05	1.85E-15	1.60E-04	3.30E-04	9.22E-10	3.41E+00	3.15E+07	1.05E-08
137mBa	2.16E+04	1.00E-02	68	5.99E+06	8.80E-06	1.47E-12	3.00E-05	6.47E-13	1.60E-04	3.30E-04	0.00E+00	0.00E+00	3.15E+07	0.00E+00
106Rh	4.16E+03	1.00E-02	68	5.99E+06	8.80E-06	1.47E-12	3.00E-05	1.25E-13	1.60E-04	3.30E-04	0.00E+00	0.00E+00	3.15E+07	0.00E+00
144mPr	0.00E+00	1.00E-02	68	5.99E+06	8.80E-06	1.47E-12	3.00E-05	0.00E+00	1.60E-04	3.30E-04	0.00E+00	0.00E+00	3.15E+07	0.00E+00
243Am	7.39E+00	1.00E-02	68	5.99E+06	8.80E-06	1.47E-12	3.00E-05	2.21E-16	1.60E-04	3.30E-04	1.52E-08	5.62E+01	3.15E+07	2.07E-08
242Cm	6.10E+00	1.00E-02	68	5.99E+06	8.80E-06	1.47E-12	3.00E-05	1.83E-16	1.60E-04	3.30E-04	9.44E-10	3.49E+00	3.15E+07	1.06E-09
243Cm	4.81E+00	1.00E-02	68	5.99E+06	8.80E-06	1.47E-12	3.00E-05	1.44E-16	1.60E-04	3.30E-04	6.29E-09	2.33E+01	3.15E+07	5.58E-09
239Np	7.39E+00	1.00E-02	68	5.99E+06	8.80E-06	1.47E-12	3.00E-05	2.21E-16	1.60E-04	3.30E-04	1.63E-11	6.03E-02	3.15E+07	2.22E-11
237Np	7.05E-02	1.00E-02	68	5.99E+06	8.80E-06	1.47E-12	3.00E-05	2.11E-18	1.60E-04	3.30E-04	1.69E-08	6.25E+01	3.15E+07	2.20E-10
242Pu	5.95E-01	1.00E-02	68	5.99E+06	8.80E-06	1.47E-12	3.00E-05	1.78E-17	1.60E-04	3.30E-04	9.45E-10	3.50E+00	3.15E+07	1.04E-10
242Am	1.69E+00	1.00E-02	68	5.99E+06	8.80E-06	1.47E-12	3.00E-05	5.06E-17	1.60E-04	3.30E-04	2.49E-12	9.21E-03	3.15E+07	7.76E-13
242mAm	1.70E+00	1.00E-02	68	5.99E+06	8.80E-06	1.47E-12	3.00E-05	5.09E-17	1.60E-04	3.30E-04	1.38E-09	5.11E+00	3.15E+07	4.33E-10
													Total	1.11E-01

MPC-68														
Normal Conditions														
Committed Effective Dose Equivalent From Inhalation														
Nuclide	Inventory (Ci/Assy)	1% for normal storage	No. Assy	MPC Vol (cm3)	L_{nor} Rate at Upstream (cm3/s)	Fraction Released per sec	Release Fraction	Release Rate (Ci/sec)	X/Q (sec/m3)	Breathing Rate (m3/sec)	DCF (Sv/Bq)	DCF (mRem/uCi)	Occ Time (sec)	CEDE (mRem)
								Gases						
H-3	8.72E+01	1.00E-02	68	5.99E+06	8.80E-06	1.47E-12	0.30	2.61E-11	1.60E-04	3.30E-04	1.73E-11	6.40E-02	3.15E+07	2.78E-06
I-129	7.72E-03	1.00E-02	68	5.99E+06	8.80E-06	1.47E-12	0.30	2.31E-15	1.60E-04	3.30E-04	3.14E-10	1.16E+00	3.15E+07	4.47E-09
Kr-85	1.43E+03	1.00E-02	68	5.99E+06	8.80E-06	1.47E-12	0.30	4.29E-10	1.60E-04	3.30E-04	0.00E+00	0.00E+00	3.15E+07	0.00E+00
								Crud						
Co-60	6.50E+01	1.00E+00	68	5.99E+06	8.80E-06	1.47E-12	0.15	9.74E-10	1.60E-04	3.30E-04	3.45E-07	1.28E+03	3.15E+07	2.07E+00
								Volatiles						
Sr-90	1.52E+04	1.00E-02	68	5.99E+06	8.80E-06	1.47E-12	2.00E-04	3.04E-12	1.60E-04	3.30E-04	2.86E-06	1.06E+04	3.15E+07	5.35E-02
Ru-106	4.16E+03	1.00E-02	68	5.99E+06	8.80E-06	1.47E-12	2.00E-04	8.31E-13	1.60E-04	3.30E-04	1.04E-06	3.85E+03	3.15E+07	5.32E-03
Cs-134	7.20E+03	1.00E-02	68	5.99E+06	8.80E-06	1.47E-12	2.00E-04	1.44E-12	1.60E-04	3.30E-04	1.18E-08	4.37E+01	3.15E+07	1.04E-04
Cs-137	2.29E+04	1.00E-02	68	5.99E+06	8.80E-06	1.47E-12	2.00E-04	4.58E-12	1.60E-04	3.30E-04	8.82E-09	3.26E+01	3.15E+07	2.48E-04
								Fines						
PU241	2.10E+04	1.00E-02	68	5.99E+06	8.80E-06	1.47E-12	3.00E-05	6.29E-13	1.60E-04	3.30E-04	7.42E-09	2.75E+01	3.15E+07	2.87E-05
Y 90	1.52E+04	1.00E-02	68	5.99E+06	8.80E-06	1.47E-12	3.00E-05	4.56E-13	1.60E-04	3.30E-04	8.89E-09	3.29E+01	3.15E+07	2.49E-05
PM147	8.88E+03	1.00E-02	68	5.99E+06	8.80E-06	1.47E-12	3.00E-05	2.66E-13	1.60E-04	3.30E-04	7.74E-08	2.86E+02	3.15E+07	1.27E-04
CE144	2.46E+03	1.00E-02	68	5.99E+06	8.80E-06	1.47E-12	3.00E-05	7.37E-14	1.60E-04	3.30E-04	1.83E-07	6.77E+02	3.15E+07	8.30E-05
PR144	2.46E+03	1.00E-02	68	5.99E+06	8.80E-06	1.47E-12	3.00E-05	7.37E-14	1.60E-04	3.30E-04	9.40E-11	3.48E-01	3.15E+07	4.26E-08
EU154	1.07E+03	1.00E-02	68	5.99E+06	8.80E-06	1.47E-12	3.00E-05	3.21E-14	1.60E-04	3.30E-04	7.92E-08	2.93E+02	3.15E+07	1.56E-05
CM244	9.30E+02	1.00E-02	68	5.99E+06	8.80E-06	1.47E-12	3.00E-05	2.79E-14	1.60E-04	3.30E-04	1.93E-05	7.14E+04	3.15E+07	3.31E-03
PU238	7.49E+02	1.00E-02	68	5.99E+06	8.80E-06	1.47E-12	3.00E-05	2.24E-14	1.60E-04	3.30E-04	1.84E-05	6.81E+04	3.15E+07	2.54E-03
SB125	6.40E+02	1.00E-02	68	5.99E+06	8.80E-06	1.47E-12	3.00E-05	1.92E-14	1.60E-04	3.30E-04	2.17E-08	8.03E+01	3.15E+07	2.56E-06
EU155	3.51E+02	1.00E-02	68	5.99E+06	8.80E-06	1.47E-12	3.00E-05	1.05E-14	1.60E-04	3.30E-04	1.19E-08	4.40E+01	3.15E+07	7.70E-07
AM241	2.20E+02	1.00E-02	68	5.99E+06	8.80E-06	1.47E-12	3.00E-05	6.59E-15	1.60E-04	3.30E-04	1.84E-05	6.81E+04	3.15E+07	7.47E-04
TE125M	1.56E+02	1.00E-02	68	5.99E+06	8.80E-06	1.47E-12	3.00E-05	4.68E-15	1.60E-04	3.30E-04	4.66E-10	1.72E+00	3.15E+07	1.34E-08
PU240	1.26E+02	1.00E-02	68	5.99E+06	8.80E-06	1.47E-12	3.00E-05	3.78E-15	1.60E-04	3.30E-04	1.73E-05	6.40E+04	3.15E+07	4.02E-04
151Sm	0.00E+00	1.00E-02	68	5.99E+06	8.80E-06	1.47E-12	3.00E-05	0.00E+00	1.60E-04	3.30E-04	3.26E-09	1.21E+01	3.15E+07	0.00E+00
239Pu	6.16E+01	1.00E-02	68	5.99E+06	8.80E-06	1.47E-12	3.00E-05	1.85E-15	1.60E-04	3.30E-04	1.73E-05	6.40E+04	3.15E+07	1.97E-04
137mBa	2.16E+04	1.00E-02	68	5.99E+06	8.80E-06	1.47E-12	3.00E-05	6.47E-13	1.60E-04	3.30E-04	0.00E+00	0.00E+00	3.15E+07	0.00E+00
106Rh	4.16E+03	1.00E-02	68	5.99E+06	8.80E-06	1.47E-12	3.00E-05	1.25E-13	1.60E-04	3.30E-04	0.00E+00	0.00E+00	3.15E+07	0.00E+00
144mPr	0.00E+00	1.00E-02	68	5.99E+06	8.80E-06	1.47E-12	3.00E-05	0.00E+00	1.60E-04	3.30E-04	0.00E+00	0.00E+00	3.15E+07	0.00E+00
243Am	7.39E+00	1.00E-02	68	5.99E+06	8.80E-06	1.47E-12	3.00E-05	2.21E-16	1.60E-04	3.30E-04	1.78E-05	6.59E+04	3.15E+07	2.43E-05
242Cm	6.10E+00	1.00E-02	68	5.99E+06	8.80E-06	1.47E-12	3.00E-05	1.83E-16	1.60E-04	3.30E-04	1.55E-05	5.74E+04	3.15E+07	1.74E-05
243Cm	4.81E+00	1.00E-02	68	5.99E+06	8.80E-06	1.47E-12	3.00E-05	1.44E-16	1.60E-04	3.30E-04	1.94E-05	7.18E+04	3.15E+07	1.72E-05
239Np	7.39E+00	1.00E-02	68	5.99E+06	8.80E-06	1.47E-12	3.00E-05	2.21E-16	1.60E-04	3.30E-04	2.36E-09	8.73E+00	3.15E+07	3.22E-09
237Np	7.05E-02	1.00E-02	68	5.99E+06	8.80E-06	1.47E-12	3.00E-05	2.11E-18	1.60E-04	3.30E-04	1.61E-05	5.96E+04	3.15E+07	2.09E-07
242Pu	5.95E-01	1.00E-02	68	5.99E+06	8.80E-06	1.47E-12	3.00E-05	1.78E-17	1.60E-04	3.30E-04	1.64E-05	6.07E+04	3.15E+07	1.80E-06
242Am	1.69E+00	1.00E-02	68	5.99E+06	8.80E-06	1.47E-12	3.00E-05	5.06E-17	1.60E-04	3.30E-04	5.20E-08	1.92E+02	3.15E+07	1.62E-08
242mAm	1.70E+00	1.00E-02	68	5.99E+06	8.80E-06	1.47E-12	3.00E-05	5.09E-17	1.60E-04	3.30E-04	4.20E-06	1.55E+04	3.15E+07	1.32E-06
													Total	2.13E+00

MPC-68														
Normal Conditions														
Committed Effective Dose Equivalent From Inhalation														
Nuclide	Inventory (Ci/Assy)	1% for normal storage	No. Assy	MPC Vol (cm3)	L_{nor} Rate at Upstream (cm3/s)	Fraction Released per sec	Release Fraction	Release Rate (Ci/sec)	X/Q (sec/m3)	Breathing Rate (m3/sec)	DCF (Sv/Bq)	DCF (mRem/uCi)	Occ Time (sec)	CEDE (mRem)
								Gases						
H-3	8.72E+01	1.00E-02	68	5.99E+06	8.80E-06	1.47E-12	0.30	2.61E-11	1.60E-04	3.30E-04	1.73E-11	6.40E-02	3.15E+07	2.78E-06
I-129	7.72E-03	1.00E-02	68	5.99E+06	8.80E-06	1.47E-12	0.30	2.31E-15	1.60E-04	3.30E-04	1.40E-10	5.18E-01	3.15E+07	1.99E-09
Kr-85	1.43E+03	1.00E-02	68	5.99E+06	8.80E-06	1.47E-12	0.30	4.29E-10	1.60E-04	3.30E-04	0.00E+00	0.00E+00	3.15E+07	0.00E+00
								Crud						
Co-60	6.50E+01	1.00E+00	68	5.99E+06	8.80E-06	1.47E-12	0.15	9.74E-10	1.60E-04	3.30E-04	1.72E-08	6.36E+01	3.15E+07	1.03E-01
								Volatiles						
Sr-90	1.52E+04	1.00E-02	68	5.99E+06	8.80E-06	1.47E-12	2.00E-04	3.04E-12	1.60E-04	3.30E-04	3.28E-08	1.21E+02	3.15E+07	6.13E-04
Ru-106	4.16E+03	1.00E-02	68	5.99E+06	8.80E-06	1.47E-12	2.00E-04	8.31E-13	1.60E-04	3.30E-04	1.76E-09	6.51E+00	3.15E+07	9.00E-06
Cs-134	7.20E+03	1.00E-02	68	5.99E+06	8.80E-06	1.47E-12	2.00E-04	1.44E-12	1.60E-04	3.30E-04	1.18E-08	4.37E+01	3.15E+07	1.04E-04
Cs-137	2.29E+04	1.00E-02	68	5.99E+06	8.80E-06	1.47E-12	2.00E-04	4.58E-12	1.60E-04	3.30E-04	8.30E-09	3.07E+01	3.15E+07	2.34E-04
								Fines						
PU241	2.10E+04	1.00E-02	68	5.99E+06	8.80E-06	1.47E-12	3.00E-05	6.29E-13	1.60E-04	3.30E-04	3.36E-06	1.24E+04	3.15E+07	1.30E-02
Y 90	1.52E+04	1.00E-02	68	5.99E+06	8.80E-06	1.47E-12	3.00E-05	4.56E-13	1.60E-04	3.30E-04	2.79E-10	1.03E+00	3.15E+07	7.82E-07
PM147	8.88E+03	1.00E-02	68	5.99E+06	8.80E-06	1.47E-12	3.00E-05	2.66E-13	1.60E-04	3.30E-04	1.61E-09	5.96E+00	3.15E+07	2.64E-06
CE144	2.46E+03	1.00E-02	68	5.99E+06	8.80E-06	1.47E-12	3.00E-05	7.37E-14	1.60E-04	3.30E-04	2.67E-08	9.88E+01	3.15E+07	1.21E-05
PR144	2.46E+03	1.00E-02	68	5.99E+06	8.80E-06	1.47E-12	3.00E-05	7.37E-14	1.60E-04	3.30E-04	1.38E-14	5.11E-05	3.15E+07	6.26E-12
EU154	1.07E+03	1.00E-02	68	5.99E+06	8.80E-06	1.47E-12	3.00E-05	3.21E-14	1.60E-04	3.30E-04	1.06E-07	3.92E+02	3.15E+07	2.09E-05
CM244	9.30E+02	1.00E-02	68	5.99E+06	8.80E-06	1.47E-12	3.00E-05	2.79E-14	1.60E-04	3.30E-04	9.38E-05	3.47E+05	3.15E+07	1.61E-02
PU238	7.49E+02	1.00E-02	68	5.99E+06	8.80E-06	1.47E-12	3.00E-05	2.24E-14	1.60E-04	3.30E-04	1.52E-04	5.62E+05	3.15E+07	2.10E-02
SB125	6.40E+02	1.00E-02	68	5.99E+06	8.80E-06	1.47E-12	3.00E-05	1.92E-14	1.60E-04	3.30E-04	5.35E-10	1.98E+00	3.15E+07	6.31E-08
EU155	3.51E+02	1.00E-02	68	5.99E+06	8.80E-06	1.47E-12	3.00E-05	1.05E-14	1.60E-04	3.30E-04	1.43E-08	5.29E+01	3.15E+07	9.26E-07
AM241	2.20E+02	1.00E-02	68	5.99E+06	8.80E-06	1.47E-12	3.00E-05	6.59E-15	1.60E-04	3.30E-04	1.74E-04	6.44E+05	3.15E+07	7.06E-03
TE125M	1.56E+02	1.00E-02	68	5.99E+06	8.80E-06	1.47E-12	3.00E-05	4.68E-15	1.60E-04	3.30E-04	3.01E-09	1.11E+01	3.15E+07	8.66E-08
PU240	1.26E+02	1.00E-02	68	5.99E+06	8.80E-06	1.47E-12	3.00E-05	3.78E-15	1.60E-04	3.30E-04	1.69E-04	6.25E+05	3.15E+07	3.93E-03
151Sm	0.00E+00	1.00E-02	68	5.99E+06	8.80E-06	1.47E-12	3.00E-05	0.00E+00	1.60E-04	3.30E-04	1.10E-08	4.07E+01	3.15E+07	0.00E+00
239Pu	6.16E+01	1.00E-02	68	5.99E+06	8.80E-06	1.47E-12	3.00E-05	1.85E-15	1.60E-04	3.30E-04	1.69E-04	6.25E+05	3.15E+07	1.92E-03
137mBa	2.16E+04	1.00E-02	68	5.99E+06	8.80E-06	1.47E-12	3.00E-05	6.47E-13	1.60E-04	3.30E-04	0.00E+00	0.00E+00	3.15E+07	0.00E+00
106Rh	4.16E+03	1.00E-02	68	5.99E+06	8.80E-06	1.47E-12	3.00E-05	1.25E-13	1.60E-04	3.30E-04	0.00E+00	0.00E+00	3.15E+07	0.00E+00
144mPr	0.00E+00	1.00E-02	68	5.99E+06	8.80E-06	1.47E-12	3.00E-05	0.00E+00	1.60E-04	3.30E-04	0.00E+00	0.00E+00	3.15E+07	0.00E+00
243Am	7.39E+00	1.00E-02	68	5.99E+06	8.80E-06	1.47E-12	3.00E-05	2.21E-16	1.60E-04	3.30E-04	1.73E-04	6.40E+05	3.15E+07	2.36E-04
242Cm	6.10E+00	1.00E-02	68	5.99E+06	8.80E-06	1.47E-12	3.00E-05	1.83E-16	1.60E-04	3.30E-04	3.90E-06	1.44E+04	3.15E+07	4.39E-06
243Cm	4.81E+00	1.00E-02	68	5.99E+06	8.80E-06	1.47E-12	3.00E-05	1.44E-16	1.60E-04	3.30E-04	1.18E-04	4.37E+05	3.15E+07	1.05E-04
239Np	7.39E+00	1.00E-02	68	5.99E+06	8.80E-06	1.47E-12	3.00E-05	2.21E-16	1.60E-04	3.30E-04	2.08E-10	7.70E-01	3.15E+07	2.83E-10
237Np	7.05E-02	1.00E-02	68	5.99E+06	8.80E-06	1.47E-12	3.00E-05	2.11E-18	1.60E-04	3.30E-04	2.62E-04	9.69E+05	3.15E+07	3.41E-06
242Pu	5.95E-01	1.00E-02	68	5.99E+06	8.80E-06	1.47E-12	3.00E-05	1.78E-17	1.60E-04	3.30E-04	1.61E-04	5.96E+05	3.15E+07	1.77E-05
242Am	1.69E+00	1.00E-02	68	5.99E+06	8.80E-06	1.47E-12	3.00E-05	5.06E-17	1.60E-04	3.30E-04	1.32E-08	4.88E+01	3.15E+07	4.11E-09
242mAm	1.70E+00	1.00E-02	68	5.99E+06	8.80E-06	1.47E-12	3.00E-05	5.09E-17	1.60E-04	3.30E-04	1.69E-04	6.25E+05	3.15E+07	5.30E-05
													Total	1.68E-01

MPC-68														
Normal Conditions														
Committed Effective Dose Equivalent From Inhalation														
Nuclide	Inventory (Ci/Assy)	1% for normal storage	No. Assy	MPC Vol (cm3)	L_{nor} Rate at Upstream (cm3/s)	Fraction Released per sec	Release Fraction	Release Rate (Ci/sec)	X/Q (sec/m3)	Breathing Rate (m3/sec)	DCF (Sv/Bq)	DCF (mRem/uCi)	Occ Time (sec)	CEDE (mRem)
								Gases						
H-3	8.72E+01	1.00E-02	68	5.99E+06	8.80E-06	1.47E-12	0.30	2.61E-11	1.60E-04	3.30E-04	1.73E-11	6.40E-02	3.15E+07	2.78E-06
I-129	7.72E-03	1.00E-02	68	5.99E+06	8.80E-06	1.47E-12	0.30	2.31E-15	1.60E-04	3.30E-04	1.38E-10	5.11E-01	3.15E+07	1.96E-09
Kr-85	1.43E+03	1.00E-02	68	5.99E+06	8.80E-06	1.47E-12	0.30	4.29E-10	1.60E-04	3.30E-04	0.00E+00	0.00E+00	3.15E+07	0.00E+00
								Crud						
Co-60	6.50E+01	1.00E+00	68	5.99E+06	8.80E-06	1.47E-12	0.15	9.74E-10	1.60E-04	3.30E-04	1.35E-08	5.00E+01	3.15E+07	8.09E-02
								Volatiles						
Sr-90	1.52E+04	1.00E-02	68	5.99E+06	8.80E-06	1.47E-12	2.00E-04	3.04E-12	1.60E-04	3.30E-04	7.09E-08	2.62E+02	3.15E+07	1.33E-03
Ru-106	4.16E+03	1.00E-02	68	5.99E+06	8.80E-06	1.47E-12	2.00E-04	8.31E-13	1.60E-04	3.30E-04	1.61E-09	5.96E+00	3.15E+07	8.23E-06
Cs-134	7.20E+03	1.00E-02	68	5.99E+06	8.80E-06	1.47E-12	2.00E-04	1.44E-12	1.60E-04	3.30E-04	1.10E-08	4.07E+01	3.15E+07	9.74E-05
Cs-137	2.29E+04	1.00E-02	68	5.99E+06	8.80E-06	1.47E-12	2.00E-04	4.58E-12	1.60E-04	3.30E-04	7.94E-09	2.94E+01	3.15E+07	2.24E-04
								Fines						
PU241	2.10E+04	1.00E-02	68	5.99E+06	8.80E-06	1.47E-12	3.00E-05	6.29E-13	1.60E-04	3.30E-04	4.20E-05	1.55E+05	3.15E+07	1.63E-01
Y 90	1.52E+04	1.00E-02	68	5.99E+06	8.80E-06	1.47E-12	3.00E-05	4.56E-13	1.60E-04	3.30E-04	2.78E-10	1.03E+00	3.15E+07	7.79E-07
PM147	8.88E+03	1.00E-02	68	5.99E+06	8.80E-06	1.47E-12	3.00E-05	2.66E-13	1.60E-04	3.30E-04	2.01E-08	7.44E+01	3.15E+07	3.29E-05
CE144	2.46E+03	1.00E-02	68	5.99E+06	8.80E-06	1.47E-12	3.00E-05	7.37E-14	1.60E-04	3.30E-04	4.54E-08	1.68E+02	3.15E+07	2.06E-05
PR144	2.46E+03	1.00E-02	68	5.99E+06	8.80E-06	1.47E-12	3.00E-05	7.37E-14	1.60E-04	3.30E-04	1.47E-14	5.44E-05	3.15E+07	6.67E-12
EU154	1.07E+03	1.00E-02	68	5.99E+06	8.80E-06	1.47E-12	3.00E-05	3.21E-14	1.60E-04	3.30E-04	5.23E-07	1.94E+03	3.15E+07	1.03E-04
CM244	9.30E+02	1.00E-02	68	5.99E+06	8.80E-06	1.47E-12	3.00E-05	2.79E-14	1.60E-04	3.30E-04	1.17E-03	4.33E+06	3.15E+07	2.01E-01
PU238	7.49E+02	1.00E-02	68	5.99E+06	8.80E-06	1.47E-12	3.00E-05	2.24E-14	1.60E-04	3.30E-04	1.90E-03	7.03E+06	3.15E+07	2.62E-01
SB125	6.40E+02	1.00E-02	68	5.99E+06	8.80E-06	1.47E-12	3.00E-05	1.92E-14	1.60E-04	3.30E-04	9.78E-10	3.62E+00	3.15E+07	1.15E-07
EU155	3.51E+02	1.00E-02	68	5.99E+06	8.80E-06	1.47E-12	3.00E-05	1.05E-14	1.60E-04	3.30E-04	1.52E-07	5.62E+02	3.15E+07	9.84E-06
AM241	2.20E+02	1.00E-02	68	5.99E+06	8.80E-06	1.47E-12	3.00E-05	6.59E-15	1.60E-04	3.30E-04	2.17E-03	8.03E+06	3.15E+07	8.80E-02
TE125M	1.56E+02	1.00E-02	68	5.99E+06	8.80E-06	1.47E-12	3.00E-05	4.68E-15	1.60E-04	3.30E-04	3.21E-08	1.19E+02	3.15E+07	9.24E-07
PU240	1.26E+02	1.00E-02	68	5.99E+06	8.80E-06	1.47E-12	3.00E-05	3.78E-15	1.60E-04	3.30E-04	2.11E-03	7.81E+06	3.15E+07	4.90E-02
151Sm	0.00E+00	1.00E-02	68	5.99E+06	8.80E-06	1.47E-12	3.00E-05	0.00E+00	1.60E-04	3.30E-04	1.38E-07	5.11E+02	3.15E+07	0.00E+00
239Pu	6.16E+01	1.00E-02	68	5.99E+06	8.80E-06	1.47E-12	3.00E-05	1.85E-15	1.60E-04	3.30E-04	2.11E-03	7.81E+06	3.15E+07	2.40E-02
137mBa	2.16E+04	1.00E-02	68	5.99E+06	8.80E-06	1.47E-12	3.00E-05	6.47E-13	1.60E-04	3.30E-04	0.00E+00	0.00E+00	3.15E+07	0.00E+00
106Rh	4.16E+03	1.00E-02	68	5.99E+06	8.80E-06	1.47E-12	3.00E-05	1.25E-13	1.60E-04	3.30E-04	0.00E+00	0.00E+00	3.15E+07	0.00E+00
144mPr	0.00E+00	1.00E-02	68	5.99E+06	8.80E-06	1.47E-12	3.00E-05	0.00E+00	1.60E-04	3.30E-04	0.00E+00	0.00E+00	3.15E+07	0.00E+00
243Am	7.39E+00	1.00E-02	68	5.99E+06	8.80E-06	1.47E-12	3.00E-05	2.21E-16	1.60E-04	3.30E-04	2.17E-03	8.03E+06	3.15E+07	2.96E-03
242Cm	6.10E+00	1.00E-02	68	5.99E+06	8.80E-06	1.47E-12	3.00E-05	1.83E-16	1.60E-04	3.30E-04	4.87E-05	1.80E+05	3.15E+07	5.48E-05
243Cm	4.81E+00	1.00E-02	68	5.99E+06	8.80E-06	1.47E-12	3.00E-05	1.44E-16	1.60E-04	3.30E-04	1.47E-03	5.44E+06	3.15E+07	1.30E-03
239Np	7.39E+00	1.00E-02	68	5.99E+06	8.80E-06	1.47E-12	3.00E-05	2.21E-16	1.60E-04	3.30E-04	2.03E-09	7.51E+00	3.15E+07	2.77E-09
237Np	7.05E-02	1.00E-02	68	5.99E+06	8.80E-06	1.47E-12	3.00E-05	2.11E-18	1.60E-04	3.30E-04	3.27E-03	1.21E+07	3.15E+07	4.25E-05
242Pu	5.95E-01	1.00E-02	68	5.99E+06	8.80E-06	1.47E-12	3.00E-05	1.78E-17	1.60E-04	3.30E-04	2.01E-03	7.44E+06	3.15E+07	2.21E-04
242Am	1.69E+00	1.00E-02	68	5.99E+06	8.80E-06	1.47E-12	3.00E-05	5.06E-17	1.60E-04	3.30E-04	1.65E-07	6.11E+02	3.15E+07	5.14E-08
242mAm	1.70E+00	1.00E-02	68	5.99E+06	8.80E-06	1.47E-12	3.00E-05	5.09E-17	1.60E-04	3.30E-04	2.12E-03	7.84E+06	3.15E+07	6.65E-04
													Total	8.75E-01

MPC-68														
Normal Conditions														
Committed Effective Dose Equivalent From Inhalation														
Nuclide	Inventory (Ci/Assy)	1% for normal storage	No. Assy	MPC Vol (cm3)	L_{nor} Rate at Upstream (cm3/s)	Fraction Released per sec	Release Fraction	Release Rate (Ci/sec)	X/Q (sec/m3)	Breathing Rate (m3/sec)	DCF (Sv/Bq)	DCF (mRem/uCi)	Occ Time (sec)	CEDE (mRem)
								Gases						
H-3	8.72E+01	1.00E-02	68	5.99E+06	8.80E-06	1.47E-12	0.30	2.61E-11	1.60E-04	3.30E-04	1.73E-11	6.40E-02	3.15E+07	2.78E-06
I-129	7.72E-03	1.00E-02	68	5.99E+06	8.80E-06	1.47E-12	0.30	2.31E-15	1.60E-04	3.30E-04	1.56E-06	5.77E+03	3.15E+07	2.22E-05
Kr-85	1.43E+03	1.00E-02	68	5.99E+06	8.80E-06	1.47E-12	0.30	4.29E-10	1.60E-04	3.30E-04	0.00E+00	0.00E+00	3.15E+07	0.00E+00
								Crud						
Co-60	6.50E+01	1.00E+00	68	5.99E+06	8.80E-06	1.47E-12	0.15	9.74E-10	1.60E-04	3.30E-04	1.62E-08	5.99E+01	3.15E+07	9.71E-02
								Volatiles						
Sr-90	1.52E+04	1.00E-02	68	5.99E+06	8.80E-06	1.47E-12	2.00E-04	3.04E-12	1.60E-04	3.30E-04	2.69E-10	9.95E-01	3.15E+07	5.03E-06
Ru-106	4.16E+03	1.00E-02	68	5.99E+06	8.80E-06	1.47E-12	2.00E-04	8.31E-13	1.60E-04	3.30E-04	1.72E-09	6.36E+00	3.15E+07	8.80E-06
Cs-134	7.20E+03	1.00E-02	68	5.99E+06	8.80E-06	1.47E-12	2.00E-04	1.44E-12	1.60E-04	3.30E-04	1.11E-08	4.11E+01	3.15E+07	9.83E-05
Cs-137	2.29E+04	1.00E-02	68	5.99E+06	8.80E-06	1.47E-12	2.00E-04	4.58E-12	1.60E-04	3.30E-04	7.93E-09	2.93E+01	3.15E+07	2.23E-04
								Fines						
PU241	2.10E+04	1.00E-02	68	5.99E+06	8.80E-06	1.47E-12	3.00E-05	6.29E-13	1.60E-04	3.30E-04	1.24E-11	4.59E-02	3.15E+07	4.80E-08
Y 90	1.52E+04	1.00E-02	68	5.99E+06	8.80E-06	1.47E-12	3.00E-05	4.56E-13	1.60E-04	3.30E-04	9.52E-12	3.52E-02	3.15E+07	2.67E-08
PM147	8.88E+03	1.00E-02	68	5.99E+06	8.80E-06	1.47E-12	3.00E-05	2.66E-13	1.60E-04	3.30E-04	1.98E-14	7.33E-05	3.15E+07	3.24E-11
CE144	2.46E+03	1.00E-02	68	5.99E+06	8.80E-06	1.47E-12	3.00E-05	7.37E-14	1.60E-04	3.30E-04	1.88E-09	6.96E+00	3.15E+07	8.53E-07
PR144	2.46E+03	1.00E-02	68	5.99E+06	8.80E-06	1.47E-12	3.00E-05	7.37E-14	1.60E-04	3.30E-04	8.47E-15	3.13E-05	3.15E+07	3.84E-12
EU154	1.07E+03	1.00E-02	68	5.99E+06	8.80E-06	1.47E-12	3.00E-05	3.21E-14	1.60E-04	3.30E-04	7.14E-09	2.64E+01	3.15E+07	1.41E-06
CM244	9.30E+02	1.00E-02	68	5.99E+06	8.80E-06	1.47E-12	3.00E-05	2.79E-14	1.60E-04	3.30E-04	1.01E-09	3.74E+00	3.15E+07	1.73E-07
PU238	7.49E+02	1.00E-02	68	5.99E+06	8.80E-06	1.47E-12	3.00E-05	2.24E-14	1.60E-04	3.30E-04	9.62E-10	3.56E+00	3.15E+07	1.33E-07
SB125	6.40E+02	1.00E-02	68	5.99E+06	8.80E-06	1.47E-12	3.00E-05	1.92E-14	1.60E-04	3.30E-04	3.24E-10	1.20E+00	3.15E+07	3.82E-08
EU155	3.51E+02	1.00E-02	68	5.99E+06	8.80E-06	1.47E-12	3.00E-05	1.05E-14	1.60E-04	3.30E-04	2.40E-10	8.88E-01	3.15E+07	1.55E-08
AM241	2.20E+02	1.00E-02	68	5.99E+06	8.80E-06	1.47E-12	3.00E-05	6.59E-15	1.60E-04	3.30E-04	1.60E-09	5.92E+00	3.15E+07	6.49E-08
TE125M	1.56E+02	1.00E-02	68	5.99E+06	8.80E-06	1.47E-12	3.00E-05	4.68E-15	1.60E-04	3.30E-04	9.93E-11	3.67E-01	3.15E+07	2.86E-09
PU240	1.26E+02	1.00E-02	68	5.99E+06	8.80E-06	1.47E-12	3.00E-05	3.78E-15	1.60E-04	3.30E-04	9.05E-10	3.35E+00	3.15E+07	2.10E-08
151Sm	0.00E+00	1.00E-02	68	5.99E+06	8.80E-06	1.47E-12	3.00E-05	0.00E+00	1.60E-04	3.30E-04	1.32E-14	4.88E-05	3.15E+07	0.00E+00
239Pu	6.16E+01	1.00E-02	68	5.99E+06	8.80E-06	1.47E-12	3.00E-05	1.85E-15	1.60E-04	3.30E-04	9.03E-10	3.34E+00	3.15E+07	1.03E-08
137mBa	2.16E+04	1.00E-02	68	5.99E+06	8.80E-06	1.47E-12	3.00E-05	6.47E-13	1.60E-04	3.30E-04	0.00E+00	0.00E+00	3.15E+07	0.00E+00
106Rh	4.16E+03	1.00E-02	68	5.99E+06	8.80E-06	1.47E-12	3.00E-05	1.25E-13	1.60E-04	3.30E-04	0.00E+00	0.00E+00	3.15E+07	0.00E+00
144mPr	0.00E+00	1.00E-02	68	5.99E+06	8.80E-06	1.47E-12	3.00E-05	0.00E+00	1.60E-04	3.30E-04	0.00E+00	0.00E+00	3.15E+07	0.00E+00
243Am	7.39E+00	1.00E-02	68	5.99E+06	8.80E-06	1.47E-12	3.00E-05	2.21E-16	1.60E-04	3.30E-04	8.29E-09	3.07E+01	3.15E+07	1.13E-08
242Cm	6.10E+00	1.00E-02	68	5.99E+06	8.80E-06	1.47E-12	3.00E-05	1.83E-16	1.60E-04	3.30E-04	9.41E-10	3.48E+00	3.15E+07	1.06E-09
243Cm	4.81E+00	1.00E-02	68	5.99E+06	8.80E-06	1.47E-12	3.00E-05	1.44E-16	1.60E-04	3.30E-04	3.83E-09	1.42E+01	3.15E+07	3.40E-09
239Np	7.39E+00	1.00E-02	68	5.99E+06	8.80E-06	1.47E-12	3.00E-05	2.21E-16	1.60E-04	3.30E-04	7.62E-12	2.82E-02	3.15E+07	1.04E-11
237Np	7.05E-02	1.00E-02	68	5.99E+06	8.80E-06	1.47E-12	3.00E-05	2.11E-18	1.60E-04	3.30E-04	1.34E-08	4.96E+01	3.15E+07	1.74E-10
242Pu	5.95E-01	1.00E-02	68	5.99E+06	8.80E-06	1.47E-12	3.00E-05	1.78E-17	1.60E-04	3.30E-04	8.79E-10	3.25E+00	3.15E+07	9.65E-11
242Am	1.69E+00	1.00E-02	68	5.99E+06	8.80E-06	1.47E-12	3.00E-05	5.06E-17	1.60E-04	3.30E-04	2.52E-12	9.32E-03	3.15E+07	7.85E-13
242mAm	1.70E+00	1.00E-02	68	5.99E+06	8.80E-06	1.47E-12	3.00E-05	5.09E-17	1.60E-04	3.30E-04	5.64E-10	2.09E+00	3.15E+07	1.77E-10
													Total	9.75E-02

MPC-68														
Normal Conditions														
Committed Effective Dose Equivalent From Inhalation														
Nuclide	Inventory (Ci/Assy)	1% for normal storage	No. Assy	MPC Vol (cm3)	L_{nor} Rate at Upstream (cm3/s)	Fraction Released per sec	Release Fraction	Release Rate (Ci/sec)	X/Q (sec/m3)	Breathing Rate (m3/sec)	DCF (Sv/Bq)	DCF (mRem/uCi)	Occ Time (sec)	CEDE (mRem)
								Gases						
H-3	8.72E+01	1.00E-02	68	5.99E+06	8.80E-06	1.47E-12	0.30	2.61E-11	1.60E-04	3.30E-04	1.73E-11	6.40E-02	3.15E+07	2.78E-06
I-129	7.72E-03	1.00E-02	68	5.99E+06	8.80E-06	1.47E-12	0.30	2.31E-15	1.60E-04	3.30E-04	4.69E-08	1.74E+02	3.15E+07	6.68E-07
Kr-85	1.43E+03	1.00E-02	68	5.99E+06	8.80E-06	1.47E-12	0.30	4.29E-10	1.60E-04	3.30E-04	0.00E+00	0.00E+00	3.15E+07	0.00E+00
								Crud		3.30E-04				
Co-60	6.50E+01	1.00E+00	68	5.99E+06	8.80E-06	1.47E-12	0.15	9.74E-10	1.60E-04	3.30E-04	5.91E-08	2.19E+02	3.15E+07	3.54E-01
								Volatiles		3.30E-04				
Sr-90	1.52E+04	1.00E-02	68	5.99E+06	8.80E-06	1.47E-12	2.00E-04	3.04E-12	1.60E-04	3.30E-04	3.51E-07	1.30E+03	3.15E+07	6.56E-03
Ru-106	4.16E+03	1.00E-02	68	5.99E+06	8.80E-06	1.47E-12	2.00E-04	8.31E-13	1.60E-04	3.30E-04	1.29E-07	4.77E+02	3.15E+07	6.60E-04
Cs-134	7.20E+03	1.00E-02	68	5.99E+06	8.80E-06	1.47E-12	2.00E-04	1.44E-12	1.60E-04	3.30E-04	1.25E-08	4.63E+01	3.15E+07	1.11E-04
Cs-137	2.29E+04	1.00E-02	68	5.99E+06	8.80E-06	1.47E-12	2.00E-04	4.58E-12	1.60E-04	3.30E-04	8.63E-09	3.19E+01	3.15E+07	2.43E-04
								Fines		3.30E-04				
PU241	2.10E+04	1.00E-02	68	5.99E+06	8.80E-06	1.47E-12	3.00E-05	6.29E-13	1.60E-04	3.30E-04	2.23E-06	8.25E+03	3.15E+07	8.64E-03
Y 90	1.52E+04	1.00E-02	68	5.99E+06	8.80E-06	1.47E-12	3.00E-05	4.56E-13	1.60E-04	3.30E-04	2.13E-09	7.88E+00	3.15E+07	5.97E-06
PM147	8.88E+03	1.00E-02	68	5.99E+06	8.80E-06	1.47E-12	3.00E-05	2.66E-13	1.60E-04	3.30E-04	1.06E-08	3.92E+01	3.15E+07	1.74E-05
CE144	2.46E+03	1.00E-02	68	5.99E+06	8.80E-06	1.47E-12	3.00E-05	7.37E-14	1.60E-04	3.30E-04	5.84E-08	2.16E+02	3.15E+07	2.65E-05
PR144	2.46E+03	1.00E-02	68	5.99E+06	8.80E-06	1.47E-12	3.00E-05	7.37E-14	1.60E-04	3.30E-04	1.17E-11	4.33E-02	3.15E+07	5.31E-09
EU154	1.07E+03	1.00E-02	68	5.99E+06	8.80E-06	1.47E-12	3.00E-05	3.21E-14	1.60E-04	3.30E-04	7.73E-08	2.86E+02	3.15E+07	1.53E-05
CM244	9.30E+02	1.00E-02	68	5.99E+06	8.80E-06	1.47E-12	3.00E-05	2.79E-14	1.60E-04	3.30E-04	6.70E-05	2.48E+05	3.15E+07	1.15E-02
PU238	7.49E+02	1.00E-02	68	5.99E+06	8.80E-06	1.47E-12	3.00E-05	2.24E-14	1.60E-04	3.30E-04	1.06E-04	3.92E+05	3.15E+07	1.46E-02
SB125	6.40E+02	1.00E-02	68	5.99E+06	8.80E-06	1.47E-12	3.00E-05	1.92E-14	1.60E-04	3.30E-04	3.30E-09	1.22E+01	3.15E+07	3.90E-07
EU155	3.51E+02	1.00E-02	68	5.99E+06	8.80E-06	1.47E-12	3.00E-05	1.05E-14	1.60E-04	3.30E-04	1.12E-08	4.14E+01	3.15E+07	7.25E-07
AM241	2.20E+02	1.00E-02	68	5.99E+06	8.80E-06	1.47E-12	3.00E-05	6.59E-15	1.60E-04	3.30E-04	1.20E-04	4.44E+05	3.15E+07	4.87E-03
TE125M	1.56E+02	1.00E-02	68	5.99E+06	8.80E-06	1.47E-12	3.00E-05	4.68E-15	1.60E-04	3.30E-04	1.52E-09	5.62E+00	3.15E+07	4.37E-08
PU240	1.26E+02	1.00E-02	68	5.99E+06	8.80E-06	1.47E-12	3.00E-05	3.78E-15	1.60E-04	3.30E-04	1.16E-04	4.29E+05	3.15E+07	2.70E-03
151Sm	0.00E+00	1.00E-02	68	5.99E+06	8.80E-06	1.47E-12	3.00E-05	0.00E+00	1.60E-04	3.30E-04	8.10E-09	3.00E+01	3.15E+07	0.00E+00
239Pu	6.16E+01	1.00E-02	68	5.99E+06	8.80E-06	1.47E-12	3.00E-05	1.85E-15	1.60E-04	3.30E-04	1.16E-04	4.29E+05	3.15E+07	1.32E-03
137mBa	2.16E+04	1.00E-02	68	5.99E+06	8.80E-06	1.47E-12	3.00E-05	6.47E-13	1.60E-04	3.30E-04	0.00E+00	0.00E+00	3.15E+07	0.00E+00
106Rh	4.16E+03	1.00E-02	68	5.99E+06	8.80E-06	1.47E-12	3.00E-05	1.25E-13	1.60E-04	3.30E-04	0.00E+00	0.00E+00	3.15E+07	0.00E+00
144mPr	0.00E+00	1.00E-02	68	5.99E+06	8.80E-06	1.47E-12	3.00E-05	0.00E+00	1.60E-04	3.30E-04	0.00E+00	0.00E+00	3.15E+07	0.00E+00
243Am	7.39E+00	1.00E-02	68	5.99E+06	8.80E-06	1.47E-12	3.00E-05	2.21E-16	1.60E-04	3.30E-04	1.19E-04	4.40E+05	3.15E+07	1.62E-04
242Cm	6.10E+00	1.00E-02	68	5.99E+06	8.80E-06	1.47E-12	3.00E-05	1.83E-16	1.60E-04	3.30E-04	4.67E-06	1.73E+04	3.15E+07	5.25E-06
243Cm	4.81E+00	1.00E-02	68	5.99E+06	8.80E-06	1.47E-12	3.00E-05	1.44E-16	1.60E-04	3.30E-04	8.30E-05	3.07E+05	3.15E+07	7.36E-05
239Np	7.39E+00	1.00E-02	68	5.99E+06	8.80E-06	1.47E-12	3.00E-05	2.21E-16	1.60E-04	3.30E-04	6.78E-10	2.51E+00	3.15E+07	9.24E-10
237Np	7.05E-02	1.00E-02	68	5.99E+06	8.80E-06	1.47E-12	3.00E-05	2.11E-18	1.60E-04	3.30E-04	1.46E-04	5.40E+05	3.15E+07	1.90E-06
242Pu	5.95E-01	1.00E-02	68	5.99E+06	8.80E-06	1.47E-12	3.00E-05	1.78E-17	1.60E-04	3.30E-04	1.11E-04	4.11E+05	3.15E+07	1.22E-05
242Am	1.69E+00	1.00E-02	68	5.99E+06	8.80E-06	1.47E-12	3.00E-05	5.06E-17	1.60E-04	3.30E-04	1.58E-08	5.85E+01	3.15E+07	4.92E-09
242mAm	1.70E+00	1.00E-02	68	5.99E+06	8.80E-06	1.47E-12	3.00E-05	5.09E-17	1.60E-04	3.30E-04	1.15E-04	4.26E+05	3.15E+07	3.61E-05
													Total	4.06E-01

MPC-68														
Off-Normal Conditions														
Committed Effective Dose Equivalent From Inhalation														
Nuclide	Inventory (Ci/Assy)	10% for off-normal storage	No. Assy	MPC Vol (cm3)	$L_{off\ nor}$ Rate at Upstream (cm3/s)	Fraction Released per sec	Release Fraction	Release Rate (Ci/sec)	X/Q (sec/m3)	Breathing Rate (m3/sec)	DCF (Sv/Bq)	DCF (mRem/uCi)	Occ Time (sec)	CEDE (mRem)
								Gases						
H-3	8.72E+01	1.00E-01	68	5.99E+06	8.80E-06	1.47E-12	0.30	2.61E-10	1.60E-04	3.30E-04	1.73E-11	6.40E-02	3.15E+07	2.78E-05
I-129	7.72E-03	1.00E-01	68	5.99E+06	8.80E-06	1.47E-12	0.30	2.31E-14	1.60E-04	3.30E-04	8.69E-11	3.22E-01	3.15E+07	1.24E-08
Kr-85	1.43E+03	1.00E-01	68	5.99E+06	8.80E-06	1.47E-12	0.30	4.29E-09	1.60E-04	3.30E-04	0.00E+00	0.00E+00	3.15E+07	0.00E+00
								Crud						
Co-60	6.50E+01	1.00E+00	68	5.99E+06	8.80E-06	1.47E-12	0.15	9.74E-10	1.60E-04	3.30E-04	4.76E-09	1.76E+01	3.15E+07	2.85E-02
								Volatiles						
Sr-90	1.52E+04	1.00E-01	68	5.99E+06	8.80E-06	1.47E-12	2.00E-04	3.04E-11	1.60E-04	3.30E-04	2.69E-10	9.95E-01	3.15E+07	5.03E-05
Ru-106	4.16E+03	1.00E-01	68	5.99E+06	8.80E-06	1.47E-12	2.00E-04	8.31E-12	1.60E-04	3.30E-04	1.30E-09	4.81E+00	3.15E+07	6.65E-05
Cs-134	7.20E+03	1.00E-01	68	5.99E+06	8.80E-06	1.47E-12	2.00E-04	1.44E-11	1.60E-04	3.30E-04	1.30E-08	4.81E+01	3.15E+07	1.15E-03
Cs-137	2.29E+04	1.00E-01	68	5.99E+06	8.80E-06	1.47E-12	2.00E-04	4.58E-11	1.60E-04	3.30E-04	8.76E-09	3.24E+01	3.15E+07	2.47E-03
								Fines						
PU241	2.10E+04	1.00E-01	68	5.99E+06	8.80E-06	1.47E-12	3.00E-05	6.29E-12	1.60E-04	3.30E-04	6.82E-07	2.52E+03	3.15E+07	2.64E-02
Y 90	1.52E+04	1.00E-01	68	5.99E+06	8.80E-06	1.47E-12	3.00E-05	4.56E-12	1.60E-04	3.30E-04	9.52E-12	3.52E-02	3.15E+07	2.67E-07
PM147	8.88E+03	1.00E-01	68	5.99E+06	8.80E-06	1.47E-12	3.00E-05	2.66E-12	1.60E-04	3.30E-04	8.25E-15	3.05E-05	3.15E+07	1.35E-10
CE144	2.46E+03	1.00E-01	68	5.99E+06	8.80E-06	1.47E-12	3.00E-05	7.37E-13	1.60E-04	3.30E-04	1.93E-09	7.14E+00	3.15E+07	8.76E-06
PR144	2.46E+03	1.00E-01	68	5.99E+06	8.80E-06	1.47E-12	3.00E-05	7.37E-13	1.60E-04	3.30E-04	2.41E-15	8.92E-06	3.15E+07	1.09E-11
EU154	1.07E+03	1.00E-01	68	5.99E+06	8.80E-06	1.47E-12	3.00E-05	3.21E-13	1.60E-04	3.30E-04	1.17E-08	4.33E+01	3.15E+07	2.31E-05
CM244	9.30E+02	1.00E-01	68	5.99E+06	8.80E-06	1.47E-12	3.00E-05	2.79E-13	1.60E-04	3.30E-04	1.59E-05	5.88E+04	3.15E+07	2.73E-02
PU238	7.49E+02	1.00E-01	68	5.99E+06	8.80E-06	1.47E-12	3.00E-05	2.24E-13	1.60E-04	3.30E-04	2.80E-05	1.04E+05	3.15E+07	3.87E-02
SB125	6.40E+02	1.00E-01	68	5.99E+06	8.80E-06	1.47E-12	3.00E-05	1.92E-13	1.60E-04	3.30E-04	3.60E-10	1.33E+00	3.15E+07	4.25E-07
EU155	3.51E+02	1.00E-01	68	5.99E+06	8.80E-06	1.47E-12	3.00E-05	1.05E-13	1.60E-04	3.30E-04	3.56E-10	1.32E+00	3.15E+07	2.30E-07
AM241	2.20E+02	1.00E-01	68	5.99E+06	8.80E-06	1.47E-12	3.00E-05	6.59E-14	1.60E-04	3.30E-04	3.25E-05	1.20E+05	3.15E+07	1.32E-02
TE125M	1.56E+02	1.00E-01	68	5.99E+06	8.80E-06	1.47E-12	3.00E-05	4.68E-14	1.60E-04	3.30E-04	1.24E-10	4.59E-01	3.15E+07	3.57E-08
PU240	1.26E+02	1.00E-01	68	5.99E+06	8.80E-06	1.47E-12	3.00E-05	3.78E-14	1.60E-04	3.30E-04	3.18E-05	1.18E+05	3.15E+07	7.39E-03
151Sm	0.00E+00	1.00E-01	68	5.99E+06	8.80E-06	1.47E-12	3.00E-05	0.00E+00	1.60E-04	3.30E-04	4.03E-14	1.49E-04	3.15E+07	0.00E+00
239Pu	6.16E+01	1.00E-01	68	5.99E+06	8.80E-06	1.47E-12	3.00E-05	1.85E-14	1.60E-04	3.30E-04	3.18E-05	1.18E+05	3.15E+07	3.61E-03
137mBa	2.16E+04	1.00E-01	68	5.99E+06	8.80E-06	1.47E-12	3.00E-05	6.47E-12	1.60E-04	3.30E-04	0.00E+00	0.00E+00	3.15E+07	0.00E+00
106Rh	4.16E+03	1.00E-01	68	5.99E+06	8.80E-06	1.47E-12	3.00E-05	1.25E-12	1.60E-04	3.30E-04	0.00E+00	0.00E+00	3.15E+07	0.00E+00
144mPr	0.00E+00	1.00E-01	68	5.99E+06	8.80E-06	1.47E-12	3.00E-05	0.00E+00	1.60E-04	3.30E-04	0.00E+00	0.00E+00	3.15E+07	0.00E+00
243Am	7.39E+00	1.00E-01	68	5.99E+06	8.80E-06	1.47E-12	3.00E-05	2.21E-15	1.60E-04	3.30E-04	3.26E-05	1.21E+05	3.15E+07	4.44E-04
242Cm	6.10E+00	1.00E-01	68	5.99E+06	8.80E-06	1.47E-12	3.00E-05	1.83E-15	1.60E-04	3.30E-04	5.70E-07	2.11E+03	3.15E+07	6.41E-06
243Cm	4.81E+00	1.00E-01	68	5.99E+06	8.80E-06	1.47E-12	3.00E-05	1.44E-15	1.60E-04	3.30E-04	2.07E-05	7.66E+04	3.15E+07	1.84E-04
239Np	7.39E+00	1.00E-01	68	5.99E+06	8.80E-06	1.47E-12	3.00E-05	2.21E-15	1.60E-04	3.30E-04	7.45E-11	2.76E-01	3.15E+07	1.02E-09
237Np	7.05E-02	1.00E-01	68	5.99E+06	8.80E-06	1.47E-12	3.00E-05	2.11E-17	1.60E-04	3.30E-04	2.96E-05	1.10E+05	3.15E+07	3.85E-06
242Pu	5.95E-01	1.00E-01	68	5.99E+06	8.80E-06	1.47E-12	3.00E-05	1.78E-16	1.60E-04	3.30E-04	3.02E-05	1.12E+05	3.15E+07	3.31E-05
242Am	1.69E+00	1.00E-01	68	5.99E+06	8.80E-06	1.47E-12	3.00E-05	5.06E-16	1.60E-04	3.30E-04	1.94E-09	7.18E+00	3.15E+07	6.05E-09
242mAm	1.70E+00	1.00E-01	68	5.99E+06	8.80E-06	1.47E-12	3.00E-05	5.09E-16	1.60E-04	3.30E-04	3.21E-05	1.19E+05	3.15E+07	1.01E-04
													Total	1.50E-01

MPC-68														
Off-Normal Conditions														
Committed Effective Dose Equivalent From Inhalation														
Nuclide	Inventory (Ci/Assy)	10% for off-normal storage	No. Assy	MPC Vol (cm3)	$L_{off\ nor}$ Rate at Upstream (cm3/s)	Fraction Released per sec	Release Fraction	Release Rate (Ci/sec)	X/Q (sec/m3)	Breathing Rate (m3/sec)	DCF (Sv/Bq)	DCF (mRem/uCi)	Occ Time (sec)	CEDE (mRem)
								Gases						
H-3	8.72E+01	1.00E-01	68	5.99E+06	8.80E-06	1.47E-12	0.30	2.61E-10	1.60E-04	3.30E-04	1.73E-11	6.40E-02	3.15E+07	2.78E-05
I-129	7.72E-03	1.00E-01	68	5.99E+06	8.80E-06	1.47E-12	0.30	2.31E-14	1.60E-04	3.30E-04	2.09E-10	7.73E-01	3.15E+07	2.98E-08
Kr-85	1.43E+03	1.00E-01	68	5.99E+06	8.80E-06	1.47E-12	0.30	4.29E-09	1.60E-04	3.30E-04	0.00E+00	0.00E+00	3.15E+07	0.00E+00
								Crud						
Co-60	6.50E+01	1.00E+00	68	5.99E+06	8.80E-06	1.47E-12	0.15	9.74E-10	1.60E-04	3.30E-04	1.84E-08	6.81E+01	3.15E+07	1.10E-01
								Volatiles						
Sr-90	1.52E+04	1.00E-01	68	5.99E+06	8.80E-06	1.47E-12	2.00E-04	3.04E-11	1.60E-04	3.30E-04	2.69E-10	9.95E-01	3.15E+07	5.03E-05
Ru-106	4.16E+03	1.00E-01	68	5.99E+06	8.80E-06	1.47E-12	2.00E-04	8.31E-12	1.60E-04	3.30E-04	1.78E-09	6.59E+00	3.15E+07	9.10E-05
Cs-134	7.20E+03	1.00E-01	68	5.99E+06	8.80E-06	1.47E-12	2.00E-04	1.44E-11	1.60E-04	3.30E-04	1.08E-08	4.00E+01	3.15E+07	9.56E-04
Cs-137	2.29E+04	1.00E-01	68	5.99E+06	8.80E-06	1.47E-12	2.00E-04	4.58E-11	1.60E-04	3.30E-04	7.84E-09	2.90E+01	3.15E+07	2.21E-03
								Fines						
PU241	2.10E+04	1.00E-01	68	5.99E+06	8.80E-06	1.47E-12	3.00E-05	6.29E-12	1.60E-04	3.30E-04	3.06E-11	1.13E-01	3.15E+07	1.19E-06
Y 90	1.52E+04	1.00E-01	68	5.99E+06	8.80E-06	1.47E-12	3.00E-05	4.56E-12	1.60E-04	3.30E-04	9.52E-12	3.52E-02	3.15E+07	2.67E-07
PM147	8.88E+03	1.00E-01	68	5.99E+06	8.80E-06	1.47E-12	3.00E-05	2.66E-12	1.60E-04	3.30E-04	3.60E-14	1.33E-04	3.15E+07	5.90E-10
CE144	2.46E+03	1.00E-01	68	5.99E+06	8.80E-06	1.47E-12	3.00E-05	7.37E-13	1.60E-04	3.30E-04	1.97E-09	7.29E+00	3.15E+07	8.94E-06
PR144	2.46E+03	1.00E-01	68	5.99E+06	8.80E-06	1.47E-12	3.00E-05	7.37E-13	1.60E-04	3.30E-04	1.05E-14	3.89E-05	3.15E+07	4.76E-11
EU154	1.07E+03	1.00E-01	68	5.99E+06	8.80E-06	1.47E-12	3.00E-05	3.21E-13	1.60E-04	3.30E-04	1.55E-08	5.74E+01	3.15E+07	3.06E-05
CM244	9.30E+02	1.00E-01	68	5.99E+06	8.80E-06	1.47E-12	3.00E-05	2.79E-13	1.60E-04	3.30E-04	1.04E-09	3.85E+00	3.15E+07	1.78E-06
PU238	7.49E+02	1.00E-01	68	5.99E+06	8.80E-06	1.47E-12	3.00E-05	2.24E-13	1.60E-04	3.30E-04	1.00E-09	3.70E+00	3.15E+07	1.38E-06
SB125	6.40E+02	1.00E-01	68	5.99E+06	8.80E-06	1.47E-12	3.00E-05	1.92E-13	1.60E-04	3.30E-04	4.16E-10	1.54E+00	3.15E+07	4.91E-07
EU155	3.51E+02	1.00E-01	68	5.99E+06	8.80E-06	1.47E-12	3.00E-05	1.05E-13	1.60E-04	3.30E-04	6.14E-10	2.27E+00	3.15E+07	3.97E-07
AM241	2.20E+02	1.00E-01	68	5.99E+06	8.80E-06	1.47E-12	3.00E-05	6.59E-14	1.60E-04	3.30E-04	2.67E-09	9.88E+00	3.15E+07	1.08E-06
TE125M	1.56E+02	1.00E-01	68	5.99E+06	8.80E-06	1.47E-12	3.00E-05	4.68E-14	1.60E-04	3.30E-04	1.07E-10	3.96E-01	3.15E+07	3.08E-08
PU240	1.26E+02	1.00E-01	68	5.99E+06	8.80E-06	1.47E-12	3.00E-05	3.78E-14	1.60E-04	3.30E-04	9.51E-10	3.52E+00	3.15E+07	2.21E-07
151Sm	0.00E+00	1.00E-01	68	5.99E+06	8.80E-06	1.47E-12	3.00E-05	0.00E+00	1.60E-04	3.30E-04	1.49E-13	5.51E-04	3.15E+07	0.00E+00
239Pu	6.16E+01	1.00E-01	68	5.99E+06	8.80E-06	1.47E-12	3.00E-05	1.85E-14	1.60E-04	3.30E-04	9.22E-10	3.41E+00	3.15E+07	1.05E-07
137mBa	2.16E+04	1.00E-01	68	5.99E+06	8.80E-06	1.47E-12	3.00E-05	6.47E-12	1.60E-04	3.30E-04	0.00E+00	0.00E+00	3.15E+07	0.00E+00
106Rh	4.16E+03	1.00E-01	68	5.99E+06	8.80E-06	1.47E-12	3.00E-05	1.25E-12	1.60E-04	3.30E-04	0.00E+00	0.00E+00	3.15E+07	0.00E+00
144mPr	0.00E+00	1.00E-01	68	5.99E+06	8.80E-06	1.47E-12	3.00E-05	0.00E+00	1.60E-04	3.30E-04	0.00E+00	0.00E+00	3.15E+07	0.00E+00
243Am	7.39E+00	1.00E-01	68	5.99E+06	8.80E-06	1.47E-12	3.00E-05	2.21E-15	1.60E-04	3.30E-04	1.52E-08	5.62E+01	3.15E+07	2.07E-07
242Cm	6.10E+00	1.00E-01	68	5.99E+06	8.80E-06	1.47E-12	3.00E-05	1.83E-15	1.60E-04	3.30E-04	9.44E-10	3.49E+00	3.15E+07	1.06E-08
243Cm	4.81E+00	1.00E-01	68	5.99E+06	8.80E-06	1.47E-12	3.00E-05	1.44E-15	1.60E-04	3.30E-04	6.29E-09	2.33E+01	3.15E+07	5.58E-08
239Np	7.39E+00	1.00E-01	68	5.99E+06	8.80E-06	1.47E-12	3.00E-05	2.21E-15	1.60E-04	3.30E-04	1.63E-11	6.03E-02	3.15E+07	2.22E-10
237Np	7.05E-02	1.00E-01	68	5.99E+06	8.80E-06	1.47E-12	3.00E-05	2.11E-17	1.60E-04	3.30E-04	1.69E-08	6.25E+01	3.15E+07	2.20E-09
242Pu	5.95E-01	1.00E-01	68	5.99E+06	8.80E-06	1.47E-12	3.00E-05	1.78E-16	1.60E-04	3.30E-04	9.45E-10	3.50E+00	3.15E+07	1.04E-09
242Am	1.69E+00	1.00E-01	68	5.99E+06	8.80E-06	1.47E-12	3.00E-05	5.06E-16	1.60E-04	3.30E-04	2.49E-12	9.21E-03	3.15E+07	7.76E-12
242mAm	1.70E+00	1.00E-01	68	5.99E+06	8.80E-06	1.47E-12	3.00E-05	5.09E-16	1.60E-04	3.30E-04	1.38E-09	5.11E+00	3.15E+07	4.33E-09
													Total	1.14E-01

MPC-68														
Off-Normal Conditions														
Committed Effective Dose Equivalent From Inhalation														
Nuclide	Inventory (Ci/Assy)	10% for off-normal storage	No. Assy	MPC Vol (cm3)	$L_{off\ nor}$ Rate at Upstream (cm3/s)	Fraction Released per sec	Release Fraction	Release Rate (Ci/sec)	X/Q (sec/m3)	Breathing Rate (m3/sec)	DCF (Sv/Bq)	DCF (mRem/uCi)	Occ Time (sec)	CEDE (mRem)
								Gases						
H-3	8.72E+01	1.00E-01	68	5.99E+06	8.80E-06	1.47E-12	0.30	2.61E-10	1.60E-04	3.30E-04	1.73E-11	6.40E-02	3.15E+07	2.78E-05
I-129	7.72E-03	1.00E-01	68	5.99E+06	8.80E-06	1.47E-12	0.30	2.31E-14	1.60E-04	3.30E-04	3.14E-10	1.16E+00	3.15E+07	4.47E-08
Kr-85	1.43E+03	1.00E-01	68	5.99E+06	8.80E-06	1.47E-12	0.30	4.29E-09	1.60E-04	3.30E-04	0.00E+00	0.00E+00	3.15E+07	0.00E+00
								Crud						
Co-60	6.50E+01	1.00E+00	68	5.99E+06	8.80E-06	1.47E-12	0.15	9.74E-10	1.60E-04	3.30E-04	3.45E-07	1.28E+03	3.15E+07	2.07E+00
								Volatiles						
Sr-90	1.52E+04	1.00E-01	68	5.99E+06	8.80E-06	1.47E-12	2.00E-04	3.04E-11	1.60E-04	3.30E-04	2.86E-06	1.06E+04	3.15E+07	5.35E-01
Ru-106	4.16E+03	1.00E-01	68	5.99E+06	8.80E-06	1.47E-12	2.00E-04	8.31E-12	1.60E-04	3.30E-04	1.04E-06	3.85E+03	3.15E+07	5.32E-02
Cs-134	7.20E+03	1.00E-01	68	5.99E+06	8.80E-06	1.47E-12	2.00E-04	1.44E-11	1.60E-04	3.30E-04	1.18E-08	4.37E+01	3.15E+07	1.04E-03
Cs-137	2.29E+04	1.00E-01	68	5.99E+06	8.80E-06	1.47E-12	2.00E-04	4.58E-11	1.60E-04	3.30E-04	8.82E-09	3.26E+01	3.15E+07	2.48E-03
								Fines						
PU241	2.10E+04	1.00E-01	68	5.99E+06	8.80E-06	1.47E-12	3.00E-05	6.29E-12	1.60E-04	3.30E-04	7.42E-09	2.75E+01	3.15E+07	2.87E-04
Y 90	1.52E+04	1.00E-01	68	5.99E+06	8.80E-06	1.47E-12	3.00E-05	4.56E-12	1.60E-04	3.30E-04	8.89E-09	3.29E+01	3.15E+07	2.49E-04
PM147	8.88E+03	1.00E-01	68	5.99E+06	8.80E-06	1.47E-12	3.00E-05	2.66E-12	1.60E-04	3.30E-04	7.74E-08	2.86E+02	3.15E+07	1.27E-03
CE144	2.46E+03	1.00E-01	68	5.99E+06	8.80E-06	1.47E-12	3.00E-05	7.37E-13	1.60E-04	3.30E-04	1.83E-07	6.77E+02	3.15E+07	8.30E-04
PR144	2.46E+03	1.00E-01	68	5.99E+06	8.80E-06	1.47E-12	3.00E-05	7.37E-13	1.60E-04	3.30E-04	9.40E-11	3.48E-01	3.15E+07	4.26E-07
EU154	1.07E+03	1.00E-01	68	5.99E+06	8.80E-06	1.47E-12	3.00E-05	3.21E-13	1.60E-04	3.30E-04	7.92E-08	2.93E+02	3.15E+07	1.56E-04
CM244	9.30E+02	1.00E-01	68	5.99E+06	8.80E-06	1.47E-12	3.00E-05	2.79E-13	1.60E-04	3.30E-04	1.93E-05	7.14E+04	3.15E+07	3.31E-02
PU238	7.49E+02	1.00E-01	68	5.99E+06	8.80E-06	1.47E-12	3.00E-05	2.24E-13	1.60E-04	3.30E-04	1.84E-05	6.81E+04	3.15E+07	2.54E-02
SB125	6.40E+02	1.00E-01	68	5.99E+06	8.80E-06	1.47E-12	3.00E-05	1.92E-13	1.60E-04	3.30E-04	2.17E-08	8.03E+01	3.15E+07	2.56E-05
EU155	3.51E+02	1.00E-01	68	5.99E+06	8.80E-06	1.47E-12	3.00E-05	1.05E-13	1.60E-04	3.30E-04	1.19E-08	4.40E+01	3.15E+07	7.70E-06
AM241	2.20E+02	1.00E-01	68	5.99E+06	8.80E-06	1.47E-12	3.00E-05	6.59E-14	1.60E-04	3.30E-04	1.84E-05	6.81E+04	3.15E+07	7.47E-03
TE125M	1.56E+02	1.00E-01	68	5.99E+06	8.80E-06	1.47E-12	3.00E-05	4.68E-14	1.60E-04	3.30E-04	4.66E-10	1.72E+00	3.15E+07	1.34E-07
PU240	1.26E+02	1.00E-01	68	5.99E+06	8.80E-06	1.47E-12	3.00E-05	3.78E-14	1.60E-04	3.30E-04	1.73E-05	6.40E+04	3.15E+07	4.02E-03
151Sm	0.00E+00	1.00E-01	68	5.99E+06	8.80E-06	1.47E-12	3.00E-05	0.00E+00	1.60E-04	3.30E-04	3.26E-09	1.21E+01	3.15E+07	0.00E+00
239Pu	6.16E+01	1.00E-01	68	5.99E+06	8.80E-06	1.47E-12	3.00E-05	1.85E-14	1.60E-04	3.30E-04	1.73E-05	6.40E+04	3.15E+07	1.97E-03
137mBa	2.16E+04	1.00E-01	68	5.99E+06	8.80E-06	1.47E-12	3.00E-05	6.47E-12	1.60E-04	3.30E-04	0.00E+00	0.00E+00	3.15E+07	0.00E+00
106Rh	4.16E+03	1.00E-01	68	5.99E+06	8.80E-06	1.47E-12	3.00E-05	1.25E-12	1.60E-04	3.30E-04	0.00E+00	0.00E+00	3.15E+07	0.00E+00
144mPr	0.00E+00	1.00E-01	68	5.99E+06	8.80E-06	1.47E-12	3.00E-05	0.00E+00	1.60E-04	3.30E-04	0.00E+00	0.00E+00	3.15E+07	0.00E+00
243Am	7.39E+00	1.00E-01	68	5.99E+06	8.80E-06	1.47E-12	3.00E-05	2.21E-15	1.60E-04	3.30E-04	1.78E-05	6.59E+04	3.15E+07	2.43E-04
242Cm	6.10E+00	1.00E-01	68	5.99E+06	8.80E-06	1.47E-12	3.00E-05	1.83E-15	1.60E-04	3.30E-04	1.55E-05	5.74E+04	3.15E+07	1.74E-04
243Cm	4.81E+00	1.00E-01	68	5.99E+06	8.80E-06	1.47E-12	3.00E-05	1.44E-15	1.60E-04	3.30E-04	1.94E-05	7.18E+04	3.15E+07	1.72E-04
239Np	7.39E+00	1.00E-01	68	5.99E+06	8.80E-06	1.47E-12	3.00E-05	2.21E-15	1.60E-04	3.30E-04	2.36E-09	8.73E+00	3.15E+07	3.22E-08
237Np	7.05E-02	1.00E-01	68	5.99E+06	8.80E-06	1.47E-12	3.00E-05	2.11E-17	1.60E-04	3.30E-04	1.61E-05	5.96E+04	3.15E+07	2.09E-06
242Pu	5.95E-01	1.00E-01	68	5.99E+06	8.80E-06	1.47E-12	3.00E-05	1.78E-16	1.60E-04	3.30E-04	1.64E-05	6.07E+04	3.15E+07	1.80E-05
242Am	1.69E+00	1.00E-01	68	5.99E+06	8.80E-06	1.47E-12	3.00E-05	5.06E-16	1.60E-04	3.30E-04	5.20E-08	1.92E+02	3.15E+07	1.62E-07
242mAm	1.70E+00	1.00E-01	68	5.99E+06	8.80E-06	1.47E-12	3.00E-05	5.09E-16	1.60E-04	3.30E-04	4.20E-06	1.55E+04	3.15E+07	1.32E-05
													Total	2.73E+00

MPC-68														
Off-Normal Conditions														
Committed Effective Dose Equivalent From Inhalation														
Nuclide	Inventory (Ci/Assy)	10% for off-normal storage	No. Assy	MPC Vol (cm3)	$L_{off\ nor}$ Rate at Upstream (cm3/s)	Fraction Released per sec	Release Fraction	Release Rate (Ci/sec)	X/Q (sec/m3)	Breathing Rate (m3/sec)	DCF (Sv/Bq)	DCF (mRem/uCi)	Occ Time (sec)	CEDE (mRem)
								Gases						
H-3	8.72E+01	1.00E-01	68	5.99E+06	8.80E-06	1.47E-12	0.30	2.61E-10	1.60E-04	3.30E-04	1.73E-11	6.40E-02	3.15E+07	2.78E-05
I-129	7.72E-03	1.00E-01	68	5.99E+06	8.80E-06	1.47E-12	0.30	2.31E-14	1.60E-04	3.30E-04	1.40E-10	5.18E-01	3.15E+07	1.99E-08
Kr-85	1.43E+03	1.00E-01	68	5.99E+06	8.80E-06	1.47E-12	0.30	4.29E-09	1.60E-04	3.30E-04	0.00E+00	0.00E+00	3.15E+07	0.00E+00
								Crud						
Co-60	6.50E+01	1.00E+00	68	5.99E+06	8.80E-06	1.47E-12	0.15	9.74E-10	1.60E-04	3.30E-04	1.72E-08	6.36E+01	3.15E+07	1.03E-01
								Volatiles						
Sr-90	1.52E+04	1.00E-01	68	5.99E+06	8.80E-06	1.47E-12	2.00E-04	3.04E-11	1.60E-04	3.30E-04	3.28E-08	1.21E+02	3.15E+07	6.13E-03
Ru-106	4.16E+03	1.00E-01	68	5.99E+06	8.80E-06	1.47E-12	2.00E-04	8.31E-12	1.60E-04	3.30E-04	1.76E-09	6.51E+00	3.15E+07	9.00E-05
Cs-134	7.20E+03	1.00E-01	68	5.99E+06	8.80E-06	1.47E-12	2.00E-04	1.44E-11	1.60E-04	3.30E-04	1.18E-08	4.37E+01	3.15E+07	1.04E-03
Cs-137	2.29E+04	1.00E-01	68	5.99E+06	8.80E-06	1.47E-12	2.00E-04	4.58E-11	1.60E-04	3.30E-04	8.30E-09	3.07E+01	3.15E+07	2.34E-03
								Fines						
PU241	2.10E+04	1.00E-01	68	5.99E+06	8.80E-06	1.47E-12	3.00E-05	6.29E-12	1.60E-04	3.30E-04	3.36E-06	1.24E+04	3.15E+07	1.30E-01
Y 90	1.52E+04	1.00E-01	68	5.99E+06	8.80E-06	1.47E-12	3.00E-05	4.56E-12	1.60E-04	3.30E-04	2.79E-10	1.03E+00	3.15E+07	7.82E-06
PM147	8.88E+03	1.00E-01	68	5.99E+06	8.80E-06	1.47E-12	3.00E-05	2.66E-12	1.60E-04	3.30E-04	1.61E-09	5.96E+00	3.15E+07	2.64E-05
CE144	2.46E+03	1.00E-01	68	5.99E+06	8.80E-06	1.47E-12	3.00E-05	7.37E-13	1.60E-04	3.30E-04	2.67E-08	9.88E+01	3.15E+07	1.21E-04
PR144	2.46E+03	1.00E-01	68	5.99E+06	8.80E-06	1.47E-12	3.00E-05	7.37E-13	1.60E-04	3.30E-04	1.38E-14	5.11E-05	3.15E+07	6.26E-11
EU154	1.07E+03	1.00E-01	68	5.99E+06	8.80E-06	1.47E-12	3.00E-05	3.21E-13	1.60E-04	3.30E-04	1.06E-07	3.92E+02	3.15E+07	2.09E-04
CM244	9.30E+02	1.00E-01	68	5.99E+06	8.80E-06	1.47E-12	3.00E-05	2.79E-13	1.60E-04	3.30E-04	9.38E-05	3.47E+05	3.15E+07	1.61E-01
PU238	7.49E+02	1.00E-01	68	5.99E+06	8.80E-06	1.47E-12	3.00E-05	2.24E-13	1.60E-04	3.30E-04	1.52E-04	5.62E+05	3.15E+07	2.10E-01
SB125	6.40E+02	1.00E-01	68	5.99E+06	8.80E-06	1.47E-12	3.00E-05	1.92E-13	1.60E-04	3.30E-04	5.35E-10	1.98E+00	3.15E+07	6.31E-07
EU155	3.51E+02	1.00E-01	68	5.99E+06	8.80E-06	1.47E-12	3.00E-05	1.05E-13	1.60E-04	3.30E-04	1.43E-08	5.29E+01	3.15E+07	9.26E-06
AM241	2.20E+02	1.00E-01	68	5.99E+06	8.80E-06	1.47E-12	3.00E-05	6.59E-14	1.60E-04	3.30E-04	1.74E-04	6.44E+05	3.15E+07	7.06E-02
TE125M	1.56E+02	1.00E-01	68	5.99E+06	8.80E-06	1.47E-12	3.00E-05	4.68E-14	1.60E-04	3.30E-04	3.01E-09	1.11E+01	3.15E+07	8.66E-07
PU240	1.26E+02	1.00E-01	68	5.99E+06	8.80E-06	1.47E-12	3.00E-05	3.78E-14	1.60E-04	3.30E-04	1.69E-04	6.25E+05	3.15E+07	3.93E-02
151Sm	0.00E+00	1.00E-01	68	5.99E+06	8.80E-06	1.47E-12	3.00E-05	0.00E+00	1.60E-04	3.30E-04	1.10E-08	4.07E+01	3.15E+07	0.00E+00
239Pu	6.16E+01	1.00E-01	68	5.99E+06	8.80E-06	1.47E-12	3.00E-05	1.85E-14	1.60E-04	3.30E-04	1.69E-04	6.25E+05	3.15E+07	1.92E-02
137mBa	2.16E+04	1.00E-01	68	5.99E+06	8.80E-06	1.47E-12	3.00E-05	6.47E-12	1.60E-04	3.30E-04	0.00E+00	0.00E+00	3.15E+07	0.00E+00
106Rh	4.16E+03	1.00E-01	68	5.99E+06	8.80E-06	1.47E-12	3.00E-05	1.25E-12	1.60E-04	3.30E-04	0.00E+00	0.00E+00	3.15E+07	0.00E+00
144mPr	0.00E+00	1.00E-01	68	5.99E+06	8.80E-06	1.47E-12	3.00E-05	0.00E+00	1.60E-04	3.30E-04	0.00E+00	0.00E+00	3.15E+07	0.00E+00
243Am	7.39E+00	1.00E-01	68	5.99E+06	8.80E-06	1.47E-12	3.00E-05	2.21E-15	1.60E-04	3.30E-04	1.73E-04	6.40E+05	3.15E+07	2.36E-03
242Cm	6.10E+00	1.00E-01	68	5.99E+06	8.80E-06	1.47E-12	3.00E-05	1.83E-15	1.60E-04	3.30E-04	3.90E-06	1.44E+04	3.15E+07	4.39E-05
243Cm	4.81E+00	1.00E-01	68	5.99E+06	8.80E-06	1.47E-12	3.00E-05	1.44E-15	1.60E-04	3.30E-04	1.18E-04	4.37E+05	3.15E+07	1.05E-03
239Np	7.39E+00	1.00E-01	68	5.99E+06	8.80E-06	1.47E-12	3.00E-05	2.21E-15	1.60E-04	3.30E-04	2.08E-10	7.70E-01	3.15E+07	2.83E-09
237Np	7.05E-02	1.00E-01	68	5.99E+06	8.80E-06	1.47E-12	3.00E-05	2.11E-17	1.60E-04	3.30E-04	2.62E-04	9.69E+05	3.15E+07	3.41E-05
242Pu	5.95E-01	1.00E-01	68	5.99E+06	8.80E-06	1.47E-12	3.00E-05	1.78E-16	1.60E-04	3.30E-04	1.61E-04	5.96E+05	3.15E+07	1.77E-04
242Am	1.69E+00	1.00E-01	68	5.99E+06	8.80E-06	1.47E-12	3.00E-05	5.06E-16	1.60E-04	3.30E-04	1.32E-08	4.88E+01	3.15E+07	4.11E-08
242mAm	1.70E+00	1.00E-01	68	5.99E+06	8.80E-06	1.47E-12	3.00E-05	5.09E-16	1.60E-04	3.30E-04	1.69E-04	6.25E+05	3.15E+07	5.30E-04
													Total	7.47E-01

MPC-68														
Off-Normal Conditions														
Committed Effective Dose Equivalent From Inhalation														
Nuclide	Inventory (Ci/Assy)	10% for off-normal storage	No. Assy	MPC Vol (cm3)	$L_{off\ nor}$ Rate at Upstream (cm3/s)	Fraction Released per sec	Release Fraction	Release Rate (Ci/sec)	X/Q (sec/m3)	Breathing Rate (m3/sec)	DCF (Sv/Bq)	DCF (mRem/uCi)	Occ Time (sec)	CEDE (mRem)
								Gases						
H-3	8.72E+01	1.00E-01	68	5.99E+06	8.80E-06	1.47E-12	0.30	2.61E-10	1.60E-04	3.30E-04	1.73E-11	6.40E-02	3.15E+07	2.78E-05
I-129	7.72E-03	1.00E-01	68	5.99E+06	8.80E-06	1.47E-12	0.30	2.31E-14	1.60E-04	3.30E-04	1.38E-10	5.11E-01	3.15E+07	1.96E-08
Kr-85	1.43E+03	1.00E-01	68	5.99E+06	8.80E-06	1.47E-12	0.30	4.29E-09	1.60E-04	3.30E-04	0.00E+00	0.00E+00	3.15E+07	0.00E+00
								Crud						
Co-60	6.50E+01	1.00E+00	68	5.99E+06	8.80E-06	1.47E-12	0.15	9.74E-10	1.60E-04	3.30E-04	1.35E-08	5.00E+01	3.15E+07	8.09E-02
								Volatiles						
Sr-90	1.52E+04	1.00E-01	68	5.99E+06	8.80E-06	1.47E-12	2.00E-04	3.04E-11	1.60E-04	3.30E-04	7.09E-08	2.62E+02	3.15E+07	1.33E-02
Ru-106	4.16E+03	1.00E-01	68	5.99E+06	8.80E-06	1.47E-12	2.00E-04	8.31E-12	1.60E-04	3.30E-04	1.61E-09	5.96E+00	3.15E+07	8.23E-05
Cs-134	7.20E+03	1.00E-01	68	5.99E+06	8.80E-06	1.47E-12	2.00E-04	1.44E-11	1.60E-04	3.30E-04	1.10E-08	4.07E+01	3.15E+07	9.74E-04
Cs-137	2.29E+04	1.00E-01	68	5.99E+06	8.80E-06	1.47E-12	2.00E-04	4.58E-11	1.60E-04	3.30E-04	7.94E-09	2.94E+01	3.15E+07	2.24E-03
								Fines						
PU241	2.10E+04	1.00E-01	68	5.99E+06	8.80E-06	1.47E-12	3.00E-05	6.29E-12	1.60E-04	3.30E-04	4.20E-05	1.55E+05	3.15E+07	1.63E+00
Y 90	1.52E+04	1.00E-01	68	5.99E+06	8.80E-06	1.47E-12	3.00E-05	4.56E-12	1.60E-04	3.30E-04	2.78E-10	1.03E+00	3.15E+07	7.79E-06
PM147	8.88E+03	1.00E-01	68	5.99E+06	8.80E-06	1.47E-12	3.00E-05	2.66E-12	1.60E-04	3.30E-04	2.01E-08	7.44E+01	3.15E+07	3.29E-04
CE144	2.46E+03	1.00E-01	68	5.99E+06	8.80E-06	1.47E-12	3.00E-05	7.37E-13	1.60E-04	3.30E-04	4.54E-08	1.68E+02	3.15E+07	2.06E-04
PR144	2.46E+03	1.00E-01	68	5.99E+06	8.80E-06	1.47E-12	3.00E-05	7.37E-13	1.60E-04	3.30E-04	1.47E-14	5.44E-05	3.15E+07	6.67E-11
EU154	1.07E+03	1.00E-01	68	5.99E+06	8.80E-06	1.47E-12	3.00E-05	3.21E-13	1.60E-04	3.30E-04	5.23E-07	1.94E+03	3.15E+07	1.03E-03
CM244	9.30E+02	1.00E-01	68	5.99E+06	8.80E-06	1.47E-12	3.00E-05	2.79E-13	1.60E-04	3.30E-04	1.17E-03	4.33E+06	3.15E+07	2.01E+00
PU238	7.49E+02	1.00E-01	68	5.99E+06	8.80E-06	1.47E-12	3.00E-05	2.24E-13	1.60E-04	3.30E-04	1.90E-03	7.03E+06	3.15E+07	2.62E+00
SB125	6.40E+02	1.00E-01	68	5.99E+06	8.80E-06	1.47E-12	3.00E-05	1.92E-13	1.60E-04	3.30E-04	9.78E-10	3.62E+00	3.15E+07	1.15E-06
EU155	3.51E+02	1.00E-01	68	5.99E+06	8.80E-06	1.47E-12	3.00E-05	1.05E-13	1.60E-04	3.30E-04	1.52E-07	5.62E+02	3.15E+07	9.84E-05
AM241	2.20E+02	1.00E-01	68	5.99E+06	8.80E-06	1.47E-12	3.00E-05	6.59E-14	1.60E-04	3.30E-04	2.17E-03	8.03E+06	3.15E+07	8.80E-01
TE125M	1.56E+02	1.00E-01	68	5.99E+06	8.80E-06	1.47E-12	3.00E-05	4.68E-14	1.60E-04	3.30E-04	3.21E-08	1.19E+02	3.15E+07	9.24E-06
PU240	1.26E+02	1.00E-01	68	5.99E+06	8.80E-06	1.47E-12	3.00E-05	3.78E-14	1.60E-04	3.30E-04	2.11E-03	7.81E+06	3.15E+07	4.90E-01
151Sm	0.00E+00	1.00E-01	68	5.99E+06	8.80E-06	1.47E-12	3.00E-05	0.00E+00	1.60E-04	3.30E-04	1.38E-07	5.11E+02	3.15E+07	0.00E+00
239Pu	6.16E+01	1.00E-01	68	5.99E+06	8.80E-06	1.47E-12	3.00E-05	1.85E-14	1.60E-04	3.30E-04	2.11E-03	7.81E+06	3.15E+07	2.40E-01
137mBa	2.16E+04	1.00E-01	68	5.99E+06	8.80E-06	1.47E-12	3.00E-05	6.47E-12	1.60E-04	3.30E-04	0.00E+00	0.00E+00	3.15E+07	0.00E+00
106Rh	4.16E+03	1.00E-01	68	5.99E+06	8.80E-06	1.47E-12	3.00E-05	1.25E-12	1.60E-04	3.30E-04	0.00E+00	0.00E+00	3.15E+07	0.00E+00
144mPr	0.00E+00	1.00E-01	68	5.99E+06	8.80E-06	1.47E-12	3.00E-05	0.00E+00	1.60E-04	3.30E-04	0.00E+00	0.00E+00	3.15E+07	0.00E+00
243Am	7.39E+00	1.00E-01	68	5.99E+06	8.80E-06	1.47E-12	3.00E-05	2.21E-15	1.60E-04	3.30E-04	2.17E-03	8.03E+06	3.15E+07	2.96E-02
242Cm	6.10E+00	1.00E-01	68	5.99E+06	8.80E-06	1.47E-12	3.00E-05	1.83E-15	1.60E-04	3.30E-04	4.87E-05	1.80E+05	3.15E+07	5.48E-04
243Cm	4.81E+00	1.00E-01	68	5.99E+06	8.80E-06	1.47E-12	3.00E-05	1.44E-15	1.60E-04	3.30E-04	1.47E-03	5.44E+06	3.15E+07	1.30E-02
239Np	7.39E+00	1.00E-01	68	5.99E+06	8.80E-06	1.47E-12	3.00E-05	2.21E-15	1.60E-04	3.30E-04	2.03E-09	7.51E+00	3.15E+07	2.77E-08
237Np	7.05E-02	1.00E-01	68	5.99E+06	8.80E-06	1.47E-12	3.00E-05	2.11E-17	1.60E-04	3.30E-04	3.27E-03	1.21E+07	3.15E+07	4.25E-04
242Pu	5.95E-01	1.00E-01	68	5.99E+06	8.80E-06	1.47E-12	3.00E-05	1.78E-16	1.60E-04	3.30E-04	2.01E-03	7.44E+06	3.15E+07	2.21E-03
242Am	1.69E+00	1.00E-01	68	5.99E+06	8.80E-06	1.47E-12	3.00E-05	5.06E-16	1.60E-04	3.30E-04	1.65E-07	6.11E+02	3.15E+07	5.14E-07
242mAm	1.70E+00	1.00E-01	68	5.99E+06	8.80E-06	1.47E-12	3.00E-05	5.09E-16	1.60E-04	3.30E-04	2.12E-03	7.84E+06	3.15E+07	6.65E-03
													Total	8.02E+00

MPC-68														
Off-Normal Conditions														
Committed Effective Dose Equivalent From Inhalation														
Nuclide	Inventory (Ci/Assy)	10% for off-normal storage	No. Assy	MPC Vol (cm3)	$L_{off\ nor}$ Rate at Upstream (cm3/s)	Fraction Released per sec	Release Fraction	Release Rate (Ci/sec)	X/Q (sec/m3)	Breathing Rate (m3/sec)	DCF (Sv/Bq)	DCF (mRem/uCi)	Occ Time (sec)	CEDE (mRem)
								Gases						
H-3	8.72E+01	1.00E-01	68	5.99E+06	8.80E-06	1.47E-12	0.30	2.61E-10	1.60E-04	3.30E-04	1.73E-11	6.40E-02	3.15E+07	2.78E-05
I-129	7.72E-03	1.00E-01	68	5.99E+06	8.80E-06	1.47E-12	0.30	2.31E-14	1.60E-04	3.30E-04	1.56E-06	5.77E+03	3.15E+07	2.22E-04
Kr-85	1.43E+03	1.00E-01	68	5.99E+06	8.80E-06	1.47E-12	0.30	4.29E-09	1.60E-04	3.30E-04	0.00E+00	0.00E+00	3.15E+07	0.00E+00
								Crud						
Co-60	6.50E+01	1.00E+00	68	5.99E+06	8.80E-06	1.47E-12	0.15	9.74E-10	1.60E-04	3.30E-04	1.62E-08	5.99E+01	3.15E+07	9.71E-02
								Volatiles						
Sr-90	1.52E+04	1.00E-01	68	5.99E+06	8.80E-06	1.47E-12	2.00E-04	3.04E-11	1.60E-04	3.30E-04	2.69E-10	9.95E-01	3.15E+07	5.03E-05
Ru-106	4.16E+03	1.00E-01	68	5.99E+06	8.80E-06	1.47E-12	2.00E-04	8.31E-12	1.60E-04	3.30E-04	1.72E-09	6.36E+00	3.15E+07	8.80E-05
Cs-134	7.20E+03	1.00E-01	68	5.99E+06	8.80E-06	1.47E-12	2.00E-04	1.44E-11	1.60E-04	3.30E-04	1.11E-08	4.11E+01	3.15E+07	9.83E-04
Cs-137	2.29E+04	1.00E-01	68	5.99E+06	8.80E-06	1.47E-12	2.00E-04	4.58E-11	1.60E-04	3.30E-04	7.93E-09	2.93E+01	3.15E+07	2.23E-03
								Fines						
PU241	2.10E+04	1.00E-01	68	5.99E+06	8.80E-06	1.47E-12	3.00E-05	6.29E-12	1.60E-04	3.30E-04	1.24E-11	4.59E-02	3.15E+07	4.80E-07
Y 90	1.52E+04	1.00E-01	68	5.99E+06	8.80E-06	1.47E-12	3.00E-05	4.56E-12	1.60E-04	3.30E-04	9.52E-12	3.52E-02	3.15E+07	2.67E-07
PM147	8.88E+03	1.00E-01	68	5.99E+06	8.80E-06	1.47E-12	3.00E-05	2.66E-12	1.60E-04	3.30E-04	1.98E-14	7.33E-05	3.15E+07	3.24E-10
CE144	2.46E+03	1.00E-01	68	5.99E+06	8.80E-06	1.47E-12	3.00E-05	7.37E-13	1.60E-04	3.30E-04	1.88E-09	6.96E+00	3.15E+07	8.53E-06
PR144	2.46E+03	1.00E-01	68	5.99E+06	8.80E-06	1.47E-12	3.00E-05	7.37E-13	1.60E-04	3.30E-04	8.47E-15	3.13E-05	3.15E+07	3.84E-11
EU154	1.07E+03	1.00E-01	68	5.99E+06	8.80E-06	1.47E-12	3.00E-05	3.21E-13	1.60E-04	3.30E-04	7.14E-09	2.64E+01	3.15E+07	1.41E-05
CM244	9.30E+02	1.00E-01	68	5.99E+06	8.80E-06	1.47E-12	3.00E-05	2.79E-13	1.60E-04	3.30E-04	1.01E-09	3.74E+00	3.15E+07	1.73E-06
PU238	7.49E+02	1.00E-01	68	5.99E+06	8.80E-06	1.47E-12	3.00E-05	2.24E-13	1.60E-04	3.30E-04	9.62E-10	3.56E+00	3.15E+07	1.33E-06
SB125	6.40E+02	1.00E-01	68	5.99E+06	8.80E-06	1.47E-12	3.00E-05	1.92E-13	1.60E-04	3.30E-04	3.24E-10	1.20E+00	3.15E+07	3.82E-07
EU155	3.51E+02	1.00E-01	68	5.99E+06	8.80E-06	1.47E-12	3.00E-05	1.05E-13	1.60E-04	3.30E-04	2.40E-10	8.88E-01	3.15E+07	1.55E-07
AM241	2.20E+02	1.00E-01	68	5.99E+06	8.80E-06	1.47E-12	3.00E-05	6.59E-14	1.60E-04	3.30E-04	1.60E-09	5.92E+00	3.15E+07	6.49E-07
TE125M	1.56E+02	1.00E-01	68	5.99E+06	8.80E-06	1.47E-12	3.00E-05	4.68E-14	1.60E-04	3.30E-04	9.93E-11	3.67E-01	3.15E+07	2.86E-08
PU240	1.26E+02	1.00E-01	68	5.99E+06	8.80E-06	1.47E-12	3.00E-05	3.78E-14	1.60E-04	3.30E-04	9.05E-10	3.35E+00	3.15E+07	2.10E-07
151Sm	0.00E+00	1.00E-01	68	5.99E+06	8.80E-06	1.47E-12	3.00E-05	0.00E+00	1.60E-04	3.30E-04	1.32E-14	4.88E-05	3.15E+07	0.00E+00
239Pu	6.16E+01	1.00E-01	68	5.99E+06	8.80E-06	1.47E-12	3.00E-05	1.85E-14	1.60E-04	3.30E-04	9.03E-10	3.34E+00	3.15E+07	1.03E-07
137mBa	2.16E+04	1.00E-01	68	5.99E+06	8.80E-06	1.47E-12	3.00E-05	6.47E-12	1.60E-04	3.30E-04	0.00E+00	0.00E+00	3.15E+07	0.00E+00
106Rh	4.16E+03	1.00E-01	68	5.99E+06	8.80E-06	1.47E-12	3.00E-05	1.25E-12	1.60E-04	3.30E-04	0.00E+00	0.00E+00	3.15E+07	0.00E+00
144mPr	0.00E+00	1.00E-01	68	5.99E+06	8.80E-06	1.47E-12	3.00E-05	0.00E+00	1.60E-04	3.30E-04	0.00E+00	0.00E+00	3.15E+07	0.00E+00
243Am	7.39E+00	1.00E-01	68	5.99E+06	8.80E-06	1.47E-12	3.00E-05	2.21E-15	1.60E-04	3.30E-04	8.29E-09	3.07E+01	3.15E+07	1.13E-07
242Cm	6.10E+00	1.00E-01	68	5.99E+06	8.80E-06	1.47E-12	3.00E-05	1.83E-15	1.60E-04	3.30E-04	9.41E-10	3.48E+00	3.15E+07	1.06E-08
243Cm	4.81E+00	1.00E-01	68	5.99E+06	8.80E-06	1.47E-12	3.00E-05	1.44E-15	1.60E-04	3.30E-04	3.83E-09	1.42E+01	3.15E+07	3.40E-08
239Np	7.39E+00	1.00E-01	68	5.99E+06	8.80E-06	1.47E-12	3.00E-05	2.21E-15	1.60E-04	3.30E-04	7.62E-12	2.82E-02	3.15E+07	1.04E-10
237Np	7.05E-02	1.00E-01	68	5.99E+06	8.80E-06	1.47E-12	3.00E-05	2.11E-17	1.60E-04	3.30E-04	1.34E-08	4.96E+01	3.15E+07	1.74E-09
242Pu	5.95E-01	1.00E-01	68	5.99E+06	8.80E-06	1.47E-12	3.00E-05	1.78E-16	1.60E-04	3.30E-04	8.79E-10	3.25E+00	3.15E+07	9.65E-10
242Am	1.69E+00	1.00E-01	68	5.99E+06	8.80E-06	1.47E-12	3.00E-05	5.06E-16	1.60E-04	3.30E-04	2.52E-12	9.32E-03	3.15E+07	7.85E-12
242mAm	1.70E+00	1.00E-01	68	5.99E+06	8.80E-06	1.47E-12	3.00E-05	5.09E-16	1.60E-04	3.30E-04	5.64E-10	2.09E+00	3.15E+07	1.77E-09
													Total	1.01E-01

MPC-68														
Off-Normal Conditions														
Committed Effective Dose Equivalent From Inhalation														
Nuclide	Inventory (Ci/Assy)	10% for off-normal storage	No. Assy	MPC Vol (cm3)	$L_{off\ nor}$ Rate at Upstream (cm3/s)	Fraction Released per sec	Release Fraction	Release Rate (Ci/sec)	X/Q (sec/m3)	Breathing Rate (m3/sec)	DCF (Sv/Bq)	DCF (mRem/uCi)	Occ Time (sec)	CEDE (mRem)
								Gases						
H-3	8.72E+01	1.00E-01	68	5.99E+06	8.80E-06	1.47E-12	0.30	2.61E-10	1.60E-04	3.30E-04	1.73E-11	6.40E-02	3.15E+07	2.78E-05
I-129	7.72E-03	1.00E-01	68	5.99E+06	8.80E-06	1.47E-12	0.30	2.31E-14	1.60E-04	3.30E-04	4.69E-08	1.74E+02	3.15E+07	6.68E-06
Kr-85	1.43E+03	1.00E-01	68	5.99E+06	8.80E-06	1.47E-12	0.30	4.29E-09	1.60E-04	3.30E-04	0.00E+00	0.00E+00	3.15E+07	0.00E+00
								Crud						
Co-60	6.50E+01	1.00E+00	68	5.99E+06	8.80E-06	1.47E-12	0.15	9.74E-10	1.60E-04	3.30E-04	5.91E-08	2.19E+02	3.15E+07	3.54E-01
								Volatiles						
Sr-90	1.52E+04	1.00E-01	68	5.99E+06	8.80E-06	1.47E-12	2.00E-04	3.04E-11	1.60E-04	3.30E-04	3.51E-07	1.30E+03	3.15E+07	6.56E-02
Ru-106	4.16E+03	1.00E-01	68	5.99E+06	8.80E-06	1.47E-12	2.00E-04	8.31E-12	1.60E-04	3.30E-04	1.29E-07	4.77E+02	3.15E+07	6.60E-03
Cs-134	7.20E+03	1.00E-01	68	5.99E+06	8.80E-06	1.47E-12	2.00E-04	1.44E-11	1.60E-04	3.30E-04	1.25E-08	4.63E+01	3.15E+07	1.11E-03
Cs-137	2.29E+04	1.00E-01	68	5.99E+06	8.80E-06	1.47E-12	2.00E-04	4.58E-11	1.60E-04	3.30E-04	8.63E-09	3.19E+01	3.15E+07	2.43E-03
								Fines						
PU241	2.10E+04	1.00E-01	68	5.99E+06	8.80E-06	1.47E-12	3.00E-05	6.29E-12	1.60E-04	3.30E-04	2.23E-06	8.25E+03	3.15E+07	8.64E-02
Y 90	1.52E+04	1.00E-01	68	5.99E+06	8.80E-06	1.47E-12	3.00E-05	4.56E-12	1.60E-04	3.30E-04	2.13E-09	7.88E+00	3.15E+07	5.97E-05
PM147	8.88E+03	1.00E-01	68	5.99E+06	8.80E-06	1.47E-12	3.00E-05	2.66E-12	1.60E-04	3.30E-04	1.06E-08	3.92E+01	3.15E+07	1.74E-04
CE144	2.46E+03	1.00E-01	68	5.99E+06	8.80E-06	1.47E-12	3.00E-05	7.37E-13	1.60E-04	3.30E-04	5.84E-08	2.16E+02	3.15E+07	2.65E-04
PR144	2.46E+03	1.00E-01	68	5.99E+06	8.80E-06	1.47E-12	3.00E-05	7.37E-13	1.60E-04	3.30E-04	1.17E-11	4.33E-02	3.15E+07	5.31E-08
EU154	1.07E+03	1.00E-01	68	5.99E+06	8.80E-06	1.47E-12	3.00E-05	3.21E-13	1.60E-04	3.30E-04	7.73E-08	2.86E+02	3.15E+07	1.53E-04
CM244	9.30E+02	1.00E-01	68	5.99E+06	8.80E-06	1.47E-12	3.00E-05	2.79E-13	1.60E-04	3.30E-04	6.70E-05	2.48E+05	3.15E+07	1.15E-01
PU238	7.49E+02	1.00E-01	68	5.99E+06	8.80E-06	1.47E-12	3.00E-05	2.24E-13	1.60E-04	3.30E-04	1.06E-04	3.92E+05	3.15E+07	1.46E-01
SB125	6.40E+02	1.00E-01	68	5.99E+06	8.80E-06	1.47E-12	3.00E-05	1.92E-13	1.60E-04	3.30E-04	3.30E-09	1.22E+01	3.15E+07	3.90E-06
EU155	3.51E+02	1.00E-01	68	5.99E+06	8.80E-06	1.47E-12	3.00E-05	1.05E-13	1.60E-04	3.30E-04	1.12E-08	4.14E+01	3.15E+07	7.25E-06
AM241	2.20E+02	1.00E-01	68	5.99E+06	8.80E-06	1.47E-12	3.00E-05	6.59E-14	1.60E-04	3.30E-04	1.20E-04	4.44E+05	3.15E+07	4.87E-02
TE125M	1.56E+02	1.00E-01	68	5.99E+06	8.80E-06	1.47E-12	3.00E-05	4.68E-14	1.60E-04	3.30E-04	1.52E-09	5.62E+00	3.15E+07	4.37E-07
PU240	1.26E+02	1.00E-01	68	5.99E+06	8.80E-06	1.47E-12	3.00E-05	3.78E-14	1.60E-04	3.30E-04	1.16E-04	4.29E+05	3.15E+07	2.70E-02
151Sm	0.00E+00	1.00E-01	68	5.99E+06	8.80E-06	1.47E-12	3.00E-05	0.00E+00	1.60E-04	3.30E-04	8.10E-09	3.00E+01	3.15E+07	0.00E+00
239Pu	6.16E+01	1.00E-01	68	5.99E+06	8.80E-06	1.47E-12	3.00E-05	1.85E-14	1.60E-04	3.30E-04	1.16E-04	4.29E+05	3.15E+07	1.32E-02
137mBa	2.16E+04	1.00E-01	68	5.99E+06	8.80E-06	1.47E-12	3.00E-05	6.47E-12	1.60E-04	3.30E-04	0.00E+00	0.00E+00	3.15E+07	0.00E+00
106Rh	4.16E+03	1.00E-01	68	5.99E+06	8.80E-06	1.47E-12	3.00E-05	1.25E-12	1.60E-04	3.30E-04	0.00E+00	0.00E+00	3.15E+07	0.00E+00
144mPr	0.00E+00	1.00E-01	68	5.99E+06	8.80E-06	1.47E-12	3.00E-05	0.00E+00	1.60E-04	3.30E-04	0.00E+00	0.00E+00	3.15E+07	0.00E+00
243Am	7.39E+00	1.00E-01	68	5.99E+06	8.80E-06	1.47E-12	3.00E-05	2.21E-15	1.60E-04	3.30E-04	1.19E-04	4.40E+05	3.15E+07	1.62E-03
242Cm	6.10E+00	1.00E-01	68	5.99E+06	8.80E-06	1.47E-12	3.00E-05	1.83E-15	1.60E-04	3.30E-04	4.67E-06	1.73E+04	3.15E+07	5.25E-05
243Cm	4.81E+00	1.00E-01	68	5.99E+06	8.80E-06	1.47E-12	3.00E-05	1.44E-15	1.60E-04	3.30E-04	8.30E-05	3.07E+05	3.15E+07	7.36E-04
239Np	7.39E+00	1.00E-01	68	5.99E+06	8.80E-06	1.47E-12	3.00E-05	2.21E-15	1.60E-04	3.30E-04	6.78E-10	2.51E+00	3.15E+07	9.24E-09
237Np	7.05E-02	1.00E-01	68	5.99E+06	8.80E-06	1.47E-12	3.00E-05	2.11E-17	1.60E-04	3.30E-04	1.46E-04	5.40E+05	3.15E+07	1.90E-05
242Pu	5.95E-01	1.00E-01	68	5.99E+06	8.80E-06	1.47E-12	3.00E-05	1.78E-16	1.60E-04	3.30E-04	1.11E-04	4.11E+05	3.15E+07	1.22E-04
242Am	1.69E+00	1.00E-01	68	5.99E+06	8.80E-06	1.47E-12	3.00E-05	5.06E-16	1.60E-04	3.30E-04	1.58E-08	5.85E+01	3.15E+07	4.92E-08
242mAm	1.70E+00	1.00E-01	68	5.99E+06	8.80E-06	1.47E-12	3.00E-05	5.09E-16	1.60E-04	3.30E-04	1.15E-04	4.26E+05	3.15E+07	3.61E-04
													Total	8.70E-01

MPC-68													
Accident Conditions													
Committed Effective Dose Equivalent From Inhalation													
Nuclide	Inventory (Ci/Assy)	No. Assy	MPC Vol (cm3)	L_{acc} Rate at Upstream (cm3/s)	Fraction Released per sec	Release Fraction	Release Rate (Ci/sec)	X/Q (sec/m3)	Breathing Rate (m3/sec)	DCF (Sv/Bq)	DCF (mRem/uCi)	Occ Time (sec)	CEDE (mRem)
							Gases						
H-3	8.72E+01	68	5.99E+06	1.25E-05	2.09E-12	0.30	3.72E-09	8.00E-03	3.30E-04	1.73E-11	6.40E-02	2.59E+06	1.63E-03
I-129	7.72E-03	68	5.99E+06	1.25E-05	2.09E-12	0.30	3.30E-13	8.00E-03	3.30E-04	8.69E-11	3.22E-01	2.59E+06	7.25E-07
Kr-85	1.43E+03	68	5.99E+06	1.25E-05	2.09E-12	0.30	6.11E-08	8.00E-03	3.30E-04	0.00E+00	0.00E+00	2.59E+06	0.00E+00
							Crud						
Co-60	6.50E+01	68	5.99E+06	1.25E-05	2.09E-12	1.00	9.25E-09	8.00E-03	3.30E-04	4.76E-09	1.76E+01	2.59E+06	1.11E+00
							Volatiles						
Sr-90	1.52E+04	68	5.99E+06	1.25E-05	2.09E-12	2.00E-04	4.33E-10	8.00E-03	3.30E-04	2.69E-10	9.95E-01	2.59E+06	2.95E-03
Ru-106	4.16E+03	68	5.99E+06	1.25E-05	2.09E-12	2.00E-04	1.18E-10	8.00E-03	3.30E-04	1.30E-09	4.81E+00	2.59E+06	3.90E-03
Cs-134	7.20E+03	68	5.99E+06	1.25E-05	2.09E-12	2.00E-04	2.05E-10	8.00E-03	3.30E-04	1.30E-08	4.81E+01	2.59E+06	6.74E-02
Cs-137	2.29E+04	68	5.99E+06	1.25E-05	2.09E-12	2.00E-04	6.52E-10	8.00E-03	3.30E-04	8.76E-09	3.24E+01	2.59E+06	1.44E-01
							Fines						
PU241	2.10E+04	68	5.99E+06	1.25E-05	2.09E-12	3.00E-05	8.97E-11	8.00E-03	3.30E-04	6.82E-07	2.52E+03	2.59E+06	1.55E+00
Y 90	1.52E+04	68	5.99E+06	1.25E-05	2.09E-12	3.00E-05	6.49E-11	8.00E-03	3.30E-04	9.52E-12	3.52E-02	2.59E+06	1.56E-05
PM147	8.88E+03	68	5.99E+06	1.25E-05	2.09E-12	3.00E-05	3.79E-11	8.00E-03	3.30E-04	8.25E-15	3.05E-05	2.59E+06	7.92E-09
CE144	2.46E+03	68	5.99E+06	1.25E-05	2.09E-12	3.00E-05	1.05E-11	8.00E-03	3.30E-04	1.93E-09	7.14E+00	2.59E+06	5.13E-04
PR144	2.46E+03	68	5.99E+06	1.25E-05	2.09E-12	3.00E-05	1.05E-11	8.00E-03	3.30E-04	2.41E-15	8.92E-06	2.59E+06	6.41E-10
EU154	1.07E+03	68	5.99E+06	1.25E-05	2.09E-12	3.00E-05	4.57E-12	8.00E-03	3.30E-04	1.17E-08	4.33E+01	2.59E+06	1.35E-03
CM244	9.30E+02	68	5.99E+06	1.25E-05	2.09E-12	3.00E-05	3.97E-12	8.00E-03	3.30E-04	1.59E-05	5.88E+04	2.59E+06	1.60E+00
PU238	7.49E+02	68	5.99E+06	1.25E-05	2.09E-12	3.00E-05	3.20E-12	8.00E-03	3.30E-04	2.80E-05	1.04E+05	2.59E+06	2.27E+00
SB125	6.40E+02	68	5.99E+06	1.25E-05	2.09E-12	3.00E-05	2.73E-12	8.00E-03	3.30E-04	3.60E-10	1.33E+00	2.59E+06	2.49E-05
EU155	3.51E+02	68	5.99E+06	1.25E-05	2.09E-12	3.00E-05	1.50E-12	8.00E-03	3.30E-04	3.56E-10	1.32E+00	2.59E+06	1.35E-05
AM241	2.20E+02	68	5.99E+06	1.25E-05	2.09E-12	3.00E-05	9.40E-13	8.00E-03	3.30E-04	3.25E-05	1.20E+05	2.59E+06	7.73E-01
TE125M	1.56E+02	68	5.99E+06	1.25E-05	2.09E-12	3.00E-05	6.66E-13	8.00E-03	3.30E-04	1.24E-10	4.59E-01	2.59E+06	2.09E-06
PU240	1.26E+02	68	5.99E+06	1.25E-05	2.09E-12	3.00E-05	5.38E-13	8.00E-03	3.30E-04	3.18E-05	1.18E+05	2.59E+06	4.33E-01
151Sm	0.00E+00	68	5.99E+06	1.25E-05	2.09E-12	3.00E-05	0.00E+00	8.00E-03	3.30E-04	4.03E-14	1.49E-04	2.59E+06	0.00E+00
239Pu	6.16E+01	68	5.99E+06	1.25E-05	2.09E-12	3.00E-05	2.63E-13	8.00E-03	3.30E-04	3.18E-05	1.18E+05	2.59E+06	2.12E-01
137mBa	2.16E+04	68	5.99E+06	1.25E-05	2.09E-12	3.00E-05	9.22E-11	8.00E-03	3.30E-04	0.00E+00	0.00E+00	2.59E+06	0.00E+00
106Rh	4.16E+03	68	5.99E+06	1.25E-05	2.09E-12	3.00E-05	1.78E-11	8.00E-03	3.30E-04	0.00E+00	0.00E+00	2.59E+06	0.00E+00
144mPr	0.00E+00	68	5.99E+06	1.25E-05	2.09E-12	3.00E-05	0.00E+00	8.00E-03	3.30E-04	0.00E+00	0.00E+00	2.59E+06	0.00E+00
243Am	7.39E+00	68	5.99E+06	1.25E-05	2.09E-12	3.00E-05	3.16E-14	8.00E-03	3.30E-04	3.26E-05	1.21E+05	2.59E+06	2.60E-02
242Cm	6.10E+00	68	5.99E+06	1.25E-05	2.09E-12	3.00E-05	2.61E-14	8.00E-03	3.30E-04	5.70E-07	2.11E+03	2.59E+06	3.76E-04
243Cm	4.81E+00	68	5.99E+06	1.25E-05	2.09E-12	3.00E-05	2.05E-14	8.00E-03	3.30E-04	2.07E-05	7.66E+04	2.59E+06	1.08E-02
239Np	7.39E+00	68	5.99E+06	1.25E-05	2.09E-12	3.00E-05	3.16E-14	8.00E-03	3.30E-04	7.45E-11	2.76E-01	2.59E+06	5.95E-08
237Np	7.05E-02	68	5.99E+06	1.25E-05	2.09E-12	3.00E-05	3.01E-16	8.00E-03	3.30E-04	2.96E-05	1.10E+05	2.59E+06	2.25E-04
242Pu	5.95E-01	68	5.99E+06	1.25E-05	2.09E-12	3.00E-05	2.54E-15	8.00E-03	3.30E-04	3.02E-05	1.12E+05	2.59E+06	1.94E-03
242Am	1.69E+00	68	5.99E+06	1.25E-05	2.09E-12	3.00E-05	7.22E-15	8.00E-03	3.30E-04	1.94E-09	7.18E+00	2.59E+06	3.54E-07
242mAm	1.70E+00	68	5.99E+06	1.25E-05	2.09E-12	3.00E-05	7.26E-15	8.00E-03	3.30E-04	3.21E-05	1.19E+05	2.59E+06	5.90E-03
												Total	8.21E+00

MPC-68													
Accident Conditions													
Committed Effective Dose Equivalent From Inhalation													
Nuclide	Inventory (Ci/Assy)	No. Assy	MPC Vol (cm3)	L_{acc} Rate at Upstream (cm3/s)	Fraction Released per sec	Release Fraction	Release Rate (Ci/sec)	X/Q (sec/m3)	Breathing Rate (m3/sec)	DCF (Sv/Bq)	DCF (mRem/uCi)	Occ Time (sec)	CEDE (mRem)
							Gases						
H-3	8.72E+01	68	5.99E+06	1.25E-05	2.09E-12	0.30	3.72E-09	8.00E-03	3.30E-04	1.73E-11	6.40E-02	2.59E+06	1.63E-03
I-129	7.72E-03	68	5.99E+06	1.25E-05	2.09E-12	0.30	3.30E-13	8.00E-03	3.30E-04	2.09E-10	7.73E-01	2.59E+06	1.74E-06
Kr-85	1.43E+03	68	5.99E+06	1.25E-05	2.09E-12	0.30	6.11E-08	8.00E-03	3.30E-04	0.00E+00	0.00E+00	2.59E+06	0.00E+00
							Crud						
Co-60	6.50E+01	68	5.99E+06	1.25E-05	2.09E-12	1.00	9.25E-09	8.00E-03	3.30E-04	1.84E-08	6.81E+01	2.59E+06	4.31E+00
							Volatiles						
Sr-90	1.52E+04	68	5.99E+06	1.25E-05	2.09E-12	2.00E-04	4.33E-10	8.00E-03	3.30E-04	2.69E-10	9.95E-01	2.59E+06	2.95E-03
Ru-106	4.16E+03	68	5.99E+06	1.25E-05	2.09E-12	2.00E-04	1.18E-10	8.00E-03	3.30E-04	1.78E-09	6.59E+00	2.59E+06	5.33E-03
Cs-134	7.20E+03	68	5.99E+06	1.25E-05	2.09E-12	2.00E-04	2.05E-10	8.00E-03	3.30E-04	1.08E-08	4.00E+01	2.59E+06	5.60E-02
Cs-137	2.29E+04	68	5.99E+06	1.25E-05	2.09E-12	2.00E-04	6.52E-10	8.00E-03	3.30E-04	7.84E-09	2.90E+01	2.59E+06	1.29E-01
							Fines						
PU241	2.10E+04	68	5.99E+06	1.25E-05	2.09E-12	3.00E-05	8.97E-11	8.00E-03	3.30E-04	3.06E-11	1.13E-01	2.59E+06	6.94E-05
Y 90	1.52E+04	68	5.99E+06	1.25E-05	2.09E-12	3.00E-05	6.49E-11	8.00E-03	3.30E-04	9.52E-12	3.52E-02	2.59E+06	1.56E-05
PM147	8.88E+03	68	5.99E+06	1.25E-05	2.09E-12	3.00E-05	3.79E-11	8.00E-03	3.30E-04	3.60E-14	1.33E-04	2.59E+06	3.45E-08
CE144	2.46E+03	68	5.99E+06	1.25E-05	2.09E-12	3.00E-05	1.05E-11	8.00E-03	3.30E-04	1.97E-09	7.29E+00	2.59E+06	5.24E-04
PR144	2.46E+03	68	5.99E+06	1.25E-05	2.09E-12	3.00E-05	1.05E-11	8.00E-03	3.30E-04	1.05E-14	3.89E-05	2.59E+06	2.79E-09
EU154	1.07E+03	68	5.99E+06	1.25E-05	2.09E-12	3.00E-05	4.57E-12	8.00E-03	3.30E-04	1.55E-08	5.74E+01	2.59E+06	1.79E-03
CM244	9.30E+02	68	5.99E+06	1.25E-05	2.09E-12	3.00E-05	3.97E-12	8.00E-03	3.30E-04	1.04E-09	3.85E+00	2.59E+06	1.05E-04
PU238	7.49E+02	68	5.99E+06	1.25E-05	2.09E-12	3.00E-05	3.20E-12	8.00E-03	3.30E-04	1.00E-09	3.70E+00	2.59E+06	8.09E-05
SB125	6.40E+02	68	5.99E+06	1.25E-05	2.09E-12	3.00E-05	2.73E-12	8.00E-03	3.30E-04	4.16E-10	1.54E+00	2.59E+06	2.88E-05
EU155	3.51E+02	68	5.99E+06	1.25E-05	2.09E-12	3.00E-05	1.50E-12	8.00E-03	3.30E-04	6.14E-10	2.27E+00	2.59E+06	2.33E-05
AM241	2.20E+02	68	5.99E+06	1.25E-05	2.09E-12	3.00E-05	9.40E-13	8.00E-03	3.30E-04	2.67E-09	9.88E+00	2.59E+06	6.35E-05
TE125M	1.56E+02	68	5.99E+06	1.25E-05	2.09E-12	3.00E-05	6.66E-13	8.00E-03	3.30E-04	1.07E-10	3.96E-01	2.59E+06	1.80E-06
PU240	1.26E+02	68	5.99E+06	1.25E-05	2.09E-12	3.00E-05	5.38E-13	8.00E-03	3.30E-04	9.51E-10	3.52E+00	2.59E+06	1.29E-05
151Sm	0.00E+00	68	5.99E+06	1.25E-05	2.09E-12	3.00E-05	0.00E+00	8.00E-03	3.30E-04	1.49E-13	5.51E-04	2.59E+06	0.00E+00
239Pu	6.16E+01	68	5.99E+06	1.25E-05	2.09E-12	3.00E-05	2.63E-13	8.00E-03	3.30E-04	9.22E-10	3.41E+00	2.59E+06	6.14E-06
137mBa	2.16E+04	68	5.99E+06	1.25E-05	2.09E-12	3.00E-05	9.22E-11	8.00E-03	3.30E-04	0.00E+00	0.00E+00	2.59E+06	0.00E+00
106Rh	4.16E+03	68	5.99E+06	1.25E-05	2.09E-12	3.00E-05	1.78E-11	8.00E-03	3.30E-04	0.00E+00	0.00E+00	2.59E+06	0.00E+00
144mPr	0.00E+00	68	5.99E+06	1.25E-05	2.09E-12	3.00E-05	0.00E+00	8.00E-03	3.30E-04	0.00E+00	0.00E+00	2.59E+06	0.00E+00
243Am	7.39E+00	68	5.99E+06	1.25E-05	2.09E-12	3.00E-05	3.16E-14	8.00E-03	3.30E-04	1.52E-08	5.62E+01	2.59E+06	1.21E-05
242Cm	6.10E+00	68	5.99E+06	1.25E-05	2.09E-12	3.00E-05	2.61E-14	8.00E-03	3.30E-04	9.44E-10	3.49E+00	2.59E+06	6.22E-07
243Cm	4.81E+00	68	5.99E+06	1.25E-05	2.09E-12	3.00E-05	2.05E-14	8.00E-03	3.30E-04	6.29E-09	2.33E+01	2.59E+06	3.27E-06
239Np	7.39E+00	68	5.99E+06	1.25E-05	2.09E-12	3.00E-05	3.16E-14	8.00E-03	3.30E-04	1.63E-11	6.03E-02	2.59E+06	1.30E-08
237Np	7.05E-02	68	5.99E+06	1.25E-05	2.09E-12	3.00E-05	3.01E-16	8.00E-03	3.30E-04	1.69E-08	6.25E+01	2.59E+06	1.29E-07
242Pu	5.95E-01	68	5.99E+06	1.25E-05	2.09E-12	3.00E-05	2.54E-15	8.00E-03	3.30E-04	9.45E-10	3.50E+00	2.59E+06	6.08E-08
242Am	1.69E+00	68	5.99E+06	1.25E-05	2.09E-12	3.00E-05	7.22E-15	8.00E-03	3.30E-04	2.49E-12	9.21E-03	2.59E+06	4.55E-10
242mAm	1.70E+00	68	5.99E+06	1.25E-05	2.09E-12	3.00E-05	7.26E-15	8.00E-03	3.30E-04	1.38E-09	5.11E+00	2.59E+06	2.53E-07
												Total	4.51E+00

MPC-68													
Accident Conditions													
Committed Effective Dose Equivalent From Inhalation													
Nuclide	Inventory (Ci/Assy)	No. Assy	MPC Vol (cm3)	L_{acc} Rate at Upstream (cm3/s)	Fraction Released per sec	Release Fraction	Release Rate (Ci/sec)	X/Q (sec/m3)	Breathing Rate (m3/sec)	DCF (Sv/Bq)	DCF (mRem/uCi)	Occ Time (sec)	CEDE (mRem)
							Gases						
H-3	8.72E+01	68	5.99E+06	1.25E-05	2.09E-12	0.30	3.72E-09	8.00E-03	3.30E-04	1.73E-11	6.40E-02	2.59E+06	1.63E-03
I-129	7.72E-03	68	5.99E+06	1.25E-05	2.09E-12	0.30	3.30E-13	8.00E-03	3.30E-04	3.14E-10	1.16E+00	2.59E+06	2.62E-06
Kr-85	1.43E+03	68	5.99E+06	1.25E-05	2.09E-12	0.30	6.11E-08	8.00E-03	3.30E-04	0.00E+00	0.00E+00	2.59E+06	0.00E+00
							Crud						
Co-60	6.50E+01	68	5.99E+06	1.25E-05	2.09E-12	1.00	9.25E-09	8.00E-03	3.30E-04	3.45E-07	1.28E+03	2.59E+06	8.08E+01
							Volatiles						
Sr-90	1.52E+04	68	5.99E+06	1.25E-05	2.09E-12	2.00E-04	4.33E-10	8.00E-03	3.30E-04	2.86E-06	1.06E+04	2.59E+06	3.13E+01
Ru-106	4.16E+03	68	5.99E+06	1.25E-05	2.09E-12	2.00E-04	1.18E-10	8.00E-03	3.30E-04	1.04E-06	3.85E+03	2.59E+06	3.12E+00
Cs-134	7.20E+03	68	5.99E+06	1.25E-05	2.09E-12	2.00E-04	2.05E-10	8.00E-03	3.30E-04	1.18E-08	4.37E+01	2.59E+06	6.12E-02
Cs-137	2.29E+04	68	5.99E+06	1.25E-05	2.09E-12	2.00E-04	6.52E-10	8.00E-03	3.30E-04	8.82E-09	3.26E+01	2.59E+06	1.45E-01
							Fines						
PU241	2.10E+04	68	5.99E+06	1.25E-05	2.09E-12	3.00E-05	8.97E-11	8.00E-03	3.30E-04	7.42E-09	2.75E+01	2.59E+06	1.68E-02
Y 90	1.52E+04	68	5.99E+06	1.25E-05	2.09E-12	3.00E-05	6.49E-11	8.00E-03	3.30E-04	8.89E-09	3.29E+01	2.59E+06	1.46E-02
PM147	8.88E+03	68	5.99E+06	1.25E-05	2.09E-12	3.00E-05	3.79E-11	8.00E-03	3.30E-04	7.74E-08	2.86E+02	2.59E+06	7.43E-02
CE144	2.46E+03	68	5.99E+06	1.25E-05	2.09E-12	3.00E-05	1.05E-11	8.00E-03	3.30E-04	1.83E-07	6.77E+02	2.59E+06	4.86E-02
PR144	2.46E+03	68	5.99E+06	1.25E-05	2.09E-12	3.00E-05	1.05E-11	8.00E-03	3.30E-04	9.40E-11	3.48E-01	2.59E+06	2.50E-05
EU154	1.07E+03	68	5.99E+06	1.25E-05	2.09E-12	3.00E-05	4.57E-12	8.00E-03	3.30E-04	7.92E-08	2.93E+02	2.59E+06	9.16E-03
CM244	9.30E+02	68	5.99E+06	1.25E-05	2.09E-12	3.00E-05	3.97E-12	8.00E-03	3.30E-04	1.93E-05	7.14E+04	2.59E+06	1.94E+00
PU238	7.49E+02	68	5.99E+06	1.25E-05	2.09E-12	3.00E-05	3.20E-12	8.00E-03	3.30E-04	1.84E-05	6.81E+04	2.59E+06	1.49E+00
SB125	6.40E+02	68	5.99E+06	1.25E-05	2.09E-12	3.00E-05	2.73E-12	8.00E-03	3.30E-04	2.17E-08	8.03E+01	2.59E+06	1.50E-03
EU155	3.51E+02	68	5.99E+06	1.25E-05	2.09E-12	3.00E-05	1.50E-12	8.00E-03	3.30E-04	1.19E-08	4.40E+01	2.59E+06	4.51E-04
AM241	2.20E+02	68	5.99E+06	1.25E-05	2.09E-12	3.00E-05	9.40E-13	8.00E-03	3.30E-04	1.84E-05	6.81E+04	2.59E+06	4.37E-01
TE125M	1.56E+02	68	5.99E+06	1.25E-05	2.09E-12	3.00E-05	6.66E-13	8.00E-03	3.30E-04	4.66E-10	1.72E+00	2.59E+06	7.85E-06
PU240	1.26E+02	68	5.99E+06	1.25E-05	2.09E-12	3.00E-05	5.38E-13	8.00E-03	3.30E-04	1.73E-05	6.40E+04	2.59E+06	2.36E-01
151Sm	0.00E+00	68	5.99E+06	1.25E-05	2.09E-12	3.00E-05	0.00E+00	8.00E-03	3.30E-04	3.26E-09	1.21E+01	2.59E+06	0.00E+00
239Pu	6.16E+01	68	5.99E+06	1.25E-05	2.09E-12	3.00E-05	2.63E-13	8.00E-03	3.30E-04	1.73E-05	6.40E+04	2.59E+06	1.15E-01
137mBa	2.16E+04	68	5.99E+06	1.25E-05	2.09E-12	3.00E-05	9.22E-11	8.00E-03	3.30E-04	0.00E+00	0.00E+00	2.59E+06	0.00E+00
106Rh	4.16E+03	68	5.99E+06	1.25E-05	2.09E-12	3.00E-05	1.78E-11	8.00E-03	3.30E-04	0.00E+00	0.00E+00	2.59E+06	0.00E+00
144mPr	0.00E+00	68	5.99E+06	1.25E-05	2.09E-12	3.00E-05	0.00E+00	8.00E-03	3.30E-04	0.00E+00	0.00E+00	2.59E+06	0.00E+00
243Am	7.39E+00	68	5.99E+06	1.25E-05	2.09E-12	3.00E-05	3.16E-14	8.00E-03	3.30E-04	1.78E-05	6.59E+04	2.59E+06	1.42E-02
242Cm	6.10E+00	68	5.99E+06	1.25E-05	2.09E-12	3.00E-05	2.61E-14	8.00E-03	3.30E-04	1.55E-05	5.74E+04	2.59E+06	1.02E-02
243Cm	4.81E+00	68	5.99E+06	1.25E-05	2.09E-12	3.00E-05	2.05E-14	8.00E-03	3.30E-04	1.94E-05	7.18E+04	2.59E+06	1.01E-02
239Np	7.39E+00	68	5.99E+06	1.25E-05	2.09E-12	3.00E-05	3.16E-14	8.00E-03	3.30E-04	2.36E-09	8.73E+00	2.59E+06	1.88E-06
237Np	7.05E-02	68	5.99E+06	1.25E-05	2.09E-12	3.00E-05	3.01E-16	8.00E-03	3.30E-04	1.61E-05	5.96E+04	2.59E+06	1.23E-04
242Pu	5.95E-01	68	5.99E+06	1.25E-05	2.09E-12	3.00E-05	2.54E-15	8.00E-03	3.30E-04	1.64E-05	6.07E+04	2.59E+06	1.05E-03
242Am	1.69E+00	68	5.99E+06	1.25E-05	2.09E-12	3.00E-05	7.22E-15	8.00E-03	3.30E-04	5.20E-08	1.92E+02	2.59E+06	9.50E-06
242mAm	1.70E+00	68	5.99E+06	1.25E-05	2.09E-12	3.00E-05	7.26E-15	8.00E-03	3.30E-04	4.20E-06	1.55E+04	2.59E+06	7.71E-04
												Total	1.20E+02

MPC-68													
Accident Conditions													
Committed Effective Dose Equivalent From Inhalation													
Nuclide	Inventory (Ci/Assy)	No. Assy	MPC Vol (cm3)	L_{acc} Rate at Upstream (cm3/s)	Fraction Released per sec	Release Fraction	Release Rate (Ci/sec)	X/Q (sec/m3)	Breathing Rate (m3/sec)	DCF (Sv/Bq)	DCF (mRem/uCi)	Occ Time (sec)	CEDE (mRem)
							Gases						
H-3	8.72E+01	68	5.99E+06	1.25E-05	2.09E-12	0.30	3.72E-09	8.00E-03	3.30E-04	1.73E-11	6.40E-02	2.59E+06	1.63E-03
I-129	7.72E-03	68	5.99E+06	1.25E-05	2.09E-12	0.30	3.30E-13	8.00E-03	3.30E-04	1.40E-10	5.18E-01	2.59E+06	1.17E-06
Kr-85	1.43E+03	68	5.99E+06	1.25E-05	2.09E-12	0.30	6.11E-08	8.00E-03	3.30E-04	0.00E+00	0.00E+00	2.59E+06	0.00E+00
							Crud						
Co-60	6.50E+01	68	5.99E+06	1.25E-05	2.09E-12	1.00	9.25E-09	8.00E-03	3.30E-04	1.72E-08	6.36E+01	2.59E+06	4.03E+00
							Volatiles						
Sr-90	1.52E+04	68	5.99E+06	1.25E-05	2.09E-12	2.00E-04	4.33E-10	8.00E-03	3.30E-04	3.28E-08	1.21E+02	2.59E+06	3.59E-01
Ru-106	4.16E+03	68	5.99E+06	1.25E-05	2.09E-12	2.00E-04	1.18E-10	8.00E-03	3.30E-04	1.76E-09	6.51E+00	2.59E+06	5.27E-03
Cs-134	7.20E+03	68	5.99E+06	1.25E-05	2.09E-12	2.00E-04	2.05E-10	8.00E-03	3.30E-04	1.18E-08	4.37E+01	2.59E+06	6.12E-02
Cs-137	2.29E+04	68	5.99E+06	1.25E-05	2.09E-12	2.00E-04	6.52E-10	8.00E-03	3.30E-04	8.30E-09	3.07E+01	2.59E+06	1.37E-01
							Fines						
PU241	2.10E+04	68	5.99E+06	1.25E-05	2.09E-12	3.00E-05	8.97E-11	8.00E-03	3.30E-04	3.36E-06	1.24E+04	2.59E+06	7.62E+00
Y 90	1.52E+04	68	5.99E+06	1.25E-05	2.09E-12	3.00E-05	6.49E-11	8.00E-03	3.30E-04	2.79E-10	1.03E+00	2.59E+06	4.58E-04
PM147	8.88E+03	68	5.99E+06	1.25E-05	2.09E-12	3.00E-05	3.79E-11	8.00E-03	3.30E-04	1.61E-09	5.96E+00	2.59E+06	1.54E-03
CE144	2.46E+03	68	5.99E+06	1.25E-05	2.09E-12	3.00E-05	1.05E-11	8.00E-03	3.30E-04	2.67E-08	9.88E+01	2.59E+06	7.10E-03
PR144	2.46E+03	68	5.99E+06	1.25E-05	2.09E-12	3.00E-05	1.05E-11	8.00E-03	3.30E-04	1.38E-14	5.11E-05	2.59E+06	3.67E-09
EU154	1.07E+03	68	5.99E+06	1.25E-05	2.09E-12	3.00E-05	4.57E-12	8.00E-03	3.30E-04	1.06E-07	3.92E+02	2.59E+06	1.23E-02
CM244	9.30E+02	68	5.99E+06	1.25E-05	2.09E-12	3.00E-05	3.97E-12	8.00E-03	3.30E-04	9.38E-05	3.47E+05	2.59E+06	9.43E+00
PU238	7.49E+02	68	5.99E+06	1.25E-05	2.09E-12	3.00E-05	3.20E-12	8.00E-03	3.30E-04	1.52E-04	5.62E+05	2.59E+06	1.23E+01
SB125	6.40E+02	68	5.99E+06	1.25E-05	2.09E-12	3.00E-05	2.73E-12	8.00E-03	3.30E-04	5.35E-10	1.98E+00	2.59E+06	3.70E-05
EU155	3.51E+02	68	5.99E+06	1.25E-05	2.09E-12	3.00E-05	1.50E-12	8.00E-03	3.30E-04	1.43E-08	5.29E+01	2.59E+06	5.42E-04
AM241	2.20E+02	68	5.99E+06	1.25E-05	2.09E-12	3.00E-05	9.40E-13	8.00E-03	3.30E-04	1.74E-04	6.44E+05	2.59E+06	4.14E+00
TE125M	1.56E+02	68	5.99E+06	1.25E-05	2.09E-12	3.00E-05	6.66E-13	8.00E-03	3.30E-04	3.01E-09	1.11E+01	2.59E+06	5.07E-05
PU240	1.26E+02	68	5.99E+06	1.25E-05	2.09E-12	3.00E-05	5.38E-13	8.00E-03	3.30E-04	1.69E-04	6.25E+05	2.59E+06	2.30E+00
151Sm	0.00E+00	68	5.99E+06	1.25E-05	2.09E-12	3.00E-05	0.00E+00	8.00E-03	3.30E-04	1.10E-08	4.07E+01	2.59E+06	0.00E+00
239Pu	6.16E+01	68	5.99E+06	1.25E-05	2.09E-12	3.00E-05	2.63E-13	8.00E-03	3.30E-04	1.69E-04	6.25E+05	2.59E+06	1.12E+00
137mBa	2.16E+04	68	5.99E+06	1.25E-05	2.09E-12	3.00E-05	9.22E-11	8.00E-03	3.30E-04	0.00E+00	0.00E+00	2.59E+06	0.00E+00
106Rh	4.16E+03	68	5.99E+06	1.25E-05	2.09E-12	3.00E-05	1.78E-11	8.00E-03	3.30E-04	0.00E+00	0.00E+00	2.59E+06	0.00E+00
144mPr	0.00E+00	68	5.99E+06	1.25E-05	2.09E-12	3.00E-05	0.00E+00	8.00E-03	3.30E-04	0.00E+00	0.00E+00	2.59E+06	0.00E+00
243Am	7.39E+00	68	5.99E+06	1.25E-05	2.09E-12	3.00E-05	3.16E-14	8.00E-03	3.30E-04	1.73E-04	6.40E+05	2.59E+06	1.38E-01
242Cm	6.10E+00	68	5.99E+06	1.25E-05	2.09E-12	3.00E-05	2.61E-14	8.00E-03	3.30E-04	3.90E-06	1.44E+04	2.59E+06	2.57E-03
243Cm	4.81E+00	68	5.99E+06	1.25E-05	2.09E-12	3.00E-05	2.05E-14	8.00E-03	3.30E-04	1.18E-04	4.37E+05	2.59E+06	6.13E-02
239Np	7.39E+00	68	5.99E+06	1.25E-05	2.09E-12	3.00E-05	3.16E-14	8.00E-03	3.30E-04	2.08E-10	7.70E-01	2.59E+06	1.66E-07
237Np	7.05E-02	68	5.99E+06	1.25E-05	2.09E-12	3.00E-05	3.01E-16	8.00E-03	3.30E-04	2.62E-04	9.69E+05	2.59E+06	2.00E-03
242Pu	5.95E-01	68	5.99E+06	1.25E-05	2.09E-12	3.00E-05	2.54E-15	8.00E-03	3.30E-04	1.61E-04	5.96E+05	2.59E+06	1.04E-02
242Am	1.69E+00	68	5.99E+06	1.25E-05	2.09E-12	3.00E-05	7.22E-15	8.00E-03	3.30E-04	1.32E-08	4.88E+01	2.59E+06	2.41E-06
242mAm	1.70E+00	68	5.99E+06	1.25E-05	2.09E-12	3.00E-05	7.26E-15	8.00E-03	3.30E-04	1.69E-04	6.25E+05	2.59E+06	3.10E-02
												Total	4.18E+01

MPC-68													
Accident Conditions													
Committed Effective Dose Equivalent From Inhalation													
Nuclide	Inventory (Ci/Assy)	No. Assy	MPC Vol (cm3)	L_{acc} Rate at Upstream (cm3/s)	Fraction Released per sec	Release Fraction	Release Rate (Ci/sec)	X/Q (sec/m3)	Breathing Rate (m3/sec)	DCF (Sv/Bq)	DCF (mRem/uCi)	Occ Time (sec)	CEDE (mRem)
							Gases						
H-3	8.72E+01	68	5.99E+06	1.25E-05	2.09E-12	0.30	3.72E-09	8.00E-03	3.30E-04	1.73E-11	6.40E-02	2.59E+06	1.63E-03
I-129	7.72E-03	68	5.99E+06	1.25E-05	2.09E-12	0.30	3.30E-13	8.00E-03	3.30E-04	1.38E-10	5.11E-01	2.59E+06	1.15E-06
Kr-85	1.43E+03	68	5.99E+06	1.25E-05	2.09E-12	0.30	6.11E-08	8.00E-03	3.30E-04	0.00E+00	0.00E+00	2.59E+06	0.00E+00
							Crud						
Co-60	6.50E+01	68	5.99E+06	1.25E-05	2.09E-12	1.00	9.25E-09	8.00E-03	3.30E-04	1.35E-08	5.00E+01	2.59E+06	3.16E+00
							Volatiles						
Sr-90	1.52E+04	68	5.99E+06	1.25E-05	2.09E-12	2.00E-04	4.33E-10	8.00E-03	3.30E-04	7.09E-08	2.62E+02	2.59E+06	7.76E-01
Ru-106	4.16E+03	68	5.99E+06	1.25E-05	2.09E-12	2.00E-04	1.18E-10	8.00E-03	3.30E-04	1.61E-09	5.96E+00	2.59E+06	4.82E-03
Cs-134	7.20E+03	68	5.99E+06	1.25E-05	2.09E-12	2.00E-04	2.05E-10	8.00E-03	3.30E-04	1.10E-08	4.07E+01	2.59E+06	5.70E-02
Cs-137	2.29E+04	68	5.99E+06	1.25E-05	2.09E-12	2.00E-04	6.52E-10	8.00E-03	3.30E-04	7.94E-09	2.94E+01	2.59E+06	1.31E-01
							Fines						
PU241	2.10E+04	68	5.99E+06	1.25E-05	2.09E-12	3.00E-05	8.97E-11	8.00E-03	3.30E-04	4.20E-05	1.55E+05	2.59E+06	9.53E+01
Y 90	1.52E+04	68	5.99E+06	1.25E-05	2.09E-12	3.00E-05	6.49E-11	8.00E-03	3.30E-04	2.78E-10	1.03E+00	2.59E+06	4.57E-04
PM147	8.88E+03	68	5.99E+06	1.25E-05	2.09E-12	3.00E-05	3.79E-11	8.00E-03	3.30E-04	2.01E-08	7.44E+01	2.59E+06	1.93E-02
CE144	2.46E+03	68	5.99E+06	1.25E-05	2.09E-12	3.00E-05	1.05E-11	8.00E-03	3.30E-04	4.54E-08	1.68E+02	2.59E+06	1.21E-02
PR144	2.46E+03	68	5.99E+06	1.25E-05	2.09E-12	3.00E-05	1.05E-11	8.00E-03	3.30E-04	1.47E-14	5.44E-05	2.59E+06	3.91E-09
EU154	1.07E+03	68	5.99E+06	1.25E-05	2.09E-12	3.00E-05	4.57E-12	8.00E-03	3.30E-04	5.23E-07	1.94E+03	2.59E+06	6.05E-02
CM244	9.30E+02	68	5.99E+06	1.25E-05	2.09E-12	3.00E-05	3.97E-12	8.00E-03	3.30E-04	1.17E-03	4.33E+06	2.59E+06	1.18E+02
PU238	7.49E+02	68	5.99E+06	1.25E-05	2.09E-12	3.00E-05	3.20E-12	8.00E-03	3.30E-04	1.90E-03	7.03E+06	2.59E+06	1.54E+02
SB125	6.40E+02	68	5.99E+06	1.25E-05	2.09E-12	3.00E-05	2.73E-12	8.00E-03	3.30E-04	9.78E-10	3.62E+00	2.59E+06	6.76E-05
EU155	3.51E+02	68	5.99E+06	1.25E-05	2.09E-12	3.00E-05	1.50E-12	8.00E-03	3.30E-04	1.52E-07	5.62E+02	2.59E+06	5.76E-03
AM241	2.20E+02	68	5.99E+06	1.25E-05	2.09E-12	3.00E-05	9.40E-13	8.00E-03	3.30E-04	2.17E-03	8.03E+06	2.59E+06	5.16E+01
TE125M	1.56E+02	68	5.99E+06	1.25E-05	2.09E-12	3.00E-05	6.66E-13	8.00E-03	3.30E-04	3.21E-08	1.19E+02	2.59E+06	5.41E-04
PU240	1.26E+02	68	5.99E+06	1.25E-05	2.09E-12	3.00E-05	5.38E-13	8.00E-03	3.30E-04	2.11E-03	7.81E+06	2.59E+06	2.87E+01
151Sm	0.00E+00	68	5.99E+06	1.25E-05	2.09E-12	3.00E-05	0.00E+00	8.00E-03	3.30E-04	1.38E-07	5.11E+02	2.59E+06	0.00E+00
239Pu	6.16E+01	68	5.99E+06	1.25E-05	2.09E-12	3.00E-05	2.63E-13	8.00E-03	3.30E-04	2.11E-03	7.81E+06	2.59E+06	1.40E+01
137mBa	2.16E+04	68	5.99E+06	1.25E-05	2.09E-12	3.00E-05	9.22E-11	8.00E-03	3.30E-04	0.00E+00	0.00E+00	2.59E+06	0.00E+00
106Rh	4.16E+03	68	5.99E+06	1.25E-05	2.09E-12	3.00E-05	1.78E-11	8.00E-03	3.30E-04	0.00E+00	0.00E+00	2.59E+06	0.00E+00
144mPr	0.00E+00	68	5.99E+06	1.25E-05	2.09E-12	3.00E-05	0.00E+00	8.00E-03	3.30E-04	0.00E+00	0.00E+00	2.59E+06	0.00E+00
243Am	7.39E+00	68	5.99E+06	1.25E-05	2.09E-12	3.00E-05	3.16E-14	8.00E-03	3.30E-04	2.17E-03	8.03E+06	2.59E+06	1.73E+00
242Cm	6.10E+00	68	5.99E+06	1.25E-05	2.09E-12	3.00E-05	2.61E-14	8.00E-03	3.30E-04	4.87E-05	1.80E+05	2.59E+06	3.21E-02
243Cm	4.81E+00	68	5.99E+06	1.25E-05	2.09E-12	3.00E-05	2.05E-14	8.00E-03	3.30E-04	1.47E-03	5.44E+06	2.59E+06	7.64E-01
239Np	7.39E+00	68	5.99E+06	1.25E-05	2.09E-12	3.00E-05	3.16E-14	8.00E-03	3.30E-04	2.03E-09	7.51E+00	2.59E+06	1.62E-06
237Np	7.05E-02	68	5.99E+06	1.25E-05	2.09E-12	3.00E-05	3.01E-16	8.00E-03	3.30E-04	3.27E-03	1.21E+07	2.59E+06	2.49E-02
242Pu	5.95E-01	68	5.99E+06	1.25E-05	2.09E-12	3.00E-05	2.54E-15	8.00E-03	3.30E-04	2.01E-03	7.44E+06	2.59E+06	1.29E-01
242Am	1.69E+00	68	5.99E+06	1.25E-05	2.09E-12	3.00E-05	7.22E-15	8.00E-03	3.30E-04	1.65E-07	6.11E+02	2.59E+06	3.01E-05
242mAm	1.70E+00	68	5.99E+06	1.25E-05	2.09E-12	3.00E-05	7.26E-15	8.00E-03	3.30E-04	2.12E-03	7.84E+06	2.59E+06	3.89E-01
												Total	4.68E+02

MPC-68													
Accident Conditions													
Committed Effective Dose Equivalent From Inhalation													
Nuclide	Inventory (Ci/Assy)	No. Assy	MPC Vol (cm3)	L_{acc} Rate at Upstream (cm3/s)	Fraction Released per sec	Release Fraction	Release Rate (Ci/sec)	X/Q (sec/m3)	Breathing Rate (m3/sec)	DCF (Sv/Bq)	DCF (mRem/uCi)	Occ Time (sec)	CEDE (mRem)
							Gases						
H-3	8.72E+01	68	5.99E+06	1.25E-05	2.09E-12	0.30	3.72E-09	8.00E-03	3.30E-04	1.73E-11	6.40E-02	2.59E+06	1.63E-03
I-129	7.72E-03	68	5.99E+06	1.25E-05	2.09E-12	0.30	3.30E-13	8.00E-03	3.30E-04	1.56E-06	5.77E+03	2.59E+06	1.30E-02
Kr-85	1.43E+03	68	5.99E+06	1.25E-05	2.09E-12	0.30	6.11E-08	8.00E-03	3.30E-04	0.00E+00	0.00E+00	2.59E+06	0.00E+00
							Crud						
Co-60	6.50E+01	68	5.99E+06	1.25E-05	2.09E-12	1.00	9.25E-09	8.00E-03	3.30E-04	1.62E-08	5.99E+01	2.59E+06	3.79E+00
							Volatiles						
Sr-90	1.52E+04	68	5.99E+06	1.25E-05	2.09E-12	2.00E-04	4.33E-10	8.00E-03	3.30E-04	2.69E-10	9.95E-01	2.59E+06	2.95E-03
Ru-106	4.16E+03	68	5.99E+06	1.25E-05	2.09E-12	2.00E-04	1.18E-10	8.00E-03	3.30E-04	1.72E-09	6.36E+00	2.59E+06	5.15E-03
Cs-134	7.20E+03	68	5.99E+06	1.25E-05	2.09E-12	2.00E-04	2.05E-10	8.00E-03	3.30E-04	1.11E-08	4.11E+01	2.59E+06	5.76E-02
Cs-137	2.29E+04	68	5.99E+06	1.25E-05	2.09E-12	2.00E-04	6.52E-10	8.00E-03	3.30E-04	7.93E-09	2.93E+01	2.59E+06	1.31E-01
							Fines						
PU241	2.10E+04	68	5.99E+06	1.25E-05	2.09E-12	3.00E-05	8.97E-11	8.00E-03	3.30E-04	1.24E-11	4.59E-02	2.59E+06	2.81E-05
Y 90	1.52E+04	68	5.99E+06	1.25E-05	2.09E-12	3.00E-05	6.49E-11	8.00E-03	3.30E-04	9.52E-12	3.52E-02	2.59E+06	1.56E-05
PM147	8.88E+03	68	5.99E+06	1.25E-05	2.09E-12	3.00E-05	3.79E-11	8.00E-03	3.30E-04	1.98E-14	7.33E-05	2.59E+06	1.90E-08
CE144	2.46E+03	68	5.99E+06	1.25E-05	2.09E-12	3.00E-05	1.05E-11	8.00E-03	3.30E-04	1.88E-09	6.96E+00	2.59E+06	5.00E-04
PR144	2.46E+03	68	5.99E+06	1.25E-05	2.09E-12	3.00E-05	1.05E-11	8.00E-03	3.30E-04	8.47E-15	3.13E-05	2.59E+06	2.25E-09
EU154	1.07E+03	68	5.99E+06	1.25E-05	2.09E-12	3.00E-05	4.57E-12	8.00E-03	3.30E-04	7.14E-09	2.64E+01	2.59E+06	8.25E-04
CM244	9.30E+02	68	5.99E+06	1.25E-05	2.09E-12	3.00E-05	3.97E-12	8.00E-03	3.30E-04	1.01E-09	3.74E+00	2.59E+06	1.01E-04
PU238	7.49E+02	68	5.99E+06	1.25E-05	2.09E-12	3.00E-05	3.20E-12	8.00E-03	3.30E-04	9.62E-10	3.56E+00	2.59E+06	7.79E-05
SB125	6.40E+02	68	5.99E+06	1.25E-05	2.09E-12	3.00E-05	2.73E-12	8.00E-03	3.30E-04	3.24E-10	1.20E+00	2.59E+06	2.24E-05
EU155	3.51E+02	68	5.99E+06	1.25E-05	2.09E-12	3.00E-05	1.50E-12	8.00E-03	3.30E-04	2.40E-10	8.88E-01	2.59E+06	9.10E-06
AM241	2.20E+02	68	5.99E+06	1.25E-05	2.09E-12	3.00E-05	9.40E-13	8.00E-03	3.30E-04	1.60E-09	5.92E+00	2.59E+06	3.80E-05
TE125M	1.56E+02	68	5.99E+06	1.25E-05	2.09E-12	3.00E-05	6.66E-13	8.00E-03	3.30E-04	9.93E-11	3.67E-01	2.59E+06	1.67E-06
PU240	1.26E+02	68	5.99E+06	1.25E-05	2.09E-12	3.00E-05	5.38E-13	8.00E-03	3.30E-04	9.05E-10	3.35E+00	2.59E+06	1.23E-05
151Sm	0.00E+00	68	5.99E+06	1.25E-05	2.09E-12	3.00E-05	0.00E+00	8.00E-03	3.30E-04	1.32E-14	4.88E-05	2.59E+06	0.00E+00
239Pu	6.16E+01	68	5.99E+06	1.25E-05	2.09E-12	3.00E-05	2.63E-13	8.00E-03	3.30E-04	9.03E-10	3.34E+00	2.59E+06	6.01E-06
137mBa	2.16E+04	68	5.99E+06	1.25E-05	2.09E-12	3.00E-05	9.22E-11	8.00E-03	3.30E-04	0.00E+00	0.00E+00	2.59E+06	0.00E+00
106Rh	4.16E+03	68	5.99E+06	1.25E-05	2.09E-12	3.00E-05	1.78E-11	8.00E-03	3.30E-04	0.00E+00	0.00E+00	2.59E+06	0.00E+00
144mPr	0.00E+00	68	5.99E+06	1.25E-05	2.09E-12	3.00E-05	0.00E+00	8.00E-03	3.30E-04	0.00E+00	0.00E+00	2.59E+06	0.00E+00
243Am	7.39E+00	68	5.99E+06	1.25E-05	2.09E-12	3.00E-05	3.16E-14	8.00E-03	3.30E-04	8.29E-09	3.07E+01	2.59E+06	6.62E-06
242Cm	6.10E+00	68	5.99E+06	1.25E-05	2.09E-12	3.00E-05	2.61E-14	8.00E-03	3.30E-04	9.41E-10	3.48E+00	2.59E+06	6.20E-07
243Cm	4.81E+00	68	5.99E+06	1.25E-05	2.09E-12	3.00E-05	2.05E-14	8.00E-03	3.30E-04	3.83E-09	1.42E+01	2.59E+06	1.99E-06
239Np	7.39E+00	68	5.99E+06	1.25E-05	2.09E-12	3.00E-05	3.16E-14	8.00E-03	3.30E-04	7.62E-12	2.82E-02	2.59E+06	6.08E-09
237Np	7.05E-02	68	5.99E+06	1.25E-05	2.09E-12	3.00E-05	3.01E-16	8.00E-03	3.30E-04	1.34E-08	4.96E+01	2.59E+06	1.02E-07
242Pu	5.95E-01	68	5.99E+06	1.25E-05	2.09E-12	3.00E-05	2.54E-15	8.00E-03	3.30E-04	8.79E-10	3.25E+00	2.59E+06	5.65E-08
242Am	1.69E+00	68	5.99E+06	1.25E-05	2.09E-12	3.00E-05	7.22E-15	8.00E-03	3.30E-04	2.52E-12	9.32E-03	2.59E+06	4.60E-10
242mAm	1.70E+00	68	5.99E+06	1.25E-05	2.09E-12	3.00E-05	7.26E-15	8.00E-03	3.30E-04	5.64E-10	2.09E+00	2.59E+06	1.04E-07
												Total	4.01E+00

MPC-68													
Accident Conditions													
Committed Effective Dose Equivalent From Inhalation													
Nuclide	Inventory (Ci/Assy)	No. Assy	MPC Vol (cm3)	L_{acc} Rate at Upstream (cm3/s)	Fraction Released per sec	Release Fraction	Release Rate (Ci/sec)	X/Q (sec/m3)	Breathing Rate (m3/sec)	DCF (Sv/Bq)	DCF (mRem/uCi)	Occ Time (sec)	CEDE (mRem)
							Gases						
H-3	8.72E+01	68	5.99E+06	1.25E-05	2.09E-12	0.30	3.72E-09	8.00E-03	3.30E-04	1.73E-11	6.40E-02	2.59E+06	1.63E-03
I-129	7.72E-03	68	5.99E+06	1.25E-05	2.09E-12	0.30	3.30E-13	8.00E-03	3.30E-04	4.69E-08	1.74E+02	2.59E+06	3.91E-04
Kr-85	1.43E+03	68	5.99E+06	1.25E-05	2.09E-12	0.30	6.11E-08	8.00E-03	3.30E-04	0.00E+00	0.00E+00	2.59E+06	0.00E+00
							Crud						
Co-60	6.50E+01	68	5.99E+06	1.25E-05	2.09E-12	1.00	9.25E-09	8.00E-03	3.30E-04	5.91E-08	2.19E+02	2.59E+06	1.38E+01
							Volatiles						
Sr-90	1.52E+04	68	5.99E+06	1.25E-05	2.09E-12	2.00E-04	4.33E-10	8.00E-03	3.30E-04	3.51E-07	1.30E+03	2.59E+06	3.84E+00
Ru-106	4.16E+03	68	5.99E+06	1.25E-05	2.09E-12	2.00E-04	1.18E-10	8.00E-03	3.30E-04	1.29E-07	4.77E+02	2.59E+06	3.87E-01
Cs-134	7.20E+03	68	5.99E+06	1.25E-05	2.09E-12	2.00E-04	2.05E-10	8.00E-03	3.30E-04	1.25E-08	4.63E+01	2.59E+06	6.48E-02
Cs-137	2.29E+04	68	5.99E+06	1.25E-05	2.09E-12	2.00E-04	6.52E-10	8.00E-03	3.30E-04	8.63E-09	3.19E+01	2.59E+06	1.42E-01
							Fines						
PU241	2.10E+04	68	5.99E+06	1.25E-05	2.09E-12	3.00E-05	8.97E-11	8.00E-03	3.30E-04	2.23E-06	8.25E+03	2.59E+06	5.06E+00
Y 90	1.52E+04	68	5.99E+06	1.25E-05	2.09E-12	3.00E-05	6.49E-11	8.00E-03	3.30E-04	2.13E-09	7.88E+00	2.59E+06	3.50E-03
PM147	8.88E+03	68	5.99E+06	1.25E-05	2.09E-12	3.00E-05	3.79E-11	8.00E-03	3.30E-04	1.06E-08	3.92E+01	2.59E+06	1.02E-02
CE144	2.46E+03	68	5.99E+06	1.25E-05	2.09E-12	3.00E-05	1.05E-11	8.00E-03	3.30E-04	5.84E-08	2.16E+02	2.59E+06	1.55E-02
PR144	2.46E+03	68	5.99E+06	1.25E-05	2.09E-12	3.00E-05	1.05E-11	8.00E-03	3.30E-04	1.17E-11	4.33E-02	2.59E+06	3.11E-06
EU154	1.07E+03	68	5.99E+06	1.25E-05	2.09E-12	3.00E-05	4.57E-12	8.00E-03	3.30E-04	7.73E-08	2.86E+02	2.59E+06	8.94E-03
CM244	9.30E+02	68	5.99E+06	1.25E-05	2.09E-12	3.00E-05	3.97E-12	8.00E-03	3.30E-04	6.70E-05	2.48E+05	2.59E+06	6.73E+00
PU238	7.49E+02	68	5.99E+06	1.25E-05	2.09E-12	3.00E-05	3.20E-12	8.00E-03	3.30E-04	1.06E-04	3.92E+05	2.59E+06	8.58E+00
SB125	6.40E+02	68	5.99E+06	1.25E-05	2.09E-12	3.00E-05	2.73E-12	8.00E-03	3.30E-04	3.30E-09	1.22E+01	2.59E+06	2.28E-04
EU155	3.51E+02	68	5.99E+06	1.25E-05	2.09E-12	3.00E-05	1.50E-12	8.00E-03	3.30E-04	1.12E-08	4.14E+01	2.59E+06	4.25E-04
AM241	2.20E+02	68	5.99E+06	1.25E-05	2.09E-12	3.00E-05	9.40E-13	8.00E-03	3.30E-04	1.20E-04	4.44E+05	2.59E+06	2.85E+00
TE125M	1.56E+02	68	5.99E+06	1.25E-05	2.09E-12	3.00E-05	6.66E-13	8.00E-03	3.30E-04	1.52E-09	5.62E+00	2.59E+06	2.56E-05
PU240	1.26E+02	68	5.99E+06	1.25E-05	2.09E-12	3.00E-05	5.38E-13	8.00E-03	3.30E-04	1.16E-04	4.29E+05	2.59E+06	1.58E+00
151Sm	0.00E+00	68	5.99E+06	1.25E-05	2.09E-12	3.00E-05	0.00E+00	8.00E-03	3.30E-04	8.10E-09	3.00E+01	2.59E+06	0.00E+00
239Pu	6.16E+01	68	5.99E+06	1.25E-05	2.09E-12	3.00E-05	2.63E-13	8.00E-03	3.30E-04	1.16E-04	4.29E+05	2.59E+06	7.72E-01
137mBa	2.16E+04	68	5.99E+06	1.25E-05	2.09E-12	3.00E-05	9.22E-11	8.00E-03	3.30E-04	0.00E+00	0.00E+00	2.59E+06	0.00E+00
106Rh	4.16E+03	68	5.99E+06	1.25E-05	2.09E-12	3.00E-05	1.78E-11	8.00E-03	3.30E-04	0.00E+00	0.00E+00	2.59E+06	0.00E+00
144mPr	0.00E+00	68	5.99E+06	1.25E-05	2.09E-12	3.00E-05	0.00E+00	8.00E-03	3.30E-04	0.00E+00	0.00E+00	2.59E+06	0.00E+00
243Am	7.39E+00	68	5.99E+06	1.25E-05	2.09E-12	3.00E-05	3.16E-14	8.00E-03	3.30E-04	1.19E-04	4.40E+05	2.59E+06	9.50E-02
242Cm	6.10E+00	68	5.99E+06	1.25E-05	2.09E-12	3.00E-05	2.61E-14	8.00E-03	3.30E-04	4.67E-06	1.73E+04	2.59E+06	3.08E-03
243Cm	4.81E+00	68	5.99E+06	1.25E-05	2.09E-12	3.00E-05	2.05E-14	8.00E-03	3.30E-04	8.30E-05	3.07E+05	2.59E+06	4.31E-02
239Np	7.39E+00	68	5.99E+06	1.25E-05	2.09E-12	3.00E-05	3.16E-14	8.00E-03	3.30E-04	6.78E-10	2.51E+00	2.59E+06	5.41E-07
237Np	7.05E-02	68	5.99E+06	1.25E-05	2.09E-12	3.00E-05	3.01E-16	8.00E-03	3.30E-04	1.46E-04	5.40E+05	2.59E+06	1.11E-03
242Pu	5.95E-01	68	5.99E+06	1.25E-05	2.09E-12	3.00E-05	2.54E-15	8.00E-03	3.30E-04	1.11E-04	4.11E+05	2.59E+06	7.14E-03
242Am	1.69E+00	68	5.99E+06	1.25E-05	2.09E-12	3.00E-05	7.22E-15	8.00E-03	3.30E-04	1.58E-08	5.85E+01	2.59E+06	2.89E-06
242mAm	1.70E+00	68	5.99E+06	1.25E-05	2.09E-12	3.00E-05	7.26E-15	8.00E-03	3.30E-04	1.15E-04	4.26E+05	2.59E+06	2.11E-02
												Total	4.41E+01

MPC-68														
Normal Conditions														
Effective Dose Equivalent From Submersion														
Nuclide	Inventory (Ci/Assy)	1% for normal storage	No. Assy	MPC Vol (cm3)	L_{nor} Rate at Upstream (cm3/s)	Fraction Released per sec	Release Fraction	Release Rate (Ci/sec)	X/Q (sec/m3)	DCF (Sv/Bq)	DCF (mRem/uCi)	Occ Time (sec)	EDE (mRem)	
								Gases						
H-3	8.72E+01	1.00E-02	68	5.99E+06	8.80E-06	1.47E-12	0.30	2.61E-11	1.60E-04	0.00E+00	0.00E+00	3.15E+07	0.00E+00	
I-129	7.72E-03	1.00E-02	68	5.99E+06	8.80E-06	1.47E-12	0.30	2.31E-15	1.60E-04	4.83E-16	1.79E-06	3.15E+07	2.08E-11	
Kr-85	1.43E+03	1.00E-02	68	5.99E+06	8.80E-06	1.47E-12	0.30	4.29E-10	1.60E-04	1.17E-16	4.33E-07	3.15E+07	9.35E-07	
								Crud						
Co-60	6.50E+01	1.00E+00	68	5.99E+06	8.80E-06	1.47E-12	0.15	9.74E-10	1.60E-04	1.23E-13	4.55E-04	3.15E+07	2.23E-03	
								Volatiles						
Sr-90	1.52E+04	1.00E-02	68	5.99E+06	8.80E-06	1.47E-12	2.00E-04	3.04E-12	1.60E-04	7.78E-18	2.88E-08	3.15E+07	4.41E-10	
Ru-106	4.16E+03	1.00E-02	68	5.99E+06	8.80E-06	1.47E-12	2.00E-04	8.31E-13	1.60E-04	0.00E+00	0.00E+00	3.15E+07	0.00E+00	
Cs-134	7.20E+03	1.00E-02	68	5.99E+06	8.80E-06	1.47E-12	2.00E-04	1.44E-12	1.60E-04	7.40E-14	2.74E-04	3.15E+07	1.99E-06	
Cs-137	2.29E+04	1.00E-02	68	5.99E+06	8.80E-06	1.47E-12	2.00E-04	4.58E-12	1.60E-04	7.96E-18	2.95E-08	3.15E+07	6.79E-10	
								Fines						
PU241	2.10E+04	1.00E-02	68	5.99E+06	8.80E-06	1.47E-12	3.00E-05	6.29E-13	1.60E-04	7.19E-20	2.66E-10	3.15E+07	8.44E-13	
Y 90	1.52E+04	1.00E-02	68	5.99E+06	8.80E-06	1.47E-12	3.00E-05	4.56E-13	1.60E-04	1.89E-16	6.99E-07	3.15E+07	1.61E-09	
PM147	8.88E+03	1.00E-02	68	5.99E+06	8.80E-06	1.47E-12	3.00E-05	2.66E-13	1.60E-04	7.48E-19	2.77E-09	3.15E+07	3.71E-12	
CE144	2.46E+03	1.00E-02	68	5.99E+06	8.80E-06	1.47E-12	3.00E-05	7.37E-14	1.60E-04	8.53E-16	3.16E-06	3.15E+07	1.17E-09	
PR144	2.46E+03	1.00E-02	68	5.99E+06	8.80E-06	1.47E-12	3.00E-05	7.37E-14	1.60E-04	1.90E-15	7.03E-06	3.15E+07	2.61E-09	
EU154	1.07E+03	1.00E-02	68	5.99E+06	8.80E-06	1.47E-12	3.00E-05	3.21E-14	1.60E-04	6.00E-14	2.22E-04	3.15E+07	3.59E-08	
CM244	9.30E+02	1.00E-02	68	5.99E+06	8.80E-06	1.47E-12	3.00E-05	2.79E-14	1.60E-04	6.90E-18	2.55E-08	3.15E+07	3.59E-12	
PU238	7.49E+02	1.00E-02	68	5.99E+06	8.80E-06	1.47E-12	3.00E-05	2.24E-14	1.60E-04	6.56E-18	2.43E-08	3.15E+07	2.75E-12	
SB125	6.40E+02	1.00E-02	68	5.99E+06	8.80E-06	1.47E-12	3.00E-05	1.92E-14	1.60E-04	1.98E-14	7.33E-05	3.15E+07	7.08E-09	
EU155	3.51E+02	1.00E-02	68	5.99E+06	8.80E-06	1.47E-12	3.00E-05	1.05E-14	1.60E-04	2.49E-15	9.21E-06	3.15E+07	4.88E-10	
AM241	2.20E+02	1.00E-02	68	5.99E+06	8.80E-06	1.47E-12	3.00E-05	6.59E-15	1.60E-04	8.58E-16	3.17E-06	3.15E+07	1.05E-10	
TE125M	1.56E+02	1.00E-02	68	5.99E+06	8.80E-06	1.47E-12	3.00E-05	4.68E-15	1.60E-04	5.96E-16	2.21E-06	3.15E+07	5.20E-11	
PU240	1.26E+02	1.00E-02	68	5.99E+06	8.80E-06	1.47E-12	3.00E-05	3.78E-15	1.60E-04	6.36E-18	2.35E-08	3.15E+07	4.48E-13	
151Sm	0.00E+00	1.00E-02	68	5.99E+06	8.80E-06	1.47E-12	3.00E-05	0.00E+00	1.60E-04	5.20E-20	1.92E-10	3.15E+07	0.00E+00	
239Pu	6.16E+01	1.00E-02	68	5.99E+06	8.80E-06	1.47E-12	3.00E-05	1.85E-15	1.60E-04	4.84E-18	1.79E-08	3.15E+07	1.67E-13	
137mBa	2.16E+04	1.00E-02	68	5.99E+06	8.80E-06	1.47E-12	3.00E-05	6.47E-13	1.60E-04	2.82E-14	1.04E-04	3.15E+07	3.40E-07	
106Rh	4.16E+03	1.00E-02	68	5.99E+06	8.80E-06	1.47E-12	3.00E-05	1.25E-13	1.60E-04	1.01E-14	3.74E-05	3.15E+07	2.35E-08	
144mPr	0.00E+00	1.00E-02	68	5.99E+06	8.80E-06	1.47E-12	3.00E-05	0.00E+00	1.60E-04	3.25E-16	1.20E-06	3.15E+07	0.00E+00	
243Am	7.39E+00	1.00E-02	68	5.99E+06	8.80E-06	1.47E-12	3.00E-05	2.21E-16	1.60E-04	2.19E-15	8.10E-06	3.15E+07	9.04E-12	
242Cm	6.10E+00	1.00E-02	68	5.99E+06	8.80E-06	1.47E-12	3.00E-05	1.83E-16	1.60E-04	7.83E-18	2.90E-08	3.15E+07	2.67E-14	
243Cm	4.81E+00	1.00E-02	68	5.99E+06	8.80E-06	1.47E-12	3.00E-05	1.44E-16	1.60E-04	5.77E-15	2.13E-05	3.15E+07	1.55E-11	
239Np	7.39E+00	1.00E-02	68	5.99E+06	8.80E-06	1.47E-12	3.00E-05	2.21E-16	1.60E-04	7.53E-15	2.79E-05	3.15E+07	3.11E-11	
237Np	7.05E-02	1.00E-02	68	5.99E+06	8.80E-06	1.47E-12	3.00E-05	2.11E-18	1.60E-04	1.04E-15	3.85E-06	3.15E+07	4.10E-14	
242Pu	5.95E-01	1.00E-02	68	5.99E+06	8.80E-06	1.47E-12	3.00E-05	1.78E-17	1.60E-04	5.34E-18	1.98E-08	3.15E+07	1.78E-15	
242Am	1.69E+00	1.00E-02	68	5.99E+06	8.80E-06	1.47E-12	3.00E-05	5.06E-17	1.60E-04	6.09E-16	2.25E-06	3.15E+07	5.75E-13	
242mAm	1.70E+00	1.00E-02	68	5.99E+06	8.80E-06	1.47E-12	3.00E-05	5.09E-17	1.60E-04	3.80E-17	1.41E-07	3.15E+07	3.61E-14	
												Total	2.24E-03	

MPC-68														
Normal Conditions														
Effective Dose Equivalent From Submersion														
Nuclide	Inventory (Ci/Assy)	1% for normal storage	No. Assy	MPC Vol (cm3)	L_{nor} Rate at Upstream (cm3/s)	Fraction Released per sec	Release Fraction	Release Rate (Ci/sec)	X/Q (sec/m3)	DCF (Sv/Bq)	DCF (mRem/uCi)	Occ Time (sec)	EDE (mRem)	
								Gases						
H-3	8.72E+01	1.00E-02	68	5.99E+06	8.80E-06	1.47E-12	0.30	2.61E-11	1.60E-04	0.00E+00	0.00E+00	3.15E+07	0.00E+00	
I-129	7.72E-03	1.00E-02	68	5.99E+06	8.80E-06	1.47E-12	0.30	2.31E-15	1.60E-04	6.66E-16	2.46E-06	3.15E+07	2.87E-11	
Kr-85	1.43E+03	1.00E-02	68	5.99E+06	8.80E-06	1.47E-12	0.30	4.29E-10	1.60E-04	1.34E-16	4.96E-07	3.15E+07	1.07E-06	
								Crud						
Co-60	6.50E+01	1.00E+00	68	5.99E+06	8.80E-06	1.47E-12	0.15	9.74E-10	1.60E-04	1.39E-13	5.14E-04	3.15E+07	2.52E-03	
								Volatiles						
Sr-90	1.52E+04	1.00E-02	68	5.99E+06	8.80E-06	1.47E-12	2.00E-04	3.04E-12	1.60E-04	9.49E-18	3.51E-08	3.15E+07	5.37E-10	
Ru-106	4.16E+03	1.00E-02	68	5.99E+06	8.80E-06	1.47E-12	2.00E-04	8.31E-13	1.60E-04	0.00E+00	0.00E+00	3.15E+07	0.00E+00	
Cs-134	7.20E+03	1.00E-02	68	5.99E+06	8.80E-06	1.47E-12	2.00E-04	1.44E-12	1.60E-04	8.43E-14	3.12E-04	3.15E+07	2.26E-06	
Cs-137	2.29E+04	1.00E-02	68	5.99E+06	8.80E-06	1.47E-12	2.00E-04	4.58E-12	1.60E-04	9.67E-18	3.58E-08	3.15E+07	8.25E-10	
								Fines						
PU241	2.10E+04	1.00E-02	68	5.99E+06	8.80E-06	1.47E-12	3.00E-05	6.29E-13	1.60E-04	8.67E-20	3.21E-10	3.15E+07	1.02E-12	
Y 90	1.52E+04	1.00E-02	68	5.99E+06	8.80E-06	1.47E-12	3.00E-05	4.56E-13	1.60E-04	2.20E-16	8.14E-07	3.15E+07	1.87E-09	
PM147	8.88E+03	1.00E-02	68	5.99E+06	8.80E-06	1.47E-12	3.00E-05	2.66E-13	1.60E-04	9.56E-19	3.54E-09	3.15E+07	4.74E-12	
CE144	2.46E+03	1.00E-02	68	5.99E+06	8.80E-06	1.47E-12	3.00E-05	7.37E-14	1.60E-04	1.01E-15	3.74E-06	3.15E+07	1.39E-09	
PR144	2.46E+03	1.00E-02	68	5.99E+06	8.80E-06	1.47E-12	3.00E-05	7.37E-14	1.60E-04	2.15E-15	7.96E-06	3.15E+07	2.96E-09	
EU154	1.07E+03	1.00E-02	68	5.99E+06	8.80E-06	1.47E-12	3.00E-05	3.21E-14	1.60E-04	6.81E-14	2.52E-04	3.15E+07	4.07E-08	
CM244	9.30E+02	1.00E-02	68	5.99E+06	8.80E-06	1.47E-12	3.00E-05	2.79E-14	1.60E-04	1.33E-17	4.92E-08	3.15E+07	6.91E-12	
PU238	7.49E+02	1.00E-02	68	5.99E+06	8.80E-06	1.47E-12	3.00E-05	2.24E-14	1.60E-04	1.27E-17	4.70E-08	3.15E+07	5.32E-12	
SB125	6.40E+02	1.00E-02	68	5.99E+06	8.80E-06	1.47E-12	3.00E-05	1.92E-14	1.60E-04	2.27E-14	8.40E-05	3.15E+07	8.12E-09	
EU155	3.51E+02	1.00E-02	68	5.99E+06	8.80E-06	1.47E-12	3.00E-05	1.05E-14	1.60E-04	2.95E-15	1.09E-05	3.15E+07	5.79E-10	
AM241	2.20E+02	1.00E-02	68	5.99E+06	8.80E-06	1.47E-12	3.00E-05	6.59E-15	1.60E-04	1.07E-15	3.96E-06	3.15E+07	1.32E-10	
TE125M	1.56E+02	1.00E-02	68	5.99E+06	8.80E-06	1.47E-12	3.00E-05	4.68E-15	1.60E-04	8.48E-16	3.14E-06	3.15E+07	7.39E-11	
PU240	1.26E+02	1.00E-02	68	5.99E+06	8.80E-06	1.47E-12	3.00E-05	3.78E-15	1.60E-04	1.23E-17	4.55E-08	3.15E+07	8.66E-13	
151Sm	0.00E+00	1.00E-02	68	5.99E+06	8.80E-06	1.47E-12	3.00E-05	0.00E+00	1.60E-04	8.80E-20	3.26E-10	3.15E+07	0.00E+00	
239Pu	6.16E+01	1.00E-02	68	5.99E+06	8.80E-06	1.47E-12	3.00E-05	1.85E-15	1.60E-04	7.55E-18	2.79E-08	3.15E+07	2.60E-13	
137mBa	2.16E+04	1.00E-02	68	5.99E+06	8.80E-06	1.47E-12	3.00E-05	6.47E-13	1.60E-04	3.22E-14	1.19E-04	3.15E+07	3.89E-07	
106Rh	4.16E+03	1.00E-02	68	5.99E+06	8.80E-06	1.47E-12	3.00E-05	1.25E-13	1.60E-04	1.16E-14	4.29E-05	3.15E+07	2.70E-08	
144mPr	0.00E+00	1.00E-02	68	5.99E+06	8.80E-06	1.47E-12	3.00E-05	0.00E+00	1.60E-04	4.20E-16	1.55E-06	3.15E+07	0.00E+00	
243Am	7.39E+00	1.00E-02	68	5.99E+06	8.80E-06	1.47E-12	3.00E-05	2.21E-16	1.60E-04	2.61E-15	9.66E-06	3.15E+07	1.08E-11	
242Cm	6.10E+00	1.00E-02	68	5.99E+06	8.80E-06	1.47E-12	3.00E-05	1.83E-16	1.60E-04	1.48E-17	5.48E-08	3.15E+07	5.05E-14	
243Cm	4.81E+00	1.00E-02	68	5.99E+06	8.80E-06	1.47E-12	3.00E-05	1.44E-16	1.60E-04	6.68E-15	2.47E-05	3.15E+07	1.80E-11	
239Np	7.39E+00	1.00E-02	68	5.99E+06	8.80E-06	1.47E-12	3.00E-05	2.21E-16	1.60E-04	8.73E-15	3.23E-05	3.15E+07	3.61E-11	
237Np	7.05E-02	1.01E+00	68	5.99E+06	8.80E-06	1.47E-12	3.00E-05	2.13E-16	1.60E-04	1.26E-15	4.66E-06	3.15E+07	5.01E-12	
242Pu	5.95E-01	2.01E+00	68	5.99E+06	8.80E-06	1.47E-12	3.00E-05	3.58E-15	1.60E-04	1.03E-17	3.81E-08	3.15E+07	6.88E-13	
242Am	1.69E+00	3.01E+00	68	5.99E+06	8.80E-06	1.47E-12	3.00E-05	1.52E-14	1.60E-04	7.30E-16	2.70E-06	3.15E+07	2.08E-10	
242mAm	1.70E+00	4.01E+00	68	5.99E+06	8.80E-06	1.47E-12	3.00E-05	2.04E-14	1.60E-04	6.01E-17	2.22E-07	3.15E+07	2.29E-11	
												Total	2.53E-03	

MPC-68														
Normal Conditions														
Effective Dose Equivalent From Submersion														
Nuclide	Inventory (Ci/Assy)	1% for normal storage	No. Assy	MPC Vol (cm3)	L_{nor} Rate at Upstream (cm3/s)	Fraction Released per sec	Release Fraction	Release Rate (Ci/sec)	X/Q (sec/m3)	DCF (Sv/Bq)	DCF (mRem/uCi)	Occ Time (sec)	EDE (mRem)	
								Gases						
H-3	8.72E+01	1.00E-02	68	5.99E+06	8.80E-06	1.47E-12	0.30	2.61E-11	1.60E-04	2.75E-18	1.02E-08	3.15E+07	1.34E-09	
I-129	7.72E-03	1.00E-02	68	5.99E+06	8.80E-06	1.47E-12	0.30	2.31E-15	1.60E-04	2.14E-16	7.92E-07	3.15E+07	9.23E-12	
Kr-85	1.43E+03	1.00E-02	68	5.99E+06	8.80E-06	1.47E-12	0.30	4.29E-10	1.60E-04	1.14E-16	4.22E-07	3.15E+07	9.11E-07	
								Crud						
Co-60	6.50E+01	1.00E+00	68	5.99E+06	8.80E-06	1.47E-12	0.15	9.74E-10	1.60E-04	1.24E-13	4.59E-04	3.15E+07	2.25E-03	
								Volatiles						
Sr-90	1.52E+04	1.00E-02	68	5.99E+06	8.80E-06	1.47E-12	2.00E-04	3.04E-12	1.60E-04	6.44E-18	2.38E-08	3.15E+07	3.65E-10	
Ru-106	4.16E+03	1.00E-02	68	5.99E+06	8.80E-06	1.47E-12	2.00E-04	8.31E-13	1.60E-04	0.00E+00	0.00E+00	3.15E+07	0.00E+00	
Cs-134	7.20E+03	1.00E-02	68	5.99E+06	8.80E-06	1.47E-12	2.00E-04	1.44E-12	1.60E-04	7.37E-14	2.73E-04	3.15E+07	1.98E-06	
Cs-137	2.29E+04	1.00E-02	68	5.99E+06	8.80E-06	1.47E-12	2.00E-04	4.58E-12	1.60E-04	6.68E-18	2.47E-08	3.15E+07	5.70E-10	
								Fines						
PU241	2.10E+04	1.00E-02	68	5.99E+06	8.80E-06	1.47E-12	3.00E-05	6.29E-13	1.60E-04	6.48E-20	2.40E-10	3.15E+07	7.61E-13	
Y 90	1.52E+04	1.00E-02	68	5.99E+06	8.80E-06	1.47E-12	3.00E-05	4.56E-13	1.60E-04	1.77E-16	6.55E-07	3.15E+07	1.50E-09	
PM147	8.88E+03	1.00E-02	68	5.99E+06	8.80E-06	1.47E-12	3.00E-05	2.66E-13	1.60E-04	5.45E-19	2.02E-09	3.15E+07	2.70E-12	
CE144	2.46E+03	1.00E-02	68	5.99E+06	8.80E-06	1.47E-12	3.00E-05	7.37E-14	1.60E-04	7.69E-16	2.85E-06	3.15E+07	1.06E-09	
PR144	2.46E+03	1.00E-02	68	5.99E+06	8.80E-06	1.47E-12	3.00E-05	7.37E-14	1.60E-04	1.90E-15	7.03E-06	3.15E+07	2.61E-09	
EU154	1.07E+03	1.00E-02	68	5.99E+06	8.80E-06	1.47E-12	3.00E-05	3.21E-14	1.60E-04	5.99E-14	2.22E-04	3.15E+07	3.58E-08	
CM244	9.30E+02	1.00E-02	68	5.99E+06	8.80E-06	1.47E-12	3.00E-05	2.79E-14	1.60E-04	7.08E-19	2.62E-09	3.15E+07	3.68E-13	
PU238	7.49E+02	1.00E-02	68	5.99E+06	8.80E-06	1.47E-12	3.00E-05	2.24E-14	1.60E-04	1.06E-18	3.92E-09	3.15E+07	4.44E-13	
SB125	6.40E+02	1.00E-02	68	5.99E+06	8.80E-06	1.47E-12	3.00E-05	1.92E-14	1.60E-04	1.95E-14	7.22E-05	3.15E+07	6.97E-09	
EU155	3.51E+02	1.00E-02	68	5.99E+06	8.80E-06	1.47E-12	3.00E-05	1.05E-14	1.60E-04	2.22E-15	8.21E-06	3.15E+07	4.35E-10	
AM241	2.20E+02	1.00E-02	68	5.99E+06	8.80E-06	1.47E-12	3.00E-05	6.59E-15	1.60E-04	6.74E-16	2.49E-06	3.15E+07	8.29E-11	
TE125M	1.56E+02	1.00E-02	68	5.99E+06	8.80E-06	1.47E-12	3.00E-05	4.68E-15	1.60E-04	2.23E-16	8.25E-07	3.15E+07	1.94E-11	
PU240	1.26E+02	1.00E-02	68	5.99E+06	8.80E-06	1.47E-12	3.00E-05	3.78E-15	1.60E-04	1.09E-18	4.03E-09	3.15E+07	7.68E-14	
151Sm	0.00E+00	1.00E-02	68	5.99E+06	8.80E-06	1.47E-12	3.00E-05	0.00E+00	1.60E-04	7.08E-21	2.62E-11	3.15E+07	0.00E+00	
239Pu	6.16E+01	1.00E-02	68	5.99E+06	8.80E-06	1.47E-12	3.00E-05	1.85E-15	1.60E-04	2.65E-18	9.81E-09	3.15E+07	9.12E-14	
137mBa	2.16E+04	1.00E-02	68	5.99E+06	8.80E-06	1.47E-12	3.00E-05	6.47E-13	1.60E-04	2.80E-14	1.04E-04	3.15E+07	3.38E-07	
106Rh	4.16E+03	1.00E-02	68	5.99E+06	8.80E-06	1.47E-12	3.00E-05	1.25E-13	1.60E-04	1.01E-14	3.74E-05	3.15E+07	2.35E-08	
144mPr	0.00E+00	1.00E-02	68	5.99E+06	8.80E-06	1.47E-12	3.00E-05	0.00E+00	1.60E-04	2.00E-16	7.40E-07	3.15E+07	0.00E+00	
243Am	7.39E+00	1.00E-02	68	5.99E+06	8.80E-06	1.47E-12	3.00E-05	2.21E-16	1.60E-04	1.92E-15	7.10E-06	3.15E+07	7.93E-12	
242Cm	6.10E+00	1.00E-02	68	5.99E+06	8.80E-06	1.47E-12	3.00E-05	1.83E-16	1.60E-04	1.13E-18	4.18E-09	3.15E+07	3.85E-15	
243Cm	4.81E+00	1.00E-02	68	5.99E+06	8.80E-06	1.47E-12	3.00E-05	1.44E-16	1.60E-04	5.50E-15	2.04E-05	3.15E+07	1.48E-11	
239Np	7.39E+00	1.00E-02	68	5.99E+06	8.80E-06	1.47E-12	3.00E-05	2.21E-16	1.60E-04	7.18E-15	2.66E-05	3.15E+07	2.97E-11	
237Np	7.05E-02	1.01E+00	68	5.99E+06	8.80E-06	1.47E-12	3.00E-05	2.13E-16	1.60E-04	9.02E-16	3.34E-06	3.15E+07	3.59E-12	
242Pu	5.95E-01	2.01E+00	68	5.99E+06	8.80E-06	1.47E-12	3.00E-05	3.58E-15	1.60E-04	9.69E-19	3.59E-09	3.15E+07	6.48E-14	
242Am	1.69E+00	3.01E+00	68	5.99E+06	8.80E-06	1.47E-12	3.00E-05	1.52E-14	1.60E-04	5.51E-15	2.04E-05	3.15E+07	1.57E-09	
242mAm	1.70E+00	4.01E+00	68	5.99E+06	8.80E-06	1.47E-12	3.00E-05	2.04E-14	1.60E-04	1.72E-17	6.36E-08	3.15E+07	6.55E-12	
												Total	2.26E-03	

MPC-68														
Normal Conditions														
Effective Dose Equivalent From Submersion														
Nuclide	Inventory (Ci/Assy)	1% for normal storage	No. Assy	MPC Vol (cm3)	L_{nor} Rate at Upstream (cm3/s)	Fraction Released per sec	Release Fraction	Release Rate (Ci/sec)	X/Q (sec/m3)	DCF (Sv/Bq)	DCF (mRem/uCi)	Occ Time (sec)	EDE (mRem)	
								Gases						
H-3	8.72E+01	1.00E-02	68	5.99E+06	8.80E-06	1.47E-12	0.30	2.61E-11	1.60E-04	0.00E+00	0.00E+00	3.15E+07	0.00E+00	
I-129	7.72E-03	1.00E-02	68	5.99E+06	8.80E-06	1.47E-12	0.30	2.31E-15	1.60E-04	1.64E-16	6.07E-07	3.15E+07	7.08E-12	
Kr-85	1.43E+03	1.00E-02	68	5.99E+06	8.80E-06	1.47E-12	0.30	4.29E-10	1.60E-04	1.09E-16	4.03E-07	3.15E+07	8.71E-07	
								Crud						
Co-60	6.50E+01	1.00E+00	68	5.99E+06	8.80E-06	1.47E-12	0.15	9.74E-10	1.60E-04	1.23E-13	4.55E-04	3.15E+07	2.23E-03	
								Volatiles						
Sr-90	1.52E+04	1.00E-02	68	5.99E+06	8.80E-06	1.47E-12	2.00E-04	3.04E-12	1.60E-04	5.44E-18	2.01E-08	3.15E+07	3.08E-10	
Ru-106	4.16E+03	1.00E-02	68	5.99E+06	8.80E-06	1.47E-12	2.00E-04	8.31E-13	1.60E-04	0.00E+00	0.00E+00	3.15E+07	0.00E+00	
Cs-134	7.20E+03	1.00E-02	68	5.99E+06	8.80E-06	1.47E-12	2.00E-04	1.44E-12	1.60E-04	7.19E-14	2.66E-04	3.15E+07	1.93E-06	
Cs-137	2.29E+04	1.00E-02	68	5.99E+06	8.80E-06	1.47E-12	2.00E-04	4.58E-12	1.60E-04	5.70E-18	2.11E-08	3.15E+07	4.86E-10	
								Fines						
PU241	2.10E+04	1.00E-02	68	5.99E+06	8.80E-06	1.47E-12	3.00E-05	6.29E-13	1.60E-04	5.63E-20	2.08E-10	3.15E+07	6.61E-13	
Y 90	1.52E+04	1.00E-02	68	5.99E+06	8.80E-06	1.47E-12	3.00E-05	4.56E-13	1.60E-04	1.62E-16	5.99E-07	3.15E+07	1.38E-09	
PM147	8.88E+03	1.00E-02	68	5.99E+06	8.80E-06	1.47E-12	3.00E-05	2.66E-13	1.60E-04	4.46E-19	1.65E-09	3.15E+07	2.21E-12	
CE144	2.46E+03	1.00E-02	68	5.99E+06	8.80E-06	1.47E-12	3.00E-05	7.37E-14	1.60E-04	6.68E-16	2.47E-06	3.15E+07	9.18E-10	
PR144	2.46E+03	1.00E-02	68	5.99E+06	8.80E-06	1.47E-12	3.00E-05	7.37E-14	1.60E-04	1.87E-15	6.92E-06	3.15E+07	2.57E-09	
EU154	1.07E+03	1.00E-02	68	5.99E+06	8.80E-06	1.47E-12	3.00E-05	3.21E-14	1.60E-04	5.87E-14	2.17E-04	3.15E+07	3.51E-08	
CM244	9.30E+02	1.00E-02	68	5.99E+06	8.80E-06	1.47E-12	3.00E-05	2.79E-14	1.60E-04	1.46E-18	5.40E-09	3.15E+07	7.59E-13	
PU238	7.49E+02	1.00E-02	68	5.99E+06	8.80E-06	1.47E-12	3.00E-05	2.24E-14	1.60E-04	1.68E-18	6.22E-09	3.15E+07	7.03E-13	
SB125	6.40E+02	1.00E-02	68	5.99E+06	8.80E-06	1.47E-12	3.00E-05	1.92E-14	1.60E-04	1.87E-14	6.92E-05	3.15E+07	6.69E-09	
EU155	3.51E+02	1.00E-02	68	5.99E+06	8.80E-06	1.47E-12	3.00E-05	1.05E-14	1.60E-04	1.85E-15	6.85E-06	3.15E+07	3.63E-10	
AM241	2.20E+02	1.00E-02	68	5.99E+06	8.80E-06	1.47E-12	3.00E-05	6.59E-15	1.60E-04	5.21E-16	1.93E-06	3.15E+07	6.41E-11	
TE125M	1.56E+02	1.00E-02	68	5.99E+06	8.80E-06	1.47E-12	3.00E-05	4.68E-15	1.60E-04	1.86E-16	6.88E-07	3.15E+07	1.62E-11	
PU240	1.26E+02	1.00E-02	68	5.99E+06	8.80E-06	1.47E-12	3.00E-05	3.78E-15	1.60E-04	1.65E-18	6.11E-09	3.15E+07	1.16E-13	
151Sm	0.00E+00	1.00E-02	68	5.99E+06	8.80E-06	1.47E-12	3.00E-05	0.00E+00	1.60E-04	1.13E-20	4.18E-11	3.15E+07	0.00E+00	
239Pu	6.16E+01	1.00E-02	68	5.99E+06	8.80E-06	1.47E-12	3.00E-05	1.85E-15	1.60E-04	2.67E-18	9.88E-09	3.15E+07	9.19E-14	
137mBa	2.16E+04	1.00E-02	68	5.99E+06	8.80E-06	1.47E-12	3.00E-05	6.47E-13	1.60E-04	2.73E-14	1.01E-04	3.15E+07	3.30E-07	
106Rh	4.16E+03	1.00E-02	68	5.99E+06	8.80E-06	1.47E-12	3.00E-05	1.25E-13	1.60E-04	9.75E-15	3.61E-05	3.15E+07	2.27E-08	
144mPr	0.00E+00	1.00E-02	68	5.99E+06	8.80E-06	1.47E-12	3.00E-05	0.00E+00	1.60E-04	1.56E-16	5.77E-07	3.15E+07	0.00E+00	
243Am	7.39E+00	1.00E-02	68	5.99E+06	8.80E-06	1.47E-12	3.00E-05	2.21E-16	1.60E-04	1.55E-15	5.74E-06	3.15E+07	6.40E-12	
242Cm	6.10E+00	1.00E-02	68	5.99E+06	8.80E-06	1.47E-12	3.00E-05	1.83E-16	1.60E-04	1.89E-18	6.99E-09	3.15E+07	6.44E-15	
243Cm	4.81E+00	1.00E-02	68	5.99E+06	8.80E-06	1.47E-12	3.00E-05	1.44E-16	1.60E-04	5.00E-15	1.85E-05	3.15E+07	1.34E-11	
239Np	7.39E+00	1.00E-02	68	5.99E+06	8.80E-06	1.47E-12	3.00E-05	2.21E-16	1.60E-04	6.50E-15	2.41E-05	3.15E+07	2.68E-11	
237Np	7.05E-02	1.00E-02	68	5.99E+06	8.80E-06	1.47E-12	3.00E-05	2.11E-18	1.60E-04	7.69E-16	2.85E-06	3.15E+07	3.03E-14	
242Pu	5.95E-01	1.00E-02	68	5.99E+06	8.80E-06	1.47E-12	3.00E-05	1.78E-17	1.60E-04	1.43E-18	5.29E-09	3.15E+07	4.76E-16	
242Am	1.69E+00	1.00E-02	68	5.99E+06	8.80E-06	1.47E-12	3.00E-05	5.06E-17	1.60E-04	4.77E-16	1.76E-06	3.15E+07	4.51E-13	
242mAm	1.70E+00	1.00E-02	68	5.99E+06	8.80E-06	1.47E-12	3.00E-05	5.09E-17	1.60E-04	1.72E-17	6.36E-08	3.15E+07	1.63E-14	
												Total	2.24E-03	

MPC-68														
Normal Conditions														
Effective Dose Equivalent From Submersion														
Nuclide	Inventory (Ci/Assy)	1% for normal storage	No. Assy	MPC Vol (cm3)	L_{nor} Rate at Upstream (cm3/s)	Fraction Released per sec	Release Fraction	Release Rate (Ci/sec)	X/Q (sec/m3)	DCF (Sv/Bq)	DCF (mRem/uCi)	Occ Time (sec)	EDE (mRem)	
								Gases						
H-3	8.72E+01	1.00E-02	68	5.99E+06	8.80E-06	1.47E-12	0.30	2.61E-11	1.60E-04	0.00E+00	0.00E+00	3.15E+07	0.00E+00	
I-129	7.72E-03	1.00E-02	68	5.99E+06	8.80E-06	1.47E-12	0.30	2.31E-15	1.60E-04	1.10E-15	4.07E-06	3.15E+07	4.75E-11	
Kr-85	1.43E+03	1.00E-02	68	5.99E+06	8.80E-06	1.47E-12	0.30	4.29E-10	1.60E-04	2.20E-16	8.14E-07	3.15E+07	1.76E-06	
								Crud						
Co-60	6.50E+01	1.00E+00	68	5.99E+06	8.80E-06	1.47E-12	0.15	9.74E-10	1.60E-04	1.78E-13	6.59E-04	3.15E+07	3.23E-03	
								Volatiles						
Sr-90	1.52E+04	1.00E-02	68	5.99E+06	8.80E-06	1.47E-12	2.00E-04	3.04E-12	1.60E-04	2.28E-17	8.44E-08	3.15E+07	1.29E-09	
Ru-106	4.16E+03	1.00E-02	68	5.99E+06	8.80E-06	1.47E-12	2.00E-04	8.31E-13	1.60E-04	0.00E+00	0.00E+00	3.15E+07	0.00E+00	
Cs-134	7.20E+03	1.00E-02	68	5.99E+06	8.80E-06	1.47E-12	2.00E-04	1.44E-12	1.60E-04	1.20E-13	4.44E-04	3.15E+07	3.22E-06	
Cs-137	2.29E+04	1.00E-02	68	5.99E+06	8.80E-06	1.47E-12	2.00E-04	4.58E-12	1.60E-04	2.29E-17	8.47E-08	3.15E+07	1.95E-09	
								Fines						
PU241	2.10E+04	1.00E-02	68	5.99E+06	8.80E-06	1.47E-12	3.00E-05	6.29E-13	1.60E-04	2.19E-19	8.10E-10	3.15E+07	2.57E-12	
Y 90	1.52E+04	1.00E-02	68	5.99E+06	8.80E-06	1.47E-12	3.00E-05	4.56E-13	1.60E-04	4.44E-16	1.64E-06	3.15E+07	3.77E-09	
PM147	8.88E+03	1.00E-02	68	5.99E+06	8.80E-06	1.47E-12	3.00E-05	2.66E-13	1.60E-04	2.18E-18	8.07E-09	3.15E+07	1.08E-11	
CE144	2.46E+03	1.00E-02	68	5.99E+06	8.80E-06	1.47E-12	3.00E-05	7.37E-14	1.60E-04	2.49E-15	9.21E-06	3.15E+07	3.42E-09	
PR144	2.46E+03	1.00E-02	68	5.99E+06	8.80E-06	1.47E-12	3.00E-05	7.37E-14	1.60E-04	2.99E-15	1.11E-05	3.15E+07	4.11E-09	
EU154	1.07E+03	1.00E-02	68	5.99E+06	8.80E-06	1.47E-12	3.00E-05	3.21E-14	1.60E-04	9.43E-14	3.49E-04	3.15E+07	5.64E-08	
CM244	9.30E+02	1.00E-02	68	5.99E+06	8.80E-06	1.47E-12	3.00E-05	2.79E-14	1.60E-04	8.82E-18	3.26E-08	3.15E+07	4.58E-12	
PU238	7.49E+02	1.00E-02	68	5.99E+06	8.80E-06	1.47E-12	3.00E-05	2.24E-14	1.60E-04	9.30E-18	3.44E-08	3.15E+07	3.89E-12	
SB125	6.40E+02	1.00E-02	68	5.99E+06	8.80E-06	1.47E-12	3.00E-05	1.92E-14	1.60E-04	3.53E-14	1.31E-04	3.15E+07	1.26E-08	
EU155	3.51E+02	1.00E-02	68	5.99E+06	8.80E-06	1.47E-12	3.00E-05	1.05E-14	1.60E-04	8.09E-15	2.99E-05	3.15E+07	1.59E-09	
AM241	2.20E+02	1.00E-02	68	5.99E+06	8.80E-06	1.47E-12	3.00E-05	6.59E-15	1.60E-04	2.87E-15	1.06E-05	3.15E+07	3.53E-10	
TE125M	1.56E+02	1.00E-02	68	5.99E+06	8.80E-06	1.47E-12	3.00E-05	4.68E-15	1.60E-04	1.22E-15	4.51E-06	3.15E+07	1.06E-10	
PU240	1.26E+02	1.00E-02	68	5.99E+06	8.80E-06	1.47E-12	3.00E-05	3.78E-15	1.60E-04	9.26E-18	3.43E-08	3.15E+07	6.52E-13	
151Sm	0.00E+00	1.00E-02	68	5.99E+06	8.80E-06	1.47E-12	3.00E-05	0.00E+00	1.60E-04	7.09E-20	2.62E-10	3.15E+07	0.00E+00	
239Pu	6.16E+01	1.00E-02	68	5.99E+06	8.80E-06	1.47E-12	3.00E-05	1.85E-15	1.60E-04	9.47E-18	3.50E-08	3.15E+07	3.26E-13	
137mBa	2.16E+04	1.00E-02	68	5.99E+06	8.80E-06	1.47E-12	3.00E-05	6.47E-13	1.60E-04	4.63E-14	1.71E-04	3.15E+07	5.59E-07	
106Rh	4.16E+03	1.00E-02	68	5.99E+06	8.80E-06	1.47E-12	3.00E-05	1.25E-13	1.60E-04	1.72E-14	6.36E-05	3.15E+07	4.00E-08	
144mPr	0.00E+00	1.00E-02	68	5.99E+06	8.80E-06	1.47E-12	3.00E-05	0.00E+00	1.60E-04	8.16E-16	3.02E-06	3.15E+07	0.00E+00	
243Am	7.39E+00	1.00E-02	68	5.99E+06	8.80E-06	1.47E-12	3.00E-05	2.21E-16	1.60E-04	7.47E-15	2.76E-05	3.15E+07	3.09E-11	
242Cm	6.10E+00	1.00E-02	68	5.99E+06	8.80E-06	1.47E-12	3.00E-05	1.83E-16	1.60E-04	1.06E-17	3.92E-08	3.15E+07	3.61E-14	
243Cm	4.81E+00	1.00E-02	68	5.99E+06	8.80E-06	1.47E-12	3.00E-05	1.44E-16	1.60E-04	1.50E-14	5.55E-05	3.15E+07	4.03E-11	
239Np	7.39E+00	1.00E-02	68	5.99E+06	8.80E-06	1.47E-12	3.00E-05	2.21E-16	1.60E-04	2.00E-14	7.40E-05	3.15E+07	8.26E-11	
237Np	7.05E-02	1.00E-02	68	5.99E+06	8.80E-06	1.47E-12	3.00E-05	2.11E-18	1.60E-04	3.20E-15	1.18E-05	3.15E+07	1.26E-13	
242Pu	5.95E-01	1.00E-02	68	5.99E+06	8.80E-06	1.47E-12	3.00E-05	1.78E-17	1.60E-04	7.90E-18	2.92E-08	3.15E+07	2.63E-15	
242Am	1.69E+00	1.00E-02	68	5.99E+06	8.80E-06	1.47E-12	3.00E-05	5.06E-17	1.60E-04	1.88E-15	6.96E-06	3.15E+07	1.78E-12	
242mAm	1.70E+00	1.00E-02	68	5.99E+06	8.80E-06	1.47E-12	3.00E-05	5.09E-17	1.60E-04	7.94E-17	2.94E-07	3.15E+07	7.54E-14	
												Total	3.24E-03	

MPC-68														
Normal Conditions														
Effective Dose Equivalent From Submersion														
Nuclide	Inventory (Ci/Assy)	1% for normal storage	No. Assy	MPC Vol (cm3)	L_{nor} Rate at Upstream (cm3/s)	Fraction Released per sec	Release Fraction	Release Rate (Ci/sec)	X/Q (sec/m3)	DCF (Sv/Bq)	DCF (mRem/uCi)	Occ Time (sec)	EDE (mRem)	
								Gases						
H-3	8.72E+01	1.00E-02	68	5.99E+06	8.80E-06	1.47E-12	0.30	2.61E-11	1.60E-04	0.00E+00	0.00E+00	3.15E+07	0.00E+00	
I-129	7.72E-03	1.00E-02	68	5.99E+06	8.80E-06	1.47E-12	0.30	2.31E-15	1.60E-04	3.86E-16	1.43E-06	3.15E+07	1.67E-11	
Kr-85	1.43E+03	1.00E-02	68	5.99E+06	8.80E-06	1.47E-12	0.30	4.29E-10	1.60E-04	1.18E-16	4.37E-07	3.15E+07	9.43E-07	
								Crud						
Co-60	6.50E+01	1.00E+00	68	5.99E+06	8.80E-06	1.47E-12	0.15	9.74E-10	1.60E-04	1.27E-13	4.70E-04	3.15E+07	2.31E-03	
								Volatiles						
Sr-90	1.52E+04	1.00E-02	68	5.99E+06	8.80E-06	1.47E-12	2.00E-04	3.04E-12	1.60E-04	7.33E-18	2.71E-08	3.15E+07	4.15E-10	
Ru-106	4.16E+03	1.00E-02	68	5.99E+06	8.80E-06	1.47E-12	2.00E-04	8.31E-13	1.60E-04	0.00E+00	0.00E+00	3.15E+07	0.00E+00	
Cs-134	7.20E+03	1.00E-02	68	5.99E+06	8.80E-06	1.47E-12	2.00E-04	1.44E-12	1.60E-04	7.57E-14	2.80E-04	3.15E+07	2.03E-06	
Cs-137	2.29E+04	1.00E-02	68	5.99E+06	8.80E-06	1.47E-12	2.00E-04	4.58E-12	1.60E-04	7.55E-18	2.79E-08	3.15E+07	6.44E-10	
								Fines						
PU241	2.10E+04	1.00E-02	68	5.99E+06	8.80E-06	1.47E-12	3.00E-05	6.29E-13	1.60E-04	6.98E-20	2.58E-10	3.15E+07	8.19E-13	
Y 90	1.52E+04	1.00E-02	68	5.99E+06	8.80E-06	1.47E-12	3.00E-05	4.56E-13	1.60E-04	1.87E-16	6.92E-07	3.15E+07	1.59E-09	
PM147	8.88E+03	1.00E-02	68	5.99E+06	8.80E-06	1.47E-12	3.00E-05	2.66E-13	1.60E-04	6.75E-19	2.50E-09	3.15E+07	3.35E-12	
CE144	2.46E+03	1.00E-02	68	5.99E+06	8.80E-06	1.47E-12	3.00E-05	7.37E-14	1.60E-04	8.33E-16	3.08E-06	3.15E+07	1.15E-09	
PR144	2.46E+03	1.00E-02	68	5.99E+06	8.80E-06	1.47E-12	3.00E-05	7.37E-14	1.60E-04	1.95E-15	7.22E-06	3.15E+07	2.68E-09	
EU154	1.07E+03	1.00E-02	68	5.99E+06	8.80E-06	1.47E-12	3.00E-05	3.21E-14	1.60E-04	6.15E-14	2.28E-04	3.15E+07	3.68E-08	
CM244	9.30E+02	1.00E-02	68	5.99E+06	8.80E-06	1.47E-12	3.00E-05	2.79E-14	1.60E-04	4.19E-18	1.55E-08	3.15E+07	2.18E-12	
PU238	7.49E+02	1.00E-02	68	5.99E+06	8.80E-06	1.47E-12	3.00E-05	2.24E-14	1.60E-04	4.01E-18	1.48E-08	3.15E+07	1.68E-12	
SB125	6.40E+02	1.00E-02	68	5.99E+06	8.80E-06	1.47E-12	3.00E-05	1.92E-14	1.60E-04	2.01E-14	7.44E-05	3.15E+07	7.19E-09	
EU155	3.51E+02	1.00E-02	68	5.99E+06	8.80E-06	1.47E-12	3.00E-05	1.05E-14	1.60E-04	2.41E-15	8.92E-06	3.15E+07	4.73E-10	
AM241	2.20E+02	1.00E-02	68	5.99E+06	8.80E-06	1.47E-12	3.00E-05	6.59E-15	1.60E-04	7.83E-16	2.90E-06	3.15E+07	9.63E-11	
TE125M	1.56E+02	1.00E-02	68	5.99E+06	8.80E-06	1.47E-12	3.00E-05	4.68E-15	1.60E-04	4.64E-16	1.72E-06	3.15E+07	4.05E-11	
PU240	1.26E+02	1.00E-02	68	5.99E+06	8.80E-06	1.47E-12	3.00E-05	3.78E-15	1.60E-04	3.92E-18	1.45E-08	3.15E+07	2.76E-13	
151Sm	0.00E+00	1.00E-02	68	5.99E+06	8.80E-06	1.47E-12	3.00E-05	0.00E+00	1.60E-04	3.58E-20	1.32E-10	3.15E+07	0.00E+00	
239Pu	6.16E+01	1.00E-02	68	5.99E+06	8.80E-06	1.47E-12	3.00E-05	1.85E-15	1.60E-04	3.88E-18	1.44E-08	3.15E+07	1.34E-13	
137mBa	2.16E+04	1.00E-02	68	5.99E+06	8.80E-06	1.47E-12	3.00E-05	6.47E-13	1.60E-04	2.88E-14	1.07E-04	3.15E+07	3.48E-07	
106Rh	4.16E+03	1.00E-02	68	5.99E+06	8.80E-06	1.47E-12	3.00E-05	1.25E-13	1.60E-04	1.03E-14	3.81E-05	3.15E+07	2.39E-08	
144mPr	0.00E+00	1.00E-02	68	5.99E+06	8.80E-06	1.47E-12	3.00E-05	0.00E+00	1.60E-04	2.81E-16	1.04E-06	3.15E+07	0.00E+00	
243Am	7.39E+00	1.00E-02	68	5.99E+06	8.80E-06	1.47E-12	3.00E-05	2.21E-16	1.60E-04	2.09E-15	7.73E-06	3.15E+07	8.63E-12	
242Cm	6.10E+00	1.00E-02	68	5.99E+06	8.80E-06	1.47E-12	3.00E-05	1.83E-16	1.60E-04	4.91E-18	1.82E-08	3.15E+07	1.67E-14	
243Cm	4.81E+00	1.00E-02	68	5.99E+06	8.80E-06	1.47E-12	3.00E-05	1.44E-16	1.60E-04	5.76E-15	2.13E-05	3.15E+07	1.55E-11	
239Np	7.39E+00	1.00E-02	68	5.99E+06	8.80E-06	1.47E-12	3.00E-05	2.21E-16	1.60E-04	7.52E-15	2.78E-05	3.15E+07	3.11E-11	
237Np	7.05E-02	1.00E-02	68	5.99E+06	8.80E-06	1.47E-12	3.00E-05	2.11E-18	1.60E-04	9.94E-16	3.68E-06	3.15E+07	3.92E-14	
242Pu	5.95E-01	1.00E-02	68	5.99E+06	8.80E-06	1.47E-12	3.00E-05	1.78E-17	1.60E-04	3.32E-18	1.23E-08	3.15E+07	1.10E-15	
242Am	1.69E+00	1.00E-02	68	5.99E+06	8.80E-06	1.47E-12	3.00E-05	5.06E-17	1.60E-04	5.94E-16	2.20E-06	3.15E+07	5.61E-13	
242mAm	1.70E+00	1.00E-02	68	5.99E+06	8.80E-06	1.47E-12	3.00E-05	5.09E-17	1.60E-04	2.95E-17	1.09E-07	3.15E+07	2.80E-14	
												Total	2.31E-03	

MPC-68														
Normal Conditions														
Effective Dose Equivalent From Submersion														
Nuclide	Inventory (Ci/Assy)	1% for normal storage	No. Assy	MPC Vol (cm3)	L_{nor} Rate at Upstream (cm3/s)	Fraction Released per sec	Release Fraction	Release Rate (Ci/sec)	X/Q (sec/m3)	DCF (Sv/Bq)	DCF (mRem/uCi)	Occ Time (sec)	EDE (mRem)	
								Gases						
H-3	8.72E+01	1.00E-02	68	5.99E+06	8.80E-06	1.47E-12	0.30	2.61E-11	1.60E-04	3.31E-19	1.22E-09	3.15E+07	1.61E-10	
I-129	7.72E-03	1.00E-02	68	5.99E+06	8.80E-06	1.47E-12	0.30	2.31E-15	1.60E-04	3.80E-16	1.41E-06	3.15E+07	1.64E-11	
Kr-85	1.43E+03	1.00E-02	68	5.99E+06	8.80E-06	1.47E-12	0.30	4.29E-10	1.60E-04	1.19E-16	4.40E-07	3.15E+07	9.51E-07	
								Crud						
Co-60	6.50E+01	1.00E+00	68	5.99E+06	8.80E-06	1.47E-12	0.15	9.74E-10	1.60E-04	1.26E-13	4.66E-04	3.15E+07	2.29E-03	
								Volatiles						
Sr-90	1.52E+04	1.00E-02	68	5.99E+06	8.80E-06	1.47E-12	2.00E-04	3.04E-12	1.60E-04	7.53E-18	2.79E-08	3.15E+07	4.26E-10	
Ru-106	4.16E+03	1.00E-02	68	5.99E+06	8.80E-06	1.47E-12	2.00E-04	8.31E-13	1.60E-04	0.00E+00	0.00E+00	3.15E+07	0.00E+00	
Cs-134	7.20E+03	1.00E-02	68	5.99E+06	8.80E-06	1.47E-12	2.00E-04	1.44E-12	1.60E-04	7.57E-14	2.80E-04	3.15E+07	2.03E-06	
Cs-137	2.29E+04	1.00E-02	68	5.99E+06	8.80E-06	1.47E-12	2.00E-04	4.58E-12	1.60E-04	7.74E-18	2.86E-08	3.15E+07	6.60E-10	
								Fines						
PU241	2.10E+04	1.00E-02	68	5.99E+06	8.80E-06	1.47E-12	3.00E-05	6.29E-13	1.60E-04	7.25E-20	2.68E-10	3.15E+07	8.51E-13	
Y 90	1.52E+04	1.00E-02	68	5.99E+06	8.80E-06	1.47E-12	3.00E-05	4.56E-13	1.60E-04	1.90E-16	7.03E-07	3.15E+07	1.61E-09	
PM147	8.88E+03	1.00E-02	68	5.99E+06	8.80E-06	1.47E-12	3.00E-05	2.66E-13	1.60E-04	6.93E-19	2.56E-09	3.15E+07	3.44E-12	
CE144	2.46E+03	1.00E-02	68	5.99E+06	8.80E-06	1.47E-12	3.00E-05	7.37E-14	1.60E-04	8.53E-16	3.16E-06	3.15E+07	1.17E-09	
PR144	2.46E+03	1.00E-02	68	5.99E+06	8.80E-06	1.47E-12	3.00E-05	7.37E-14	1.60E-04	1.95E-15	7.22E-06	3.15E+07	2.68E-09	
EU154	1.07E+03	1.00E-02	68	5.99E+06	8.80E-06	1.47E-12	3.00E-05	3.21E-14	1.60E-04	6.14E-14	2.27E-04	3.15E+07	3.67E-08	
CM244	9.30E+02	1.00E-02	68	5.99E+06	8.80E-06	1.47E-12	3.00E-05	2.79E-14	1.60E-04	4.91E-18	1.82E-08	3.15E+07	2.55E-12	
PU238	7.49E+02	1.00E-02	68	5.99E+06	8.80E-06	1.47E-12	3.00E-05	2.24E-14	1.60E-04	4.88E-18	1.81E-08	3.15E+07	2.04E-12	
SB125	6.40E+02	1.00E-02	68	5.99E+06	8.80E-06	1.47E-12	3.00E-05	1.92E-14	1.60E-04	2.02E-14	7.47E-05	3.15E+07	7.23E-09	
EU155	3.51E+02	1.00E-02	68	5.99E+06	8.80E-06	1.47E-12	3.00E-05	1.05E-14	1.60E-04	2.49E-15	9.21E-06	3.15E+07	4.88E-10	
AM241	2.20E+02	1.00E-02	68	5.99E+06	8.80E-06	1.47E-12	3.00E-05	6.59E-15	1.60E-04	8.18E-16	3.03E-06	3.15E+07	1.01E-10	
TE125M	1.56E+02	1.00E-02	68	5.99E+06	8.80E-06	1.47E-12	3.00E-05	4.68E-15	1.60E-04	4.53E-16	1.68E-06	3.15E+07	3.95E-11	
PU240	1.26E+02	1.00E-02	68	5.99E+06	8.80E-06	1.47E-12	3.00E-05	3.78E-15	1.60E-04	4.75E-18	1.76E-08	3.15E+07	3.34E-13	
151Sm	0.00E+00	1.00E-02	68	5.99E+06	8.80E-06	1.47E-12	3.00E-05	0.00E+00	1.60E-04	3.61E-20	1.34E-10	3.15E+07	0.00E+00	
239Pu	6.16E+01	1.00E-02	68	5.99E+06	8.80E-06	1.47E-12	3.00E-05	1.85E-15	1.60E-04	4.24E-18	1.57E-08	3.15E+07	1.46E-13	
137mBa	2.16E+04	1.00E-02	68	5.99E+06	8.80E-06	1.47E-12	3.00E-05	6.47E-13	1.60E-04	2.88E-14	1.07E-04	3.15E+07	3.48E-07	
106Rh	4.16E+03	1.00E-02	68	5.99E+06	8.80E-06	1.47E-12	3.00E-05	1.25E-13	1.60E-04	1.04E-14	3.85E-05	3.15E+07	2.42E-08	
144mPr	0.00E+00	1.00E-02	68	5.99E+06	8.80E-06	1.47E-12	3.00E-05	0.00E+00	1.60E-04	2.79E-16	1.03E-06	3.15E+07	0.00E+00	
243Am	7.39E+00	1.00E-02	68	5.99E+06	8.80E-06	1.47E-12	3.00E-05	2.21E-16	1.60E-04	2.18E-15	8.07E-06	3.15E+07	9.00E-12	
242Cm	6.10E+00	1.00E-02	68	5.99E+06	8.80E-06	1.47E-12	3.00E-05	1.83E-16	1.60E-04	5.69E-18	2.11E-08	3.15E+07	1.94E-14	
243Cm	4.81E+00	1.00E-02	68	5.99E+06	8.80E-06	1.47E-12	3.00E-05	1.44E-16	1.60E-04	5.88E-15	2.18E-05	3.15E+07	1.58E-11	
239Np	7.39E+00	1.00E-02	68	5.99E+06	8.80E-06	1.47E-12	3.00E-05	2.21E-16	1.60E-04	7.69E-15	2.85E-05	3.15E+07	3.18E-11	
237Np	7.05E-02	1.00E-02	68	5.99E+06	8.80E-06	1.47E-12	3.00E-05	2.11E-18	1.60E-04	1.03E-15	3.81E-06	3.15E+07	4.06E-14	
242Pu	5.95E-01	1.00E-02	68	5.99E+06	8.80E-06	1.47E-12	3.00E-05	1.78E-17	1.60E-04	4.01E-18	1.48E-08	3.15E+07	1.33E-15	
242Am	1.69E+00	1.00E-02	68	5.99E+06	8.80E-06	1.47E-12	3.00E-05	5.06E-17	1.60E-04	6.15E-16	2.28E-06	3.15E+07	5.81E-13	
242mAm	1.70E+00	1.00E-02	68	5.99E+06	8.80E-06	1.47E-12	3.00E-05	5.09E-17	1.60E-04	3.17E-17	1.17E-07	3.15E+07	3.01E-14	
												Total	2.29E-03	

MPC-68														
Normal Conditions														
Effective Dose Equivalent From Submersion														
Nuclide	Inventory (Ci/Assy)	1% for normal storage	No. Assy	MPC Vol (cm3)	L_{nor} Rate at Upstream (cm3/s)	Fraction Released per sec	Release Fraction	Release Rate (Ci/sec)	X/Q (sec/m3)	DCF (Sv/Bq)	DCF (mRem/uCi)	Occ Time (sec)	EDE (mRem)	
								Gases						
H-3	8.72E+01	1.00E-02	68	5.99E+06	8.80E-06	1.47E-12	0.30	2.61E-11	1.60E-04	0.00E+00	0.00E+00	3.15E+07	0.00E+00	
I-129	7.72E-03	1.00E-02	68	5.99E+06	8.80E-06	1.47E-12	0.30	2.31E-15	1.60E-04	1.10E-15	4.07E-06	3.15E+07	4.75E-11	
Kr-85	1.43E+03	1.00E-02	68	5.99E+06	8.80E-06	1.47E-12	0.30	4.29E-10	1.60E-04	1.32E-14	4.88E-05	3.15E+07	1.05E-04	
								Crud						
Co-60	6.50E+01	1.00E+00	68	5.99E+06	8.80E-06	1.47E-12	0.15	9.74E-10	1.60E-04	1.45E-13	5.37E-04	3.15E+07	2.63E-03	
								Volatiles						
Sr-90	1.52E+04	1.00E-02	68	5.99E+06	8.80E-06	1.47E-12	2.00E-04	3.04E-12	1.60E-04	9.20E-15	3.40E-05	3.15E+07	5.21E-07	
Ru-106	4.16E+03	1.00E-02	68	5.99E+06	8.80E-06	1.47E-12	2.00E-04	8.31E-13	1.60E-04	0.00E+00	0.00E+00	3.15E+07	0.00E+00	
Cs-134	7.20E+03	1.00E-02	68	5.99E+06	8.80E-06	1.47E-12	2.00E-04	1.44E-12	1.60E-04	9.45E-14	3.50E-04	3.15E+07	2.54E-06	
Cs-137	2.29E+04	1.00E-02	68	5.99E+06	8.80E-06	1.47E-12	2.00E-04	4.58E-12	1.60E-04	8.63E-15	3.19E-05	3.15E+07	7.36E-07	
								Fines						
PU241	2.10E+04	1.00E-02	68	5.99E+06	8.80E-06	1.47E-12	3.00E-05	6.29E-13	1.60E-04	1.17E-19	4.33E-10	3.15E+07	1.37E-12	
Y 90	1.52E+04	1.00E-02	68	5.99E+06	8.80E-06	1.47E-12	3.00E-05	4.56E-13	1.60E-04	6.24E-14	2.31E-04	3.15E+07	5.30E-07	
PM147	8.88E+03	1.00E-02	68	5.99E+06	8.80E-06	1.47E-12	3.00E-05	2.66E-13	1.60E-04	8.11E-16	3.00E-06	3.15E+07	4.02E-09	
CE144	2.46E+03	1.00E-02	68	5.99E+06	8.80E-06	1.47E-12	3.00E-05	7.37E-14	1.60E-04	2.93E-15	1.08E-05	3.15E+07	4.03E-09	
PR144	2.46E+03	1.00E-02	68	5.99E+06	8.80E-06	1.47E-12	3.00E-05	7.37E-14	1.60E-04	8.43E-14	3.12E-04	3.15E+07	1.16E-07	
EU154	1.07E+03	1.00E-02	68	5.99E+06	8.80E-06	1.47E-12	3.00E-05	3.21E-14	1.60E-04	8.29E-14	3.07E-04	3.15E+07	4.96E-08	
CM244	9.30E+02	1.00E-02	68	5.99E+06	8.80E-06	1.47E-12	3.00E-05	2.79E-14	1.60E-04	3.91E-17	1.45E-07	3.15E+07	2.03E-11	
PU238	7.49E+02	1.00E-02	68	5.99E+06	8.80E-06	1.47E-12	3.00E-05	2.24E-14	1.60E-04	4.09E-17	1.51E-07	3.15E+07	1.71E-11	
SB125	6.40E+02	1.00E-02	68	5.99E+06	8.80E-06	1.47E-12	3.00E-05	1.92E-14	1.60E-04	2.65E-14	9.81E-05	3.15E+07	9.48E-09	
EU155	3.51E+02	1.00E-02	68	5.99E+06	8.80E-06	1.47E-12	3.00E-05	1.05E-14	1.60E-04	3.39E-15	1.25E-05	3.15E+07	6.65E-10	
AM241	2.20E+02	1.00E-02	68	5.99E+06	8.80E-06	1.47E-12	3.00E-05	6.59E-15	1.60E-04	1.28E-15	4.74E-06	3.15E+07	1.57E-10	
TE125M	1.56E+02	1.00E-02	68	5.99E+06	8.80E-06	1.47E-12	3.00E-05	4.68E-15	1.60E-04	1.94E-15	7.18E-06	3.15E+07	1.69E-10	
PU240	1.26E+02	1.00E-02	68	5.99E+06	8.80E-06	1.47E-12	3.00E-05	3.78E-15	1.60E-04	3.92E-17	1.45E-07	3.15E+07	2.76E-12	
151Sm	0.00E+00	1.00E-02	68	5.99E+06	8.80E-06	1.47E-12	3.00E-05	0.00E+00	1.60E-04	1.90E-20	7.03E-11	3.15E+07	0.00E+00	
239Pu	6.16E+01	1.00E-02	68	5.99E+06	8.80E-06	1.47E-12	3.00E-05	1.85E-15	1.60E-04	1.86E-17	6.88E-08	3.15E+07	6.40E-13	
137mBa	2.16E+04	1.00E-02	68	5.99E+06	8.80E-06	1.47E-12	3.00E-05	6.47E-13	1.60E-04	3.73E-14	1.38E-04	3.15E+07	4.50E-07	
106Rh	4.16E+03	1.00E-02	68	5.99E+06	8.80E-06	1.47E-12	3.00E-05	1.25E-13	1.60E-04	1.09E-13	4.03E-04	3.15E+07	2.53E-07	
144mPr	0.00E+00	1.00E-02	68	5.99E+06	8.80E-06	1.47E-12	3.00E-05	0.00E+00	1.60E-04	5.08E-16	1.88E-06	3.15E+07	0.00E+00	
243Am	7.39E+00	1.00E-02	68	5.99E+06	8.80E-06	1.47E-12	3.00E-05	2.21E-16	1.60E-04	2.75E-15	1.02E-05	3.15E+07	1.14E-11	
242Cm	6.10E+00	1.00E-02	68	5.99E+06	8.80E-06	1.47E-12	3.00E-05	1.83E-16	1.60E-04	4.29E-17	1.59E-07	3.15E+07	1.46E-13	
243Cm	4.81E+00	1.00E-02	68	5.99E+06	8.80E-06	1.47E-12	3.00E-05	1.44E-16	1.60E-04	9.79E-15	3.62E-05	3.15E+07	2.63E-11	
239Np	7.39E+00	1.00E-02	68	5.99E+06	8.80E-06	1.47E-12	3.00E-05	2.21E-16	1.60E-04	1.60E-14	5.92E-05	3.15E+07	6.61E-11	
237Np	7.05E-02	1.00E-02	68	5.99E+06	8.80E-06	1.47E-12	3.00E-05	2.11E-18	1.60E-04	1.54E-15	5.70E-06	3.15E+07	6.07E-14	
242Pu	5.95E-01	1.00E-02	68	5.99E+06	8.80E-06	1.47E-12	3.00E-05	1.78E-17	1.60E-04	3.27E-17	1.21E-07	3.15E+07	1.09E-14	
242Am	1.69E+00	1.00E-02	68	5.99E+06	8.80E-06	1.47E-12	3.00E-05	5.06E-17	1.60E-04	8.20E-15	3.03E-05	3.15E+07	7.74E-12	
242mAm	1.70E+00	1.00E-02	68	5.99E+06	8.80E-06	1.47E-12	3.00E-05	5.09E-17	1.60E-04	1.36E-16	5.03E-07	3.15E+07	1.29E-13	
												Total	2.74E-03	

MPC-68													
Off-Normal Conditions													
Effective Dose Equivalent From Submersion													
Nuclide	Inventory (Ci/Assy)	10% for off normal storage	No. Assy	MPC Vol (cm3)	L_{offnor} Rate at Upstream (cm3/s)	Fraction Released per sec	Release Fraction	Release Rate (Ci/sec)	X/Q (sec/m3)	DCF (Sv/Bq)	DCF (mRem/uCi)	Occ Time (sec)	EDE (mRem)
								Gases					
H-3	8.72E+01	1.00E-01	68	5.99E+06	8.80E-06	1.47E-12	0.30	2.61E-10	1.60E-04	0.00E+00	0.00E+00	3.15E+07	0.00E+00
I-129	7.72E-03	1.00E-01	68	5.99E+06	8.80E-06	1.47E-12	0.30	2.31E-14	1.60E-04	4.83E-16	1.79E-06	3.15E+07	2.08E-10
Kr-85	1.43E+03	1.00E-01	68	5.99E+06	8.80E-06	1.47E-12	0.30	4.29E-09	1.60E-04	1.17E-16	4.33E-07	3.15E+07	9.35E-06
								Crud					
Co-60	6.50E+01	1.00E+00	68	5.99E+06	8.80E-06	1.47E-12	0.15	9.74E-10	1.60E-04	1.23E-13	4.55E-04	3.15E+07	2.23E-03
								Volatiles					
Sr-90	1.52E+04	1.00E-01	68	5.99E+06	8.80E-06	1.47E-12	2.00E-04	3.04E-11	1.60E-04	7.78E-18	2.88E-08	3.15E+07	4.41E-09
Ru-106	4.16E+03	1.00E-01	68	5.99E+06	8.80E-06	1.47E-12	2.00E-04	8.31E-12	1.60E-04	0.00E+00	0.00E+00	3.15E+07	0.00E+00
Cs-134	7.20E+03	1.00E-01	68	5.99E+06	8.80E-06	1.47E-12	2.00E-04	1.44E-11	1.60E-04	7.40E-14	2.74E-04	3.15E+07	1.99E-05
Cs-137	2.29E+04	1.00E-01	68	5.99E+06	8.80E-06	1.47E-12	2.00E-04	4.58E-11	1.60E-04	7.96E-18	2.95E-08	3.15E+07	6.79E-09
								Fines					
PU241	2.10E+04	1.00E-01	68	5.99E+06	8.80E-06	1.47E-12	3.00E-05	6.29E-12	1.60E-04	7.19E-20	2.66E-10	3.15E+07	8.44E-12
Y 90	1.52E+04	1.00E-01	68	5.99E+06	8.80E-06	1.47E-12	3.00E-05	4.56E-12	1.60E-04	1.89E-16	6.99E-07	3.15E+07	1.61E-08
PM147	8.88E+03	1.00E-01	68	5.99E+06	8.80E-06	1.47E-12	3.00E-05	2.66E-12	1.60E-04	7.48E-19	2.77E-09	3.15E+07	3.71E-11
CE144	2.46E+03	1.00E-01	68	5.99E+06	8.80E-06	1.47E-12	3.00E-05	7.37E-13	1.60E-04	8.53E-16	3.16E-06	3.15E+07	1.17E-08
PR144	2.46E+03	1.00E-01	68	5.99E+06	8.80E-06	1.47E-12	3.00E-05	7.37E-13	1.60E-04	1.90E-15	7.03E-06	3.15E+07	2.61E-08
EU154	1.07E+03	1.00E-01	68	5.99E+06	8.80E-06	1.47E-12	3.00E-05	3.21E-13	1.60E-04	6.00E-14	2.22E-04	3.15E+07	3.59E-07
CM244	9.30E+02	1.00E-01	68	5.99E+06	8.80E-06	1.47E-12	3.00E-05	2.79E-13	1.60E-04	6.90E-18	2.55E-08	3.15E+07	3.59E-11
PU238	7.49E+02	1.00E-01	68	5.99E+06	8.80E-06	1.47E-12	3.00E-05	2.24E-13	1.60E-04	6.56E-18	2.43E-08	3.15E+07	2.75E-11
SB125	6.40E+02	1.00E-01	68	5.99E+06	8.80E-06	1.47E-12	3.00E-05	1.92E-13	1.60E-04	1.98E-14	7.33E-05	3.15E+07	7.08E-08
EU155	3.51E+02	1.00E-01	68	5.99E+06	8.80E-06	1.47E-12	3.00E-05	1.05E-13	1.60E-04	2.49E-15	9.21E-06	3.15E+07	4.88E-09
AM241	2.20E+02	1.00E-01	68	5.99E+06	8.80E-06	1.47E-12	3.00E-05	6.59E-14	1.60E-04	8.58E-16	3.17E-06	3.15E+07	1.05E-09
TE125M	1.56E+02	1.00E-01	68	5.99E+06	8.80E-06	1.47E-12	3.00E-05	4.68E-14	1.60E-04	5.96E-16	2.21E-06	3.15E+07	5.20E-10
PU240	1.26E+02	1.00E-01	68	5.99E+06	8.80E-06	1.47E-12	3.00E-05	3.78E-14	1.60E-04	6.36E-18	2.35E-08	3.15E+07	4.48E-12
151Sm	0.00E+00	1.00E-01	68	5.99E+06	8.80E-06	1.47E-12	3.00E-05	0.00E+00	1.60E-04	5.20E-20	1.92E-10	3.15E+07	0.00E+00
239Pu	6.16E+01	1.00E-01	68	5.99E+06	8.80E-06	1.47E-12	3.00E-05	1.85E-14	1.60E-04	4.84E-18	1.79E-08	3.15E+07	1.67E-12
137mBa	2.16E+04	1.00E-01	68	5.99E+06	8.80E-06	1.47E-12	3.00E-05	6.47E-12	1.60E-04	2.82E-14	1.04E-04	3.15E+07	3.40E-06
106Rh	4.16E+03	1.00E-01	68	5.99E+06	8.80E-06	1.47E-12	3.00E-05	1.25E-12	1.60E-04	1.01E-14	3.74E-05	3.15E+07	2.35E-07
144mPr	0.00E+00	1.00E-01	68	5.99E+06	8.80E-06	1.47E-12	3.00E-05	0.00E+00	1.60E-04	3.25E-16	1.20E-06	3.15E+07	0.00E+00
243Am	7.39E+00	1.00E-01	68	5.99E+06	8.80E-06	1.47E-12	3.00E-05	2.21E-15	1.60E-04	2.19E-15	8.10E-06	3.15E+07	9.04E-11
242Cm	6.10E+00	1.00E-01	68	5.99E+06	8.80E-06	1.47E-12	3.00E-05	1.83E-15	1.60E-04	7.83E-18	2.90E-08	3.15E+07	2.67E-13
243Cm	4.81E+00	1.00E-01	68	5.99E+06	8.80E-06	1.47E-12	3.00E-05	1.44E-15	1.60E-04	5.77E-15	2.13E-05	3.15E+07	1.55E-10
239Np	7.39E+00	1.00E-01	68	5.99E+06	8.80E-06	1.47E-12	3.00E-05	2.21E-15	1.60E-04	7.53E-15	2.79E-05	3.15E+07	3.11E-10
237Np	7.05E-02	1.00E-01	68	5.99E+06	8.80E-06	1.47E-12	3.00E-05	2.11E-17	1.60E-04	1.04E-15	3.85E-06	3.15E+07	4.10E-13
242Pu	5.95E-01	1.00E-01	68	5.99E+06	8.80E-06	1.47E-12	3.00E-05	1.78E-16	1.60E-04	5.34E-18	1.98E-08	3.15E+07	1.78E-14
242Am	1.69E+00	1.00E-01	68	5.99E+06	8.80E-06	1.47E-12	3.00E-05	5.06E-16	1.60E-04	6.09E-16	2.25E-06	3.15E+07	5.75E-12
242mAm	1.70E+00	1.00E-01	68	5.99E+06	8.80E-06	1.47E-12	3.00E-05	5.09E-16	1.60E-04	3.80E-17	1.41E-07	3.15E+07	3.61E-13
												Total	2.27E-03

MPC-68													
Off-Normal Conditions													
Effective Dose Equivalent From Submersion													
Nuclide	Inventory (Ci/Assy)	10% for off normal storage	No. Assy	MPC Vol (cm3)	L_{offnor} Rate at Upstream (cm3/s)	Fraction Released per sec	Release Fraction	Release Rate (Ci/sec)	X/Q (sec/m3)	DCF (Sv/Bq)	DCF (mRem/uCi)	Occ Time (sec)	EDE (mRem)
								Gases					
H-3	8.72E+01	1.00E-01	68	5.99E+06	8.80E-06	1.47E-12	0.30	2.61E-10	1.60E-04	0.00E+00	0.00E+00	3.15E+07	0.00E+00
I-129	7.72E-03	1.00E-01	68	5.99E+06	8.80E-06	1.47E-12	0.30	2.31E-14	1.60E-04	6.66E-16	2.46E-06	3.15E+07	2.87E-10
Kr-85	1.43E+03	1.00E-01	68	5.99E+06	8.80E-06	1.47E-12	0.30	4.29E-09	1.60E-04	1.34E-16	4.96E-07	3.15E+07	1.07E-05
								Crud					
Co-60	6.50E+01	1.00E+00	68	5.99E+06	8.80E-06	1.47E-12	0.15	9.74E-10	1.60E-04	1.39E-13	5.14E-04	3.15E+07	2.52E-03
								Volatiles					
Sr-90	1.52E+04	1.00E-01	68	5.99E+06	8.80E-06	1.47E-12	2.00E-04	3.04E-11	1.60E-04	9.49E-18	3.51E-08	3.15E+07	5.37E-09
Ru-106	4.16E+03	1.00E-01	68	5.99E+06	8.80E-06	1.47E-12	2.00E-04	8.31E-12	1.60E-04	0.00E+00	0.00E+00	3.15E+07	0.00E+00
Cs-134	7.20E+03	1.00E-01	68	5.99E+06	8.80E-06	1.47E-12	2.00E-04	1.44E-11	1.60E-04	8.43E-14	3.12E-04	3.15E+07	2.26E-05
Cs-137	2.29E+04	1.00E-01	68	5.99E+06	8.80E-06	1.47E-12	2.00E-04	4.58E-11	1.60E-04	9.67E-18	3.58E-08	3.15E+07	8.25E-09
								Fines					
PU241	2.10E+04	1.00E-01	68	5.99E+06	8.80E-06	1.47E-12	3.00E-05	6.29E-12	1.60E-04	8.67E-20	3.21E-10	3.15E+07	1.02E-11
Y 90	1.52E+04	1.00E-01	68	5.99E+06	8.80E-06	1.47E-12	3.00E-05	4.56E-12	1.60E-04	2.20E-16	8.14E-07	3.15E+07	1.87E-08
PM147	8.88E+03	1.00E-01	68	5.99E+06	8.80E-06	1.47E-12	3.00E-05	2.66E-12	1.60E-04	9.56E-19	3.54E-09	3.15E+07	4.74E-11
CE144	2.46E+03	1.00E-01	68	5.99E+06	8.80E-06	1.47E-12	3.00E-05	7.37E-13	1.60E-04	1.01E-15	3.74E-06	3.15E+07	1.39E-08
PR144	2.46E+03	1.00E-01	68	5.99E+06	8.80E-06	1.47E-12	3.00E-05	7.37E-13	1.60E-04	2.15E-15	7.96E-06	3.15E+07	2.96E-08
EU154	1.07E+03	1.00E-01	68	5.99E+06	8.80E-06	1.47E-12	3.00E-05	3.21E-13	1.60E-04	6.81E-14	2.52E-04	3.15E+07	4.07E-07
CM244	9.30E+02	1.00E-01	68	5.99E+06	8.80E-06	1.47E-12	3.00E-05	2.79E-13	1.60E-04	1.33E-17	4.92E-08	3.15E+07	6.91E-11
PU238	7.49E+02	1.00E-01	68	5.99E+06	8.80E-06	1.47E-12	3.00E-05	2.24E-13	1.60E-04	1.27E-17	4.70E-08	3.15E+07	5.32E-11
SB125	6.40E+02	1.00E-01	68	5.99E+06	8.80E-06	1.47E-12	3.00E-05	1.92E-13	1.60E-04	2.27E-14	8.40E-05	3.15E+07	8.12E-08
EU155	3.51E+02	1.00E-01	68	5.99E+06	8.80E-06	1.47E-12	3.00E-05	1.05E-13	1.60E-04	2.95E-15	1.09E-05	3.15E+07	5.79E-09
AM241	2.20E+02	1.00E-01	68	5.99E+06	8.80E-06	1.47E-12	3.00E-05	6.59E-14	1.60E-04	1.07E-15	3.96E-06	3.15E+07	1.32E-09
TE125M	1.56E+02	1.00E-01	68	5.99E+06	8.80E-06	1.47E-12	3.00E-05	4.68E-14	1.60E-04	8.48E-16	3.14E-06	3.15E+07	7.39E-10
PU240	1.26E+02	1.00E-01	68	5.99E+06	8.80E-06	1.47E-12	3.00E-05	3.78E-14	1.60E-04	1.23E-17	4.55E-08	3.15E+07	8.66E-12
151Sm	0.00E+00	1.00E-01	68	5.99E+06	8.80E-06	1.47E-12	3.00E-05	0.00E+00	1.60E-04	8.80E-20	3.26E-10	3.15E+07	0.00E+00
239Pu	6.16E+01	1.00E-01	68	5.99E+06	8.80E-06	1.47E-12	3.00E-05	1.85E-14	1.60E-04	7.55E-18	2.79E-08	3.15E+07	2.60E-12
137mBa	2.16E+04	1.00E-01	68	5.99E+06	8.80E-06	1.47E-12	3.00E-05	6.47E-12	1.60E-04	3.22E-14	1.19E-04	3.15E+07	3.89E-06
106Rh	4.16E+03	1.00E-01	68	5.99E+06	8.80E-06	1.47E-12	3.00E-05	1.25E-12	1.60E-04	1.16E-14	4.29E-05	3.15E+07	2.70E-07
144mPr	0.00E+00	1.00E-01	68	5.99E+06	8.80E-06	1.47E-12	3.00E-05	0.00E+00	1.60E-04	4.20E-16	1.55E-06	3.15E+07	0.00E+00
243Am	7.39E+00	1.00E-01	68	5.99E+06	8.80E-06	1.47E-12	3.00E-05	2.21E-15	1.60E-04	2.61E-15	9.66E-06	3.15E+07	1.08E-10
242Cm	6.10E+00	1.00E-01	68	5.99E+06	8.80E-06	1.47E-12	3.00E-05	1.83E-15	1.60E-04	1.48E-17	5.48E-08	3.15E+07	5.05E-13
243Cm	4.81E+00	1.00E-01	68	5.99E+06	8.80E-06	1.47E-12	3.00E-05	1.44E-15	1.60E-04	6.68E-15	2.47E-05	3.15E+07	1.80E-10
239Np	7.39E+00	1.00E-01	68	5.99E+06	8.80E-06	1.47E-12	3.00E-05	2.21E-15	1.60E-04	8.73E-15	3.23E-05	3.15E+07	3.61E-10
237Np	7.05E-02	1.00E-01	68	5.99E+06	8.80E-06	1.47E-12	3.00E-05	2.11E-17	1.60E-04	1.26E-15	4.66E-06	3.15E+07	4.96E-13
242Pu	5.95E-01	1.00E-01	68	5.99E+06	8.80E-06	1.47E-12	3.00E-05	1.78E-16	1.60E-04	1.03E-17	3.81E-08	3.15E+07	3.43E-14
242Am	1.69E+00	1.00E-01	68	5.99E+06	8.80E-06	1.47E-12	3.00E-05	5.06E-16	1.60E-04	7.30E-16	2.70E-06	3.15E+07	6.89E-12
242mAm	1.70E+00	1.00E-01	68	5.99E+06	8.80E-06	1.47E-12	3.00E-05	5.09E-16	1.60E-04	6.01E-17	2.22E-07	3.15E+07	5.71E-13
												Total	2.56E-03

MPC-68													
Off-Normal Conditions													
Effective Dose Equivalent From Submersion													
Nuclide	Inventory (Ci/Assy)	10% for off normal storage	No. Assy	MPC Vol (cm3)	L_{offnor} Rate at Upstream (cm3/s)	Fraction Released per sec	Release Fraction	Release Rate (Ci/sec)	X/Q (sec/m3)	DCF (Sv/Bq)	DCF (mRem/uCi)	Occ Time (sec)	EDE (mRem)
								Gases					
H-3	8.72E+01	1.00E-01	68	5.99E+06	8.80E-06	1.47E-12	0.30	2.61E-10	1.60E-04	2.75E-18	1.02E-08	3.15E+07	1.34E-08
I-129	7.72E-03	1.00E-01	68	5.99E+06	8.80E-06	1.47E-12	0.30	2.31E-14	1.60E-04	2.14E-16	7.92E-07	3.15E+07	9.23E-11
Kr-85	1.43E+03	1.00E-01	68	5.99E+06	8.80E-06	1.47E-12	0.30	4.29E-09	1.60E-04	1.14E-16	4.22E-07	3.15E+07	9.11E-06
								Crud					
Co-60	6.50E+01	1.00E+00	68	5.99E+06	8.80E-06	1.47E-12	0.15	9.74E-10	1.60E-04	1.24E-13	4.59E-04	3.15E+07	2.25E-03
								Volatiles					
Sr-90	1.52E+04	1.00E-01	68	5.99E+06	8.80E-06	1.47E-12	2.00E-04	3.04E-11	1.60E-04	6.44E-18	2.38E-08	3.15E+07	3.65E-09
Ru-106	4.16E+03	1.00E-01	68	5.99E+06	8.80E-06	1.47E-12	2.00E-04	8.31E-12	1.60E-04	0.00E+00	0.00E+00	3.15E+07	0.00E+00
Cs-134	7.20E+03	1.00E-01	68	5.99E+06	8.80E-06	1.47E-12	2.00E-04	1.44E-11	1.60E-04	7.37E-14	2.73E-04	3.15E+07	1.98E-05
Cs-137	2.29E+04	1.00E-01	68	5.99E+06	8.80E-06	1.47E-12	2.00E-04	4.58E-11	1.60E-04	6.68E-18	2.47E-08	3.15E+07	5.70E-09
								Fines					
PU241	2.10E+04	1.00E-01	68	5.99E+06	8.80E-06	1.47E-12	3.00E-05	6.29E-12	1.60E-04	6.48E-20	2.40E-10	3.15E+07	7.61E-12
Y 90	1.52E+04	1.00E-01	68	5.99E+06	8.80E-06	1.47E-12	3.00E-05	4.56E-12	1.60E-04	1.77E-16	6.55E-07	3.15E+07	1.50E-08
PM147	8.88E+03	1.00E-01	68	5.99E+06	8.80E-06	1.47E-12	3.00E-05	2.66E-12	1.60E-04	5.45E-19	2.02E-09	3.15E+07	2.70E-11
CE144	2.46E+03	1.00E-01	68	5.99E+06	8.80E-06	1.47E-12	3.00E-05	7.37E-13	1.60E-04	7.69E-16	2.85E-06	3.15E+07	1.06E-08
PR144	2.46E+03	1.00E-01	68	5.99E+06	8.80E-06	1.47E-12	3.00E-05	7.37E-13	1.60E-04	1.90E-15	7.03E-06	3.15E+07	2.61E-08
EU154	1.07E+03	1.00E-01	68	5.99E+06	8.80E-06	1.47E-12	3.00E-05	3.21E-13	1.60E-04	5.99E-14	2.22E-04	3.15E+07	3.58E-07
CM244	9.30E+02	1.00E-01	68	5.99E+06	8.80E-06	1.47E-12	3.00E-05	2.79E-13	1.60E-04	7.08E-19	2.62E-09	3.15E+07	3.68E-12
PU238	7.49E+02	1.00E-01	68	5.99E+06	8.80E-06	1.47E-12	3.00E-05	2.24E-13	1.60E-04	1.06E-18	3.92E-09	3.15E+07	4.44E-12
SB125	6.40E+02	1.00E-01	68	5.99E+06	8.80E-06	1.47E-12	3.00E-05	1.92E-13	1.60E-04	1.95E-14	7.22E-05	3.15E+07	6.97E-08
EU155	3.51E+02	1.00E-01	68	5.99E+06	8.80E-06	1.47E-12	3.00E-05	1.05E-13	1.60E-04	2.22E-15	8.21E-06	3.15E+07	4.35E-09
AM241	2.20E+02	1.00E-01	68	5.99E+06	8.80E-06	1.47E-12	3.00E-05	6.59E-14	1.60E-04	6.74E-16	2.49E-06	3.15E+07	8.29E-10
TE125M	1.56E+02	1.00E-01	68	5.99E+06	8.80E-06	1.47E-12	3.00E-05	4.68E-14	1.60E-04	2.23E-16	8.25E-07	3.15E+07	1.94E-10
PU240	1.26E+02	1.00E-01	68	5.99E+06	8.80E-06	1.47E-12	3.00E-05	3.78E-14	1.60E-04	1.09E-18	4.03E-09	3.15E+07	7.68E-13
151Sm	0.00E+00	1.00E-01	68	5.99E+06	8.80E-06	1.47E-12	3.00E-05	0.00E+00	1.60E-04	7.08E-21	2.62E-11	3.15E+07	0.00E+00
239Pu	6.16E+01	1.00E-01	68	5.99E+06	8.80E-06	1.47E-12	3.00E-05	1.85E-14	1.60E-04	2.65E-18	9.81E-09	3.15E+07	9.12E-13
137mBa	2.16E+04	1.00E-01	68	5.99E+06	8.80E-06	1.47E-12	3.00E-05	6.47E-12	1.60E-04	2.80E-14	1.04E-04	3.15E+07	3.38E-06
106Rh	4.16E+03	1.00E-01	68	5.99E+06	8.80E-06	1.47E-12	3.00E-05	1.25E-12	1.60E-04	1.01E-14	3.74E-05	3.15E+07	2.35E-07
144mPr	0.00E+00	1.00E-01	68	5.99E+06	8.80E-06	1.47E-12	3.00E-05	0.00E+00	1.60E-04	2.00E-16	7.40E-07	3.15E+07	0.00E+00
243Am	7.39E+00	1.00E-01	68	5.99E+06	8.80E-06	1.47E-12	3.00E-05	2.21E-15	1.60E-04	1.92E-15	7.10E-06	3.15E+07	7.93E-11
242Cm	6.10E+00	1.00E-01	68	5.99E+06	8.80E-06	1.47E-12	3.00E-05	1.83E-15	1.60E-04	1.13E-18	4.18E-09	3.15E+07	3.85E-14
243Cm	4.81E+00	1.00E-01	68	5.99E+06	8.80E-06	1.47E-12	3.00E-05	1.44E-15	1.60E-04	5.50E-15	2.04E-05	3.15E+07	1.48E-10
239Np	7.39E+00	1.00E-01	68	5.99E+06	8.80E-06	1.47E-12	3.00E-05	2.21E-15	1.60E-04	7.18E-15	2.66E-05	3.15E+07	2.97E-10
237Np	7.05E-02	1.00E-01	68	5.99E+06	8.80E-06	1.47E-12	3.00E-05	2.11E-17	1.60E-04	9.02E-16	3.34E-06	3.15E+07	3.55E-13
242Pu	5.95E-01	1.00E-01	68	5.99E+06	8.80E-06	1.47E-12	3.00E-05	1.78E-16	1.60E-04	9.69E-19	3.59E-09	3.15E+07	3.22E-15
242Am	1.69E+00	1.00E-01	68	5.99E+06	8.80E-06	1.47E-12	3.00E-05	5.06E-16	1.60E-04	5.51E-15	2.04E-05	3.15E+07	5.20E-11
242mAm	1.70E+00	1.00E-01	68	5.99E+06	8.80E-06	1.47E-12	3.00E-05	5.09E-16	1.60E-04	1.72E-17	6.36E-08	3.15E+07	1.63E-13
												Total	2.29E-03

MPC-68													
Off-Normal Conditions													
Effective Dose Equivalent From Submersion													
Nuclide	Inventory (Ci/Assy)	10% for off normal storage	No. Assy	MPC Vol (cm3)	L_{offnor} Rate at Upstream (cm3/s)	Fraction Released per sec	Release Fraction	Release Rate (Ci/sec)	X/Q (sec/m3)	DCF (Sv/Bq)	DCF (mRem/uCi)	Occ Time (sec)	EDE (mRem)
								Gases					
H-3	8.72E+01	1.00E-01	68	5.99E+06	8.80E-06	1.47E-12	0.30	2.61E-10	1.60E-04	0.00E+00	0.00E+00	3.15E+07	0.00E+00
I-129	7.72E-03	1.00E-01	68	5.99E+06	8.80E-06	1.47E-12	0.30	2.31E-14	1.60E-04	1.64E-16	6.07E-07	3.15E+07	7.08E-11
Kr-85	1.43E+03	1.00E-01	68	5.99E+06	8.80E-06	1.47E-12	0.30	4.29E-09	1.60E-04	1.09E-16	4.03E-07	3.15E+07	8.71E-06
								Crud					
Co-60	6.50E+01	1.00E+00	68	5.99E+06	8.80E-06	1.47E-12	0.15	9.74E-10	1.60E-04	1.23E-13	4.55E-04	3.15E+07	2.23E-03
								Volatiles					
Sr-90	1.52E+04	1.00E-01	68	5.99E+06	8.80E-06	1.47E-12	2.00E-04	3.04E-11	1.60E-04	5.44E-18	2.01E-08	3.15E+07	3.08E-09
Ru-106	4.16E+03	1.00E-01	68	5.99E+06	8.80E-06	1.47E-12	2.00E-04	8.31E-12	1.60E-04	0.00E+00	0.00E+00	3.15E+07	0.00E+00
Cs-134	7.20E+03	1.00E-01	68	5.99E+06	8.80E-06	1.47E-12	2.00E-04	1.44E-11	1.60E-04	7.19E-14	2.66E-04	3.15E+07	1.93E-05
Cs-137	2.29E+04	1.00E-01	68	5.99E+06	8.80E-06	1.47E-12	2.00E-04	4.58E-11	1.60E-04	5.70E-18	2.11E-08	3.15E+07	4.86E-09
								Fines					
PU241	2.10E+04	1.00E-01	68	5.99E+06	8.80E-06	1.47E-12	3.00E-05	6.29E-12	1.60E-04	5.63E-20	2.08E-10	3.15E+07	6.61E-12
Y 90	1.52E+04	1.00E-01	68	5.99E+06	8.80E-06	1.47E-12	3.00E-05	4.56E-12	1.60E-04	1.62E-16	5.99E-07	3.15E+07	1.38E-08
PM147	8.88E+03	1.00E-01	68	5.99E+06	8.80E-06	1.47E-12	3.00E-05	2.66E-12	1.60E-04	4.46E-19	1.65E-09	3.15E+07	2.21E-11
CE144	2.46E+03	1.00E-01	68	5.99E+06	8.80E-06	1.47E-12	3.00E-05	7.37E-13	1.60E-04	6.68E-16	2.47E-06	3.15E+07	9.18E-09
PR144	2.46E+03	1.00E-01	68	5.99E+06	8.80E-06	1.47E-12	3.00E-05	7.37E-13	1.60E-04	1.87E-15	6.92E-06	3.15E+07	2.57E-08
EU154	1.07E+03	1.00E-01	68	5.99E+06	8.80E-06	1.47E-12	3.00E-05	3.21E-13	1.60E-04	5.87E-14	2.17E-04	3.15E+07	3.51E-07
CM244	9.30E+02	1.00E-01	68	5.99E+06	8.80E-06	1.47E-12	3.00E-05	2.79E-13	1.60E-04	1.46E-18	5.40E-09	3.15E+07	7.59E-12
PU238	7.49E+02	1.00E-01	68	5.99E+06	8.80E-06	1.47E-12	3.00E-05	2.24E-13	1.60E-04	1.68E-18	6.22E-09	3.15E+07	7.03E-12
SB125	6.40E+02	1.00E-01	68	5.99E+06	8.80E-06	1.47E-12	3.00E-05	1.92E-13	1.60E-04	1.87E-14	6.92E-05	3.15E+07	6.69E-08
EU155	3.51E+02	1.00E-01	68	5.99E+06	8.80E-06	1.47E-12	3.00E-05	1.05E-13	1.60E-04	1.85E-15	6.85E-06	3.15E+07	3.63E-09
AM241	2.20E+02	1.00E-01	68	5.99E+06	8.80E-06	1.47E-12	3.00E-05	6.59E-14	1.60E-04	5.21E-16	1.93E-06	3.15E+07	6.41E-10
TE125M	1.56E+02	1.00E-01	68	5.99E+06	8.80E-06	1.47E-12	3.00E-05	4.68E-14	1.60E-04	1.86E-16	6.88E-07	3.15E+07	1.62E-10
PU240	1.26E+02	1.00E-01	68	5.99E+06	8.80E-06	1.47E-12	3.00E-05	3.78E-14	1.60E-04	1.65E-18	6.11E-09	3.15E+07	1.16E-12
151Sm	0.00E+00	1.00E-01	68	5.99E+06	8.80E-06	1.47E-12	3.00E-05	0.00E+00	1.60E-04	1.13E-20	4.18E-11	3.15E+07	0.00E+00
239Pu	6.16E+01	1.00E-01	68	5.99E+06	8.80E-06	1.47E-12	3.00E-05	1.85E-14	1.60E-04	2.67E-18	9.88E-09	3.15E+07	9.19E-13
137mBa	2.16E+04	1.00E-01	68	5.99E+06	8.80E-06	1.47E-12	3.00E-05	6.47E-12	1.60E-04	2.73E-14	1.01E-04	3.15E+07	3.30E-06
106Rh	4.16E+03	1.00E-01	68	5.99E+06	8.80E-06	1.47E-12	3.00E-05	1.25E-12	1.60E-04	9.75E-15	3.61E-05	3.15E+07	2.27E-07
144mPr	0.00E+00	1.00E-01	68	5.99E+06	8.80E-06	1.47E-12	3.00E-05	0.00E+00	1.60E-04	1.56E-16	5.77E-07	3.15E+07	0.00E+00
243Am	7.39E+00	1.00E-01	68	5.99E+06	8.80E-06	1.47E-12	3.00E-05	2.21E-15	1.60E-04	1.55E-15	5.74E-06	3.15E+07	6.40E-11
242Cm	6.10E+00	1.00E-01	68	5.99E+06	8.80E-06	1.47E-12	3.00E-05	1.83E-15	1.60E-04	1.89E-18	6.99E-09	3.15E+07	6.44E-14
243Cm	4.81E+00	1.00E-01	68	5.99E+06	8.80E-06	1.47E-12	3.00E-05	1.44E-15	1.60E-04	5.00E-15	1.85E-05	3.15E+07	1.34E-10
239Np	7.39E+00	1.00E-01	68	5.99E+06	8.80E-06	1.47E-12	3.00E-05	2.21E-15	1.60E-04	6.50E-15	2.41E-05	3.15E+07	2.68E-10
237Np	7.05E-02	1.00E-01	68	5.99E+06	8.80E-06	1.47E-12	3.00E-05	2.11E-17	1.60E-04	7.69E-16	2.85E-06	3.15E+07	3.03E-13
242Pu	5.95E-01	1.00E-01	68	5.99E+06	8.80E-06	1.47E-12	3.00E-05	1.78E-16	1.60E-04	1.43E-18	5.29E-09	3.15E+07	4.76E-15
242Am	1.69E+00	1.00E-01	68	5.99E+06	8.80E-06	1.47E-12	3.00E-05	5.06E-16	1.60E-04	4.77E-16	1.76E-06	3.15E+07	4.51E-12
242mAm	1.70E+00	1.00E-01	68	5.99E+06	8.80E-06	1.47E-12	3.00E-05	5.09E-16	1.60E-04	1.72E-17	6.36E-08	3.15E+07	1.63E-13
												Total	2.27E-03

MPC-68													
Off-Normal Conditions													
Effective Dose Equivalent From Submersion													
Nuclide	Inventory (Ci/Assy)	10% for off normal storage	No. Assy	MPC Vol (cm3)	L_{offnor} Rate at Upstream (cm3/s)	Fraction Released per sec	Release Fraction	Release Rate (Ci/sec)	X/Q (sec/m3)	DCF (Sv/Bq)	DCF (mRem/uCi)	Occ Time (sec)	EDE (mRem)
								Gases					
H-3	8.72E+01	1.00E-01	68	5.99E+06	8.80E-06	1.47E-12	0.30	2.61E-10	1.60E-04	0.00E+00	0.00E+00	3.15E+07	0.00E+00
I-129	7.72E-03	1.00E-01	68	5.99E+06	8.80E-06	1.47E-12	0.30	2.31E-14	1.60E-04	1.10E-15	4.07E-06	3.15E+07	4.75E-10
Kr-85	1.43E+03	1.00E-01	68	5.99E+06	8.80E-06	1.47E-12	0.30	4.29E-09	1.60E-04	2.20E-16	8.14E-07	3.15E+07	1.76E-05
								Crud					
Co-60	6.50E+01	1.00E+00	68	5.99E+06	8.80E-06	1.47E-12	0.15	9.74E-10	1.60E-04	1.78E-13	6.59E-04	3.15E+07	3.23E-03
								Volatiles					
Sr-90	1.52E+04	1.00E-01	68	5.99E+06	8.80E-06	1.47E-12	2.00E-04	3.04E-11	1.60E-04	2.28E-17	8.44E-08	3.15E+07	1.29E-08
Ru-106	4.16E+03	1.00E-01	68	5.99E+06	8.80E-06	1.47E-12	2.00E-04	8.31E-12	1.60E-04	0.00E+00	0.00E+00	3.15E+07	0.00E+00
Cs-134	7.20E+03	1.00E-01	68	5.99E+06	8.80E-06	1.47E-12	2.00E-04	1.44E-11	1.60E-04	1.20E-13	4.44E-04	3.15E+07	3.22E-05
Cs-137	2.29E+04	1.00E-01	68	5.99E+06	8.80E-06	1.47E-12	2.00E-04	4.58E-11	1.60E-04	2.29E-17	8.47E-08	3.15E+07	1.95E-08
								Fines					
PU241	2.10E+04	1.00E-01	68	5.99E+06	8.80E-06	1.47E-12	3.00E-05	6.29E-12	1.60E-04	2.19E-19	8.10E-10	3.15E+07	2.57E-11
Y 90	1.52E+04	1.00E-01	68	5.99E+06	8.80E-06	1.47E-12	3.00E-05	4.56E-12	1.60E-04	4.44E-16	1.64E-06	3.15E+07	3.77E-08
PM147	8.88E+03	1.00E-01	68	5.99E+06	8.80E-06	1.47E-12	3.00E-05	2.66E-12	1.60E-04	2.18E-18	8.07E-09	3.15E+07	1.08E-10
CE144	2.46E+03	1.00E-01	68	5.99E+06	8.80E-06	1.47E-12	3.00E-05	7.37E-13	1.60E-04	2.49E-15	9.21E-06	3.15E+07	3.42E-08
PR144	2.46E+03	1.00E-01	68	5.99E+06	8.80E-06	1.47E-12	3.00E-05	7.37E-13	1.60E-04	2.99E-15	1.11E-05	3.15E+07	4.11E-08
EU154	1.07E+03	1.00E-01	68	5.99E+06	8.80E-06	1.47E-12	3.00E-05	3.21E-13	1.60E-04	9.43E-14	3.49E-04	3.15E+07	5.64E-07
CM244	9.30E+02	1.00E-01	68	5.99E+06	8.80E-06	1.47E-12	3.00E-05	2.79E-13	1.60E-04	8.82E-18	3.26E-08	3.15E+07	4.58E-11
PU238	7.49E+02	1.00E-01	68	5.99E+06	8.80E-06	1.47E-12	3.00E-05	2.24E-13	1.60E-04	9.30E-18	3.44E-08	3.15E+07	3.89E-11
SB125	6.40E+02	1.00E-01	68	5.99E+06	8.80E-06	1.47E-12	3.00E-05	1.92E-13	1.60E-04	3.53E-14	1.31E-04	3.15E+07	1.26E-07
EU155	3.51E+02	1.00E-01	68	5.99E+06	8.80E-06	1.47E-12	3.00E-05	1.05E-13	1.60E-04	8.09E-15	2.99E-05	3.15E+07	1.59E-08
AM241	2.20E+02	1.00E-01	68	5.99E+06	8.80E-06	1.47E-12	3.00E-05	6.59E-14	1.60E-04	2.87E-15	1.06E-05	3.15E+07	3.53E-09
TE125M	1.56E+02	1.00E-01	68	5.99E+06	8.80E-06	1.47E-12	3.00E-05	4.68E-14	1.60E-04	1.22E-15	4.51E-06	3.15E+07	1.06E-09
PU240	1.26E+02	1.00E-01	68	5.99E+06	8.80E-06	1.47E-12	3.00E-05	3.78E-14	1.60E-04	9.26E-18	3.43E-08	3.15E+07	6.52E-12
151Sm	0.00E+00	1.00E-01	68	5.99E+06	8.80E-06	1.47E-12	3.00E-05	0.00E+00	1.60E-04	7.09E-20	2.62E-10	3.15E+07	0.00E+00
239Pu	6.16E+01	1.00E-01	68	5.99E+06	8.80E-06	1.47E-12	3.00E-05	1.85E-14	1.60E-04	9.47E-18	3.50E-08	3.15E+07	3.26E-12
137mBa	2.16E+04	1.00E-01	68	5.99E+06	8.80E-06	1.47E-12	3.00E-05	6.47E-12	1.60E-04	4.63E-14	1.71E-04	3.15E+07	5.59E-06
106Rh	4.16E+03	1.00E-01	68	5.99E+06	8.80E-06	1.47E-12	3.00E-05	1.25E-12	1.60E-04	1.72E-14	6.36E-05	3.15E+07	4.00E-07
144mPr	0.00E+00	1.00E-01	68	5.99E+06	8.80E-06	1.47E-12	3.00E-05	0.00E+00	1.60E-04	8.16E-16	3.02E-06	3.15E+07	0.00E+00
243Am	7.39E+00	1.00E-01	68	5.99E+06	8.80E-06	1.47E-12	3.00E-05	2.21E-15	1.60E-04	7.47E-15	2.76E-05	3.15E+07	3.09E-10
242Cm	6.10E+00	1.00E-01	68	5.99E+06	8.80E-06	1.47E-12	3.00E-05	1.83E-15	1.60E-04	1.06E-17	3.92E-08	3.15E+07	3.61E-13
243Cm	4.81E+00	1.00E-01	68	5.99E+06	8.80E-06	1.47E-12	3.00E-05	1.44E-15	1.60E-04	1.50E-14	5.55E-05	3.15E+07	4.03E-10
239Np	7.39E+00	1.00E-01	68	5.99E+06	8.80E-06	1.47E-12	3.00E-05	2.21E-15	1.60E-04	2.00E-14	7.40E-05	3.15E+07	8.26E-10
237Np	7.05E-02	1.00E-01	68	5.99E+06	8.80E-06	1.47E-12	3.00E-05	2.11E-17	1.60E-04	3.20E-15	1.18E-05	3.15E+07	1.26E-12
242Pu	5.95E-01	1.00E-01	68	5.99E+06	8.80E-06	1.47E-12	3.00E-05	1.78E-16	1.60E-04	7.90E-18	2.92E-08	3.15E+07	2.63E-14
242Am	1.69E+00	1.00E-01	68	5.99E+06	8.80E-06	1.47E-12	3.00E-05	5.06E-16	1.60E-04	1.88E-15	6.96E-06	3.15E+07	1.78E-11
242mAm	1.70E+00	1.00E-01	68	5.99E+06	8.80E-06	1.47E-12	3.00E-05	5.09E-16	1.60E-04	7.94E-17	2.94E-07	3.15E+07	7.54E-13
												Total	3.29E-03

MPC-68													
Off-Normal Conditions													
Effective Dose Equivalent From Submersion													
Nuclide	Inventory (Ci/Assy)	10% for off normal storage	No. Assy	MPC Vol (cm3)	L_{offnor} Rate at Upstream (cm3/s)	Fraction Released per sec	Release Fraction	Release Rate (Ci/sec)	X/Q (sec/m3)	DCF (Sv/Bq)	DCF (mRem/uCi)	Occ Time (sec)	EDE (mRem)
								Gases					
H-3	8.72E+01	1.00E-01	68	5.99E+06	8.80E-06	1.47E-12	0.30	2.61E-10	1.60E-04	0.00E+00	0.00E+00	3.15E+07	0.00E+00
I-129	7.72E-03	1.00E-01	68	5.99E+06	8.80E-06	1.47E-12	0.30	2.31E-14	1.60E-04	3.86E-16	1.43E-06	3.15E+07	1.67E-10
Kr-85	1.43E+03	1.00E-01	68	5.99E+06	8.80E-06	1.47E-12	0.30	4.29E-09	1.60E-04	1.18E-16	4.37E-07	3.15E+07	9.43E-06
								Crud					
Co-60	6.50E+01	1.00E+00	68	5.99E+06	8.80E-06	1.47E-12	0.15	9.74E-10	1.60E-04	1.27E-13	4.70E-04	3.15E+07	2.31E-03
								Volatiles					
Sr-90	1.52E+04	1.00E-01	68	5.99E+06	8.80E-06	1.47E-12	2.00E-04	3.04E-11	1.60E-04	7.33E-18	2.71E-08	3.15E+07	4.15E-09
Ru-106	4.16E+03	1.00E-01	68	5.99E+06	8.80E-06	1.47E-12	2.00E-04	8.31E-12	1.60E-04	0.00E+00	0.00E+00	3.15E+07	0.00E+00
Cs-134	7.20E+03	1.00E-01	68	5.99E+06	8.80E-06	1.47E-12	2.00E-04	1.44E-11	1.60E-04	7.57E-14	2.80E-04	3.15E+07	2.03E-05
Cs-137	2.29E+04	1.00E-01	68	5.99E+06	8.80E-06	1.47E-12	2.00E-04	4.58E-11	1.60E-04	7.55E-18	2.79E-08	3.15E+07	6.44E-09
								Fines					
PU241	2.10E+04	1.00E-01	68	5.99E+06	8.80E-06	1.47E-12	3.00E-05	6.29E-12	1.60E-04	6.98E-20	2.58E-10	3.15E+07	8.19E-12
Y 90	1.52E+04	1.00E-01	68	5.99E+06	8.80E-06	1.47E-12	3.00E-05	4.56E-12	1.60E-04	1.87E-16	6.92E-07	3.15E+07	1.59E-08
PM147	8.88E+03	1.00E-01	68	5.99E+06	8.80E-06	1.47E-12	3.00E-05	2.66E-12	1.60E-04	6.75E-19	2.50E-09	3.15E+07	3.35E-11
CE144	2.46E+03	1.00E-01	68	5.99E+06	8.80E-06	1.47E-12	3.00E-05	7.37E-13	1.60E-04	8.33E-16	3.08E-06	3.15E+07	1.15E-08
PR144	2.46E+03	1.00E-01	68	5.99E+06	8.80E-06	1.47E-12	3.00E-05	7.37E-13	1.60E-04	1.95E-15	7.22E-06	3.15E+07	2.68E-08
EU154	1.07E+03	1.00E-01	68	5.99E+06	8.80E-06	1.47E-12	3.00E-05	3.21E-13	1.60E-04	6.15E-14	2.28E-04	3.15E+07	3.68E-07
CM244	9.30E+02	1.00E-01	68	5.99E+06	8.80E-06	1.47E-12	3.00E-05	2.79E-13	1.60E-04	4.19E-18	1.55E-08	3.15E+07	2.18E-11
PU238	7.49E+02	1.00E-01	68	5.99E+06	8.80E-06	1.47E-12	3.00E-05	2.24E-13	1.60E-04	4.01E-18	1.48E-08	3.15E+07	1.68E-11
SB125	6.40E+02	1.00E-01	68	5.99E+06	8.80E-06	1.47E-12	3.00E-05	1.92E-13	1.60E-04	2.01E-14	7.44E-05	3.15E+07	7.19E-08
EU155	3.51E+02	1.00E-01	68	5.99E+06	8.80E-06	1.47E-12	3.00E-05	1.05E-13	1.60E-04	2.41E-15	8.92E-06	3.15E+07	4.73E-09
AM241	2.20E+02	1.00E-01	68	5.99E+06	8.80E-06	1.47E-12	3.00E-05	6.59E-14	1.60E-04	7.83E-16	2.90E-06	3.15E+07	9.63E-10
TE125M	1.56E+02	1.00E-01	68	5.99E+06	8.80E-06	1.47E-12	3.00E-05	4.68E-14	1.60E-04	4.64E-16	1.72E-06	3.15E+07	4.05E-10
PU240	1.26E+02	1.00E-01	68	5.99E+06	8.80E-06	1.47E-12	3.00E-05	3.78E-14	1.60E-04	3.92E-18	1.45E-08	3.15E+07	2.76E-12
151Sm	0.00E+00	1.00E-01	68	5.99E+06	8.80E-06	1.47E-12	3.00E-05	0.00E+00	1.60E-04	3.58E-20	1.32E-10	3.15E+07	0.00E+00
239Pu	6.16E+01	1.00E-01	68	5.99E+06	8.80E-06	1.47E-12	3.00E-05	1.85E-14	1.60E-04	3.88E-18	1.44E-08	3.15E+07	1.34E-12
137mBa	2.16E+04	1.00E-01	68	5.99E+06	8.80E-06	1.47E-12	3.00E-05	6.47E-12	1.60E-04	2.88E-14	1.07E-04	3.15E+07	3.48E-06
106Rh	4.16E+03	1.00E-01	68	5.99E+06	8.80E-06	1.47E-12	3.00E-05	1.25E-12	1.60E-04	1.03E-14	3.81E-05	3.15E+07	2.39E-07
144mPr	0.00E+00	1.00E-01	68	5.99E+06	8.80E-06	1.47E-12	3.00E-05	0.00E+00	1.60E-04	2.81E-16	1.04E-06	3.15E+07	0.00E+00
243Am	7.39E+00	1.00E-01	68	5.99E+06	8.80E-06	1.47E-12	3.00E-05	2.21E-15	1.60E-04	2.09E-15	7.73E-06	3.15E+07	8.63E-11
242Cm	6.10E+00	1.00E-01	68	5.99E+06	8.80E-06	1.47E-12	3.00E-05	1.83E-15	1.60E-04	4.91E-18	1.82E-08	3.15E+07	1.67E-13
243Cm	4.81E+00	1.00E-01	68	5.99E+06	8.80E-06	1.47E-12	3.00E-05	1.44E-15	1.60E-04	5.76E-15	2.13E-05	3.15E+07	1.55E-10
239Np	7.39E+00	1.00E-01	68	5.99E+06	8.80E-06	1.47E-12	3.00E-05	2.21E-15	1.60E-04	7.52E-15	2.78E-05	3.15E+07	3.11E-10
237Np	7.05E-02	1.00E-01	68	5.99E+06	8.80E-06	1.47E-12	3.00E-05	2.11E-17	1.60E-04	9.94E-16	3.68E-06	3.15E+07	3.92E-13
242Pu	5.95E-01	1.00E-01	68	5.99E+06	8.80E-06	1.47E-12	3.00E-05	1.78E-16	1.60E-04	3.32E-18	1.23E-08	3.15E+07	1.10E-14
242Am	1.69E+00	1.00E-01	68	5.99E+06	8.80E-06	1.47E-12	3.00E-05	5.06E-16	1.60E-04	5.94E-16	2.20E-06	3.15E+07	5.61E-12
242mAm	1.70E+00	1.00E-01	68	5.99E+06	8.80E-06	1.47E-12	3.00E-05	5.09E-16	1.60E-04	2.95E-17	1.09E-07	3.15E+07	2.80E-13
												Total	2.34E-03

MPC-68													
Off-Normal Conditions													
Effective Dose Equivalent From Submersion													
Nuclide	Inventory (Ci/Assy)	10% for off normal storage	No. Assy	MPC Vol (cm3)	L_{offnor} Rate at Upstream (cm3/s)	Fraction Released per sec	Release Fraction	Release Rate (Ci/sec)	X/Q (sec/m3)	DCF (Sv/Bq)	DCF (mRem/uCi)	Occ Time (sec)	Effective Dose (mRem)
								Gases					
H-3	8.72E+01	1.00E-01	68	5.99E+06	8.80E-06	1.47E-12	0.30	2.61E-10	1.60E-04	3.31E-19	1.22E-09	3.15E+07	1.61E-09
I-129	7.72E-03	1.00E-01	68	5.99E+06	8.80E-06	1.47E-12	0.30	2.31E-14	1.60E-04	3.80E-16	1.41E-06	3.15E+07	1.64E-10
Kr-85	1.43E+03	1.00E-01	68	5.99E+06	8.80E-06	1.47E-12	0.30	4.29E-09	1.60E-04	1.19E-16	4.40E-07	3.15E+07	9.51E-06
								Crud					
Co-60	6.50E+01	1.00E+00	68	5.99E+06	8.80E-06	1.47E-12	0.15	9.74E-10	1.60E-04	1.26E-13	4.66E-04	3.15E+07	2.29E-03
								Volatiles					
Sr-90	1.52E+04	1.00E-01	68	5.99E+06	8.80E-06	1.47E-12	2.00E-04	3.04E-11	1.60E-04	7.53E-18	2.79E-08	3.15E+07	4.26E-09
Ru-106	4.16E+03	1.00E-01	68	5.99E+06	8.80E-06	1.47E-12	2.00E-04	8.31E-12	1.60E-04	0.00E+00	0.00E+00	3.15E+07	0.00E+00
Cs-134	7.20E+03	1.00E-01	68	5.99E+06	8.80E-06	1.47E-12	2.00E-04	1.44E-11	1.60E-04	7.57E-14	2.80E-04	3.15E+07	2.03E-05
Cs-137	2.29E+04	1.00E-01	68	5.99E+06	8.80E-06	1.47E-12	2.00E-04	4.58E-11	1.60E-04	7.74E-18	2.86E-08	3.15E+07	6.60E-09
								Fines					
PU241	2.10E+04	1.00E-01	68	5.99E+06	8.80E-06	1.47E-12	3.00E-05	6.29E-12	1.60E-04	7.25E-20	2.68E-10	3.15E+07	8.51E-12
Y 90	1.52E+04	1.00E-01	68	5.99E+06	8.80E-06	1.47E-12	3.00E-05	4.56E-12	1.60E-04	1.90E-16	7.03E-07	3.15E+07	1.61E-08
PM147	8.88E+03	1.00E-01	68	5.99E+06	8.80E-06	1.47E-12	3.00E-05	2.66E-12	1.60E-04	6.93E-19	2.56E-09	3.15E+07	3.44E-11
CE144	2.46E+03	1.00E-01	68	5.99E+06	8.80E-06	1.47E-12	3.00E-05	7.37E-13	1.60E-04	8.53E-16	3.16E-06	3.15E+07	1.17E-08
PR144	2.46E+03	1.00E-01	68	5.99E+06	8.80E-06	1.47E-12	3.00E-05	7.37E-13	1.60E-04	1.95E-15	7.22E-06	3.15E+07	2.68E-08
EU154	1.07E+03	1.00E-01	68	5.99E+06	8.80E-06	1.47E-12	3.00E-05	3.21E-13	1.60E-04	6.14E-14	2.27E-04	3.15E+07	3.67E-07
CM244	9.30E+02	1.00E-01	68	5.99E+06	8.80E-06	1.47E-12	3.00E-05	2.79E-13	1.60E-04	4.91E-18	1.82E-08	3.15E+07	2.55E-11
PU238	7.49E+02	1.00E-01	68	5.99E+06	8.80E-06	1.47E-12	3.00E-05	2.24E-13	1.60E-04	4.88E-18	1.81E-08	3.15E+07	2.04E-11
SB125	6.40E+02	1.00E-01	68	5.99E+06	8.80E-06	1.47E-12	3.00E-05	1.92E-13	1.60E-04	2.02E-14	7.47E-05	3.15E+07	7.23E-08
EU155	3.51E+02	1.00E-01	68	5.99E+06	8.80E-06	1.47E-12	3.00E-05	1.05E-13	1.60E-04	2.49E-15	9.21E-06	3.15E+07	4.88E-09
AM241	2.20E+02	1.00E-01	68	5.99E+06	8.80E-06	1.47E-12	3.00E-05	6.59E-14	1.60E-04	8.18E-16	3.03E-06	3.15E+07	1.01E-09
TE125M	1.56E+02	1.00E-01	68	5.99E+06	8.80E-06	1.47E-12	3.00E-05	4.68E-14	1.60E-04	4.53E-16	1.68E-06	3.15E+07	3.95E-10
PU240	1.26E+02	1.00E-01	68	5.99E+06	8.80E-06	1.47E-12	3.00E-05	3.78E-14	1.60E-04	4.75E-18	1.76E-08	3.15E+07	3.34E-12
151Sm	0.00E+00	1.00E-01	68	5.99E+06	8.80E-06	1.47E-12	3.00E-05	0.00E+00	1.60E-04	3.61E-20	1.34E-10	3.15E+07	0.00E+00
239Pu	6.16E+01	1.00E-01	68	5.99E+06	8.80E-06	1.47E-12	3.00E-05	1.85E-14	1.60E-04	4.24E-18	1.57E-08	3.15E+07	1.46E-12
137mBa	2.16E+04	1.00E-01	68	5.99E+06	8.80E-06	1.47E-12	3.00E-05	6.47E-12	1.60E-04	2.88E-14	1.07E-04	3.15E+07	3.48E-06
106Rh	4.16E+03	1.00E-01	68	5.99E+06	8.80E-06	1.47E-12	3.00E-05	1.25E-12	1.60E-04	1.04E-14	3.85E-05	3.15E+07	2.42E-07
144mPr	0.00E+00	1.00E-01	68	5.99E+06	8.80E-06	1.47E-12	3.00E-05	0.00E+00	1.60E-04	2.79E-16	1.03E-06	3.15E+07	0.00E+00
243Am	7.39E+00	1.00E-01	68	5.99E+06	8.80E-06	1.47E-12	3.00E-05	2.21E-15	1.60E-04	2.18E-15	8.07E-06	3.15E+07	9.00E-11
242Cm	6.10E+00	1.00E-01	68	5.99E+06	8.80E-06	1.47E-12	3.00E-05	1.83E-15	1.60E-04	5.69E-18	2.11E-08	3.15E+07	1.94E-13
243Cm	4.81E+00	1.00E-01	68	5.99E+06	8.80E-06	1.47E-12	3.00E-05	1.44E-15	1.60E-04	5.88E-15	2.18E-05	3.15E+07	1.58E-10
239Np	7.39E+00	1.00E-01	68	5.99E+06	8.80E-06	1.47E-12	3.00E-05	2.21E-15	1.60E-04	7.69E-15	2.85E-05	3.15E+07	3.18E-10
237Np	7.05E-02	1.00E-01	68	5.99E+06	8.80E-06	1.47E-12	3.00E-05	2.11E-17	1.60E-04	1.03E-15	3.81E-06	3.15E+07	4.06E-13
242Pu	5.95E-01	1.00E-01	68	5.99E+06	8.80E-06	1.47E-12	3.00E-05	1.78E-16	1.60E-04	4.01E-18	1.48E-08	3.15E+07	1.33E-14
242Am	1.69E+00	1.00E-01	68	5.99E+06	8.80E-06	1.47E-12	3.00E-05	5.06E-16	1.60E-04	6.15E-16	2.28E-06	3.15E+07	5.81E-12
242mAm	1.70E+00	1.00E-01	68	5.99E+06	8.80E-06	1.47E-12	3.00E-05	5.09E-16	1.60E-04	3.17E-17	1.17E-07	3.15E+07	3.01E-13
												Total	2.32E-03

MPC-68													
Off-Normal Conditions													
Effective Dose Equivalent From Submersion													
Nuclide	Inventory (Ci/Assy)	10% for off normal storage	No. Assy	MPC Vol (cm3)	L_{offnor} Rate at Upstream (cm3/s)	Fraction Released per sec	Release Fraction	Release Rate (Ci/sec)	X/Q (sec/m3)	DCF (Sv/Bq)	DCF (mRem/uCi)	Occ Time (sec)	Effective Dose (mRem)
								Gases					
H-3	8.72E+01	1.00E-01	68	5.99E+06	8.80E-06	1.47E-12	0.30	2.61E-10	1.60E-04	0.00E+00	0.00E+00	3.15E+07	0.00E+00
I-129	7.72E-03	1.00E-01	68	5.99E+06	8.80E-06	1.47E-12	0.30	2.31E-14	1.60E-04	1.10E-15	4.07E-06	3.15E+07	4.75E-10
Kr-85	1.43E+03	1.00E-01	68	5.99E+06	8.80E-06	1.47E-12	0.30	4.29E-09	1.60E-04	1.32E-14	4.88E-05	3.15E+07	1.05E-03
								Crud					
Co-60	6.50E+01	1.00E+00	68	5.99E+06	8.80E-06	1.47E-12	0.15	9.74E-10	1.60E-04	1.45E-13	5.37E-04	3.15E+07	2.63E-03
								Volatiles					
Sr-90	1.52E+04	1.00E-01	68	5.99E+06	8.80E-06	1.47E-12	2.00E-04	3.04E-11	1.60E-04	9.20E-15	3.40E-05	3.15E+07	5.21E-06
Ru-106	4.16E+03	1.00E-01	68	5.99E+06	8.80E-06	1.47E-12	2.00E-04	8.31E-12	1.60E-04	0.00E+00	0.00E+00	3.15E+07	0.00E+00
Cs-134	7.20E+03	1.00E-01	68	5.99E+06	8.80E-06	1.47E-12	2.00E-04	1.44E-11	1.60E-04	9.45E-14	3.50E-04	3.15E+07	2.54E-05
Cs-137	2.29E+04	1.00E-01	68	5.99E+06	8.80E-06	1.47E-12	2.00E-04	4.58E-11	1.60E-04	8.63E-15	3.19E-05	3.15E+07	7.36E-06
								Fines					
PU241	2.10E+04	1.00E-01	68	5.99E+06	8.80E-06	1.47E-12	3.00E-05	6.29E-12	1.60E-04	1.17E-19	4.33E-10	3.15E+07	1.37E-11
Y 90	1.52E+04	1.00E-01	68	5.99E+06	8.80E-06	1.47E-12	3.00E-05	4.56E-12	1.60E-04	6.24E-14	2.31E-04	3.15E+07	5.30E-06
PM147	8.88E+03	1.00E-01	68	5.99E+06	8.80E-06	1.47E-12	3.00E-05	2.66E-12	1.60E-04	8.11E-16	3.00E-06	3.15E+07	4.02E-08
CE144	2.46E+03	1.00E-01	68	5.99E+06	8.80E-06	1.47E-12	3.00E-05	7.37E-13	1.60E-04	2.93E-15	1.08E-05	3.15E+07	4.03E-08
PR144	2.46E+03	1.00E-01	68	5.99E+06	8.80E-06	1.47E-12	3.00E-05	7.37E-13	1.60E-04	8.43E-14	3.12E-04	3.15E+07	1.16E-06
EU154	1.07E+03	1.00E-01	68	5.99E+06	8.80E-06	1.47E-12	3.00E-05	3.21E-13	1.60E-04	8.29E-14	3.07E-04	3.15E+07	4.96E-07
CM244	9.30E+02	1.00E-01	68	5.99E+06	8.80E-06	1.47E-12	3.00E-05	2.79E-13	1.60E-04	3.91E-17	1.45E-07	3.15E+07	2.03E-10
PU238	7.49E+02	1.00E-01	68	5.99E+06	8.80E-06	1.47E-12	3.00E-05	2.24E-13	1.60E-04	4.09E-17	1.51E-07	3.15E+07	1.71E-10
SB125	6.40E+02	1.00E-01	68	5.99E+06	8.80E-06	1.47E-12	3.00E-05	1.92E-13	1.60E-04	2.65E-14	9.81E-05	3.15E+07	9.48E-08
EU155	3.51E+02	1.00E-01	68	5.99E+06	8.80E-06	1.47E-12	3.00E-05	1.05E-13	1.60E-04	3.39E-15	1.25E-05	3.15E+07	6.65E-09
AM241	2.20E+02	1.00E-01	68	5.99E+06	8.80E-06	1.47E-12	3.00E-05	6.59E-14	1.60E-04	1.28E-15	4.74E-06	3.15E+07	1.57E-09
TE125M	1.56E+02	1.00E-01	68	5.99E+06	8.80E-06	1.47E-12	3.00E-05	4.68E-14	1.60E-04	1.94E-15	7.18E-06	3.15E+07	1.69E-09
PU240	1.26E+02	1.00E-01	68	5.99E+06	8.80E-06	1.47E-12	3.00E-05	3.78E-14	1.60E-04	3.92E-17	1.45E-07	3.15E+07	2.76E-11
151Sm	0.00E+00	1.00E-01	68	5.99E+06	8.80E-06	1.47E-12	3.00E-05	0.00E+00	1.60E-04	1.90E-20	7.03E-11	3.15E+07	0.00E+00
239Pu	6.16E+01	1.00E-01	68	5.99E+06	8.80E-06	1.47E-12	3.00E-05	1.85E-14	1.60E-04	1.86E-17	6.88E-08	3.15E+07	6.40E-12
137mBa	2.16E+04	1.00E-01	68	5.99E+06	8.80E-06	1.47E-12	3.00E-05	6.47E-12	1.60E-04	3.73E-14	1.38E-04	3.15E+07	4.50E-06
106Rh	4.16E+03	1.00E-01	68	5.99E+06	8.80E-06	1.47E-12	3.00E-05	1.25E-12	1.60E-04	1.09E-13	4.03E-04	3.15E+07	2.53E-06
144mPr	0.00E+00	1.00E-01	68	5.99E+06	8.80E-06	1.47E-12	3.00E-05	0.00E+00	1.60E-04	5.08E-16	1.88E-06	3.15E+07	0.00E+00
243Am	7.39E+00	1.00E-01	68	5.99E+06	8.80E-06	1.47E-12	3.00E-05	2.21E-15	1.60E-04	2.75E-15	1.02E-05	3.15E+07	1.14E-10
242Cm	6.10E+00	1.00E-01	68	5.99E+06	8.80E-06	1.47E-12	3.00E-05	1.83E-15	1.60E-04	4.29E-17	1.59E-07	3.15E+07	1.46E-12
243Cm	4.81E+00	1.00E-01	68	5.99E+06	8.80E-06	1.47E-12	3.00E-05	1.44E-15	1.60E-04	9.79E-15	3.62E-05	3.15E+07	2.63E-10
239Np	7.39E+00	1.00E-01	68	5.99E+06	8.80E-06	1.47E-12	3.00E-05	2.21E-15	1.60E-04	1.60E-14	5.92E-05	3.15E+07	6.61E-10
237Np	7.05E-02	1.00E-01	68	5.99E+06	8.80E-06	1.47E-12	3.00E-05	2.11E-17	1.60E-04	1.54E-15	5.70E-06	3.15E+07	6.07E-13
242Pu	5.95E-01	1.00E-01	68	5.99E+06	8.80E-06	1.47E-12	3.00E-05	1.78E-16	1.60E-04	3.27E-17	1.21E-07	3.15E+07	1.09E-13
242Am	1.69E+00	1.00E-01	68	5.99E+06	8.80E-06	1.47E-12	3.00E-05	5.06E-16	1.60E-04	8.20E-15	3.03E-05	3.15E+07	7.74E-11
242mAm	1.70E+00	1.00E-01	68	5.99E+06	8.80E-06	1.47E-12	3.00E-05	5.09E-16	1.60E-04	1.36E-16	5.03E-07	3.15E+07	1.29E-12
												Total	3.74E-03

MPC-68													
Accident Conditions													
Effective Dose Equivalent From Submersion													
Nuclide	Inventory (Ci/Assy)	No. Assy	MPC Vol (cm3)	L_{acc} Rate at Upstream (cm3/s)	Fraction Released per sec	Release Fraction	Release Rate (Ci/sec)	X/Q (sec/m3)	DCF (Sv/Bq)	DCF (mRem/uCi)	Occ Time (sec)	EDE (mRem)	
							Gases						
H-3	8.72E+01	68	5.99E+06	1.25E-05	2.09E-12	0.30	3.72E-09	8.00E-03	0.00E+00	0.00E+00	2.59E+06	0.00E+00	
I-129	7.72E-03	68	5.99E+06	1.25E-05	2.09E-12	0.30	3.30E-13	8.00E-03	4.83E-16	1.79E-06	2.59E+06	1.22E-08	
Kr-85	1.43E+03	68	5.99E+06	1.25E-05	2.09E-12	0.30	6.11E-08	8.00E-03	1.17E-16	4.33E-07	2.59E+06	5.48E-04	
							Crud						
Co-60	6.50E+01	68	5.99E+06	1.25E-05	2.09E-12	1.00	9.25E-09	8.00E-03	1.23E-13	4.55E-04	2.59E+06	8.73E-02	
							Volatiles						
Sr-90	1.52E+04	68	5.99E+06	1.25E-05	2.09E-12	2.00E-04	4.33E-10	8.00E-03	7.78E-18	2.88E-08	2.59E+06	2.58E-07	
Ru-106	4.16E+03	68	5.99E+06	1.25E-05	2.09E-12	2.00E-04	1.18E-10	8.00E-03	0.00E+00	0.00E+00	2.59E+06	0.00E+00	
Cs-134	7.20E+03	68	5.99E+06	1.25E-05	2.09E-12	2.00E-04	2.05E-10	8.00E-03	7.40E-14	2.74E-04	2.59E+06	1.16E-03	
Cs-137	2.29E+04	68	5.99E+06	1.25E-05	2.09E-12	2.00E-04	6.52E-10	8.00E-03	7.96E-18	2.95E-08	2.59E+06	3.98E-07	
							Fines						
PU241	2.10E+04	68	5.99E+06	1.25E-05	2.09E-12	3.00E-05	8.97E-11	8.00E-03	7.19E-20	2.66E-10	2.59E+06	4.94E-10	
Y 90	1.52E+04	68	5.99E+06	1.25E-05	2.09E-12	3.00E-05	6.49E-11	8.00E-03	1.89E-16	6.99E-07	2.59E+06	9.41E-07	
PM147	8.88E+03	68	5.99E+06	1.25E-05	2.09E-12	3.00E-05	3.79E-11	8.00E-03	7.48E-19	2.77E-09	2.59E+06	2.17E-09	
CE144	2.46E+03	68	5.99E+06	1.25E-05	2.09E-12	3.00E-05	1.05E-11	8.00E-03	8.53E-16	3.16E-06	2.59E+06	6.87E-07	
PR144	2.46E+03	68	5.99E+06	1.25E-05	2.09E-12	3.00E-05	1.05E-11	8.00E-03	1.90E-15	7.03E-06	2.59E+06	1.53E-06	
EU154	1.07E+03	68	5.99E+06	1.25E-05	2.09E-12	3.00E-05	4.57E-12	8.00E-03	6.00E-14	2.22E-04	2.59E+06	2.10E-05	
CM244	9.30E+02	68	5.99E+06	1.25E-05	2.09E-12	3.00E-05	3.97E-12	8.00E-03	6.90E-18	2.55E-08	2.59E+06	2.10E-09	
PU238	7.49E+02	68	5.99E+06	1.25E-05	2.09E-12	3.00E-05	3.20E-12	8.00E-03	6.56E-18	2.43E-08	2.59E+06	1.61E-09	
SB125	6.40E+02	68	5.99E+06	1.25E-05	2.09E-12	3.00E-05	2.73E-12	8.00E-03	1.98E-14	7.33E-05	2.59E+06	4.15E-06	
EU155	3.51E+02	68	5.99E+06	1.25E-05	2.09E-12	3.00E-05	1.50E-12	8.00E-03	2.49E-15	9.21E-06	2.59E+06	2.86E-07	
AM241	2.20E+02	68	5.99E+06	1.25E-05	2.09E-12	3.00E-05	9.40E-13	8.00E-03	8.58E-16	3.17E-06	2.59E+06	6.18E-08	
TE125M	1.56E+02	68	5.99E+06	1.25E-05	2.09E-12	3.00E-05	6.66E-13	8.00E-03	5.96E-16	2.21E-06	2.59E+06	3.04E-08	
PU240	1.26E+02	68	5.99E+06	1.25E-05	2.09E-12	3.00E-05	5.38E-13	8.00E-03	6.36E-18	2.35E-08	2.59E+06	2.62E-10	
151Sm	0.00E+00	68	5.99E+06	1.25E-05	2.09E-12	3.00E-05	0.00E+00	8.00E-03	5.20E-20	1.92E-10	2.59E+06	0.00E+00	
239Pu	6.16E+01	68	5.99E+06	1.25E-05	2.09E-12	3.00E-05	2.63E-13	8.00E-03	4.84E-18	1.79E-08	2.59E+06	9.76E-11	
137mBa	2.16E+04	68	5.99E+06	1.25E-05	2.09E-12	3.00E-05	9.22E-11	8.00E-03	2.82E-14	1.04E-04	2.59E+06	1.99E-04	
106Rh	4.16E+03	68	5.99E+06	1.25E-05	2.09E-12	3.00E-05	1.78E-11	8.00E-03	1.01E-14	3.74E-05	2.59E+06	1.38E-05	
144mPr	0.00E+00	68	5.99E+06	1.25E-05	2.09E-12	3.00E-05	0.00E+00	8.00E-03	3.25E-16	1.20E-06	2.59E+06	0.00E+00	
243Am	7.39E+00	68	5.99E+06	1.25E-05	2.09E-12	3.00E-05	3.16E-14	8.00E-03	2.19E-15	8.10E-06	2.59E+06	5.30E-09	
242Cm	6.10E+00	68	5.99E+06	1.25E-05	2.09E-12	3.00E-05	2.61E-14	8.00E-03	7.83E-18	2.90E-08	2.59E+06	1.56E-11	
243Cm	4.81E+00	68	5.99E+06	1.25E-05	2.09E-12	3.00E-05	2.05E-14	8.00E-03	5.77E-15	2.13E-05	2.59E+06	9.09E-09	
239Np	7.39E+00	68	5.99E+06	1.25E-05	2.09E-12	3.00E-05	3.16E-14	8.00E-03	7.53E-15	2.79E-05	2.59E+06	1.82E-08	
237Np	7.05E-02	68	5.99E+06	1.25E-05	2.09E-12	3.00E-05	3.01E-16	8.00E-03	1.04E-15	3.85E-06	2.59E+06	2.40E-11	
242Pu	5.95E-01	68	5.99E+06	1.25E-05	2.09E-12	3.00E-05	2.54E-15	8.00E-03	5.34E-18	1.98E-08	2.59E+06	1.04E-12	
242Am	1.69E+00	68	5.99E+06	1.25E-05	2.09E-12	3.00E-05	7.22E-15	8.00E-03	6.09E-16	2.25E-06	2.59E+06	3.37E-10	
242mAm	1.70E+00	68	5.99E+06	1.25E-05	2.09E-12	3.00E-05	7.26E-15	8.00E-03	3.80E-17	1.41E-07	2.59E+06	2.12E-11	
											Total	8.92E-02	

MPC-68													
Accident Conditions													
Effective Dose Equivalent From Submersion													
Nuclide	Inventory (Ci/Assy)	No. Assy	MPC Vol (cm3)	L_{acc} Rate at Upstream (cm3/s)	Fraction Released per sec	Release Fraction	Release Rate (Ci/sec)	X/Q (sec/m3)	DCF (Sv/Bq)	DCF (mRem/uCi)	Occ Time (sec)	EDE (mRem)	
							Gases						
H-3	8.72E+01	68	5.99E+06	1.25E-05	2.09E-12	0.30	3.72E-09	8.00E-03	0.00E+00	0.00E+00	2.59E+06	0.00E+00	
I-129	7.72E-03	68	5.99E+06	1.25E-05	2.09E-12	0.30	3.30E-13	8.00E-03	6.66E-16	2.46E-06	2.59E+06	1.68E-08	
Kr-85	1.43E+03	68	5.99E+06	1.25E-05	2.09E-12	0.30	6.11E-08	8.00E-03	1.34E-16	4.96E-07	2.59E+06	6.27E-04	
							Crud						
Co-60	6.50E+01	68	5.99E+06	1.25E-05	2.09E-12	1.00	9.25E-09	8.00E-03	1.39E-13	5.14E-04	2.59E+06	9.86E-02	
							Volatiles						
Sr-90	1.52E+04	68	5.99E+06	1.25E-05	2.09E-12	2.00E-04	4.33E-10	8.00E-03	9.49E-18	3.51E-08	2.59E+06	3.15E-07	
Ru-106	4.16E+03	68	5.99E+06	1.25E-05	2.09E-12	2.00E-04	1.18E-10	8.00E-03	0.00E+00	0.00E+00	2.59E+06	0.00E+00	
Cs-134	7.20E+03	68	5.99E+06	1.25E-05	2.09E-12	2.00E-04	2.05E-10	8.00E-03	8.43E-14	3.12E-04	2.59E+06	1.32E-03	
Cs-137	2.29E+04	68	5.99E+06	1.25E-05	2.09E-12	2.00E-04	6.52E-10	8.00E-03	9.67E-18	3.58E-08	2.59E+06	4.83E-07	
							Fines						
PU241	2.10E+04	68	5.99E+06	1.25E-05	2.09E-12	3.00E-05	8.97E-11	8.00E-03	8.67E-20	3.21E-10	2.59E+06	5.96E-10	
Y 90	1.52E+04	68	5.99E+06	1.25E-05	2.09E-12	3.00E-05	6.49E-11	8.00E-03	2.20E-16	8.14E-07	2.59E+06	1.09E-06	
PM147	8.88E+03	68	5.99E+06	1.25E-05	2.09E-12	3.00E-05	3.79E-11	8.00E-03	9.56E-19	3.54E-09	2.59E+06	2.78E-09	
CE144	2.46E+03	68	5.99E+06	1.25E-05	2.09E-12	3.00E-05	1.05E-11	8.00E-03	1.01E-15	3.74E-06	2.59E+06	8.13E-07	
PR144	2.46E+03	68	5.99E+06	1.25E-05	2.09E-12	3.00E-05	1.05E-11	8.00E-03	2.15E-15	7.96E-06	2.59E+06	1.73E-06	
EU154	1.07E+03	68	5.99E+06	1.25E-05	2.09E-12	3.00E-05	4.57E-12	8.00E-03	6.81E-14	2.52E-04	2.59E+06	2.39E-05	
CM244	9.30E+02	68	5.99E+06	1.25E-05	2.09E-12	3.00E-05	3.97E-12	8.00E-03	1.33E-17	4.92E-08	2.59E+06	4.05E-09	
PU238	7.49E+02	68	5.99E+06	1.25E-05	2.09E-12	3.00E-05	3.20E-12	8.00E-03	1.27E-17	4.70E-08	2.59E+06	3.11E-09	
SB125	6.40E+02	68	5.99E+06	1.25E-05	2.09E-12	3.00E-05	2.73E-12	8.00E-03	2.27E-14	8.40E-05	2.59E+06	4.76E-06	
EU155	3.51E+02	68	5.99E+06	1.25E-05	2.09E-12	3.00E-05	1.50E-12	8.00E-03	2.95E-15	1.09E-05	2.59E+06	3.39E-07	
AM241	2.20E+02	68	5.99E+06	1.25E-05	2.09E-12	3.00E-05	9.40E-13	8.00E-03	1.07E-15	3.96E-06	2.59E+06	7.71E-08	
TE125M	1.56E+02	68	5.99E+06	1.25E-05	2.09E-12	3.00E-05	6.66E-13	8.00E-03	8.48E-16	3.14E-06	2.59E+06	4.33E-08	
PU240	1.26E+02	68	5.99E+06	1.25E-05	2.09E-12	3.00E-05	5.38E-13	8.00E-03	1.23E-17	4.55E-08	2.59E+06	5.07E-10	
151Sm	0.00E+00	68	5.99E+06	1.25E-05	2.09E-12	3.00E-05	0.00E+00	8.00E-03	8.80E-20	3.26E-10	2.59E+06	0.00E+00	
239Pu	6.16E+01	68	5.99E+06	1.25E-05	2.09E-12	3.00E-05	2.63E-13	8.00E-03	7.55E-18	2.79E-08	2.59E+06	1.52E-10	
137mBa	2.16E+04	68	5.99E+06	1.25E-05	2.09E-12	3.00E-05	9.22E-11	8.00E-03	3.22E-14	1.19E-04	2.59E+06	2.28E-04	
106Rh	4.16E+03	68	5.99E+06	1.25E-05	2.09E-12	3.00E-05	1.78E-11	8.00E-03	1.16E-14	4.29E-05	2.59E+06	1.58E-05	
144mPr	0.00E+00	68	5.99E+06	1.25E-05	2.09E-12	3.00E-05	0.00E+00	8.00E-03	4.20E-16	1.55E-06	2.59E+06	0.00E+00	
243Am	7.39E+00	68	5.99E+06	1.25E-05	2.09E-12	3.00E-05	3.16E-14	8.00E-03	2.61E-15	9.66E-06	2.59E+06	6.32E-09	
242Cm	6.10E+00	68	5.99E+06	1.25E-05	2.09E-12	3.00E-05	2.61E-14	8.00E-03	1.48E-17	5.48E-08	2.59E+06	2.96E-11	
243Cm	4.81E+00	68	5.99E+06	1.25E-05	2.09E-12	3.00E-05	2.05E-14	8.00E-03	6.68E-15	2.47E-05	2.59E+06	1.05E-08	
239Np	7.39E+00	68	5.99E+06	1.25E-05	2.09E-12	3.00E-05	3.16E-14	8.00E-03	8.73E-15	3.23E-05	2.59E+06	2.11E-08	
237Np	7.05E-02	68	5.99E+06	1.25E-05	2.09E-12	3.00E-05	3.01E-16	8.00E-03	1.26E-15	4.66E-06	2.59E+06	2.91E-11	
242Pu	5.95E-01	68	5.99E+06	1.25E-05	2.09E-12	3.00E-05	2.54E-15	8.00E-03	1.03E-17	3.81E-08	2.59E+06	2.01E-12	
242Am	1.69E+00	68	5.99E+06	1.25E-05	2.09E-12	3.00E-05	7.22E-15	8.00E-03	7.30E-16	2.70E-06	2.59E+06	4.04E-10	
242mAm	1.70E+00	68	5.99E+06	1.25E-05	2.09E-12	3.00E-05	7.26E-15	8.00E-03	6.01E-17	2.22E-07	2.59E+06	3.35E-11	
											Total	1.01E-01	

MPC-68													
Accident Conditions													
Effective Dose Equivalent From Submersion													
Nuclide	Inventory (Ci/Assy)	No. Assy	MPC Vol (cm3)	L_{acc} Rate at Upstream (cm3/s)	Fraction Released per sec	Release Fraction	Release Rate (Ci/sec)	X/Q (sec/m3)	DCF (Sv/Bq)	DCF (mRem/uCi)	Occ Time (sec)	EDE (mRem)	
							Gases						
H-3	8.72E+01	68	5.99E+06	1.25E-05	2.09E-12	0.30	3.72E-09	8.00E-03	2.75E-18	1.02E-08	2.59E+06	7.85E-07	
I-129	7.72E-03	68	5.99E+06	1.25E-05	2.09E-12	0.30	3.30E-13	8.00E-03	2.14E-16	7.92E-07	2.59E+06	5.41E-09	
Kr-85	1.43E+03	68	5.99E+06	1.25E-05	2.09E-12	0.30	6.11E-08	8.00E-03	1.14E-16	4.22E-07	2.59E+06	5.34E-04	
							Crud						
Co-60	6.50E+01	68	5.99E+06	1.25E-05	2.09E-12	1.00	9.25E-09	8.00E-03	1.24E-13	4.59E-04	2.59E+06	8.80E-02	
							Volatiles						
Sr-90	1.52E+04	68	5.99E+06	1.25E-05	2.09E-12	2.00E-04	4.33E-10	8.00E-03	6.44E-18	2.38E-08	2.59E+06	2.14E-07	
Ru-106	4.16E+03	68	5.99E+06	1.25E-05	2.09E-12	2.00E-04	1.18E-10	8.00E-03	0.00E+00	0.00E+00	2.59E+06	0.00E+00	
Cs-134	7.20E+03	68	5.99E+06	1.25E-05	2.09E-12	2.00E-04	2.05E-10	8.00E-03	7.37E-14	2.73E-04	2.59E+06	1.16E-03	
Cs-137	2.29E+04	68	5.99E+06	1.25E-05	2.09E-12	2.00E-04	6.52E-10	8.00E-03	6.68E-18	2.47E-08	2.59E+06	3.34E-07	
							Fines						
PU241	2.10E+04	68	5.99E+06	1.25E-05	2.09E-12	3.00E-05	8.97E-11	8.00E-03	6.48E-20	2.40E-10	2.59E+06	4.46E-10	
Y 90	1.52E+04	68	5.99E+06	1.25E-05	2.09E-12	3.00E-05	6.49E-11	8.00E-03	1.77E-16	6.55E-07	2.59E+06	8.81E-07	
PM147	8.88E+03	68	5.99E+06	1.25E-05	2.09E-12	3.00E-05	3.79E-11	8.00E-03	5.45E-19	2.02E-09	2.59E+06	1.58E-09	
CE144	2.46E+03	68	5.99E+06	1.25E-05	2.09E-12	3.00E-05	1.05E-11	8.00E-03	7.69E-16	2.85E-06	2.59E+06	6.19E-07	
PR144	2.46E+03	68	5.99E+06	1.25E-05	2.09E-12	3.00E-05	1.05E-11	8.00E-03	1.90E-15	7.03E-06	2.59E+06	1.53E-06	
EU154	1.07E+03	68	5.99E+06	1.25E-05	2.09E-12	3.00E-05	4.57E-12	8.00E-03	5.99E-14	2.22E-04	2.59E+06	2.10E-05	
CM244	9.30E+02	68	5.99E+06	1.25E-05	2.09E-12	3.00E-05	3.97E-12	8.00E-03	7.08E-19	2.62E-09	2.59E+06	2.16E-10	
PU238	7.49E+02	68	5.99E+06	1.25E-05	2.09E-12	3.00E-05	3.20E-12	8.00E-03	1.06E-18	3.92E-09	2.59E+06	2.60E-10	
SB125	6.40E+02	68	5.99E+06	1.25E-05	2.09E-12	3.00E-05	2.73E-12	8.00E-03	1.95E-14	7.22E-05	2.59E+06	4.09E-06	
EU155	3.51E+02	68	5.99E+06	1.25E-05	2.09E-12	3.00E-05	1.50E-12	8.00E-03	2.22E-15	8.21E-06	2.59E+06	2.55E-07	
AM241	2.20E+02	68	5.99E+06	1.25E-05	2.09E-12	3.00E-05	9.40E-13	8.00E-03	6.74E-16	2.49E-06	2.59E+06	4.85E-08	
TE125M	1.56E+02	68	5.99E+06	1.25E-05	2.09E-12	3.00E-05	6.66E-13	8.00E-03	2.23E-16	8.25E-07	2.59E+06	1.14E-08	
PU240	1.26E+02	68	5.99E+06	1.25E-05	2.09E-12	3.00E-05	5.38E-13	8.00E-03	1.09E-18	4.03E-09	2.59E+06	4.50E-11	
151Sm	0.00E+00	68	5.99E+06	1.25E-05	2.09E-12	3.00E-05	0.00E+00	8.00E-03	7.08E-21	2.62E-11	2.59E+06	0.00E+00	
239Pu	6.16E+01	68	5.99E+06	1.25E-05	2.09E-12	3.00E-05	2.63E-13	8.00E-03	2.65E-18	9.81E-09	2.59E+06	5.34E-11	
137mBa	2.16E+04	68	5.99E+06	1.25E-05	2.09E-12	3.00E-05	9.22E-11	8.00E-03	2.80E-14	1.04E-04	2.59E+06	1.98E-04	
106Rh	4.16E+03	68	5.99E+06	1.25E-05	2.09E-12	3.00E-05	1.78E-11	8.00E-03	1.01E-14	3.74E-05	2.59E+06	1.38E-05	
144mPr	0.00E+00	68	5.99E+06	1.25E-05	2.09E-12	3.00E-05	0.00E+00	8.00E-03	2.00E-16	7.40E-07	2.59E+06	0.00E+00	
243Am	7.39E+00	68	5.99E+06	1.25E-05	2.09E-12	3.00E-05	3.16E-14	8.00E-03	1.92E-15	7.10E-06	2.59E+06	4.65E-09	
242Cm	6.10E+00	68	5.99E+06	1.25E-05	2.09E-12	3.00E-05	2.61E-14	8.00E-03	1.13E-18	4.18E-09	2.59E+06	2.26E-12	
243Cm	4.81E+00	68	5.99E+06	1.25E-05	2.09E-12	3.00E-05	2.05E-14	8.00E-03	5.50E-15	2.04E-05	2.59E+06	8.66E-09	
239Np	7.39E+00	68	5.99E+06	1.25E-05	2.09E-12	3.00E-05	3.16E-14	8.00E-03	7.18E-15	2.66E-05	2.59E+06	1.74E-08	
237Np	7.05E-02	68	5.99E+06	1.25E-05	2.09E-12	3.00E-05	3.01E-16	8.00E-03	9.02E-16	3.34E-06	2.59E+06	2.08E-11	
242Pu	5.95E-01	68	5.99E+06	1.25E-05	2.09E-12	3.00E-05	2.54E-15	8.00E-03	9.69E-19	3.59E-09	2.59E+06	1.89E-13	
242Am	1.69E+00	68	5.99E+06	1.25E-05	2.09E-12	3.00E-05	7.22E-15	8.00E-03	5.51E-15	2.04E-05	2.59E+06	3.05E-09	
242mAm	1.70E+00	68	5.99E+06	1.25E-05	2.09E-12	3.00E-05	7.26E-15	8.00E-03	1.72E-17	6.36E-08	2.59E+06	9.57E-12	
											Total	8.99E-02	

MPC-68													
Accident Conditions													
Effective Dose Equivalent From Submersion													
Nuclide	Inventory (Ci/Assy)	No. Assy	MPC Vol (cm3)	L_{acc} Rate at Upstream (cm3/s)	Fraction Released per sec	Release Fraction	Release Rate (Ci/sec)	X/Q (sec/m3)	DCF (Sv/Bq)	DCF (mRem/uCi)	Occ Time (sec)	EDE (mRem)	
							Gases						
H-3	8.72E+01	68	5.99E+06	1.25E-05	2.09E-12	0.30	3.72E-09	8.00E-03	0.00E+00	0.00E+00	2.59E+06	0.00E+00	
I-129	7.72E-03	68	5.99E+06	1.25E-05	2.09E-12	0.30	3.30E-13	8.00E-03	1.64E-16	6.07E-07	2.59E+06	4.15E-09	
Kr-85	1.43E+03	68	5.99E+06	1.25E-05	2.09E-12	0.30	6.11E-08	8.00E-03	1.09E-16	4.03E-07	2.59E+06	5.10E-04	
							Crud						
Co-60	6.50E+01	68	5.99E+06	1.25E-05	2.09E-12	1.00	9.25E-09	8.00E-03	1.23E-13	4.55E-04	2.59E+06	8.73E-02	
							Volatiles						
Sr-90	1.52E+04	68	5.99E+06	1.25E-05	2.09E-12	2.00E-04	4.33E-10	8.00E-03	5.44E-18	2.01E-08	2.59E+06	1.80E-07	
Ru-106	4.16E+03	68	5.99E+06	1.25E-05	2.09E-12	2.00E-04	1.18E-10	8.00E-03	0.00E+00	0.00E+00	2.59E+06	0.00E+00	
Cs-134	7.20E+03	68	5.99E+06	1.25E-05	2.09E-12	2.00E-04	2.05E-10	8.00E-03	7.19E-14	2.66E-04	2.59E+06	1.13E-03	
Cs-137	2.29E+04	68	5.99E+06	1.25E-05	2.09E-12	2.00E-04	6.52E-10	8.00E-03	5.70E-18	2.11E-08	2.59E+06	2.85E-07	
							Fines						
PU241	2.10E+04	68	5.99E+06	1.25E-05	2.09E-12	3.00E-05	8.97E-11	8.00E-03	5.63E-20	2.08E-10	2.59E+06	3.87E-10	
Y 90	1.52E+04	68	5.99E+06	1.25E-05	2.09E-12	3.00E-05	6.49E-11	8.00E-03	1.62E-16	5.99E-07	2.59E+06	8.06E-07	
PM147	8.88E+03	68	5.99E+06	1.25E-05	2.09E-12	3.00E-05	3.79E-11	8.00E-03	4.46E-19	1.65E-09	2.59E+06	1.30E-09	
CE144	2.46E+03	68	5.99E+06	1.25E-05	2.09E-12	3.00E-05	1.05E-11	8.00E-03	6.68E-16	2.47E-06	2.59E+06	5.38E-07	
PR144	2.46E+03	68	5.99E+06	1.25E-05	2.09E-12	3.00E-05	1.05E-11	8.00E-03	1.87E-15	6.92E-06	2.59E+06	1.51E-06	
EU154	1.07E+03	68	5.99E+06	1.25E-05	2.09E-12	3.00E-05	4.57E-12	8.00E-03	5.87E-14	2.17E-04	2.59E+06	2.06E-05	
CM244	9.30E+02	68	5.99E+06	1.25E-05	2.09E-12	3.00E-05	3.97E-12	8.00E-03	1.46E-18	5.40E-09	2.59E+06	4.45E-10	
PU238	7.49E+02	68	5.99E+06	1.25E-05	2.09E-12	3.00E-05	3.20E-12	8.00E-03	1.68E-18	6.22E-09	2.59E+06	4.12E-10	
SB125	6.40E+02	68	5.99E+06	1.25E-05	2.09E-12	3.00E-05	2.73E-12	8.00E-03	1.87E-14	6.92E-05	2.59E+06	3.92E-06	
EU155	3.51E+02	68	5.99E+06	1.25E-05	2.09E-12	3.00E-05	1.50E-12	8.00E-03	1.85E-15	6.85E-06	2.59E+06	2.13E-07	
AM241	2.20E+02	68	5.99E+06	1.25E-05	2.09E-12	3.00E-05	9.40E-13	8.00E-03	5.21E-16	1.93E-06	2.59E+06	3.75E-08	
TE125M	1.56E+02	68	5.99E+06	1.25E-05	2.09E-12	3.00E-05	6.66E-13	8.00E-03	1.86E-16	6.88E-07	2.59E+06	9.50E-09	
PU240	1.26E+02	68	5.99E+06	1.25E-05	2.09E-12	3.00E-05	5.38E-13	8.00E-03	1.65E-18	6.11E-09	2.59E+06	6.81E-11	
151Sm	0.00E+00	68	5.99E+06	1.25E-05	2.09E-12	3.00E-05	0.00E+00	8.00E-03	1.13E-20	4.18E-11	2.59E+06	0.00E+00	
239Pu	6.16E+01	68	5.99E+06	1.25E-05	2.09E-12	3.00E-05	2.63E-13	8.00E-03	2.67E-18	9.88E-09	2.59E+06	5.38E-11	
137mBa	2.16E+04	68	5.99E+06	1.25E-05	2.09E-12	3.00E-05	9.22E-11	8.00E-03	2.73E-14	1.01E-04	2.59E+06	1.93E-04	
106Rh	4.16E+03	68	5.99E+06	1.25E-05	2.09E-12	3.00E-05	1.78E-11	8.00E-03	9.75E-15	3.61E-05	2.59E+06	1.33E-05	
144mPr	0.00E+00	68	5.99E+06	1.25E-05	2.09E-12	3.00E-05	0.00E+00	8.00E-03	1.56E-16	5.77E-07	2.59E+06	0.00E+00	
243Am	7.39E+00	68	5.99E+06	1.25E-05	2.09E-12	3.00E-05	3.16E-14	8.00E-03	1.55E-15	5.74E-06	2.59E+06	3.75E-09	
242Cm	6.10E+00	68	5.99E+06	1.25E-05	2.09E-12	3.00E-05	2.61E-14	8.00E-03	1.89E-18	6.99E-09	2.59E+06	3.77E-12	
243Cm	4.81E+00	68	5.99E+06	1.25E-05	2.09E-12	3.00E-05	2.05E-14	8.00E-03	5.00E-15	1.85E-05	2.59E+06	7.87E-09	
239Np	7.39E+00	68	5.99E+06	1.25E-05	2.09E-12	3.00E-05	3.16E-14	8.00E-03	6.50E-15	2.41E-05	2.59E+06	1.57E-08	
237Np	7.05E-02	68	5.99E+06	1.25E-05	2.09E-12	3.00E-05	3.01E-16	8.00E-03	7.69E-16	2.85E-06	2.59E+06	1.78E-11	
242Pu	5.95E-01	68	5.99E+06	1.25E-05	2.09E-12	3.00E-05	2.54E-15	8.00E-03	1.43E-18	5.29E-09	2.59E+06	2.79E-13	
242Am	1.69E+00	68	5.99E+06	1.25E-05	2.09E-12	3.00E-05	7.22E-15	8.00E-03	4.77E-16	1.76E-06	2.59E+06	2.64E-10	
242mAm	1.70E+00	68	5.99E+06	1.25E-05	2.09E-12	3.00E-05	7.26E-15	8.00E-03	1.72E-17	6.36E-08	2.59E+06	9.57E-12	
											Total	8.91E-02	

MPC-68													
Accident Conditions													
Effective Dose Equivalent From Submersion													
Nuclide	Inventory (Ci/Assy)	No. Assy	MPC Vol (cm3)	L_{acc} Rate at Upstream (cm3/s)	Fraction Released per sec	Release Fraction	Release Rate (Ci/sec)	X/Q (sec/m3)	DCF (Sv/Bq)	DCF (mRem/uCi)	Occ Time (sec)	EDE (mRem)	
							Gases						
H-3	8.72E+01	68	5.99E+06	1.25E-05	2.09E-12	0.30	3.72E-09	8.00E-03	0.00E+00	0.00E+00	2.59E+06	0.00E+00	
I-129	7.72E-03	68	5.99E+06	1.25E-05	2.09E-12	0.30	3.30E-13	8.00E-03	1.10E-15	4.07E-06	2.59E+06	2.78E-08	
Kr-85	1.43E+03	68	5.99E+06	1.25E-05	2.09E-12	0.30	6.11E-08	8.00E-03	2.20E-16	8.14E-07	2.59E+06	1.03E-03	
							Crud						
Co-60	6.50E+01	68	5.99E+06	1.25E-05	2.09E-12	1.00	9.25E-09	8.00E-03	1.78E-13	6.59E-04	2.59E+06	1.26E-01	
							Volatiles						
Sr-90	1.52E+04	68	5.99E+06	1.25E-05	2.09E-12	2.00E-04	4.33E-10	8.00E-03	2.28E-17	8.44E-08	2.59E+06	7.56E-07	
Ru-106	4.16E+03	68	5.99E+06	1.25E-05	2.09E-12	2.00E-04	1.18E-10	8.00E-03	0.00E+00	0.00E+00	2.59E+06	0.00E+00	
Cs-134	7.20E+03	68	5.99E+06	1.25E-05	2.09E-12	2.00E-04	2.05E-10	8.00E-03	1.20E-13	4.44E-04	2.59E+06	1.89E-03	
Cs-137	2.29E+04	68	5.99E+06	1.25E-05	2.09E-12	2.00E-04	6.52E-10	8.00E-03	2.29E-17	8.47E-08	2.59E+06	1.14E-06	
							Fines						
PU241	2.10E+04	68	5.99E+06	1.25E-05	2.09E-12	3.00E-05	8.97E-11	8.00E-03	2.19E-19	8.10E-10	2.59E+06	1.51E-09	
Y 90	1.52E+04	68	5.99E+06	1.25E-05	2.09E-12	3.00E-05	6.49E-11	8.00E-03	4.44E-16	1.64E-06	2.59E+06	2.21E-06	
PM147	8.88E+03	68	5.99E+06	1.25E-05	2.09E-12	3.00E-05	3.79E-11	8.00E-03	2.18E-18	8.07E-09	2.59E+06	6.34E-09	
CE144	2.46E+03	68	5.99E+06	1.25E-05	2.09E-12	3.00E-05	1.05E-11	8.00E-03	2.49E-15	9.21E-06	2.59E+06	2.01E-06	
PR144	2.46E+03	68	5.99E+06	1.25E-05	2.09E-12	3.00E-05	1.05E-11	8.00E-03	2.99E-15	1.11E-05	2.59E+06	2.41E-06	
EU154	1.07E+03	68	5.99E+06	1.25E-05	2.09E-12	3.00E-05	4.57E-12	8.00E-03	9.43E-14	3.49E-04	2.59E+06	3.30E-05	
CM244	9.30E+02	68	5.99E+06	1.25E-05	2.09E-12	3.00E-05	3.97E-12	8.00E-03	8.82E-18	3.26E-08	2.59E+06	2.69E-09	
PU238	7.49E+02	68	5.99E+06	1.25E-05	2.09E-12	3.00E-05	3.20E-12	8.00E-03	9.30E-18	3.44E-08	2.59E+06	2.28E-09	
SB125	6.40E+02	68	5.99E+06	1.25E-05	2.09E-12	3.00E-05	2.73E-12	8.00E-03	3.53E-14	1.31E-04	2.59E+06	7.40E-06	
EU155	3.51E+02	68	5.99E+06	1.25E-05	2.09E-12	3.00E-05	1.50E-12	8.00E-03	8.09E-15	2.99E-05	2.59E+06	9.30E-07	
AM241	2.20E+02	68	5.99E+06	1.25E-05	2.09E-12	3.00E-05	9.40E-13	8.00E-03	2.87E-15	1.06E-05	2.59E+06	2.07E-07	
TE125M	1.56E+02	68	5.99E+06	1.25E-05	2.09E-12	3.00E-05	6.66E-13	8.00E-03	1.22E-15	4.51E-06	2.59E+06	6.23E-08	
PU240	1.26E+02	68	5.99E+06	1.25E-05	2.09E-12	3.00E-05	5.38E-13	8.00E-03	9.26E-18	3.43E-08	2.59E+06	3.82E-10	
151Sm	0.00E+00	68	5.99E+06	1.25E-05	2.09E-12	3.00E-05	0.00E+00	8.00E-03	7.09E-20	2.62E-10	2.59E+06	0.00E+00	
239Pu	6.16E+01	68	5.99E+06	1.25E-05	2.09E-12	3.00E-05	2.63E-13	8.00E-03	9.47E-18	3.50E-08	2.59E+06	1.91E-10	
137mBa	2.16E+04	68	5.99E+06	1.25E-05	2.09E-12	3.00E-05	9.22E-11	8.00E-03	4.63E-14	1.71E-04	2.59E+06	3.27E-04	
106Rh	4.16E+03	68	5.99E+06	1.25E-05	2.09E-12	3.00E-05	1.78E-11	8.00E-03	1.72E-14	6.36E-05	2.59E+06	2.34E-05	
144mPr	0.00E+00	68	5.99E+06	1.25E-05	2.09E-12	3.00E-05	0.00E+00	8.00E-03	8.16E-16	3.02E-06	2.59E+06	0.00E+00	
243Am	7.39E+00	68	5.99E+06	1.25E-05	2.09E-12	3.00E-05	3.16E-14	8.00E-03	7.47E-15	2.76E-05	2.59E+06	1.81E-08	
242Cm	6.10E+00	68	5.99E+06	1.25E-05	2.09E-12	3.00E-05	2.61E-14	8.00E-03	1.06E-17	3.92E-08	2.59E+06	2.12E-11	
243Cm	4.81E+00	68	5.99E+06	1.25E-05	2.09E-12	3.00E-05	2.05E-14	8.00E-03	1.50E-14	5.55E-05	2.59E+06	2.36E-08	
239Np	7.39E+00	68	5.99E+06	1.25E-05	2.09E-12	3.00E-05	3.16E-14	8.00E-03	2.00E-14	7.40E-05	2.59E+06	4.84E-08	
237Np	7.05E-02	68	5.99E+06	1.25E-05	2.09E-12	3.00E-05	3.01E-16	8.00E-03	3.20E-15	1.18E-05	2.59E+06	7.39E-11	
242Pu	5.95E-01	68	5.99E+06	1.25E-05	2.09E-12	3.00E-05	2.54E-15	8.00E-03	7.90E-18	2.92E-08	2.59E+06	1.54E-12	
242Am	1.69E+00	68	5.99E+06	1.25E-05	2.09E-12	3.00E-05	7.22E-15	8.00E-03	1.88E-15	6.96E-06	2.59E+06	1.04E-09	
242mAm	1.70E+00	68	5.99E+06	1.25E-05	2.09E-12	3.00E-05	7.26E-15	8.00E-03	7.94E-17	2.94E-07	2.59E+06	4.42E-11	
											Total	1.30E-01	

MPC-68													
Accident Conditions													
Effective Dose Equivalent From Submersion													
Nuclide	Inventory (Ci/Assy)	No. Assy	MPC Vol (cm3)	L_{acc} Rate at Upstream (cm3/s)	Fraction Released per sec	Release Fraction	Release Rate (Ci/sec)	X/Q (sec/m3)	DCF (Sv/Bq)	DCF (mRem/uCi)	Occ Time (sec)	EDE (mRem)	
							Gases						
H-3	8.72E+01	68	5.99E+06	1.25E-05	2.09E-12	0.30	3.72E-09	8.00E-03	0.00E+00	0.00E+00	2.59E+06	0.00E+00	
I-129	7.72E-03	68	5.99E+06	1.25E-05	2.09E-12	0.30	3.30E-13	8.00E-03	3.86E-16	1.43E-06	2.59E+06	9.76E-09	
Kr-85	1.43E+03	68	5.99E+06	1.25E-05	2.09E-12	0.30	6.11E-08	8.00E-03	1.18E-16	4.37E-07	2.59E+06	5.52E-04	
							Crud						
Co-60	6.50E+01	68	5.99E+06	1.25E-05	2.09E-12	1.00	9.25E-09	8.00E-03	1.27E-13	4.70E-04	2.59E+06	9.01E-02	
							Volatiles						
Sr-90	1.52E+04	68	5.99E+06	1.25E-05	2.09E-12	2.00E-04	4.33E-10	8.00E-03	7.33E-18	2.71E-08	2.59E+06	2.43E-07	
Ru-106	4.16E+03	68	5.99E+06	1.25E-05	2.09E-12	2.00E-04	1.18E-10	8.00E-03	0.00E+00	0.00E+00	2.59E+06	0.00E+00	
Cs-134	7.20E+03	68	5.99E+06	1.25E-05	2.09E-12	2.00E-04	2.05E-10	8.00E-03	7.57E-14	2.80E-04	2.59E+06	1.19E-03	
Cs-137	2.29E+04	68	5.99E+06	1.25E-05	2.09E-12	2.00E-04	6.52E-10	8.00E-03	7.55E-18	2.79E-08	2.59E+06	3.77E-07	
							Fines						
PU241	2.10E+04	68	5.99E+06	1.25E-05	2.09E-12	3.00E-05	8.97E-11	8.00E-03	6.98E-20	2.58E-10	2.59E+06	4.80E-10	
Y 90	1.52E+04	68	5.99E+06	1.25E-05	2.09E-12	3.00E-05	6.49E-11	8.00E-03	1.87E-16	6.92E-07	2.59E+06	9.31E-07	
PM147	8.88E+03	68	5.99E+06	1.25E-05	2.09E-12	3.00E-05	3.79E-11	8.00E-03	6.75E-19	2.50E-09	2.59E+06	1.96E-09	
CE144	2.46E+03	68	5.99E+06	1.25E-05	2.09E-12	3.00E-05	1.05E-11	8.00E-03	8.33E-16	3.08E-06	2.59E+06	6.71E-07	
PR144	2.46E+03	68	5.99E+06	1.25E-05	2.09E-12	3.00E-05	1.05E-11	8.00E-03	1.95E-15	7.22E-06	2.59E+06	1.57E-06	
EU154	1.07E+03	68	5.99E+06	1.25E-05	2.09E-12	3.00E-05	4.57E-12	8.00E-03	6.15E-14	2.28E-04	2.59E+06	2.15E-05	
CM244	9.30E+02	68	5.99E+06	1.25E-05	2.09E-12	3.00E-05	3.97E-12	8.00E-03	4.19E-18	1.55E-08	2.59E+06	1.28E-09	
PU238	7.49E+02	68	5.99E+06	1.25E-05	2.09E-12	3.00E-05	3.20E-12	8.00E-03	4.01E-18	1.48E-08	2.59E+06	9.83E-10	
SB125	6.40E+02	68	5.99E+06	1.25E-05	2.09E-12	3.00E-05	2.73E-12	8.00E-03	2.01E-14	7.44E-05	2.59E+06	4.21E-06	
EU155	3.51E+02	68	5.99E+06	1.25E-05	2.09E-12	3.00E-05	1.50E-12	8.00E-03	2.41E-15	8.92E-06	2.59E+06	2.77E-07	
AM241	2.20E+02	68	5.99E+06	1.25E-05	2.09E-12	3.00E-05	9.40E-13	8.00E-03	7.83E-16	2.90E-06	2.59E+06	5.64E-08	
TE125M	1.56E+02	68	5.99E+06	1.25E-05	2.09E-12	3.00E-05	6.66E-13	8.00E-03	4.64E-16	1.72E-06	2.59E+06	2.37E-08	
PU240	1.26E+02	68	5.99E+06	1.25E-05	2.09E-12	3.00E-05	5.38E-13	8.00E-03	3.92E-18	1.45E-08	2.59E+06	1.62E-10	
151Sm	0.00E+00	68	5.99E+06	1.25E-05	2.09E-12	3.00E-05	0.00E+00	8.00E-03	3.58E-20	1.32E-10	2.59E+06	0.00E+00	
239Pu	6.16E+01	68	5.99E+06	1.25E-05	2.09E-12	3.00E-05	2.63E-13	8.00E-03	3.88E-18	1.44E-08	2.59E+06	7.83E-11	
137mBa	2.16E+04	68	5.99E+06	1.25E-05	2.09E-12	3.00E-05	9.22E-11	8.00E-03	2.88E-14	1.07E-04	2.59E+06	2.04E-04	
106Rh	4.16E+03	68	5.99E+06	1.25E-05	2.09E-12	3.00E-05	1.78E-11	8.00E-03	1.03E-14	3.81E-05	2.59E+06	1.40E-05	
144mPr	0.00E+00	68	5.99E+06	1.25E-05	2.09E-12	3.00E-05	0.00E+00	8.00E-03	2.81E-16	1.04E-06	2.59E+06	0.00E+00	
243Am	7.39E+00	68	5.99E+06	1.25E-05	2.09E-12	3.00E-05	3.16E-14	8.00E-03	2.09E-15	7.73E-06	2.59E+06	5.06E-09	
242Cm	6.10E+00	68	5.99E+06	1.25E-05	2.09E-12	3.00E-05	2.61E-14	8.00E-03	4.91E-18	1.82E-08	2.59E+06	9.81E-12	
243Cm	4.81E+00	68	5.99E+06	1.25E-05	2.09E-12	3.00E-05	2.05E-14	8.00E-03	5.76E-15	2.13E-05	2.59E+06	9.07E-09	
239Np	7.39E+00	68	5.99E+06	1.25E-05	2.09E-12	3.00E-05	3.16E-14	8.00E-03	7.52E-15	2.78E-05	2.59E+06	1.82E-08	
237Np	7.05E-02	68	5.99E+06	1.25E-05	2.09E-12	3.00E-05	3.01E-16	8.00E-03	9.94E-16	3.68E-06	2.59E+06	2.29E-11	
242Pu	5.95E-01	68	5.99E+06	1.25E-05	2.09E-12	3.00E-05	2.54E-15	8.00E-03	3.32E-18	1.23E-08	2.59E+06	6.47E-13	
242Am	1.69E+00	68	5.99E+06	1.25E-05	2.09E-12	3.00E-05	7.22E-15	8.00E-03	5.94E-16	2.20E-06	2.59E+06	3.29E-10	
242mAm	1.70E+00	68	5.99E+06	1.25E-05	2.09E-12	3.00E-05	7.26E-15	8.00E-03	2.95E-17	1.09E-07	2.59E+06	1.64E-11	
											Total	9.21E-02	

MPC-68													
Accident Conditions													
Effective Dose Equivalent From Submersion													
Nuclide	Inventory (Ci/Assy)	No. Assy	MPC Vol (cm3)	L_{acc} Rate at Upstream (cm3/s)	Fraction Released per sec	Release Fraction	Release Rate (Ci/sec)	X/Q (sec/m3)	DCF (Sv/Bq)	DCF (mRem/uCi)	Occ Time (sec)	EDE (mRem)	
							Gases						
H-3	8.72E+01	68	5.99E+06	1.25E-05	2.09E-12	0.30	3.72E-09	8.00E-03	3.31E-19	1.22E-09	2.59E+06	9.45E-08	
I-129	7.72E-03	68	5.99E+06	1.25E-05	2.09E-12	0.30	3.30E-13	8.00E-03	3.80E-16	1.41E-06	2.59E+06	9.60E-09	
Kr-85	1.43E+03	68	5.99E+06	1.25E-05	2.09E-12	0.30	6.11E-08	8.00E-03	1.19E-16	4.40E-07	2.59E+06	5.57E-04	
							Crud						
Co-60	6.50E+01	68	5.99E+06	1.25E-05	2.09E-12	1.00	9.25E-09	8.00E-03	1.26E-13	4.66E-04	2.59E+06	8.94E-02	
							Volatiles						
Sr-90	1.52E+04	68	5.99E+06	1.25E-05	2.09E-12	2.00E-04	4.33E-10	8.00E-03	7.53E-18	2.79E-08	2.59E+06	2.50E-07	
Ru-106	4.16E+03	68	5.99E+06	1.25E-05	2.09E-12	2.00E-04	1.18E-10	8.00E-03	0.00E+00	0.00E+00	2.59E+06	0.00E+00	
Cs-134	7.20E+03	68	5.99E+06	1.25E-05	2.09E-12	2.00E-04	2.05E-10	8.00E-03	7.57E-14	2.80E-04	2.59E+06	1.19E-03	
Cs-137	2.29E+04	68	5.99E+06	1.25E-05	2.09E-12	2.00E-04	6.52E-10	8.00E-03	7.74E-18	2.86E-08	2.59E+06	3.87E-07	
							Fines						
PU241	2.10E+04	68	5.99E+06	1.25E-05	2.09E-12	3.00E-05	8.97E-11	8.00E-03	7.25E-20	2.68E-10	2.59E+06	4.98E-10	
Y 90	1.52E+04	68	5.99E+06	1.25E-05	2.09E-12	3.00E-05	6.49E-11	8.00E-03	1.90E-16	7.03E-07	2.59E+06	9.46E-07	
PM147	8.88E+03	68	5.99E+06	1.25E-05	2.09E-12	3.00E-05	3.79E-11	8.00E-03	6.93E-19	2.56E-09	2.59E+06	2.01E-09	
CE144	2.46E+03	68	5.99E+06	1.25E-05	2.09E-12	3.00E-05	1.05E-11	8.00E-03	8.53E-16	3.16E-06	2.59E+06	6.87E-07	
PR144	2.46E+03	68	5.99E+06	1.25E-05	2.09E-12	3.00E-05	1.05E-11	8.00E-03	1.95E-15	7.22E-06	2.59E+06	1.57E-06	
EU154	1.07E+03	68	5.99E+06	1.25E-05	2.09E-12	3.00E-05	4.57E-12	8.00E-03	6.14E-14	2.27E-04	2.59E+06	2.15E-05	
CM244	9.30E+02	68	5.99E+06	1.25E-05	2.09E-12	3.00E-05	3.97E-12	8.00E-03	4.91E-18	1.82E-08	2.59E+06	1.50E-09	
PU238	7.49E+02	68	5.99E+06	1.25E-05	2.09E-12	3.00E-05	3.20E-12	8.00E-03	4.88E-18	1.81E-08	2.59E+06	1.20E-09	
SB125	6.40E+02	68	5.99E+06	1.25E-05	2.09E-12	3.00E-05	2.73E-12	8.00E-03	2.02E-14	7.47E-05	2.59E+06	4.23E-06	
EU155	3.51E+02	68	5.99E+06	1.25E-05	2.09E-12	3.00E-05	1.50E-12	8.00E-03	2.49E-15	9.21E-06	2.59E+06	2.86E-07	
AM241	2.20E+02	68	5.99E+06	1.25E-05	2.09E-12	3.00E-05	9.40E-13	8.00E-03	8.18E-16	3.03E-06	2.59E+06	5.89E-08	
TE125M	1.56E+02	68	5.99E+06	1.25E-05	2.09E-12	3.00E-05	6.66E-13	8.00E-03	4.53E-16	1.68E-06	2.59E+06	2.31E-08	
PU240	1.26E+02	68	5.99E+06	1.25E-05	2.09E-12	3.00E-05	5.38E-13	8.00E-03	4.75E-18	1.76E-08	2.59E+06	1.96E-10	
151Sm	0.00E+00	68	5.99E+06	1.25E-05	2.09E-12	3.00E-05	0.00E+00	8.00E-03	3.61E-20	1.34E-10	2.59E+06	0.00E+00	
239Pu	6.16E+01	68	5.99E+06	1.25E-05	2.09E-12	3.00E-05	2.63E-13	8.00E-03	4.24E-18	1.57E-08	2.59E+06	8.55E-11	
137mBa	2.16E+04	68	5.99E+06	1.25E-05	2.09E-12	3.00E-05	9.22E-11	8.00E-03	2.88E-14	1.07E-04	2.59E+06	2.04E-04	
106Rh	4.16E+03	68	5.99E+06	1.25E-05	2.09E-12	3.00E-05	1.78E-11	8.00E-03	1.04E-14	3.85E-05	2.59E+06	1.42E-05	
144mPr	0.00E+00	68	5.99E+06	1.25E-05	2.09E-12	3.00E-05	0.00E+00	8.00E-03	2.79E-16	1.03E-06	2.59E+06	0.00E+00	
243Am	7.39E+00	68	5.99E+06	1.25E-05	2.09E-12	3.00E-05	3.16E-14	8.00E-03	2.18E-15	8.07E-06	2.59E+06	5.27E-09	
242Cm	6.10E+00	68	5.99E+06	1.25E-05	2.09E-12	3.00E-05	2.61E-14	8.00E-03	5.69E-18	2.11E-08	2.59E+06	1.14E-11	
243Cm	4.81E+00	68	5.99E+06	1.25E-05	2.09E-12	3.00E-05	2.05E-14	8.00E-03	5.88E-15	2.18E-05	2.59E+06	9.26E-09	
239Np	7.39E+00	68	5.99E+06	1.25E-05	2.09E-12	3.00E-05	3.16E-14	8.00E-03	7.69E-15	2.85E-05	2.59E+06	1.86E-08	
237Np	7.05E-02	68	5.99E+06	1.25E-05	2.09E-12	3.00E-05	3.01E-16	8.00E-03	1.03E-15	3.81E-06	2.59E+06	2.38E-11	
242Pu	5.95E-01	68	5.99E+06	1.25E-05	2.09E-12	3.00E-05	2.54E-15	8.00E-03	4.01E-18	1.48E-08	2.59E+06	7.81E-13	
242Am	1.69E+00	68	5.99E+06	1.25E-05	2.09E-12	3.00E-05	7.22E-15	8.00E-03	6.15E-16	2.28E-06	2.59E+06	3.40E-10	
242mAm	1.70E+00	68	5.99E+06	1.25E-05	2.09E-12	3.00E-05	7.26E-15	8.00E-03	3.17E-17	1.17E-07	2.59E+06	1.76E-11	
											Total	9.14E-02	

MPC-68													
Accident Conditions													
Effective Dose Equivalent From Submersion													
Nuclide	Inventory (Ci/Assy)	No. Assy	MPC Vol (cm3)	L_{acc} Rate at Upstream (cm3/s)	Fraction Released per sec	Release Fraction	Release Rate (Ci/sec)	X/Q (sec/m3)	DCF (Sv/Bq)	DCF (mRem/uCi)	Occ Time (sec)	EDE (mRem)	
							Gases						
H-3	8.72E+01	68	5.99E+06	1.25E-05	2.09E-12	0.30	3.72E-09	8.00E-03	0.00E+00	0.00E+00	2.59E+06	0.00E+00	
I-129	7.72E-03	68	5.99E+06	1.25E-05	2.09E-12	0.30	3.30E-13	8.00E-03	1.10E-15	4.07E-06	2.59E+06	2.78E-08	
Kr-85	1.43E+03	68	5.99E+06	1.25E-05	2.09E-12	0.30	6.11E-08	8.00E-03	1.32E-14	4.88E-05	2.59E+06	6.18E-02	
							Crud						
Co-60	6.50E+01	68	5.99E+06	1.25E-05	2.09E-12	1.00	9.25E-09	8.00E-03	1.45E-13	5.37E-04	2.59E+06	1.03E-01	
							Volatiles						
Sr-90	1.52E+04	68	5.99E+06	1.25E-05	2.09E-12	2.00E-04	4.33E-10	8.00E-03	9.20E-15	3.40E-05	2.59E+06	3.05E-04	
Ru-106	4.16E+03	68	5.99E+06	1.25E-05	2.09E-12	2.00E-04	1.18E-10	8.00E-03	0.00E+00	0.00E+00	2.59E+06	0.00E+00	
Cs-134	7.20E+03	68	5.99E+06	1.25E-05	2.09E-12	2.00E-04	2.05E-10	8.00E-03	9.45E-14	3.50E-04	2.59E+06	1.49E-03	
Cs-137	2.29E+04	68	5.99E+06	1.25E-05	2.09E-12	2.00E-04	6.52E-10	8.00E-03	8.63E-15	3.19E-05	2.59E+06	4.31E-04	
							Fines						
PU241	2.10E+04	68	5.99E+06	1.25E-05	2.09E-12	3.00E-05	8.97E-11	8.00E-03	1.17E-19	4.33E-10	2.59E+06	8.04E-10	
Y 90	1.52E+04	68	5.99E+06	1.25E-05	2.09E-12	3.00E-05	6.49E-11	8.00E-03	6.24E-14	2.31E-04	2.59E+06	3.11E-04	
PM147	8.88E+03	68	5.99E+06	1.25E-05	2.09E-12	3.00E-05	3.79E-11	8.00E-03	8.11E-16	3.00E-06	2.59E+06	2.36E-06	
CE144	2.46E+03	68	5.99E+06	1.25E-05	2.09E-12	3.00E-05	1.05E-11	8.00E-03	2.93E-15	1.08E-05	2.59E+06	2.36E-06	
PR144	2.46E+03	68	5.99E+06	1.25E-05	2.09E-12	3.00E-05	1.05E-11	8.00E-03	8.43E-14	3.12E-04	2.59E+06	6.79E-05	
EU154	1.07E+03	68	5.99E+06	1.25E-05	2.09E-12	3.00E-05	4.57E-12	8.00E-03	8.29E-14	3.07E-04	2.59E+06	2.90E-05	
CM244	9.30E+02	68	5.99E+06	1.25E-05	2.09E-12	3.00E-05	3.97E-12	8.00E-03	3.91E-17	1.45E-07	2.59E+06	1.19E-08	
PU238	7.49E+02	68	5.99E+06	1.25E-05	2.09E-12	3.00E-05	3.20E-12	8.00E-03	4.09E-17	1.51E-07	2.59E+06	1.00E-08	
SB125	6.40E+02	68	5.99E+06	1.25E-05	2.09E-12	3.00E-05	2.73E-12	8.00E-03	2.65E-14	9.81E-05	2.59E+06	5.55E-06	
EU155	3.51E+02	68	5.99E+06	1.25E-05	2.09E-12	3.00E-05	1.50E-12	8.00E-03	3.39E-15	1.25E-05	2.59E+06	3.90E-07	
AM241	2.20E+02	68	5.99E+06	1.25E-05	2.09E-12	3.00E-05	9.40E-13	8.00E-03	1.28E-15	4.74E-06	2.59E+06	9.22E-08	
TE125M	1.56E+02	68	5.99E+06	1.25E-05	2.09E-12	3.00E-05	6.66E-13	8.00E-03	1.94E-15	7.18E-06	2.59E+06	9.91E-08	
PU240	1.26E+02	68	5.99E+06	1.25E-05	2.09E-12	3.00E-05	5.38E-13	8.00E-03	3.92E-17	1.45E-07	2.59E+06	1.62E-09	
151Sm	0.00E+00	68	5.99E+06	1.25E-05	2.09E-12	3.00E-05	0.00E+00	8.00E-03	1.90E-20	7.03E-11	2.59E+06	0.00E+00	
239Pu	6.16E+01	68	5.99E+06	1.25E-05	2.09E-12	3.00E-05	2.63E-13	8.00E-03	1.86E-17	6.88E-08	2.59E+06	3.75E-10	
137mBa	2.16E+04	68	5.99E+06	1.25E-05	2.09E-12	3.00E-05	9.22E-11	8.00E-03	3.73E-14	1.38E-04	2.59E+06	2.64E-04	
106Rh	4.16E+03	68	5.99E+06	1.25E-05	2.09E-12	3.00E-05	1.78E-11	8.00E-03	1.09E-13	4.03E-04	2.59E+06	1.48E-04	
144mPr	0.00E+00	68	5.99E+06	1.25E-05	2.09E-12	3.00E-05	0.00E+00	8.00E-03	5.08E-16	1.88E-06	2.59E+06	0.00E+00	
243Am	7.39E+00	68	5.99E+06	1.25E-05	2.09E-12	3.00E-05	3.16E-14	8.00E-03	2.75E-15	1.02E-05	2.59E+06	6.65E-09	
242Cm	6.10E+00	68	5.99E+06	1.25E-05	2.09E-12	3.00E-05	2.61E-14	8.00E-03	4.29E-17	1.59E-07	2.59E+06	8.57E-11	
243Cm	4.81E+00	68	5.99E+06	1.25E-05	2.09E-12	3.00E-05	2.05E-14	8.00E-03	9.79E-15	3.62E-05	2.59E+06	1.54E-08	
239Np	7.39E+00	68	5.99E+06	1.25E-05	2.09E-12	3.00E-05	3.16E-14	8.00E-03	1.60E-14	5.92E-05	2.59E+06	3.87E-08	
237Np	7.05E-02	68	5.99E+06	1.25E-05	2.09E-12	3.00E-05	3.01E-16	8.00E-03	1.54E-15	5.70E-06	2.59E+06	3.55E-11	
242Pu	5.95E-01	68	5.99E+06	1.25E-05	2.09E-12	3.00E-05	2.54E-15	8.00E-03	3.27E-17	1.21E-07	2.59E+06	6.37E-12	
242Am	1.69E+00	68	5.99E+06	1.25E-05	2.09E-12	3.00E-05	7.22E-15	8.00E-03	8.20E-15	3.03E-05	2.59E+06	4.54E-09	
242mAm	1.70E+00	68	5.99E+06	1.25E-05	2.09E-12	3.00E-05	7.26E-15	8.00E-03	1.36E-16	5.03E-07	2.59E+06	7.57E-11	
											Total	1.68E-01	